

Studies in organic and medicinal chemistry:
(i) Synthesis, antimicrobial evaluation, and photophysical studies of novel conjugated systems; (ii) Antimicrobial evaluation of pyrazolopyrimidinone heterocycles.

A thesis submitted by

Amanda Doyle B.Sc. (Hons.)

to

Maynooth University

for the degree of Doctor of Philosophy.



**Maynooth
University**
National University
of Ireland Maynooth

Volume 1 of 2

Based on the research carried out in the
Department of Chemistry, Faculty of Science and Engineering,
Maynooth University
under the supervision of
Prof. John C. Stephens
October 2020

Table of contents

Abstract	1
List of Abbreviations	4
Chapter One. Antimicrobial agents: Cinnamaldehydes and pyrazolopyrimidinones	6
1.1 Introduction	6
1.1.1 Antimicrobial agents	6
1.1.2 Natural products	6
1.1.3 Commercial use of <i>trans</i> -cinnamaldehyde	7
1.1.4 Limitations of <i>trans</i> -cinnamaldehyde for commercial applications	7
1.1.5 General medicinal properties of cinnamaldehyde and its derivatives	8
1.1.6 Molecular mechanism: Cinnamaldehyde as an electrophile	9
1.1.7 Antibacterial activity of cinnamaldehyde and its derivatives	11
1.1.7.1 General antibacterial activity of cinnamaldehyde and its derivatives	11
1.1.7.2 Antibacterial mechanisms of action displayed by cinnamaldehyde and its derivatives	12
1.1.8 Access to cinnamaldehydes – overview of some synthetic routes	13
1.1.8.1 Oxidative enamine catalysis	13
1.1.8.2 Palladium-catalyzed Heck-Saegusa reaction	14
1.1.8.3 Dess-Martin oxidation of alcohols	15
1.1.8.4 Wittig procedure	15
1.1.9 Synthetic versus natural medicinal agents	16
1.1.10 Pyrazolopyrimidinones as medicinal agents	17
1.1.11 Antimicrobial activity of pyrazolo[1,5- <i>a</i>]pyrimidines	18
1.1.12 Synthesis of 4- <i>H</i> -pyrazolo[1,5- <i>a</i>]pyrimidin-7-ones	19
1.1.13 Aims of our antimicrobial research	20
1.2 Cinnamaldehydes Results and Discussion	21
1.2.1 Synthesis of cinnamaldehydes	21
1.2.2 Overview of synthetic strategies to access cinnamaldehydes	22
1.2.3 Wittig reaction mechanism	24
1.2.4 Synthesis of 4-methylcinnamaldehyde	27
1.2.5 Structural characterization of a cinnamaldehyde – 4-cyanocinnamaldehyde 38	30
1.2.6 Methods for determining antimicrobial activity – antimicrobial susceptibility tests (ASTs)	32
1.2.6.1 Microdilution – an AST dilution method	32
1.2.6.2 Agar Disk Diffusion method – an AST diffusion method	34
1.2.6.3 Biological evaluation of cinnamaldehydes by microdilution	35
1.2.7 Comparison of electrophilicity of cinnamaldehydes	36
1.2.7.1 Assessment of antibacterial activity of cinnamaldehydes in relation to electrophilicity	37

1.2.8	Cysteamine assay	40
1.2.9	<i>Galleria mellonella</i> <i>in vivo</i> toxicity study	44
1.2.10	Preliminary mechanism of action study	46
1.3	Pyrazolo[1,5-<i>a</i>]pyrimidin-7-ones Results and Discussion	49
1.3.1	Antimicrobial evaluation of group 1a pyrazolo[1,5- <i>a</i>]pyrimidin-7-ones	52
1.3.2	Antimicrobial evaluation of group 1b pyrazolo[1,5- <i>a</i>]pyrimidin-7-ones	54
1.3.3	Antimicrobial evaluation of group 1c pyrazolo[1,5- <i>a</i>]pyrimidin-7-ones	57
1.3.4	Antimicrobial evaluation of group 2a pyrazolo[1,5- <i>a</i>]pyrimidin-7-ones	59
1.3.5	Antimicrobial evaluation of group 2b pyrazolo[1,5- <i>a</i>]pyrimidin-7-ones	61
1.3.6	Antibacterial evaluation of select pyrazolo[1,5- <i>a</i>]pyrimidin-7-ones against clinically-relevant MRSA and <i>P. aeruginosa</i> .	65
1.3.7	Antibacterial evaluation of select pyrazolo[1,5- <i>a</i>]pyrimidin-7-ones against clinically-relevant MRSA	66
1.3.8	Antibacterial evaluation of select pyrazolo[1,5- <i>a</i>]pyrimidin-7-ones against clinically-relevant <i>P. aeruginosa</i>	68
1.3.9	<i>Galleria mellonella</i> <i>in vivo</i> toxicity study	70
1.3.10	Therapeutic effect - <i>Galleria mellonella</i> <i>in vivo</i> study	71
1.4	Conclusion	79
1.5	Experimental Procedure	82
1.5.1	General information for chemical synthesis	82
1.5.2	General procedure and experimental details for the synthesis of (<i>E</i>)-cinnamaldehyde analogues	82
1.5.3	Procedures for the synthesis of cinnamaldehyde analogues deviating from general procedure	86
1.5.4	Cysteamine assay protocols	88
1.5.5	Biological evaluation of <i>trans</i> -cinnamaldehydes	89
1.5.5.1	<i>In vitro</i> bacterial screening of <i>trans</i> -cinnamaldehydes	89
1.5.5.1.1	Materials and methods for <i>trans</i> -cinnamaldehydes	89
1.5.5.1.2	Susceptibility assay for <i>trans</i> -cinnamaldehydes	90
1.5.5.2	Cell constituent release assessment for <i>trans</i> -cinnamaldehydes	90
1.5.5.3	<i>Galleria mellonella</i> <i>in vivo</i> compound toxicity assay for <i>trans</i> -cinnamaldehydes	91
1.5.6	Biological evaluation of pyrazolo[1,5- <i>a</i>]pyrimidin-7-ones	92
1.5.6.1	<i>In vitro</i> antimicrobial screening of pyrazolo[1,5- <i>a</i>]pyrimidin-7-ones	92
1.5.6.1.1	Materials and methods for pyrazolo[1,5- <i>a</i>]pyrimidin-7-ones	92
1.5.6.1.2	Susceptibility assay for pyrazolo[1,5- <i>a</i>]pyrimidin-7-ones	92
1.5.6.2	<i>Galleria mellonella</i> <i>in vivo</i> toxicity assay for pyrazolo[1,5- <i>a</i>]pyrimidin-7-ones	93

1.5.6.3	<i>Galleria mellonella</i> in vivo therapeutic assessment for pyrazolo[1,5- <i>a</i>]pyrimidin-7-ones	94
---------	--	----

Chapter Two: Synthesis of trienes 95

2.1	Introduction	95
2.1.1	Applications of trienes	95
2.1.1.1	Trienes as motifs in biologically active compounds	95
2.1.1.2	Trienes as reactants in synthetic applications	98
2.1.2	Synthetic methodologies used to access trienes	99
2.1.2.1	Synthetic strategies using transition metals to access 1,3,5-hexatrienes	100
2.1.2.2	Access to 1,3,5-hexatrienes using synthetic methodologies that do not incorporate transition metals	102
2.1.3	Traditional Knoevenagel-condensation	104
2.1.3.1	Emil Knoevenagel publications (1894-1898)	104
2.1.3.2	Limitations of the Knoevenagel-condensation	106
2.1.4	Knoevenagel-type condensation	107
2.1.5	Aluminium oxide (alumina) as a catalyst	108
2.1.6	Aims of triene synthesis	109
2.2	Results and Discussion	110
2.2.1	Synthesis of 1,3,5-hexatrienes	110
2.2.2	(1 <i>E</i> ,3 <i>E</i> ,5 <i>E</i>)-1,3-Bis-phenylsulfonyl-6-phenyl-hexa-1,3,5-triene percentage conversion estimation using quantitative NMR (qNMR)	112
2.2.2.1	Effect of base on the synthesis of (1 <i>E</i> ,3 <i>E</i> ,5 <i>E</i>)-1,3-bis-phenylsulfonyl-6-phenyl-hexa-1,3,5-triene 105	115
2.2.2.2	Effect of solvent on the synthesis of (1 <i>E</i> ,3 <i>E</i> ,5 <i>E</i>)-1,3-bis-phenylsulfonyl-6-phenyl-hexa-1,3,5-triene 105	117
2.2.2.3	Effect of base equivalents on the synthesis of (1 <i>E</i> ,3 <i>E</i> ,5 <i>E</i>)-1,3-bis-phenylsulfonyl-6-phenyl-hexa-1,3,5-triene 105	117
2.2.2.4	Effect of temperature on the synthesis of (1 <i>E</i> ,3 <i>E</i> ,5 <i>E</i>)-1,3-bis-phenylsulfonyl-6-phenyl-hexa-1,3,5-triene 105	118
2.2.3	Knoevenagel-type condensation reaction mechanism	119
2.2.4	Reaction scope: Variation of the cinnamaldehyde	120
2.2.5	Structural characterization of (1 <i>E</i> ,3 <i>E</i> ,5 <i>E</i>)-1,3-bis-phenylsulfonyl-(6- <i>p</i> -dimethylaminophenyl)-hexa-1,3,5-triene 110	122
2.2.5.1	Use of NMR spectroscopic data to characterize (1 <i>E</i> ,3 <i>E</i> ,5 <i>E</i>)-1,3-bis-phenylsulfonyl-(6- <i>p</i> -dimethylaminophenyl)-hexa-1,3,5-triene 110	122
2.2.5.2	IR spectroscopy and MS analysis for structural characterization of (1 <i>E</i> ,3 <i>E</i> ,5 <i>E</i>)-1,3-bis-phenylsulfonyl-(6- <i>p</i> -dimethylaminophenyl)-hexa-1,3,5-triene 110	134
2.2.6	Structural characterization of (1 <i>E</i> ,3 <i>E</i> ,5 <i>E</i>)-1,3-bis-phenylsulfonyl-(6- <i>p</i> -nitrophenyl)-hexa-1,3,5-triene 109	136
2.2.7	Structural characterization of (1 <i>E</i> ,3 <i>E</i> ,5 <i>E</i>)-1,3-bis-phenylsulfonyl-(6- <i>m</i> -bromophenyl)-hexa-1,3,5-triene 115	138

2.2.8	Structural characterization of (1 <i>E</i> ,3 <i>E</i> ,5 <i>E</i>)-1,3-bis-phenylsulfonyl-6-(thiophene)-hexa-1,3,5-triene 120	140
2.2.9	Reaction scope: Variation of the propene electron-withdrawing group	141
2.2.9.1	Synthesis of cyano and ester propenes	142
2.2.9.2	Attempted synthesis of methyl 7-phenyl-4-(phenylsulfonyl)hepta-2,4,6-trienoate 124 from (<i>E</i>)-4-(phenylsulfonyl)but-2-enoate 123	144
2.2.9.3	Synthesis of cyano-sulfonyl trienes	147
2.2.9.4	Attempted synthesis of bis(methyl ester) triene	148
2.3	Conclusion	154
2.4	Experimental Procedure	156
2.4.1	General information for chemical synthesis	156
2.4.2	Synthesis of precursor molecules	156
2.4.3	General protocol for reactions carried out as part of the optimization study to determine preferred reaction conditions for triene synthesis – qNMR	158
2.4.4	General procedure for the synthesis of trienes	161
2.4.5	Experiments using traditional Knoevenagel-condensation reaction conditions	172
2.4.5.1	Attempted synthesis of bis(methyl ester) triene	172
2.4.5.2	General procedure for traditional Knoevenagel-condensation reaction	174
	Chapter Three: Biaryl synthesis and photophysical study	176
3.1	Introduction	176
3.1.1	Importance and applications of biaryl-containing compounds	176
3.1.1.1	Medicinal applications of biaryls	176
3.1.1.2	Application of biaryls in OLEDs	178
3.1.2	Transition metal-free approaches to biaryl synthesis	180
3.1.2.1	Transition metal-free approach of Xu <i>et al.</i> (2015)	180
3.1.2.2	Transition metal-free approach of Walia <i>et al.</i> (2018)	181
3.1.3	Synthesis of biaryls: Strategies involving transition metals	182
3.1.3.1	Suzuki coupling to access biaryl molecules	182
3.1.3.1.1	Suzuki approach of Barbero and Dughera (2018)	183
3.1.3.2	Stille coupling methodologies to access biaryls	184
3.1.3.2.1	Stille approach of Wang <i>et al.</i> (2016)	184
3.1.3.3	Negishi coupling to access biaryls	186
3.1.3.3.1	Negishi approach of Wang and Liu (2019)	186
3.1.4	Aims of biaryl synthesis	187
3.2	Results and Discussion	188
3.2.1	Development of synthetic methodology to access biaryls	188
3.2.2	Application of Woodward-Hoffman rules to our thermally induced electrocyclization	192

3.2.3	Investigation of optimal procedure for biaryl synthesis	194
3.2.3.1	Optimization study: Investigation of heating methodology	194
3.2.3.2	Optimization study: Purification attempts using sublimation	195
3.2.3.3	Optimization study: Microwave heating	197
3.2.3.3.1	Microwave heating and choice of solvent	197
3.2.3.3.2	Microwave heating and variations in temperature used	198
3.2.3.3.3	Microwave heating and concentration of triene	198
3.2.3.4	Optimisation study: UV experiment	199
3.2.4	Substrate scope investigation of the thermal electrocyclization of 1,3,5-hexatrienes	200
3.2.5	Structural characterization of 1-(4-methyl ester phenyl)-4-(phenylsulfonyl)benzene 139	201
3.2.5.1	NMR analysis of 1-(4-methyl ester phenyl)-4-(phenylsulfonyl)benzene 139	202
3.2.5.2	IR spectroscopy and MS analysis used to fully characterize 1-(4-methyl ester phenyl)-4-(phenylsulfonyl)benzene 139	213
3.2.6	Structural characterisation of 1-(4-dimethylaminophenyl)-4-(phenylsulfonyl)benzene 138	214
3.2.7	Fluorescence	215
3.2.7.1	Fluorescence reported for structurally similar biaryls	217
3.2.7.2	Investigation of fluorescent properties of our biaryls	218
3.2.7.3	Effect of solvent on emission spectra	224
3.2.7.4	Measurement of molar extinction coefficient (ϵ)	230
3.2.7.5	Quantum yield calculation	231
3.3	Conclusion	236
3.4	Experimental Procedure	238
3.4.1	General information for chemical synthesis	238
3.4.2	Optimization study to determine preferred reaction conditions for biaryl synthesis	238
3.4.3	General procedure for synthesis of biaryls	242
3.4.4	General methods for the photophysical study of biaryls	247
	References	248

Acknowledgements

Firstly, I would like to thank my supervisor Prof John Stephens for the opportunity to do this PhD project in the first place. There's no doubt that I have grown as a person and as a researcher over the last four years and I want to thank you for allowing me to develop as the independent researcher I have become.

Next, thanks to my internal examiner Dr Trinidad Velasco-Torrijos and external examiner Prof Marc Devocelle for reading my thesis and for the constructive feedback they will provide in order to improve my work. Getting opinions from highly respected researchers like the two of you means a great deal and will ensure that my thesis is the best that it can possibly be.

To Kevin Kavanagh and all of the medical mycology lab in the department of biology who have put up with my limitless questions and have spent time training me in new techniques, I am very grateful.

To all of the staff in the chemistry department who have always been willing to lend a hand and offer advice when I needed help, I will always appreciate it.

A huge thank you to the postgrads for being a part of my journey over the last four years. There have been ups and downs but it always meant a lot that we went through them all together (I can't help but think of 'sad, but sad together' as I write this). To Dr Harlei Martin, thank you for being the first postgrad to introduce themselves to me when I started. Had you not approached me, I probably would have stayed silent for the first year of my PhD, and what insightful tea-time chats I would have missed out on! To Luke Marchetti, I know you requested a paragraph of my acknowledgements, but it has been a long process putting this thesis together and I am very stuck for words, so I'm afraid it's just a few sentences! Nearly as soon as you started, we formed a friendship very early on and I am very grateful for that, and for you constantly listening to my rants. You helped me to get over my fear of talking in the tea room, and have always made yourself available for a chat and so, when I say thank you, there is a lot of ground that that is covering. To all the other postgrads especially in their early years, Colm, Conor G, Conor W, Eoin, Kyle, Tian, Clara E, Sinead, Luke B, Darren, Kobi, Caitlyn, Hua, Jason, and Stephen, best of luck with all the research that is ahead of you. I have memories of you all from both postgrad and undergraduate, and I have no doubt you'll all get through to the other side.

Last, but definitely not least, I have to say the biggest thank you to my partner Stephen Mc Guire. There will never be enough sorrys, or enough thank yous, to cover the last four years (well 6 years really!). I'm sorry for all the time we've missed out on because I threw everything into the PhD, I'm sorry for all the lost weekends and experiences we could have had during that time, and for all the times even when I was physically there that I was mentally trying to tick something else off my never-ending to do list. Thank you for always having my back, it never mattered what I had to do or when, you always stood behind me and supported me. There is no doubt in my mind that I couldn't have done this

without you, you are my rock and my best friend, and I'm so looking forward to our life together when neither of us are students!

Abstract

This thesis is divided into three distinct chapters. The first chapter highlights the synthesis of a family of *trans*-cinnamaldehydes using a Wittig methodology, and their evaluation as antibacterial agents against Gram-positive *Staphylococcus aureus* (*S. aureus*) and Gram-negative *Escherichia coli* (*E. coli*) *in vitro*. Cinnamaldehydes are known electrophiles, with some literature reports suggesting a Michael acceptor role as part of their antibacterial mode of action. The electrophilicities of our family of *trans*-cinnamaldehydes were calculated, and a relationship between electrophilicity and observed antibacterial activity was considered. Here, the more electrophilic cinnamaldehydes appeared to be more active in our antibacterial assays. An *in vivo* toxicity assessment of a selection of these *trans*-cinnamaldehydes was undertaken using *Galleria mellonella* larvae, and an initial mechanism of action study was performed using protein and amino acid leakage as an indication of the effect the *trans*-cinnamaldehydes might have on the integrity of the bacterial cell wall and/or membrane. The *trans*-cinnamaldehydes studied were non-toxic and did show some protein and amino acid leakage, although the results were such that the cell wall/membrane disruption may not be the primary or only mechanism of action. Overall, the antibacterial activity of the *trans*-cinnamaldehydes was modest to low. They were non-toxic and displayed both an interesting relationship to electrophilicity and an ability to disrupt the cell wall/membrane. However, they are not strong candidates for further development as antibacterial agents and would require further structural modification to improve efficacy.

A second antimicrobial study was undertaken with the aim of identifying novel potent antimicrobial agents. An initial screen of novel structures, which was available in the Stephens group, identified a pyrazolo[1,5-*a*]pyrimidin-7-one family of compounds with antibacterial potential. This family of pyrazolo[1,5-*a*]pyrimidin-7-ones were synthesized by other group members and I carried out the antimicrobial activity study. One member of this family, 2-butyl-5-(3,5-bis(trifluoromethyl))phenylpyrazolo[1,5-*a*]pyrimidin-7(4*H*)-one, was identified as a leading hit compound against *S. aureus* in the preliminary study. The family of thirty-five pyrazolo[1,5-*a*]pyrimidin-7-ones was divided into groups based on their structure as part of a structure activity relationship (SAR) study, and each member was tested *in vitro* against *S. aureus* (Gram-positive bacteria), *E. coli* (Gram-negative bacteria), and *Candida albicans* (representative fungus). The pyrazolo[1,5-*a*]pyrimidin-7-ones showed more potent antibacterial activity than antifungal activity. The SAR studies resulted in the identification of a leading hit pyrazolo[1,5-*a*]pyrimidin-7-one, 2-isopropyl-5-(3,5-bis(trifluoromethyl))phenylpyrazolo[1,5-*a*]pyrimidin-7(4*H*)-one, which showed the highest activity against *S. aureus*, MIC₅₀ of 1.2 μM. The activity of 2-isopropyl-5-(3,5-bis(trifluoromethyl))phenylpyrazolo[1,5-*a*]pyrimidin-7(4*H*)-one was superior to that of the commercial antibiotics tested against *S. aureus*, in that, a MIC₅₀ of 21.8 μM, 11.03 μM, and 5.22 μM was obtained for ampicillin trihydrate, tetracycline, and streptomycin sulfate, respectively. A selection of pyrazolo[1,5-*a*]pyrimidin-7-ones, including our most active candidates, were then evaluated against more clinically-relevant bacterial strains, namely methicillin-resistant *S. aureus* (MRSA, Gram-positive),

and *Pseudomonas aeruginosa* (Gram-negative). The most active compound was 2-(4-trifluoromethylphenyl)-5-(3,5-bis(trifluoromethyl))phenylpyrazolo[1,5-*a*]pyrimidin-7(4*H*)-one, with an MIC₅₀ of 1.88 μM against MRSA, and compares favourably to the MIC₅₀ of 2.33 mM and 291.72 μM for the commercial antibiotics ampicillin trihydrate and tetracycline, respectively. An *in vivo* toxicity assessment and an *in vivo* therapeutic evaluation of the most active compounds was completed, using *Galleria mellonella* and infected *Galleria mellonella* respectively. Here, the pyrazolo[1,5-*a*]pyrimidin-7-ones evaluated were shown to be non-toxic and, in the therapeutic evaluation study, where *Galleria mellonella* were infected with MRSA and subsequently treated with was 2-(4-trifluoromethylphenyl)-5-(3,5-bis(trifluoromethyl))phenylpyrazolo[1,5-*a*]pyrimidin-7(4*H*)-one, the survival rate improved by 25% for the treated *Galleria mellonella* over the non-treated.

Chapter two is dedicated to the development of a synthetic methodology that allows access to electron deficient trienes. Important applications of trienes can be broadly divided into (i) medicinal applications and (ii) synthetic applications. An initial attempt to access (1*E*,3*E*,5*E*)-1,3-bis-phenylsulfonyl-6-phenyl-hexa-1,3,5-triene from *trans*-cinnamaldehyde and (*E*)-1,3-bis-phenylsulfonylprop-1-ene, using traditional Knoevenagel-condensation reaction conditions, was unsuccessful. We then undertook a study to determine Knoevenagel-type condensation reaction conditions that would allow access to the desired triene. The model reaction chosen was that between *trans*-cinnamaldehyde and (*E*)-1,3-bis-phenylsulfonylprop-1-ene. The study explored reaction variables such as solvent, base, equivalents of base, and temperature, with conversion to triene estimated using quantitative NMR. This allowed us to establish the preferred reaction conditions for our Knoevenagel-type condensation synthetic strategy which used DCM as solvent, 20 °C, and 15 equivalents of Al₂O₃ as base. The desired triene was generated in 93% isolated yield and the methodology was successfully applied to the synthesis of 20 trienes. All of these novel compounds underwent full structural characterization using NMR spectroscopy, liquid chromatography-mass spectrometry (LC-MS), high resolution-mass spectrometry (HR-MS), and infrared (IR) spectroscopy. In terms of substrate scope, our synthetic strategy allowed for variation of the starting cinnamaldehyde, and some variation of the starting propene (nitrile and sulfonyl electron withdrawing groups). However, our studies to date suggest that employing esters as an electron withdrawing group on the propene may not be well tolerated. Within our attempts to employ the esters, an alternative biaryl product was generated when dimethyl glutaconate was employed as the starting ester propene. Other ester variations resulted in the generation of complex mixtures.

In chapter three we report a thermal electrocyclization of our electron poor trienes in the synthesis of a family of phenylsulfonyl biaryls. An optimization study led to the identification of preferred reaction conditions and an isolated yield of 88% for our model reaction was obtained using (1*E*,3*E*,5*E*)-1,3-bis-phenylsulfonyl-6-phenyl-hexa-1,3,5-triene as the substrate. This allowed us to access nine phenylsulfonyl biaryl products. All novel compounds underwent full structural characterization using NMR spectroscopy, LC-MS, HR-MS, and IR spectroscopy. A photophysical study was also performed, as the structure of the biaryls suggested that they may possess some interesting fluorescent

properties via a possible twisted intramolecular charge transfer (TICT) process. The dimethylamino derivative showed the greatest sensitivity to solvent choice. In terms of the molar extinction coefficient (ϵ), values of between 17332 and 37964 $\text{M}^{-1} \text{cm}^{-1}$ were recorded in chloroform. The highest value was obtained for the choro derivative, and the lowest value for the dimethylamino substituted derivative. The derivative with the highest quantum yield of 0.92 was also the dimethylamino derivative, but this was only observed in the aprotic solvent chloroform. In methanol, the quantum yield dropped dramatically for the dimethylamino derivative due to a suspected hydrogen bonding effect. The preliminary photophysical properties suggest that these biaryls are potentially useful and versatile fluorescent small molecules.

List of abbreviations

2D	Two Dimensional
AI	Autoinducer
Ar	Aryl
AST	Antimicrobial Susceptibility Test
CDC	Centers for Disease Control and Prevention
CFU	Colony-forming unit
CLSI	Clinical & Laboratory Standards Institute
COSY	¹ H- ¹ H Correlation Spectroscopy
DCM	Dichloromethane
DEPT	Distortionless Enhancement by Polarization Transfer
DIBAL-H	Di- <i>isobutyl</i> Aluminium Hydride
DMF	N,N-Dimethylformamide
DMP	Dess-Martin Periodinane
DMSO	Dimethyl sulfoxide
DNA	Deoxyribonucleic acid
EA	Electron Affinity
Eq.	Equivalent(s)
ESI	Electrospray ionization
EU	European Union
FDA	United States Food & Drug Administration
FtsZ	Filamentation temperature sensitive protein Z
GA	γ -aminobutyric acid
GRAS	Generally Regarded as Safe
HOMO	Highest Occupied Molecular Orbital
HMBC	¹ H- ¹³ C Heteronuclear Multiple Bond Correlation
HSQC	Heteronuclear Single Quantum Coherence
IBX	2-Iodoxybenzoic acid
ICR	Institute of Cancer Research
IP	Ionization Potential
ISO	International Organization for Standardization
LC	Liquid Chromatography
LUMO	Lowest Unoccupied Molecular Orbital
Me	Methyl
MIC	Minimum Inhibitory Concentration
MRSA	Methicillin-resistant <i>Staphylococcus aureus</i>
MS	Mass Spectrometry
NMR	Nuclear Magnetic Resonance
NOAEL	No Observed Adverse Effect Level
OLED	Organic Light Emitting Diode

Ph	Phenyl
qNMR	Quantitative Nuclear Magnetic Resonance
RT	Room Temperature
SAR	Structure Activity Relationship
TC	<i>Trans</i> -cinnamaldehyde
THF	Tetrahydrofuran
TLC	Thin Layer Chromatography
TMS	Tetramethylsilane
UV	Ultraviolet
Vis	Visible

Chapter One. Antimicrobial agents: Cinnamaldehydes and pyrazolopyrimidinones

1.1 Introduction

1.1.1 Antimicrobial agents

Antibiotics and antimicrobial agents are those substances that inhibit the growth of bacteria, with many disrupting vital cellular functions thereby causing rapid bacterial cell death.¹ In the last forty years, antibiotics have been over-used by humans, not only by direct consumption, but also through their extensive use in animal feed.² Consequentially, antibiotic resistance in several pathogenic organisms has occurred,² with a corresponding reduction in the efficacy of antibiotics that are currently on the market. This has resulted in antibiotic resistance becoming a global health issue.¹ The American Centers for Disease Control and Prevention (CDC) has reported, to date, that more than two million diseases have been caused by microorganisms that are resistant to more than one class of antibiotics.³ Antibiotic resistance also causes a substantial economic burden, incurring approximately €1.5 billion in additional health care costs annually within the European Union (EU).¹ Moreover, this resistance has a high associated mortality rate. Based on data collected between January 1st 2015 and December 31st 2015, it is estimated that infections involving antibiotic-resistant bacteria accounted for 33,110 attributable deaths in the EU and EEA (European Economic Area).⁴ This high mortality rate is due to the fact that these related infections have become extremely difficult to treat, where examples include extensively drug-resistant tuberculosis (XDR-TB) and community-associated methicillin-resistant *Staphylococcus aureus* (MRSA). Infections such as these pose a monumental challenge to clinicians.²

1.1.2 Natural products

Aside from the emergence of bacterial antibiotic resistance, negative consumer attitudes towards synthetic food preservatives has resulted in a growing consumer popularity towards the use of natural products, such as plant components containing essential oils and essences, which similarly help to protect from harmful pathogens and prevent food spoilage.^{5,6} This consumer trend is in part due to perceived nutritional and safety qualities of natural products.⁷⁻⁹ As a result, there has been a renewed interest by food scientists in the use of spices and natural preservatives derived from plant sources as alternative antimicrobial agents.^{7,8} Historically, plants, spices and their essential oils have been used in traditional medicine.¹⁰ From an ecological viewpoint, the use of plants as a source of antimicrobial agents is a sensible strategy since plants naturally produce an array of secondary metabolites that defend the host from microbiological invasion.^{3,6} In addition, plants can contain chemical entities that have diverse features such as complex structures that synthetically would be difficult to obtain.

Cinnamon spice is obtained from the inner bark of several trees within the genus *Cinnamomum*, which itself is comprised of approximately 250 plant species.^{11, 12} The most common species are *C. cassia* (Chinese cinnamon, commonly referred to as Cassia) and *C. verum* (also called *C. zeylanicum*, commonly referred to as true cinnamon). These two species contain a varying percentage of cinnamaldehyde with up to 85.3% and 90.5% reported, respectively.¹¹ *trans*-Cinnamaldehyde has been identified as the component that gives rise to much of the reported antimicrobial properties of this spice.^{9, 12-16} Isolated cinnamaldehyde has been shown to effectively inhibit the growth of an array of microorganisms such as bacteria, moulds, and yeasts, as well as having been reported to inhibit toxin production by microorganisms.^{8, 9, 13, 17, 18}

1.1.3 Commercial use of *trans*-cinnamaldehyde

trans-Cinnamaldehyde is Generally Recognized as Safe (GRAS) by the United States Food and Drug Administration (FDA), and Flavour and Extract Manufacturer's Association (FEMA), and has been granted A status (i.e. may be used in foodstuffs) by the Council of Europe.¹⁷ On this basis, *trans*-cinnamaldehyde can be viewed as a safe food and flavour additive, with a pleasant taste and odour, and has found many commercial food uses.^{15, 17} Cinnamon has been a useful spice since biblical times, when it was utilized as a perfume in rubbing oils.¹¹ Ancient Egyptians employed cinnamon as a fragrance for preserving bodies,¹¹ and more recently, *trans*-cinnamaldehyde has been used agriculturally as a fungicide.¹⁹ Cinnamaldehyde has also been incorporated into edible antimicrobial films, prepared from foodstuffs such as fruit and vegetables, and has inactivated foodborne pathogens either by direct contact or by vapours released from the films in closed containers.²⁰ These films have also been shown to reduce the presence of non-pathogenic spoilage organisms that impact food quality.¹⁷ This correlates with a growing interest in natural antimicrobials that not only prevent the growth of foodborne pathogens and spoilage microorganisms, but can also enhance the flavour and quality of foods.²¹ Thus, in light of *trans*-cinnamaldehyde being a safe additive that is already being added to foods to enhance flavour, related cinnamaldehyde derivatives have the potential to be cost-effective, food-compatible, broad-spectrum antimicrobial additives that could be used against an array of pathogenic microorganisms,¹⁷ and hence have sparked the interest of researchers across the globe.

1.1.4 Limitations of *trans*-cinnamaldehyde for commercial applications

There have been some undesirable aspects reported for *trans*-cinnamaldehyde that has limited its commercial use. For one, the solubility of this compound in water is low at approximately 1.1 g/L at 20 °C.¹⁹ It is also sensitive when exposed to light and air for prolonged periods.¹⁹ *In vivo*, it is possible that *trans*-cinnamaldehyde decomposes to cinnamic acid by enzyme catalysis before it is able to elicit its antibacterial activity, hence could be considered unstable in blood.¹² Additionally, Visvalingham *et al.*⁹ were the first

to show that *Escherichia coli* O157:H7 can convert cinnamaldehyde to cinnamic alcohol using dehydrogenase/reductase enzymes.⁹ Cinnamaldehyde is a known sensitizer in humans and the North American Contact Dermatitis Research group have reported that cinnamaldehyde is a frequent cause of allergic reactions as a constituent of perfumes and cosmetics.¹¹ In human dermatological studies, the No-Observed-Adverse-Effect-Level (NOAEL) for cinnamaldehyde sensitization has been set at 0.5%.¹¹ For this reason, the International Fragrance Research Association (IFRA) has limited its use to 0.05%.¹¹ This all highlights the need for research into cinnamaldehyde derivatives that have lower sensitization effects, lower toxicity, but improved antibacterial activity to that of *trans*-cinnamaldehyde.

1.1.5 General medicinal properties of cinnamaldehyde and its derivatives

Extensive research has been carried out investigating the broad scope of medicinal applications associated with cinnamaldehyde and its natural and synthetic derivatives. A number of excellent reviews have been published with respect to the medicinal properties associated with *trans*-cinnamaldehyde itself (Figure 1, structure **1**),^{12, 17, 19} including its anti-inflammatory properties,²²⁻²⁴ anti-fungal activity,²⁵⁻²⁷ and thermogenic and metabolic effects.²⁸⁻³² Other applications for *trans*-cinnamaldehyde including anti-mold, anti-diabetic, neuroprotective, cardioprotective, anticancer and anti-oxidant functions, have all been discussed previously in the literature.³³⁻⁵⁵ In addition, reviews on cinnamaldehyde derivatives and their associated medicinal properties have been published, including noteworthy examples by Chen *et al.*³³ and Shreaz *et al.*¹¹, and numerous studies have been implemented by other groups with results indicating the potential of cinnamaldehyde derivatives as medicinal agents.^{56, 34, 57, 58}

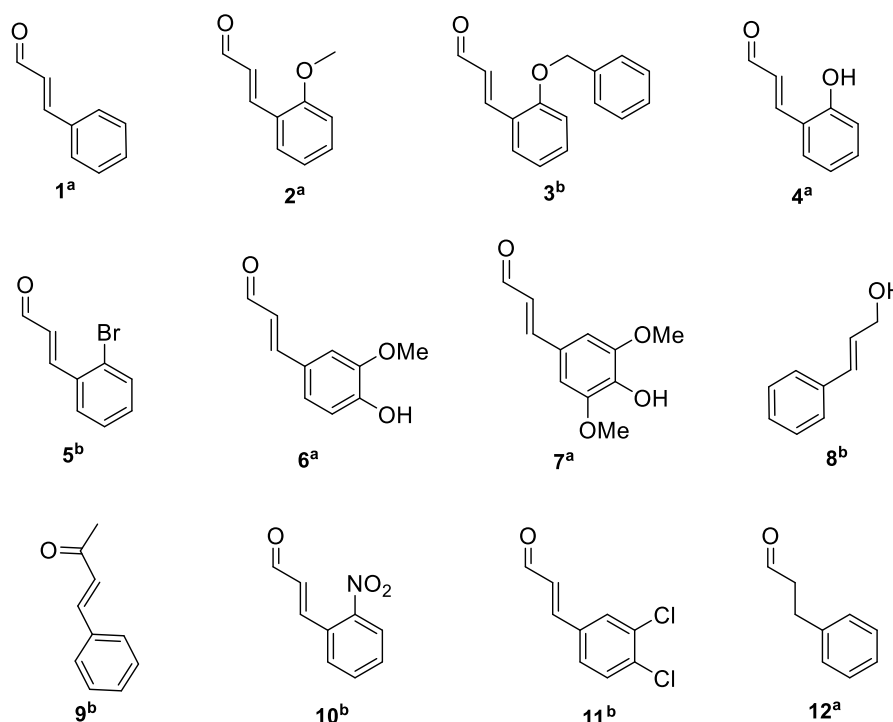


Figure 1. Examples of cinnamaldehyde derivatives from the literature that have reported medicinal properties. ^a Denotes a naturally occurring cinnamaldehyde, ^b denotes a synthetic cinnamaldehyde derivative.

1.1.6 Molecular mechanism: Cinnamaldehyde as an electrophile

Cinnamaldehyde has two electrophilic reactive sites, the β -carbon on the conjugated double bond and the carbon of the aldehyde carbonyl group.¹⁷ A number of previous studies have related the bioactivity of cinnamaldehyde, and its derivatives, to its potential Michael acceptor ability, i.e. nucleophilic attack at the β -carbon. For example, Cabello *et al.*⁴⁹ related the Michael acceptor ability of *trans*-cinnamaldehyde (Figure 1, compound **1**), and a range of its derivatives to their ability to impair melanoma cell proliferation, viability, invasiveness, and NF- κ B transcriptional activity. They observed that **1**, but not structurally similar compounds devoid of Michael acceptor ability such as cinnamyl alcohol (Figure 1, compound **8**), possessed this ability.⁴⁹ A related example can be found in the findings of Motohashi *et al.*⁵⁰ who conducted a structure activity relationship (SAR) study using antimutagenic benzalacetone (Figure 1, compound **9**), as well as a number of cinnamaldehydes and cinnamic acids. This group similarly found that the presence of the unsaturated bonded-carbonyl system is necessary for biological activity, namely the inhibition of mutagenesis activity.⁵⁰

Brackman *et al.*⁵⁹ conducted a SAR study of cinnamaldehyde analogues as AI (autoinducer)-2 based quorum sensing inhibitors in *Vibrio spp.* It was suggested that those analogues containing an α,β -unsaturated acyl group with potential to act as Michael acceptors (for example 2-nitrocinnamaldehyde **10**, 3,4-dichlorocinnamaldehyde **11**, and

1, Figure 1), were found to possess greater activity with respect to the inhibition of bioluminescence of *Vibrio harveyi* BB170. However, analogues that did not possess an α,β -unsaturated acyl group, such as 3-phenylpropionaldehyde (Figure 1, compound **12**), did not result in a significant inhibition of the bioluminescence signal. The group proposed that these effects may be as a result of a Michael-addition reaction in the mechanism of action, allowing **1** and its analogues to act as LuxR-ligands. This could yield a modified protein that likely resulted in the reduced ability to bind to DNA. The reduced DNA binding was observed experimentally and measured in terms of K_d values, which refer to the respective concentrations of LuxR at the half-maximal fractional change in fluorescence anisotropy.⁵⁹

More recent studies have however indicated, perhaps surprisingly, that it is the carbonyl carbon that is more significant in terms of reactivity than the β -carbon. For example, Sadofsky *et al.*⁶⁰ investigated the mechanism leading to the activation of TRPA1 (transient receptor potential ankyrin 1) of cysteine residues. This group noted that cinnamic acid, acrylic acid, and acrylamide caused little or no TRPA1 activation in concentrations up to 300 μ M, where these compounds contain both a carbonyl carbon and an unsaturated β -carbon, but are weakly electrophilic at the carbonyl carbon. In contrast, those compounds such as acrolein and **1**, which can react via either conjugate addition at the β -carbon, or reversible direct addition at the carbonyl carbon, caused TRPA1 activation in a concentration dependent manner. With respect to these reactive aldehydes, the authors indicate that it is the reversible direct addition that is responsible for the channel activation, which would explain why TRPA1 agonists such as cinnamaldehyde acted in a manner compatible with reversible, competitive agonism. Similarly, both hydrocinnamic acid NHS ester and propionic acid NHS ester, which are only capable of direct addition, activated TRPA1 expressed in HEK293 cells.⁶⁰

Autelitano *et al.*⁶¹ investigated the reaction of cinnamaldehyde and cinnam(o)yl derivatives with thiols. Here dodecanethiol was employed as a model of simple thiols, with cysteamine utilized as a model of reactive protein thiols in an NMR assay as developed by Avonto *et al.*⁶² This study was carried out to probe the selective reactivity of **1** at both the carbonyl carbon and the β -carbon. Compound **1**, when reacted with cysteamine, afforded a mixture of a thiazoline derivative and compounds of multiple addition at both the carbonyl and β -carbon. The reaction with dodecanethiol gave a bis-dithioacetal via direct addition, but no reaction occurred between dodecanethiol and saturated compound **12**. A possible explanation was given in that for **1** (versus **12**), conjugation to a phenyl reduces the hardness of the carbonyl to the point of making it possible for a weak and soft nucleophile like sulfur to attack it without any previous catalysis. These surprising results suggest that **1** can trap simple thiols via direct addition, and can also trap cysteamine-type thiols, but only after imine formation with the amino motif.⁶¹

1.1.7 Antibacterial activity of cinnamaldehyde and its derivatives

trans-Cinnamaldehyde, **1**, has known antibacterial properties that have been established across an array of Gram-positive and -negative bacteria, including *Escherichia coli*,^{6, 10, 12, 34, 63} *Bacillus subtilis*,^{10, 12, 63} *Staphylococcus* spp.,^{12, 17, 34, 63} *Listeria* spp. and *Salmonella* spp.,^{6, 10, 12, 17, 63} *Lactobacillus sakei*,⁶³ *Campylobacter jejuni*,^{6, 64} *Vibrio* spp.,^{3, 10, 12} *Pseudomonas* spp.,^{3, 10, 12, 34} *Porphyromonas gingivalis*,¹² *Streptococcus pyogenes*,³ and *Cronobacter sakazakii*.^{12, 17} Some studies investigate the general antibacterial activity of cinnamaldehyde and its derivatives, while others focus on a particular mechanism of action. The following will highlight some of the relevant publications in each category and discuss them in separate sections.

1.1.7.1 General antibacterial activity of cinnamaldehyde and its derivatives

Some recent research has utilized *trans*-cinnamaldehyde, **1**, as a hit compound, from which a range of derivatives have been synthesized and tested for their antibacterial activity, as is the case with the following examples. One such case is that of Wei *et al.*,²⁵ who developed nine Schiff base cinnamaldehyde compounds and tested them, along with cinnamaldehyde, against *Bacillus subtilis* (*B. subtilis*) and *Escherichia coli* (*E. coli*). The antimicrobial activity of the Schiff base adducts were very near or higher than cinnamaldehyde.²⁵ Following on from this work, Wang *et al.*⁶⁵ synthesized twenty four Schiff base cinnamaldehyde analogues using **1**, 4-chlorocinnamaldehyde (Figure 2, compound **13**), and 4-methoxycinnamaldehyde (Figure 2, compound **14**), as the cinnamaldehyde component. The three cinnamaldehydes were combined with one of eight amino acids to generate the corresponding Schiff base. Results indicate that all compounds inhibited the growth of the two bacteria *Staphylococcus aureus* (*S. aureus*) and *E. coli*, but compounds **15** and **16** (Figure 2) exhibited the best antibacterial activity. Two mold fungi were also examined in this study and it was found that they were more sensitive to the cinnamaldehyde derivatives than the two test bacteria.⁶⁵

In 2016, Liu *et al.*⁶⁶ synthesized Schiff base cinnamaldehyde metal complexes using γ -aminobutyric acid (GA) and cinnamaldehyde, as well as copper (Cu²⁺) and zinc (Zn²⁺). The Schiff base-metal complexes were evaluated for their inhibitory effect against *S. aureus* and *E. coli*. The cinnamaldehyde-GA Schiff base was shown to possess better antibacterial activity against *S. aureus* than *E. coli*, as assessed by MBC (minimal bactericidal concentration) values. For *S. aureus*, both metal complexes of cinnamaldehyde-GA were shown to enhance the antimicrobial activity compared to the cinnamaldehyde-GA Schiff base alone.⁶⁶

Shen *et al.*⁶⁷ investigated the ability of cinnamaldehyde and its derivatives to eradicate persisters in *E. coli*. Persisters lead to recurring infections and relapse after

treatment and are widely occurring throughout bacteria, as well as fungi and parasites.⁶⁷ In this study, α -bromocinnamaldehyde (Figure 2, structure **17**) was shown to exhibit the best activity of those compounds evaluated. Interestingly, α -methylcinnamaldehyde (Figure 2, structure **18**) was shown not to display any bactericidal activity at any concentration examined.⁶⁷

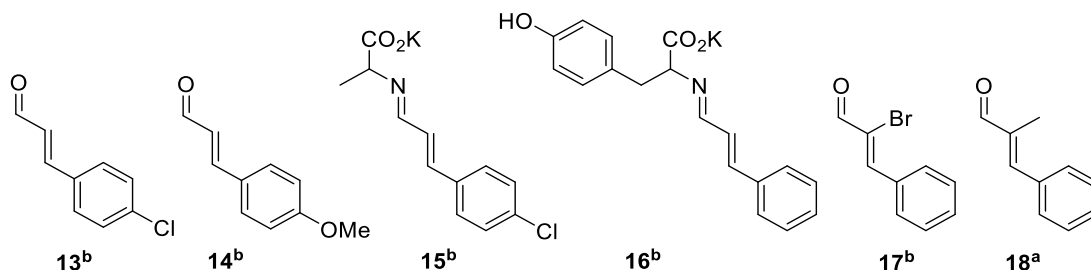


Figure 2. Cinnamaldehyde derivatives shown to possess general antibacterial activity.^{25, 65, 67} ^a Denotes a naturally occurring cinnamaldehyde, ^b denotes a synthetic cinnamaldehyde derivative.

1.1.7.2 Antibacterial mechanisms of action displayed by cinnamaldehyde and its derivatives

Although there have been many studies collectively describing the antibacterial activity exhibited by **1** and its derivatives, there are fewer that discuss the mechanism of action, particularly with respect to cinnamaldehyde derivatives. Graphically depicted in Figure 3 are a few of the mechanisms of action for which **1**, and in some cases its' derivatives, have been investigated. A full discussion of these antibacterial mechanisms is available in our literature review of this particular subject and include quorum sensing inhibition, FtsZ inhibition, biofilm inhibition, inhibition of ATP and ATPase, membrane permeabilization and cell constituents release.⁶⁸ The mechanism of action we investigated experimentally was related to the membrane permeabilization abilities of **1**, and some of its derivatives, and discussion of our findings on the topic will be restricted to the results and discussion, section 1.2.10, later in the chapter.

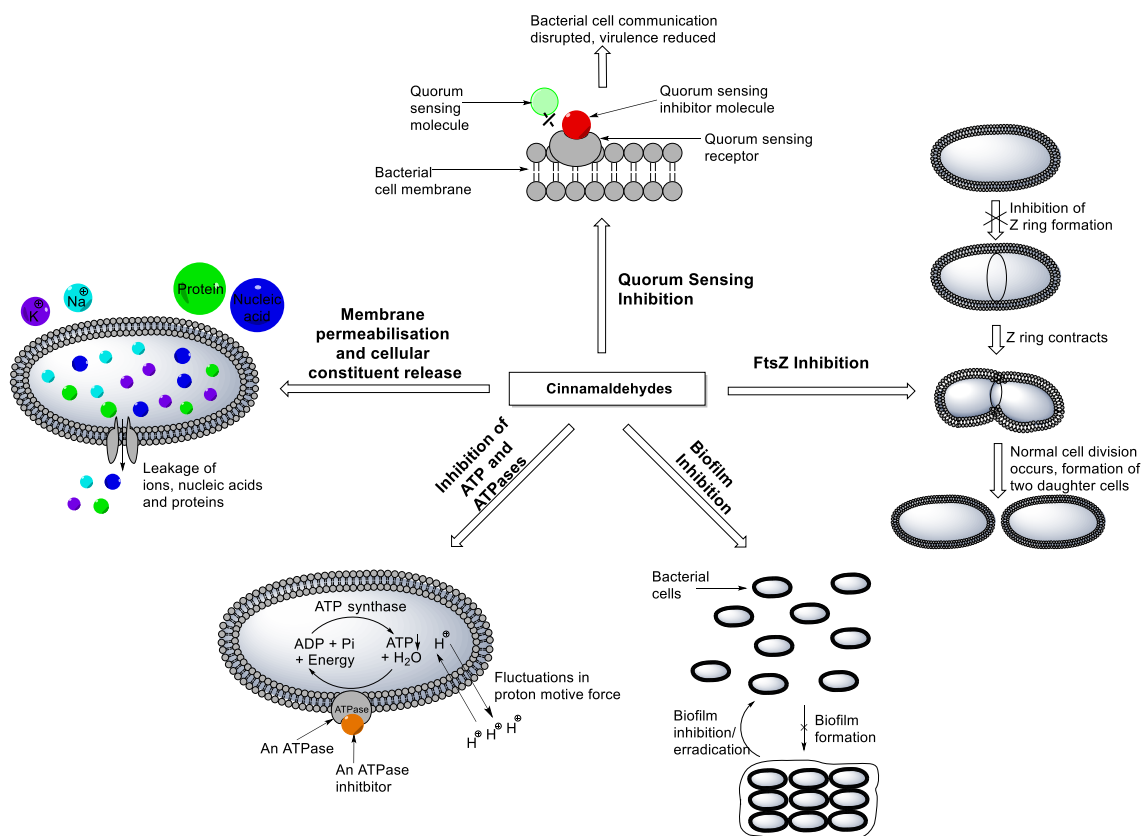


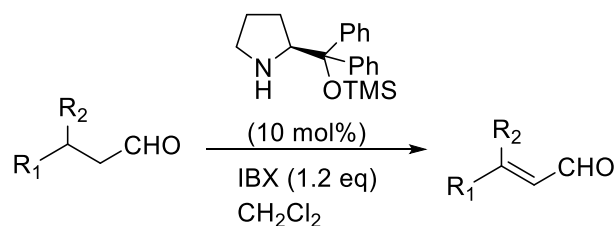
Figure 3. Graphical depiction of antibacterial mechanisms of action exhibited by cinnamaldehydes.

1.1.8 Access to cinnamaldehydes – overview of some synthetic routes

Several synthetic methods have been reported for the generation of cinnamaldehydes, including oxidative enamine catalysis,^{69, 70} the use of a palladium-catalyzed Heck-Saegusa reaction,⁷¹ and Dess-Martin oxidation of alcohols.^{72, 73}

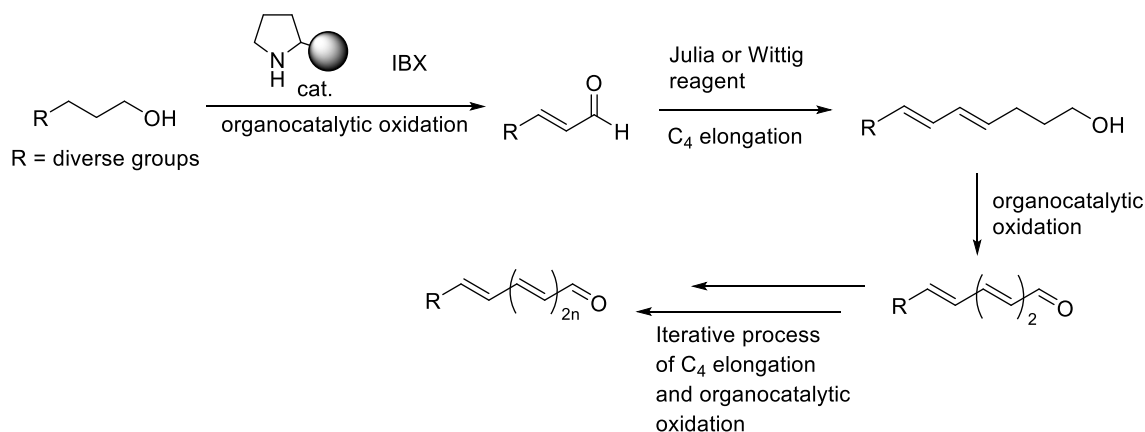
1.1.8.1 Oxidative enamine catalysis

The oxidative enamine catalysis described by Zhang *et al.*⁶⁹ consists of an amine-catalyzed, IBX-mediated oxidation of simple aldehydes to *E*-selective α,β -unsaturated aldehydes in 14-84% yield. This catalysis involves an oxidation of an enamine, derived from a saturated aldehyde, into a corresponding α,β -iminium ion by means of 2-iodoxybenzoic acid (IBX)-mediated oxidation via a 2 electron transfer. Building on the catalysis that had been developed previously by the Zhang group,⁷⁴ it was modified so as to synthesize C=C double bonds. This was done by utilizing the intermediate iminium ion, which undergoes hydrolysis without the presence of a nucleophile, to produce the desired α,β -unsaturated aldehydes. In this case, an additional advantage of this method is the implementation of mild reaction conditions, Scheme 1.⁶⁹



Scheme 1. Reaction scheme showing conditions implemented by Zhang *et al.*⁶⁹ R₁ = non-/substituted phenyl ring or pyridine, R₂ = H or Me

This oxidative enamine catalysis strategy can be used as a complementary method in order to obtain a variety of alternative products. For example, Chen *et al.*⁷⁰ alternatively started with saturated alcohols to form intermediate α,β -unsaturated aldehydes in 78–92% yields, to which C₄ elongation using olefination reagents, such as a Julia or Wittig reagent were systematically repeated in order to attain highly conjugated polyene architectures.⁷⁰

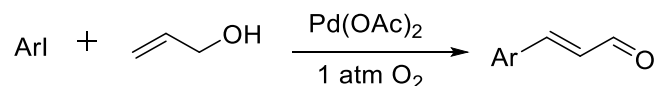


Scheme 2. Reaction scheme showing conditions implemented by Chen *et al.*⁷⁰

1.1.8.2 Palladium-catalyzed Heck-Saegusa reaction

Liu *et al.*⁷¹ used a different synthetic methodology to attain a variety of cinnamaldehydes – a novel one-pot palladium-catalyzed Heck–Saegusa reaction.⁷¹ This group had previously developed an amine–palladium(II) acetate (Pd(OAc)₂) co-catalyzed direct Saegusa oxidation which was applied to β -aryl aldehydes, rather than enol silyl ethers which are typically used in a traditional Saegusa oxidation reaction. This strategy gave access to α,β -unsaturated aldehydes in 41–62% yield.⁷⁵ Liu *et al.*⁷¹ were then successful in merging this method with the Heck reaction in order to give the same product but using a one-pot approach. Rather than starting with β -aryl aldehydes, an allyl alcohol is used which is coupled to an aryl iodide by means of the palladium-catalyzed Heck mechanism, producing β -aryl aldehydes. These then serve as starting materials for the subsequent Saegusa reaction to directly produce enals, given that Pd(OAc)₂ is used as a promoter in both reactions which facilitates the one-pot approach. Not only is this strategy performed

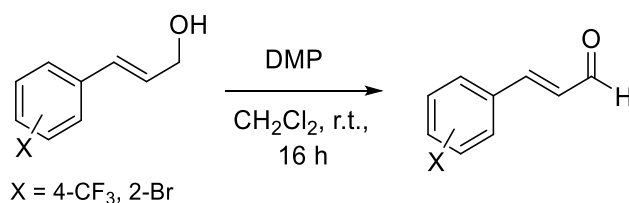
under mild reaction conditions and the starting materials are readily commercially available, but the cascade reactions are compatible with a variety of functional groups on the aryl ring and alternatively with heterocycles in 57-82% yield,⁷¹ making this a very attractive synthetic strategy for accessing enals.



Scheme 3. Reaction scheme showing conditions implemented by Liu *et al.*⁷¹

1.1.8.3 Dess-Martin oxidation of alcohols

Dess-Martin periodinane (DMP) is a mild, readily prepared and relatively inexpensive 12-I-5 organoiodine compound that is used in the selective oxidation of primary and secondary alcohols to aldehydes and ketones.⁷⁶ The advantages of the Dess-Martin oxidation procedure, relative to other methods in which alcohols are oxidised, include the shorter reaction times, ease of workups, and it avoids the use of a large excess of the oxidizing agent.⁷⁶ This type of method has been used by groups such as Morack *et al.*⁷³, who obtained the desired α,β -unsaturated aldehydes from the corresponding cinnamyl alcohols in 57-63% yield. Kim *et al.*⁷² is another example of a group that used this method. However, they did not disclose the yields obtained given that they used the cinnamaldehydes as intermediates in further synthetic applications.



Scheme 4. Reaction scheme showing conditions implemented by Morack *et al.*⁷³

1.1.8.4 Wittig procedure

The Wittig reaction occurs between a carbonyl compound, generally an aldehyde or ketone, and a phosphonium ylide to give an alkene with phosphine oxide generated as a by-product.⁷⁷ Wittig and Geissler⁷⁸ first reported this reaction in 1953, yet it is still a very valuable reaction with widespread use. Some of the reasons for this include its regioselectivity and stereoselectivity, the incorporation of mild reaction conditions, the readily available starting materials, and ylides are tolerant of a number of different functional groups, meaning the reaction has a broad scope and is useful in generating a wide range of target molecules.⁷⁷ In light of this, the Wittig reaction remains the subject of many modern publications,⁷⁷ and has been widely applied in the synthesis of cinnamaldehydes. The procedures applied have slightly variable conditions. For example,

some groups have used the benzaldehyde starting material in excess,^{79, 80} while others use the phosphonium ylide in excess.⁸¹⁻⁸⁷ Different solvents have been incorporated, such as toluene,^{79, 80, 85, 86} dry benzene,^{81, 84} dry DMF,⁸² DCM, or THF.⁸³ Generally, reaction times from 16 hours to 24 hours are employed,^{79-82, 84, 87} but shorter reaction times of 2 hours,⁸⁵ and longer reaction times of over 35 hours,⁸⁶ have been reported. In general, the temperature implemented is approximately 80 °C,^{79-81, 84-87} but reactions employed at room temperature,⁸² or initially at 0 °C followed by reaction at 25 °C have been recorded.⁸³ The procedure for purification generally involves flash chromatography.^{79, 80, 83-87} Alternatively, a work-up has been documented in the literature.⁸² This method was chosen to access a family of cinnamaldehydes, as will be described later in the experimental procedure, and more details on the Wittig procedure, such as mechanistic details, will be explored later in the results and discussion of this chapter, sections 1.2.1-1.2.3.

1.1.9 Synthetic versus natural medicinal agents

While natural products, as previously described in section 1.1.2, exhibit a number of advantages that make their incorporation as the major components of therapeutic agents highly desirable, synthetic medicinal agents are, in addition, valuable. With natural diversity being depleted by environmental factors, including global warming and toxic waste, including heavy metals,⁸⁸ it is essential that drugs can also be accessed via a purely synthetic route. Additionally, multidrug resistance to traditional natural medicines is high.⁸⁸ Furthermore, herbal drugs are generally considered as very safe and free from side effects, but this statement is false,⁸⁹ as there have been two kinds of side effects reported for herbal medicines.⁸⁹ The first is associated with the drugs themselves and is mainly related to over-dosage and/or interaction with conventional drugs, which leads to associated allergic reactions being reported for herbal drugs. The second is associated with the manufacturing of these natural medicinal agents and issues related to this, such as the misidentification of plants, lack of standardization, and failure of good manufacturing practice.⁸⁹ This is not aided by that fact that, in some countries including the United States, botanical products are marketed as “dietary supplement” and therefore their manufacture is not treated in the same manner as that for drugs, which must be registered and tested rigorously to prove their safety and clinical efficacy.⁸⁹ Synthetic drugs address symptoms caused by specific diseases as understood by scientific pathology,⁹⁰ and are comprised of small chemical building blocks which are not found in nature. Instead, they are produced with the help of areas such as computational chemistry and through the incorporation of different chemical sources.⁸⁸ Pyrazolopyrimidinones are made up of purely synthetic building blocks, and thus, represents this other class of medicinal agents investigated in this chapter and will be further described in the following section.

1.1.10 Pyrazolopyrimidinones as medicinal agents

4-*H*-Pyrazolo[1,5-*a*]pyrimidin-7-one is a fused nitrogen-containing heterocyclic system,⁹¹ Figure 4, that has served both as the core in numerous medicinal products and as a versatile synthetic intermediate.⁹²

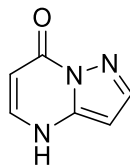


Figure 4. 4-*H*-pyrazolo[1,5-*a*]pyrimidin-7-one core.

Its derivatives have found such uses in the pharmaceutical industry as anti-cancer, antiviral, antiobesity,⁹¹ anti-inflammatory and anti-schistosomal agents,⁹² Figure 5.

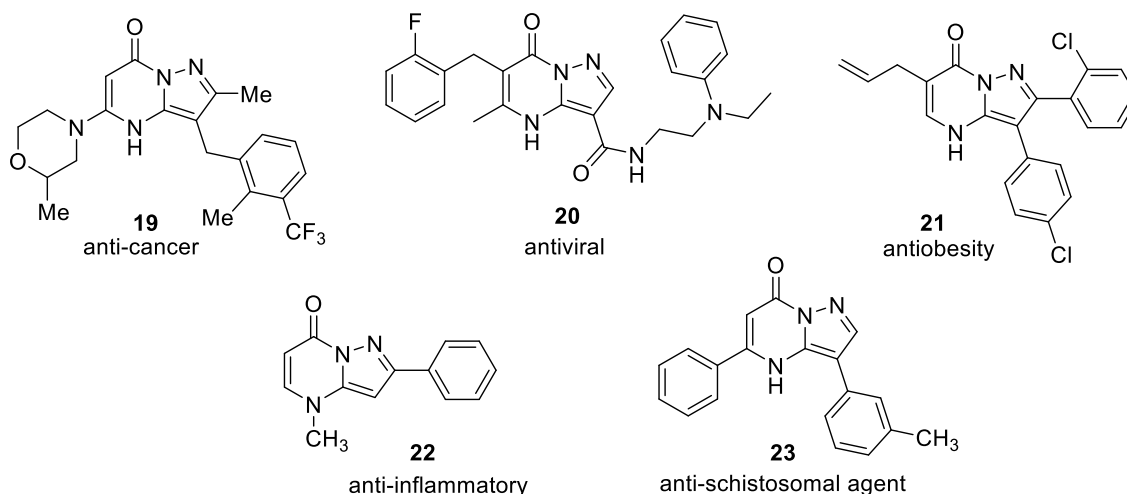


Figure 5. Pharmaceutical drugs with various therapeutic actions that all contain the same pyrazolo[1,5-*a*]pyrimidin-7-one core.^{91, 92}

Despite the range of medicinal applications elicited by this class of compounds, to the best of our knowledge, based on our search of the literature, there have been no antimicrobial investigations conducted. However, there have been such reports for structurally similar pyrazolo[1,5-*a*]pyrimidine,⁹³⁻⁹⁵ Figure 6, and pyrazolo[3,4-*d*]pyrimidine alternatives.

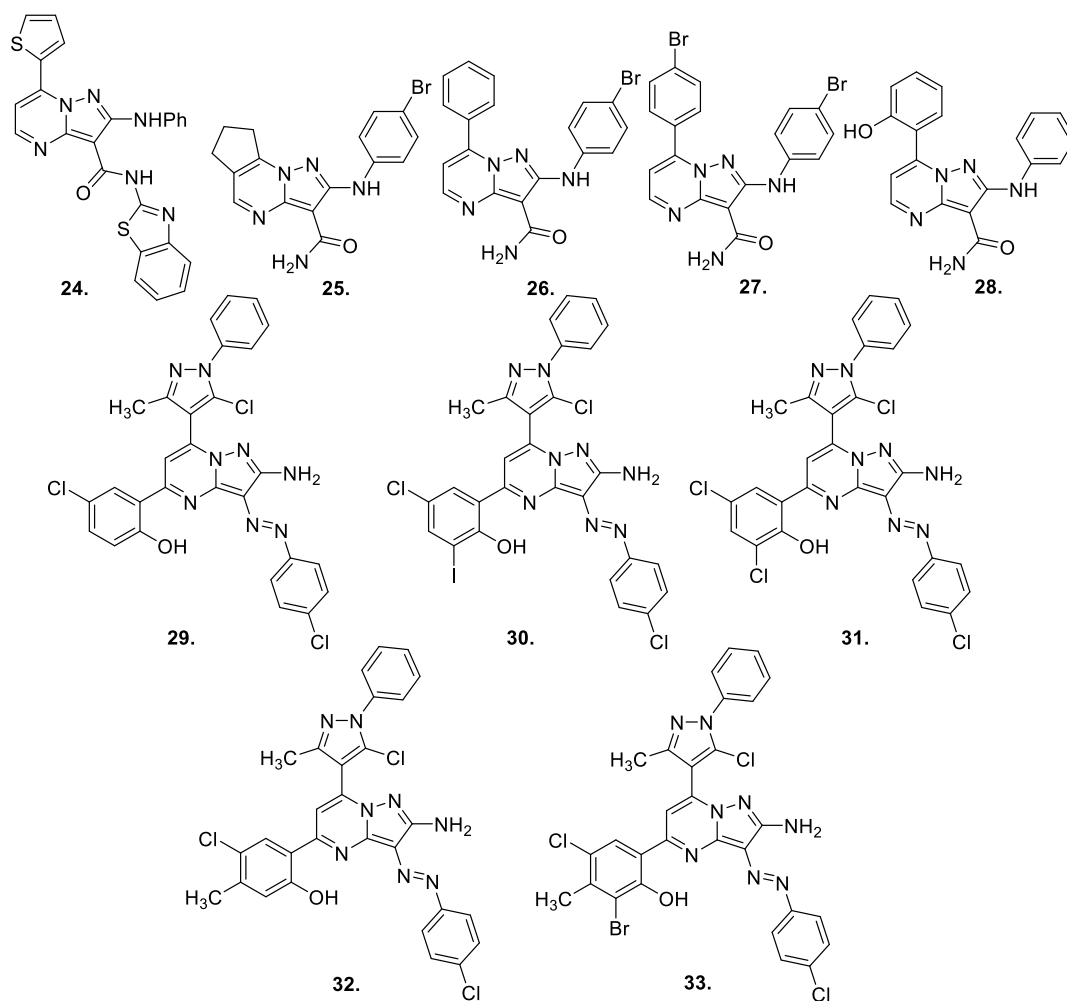


Figure 6. Structurally similar pyrazolo[1,5-*a*]pyrimidines that have exhibited potent antimicrobial activity.⁹³⁻⁹⁵

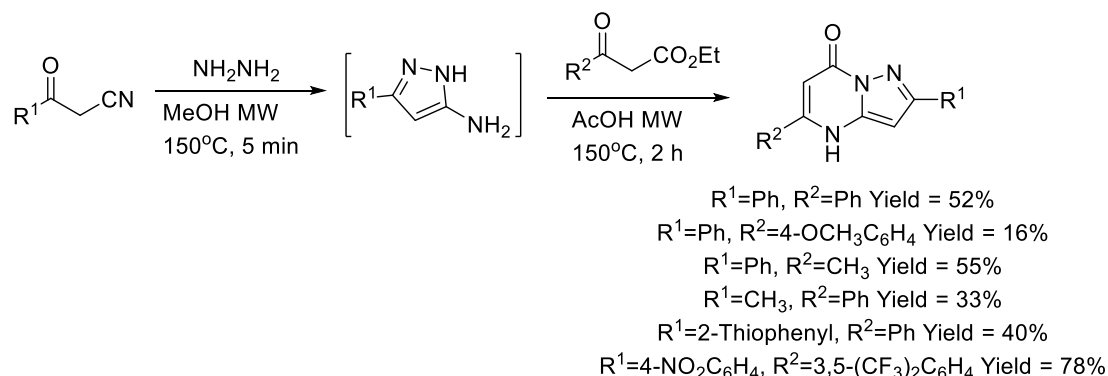
1.1.11 Antimicrobial activity of pyrazolo[1,5-*a*]pyrimidines

Bondock *et al.*⁹³ report that compound **24** (Figure 6) demonstrated significant *in vitro* anti-fungal activity against *Fusarium oxysporum* and *Aspergillus fumigatus*, exhibiting an MIC value of 6.25 µg/mL in both cases.⁹³ Of the family of pyrazolo[1,5-*a*]pyrimidines synthesized by Abdallah and Elgemeie,⁹⁴ compounds **25** and **26** (Figure 6) had potent activity against *B. subtilis*, *E. coli*, and *Pseudomonas aeruginosa* (*P. aeruginosa*). Additionally, compounds **27** and **28** (Figure 6) were effective against *S. aureus*. The largest inhibition zone diameters were recorded when compound **27** was used with respect to all four bacteria, with a 14 mm diameter being recorded per milligram of compound with respect to the two Gram-positive bacteria and 12 mm in the cases of both Gram-negative bacteria. This was relative to diameters of between 21 and 26 mm recorded when ampicillin was used. Interestingly, none of the pyrazolo[1,5-*a*]pyrimidines synthesized demonstrated any antifungal activity with respect to the two antifungal strains investigated, *Aspergillus flavus* and *Candida albicans*.⁹⁴ Shaikh *et al.*⁹⁵ similarly

synthesized a range of pyrazolo[1,5-*a*]pyrimidines, and compounds **29-31** (Figure 6) exhibited the best activity against at least one strain tested out of *B. subtilis*, *S. aureus* (both Gram-positive), *E. coli* and *Salmonella typhi* (both Gram-negative), *Aspergillus niger*, *Aspergillus flavus*, *Candida albicans*, and *Penicillium chrysogenum* (fungi). For example, **33** (Figure 6) was the most effective against *E. coli* and *Aspergillus flavus*, with inhibition zone diameters of 19 and 17 mm being recorded against each respective strain, relative to 20 and 18 mm when the reference compounds penicillin and nystatin were used, respectively. In most cases, the synthesized compounds had comparable activity to the commercial agent employed as a reference compound, showing that these pyrazolo[1,5-*a*]pyrimidines have potent antimicrobial activities across a range of microbial strains.⁹⁵

1.1.12 Synthesis of 4-*H*-pyrazolo[1,5-*a*]pyrimidin-7-ones

Our group have synthesized a range of 4-*H*-pyrazolo[1,5-*a*]pyrimidin-7-ones using one-pot microwave-assisted synthetic methodology, in which ketonitrile, hydrazine, and methanol were heated using microwave conditions (100 W, 150 °C) for 5 minutes followed by the addition of acetic acid and ketoester, then heated under the same microwave conditions for a further 2 hours.⁹¹



Scheme 5. Examples of 4-*H*-pyrazolo[1,5-*a*]pyrimidin-7-one compounds that have been synthesized by this method, adapted from the work of Kelada *et al.*⁹¹.

As a result of this synthetic work by colleagues in our group,⁹¹ a family of 4-*H*-pyrazolo[1,5-*a*]pyrimidin-7-one compounds were at our disposal, and so, given the lack of prior studies assessing the antimicrobial activity of this type of compound, we thought this warranted investigation. The results of the antimicrobial studies related to this family of compounds is included later in the results and discussion section of this chapter, section 1.3.

1.1.13 Aims of our antimicrobial research.

The aims of this part of the PhD project include:

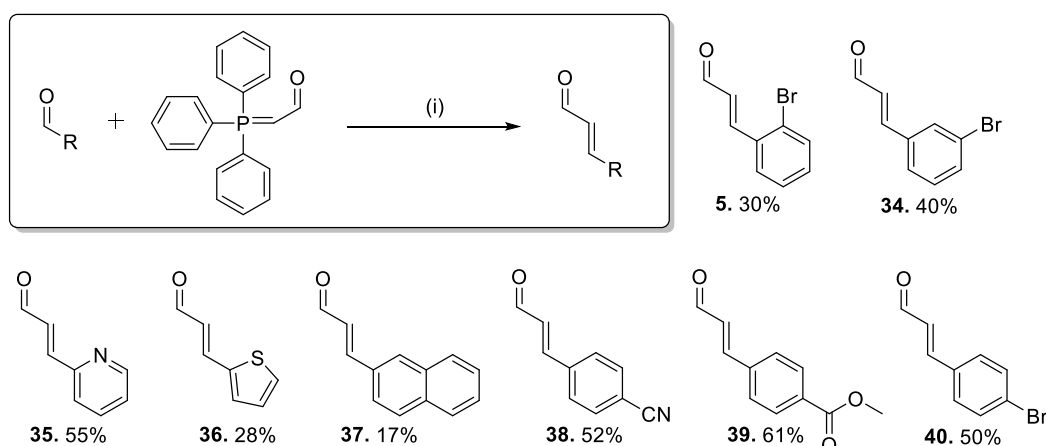
- (i) To synthesize a family of cinnamaldehydes, explore their electrophilicity as well as their antibacterial activity against *S. aureus* (Gram-positive) and *E. coli* (Gram-negative), and assess if any relationship exists between the two. Additionally, an initial investigation into a possible antibacterial mechanism of action is to be conducted, as well as an *in vivo* toxicity assessment of a selection of the cinnamaldehydes using *Galleria mellonella* (*G. mellonella*).
- (ii) To conduct an antimicrobial evaluation of 35 4-*H*-pyrazolo[1,5-*a*]pyrimidin-7-ones against *S. aureus*, *E. coli*, and *Candida albicans* (a representative fungus). This is to include evaluating leading hit candidates against clinically relevant strains of methicillin-resistant *Staphylococcus aureus* and *Pseudomonas aeruginosa*. Additionally, an *in vivo* toxicity assessment and an *in vivo* therapeutic evaluation of the most active compounds is to be completed, using *G. mellonella* and infected *G. mellonella* respectively.

1.2 Cinnamaldehydes Results and Discussion.

1.2.1 Synthesis of cinnamaldehydes

As previously highlighted in the introduction, sections 1.1.6 and 1.1.7, *trans*-cinnamaldehyde has been described in the literature as both an antimicrobial agent and as a Michael acceptor.^{3, 6, 8-10, 12-14, 17, 18, 59, 63, 96, 97} However, to the best of our knowledge, a systematic study exploring how the chemical structure and electrophilicity of its derivatives relates to antimicrobial activity had not been reported. Thus, the first half of this results and discussion section is dedicated to elucidating the synthesis, antibacterial evaluation, and an initial mechanism of action study for a family of *trans*-cinnamaldehydes, as reported in our experimental paper ‘Cinnamaldehydes: Synthesis, antibacterial evaluation, and the effect of molecular structure on antibacterial activity’ which appeared in the peer-reviewed journal *Results in Chemistry*,⁹⁸ and our literature review ‘A review of cinnamaldehyde and its derivatives as antibacterial agents’, which was published in the peer-reviewed journal *Fitoterapia*.⁶⁸

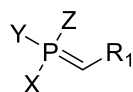
The *trans*-cinnamaldehydes were selected based on their predicted electrophilicities in order to better understand how this might affect their antimicrobial activities. For our study, nine of the fifteen *trans*-cinnamaldehydes were synthesized, and, in all but one case, this was achieved using a modified Wittig procedure.⁸⁷ The nine synthesised cinnamaldehydes are literature compounds, see sections 1.4.2 and 1.4.3 of the experimental procedure, and our yields are shown in Scheme 6. The remaining cinnamaldehydes were purchased from commercial sources.



Scheme 6. (i) Arylaldehyde (0.628 mmol, 1 eq.), (triphenylphosphoranylidene) acetaldehyde (0.690 mmol, 1.1 eq), toluene (5 mL), 80 °C, 24 h.⁹⁸

Our Wittig synthetic methodology employed a low-cost commercially available ylide, (triphenylphosphoranylidene)acetaldehyde. A triphenylphosphine-derived ylide, in which R¹ (Figure 7) is a carbonyl, is classified as a stabilized ylide. Ylides are typically

categorised as stabilized, semi-stabilized and non-stabilized, depending on the nature of this R¹ group.



X, Y, Z = aryl or alkyl

Figure 7. Structural motif of a general ylide, adapted from Byrne and Gilheany.⁷⁷

As per Figure 7, if R¹ is a conjugating group, it is a stabilized ylide, if it is an aryl or alkenyl group, it is semi-stabilized and if it is an alkyl group, it is non-stabilized. Stabilized ylides are so-called because the conjugating group means that they are typically more stable to hydrolysis in air. Other common examples of conjugating groups present in stabilized ylides are esters, sulfones and nitriles.⁷⁷ The nature of the ylide is significant because it affects its reactivity and certain trends have been reported in the literature depending on the class of ylide in terms of *E/Z*-selectivity observed in the product for example.

1.2.2 Overview of synthetic strategies to access cinnamaldehydes

As discussed previously in the introduction, section 1.1.8, there have been various synthetic strategies used to access cinnamaldehydes, including oxidative enamine catalysis,^{69, 70} the use of a palladium-catalyzed Heck-Saegusa reaction,⁷¹ and Dess-Martin oxidation of alcohols.^{72, 73}

The oxidative enamine catalysis described by both Zhang *et al.*⁶⁹ and Chen *et al.*⁷⁰ consists of an amine-catalyzed, 2-iodoxybenzoic acid (IBX)-mediated oxidation of aldehydes,⁶⁹ or alcohols,⁷⁰ to α,β -unsaturated aldehydes. Of the cinnamaldehydes we synthesized, three were accessed by Zhang *et al.*⁶⁹, 4-bromocinnamaldehyde **40**, 4-cyanocinnamaldehyde **38**, and 3-(pyridin-2-yl)acrylaldehyde **35** (Scheme 6) in 82, 79 and 75% yield, respectively. Chen *et al.*⁷⁰ also synthesized compound **40** in a superior yield of 91%.⁷⁰ In all cases, the *E* isomer only was synthesized. Both groups employed room temperature for all these conversions but Zhang *et al.*⁶⁹ used DCM as a solvent, 10 mol% catalyst and 1.2 equivalents of IBX, whereas Chen *et al.*⁷⁰ employed DMSO and acetonitrile (1:1.5) as co-solvent, 20 mol% catalyst and 2.5 equivalents of IBX. In particular, with respect to the synthesis of **40**, Chen *et al.*⁷⁰ used a longer reaction time of 9 hours, relative to 4 hours in the case of Zhang *et al.*⁶⁹

Traditionally, one of the biggest issues with the use of IBX was its limited solubility in common organic solvents except DMSO,⁹⁹ although this was overcome by Zhang *et al.*⁶⁹. Additionally, the methods required for the synthesis of IBX were potassium bromate (KBrO₃)-based.⁹⁹ KBrO₃ is classified as a carcinogen, and entailed other unappealing aspects such as the performance of the reaction in hot aqueous sulfuric acid (0.73 M).⁹⁹

Nowadays, a simple one-step preparation from 2-iodobenzoic acid is used, with Oxone[®] being employed as an environmentally friendly oxidant.¹⁰⁰ Despite the high yields being reported by application of this method, the extra step required to prepare IBX, particularly when the method required Oxone[®] which, according to its MSDS is corrosive to the skin (sub-category 1B) and causes serious eye damage (category 1), was not of interest to us and so, we looked for alternative methods.

Dess-Martin oxidation is an alternative to IBX-mediated oxidation, as described previously in section 1.1.8.3 of the introduction. Dess-Martin periodinane (DMP) is an acylated derivation of IBX, which is far more soluble than IBX in organic solvents.⁹⁹ IBX has been used as a precursor to access DMP.^{99, 100} The Dess-Martin oxidation method has been used by groups such as Morack *et al.*⁷³ who obtained the desired α,β -unsaturated aldehydes from corresponding cinnamyl alcohols in 57-63% yield. The only cinnamaldehyde synthesized by this group which we also synthesized was compound **5** (2-bromocinnamaldehyde) which was obtained in 63% yield, superior to our yield of 30%. However, DMP has a number of disadvantages relative to IBX, such as its higher cost and lower stability,¹⁰⁰ and so, this was also discounted as a synthetic strategy to access cinnamaldehydes.

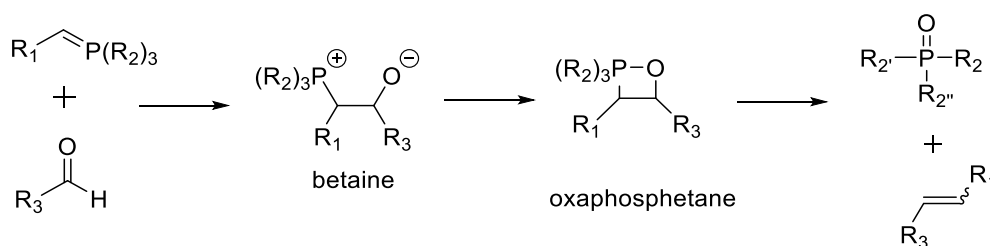
The use of a palladium-catalyzed reaction, such as the Heck-Saegusa reaction,⁷¹ was also considered as a potential synthesis, see section 1.1.8.2 of the introduction. The cinnamaldehydes synthesized by this method, which we also synthesized, were compounds **38**, **39** (Scheme 6), and **37** obtained in 68, 80 and 82% yield, respectively. Despite the high yields of cinnamaldehydes possible via this methodology, the requirement for such a precious, expensive catalyst,¹⁰¹ as palladium, and the desire for a more environmentally friendly method than one which requires a toxic, metal reagent,¹⁰⁰ led us to explore an alternative method.

The Wittig methodology avoids the issues encountered through the use of these aforementioned synthetic strategies. The benzaldehyde substrate and (triphenylphosphoranylidene)acetaldehyde were commercially available, avoiding the requirement to prepare either separately and hence, requiring fewer steps in this synthesis. Additionally, the requirement for a transition-metal catalyst was avoided, which was of significant economic and environmental benefit, and the safe and convenient nature of this synthesis without the implementation of anhydrous conditions was appealing to us. We implemented a modified procedure of Knölker *et al.*⁸⁷, who used **1**, **14**, and **38** as substrates to access a range of 1-azabuta-1,3-dienes. We modified this procedure by using a smaller scale of reagents, and an alternative mobile phase for column chromatography. Alternative Wittig procedures to that reported by Knölker *et al.*⁸⁷ to access cinnamaldehydes have been reported,^{81-86, 102} see section 1.1.8.4 of the introduction, but the requirement for higher temperatures,⁸¹ more toxic solvents such as DMF or benzene,^{82, 102} or lack of clarity regarding the stereochemical outcome of the reaction,⁸³ led us to the use the modified procedure of Knölker *et al.*⁸⁷

1.2.3 Wittig reaction mechanism

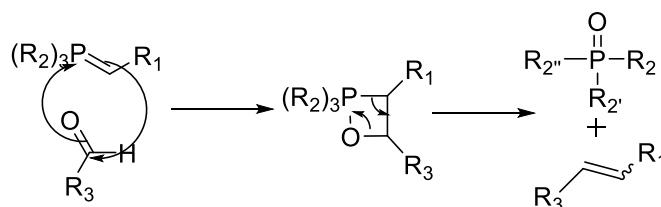
There have been multiple mechanisms proposed in order to explain the Wittig reaction, a large number of which have been summarised in the excellent review paper by Byrne and Gilheany.⁷⁷ The focus in this discussion will be limited to the original betaine mechanism, as it is a mechanism that is still quite prevalent throughout the literature related to this topic, and the cycloaddition mechanism put forward by Vedejs *et al.*^{103, 104} as it lays the foundation for the modern understanding of the Wittig reaction mechanism.

The betaine mechanism is comprised of nucleophilic addition of the ylide to the aldehyde carbonyl to form a betaine intermediate. Subsequent ring closure leads to the formation of an oxaphosphetane, which decomposes to give the alkene and phosphine oxide as a by-product. The earliest proposal of the Wittig mechanism by Wittig and Schöllkopf included betaine as an intermediate of the reaction.¹⁰⁵ However, although a betaine-LiBr complex has been detected by NMR,¹⁰³ non-complexed betaine has not been identified by any spectroscopic means in a Wittig reaction mixture.⁷⁷ In light of this, the formation of the betaine intermediate has been largely discounted.^{77, 106}



Scheme 7. Original betaine mechanistic overview, adapted from Byrne and Gilheany.⁷⁷

Thus, a more modern explanation for the Wittig reaction mechanism is that presented by Vedejs *et al.*,¹⁰⁴ who were the first group to advance the idea of a direct irreversible [2+2] cycloaddition of the ylide and aldehyde to give an oxaphosphetane. The oxaphosphetane then undergoes irreversible and stereospecific cycloreversion to give phosphine oxide and the alkene, as per Scheme 8.



Scheme 8. [2+2] Cycloaddition mechanistic overview, adapted from Byrne and Gilheany.⁷⁷

This mechanism has been further developed to include an explanation of the stereochemistry of the alkene product and how this is dictated at the transition state of the cycloaddition step. The use of different ylides leads to different transition state shapes,

which in turn affects the stereochemistry of the resulting alkene. Reactions of aldehydes with non-stabilized ylides were proposed to proceed via an early puckered transition state (Figure 8 (a)) in which both bond formation and rehybridization about the forming ring occur at an early stage. Conversely, reactions of aldehydes with stabilized ylides were proposed to proceed via a later transition state, (Figure 8 (b)) and are *trans*-selective. The possible (late) *cis*-selective transition states (planar and puckered) in these reactions of stabilized ylides (Figure 8 (c) and (d)) were found to be significantly higher in energy, using the Jaguar 4.0 pseudospectral program package,¹⁰⁷ than the *trans*-selective transition state (Figure 8 (b)).

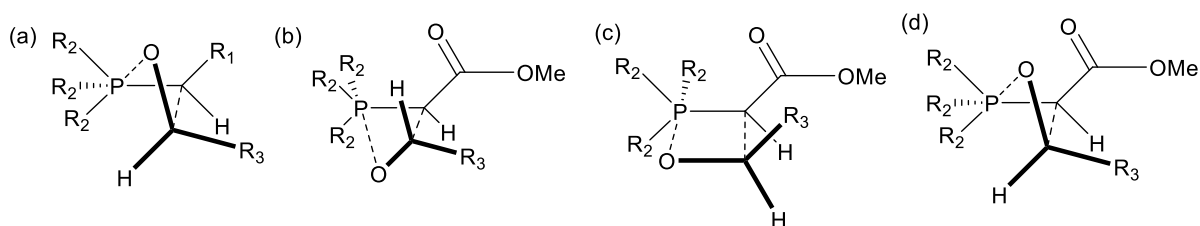
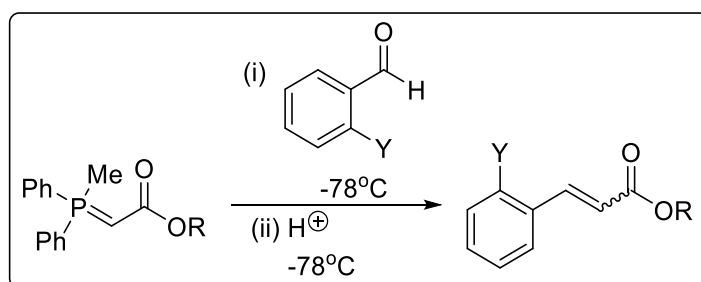


Figure 8. Proposed [2+2] cycloaddition transition states for various Wittig reactions, adapted from Byrne and Gilheany.¹⁰⁶

As was evident by Scheme 6 previously, the yields of desired cinnamaldehydes, with selective *E*-geometry, varied greatly in our study from 17- 61%. Generally, electron-withdrawing groups in the *para*-position were well tolerated while electron-donating groups in this position were less so. An alkyl substituent in the *para* position, namely the 4-methylcinnamaldehyde derivative **41**, could not be adequately isolated using this method, where a small amount of product could be seen in the ¹H NMR spectrum of the crude mixture, in addition to a complex mixture, and consequently a low yield of only 4% pure product resulted. Thus, the alternative synthetic approach used for **41** will be discussed separately. Although (*E*)-3-(pyridine-2-yl)acrylaldehyde **35** was successfully obtained in 55% yield, replacement of the phenyl ring with either a thiophene or naphthalene were not as successful, with lower yields of 28% (**36**) and 17% (**37**) obtained, respectively. The lower yield was due to a reduction in reactivity, as evidenced by some starting material in crude NMR spectra, as well as the generation of a complex mixture of other products. This indicates that the nature of the substituent on the phenyl ring, or replacement of it with another carbocycle or heterocycle, influences the yield obtained by implementation of the Wittig procedure.

In addition, the above reaction scope indicates that the position of the substituent on the phenyl ring is a factor that affects the yield, given that 4-bromocinnamaldehyde, **40**, was obtained in 50% yield while 3-bromocinnamaldehyde, **34**, was obtained in 40% yield and 2-bromocinnamaldehyde, **5**, was obtained in the lowest yield of the bromo-substituted cinnamaldehydes at 30% yield. This is something that has been well-documented by groups such as Byrne and Gilheany,¹⁰⁶ whose research has contributed to the elucidation

of the true mechanism of the Wittig reaction.⁷⁷ In their work investigating the reactions of substituted aldehydes with all phosphonium ylide types, an observation was recorded noting that lone-pair bearing *ortho*-substituents on benzaldehydes resulted in significantly enhanced *Z*-selectivity when both semi- and stabilized ylides were employed. Given that a stabilized ylide was implemented in our synthetic approach to access cinnamaldehydes, discussion will be limited to this type of ylide, depicted as Scheme 9 below, which has been adapted from the literature.¹⁰⁶



Ylide OR	Aldehyde Y	Enoate <i>Z</i> : <i>E</i> ratio
OEt	H	36:64
OEt	OMe	66:34
OEt	Cl	77:23
OEt	Br	83:17

Scheme 9. Summary of the yields obtained by Byrne and Gilheany¹⁰⁶ when a stabilized ylide was reacted with various *ortho*-heteroatom-substituted benzaldehydes.

As is evident by the above scheme, the reaction between benzaldehyde and the stabilized ylide showed good *E*-selectivity, but reaction of the same ylide with *ortho*-heteroatom-substituted benzaldehydes resulted in enhanced *Z*-selectivity. This was most prominent in the case of the larger bromo substituent, which showed the highest *Z*-selectivity and this, the authors note, is consistent with the reaction occurring under kinetic control.¹⁰⁶ The yields obtained as depicted in Scheme 9 by Byrne and Gilheany¹⁰⁶ were the result of the implementation of a standard set of conditions. The use of a standard set of reaction conditions ensured that the experiment was carried out under kinetic control, and they avoided the possibility of stereochemical drift. They also ensured that the *Z/E* ratio of the alkene product at the end of the reaction remained unchanged once formed.¹⁰⁶ This last consideration is particularly important because this group note how the *Z/E* ratio is fragile and can change after a reaction has come to completion.¹⁰⁶ The reaction mixture being allowed to stand for a period of time, exposure to sunlight or heat, the solvent employed or the presence of acids have all been implicated as factors affecting this ratio.¹⁰⁶

With our cinnamaldehydes, the major isomer was the *E* isomer in all analyzed cases. The crude ¹H NMR spectra, of those cinnamaldehydes that were analyzed, showed the presence of both the *E* and *Z* isomers, as well as unreacted starting aldehyde. The ratios

of starting aldehyde : *E* cinnamaldehyde : *Z* cinnamaldehyde for eight cinnamaldehydes is shown in Table 1. We focused on the isolation of the *E*-isomer only as this was the geometry present in the naturally occurring *trans*-cinnamaldehyde, **1**. We wanted this geometry to be retained in our target cinnamaldehydes for the purposes of comparative antibacterial activity assessment.

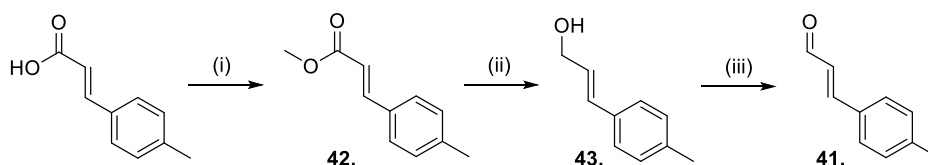
Table 1. The ratios of starting aldehyde : *E* cinnamaldehyde : *Z* cinnamaldehyde in the crude mixtures of eight cinnamaldehydes that we synthesized.

Compound number	Cinnamaldehyde	Starting aldehyde : <i>E</i> cinnamaldehyde : <i>Z</i> cinnamaldehyde ^a
5	2-Bromocinnamaldehyde	1.5:4:1
34	3-Bromocinnamaldehyde	2:5:1
35	3-(Pyridin-2-yl)acrylaldehyde	3:26:1
36	3-(Thiophen-2-yl)acrylaldehyde	3:5:1
37	3-(Naphthalen-1-yl)acrylaldehyde	6:2:1
38	4-Cyanocinnamaldehyde	1:9:1
39	4-(Methyl ester) cinnamaldehyde	2:7:1
40	4-Bromocinnamaldehyde	3:6:1

^a Ratio determined by integration of the aldehyde signal in the crude ¹H NMR spectrum, using the modified procedure of Knölker *et al.*⁸⁷, specifically arylaldehyde (0.628 mmol, 1 eq.), (triphenylphosphoranylidene) acetaldehyde (0.690 mmol, 1.1 eq), toluene (5 mL), 80 °C, 24 h. See Appendix 1. Figures A38-A53

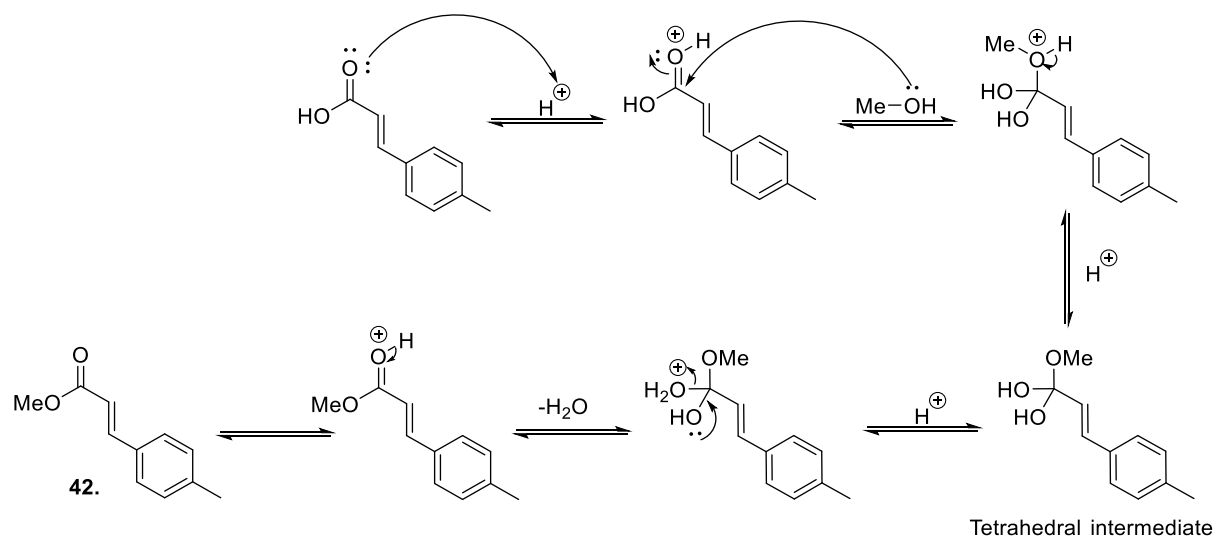
1.2.4 Synthesis of 4-methylcinnamaldehyde

When the Wittig procedure was applied to the synthesis of *p*-methylcinnamaldehyde, **41**, a complex mixture resulted, which made isolation of the desired product difficult, and a 4% yield was obtained. An alternative synthetic strategy was therefore required, Scheme 10.^{108, 109} This involved Fischer esterification of the starting carboxylic acid, followed by reduction using di-*isobutyl* aluminum hydride (DIBAL-H). The final oxidation by activated manganese dioxide (MnO₂) furnished the desired *p*-methylcinnamaldehyde, **41**, in an overall yield of 79% over the three steps.



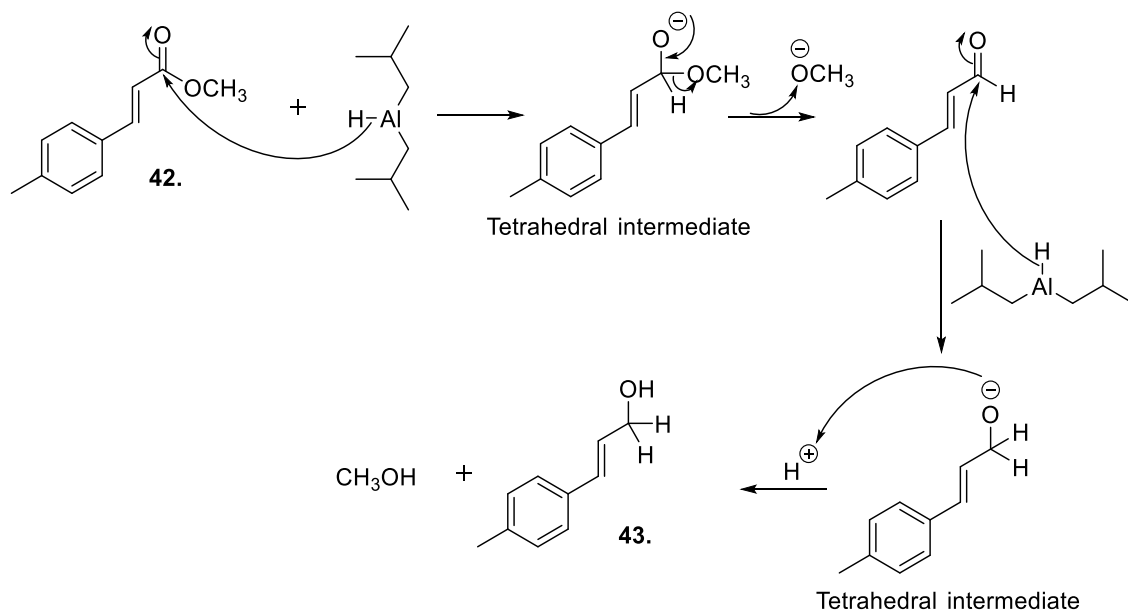
Scheme 10. (i) H₂SO₄, MeOH, 6 hr, reflux 85% yield; (ii) DIBAL-H, toluene, 0 °C, 93% yield; (iii) MnO₂, DCM, 35 °C, 7 hr, 99.6% yield. A 79% overall yield for the three steps.

Adapted from the literature,¹⁰⁸ we used a Fischer esterification to convert 4-methylcinnamic acid (predominantly *trans*, purchased from commercial sources) to its corresponding ester, **42**. Originally proposed by Emil Fischer and Arthur Speier,¹¹⁰ the mechanism involves a two-step process and proceeds via the formation of a tetrahedral intermediate,¹¹¹ Scheme 11.



Scheme 11. Fischer esterification mechanism.¹¹¹

Once the cinnamic ester **42** was accessed, it was then reduced by DIBAL-H, using a procedure adapted from the literature,¹⁰⁹ to produce its corresponding primary alcohol **43**. A proposed mechanism is shown in Scheme 12. This mechanism consists of a nucleophilic acyl substitution, followed by nucleophilic addition of a second equivalent of DIBAL-H to the aldehyde intermediate.¹¹² DIBAL-H has been reported as an effective reducing agent since as early as 1959 by Miller *et al.*¹¹³, for example in the reduction of methyl benzoate to benzyl alcohol in a 90% yield.



Scheme 12. Proposed mechanism of DIBAL-H reduction.

The final step of this three-step process was the conversion of the primary alcohol to the desired 4-methylcinnamaldehyde product, **41**. This was done via oxidation using activated MnO_2 , implementing a procedure adapted from the literature.¹⁰⁹ Activated MnO_2 has found widespread use as a mild oxidant in organic chemistry, something which can be attributed to any of a number of reasons including its low associated toxicity, wide commercial availability and low cost.¹¹⁴ In addition, in light of its nature as a heterogeneous substance, this facilitates a convenient workup process consisting of simple filtration followed by the evaporation of solvent.¹¹⁴ The precise mechanism of oxidation by MnO_2 has been difficult to elucidate,¹¹⁵ both free-radical and ionic mechanisms have been proposed,¹¹⁵ and it is beyond the scope of this thesis to probe the mechanism further. However, its application was successful in our case with the desired product, **41**, being isolated in a high yield. Patil *et al.*¹⁰⁹ used a similar three-step method to access a range of cinnamaldehydes, including **41**. However, this group started with the corresponding benzaldehyde in each case, and reacted this with triethyl phosphonate and sodium hydride to convert from the aldehyde to an α,β -unsaturated ester. Then, using DIBAL-H, they isolated the corresponding alcohol and finally, they oxidised this using activated MnO_2 to produce the final cinnamaldehyde. This group achieved an overall yield of 58% using their three-step method, compared with our 79% yield over three-steps, but they did not include a percentage yield for each step undertaken.

1.2.5 Structural characterization of a cinnamaldehyde – 4-cyanocinnamaldehyde, **38**

As mentioned previously, all of the cinnamaldehydes we synthesized were literature compounds, and hence, structural characterization was performed by comparison of our collected NMR spectroscopic data with the literature. Our data consistently matched the existing literature data for all cinnamaldehydes. A brief discussion on the structural characterization of 4-cyanocinnamaldehyde, compound **38**, as an example cinnamaldehyde is included here. The structure of this compound, with atoms labelled for ease of discussion, is shown in Figure 9.

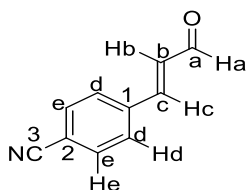


Figure 9. Structure of **38**, with atoms labelled.

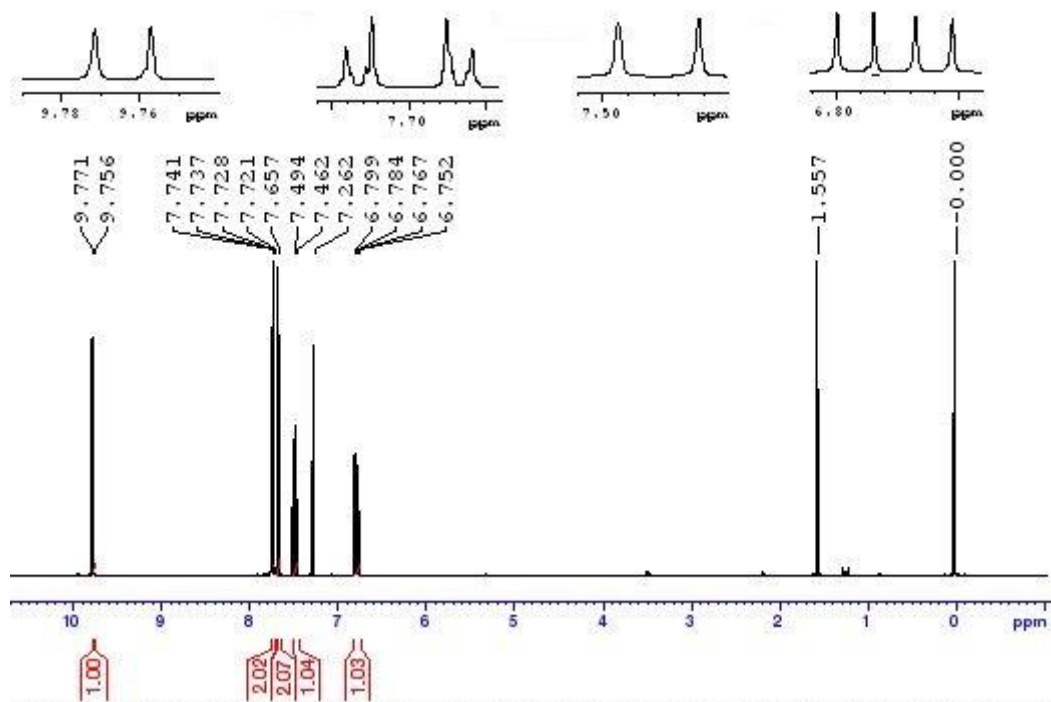


Figure 10. ^1H NMR spectrum of **38**, with zoomed in images of signal multiplicities, in order of ppm.

All proton assignments can be made on the basis of the ^1H NMR spectrum of **38** alone. The most deshielded signal belongs to Ha (Figure 9), the aldehyde proton signal that is deshielded due to its proximity to the electron-withdrawing carbonyl group. Moving upfield, the signal integrating for two protons belongs to He, which is more deshielded than Hd, the next signal integrating for two protons moving upfield, because of its position on the ring in relation to the electron-withdrawing cyano group. Next, the doublet at 7.49 ppm belongs to Hc and finally the only doublet of doublets signal belongs to Hb,

which couples to Ha ($J = 7.4$ Hz) and Hc ($J = 16.1$ Hz), as confirmed by assessment of the COSY spectrum (Appendix 1, Figure A3).

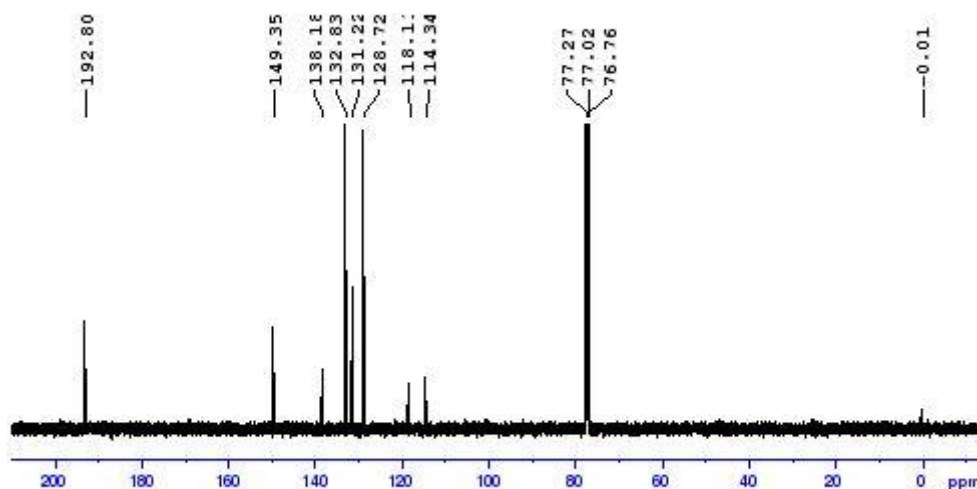


Figure 11. ^{13}C NMR spectrum of **38**.

With regard to the above ^{13}C NMR spectrum, the signal at 192.8 ppm is accounted for by the aldehyde carbonyl carbon (Ca, Figure 9), again, due to the electron-withdrawing nature of this group, it has a deshielding effect on the carbon signal. Comparing this spectrum to the DEPT-135 spectrum, three quaternary carbons can be identified, as expected from the structure **38**, at 138.2 ppm, 118.1 ppm and 114.3 ppm. See Appendix 1, Figure A6 for the DEPT-135 spectrum.

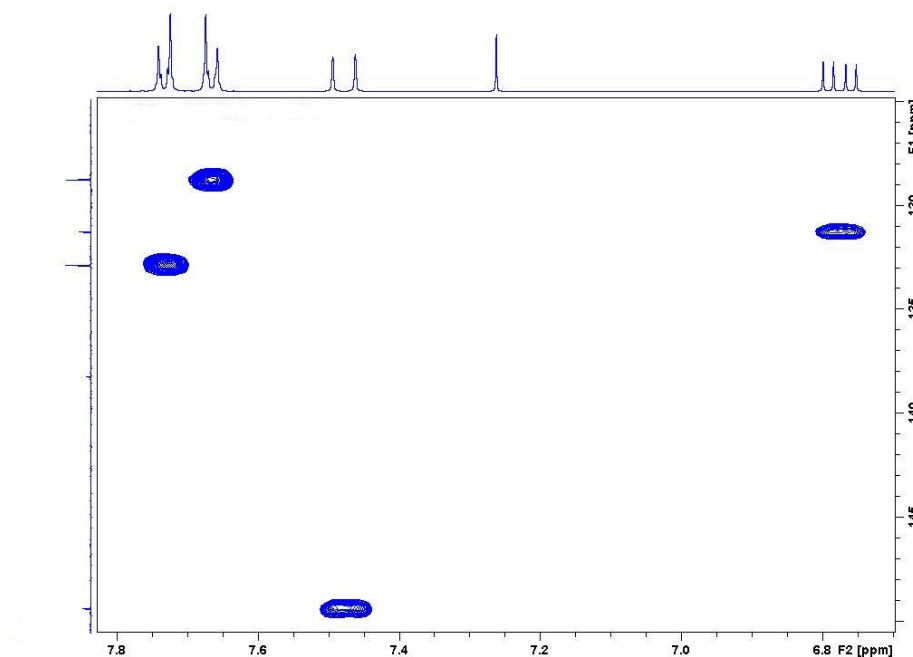


Figure 12. HSQC NMR spectrum of **38**.

The majority of carbon assignments can be made from examination of the HSQC spectrum, Figure 12. The signal at 149.4 ppm is accounted for by Cc (Figure 9), 132.8 ppm by Ce, 131.2 ppm by Hb and 128.7 ppm by Hd. The HMBC spectrum, see Appendix 1, Figure A5, shows coupling between the carbon signal at 138.2 ppm with Hb, Hc and He, making this likely to be the signal of C1, as C2 and C3 are too far away from either Hb or Hc to experience coupling with these protons. The quaternary carbon at 118.1 ppm is likely to be the cyano carbon (C3) as this shows coupling to He and a smaller coupling to Hd, consistent with He being closer in proximity and hence, a stronger coupling than to Hd which is four bonds away. This makes C2 the signal appearing at 114.3 ppm. These assignments are all consistent with those assigned by Knölker *et al.*⁸⁷ for this compound. All NMR assignments we made with respect to the cinnamaldehydes were consistent with the respective literature data available for each compound, as referenced in the experimental procedure data for each cinnamaldehyde.

1.2.6 Methods for determining antimicrobial activity – antimicrobial susceptibility tests (ASTs)

Antimicrobial susceptibility tests (ASTs) are used to determine antimicrobial resistance,¹¹⁶⁻¹¹⁸ and to ascertain the susceptibility of microorganisms to novel or conventional antimicrobial agents.^{116, 117} First introduced in 1929, *in vitro* AST methods are still considered key to determining the effectiveness of antimicrobial agents against microorganisms.¹¹⁸ A variety of laboratory methods have been used to assess the *in vitro* antimicrobial activity of a compound. The most known and widely used methods are the disk-diffusion and broth or agar dilution methods.¹¹⁹ Other methods used include time-kill test and flow cytometric methods.¹¹⁹ In general, *in vitro* antimicrobial susceptibility methods combine one or more antimicrobial agents with a microorganism, such as bacteria, to assess the growth of that microorganism as a result of treatment.¹¹⁸ All *in vitro* AST methods provide a qualitative result, including the response of a microorganism to an agent within the categories of susceptible, intermediate, or resistant,¹¹⁷ which is determined by eye. Some methods provide quantitative results, such as a minimum inhibitory concentration (MIC) value.¹¹⁷ The fact that there are a variety of ASTs implemented could lead to variations in results obtained.¹²⁰ Each method has advantages and disadvantages.¹¹⁷ A selection of these methods can be classified as gold-standard clinical antimicrobial susceptibility testing methods, including the agar dilution method, broth micro/macrodilution method, disc diffusion method, and polymerase chain reaction (PCR)-based techniques. As gold-standard clinical antimicrobial susceptibility testing methods, they focus on the determination of the MIC or growth curve using a simple readout procedure and have been standardized by various organisations including the Clinical and Laboratory Standards Institute (CLSI) and the International Organization for Standardization (ISO).¹¹⁸ For convenience, these methods can be broadly divided into

diffusion and dilution,¹¹⁹ and an example of each type will be explained in the following section.

1.2.6.1 Microdilution – an AST dilution method

The microdilution assay format was developed in 1977.¹¹⁸ The macrodilution format was developed prior to this, a method in which two-fold dilutions, i.e. a dilution of a half, of the antibiotic agents (for example, 1, 2, 4, 8, and 16 µg/mL) in a nutrient broth medium in test tubes containing a minimum volume of 2 mL were prepared.^{117, 119} These test tubes were then inoculated with a standardised bacterial suspension and allowed to incubate overnight at 35 °C. The tubes were then examined for bacterial growth by eye using turbidity (i.e. apparent cloudiness of the medium) as a qualitative measurement,¹¹⁷ where the greater the extent of turbidity, the larger the number of cells in the culture. A MIC value could be assessed using this method and was quantified as the lowest concentration of the antibiotic agent that prevented bacterial growth. The ability to ascertain this value was the biggest advantage of this method. However, the necessity to manually prepare each of the antibiotic solutions,^{117, 119} as well as the associated risk of errors in preparing each of these solutions,¹¹⁹ and the relatively large amounts of reagents and space required for each test,^{117, 119} were some of the major disadvantages of this method. The miniaturization and mechanization of this test through the use of small, disposable, plastic ‘microdilution’ trays made the broth microdilution method a widely popular and practiced technique. In this method, trays consisting of 96 wells which each contain a volume of 0.1 mL are used. This facilitates up to 12 antibiotics being tested on a single plate in the range of 8 two-fold dilutions.^{117, 118} After manually, or automatically, dispensing a small amount of bacteria to each well,¹¹⁸ typically done using dispensing instruments that aliquot accurate volumes,¹¹⁷ the plate is incubated overnight and analyzed subsequently for the determination of a MIC value.¹¹⁸ Manual, or automatic, viewing devices, or alternatively the use of colorimetric methods using dye reagents, have been used in conjunction with the microdilution method to ensure reproducible results with respect to the determination of MIC values. These are determined by fluorescence intensity or turbidity measurements.^{118, 119} The development of the microdilution method has increased reproducibility, requires fewer reagents and less space, and entails less time to prepare samples, relative to the macrodilution procedure, all of which are major advantages to this method.^{118, 119} With a higher degree of automation, where plates can even be purchased containing different concentrations of the dry agent pre-prepared in each well, microdilution is now preferred over broth macrodilution.¹¹⁸ However, the main disadvantage of this method is the inflexibility of drug selections available in standard commercial panels,¹¹⁹ thus manual preparation of samples is still necessary in a large number of cases. The microdilution method however can tolerate a wide range of microorganisms for analysis and is standardized by the CLSI for both anaerobic and aerobic bacteria.¹¹⁸

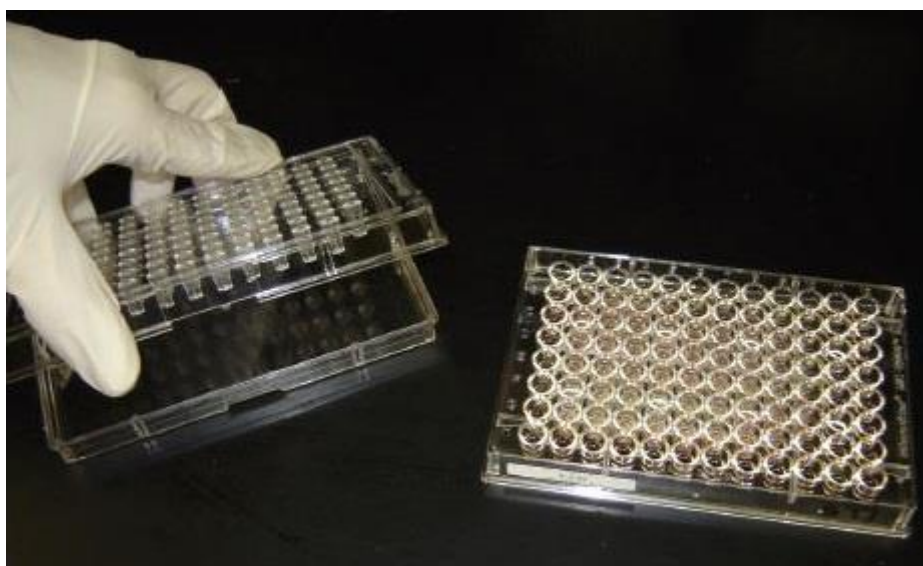


Figure 13. A broth microdilution susceptibility panel containing 96 reagent wells and a disposable tray inoculator, taken from Jorgensen *et al.*¹¹⁷

1.2.6.2 Agar Disk Diffusion method – an AST diffusion method

The agar disk diffusion technique, developed in 1940,¹²⁰ is used in many clinical microbiology laboratories for regular antimicrobial susceptibility testing.¹¹⁹ Using a cotton swab,¹¹⁸ a standardized inoculum of the test microorganism of approximately $1-2 \times 10^8$ CFU/mL is applied to a large (150 mm diameter) Petri dish containing a suitable agar medium,¹¹⁷ usually Mueller-Hinton, though researchers have also used Trypton soy agar or Nutrient agar.¹¹⁶ Up to twelve paper disks are then placed onto the agar surface,¹¹⁷ usually 6 mm sterilized filter paper disks (Whatmann No. 1),¹²⁰ saturated with the test compound at a desired concentration.¹¹⁹ There has been some variation reported as to whether the disks are saturated with the antimicrobial substance before or after being placed on the inoculated agar plate.¹¹⁶ Plates are then incubated under suitable conditions, for example at 37 °C for 24 hours in the case of bacteria and 48 hours at 25 °C for fungi.¹²⁰ If the concentration of the antimicrobial agent is sufficient, it diffuses into the agar and inhibits the growth of the test microorganism.^{118, 119} This results in a zone of inhibition around the paper disk which is measured to the nearest millimetre.^{117, 120} The zone diameters of each drug are analyzed using the criteria issued by the CLSI or the FDA in cases where FDA-approved product inserts are used for the paper disks.¹¹⁷ Typically, the zone of inhibition is measured from the circumference of the paper disk to the circumference of the inhibition zone.¹¹⁶ Alternatively, it can be recorded as the difference in diameter between the paper disk and the inhibition zone around the disk.¹¹⁶

The agar disk diffusion method provides qualitative results, in that a category of susceptibility (i.e. susceptible, intermediate, or resistant) is assigned to the test microorganism on the basis of the size of the zone of inhibition recorded.¹¹⁷⁻¹¹⁹ This

method offers distinct advantages over other methods such as its simplicity,¹¹⁷⁻¹¹⁹ the ability to test large numbers of microorganisms and antimicrobial agents.¹¹⁹ Furthermore, it does not require any specialist equipment,^{117, 118} and the qualitative nature of the results it provides can be easily interpreted by all clinicians.^{117, 119} Additionally, this AST method has the lowest associated cost,^{117, 118} at approximately \$2.50-\$5 for materials per test.¹¹⁷ These factors have contributed to its widespread use in the antimicrobial screening of plant extracts, essential oils, and other drugs.¹¹⁹

However, there are a number of disadvantages associated with the use of this susceptibility test method. For one, although the inhibitory ability of antimicrobial agents can be visualised, since the microbial growth inhibition does not necessarily correlate to cell death, this method cannot distinguish between bactericidal and bacteriostatic effects.^{116, 119} Since this test is dependent on appropriate diffusion, the molecular weight of the microbial agent being examined is a crucial factor to be considered when applying this method.¹¹⁸ In light of this, the agar disk diffusion method can only be used to ascertain the antimicrobial susceptibility of pure substances because, if it was applied to a mixture of different constituents that exhibit different diffusion rates, the results exhibited may be unreliable.¹¹⁶ Furthermore, any unevenness or any other imperfections of the agar plate can affect diffusion and therefore lead to false results.¹¹⁸ The lack of mechanisation or automation of the test also poses a disadvantage.¹¹⁷ The agar disk diffusion test is generally considered not applicable in the determination of MIC values as it is impossible to quantify the amount of antimicrobial agent that has diffused into the agar medium,¹¹⁹ nor is the amount of antimicrobial agent that adheres to the disk quantitatively determined.¹¹⁶ Thus, the nature of the results this test provides mean it can facilitate the identification of lead compounds but it is not useful for the quantification of bioactivity.¹¹⁶

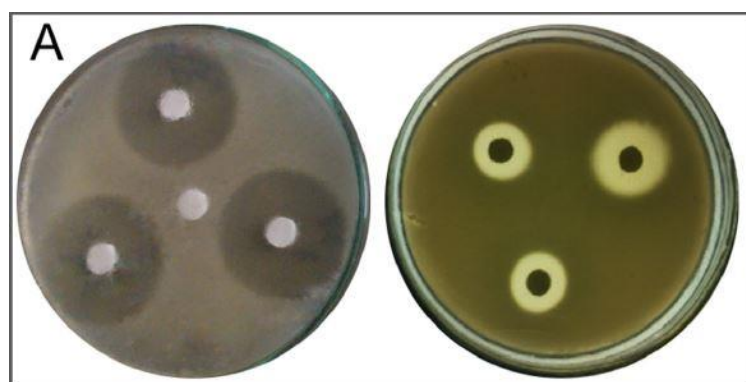


Figure 14. Agar disk-diffusion method of microbial extract using *C. albicans* as test microorganism, taken from Balouiri *et al.*¹¹⁹

1.2.6.3 Biological evaluation of cinnamaldehydes by microdilution

Once the family of cinnamaldehydes were synthesized, they were assessed for their *in vitro* antibacterial activity in collaboration with Professor Kevin Kavanagh using a

standard broth microdilution method, following CLSI guidelines.¹²¹ This method was chosen, taking into consideration all the information presented above. We had access to the equipment required for both (Petri dishes and 96-well plates/ a suitable plate reader). However, the microdilution method allowed for a larger sample set to be considered, where seven replicates of a single sample are run in one plate as opposed to just a single data set which would be run using the disk diffusion method. Thus, on duplication of the experiment, a total of eighteen sample sets can be considered, which is a better representative of antimicrobial activity. In addition, the quantitative nature of the result obtained from the use of the microdilution method, relative to a qualitative result, was appealing to us for the purposes of our comparative antibacterial assessment study.

Ampicillin trihydrate, tetracycline, and streptomycin sulfate were selected as the reference agents in this test. The bacterial strains tested were *Staphylococcus aureus* (*S. aureus*) (a clinical isolate from a urinary tract infection, St. James Hospital, Dublin) and *Escherichia coli* (*E. coli*) (a clinical isolate from a gastro-intestinal tract infection, St. James Hospital, Dublin). These bacteria were chosen as representatives of Gram-positive and -negative bacteria, respectively. The fifteen cinnamaldehydes examined in this respect were so chosen in order to explore the potential effect that electrophilicity has on antibacterial activity. As highlighted previously in the introduction, section 1.1.7, compound **1** possesses antibacterial properties across an array of Gram-negative and Gram-positive bacteria, including *E. coli*,^{6, 10, 12, 34, 63} and *Staphylococcus* spp.,^{12, 17, 34, 63}, respectively. In light of this, we wondered whether we could use **1** as a leading hit compound for antibacterial activity assessment and, by changing the substituent on the phenyl ring or replacing the phenyl ring with another carbocycle or heterocycle, assess whether changing the electrophilicity has an effect on antibacterial activity observed.

1.2.7 Comparison of electrophilicity of cinnamaldehydes

To this effect, our collaborator Dr Tobias Krämer assessed *trans*-cinnamaldehyde, compound **1**, and our derivatives in terms of global electrophilicity indices. The global electrophilicity index ω , introduced by Parr *et al.*¹²², is generally expressed in the form $\omega = \mu^2/2\eta$, where μ is the chemical potential and η the chemical hardness of the system. The μ and η terms can be related to the ionization potentials (IP) and electron affinities (EA) of the molecule, or alternatively to the energies of the Lowest Unoccupied Molecular Orbital (ϵ_{LUMO}) and Highest Occupied Molecular Orbital (ϵ_{HOMO}). Therefore, ω provides a measure for the ability of a molecule to accept electrons from its environment. By evaluating **1** and its derivatives in terms of the frontier orbital energies, and also the IPs/EAs at the ground state of the molecules using the B3LYP/6-31G(d,p) level of theory, qualitatively similar results were obtained with either approach, as presented in Figure 15.

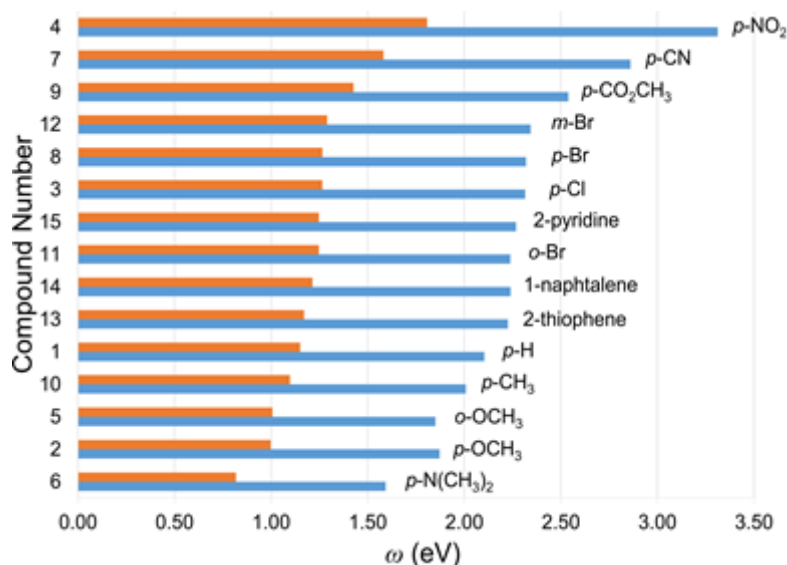


Figure 15. Global electrophilicities of various cinnamaldehyde derivatives computed by IP/EA method (orange bars) or by frontier orbital method (blue bars), taken from our publication.⁹⁸

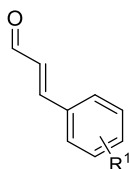
The ranking of the molecules according to their electrophilicity (top to bottom) can be rationalized in terms of substituent effects induced by electron-withdrawing and electron-donating substituents which result in electrophilic activation or deactivation of the C=C double bond, respectively. Using **1** as a reference, the introduction of electron-donating groups such as (–OCH₃, –CH₃, –N(CH₃)₂) into the *para*- or *ortho*-position of the phenyl ring causes ω , and therefore the electrophilicity, to decrease. In contrast, halide or electron-withdrawing residues attached to the phenyl ring cause moderate (–Br, –Cl) or large (–NO₂, –CN, –CO₂CH₃) electrophilic activation, as seen from the increase in ω in Figure 15. For the series of halide derivatives the exact location of the –Br substituent at either the *o*-, *p*- or *m*-position of the phenyl ring only has a very small influence on the degree of activation, and these compounds share very similar ω values. Replacement of the phenyl ring in **1** by carbocyclic or heterocyclic substituents leads to relatively moderate electrophilic activation in all cases.

1.2.7.1 Assessment of antibacterial activity of cinnamaldehydes in relation to electrophilicity

The antibacterial results have been separated into three tables. Table 2: *para*-substituted *trans*-cinnamaldehydes; Table 3: where the importance of substituent position on the phenyl ring is explored; Table 4: where the replacement of the phenyl ring with another hetero- or carbocycle is explored. In Table 2, we ordered the cinnamaldehydes based on their MIC₅₀ values against *S. aureus* (and *E. coli*), with the *p*-Br derivative, compound **40**, having the lowest MIC₅₀ and the *p*-(NCH₃)₂ showing no inhibition. Examples of the

antimicrobial graphs from which this data has been extracted can be found in Appendix 1, Figures A59-A64.

Table 2. MIC₅₀ (mM) against *S. aureus* and *E. coli* and calculated global electrophilicities.



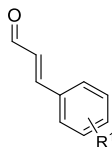
Compound number	R ¹	<i>S. aureus</i> MIC ₅₀ (mM)	<i>E. coli</i> MIC ₅₀ (mM)	ω (eV) ^a	ω (eV) ^b
40	<i>p</i> -Br	0.51	0.511	2.32	1.27
38	<i>p</i> -CN	0.94	0.97	2.86	1.58
39	<i>p</i> -CO ₂ CH ₃	1.75	2.05	2.54	1.43
13	<i>p</i> -Cl	1.83	3.16	2.32	1.26
44	<i>p</i> -NO ₂	1.84	1.18	3.31	1.81
1	<i>p</i> -H	2.32	1.93	2.10	1.15
41	<i>p</i> -CH ₃	3.14	3.31	2.01	1.10
14	<i>p</i> -OCH ₃	8.57	4.86	1.87	1.00
45	<i>p</i> -N(CH ₃) ₂	No inhibition observed	No inhibition above 12%	1.59	0.82

Commercial antibiotics ampicillin trihydrate, tetracycline and streptomycin sulfate were used as controls (see Appendix 1, Figures A71-A73 for example graphs). ^a Global Electrophilicity Index calculated via ϵ_{HOMO} and ϵ_{LUMO} . ^b Global Electrophilicity Index calculated via IP and EA.

Although the activity levels are modest, with the most active derivative giving an MIC₅₀ of ~0.5 mM, a relationship can be observed in Table 2 with respect to *S. aureus*, where all *trans*-cinnamaldehydes that are more electrophilic than compound **1** itself, are also more biologically active. For example, *p*-bromocinnamaldehyde, **40**, is nearly five times more active than **1**, with the less electrophilic *p*-methoxycinnamaldehyde, **14**, almost 17 times less active than **1**, and *p*-dimethylaminocinnamaldehyde, **45**, showed no antibacterial activity. However, the most electrophilic derivatives *p*-nitro and *p*-cyanocinnamaldehyde **44** and **38**, while more active than **1** were not the most active derivatives tested. This could be due to differences in their cellular uptake or other cellular processes. A similar overall effect can be seen in *E. coli*, where **40** again proved to be the most active derivative, although here both *p*-Cl, **13**, and *p*-CO₂CH₃, **39**, are less active than **1** even though they are more electrophilic. Potentially the difference in activity for the **13** versus the **40** could be as a result of discrepancies in cellular uptake. *E. coli* is Gram-negative, where the bacterial cell wall is more complex than that of *S. aureus*, and consists of a thin layer of peptidoglycan that is surrounded by an outer membrane.¹⁰ *S.*

aureus is a Gram-positive bacteria where the cell wall consists largely of peptidoglycan and more easily facilitates the access of hydrophobic molecules to both the cell wall and the cytoplasm within.¹⁰ Thus, variation in antimicrobial activity could be expected when comparing *S. aureus* and *E. coli* and such variation may be related to a compounds ability to pass through the outer membrane in order to exert their effect.

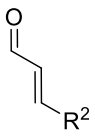
Table 3. MIC₅₀ (mM) against *S. aureus* and *E.coli*, and calculated global electrophilicities



Compound number	R ¹	<i>S. aureus</i> MIC ₅₀ (mM)	<i>E. coli</i> MIC ₅₀ (mM)	ω (eV) ^a	ω (eV) ^b
40	<i>p</i> -Br	0.51	0.511	2.32	1.27
34	<i>m</i> -Br	0.57	1.51	2.34	1.29
5	<i>o</i> -Br	6.59	5.64	2.24	1.25
14	<i>p</i> -OCH ₃	8.57	4.86	1.87	1.00
2	<i>o</i> -OCH ₃	9.63	7.26	1.85	1.01

^a Global Electrophilicity Index calculated via ϵ_{HOMO} and ϵ_{LUMO} .^b Global Electrophilicity Index calculated via IP and EA.

Table 3 examines the position of the substituent on the phenyl ring, and again is ordered based on the cinnamaldehydes MIC₅₀ against *S. aureus*. While *p*-bromocinnamaldehyde, **40**, and *o*-bromocinnamaldehyde, **5**, have very similar electronic properties, the bacterial inhibition observed varied greatly, with **5** proving to be 10 times less active than the *para* derivative. Although a limited number of *ortho* and *meta* substituted derivatives were studied, this result could suggest that sterics may also play an important role. The associated steric bulk of the bromo substituent at the *ortho*-position could be expected to block the electrophilic β -carbon site, preventing nucleophilic attack and thus hindering the reactivity of the cinnamaldehyde. Thus, the observed antimicrobial activity against both *S. aureus* and *E. coli*, with respect to the bromo-substituted cinnamaldehydes, decreased from *para*- to *meta*- to *ortho*-substituted, Table 2, as steric hindrance increased. This same steric effect is observed with respect to *p*-methoxycinnamaldehyde, **14**, where the *o*-methoxycinnamaldehyde **2** was less active against both *S. aureus* and *E. coli*, Table 3.

Table 4. MIC₅₀ (mM) against *S. aureus* and *E. coli*, and calculated global electrophilicities


Compound number	R ²	<i>S. aureus</i> MIC ₅₀ (mM)	<i>E. coli</i> MIC ₅₀ (mM)	ω (eV) ^a	ω (eV) ^b
37	1-Napthalene	3.55	9.88	2.24	1.21
35	2-Pyridine	No inhibition above 49.5%	1.12	2.27	1.25
36	2-Thiophene	No inhibition above 25.1%	8.57	2.23	1.17

^a Global Electrophilicity Index calculated via ϵ_{HOMO} and ϵ_{LUMO} . ^b Global Electrophilicity Index calculated via IP and EA.

The effect of replacement of the phenyl ring with an alternative hetero- or carbocycle was also examined, where the new derivatives were shown to be much less active against *S. aureus* than those derivatives with a phenyl ring, Tables 2 and 3. Here, only the 1-naphthalene, derivative, **37**, exhibited sufficient inhibition to attain an MIC₅₀ value against *S. aureus*. With respect to activity against *E. coli*, only the 2-pyridine derivative, **35**, exhibited superior activity to compound **1**. This difference in biological activity observed on testing the same analogues against *S. aureus* and *E. coli* may, as discussed earlier, be a reflection of the differences between Gram-positive and Gram-negative bacterial cells and the structure of their cell walls.¹⁰

1.2.8 Cysteamine assay

The ability of compound **1**, to act as a Michael acceptor has been pointed to in the literature as being attributable to its antimicrobial activity, something which was discussed in the introduction to this chapter, section 1.1.6. Briefly, Mousavi *et al.*⁹⁷, for instance, notes that the presence of a structure bearing an aldehyde conjugated to a carbon double bond, affects biological processes involving electron transfers. This group suggest that by covalently bonding to nitrogen-containing structures such as DNA, via an amine group, cinnamaldehyde-type structures can prevent normal metabolic functions from being executed.⁹⁷ Specifically, Brackman *et al.*⁵⁹ have hypothesized that cinnamaldehyde and cinnamaldehyde analogues bind to LuxR residues, a type of quorum-sensing response regulator, in a Michael-type addition reaction, forming irreversible cinnamaldehyde-receptor conjugates that limit the DNA binding ability of LuxR.⁵⁹ In general, Brackman *et al.*⁵⁹ reported that compounds containing electron-withdrawing groups were found to exhibit greater activity against *Vibrio* spp.⁵⁹

On this basis, we wanted to further probe the ability of *trans*-cinnamaldehyde derivatives to act as electrophilic agents. To this effect, we utilized a cysteamine based NMR assay system to identify thiol-trapping agents, as described by Appendino and co-workers.⁶² The same group also reported using this assay system to establish **1** as a thiol-trapping agent, where **1** reacted with cysteamine at the β carbon and at the carbonyl carbon.⁶¹ This is consistent with a mechanism proposed by Friedman¹⁷ in his literature review of the antibacterial mechanisms of **1**, in which the enzyme cytochrome CYP2A6 becomes inactivated by interacting with **1** at two different sites,¹⁷ Figure 16.

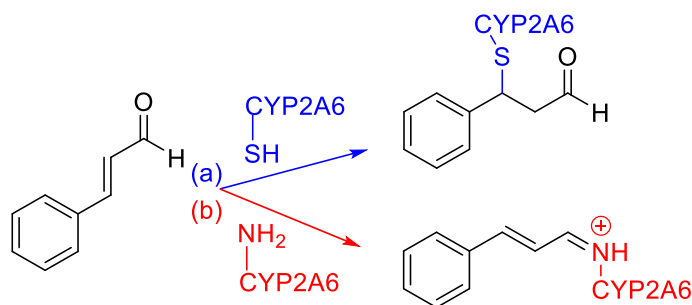


Figure 16. Possible mechanism of CYP2A6 inactivation *in vivo* by cinnamaldehyde via nucleophilic addition by (a) an SH group of a cysteine residue via the β -carbon to form a cysteine adduct, or (b) by an NH₂ group of a lysine side chain to the aldehyde group to form an aldimine (Schiff base) derivative, adapted from Friedman.¹⁷

In our hands, employment of the cysteamine assay system on **1** produced the same result to that obtained by the Appendino group,⁶¹ i.e. complete consumption of **1** in under 5 minutes at room temperature, Figure 17. Its application to *p*-bromocinnamaldehyde, **40**, and *p*-nitrocinnamaldehyde, **44**, also showed complete consumption of the respective cinnamaldehyde, Appendix 1, Figures A55-58.

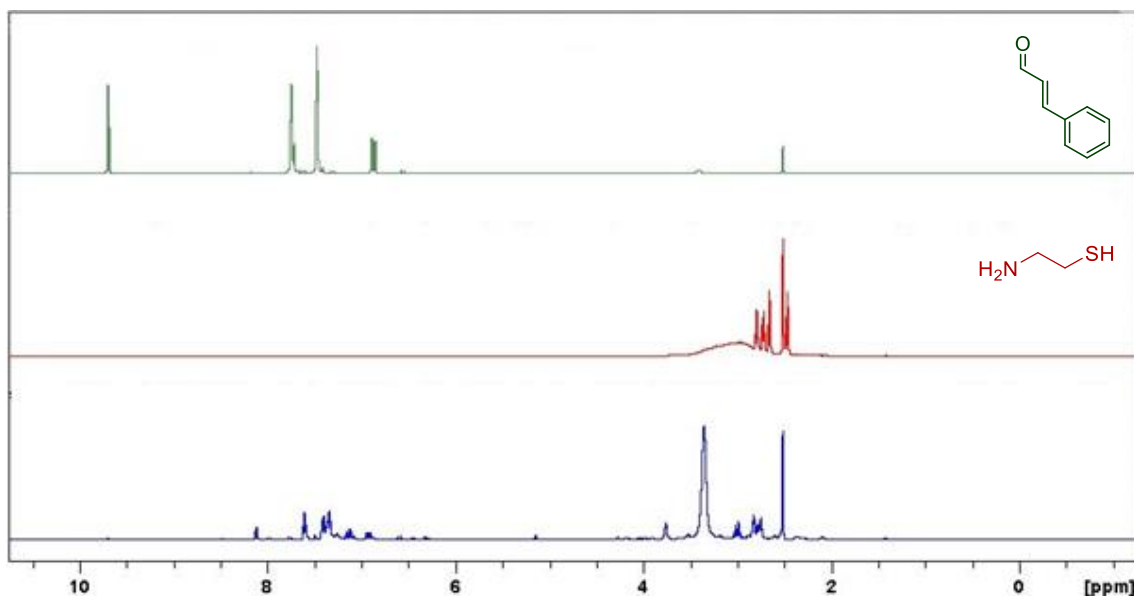


Figure 17. ^1H NMR of (a) *trans*-cinnamaldehyde **1** dissolved in DMSO-d_6 (green), (b) cysteamine dissolved in DMSO-d_6 (red), and (c) the reaction between cysteamine and **1** at room temperature (after ~ 5 minutes) in DMSO-d_6 (blue), where there is no evidence of **1** or cysteamine remaining.

Appendino *et al.*⁶¹ were effectively able to separate out the products that occurred as a result of the reaction between **1** and cysteamine, and confirmed in their study that **1** acts as a multidentate electrophile (i.e. can react at the carbonyl-, alpha- or beta-carbon, Figure 18).

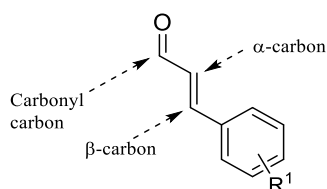


Figure 18. Potential electrophilic sites of cinnamaldehyde derivatives.

The reaction of **1** at more than one site is inferred by comparison of the NMR data we obtained to that of the products obtained by Appendino *et al.*⁶¹. For example, analysis of our complex mixture of products suggests traces of compounds 5a and/or b (Figure 19) from their work, which this group suggest is the result of a reaction between two molecules of cinnamaldehyde and three molecules of cysteamine.⁶¹

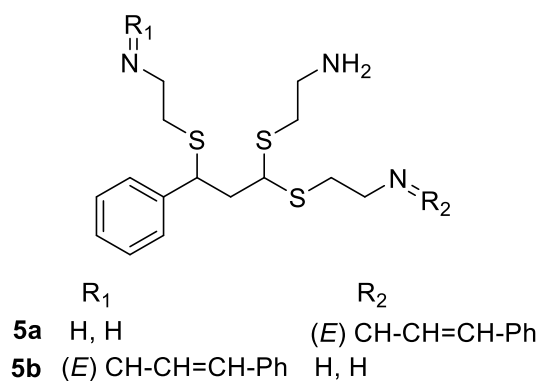


Figure 19. Compound 5a and b taken from the work of Appendino *et al.*⁶¹

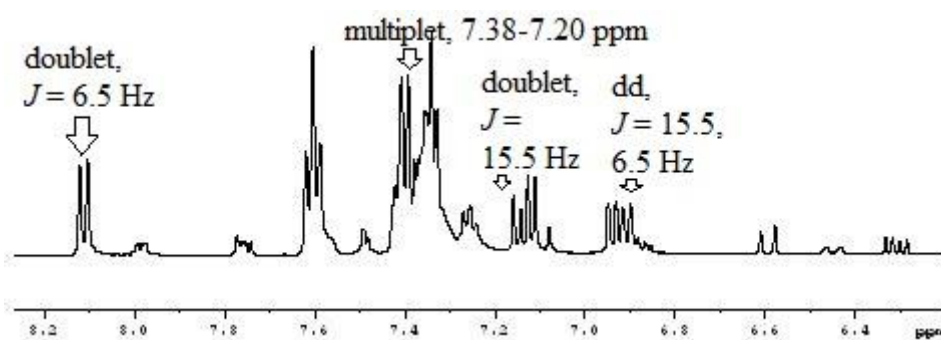


Figure 20. Zoomed in ^1H NMR spectrum of the reaction between **1** and cysteamine, showing a few of the distinct signals that suggest the presence of compound 5a/b in our mixture

Only a few of the distinct NMR signals suggested by Appendino *et al.*⁶¹ have been included here, to highlight the potential presence of compounds 5a and/or 5b in our complex mixture. The doublet signal appearing at 8.10 ppm with a J value of 6.5 Hz could be due to the proton on the first carbon of R^2 (or R^1) of compound 5a (and b, respectively), Figure 19, nearest the N atom. This would have geminal coupling to the alkene proton adjacent to it, explaining the observed coupling constant. Moving upfield, the multiplet is likely due to the overlap of aromatic proton signals, as there are two phenyl rings present in compound 5a and another two in compound 5b, Figure 19. The doublet signal appearing at 7.15 ppm with a J value of 15.5 Hz could be due to the alkene proton adjacent to the phenyl ring in R^2 (or R^1) of compound 5a (and b, respectively). Finally, the doublet of doublets signal at 6.86 ppm with J values of 6.5 and 15.5 Hz could be due to the alkene proton of R^2 (or R^1) of compound 5a (and b, respectively), which shows geminal coupling to one proton within three bonds and *trans* coupling to the other proton within three bonds. However, there was a lot of overlap of signals that appeared between 2 and 4.5 ppm and so, we cannot say with 100% certainty that this product was formed. Furthermore, we did not separate this complex mixture of products and isolate individual components so we cannot definitively determine the products formed as a result of this

reaction. All we can conclusively point to was the consumption of **1** and cysteamine under these conditions.

Thus, while we cannot verify that it is the Michael acceptor ability of *trans*-cinnamaldehyde derivatives alone that relates to their antibacterial properties, our studies suggest that a relationship could be observed between electrophilicity and bacteriostatic activity, where *trans*-cinnamaldehydes that are more electrophilic than **1** tend to be more biologically active, particularly with respect to *S. aureus* activity. The positive results obtained from the implementation of the cysteamine assay, along with the relationship between electrophilicity and antibacterial activity, we believe offers some further insight into a possible antimicrobial mechanism of action for *trans*-cinnamaldehydes at a molecular level, where cinnamaldehydes could act as electrophilic species.

1.2.9 *Galleria mellonella* in vivo toxicity study

An *in vivo* toxicity study was carried out using the larvae of the Greater wax moth, *Galleria mellonella* (*G. mellonella*, Figure 21), as described by Rowan *et al.*¹²³ (see experimental procedure for details, section 1.4.5.3). Conventional *in vivo* assays, which have incorporated a range of mammalian species, have been valuable in elucidating the immune mechanism(s) involved in the host's response to pathogens, but they are expensive, time consuming and involve extensive monitoring of the infected animals.¹²³ The larvae of *G. mellonella* presents an alternative, non-mammalian system that provides comparable preliminary data without the need to use mammals for *in vivo* testing.¹²³ They have been used as an *in vivo* model in a number of studies to investigate the virulence of human pathogens¹²⁴⁻¹²⁶ due to similarities between the innate immune system of insects and mammals.^{127, 128} *G. mellonella* are a useful infection model, offering numerous advantages including their low associated rearing costs,¹²⁶ practical injection feasibility,¹²⁶ (in which pathogens are injected directly into the hemocoel (a body cavity that functions as part of the circulatory system of *G. mellonella*) and therefore the larvae receive a known amount of pathogen,¹²⁵) and their status as an ethically acceptable animal model.¹²⁶ The results obtained using these larvae also consistently correlate with those of alternative mammalian models.¹²⁴ *G. mellonella* larvae have also been used in studies that evaluated the therapeutic effect of current and novel antimicrobial agents, as well as the *in vivo* tolerance of novel antimicrobial agents.¹²⁹⁻¹³²

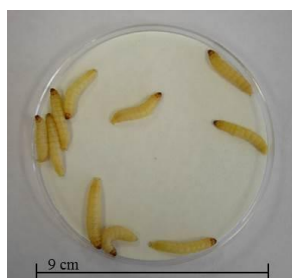


Figure 21. *G. mellonella* larvae.¹³³

Three test concentrations (1 mM, 10 mM, 25 mM) were used for each of *trans*-cinnamaldehyde, **1**, *p*-bromocinnamaldehyde, **40**, *m*-bromocinnamaldehyde, **34**, and *o*-bromocinnamaldehyde, **5**. We wanted to compare the toxicity of compounds that exhibited a range of activity to that of naturally occurring compound **1**, which, as per section 1.1.3 of the introduction, has found numerous commercial applications. This would allow us to assess if those compounds that exhibited better antibacterial activity selectively targeted the bacteria, or whether they were cytotoxic to all cells. These concentrations were chosen to represent a concentration near, above and well above their MIC₅₀ concentrations, as a fair representative of potential toxicity. After injection, the larvae were incubated at 37 °C for three days, and monitored for survival and melanisation at 24-hour intervals. High survival rates were observed in all cases, Table 5, indicating the low toxicity of **1** and the bromo derivatives, and that the enhanced activity of **40** relative to **1**, the most active derivatives of all those investigated, is not due to a toxic effect. This can be determined on the basis that as many larvae survived post-injection of the **40** as did those post-injection of **1**. As mentioned previously, **1** is Generally Recognized as Safe (GRAS) by the United States Food and Drug Administration (FDA) and Flavour and Extract Manufacturer’s Association (FEMA), and has been granted A status (i.e. may be used in foodstuffs) by the Council of Europe.¹⁷ This toxicity evaluation was run in triplicate.

Table 5. Summary of the survival of *G. mellonella* larvae (expressed as %) post injection at 24, 48, and 72 hours

Compound number	Compound name	Dosage concentration (mM)	<i>G. mellonella</i> survival (%)		
			24 h	48 h	72 h
1	<i>Trans</i> -cinnamaldehyde	25	100	88	88
		10	100	100	96
		1	100	100	100
5	<i>o</i> -Bromocinnamaldehyde	25	100	92	84
		10	100	100	100
		1	100	96	96
34	<i>m</i> -Bromocinnamaldehyde	25	100	100	100
		10	100	100	100
		1	100	100	100

40	<i>p</i> -Bromocinnamaldehyde	25	100	96	88
		10	100	100	100
		1	100	100	96

An n = 3 was employed

1.2.10 Preliminary mechanism of action study

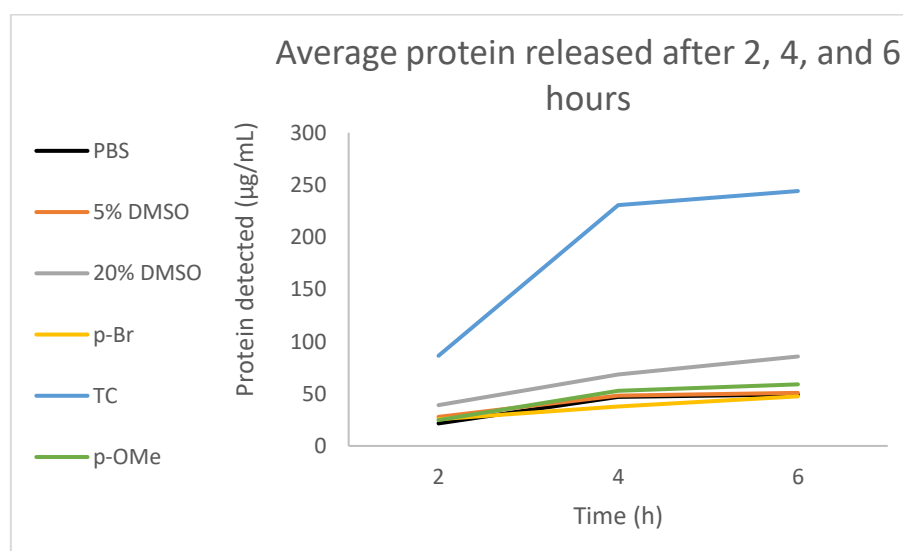
As mentioned previously in the introduction, section 1.1.7.2, multiple mechanisms of action have been reported for *trans*-cinnamaldehyde, **1**, in the literature, including binding to FtsZ (filamentation temperature sensitive protein Z),¹³⁴ lowering the uptake or use of glucose,¹³⁵ and altering bacterial cell membrane integrity and permeability.¹³⁶ We found this latter mechanism interesting and wanted to see how this translated to other derivatives included in our study, given that it has been shown to apply to **1**.¹³⁶ In their recent review on essential oils as antimicrobials in foods, Rao *et al.*¹³⁷ discussed how the disruption of the cell membrane permeability inactivates the bacteria by facilitating the infiltration of ions and organic molecules from outside the cell. This eventually leads to the loss of membrane integrity, which is critical for microbial survival.¹³⁷ Additionally, when the cell membrane is disrupted some of the intracellular constituents are released, and the monitoring of this release can serve as a means of evaluating the effectiveness of antimicrobial agents, as well as giving valuable insight into its mechanism of action.^{137, 138}

The release of cell constituents can be experimentally monitored in various ways. One such method is to monitor the release of microbial cell constituents by measuring the UV-absorbance of cell cultures at 260 nm, which is the wavelength at which materials such as proteins and nucleic acids get absorbed.^{139, 140} Proteins and nucleic acids are present throughout the membrane and cytoplasm of the bacterial cells. Proteins facilitate key structural functions, while nucleic acids carry unique genetic information, and both are involved in critical processes such as translation, transcription, and DNA replication.¹³⁸ This approach has been used by Oussalah *et al.*¹⁴¹ to measure the release of cell constituents from *Escherichia coli* (*E. coli*) O157:H7 as well as *Listeria monocytogenes* after treatment with Chinese cinnamon, the major component of which is cinnamaldehyde. A significant release of cell constituents was recorded across all concentrations of Chinese cinnamon administered, the highest being observed at 0.1% v/v at which the OD_{260nm} recorded increased by approximately 4-fold for both bacteria, relative to the control. The release of cellular constituents was also observed to increase with increasing concentration of Chinese cinnamon essential oil.¹⁴¹

Shen *et al.*¹⁴² studied the mechanism of action of cinnamaldehyde on *S. aureus* and *E. coli* by measuring the UV-absorbance of cell cultures at 260 nm and similarly observed the significant release of 260 nm absorbing materials from both strains. This occurred quickly after they were exposed to cinnamaldehyde and reached a plateau after 2 and 4 hours, respectively. The absorption values, at 4 hours, for the *E. coli* treated with

0.31 mg/mL cinnamaldehyde was 3.55, which is considerably higher than the control of approximately 0.1 at the same timepoint. The absorption value at 2 hours for the *S. aureus* treated with 0.31 mg/mL cinnamaldehyde was 3.00, which was also considerably higher than the control of approximately 0.25 at the same timepoint.¹⁴² Kwon *et al.*¹³ also measured the UV-absorbance of cell cultures at 260 nm. This group noted the significant leakage of proteins by *S. aureus*, but not *B. cereus*, over a 120-minute incubation period after exposure to cinnamaldehyde and used the Bradford method to investigate this.¹³ The principle of this method is that the binding of protein molecules to Coomassie dye under acidic conditions results in a colour change from brown to blue,¹⁴³ and hence, can be used to assess the occurrence of protein leakage. Protein leakage was recorded as 9 $\mu\text{g/mL}$ after exposure to 0.4 mL/L cinnamaldehyde after 120 min of incubation.¹³ This was approximately 3 $\mu\text{g/mL}$ higher than the control. In addition, the protein leakage from *S. aureus* was observed to increase gradually during the 120 minute incubation period.¹³

On the basis that **1** has an established ability to permeabilize bacterial cell membranes and there have been previous studies involving both *S. aureus* and *E. coli*, the two bacteria we were investigating, we wanted to explore this mechanism of action further to include our *p*-bromocinnamaldehyde, **40**, (most active derivative) and *p*-methoxycinnamaldehyde, **14**, (one of the least active derivatives) derivatives. The effect of the derivatives on the cell wall/membrane after being added to a *S. aureus* or *E. coli* culture, was monitored after 2-, 4- and 6-hours incubation, with results expressed in terms of protein and amino acid leakage, Figures 22 and 23.



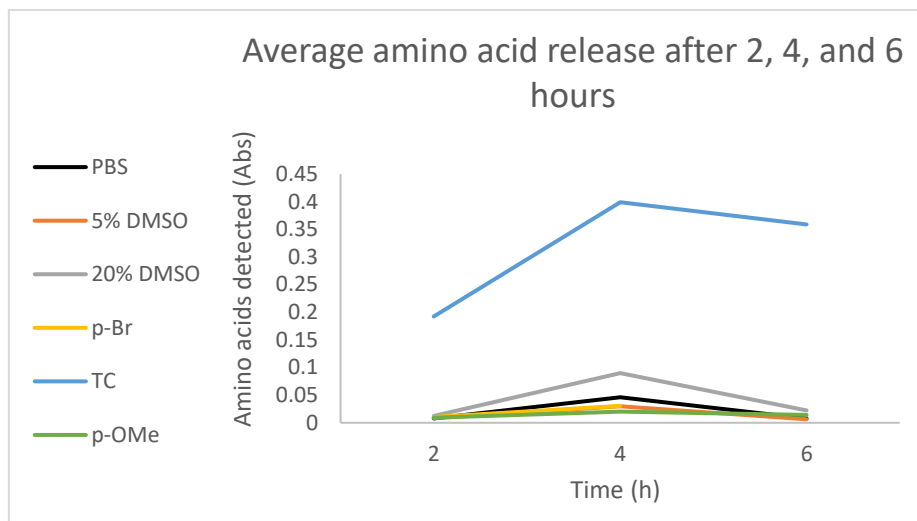
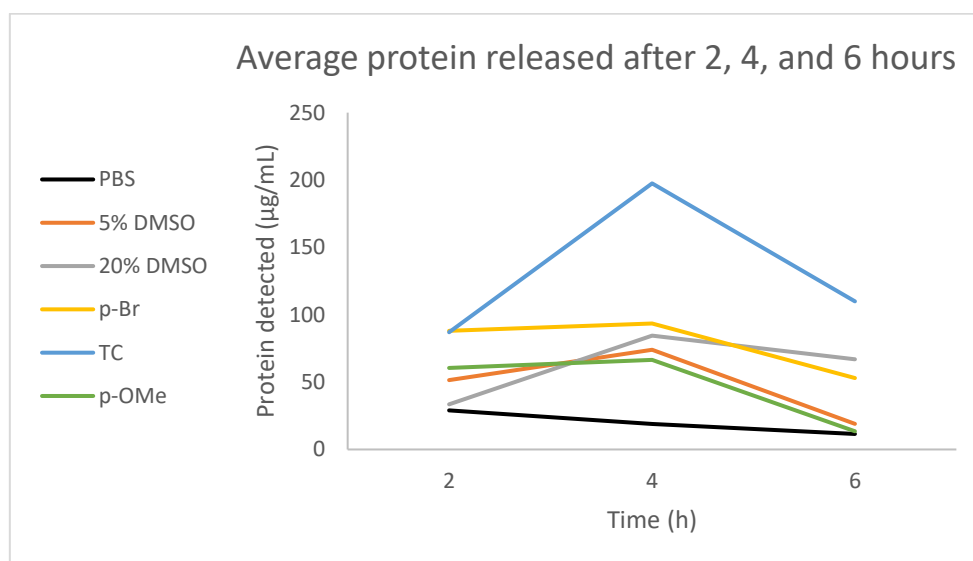


Figure 22(a) and (b). (a) Protein leakage in *S. aureus* as observed over a six-hour incubation period and (b) Amino acid leakage in *S. aureus* as observed over a six-hour incubation period. PBS: phosphate buffered saline, vehicle control: 5% DMSO, positive control: 20% DMSO, *p*-Br: *para*-bromocinnamaldehyde compound **40**, TC: *trans*-cinnamaldehyde compound **1**, *p*-OMe: *para*-methoxycinnamaldehyde compound **14**.



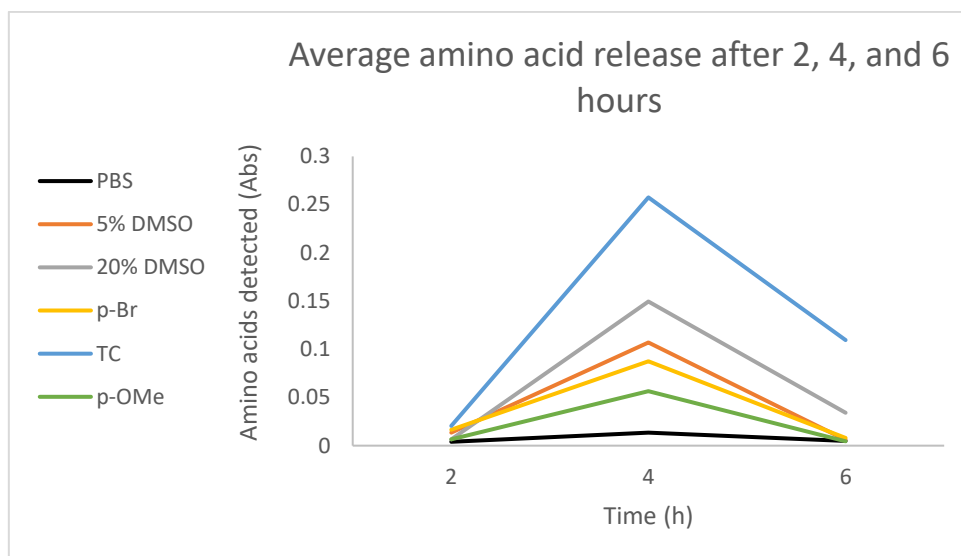


Figure 23(a) and (b). (a) Protein leakage in *E. coli* as observed over a six-hour incubation period and (b) Amino acid leakage in *E. coli* as observed over a six-hour incubation period. PBS: phosphate buffered saline, vehicle control: 5% DMSO, positive control: 20% DMSO, *p*-Br: *para*-bromocinnamaldehyde compound **40**, TC: *trans*-cinnamaldehyde compound **1**, *p*-OMe: *para*-methoxycinnamaldehyde compound **14**.

Much higher leakage was observed in terms of both proteins and amino acids for the Gram-negative *E. coli* compared to the Gram-positive *S. aureus*, something which has been noted previously in the literature.¹⁴⁴ This leaked material may consist of constituents of the membrane itself or cell wall-related material, since the cell wall of Gram-negative bacteria is thin. Proteomic analysis would be required to identify the leaked material and determine the extent to which the bacteria cell is disrupted. The amount of leakage observed was very different across the three cinnamaldehydes examined. For both bacteria, **1** caused the highest leakage of amino acids and proteins. The ability of **1** to cause leakage was expected, given the previous studies documenting this, as above. However, we found it interesting that while **40** exhibited the greatest inhibition of all fifteen cinnamaldehydes evaluated, it did not correlate to an ability to induce leakage, generating less leakage than **1**. This is particularly evident with respect to protein leakage by *E. coli*, where **40** produced less leakage than **1**, but is fast-acting, inducing relatively high leakage by the first two-hour time point, Figure 23. This may indicate that while this compound is capable of interacting with the cell wall of both bacteria it is not the primary mechanism of action. These observations coincide with previous reports regarding the multiple possible modes of action of **1**.^{10, 18, 142}

1.3 Pyrazolopyrimidinones Results and Discussion

As part of the groups research into novel antimicrobial agents, we conducted a preliminary antibacterial screen of four compounds that represented four different structural families available in our group, Figure 24.

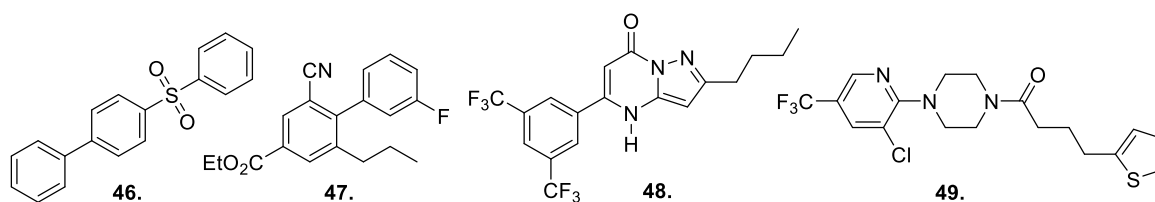


Figure 24. Compounds used in preliminary antibacterial screen. Compound **46**, 4-phenylsulfonyl-1,1'-biphenyl, a representative phenylsulfonyl biphenyl, compound **47**, ethyl 2-cyano-3'-fluoro-6-propyl-[1,1'-biphenyl]-4-carboxylate, a representative cyano-substituted biphenyl, compound **48**, 2-butyl-5-(3,5-bis(trifluoromethyl)phenyl)pyrazolo[1,5-*a*]pyrimidin-7(*4H*)-one, a representative pyrazolopyrimidinone, compound **49**, 1-(4-(2-chloro-4-(trifluoromethyl)pyridin-2-yl)piperazin-1-yl)-4-(thiophen-2-yl)butan-1-one, a representative aryl piperazine.

This preliminary screen indicated that compound **48** (Figure 24) was the most active with an MIC₅₀ of 3.54 μg against *S. aureus*. Compounds **46**, **47**, and **49** (Figure 24) did not demonstrate any bacteriostatic activity, see Figures A65-A68 in Appendix 1 for the corresponding data. As compound **48** showed the most promising level of antibacterial activity, it became our initial hit compound and the focus of our antimicrobial study.

Compound **48** is a pyrazolo[1,5-*a*]pyrimidin-7-one and, as mentioned previously in section 1.1.12 of the introduction, a large family of pyrazolo[1,5-*a*]pyrimidin-7-one compounds (Figure 25 (a)) have previously been synthesized by our group.⁹¹ These pyrazolopyrimidinones, until this project, had not been evaluated for antimicrobial activity. However, there have been reports of structurally similar pyrazolo[1,5-*a*]pyrimidine,⁹³⁻⁹⁵ (Figure 25 (b)) and pyrazolo[3,4-*d*]pyrimidines (Figure 25 (c)),¹⁴⁵ which have been shown to possess potent antifungal properties against *Fusarium oxysporum*,⁹³ *Aspergillus niger*,^{95,145} *Candida albicans*,⁹⁵ and *Aspergillus fumigatus*.^{93, 95} In addition, these compounds have shown antibacterial activity against Gram-positive *S. aureus* and *B. subtilis*,^{94, 95} and Gram-negative *E. coli*,^{94, 95, 145} *Salmonella typhi*,⁹⁵ and *Pseudomonas aeruginosa* (*P. aeruginosa*).⁹⁴ Therefore, it was unsurprising to us that, in our preliminary screen of the compounds shown above in Figure 24, compound **48** exhibited the best activity against *S. aureus* of the four compounds evaluated. On this basis, and as part of an initial Structure Activity Relationship (SAR) study, we evaluated a family of pyrazolo[1,5-*a*]pyrimidin-7-one compounds against *S. aureus* and *E. coli* for biological activity using the standard broth microdilution method, following CLSI guidelines,¹²¹ exactly as described above with respect to *trans*-cinnamaldehydes, using the same strains of *S. aureus* and *E. coli*, see Experimental Procedure for details. Additionally, in this case, the pyrazolo[1,5-*a*]pyrimidin-7-ones were screened for activity against *Candida albicans*, in order to assess both antibacterial and antifungal activity, given the wide range of pathogens that structurally similar compounds were active against.

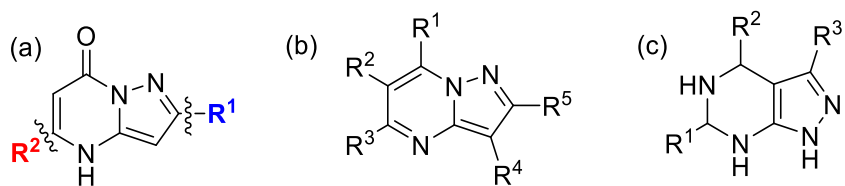


Figure 25. (a) Structure of pyrazolo[1,5-*a*]pyrimidin-7-ones that allow variation at R¹ and R²,⁹¹ (b) general structure of pyrazolo[1,5-*a*]pyrimidines,⁹³⁻⁹⁵ and (c) general structure of pyrazolo[3,4-*d*]pyrimidines.¹⁴⁵

We progressed with a SAR study (a two stage process), initially using compound **48** as a hit compound, in order to better understand what structural elements of this compound were important for its antimicrobial activity and to see if a more active molecule could be identified, Figure 26. Stage one of the SAR study involved groups 1a, 1b, and 1c and allowed variation at R¹. Here we changed R¹ to an alkyl chain (group 1a), substituted phenyl (group 1b), or heterocycle (group 1c), but kept the 3,5-bis-(trifluoromethyl)phenyl group as R². On the basis of the results generated from stage one of the SAR study, a new hit compound was identified, compound **50** (Figure 26). Stage two of the SAR study involved groups 2a and 2b. Here we allowed variation at R² but kept an isopropyl group as R¹ (as found in compound **50**). In all cases, each compound was made up to a concentration of 3 mM so that the first concentration examined in the antimicrobial evaluation was 0.75 mM with respect to each compound evaluated. It was envisaged that the final leading hit compounds identified by the two stage SAR study would also be evaluated for activity against more clinically relevant, resistant strains methicillin-resistant *Staphylococcus aureus* (MRSA, Gram-positive bacteria) and *P. aeruginosa* (Gram-negative bacteria). In addition, the same leading hit compounds would be evaluated for *in vivo* toxicity and evaluated for therapeutic effect *in vivo*, using *Galleria mellonella* larvae in both cases.

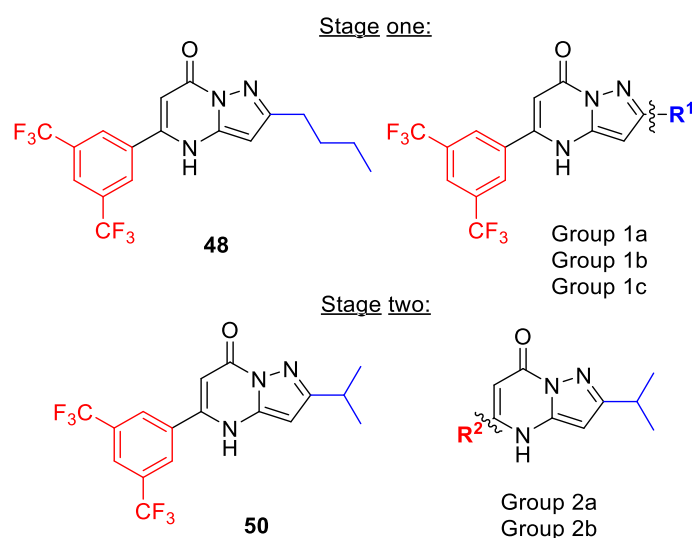


Figure 26. A two-stage SAR study approach used in the antimicrobial evaluation of pyrazolo[1,5-*a*]pyrimidin-7-ones, using compound **48**, and subsequently **50**, as a hit compound.

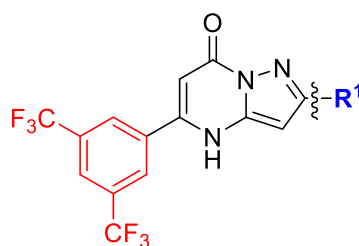
1.3.1 Antimicrobial evaluation of group 1a pyrazolo[1,5-*a*]pyrimidin-7-ones

Group 1a was established to undertake an initial examination of the nature of R¹, with a focus on the importance of the *n*-butyl chain. For example, replacement of the *n*-butyl chain with shorter linear alkyl chains, such as compounds **51**, **53**, and **55**, or branched alkyl chains, such as compounds **50**, **52**, and **54** were investigated, Table 6. The 3,5-bis-(trifluoromethyl)phenyl group was retained at R² for all compounds in group 1a and allowed us to study the effects of changing R¹ alone on observed antimicrobial activity. Against *S. aureus*, the most promising antibacterial activity was exhibited by compound **50**, in which the *n*-butyl group was replaced by an *iso*-propyl group. This was 1.5 times more active than the initial hit compound **48** in terms of its MIC₅₀ value and also exhibited superior activity in terms of MIC₈₀. Compound **50** generated an MIC₈₀ of 6.4 μM, and compares favorably with our initial hit compound **48**, which did not inhibit growth by 80% in our study. Compound **51**, with R¹ as an ethyl group, demonstrated the best activity against Gram-negative *E. coli* of all the compounds examined as part of group 1a. However, compound **51** was more active against *S. aureus* than *E. coli* (200 times more active in terms of MIC₅₀ values), but still not as active as compound **50** against *S. aureus* (compound **50** being 1.5 times more active in terms of MIC₅₀ values), Table 6(a). The fact that there is a large difference between *S. aureus* and *E. coli* activity is not completely unexpected and may be due to differences in cell uptake as a result of the structural differences between the two bacteria. *E. coli* is Gram-negative, where the bacterial cell wall is more complex than that of *S. aureus*, and consists of a thin layer of peptidoglycan that is surrounded by an outer membrane.¹⁰ *S. aureus* is a Gram-positive bacteria where the cell wall consists largely of peptidoglycan and more easily facilitates the access of hydrophobic molecules to both the cell wall and the cytoplasm within.¹⁰ Thus, variation in antimicrobial activity could be expected when comparing *S. aureus* and *E. coli* and such variation may be related to a compounds ability to pass through the outer membrane in order to exert their effect. Commercial antibiotics ampicillin trihydrate, tetracycline, and streptomycin sulfate were used as controls and also showed this difference in *E. coli* versus *S. aureus* activity. Here MIC₅₀ values of 21.8 μM, 11.03 μM, and 5.22 μM were obtained against *S. aureus*, respectively and higher MIC₅₀ values of 2.55 mM, 56.25 μM, and 6.18 μM against *E. coli*, respectively. The activity of compound **50** against *S. aureus* was a stronger and more interesting result for us, than the activity of compound **51** against *E. coli*, as the activity of compound **50** showed superior results to the commercial antibiotics investigated in our antimicrobial screen. It is noteworthy that three other compounds in group 1a demonstrated superior activity to these commercial antibiotics in terms of activity against *S. aureus*, specifically compounds **48**, **51** and **52**, with respect to MIC₅₀ values. This indicates the potential of this family of compounds in terms of activity against *S. aureus* in particular.

Notably, hit compound **48** showed the best activity against *C. albicans* with a MIC₅₀ value of 190 μM. However, this activity was 106 times less potent than the activity of this same compound against *S. aureus*. All other compounds tested as part of group 1a were much

less active than compound **48**, and hence, this indicated that the pyrazolo[1,5-a]pyrimidin-7-ones may not be very active against *C. albicans*, given that the MIC₅₀ of the commercial antifungal agent fluconazole is reported as 3.27 μM (1 μg/mL) by Clancy *et al.*¹⁴⁶ All results relevant to the antimicrobial evaluation of group 1a are included in Table 6(a) and (b).

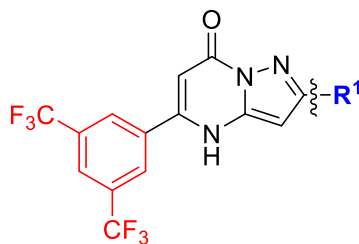
Table 6(a). Antibacterial (*S. aureus* and *E. coli*) activity of group 1a pyrazolo[1,5-a]pyrimidin-7-one analogues as MIC₅₀/ MIC₈₀ values.



Code	R ¹	<i>S. aureus</i>				<i>E. coli</i>			
		MIC ₅₀ (μM)	MIC ₅₀ (μg/ mL)	MIC ₈₀ (μM)	MIC ₈₀ (μg/ mL)	MIC ₅₀ (μM)	MIC ₅₀ (μg/ mL)	MIC ₈₀ (μM)	MIC ₈₀ (μg/ mL)
48		1.8	0.73	N/A	N/A	N/A	N/A	N/A	N/A
50		1.2	0.47	6.4	2.49	584	227.35	N/A	N/A
51	Et	1.78	0.67	10	3.75	355	133.22	N/A	N/A
52		2.2	0.89	N/A	N/A	628	253.29	N/A	N/A
53	Me	85	30.71	N/A	N/A	532	192.19	N/A	N/A
54		47	18.96	N/A	N/A	522	210.54	748	301.69
55		35	13.63	N/A	N/A	N/A	N/A	N/A	N/A

N/A denotes that the minimum inhibitory concentration recorded was lower than MIC₅₀ or MIC₈₀. With respect to the activity of compound **54** against *E. coli*, note that the concentration of DMSO was greater than 5% (v/v) at the concentration recorded as MIC₈₀.

Table 6(b). Antifungal (*C. albicans*) activity of group 1a pyrazolo[1,5-a]pyrimidin-7-one analogues as MIC₅₀/MIC₈₀ values.



		<i>C. albicans</i>			
Code	R ¹	MIC ₅₀ (μM)	MIC ₅₀ (μg/ mL)	MIC ₈₀ (μM)	MIC ₈₀ (μg/ mL)
48		190	76.63	350	141.17
50		337	131.19	N/A	N/A
51	Et	300	112.58	536	201.14
52		343	138.34	611	246.43
53	Me	343	123.91	606	218.92
54		321	129.47	635	256.11
55		N/A	N/A	N/A	N/A

N/A denotes that the minimum inhibitory concentration recorded was lower than MIC₅₀ or MIC₈₀.

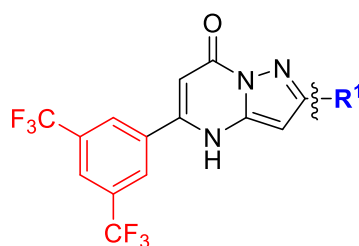
1.3.2 Antimicrobial evaluation of group 1b pyrazolo[1,5-a]pyrimidin-7-ones

Group 1b, like group 1a, was established to examine the importance of the *n*-butyl chain at R¹. This group examined the effects of replacement of the *n*-butyl chain with a substituted phenyl group on observed antimicrobial activity. As with group 1a, the 3,5-bis-(trifluoromethyl)phenyl group was retained at R², to allow us to study the effects of R¹ alone on observed antimicrobial activity. In general, group 1b were far less active against *S. aureus* than group 1a, with activity so low that it was not possible for a MIC₅₀ to be recorded for the majority of compounds in this group, compounds **61-66**, Table 7(a). Low MIC₅₀ values were recorded when R¹ was 2-chlorophenyl, compound **56**, or 4-(trifluoromethyl)phenyl, compound **57**, of 2.8 and 3.8 μM, respectively. However, activity was insufficient for a MIC₈₀ value to be recorded in either case. This suggests that a substituted phenyl is not a good replacement for the *n*-butyl chain in terms of activity against *S. aureus*. The general activity of group 1b against *E. coli* was very poor,

with the majority again incapable of inhibiting bacterial growth by 50%, compounds **57-65**, Table 7(a). The only two compounds that did inhibit *E. coli* growth showed moderate activity, with MIC₅₀ values of 390 and 424 μM when R¹ was 2-chlorophenyl (compound **56**) or 4-methoxyphenyl (compound **66**), respectively. Given that compounds **56**, **58**, and **64** all have a chloro-substituent that only differs in its position on the phenyl ring, and yet these three compounds all exhibit very different bacteriostatic activities. This may suggest that it is not just the nature of the substituent on the phenyl ring that is important for activity, but also its position on the phenyl ring. When this chloro-substituent is in the *ortho*-position, there is observed activity against both *S. aureus* and *E. coli*, but when this same position is in the *meta*-position, this analogue is nearly 104 times less active against *S. aureus* (in terms of MIC₅₀ values) and shows no activity against *E. coli*. When this chloro-substituent is in the *para*-position, no activity is observed against either bacteria. A similar observation can be made with respect to compounds **59**, **63**, and **66** regarding the methoxy-substituent on the phenyl ring, pointing us towards the hypothesis that both the position and nature of the substituent is important to exhibit bacteriostatic activity. In any case, all compounds evaluated in group 1b were less active than our current hit compound **48**.

Conversely, activity with respect to *C. albicans* improved as a result of the replacement of the *n*-butyl chain with a substituted phenyl ring, with moderate activity observed across all members of group 1b. The best activity was observed with respect to compound **56** for which a MIC₈₀ of 182 μM was recorded, over 1.9 times more potent than the most active member of group 1a, compound **48**. However, this antifungal activity is still not very potent, and so, we were less interested in pursuing the pyrazolo[1,5-*a*]pyrimidin-7-ones as anti-fungal agents. All results relevant to the antimicrobial evaluation of group 1b are included in Tables 7(a) and (b).

Table 7(a). Antibacterial (*S. aureus* and *E. coli*) activity of group 1b pyrazolo[1,5-*a*]pyrimidin-7-one analogues as MIC₅₀/MIC₈₀ values

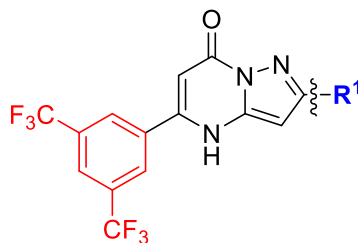


Code	R ¹	<i>S. aureus</i>				<i>E. coli</i>			
		MIC ₅₀ (μM)	MIC ₅₀ (μg/ mL)	MIC ₈₀ (μM)	MIC ₈₀ (μg/ mL)	MIC ₅₀ (μM)	MIC ₅₀ (μg/ mL)	MIC ₈₀ (μM)	MIC ₈₀ (μg/ mL)

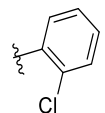
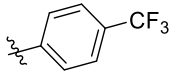
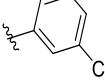
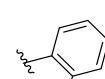
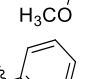
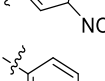
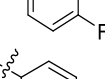
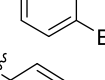
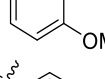
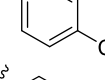
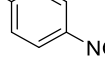
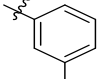
56		2.8	1.28	N/A	N/A	390	178.53	N/A	N/A
57		3.6	1.77	N/A	N/A	N/A	N/A	N/A	N/A
58		291	133.21	N/A	N/A	N/A	N/A	N/A	N/A
59		299	135.55	N/A	N/A	N/A	N/A	N/A	N/A
60		300	140.50	N/A	N/A	N/A	N/A	N/A	N/A
61		N/A	N/A	N/A	N/A	N/A	N/A	N/A	N/A
62		N/A	N/A	N/A	N/A	N/A	N/A	N/A	N/A
63		N/A	N/A	N/A	N/A	N/A	N/A	N/A	N/A
64		N/A	N/A	N/A	N/A	N/A	N/A	N/A	N/A
65		N/A	N/A	N/A	N/A	N/A	N/A	N/A	N/A
66		N/A	N/A	N/A	N/A	424	192.22	N/A	N/A

N/A denotes that the minimum inhibitory concentration recorded was lower than MIC₅₀ or MIC₈₀

Table 7(b). Antifungal (*C. albicans*) activity of group 1b pyrazolo[1,5-a]pyrimidin-7-one analogues as MIC₅₀/ MIC₈₀ values.



Code	R ¹	<i>C. albicans</i>			
		MIC ₅₀ (μM)	MIC ₅₀ (μg/ mL)	MIC ₈₀ (μM)	MIC ₈₀ (μg/ mL)

56		149	68.21	182	83.31
57		283	139.04	N/A	N/A
58		164	75.07	349	159.76
59		160	72.53	375	170.00
60		266	124.57	N/A	N/A
61		174	76.79	341	150.49
62		243	122.04	367	184.31
63		160	72.53	N/A	N/A
64		254	116.27	370	169.37
65		238	111.46	372	174.22
66		238	107.89	366	165.92
					

N/A denotes that the minimum inhibitory concentration recorded was lower than MIC₅₀ or MIC₈₀

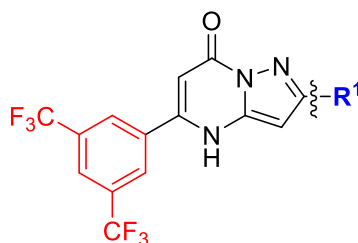
1.3.3 Antimicrobial evaluation of group 1c pyrazolo[1,5-*a*]pyrimidin-7-ones

Group 1c, like groups 1a and 1b, was established to examine the importance of the *n*-butyl chain as R¹. This group examined the effects of replacement of the *n*-butyl chain with a heterocycle on observed antimicrobial activity. As with groups 1a and 1b, the 3,5-bis-(trifluoromethyl)phenyl group was retained at R², to allow us to study the effects of R¹ alone on observed antimicrobial activity. In terms of *S. aureus*, replacement of the *n*-butyl chain with 2-furan as R¹, compound **67**, resulted in a reduction in activity by a factor of 6.7 (based on MIC₅₀ values), and with 2-thiophene as R¹, compound **68**, resulted in a further reduction by a factor of 289 (based on MIC₅₀ values). These results indicated that heterocycles are not optimal substituents at R¹ for *S. aureus* activity. In terms of *E. coli*, replacement of the *n*-butyl chain with 2-furan resulted in improved activity, in that a MIC₅₀ value was recorded for this compound. This was not possible for compound **48**. However, this compound was still less active than the most active compound against *E.*

coli (compound **51** group 1a). A MIC₅₀ against *E. coli* could not be obtained with 2-thiophene at R¹. This indicates that having a heterocycle at R¹ is also not optimal for activity against *E. coli*.

In terms of activity against *C. albicans*, compound **67** resulted in reduced activity relative to compound **48**. The MIC₅₀ recorded for compound **68** was slightly lower than that of compound **48**, but not as low as the MIC₅₀ recorded for compound **56** of group 1b. Of the compounds evaluated thus far, compound **56** has displayed the best activity against *C. albicans*. As such, there are no major advantages to having R¹ as a heterocycle for general antimicrobial activity. All results relevant to the antimicrobial evaluation of group 1c are included in Tables 8(a) and (b).

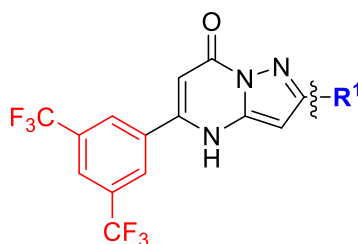
Table 8(a). Antibacterial (*S. aureus* and *E. coli*) activity of group 1c pyrazolo[1,5-a]pyrimidin-7-one analogues as MIC₅₀/MIC₈₀ values.

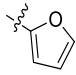
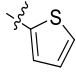


Code	R ¹	<i>S. aureus</i>				<i>E. coli</i>			
		MIC ₅₀ (μM)	MIC ₅₀ (μg/mL)	MIC ₈₀ (μM)	MIC ₈₀ (μg/mL)	MIC ₅₀ (μM)	MIC ₅₀ (μg/mL)	MIC ₈₀ (μM)	MIC ₈₀ (μg/mL)
67		12	4.96	N/A	N/A	376	155.39	N/A	N/A
68		520	223.26	N/A	N/A	N/A	N/A	N/A	N/A

N/A denotes that the minimum inhibitory concentration recorded was lower than MIC₅₀ or MIC₈₀

Table 8(b). Antifungal (*C. albicans*) activity of group 1c pyrazolo[1,5-a]pyrimidin-7-one analogues as MIC₅₀/MIC₈₀ values



Code	R ¹	<i>C. albicans</i>			
		MIC ₅₀ (μM)	MIC ₅₀ (μg/ mL)	MIC ₈₀ (μM)	MIC ₈₀ (μg/ mL)
67		320	132.25	N/A	N/A
68		184	79.00	374	160.57

N/A denotes that the minimum inhibitory concentration recorded was lower than MIC₅₀ or MIC₈₀

Given that the lowest MIC₈₀ values, and the most promising results, were recorded for compound **50** against *S. aureus*, we decided to move forward to phase two of the SAR study with compound **50** as our leading hit compound. Compound **50** (Group 1a) exhibited the best activity against *S. aureus* and was even superior to the commercial antibiotics evaluated in our study. As such, we further examined the structural elements that were important for its activity. The effect changes to R¹ had on antimicrobial activity was examined using groups 1a-c in stage one of our SAR study. For stage two, we wanted to explore structural changes at R², while keeping R¹ as an *iso*-propyl group, as found in compound **50**. To do this we established groups 2a and 2b.

1.3.4 Antimicrobial evaluation of group 2a pyrazolo[1,5-*a*]pyrimidin-7-ones

In compound **50**, like in compound **48**, R² was a 3,5-bis-(trifluoromethyl)phenyl group. Thus, our first stage two group, group 2a, was designed to allow us to explore the relationship between structure and activity by making some initial changes to R². For group 2a we wanted to explore the role of the CF₃ groups. To do this, we replaced them with smaller and less hydrophobic methyl groups (compound **72**), as well as removing them and replacing them with simple hydrogen atoms (compound **71**), Table 9.

Group 2a also includes compound **70**, where the entire 3,5-bis-(trifluoromethyl)phenyl group was replaced with the smaller and less hydrophobic methyl group, in addition to compound **69**, where the entire 3,5-bis-(trifluoromethyl)phenyl group was removed and replaced with a simple hydrogen atom, Table 9.

The antibacterial activity results for group 2a can be found in Table 9(a), where we included the results for compound **50** for ease of comparison. In terms of *S. aureus* activity, this could not be improved by any of the group 2a changes to R². Compound **71** exhibited the best activity against *S. aureus* of the four, but this was still 75 times less potent than compound **50** in terms of MIC₅₀ values. Replacing the entire 3,5-bis-(trifluoromethyl)phenyl group with either a hydrogen (compound **69**) or a methyl (compound **70**) resulted in a severe decrease in activity against *S. aureus*. The 3,5-

dimethylphenyl derivative, compound **72**, led to insufficient activity for a MIC₅₀ to be recorded. With respect to activity against *E. coli*, activity was improved by a factor of 1.57 when the 3,5-bis-(trifluoromethyl)phenyl was replaced by either a methyl (compound **70**, MIC₅₀ of 373 μM), or phenyl group (compound **71**, MIC₅₀ of 373 μM), in terms of MIC₅₀ values. However, this activity was still not as good as that recorded for compound **51** of group 1a, which had an MIC₅₀ of 355 μM (Table 6(a)).

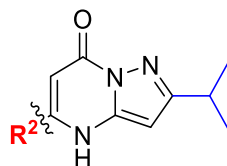
In terms of activity against *C. albicans*, changing R² to any of the four alternative substituents within this group improved activity, in that lower MIC₅₀ values were recorded for compound **69-72** relative to that recorded for compound **50**. However, compound **69** with an MIC₅₀ value of 305 μM, was over 2 times less active than compound **56** of group 1b (MIC₅₀ of 149 μM, Table 7(b)), and compound **56** was in turn nearly 46 times less potent than the commercial antifungal agent fluconazole (MIC₅₀ of 3.27 μM)¹⁴⁶. As such, the antifungal activity of the pyrazolo[1,5-a]pyrimidin-7-one family remained less interesting to us when compared to the antibacterial activity being displayed against *S. aureus*. All results relevant to the antimicrobial evaluation of group 2a are included in Tables 9(a) and (b).

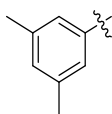
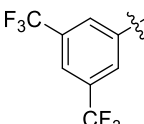
Table 9(a). Antibacterial (*S. aureus* and *E. coli*) activity of group 2a pyrazolo[1,5-a]pyrimidin-7-one analogues as MIC₅₀/ MIC₈₀ values.

Code	R ²	<i>S. aureus</i>				<i>E. coli</i>			
		MIC ₅₀ (μM)	MIC ₅₀ (μg/ mL)	MIC ₈₀ (μM)	MIC ₈₀ (μg/ mL)	MIC ₅₀ (μM)	MIC ₅₀ (μg/mL)	MIC ₈₀ (μM)	MIC ₈₀ (μg/mL)
69	H	662	117.31	N/A	N/A	626	110.93	N/A	N/A
70	Me	698	133.48	N/A	N/A	373	71.33	733	140.17
71	Ph	90	22.80	N/A	N/A	373	94.48	733	185.67
72		N/A	N/A	N/A	N/A	594	167.13	N/A	N/A
50		1.2	0.47	6.4	2.49	584	227.35	N/A	N/A

N/A denotes that the minimum inhibitory concentration recorded was lower than MIC₅₀ or MIC₈₀

Table 9(b). Antifungal (*C. albicans*) activity of group 2a pyrazolo[1,5-a]pyrimidin-7-one analogues as MIC₅₀/ MIC₈₀ values.



Code	R ²	<i>C. albicans</i>			
		MIC ₅₀ (μM)	MIC ₅₀ (μg/ mL)	MIC ₈₀ (μM)	MIC ₈₀ (μg/ mL)
69	H	305	54.05	415	73.54
70	Me	313	59.85	375	71.71
71	Ph	332	84.10	374	94.73
72		327	92.00	447	125.77
50		337	131.19	N/A	N/A

N/A denotes that the minimum inhibitory concentration recorded was lower than MIC₅₀ or MIC₈₀

1.3.5 Antimicrobial evaluation of group 2b pyrazolo[1,5-a]pyrimidin-7-ones

Again, with our primary focus remaining on exploring the activity against *S. aureus*, we decided to further explore structural changes at R² using group 2b, and again keeping R¹ as an *iso*-propyl group. Given that the results from group 2a show that activity of compound **50**, with R² as 3,5-bis-(trifluoromethyl)phenyl, was significantly greater than that of compounds **69**, **70**, **71** or **72**, we decided to investigate if alternative substituents on the phenyl ring could improve activity. To this end, in group 2b we examined a range of substituted phenyl groups at R², Tables 10(a) and (b).

The results for group 2b are shown in Table 10(a) and are ordered from most active to least active based on MIC₅₀ values against *S. aureus*. Looking at those MIC₅₀ values for activity against *S. aureus*, the most active group 2b compounds were when R² was a 3,5-dichlorophenyl, compound **73**, and a 3-trifluoromethylphenyl, compound **74**, at 2.2 and 2.3 μM respectively. However, activity was insufficient to allow an MIC₈₀ to be determined for either compound. The lowest MIC₈₀ recorded was that for compound **78**

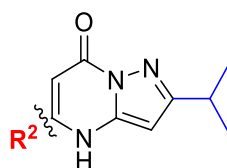
but this was 56 times higher than the MIC₈₀ of the most active pyrazolo[1,5-a]pyrimidin-7-one against *S. aureus*, compound **50**.

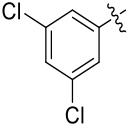
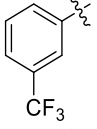
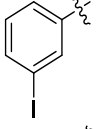
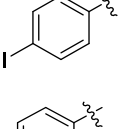
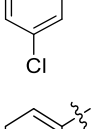
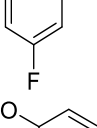
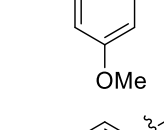
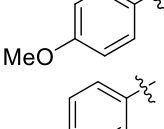
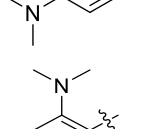
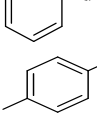
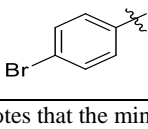

Upon further examination of group 2b activities against *S. aureus*, it appears as though electron-withdrawing groups, specifically trifluoromethyl, compound **74**, and groups with mild electronic effects (i.e. the halogens), compounds **73**, **75**, **76**, **77**, and **78**, generally resulted in better activity than electron-donating groups, compounds **70**, **80**, **81**, and **82**, Table 10(a). The exceptions to this are compounds **83** and **84**, in which the chloro- and bromo-substituent, respectively, are in the *para*-position. This could suggest that the activity of such halogenated compounds is highest when the halogens are in the *meta*-position. This is supported, for example, by the superior activity of compounds **73** and **77**.

With respect to *E. coli* activity, the two lowest MIC₈₀ values of all compounds examined in this study were recorded by compounds **78** and **79** in group 2b. These two compounds, bearing a 3,5-dimethoxyphenyl or 3-fluorophenyl, at R² respectively, are quite different in their electronic properties. However, both oxygen and fluorine are capable of forming hydrogen bonds (H-bond acceptors), with fluorine forming considerably weaker hydrogen bonds, and perhaps this has an effect on the observed antibacterial activity. Coinciding with this, compound **82**, with an *ortho*-dimethylamino group on the phenyl ring, exhibited the lowest MIC₅₀ of all the compounds tested against *E. coli*. Nitrogen is also a H-bond acceptor, but a MIC₈₀ could not be recorded for this compound. The same substituent in the *para*-position on the ring, compound **81**, was much less effective and so, perhaps like with *S. aureus* activity, we could postulate that the *ortho*- or *meta*- position might be more important for activity than the *para*- position.

Concerning activity against *C. albicans*, the most active pyrazolo[1,5-a]pyrimidin-7-ones were compounds **78** and **79**. As above, perhaps it is the hydrogen bonding ability of the oxygen and fluorine atoms that results in increased activity, but this is not conclusive. In any case, neither of these compounds, which were the most active against *C. albicans* as suggested by our SAR study, were close to the activity levels found for the commercial anti-fungal agent fluconazole.¹⁴⁶ Therefore, we shifted the focus of further studies completely to an investigation of the pyrazolo[1,5-a]pyrimidin-7-one family as antibacterial agents. All results relevant to the antimicrobial evaluation of group 2b are included in Tables 10(a) and (b).

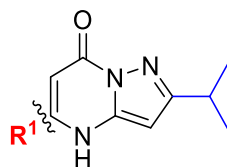
Table 10(a). Antibacterial (*S. aureus* and *E. coli*) activity of group 2b pyrazolo[1,5-a]pyrimidin-7-one analogues as MIC₅₀/ MIC₈₀ values.



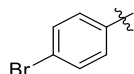
Code	R ²	<i>S. aureus</i>				<i>E. coli</i>			
		MIC ₅₀ (μM)	MIC ₅₀ (μg/ mL)	MIC ₈₀ (μM)	MIC ₈₀ (μg/ mL)	MIC ₅₀ (μM)	MIC ₅₀ (μg/ mL)	MIC ₈₀ (μM)	MIC ₈₀ (μg/ mL)
73		2.2	0.71	N/A	N/A	641	206.52	N/A	N/A
74		2.3	0.74	N/A	N/A	N/A	N/A	N/A	N/A
75		4.2	1.59	N/A	N/A	N/A	N/A	N/A	N/A
76		8.4	3.19	N/A	N/A	N/A	N/A	N/A	N/A
77		10	2.88	N/A	N/A	631	181.57	N/A	N/A
78		19	5.15	360	97.67	193	52.36	410	111.23
79		250	78.34	370	115.94	310	97.14	420	131.612
80		375	106.25	N/A	N/A	643	182.18	N/A	N/A
81		415	122.99	N/A	N/A	719	213.09	N/A	N/A
82		483	143.15	N/A	N/A	146	43.27	N/A	N/A
83		N/A	N/A	N/A	N/A	702	202.00	N/A	N/A
84		N/A	N/A	N/A	N/A	717	230.55	N/A	N/A

N/A denotes that the minimum inhibitory concentration recorded was lower than MIC₅₀ or MIC₈₀

Table 10(b). Antifungal (*C. albicans*) activity of group 2b pyrazolo[1,5-a]pyrimidin-7-one analogues as MIC₅₀/ MIC₈₀ values



Code	R ²	<i>C. albicans</i>			
		MIC ₅₀ (μM)	MIC ₅₀ (μg/ mL)	MIC ₈₀ (μM)	MIC ₈₀ (μg/ mL)
73		332	106.97	549	176.88
74		283	90.93	750	240.98
75		313	118.69	N/A	N/A
76		N/A	N/A	N/A	N/A
77		N/A	N/A	N/A	N/A
78		250	67.83	343	93.06
79		172	53.90	300	94.01
80		345	97.75	662	187.56
81		316	93.65	500	148.19
82		329	97.51	547	162.11
83		351	101.00	N/A	N/A



N/A denotes that the minimum inhibitory concentration recorded was lower than MIC₅₀ or MIC₈₀

To summarize, in our SAR study investigating pyrazolo[1,5-a]pyrimidin-7-ones, 35 members of this family were screened for activity against *S. aureus*, *E. coli* and *C. albicans*. It is noteworthy how, overall, these compounds displayed much more potent antimicrobial activity than the previously tested *trans*-cinnamaldehydes. Variation at R¹ of the pyrazolo[1,5-a]pyrimidin-7-ones, Figure 26 previously, was explored through groups 1a-c, using compound **48** as the leading hit compound. Variation at R² was explored through groups 2a and b, using compound **50** as the leading hit compound. Against *S. aureus*, four compounds demonstrated activity superior to commercial antibiotics, namely **48**, **50**, **51**, and **52**. Thus, for activity against *S. aureus*, preliminary results from our SAR study would suggest that the 3,5-bis-(trifluoromethyl)phenyl substituent as R² is important, with a relatively short alkyl chain as R¹.

Against both *E. coli* and *C. albicans*, two members of group 2b exhibited the highest activities, namely compounds **77** and **78**, suggesting in these cases that the 3,5-bis-(trifluoromethyl)phenyl substituent as R² is less important for activity, with either a 3-fluorophenyl or 3,5-dimethoxyphenyl substituent as R², with an *iso*-propyl group as R¹, giving better levels of activity. Overall, it was observed that this family of compounds were much more active against *S. aureus* than either *E. coli* or *C. albicans*, with very low micromolar MIC values demonstrated. As such, we were very interested to investigate the activity of these pyrazolo[1,5-a]pyrimidin-7-ones against more clinically-relevant MRSA. In collaboration with Professor Kavanagh, we felt that in general the antibacterial activity of these compounds was more potent than their antifungal activity and so, along with MRSA, we also tested a selection of these compounds against the more resistant Gram-negative bacteria *P. aeruginosa*.

1.3.6 Antibacterial evaluation of select pyrazolo[1,5-a]pyrimidin-7-ones against clinically-relevant MRSA and *P. aeruginosa*

MRSA and *P. aeruginosa* exemplify some of the more problematic drug-resistant pathogens encountered today in clinical settings.^{147, 148} MRSA is a major pathogen in skin and soft tissue infections and can be either hospital- or community-acquired.¹⁴⁷ However, the majority of people who acquire MRSA do so as a result of a previous (recent) hospital admission or similar healthcare setting.¹⁴⁷ The most common MRSA carriage sites are the nose, skin, throat and, possibly, the gastro-intestinal tract.¹⁴⁷ *P. aeruginosa* is a ubiquitous organism that is present in a range of environmental settings but is rarely a member of the normal microbial flora in humans.¹⁴⁸ Serious infections associated with this organism are largely hospital acquired, and patients with impaired immunity have an increased risk for

colonization.¹⁴⁸ Given that the *P. aeruginosa* and MRSA bacteria are more resistant to currently available treatments, then it could not be assumed that the mechanism of resistance that was at play by *E. coli* and *S. aureus*, respectively would be the same as that displayed by the two clinically-relevant bacteria. As such, we chose compounds that displayed good, moderate, and no activity against *E. coli* and *S. aureus* in the preliminary study, on the basis of MIC₅₀ and MIC₈₀ values, in case activity did not directly translate across the bacteria. We also chose at least one compound from each of the groups 1a-c and groups 2a,b so that we could preliminarily explore some structural effects. The majority of compounds chosen for testing against the more clinically relevant bacteria were those that displayed the highest or second highest activity out of all compounds within each group examined (taking both MIC₅₀ and MIC₈₀ values into consideration). One compound was chosen in the screen against each of the clinically-relevant bacteria that did not exhibit any activity in the preliminary screen, and this was to ensure that the screening process was effective in choosing good drug candidates for further testing and eliminating those that would be ineffective.

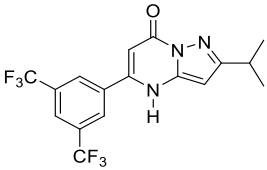
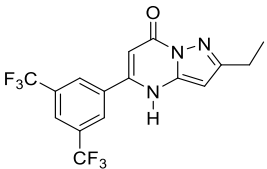
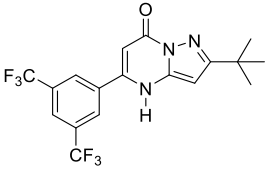
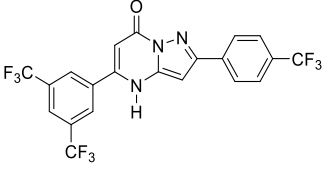
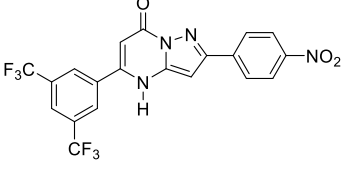
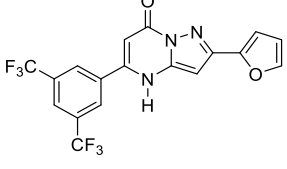
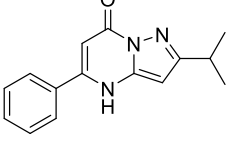
1.3.6.1 Antibacterial evaluation of select pyrazolo[1,5-*a*]pyrimidin-7-ones against clinically-relevant MRSA

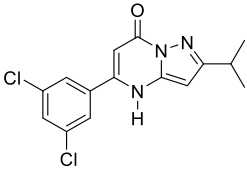
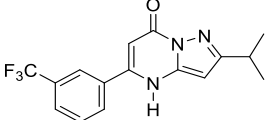
Starting with MRSA, the compounds tested and the results obtained are shown in Table 11. Taking into consideration MIC₈₀ values only as a measure of activity, compound **57** was shown to be the most active compound in terms of micromolar activity, with an MIC₈₀ value of 2.93 μ M. This compound was found to be the second most active compound in group 1b against *S. aureus* in our SAR study, but did not have the highest activity in terms of inhibition of *S. aureus* growth overall. It is interesting that it is the most active compound against MRSA, out of our selection of compounds. This may indicate an alternative mechanism of resistance of *S. aureus* relative to MRSA. Interestingly, only our most active compound, compound **57**, was capable of inhibiting MRSA growth by 80%. This is consistent with MRSA being more resistant than *S. aureus*.

The next most active compound, compound **74** of group 2b, inhibited growth by 77%. This compound was unable to inhibit *S. aureus* growth by 80% in the SAR study, therefore it being unable to inhibit MRSA growth by 80% is not surprising. However, its very low MIC₅₀ value against *S. aureus* warranted its screening against MRSA and was found to be the second most active compound. Despite compounds from group 1a generally being the most active against *S. aureus* in the SAR study, it is interesting that they were not the most active against MRSA. It was thought from the SAR study with *S. aureus* that the presence of 3,5-bis-(trifluoromethyl)phenyl as R² was an important structural feature for activity, so it is noteworthy that it is also present in our most active compound against MRSA. The compound that showed no activity against *S. aureus* also showed no activity against MRSA, compound **65**, suggesting that that our *S. aureus*

screening process appeared effective at selecting candidates for evaluation against MRSA.

Table 11. Antibacterial activity of pyrazolo[1,5-a]pyrimidin-7-one analogues from preliminary study against MRSA as MIC₅₀/ MIC₈₀ values

<i>Code</i>	<i>Group</i>	<i>Structure</i>	MIC ₅₀ (μ M)	MIC ₅₀ (μ g/ mL)	MIC _{XX} (μ M)	MIC _{XX} (μ g/ mL)
50	1a		8.01	3.14	MIC ₇₁ = 105.45	MIC ₇₁ = 41.05
51	1a		3.01	1.13	MIC ₆₆ = 155.85	MIC ₆₆ = 58.49
52	1a		3.68	1.49	MIC ₇₅ = 17.55	MIC ₇₅ = 7.08
57	1b		1.88	0.923	MIC ₈₀ = 2.93	MIC ₈₀ = 1.44
65	1b		N/A	N/A	N/A	N/A
67	1c		10.42	4.31	MIC ₇₄ = 23.42	MIC ₇₄ = 9.68
71	2a		224.35	56.82	MIC ₆₄ = 375	MIC ₆₄ = 94.99

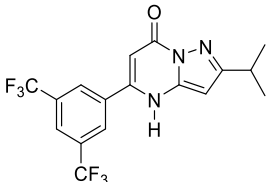
73	2b		32.51	10.475	MIC ₆₀ = 46.9	MIC ₆₀ = 15.11
74	2b		4.83	1.56	MIC ₇₇ = 8.78	MIC ₇₇ = 2.82

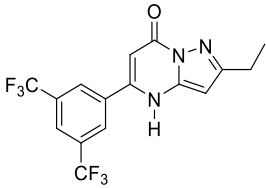
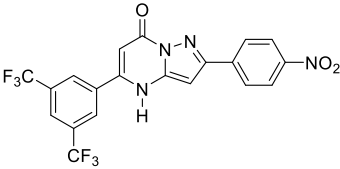
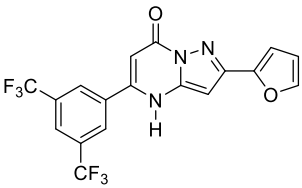
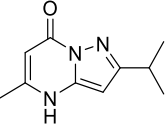
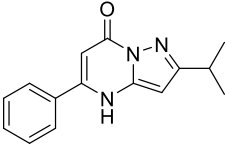
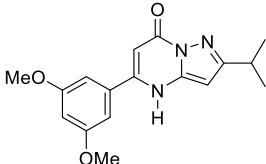
N/A denotes that bacterial growth was not inhibited by this compound.

1.3.6.2 Antibacterial evaluation of select pyrazolo[1,5-a]pyrimidin-7-ones against clinically-relevant *P. aeruginosa*

With respect to *P. aeruginosa*, the compounds tested and the results obtained, are included in Table 12. Taking into consideration MIC₈₀ values only as a measure of activity against *P. aeruginosa*, compound **71** of group 2a was shown to be the most active compound in terms of micromolar activity, with an MIC₈₀ value of 692.3 μM. In our SAR study against *E. coli*, this compound was also found to be the most active compound in group 2a (tied with compound **70**) and appeared in the top 5 most active compounds overall in terms of inhibition of *E. coli* growth. However, looking across the selection of compounds chosen for further testing, results from the SAR study did not directly translate across for *P. aeruginosa* in all cases. For example, compound **51** of group 1a was found to be the most active compound against *E. coli* but could not inhibit the growth of *P. aeruginosa* by 80%. This demonstrates that different mechanisms of action can be at play. Pleasingly, the compound that showed no activity against *E. coli*, compound **65**, also showed no activity against *P. aeruginosa*. Overall, the results suggest that a preliminary screening process using *E. coli* could be helpful in identifying compounds for further testing against more resistant strains.

Table 12. Antibacterial activity of pyrazolo[1,5-a]pyrimidin-7-one analogues from preliminary study against *P. aeruginosa* as MIC₅₀/ MIC₈₀ values

Code	Group	Structure	MIC ₅₀ (μM)	MIC ₅₀ (μg/ mL)	MIC ₈₀ (μM)	MIC ₈₀ (μg/ mL)
50	1a		489.9	190.70	N/A	N/A

51	1a		343.0	128.72	749.3 ^a	281.45 ^a
65	1b		N/A	N/A	N/A	N/A
67	1c		667.0	275.64	N/A	N/A
70	2a		488.6	93.43	693.9	132.70
71	2a		477.5	120.94	692.3	175.44
79	2b		535.3	167.73	726.4	227.63

N/A denotes that bacterial growth was not inhibited by this compound. ^aThis compound inhibited bacterial growth by 76%, not 80%, and as such was recorded as a MIC₇₆ value.

However, as suspected from the results of our SAR study where better antibacterial activity was observed against the Gram positive (*S. aureus*) over Gram negative (*E. coli*) bacteria, the activity of pyrazolo[1,5-a]pyrimidin-7-ones was much higher against MRSA (Gram positive) than *P. aeruginosa* (Gram negative). For example, the MIC₈₀ of the most active compound against MRSA, compound **57**, was over 236 times lower than the MIC₈₀ of the most active compound against *P. aeruginosa*, compound **71**. This is consistent with comparison of these compounds with the activities of commercial antibiotics. With respect to MRSA, the commercial antibiotics used were ampicillin trihydrate and tetracycline, which gave MIC₅₀ values of 2.33 mM (941.1 µg/mL) and 291.72 µM (129.65 µg/mL), a MIC₈₀ was not recorded in either case. Regarding *P. aeruginosa*, the

commercial antibiotic used was streptomycin sulfate, which gave MIC₅₀ and MIC₈₀ values of 6.44 μ M (4.69 μ g/mL) and 40.41 μ M (29.45 μ g/mL) respectively. Compound **57** had far superior activity against MRSA compared to the commercial antibacterial agents we examined, while the activity of compound **71** against *P. aeruginosa* was much less potent relative to that of commercial streptomycin sulfate. Therefore, evaluation of pyrazolo[1,5-a]pyrimidin-7-ones against *S. aureus* and *E. coli* appears to have been successful in identifying candidates for testing against more clinically relevant bacteria. The most active compound against MRSA was identified as compound **57**, and against *P. aeruginosa* was identified as compound **71**. However, we wanted to ensure that the activities observed in both cases were not as a result of non-selective toxic effects of these compounds and, to this effect, we did an *in vivo* toxicity study using *Galleria mellonella* (*G. mellonella*) larvae, section 1.3.7.

1.3.7 *Galleria mellonella in vivo* toxicity study

It was important to ensure that the antibacterial activity displayed was not simply due to the compounds being toxic in nature (i.e. not selective for bacteria). To explore this, an *in vivo* toxicity study was carried out using the larvae of the Greater wax moth, *G. mellonella*, as described and employed in our toxicity assessment of the *trans*-cinnamaldehydes, section 1.2.9. For each compound tested, five healthy *G. mellonella* larvae, in the sixth developmental stage, were injected into the last left pro-leg, directly into the haemocoel, with 20 μ L of each test solution. The concentration of each test solution was decided on the basis of the respective MIC₈₀ values of the two most active compounds identified by our screening process. With respect to compound **57**, this had an MIC₈₀ value of 2.93 μ M against MRSA and so, three different test solutions were made, one consisting of 1 μ M, another of 2 μ M and a final solution of 4 μ M. These concentrations were selected in order to assess the toxicity of this compound at a concentration lower than, similar to, and above its MIC₈₀. Similarly, regarding compound **71** that had an MIC₈₀ value of 692.3 μ M against *P. aeruginosa*, three test solutions of different concentrations were made, one consisting of 400 μ M, another of 600 μ M and a final solution of 800 μ M. Again, these concentrations were selected in order to assess the toxicity of this compound at a concentration lower than, similar to, and above its MIC₈₀. After injection, the larvae were incubated at 37 °C for a total of three days. As with the *trans*-cinnamaldehyde toxicity assay, larvae were monitored for survival and melanisation at 24-hour intervals. The results of this toxicity evaluation are summarized in Table 13, which was run at least in triplicate, see experimental section for further details, section 1.4.6.2.

Table 13. Summary of the survival of *G. mellonella* larvae (expressed as %) post injection at 24, 48, and 72 hrs.

Compound	Dosage concentration (μM)	G. mellonella survival (%)		
		24 h	48 h	72 h
57	1	100	100	93
	2	100	93	93
	4	93	93	90
71	400	93	87	73
	600	93	93	93
	800	100	100	100
^a DMSO : Distilled water (5: 95 (v/v))		100	93	90

^a5:95 (v/v) DMSO: Distilled water was the vehicle control used in this study. An n = 4 was employed.

It is evident from the results in Table 13 that high survival rates were observed in all cases and therefore it is not a toxic effect causing the antibacterial activity of either compound. This can be determined on the basis that for compounds **57** and **71** at the highest and second highest concentrations administered, the same amount of larvae or more larvae, survived post-injection of the vehicle control as did those post-injection of either compound. Thus, both compounds that have associated promising antibacterial activity were also well tolerated *in vivo*. This toxicity assay also allowed us to determine appropriate concentrations to administer for the *in vivo* therapeutic evaluation, section 1.2.14

1.3.8 Therapeutic effect – *Galleria mellonella* *in vivo* study

Having established the non-toxicity of our two most active compounds, we then evaluated their therapeutic effect *in vivo*. The first step in doing this was to establish a concentration of bacteria which, when injected, would kill roughly 50% of the *G. mellonella* larvae. Establishing this concentration is an important step in evaluating the therapeutic effect of a potential drug candidate because it prevents the issues associated with either too many or too few of the bacteria being injected. For example, if too many bacteria are added, and result in the death of all the larvae within a 24-hour period, the drug might not get a chance to elicit its mechanism of action, and hence, this is not a reasonable assessment of the effect of the candidate. In contrast, if too few bacteria are added, then the infection might not take hold and so, the true effect of the drug might be masked. Thus, time was taken to establish the optimal bacterial dose and a number of different concentrations of each clinically relevant bacteria were considered in this process. The concentration of each bacteria culture, grown in nutrient broth over a 48-hour period, was approximated

by using optical density. This was done by measuring the absorbance of each original stock solution of bacteria, read at 600 nm using a UV/Vis spectrometer. For MRSA cultures, the optical density measured was typically 1.3 absorbance units, and for *P. aeruginosa* it was typically 0.9 absorbance units. This in each case, without dilution, is referred to as the ‘stock solution’. This was then diluted by a factor of 10 by taking 100 µL of ‘stock solution’ and diluting this in 900 µL PBS, which is referred to as the ‘1/10 dilution’. This, in turn, was diluted by a factor of 10 by taking 100 µL of the ‘1/10 dilution’ solution and diluting in 900 µL PBS, which is referred to as the ‘1/100 dilution’. This process continued so that a range of concentrations between the 1/10,000 and the 1/10,000,000 dilution of ‘stock solution’ were investigated for *P. aeruginosa*. Similarly, MRSA was investigated between the 1/1,000 and the 1/1,000,000 dilution of ‘stock solution’. In each case, concentrations differed by a factor a ten. The results obtained from this are included in Table 14. In each case 5 healthy larvae were injected with a solution of the respective bacteria and examined every 24 hours over a 72-hour period. Again, results were obtained at least in triplicate, see experimental section for further details, section 1.4.6.3.

Table 14. Summary of the survival of *G. mellonella* larvae (expressed as %) post injection at 24, 48, and 72 hrs.

Bacteria	Dosage concentration (dilution relative to ‘stock solution’)	G. mellonella survival (%)		
		24 h	48 h	72 h
<i>P. aeruginosa</i>	1/10,000	0	0	0
	1/100,000	27	7	7
	1/1,000,000	45	45	40
	1/10,000,000	100	100	100
MRSA	No dilution	65	60	60
	1/10	100	100	80
	1/1,000	100	80	80
	1/10,000	100	90	90
	1/100,000	100	100	100
	1/1,000,000	100	100	100

An n = 4 was employed.

It is evident from the above results that much lower concentrations of *P. aeruginosa* were required to kill the *G. mellonella* larvae relative to MRSA. This is justified as the

sensitivity of *G. mellonella* to *P. aeruginosa*, when it is injected to the hemolymph,¹⁴⁹ which has been described in the literature. A 50% lethal dose (LD₅₀) of fewer than 10 bacteria has been reported in a number of studies.¹⁴⁹ Based on these results, it was decided that the dose of *P. aeruginosa* to be administered as part of the therapeutic evaluation would be the 1/1,000,000 dilution of ‘stock solution’ of *P. aeruginosa*, as this was the closest to a LD₅₀ that was observed in our screening. As above, this stock had an absorbance of roughly 0.9 absorbance units when read at 600 nm using a UV/Vis-spectrometer and had been grown for 48 hours at 37 °C prior to injection of five healthy *Galleria* larvae on each occasion. After injection with the bacteria, the larvae were left for 30 minutes, then injected with ‘treatment’. This treatment consisted of the highest concentration of compound **71** examined previously in the toxicity assay which was determined as non-toxic. Specifically, 800 µL of compound **71** was made up using 5% DMSO (95% deionised water) as the vehicle control, and once this ‘treatment’ was injected into each larvae, they were subsequently allowed to incubate at 37 °C for 72-hours. They were checked at 24-hour intervals.

As the larvae were not as susceptible to MRSA, the dose administered as part of the therapeutic evaluation was simply an injection of MRSA in nutrient broth without dilution, as this was the closest to a LD₅₀ that was observed in our screening. As above, this ‘stock solution’ had an absorbance of roughly 1.3 absorbance units when read at 600 nm using a UV/Vis-spectrometer and had been grown for 48 hours at 37 °C prior to the injection of five healthy *Galleria* larvae on each occasion. As was the case for *P. aeruginosa*, once injected, the larvae were left for 30 minutes, at which point they were injected with a 4 µM solution of compound **57**. This concentration was chosen as it was the highest concentration of compound **57** that was determined as non-toxic in our toxicity study. As above, compound **57** was made up using 5% DMSO (95% deionised water) as the vehicle control, and once this ‘treatment’ was injected into each larvae, they were allowed to incubate at 37 °C for 72-hours and checked at 24-hour intervals. The results obtained from these studies are included in Table 15, see experimental section for further details, section 1.4.6.3.

Table 15. Summary of the survival of *G. mellonella* larvae (expressed as %) post injection at 24, 48, and 72 hrs.

Treatment	<i>G. mellonella</i> survival (%)		
	24 h	48 h	72 h
Compound 71 (800 µM) + <i>P. aeruginosa</i> (1/1,000,000 dilution)	30	25	20
<i>P. aeruginosa</i> (1/1,000,000 dilution)	25	25	20
Compound 71 (800 µM)	100	100	100

Compound 57 (4 μ M) + MRSA (no dilution)	90	80	75
MRSA (no dilution)	55	50	50
Compound 57 (4 μ M)	93	93	90
^a DMSO : Distilled water (5: 95 (v/v))	100	93	93

^a5:95 (v/v) DMSO: Distilled water was the vehicle control used in this study. An n = 4 was employed.

As can be observed from the above table of results, the percentage survival of *G. mellonella* larvae was largely unaffected by the administration of compound **71** relative to those just administered with *P. aeruginosa*. There was a slight exception in the case of the 24-hour mark, in which there was a slightly higher percentage survival observed in those larvae to which compound **71** was administered after *P. aeruginosa*, relative to larvae to which *P. aeruginosa* only was administered. These results altogether indicate that although this compound inhibits bacterial growth *in vitro* and is not toxic *in vivo*, it appears unlikely to result in an effective therapy *in vivo*. This may be somewhat expected given the relatively high MIC₈₀ value recorded *in vitro*. Additionally, differences in *in vitro* and *in vivo* antimicrobial activity are often observed,¹⁵⁰ and may be because *in vitro* models lack host factors such as its cellular immunity and the occurrence of protein binding, for example.¹⁵⁰ With respect to *G. mellonella* specifically, its immune system is innate and is divided into a cellular component, which is mediated by hemocytes (the blood cells of *G. mellonella*), and a humoral component, which is composed of antimicrobial peptides and lytic enzymes, for example.¹⁵¹ *In vivo*, our treatment might be interacting with one or more of the components of the innate immune system of *G. mellonella*, which may lead to inactivation of compound **71**. The occurrence of factors such as these may explain the differences observed in activity *in vitro* relative to *in vivo* against *P. aeruginosa*. Photographs of the larvae observed over the course of one three-day experiment are included below as Figure 27 (a)-(c), as representative examples of the results obtained.

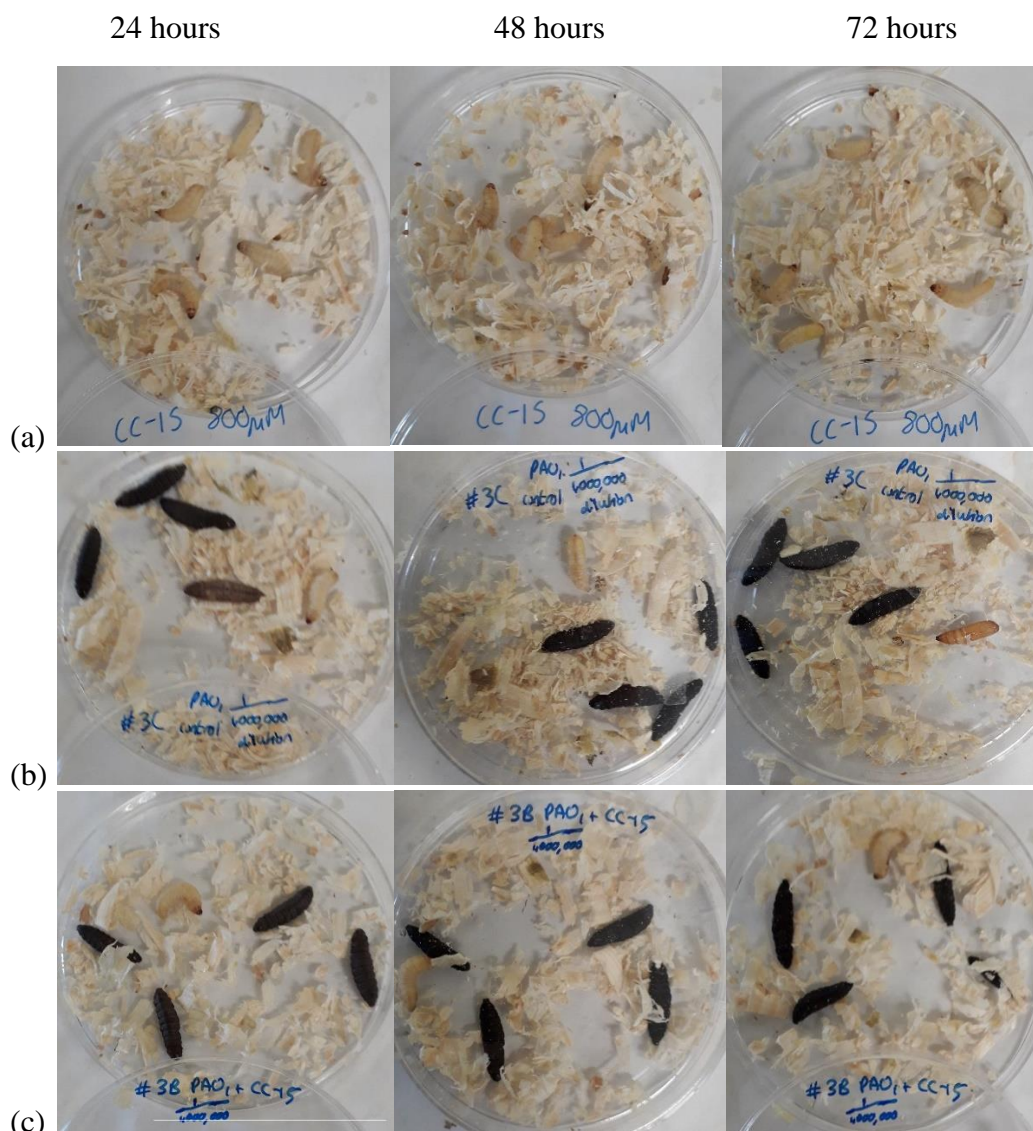
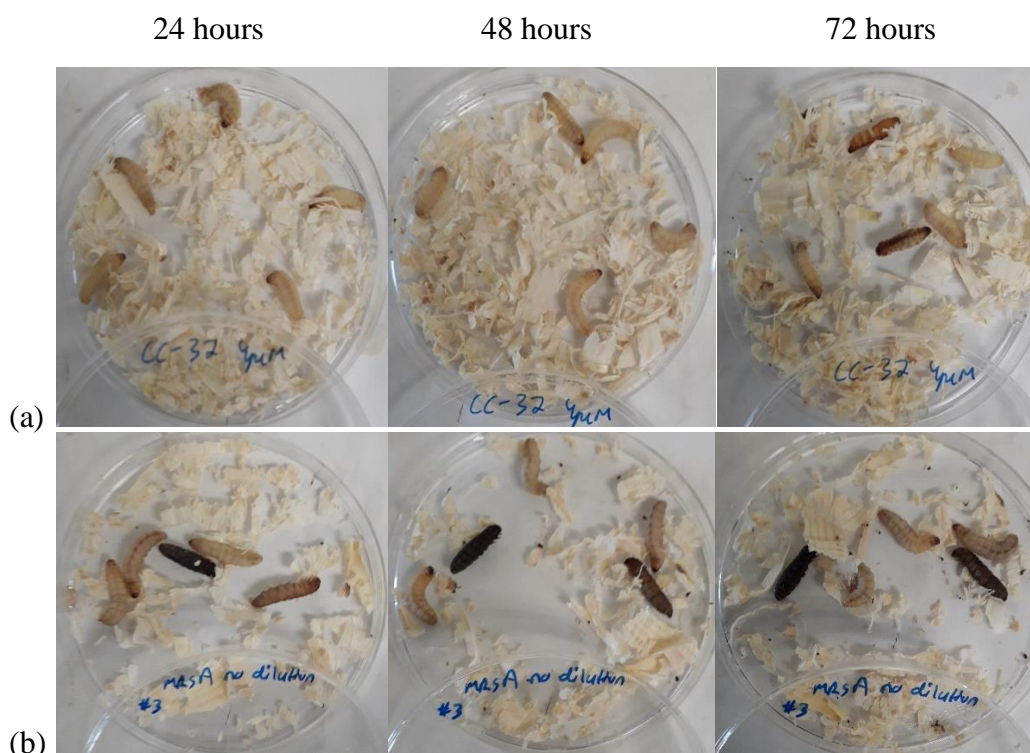


Figure 27 (a). *G. mellonella* larvae injected with 800 μ M compound **71** as observed after a 24-, 48- and 72-hour incubation period, reading from left to right. **(b)** *G. mellonella* larvae injected with a 1/1,000,000 dilution of *P. aeruginosa* stock, as observed after a 24-, 48- and 72-hour incubation period, reading from left to right. **(c)** *G. mellonella* larvae injected with a 1/1,000,000 dilution of *P. aeruginosa* stock, left for 30 minutes then injected with 800 μ M compound **71**, as observed after a 24-, 48- and 72-hour incubation period, reading from left to right.

A different set of observations were made with respect to the effect of compound **57** as a treatment *in vivo*. Relative to those larvae to which MRSA only was administered, see results in Table 14 previously, the percentage survival of *G. mellonella* larvae increased as a result of the administration of 4 μ M compound **57**. This was significant change, with a 25% increase in survival of *G. mellonella* evident three days after injection of the larvae with MRSA, followed by treatment with compound **57**, relative to those larvae to which MRSA only was injected. This was observed over four different occasions, giving a final sample set value of 20. The percentage survival as a result of the treatment administered

was observed to decrease over the course of the three-day period (from 90% to 75%) suggesting that, at the very least, this compound slows the spread of the infection, resulting in an overall effect of increased survival rates relative to the larvae to which MRSA was administered alone. This is an important result and implies that compound **57**, at a relatively low dose of just 4 μM , may be sufficient to have a therapeutic effect *in vivo*. A study by Desbois and Coote¹³¹ showed that commercial antibiotics, such as vancomycin, improved the survival rate of *G. mellonella* larvae that were inoculated with a dose of 1, 10 and 50 mg/kg 2 hours after the injection of MRSA, relative to those injected with PBS and MRSA subsequently. These survival rates improved in a dose-dependent manner. For example, after three days, 65% of the larvae to which 1 mg/kg vancomycin was administered survived, relative to 100% survival in the larvae to which 50 mg/kg vancomycin was administered. The larvae were studied over the course of five days, over which time the survival rates decreased with respect to the 1 and 10 mg/kg treatments,¹³¹ similar to what we observed in our assessment. However, in this study, treatments were administered at 24, 48, and 72-hour timepoints.¹³¹ Photographs of the larvae observed over the course of one three-day experiment is included below as Figure 28 (a)-(c), as representative examples of the results we obtained.



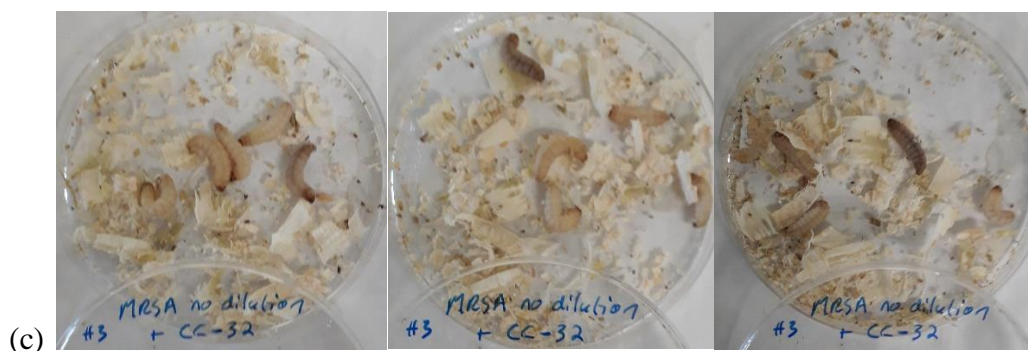


Figure 28 (a). *G. mellonella* larvae injected with 4 μM compound **57** as observed after a 24-, 48- and 72-hour incubation period, reading from left to right. **(b)** *G. mellonella* larvae injected with a MRSA culture without dilution, as observed after a 24-, 48- and 72-hour incubation period, reading from left to right. **(c)** *G. mellonella* larvae injected with a MRSA culture without dilution, left for 30 minutes then injected with 4 μM compound **57**, as observed after a 24-, 48- and 72-hour incubation period, reading from left to right.

To summarize, from our preliminary screen of four compounds, one each from a structurally different family of compounds, compound **48** as a representative pyrazolo[1,5-*a*]pyrimidin-7-one demonstrated promising antibacterial activity against *S. aureus*. Thirty-five compounds from this family were then evaluated as part of a SAR study for their antimicrobial activity against *S. aureus*, *E. coli*, and *C. albicans*. Structural changes were divided into groups based on the change made, and explored different substitution and structural modifications at a number of locations on the pyrazolo[1,5-*a*]pyrimidin-7-ones. Compound **48** was used as the initial hit compound. Antibacterial activity was shown to be superior to observed antifungal activities across the pyrazolo[1,5-*a*]pyrimidin-7-ones and so, a selection of compounds were chosen based on the results of the SAR study with a focus on their antibacterial activity. This selection of compounds then underwent further evaluation against the more clinically relevant bacterial strains MRSA and *P. aeruginosa*. As suggested by the SAR study against *S. aureus* and *E. coli*, MRSA activity was much higher than that against *P. aeruginosa*, where the activity of the most active compound, compound **57**, was superior to the commercial antibiotics examined in this screen. Compound **71** was found to be the most active compound against *P. aeruginosa*, and these two compounds were examined for toxicity *in vivo* using *G. mellonella* larvae. Across three different concentrations, chosen based on their respective MIC₈₀ concentration, compounds **57** and **71** were shown to be non-toxic, at concentrations of 1-4 μM and 400-800 μM , respectively. Having established non-toxicity, the highest dose of each compound was then used as a treatment and injected into *G. mellonella* larvae that had been infected with MRSA or *P. aeruginosa* 30 minutes prior to treatment. After monitoring for three days at 24-hour intervals, it was observed that compound **71** did not result in any significant increase in survival rate of *G. mellonella* larvae as compared with those infected with bacteria and no treatment. However, compound **57** resulted in a 25% increase in survival, three days after the injection of both MRSA and 4 μM of this compound. After three days, 75% survival was evident in *G. mellonella* to which both MRSA and treatment was administered, relative

to 50% survival when the same dose of MRSA only was administered. The survival rate after treatment did decrease over a three day-period, starting at 90% survival, then 80%, and finally 75%. Comparing this to the results for injection of compound **57** alone to larvae that were not infected (93% survival rate at day three), suggests that the treatment did not fully eliminate the infection, but does appear to slow down the rate of MRSA infection, resulting in a net increase in survival rate over three day examination period. This suggests that compound **57**, even at a dose as low as 4 μ M, has potential as an effective anti-MRSA agent *in vivo*. Taken together with the excellent *in vitro* activity and non-toxicity demonstrated *in vivo*, compound **57** may represent a potential new drug or lead candidate for the treatment of MRSA infections. However, further studies using alternative mammalian models, such as mice, would be required to demonstrate its efficacy as a treatment and further study its non-toxicity *in vivo*. This is important so as to ensure that the observations we recorded in *G. mellonella* larvae translates to other, more complex mammalian systems. Additionally, proteomic analysis would also be required to elucidate the antibacterial mechanism of action on MRSA cells,¹⁵² as this work only demonstrates that compound **57** has a bacteriostatic effect on MRSA *in vitro*. *In vivo*, the results obtained above suggest that compound **57** slows down the rate of MRSA infection, but we cannot postulate at this stage on its mechanism of action. The work presented here indicates that compound **57**, at least in a preliminary context, represents a potent, non-toxic anti-MRSA compound that displays activity both *in vitro* and *in vivo*, with further study required to prove its efficacy as a potential therapeutic agent.

1.4 Conclusion

The first half of this chapter described the synthesis of *trans*-cinnamaldehydes, their subsequent biological evaluation as antibacterial agents, and a consideration of how their ability as electrophilic agents related to antibacterial activity. The synthesis of the *trans*-cinnamaldehydes was achieved using a Wittig procedure in all but one case. The yields of pure *E*-isomer varied greatly from 17-61%, with factors that may explain this variation in yield being considered in this chapter, such as the presence of lone pair-bearing substituents on the *ortho*-position of the phenyl ring, and the occurrence of the alternative *Z*-isomer in the crude mixture.

Once synthesized, this family of nine *trans*-cinnamaldehydes, as well as six other *trans*-cinnamaldehydes which were purchased commercially, were subjected to antibacterial evaluation using the established microdilution methodology. In total, fifteen *trans*-cinnamaldehydes were evaluated against Gram-positive (*Staphylococcus aureus*, *S. aureus*) and Gram-negative (*Escherichia coli*, *E. coli*) bacteria. It was found that biological activity was modest, with millimolar concentrations of cinnamaldehydes required in all cases to inhibit bacterial growth by 50%. However, not all of the *trans*-cinnamaldehydes evaluated in this study were capable of inhibiting growth by 50%. The antibacterial activity we observed showed a general relationship with electrophilicity, particularly with respect to activity against *S. aureus*. Here, compounds that were more electrophilic (electrophilicity was determined by our collaborator using computational methods) than the parent *trans*-cinnamaldehyde, **1**, required lower concentrations to inhibit the bacterial growth by 50%, or in some cases by 80%. (*E*)-4-Bromocinnamaldehyde, compound **40**, was shown to be the most active compound demonstrating activity nearly 5 times more potent than **1**. A preliminary mechanism of action study indicated that the *trans*-cinnamaldehydes investigated could induce cellular leakage, as indicated by the observed leakage of amino acids and protein over a 6-hour period. This was somewhat expected from our assessment of the literature with respect to the parent compound **1**. However, the most active compound, **40**, did not induce the most leakage, and so, it was concluded that this may not be the preliminary mechanism of antibacterial activity employed by *trans*-cinnamaldehydes. This coincided with literature reports for **1**, which suggested that it exerts multiple antibacterial mechanisms of action. A NMR-based cysteamine assay has been reported by Appendino *et al.*⁶¹ to show that **1** could act as a thiol-trap *in vivo* by reacting at its multiple electrophilic sites. We replicated this assay and preliminary data suggested we obtained the same result, with some evidence of the same products described by this group evident in our crude mixture after the reaction between **1** and cysteamine. In our replication of this assay, **1** was also completely consumed within 5 minutes at room temperature, and this was also the case for compound **40** and 4-nitrocinnamaldehyde, compound **44**. Additionally, an *in vivo* study using *Galleria mellonella* indicated that the *trans*-cinnamaldehydes investigated were non-toxic, with our most active compound, **40**, resulting in the same high survival rates

in larvae as shown by the parent compound **1**. Compound **1** has been granted GRAS status by the FDA and is therefore generally regarded as safe.

As part of our research groups efforts to identify new antimicrobial agents, we undertook an antimicrobial screen of four compounds, each a representative of different compound classes. Out of the four structurally distinct compounds that were evaluated, compound **48**, as a representative pyrazolo[1,5-*a*]pyrimidin-7-one, exhibited good antibacterial activity against *S. aureus* (being the only compound of the four to do so). This prompted us to further examining the antimicrobial properties of this family of pyrazolo[1,5-*a*]pyrimidin-7-one compounds that were available within our research group.

As a result, we conducted a SAR study to probe the important structural features of compound **48** that might have an effect on the antimicrobial activity. This family of pyrazolo[1,5-*a*]pyrimidin-7-ones were divided into five groups on this basis, and our SAR study of this family of thirty-five compounds against *S. aureus*, *E. coli* and *Candida albicans* (as a representative of yeast) showed promising levels of antibacterial activity. In some cases, very low micromolar concentrations were required to inhibit 80% of growth with respect to *S. aureus*. Notably, the observed activity of some compounds, generally in group 1a, was superior to the commercial antibacterial agents investigated in this study, specifically ampicillin trihydrate, tetracycline and streptomycin sulfate. In addition, we identified a compound whose activity against *S. aureus* was superior to compound **48** and, as such, compound **50** became our new leading hit compound. Although activity was observed by some of these compounds against *E. coli* and *C. albicans*, this activity was lower than that found against *S. aureus*. As a result, we became focused on the antibacterial properties of these compounds and investigations involving *C. albicans* did not progress beyond the initial SAR study. Based on the results of our SAR study of the pyrazolo[1,5-*a*]pyrimidin-7-ones, a selection of these compounds were tested against clinically relevant resistant strains of a Gram-positive and a Gram-negative bacteria, namely methicillin-resistant *Staphylococcus aureus* (MRSA) and *Pseudomonas aeruginosa* (*P. aeruginosa*) respectively. *P. aeruginosa* is resistant to a variety of antibiotics, including aminoglycosides, quinolones and β -lactams.¹⁵³ The activity against the resistant strains was also quite high with micromolar concentrations required to inhibit 80% bacterial growth in both cases. However, this family of pyrazolo[1,5-*a*]pyrimidin-7-ones were shown to be much more effective against Gram-positive bacteria, as expected based on the results of our SAR study. A much lower concentration of the most active compound, **57**, was required to inhibit 80% of MRSA growth, specifically 2.93 μ M. This can be compared to the higher amount required to inhibit the same percentage growth in *P. aeruginosa*, specifically 692.3 μ M for compound **71**. These two compounds, being the most active against the two clinically relevant bacteria, underwent subsequent *in vivo* toxicity assessment using *G. mellonella*. Both were shown to be non-toxic across three concentrations with high survival rates recorded over a three-day observation period. Once the non-toxicity of the compounds was established, the highest concentration of

each compound evaluated in the toxicity assay, specifically 4 μM for compound **57** and 800 μM for compound **71**, was then used in a therapeutic assessment of the compounds *in vivo*, again using *G. mellonella* larvae. After establishing the optimal concentration of MRSA and *P. aeruginosa*, which would kill roughly 50% of the larvae after infection, five healthy *G. mellonella* larvae (on four separate occasions) were injected with one of the two bacteria. They were then left for 30 minutes, injected with the respective most active compound, and then observed over a three-day period to assess any discrepancies in survival rates between larvae administered with and without the respective treatment. Although 800 μM compound **71** did not elicit a significant difference *in vivo*, 4 μM compound **57** resulted in a 25% increase in survival rates after the three-day period, compared with *G. mellonella* that were injected with MRSA only. A 75% survival rate of the larvae was observed three days after treatment, relative to a 50% survival rate without. Compound **57** therefore showed excellent *in vitro* activity against MRSA, demonstrated non-toxicity *in vivo*, and increased survival rates *in vivo* compared with *Galleria* larvae injected with MRSA but without compound **57**. Overall, these preliminary findings suggest that this compound may represent a potential new drug candidate for treating MRSA. However, further studies would be needed to confirm its efficacy, such as an investigation of its *in vivo* activity in mammalian models, such as mice. An elucidation of its mechanism(s) of action would also be necessary using proteomic analysis which is beyond the scope of this PhD project.

Thus, in this chapter, two different classes of compounds were investigated for their antimicrobial activity, with the pyrazolo[1,5-*a*]pyrimidin-7-ones showing much more potent activity than the *trans*-cinnamaldehydes. Compound **57** in particular showed excellent activity against *S. aureus* and MRSA and may be the subject of future studies to investigate its potential as a new antimicrobial agent.

1.5 Experimental Procedure

1.5.1 General information for chemical synthesis

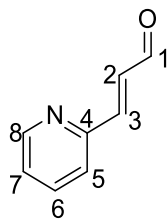
All starting materials and solvents were obtained from commercial suppliers and used without further purification. TLC was performed on Merck Silica Gel F254 plates and visualised under UV light ($\lambda=254$ nm). NMR spectra were recorded on a Bruker Ascend 500 NMR spectrometer at 20 °C (unless otherwise specified) using either CDCl₃ or (CD₃)₂S=O solutions with tetramethylsilane (TMS) as the internal standard. Assignments of the NMR spectra were deduced using ¹H NMR and ¹³C NMR, along with 2D experiments (COSY, HSQC and HMBC) and DEPT-135. Data for ¹H are reported as follows: chemical shifts (δ) are given in ppm, multiplicity is given as s = singlet, d = doublet, t = triplet, q = quartet, dd = doublet of doublets, dt – doublet of triplets and/or m = multiplet as appropriate and *J* values are given in Hz. Data for ¹³C NMR are reported as ppm. Column chromatography was performed using Merck Silica Gel 60. Uncorrected melting points (m.p.) were determined using a Stewart Scientific SMP 1 melting point machine. LC-MS was performed on an Agilent Technologies 1200 Series instrument consisting of a G1322A Quaternary pump and a G1314B UV detector (254 nm) coupled to an Advion Expression L Compact Mass spectrometer (ESI) operating in positive mode. Separations were performed on a Waters Xbridge OST 2.5 μ m, 4.6 x 50 mm column (C18) operating at a flow rate of 0.2 mL/min. Separations were performed using a mobile phase of 0.1% formic acid in water (solvent A) and 0.1% formic acid in acetonitrile (solvent B) and a linear gradient of 0-100% B over 50 minutes.

The Wittig methodology was used to synthesize a family of *trans*-cinnamaldehydes. Those not synthesized were *trans*-cinnamaldehyde, **1**, 2-methoxycinnamaldehyde, **2**, 4-chlorocinnamaldehyde, **13**, 4-methoxycinnamaldehyde, **14**, 4-nitrocinnamaldehyde, **44**, and 4-dimethylaminocinnamaldehyde, **45**, were purchased from commercial sources and used without further purification.

1.5.2 General procedure and experimental details for the synthesis of (*E*)-cinnamaldehyde analogues

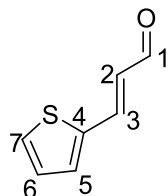
Adapted from the work of H.-J. Knölker *et al.*,⁸⁷ the general procedure for the synthesis of cinnamaldehyde analogues is as follows: A solution of substituted benzaldehyde (0.628 mmol, 1 eq.) and (triphenylphosphoranylidene) acetaldehyde (0.690 mmol, 1.1 eq) in toluene (5 mL) was stirred at 80 °C for 24 hours. The resulting solution was evaporated under reduced pressure and purified using flash chromatography on silica gel, eluting generally with ethyl acetate/petroleum ether (as indicated by TLC in order to give best separation for each compound) to attain the *E*-isomer of the product only which was used without further purification.

(E)-3-(Pyridin-2-yl)acrylaldehyde, 35



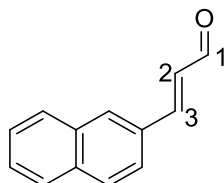
For **35**, the starting benzaldehyde was 2-pyridine carboxaldehyde. The product was eluted with ethyl acetate/petroleum ether (35:65). Black solid (93 mg, 55%); m.p. 46-48°C (lit. m.p. 46-49°C)¹⁵⁴; ¹H NMR (500 MHz, CDCl₃) δ 9.81 (d, 1H, *J* = 7.80 Hz, H1), 8.71 (d, 1H, *J* = 4.7 Hz, H8) 7.79-7.76 (td, 1H, *J* = 7.7 Hz, *J* = 1.8 Hz, H6), 7.56-7.52 (m, 2H, (H5) and (H3)), 7.34-7.31 (m, 1H, H7), 7.12-7.07 (dd, 1H, *J* = 7.80 Hz, *J* = 15.80 Hz, H2); ¹³C NMR (125 MHz, CDCl₃) δ 193.6 (C1), 152.7 (C4), 151.1 (C3), 150.4 (C8), 136.9 (C6), 131.6 (C2), 124.8 (C7), 124.2 (C5). NMR data recorded is consistent with NMR data previously reported.⁶⁹ LC-MS: purity 100% *t*_R = 13.80, (ESI) *m/z* [M+H]⁺ 134.00.

(E)-3-(Thiophen-2-yl)acrylaldehyde, 36



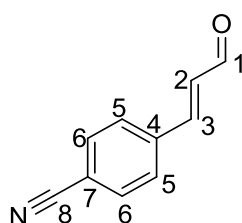
For **36**, the starting benzaldehyde was 2-thiophenecarboxaldehyde. The product was eluted with ethyl acetate/petroleum ether (1:9). Brown oil (49 mg, 28%); m.p. not applicable; ¹H NMR (500 MHz, CDCl₃) δ 9.64 (d, 1H, *J* = 7.7 Hz, H1), 7.61 (d, 1H, *J* = 15.6 Hz, H3), 7.52-7.51 (m, 1H, *J* = 5.1 Hz, H7), 7.38-7.47 (m, 1H, H5), 7.13 (dd, 1H, *J* = 3.7 Hz, *J* = 5.1 Hz, H6), 6.55 (dd, 1H, *J* = 7.7 Hz, *J* = 15.6 Hz, H2); ¹³C NMR (125 MHz, CDCl₃) δ 193.0 (C1), 144.5 (C3), 139.3 (C4), 132.1 (C5), 130.4 (C7), 128.5 (C6), 127.4 (C2). NMR data recorded is consistent with NMR data previously reported.¹⁵⁵ LC-MS: purity 98.5% *t*_R = 23.29, (ESI) *m/z* [M+H]⁺ 138.80.

(E)-3-(Naphthalen-1-yl)acrylaldehyde, 37



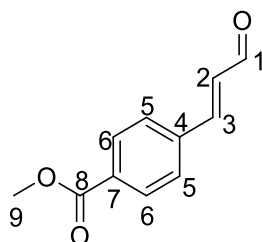
For **37**, the starting benzaldehyde was α -naphthaldehyde. The product was eluted with ethyl acetate/petroleum ether (7:93). Yellow solid (20 mg, 18%); m.p. 121-123°C (lit. m.p. 122-124°C)⁷¹; ¹H NMR (500 MHz, CDCl₃) δ 9.87 (d, 1H, J = 7.7 Hz, H1), 8.35 (d, 1H, J = 15.8 Hz, H3) 8.20 (d, 1H, J = 8.6 Hz, ArCH), 7.97 (d, 1H, J = 8.2 Hz, ArCH), 7.92 (d, 1H, J = 8.1 Hz, ArCH), 7.84 (d, 1H, J = 7.2 Hz, ArCH), 7.65-7.61 (m, 1H, ArCH), 7.59-7.52 (m, 2H, ArCH), 6.88 (dd, 1H, J = 7.7, J = 15.8, H2); ¹³C NMR (125 MHz, CDCl₃) δ 193.8 (C1), 149.4 (C3), 133.7 (ArC), 131.7 (ArCH), 131.2 (ArC), 130.9 (ArC), 130.89 (C2), 129.0 (ArCH), 127.3 (ArCH), 126.4 (ArCH), 125.7 (ArCH), 125.5 (ArCH), 122.8 (ArCH). NMR data recorded is consistent with NMR data previously reported.⁷¹ LC-MS: purity 96.5% t_R = 26.58, (ESI) m/z [M+H]⁺ 182.80.

(E)-p-Cyanocinnamaldehyde, 38



For **38** the starting benzaldehyde was *p*-formylbenzonitrile. The product was eluted with a gradient of ethyl acetate/petroleum ether (15:85 until the first spot was removed, then 20:80 until product eluted). Off-white solid (51 mg, 52%); m.p. 128-130°C (lit. m.p. 132°C)⁸⁷; ¹H NMR (500 MHz, CDCl₃) δ 9.77 (d, 1H, J = 7.4 Hz, H1), 7.74-7.72 (m, 2H, (H6), 7.67-7.66 (m, 2H, H5), 7.49 (d, 1H, J = 16.1 Hz, H3), 6.80 (dd, 1H, J = 7.4 Hz, J = 16.1 Hz, H2); ¹³C NMR (125 MHz, CDCl₃) δ 192.8 (C1), 149.4 (C3), 138.2 (C4), 132.8 (C6), 131.2 (C2), 128.7 (C5), 118.1 (C8) 114.3 (C7). NMR data recorded is consistent with NMR data previously reported.^{87,156} LC-MS: purity 99.1% t_R = 23.80, (ESI) m/z [M+H]⁺ 158.20.

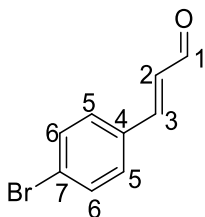
(E)-p-(Methyl ester) cinnamaldehyde, 39



For **39**, the starting benzaldehyde was methyl *p*-formylbenzoate. The product was eluted with ethyl acetate/petroleum ether (1:5). Yellow solid (72 mg, 61%); m.p. 103-105°C, (lit. m.p. 103-104°C)¹⁵⁷; ¹H NMR (500 MHz, CDCl₃) δ 9.76 (d, 1H, J = 7.6 Hz, H1), 8.11-8.08 (m, 2H, H6), 7.65-7.62 (m, 2H, H5), 7.52 (d, 1H, J = 16.01 Hz, H3), 6.81 (dd, 1H, J

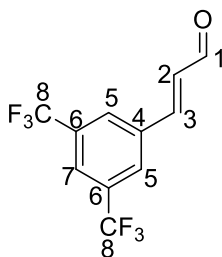
= 7.6 Hz, $J = 16.01$ Hz, H2), 3.95 (s, 3H, H9); ^{13}C NMR (125 MHz, CDCl_3) δ 193.3 (C1), 166.3 (C8), 150.9 (C3), 138.1 (C4), 132.2 (C7), 130.4 (C2), 130.3 (C6), 128.3 (C5), 52.4 (C9). NMR data recorded is consistent with NMR data previously reported.¹⁵⁷ LC-MS: purity 96.1% $t_{\text{R}} = 24.55$, (ESI) m/z $[\text{M}+\text{H}]^+$ 191.20.

(*E*)-*p*-Bromocinnamaldehyde, **40**



For **40**, the starting benzaldehyde was *p*-bromobenzaldehyde. The product was eluted with ethyl acetate/petroleum ether (88:12). Off-white solid (66 mg, 50%); m.p. 80-81°C (lit. m.p. 81-82°C)¹⁵⁸; ^1H NMR (500 MHz, CDCl_3) δ 9.71 (d, 1H, $J = 7.6$ Hz, H1), 7.59-7.56 (m, 2H, H6), 7.44-7.39 (m, 3H, H5 and H3, $J = 16.0$ Hz), 6.73-6.68 (dd, 1H, $J = 7.6$ Hz, $J = 16.0$ Hz, H2); ^{13}C NMR (125 MHz, CDCl_3) δ 193.3 (C1), 151.1 (C3), 132.9 (C4), 132.4 (C6), 129.8 (C5), 129.1 (C2), 125.7 (C7). NMR data recorded is consistent with NMR data previously reported.⁷⁰ LC-MS: purity 96.9% $t_{\text{R}} = 25.44$, (ESI) m/z $[\text{M}+\text{H}]^+$ 212.1.

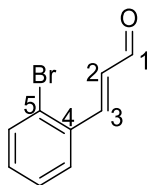
Synthesis of (*E*)-3,5-bis(trifluoromethyl)cinnamaldehyde, **86**



For **86**, the starting benzaldehyde was 3,5-bis(trifluoromethyl)benzaldehyde. The product was eluted with ethyl acetate/petroleum ether (2:8). Yellow solid (81 mg, 50%); m.p. 79-81°C, (lit. m.p. 80-81°C)¹⁰²; ^1H NMR (500 MHz, CDCl_3) δ 9.79 (d, 1H, $J = 7.3$ Hz, H1), 7.99 (s, 2H, H5), 7.94 (s, 1H, H7), 7.55 (d, 1H, $J = 16.1$ Hz, H3), 6.86 (dd, 1H, $J = 7.30$ Hz, $J = 16.1$ Hz, H2); ^{13}C NMR (125 MHz, CDCl_3) δ 192.4 (C1), 147.9 (C3), 136.1 (C4), 132.7 (q, $J_{\text{CF}} = 34$ Hz, C6), 131.5 (C2), 127.9 (d, $J_{\text{CF}} = 3.3$ Hz, C5), 124.2 (q, $J_{\text{CF}} = 3.7$ Hz, C7), 124.0 (d, $J_{\text{CF}} = 273$ Hz, C8). NMR data recorded is consistent with NMR data previously reported.¹⁰² LC-MS: purity 99.5% $t_{\text{R}} = 30.82$ min, (ESI) m/z $[\text{M}+\text{Na}]^+$ 291.4.

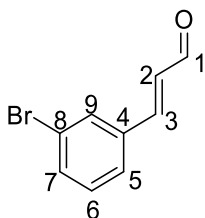
1.5.3 Procedures for the synthesis of cinnamaldehyde analogues deviating from general procedure

(E)-*o*-Bromocinnamaldehyde, 5



A solution of *o*-bromobenzaldehyde (128 mg, 6.9 mmol) and (triphenylphosphoranylidene) acetaldehyde (191 mg, 6.28 mmol) in toluene (5 mL) was stirred at 80°C for 24 hours. The resulting solution was evaporated under reduced pressure and then purified using flash chromatograph on silica gel, eluting with petroleum ether/diethyl ether (9:1). Off-white solid (55 mg, 41%); m.p. 66-68°C, (lit. m.p. 67-69°C)¹⁵⁹; ¹H NMR (500 MHz, CDCl₃) δ 9.78 (d, 1H, *J* = 7.7 Hz, H1), 7.91 (d, 1H, *J* = 16.0 Hz, H3), 7.67-7.65 (m, 2H, ArCH), 7.39-7.36 (m, 1H, ArCH), 7.30-7.27 (m, 1H, ArCH) 6.70 (dd, 1H, *J* = 7.7 Hz, *J* = 16.0 Hz, H2); ¹³C NMR (125 MHz, CDCl₃) δ 193.5 (C1), 150.6 (C3), 133.9 (C4), 133.7 (ArCH), 132.1 (ArCH), 130.8 (C2) 128.1 (ArCH), 128.0 (ArCH), 125.7 (C5). NMR data recorded is consistent with NMR data previously reported.¹⁵⁹ LC-MS: purity 99.9% *t*_R = 27.79, (ESI) *m/z* [M+H]⁺ 212.70.

(E)-*m*-Bromocinnamaldehyde, 34

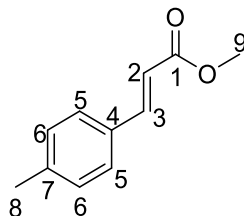


A solution of *m*-bromobenzaldehyde (73.2 μL, 6.28 mmol) and (triphenylphosphoranylidene) acetaldehyde (210 mg, 6.9 mmol) in toluene (5 mL) was refluxed for 48 hours. The resulting solution was evaporated under reduced pressure and then purified using flash chromatograph on silica gel, eluting with ethyl acetate/petroleum ether (12:88). Off-white solid (62 mg, 46%); m.p. 129-132°C, (no lit. m.p. found); ¹H NMR (500 MHz, CDCl₃) δ 9.71 (d, 1H, *J* = 7.6 Hz, H1), 7.71-7.70 (m, 1H, H9), 7.58-7.56 (m, 1H, H7), 7.51-7.49 (m, 1H, H5), 7.42-7.39 (d, 1H, *J* = 16.0 Hz, H3), 7.33-7.30 (m, 1H, H6), 6.73-6.68 (dd, 1H, *J* = 7.6 Hz, *J* = 16.0 Hz, H2), ¹³C NMR (125 MHz, CDCl₃) δ 193.3 (C1), 150.7 (C3), 136.1 (C4), 134.0 (C7), 131.2 (C9), 130.6 (C6), 129.7 (C2), 126.9 (C5), 123.3 (C8). NMR data recorded is consistent with NMR data previously reported.⁷² (Note: A HPLC chromatogram of (E)-*m*-bromocinnamaldehyde could not be obtained as it degraded on the HPLC column).

(E)-p-Methyl cinnamaldehyde

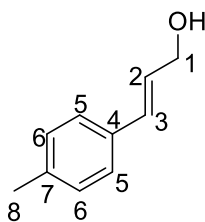
This synthesis comprised of three separate steps;

(i) Synthesis of (E)-p-methyl cinnamate, 42



The method used to synthesize **42** was adapted from the work of K. Sunnerheim *et al.*¹⁰⁸ and consists of the following: To a solution of *p*-methyl cinnamic acid (389 mg, 2.4 mmol) dissolved in methanol (22 mL) was added 6 drops of concentrated sulphuric acid, and the resulting mixture was refluxed for 6 hours. This was then concentrated *in vacuo*, diluted with water and diethyl ether (60 mL), then washed with Na₂CO₃ (10 mL). The organic layer was then dried over MgSO₄, filtered and concentrated under reduced pressure. White crystals (358 mg, 85%); m.p. 52-53°C (lit. m.p. 55°C)¹⁶⁰; ¹H NMR (500 MHz, CDCl₃) δ 7.69 (d, *J* = 16.0 Hz, 1H, H3), 7.42 (d, *J* = 8.0 Hz, 2H, H5), 7.19 (d, *J* = 8.0 Hz, 2H, H6), 6.41 (d, *J* = 16.0 Hz, 1H, H2), 3.80 (s, 3H, H9), 2.37 (s, 3H, H8); ¹³C NMR (125 MHz, CDCl₃) δ 167.6 (C1), 144.9 (C3), 140.7 (C7), 131.7 (C4), 129.6 (C6), 128.1 (C5), 116.8 (C2), 51.6 (C9), 21.4 (C8). NMR data consisted with that reported in literature.¹⁶⁰

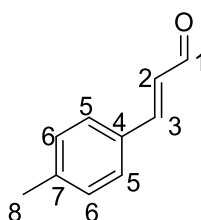
(ii) Synthesis of (E)-3-p-tolylprop-2-en-1-ol, 43



The method used to synthesize **43** was adapted from the work of N.T. Patil *et al.*¹⁰⁹ and consists of the following: A solution of DIBAL-H (25% weight solution in toluene (700g bottle), 2 mL, 2 eq.) was added dropwise to a stirring solution of **42** (268 mg, 1.52 mmol) in dried toluene (dried with molecular sieves) at 0°C in a Schlenk tube that had been dried with a heat gun and contained an atmosphere of argon. The reaction mixture was allowed to stir for one hour, at which point a TLC was done that indicated the completion of the reaction. The reaction mixture was then diluted with ethyl acetate and distilled water (20 mL of each), as well as 1 M HCl (5 mL) which was used to help separate out the aqueous and organic layers. The aqueous layer was subsequently extracted twice with ethyl acetate. The combined organic layers were then dried over Na₂SO₄, concentrated under vacuum and the colourless solid product was used without further purification.

Colourless solid (210 mg, 93%); m.p. 49-51°C (lit. m.p. 52°C)¹⁵⁶; ¹H NMR (500 MHz, CDCl₃) δ 7.30 (2H, d, *J* = 8.0 Hz, H5), 7.14 (2H, d, *J* = 8.0 Hz, H6), 6.60 (1H, d, *J* = 15.9 Hz, H3), 6.35 (1H, dt, *J* = 5.9 Hz, 15.9 Hz, H2), 4.31 (2H, dd, *J* = 1.4 Hz, *J* = 5.9 Hz, H1), 2.35 (3H, s, H8), 1.80 (1H, broad s, OH); ¹³C NMR (125 MHz, CDCl₃) δ 137.6 (C7), 133.9 (C4), 131.3 (C3), 129.3 (C6) 127.5 (C2), 126.4 (C5), 63.9 (C1), 21.2 (C8). NMR data consisted with that reported in literature.¹⁶¹

(iii) Synthesis of (*E*)-*p*-methylcinnamaldehyde, **41**



The method used to synthesize **41** was adapted from the work of N.T. Patil et al.¹³ and consists of the following: Activated manganese dioxide (IV) (10 eq., 5.53 mmol) was added to a stirring solution of **43** (1 eq., 0.553 mmol) dissolved in DCM (8.8 mL) and left stirring at 35°C for 7 hours, the completion of this reaction being indicated by TLC. The suspension was filtered through a celite pad and the filtrate was concentrated *in vacuo*. The resulting off-white solid obtained was used without further purification. Off-white solid (80.6 mg, 99.6%); m.p. 44-46°C (lit. m.p. 43-45°C)¹⁵⁹; ¹H NMR (500 MHz, CDCl₃) δ 9.67 (d, 1H, *J* = 7.7 Hz, H1), 7.46-7.42 (m, 3H, H5 and H3, *J* = 15.9 Hz), 7.24-7.22 (m, 2H, H6) 6.69-6.65 (dd, 1H, *J* = 7.7 Hz, *J* = 15.9 Hz, H2), 2.39 (s, 1H, H8); ¹³C NMR (125 MHz, CDCl₃) δ 192.7 (C1), 151.9 (C3), 140.9 (C4), 130.3 (C7), 128.8 (C6), 127.5 (C5), 126.7 (C2), 20.5 (C8). NMR data consisted with that reported in literature.¹⁵⁹ LC-MS: purity 99.3% *t*_R = 26.54, (ESI) *m/z* [M+H]⁺ 147.10.

1.5.4 Cysteamine assay protocols

Cysteamine assay – *trans*-cinnamaldehyde plus cysteamine

trans-Cinnamaldehyde, **1** (5 μL, 0.0397 mmol, 1 eq.) was added using a micropipette to a NMR tube, to which 200 μL of DMSO-d₆ was used to ensure all of **1** was added to the bottom of the NMR tube. Cysteamine (6.13 mg, 0.0794 mmol, 2 eq.) was then diluted in 200 μL of DMSO-d₆ and added to the NMR tube containing **1**. A stopwatch was used to note the point at which this addition occurred. A further 100 μL of DMSO-d₆ was added to the NMR so that the total DMSO-d₆ content of the flask was 500 μL. The first acquisition by the NMR instrument occurred 4 minutes and 55 seconds after initial addition of the cysteamine. This was complete 9 minutes and 45 seconds after the initial

addition cysteamine, at which point the ^1H NMR spectrum showed complete consumption of **1**.

Cysteamine assay– (E)-4-bromocinnamaldehyde plus cysteamine

(E)-4-Bromocinnamaldehyde, **40** (5.25 mg, 0.02487 mmol, 1 eq.) was added using a micropipette to a NMR tube, to which 200 μL of DMSO- d_6 was used to ensure all of **40** was added to the bottom of the NMR tube. Cysteamine (6.13 mg, 0.0794 mmol, 2 eq.) was then diluted in 200 μL of DMSO- d_6 and added to the NMR tube containing **40**. A stopwatch was used to note the point at which this addition occurred. A further 100 μL of DMSO- d_6 was added to the NMR so that the total DMSO- d_6 content of the flask was 500 μL . The first acquisition, by the NMR instrument, occurred 4 minutes and 42 seconds after initial addition of the cysteamine. This was complete 8 minutes and 45 seconds after the initial addition cysteamine, at which point the ^1H NMR spectrum showed complete consumption of **40**.

Cysteamine assay– (E)-4-nitrocinnamaldehyde plus cysteamine

(E)-4-Nitrocinnamaldehyde, **44** (5.25 mg, 0.02963 mmol, 1 eq.) was added using a micropipette to a NMR tube, to which 200 μL of DMSO- d_6 was used to ensure all of **44** was added to the bottom of the NMR tube. Cysteamine (4.57 mg, 0.0593 mmol, 2 eq.) was then diluted in 200 μL of DMSO- d_6 and added to the NMR tube containing **44**. A stopwatch was used to note the point at which this addition occurred. A further 100 μL of DMSO- d_6 was added to the NMR so that the total DMSO- d_6 content of the flask was 500 μL . The first acquisition, by the NMR instrument, occurred 4 minutes and 49 seconds after initial addition of the cysteamine. This was complete 9 minutes and 5 seconds after the initial addition cysteamine, at which point the ^1H NMR spectrum showed complete consumption of **44**.

1.5.5 Biological evaluation of trans-cinnamaldehydes

1.5.5.1 In vitro bacterial screening of trans-cinnamaldehydes

1.5.5.1.1 Materials and methods for trans-cinnamaldehydes

Nutrient Broth was obtained from Oxoid Ltd., Basingstoke, UK, and made up according to the manufacturer's instructions (13 g in 1 L deionised water). Optical density was read using a microplate reader (Bio-Tek. Synergy HT Spectrophotometer) at 600 nm. *S. aureus*

(a clinical isolate from a urinary tract infection, St. James Hospital, Dublin) and *E. coli* (a clinical isolate from a gastro-intestinal tract infection, St. James Hospital, Dublin) were used in this study. All bacteria were grown on nutrient broth agar plates at 37 °C and maintained at 4 °C for short term storage. Cultures were routinely sub-cultured every 4-6 weeks. All assays were run in duplicate.

1.5.5.1.2 Susceptibility assay for *trans*-cinnamaldehydes

All workspaces were washed down with 70% (v/v) ethanol prior to use. Bacterial strains were taken from nutrient agar plates and cultures were grown in nutrient broth overnight in an orbital shaker at 37 °C and 200 rpm, in a fully aerated conical flask.

Fresh solutions (10mM) of the compounds were prepared using distilled water and DMSO (95:5 v/v) and made up immediately prior to testing. Compounds with low solubility were tested as fine suspensions.

Nutrient broth (100 µL) was added to each well of a 96-well flat-bottomed microtitre plate. Serial dilutions (1:1) of the test complex were made from columns 3-11 giving a test concentration range of 10–0.039 mM. Bacteria suspensions (100 µL) were added to each well and the plate was incubated for 24 hours at 37 °C. The optical density was read at $\lambda_{\text{max}} = 600 \text{ nm}$ and growth was then quantified as a percentage of control (bacterial suspension without the addition of a test compound). Assays were run in duplicate. The results were analysed using Excel[®].

The MIC₅₀ was taken to signify the concentration of compound that would inhibit the growth of the microorganism in question by 50% and MIC₈₀ was similarly taken to signify the concentration of compound that would inhibit the growth of the microorganism in question by 80%. The active pharmaceutical ingredients of some commercial antibiotics, namely ampicillin trihydrate, tetracycline and streptomycin sulfate, were used as controls and gave MIC₅₀ values of 8.8 µg/mL (21.8 µM), 4.9 µg/mL (11 µM) and 3.8 µg/mL (5.2 µM) against *S. aureus*, respectively and MIC₅₀ values of 1.03 mg/mL (2.6 mM), 25 µg/mL (56.3 µM) and 4.5 µg/mL (6.2 µM) against *E. coli*, respectively.

1.5.5.2 Cell constituent release assessment for *trans*-cinnamaldehydes

Forty-eight-hour-old cultures (35 ml) of either *S. aureus* or *E. coli* were harvested by centrifugation (2150 g, 8 minutes), washed in PBS (phosphate buffered saline) and the hyphal mass resuspended in PBS, DMSO (Sigma-Aldrich) (5% or 20% v/v), *p*-bromocinnamaldehyde, **39** (0.51 or 0.511 mM), *trans*-cinnamaldehyde, **1** (2.32 mM or 1.93 mM) or *p*-methoxycinnamaldehyde, **40** (8.57 mM or 4.86 mM). These concentrations of samples were chosen as they had been established to be the MIC₅₀ values against *S.*

aureus and *E. coli* respectively. All three cinnamaldehyde samples were made up as 5% DMSO 95% PBS solutions (v/v).

The cultures were then incubated at 37 °C and 200 r.p.m. in an orbital shaker for a further 2, 4 or 6 h. At each time point a culture was removed and the contents filtered through a 0.45 µM syringe filter (Sartorius) and free amino acids or protein were measured as described below.

Amino acid concentration was determined by the ninhydrin colorimetric method. A ninhydrin (Sigma-Aldrich) solution (200 µL; stock: 0.35 g in 100 ml ethanol) was added to each sample (1 mM) and heated to 95 °C for 4 min. After cooling to room temperature in an ice bath, the absorbance at 600 nm was recorded on a spectrophotometer (Beckman DU 640).

To determine the quantity of protein released from the hyphal mass, samples were assayed using the Bradford reagent (Bio-Rad) and the absorbance at 570 nm was recorded on a spectrophotometer (Beckman DU 640).

1.5.5.3 *Galleria mellonella* in vivo compound toxicity assay for *trans*-cinnamaldehydes

Galleria mellonella (*G. mellonella*) in the sixth developmental stage were obtained from The Mealworm Company (Sheffield, England) and stored in wood shavings, in the dark, at 15 °C.¹²³

The experiments were carried out using ten healthy *G. mellonella* larvae (between 0.19-0.25 g in weight) placed in sterile, 9 cm petri dishes containing a sheet of Whatman filter paper and wood shavings. Test compound solutions were made fresh on the day of testing, prior to administration. Each compound was dissolved in DMSO and added to sterile, distilled water to give stock solutions consisting of 10% (v/v) DMSO. The compounds were tested across the concentration range of 1-25mM. Using a 1000 µL Thermo Myjector syringe, test solutions (20 µL) were administered to the larvae by injection into the last, left pro-leg of the *G. mellonella* larvae, directly into the haemocoel.

After injection, the larvae were incubated at 37 °C for a total of three days. Larvae were monitored for survival and melanisation, at 24 hour intervals. Death was assessed based on the lack of movement in response to stimulation together with discolouration of the cuticle. Two controls were employed for the assay:

- (1) untreated larvae maintained under the same conditions as the treated larvae,
- (2) larvae treated with 20 µL of sterile water/DMSO solution (90:10 v/v).

The results are presented as the mean percentage survival of *G. mellonella* larvae, as a function of the test compounds administered dosage. The aim of the experiment was to determine if the compounds are non-toxic and the doses given were across a range, with

concentrations of 1 mM, 10 mM, and 25 mM used, with results indicating that they are non-toxic, which suggest they may be non-toxic in mammals.^{131, 162} All experiments were run in triplicate.

1.5.6 Biological evaluation of pyrazolo[1,5-*a*]pyrimidin-7-ones

1.5.6.1 *In vitro* antimicrobial screening of pyrazolo[1,5-*a*]pyrimidin-7-ones

1.5.6.1.1 Materials and methods for pyrazolo[1,5-*a*]pyrimidin-7-ones

See section 1.5.5.1.1 previously for full details. Additionally, *Pseudomonas aeruginosa* (American Type Culture Collection (ATCC) 10145) was used in this study. *C. albicans* was maintained on yeast extract–peptone–dextrose (YEPD) agar and grown for approximately 24 hours in YEPD broth [2% (w/v) glucose, 2% (w/v) bacteriological peptone (Difco Laboratories), 1% (w/v) yeast extract (Oxoid Ltd, Basingstoke, UK) to the stationary phase (approximately $2 \times 10^8 \text{ ml}^{-1}$). *C. albicans* cells were washed twice in sterile phosphate-buffered saline (PBS) before use and enumerated by haemocytometry. All assays were run in duplicate in the SAR study, meaning that each set of results were obtained on two separate occasions (on two separate days) and the results presented are an average of the two recordings for each sample. All assays were run triplicate when examined against MRSA and *Pseudomonas aeruginosa*, meaning that each set of results were obtained on three separate occasions (on three separate days) and the results presented are an average of the three recordings for each sample.

1.5.6.1.2 Susceptibility assay for pyrazolo[1,5-*a*]pyrimidin-7-ones

All workspaces were washed down with 70% (v/v) ethanol prior to use. Bacterial strains and *C. albicans* were taken from nutrient agar plates and cultures were grown in nutrient/YEPD broth overnight in an orbital shaker at 37 °C and 200 rpm, in a fully aerated conical flask.

Fresh solutions (3 mM) of the compounds were prepared using distilled water and DMSO (90:10 v/v) and made up immediately prior to testing. Compounds with low solubility were tested as fine suspensions.

Nutrient broth (100 μL) was added to each well of a 96-well flat-bottomed microtitre plate. Serial dilutions (1:1) of the test complex were made from columns 3-11 giving a test concentration range of 750–2.93 μM . Bacteria suspensions or suspensions of *C. albicans* (100 μL) were added to each well and the plate was incubated for 24 hours at 37 °C. The optical density was read at $\lambda_{\text{max}} = 600 \text{ nm}$ and growth was then quantified as a

percentage of control (bacterial suspension or suspensions of *C. albicans* without the addition of a test compound). The results were analysed using Excel[®] and Origin software.

The MIC₅₀ (Minimum Inhibitory Concentration) was taken to signify the concentration of compound that would inhibit the growth of the microorganism in question by 50%, and the MIC₈₀ was taken to signify the concentration of compound that would inhibit the growth of the microorganism in question by 80%.

Commercial antibiotics ampicillin trihydrate, tetracycline and streptomycin sulfate were used as controls and gave MIC₅₀ values of 8.8 µg/mL (21.8 µM), 4.9 µg/mL (11.03 µM) and 3.8 µg/mL (5.22 µM) against *S. aureus*, respectively and MIC₅₀ values of 1.027 mg/mL (2.55 mM), 25 µg/mL (56.25 µM) and 4.5 µg/mL (6.18 µM) against *E. coli*, respectively. In terms of MIC₈₀ values, those recorded for ampicillin trihydrate, tetracycline and streptomycin sulfate were 0.4384 mg/mL (1.09 mM), 5.6 µg/mL (12.6 µM) and 0.1537 mg/mL (210.9 µM) against *S. aureus*, respectively. MIC₈₀ values of 0.1348 mg/mL (303.3 µM) and 7.83 µg/mL (10.75 µM) were recorded in the case of tetracycline and streptomycin sulfate against *E. coli*, respectively.

The commercial antibiotics used against MRSA were ampicillin trihydrate and tetracycline, which gave MIC₅₀ values of 941.1 µg/mL (2.33 mM) and 129.65 µg/mL (291.72 µM), a MIC₈₀ was not recorded in either case. The commercial antibiotic used against *P. aeruginosa* was streptomycin sulfate, which gave MIC₅₀ and MIC₈₀ values of 4.69 µg/mL (6.44 µM) and 29.45 µg/mL (40.41 µM), respectively.

1.5.6.2 Galleria mellonella in vivo toxicity assay for pyrazolo[1,5-a]pyrimidin-7-ones

See section 1.4.5.3 previously for full details. The compounds were tested across the concentration range of 1-4 µM with respect to **57** and 400-800 µM with respect to **71**, on the basis of the MIC₈₀ value obtained *in vitro* against MRSA and *P. aeruginosa*, respectively. Using a 1000 µL Thermo Myjector syringe, test solutions (20 µL) were administered to the larvae by injection into the last, left pro-leg of the *G. mellonella* larvae, directly into the haemocoel.

After injection, the larvae were incubated at 37 °C for a total of three days. Larvae were monitored for survival and melanisation, at 24-hour intervals. Death was assessed based on the lack of movement in response to stimulation together with discolouration of the cuticle. Two controls were employed for the assay:

- (1) untreated larvae maintained under the same conditions as the treated larvae,
- (2) larvae treated with 10 µL of sterile water/DMSO solution (95:5 v/v).

The results were presented as the mean percentage survival of *G. mellonella* larvae, as a function of the test compounds administered dosage. All experiments were run in triplicate.

1.5.6.3 *Galleria mellonella* in vivo therapeutic assessment for pyrazolo[1,5-*a*]pyrimidin-7-ones

Firstly, the concentration of *P. aeruginosa* and MRSA required to kill 50% of the galleria (a LD₅₀ value) was established for each bacteria. This was done by measuring the absorbance of a stock solution of each bacteria in nutrient broth, which had been grown for 48 hours in each case before reading at 600 nm using a UV/Vis spectrometer. The *P. aeruginosa* stock had an absorbance of roughly 0.9 absorbance units, and the MRSA stock had an absorbance of roughly 1.3 absorbance units before use. These two stock solutions were then diluted by a factor of 10 by taking 100 µL and diluting in 900 µL PBS, giving a 1/10 dilution of respective original stock solution. 100 µL of this solution was taken and diluted in 900 µL PBS to give a 1/100 dilution of original stock solution. This process continued so that a range of concentrations were injected into five healthy *G. mellonella*, as above, such that a dilution range of 1/10,000 – 1/10,000,000 of original stock solution was investigated for *P. aeruginosa* and a dilution range of 1/1,000 – 1/1,000,000 of original stock solution was investigated for MRSA. A LD₅₀ value was recorded when a 1/1,000,000 dilution of original *P. aeruginosa* stock was injected into the *G. Mellonella* larvae. A LD₅₀ value was recorded when no dilution of MRSA stock in nutrient broth was injected into the *G. Mellonella* larvae. These respective concentrations of each bacteria were injected into five healthy *G. mellonella* larvae which were then incubated for 30 minutes at 37 °C, after which time the highest concentration of each compound investigated in the *in vivo* toxicity assay was injected into each larvae additionally, then checked after 24-, 48- and 72 hours for melanisation and survival. All experiments were run in triplicate.

Chapter Two: Synthesis of trienes

2.1 Introduction

In this chapter the synthesis of a number of trienes is described, mainly 1,3,5-hexatrienes but some 2,4,6-heptatrienes in addition, Figure 29. The two vary in the number of carbon atoms making up the longest chain and therefore, in the position of the alternating carbon-carbon double bonds. As each of the double bonds present in trienes are separated by the presence of one single bond, the molecule therefore consists of alternating single and double bonds. As such, the trienes synthesized can be described as a conjugated system. The synthesis of these molecules requires the use of alkenes as substrates, Figure 29. An alkene is the term used for a carbon-based molecule containing one carbon-carbon double bond. This introduction describes some of the current applications and syntheses of trienes in the literature and then focuses on one type of synthetic strategy, the Knoevenagel-condensation reaction, which is relevant to the experimental investigations described in the results and discussion section, starting from section 2.2.1, later in this chapter.

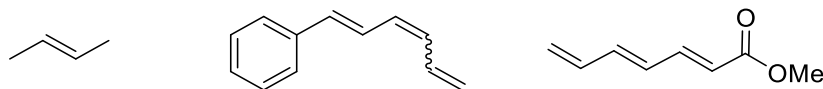


Figure 29. From left to right an example of an alkene,¹⁶³ diene,¹⁶⁴ 1,3,5-hexatriene,¹⁶⁴ and 2,4,6-heptatriene,¹⁶⁵ respectively, from the literature.

2.1.1 Applications of trienes

Important applications of trienes can be broadly divided into (i) medicinal properties, and (ii) synthetic applications, such as Diels Alder reactions and 1,8-conjugate addition reactions. Each of these applications will be explored further in the following sections. The use of trienes as substrates for electrocyclization reactions has also been reported, and this will be discussed as part of Chapter Three, section 3.2.1.

2.1.1.1 Trienes as motifs in biologically active compounds

Conjugated trienes are important structural units in many biologically important polyene natural products.¹⁶⁶ Natural products containing conjugated double bonds represent a large and structurally diverse group of compounds.¹⁶⁷ These polyenes are derived from a variety of sources, such as marine organisms, fungi, and plants, and are often produced as a natural means of chemical defense. In light of this, some polyenes have been shown to possess a variety of biological activities, including antibacterial, antifungal, and antitumour activity.¹⁶⁷ A few examples of such polyenes that contain the hexatriene unit are shown in Figure 30.

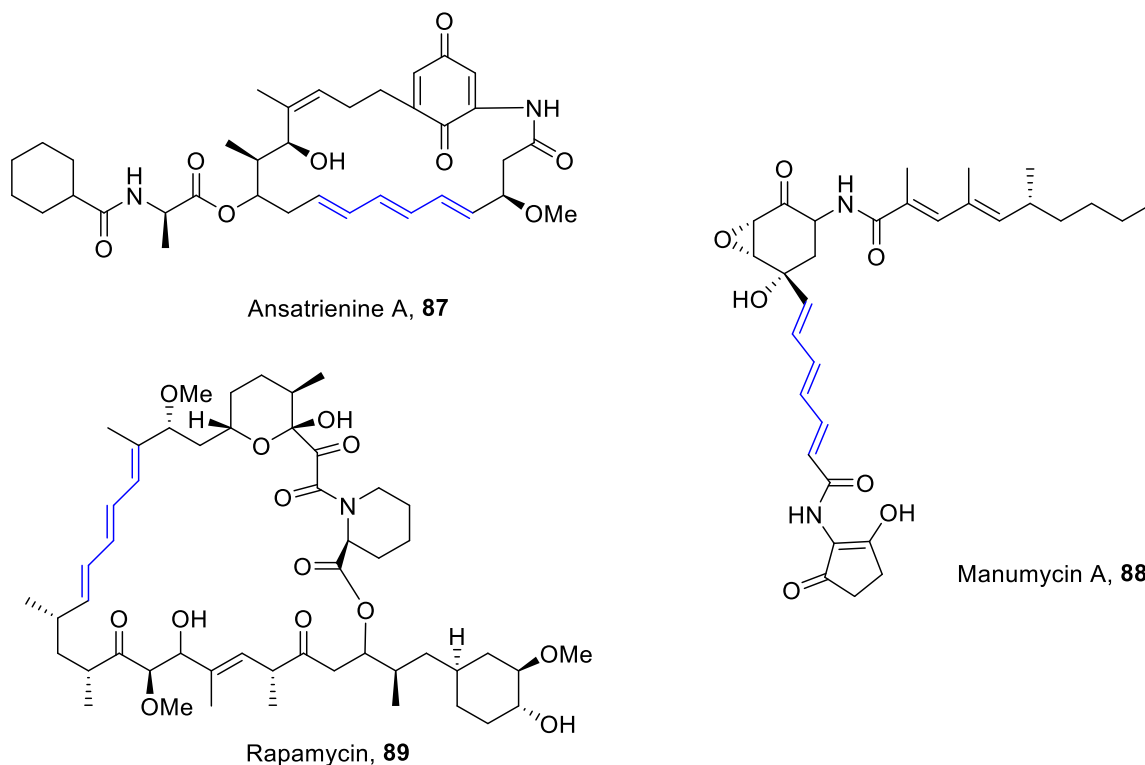


Figure 30. Examples of triene-containing molecules that possess biological activity, adapted from Thirsk and Whiting,¹⁶⁷

Miranda *et al.*¹⁶⁸ have composed an excellent review of studies involving conjugated linolenic acid (CLNA). CLNAs are a particular group of conjugated fatty acids that have been previously reported to reduce body fat, as well as possessing other attributes that are beneficial to health.³ CLNA is a collective term for a group of positional and geometric isomers of linolenic acid, in which at least two double bonds are conjugated, Figure 31.

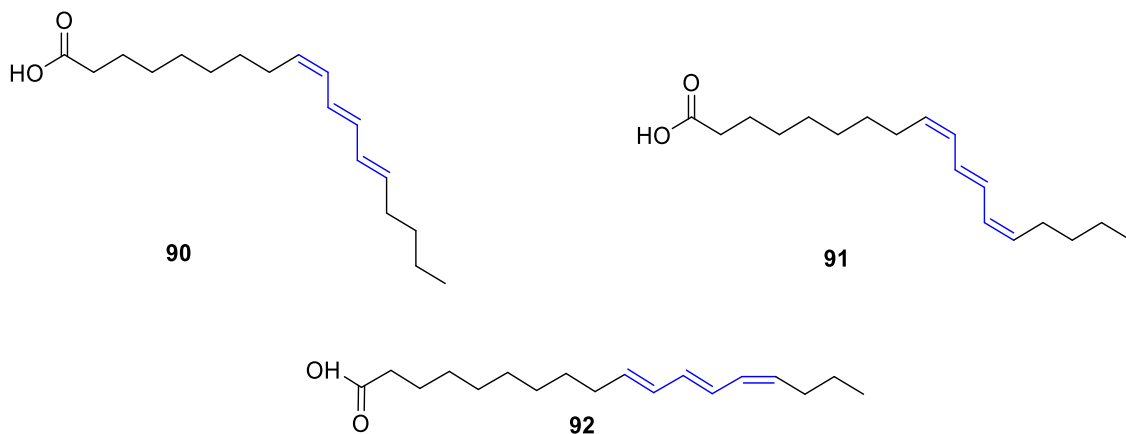


Figure 31. Examples of CLNAs containing the 1,3,5-hexatriene motif, adapted from the work of Miranda *et al.*¹⁶⁸

In vitro studies conducted on 3T3-L1 (mice) adipocytes and HepG2 (human) cells have suggested that certain plant-derived CLNA isomers, such as α -eleostearic acid and punicic acid (Figure 31, **90** and **91**, respectively), have been shown to decrease inflammation associated with obesity, for example.¹⁶⁸ Calendic acid, Figure 31 compound **92**, has also been reported to have caused a greater body fat decrease in ICR male mice (A type of albino mice named after the Institute of Cancer Research in the United States) relative to those on a control diet.¹⁶⁸ Interestingly, punicic acid, **91**, which is found in large amounts in the peels, juice and seed oil of the pomegranate fruit, has also been reported to possess anti-cancer properties.¹⁶⁹

Oh *et al.*¹⁷⁰ synthesized twenty-five novel synthetic (1*E*,3*E*,5*E*)-1,6-bis(substituted phenyl)hexa-1,3,5-triene analogs and evaluated their anti-melanogenic activity in B16F10 murine melanoma cells and zebrafish embryos. The derivatives shown in Figure 32 demonstrated promising anti-melanogenic activity and were also found by Oh *et al.*¹⁷⁰ to possess negligible toxicity at the maximum concentration evaluated of 12.5 μ M. Compound **93** was proposed as the most potent anti-melanogenic agent.¹⁷⁰

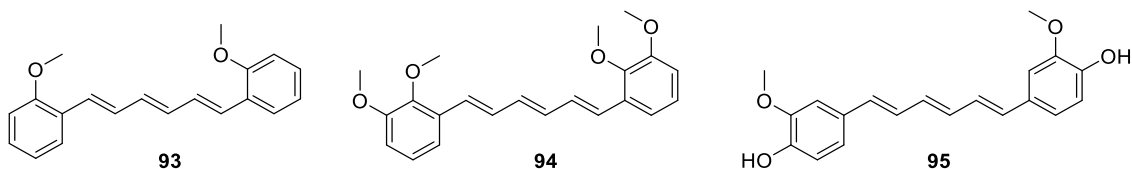


Figure 32. The above (1*E*,3*E*,5*E*)-1,6-bis(substituted phenyl)hexa-1,3,5-triene analogs demonstrated promising anti-melanogenic activity, adapted from the work of Oh *et al.*¹⁷⁰

Another study conducted by Ha *et al.*¹⁷¹ investigated a range of novel (1*E*,3*E*,5*E*)-1,6-bis(substituted phenyl)hexa-1,3,5-trienes as potential tyrosinase inhibitors. The most promising derivatives are shown in Figure 33. It was found that these compounds showed

similar or better inhibition than kojic acid, which was the positive control utilized as it is a well-known tyrosinase inhibitor.

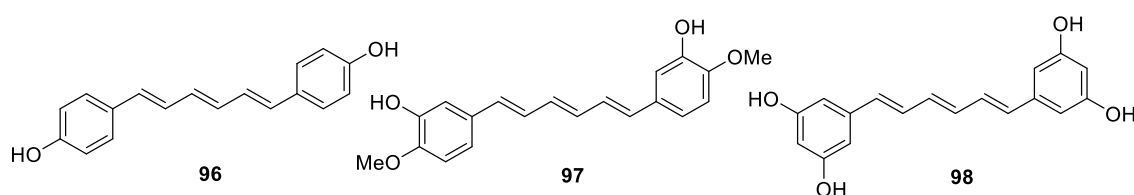


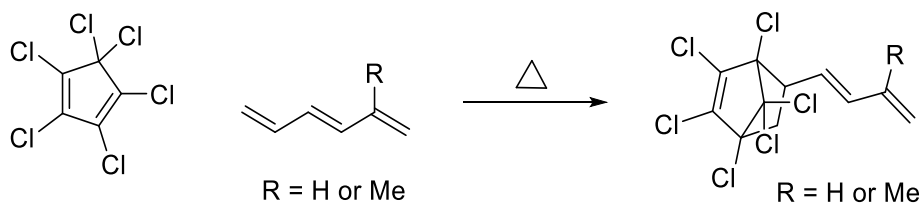
Figure 33. The above novel (1*E*,3*E*,5*E*)-1,6-bis(substituted phenyl)hexa-1,3,5-triene analogs have been investigated as potential tyrosinase inhibitors, adapted from the work of Ha *et al.*¹⁷¹

2.1.1.2 Trienes as reactants in synthetic applications

Trienes have been used as substrates in a number of syntheses, two of which are the Diels-Alder reaction and 1,8-conjugate addition.

Named after the two scientists Diels and Alder who discovered it,¹⁷² the Diels-Alder reaction is one of the most useful synthetic reactions.¹⁷³ It is a concerted, stereospecific cycloaddition reaction, which can simultaneously establish two bonds and up to four stereogenic centers.¹⁷⁴ Diels-Alder reactions can be classified as “normal-electron-demand” or “inverse-electron-demand” according to the electron density of the dienes and dienophiles involved.⁹ Trienes are a versatile synthetic intermediate, and it is interesting that in different Diels-Alder reactions, they have been used as both dienes and dienophiles.¹⁷⁵⁻¹⁷⁷

1,3,5-Hexatriene and 2-methyl-1,3,5-hexatriene, Scheme 13, were found by Burshtein *et al.*¹⁷⁵ to behave as dienophiles in their respective reaction with hexachlorocyclopentadiene.



Scheme 13. This reaction is an example of where 1,3,5-hexatrienes act as a dienophile in Diels-Alder reactions, adapted from the work of Burshtein *et al.*¹⁷⁵

The group carried out quantum chemical calculations and found that the introduction of the chlorine atom onto the cyclopentadiene molecule lowers the HOMO and LUMO levels, indicating that hexachlorocyclopentadiene is much more reactive as a diene than the more common cyclopentadiene. In addition, they indicated that the reaction between hexachlorocyclopentadiene and each of the two 1,3,5-hexatrienes investigated are inverse electron-demand Diels-Alder reactions. These observations were supported by the later

work of Veliev *et al.*¹⁷⁷ who made the same experimental observations in their publication but added that, while 1,3,5-hexatriene and 2-methyl-1,3,5-hexatriene did react with hexachlorocyclopentadiene, they did not react with cyclopentadiene.¹⁷⁷

Polyenic electron-deficient alkenes also act as Michael acceptors and are of high synthetic interest.¹⁷⁸ They can undergo successive nucleophilic additions and therefore enable the generation of several new chiral centers. The main challenge associated with polyenic Michael acceptors lies within the regiocontrol of the nucleophilic attack.¹⁷⁸ Figure 34 depicts the various sites where nucleophilic attack could occur with a substrate containing the 1,3,5-hexatriene motif.

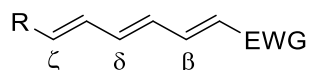
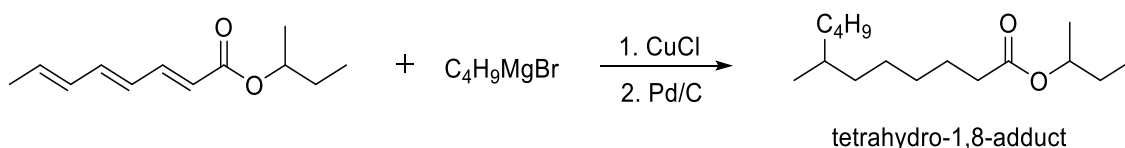


Figure 34. The structure of species containing the 1,3,5-hexatriene motif as an extended Michael acceptor with potential sites for nucleophilic attack highlighted.

1,8-Conjugate addition refers to nucleophilic addition at the ζ -carbon. Trienes have been investigated as substrates for this type of reaction. One such example is the copper-catalysed 1,8-conjugate addition involving *sec*-butyl octa-2,4,6-trienoate and the Grignard reagent butylmagnesium bromide, which was investigated as early as 1963 by Jacobsen *et al.*¹⁷⁹ The uncatalyzed reaction gave only a trace amount of simple conjugate addition product, whereas the use of copper(I) chloride as a catalyst increased the yield to 25% of exclusively 1,8-adduct, a butyloctadienoic ester (as opposed to the possible 1,4- or 1,6-adducts that could have been formed), Scheme 14.



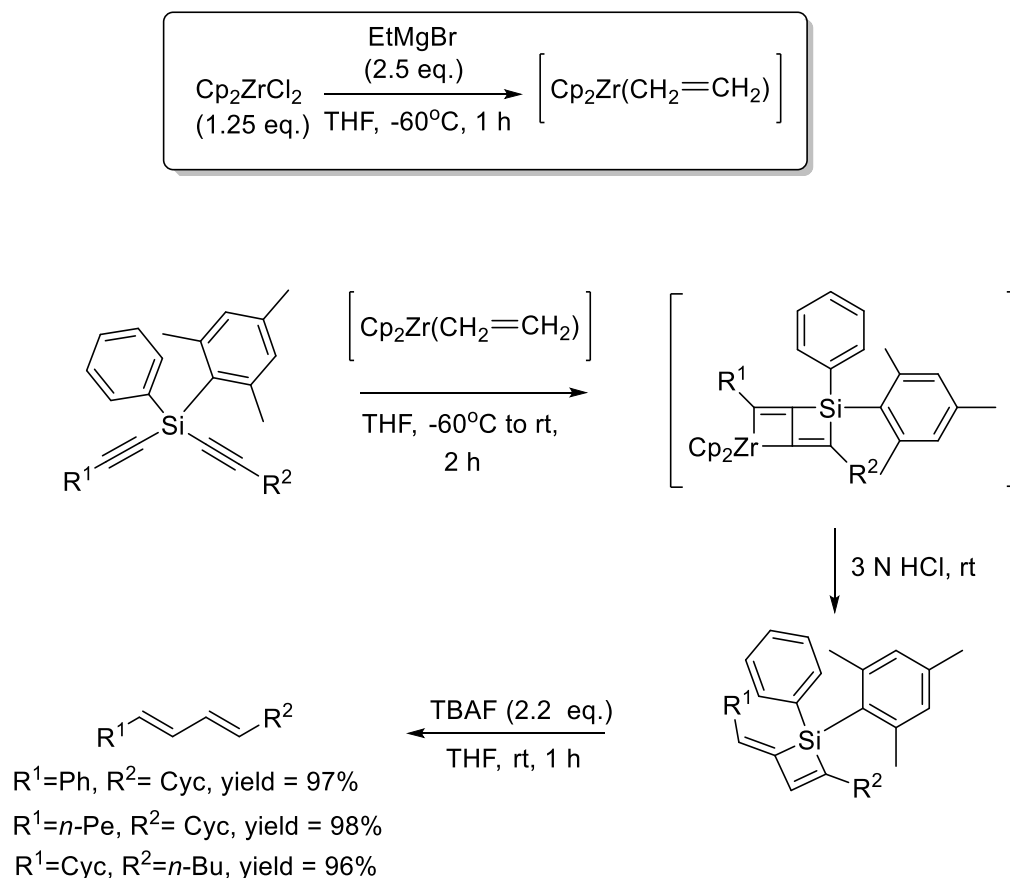
Scheme 14. The 1,8-conjugate addition involving *sec*-butyl octa-2,4,6-trienoate and butylmagnesium bromide, catalysed by copper(I), adapted from the work of Jacobsen *et al.*¹⁷⁹

2.1.2 Synthetic methodologies used to access trienes

Numerous methods have been used to access 1,3,5-hexatriene molecules and these synthetic methodologies can be broadly divided into those that incorporate a transition metal and those that do not.

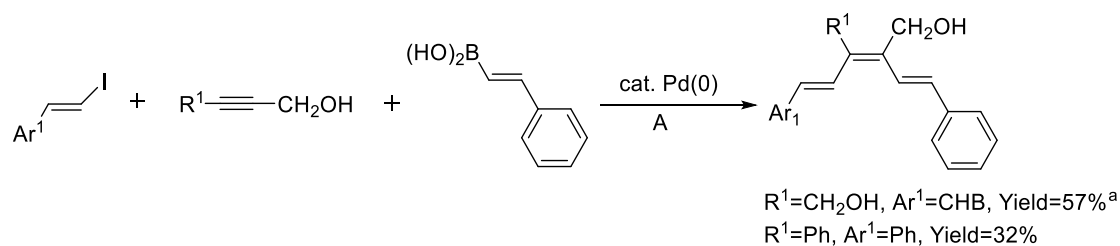
2.1.2.1 Synthetic strategies using transition metals to access 1,3,5-hexatrienes

Jin *et al.*¹⁸⁰ have developed a novel method for synthesizing unsymmetrical conjugated (*1E,3E*)-trienes that involves the reaction of different kinds of alkynyl-substituted dialkynyldiarylsilanes with an *in situ* generated zirconocene–ethylene complex $\text{Cp}_2\text{Zr}(\text{CH}_2=\text{CH}_2)$ (Takahashi reagent) to form silacyclobutenes. These silacyclobutenes are then reacted with tetrabutylammonium fluoride (TBAF) as shown in Scheme 15 to give 1,3,5-hexatrienes.



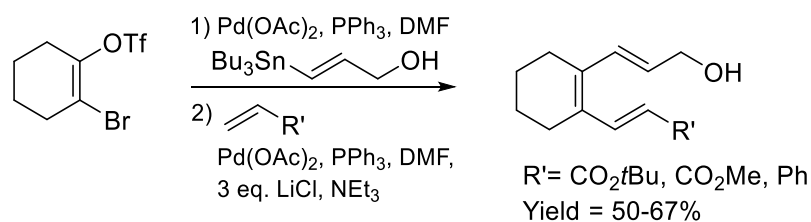
Scheme 15. Example trienes that have been made using the transition metal zirconium. Ph = phenyl, Cyc = cyclohexene, *n*-Pe = *n*-pentyl, *n*-Bu = *n*-butyl. Adapted from the work of Jin *et al.*¹⁸⁰

Zhang *et al.*¹⁸¹ have stereoselectively synthesized some tetra-substituted 1,3,5-hexatrienes using a one-pot, intermolecular, palladium-catalyzed Suzuki coupling of vinylic halides, internal alkynes, and vinylic boron organometallics, Scheme 16.



Scheme 16. Example trienes that have been made using the transition metal palladium. A: 1 equivalent of vinylic halide, 2 equivalents of internal alkyne, 2 equivalents of arylboronic acid, 5 mol % of PdCl₂, 2 equivalents of KF, and 5:1 DMF/H₂O as the solvent at 100 °C in the presence of air. ^a 57% was achieved when 6 equivalents of KF were employed. CHB = cyclohexylbenzene, Ph = phenyl. Adapted from the work of Zhang *et al.*¹⁸¹

Unsymmetrically 1,6-disubstituted 1,3,5-hexatrienes have been accessed by de Meijere *et al.*¹⁸² using a sequence of chemoselective Stille cross-coupling reactions. Here a 2-bromocycloalk-1-enyl triflate is coupled with an alkenylstannane and a subsequent Heck coupling on the resulting 2-bromo-1,3-butadiene gives the final triene, Scheme 17.^{182, 183}

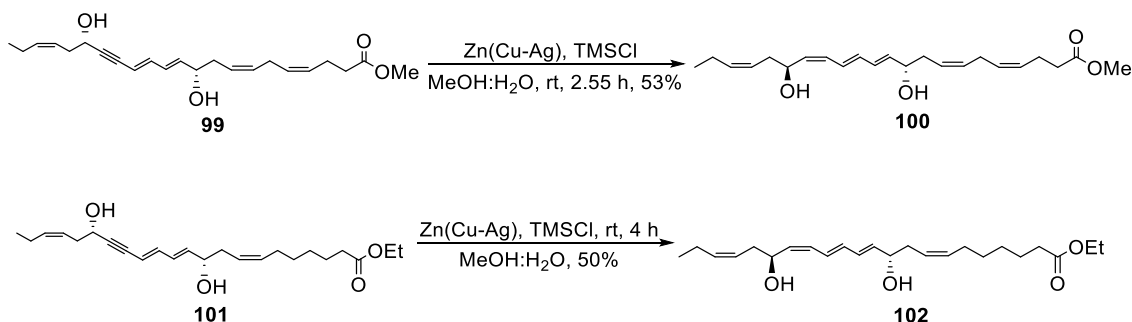


Scheme 17. Example trienes have been made using a sequence of Stille and Heck couplings via Palladium catalysis, adapted from the work of de Meijere *et al.*¹⁸²

This synthetic approach is desirable as it is chemoselective and can be achieved by a one-pot experimental set-up, once a fresh sample of the catalyst and triphenylphosphine (PPh₃) is added before the Heck reaction is initiated. A one-pot procedure is possible because the same active catalyst is present in both reactions, a 14-electron palladium(0) complex.¹⁸²

The Hansen methodology,¹⁸⁴ a modified Boland protocol,¹⁸⁵ is an example of hydrolysis of metallocyclopropene complexes using zinc, as categorized by Oger *et al.*¹⁸⁶ Activated zinc, in the presence of a solvent containing alcohol groups, reduces alkynes to *cis*-alkenes stereospecifically.¹⁸⁶ Boland *et al.* developed a Zn(Cu/Ag) system,¹⁸⁵ which, as of 2013, was the most used Zn(Cu) system, as according to the excellent review by Oger *et al.*¹⁸⁶ This is despite the catalyst being pyrophoric.¹⁸⁶ The protocol developed by Boland *et al.*¹⁸⁵ to stereospecifically reduce conjugated alkynes to *Z*-alkenes was then modified by Mohamed and Hansen,¹⁸⁴ who included 10 equivalents of trimethylsilyl chloride (TMSCl) together with copper/silver activated zinc in aqueous methanol. This modification improved the reaction rate as compared to that of the Boland protocol.¹⁸⁴

These reaction conditions were then employed by Dayaker *et al.*,¹⁸⁷ who termed this the Hansen procedure. Two examples of conjugated trienes synthesized by Dayaker *et al.*¹⁸⁷ is given in Scheme 18, each of which contains a conjugated *E,E,Z* triene subunit.

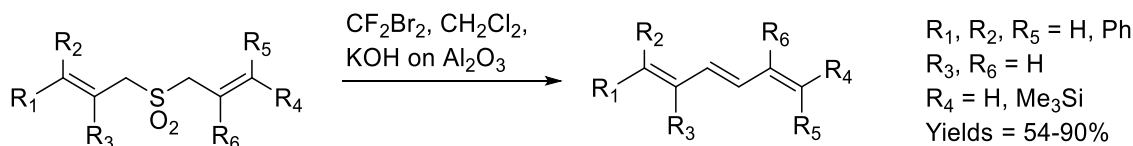


Scheme 18. Example trienes that have been made using a Zn (Ag/Cu) catalyst, adapted from the work of Dayaker *et al.*¹⁸⁷

The benefit of the Hansen procedure is the ability to chemoselectively reduce the triple bond in ynedienes **99** and **101** to the *cis*-double bond in **100** and **102** in the presence of the additional conjugated and isolated double bonds and avoid over-reduction.¹⁸⁷

2.1.2.2 Access to 1,3,5-hexatrienes using synthetic methodologies that do not incorporate transition metals

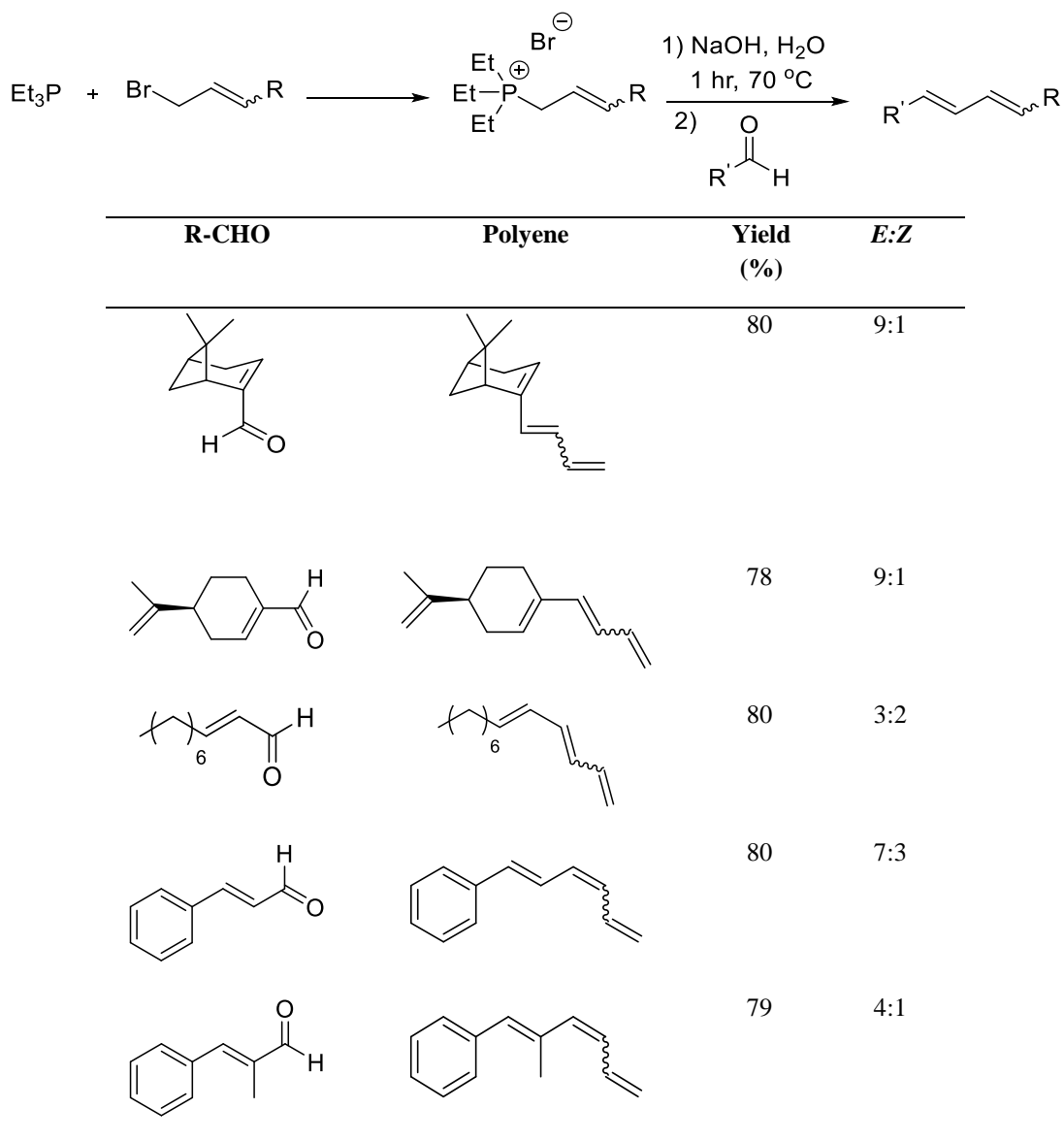
In 1994, Chan *et al.*¹⁸⁸ reported new conditions for the Ramberg-Bäcklund reaction,^{189,190} which is used to generate alkenes. These new conditions employed aluminium oxide-supported potassium hydroxide in the presence of dibromodifluoromethane and *tert*-butyl alcohol.¹⁸⁸ This allowed sulfones that possessed both α - and α' -hydrogens, regardless of structural types, to be uniformly converted into alkenes in good yields.¹⁸⁸ Using this modified Ramberg-Bäcklund reaction, Cao *et al.*¹⁹¹ have accessed a range of (*E,E,E*)-, (*Z,E,Z*)- and (*E,E,Z*)-conjugated 1,3,5-trienes, Scheme 19.



Scheme 19. Example trienes that have been made without the use of a transition metal catalyst. The geometry of the C=C bonds were different for each product. Adapted from the work of Cao *et al.*¹⁹¹

The Wittig reaction has been used by groups such as McNulty and Das,¹⁶⁴ to access 1,3,5-trienes, as well as 1,3-dienes. The proposed synthesis includes the first examples of an aqueous Wittig reaction of trialkyl-allylphosphonium salt-derived semi-stabilized ylides to produce a range of functionalized 1,3-dienes and 1,3,5-trienes in water using NaOH as

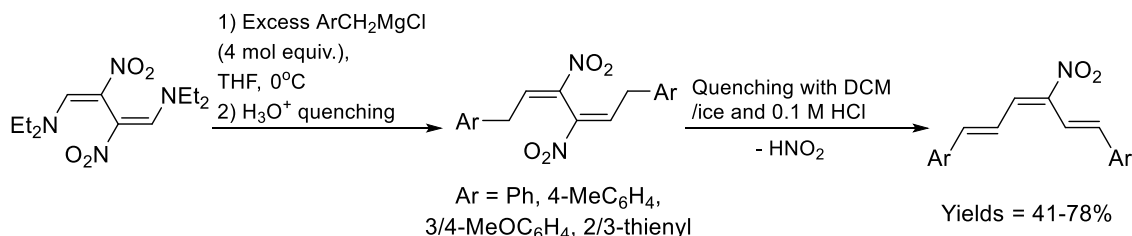
base. The use of α,β -unsaturated aldehydes facilitates access to the corresponding 1,3,5-trienes from a variety of aldehyde skeletons including monoterpeneoid, aliphatic, and aromatic derivatives. This synthetic methodology can incorporate a broad substrate scope with respect to the choice of aldehyde, with isolated yields of 78-80%, and *E*-stereoselectivity being observed,¹⁶⁴ Scheme 20.



Scheme 20. A summary of the aqueous Wittig reaction of ylides derived from triethylallylphosphonium bromide with a series of α,β -unsaturated aldehydes to form the corresponding 1,3,5-hexatrienes. Adapted from the work of McNulty and Das.¹⁶⁴

The use of Grignard reagents to access 1,3,5-hexatrienes has also been reported. Discovered by Victor Grignard at the University of Lyon in France in 1900,¹⁹² Grignard reagents are probably the most widely used organometallic reagents in light of their ease of preparation and their broad applications in organic and organometallic synthesis.¹⁹² Dell'Erba *et al.*¹⁹³ reported that good yields of (*E,E,E*)-1,6-diaryl-3-nitro-1,3,5-

hexatrienes were obtained from the reaction of 1,2-bis(diethylamino)-2,3-dinitro-1,3-butadiene and arylmethylmagnesium chloride, a benzyl Grignard reagent, in THF at 0 °C, Scheme 21.



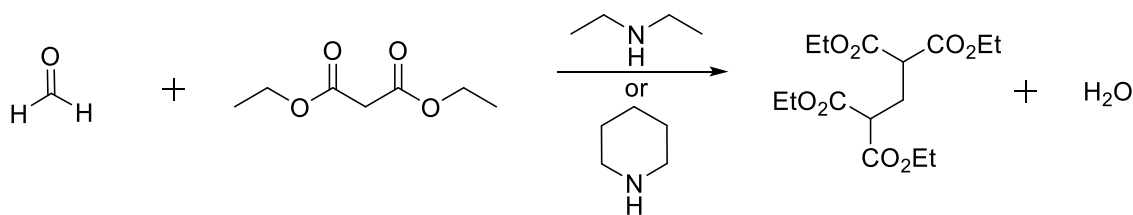
Scheme 21. Example reactions using Grignard reagents to access 1,3,5-hexatrienes. Adapted from the work of Dell’Erba et al.¹⁹³

2.1.3 Traditional Knoevenagel-condensation

The Knoevenagel-condensation is one of the most valuable reactions in organic chemistry for carbon–carbon bond formation,¹⁹⁴ especially those carrying one or two electron-withdrawing groups.¹⁹⁵ In a series of publications starting in 1894, Emil Knoevenagel found that primary and secondary amines, as well as their salts, catalyzed the aldol condensation of β -ketoesters or malonates with aldehydes or ketones.¹⁹⁶⁻¹⁹⁸ This became known as the Knoevenagel-condensation reaction, and thus, could be defined as the reaction between an aldehyde or ketone and any compound that possesses an active methylene group. The Knoevenagel-condensation can be catalyzed by an organic base,¹⁹⁹ such as piperidine,¹⁹⁴ or ammonia or their salts.¹⁹⁹ Since its original publication, there have been many reports of the Knoevenagel-condensation,¹⁹⁴ with numerous variations from the traditional Knoevenagel-condensation reaction conditions being reported. It is important to acknowledge that Knoevenagel’s seminal discovery and mechanistic interpretation of his reaction laid the foundation for the development of modern aminocatalysis,²⁰⁰ so a brief discussion of Knoevenagel’s work is included. However, more focus will be placed on examples of variations of the Knoevenagel-condensation reaction, or as they are hereby termed, ‘Knoevenagel-type’ condensations. Although these reactions deviate from the traditional reaction conditions employed by Knoevenagel, they still embody, at least in part, the mechanisms proposed by early work on this reaction and will be discussed in the subsequent section.

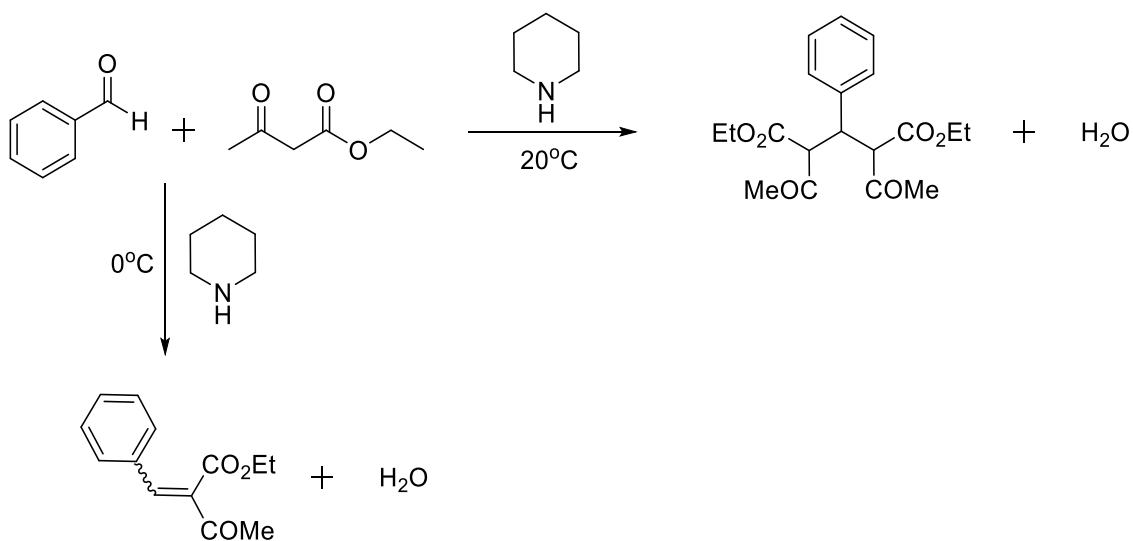
2.1.3.1 Emil Knoevenagel publications (1894-1898)

From 1894, Knoevenagel published several papers in this field in which he described the condensation of different species. In one such publication, he presents the condensation of formaldehyde with two equivalents of dimethyl malonate.¹⁹⁷ This reaction gave a bis-substituted product and was catalyzed by diethylamine or piperidine.¹⁹⁷



Scheme 22. Knoevenagel condensation reaction of formaldehyde with two equivalents of diethyl malonate, adapted from the work of Knoevenagel.¹⁹⁷

In his other publications, Knoevenagel showed that a number of other aldehydes, including benzaldehyde and acetaldehyde,¹⁹⁸ reacted with such activated methylene species diethyl malonate,²⁰¹ ethyl benzoylacetate,¹⁹⁸ ethyl benzoylpyruvate,¹⁹⁸ and acetylacetone^{198, 202} in a similar manner. They all formed bis-substituted products,¹⁹⁹ and were catalyzed by different primary and secondary amines, including those shown in Scheme 22, as well as dimethylamine and aniline.¹⁹⁸ In 1896, Knoevenagel showed that the condensation of benzaldehyde with ethyl acetoacetate gave the bis-substituted product when conducted at room temperature, whereas the same reaction conducted at 0°C gave benzylidene-1,3-dicarbonyl,^{196, 203} as per Scheme 23.

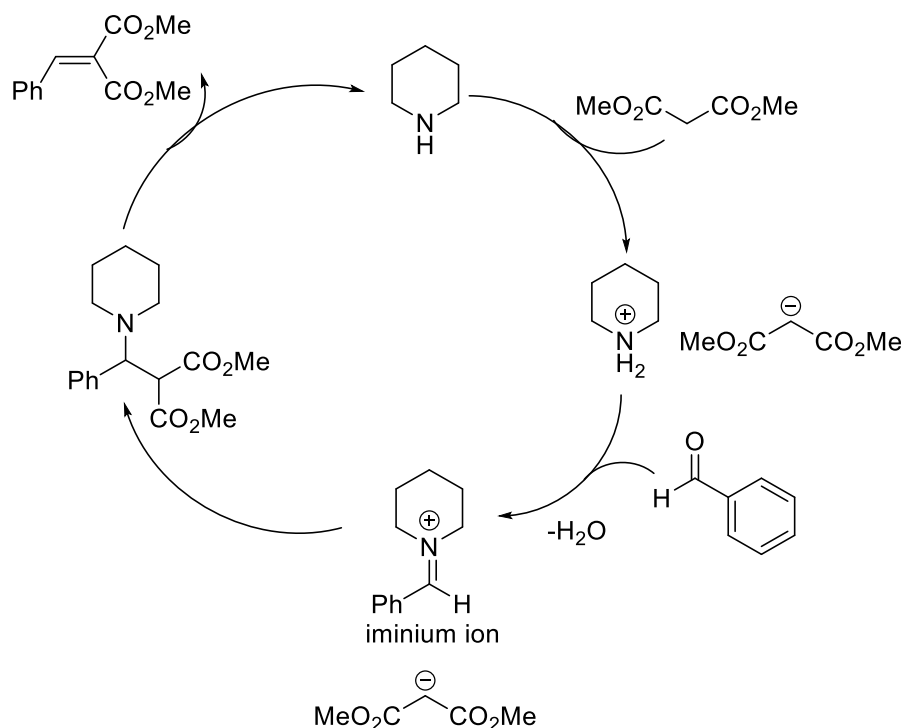


Scheme 23. Adapted from the work of Knoevenagel,¹⁹⁶ this reaction demonstrates how two different products could be obtained using the same reagents but at a different temperature.

This reaction was significant because its subsequent investigation exhibited the broad scope of this reaction.¹⁹⁹

Although Knoevenagel himself did not fully elucidate the mechanism of the condensation reaction, he did carry out mechanistic studies in which he attempted to obtain possible intermediates in the reaction.¹⁹⁹ Some of the intermediates he suggested were later

discovered to form part of the modern mechanism proposed for this reaction. This is represented as the following catalytic cycle, Scheme 24.^{200, 201, 204, 205}



Scheme 24. A modern catalytic cycle explaining the mechanism for a reaction conducted by Knoevenagel himself,¹⁹⁶ adapted from the work of List.²⁰⁰

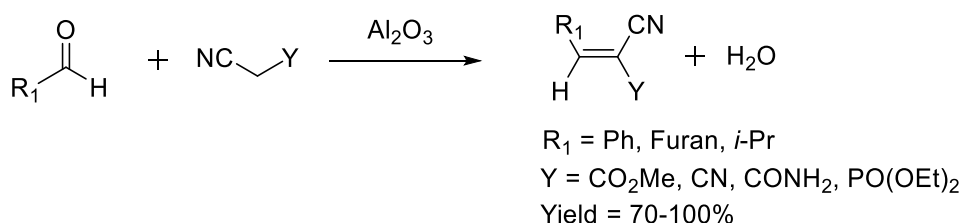
2.1.3.2 Limitations of the Knoevenagel-condensation

Although the Knoevenagel-condensation is often the method of choice for the preparation of α,β -unsaturated dicarbonyl and related compounds, and has several applications including the synthesis of natural and heterocyclic products, drugs and dyes for example,²⁰³ there are some limitations. For instance, with the traditional Knoevenagel-condensation, there are problems with the reactivity of ketones, where the competitive Michael addition can occur in the reaction of some active methylene compounds, leading to secondary products.²⁰³ There is also a problem with stereocontrol in the synthesis of Knoevenagel products from unsymmetrical 1,3-dicarbonyl compounds.²⁰³ This leads us on to discuss some modifications to the traditional Knoevenagel-condensation, where changes have been made to the nature of the base or the experimental set-up, for example. A few of these Knoevenagel-type condensation reactions will be highlighted in the next section.

2.1.4 Knoevenagel-type condensation

As early as the 1950s, modification of the traditional Knoevenagel-condensation reaction has been reported. These include minor changes, such as changing the nature of the base beyond the scope of what was traditionally defined as a catalyst for the Knoevenagel-condensation. One such example was the introduction of potassium fluoride as a catalyst for the Knoevenagel-condensation in 1958 by Midorikawa *et al.*²⁰⁶ In 1974, Lehnert²⁰⁷ introduced a mixture of titanium tetrachloride and a tertiary organic base,²⁰³ such as pyridine, using THF or dioxane as the solvent.²⁰⁷ Such procedures have been used since this time, and have been found to be more successful relative to the implementation of traditional Knoevenagel-condensation conditions.²⁰³ One such example where this is the case is the work of Courtheyn *et al.*²⁰⁸, in which a series of γ,γ -dichloro- α,β -unsaturated esters were formed from the condensation of 2,2-dichloro aldehydes with active methylene species in the presence of titanium-pyridine. In this same study, the use of piperidinium acetate as the catalyst, which would be considered a typical catalyst in Knoevenagel-condensation reactions, gave no reaction.²⁰⁸

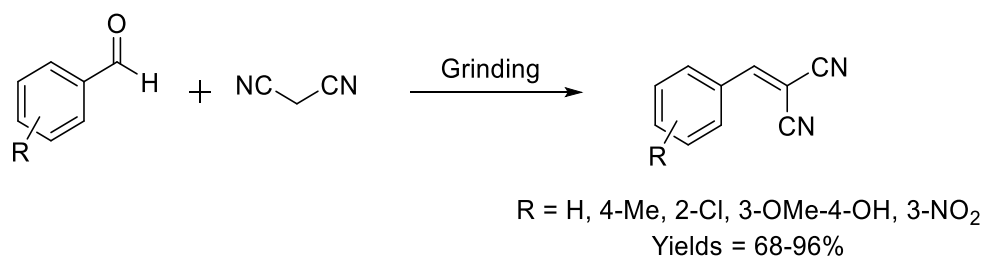
The use of inorganic solids and solid supports as catalysts in modifications of the Knoevenagel-condensation has gained popularity,²⁰³ since the introduction of dry alumina for this purpose in 1982.²⁰⁹ Texier-Boullet and Foucaud²⁰⁹ found that Knoevenagel condensations could be achieved in the presence of dry alumina using mild reaction conditions, generally the use of room temperature for 2-10 minutes. They did not use an organic solvent, the reagents were simply adsorbed onto the alumina. Specifically, the condensation of various aldehydes with active methylene species malononitrile, cyanoacetic esters, cyanoacetamide and cyanophosphonates was achieved,²⁰⁹ Scheme 25.



Scheme 25. Examples of Knoevenagel-condensation reactions carried out using aluminium oxide as the base/catalyst. Ph = phenyl, *i*-Pr = *isopropyl*. Adapted from the work of Texier-Boullet and Foucaud.²⁰⁹

The Knoevenagel-condensation reaction is still an active research area, particularly in the context of the development of environmentally friendly routes.¹⁹⁵ The development of more environmentally friendly synthetic methodologies has been receiving considerable attention because of growing worldwide concerns over chemical wastes and future resources, as well as growing requirements for green chemistry.^{210, 211} An example of a Knoevenagel-type condensation method that is more environmentally friendly than the traditional Knoevenagel-condensation is that developed by Ren *et al.*²¹¹ In their work, they report the condensation of several aldehydes with malononitrile by means of

grinding the two reagents together at room temperature, in the absence of both solvents and catalysts, Scheme 26.



Scheme 26. Examples exhibiting the development of an environmentally friendly Knoevenagel-condensation procedure, adapted from the work of Ren *et al.*²¹¹

Thus, the Knoevenagel-condensation has been modified to very different extents since its discovery but is still an active research area facilitating access to numerous products.

2.1.5 Aluminium oxide (alumina) as a catalyst

The performance of reactions on the surface of solids not only eliminates the necessity of solvents but can offer significant advantages, such as shorter reaction times and/or the generation of higher yields in comparison to the same reaction carried out in solution.²¹² Organic reactions have been carried out on the surfaces of many solids, one notable example of which is alumina.²¹² The term alumina refers to a series of ionic solids which have the formula $Al_2O_3 \cdot (H_2O)_n$, where $n = 0, 1, 2$ or 3 .²¹² Several polymorphs of alumina exist, such as γ -, η -, χ -, δ -, θ -, κ -, and α - Al_2O_3 , all of which possess different characteristics including the amount and nature of impurities, specific surface area, pore volume and pore-size distribution. The different characteristics of each polymorph is determined by their individual structure and morphology, which, in turn, is affected by the preparation conditions.²¹³ One example of these conditions is activation temperature, where different temperatures lead to the formation of different aluminas. For example, by heating the reagents used to access alumina above 1100 °C, an “endpoint” is reached, which is a type of alumina called corundum,²¹² or α - Al_2O_3 , which is the densest form of alumina.²¹⁴ The other aluminas which are formed at temperatures lower than 1100 °C are referred to as “transition aluminas”, as they are made in the transition between aluminium hydroxides and corundum.²¹⁴

Alumina can be used as a catalyst, support and reagent,²¹² and this it makes it a very versatile substance. Notably, alumina is a bifunctional catalyst, and is reported to contain both acidic and basic sites.²¹⁵ It is the chemical nature of the surface of aluminium oxide that is mainly responsible for its multiple purposes, such as its adsorption and catalytic properties.²¹³ Assuming that there are three dominant species on the surface of aluminium oxide, ^-OH , O^{2-} and Al^{3+} , whose concentrations are interdependent and controlled by the

activation temperature, then, on this basis, the surface can exhibit a variety of properties.²¹² ^{-}OH can act as a base and possibly a nucleophile, O^{2-} should be a strong base and nucleophile, and Al^{3+} is a Lewis acid.²¹² Since the ions that make up the surface of alumina are immobile at the temperatures typically used to carry out organic reactions, an activated solid will possess strongly basic and acidic sites adjacent to each other, something which is not possible to achieve in a liquid solution.²¹² These adjacent sites may act cooperatively in such reactions.²¹² In addition to serving catalytic roles, the surface components may also serve as reagents, donating species such as hydrogen, hydroxyl, oxide, or water.²¹²

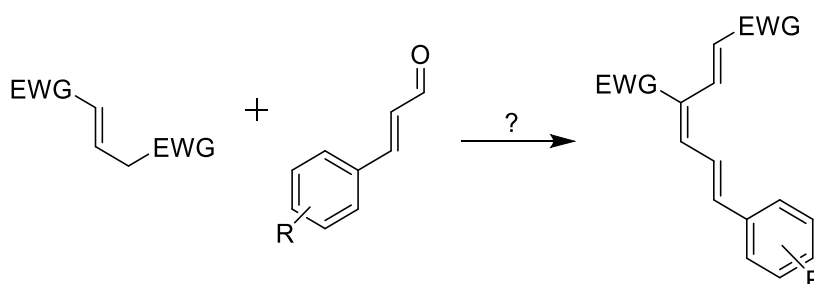
It is important to note that, because reactions occur on the surface of alumina, chemical modifications to its surface can lead to big fluctuations in its catalytic properties.²¹⁴ These modifications can be unintentional, caused by the contamination of an alumina surface with sodium ions that turn alumina into a less acidic catalyst,²¹⁴ for example. Otherwise, they may be intentional, in which alumina is doped with an inorganic entity, such as the doping of an alumina surface with a small amount of silicon (Si^{4+}) or chloride (Cl^{-}) ions, which significantly increases its acidity.²¹⁴

The above examples and discussion show that not only is aluminium oxide an effective amphoteric catalyst but, because of the diverse nature of its surface, can serve a multitude of other purposes.

2.1.6 Aims of triene synthesis.

The aims of this part of the PhD project include:

- (i) To investigate the Knoevenagel condensation as a method to access a bis(phenylsulfonyl) triene.
- (ii) To establish improved reaction conditions for this Knoevenagel approach and to use this method to synthesize a family of novel bis(phenylsulfonyl) trienes.
- (iii) To explore the substrate scope of the developed methodology through variation of the propene electron withdrawing groups and variation of the cinnamaldehyde, Scheme 27.
- (iv) To complete full structural characterization of all novel products using NMR spectroscopy, LCMS, HRMS, and IR spectroscopy.

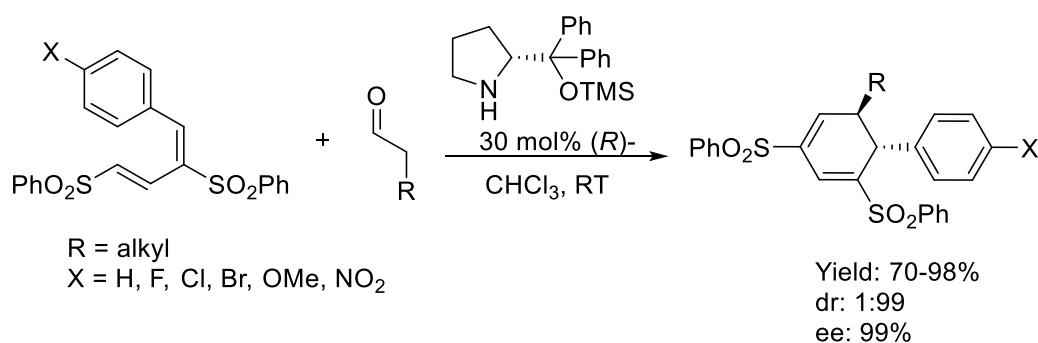


Scheme 27. General scheme for the synthesis of 1,3,5-hexatrienes. EWG = electron withdrawing group

2.2 Results and Discussion

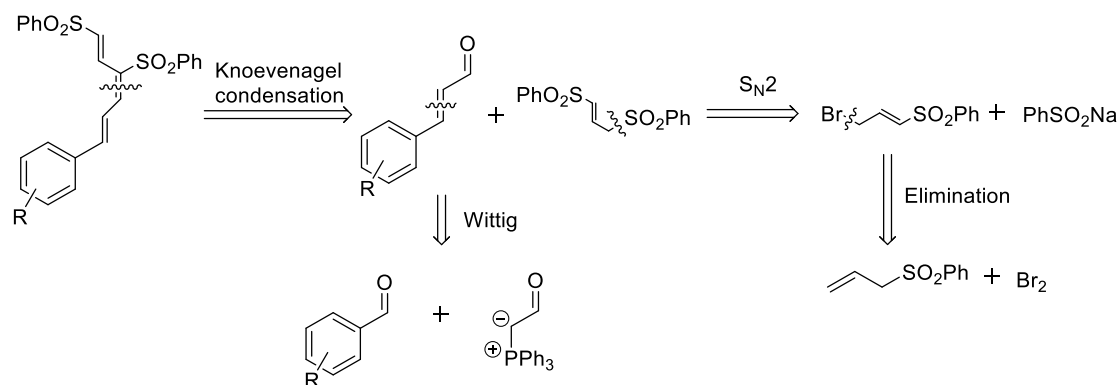
2.2.1 Synthesis of 1,3,5-hexatrienes

Extended conjugated systems are of significant interest to organic chemists and the last few years has seen major advancements in the development of organic conjugated molecules.²¹⁶ Not only has this led to the development of novel π -conjugated systems, but also in their application as part of organic electronic devices. For example, organic light emitting diodes (OLEDs) and organic photodetectors (OTDs) are reported to have applications in electroluminescent devices,²¹⁷ night vision,²¹⁸ photo and video imaging,²¹⁸ and biosensing.²¹⁸ The Stephens group at Maynooth University is interested in the development and application of such conjugated systems. Previously in our laboratory, various electron poor conjugated butadiene systems were synthesized, including 1,3-bis-(sulfonyl)butadienes and 1,3-bis(alkyl carboxylate)butadienes, and applied in an organocatalysed annulation that allowed access to chiral polysubstituted cyclohexa-1,3-dienes in high yield and high enantio- and diastereoselectivity, Scheme 28.^{219, 220}



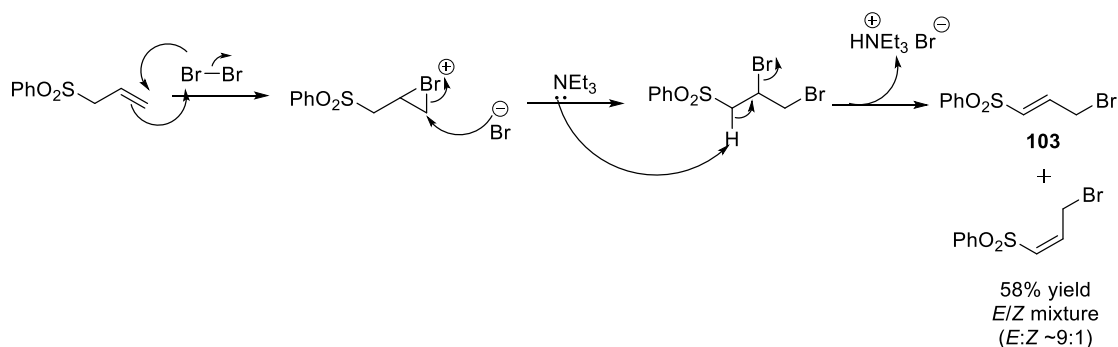
Scheme 28. Adapted from Murphy *et al.*²¹⁹, organocatalysed annulation of electron poor butadienes.

The ability to synthesize heavily functionalized polyenes is highly desirable in organic chemistry,¹⁶⁴ and building on previous findings within the group, we wanted to develop a synthetic route to 1,3,5-hexatriene systems. 1,3,5-Hexatrienes have found application in multiple fields including as motifs in medicinal products and as synthetic substrates in reactions such as Diels-Alder and 1,8-conjugate additions, as discussed in sections 2.1.1.1 and 2.1.1.2 of the introduction, respectively. Using retrosynthetic analysis, as shown in Scheme 29, we envisioned accessing the desired hexatrienes by reacting a bis-phenylsulfonyl propene with functionalized cinnamaldehydes using a Knoevenagel-type condensation. The family of cinnamaldehydes could be accessed via Wittig chemistry and the bis-phenylsulfonyl propene via a combination of S_N2 chemistry and an elimination reaction, Scheme 29. This approach would also allow access to hexatrienes with electron withdrawing groups other than sulfones through the generation of other propenes, such as ester propenes and cyano propenes.



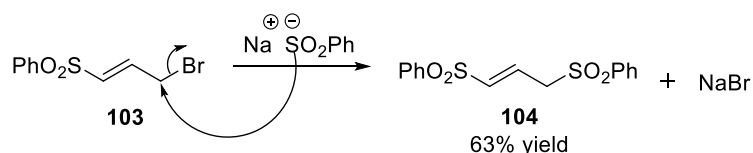
Scheme 29. Retrosynthetic analysis leading to the desired 1,3,5-hexatriene.

We first needed to access the precursor molecules, namely the (*E*)-3-bromo-1-phenylsulfonylprop-1-ene, **103**, which was subsequently used to synthesize (*E*)-1,3-bis-phenylsulfonylprop-1-ene, **104**. The synthesis of **103** first required the treatment of allyl phenylsulfone with elemental bromine and subsequently, a selective elimination (*E*2) of the secondary halide using triethylamine, Scheme 30. The reaction was performed on 29 mmol scale using allyl phenylsulfone (1 equivalent), elemental bromine (1.1 equivalents) in DCM (98 mL), at room temperature for 4 hours. Following this, the intermediate dibromide was isolated, dissolved in chloroform (98 mL), treated dropwise with triethylamine (1 equivalent) at 0 °C, stirred for 5 minutes on ice and then for ~15 minutes on removal of the ice (until the solution returned to room temperature). This gave a crude mixture of isomers. Crystallization of this crude mixture gave the *E* isomer exclusively.



Scheme 30. Proposed mechanism for the generation of **103**

103 was then reacted with the sodium salt of benzenesulfonic acid in a S_N2 reaction to generate **104**, Scheme 31. The reaction was performed on 7.5 mmol scale using **103** (1 eq.) and benzenesulfonic acid sodium salt (2.3 eq.) in methanol (22.5 mL) at reflux for 1.5 hours. Crystallization gave the product as a single *E*-isomer.



Scheme 31. Proposed mechanism for the generation of **104**.

With these precursor molecules in hand, we were able to focus on the development and application of a Knoevenagel-type condensation in order to access a series of novel 1,3,5-hexatrienes. To do this, we wanted to undertake a study to optimize reaction conditions and explore the use of different solvents, bases, and temperatures. To do this efficiently, we developed a quantitative NMR spectroscopic method to estimate reaction yield and the synthesis of (1*E*,3*E*,5*E*)-1,3-bis-phenylsulfonyl-6-phenyl-hexa-1,3,5-triene, **105**, Figure 35, was chosen as the model reaction.

The geometry of the final triene product was elucidated by an x-ray crystal structure obtained by a previous group member of the Stephens group,²²⁶ Figure 35, in collaboration with Prof. Patrick McArdles' group in the National University of Ireland, Galway.²²⁷ In addition, analysis of the NMR spectra of this compound confirmed the geometry assigned by examination of splitting of signals and accompanying *J* values. The analysis of the relevant spectra of a representative triene is included later in section 2.2.5.1.

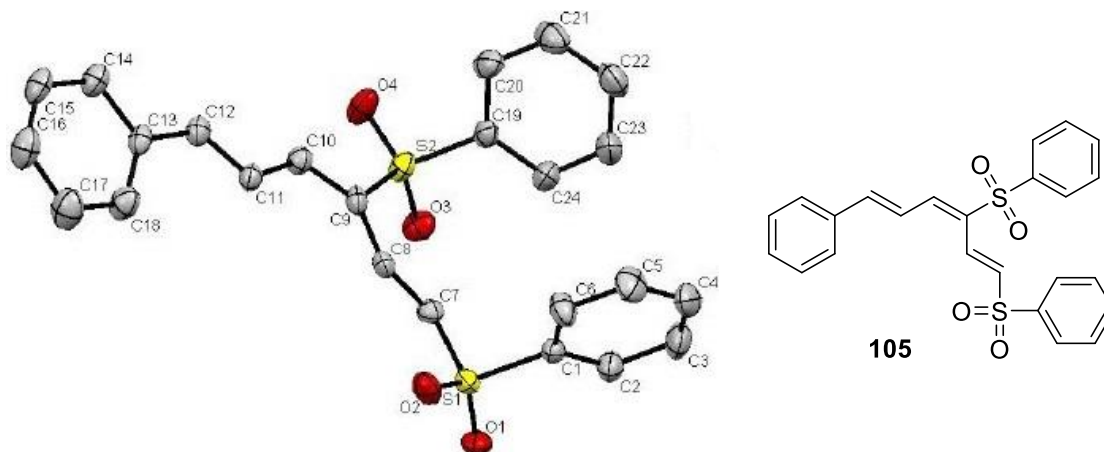


Figure 37. X-ray crystal structure of **105**,²²⁶ confirming (*E,E,E*) geometry assignment.

On the basis of X-ray crystal structures and/or information obtained from NMR spectra, the (*E,E,E*) geometry has been assigned for all 1,3,5-hexatrienes synthesized.

2.2.2 (1E,3E,5E)-1,3-Bis-phenylsulfonyl-6-phenyl-hexa-1,3,5-triene yield estimation using quantitative NMR (qNMR)

Quantitative NMR (qNMR) was employed as part of an investigation to find the optimal reaction conditions for the synthesis of (1E,3E,5E)-1,3-bis-phenylsulfonyl-6-phenyl-hexa-1,3,5-triene, **105**. Proton NMR spectroscopy was first reported as a tool for quantitative analysis in 1963 by Jungnickel and Forbes.²²¹ This group used qNMR to determine the apparent percentages of total hydrogen content in 26 pure compounds by integrating non-equivalent groups of protons. The relative standard deviation from theoretical values for the means of three determinations of each of the 26 compounds, including aniline, ethanol and pyrrolidine, was 0.3%, demonstrating that accurate quantitative analysis could be done using this method.²²¹ In the same year, Hollis²²² analyzed several known and some commercial samples of aspirin, phenacetine, and caffeine using qNMR and determined that the average deviations from the correct results were 1.1%, 2.2%, and 3.2% respectively.²²²

There has been growing interest in qNMR in the past three decades.²²³ For example, its use has grown significantly in metabolomics as it provides absolute and relative quantification of several metabolites in biological samples without requiring the separation of individual components.²²³ Thus, it has found applications in such areas as environmental toxicity, drug toxicity, cancer metabolism, drug metabolism, and investigations of cell-virus interactions.²²³ Compared to the traditional chromatographic methods that are still favoured in routine quantitative analyses, qNMR has certain advantages including the facile sample preparation, relatively short measurement times, the non-destructive nature of the method, and the lack of need to isolate the analyte present in a mixture prior to analysis.²²⁴ In addition, the uncertainty in quantification measurement by NMR spectroscopy is low,²²⁴ less than 2.0%,²²³ which is an acceptable limit for precise, accurate quantification.²²³

The basic principle which permits the use of NMR spectroscopy as a quantitative measure of a particular substance is that peak areas are proportional to the number of corresponding nuclei giving rise to the signals.²²⁴ Thus, it is a primary ratio method of measurement.²²⁴ In qNMR a reference standard of the analyte is not needed, the quantification may be performed using an internal standard.²²⁴ Various internal standards have been used in qNMR, including 3,4,5-trichloropyridine, 1,4-dinitrobenzene, and 2,3,5-triiodobenzoic acid and are usually co-dissolved with the analyte.²²⁴ To obtain an accurate analysis of results, the analyte and internal standard peaks should not interfere with each other's signals.²²⁵ 1,3,5-Trimethoxybenzene was chosen as an internal standard for this qNMR study because it is soluble in deuterated chloroform, thus could be co-dissolved with the triene analyte, and also because its proton signals do not overlap with any of those from the triene. There are two characteristic signals for 1,3,5-trimethoxybenzene, a singlet at 6.08 ppm (3H, the aromatic protons) and another singlet at 3.78 ppm (9H, the methoxy protons). As such, if a known concentration of the internal

standard is made, either of these signals can be used to quantify the protons causing a signal in the analyte (the triene) by comparing the integral ratio of protons. Hence, the unknown concentration can be deduced if you know the actual number of protons that the analyte signal should represent. This is known as relative quantitation and means that the molar ratio M_X/M_Y between two compounds X and Y can be calculated through the use of the following expression, Figure 36.

$$\frac{M_x}{M_y} = \frac{I_x}{I_y} \cdot \frac{N_y}{N_x}$$

Figure 36. Taken from Bharti and Roy,²²³ this expression was used to solve for the concentration of triene, and therefore, percentage conversion to triene, achieved in our qNMR studies. I is the integral observed, N is the number of nuclei giving rise to the signal, M_x/M_y is the molar ratio of compound X to compound Y.

Essentially, the signals of interest were integrated, normalized for the number of protons, and a simple ratio analysis was performed. In our experiments, the analyte was a crude reaction mixture generated from reacting *trans*-cinnamaldehyde, **1** (1.1 mmol), (*E*)-1,3-bis(phenylsulfonyl)prop-1-ene, **104** (1 mmol), and base in a given solvent at a specified temperature for a specified time. In the ¹H NMR spectrum of pure **105**, one finds a multiplet integrating to 1H at 7.67-7.63 ppm. It was chosen as the triene signal to use in the comparative ratio with the 9 methoxy protons of the 1,3,5-trimethoxybenzene internal standard (3.77 ppm).

We tested the efficiency of this process for the purposes of relative quantitation by making up a known concentration of pure triene **105** (90 mM) and using the internal standard to approximate the conversion of starting materials to desired triene **105**. Both solutions were made up to 10 mL volumes using deuterated chloroform as the solvent and then 500 μL of each solution was transferred to an NMR tube for analysis. Knowing that the internal standard concentration was 10 mM before addition to the NMR tube, and using the ¹H NMR spectrum generated from the NMR sample containing pure **105** and the internal standard, Figure 36, we calculated that a 88% conversion to **105** had been achieved, corresponding to a 88.24 mM solution of the triene. The calculation of this will be explained in the following.

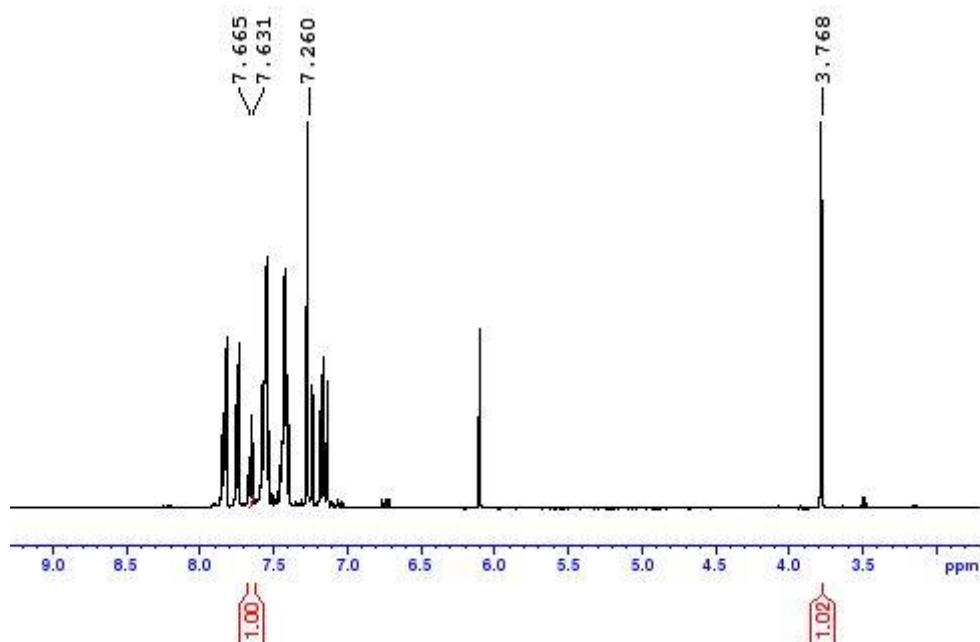


Figure 37. ^1H NMR spectrum of crude mixture containing a known concentration of (1*E*,3*E*,5*E*)-1,3-bis phenylsulfonyl-6-phenyl-hexa-1,3,5-triene, **105**, and internal standard 1,3,5-trimethoxybenzene.

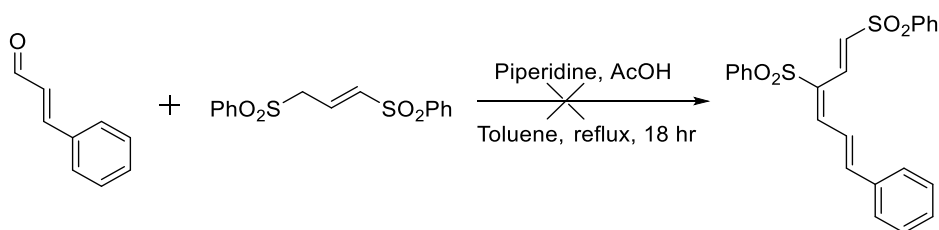
Referring to the equation previously given as Figure 35, in this case and in all future cases compound X refers to triene **105** and compound Y refers to the internal standard. I_x is 1 and I_y is 1.02 as observed in the ^1H NMR spectrum above, Figure 36. N_y is 9 as we know there are 9 protons that make up the compound Y signal appearing at 3.77 ppm. N_x is 1 as we know there is 1 proton that makes up the compound X signal appearing at 7.66-7.63 ppm. While a 10 mM solution of compound Y was made up to a 10 mL volume, 500 μL of this solution was transferred to an NMR tube containing 500 μL of a solution of compound X. Thus, the final concentration of compound Y in the NMR tube is half of its original concentration, as the volume of deuterated chloroform has been doubled from 500 μL to 1 mL. This means $(M_x/5) = (1/1.02) \cdot (9/1)$, and therefore $M_x = 44.12$ mM where M_x is the calculated concentration of triene **105** in the NMR tube. However, as this concentration has been diluted by a factor of two relative to that made up to 10 mL (due to the addition of 500 μL of each solution X and Y to the NMR tube, made up in the same solvent), the true concentration of solution X in the 10 mL volumetric flask would be double with respect to that in the NMR tube so $44.11765 \times 2 = 88.24$ mM. This compared favourably with the actual known concentration of 90 mM. This inferred an error of 1.96 %, which we deemed sufficiently accurate to implement the qNMR technique for relative quantitation assessment.

Given that 1 mmol is the moles of the limiting reagent (**104**) and the molecular weight of the triene **105** is 436.5432 g/mol, we can calculate a theoretical 100% conversion for this reaction to be equivalent to 437 mg of **105** and would correspond to the generation of a

100.11 mM solution. In a 88.24 mM solution of **105**, the mass corresponds to 385 mg (in 10 mL) and therefore a 88% conversion is achieved.

2.2.2.1 Effect of base on the synthesis of (1*E*,3*E*,5*E*)-1,3-bis-phenylsulfonyl-6-phenyl-hexa-1,3,5-triene **105**

Many versions of the Knoevenagel condensation reaction have been described with piperidine having been reported as base in many cases.¹⁹⁴ Thus, we first attempted a Knoevenagel condensation reaction whereby *trans*-cinnamaldehyde, **1** (1.1 mmol) and (*E*)-1,3-bis(phenylsulfonyl)prop-1-ene, **104** (1 mmol) were dissolved in toluene (10 mL) to which piperidine and acetic acid (1 equivalent of each) were added and the mixture allowed to reflux for 18 hours, Scheme 32.



Scheme 32. Unsuccessful attempted triene **105** synthesis using traditional Knoevenagel condensation reaction conditions.

Evidence of conversion to triene **105** was not detected. A complex crude mixture was obtained with uninterpretable NMR spectra and hence qNMR could not be used. To ensure that there was no trace amount of triene in this complex mixture we undertook a purification process using column chromatography. No triene product was obtained and piperidine was excluded as a possible choice of base.

A previous group member arrived at the same conclusion and explored the literature for an alternative base.²²⁶ There are reports in the literature from some groups where they have used aluminium oxide (Al₂O₃) as a base in the reaction of carbonyl-containing compounds with activated methylene compounds.^{209, 228, 229} As discussed previously in section 2.1.5, it was then hypothesized that Al₂O₃ was a suitable base for our reaction. We then tried this base as part of our reaction optimization study. Here we used **1** (1.1 mmol) and **104** (1 mmol) dissolved in DCM (10 mL) using 15 equivalents of Al₂O₃ as a base and found it successfully produced the desired triene (compound **105**) in a quantitative conversion (by qNMR, corresponding to the generation of a 105.88 mM solution). Since the crude mixture generated a sufficiently clean ¹H NMR spectrum in which both the triene signal and internal standard signal could be integrated and therefore compared, a qNMR estimation of the yield was possible using the information obtained from the ¹H spectrum found in Appendix 2, Figure A96.

Briefly, the calculation of the yield can be explained as follows. Referring to the equation previously given as Figure 35, compound X refers to triene **105** and compound Y refers to the internal standard. I_x was found to be 1 and I_y was 0.85, Appendix 2 Figure A96. N_y is 9 and N_x is 1. The 10 mM of compound Y is diluted by a factor of 2 when added to the NMR tube (i.e. 5 mM), so $(M_x/5) = (1/0.85).(9/1)$, and therefore $M_x = 52.94$ mM. This is the concentration of **105** in the NMR tube, made up in 500 μ L of deuterated chloroform. However, as per section 2.2.2, the concentration of this solution was diluted by a factor of two, relative to the solution of **105** made up in the 10 mL volumetric flask, because the NMR tube contained an additional 500 μ L deuterated chloroform from solution Y. Therefore, the true concentration, M_x , is $52.94 \times 2 = 105.88$ mM. Full experimental details can be found in Section 2.4.3 of the Experimental Procedure. Given that 1 mmol is the moles of the limiting reagent and the molecular weight of the triene is 436.5432 g/mol, then we can calculate a theoretical 100% conversion for this reaction to be equivalent to 437 mg, corresponding to a 100.11 mM solution. In a 105.88 mM solution, the mass corresponds to 462 mg and therefore a quantitative conversion is achieved. By this calculation, however, over 100% conversion was obtained, something that can be explained by crude nature of the product, therefore having some impurities which are later removed when the product is recrystallized. In addition, there is roughly a 2% error associated with this method, as calculated previously.

Therefore, Al_2O_3 was found to be a suitable base for this reaction and was used in all further reactions for triene synthesis.

2.2.2.2 Effect of solvent on the synthesis of (1E,3E,5E)-1,3-bis-phenylsulfonyl-6-phenyl-hexa-1,3,5-triene **105**

The next variable investigated was the choice of solvent. DCM, methanol, acetonitrile, and toluene were all investigated using the same experimental set up and reaction time. qNMR was used to estimate the percentage conversion achieved from the use of each solvent, and the spectra obtained can be found in Appendix 2, Figures A97-A99. As DCM was used in the reaction described above (section 2.2.2.1), the result is the same i.e. a quantitative conversion to triene corresponding to a 105.88 mM solution of **105** was generated when DCM was used as the solvent. By applying the same reaction conditions, but replacing 10 mL DCM with toluene, and performing the calculations above, a 62% conversion (or 61.22 mM solution) was obtained. Using methanol as the solvent gave a 66% conversion (or 65.7 mM solution), whereas the use of acetonitrile resulted in a 43% conversion (or 42.46 mM solution). Thus, DCM was chosen as the preferred solvent and used when varying the remaining reaction conditions.

2.2.2.3 Effect of base equivalents on the synthesis of (1E,3E,5E)-1,3-bis-phenylsulfonyl-6-phenyl-hexa-1,3,5-triene **105**

After finding the preferred base and solvent, we next investigated whether changing the equivalents of base would increase the percentage conversion to triene. We compared the reaction carried out using 30, 15, 5 and 1 equivalent of Al₂O₃. qNMR was used to estimate percentage conversion and the NMR spectra can be found in Appendix 2, Figures A96, A100-102. As 15 equivalents of Al₂O₃ was used in the reaction described in section 2.2.2.1, a quantitative conversion corresponding to a 105.88 mM solution of **105** was generated in this case. When 30 equivalents of Al₂O₃ was used, a 59% conversion corresponding to a 59.22 mM solution of **105** was generated. When 5 equivalents were used, a 96% conversion corresponding to a 95.74 mM solution was obtained. Unfortunately, when 1 equivalent of Al₂O₃ was employed, there was overlap between the triene proton signal and that of the propene starting material, where a lot of unreacted material was evident in the ¹H NMR. As such, it was not possible to accurately integrate the triene signal, so qNMR could not be employed in this case. Given the large amount of starting material present in the spectrum, which is not visible to the same extent when any of the other conditions were investigated, it is likely that triene formation was low and so, not a viable condition to employ in future reactions.

Thus, 15 equivalents of Al₂O₃ was chosen as the preferred equivalents of base to be used in future reactions.

2.2.2.4 Effect of temperature on the synthesis of (1*E*,3*E*,5*E*)-1,3-bis-phenylsulfonyl-6-phenyl-hexa-1,3,5-triene **105**

Finally, we investigated whether an increase in temperature would affect the yield. The reaction carried out at room temperature was compared to that carried out at the reflux temperature of DCM (~40 °C). qNMR was again used to estimate the percentage conversion to triene and the corresponding NMR spectra can be found in Appendix 2, Figures A96 and A103. The reaction which resulted in quantitative conversion to triene was performed at 20 °C (section 2.2.2.1) and so, the percentage conversion achieved, when reflux temperature was applied, was compared to this. We found that the higher temperature was less effective in producing the triene, giving a 25.72 mM solution corresponding to a 26% conversion. A complex mixture of alternative side products was also formed, as evident from the analysis of the ¹H NMR spectrum of the crude mixture, Appendix 2, Figure A103. Thus, 20 °C was employed for future reactions.

In conclusion, there were four variables investigated in this optimization study, as summarized by Table 16. When an appropriate internal standard is chosen, qNMR represents a convenient method for relative quantitative assessment, which suited the goal of this optimization study. As *I_y* is the only variable that changes in the equation, given previously as Figure 35, and it can be obtained by examining the relevant ¹H NMR spectra, the molar ratio of internal standard to **105** can be easily determined. This allows for an accurate assessment of the effect of systematically varying reaction conditions on

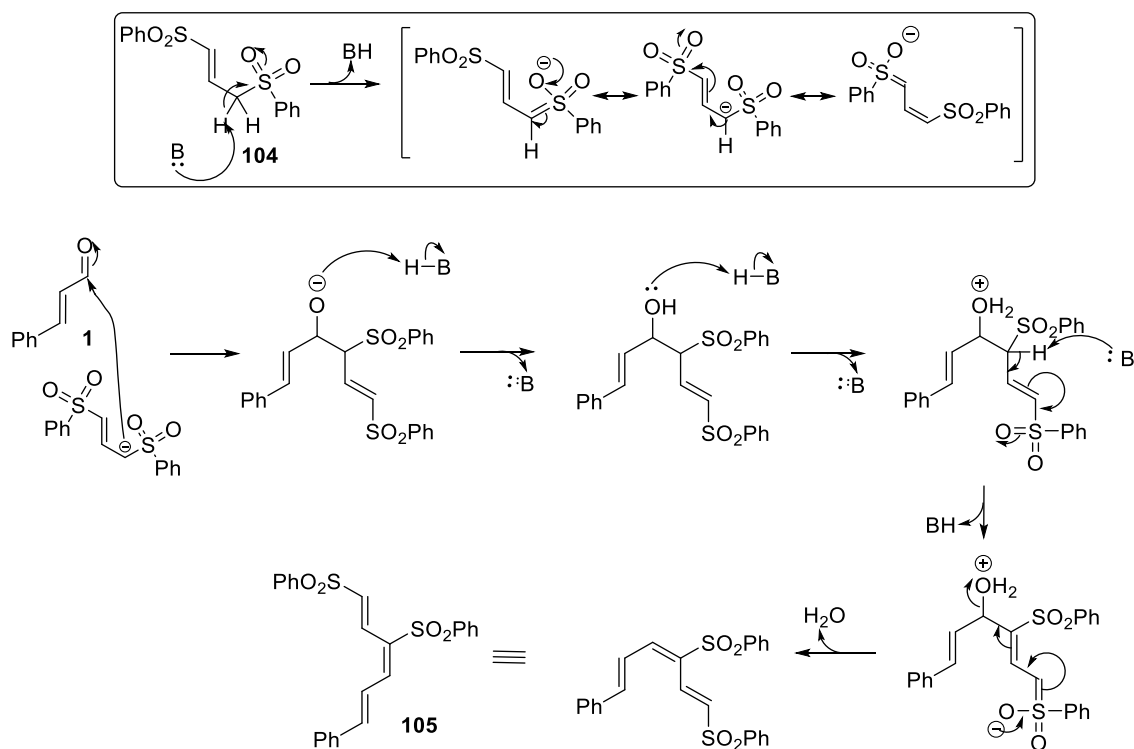
the percentage conversion to product. Based on our implementation of qNMR, we have found that the preferred conditions for our Knoevenagel-type condensation reaction are the use of DCM as the solvent with 15 equivalents of Al₂O₃ as base, and the reaction being allowed to take place over 24 hours at 20 °C. Therefore, we have established these conditions as the standard conditions to be implemented in our synthetic protocol.

Table 16. Variables explored in this optimization study

Solvent	Temperature	Base	Equivalents of base (Al ₂ O ₃)
Dichloromethane	20°C	Al ₂ O ₃	30
Methanol	Reflux	Piperidine	15
Acetonitrile			5
Toluene			1

2.2.3 Knoevenagel-type condensation reaction mechanism

The formation of *(1E,3E,5E)*-1,3-bis-phenylsulfonyl-6-phenyl-hexa-1,3,5-triene, **105**, can be explained by the occurrence of the following Knoevenagel-type condensation, and a proposed mechanism is given in Scheme 33.



Scheme 33. Proposed mechanism explaining the formation of *(1E,3E,5E)*-1,3-bis-phenylsulfonyl-6-phenyl-hexa-1,3,5-triene, **105**

The differences between the traditional Knoevenagel-condensation and a Knoevenagel-type condensation reaction have been discussed in depth in the introduction section of this chapter, sections 2.1.3 and 2.1.4. Briefly, the proposed mechanism differs from that of a traditional Knoevenagel-condensation, in that, one of the reagents is not a typical activated methylene but a bis-phenylsulfonyl propene, **104**. When an activated methylene is used, Patai and Zabicky²³⁰ determined that the dissociation of the C-H bond, and consequential anion formation, is the first step in the Knoevenagel-condensation mechanism on the basis of kinetic studies.²³⁰ This group investigated the kinetics of the reaction of malononitrile with five aromatic aldehydes in 95% ethanol and it was found that, while the reaction follows second-order kinetics, it still showed the distinctive features of an ionization reaction. The concentration of the carbanion produced, as a result of the dissociation of the carbon-hydrogen bond of the active methylene group, was found to reach equilibrium practically instantaneously on dissolution in ethanol.²³⁰ We can postulate that the first step in our mechanism proceeds in a similar manner, perhaps not by dissociation of the C-H bond given the difference in solvent/substrate, but we can hypothesize that formation of the anion is the first step in our proposed mechanism also. Additionally, the base is not a usual amine base (e.g. piperidine) but has been substituted by activated Al₂O₃ and so, there is no iminium ion formation in our Knoevenagel-type condensation mechanism.

In the above mechanism, an anion is generated by abstraction of the most acidic proton of the propene, presumably by the base, which is in equilibrium with its other resonance structures. This anion then acts as a nucleophile and undergoes direct addition with the carbonyl carbon of *trans*-cinnamaldehyde, **1**. A series of protonation and deprotonation steps by the base (Al₂O₃) followed by dehydration leads to the desired 1,3-bis-phenylsulfonyl-6-phenyl-hexa-1,3,5-triene, **105**.

2.2.4 Reaction scope: Variation of the cinnamaldehyde

We then investigated the substrate scope of our developed methodology. We retained (*E*)-1,3-bisphenylsulfonylprop-1-ene, **104**, as the propene and, using the preferred reaction conditions, introduced variety in the products by reacting this propene with different cinnamaldehydes. The synthesis of these cinnamaldehydes has already been discussed in chapter 1, specifically in sections 1.2.1-1.2.3 of the results and discussion, and I was first author in the publication relating to this work.⁹⁸ The triene products obtained are novel and are shown with isolated yields in Figure 38.

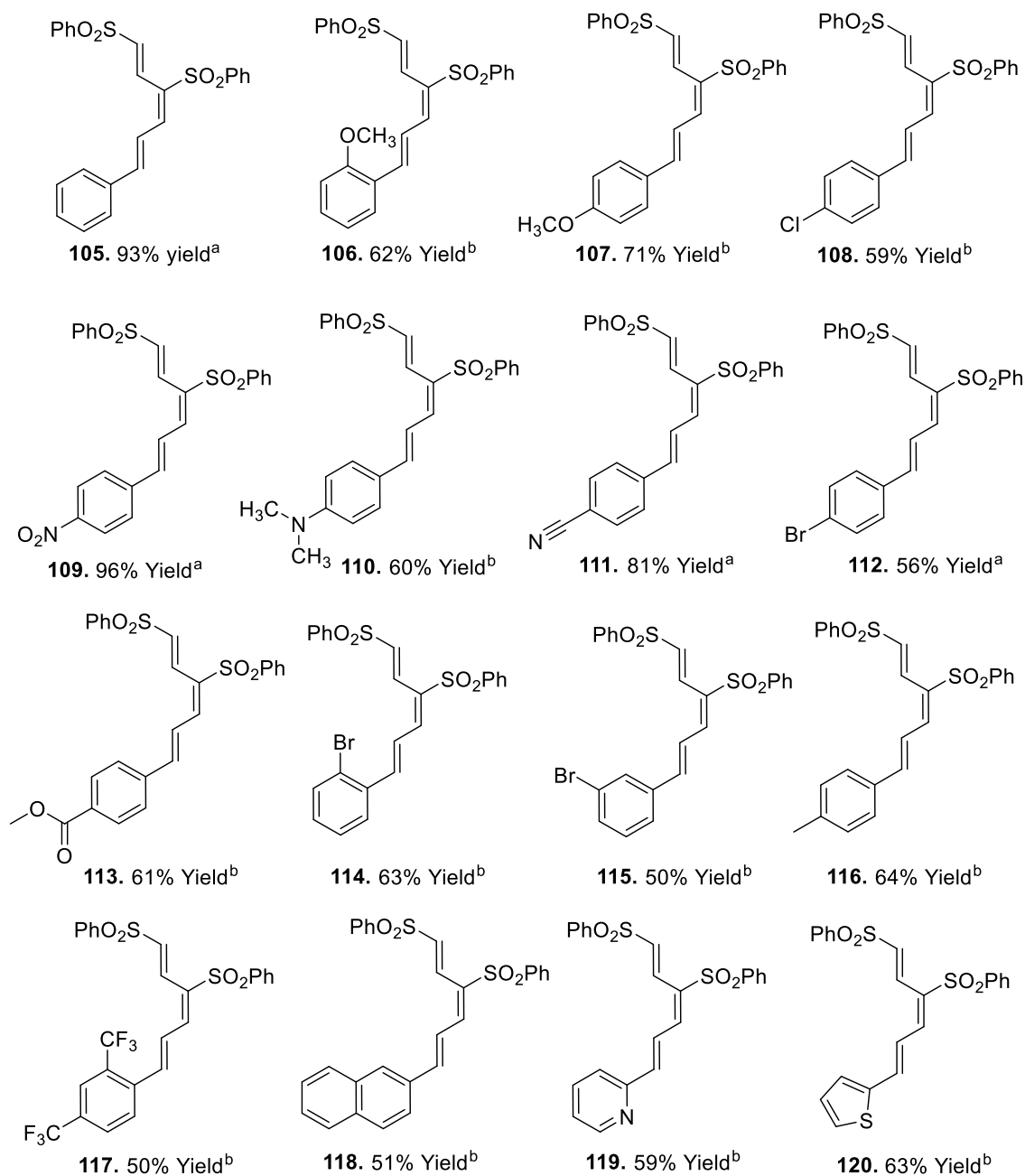


Figure 38. Range of 1,3,5-hexatrienes synthesized using the respective *trans*-cinnamaldehyde (1.1 eq.), **104** (1 eq), DCM (10 mL) and Al₂O₃ (15 eq.) at room temperature for 24 hr. ^a Reactions were performed at 1 mmol scale. ^b Reactions were performed at 0.5 mmol scale.

The developed aluminium oxide methodology appears to tolerate a broad range of substituted cinnamaldehydes. The yields obtained ranged from 50-96%, but importantly all sixteen cinnamaldehydes were successfully converted to their corresponding 1,3,5-hexatriene. This is encouraging because, by changing the cinnamaldehyde component alone, a large range of 1,3,5-hexatriene species can be accessed, demonstrating versatility in the synthetic methodology developed. The structures of the triene products were

confirmed by NMR spectroscopy, HRMS, and IR analysis. Further details and discussion of the structural characterization, including assignment of the geometry, can be found in the following section (section 2.2.5).

There were no clear trends observed relating substituent choice and yield, although substrates containing an electron-withdrawing group in the *para*-position of the phenyl ring appear to be the best tolerated, compounds **109**, **111**, and **113** (NO₂, CN, CO₂Me, respectively, Figure 38) and the yields obtained ranged from 60-96%. This may relate to the influence that these electron-withdrawing *para*-substituents have on increasing the electrophilicity of the carbonyl carbon atom²³⁰ of the cinnamaldehyde. Two trienes were synthesized containing an electron-donating group in the *para*-position of the phenyl ring and one with an alkyl group in the same position, compounds **107**, **110**, and **116** (OMe, NMe₂, Me, respectively, Figure 38). The yields of these trienes were in the range of 60-71%. The yield of the non-substituted triene, **105**, was 93%. Halogen substituents at the *para* position appear to produce slightly lower yields compared with electron-donating groups, with yields of 57% and 59% obtained for the *p*-bromo, **112**, and *p*-chloro-substituted, **108**, trienes respectively. A similar observation was made when the phenyl ring was replaced with other aromatic and heterocyclic rings. Here, replacement of the phenyl ring with α -naphthalene led to the lowest yield of the three examples at 51%, followed then by 2-pyridine at 59% and then 2-thiophene at 63% (compounds **118**, **119**, and **120**, respectively, Figure 38). The only bis-substituted phenyl example explored was that synthesized with two CF₃ substituents, compound **117**, Figure 38. This gave the lowest yielding reaction at 50%.

We did not access a large range of triene products where the substituent on the phenyl ring was in a position other than *para*-, but there are three examples that can be discussed. The movement of the methoxy substituent from the *para*-, **107**, to the *ortho*-position, **106**, saw the yield drop by 9%. Conversely, the movement of the bromo-substituent from the *para*- to the *ortho*-position saw an increase in yield of 7%, from 56%, **112**, to 63%, **114**, respectively. When the bromo substituent was moved to the *meta*-position, **115**, the yield dropped to 50%. This would preliminarily indicate that the position of the substituent on the phenyl ring does have an effect on the overall yield of the corresponding triene, with substitution at the *meta*-position of the phenyl ring less well tolerated. However, more data sets would need to be obtained using different substituents in order to conclusively show this to be the case.

Some reactions were performed at 1 mmol, while the majority were performed at 0.5 mmol. In order to publish with the American Chemical Society journals, it is necessary to demonstrate at least one new reaction on a 1 mmol scale. Reactions with *trans*-cinnamaldehyde, **1**, *p*-nitrocinnamaldehyde, **44**, *p*-cyanocinnamaldehyde, **38**, and *p*-bromocinnamaldehyde, **40**, were all performed at the 1 mmol scale. The yield of triene using **109** was recorded as an excellent 96%, with the **111** and **112** triene derivatives generating isolated yields of 81% and 56% respectively.

2.2.5 Structural characterization of *(1E,3E,5E)*-1,3-bis-phenylsulfonyl-(6-*p*-dimethylaminophenyl)-hexa-1,3,5-triene **110**

A combination of ^1H NMR, ^{13}C NMR, 2D NMR, IR spectroscopy, and MS analysis were used to fully characterize *(1E,3E,5E)*-1,3-bis-phenylsulfonyl-(6-*p*-dimethylaminophenyl)-hexa-1,3,5-triene, **110**, and other trienes. The characterization of **110** will be considered first, using a detailed explanation of the NMR spectroscopic analysis of this compound as an example of how all 1,3,5-hexatrienes were characterized.

2.2.5.1 Use of NMR spectroscopic data to characterize *(1E,3E,5E)*-1,3-bis-phenylsulfonyl-(6-*p*-dimethylaminophenyl)-hexa-1,3,5-triene **110**

For ease of explanation, an atom labelling system has been employed and is shown in Figure 39.

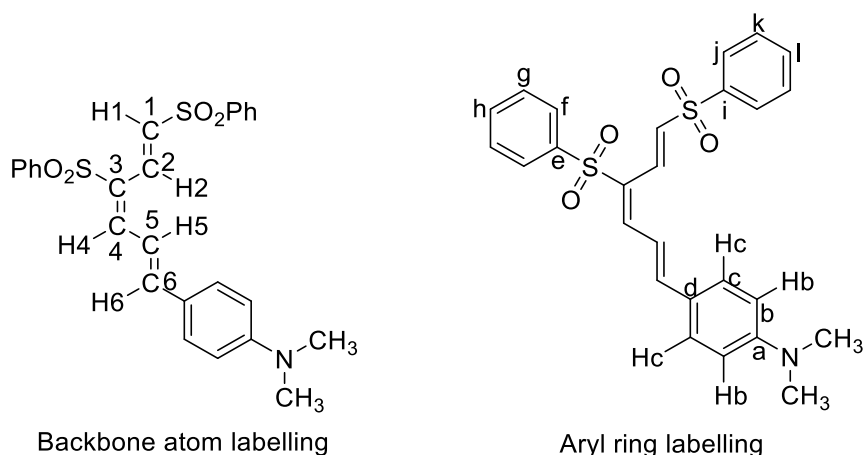


Figure 39. The structure of *(1E,3E,5E)*-1,3-bis-phenylsulfonyl-(6-*p*-dimethylaminophenyl)-hexa-1,3,5-triene (compound **110**, Figure 38), with atoms labelled for ease of discussion.

Comparing the ^{13}C and DEPT-135 spectra (Figure 40 and 41, respectively), the quaternary carbons can be identified at 152.3, 140.5 (x2), 127.5, 122.9 ppm as these signals disappear in the DEPT-135.

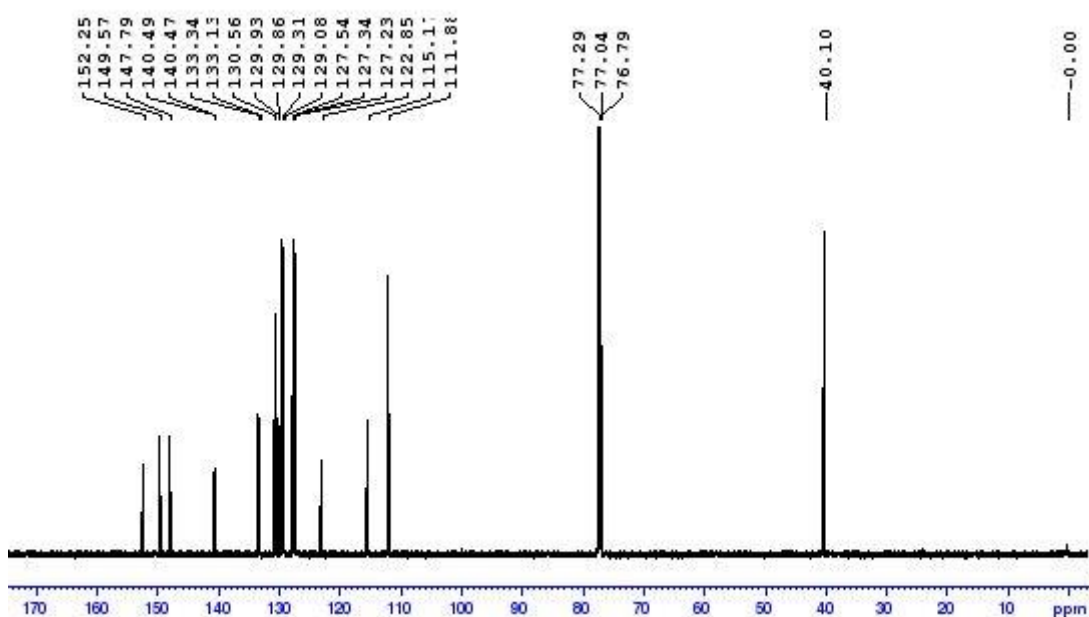


Figure 40. Full ^{13}C spectrum of compound **110**.

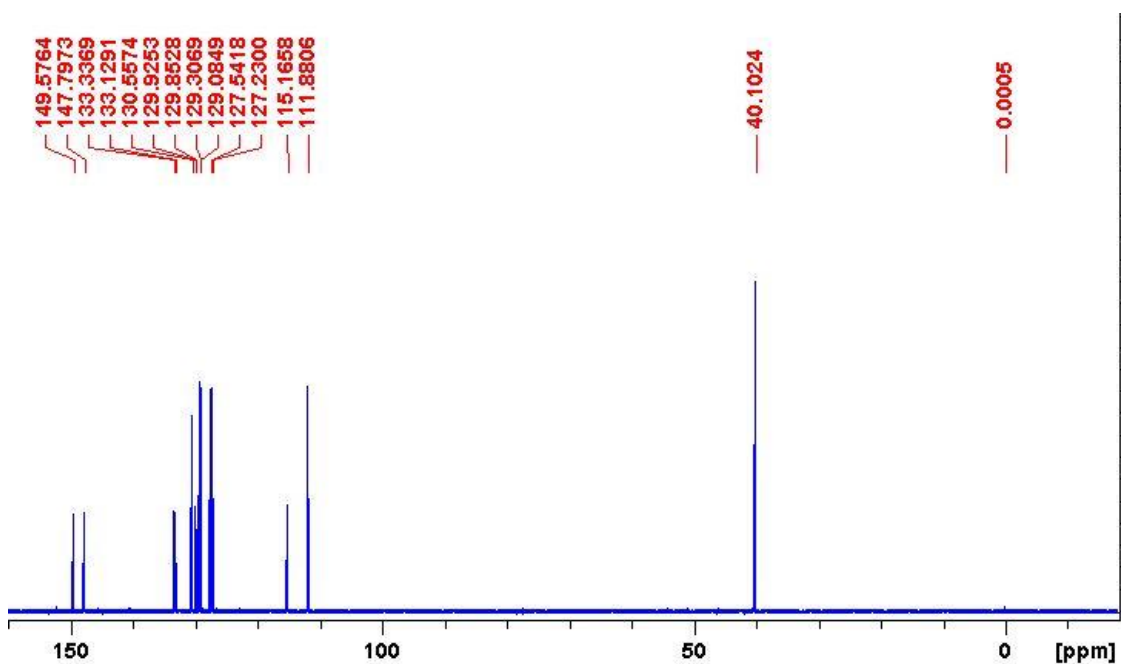


Figure 41. Full DEPT-135 spectrum of compound **110**.

Looking at the structure of (1*E*,3*E*,5*E*)-1,3-bis-phenylsulfonyl-(6-*p*-dimethylaminophenyl)-hexa-1,3,5-triene, compound **110**, there are 26 carbon atoms but as one would expect due to symmetry in the aryl rings, the ^{13}C NMR spectrum shows only 19 carbon signals. In addition, only one signal is present for the $\text{N}(\text{CH}_3)_2$ methyl carbons, as expected.

With compound **110**, one would expect the most shielded proton signal in the ^1H NMR spectrum (a doublet at 6.70-6.68 ppm) to be that of Hb (Figure 39) and to integrate for two hydrogens.

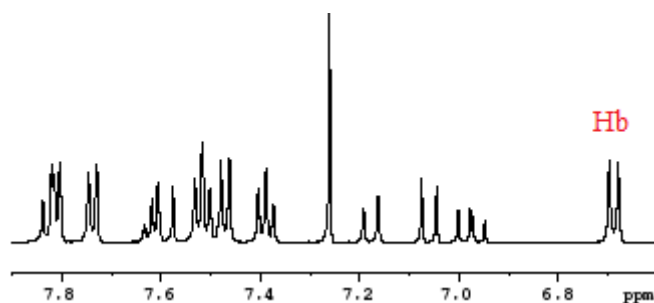


Figure 42. Expanded ^1H spectrum of compound **110** showing Hb.

This shielding is due to the ability of the lone pair on the nitrogen of the dimethylamino group to delocalize, thereby increasing the electron density at Cb, which has a shielding effect on Hb. Shielding effects at the *ortho* position are significant for strongly electron-donating groups,²³¹ dimethylamino being a good example, but interestingly the extent of the deshielding effects of electron-withdrawing groups at the same position are reported to be mixed.²³¹

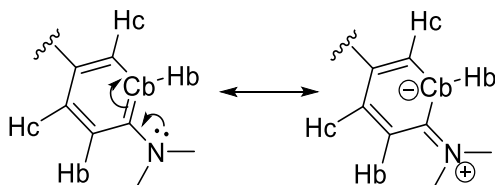


Figure 43. Resonance structures of the B-C aryl system of compound **110**, showing the shielding effect that the dimethylamino substituent has on the *ortho* position.

The COSY spectrum can then be used to identify Hc as the signal at 7.48-7.46 ppm, which also integrates for two protons. Hc is coupled to Hb in the COSY spectrum (Figure 44), as one would expect for such a B-C aryl system. Hc is also expected to appear as a doublet due to the splitting by Hb, and vice versa.

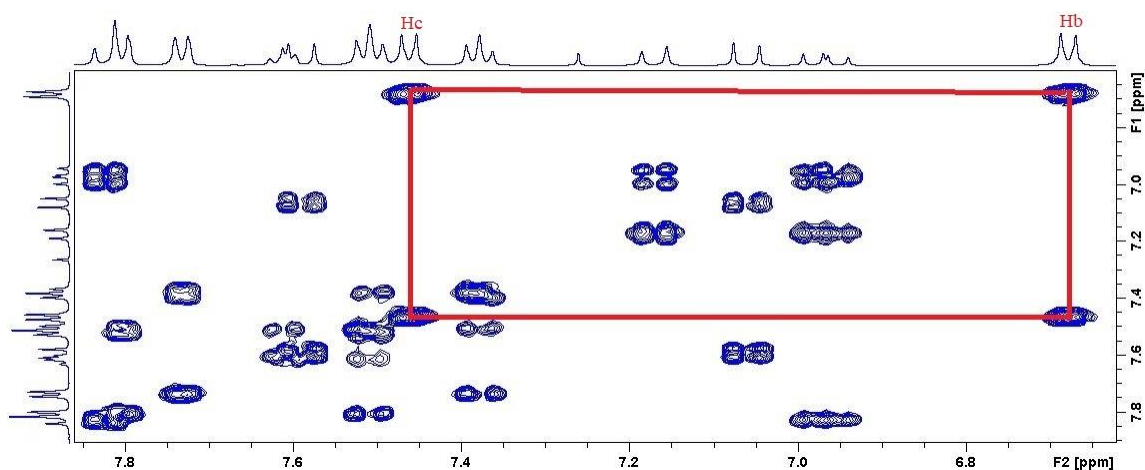


Figure 44. Expanded COSY spectrum of compound **110**, showing Hb and Hc coupling.

Using HSQC (Figure 45), one can see that Hb couples to the carbon signal at 111.9 ppm (hence assigned to Cb) and that Hc couples to carbon signal at 130.6 ppm (hence assigned to Cc).

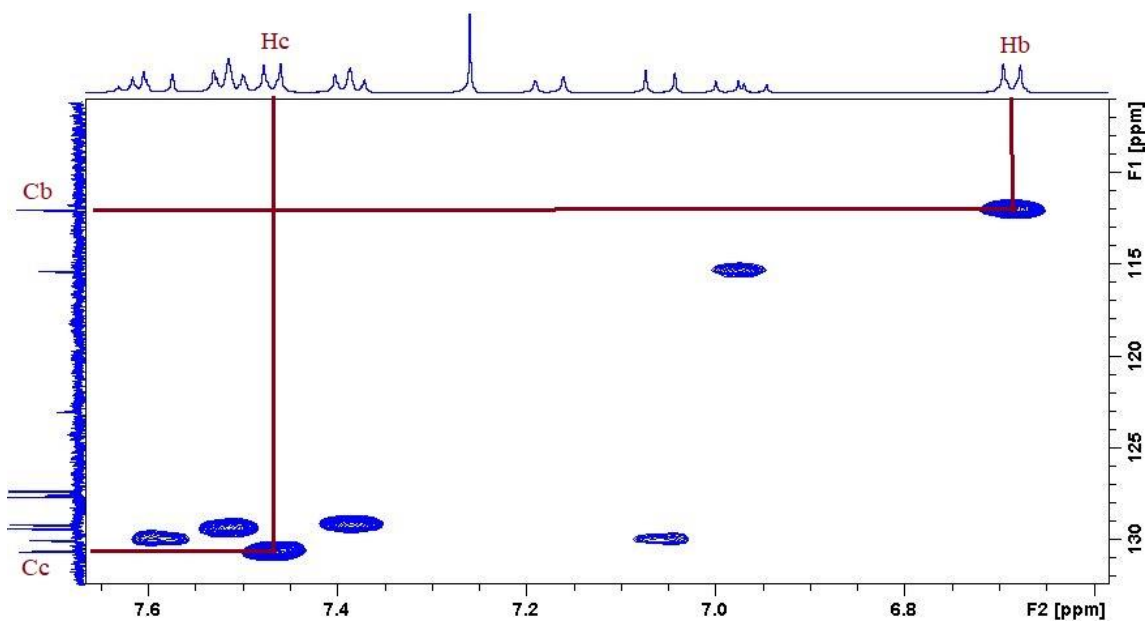


Figure 45. Expanded HSQC spectrum of compound **110**, showing Hb and Hc couplings to Cb and Cc, respectively.

Looking at the ^{13}C spectrum, the most deshielded carbon signal is also a quaternary carbon occurring at 152.3 ppm, and this was assigned as $\text{C}-\text{N}(\text{CH}_3)_2$ (Ca). A *para* $\text{N}(\text{CH}_3)_2$ group will have a significant deshielding effect on its *ipso* carbon (Ca in this case). The chemical shift of the *ipso* carbon is determined primarily by the inductive effect of the substituent.²³¹ Electronegative atoms directly bonded to the *ipso* carbon have a strong inductive effect at the *ipso* carbon and the result is a significant downfield shift for the

ipso carbon,²³¹ in contrast to the resonance effect we observed earlier with respect to the *ortho* position.

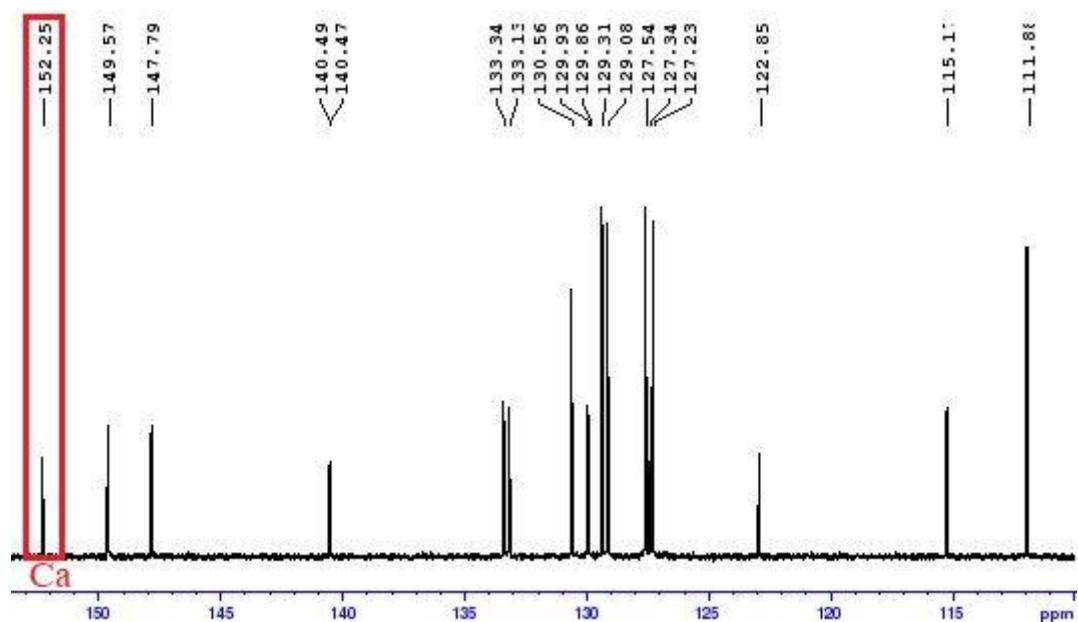


Figure 46. Expanded ^{13}C spectrum of compound **110**, showing assignment of Ca (*ipso* carbon attached to the dimethylamino substituent).

Examining the HMBC spectrum (Figure 47), Ca is coupled to both Hc and the methyl proton signal, as both are within four bonds of Ca. This acts as further confirmation of this signals' assignment as Ca.

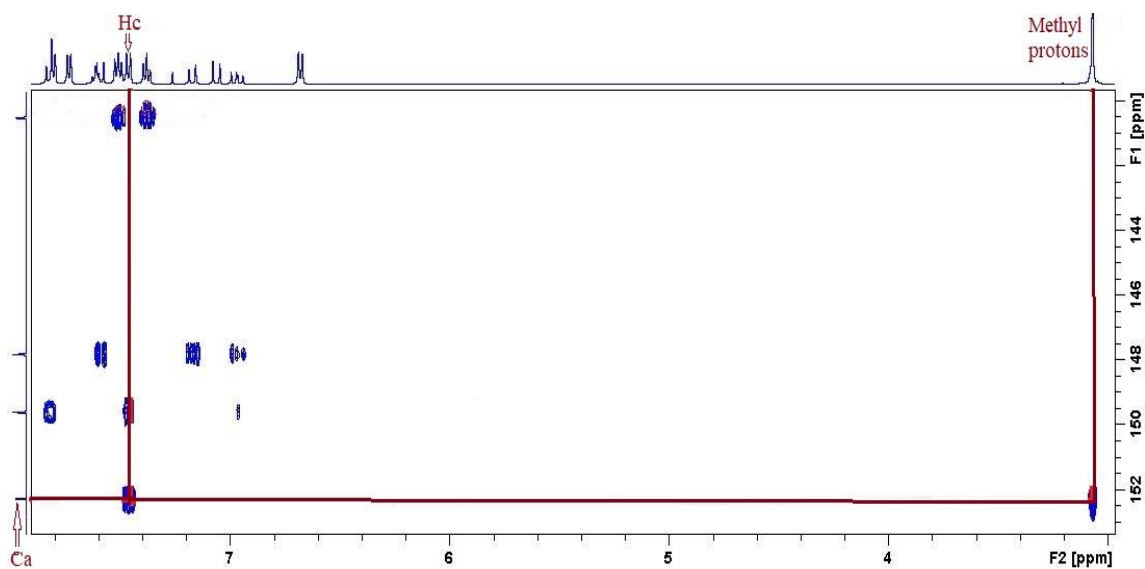


Figure 47. Expanded HMBC spectrum of compound **110**, showing the long-range coupling of Ca to Hc and the methyl protons.

In the HMBC spectrum, Hb has long range coupling to the quaternary carbon at 122.9 ppm. Apart from Ca, the only other quaternary carbon in the vicinity is Cd, the aromatic carbon adjacent to the olefin double bond, and therefore this can be assigned as the signal at 122.9 ppm. The HMBC spectrum also shows coupling between Cd and another signal at 7.00-6.95 ppm, which integrates for one hydrogen (as well as a smaller coupling to a proton at 7.19-7.16 ppm, which is later assigned as H6).

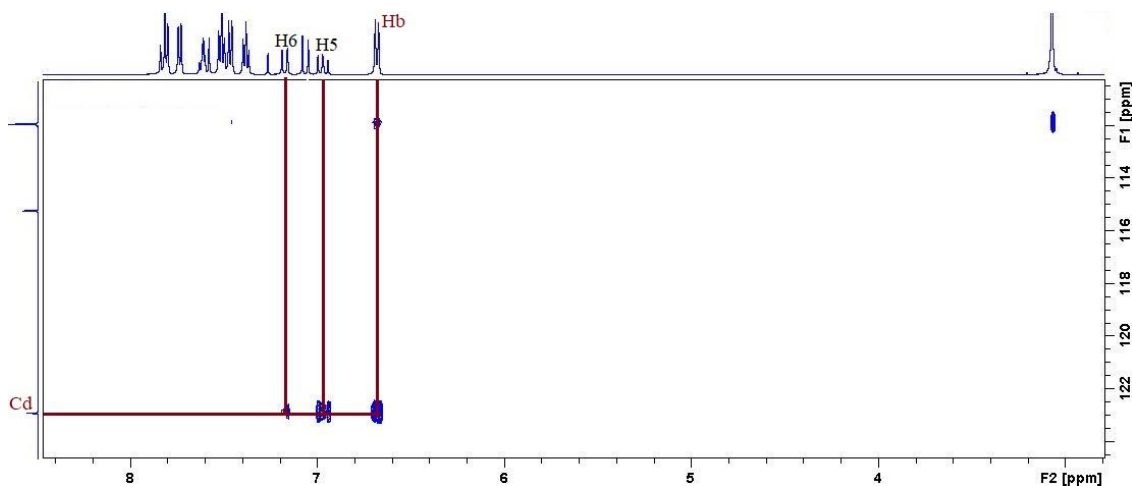


Figure 48. Expanded HMBC spectrum of compound **110**, showing the long range coupling between Hb, H5 and H6 to Cd.

We can assume the signal at 7.00-6.95 ppm is caused by H5 because it appears as a doublet of doublets and shows coupling constants of $J = 11.9$ Hz and $J = 14.9$ Hz (Figure 49).

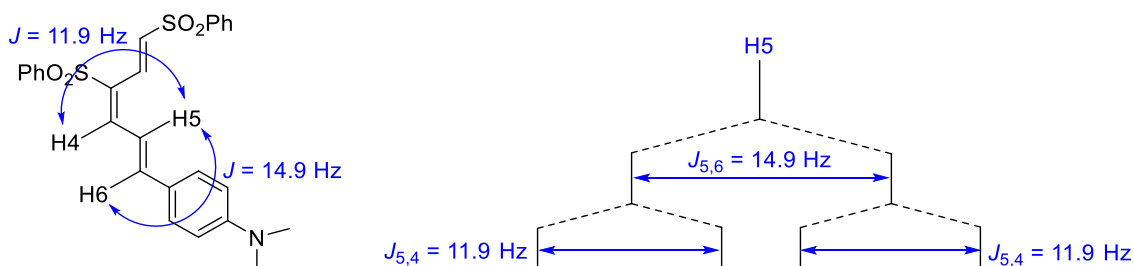


Figure 49. H5 coupling to H4 and H6 and corresponding splitting tree diagram.

This is consistent with a proton that is within three bonds of another proton, as H₅ is with H₄, and with a third proton H₆. The coupling of H₅ to H₆ is a *trans* coupling and gives the expected coupling constant of 14.9 Hz. Thus, H₅ is assigned as the pair of doublets at 7.00-6.95 ppm in the ¹H NMR spectrum.

With H₅ assigned as the signal at 7.00-6.95 ppm, we utilized the COSY spectrum (Figure 50) to confirm the assignment of the signal at 7.19-7.16 ppm as H₆, and the signal at

7.84-7.80 ppm as an overlapping signal for H4 and two aromatic protons. Further confirmation of the H6 assignment can be found in the ^1H NMR spectrum where the signal appears as the expected doublet with the expected *trans* coupling constant of 14.9 Hz. A coupling constant this large would not arise due to coupling with H4, as H4 is not *trans* relative to H5, and hence H6 is the doublet at 7.19-7.16 ppm. Additionally, one might expect H4 to be more deshielded than H6, as H4 is within three bonds of an electron-withdrawing sulfonyl group.

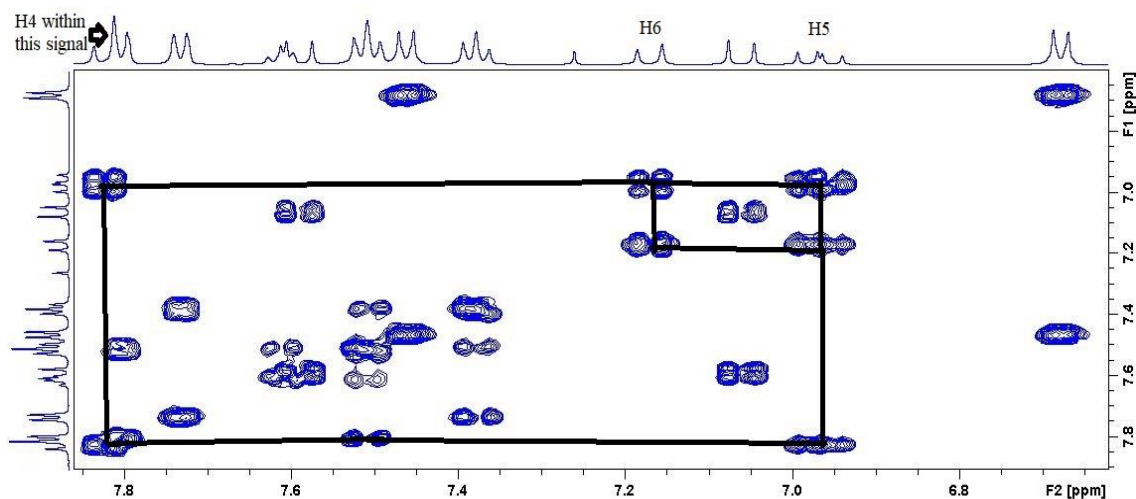


Figure 50. Expanded COSY spectrum of compound **110**, showing H5 coupling to both H4 and H6.

Using the HSQC spectrum (Figure 51) we can assign C5 and C6 as the ^{13}C NMR signals at 115.2 ppm and 149.5 ppm respectively, due to coupling with H5 and H6. The HSQC, spectrum (Figure 51) shows the overlapping H4-aromatic proton signals coupling to two carbon signals at 127.5 or 147.8 ppm.

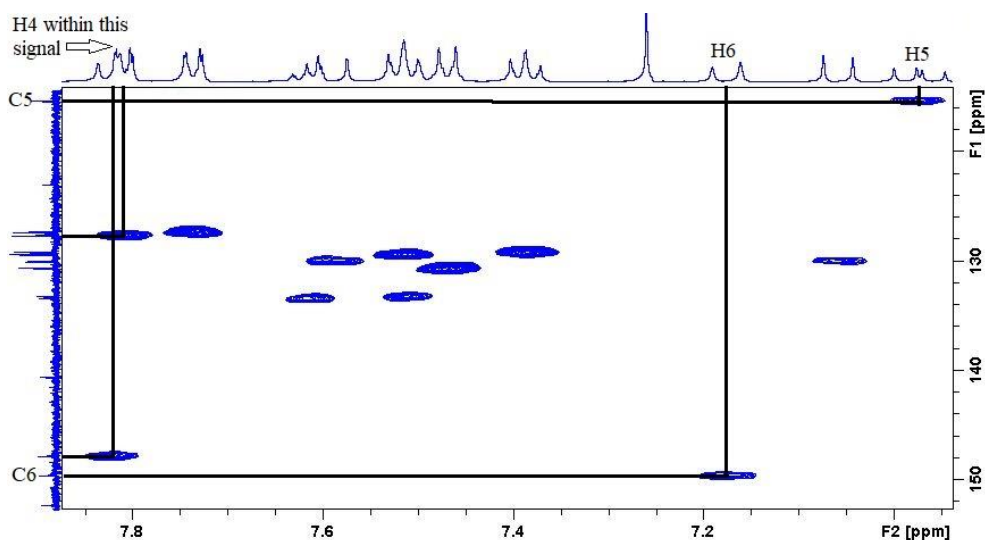


Figure 51. Expanded HSQC spectrum of compound **110**, showing H5 and H6 couplings to C5 and C6, respectively. It also shows the coupling of the signal containing H4 to two carbon signals at 127.5 and 147.8 ppm.

To assign C4 we need to consider the HMBC spectrum, (Figure 52). Here the carbon at 147.8 ppm shows long-range coupling to H6 (as well as another to proton at 7.63-7.57 ppm). This would be expected for the C4 carbon attached to H4. In the HMBC spectrum (Figure 52), the carbon at 127.5 ppm shows no long-range coupling to any of the olefin protons you would expect if it were due to C4, though it does show coupling to a proton within the 7.84-7.80 ppm signal. However, in the ^{13}C NMR spectrum this carbon signal (at 127.5 ppm) is one of the four tallest peaks, meaning it is likely due to an aromatic carbon, Cf, Cg, Cj or Ck, which one would expect to be a taller signal as it is due to two aromatic CHs as opposed to one olefin CH. Thus, the signal at 147.8 ppm is assigned as C4, Figure 53.

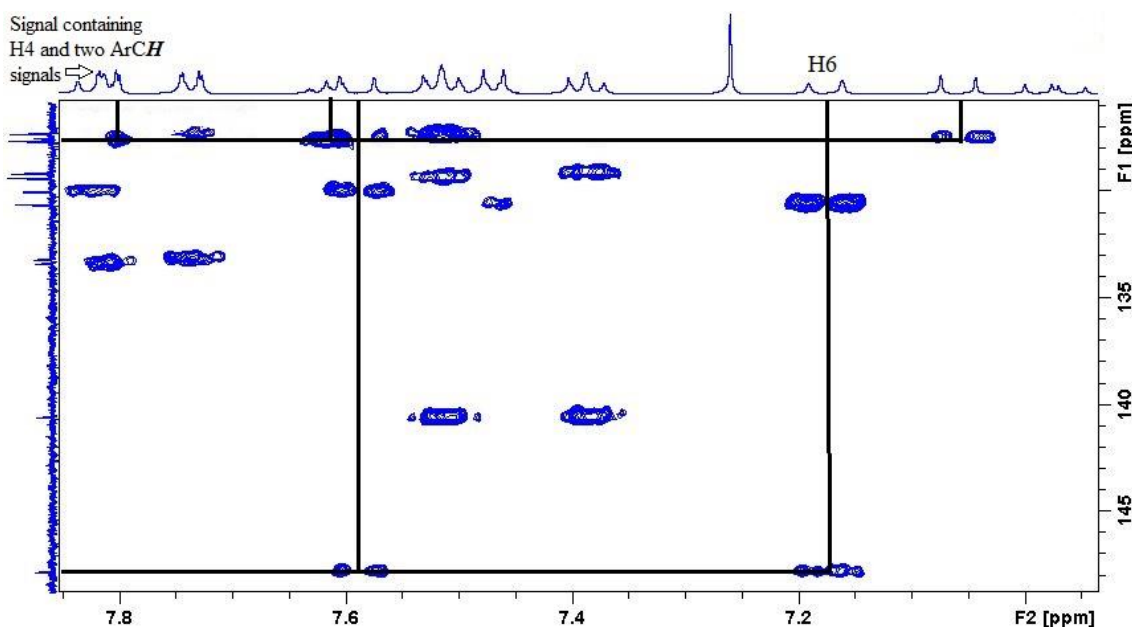


Figure 52. Expanded HMBC spectrum of compound **110**, showing long range couplings of the carbon signals at 127.5 and 147.8 ppm (C4).

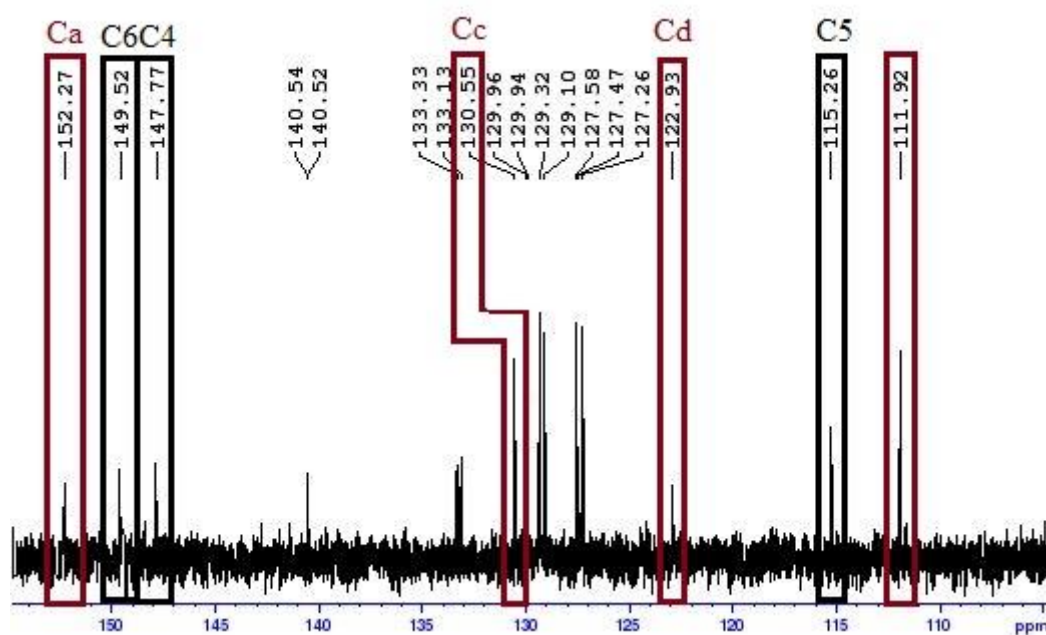


Figure 53. Expanded ^{13}C spectrum of compound **110**, showing assignment of the ^{13}C signals thus far within this ppm range.

With respect to the HMBC spectrum of C4, there was a third coupling evident, that to a proton at 7.63-7.57 ppm that integrates for two protons. A doublet can be observed within this overlapping multiplet signal that has a coupling constant of 15.4 Hz, thus is most likely due to either H₁ or H₂, i.e. a *trans* olefin coupling constant.

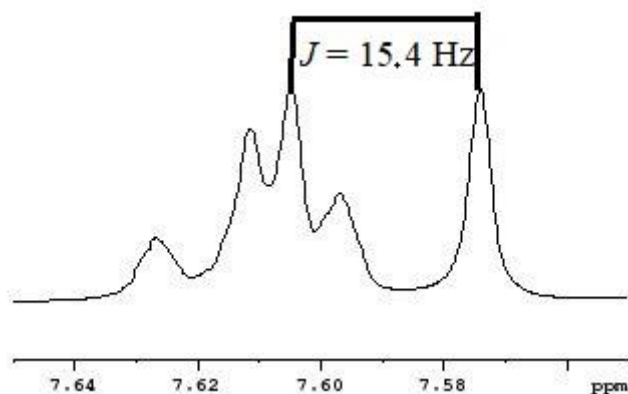


Figure 54. Expanded ^1H NMR spectrum of compound **110**, showing signal at 7.63-7.57 ppm, within which there is a doublet with a *trans* coupling constant.

Examining the HMBC (Figure 55) with respect to this signal, long-range coupling to C4 (four bonds away) is evident and therefore we assign this signal to H₂. Thus, the peak at 7.60-7.58 ppm contains H₂ and an aromatic proton of a phenyl sulfonyl group.

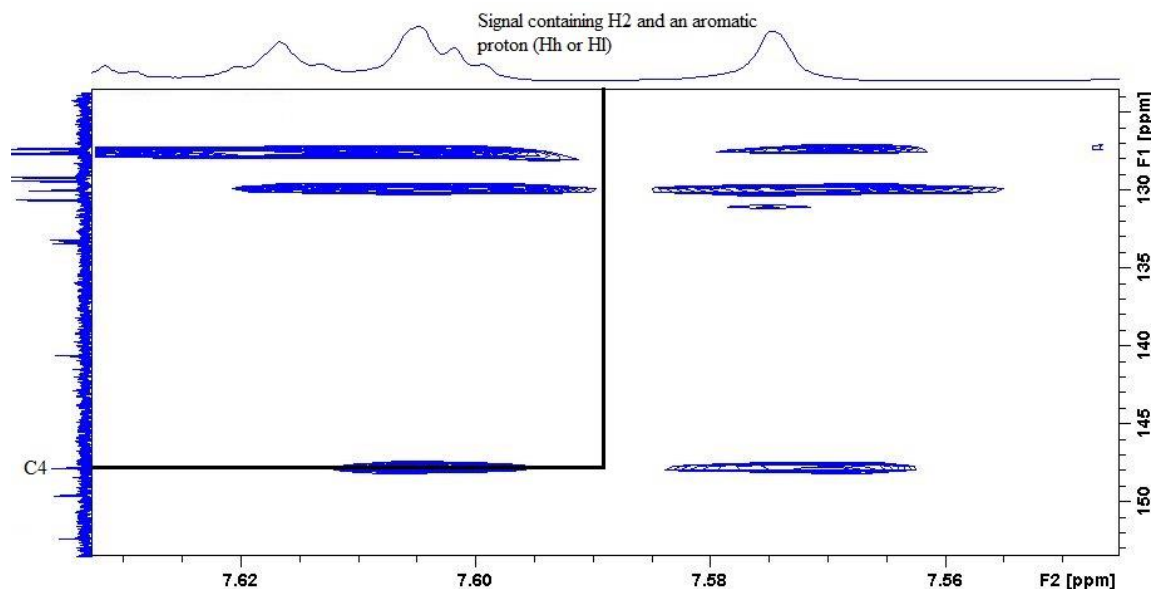


Figure 55. Expanded HMBC spectrum of compound **110**, showing long range couplings of C4 to a *trans* olefin signal, confirming this signal contains H2.

The COSY spectrum (Figure 56) can then be used to identify H1 as the doublet signal at 7.07-7.04 ppm, which couples to H2. The signal for H1 integrates for one proton and has a coupling constant $J = 15.4$ Hz. One would also expect H2 to be more deshielded than H1 due to the effect of both electron withdrawing sulfones on C2.

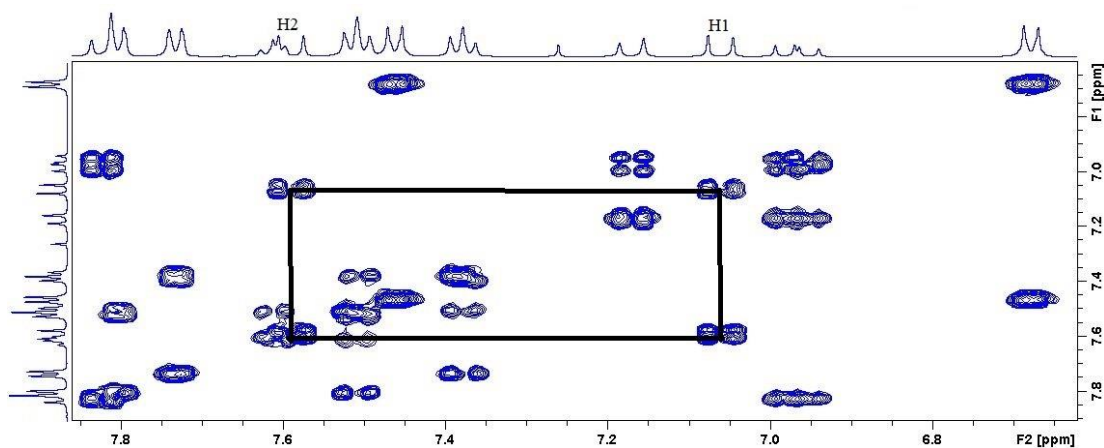


Figure 56. Expanded COSY spectrum of compound **110**, showing H1 coupling to H2.

Looking at the HSQC spectrum (Figure 57), we can see H1 is coupled to the carbon signal at 129.86 ppm, and hence is assigned as C1, while H2 is coupled to the carbon signal at 129.9 ppm, and hence is assigned as C2.

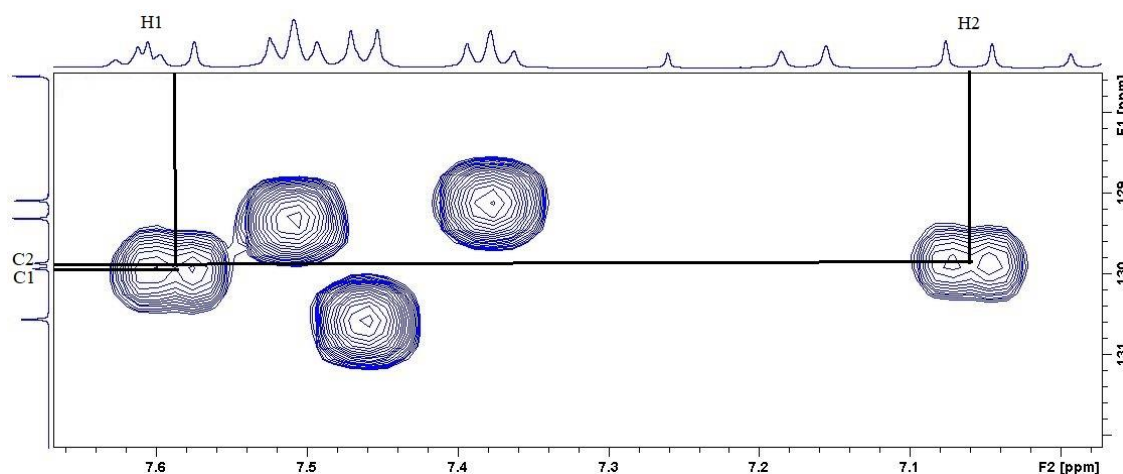


Figure 57. Expanded HSQC spectrum of compound **110**, showing H1 and H2 couplings to C1 and C2, respectively.

There are three quaternary carbons that need assignment, those at 140.49, 140.47 and 127.5 ppm. The HMBC spectrum (Figure 58) shows that the carbon signal at 127.5 ppm has several long-range couplings. These couplings would all suggest that the signal at 127.5 ppm is due to C3. In addition, it makes sense that the two quaternary carbons in the phenylsulfonyl groups would have similar chemical shifts, due to the similarities of their chemical environment. Therefore, the signals at 140.49 and 140.47 ppm can be assigned as these quaternary carbons in the phenylsulfonyl groups.

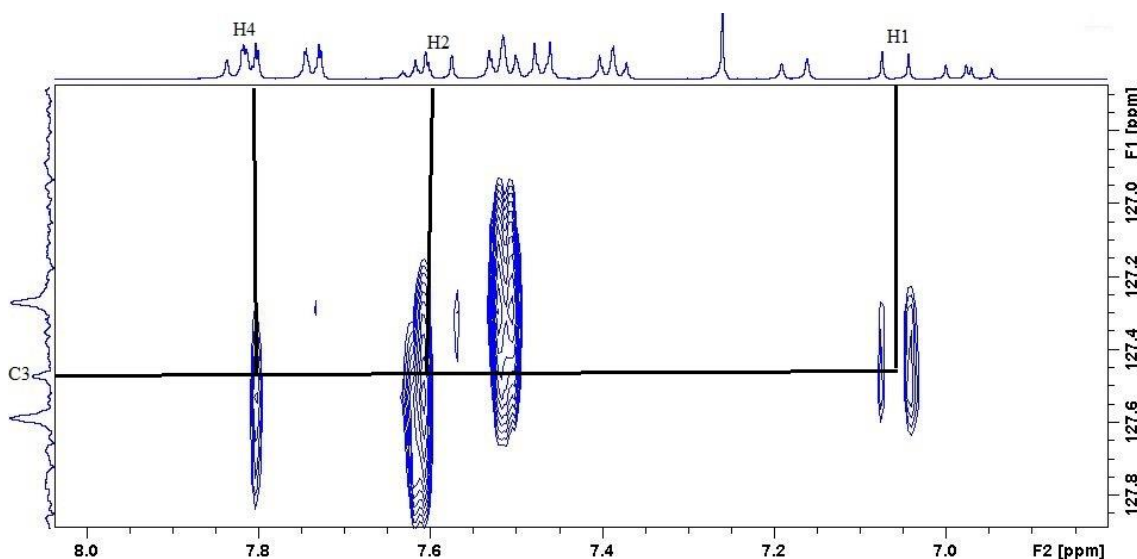


Figure 58. Expanded HMBC spectrum of compound **110**, showing numerous long range couplings of carbon at 127.5 ppm, confirming this signal is that of C3.

Thus, all alkene protons and carbons, as well as the four distinct aromatic carbon and proton signals of the *p*-dimethylamino substituted phenyl ring, can be assigned. The ten

protons of the phenylsulfonyl groups can be identified as generating the remaining protons signals, (i.e. those at 7.84-7.80, 7.75-7.73, 7.63-7.57, 7.53-7.50, 7.40-7.37 ppm). Further assignment of these signals is not possible due to the similarity of the protons responsible for their generation. This is also the case for the corresponding phenylsulfonyl carbons signals, which appear at 133.3, 133.1, 129.3, 129.1, 127.6 and 127.2 ppm. A summary of the assignments is shown in Figure 59.

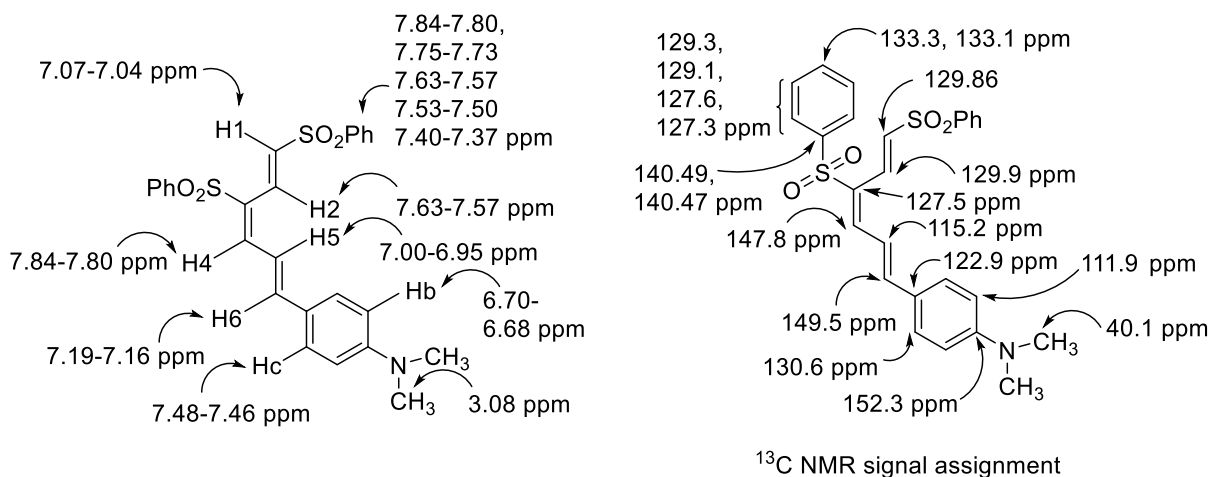


Figure 59. Summary of NMR spectroscopy signal assignment for (1*E*,3*E*,5*E*)-1,3-bis-phenylsulfonyl-(6-*p*-dimethylaminophenyl)-hexa-1,3,5-triene, **110**.

2.2.5.2 IR spectroscopy and MS analysis for structural characterization of (1*E*,3*E*,5*E*)-1,3-bis-phenylsulfonyl-(6-*p*-dimethylaminophenyl)-hexa-1,3,5-triene **110**

In addition to the use of NMR spectroscopy, IR spectroscopy and MS analysis were used to fully characterize (1*E*,3*E*,5*E*)-1,3-bis-phenylsulfonyl-(6-*p*-dimethylaminophenyl)-hexa-1,3,5-triene, **110**. The IR spectrum of compound **110** is included as Figure 60.

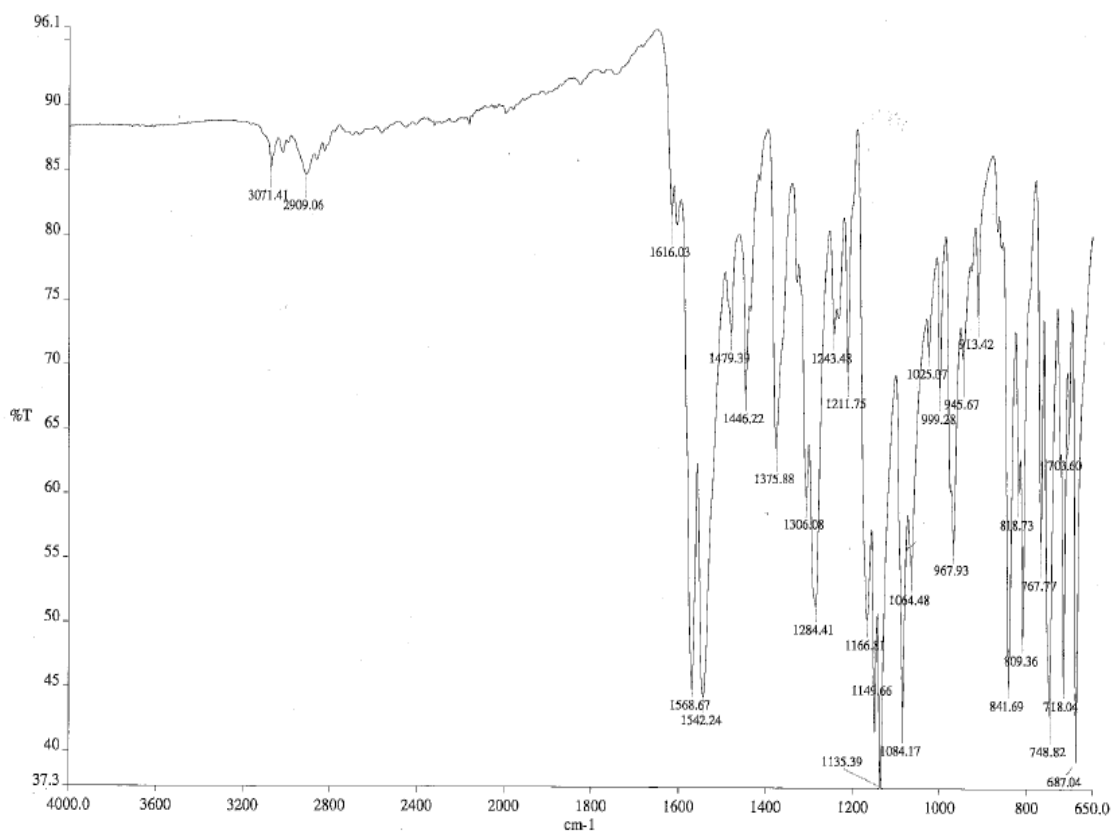


Figure 60. IR spectrum of **110**.

As expected from the structure of compound **110**, there are a series of bands associated with the presence of aromatic C=C, C-C and =C-H bonds. These include the band at 3071 cm⁻¹, characteristic of an aromatic C-H stretch, the bands at 1569, 1542, and 1479 cm⁻¹, characteristic of an aromatic C-C stretches, and the bands at 999 and 913 cm⁻¹, which are associated with =C-H bends. There are overtones associated with the presence of aromatic rings that occur between 2000-1650 cm⁻¹ also. Additionally, the 1,4-disubstituted (*para*) phenyl ring portion of **110** produces the strong band at 842 cm⁻¹. The conjugated alkene portion of the molecule is responsible for the appearance of such bands as those at 1616 cm⁻¹, as a result of C=C stretching, and 749 cm⁻¹, as a result of out of plane C-H bending. The sulfone S=O asymmetric stretch is apparent at 1284 cm⁻¹ and its symmetric stretch at 1135 cm⁻¹. The bands mentioned so far can be expected to be present in all 1,3-bis-phenylsulfonyl-(6-substituted phenyl)-hexa-1,3,5-triene molecules. Specific to (1*E*,3*E*,5*E*)-1,3-bis-phenylsulfonyl-(6-*p*-dimethylaminophenyl)-hexa-1,3,5-triene, compound **110**, the presence of two methyl groups also causes certain bands, such as that at 2909 cm⁻¹ as a result of a C-H stretch, 1446 cm⁻¹ associated with C-H scissoring, 1376 cm⁻¹ corresponding to C-H rocking and the bands at 1064 and 1025 cm⁻¹ relating to in plane C-H bending. Additionally, the amine C-N stretch accounts for the band at 1149 cm⁻¹.²³²

The MS analysis can be broken down into LC-MS (Liquid Chromatography – Mass Spectrometry) and HR-MS (High Resolution – Mass spectrometry). LC-MS incorporates HPLC (High Performance Liquid Chromatography), which allows the individual components in a molecule to be separated and then ionized by an Electrospray Ionization Source (ESI). The separation of the ions occurs on the basis of their respective mass/charge ratio.²³³ The LC-ESI-MS spectrum of compound **110** showed it has m/z $[M+H]^+$ 480.3, see Appendix 2 Figure A161. The LC-MS is coupled to a UV detector, and this can be used to give information about the purity of compound **110**. The chromatogram shows a single peak with a retention time of 32.7 minutes, see Appendix 2 Figure A162.

HR-MS was also applied to compound **110**, in order to confirm the molecular formula assigned. Mass errors of between -5.00 and 5.00 ppm with isotope match scores above 60% are considered confirmation of molecular formulae. Compound **110** showed a mass error of -0.22 ppm, thus it is very likely that this molecular formula assigned is that of the molecule analyzed, see Appendix 2 Figure A163 for this data. Taken together, all of the results from NMR spectrometry, IR and MS analysis all confirm the structural characterization of compound **110**.

All the (1*E*,3*E*,5*E*)-1,3-bis-phenylsulfonyl-(6-substituted phenyl)-hexa-1,3,5-trienes synthesized were analyzed in the same manner using a combination of the analytical techniques at our disposal. It is beyond the scope of this thesis to fully explain the analysis of each member of this family of sixteen 1,3,5-hexatrienes, so an example of each type of substituent on the phenyl ring attached to the alkene carbon 6, as depicted in Figure 39 previously, will be briefly explained in the following. The analysis of **110**, can be used as an example of how those trienes bearing an electron-donating group were analyzed and fully characterized.

2.2.6 Structural characterization of (1*E*,3*E*,5*E*)-1,3-bis-phenylsulfonyl-(6-*p*-nitrophenyl)-hexa-1,3,5-triene **109**

(1*E*,3*E*,5*E*)-1,3-Bis-phenylsulfonyl-(6-*p*-nitrophenyl)-hexa-1,3,5-triene **109** can be used as an example of triene bearing an electron-withdrawing group on the phenyl ring. In terms of NMR spectroscopy, the major difference between these spectra and those of 1,3-bis-phenylsulfonyl-(6-*p*-dimethylaminophenyl)-hexa-1,3,5-triene, **110**, is the position of the *ipso*-carbon (Ca, Figure 61) which occurs at 147.5 ppm due to the inductive effect of the nitro group.²³¹ The carbon *ortho* to the nitro substituent (Cb, Figure 61) can be identified at 123.3 ppm and the attached proton (Hb, Figure 61) appears as the multiplet at 8.28-8.26 ppm, integrating for two protons. This was deduced based on the long range couplings apparent in the HMBC spectrum of Ca, showing the coupling to Hb, which is expected to be the most deshielded signal, as a result of its proximity to the electron-withdrawing nitro group which withdraws electron density by resonance. The HSQC

spectrum was then used to identify Cb. The COSY spectrum shows coupling between Hb, and the protons on the carbon *meta* to the nitro substituent (Hc, Figure 61), which appears within the multiplet at 7.59-7.53, and this integrates for four protons. Using the HSQC spectrum, the carbons attached to these protons can be observed at 127.6 ppm (Cc, Figure 61). The other quaternary carbon in this system (Cd, Figure 61) is identified as that at 139.8 ppm, which shows coupling to Hc in the HMBC spectrum. All NMR spectra relating to this compound can be found in Appendix 2, Figures A104 and A105.

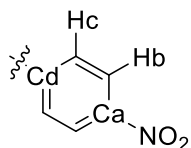


Figure 61. Structure of aryl system within **109**, with protons and carbons labelled for ease of discussion.

The notable IR bands that appear in the spectrum of **109**, that do not appear in the spectrum of **110**, are those that appear at 1516 and 1342 cm^{-1} (Figure 62). These are accounted for by the occurrence of NO_2 stretching.

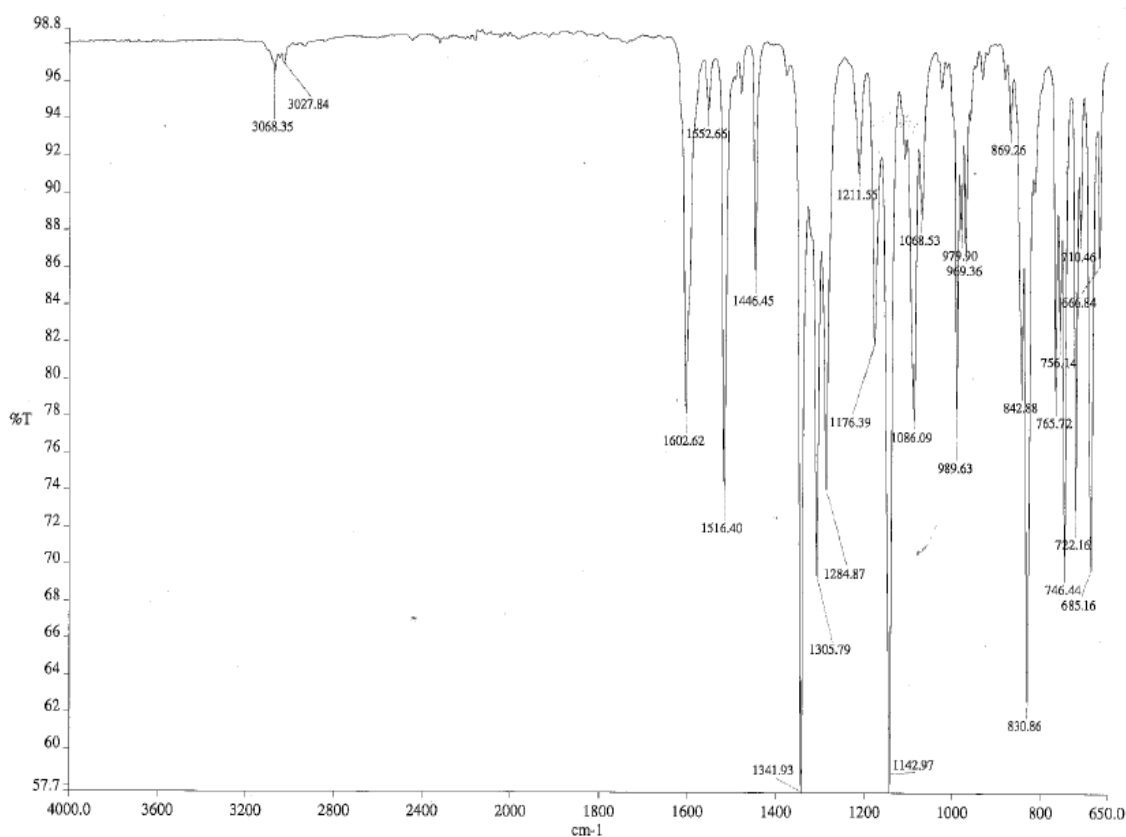


Figure 62. IR spectrum of **109**.

The LC-ESI-MS spectrum of compound **109** showed it has m/z $[M+Na]^+$ 504.4 and the LC chromatogram obtained indicated the purity of this compound as 98.8%, and had a retention time of 31.7 minutes. The corresponding data can be found in Appendix 2 Figures A151 and A152. HR-MS was also applied compound **109**, in order to confirm the molecular formula assigned. A mass error of -3.26 ppm was found and, as before, with a mass error of less than 5.00 ppm it is likely that this molecular formula assigned is that of the molecule analyzed. The corresponding data can be found in Appendix 2 Figure A153. Taken together, all of the results from NMR spectrometry, IR and MS analysis all confirm the structural characterization of (1*E*,3*E*,5*E*)-1,3-bis-phenylsulfonyl-(6-*p*-nitrophenyl)-hexa-1,3,5-triene compound **109** as a representative of trienes bearing an electron-withdrawing substituent in the phenyl ring.

2.2.7 Structural characterization of (1*E*,3*E*,5*E*)-1,3-bis-phenylsulfonyl-(6-*m*-bromophenyl)-hexa-1,3,5-triene **115**

(1*E*,3*E*,5*E*)-1,3-Bis-phenylsulfonyl-(6-*m*-bromophenyl)-hexa-1,3,5-triene **115** can be used as an example of a triene bearing a halogen on the phenyl ring attached to alkene carbon 6, as depicted in Figure 39 previously. In terms of NMR spectroscopy, the major difference between these spectra, and those of either triene discussed above, is the position of the *ipso*-carbon (Ca, Figure 63), which occurs at 123.3 ppm due to the inductive effect of the bromo group, and corresponds with the chemical shift reported in the literature for a ^{13}C atom directly attached to Br.²³¹ Unfortunately, due to the nature of this substituent, there are no distinguishing proton groups in the 1H NMR spectrum, and a lot of proton signals overlap, making it difficult to definitively assign all the NMR signals for this particular triene, or any of the halogen-substituted trienes. However, the HMBC spectrum does reveal that Ca is coupled to protons to a signal within the multiplet at 7.67-7.64 ppm integrating for two protons, the multiplet at 7.57-7.51 ppm integrating for five protons, the doublet at 7.48-7.46 ppm integrating for one proton, and the pseudo triplet at 7.31-7.28 ppm integrating for one proton. These signals likely make up the protons of the same phenyl ring, Figure 63.

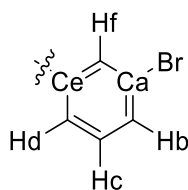


Figure 63. Structure of aryl system within **115** with protons and carbons labelled for ease of discussion.

The pseudo triplet at 7.31-7.28 ppm integrating for one proton is likely to be the signal of Hc, then Cc, by analysis of the HSQC spectrum, appears at 130.6 ppm. In the COSY spectrum, Hc couples to the multiplet at 7.57-7.51 ppm and the doublet at 7.48-7.46 ppm,

making it likely that within these two signals are Hb and Hd. Since the lone pair of electrons on the bromo substituent can delocalize onto Cb (or Cf), this would result in a negative charge and consequently, Hb (and Hf) would experience a shielding effect. Therefore, we might speculate that Hb accounts for the signal of lower chemical shift (i.e. 7.48-7.46 ppm), making Cb the signal appearing at 126.6 ppm, by analysis of the HSQC spectrum. Therefore, within the multiplet at 7.57-7.51 ppm lies Hd but, given the number of protons that this signal accounts for, it is impossible to assign Cd. Hf, by process of elimination, is likely within the multiplet at 7.67-7.64 ppm integrating for two protons. Cf, by analysis of the HSQC spectrum, is either 130.8 or 133.8 ppm. The quaternary carbon at 137.0 ppm, assigned as such by comparison of the ^{13}C NMR and DEPT-135 spectra, shows long range coupling to Hc in the HMBC spectrum, and therefore can be assigned as Ce. All NMR spectra relating to this compound can be found in Appendix 2, Figures A204-A209.

The notable IR bands that appear in the spectrum of **115**, that do not appear in the spectra of either triene previously analyzed above, is that appearing at 1083 cm^{-1} (Figure 64), which is a strong band accounted for by C-Br stretching as part of an aromatic halide.²³²

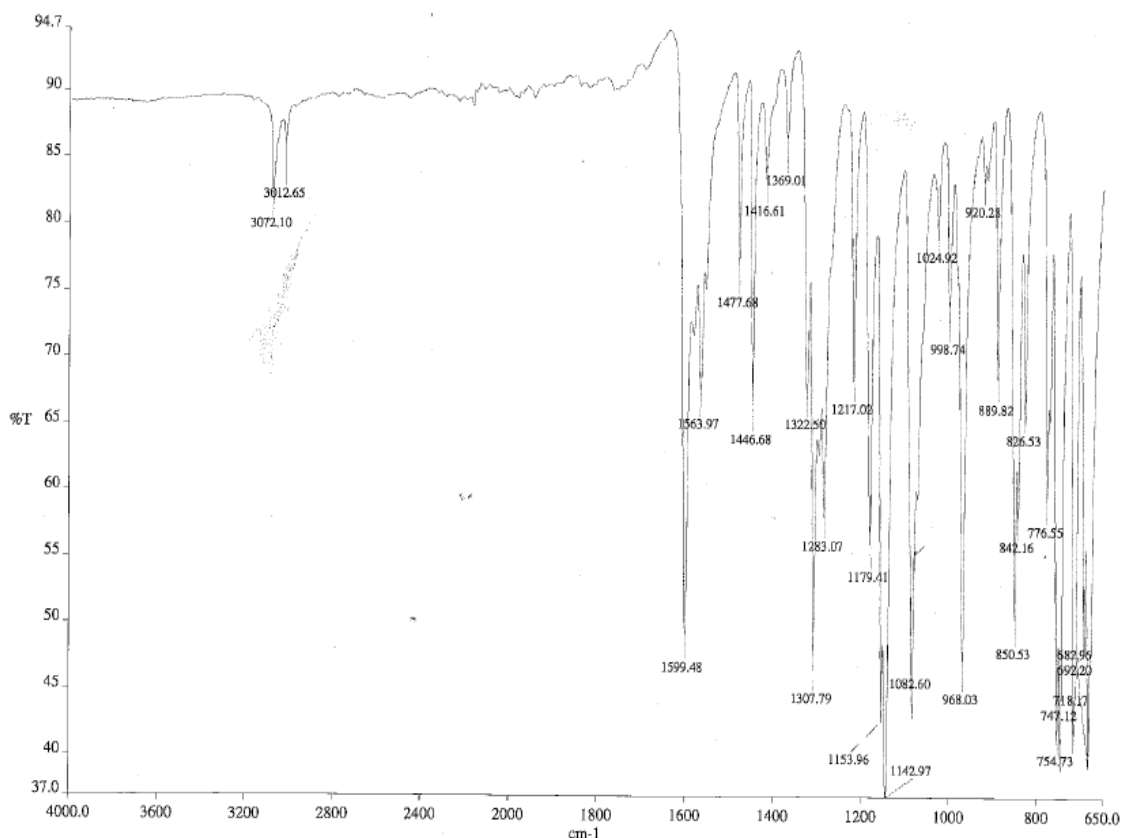


Figure 64. IR spectrum of **115**.

The LC-ESI-MS spectrum of compound **115** shows it has m/z $[\text{M}+\text{H}]^+$ 516.2, and the LC chromatogram obtained indicated the purity of this compound as 99.5% and has a

retention time of 33.7 minutes. The corresponding data can be found in Appendix 2 A211 and A212.

HR-MS was also applied to compound **115**, in order to confirm the molecular formula assigned. A mass error of -0.50 ppm was found and so, it is very likely that this molecular formula assigned is that of the molecule analyzed, see Appendix 2 Figure A213 for the corresponding data. Taken together, all of the results from NMR spectrometry, IR and MS analysis all confirm the structural characterization of (1*E*,3*E*,5*E*)-1,3-bis-phenylsulfonyl-(6-*m*-bromophenyl)-hexa-1,3,5-triene **115** as a representative of trienes bearing an halogen substituent on the phenyl ring.

2.2.8 Structural characterization of (1*E*,3*E*,5*E*)-1,3-bis-phenylsulfonyl-6-(thiophene)-hexa-1,3,5-triene **120**

(1*E*,3*E*,5*E*)-1,3-Bis-phenylsulfonyl-6-(thiophene)-hexa-1,3,5-triene **120** can be used as an example of a triene bearing a heterocycle instead of a phenyl ring attached to alkene carbon 6, as depicted in Figure 39 previously. In terms of NMR spectroscopy, the major difference are the signals that appear as a result of the heterocycle, Figure 65.

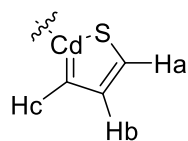


Figure 65. Structure of aryl system within **120**, with protons and carbons labelled for ease of discussion.

Hb can be identified in the ^1H NMR spectrum as a doublet of doublets signal appearing at 7.11-7.09 ppm and integrates for one proton. This is distinguishable as the signal for Hb due to its small coupling constants of 3.7 Hz and 5.0 Hz, and this is typical for protons within such heterocycles.²³¹ Based on the HSQC spectrum, Cb is identified as the carbon appearing at 128.6 ppm. Using the COSY spectrum, Hc can be identified within the multiplet at 7.49-7.47 ppm, which integrates for 2 protons, and Ha can be identified as the multiplet appearing at 7.30-7.29 ppm. The corresponding Cc and Ca can be identified at 130.0 and 131.5 ppm, respectively, by the HSQC spectrum. In the HMBC spectrum, Hb shows long-range coupling to Ca, Cc, and another carbon that appears at 139.8 ppm. This is a quaternary carbon, so identified by its absence in the DEPT-135 spectrum and presence in the ^{13}C spectrum. This signal likely corresponds to that of Cd. All NMR spectra relating to this compound can be found in Appendix 2 Figures A254-A259.

The notable IR bands that appear in the spectrum of **120**, that do not appear in the spectra of any triene previously discussed above, are those appearing at 979, 849 and 680 cm^{-1} (Figure 66), which are strong bands accounted for by C-S bond stretching as part of the heterocycle.²³⁴

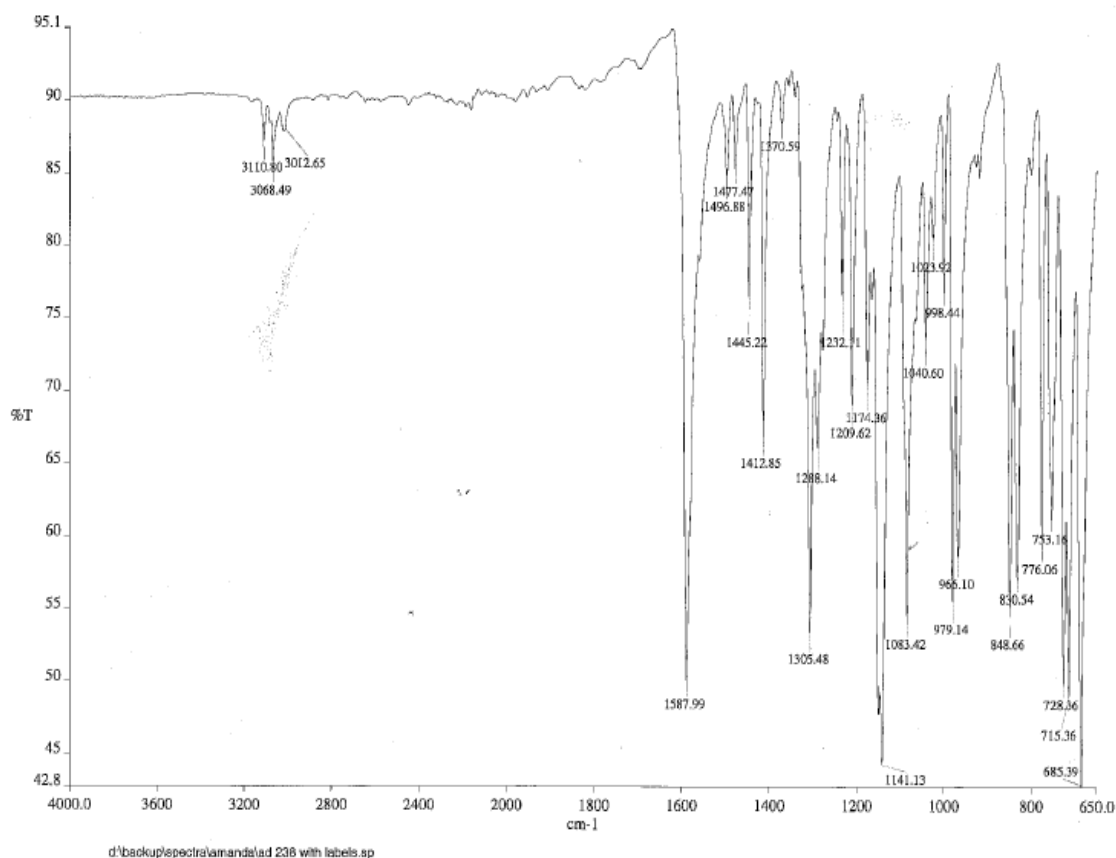


Figure 66. IR spectrum of **120**.

The LC-ESI-MS spectrum shows that compound **120** has m/z $[M+Na]^+$ 465.2 and the LC chromatogram obtained indicated the purity of this compound as 98.8%, with a retention time of 31.2 minutes. See Appendix 2, Figures A261 and A262 for corresponding data. HR-MS was also applied to compound **120** in order to confirm the molecular formula assigned. The result obtained showed that this compound has a mass error of 0.46 ppm, thus it is very likely that this molecular formula assigned is that of the molecule analyzed (see Appendix 2 Figure A263 for corresponding data). Taken together, all of the results from NMR spectrometry, IR and MS analysis all confirm the structural characterization of (1*E*,3*E*,5*E*)-1,3-bis-phenylsulfonyl-6-(thiophene)-hexa-1,3,5-triene **120** as a representative of trienes bearing a heterocycle as an alternative to the phenyl ring.

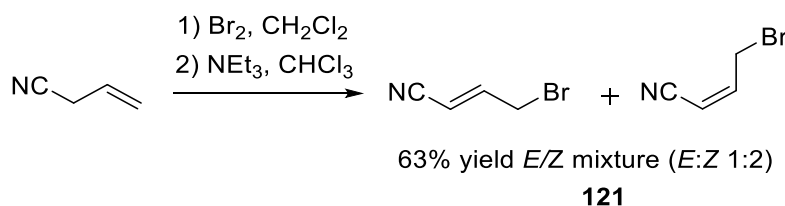
2.2.9 Reaction scope: Variation of the propene electron-withdrawing group

We then investigated if we could increase the substrate scope further by changing the electron-withdrawing group on the propene. However, before these reactions could be investigated, the corresponding propenes first had to be synthesized.

2.2.9.1 Synthesis of cyano and ester propenes

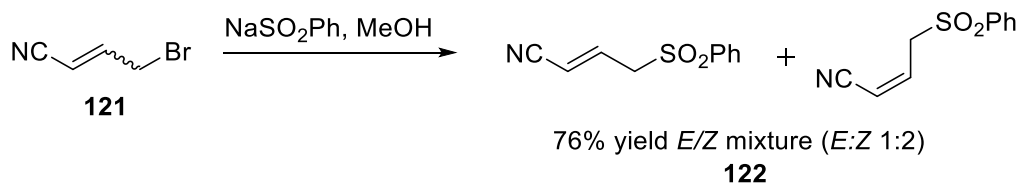
A proposed method and mechanism for the synthesis of (*E*)-3-bromo-1-phenylsulfonylprop-1-ene **103**²³⁵ has been discussed previously in section 2.2.1. The same method of bromination, followed by E2 elimination, was applied in the synthesis of (*E/Z*)-4-bromo-but-2-enenitrile **121** using allyl cyanide as the starting material, Scheme 34. The reaction was performed on 37.3 mmol scale using allyl cyanide (1 equivalent), elemental bromine (1.1 equivalents) in DCM (50 mL) on ice for 15 minutes, then at room temperature for 4 hours. Following this, the intermediate dibromide was isolated, dissolved in chloroform (50 mL), and treated dropwise with triethylamine (1 equivalent). This solution was then stirred for 5 minutes on ice and then for a further ~15 minutes on removal of the ice (until the solution returned to room temperature) to give a crude mixture of isomers.

The desired product was obtained in a 63% yield (1:2 ratio of *E/Z* isomers obtained, respectively) after purification. Short-path distillation of the crude product using a Kugelrohr apparatus gave pure product as a colourless liquid, albeit as a 1:2 mixture of isomers. Further attempts to separate the *E/Z* isomers, including separation by crystallization and by column chromatography were futile.



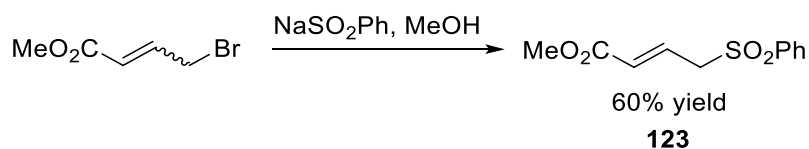
Scheme 34. Synthesis of (*E/Z*)-4-bromo-but-2-enenitrile, **121**.

Compound **121** was then used to synthesize (*E/Z*)-4-phenylsulfonyl-but-2-enenitrile, **122**, following the same procedure as described for the synthesis of (*E*)-1,3-bis-phenylsulfonylprop-1-ene **103** see section 2.2.1. The procedure incorporates a S_N2 mechanism with benzenesulfinic acid sodium salt, and was adapted from literature.²³⁶ When it was implemented using **121**, the yield of **122** was 76%, where the ratio of *E:Z* isomers was 1:2, respectively, Scheme 35. The product was purified by crystallization of the crude residue using a dichloromethane/*n*-hexane mixture on a salt/acetone ice bath.



Scheme 35. Synthesis of (*E/Z*)-4-phenylsulfonyl-but-2-enitrile, **122**. The experimental procedure was adapted from the literature.²³⁶ Reaction was performed on 13.7 mmol scale using **121** (1 eq.) and benzenesulfinic acid sodium salt (2.3 eq.) in methanol (35 mL) at reflux for 3.5 hours.

The synthesis of methyl (*E*)-4-(phenylsulfonyl)but-2-enoate **123** from methyl 4-bromocrotonate (which was predominately *trans*- and purchased commercially) followed the same procedure, Scheme 36. In this case, the *E*-isomer was exclusively formed, as shown by ¹H NMR spectroscopy, on crystallization of the crude oil from a dichloromethane/*n*-hexane mixture using an ice/acetone/salt bath. The desired product **123** was isolated in a 60% yield.



Scheme 36. Synthesis of methyl (*E*)-4-(phenylsulfonyl)but-2-enoate, **123**. The experimental procedure was adapted from the literature.²³⁶ Reaction was performed on 7.5 mmol scale using (*E/Z*)-methyl 4-bromocrotonate (1 eq.) and benzenesulfinic acid sodium salt (2.3 eq.) in methanol (20 mL) at reflux for 3.5 hours.

All three propenes were structural characterized using NMR spectroscopy and LC-MS. The NMR characterization of (*E/Z*)-4-phenylsulfonyl-but-2-enitrile **122** can be used as an example. For ease of explanation, an atom labelling system has been employed and is shown in Figure 67.

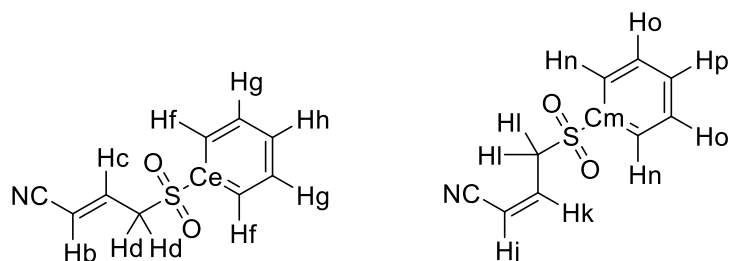


Figure 67. The structure of (*E/Z*)-4-phenylsulfonyl-but-2-enenitrile (compound **122**, Scheme 35), with atoms labelled for ease of discussion.

Starting with the *E*-isomer, Hb can be identified as a doublet of triplets signal and, using coupling constants, can be distinguished from the alternative *Z*-isomer whose equivalent Hj exhibits the same splitting pattern but with a smaller coupling constant. With coupling constants of 1.4 Hz and 16.3 Hz, Hb corresponds to the doublet of triplets (dt) signal at 5.45 ppm integrating for one proton. Cb can be identified as the signal at 108.2 ppm using the HSQC spectrum. Using the COSY spectrum, Hd can be identified as the doublet of doublets signal at 3.95 ppm and Hc can be expected to be a dt signal also but, due to overlapping of its signal with that of Hl from the alternative *Z*-isomer, appears as a multiplet at 6.59-6.53 ppm. Using the HSQC spectrum, Cd is the signal at 59.5 ppm and Cc appears at 139.9 ppm. Ca (the nitrile carbon) can be predicted to be the more upfield ^{13}C signal of the two quaternary carbon signals, the other being Ce. Due to being bonded directly to a nitrogen atom, an inductive effect makes Ca more deshielded than a typical alkyne carbon, but it appears more upfield than Ce nonetheless as Ce is an aromatic carbon. By comparison of the DEPT-135 and ^{13}C spectra, the quaternary carbons can be identified as 137.7 and 115.6 ppm and, based on the above, as Ce and Ca, respectively. With respect to the phenyl ring, Hf can be found within the multiplet at 7.92-7.87 ppm, which can be explained due to its proximity to the electron-withdrawing sulfonyl group, and so, would be more deshielded than Hg or Hh. Hg, which shows coupling to both Hf and Hh, appears within the multiplet at 7.64-7.59 ppm and Hh appears within the multiplet at 7.75-7.70 ppm, as identified using the COSY spectrum. Using the HSQC spectrum, Cf, Cg and Ch can be identified as the signals at 129.62, 128.3 and 134.6, respectively. The corresponding protons and carbons of the *Z*- isomer can be assigned in the same way. All spectra relevant to compound **122** can be found in Appendix 2, Figures A88-A93.

2.2.9.2 Attempted synthesis of methyl 7-phenyl-4-(phenylsulfonyl)hepta-2,4,6-trienoate **124** from (*E*)-4-(phenylsulfonyl)but-2-enoate **123**

The attempted synthesis of methyl 7-phenyl-4-(phenylsulfonyl)hepta-2,4,6-trienoate **124** using methyl (*E*)-4-(phenylsulfonyl)but-2-enoate **123** under our now standard Knoevenagel-type condensation reaction conditions, resulted in a complex mixture. The crude reaction mixture was a yellow oil and, even after being subjected to column

chromatography, a complex mixture was obtained which we were unable to separate. The ^1H NMR spectrum of some of the fractions collected are shown in Figure 68 and the spectrum does appear to show the presence of the desired triene product, along with inseparable impurities.

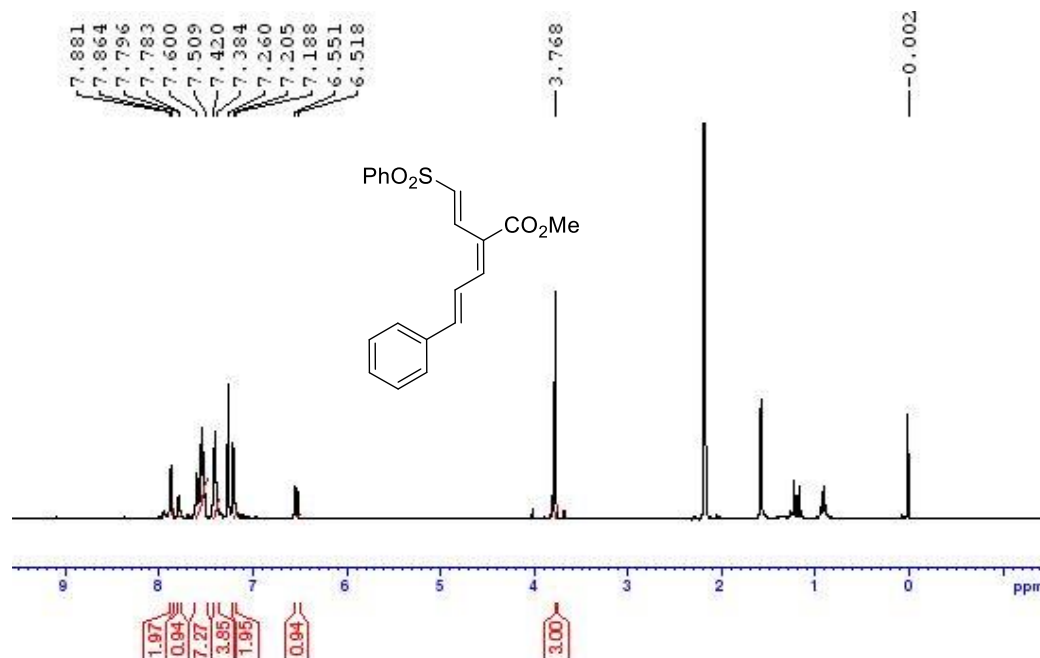


Figure 68. ^1H NMR spectrum of fractions 17-20 corresponding to 17 mg of material containing impure compound **124**. This correlates to a crude yield of 10%.

The ^1H NMR spectrum shows some diagnostic triene signals including a CO_2Me signal at 3.77 ppm, a possible olefin doublet at 6.55-6.52 ppm which has a coupling constant of 16.1 Hz, and an additional olefin signal within the multiplet at 7.60-7.51 ppm with the same coupling constant. This is supported by the COSY spectrum, which shows coupling between these two signals, Figure 69.

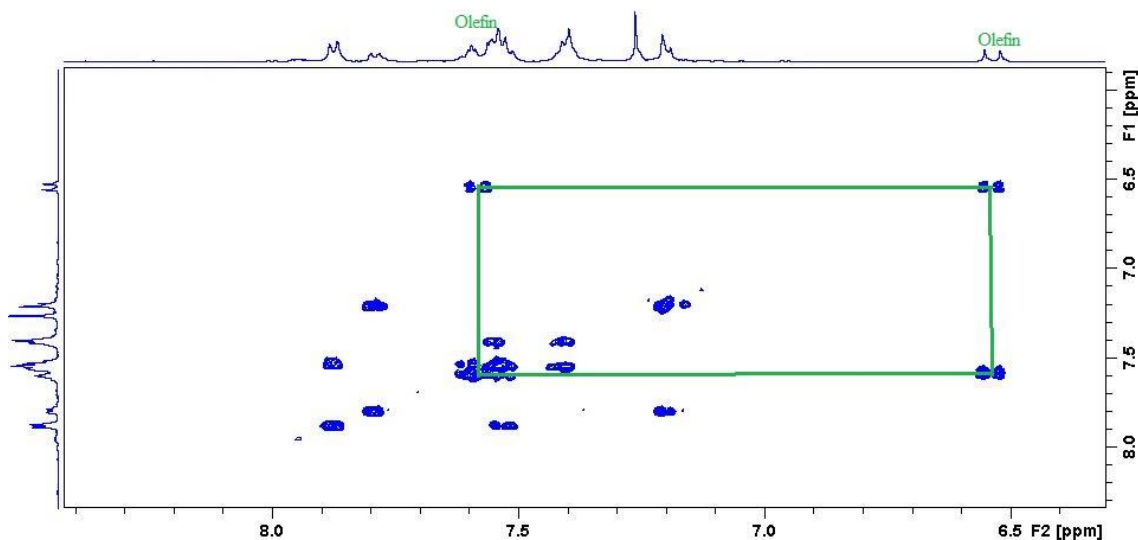


Figure 69. COSY spectrum of fractions 17-20 containing impure **124**.

Examination of the ^{13}C NMR spectrum supported the conclusion that triene **124** was present as 16 distinct carbon signals are evident, as well as the major impurity of acetone, which shows signals at δ 207.0 and 30.9 ppm, Figure 70. Expected ^{13}C NMR signals appeared at 166.7 ppm corresponding to the carbonyl carbon, the methyl component of the CO_2Me signal appearing at 52.0 ppm, and two taller carbon peaks at 129.3 and 129.1 ppm. These are typical for phenylsulfonyl carbons as they represent two carbons rather than one, as a result of symmetry in the molecule.

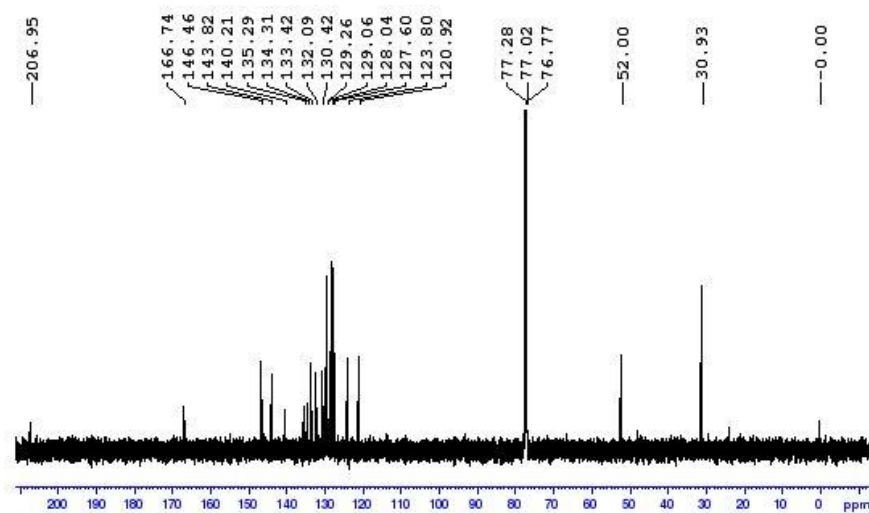


Figure 70. ^{13}C NMR spectrum of fractions 17-20, containing impure **124**.

When the propene was changed, (i.e. an ester was introduced in place of a phenylsulfonyl group), the reactivity of the anion formed in the first step of triene synthesis, given as Scheme 33 previously, may also change, resulting in a diminished yield in comparison to the use of bis(phenylsulfonyl)propene, **104**. The lower reactivity of this anion, relative to that formed when **104** was used, is supported by the fact that some starting material (*E*)-4-(phenylsulfonyl)but-2-enoate was also recovered (20%). This implies that, in addition to a complex mixture, we also had incomplete conversion to products.

2.2.9.3 Synthesis of cyano-sulfonyl trienes

Our attempted synthesis of cyano-sulfonyl trienes was more successful. We employed our now standard reaction conditions of (*E/Z*)-4-(phenylsulfonyl)but-2-enenitrile, **122**, (1 equivalent), corresponding cinnamaldehyde (1.1 equivalents), activated aluminium oxide (15 equivalents) in anhydrous dichloromethane (10 mL) under nitrogen for 24 hours. This allowed us to gain access to a family of trienes using an *E*- and *Z*- mixture of **122** and different cinnamaldehydes as starting materials, Figure 71.

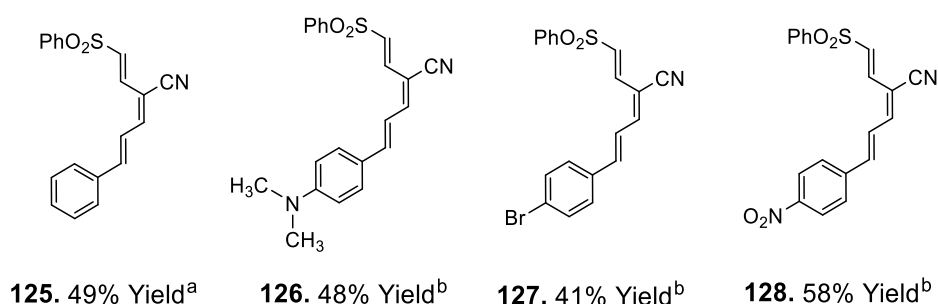


Figure 71. Cyano-sulfonyl trienes synthesized. ^a Reaction was performed at 1 mmol scale. ^b Reaction was performed at 0.5 mmol scale.

We chose these four trienes as they include an electron-donating group (NMe₂), an electron-withdrawing group (NO₂), a halogen (Br), and the parent phenyl ring. The yields obtained ranged from 41% to 58%. As was the case with respect to the bis(phenylsulfonyl) trienes, the most electrophilic cinnamaldehyde used (*p*-nitrophenyl cinnamaldehyde **44**, see section 2.2.4) gave the highest yield at 58%. Of note is the fact that, despite the use of a propene which contained a mixture of isomers, **122**, preliminary data provided by NMR spectroscopy suggests that the (*2E,4E,6E*)-isomer was isolated exclusively in each case. The preferential formation of (*E,E*)-diene or (*E,E,E*)-triene isomers have been previously described by other groups.^{164, 191, 209, 237} However, in general, the yields were lower than when (*E*)-1,3-bis(phenylsulfonyl)prop-1-ene, **104**, was employed as the propene. This may have been due to issues with crystallization in order to obtain a pure product as the crystals were more difficult to obtain, compared with the corresponding bis(phenylsulfonyl)-containing triene. This may be explained by the

presence of a complex mixture in the crude ^1H NMR spectrum (see Appendix 2, Figure A264). It was pleasing to see that a family of cyano sulfonyl trienes could also be accessed using our now standard reaction conditions, and that both electron-donating and electron-withdrawing substituents were tolerated.

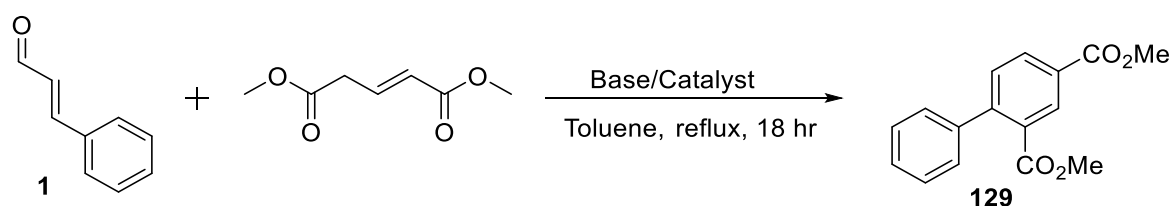
2.2.9.4 Attempted synthesis of bis(methyl ester) triene

A fourth propene, dimethyl glutaconate (Scheme 37), was also applied in our aluminium oxide (Al_2O_3) methodology. Dimethyl glutaconate, which was purchased commercially, was used without further purification and consisted mostly of the *E*-isomer. Our three other propenes all contained at least one phenylsulfonyl group and we thought it would be interesting to include a propene which contained two different electron-withdrawing groups. Surprisingly, when dimethyl glutaconate was used as the propene, the desired triene was not produced in any amount. In fact, no reaction took place under these conditions and returned starting material was observed as evidence by ^1H NMR spectroscopy (see Appendix 2, Figure A323).

On the basis of the complex product mixture and low yield of triene obtained when (*E*)-4-(phenylsulfonyl)but-2-enoate, **123**, was utilized as the propene, we had expected a similar occurrence with the use of dimethyl glutaconate, rather than no reaction at all. Taken together, this indicates that the developed Al_2O_3 methodology may not be suitable for esters, and that other types of electron-withdrawing groups are better tolerated, such as phenylsulfonyl or cyano groups.

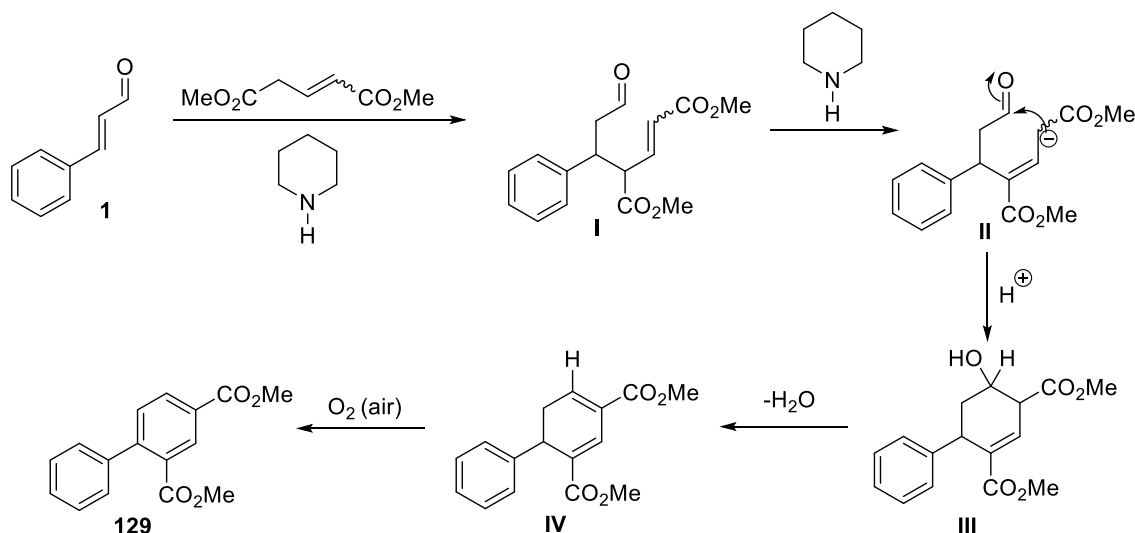
Given the lack of reaction between dimethyl glutaconate and *trans*-cinnamaldehyde, **1**, using our preferred aluminium oxide methodology, we wanted to see if the traditional Knoevenagel-condensation conditions would be more successful. This was attempted through the use of an amine base, piperidine. The solvent was changed to toluene and the mixture was allowed to reflux for 18 hours, rather than reacting at 20 °C for 24 hours. This did lead to a reaction between dimethyl glutaconate and **1**, but the triene was not formed. Instead a biaryl product, previously reported by Diallo *et al.*²³⁸, was formed, Scheme 37, though this group used NaOH as a base rather than the piperidine.²³⁸ As expected in the ^1H NMR spectrum (Appendix 2, Figure A324), the proton between the two esters is the most deshielded signal, appearing at 8.49 ppm, and integrates for one proton. The next signal, reading upfield, corresponds to the proton *meta*-to the most deshielded proton as this proton is within three bonds of one of the esters and hence, is shifted downfield relative to the last proton in the aryl system. It appears as a doublet of doublets due to coupling between this proton and the two others on this aryl ring, with coupling constants of 1.8 Hz and 8.1 Hz. The remaining proton in this aromatic ring appears at 7.47 ppm and those protons that make up the second aryl system appear as multiplets at 7.47-7.38 ppm and 7.33-7.31 ppm. The two methyl groups on the esters appear as singlets, as expected, at 3.96 and 3.68 ppm. All of this matches the NMR data

reported by Diallo *et al.*²³⁸ However, the signal that appears at 8.49 ppm in our ¹H NMR spectrum appears as a doublet with a coupling constant of 1.8 Hz, whereas, Diallo *et al.*²³⁸ record this as a singlet, and the signal at 7.47 ppm appears in our ¹H NMR spectrum as a doublet with a coupling constant of 8.1 Hz, whereas, Diallo *et al.*²³⁸ record this as a doublet of doublets with coupling constants of 8.5 Hz and 1.5 Hz. We did use HR-MS to confirm the molecular formula assignment of this product (see Appendix 2, Figure A326) and, with a mass error of 1.67 ppm, we are confident that dimethyl biphenyl-2,4-dicarboxylate, **129**, is the product produced as a result of this reaction.



Scheme 37. Reaction that occurred when **1** was reacted with dimethyl glutaconate in the presence of either piperidine and acetic acid, *DL*-proline, or pyrrolidine. The use of pyridine led to no reaction and returned starting material.

A number of different bases were then investigated, namely *DL*-proline, pyrrolidine and pyridine. However, in all cases where a reaction occurred, the same biaryl product was produced. A proposed mechanism, based on that suggested by Diallo *et al.*²³⁸, is given in Scheme 38.



Scheme 38. Adapted from the work of Diallo *et al.*,²³⁸ a proposed mechanism for biaryl formation.

According to this mechanism, the biaryl product is formed as a result of a based-catalyzed [3+3] oxidative benzannulation reaction between α,β -unsaturated carbonyl compounds

and dimethyl glutaconate. It starts with the intermolecular Michael addition of dimethyl glutaconate to the aldehyde, in our case *trans*-cinnamaldehyde **1**, to give the intermediate **I**. The intermediate **II** is generated via C=C double bond isomerization of intermediate **I** under basic conditions, and this intermediate subsequently undergoes an intramolecular aldol cyclization to produce the six-membered alcohol intermediate **III**. The final biaryl product is formed via a sequential dehydration and oxidative aromatization with molecular oxygen (from air).²³⁸ The pKa of (the amino component of the) protonated *DL*-proline, pyrrolidine, and piperidine are all approximately 11. However, the pKa of the protonated form of pyridine is approximately 5. This makes its conjugate base, being pyridine, a much weaker base than those listed above. This might explain why the reaction shown above does not take place with respect to pyridine but does when any of the other bases are used. Different variations of this reaction were attempted, including changing the solvent to ethanol, an investigation of different temperatures, 20 °C, 50 °C and 80 °C and different equivalents of base, Tables 17(a)-(d). In all cases, the biaryl product formed and the best yield was obtained using toluene as the solvent, piperidine as the base, and a reflux temperature of ~112 °C for 18 hours. Hence, it was decided that we could not access this particular triene using the Knoevenagel condensation reaction, traditional or otherwise.

Table 17(a). Number of equivalents of base explored as part of the variations of the traditional Knoevenagel-condensation reaction

Equivalents of base ^a	Yield of pure biaryl (%) ^b
0.25 eq. piperidine and acetic acid	42
0.5 eq. piperidine and acetic acid	45
1 eq. piperidine and acetic acid	51
1.5 eq. piperidine and acetic acid	47

^a In varying the conditions for application of the traditional Knoevenagel-condensation, dimethyl glutaconate (1 mmol) and *trans*-cinnamaldehyde, **1** (1 mmol) were employed, using piperidine and acetic acid (varying equivalents), and allowed to reflux in toluene for 18 hours. ^b Isolated yield obtained after column chromatography.

Table 17(b). Solvents explored as part of the variations of the traditional Knoevenagel-condensation reaction

Solvent ^a	Yield of pure biaryl (%) ^b
Toluene	51
Ethanol	21

^a In varying the conditions for application of the traditional Knoevenagel-condensation, dimethyl glutaconate (1 mmol) and **1** (1 mmol) were employed, using piperidine and acetic acid (1 eq.), and allowed to reflux in different solvents for 18 hours. ^b Isolated yield obtained after column chromatography.

Table 17(c). Temperatures explored as part of the variations of the traditional Knoevenagel-condensation reaction

Temperature (°C) ^a	Yield of pure biaryl (%) ^b
~ 112 (Reflux)	51
80	44
30	Product not obtained by crude NMR, returned starting materials

^a In varying the conditions for application of the traditional Knoevenagel-condensation, dimethyl glutaconate (1 mmol) and **1** (1 mmol) were employed, using piperidine and acetic acid (1 eq.), and allowed to react at different temperatures in toluene for 18 hours. ^b Isolated yield obtained after column chromatography.

Table 17(d). Bases explored as part of the variations of the traditional Knoevenagel-condensation reaction

Base ^a	Yield of pure biaryl (%) ^b
Piperidine and acetic acid	51
<i>DL</i> -proline	9
Pyrrolidine	19
Pyridine	Product not obtained by crude NMR, returned starting materials

^a In varying the conditions for application of the traditional Knoevenagel-condensation, dimethyl glutaconate (1 mmol) and **1** (1 mmol) were employed, using different bases (1 eq.), and allowed to reflux in toluene for 18 hours. ^b Isolated yield obtained after column chromatography.

We then wanted to consider if changing the electronics of the reacting species might enable triene formation. The phenyl ring on *trans*-cinnamaldehyde, **1**, was replaced with one containing an electron-withdrawing group at the *para* position (a nitro group). All other conditions remained the same (i.e. dimethyl glutaconate (1 mmol) and **44** (1 mmol) reacted using piperidine as the base (1 equivalent), and acetic acid (1 equivalent) and allowed to reflux in toluene for 18 hours). Again, it appears that it is the biaryl product, **130**, (Figure 72(a)) that is formed rather than the triene. This is a novel biaryl to the best

of our knowledge, although Diallo *et al.*²³⁸ did report the formation of a very similar product, Figure 72(b), whose reported spectra align very well with our data.

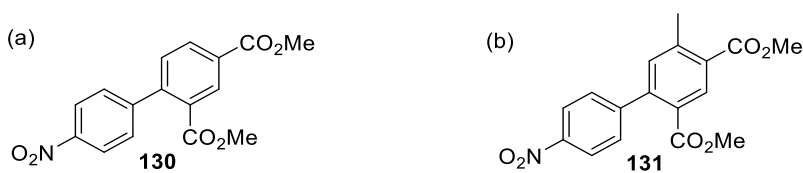


Figure 72. (a) The proposed product **130** formed from the reaction 4-nitrocinnamaldehyde, **44**, and dimethyl glutaconate in our attempts at triene synthesis. (b) The dimethyl 5-methyl-4'-nitrophenyl-2,4-dicarboxylate product, **131**, formed by Diallo *et al.*²³⁸

The analysis of the ¹H NMR spectrum (Figure 73), is very clear for the assignment of the NMR data of compound **130** and so this will be the focus of the discussion here.

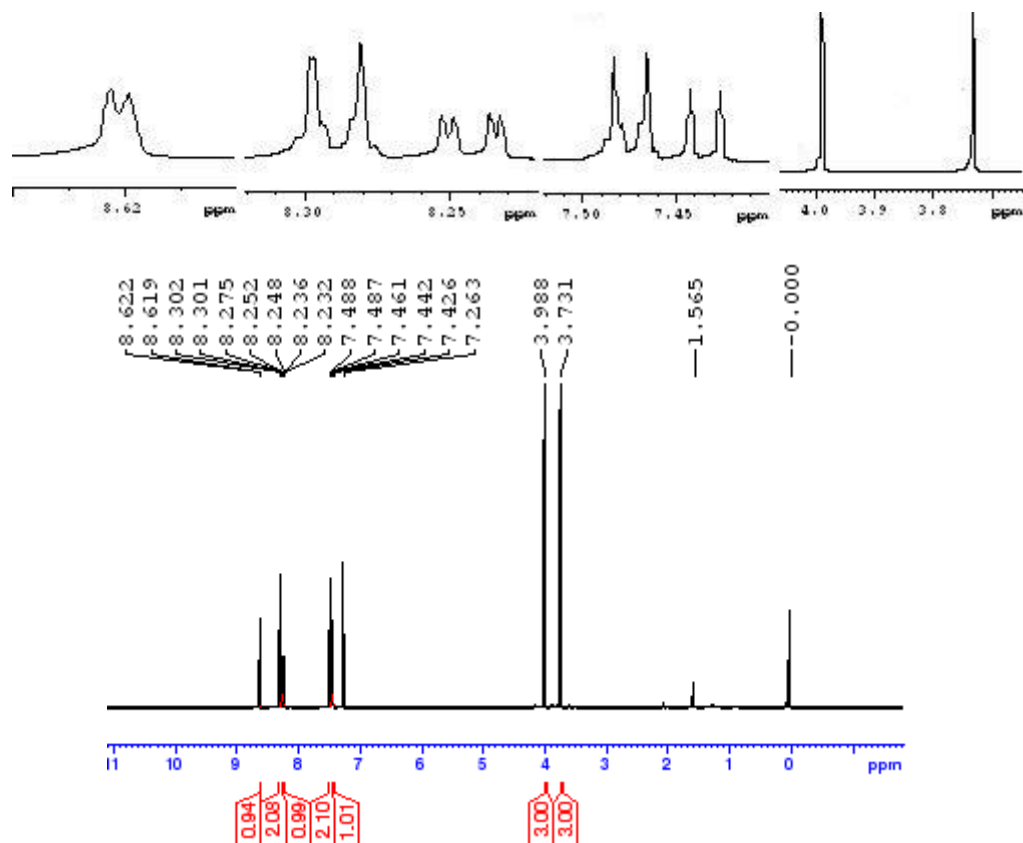


Figure 73. ¹H NMR spectrum of dimethyl 4'-nitrophenyl-2,4-dicarboxylate, **130**, with zoomed in images of signal multiplicities, in order of ppm.

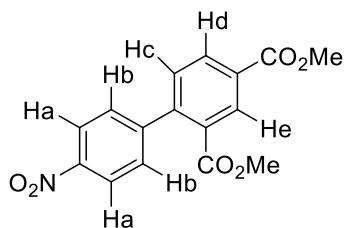


Figure 74. The proposed biaryl product with protons assigned with labels.

Hc (Figure 74) is the most shielded aromatic proton and therefore appears the most upfield after the two methyl groups, which are assigned as the two singlets at 3.99 and 3.73 ppm. This is because Hc is over three bonds away from either of the two methyl ester electron-withdrawing groups, and hence, does not experience the deshielding effect that either Hd or He experiences. The next signal, reading downfield, is that of a set of protons on the other aromatic ring. We know that the nitro group is a strongly electron-withdrawing group so Ha would be more deshielded for that reason. Hence the signal that is slightly more downfield to Hc must belong to the two Hb protons. They would not be exactly chemically equivalent, but on the basis of their chemical shifts being so close, it is easier for the purposes of NMR analysis to assign them the same label. Hd can be easily assigned because it is the only proton that could generate a doublet of doublets, being coupled to Hc and He, and the coupling constants observed of 8.0 Hz (d-c coupling) and 1.8 Hz (d-e coupling) is justified on the basis of its proximity to these two protons. Ha is the next signal, reading downfield, which is a multiplet integrating for two protons. It is quite downfield because of proximity to the *para*-nitro substituent as mentioned previously. He therefore appears as the most deshielded signal, which is also justified based on its location between two electron-withdrawing groups. The ^{13}C NMR and 2D-spectra confirm the formation of this product. For example, the COSY spectrum shows the coupling of Hd to Hc and He, and the coupling between Ha and Hb. These spectra are included in Appendix 2, Figures A327-A332.

Our final attempt to synthesize the bisester triene involved the reaction of 4-methoxycinnamaldehyde, **14**, (cinnamaldehyde with an electron-donating OMe substituent) with dimethyl glutaconate. Unfortunately, the traditional Knoevenagel-condensation reaction conditions led to a complex mixture, which we were unable to separate.

2.3 Conclusion

To conclude, in this chapter we have described the development and application of a Knoevenagel-type condensation reaction for the synthesis of a family of novel electron poor trienes. Trienes are interesting because of their presence in a range of medicinal products that exhibit a wide range of properties including antibacterial and anti-melanogenic, as well as their ability to act as substrates in reactions such as Diels Alder and 1,8-conjugate additions. Our approach involved the Knoevenagel-type condensation of a propene with a *trans*-cinnamaldehyde to give the target triene, with the synthesis of both the starting propene and *trans*-cinnamaldehyde required in most cases. The development of this methodology involved an initial attempt to use traditional Knoevenagel-condensation reaction conditions of piperidine and acetic acid. However, in our model/test reaction this did not lead to the synthesis of the desired (1*E*,3*E*,5*E*)-1,3-bis-phenylsulfonyl-6-phenyl-hexa-1,3,5-triene, **105**, and prompted us to search for alternative reaction conditions. As a result, we undertook an optimisation study, with percentage conversion to triene estimated by qNMR, where we explored choice of solvent, choice of base, and temperature. One of the reaction conditions we explored involved the use of activated aluminium oxide as a base. The use of activated aluminium oxide in Knoevenagel-type condensations has been reported previously in the literature but its application to (*E*)-1,3-bis-phenylsulfonyl-prop-1-ene, **104**, is, to the best of our knowledge, a novel application of this synthetic approach. The optimization study was successful in that preferred reaction conditions using activated aluminium oxide were established which allowed the synthesis of the desired triene **105**. The geometry of this compound was confirmed by a previous group member, through X-ray crystallography, and correlated with the NMR spectroscopic evidence we had obtained, for example, through the calculation of coupling constants. Our preferred reaction conditions are 1 equivalent of propene and 1.1 equivalent of the *trans*-cinnamaldehyde, reacted at 20 °C for 24 hours, using 15 equivalents of aluminium oxide as the base and DCM as the solvent.

The application of our preferred aluminium oxide reaction conditions, and a variety of *trans*-cinnamaldehydes, allowed us to access a family of novel 1,3,5-bis(phenylsulfonyl)hexatrienes, compounds **106-120**. As an example of our approach to structural characterization, a detailed discussion of the NMR analysis of one representative 1,3,5-hexatriene species, **110**, is included. This methodology was successful in the incorporation of a number of different *trans*-cinnamaldehydes, with different electron donating and withdrawing groups on the aryl ring, as well as replacement of the aryl ring with other heterocyclic and aryl systems. This was important as it showed the substrate scope of our methodology, and all *trans*-cinnamaldehyde that were employed resulted in the generation of the respective triene. Yields of 50-96% were achieved with respect to the family of bis(phenylsulfonyl) trienes, with cinnamaldehydes bearing an electron-withdrawing group in the *para*-position of the phenyl ring producing the highest yields of trienes.

The use of propene (*E/Z*)-4-phenylsulfonyl-but-2-enenitrile, **122**, as starting material, in place of **104**, resulted in the generation of a small family of 2,4,6-heptatrienes, albeit in lower yields than the bis(phenylsulfonyl) trienes, at 41-58%. Here we explored both electron donating and electron withdrawing groups on the aryl ring of the *trans*-cinnamaldehyde. Again, the *trans*-cinnamaldehyde bearing an electron-withdrawing group in the *para*-position of the aryl ring (a nitro substituent) produced the highest yield (58%) of the respective triene, **128**. The incorporation of an alternative to **104** was important as it demonstrates the ability to increase the substrate scope further, where variations of both the *trans*-cinnamaldehyde and propene are tolerated. All twenty trienes reported in this chapter are novel in the literature, and full characterization of each was successfully completed using a combination of NMR spectroscopy, LC-MS, HR-MS and IR analysis (and X-ray crystallography, where possible).

However, we did find that there were limitations in terms of substrate scope regarding the nature of the propene used. Our research to date indicates that the presence of an ester on the propene substrate largely diminishes and even prevents the formation of the desired triene product. For instance, the attempted synthesis of methyl 7-phenyl-4-(phenylsulfonyl)hepta-2,4,6-trienoate, **124**, using the propene methyl (*E*)-4-(phenylsulfonyl)but-2-enoate, **123**, resulted in a complex mixture. Despite column chromatography, the desired triene product was isolated with inseparable impurities in a very low yield of 10%. Additionally, the use of dimethyl glutaconate as the propene was completely unsuccessful, with respect to its application in our aluminium oxide methodology, as just returned starting materials was observed, evident by NMR spectroscopic analysis after the 24-hour reaction. In this case, a traditional Knoevenagel approach was attempted using piperidine but, despite attempts at varying the reaction conditions by changing the base, solvent and temperature, the desired triene could not be synthesized. An alternative biaryl product, dimethyl biphenyl-2,4-dicarboxylate **129**, was obtained when the traditional Knoevenagel-condensation reaction conditions were employed. This product was previously reported by Diallo *et al.*,²³⁸ though this group used NaOH as a base rather than the piperidine. NMR analysis was used to confirm the structure of this biaryl, as well as HR-MS.

Thus, there is an apparent limitation in terms of substrate scope that suggests the developed aluminium oxide methodology may not be suitable for propenes containing esters, and that other types of electron-withdrawing groups in the propene component are better tolerated, such as phenylsulfonyl or cyano groups. This is an important consideration in terms of any future potential applications of this procedure. However, overall this proposed methodology is a convenient synthetic protocol that allows for the generation of a range of trienes under mild conditions without the need for column chromatography. This method tolerates a wide range of cinnamaldehydes, and a smaller range of propenes, and is a new synthetic methodology for the synthesis of novel electron poor triene systems.

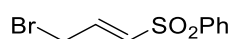
2.4 Experimental Procedure

2.4.1 General information for chemical synthesis

See section 1.4.1 for full details. Additionally, infrared spectra were obtained via ATR as a solid on a zinc selenide crystal in the region 4000-400 cm^{-1} on a Perkin Elmer Spectrum 100 FT-IR spectrophotometer.

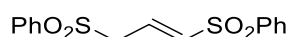
2.4.2 Synthesis of precursor molecules

2.4.2.1 Procedure for the synthesis of (*E*)-3-bromo-1-phenylsulfonylprop-1-ene, **103**



This procedure was modified from literature.²³⁵ Elemental bromine (1.66 mL, 32.3 mmol, 1.1 eq.) was added to a stirring solution of allyl phenylsulfone (4.5 mL, 29 mmol, 1 eq.) and dichloromethane (98 mL) and the resulting mixture was stirred at room temperature for 4 hours. The solvent, and excess bromine, were removed *in vacuo* and the residue was suspended in cold diethyl ether (50 mL). The intermediate dibromide was isolated as a white solid after vacuum filtration. This solid was dissolved in chloroform (98 mL) and triethylamine (4.10 mL, 29.4 mmol, 1 eq.) was added dropwise to the solution on ice. The reaction was stirred for 5 minutes, and then for a further 10 minutes on removal of the ice, until the solution returned to room temperature. The resulting mixture was washed, first with 1 M HCl (50 mL) and then with distilled water (50 mL). The organic layer was removed, dried over anhydrous Na_2SO_4 , and concentrated *in vacuo* to give a colourless residue. This was crystallised from a diethyl ether/n-hexane mixture on ice, which was then left in the freezer for 3 hours to give colourless needles, 4.039 g (53%). ^1H NMR (500 MHz, CDCl_3): δ 7.95-7.88 (m, 2H), 7.66-7.54 (m, 3H), 7.03 (dt, 1H, $J = 6.8$ Hz, $J = 14.8$ Hz), 6.57 (dt, 1H, $J = 1.4$ Hz, $J = 14.8$ Hz), 4.01 (dd, 2H, $J = 1.4$ Hz, $J = 6.8$ Hz); ^{13}C NMR (125 MHz, CDCl_3) δ 139.7, 139.5, 134.1, 133.8, 129.5, 127.9, 27.3 ppm NMR data matches with literature.²³⁵; LC-MS: purity 99.0% $t_{\text{R}} = 25.59$ min, (ESI) m/z $[\text{M}+\text{NH}_4]^+$ 278.2.

2.4.2.2 Procedure for the synthesis of (*E*)-1,3-bis-phenylsulfonylprop-1-ene, **104**



The procedure was modified from literature.²³⁶ **103** (1.958 g, 7.5 mmol, 1 eq.) was dissolved in methanol (22.5 mL) by stirring at room temperature. Benzenesulfinic acid sodium salt (2.831 g, 17.25 mmol, 2.3 eq.) was added and the mixture was refluxed for 1.5 hours. The solvent was removed *in vacuo*, leaving a white solid, which was partitioned

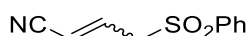
between dichloromethane (37.5 cm³) and distilled water (37.5 cm³). The organic layer was separated and dried over anhydrous Na₂SO₄. The mixture was then filtered and concentrated *in vacuo* to give a colourless residue that solidifies on standing. The product was crystallised from a dichloromethane/n-hexane mixture on a salt/acetone ice bath, which then gave colourless needles after being left in the freezer for 24 hours, 1.517 g (63%). ¹H NMR (500 MHz, CDCl₃) δ 7.83-7.81 (m, 2 H), 7.77-7.75 (m, 2H), 7.69-7.66 (m, 1 H), 7.65-7.61 (m, 1H), 7.59-7.55 (m, 2 H), 7.49-7.45 (m, 2H), 6.84 (overlapping dt, 1 H, *J* = 7.7 Hz, *J* = 15.2 Hz), 6.38 (dt, 1 H, *J* = 1.2 Hz, *J* = 15.1 Hz, CHCH), 3.95 (dd, 2 H, *J* = 7.8 Hz, *J* = 1.3 Hz); ¹³C NMR (125MHz, CDCl₃) δ 139.3, 138.6, 137.6, 134.34, 134.0, 131.3, 129.5, 129.4, 128.3, 128.0, 57.8 ppm, NMR data matches with literature.^{236, 239}; LC-MS: purity 99.2% t_R = 24.97 min, (ESI) m/z [M+NH₄]⁺ 340.1.

2.4.2.3 Procedure for the synthesis of (*E/Z*)-4-bromo-but-2-enenitrile, **121**



This procedure was modified from literature.²³⁵ Elemental bromine (2.2 mL, 41.03 mmol, 1.1 eq.) was added to a stirring solution of allyl cyanide (3 mL, 37.3 mmol, 1 eq.) and dichloromethane (50 mL) on ice, stirred for 15 minutes after all the bromine was added and then resulting mixture was then stirred at room temperature for 4 hours. The solvent, and excess bromine, were removed *in vacuo* and the residue was dissolved in chloroform (50 mL) and triethylamine (4.10 mL, 29.4 mmol, 1 eq.) was added dropwise to the solution on ice. The reaction was stirred for 5 minutes, and then for a further 10 minutes on removal of the ice, until the solution returned to room temperature. The resulting mixture was washed first with 1 M HCl (50 mL) and then with distilled water (50 mL). The organic layer was removed, dried over anhydrous Na₂SO₄, and concentrated *in vacuo* to give a brown liquid. This was then subjected to short-path distillation using a Kugelrohr apparatus to give a colourless liquid containing a mixture of isomers, 3.498g. (*Z:E* 2:1, 63%). ¹H NMR (500 MHz, CDCl₃): *E*-isomer: δ 6.85 (dt, 1H, *J* = 7.2 Hz, *J* = 16.0 Hz), 5.70 (dt, 1H, *J* = 1.4 Hz, *J* = 16.0 Hz), 4.07 (dd, 2H, *J* = 1.4 Hz, *J* = 7.2 Hz); *Z*-isomer: δ 6.74 (dt, 1H, *J* = 8.2 Hz, *J* = 10.7 Hz), 5.53 (dt, 1H, *J* = 0.8 Hz, *J* = 10.7 Hz), 4.18 (dd, 2H, *J* = 0.8 Hz, *J* = 8.2 Hz); ¹³C NMR (125 MHz, CDCl₃) *E*-isomer: δ 148.6, 116.4, 103.5, 29.5 ppm, *Z*-isomer: δ 147.7, 114.6, 102.5, 26.9 ppm, NMR data matches with literature.^{240, 241}.

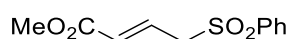
2.4.2.4 Procedure for the synthesis of (*E/Z*)-4-phenylsulfonyl-but-2-enenitrile, **122**



The procedure was modified from literature.²³⁶ **121** (2 g, 13.7 mmol, 1 eq.) was dissolved in methanol (35 mL) by stirring at room temperature. Benzenesulfinic acid sodium salt (5.173 g, 31.5 mmol, 2.3 eq.) was added and the mixture was refluxed for 3.5 hours. The

solvent was removed *in vacuo*, leaving an oily residue, which was partitioned between dichloromethane (60 cm³) and distilled water (60 cm³). The organic layer was separated and dried over anhydrous Na₂SO₄. The mixture was then filtered and concentrated *in vacuo* to give a colourless residue that solidifies on standing. The product was crystallised from a dichloromethane/n-hexane mixture on a salt/acetone ice bath, which then gave a brown-tinted solid after being left in the freezer for 24 hours which contained both isomers, 2.16 g (*Z:E* 66:33, 76%). ¹H NMR (500 MHz, CDCl₃) *Z* isomer: δ 7.92-7.87 (m, 2 H), δ 7.75-7.70 (m, 1 H) 7.64-7.59 (m, 2 H), 6.59-6.53 (m, 1 H), 5.60 (dt, 1H, *J* = 1.1 Hz, *J* = 10.9 Hz), 4.19 (dd, 2H, *J* = 1.1 Hz, *J* = 7.9 Hz); *E* isomer: δ 7.92-7.87 (m, 2 H), 7.75-7.70 (m, 1 H), 7.64-7.59 (m, 2 H), 6.59-6.53 (m, 1 H), 5.45 (dt, 1H, *J* = 1.4 Hz, *J* = 16.3 Hz), 3.95 (dd, 2H, *J* = 1.4 Hz, *J* = 7.7 Hz); ¹³C NMR (125 MHz, CDCl₃) *E* isomer: δ 139.9, 137.7, 134.6, 129.62, 128.3, 115.6, 108.2, 59.5 ppm, *Z* isomer: δ 139.4, 137.5, 134.58, 129.6, 128.4, 113.9, 107.2, 58.3 ppm; LC-MS (ESI) *m/z* [M+K]⁺ 246.1.

2.4.2.5 Procedure for the synthesis of (*E*)-4-(phenylsulfonyl)but-2-enoate, **123**



The procedure was modified from literature.²³⁶ Methyl 4-bromocrotonate (882 μL, 7.5 mmol, 1 eq.), which was predominately *trans*- and purchased commercially was dissolved in methanol (20 mL) by stirring at room temperature. Benzenesulfinic acid sodium salt (2.832 g, 17.25 mmol, 2.3 eq.) was added and the mixture was refluxed for 3.5 hours. The solvent was removed *in vacuo*, leaving an oily residue, which was partitioned between dichloromethane (60 cm³) and distilled water (60 cm³). The organic layer was separated and dried over anhydrous Na₂SO₄. The mixture was then filtered and concentrated *in vacuo* to give a colourless residue that solidifies on standing. The product was crystallised from a dichloromethane/n-hexane mixture on a salt/acetone ice bath, 1.085 g (60%). ¹H NMR (500 MHz, CDCl₃) *E* isomer: δ 7.88 (d, *J* = 7.4 Hz, 2H), 7.69 (t, *J* = 7.4 Hz, 1H), 7.59 (t, *J* = 7.8 Hz, 2H), 6.82 (overlapping dt, *J* = 15.6, 7.8 Hz, 1H), 5.91 (dd, *J* = 15.6, 1.1 Hz, 1H), 4.00 (d, *J* = 7.8 Hz, 2H), 3.72 (s, 3H); ¹³C NMR (125 MHz, CDCl₃) *E* isomer: δ 165.2, 138.1, 134.2, 133.2, 129.4, 129.0, 128.2, 58.9, 51.9 ppm. NMR data matches with literature.²³⁶

2.4.3 General protocol for reactions carried out as part of the optimization study to determine preferred reaction conditions for triene synthesis - qNMR

In order to develop a Knoevenagel-type condensation reaction, different solvent, bases, and temperatures were investigated using the synthesis of (1*E*,3*E*,5*E*)-1,3-bis-phenylsulfonyl-6-phenyl-hexa-1,3,5-triene **105** as a model reaction. In order to determine a set of preferred reaction conditions for our triene synthetic methodology, a quantitative NMR spectroscopic (qNMR) method was used to estimate percentage conversion of triene achieved by implementation of each reaction. In each case, *trans*-cinnamaldehyde, **1**, (140 μL, 1.1 mmol, 1.1 eq.) and (*E*)-1,3-bis(phenylsulfonyl)prop-1-ene, **104**, (324 mg,

1 mmol, 1 eq.) were dissolved in a solvent and a particular base, then the mixture was allowed to stir for a particular amount of time at a certain temperature. After this time had elapsed, the reaction mixture was reduced *in vacuo* to give the crude triene product **105**, all of which was transferred to a 10 mL volumetric flask and made up to the calibration mark using deuterated chloroform. A 10 mM solution of 1,3,5-trimethoxybenzene was made up by dissolving 16.819 mg of the solid in a 10 mL volumetric flask, using deuterated chloroform, and making up to the calibration mark. This solution was used as the internal standard for the experiment. 500 μL of each solution (of crude triene **105** and of the internal standard) was then transferred to a NMR tube which was capped and inverted several times to ensure homogeneous mixing of the two solutions. This solution was then subjected to ^1H NMR spectroscopy.

2.4.3.1 Exploration of base

2.4.3.1.1 Use of piperidine

As above, in section 2.4.3, piperidine (73 μL , 1 eq.) and acetic acid (63 μL , 1 eq.) were added to toluene (10 mL) and the mixture was allowed to reflux for 18 hours. A complex crude mixture was obtained with uninterpretable NMR spectra and hence, qNMR could not be applied to quantify the percentage conversion to **105** in this case.

2.4.3.1.2 Use of aluminium oxide (Al_2O_3)

As above, in section 2.4.3, Al_2O_3 (1.53 g, 15 eq.) was used as a base, which was added to DCM (10 mL) and the mixture was allowed to stir at 20 $^\circ\text{C}$ for 24 hours under nitrogen. The desired triene, **105** was produced in a quantitative conversion, corresponding to the generation of a 105.88 mM solution.

2.4.3.2. Exploration of solvent

2.4.3.2.1. Use of DCM

Exactly as above in section 2.4.3.1.2

2.4.3.2.2. Use of toluene

As above in section 2.4.3.1.2, Al_2O_3 (1.53 g, 15 eq.) was used as a base, which was added to toluene (10 mL) and the mixture was allowed to stir at 20 $^\circ\text{C}$ for 24 hours under

nitrogen. The desired triene **105** was produced, corresponding to a 62% conversion, in turn, corresponding to the generation of a 61.22 mM solution.

2.4.3.2.3. Use of methanol

As above in section 2.4.3.1.2, Al₂O₃ (1.53 g, 15 eq.) was used as a base, which was added to methanol (10 mL) and the mixture was allowed to stir at 20 °C for 24 hours under nitrogen. The desired triene **105** was produced, corresponding to a 66% conversion, in turn, corresponding to the generation of a 65.7 mM solution.

2.4.3.2.4. Use of acetonitrile

As above in section 2.4.3.1.2, Al₂O₃ (1.53 g, 15 eq.) was used as a base, which was added to acetonitrile (10 mL) and the mixture was allowed to stir at 20 °C for 24 hours under nitrogen. The desired triene **105** was produced, corresponding to a 43% conversion, in turn, corresponding to the generation of a 42.46 mM solution.

2.4.3.3 Exploration of number of equivalents of Al₂O₃

2.4.3.3.1 Use of 15 equivalents of Al₂O₃

Exactly as above in section 2.4.3.1.2

2.4.3.3.2 Use of 30 equivalents of Al₂O₃

As above in section 2.4.3.1.2, (3.06 g, 15 eq.) was used as a base, which was added to DCM (10 mL) and the mixture was allowed to stir at 20 °C for 24 hours under nitrogen. The desired triene **105** was produced, corresponding to a 59% conversion, in turn, corresponding to the generation of a 59.22 mM solution.

2.4.3.3.3 Use of 5 equivalents of Al₂O₃

As above in section 2.4.3.1.2, (0.51 g, 5 eq.) was used as a base, which was added to DCM (10 mL) and the mixture was allowed to stir at 20 °C for 24 hours under nitrogen. The triene **105** was produced, corresponding to a 96% conversion, in turn, corresponding to the generation of a 95.74 mM solution.

2.4.3.3.4 Use of 1 equivalent of Al₂O₃

As above in section 2.4.3.1.2, Al₂O₃ (0.10 g, 1 eq.) was used as a base, which was added to DCM (10 mL) and the mixture was allowed to stir at 20 °C for 24 hours under nitrogen. A complex crude mixture was obtained with uninterpretable NMR spectra and hence, qNMR could not be applied to quantify the percentage conversion to **105** in this case.

2.4.3.4 Exploration of reaction temperature

2.4.3.4.1 Use of 20 °C

Exactly as above in section 2.4.3.1.2

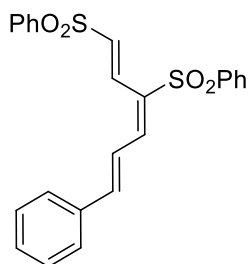
2.4.3.4.2 Use of ~40 °C (reflux)

As above in section 2.4.3.1.2, Al₂O₃ (1.53 g, 15 eq.) was used as a base, which was added to DCM (10 mL) and the mixture was allowed to reflux for 24 hours under nitrogen. The desired triene **105** was produced, corresponding to a 26% conversion, in turn, corresponding to the generation of a 25.72 mM solution.

2.4.4 General procedure for the synthesis of trienes

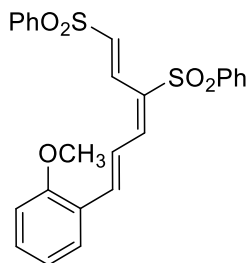
Activated aluminium oxide (0.765 g, 7.5 mmol, 15 eq.) was suspended in anhydrous dichloromethane (5 mL). The mixture was stirred in an ice bath for 10 minutes, at which point **104** (162 mg, 0.5 mmol, 1 eq.) was added followed by the corresponding cinnamaldehyde (0.55 mmol, 1.1 eq.). Alternatively, the reaction was performed at 1 mmol scale, thus the same conditions apply but all reagents mentioned thus far were doubled in quantity. The reaction was stirred for 24 hours at 20 °C. The resulting suspension was then filtered through a pad of Celite and washed with dichloromethane (25 mL). The solvent was removed *in vacuo* using a water bath set to 30 °C to afford the crude product. Dichloromethane was added to facilitate dissolution of the crude product and n-hexane (approximately 0.5 mL) was added. The solution was stored in the freezer overnight and the precipitate was filtered and washed with ice-cold methanol (2.5 mL) to yield a solid.

Synthesis of (1*E*,3*E*,5*E*)-1,3-bis-phenylsulfonyl-6-phenyl-hexa-1,3,5-triene, 105



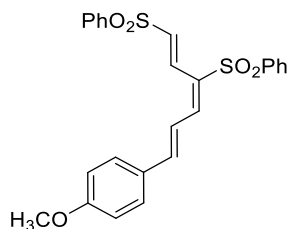
This compound was synthesized using *trans*-cinnamaldehyde, **1** (140 μ L, 1.1 mmol, 1.1 eq.) according to the general procedure at 1 mmol scale. A bright yellow solid was obtained, 403 mg (93%). ^1H NMR (500 MHz, CDCl_3) δ 7.84-7.81 (m, 3 H), 7.75-7.73 (m, 2 H), 7.66-7.63 (m, 1 H), 7.57-7.52 (m, 6 H), 7.43-7.39 (m, 5 H), 7.26-7.23 (d, 1 H), 7.18-7.13 (m, 2 H); ^{13}C NMR (125 MHz, CDCl_3) δ 147.8, 145.5, 134.0, 139.8, 135.0, 133.7, 133.6, 133.0, 132.3, 130.8, 129.4, 129.3, 129.2, 128.3, 127.7, 127.5, 120.3; HRMS (ESI-MS) Calc. for $\text{C}_{24}\text{H}_{21}\text{O}_4\text{S}_2$ ($\text{M}+\text{H}$) $^+$: 437.0876; found: 437.0862; IR (ATR): ν_{max} 3079, 3033, 1589, 1575, 1555, 1446, 1309, 1287, 1213, 1178, 1143, 1083, 977, 962, 873, 848, 817, 743, 719, 686 cm^{-1} ; LC-MS: purity 100% t_{R} = 31.59 min, (ESI) m/z [$\text{M}+\text{K}$] $^+$ 475.6.

Synthesis of (1*E*,3*E*,5*E*)-1,3-bis-phenylsulfonyl-(6-*o*-methoxyphenyl)-hexa-1,3,5-triene, 106



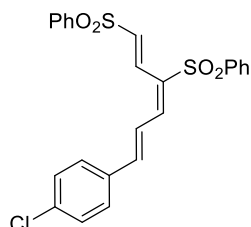
This compound was synthesized using 2-methoxy cinnamaldehyde, **2** (predominantly *trans*) (89 mg, 0.55 mmol, 1.1 eq.) according to the general procedure. A yellow solid was obtained, 163 mg (71%). ^1H NMR (500 MHz, CDCl_3) δ 7.86-7.80 (m, 3 H), 7.75-7.73 (m, 2 H), 7.65-7.62 (m, 1 H), 7.60-7.51 (m, 6H), 7.42-7.37 (m, 3 H), 7.31-7.26 (m, 1 H), 7.13-7.10 (d, 1 H), 7.02-6.99 (t, 1 H), 6.95-6.93 (d, 1 H) 3.92 (s, 3 H); ^{13}C NMR (125 MHz, CDCl_3) δ 158.4, 146.8, 143.5, 140.1, 140.0, 133.6, 133.4, 132.3, 132.2, 131.2, 129.6, 129.4, 129.2, 128.9, 127.7, 127.5, 124.0, 121.1, 121.0, 111.3, 55.7; HRMS (ESI-MS) Calc. for $\text{C}_{25}\text{H}_{23}\text{O}_5\text{S}_2$ ($\text{M}+\text{Na}$) $^+$: 489.0801; found 489.0797; IR (ATR): ν_{max} 3068, 3018, 1584, 1563, 1482, 1462, 1444, 1289, 1247, 1213, 1181, 1139, 1085, 1022, 984, 958, 841, 819, 741, 717, 687 cm^{-1} ; LC-MS: purity 97.1% t_{R} = 32.34 min, (ESI) m/z [$\text{M}+\text{H}$] $^+$ 467.4.

Synthesis of (1*E*,3*E*,5*E*)-1,3-bis-phenylsulfonyl-(6-*p*-methoxyphenyl)-hexa-1,3,5-triene, 107



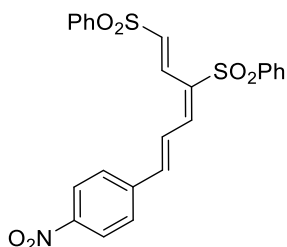
This compound was synthesized using *trans*-4-methoxy cinnamaldehyde, **14** (89 mg, 0.55 mmol, 1.1 eq.) according to the general procedure. A light brown solid was obtained, 145 mg (62%). ¹H NMR (500 MHz, CDCl₃) δ 7.83-7.80 (m, 3 H), 7.74-7.72 (m, 2 H), 7.66-7.62 (m, 1 H), 7.58-7.51 (m, 6 H) 7.42-7.38 (m, 2 H), 7.21-7.18 (d, 1 H), 7.13-7.10 (d, 1 H), 7.06-7.00 (dd, 1 H, *J* = 11.7 Hz, *J* = 15.0 Hz), 6.96-6.93 (m, 2H), 3.87 (s, 3H); ¹³C NMR (125 MHz, CDCl₃) δ 162.0, 147.9, 146.4, 140.1, 140.0, 133.6, 133.4, 131.9, 130.5, 130.2, 129.4, 129.2, 127.8, 127.7, 127.4, 118.1, 114.7, 55.5; HRMS (ESI-MS) Calc. for C₂₅H₂₂O₅S₂ (M+H)⁺: 466.0909; found 466.0907; IR (ATR): ν_{max} 3072, 3023, 1587, 1551, 1508, 1468, 1446, 1306, 1287, 1255, 1216, 1168, 1144, 1108, 1084, 1024, 975, 962, 850, 827, 782, 752, 739, 717, 684 cm⁻¹; LC-MS: purity 100% t_R = 31.89 min, (ESI) m/z [M+H]⁺ 467.2.

Synthesis of (1*E*,3*E*,5*E*)-1,3-bis-phenylsulfonyl-(6-*p*-chlorophenyl)-hexa-1,3,5-triene, 108



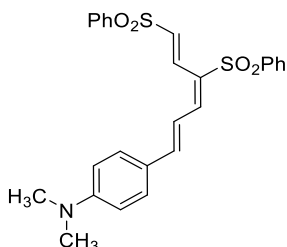
This compound was synthesized using *trans*-4-chloro cinnamaldehyde, **43** (92 mg, 0.55 mmol, 1.1 eq.) according to the general procedure. A yellow solid was obtained, 139 mg (59%). ¹H NMR (500 MHz, CDCl₃) δ 7.82-7.79 (m, 3 H), 7.74-7.72 (m, 2 H), 7.67-7.64 (m, 1H), 7.57-7.52 (m, 4 H), 7.50-7.47 (m, 2 H), 7.42-7.38 (m, 4 H), 7.20-7.08 (m, 3 H); ¹³C NMR (125 MHz, CDCl₃) δ 146.0, 144.9, 139.9, 139.6, 136.8, 133.7, 133.6, 133.5, 133.3, 132.8, 129.5, 129.3, 129.3, 129.0, 127.7, 127.6, 120.8; HRMS (ESI-MS) Calc. for C₂₄H₂₀O₄S₂Cl (M+H)⁺: 471.0486; found 471.0469; IR (ATR): ν_{max} 3066, 3038, 1600, 1586, 1567, 1545, 1490, 1446, 1307, 1285, 1210, 1176, 1141, 1083, 983, 946, 843, 813, 767, 749, 720, 687 cm⁻¹, LC-MS: purity 99.5% t_R = 19.21 min, (ESI) m/z [M+H]⁺ 472.2.

Synthesis of (1*E*,3*E*,5*E*)-1,3-bis-phenylsulfonyl-(6-*p*-nitrophenyl)-hexa-1,3,5-triene, 109



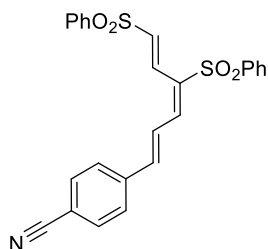
This compound was synthesized using *trans*-4-nitro cinnamaldehyde, **44** (195 mg, 1.1 mmol, 1.1 eq.) according to the general procedure, performed at 1 mmol scale. A light brown solid was obtained, 463 mg (96%). ¹H NMR (500 MHz, CDCl₃) δ 8.28-8.26 (m, 2 H), 7.83-7.81 (m, 3 H), 7.74-7.66 (m, 5 H), 7.59-7.53 (m, 4 H), 7.43-7.40 (m, 2 H), 7.28-7.24 (m, 2 H), 7.21-7.18 (m, 1 H); ¹³C NMR (125 MHz, CDCl₃) δ 147.5, 142.8, 142.3, 139.8, 138.6, 138.2, 134.2, 133.6, 132.9, 132.8, 128.5, 128.4, 127.61, 127.60, 126.8, 126.7, 123.3, 123.2; HRMS (ESI-MS) Calc. for C₂₄H₁₉O₆S₂N (M+H)⁺: 481.0654; found 481.0638; IR (ATR): ν_{max} 3068, 3028, 1603, 1516, 1447, 1342, 1306, 1285, 1212, 1176, 1142, 1086, 990, 969, 843, 831, 766, 746, 722, 685, 667 cm⁻¹; LC-MS: purity 98.8% t_R= 31.60 min, (ESI) m/z [M+Na]⁺ 504.4.

Synthesis of (1*E*,3*E*,5*E*)-1,3-bis-phenylsulfonyl-(4-*p*-dimethylaminophenyl)-hexa-1,3,5-triene, 110



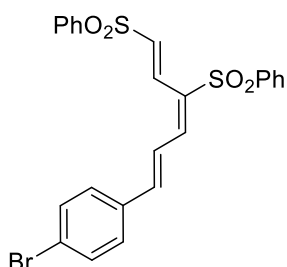
This compound was synthesized using *trans*-*p*-dimethylaminocinnamaldehyde, **45** (96 mg, 0.55 mmol, 1.1 eq.) according to the general procedure, with the exception that tinfoil was used to cover the reaction flask as *trans*-*p*-dimethylaminocinnamaldehyde is light sensitive. A bright red solid was obtained, 144 mg (60%) ¹H NMR (500 MHz, CDCl₃) δ 7.84-7.80 (m, 3 H), 7.75-7.73 (m, 2 H), 7.63-7.57 (m, 2 H), 7.53-7.50 (m, 3 H), 7.48-7.46 (m, 2 H), 7.40-7.37 (m, 2 H), 7.19-7.16 (d, 1 H, *J* = 14.9 Hz), 7.07-7.04 (d, 1 H, *J* = 15.1 Hz), 7.00-6.95 (dd, 1 H, *J* = 11.9 Hz, *J* = 14.9 Hz), 6.70-6.68 (m, 2H), 3.08 (s, 6H); ¹³C NMR (125 MHz, CDCl₃) δ 152.3, 149.6, 147.8, 140.5, 140.47, 133.3, 133.1, 130.6, 129.9, 129.86, 129.3, 129.1, 127.5, 127.3, 127.2, 122.9, 115.2, 111.9, 40.1; HRMS (ESI-MS) Calc. for C₂₆H₂₅O₄S₂N (M+H)⁺: 479.1225; found 479.1225; IR (ATR): ν_{max} 3068, 3018, 1568, 1542, 1480, 1446, 1376, 1306, 1285, 1244, 1212, 1166, 1150, 1136, 1084, 1065, 999, 968, 914, 842, 810, 768, 749, 718, 704, 687 cm⁻¹; LC-MS: purity 100% t_R= 32.71 min, (ESI) m/z [M+H]⁺ 480.3.

Synthesis of (1*E*,3*E*,5*E*)-1,3-bis-phenylsulfonyl-(6-*p*-cyanophenyl)-hexa-1,3,5-triene, 111



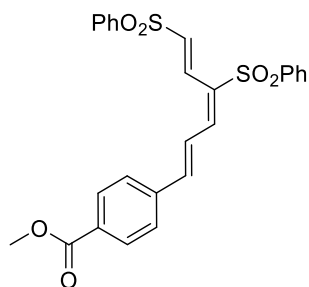
This compound was synthesized using *trans* 4-cyanocinnamaldehyde, **38** (173 mg, 1.1 mmol, 1.1 eq.) according to the general procedure, performed at 1 mmol scale. A yellow-tinted solid was obtained, 231 mg (81%). ¹H NMR (500 MHz, CDCl₃) δ 7.85-7.79 (m, 3 H), 7.73-7.62 (m, 7 H), 7.58-7.51 (m, 4 H), 7.43-7.40 (m, 2H), 7.21-7.16 (m, 3H); ¹³C NMR (125 MHz, CDCl₃) δ 144.4, 143.6, 139.6, 139.3, 139.1, 134.9, 134.4, 133.9, 133.8, 132.8, 129.5, 129.4, 128.6, 128.4, 127.8, 127.7 123.5, 118.3, 113.6; HRMS (ESI-MS) Calc. for C₂₅H₁₉S₂O₄N (M+Na⁺): 484.0648; found 484.0661; IR (ATR): ν_{max} 3070, 2222, 1604, 1560, 1478, 1445, 1412, 1318, 1307, 1287, 1213, 1177, 1154, 1143, 1084, 1022, 999, 984, 971, 958, 865, 845, 820, 771, 749, 718, 700, 686 cm⁻¹; LC-MS: purity 99.3% t_R = 30.86 min, (ESI) m/z [M+Na]⁺ 484.3.

Synthesis of (1*E*,3*E*,5*E*)-1,3-bis-phenylsulfonyl-6-(*p*-bromophenyl)-hexa-1,3,5-triene, 112



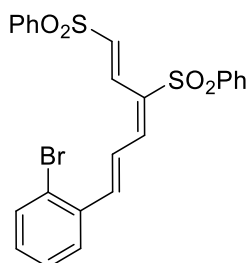
This compound was synthesized using *trans*-4-bromo cinnamaldehyde, **40** (232 mg, 1.1 mmol, 1.1 eq.) according to the general procedure performed at 1 mmol scale. A yellow solid was obtained, 287 mg (56%). ¹H NMR (500 MHz, CDCl₃) δ 7.85-7.79 (m, 3 H), 7.75-7.70 (m, 2 H), 7.67-7.64 (m, 1H), 7.60-7.51 (m, 6 H), 7.45-7.39 (m, 4 H), 7.21-7.10 (m, 3 H); ¹³C NMR (125 MHz, CDCl₃) δ 146.1, 144.9, 139.9, 139.6, 133.9, 133.7, 133.6, 133.3, 132.9, 132.4, 129.50, 129.47, 129.3, 129.0, 127.8, 127.6, 125.2 120.9; HRMS (ESI-MS) Calc. for C₂₄H₁₉S₂O₄Br (M+Na⁺): 538.9774; found 538.9781; IR (ATR): ν_{max} 3065, 1599, 1583, 1563, 1546, 1485, 1446, 1403, 1307, 1285, 1208, 1174, 1141, 1083, 1068, 1023, 1007, 982, 967, 926, 843, 806, 767, 745, 719, 685, 658 cm⁻¹; LC-MS: purity 99.4% t_R = 19.27 min, (ESI) m/z [M+H]⁺ 516.2.

Synthesis of (1E,3E,5E)-1,3-bis-phenylsulfonyl-6-(p-methyl benzoate)-hexa-1,3,5-triene, 113



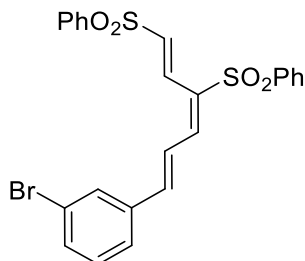
This compound was synthesized using *trans* 4-methyl benzoate cinnamaldehyde, **39** (105 mg, 0.55 mmol, 1.1 eq.) according to the general procedure. A yellow solid was obtained, 151 mg (61%). ¹H NMR (500 MHz, CDCl₃) δ 8.08-8.06 (m, 2 H), 7.83-7.81 (m, 3 H), 7.74-7.73 (m, 2 H), 7.68-7.65 (m, 1 H), 7.61-7.53 (m, 6 H), 7.43-7.40 (m, 2H), 7.26-7.23 (m, 2 H) 7.21-7.15 (m, 1 H), 3.95 ppm (s, 3 H); ¹³C NMR (125 MHz, CDCl₃) δ 166.3, 145.9, 144.4, 139.8, 139.5, 139.0, 133.9, 133.8, 133.7, 131.7, 130.3, 129.5, 129.3, 128.9, 128.0, 127.8, 127.6, 122.4, 52.4 ppm; HRMS (ESI-MS) Calc. for C₂₆H₂₂O₆S₂ (M+Na⁺): 517.0750; found: 517.0738; IR (ATR): ν_{max} 3071, 3030, 1715, 1605, 1553, 1478, 1446, 1429, 1411, 1358, 1306, 1282, 1215, 1178, 1144, 1106, 1083, 1012, 998, 959, 912, 871, 851, 829, 813, 765, 755, 745, 718, 685, 665 cm⁻¹; LC-MS: purity 99.6% t_R = 18.43 min, (ESI) m/z [M+Na]⁺ 517.3.

Synthesis of (1E,3E,5E)-1,3-bis-phenylsulfonyl-6-(o-bromophenyl)-hexa-1,3,5-triene, 114



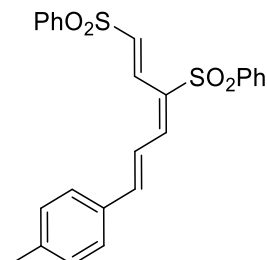
This compound was synthesized using *trans*-2-bromo cinnamaldehyde, **5** (116 mg, 0.55 mmol, 1.1 eq.) according to the general procedure. A yellow solid was obtained, 163 mg (63%). ¹H NMR (500 MHz, CDCl₃) δ 7.88-7.84 (m, 1 H), 7.82-7.78 (m, 2 H), 7.75-7.72 (m, 2 H), 7.68-7.60 (m, 4 H), 7.57-7.50 (m, 4 H), 7.43-7.34 (m, 3H), 7.26-7.23 (m, 1H), 7.18-7.05 (m, 2H); ¹³C NMR (125 MHz, CDCl₃) δ 145.5, 144.8, 139.8, 139.5, 134.7, 133.7, 133.66, 133.6, 133.5, 131.6, 129.5, 129.3, 129.0, 127.9, 127.8, 127.7, 127.6, 125.6, 122.6; HRMS (ESI-MS) Calc. for C₂₄H₁₉S₂O₄Br (M+Na⁺): 513.9908; found 513.9906; IR (ATR): ν_{max} 3069, 3023, 1598, 1582, 1564, 1478, 1463, 1446, 1368, 1309, 1281, 1218, 1179, 1144, 1084, 1024, 999, 969, 921, 867, 842, 825, 764, 750, 719, 682, 672 cm⁻¹; LC-MS: purity 99.3% t_R = 33.80 min, (ESI) m/z [M+NH₄]⁺ 533.3.

Synthesis of (1E,3E,5E)-1,3-bis-phenylsulfonyl-6-(m-bromophenyl)-hexa-1,3,5-triene, 115



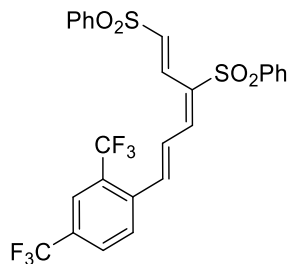
This compound was synthesized using *trans*-3-bromo cinnamaldehyde, **34** (116 mg, 0.55 mmol, 1.1 eq.) according to the general procedure. A yellow solid was obtained, 143 mg (55%). ¹H NMR (500 MHz, CDCl₃) δ 7.83-7.78 (m, 3 H), 7.74-7.72 (m, 2 H) 7.67-7.64 (m, 2 H), 7.57-7.51 (m, 5 H), 7.48-7.46 (d, 1 H, *J* = 7.9 Hz), 7.43-7.40 (m, 2 H), 7.31-7.28 (t, 1H, *J* = 7.9 Hz), 7.18-7.07 ppm (m, 3H); ¹³C NMR (125 MHz, CDCl₃) δ 145.6, 144.6, 139.8, 139.5, 137.0, 133.8, 133.7, 133.6, 133.5, 133.4, 130.8, 130.6, 129.5, 129.3, 128.9, 127.8, 127.6, 126.6, 123.3, 121.5 ppm; HRMS (ESI-MS) Calc. for C₂₄H₁₉S₂O₄Br (M+H⁺): 513.9908; found 513.9906; IR (ATR): ν_{max} 3072, 3013, 1600, 1564, 1478, 1447, 1417, 1369, 1323, 1308, 1283, 1217, 1179, 1154, 1140, 1083, 1025, 999, 968, 920, 890, 851, 842, 827, 777, 755, 747, 718, 692, 683 cm⁻¹; LC-MS: purity 99.5% t_R = 33.74 min, (ESI) m/z [M+H]⁺ 516.2.

Synthesis of (1E,3E,5E)-1,3-bis-phenylsulfonyl-6-(p-methylphenyl)-hexa-1,3,5-triene, 116



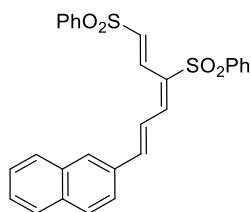
This compound was synthesized using (*E*)-*p*-methylcinnamaldehyde, **41** (80 mg, 0.55 mmol, 1.1 eq.) according to the general procedure. A yellow solid was obtained, 147 mg (65%). ¹H NMR (500 MHz, CDCl₃) δ 7.83-7.81 (m, 3 H), 7.75-7.73 (m, 2 H) 7.66-7.63 (m, 1 H), 7.57-7.52 (m, 4 H), 7.46-7.44 (m, 2 H), 7.42-7.39 (m, 2 H), 7.24-7.20 (m, 3 H), 7.15-7.14 (m, 1 H), 7.11-7.08 (m, 1 H), 2.41 ppm (s, 3 H); ¹³C NMR (125 MHz, CDCl₃) δ 148.1, 145.9, 141.6, 140.1, 139.9, 133.6, 133.5, 132.6, 132.3, 131.5, 129.9, 129.4, 129.3, 129.2, 128.3, 127.7, 127.5, 119.4, 21.6 ppm; HRMS (ESI-MS) Calc. for C₂₅H₂₂O₄S₂ (M+Na⁺): 473.0837; found: 473.0852; IR (ATR): ν_{max} 3070, 3028, 1590, 1549, 1478, 1445, 1306, 1289, 1207, 1177, 1140, 1083, 1023, 998, 988, 960, 866, 848, 819, 809, 782, 755, 739, 717, 687 cm⁻¹; LC-MS: purity 100% t_R = 33.31, (ESI) m/z [M+Na]⁺ 473.3.

Synthesis of (1*E*,3*E*,5*E*)-1,3-bis-phenylsulfonyl-6-(3,5-bis(trifluoromethyl)-hexa-1,3,5-triene, 117



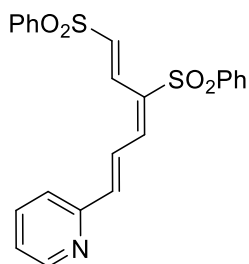
This compound was synthesized using (*E*)-3,5-bis(trifluoromethyl)cinnamaldehyde, **86** (133 mg, 0.55 mmol, 1.1 eq.) according to the general procedure. A very pale yellow solid was obtained, 143 mg (50%). ¹H NMR (500 MHz, CDCl₃) δ 7.94 (s, 2H), 7.89 (s, 1H), 7.84-7.80 (m, 3H), 7.74-7.71 (m, 2H), 7.69-7.66 (m, 1H), 7.59-7.50 (m, 4H), 7.44-7.41 (m, 2H), 7.24-7.18 ppm (m, 3H); ¹³C NMR (125 MHz, CDCl₃) δ 143.2, 143.16, 139.5, 139.2, 136.9, 135.3, 134.7, 133.9, 133.88, 132.9, 132.6, 129.5, 129.4, 128.4, 127.8, 127.7, 127.6, 124.0, 123.7, 121.9 ppm; HRMS (ESI-MS) Calc. for C₂₅H₂₂O₄S₂ (M+Na⁺): 595.0476; found: 595.0442; IR (ATR): ν_{max} 3069, 3018, 1606, 1585, 1560, 1479, 1447, 1382, 1362, 1310, 1282, 1217, 1169, 1143, 1123, 1109, 1084, 1023, 999, 978, 945, 931, 899, 846, 770, 749, 732, 720, 709, 682, 658 cm⁻¹; LC-MS: purity 100% t_R = 33.15 min, (ESI) m/z [M+Na]⁺ 595.3.

Synthesis of (1*E*,3*E*,5*E*)-1,3-bis-phenylsulfonyl-6-(naphthalene)-hexa-1,3,5-triene, 118



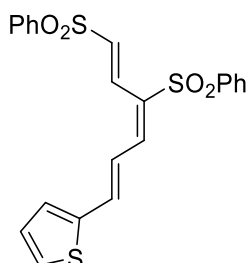
This compound was synthesized using (*E*)-3-(naphthalen-1-yl)acrylaldehyde, **37** (100 mg, 0.55 mmol, 1.1 eq.) according to the general procedure. A yellow solid was obtained, 124 mg (51%). ¹H NMR (500 MHz, CDCl₃) δ 8.17-8.15 (d, 1 H, *J* = 8.5 Hz), 8.11-8.08 (d, 1 H, *J* = 15.1 Hz), 8.00-7.97 (d, 1H, *J* = 11.8 Hz), 7.95-7.90 (m, 2 H), 7.87-7.85 (d, 1 H, *J* = 7.4 Hz), 7.83-7.81 (m, 2 H), 7.79-7.70 (m, 2 H), 7.66-7.52 (m, 8 H), 7.44-7.41 (m, 2 H), 7.30-7.24 (dd, 1H, *J* = 11.8 Hz, *J* = 15.1 Hz), 7.20-7.16 ppm (d, 1H, *J* = 15.1 Hz); ¹³C NMR (125 MHz, CDCl₃) δ 145.5, 144.3, 139.9, 139.7, 133.8, 133.7, 133.6, 133.0, 132.4, 132.0, 131.4, 131.3, 129.4, 129.3, 129.2, 129.0, 127.7, 127.6, 127.3, 126.4, 125.6, 125.4, 122.8, 122.5 ppm; HRMS (ESI-MS) Calc. for C₂₈H₂₂O₄S₂ (M+Na⁺): 509.0874; found: 509.0849; IR (ATR): ν_{max} 3071, 3028, 1595, 1568, 1557, 1509, 1479, 1446, 1343, 1311, 1305, 1243, 1214, 1189, 1153, 1141, 1083, 1024, 999, 964, 915, 883, 845, 825, 793, 772, 758, 749, 738, 717, 680 cm⁻¹; LC-MS: purity 98.8% t_R = 34.00 min, (ESI) m/z [M+Na]⁺ 509.4.

Synthesis of (1*E*,3*E*,5*E*)-1,3-bis-phenylsulfonyl-6-(2-pyridine)-hexa-1,3,5-triene, **119**



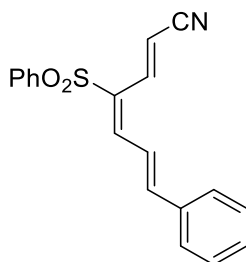
This compound was synthesized using (*E*)-3-(pyridin-2-yl)acrylaldehyde, **35** (73 mg, 0.55 mmol, 1.1 eq.) according to the general procedure. A brown solid was obtained, 130mg (59%). ¹H NMR (500 MHz, CDCl₃) δ 8.68-8.67 (m, 1 H), 7.86-7.81 (m, 3 H), 7.75-7.70 (m, 4 H), 7.66-7.60 (m, 2 H), 7.57-7.52 (m, 3 H), 7.43-7.39 (m, 3 H), 7.29-7.26 (m, 1 H), 7.25-7.22 (d, 1 H, *J* = 14.7 Hz), 7.20-7.17 (d, 1 H, *J* = 15.5 Hz); ¹³C NMR (125 MHz, CDCl₃) δ 153.0, 150.4, 145.6, 144.5, 139.9, 139.5, 136.8, 134.5, 133.7, 129.4, 129.3, 129.0, 127.8, 127.6, 124.6, 124.3, 124.1 ppm; HRMS (ESI-MS) Calc. for C₂₃H₁₉O₄S₂N (M+H⁺): 438.0814; found: 438.0830; IR (ATR): ν_{max} 3069, 3028, 1596, 1581, 1548, 1471, 1446, 1434, 1318, 1307, 1290, 1235, 1218, 1206, 1173, 1140, 1083, 1024, 987, 978, 966, 927, 869, 847, 823, 779, 769, 746, 717, 685 cm⁻¹; LC-MS: purity 99.7% t_R = 28.37, (ESI) m/z [M+Na]⁺ 465.2.

Synthesis of (1*E*,3*E*,5*E*)-1,3-bis-phenylsulfonyl-6-(2-thiophene)-hexa-1,3,5-triene, **120**



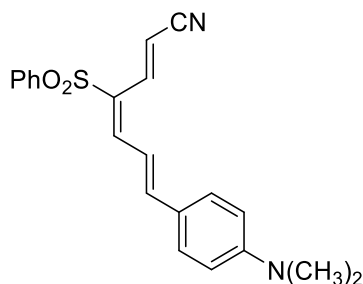
This compound was synthesized using (*E*)-3-(thiophen-2-yl)acrylaldehyde, **36** (76 mg, 0.55 mmol, 1.1 eq.) according to the general procedure. A yellow/orange solid was obtained, 140 mg (63%). ¹H NMR (500 MHz, CDCl₃) δ 7.85-7.81 (m, 2 H), 7.78-7.75 (d, 1 H, *J* = 11.9 Hz) 7.73-7.71 (m, 2 H), 7.66-7.63 (m, 1 H), 7.55-7.52 (m, 3H), 7.49-7.47 (m, 2 H), 7.42-7.38 (m, 2 H), 7.37-7.34 (d, 1 H, *J* = 15.1 Hz), 7.30-7.29 (m, 1 H), 7.15-7.12 (d, 1 H, *J* = 15.1 Hz), 7.11-7.09 (dd, 1 H, *J* = 3.7 Hz, *J* = 5.0 Hz), 6.93-6.87 (dd, 1 H, *J* = 11.9 Hz, *J* = 15.1 Hz); ¹³C NMR (125 MHz, CDCl₃) δ 145.4, 140.5, 140.0, 139.9, 139.8, 133.6, 133.5, 132.4, 131.5, 131.3, 130.0, 129.4, 129.2, 129.1, 128.6, 127.7, 127.5, 119.5 ppm; HRMS (ESI-MS) Calc. for C₂₂H₁₈O₄S₃ (M+Na⁺): 465.0291; found: 465.0262; IR (ATR): ν_{max} 3111, 3069, 3013, 1588, 1497, 1478, 1445, 1413, 1371, 1306, 1288, 1232, 1210, 1174, 1141, 1083, 1041, 1024, 998, 979, 966, 918, 849, 831, 776, 753, 728, 715, 680 cm⁻¹; LC-MS: purity 98.8% t_R = 31.16, (ESI) m/z [M+Na]⁺ 465.2.

Synthesis of (2*E*,4*E*,6*E*)-1-cyano-4-phenylsulfonyl-7-phenyl-hepta-2,4,6-triene, 125



This compound was synthesized using *trans*-cinnamaldehyde, **1** (140 μ L, 1.1 mmol, 1.1 eq.) according to the general procedure with (*E/Z*)-4-phenylsulfonyl-but-2-enenitrile, **122**, substituted for (*E*)-3-bromo-1-phenylsulfonylprop-1-ene, **104**, performed at 1 mmol scale. A bright orange solid was obtained, 158 mg (49%). ^1H NMR (500 MHz, CDCl_3) δ 7.93-7.91 (m, 2 H), 7.67-7.64 (m, 1 H), 7.59-7.55 (m, 4 H), 7.41-7.40 (m, 3 H), 7.35-7.32 (m, 1 H), 7.26-7.23 (m, 2 H), 7.16-7.10 (m, 1 H), 6.77-6.74 ppm (m, 1 H); ^{13}C NMR (125 MHz, CDCl_3) δ 152.0, 146.4, 140.0, 137.6, 134.9, 133.8, 130.9, 130.7, 129.5, 129.1, 128.3, 127.8, 123.8, 114.2, 108.3 ppm; HRMS (ESI-MS) Calc. for $\text{C}_{19}\text{H}_{15}\text{O}_2\text{SN}$ ($\text{M}+\text{Na}$) $^+$: 344.0716; found: 344.0719; IR (ATR): ν_{max} 3046, 2222, 1585, 1574, 1447, 1305, 1286, 1274, 1219, 1197, 1178, 1140, 1083, 1023, 991, 983, 953, 866, 836, 798, 764, 750, 726, 687 cm^{-1} ; LC-MS: purity 96.3% $t_{\text{R}}= 29.76$ min, (ESI) m/z $[\text{M}+\text{H}]^+$ 322.0.

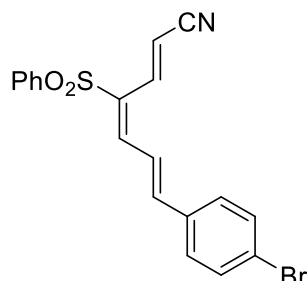
Synthesis of (2*E*,4*E*,6*E*)-1-cyano-4-phenylsulfonyl-7-(*p*-dimethylaminophenyl)-hepta-2,4,6-triene, 126



This compound was synthesized using *trans*-*p*-dimethylaminocinnamaldehyde, **45** (96 mg, 0.55 mmol, 1.1 eq.) according to the general procedure, with the exception that tin foil was used to cover the reaction flask as *trans*-*p*-dimethylaminocinnamaldehyde is light sensitive, and with compound **122** substituted for compound **104**. A bright red solid was obtained, 88 mg (48%). ^1H NMR (500 MHz, CDCl_3) δ 7.92-7.90 (m, 2 H), 7.64-7.61 (m, 1 H), 7.57-7.54 (m, 2 H), 7.45-7.44 (m, 2 H), 7.32-7.29 (m, 1 H), 7.19-7.17 (m, 1 H), 7.06-6.99 (m, 2 H), 6.67-6.65 (m, 2 H), 6.62 (d, 1 H, $J = 14.7$ Hz), 3.06 ppm (s, 6 H); ^{13}C NMR (125 MHz, CDCl_3) δ 153.4, 152.2, 147.8, 140.6, 138.9, 133.5, 130.5, 129.4, 127.6, 127.5, 122.8, 119.0, 115.1, 111.9, 103.5, 40.1 ppm; HRMS (ESI-MS) Calc. for $\text{C}_{21}\text{H}_{20}\text{O}_2\text{SN}_2$ ($\text{M}+\text{H}$) $^+$: 365.1318; found: 365.1319; IR (ATR): ν_{max} 2970, 2921, 2802, 2738, 2220, 1738, 1659, 1594, 1571, 1524, 1486, 1446, 1368, 1306, 1266, 1231, 1215, 1177, 1137, 1083, 1068, 1007, 972, 943, 837, 810, 758, 733, 687 cm^{-1} . (Note: A HPLC

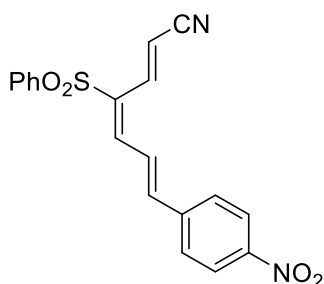
chromatogram of (1*E*,3*E*,5*E*)-1-cyano-3-phenylsulfonyl-6-(*p*-dimethylaminophenyl)-hexa-1,3,5-triene could not be obtained as it degraded on the HPLC column).

Synthesis of (2*E*,4*E*,6*E*)-1-cyano-4-phenylsulfonyl-7-(*p*-bromophenyl)-hepta-2,4,6-triene, **127**



This compound was synthesized using *trans*-4-bromo cinnamaldehyde, **40** (116 mg, 0.55 mmol, 1.1 eq.) according to the general procedure with compound **122** substituted for compound **104**. A yellow solid was obtained, 82 mg (41%). ¹H NMR (500 MHz, CDCl₃) δ 7.92-7.91 (m, 2 H), 7.67-7.64 (m, 1 H), 7.59-7.53 (m, 4 H), 7.42-7.40 (m, 2 H), 7.34-7.31 (m, 1 H), 7.23-7.19 (m, 2 H), 7.08-7.04 (m, 1 H), 6.78-6.75 ppm (m, 1 H); ¹³C NMR (125 MHz, CDCl₃) δ 151.4, 144.7, 139.9, 137.4, 133.9, 133.8, 132.4, 131.2, 129.5, 129.49, 127.8, 125.3, 124.3, 114.1, 108.9 ppm; HRMS (ESI-MS) Calc. for C₁₉H₁₄O₂SNBr (M+Na)⁺: 423.9802; found: 423.9800; IR (ATR): ν_{max} 3016, 2970, 2231, 1739, 1613, 1581, 1568, 1488, 1445, 1407, 1365, 1313, 1280, 1269, 1227, 1217, 1191, 1180, 1165, 1085, 1069, 1022, 995, 964, 906, 882, 864, 839, 813, 797, 754, 725, 686 cm⁻¹; LC-MS: purity 96% t_R = 33.12 min, (ESI) m/z [M+Na]⁺ 423.2.

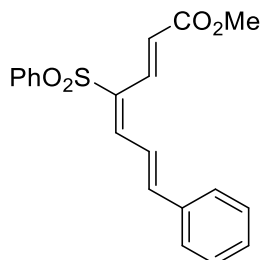
Synthesis of (2*E*,4*E*,6*E*)-1-cyano-4-phenylsulfonyl-(7-*p*-nitrophenyl)-hepta-2,4,6-triene, **128**



This compound was synthesized using *trans*-4-nitro cinnamaldehyde, **44** (97 mg, 0.55 mmol, 1.1 eq.) according to the general procedure with compound **122** substituted for compound **104**. A light brown solid was obtained, 106 mg (58%). ¹H NMR (500 MHz, CDCl₃) δ 8.27-8.25 (m, 2 H), 7.94-7.92 (m, 2 H), 7.71-7.67 (m, 3 H), 7.61-7.58 (m, 2 H), 7.38-7.33 (m, 2 H), 7.29 (d, 1 H, *J* = 11.5 Hz), 7.18 (d, 1 H, *J* = 15.1 Hz), 6.85 ppm (d, 1 H, *J* = 15.1 Hz); ¹³C NMR (125 MHz, CDCl₃) δ 150.2, 148.5, 142.5, 140.8, 139.6, 136.8, 134.0, 132.6, 129.6, 128.7, 127.9, 127.5, 124.4, 113.7, 111.2 ppm; HRMS (ESI-MS) Calc. for C₁₉H₁₄O₄N₂S (M-H)⁺: 366.0674; found: 366.0676; IR (ATR): ν_{max} 3050, 2225, 1682,

1595, 1509, 1448, 1378, 1341, 1318, 1310, 1207, 1194, 1143, 1111, 1088, 1022, 1011, 981, 921, 874, 833, 804, 759, 745, 729, 688, 656 cm^{-1} ; LC-MS: purity 97.6% $t_R = 30.29$ min, (ESI) m/z $[\text{M}+\text{H}]^+$ 367.5.

Attempted synthesis of methyl 7-phenyl-4-(phenylsulfonyl)hepta-2,4,6-trienoate, **124**



The attempt to synthesize this compound was done using *trans*-cinnamaldehyde, **1** (140 μL , 1.1 mmol, 1.1 eq.) according to the general procedure with (*E*)-4-(phenylsulfonyl)but-2-enoate, **123** substituted for **104**, performed at 0.5 mmol scale. This produced a complex mixture consisting of a yellow oil which, even after being subjected to column chromatography using 25:75 ethyl acetate: petroleum ether as mobile phase, we were unable to separate.

2.4.5 Experiments using traditional Knoevenagel-condensation reaction conditions

2.4.5.1 Attempted synthesis of bis(methyl ester) triene

In our attempts to synthesize the bis(methyl ester) triene, different solvents, bases, and temperatures were investigated. In each case, *trans*-cinnamaldehyde (1 mmol) and dimethyl glutaconate (1 mmol) were dissolved in a solvent and a particular base, then the mixture was allowed to stir for a particular amount of time at a certain temperature. Subsequently, saturated ammonium chloride (20 mL) was added and the mixture was extracted three times with dichloromethane (30 mL). The organic layer was next washed with saturated sodium bicarbonate (100 mL) and deionised water (100 mL), and then concentrated under reduced pressure to yield the crude product. This was subjected to column chromatography using the mobile phase that gave the best separation, as indicated by TLC.

2.4.5.1.1 Exploration of equivalents of base

2.4.5.1.1.1 0.25 equivalents of piperidine

As per section 2.4.5.1, using piperidine as base (24.7 μL , 0.25 eq.), with acetic acid (14.3 μL , 0.25 eq.), and the mixture was allowed to reflux in toluene for 18 hours. Dimethyl biphenyl-2,4-dicarboxylate (colourless oil) was obtained, 113 mg (42% yield).

2.4.5.1.1.2 0.5 equivalents of piperidine

As per section 2.4.5.1, using piperidine as base (49.4 μL , 0.5 eq.), with acetic acid (28.6 μL , 0.5 eq.), and the mixture was allowed to reflux in toluene for 18 hours. Dimethyl biphenyl-2,4-dicarboxylate (colourless oil) was obtained, 122 mg (45% yield).

2.4.5.1.1.3 1 equivalent of piperidine

As per section 2.4.5.1, using piperidine as base (98.8 μL , 1 eq.), with acetic acid (57.2 μL , 1 eq.), and the mixture was allowed to reflux in toluene for 18 hours. Dimethyl biphenyl-2,4-dicarboxylate (colourless oil) obtained, 138 mg (51% yield).

2.4.5.1.1.4 1.5 equivalents of piperidine

As per section 2.4.5.1, using piperidine as base (148 μL , 1.5 eq.), with acetic acid (85.8 μL , 1.5 eq.), and the mixture was allowed to reflux in toluene for 18 hours. Dimethyl biphenyl-2,4-dicarboxylate (colourless oil) obtained, 127 mg (47% yield)

2.4.5.1.2 Exploration of solvent

2.4.5.1.2.1 Use of toluene

Exactly as per section 2.4.5.1.1.3

2.4.5.1.2.2 Use of ethanol

As per section 2.4.5.1, using piperidine as base (98.8 μL , 1 eq.), with acetic acid (57.2 μL , 1 eq.), and the mixture was allowed to reflux in ethanol for 18 hours. Dimethyl biphenyl-2,4-dicarboxylate (colourless oil) obtained, 56 mg (21% yield).

2.4.5.1.3 Exploration of reaction temperature

2.4.5.1.3.1 Use of ~112 °C (Reflux)

Exactly as per section 2.4.5.1.1.3

2.4.5.1.3.2 Use of 80 °C

As per section 2.4.5.1, using piperidine as base (98.8 μL , 1 eq.), with acetic acid (57.2 μL , 1 eq.), and the mixture was allowed to stir in toluene for 18 hours at 80 °C. Dimethyl biphenyl-2,4-dicarboxylate (colourless oil) obtained, 119 mg (44% yield).

2.4.5.1.3.3 Use of 30 °C

As per section 2.4.5.1, using piperidine as base (98.8 μL , 1 eq.), with acetic acid (57.2 μL , 1 eq.), and the mixture was allowed to stir in toluene for 18 hours at 30 °C. No reaction occurred, returned starting material visible by ^1H NMR.

2.4.5.1.4 Exploration of base

2.4.5.1.4.1 Use of piperidine (and acetic acid)

Exactly as per section 2.4.5.1.1.3

2.4.5.1.4.2 Use of *DL*-proline

As per section 2.4.5.1, using *DL*-proline as base (115 mg, 1 eq.), and the mixture was allowed to reflux in toluene for 18 hours. Dimethyl biphenyl-2,4-dicarboxylate (colourless oil) obtained, 23 mg (9% yield).

2.4.5.1.4.3 Use of pyrrolidine

As per section 2.4.5.1, using pyrrolidine as base (82.1 μL , 1 eq.), and the mixture was allowed to reflux in toluene for 18 hours. Dimethyl biphenyl-2,4-dicarboxylate (colourless oil) obtained, 52 mg (19% yield).

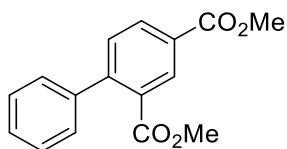
2.4.5.1.4.4 Use of pyridine

As per section 2.4.5.1, using pyridine as base (80.5 μL , 1 eq.), and the mixture was allowed to reflux in toluene for 18 hours. No reaction occurred, returned starting material visible by ^1H NMR.

2.4.5.2 General procedure for traditional Knoevenagel-condensation reaction

Dimethyl glutaconate (141 μL , 1 mmol, 1 eq.), toluene (20 mL), 4 Å molecular sieves (1 g), piperidine (98.8 μL) and AcOH (57.2 μL) and the relevant cinnamaldehyde (1 mmol, 1 eq.), were all allowed to reflux for 18 hours. Subsequently, saturated ammonium chloride (20 mL) was added and the mixture was extracted three times with dichloromethane (30 mL). The organic layer was next washed with saturated sodium bicarbonate (100 mL) and deionised water (100 mL), and then concentrated under reduced pressure to yield the crude product. This was subjected to column chromatography using the mobile phase that gave the best separation, as indicated by TLC.

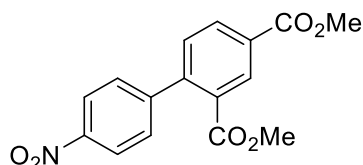
Synthesis of dimethyl biphenyl-2,4-dicarboxylate, **129**



According to general procedure using *trans*-cinnamaldehyde, **1** (126 μL , 1 mmol, 1 eq.). The mobile phase used for column chromatography was a 91:9 petroleum ether: ethyl acetate solution. A colourless oil was obtained, 138 mg (51%). ^1H NMR (500 MHz, CDCl_3) δ 8.49-8.48 (d, $J = 1.8$ Hz, 1 H), 8.19 (dd, $J = 1.8$ Hz, 8.1 Hz, 1 H), 7.47 (d, $J =$

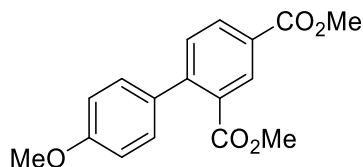
8.0 Hz, 1 H), 7.47-7.38 (m, 3 H), 7.33-7.31 (m, 2 H), 3.96 (s, 3 H), 3.68 (s, 3 H) ppm; ^{13}C NMR (125 MHz, CDCl_3) δ 168.2, 166.1, 146.8, 140.3, 132.1, 131.2, 131.1, 131.0, 129.1, 128.2 (2C), 128.18 (2C), 127.9, 52.4, 52.2 ppm, NMR data matches with literature.²³⁸; HRMS (ESI-MS) Calc. for $\text{C}_{16}\text{H}_{14}\text{O}_4$ ($\text{M}+\text{Na}$) $^+$: 270.0892; found: 270.0897.

Synthesis of dimethyl 4'-nitrobiphenyl-2,4-dicarboxylate, **130**



According to general procedure using *trans* 4-nitrocinnamaldehyde, **45** (177 mg, 1 mmol, 1 eq.). The mobile phase used for column chromatography was a 86:14 petroleum ether: ethyl acetate solution. An off-white crystalline solid was obtained, 103 mg (57%). ^1H NMR (500 MHz, CDCl_3) 8.622-8.619 (m, 1H), 8.302-8.301 (m, 2H), 8.25 (dd, $J = 1.8$ Hz, 8.0 Hz, 1H), 7.48-7.46 (m, 2H), 7.44 (d, $J = 8.0$ Hz, 1H), 3.99 (s, 3H, CH_3), δ 3.73 (s, 3H, CH_3) ppm; ^{13}C NMR (125 MHz, CDCl_3) δ 166.9, 165.7, 147.5, 147.3, 144.9, 132.6, 131.8, 130.9, 130.5, 130.4, 129.2, 123.4, 52.6, 52.4 ppm; IR (ATR): ν_{max} 3076, 2964, 1718, 1612, 1599, 1513, 1433, 1397, 1344, 1257, 1239, 1148, 1091, 1023, 994, 959, 930, 872, 851, 810, 775, 752, 720, 693 cm^{-1} . LC-MS: purity 97.1% $t_{\text{R}} = 29.87$ min, (ESI) m/z [$\text{M}+\text{NH}_4$] $^+$ 333.1.

Attempted synthesis of dimethyl 4'-methoxybiphenyl-2,4-dicarboxylate



According to general procedure using 4-methoxycinnamaldehyde (162 mg, 1 mmol, 1 eq.). The mobile phase used for column chromatography was 8:2 petroleum ether: ethyl acetate. A complex crude mixture was obtained with uninterpretable NMR spectra.

Chapter Three: Biaryl synthesis and photophysical study

3.1 Introduction

3.1.1 Importance and applications of biaryl-containing compounds

Biaryls, or biphenyls, consist of two adjacent phenyl rings attached at their 1,1'-positions,²⁴² a general structure of which is given in Figure 75.

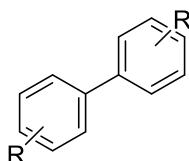
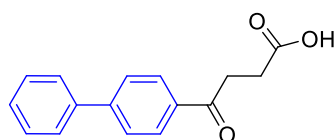


Figure 75. Motif of a biaryl compound

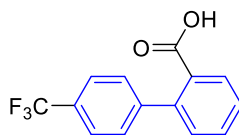
The biaryl motif is prevalent in pharmaceuticals,²⁴²⁻²⁴⁵ natural products²⁴²⁻²⁴⁵ including alkaloids, terpenes and peptides,²⁴⁶ polymers,²⁴³ and advanced materials.^{244, 245} It can also be found as a central building block in a variety of molecules of value such as agrochemicals,²⁴⁴ chiral reagents,^{242, 246} and liquid crystals.^{1,3,5} They also serve as inflexible “spacers” between two parts of a molecule,²⁴² and as the emissive layer in organic light emitting diodes (OLEDs).²⁴²

3.1.1.1 Medicinal applications of biaryls

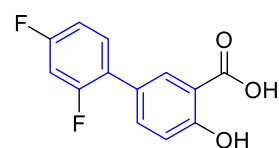
Biaryls have found many useful applications as part of medicinally relevant molecules. The biaryl motif is considered a privileged structure, which can be defined as “a single molecular framework able to provide ligands for diverse receptors”. This is because molecules containing the biaryl subunit have been shown to bind to multiple receptors with high affinity.²⁴⁷ Biaryl compounds have been investigated for their antimicrobial,²⁴⁸ antidiabetic,²⁴⁸ immunosuppressant,²⁴⁸ antitumour,²⁴⁷ antihypertensive,²⁴⁷ analgesic,²⁴⁸ and anti-inflammatory properties,²⁴⁸ to name a few. Some examples of pharmaceutical drugs that contain the biaryl motif are shown in Figure 76.



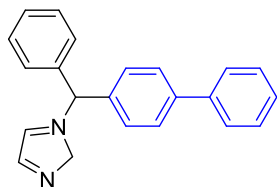
Fenbufen - an anti-inflammatory drug



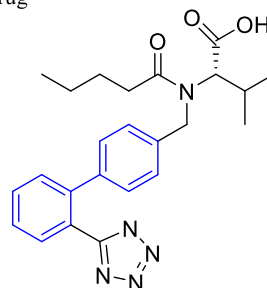
Xenalipin - an antihyperlipidemic (lipid-lowering) drug



Diflunisal - an analgesic



Bifonazole - an antifungal drug



Valsartan - an antihypertensive drug

Figure 76. Examples of pharmaceutical drugs containing the biaryl subunit,²⁴⁹⁻²⁵³ each of which effect a different therapeutic action.

In 2003, the biaryl motif was found to be present in 4.3% of all known drugs.²⁴⁷ It is no coincidence that the biaryl sub-structure is so prevalent in pharmaceuticals and can, in part, be attributed to the versatility of binding interactions shown by biaryl compounds *in vivo*. Drugs consisting of aromatic components bind to proteins through largely aromatic and hydrophobic interactions.²⁴⁷ However, these aromatic components have also been shown to form favourable interactions with polar substituents and even with positively charged groups.²⁴⁷ This is what makes biaryl-containing compounds so useful in terms of medicinal application and as such, they have been incorporated into many different scaffolds.²⁴⁷

An important example of a medicinal product containing the biaryl motif are the vancomycin group of antibiotics.²⁴⁶ These glycopeptides are employed in clinical settings in the treatment of bacterial pathogens that are resistant to other antibiotics. Arguably, the most important among this group of antibiotics is vancomycin itself, Figure 77, which is still used as an antibiotic of last resort.²⁴⁶

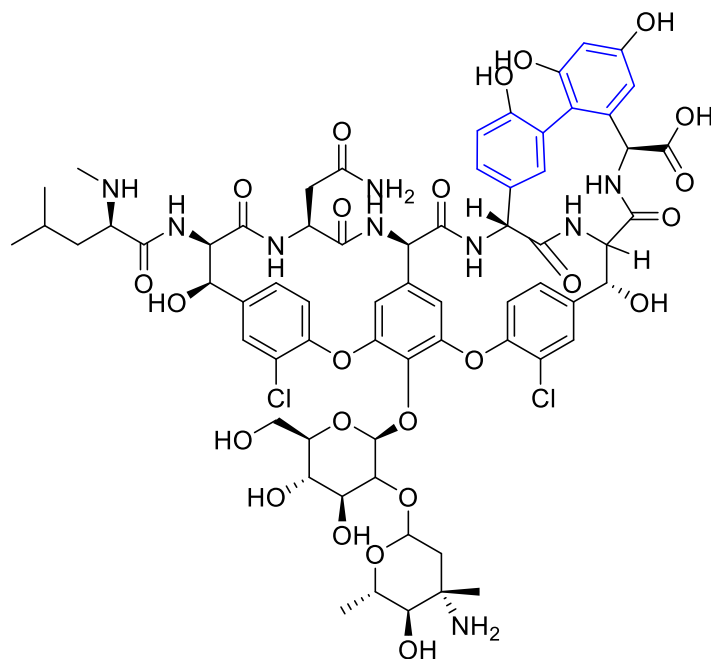


Figure 77. The structure of the important antibiotic vancomycin, which contains a biaryl subunit, adapted from the work of Vardanyan and Hruby.²⁵⁴

3.1.1.2 Application of biaryls in OLEDs

Another application that biaryls have been investigated for is as the emissive layer (EL) in OLEDs.^{255, 256} OLEDs have potential applications in display,²⁵⁵ such as full-coloured flat screen displays,^{256, 257} and solid-state lighting.^{255, 256} Devices like OLEDs exhibit several advantages relative to their inorganic alternatives, such as light weight, low cost, and flexibility.²⁵⁷ Blue-, green-, and red-emitting materials provide the three main colours required for the application of OLEDs.²⁵⁵ Of these three, progress on blue emitters that possess good stability and high efficiency is necessary so that light-emitting device technology can be advanced.^{255, 256}

There are various structures of OLEDs possible, which differ in the way electroluminescence is generated. Using a three-layer OLED as an example, Figure 78, the EL lies between the hole transporting layer (HTL) and the electron-transporting layer (ETL) and acts as the main site of hole-electron recombination, and thus, is an important site for the resulting electroluminescence.²⁵⁸ The HTL is important to facilitate the transport of holes and the blocking of electrons, thus preventing the electrons from reaching the opposite electrode before recombining with the holes. In contrast, the ETL is important to facilitate the transport of electrons and the blocking of holes. In this type of OLED structure, the HTL and the ELT lie between a cathode and an anode also.²⁵⁸

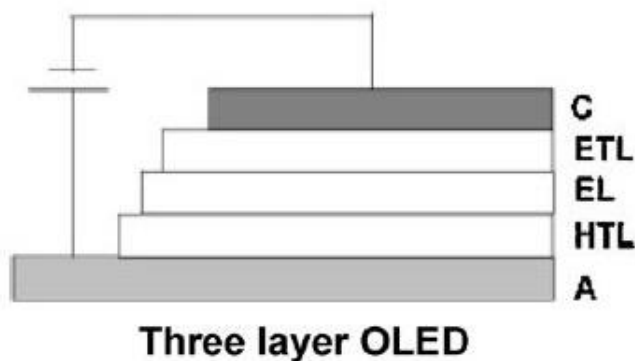


Figure 78. The structure of a three layer OLED consisting of a cathode (C - typically consisting of aluminium), an electron transport layer (ETL), an emitting layer (EL), a hole transport layer (HTL) and an anode (A – typically consisting of small molecules). Adapted from the work of Kalyani and Dhoble.²⁵⁸

When voltage is applied across the OLED, the current flows through the device and, as a result, the cathode gives electrons to the emissive layer, and holes are injected from the anode.²⁵⁸ Where the holes and electrons recombine, exciton pairs are formed in the emissive layer. Light emission occurs when the charges in exciton pairs are combined. The colour of this light essentially corresponds to the energy difference between the HOMO (highest occupied molecular orbital) and the LUMO (lowest unoccupied molecular orbital) and thus, to the nature of the organic molecule. The brightness/intensity of light produced relates to the amount of electrical current applied.²⁵⁸

Figure 79 gives two examples of organic molecules being used as part of the EL in blue-OLEDs, both of which incorporate the biaryl subunit.^{255, 256}

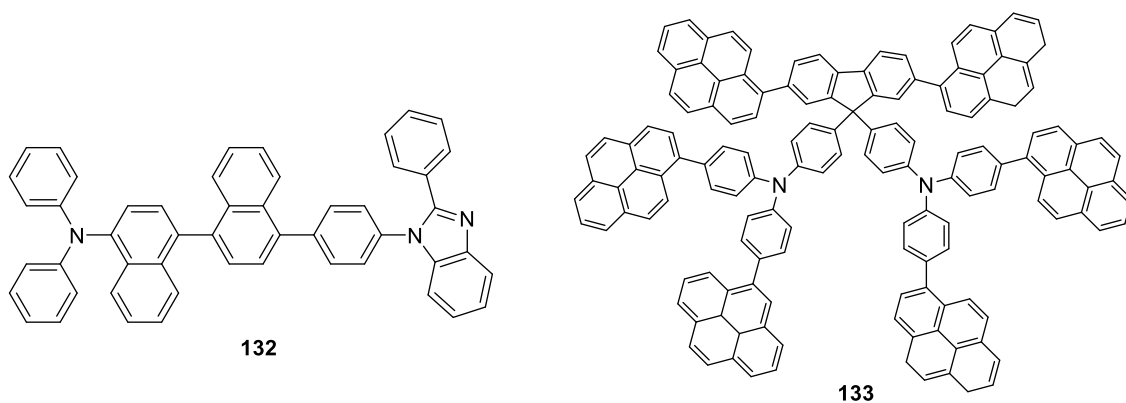


Figure 79. Examples of organic structures containing the biaryl motif that are being used as EL in OLEDs (a) BINAPN, synthesized by Muangpaisal *et al.*²⁵⁵ and (b) 9,9-bis(4-di[4-(pyren-2-yl)phenyl]aminophenyl)-2,7-di(pyren-2-yl)fluorene (PFT), synthesized by Prachumrak *et al.*²⁵⁶.

Thus, compounds containing the biaryl motif are important structures that serve a variety of purposes. In light of this, they are important synthetic targets and many methods for their synthesis have been described.²⁴⁶ These synthetic methodologies can broadly be

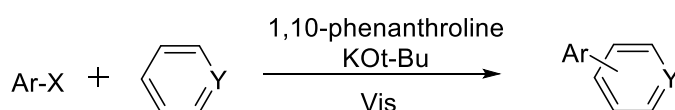
divided into two types of methods, those that incorporate a transition metal and those that do not. Examples of both types will be explored in the following sections.

3.1.2 Transition metal-free approaches to biaryl synthesis

As has been mentioned previously with respect to triene synthesis, there is a growing interest in the development of sustainable synthetic methods. This is also true with respect to biaryl synthesis, where there is a particular interest in synthetic methodologies that avoid the use of expensive and scarce transition metals.^{244, 259} This is not only because of their associated high cost, but also because their use can result in the presence of transition-metal impurities in the final product.²⁵⁹ The potential environmental issues that can be related to metal waste is also of some concern.²⁶⁰ Additionally, due to the highly reactive nature of many aryl metal reactants, methods that avoid their use are desirable.²⁴⁴ Earlier attempts at metal-free biaryl synthetic strategies often required harsh reaction conditions and/or operationally complex protocols to achieve the same selective coupling as their organometallic counterparts. We will limit our summary to a few recent examples of metal-free approaches to biaryl synthesis, with a focus on those that avoided the implementation of harsh conditions or complex protocols.

3.1.2.1 Transition metal-free approach of Xu *et al.* (2015)

Xu *et al.*²⁵⁹ have employed a strategy whereby a photosensitive complex of potassium tert-butoxide (KO*t*-Bu) and nitrogenous heterocyclic bidentate chelating ligands are excited by visible light irradiation with a xenon lamp ($\lambda \geq 420\text{nm}$). This then initiates a series of coupling reactions incorporating a single-electron-transfer (SET) process.²⁵⁹ An overview of the reaction scope of this strategy is given by Scheme 39.



Ar = C₆H₅, Y = CH Yield = 72%

Ar = 4-CH₃C₆H₄, Y = CH, Yield = 73%

Ar = 4-OCH₃C₆H₄, Y = CH, Yield = 90%

Ar = 2-CH₃C₆H₄, Y = CH, Yield = 15%

Ar = 2-OCH₃C₆H₄, Y = CH, Yield = 76%

Ar = 4-CH₃C₆H₄, Y = CH, Yield = 20%

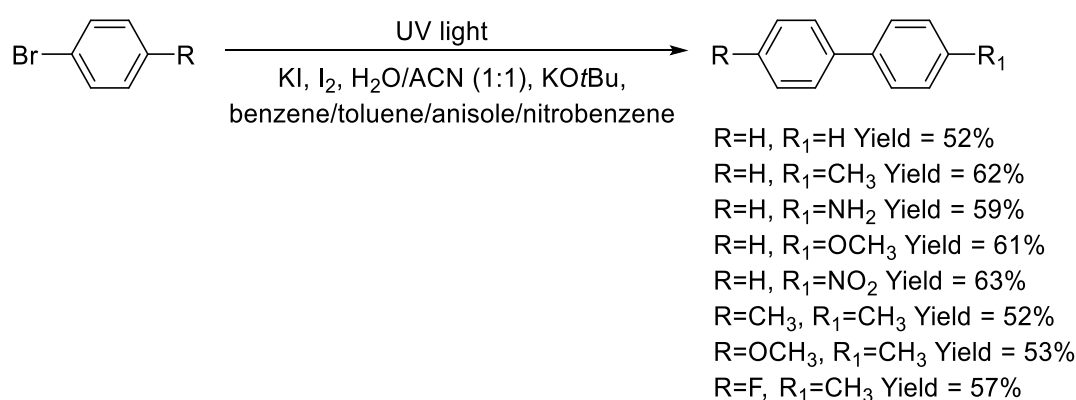
Ar = 4-CH₃C₆H₄, Y = N, Yield = 95%^a

Scheme 39. Examples of biaryl products obtained via this synthetic strategy. General reaction conditions that were employed: Aryl halide ArX (0.1 mmol), benzene (1 mL), KO*t*-Bu (4 eq.), 1,10-phenanthroline (50 mol %), temperature (18 °C, cycle water cooling), N₂ atmosphere, visible light irradiation (420 nm < λ < 780 nm, 400 mW cm⁻², 24 h). ^a ArX (0.5 mmol) and pyridine (5 mL) were used in this case and an isomer ratio: *o*/*m*/*p* = 1.0/1.2/3.9 was determined by NMR for this product. Adapted from the work of Xu *et al.*²⁵⁹

The advantages of this approach include the use of an inexpensive catalyst (1,10-phenanthroline), abundant visible light, and relatively mild reaction conditions.²⁵⁹ All of these attributes make this approach a more sustainable and environmentally friendly approach to biaryl synthesis. A variety of aryl halide substrates were successfully employed, including those with electron-donating and electron-withdrawing groups, as well as an halopyridine, though the yields did vary considerably depending on what substrate was used.²⁵⁹ A drawback to this method is that the biaryls produced are not heavily functionalized.²⁵⁹

3.1.2.2 Transition metal-free approach of Walia *et al.*²⁶⁰ (2018)

Walia *et al.*²⁶⁰, similarly to Xu *et al.*,²⁵⁹ have developed a transition metal-free light-mediated protocol that facilitates the synthesis of biaryls, as well as aryl iodides (and alkynes), from aryl bromides. The work of Xu *et al.*²⁵⁹ is specifically mentioned, where the authors mention that, although their base and light-assisted strategy for biaryl synthesis is economic and eco-friendly, the requirement of excess amount of ligand (50 mol %) necessitates additional efforts for the development of a “green” protocol for the synthesis of biaryls.²⁶⁰ In addition, they acknowledge the need for a simple strategy that facilitates access to aryl iodides, given that most methodologies used for biaryl synthesis are optimal when aromatic iodides are used as one of the coupling partners. Under green conditions, this group successfully incorporated ultraviolet irradiation and basic aqueous media to facilitate the transformation of aryl bromides to target biaryl molecules via a cascade reaction,²⁶⁰ Scheme 40.



Scheme 40. Examples of biaryl products obtained via this synthetic strategy, adapted from the work of Walia *et al.*²⁶⁰

This group utilized an aromatic Finkelstein reaction and biaryl coupling in a single step via a cascade reaction strategy.²⁶⁰ The Finkelstein reaction is one in which an alkyl halide is converted into another alkyl halide by reacting with a metal halide salt via a bimolecular

nucleophilic substitution reaction (S_N2) mechanism.²⁶¹ The use of a UV-mediated aromatic Finkelstein reaction had been reported by other groups, but Walia *et al.*²⁶⁰ were the first to propose the same photoinduced SET process under argon-free conditions. This report is the first where an aromatic Finkelstein reaction/biaryl coupling have been demonstrated in a one-pot cascade reaction. Thus, this synthetic methodology is an example of a simple and greener strategy for biaryl synthesis.

3.1.3 Synthesis of biaryls: Strategies involving transition metals

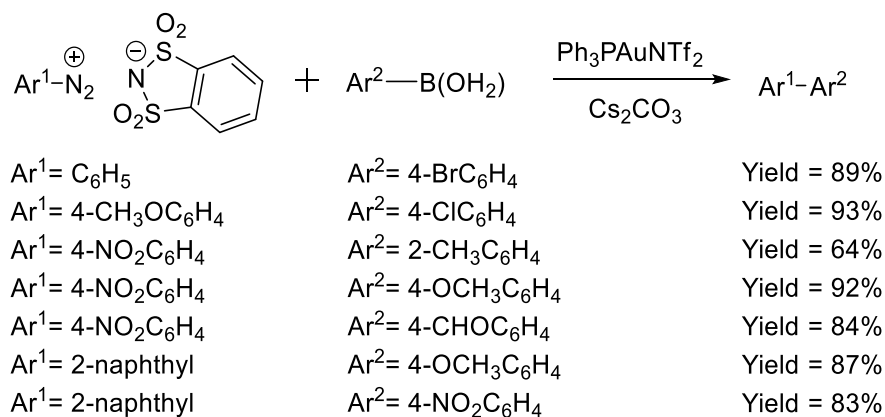
It is widely recognized that palladium has significantly changed organic synthesis over the last few decades.²⁶² Correspondingly, palladium(0)-catalyzed crossed coupling reactions using aryltin and especially arylboron reagents are among the most important carbon-carbon bond-forming reactions available to the organic chemist.²⁴⁶ The three prominent palladium-catalyzed reactions used in biaryl synthesis are the Stille,²⁶² Negishi,²⁴³ and Suzuki coupling reactions,²⁶² which utilize aryltin,²⁶² arylzinc,²⁴³ and arylboron reagents,²⁶² respectively. They are versatile reactions and tolerate a much wider range of structural diversity than alternative methods.²⁴⁶ Mechanistically these reactions are complex, but in general they are thought to proceed via oxidative addition of the catalyst to the aryl halide, followed by a transmetalation step that gives a diaryl palladium species. Reductive elimination of this then produces the biaryl compound and regenerates the palladium catalyst in the 0-oxidation state, which can re-enter the catalytic cycle.²⁴⁶ Although palladium catalysts have been traditionally applied in these coupling reactions,^{262, 263} the use of alternative catalysts, and therefore modifications to these traditional synthetic methodologies, have also been documented.^{245, 264} These three synthetic methodologies will be discussed in the following sections, where a general description of these coupling reactions will be given but only recent, relevant examples of modifications will be included. This goes to demonstrate how, even decades after their initial discovery, these reactions are still being investigated and developed.

3.1.3.1 Suzuki coupling to access biaryl molecules

The transition metal-catalyzed Suzuki reaction has been well developed and accepted as one of the most efficient methodologies for the synthesis of biaryls in both laboratory and industry settings.²⁴⁵ For example, this reaction has found extensive use in natural product synthesis.²⁴³ Boronic acids ($Ar^1B(OH)_2$) are the usual substrates in this reaction, which react with aryl halides or triflates (Ar^2X , $X = \text{halogen or triflate}$), although the esters of boronic acids and arylboranes have been used.²⁴³ Importantly, both carbocyclic and heterocyclic halides can be incorporated as reagents in this reaction.²⁴³ The Suzuki reaction has been adapted in literature in previous years, an example of which has been included in the following.

3.1.3.1.1 Suzuki approach of Barbero and Dughera (2018)

Research by Barbero and Dughera²⁶⁴ utilized the reactivity of arenediazonium *o*-benzenedisulfonimides synthesized by their group as electrophilic partners in Au(I)-catalyzed Suzuki coupling reactions, Scheme 41. This synthetic strategy was proposed on the basis of previous research which suggested that the generation of aryl radicals is useful in gold-catalysed cross-coupling reactions. This is because aryl radicals can operate as both oxidants and coupling partners, thereby eliminating the requirement for external oxidants.²⁶⁴ This is consistent with the work of Barbero and Dughera²⁶⁴ in that no external oxidants, photocatalysts, or light were necessary for the reaction to occur under the proposed conditions, where a reaction was even performed successfully in the dark. This is unlike other gold-catalyzed Suzuki reactions that had been reported up to the time of their publication.²⁶⁴ This synthetic methodology is summarized by Scheme 41 below.



Scheme 41. A selection of the 60 examples of the successful application of this groups' synthetic methodology to biaryl synthesis. All reactions were performed in THF at room temperature under nitrogen flow in the presence of Cs₂CO₃ (1 mmol) and Ph₃PAuNTf₂ (5 mol%). The diazonium salt (0.5 mmol): boronic acid ratio was 1:1.1. Adapted from the work of Barbero and Dughera.²⁶⁴

The generally high yields of biaryls obtained, short reaction time, the mild reaction conditions required, as well as simplicity of the procedure and lack of external oxidants, makes this a welcome addition to the synthetic toolkit for the synthesis of biaryls.²⁶⁴ Furthermore, this synthetic methodology is chemoselective, with negligible amounts of by-products produced, versatile, and has a broad scope in that variously substituted diazonium salts and boronic acids can be incorporated, as evidenced by Scheme 41. The reaction was not affected by electronic effects as the presence of electron-donating and/or electron-withdrawing groups on either coupling partner led to the synthesis of biaryls in satisfactory yields, Scheme 41. However, sterics had a much more pronounced effect, where the presence of a substituent in the *ortho* position of either coupling partner drastically reduced the yield, as observed in the case of Ar¹ = 4-NO₂C₆H₄ and Ar² = 2-CH₃C₆H₄ for example, Scheme 41. Additionally, reactions carried out with heteroaryl boronic acids failed. As a result, four heteroarenediazonium salts were synthesized and

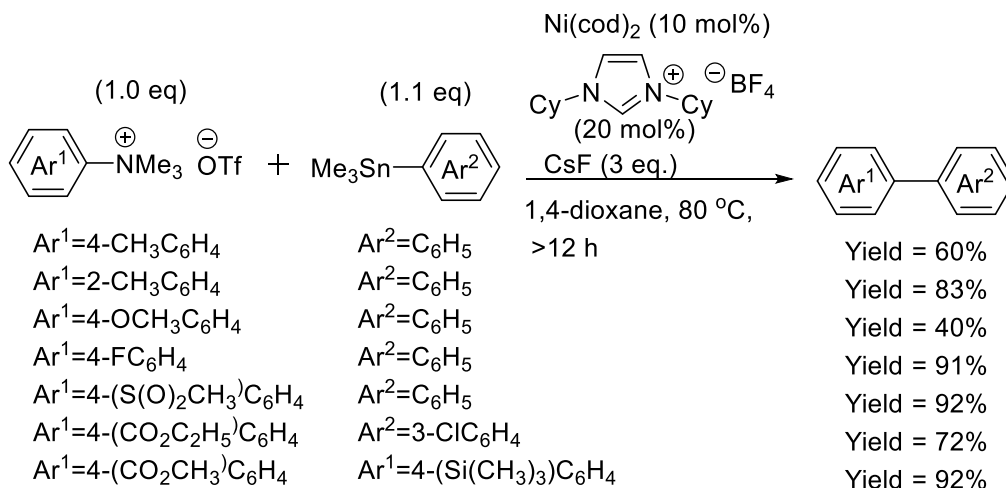
used as the electrophilic partners, which enabled the target compounds to be synthesized using this methodology.²⁶⁴

3.1.3.2 Stille coupling methodologies to access biaryls

The Stille reaction traditionally utilizes arylstannanes and either aryl halides or triflates as the coupling partners in order to synthesize biaryls. This reaction is extremely versatile, proceeds under neutral conditions, and can tolerate a wide range of substituents on both coupling partners. Both carbocyclic and heterocyclic halides can be incorporated as reagents in this reaction.²⁴³ The major disadvantage of the Stille reaction is the toxicity associated with the required organotin reagents and the by-products that result.²⁴³ However, there have been modifications to this traditional protocol, an example of which will be discussed in the following sub-section.

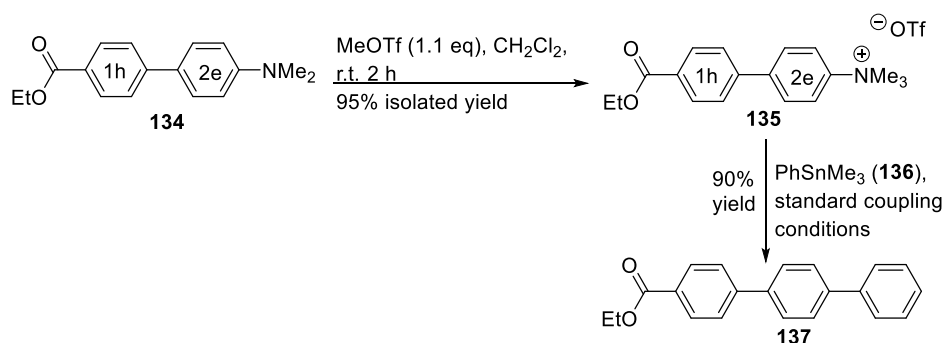
3.1.3.2.1 Stille approach of Wang *et al.* (2016)

The Stille palladium catalyzed cross-coupling reaction is another one of the most widely used cross-coupling methods for the synthesis of functional molecules and polymers, both in laboratory research and in industry.²⁶⁵ However, in 2016, Stille coupling utilizing C–O and C–N bond cleavage was under explored.²⁶⁵ As such, Wang *et al.*²⁶⁵ developed the first nickel-catalyzed Stille cross-coupling reaction of quaternary organo-ammonium salts via C–N bond cleavage. As part of their investigations, they determined the preferred reaction conditions as heating a mixture of quaternary organo-ammonium salts (as triflate) and aryltrimethylstannanes in 1:1 ratio in dioxane, with caesium fluoride as base, commercially available bis(cyclooctadiene)nickel(0) (Ni(cod)₂) as a catalyst, and 1,3-dicyclohexylimidazol-2-ylidene (ICy) as a ligand. This methodology was shown to provide high synthetic efficiency and afforded the corresponding biaryl with broad functional group compatibility,²⁶⁵ Scheme 42(a).²⁶⁵



Scheme 42(a). Some examples of the application of Stille cross-coupling reactions of quaternary organo-ammonium salts with aryltrimethylstannanes to give biaryl products. Adapted from the work of Wang *et al.*²⁶⁵

In addition to reporting a novel methodology, which led to a broad range of biaryl products, the group demonstrated how these products could be applied in subsequent reactions in order to selectively prepare functional molecules.²⁶⁵ An example of one such reaction is given in Scheme 42(b), in which compound **134** is converted to the ammonium salt (**135**), which undergoes further coupling with a stannane (**136**) to generate the *p*-terphenyl derivative (**137**).



Scheme 42(b). The sequential cross-coupling of a biaryl product formed by implementation of the standard coupling conditions can produce more functionalised molecules, adapted from the work of Wang *et al.*²⁶⁵

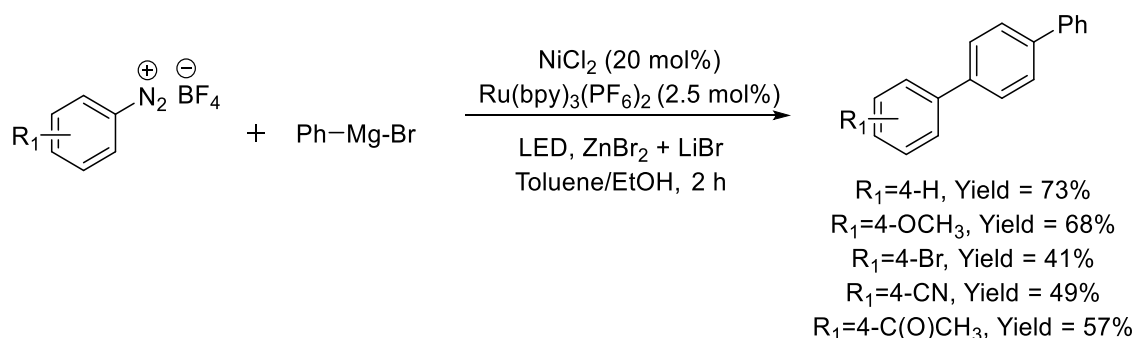
Therefore, this group were the first to develop a Stille reaction that occurs via C–N bond cleavage by incorporating quaternary ammonium salts and is catalyzed by a commercially available Ni-catalyst/ligand. This synthetic methodology is predicted to be useful for straightforward transformations of various aromatic amines/quaternary ammonium salts into multi-aromatic compounds and oligo(arylene)s, the products of which would have useful industrial applications.²⁶⁵

3.1.3.3 Negishi coupling to access biaryls

The Negishi reaction represents one of the most widely used coupling protocols.²⁶² Furthermore, this methodology is one of the most commonly used approaches to access biaryls specifically.²⁴³ This reaction utilizes arylzinc reagents (Ar^1ZnX , $\text{X} = \text{halogen}$) and aryl halides or triflates (Ar^2X , $\text{X} = \text{halogen or triflate}$), where a broad range of functional groups are tolerated in both coupling partners.²⁴³ The Negishi reaction has also been used to prepare various heterobiaryls.²⁴³ Modifications to the traditional Negishi coupling reaction have been reported, and one example of a recent development in this coupling methodology is included in the following sub-section.

3.1.3.3.1 Negishi approach of Wang and Liu (2019)

The efforts of Wang and Liu²⁶⁶ have resulted in the development of a one-pot Nickel-catalyzed Negishi coupling reaction that is accelerated by visible-light and therefore can occur at room temperature within a short reaction time (< 2 h). Diazonium salts were used in addition to Ar_2Zn species that were generated *in situ* from Grignard reagents and zinc bromide.²⁶⁶ This has facilitated the synthesis of a broad range of biaryls, which can be accessed by varying the aryldiazonium salt used, Scheme 43.



Scheme 43. Some examples of Negishi coupling to access biaryls. Reaction conditions: Diazonium salts (0.25 mmol), Grignard reagent (0.5 mmol), NiCl_2 (0.05 mmol, 20 mol%), ZnBr_2 (0.25 mmol), LiBr (0.38 mmol), $\text{Ru}(\text{bpy})_3(\text{PF}_6)_2$ (0.00625 mmol, 2.5 mol%), 3.0 mL toluene/3.0 mL ethanol at room temperature in open air under blue LED irradiation. Adapted from the work of Wang and Liu.²⁶⁶

A wide variety of aryldiazonium salts and Grignard reagents are suitable substrates for this Negishi coupling reaction, and provided the desired products in moderate to good yields.²⁶⁶ Up to the time of their publication, the use of the nickel catalyst in Negishi coupling reactions had been described but only in conjunction with well-designed ligands and at high temperatures of over 60 °C. Thus, Wang and Liu²⁶⁶ have achieved a novel, mild, one-pot protocol for a nickel-catalyzed Negishi reaction, which is accelerated by photocatalysis, proceeds at room temperature, and is compatible with a range of functional groups.²⁶⁶

3.1.4 Aims of biaryl synthesis.

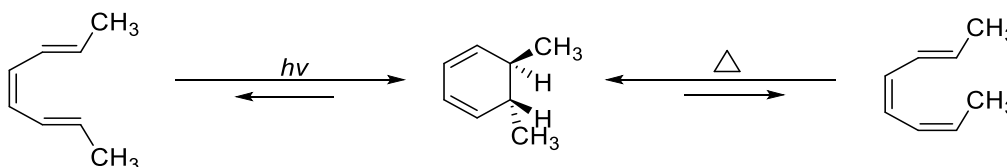
The aims of this part of the PhD project include:

- (i) To investigate a metal-free approach to synthesize biaryl molecules. To do this, we aim to explore the use of our trienes as substrates in a thermally induced electrocyclization.
- (ii) To carry out a reaction optimization study in order to determine preferred reaction conditions for this approach and to use these preferred reaction conditions to synthesize a family of novel biaryls. The biaryls will be characterized using NMR spectroscopy, LC-MS, HR-MS, and IR spectroscopy.
- (iii) To conduct a preliminary photophysical study of the biaryls synthesized.

3.2 Results & Discussion

3.2.1 Development of synthetic methodology to access biaryls

1,3,5-Hexatriene systems have been reported to undergo 6π electrocyclizations, such as that described by Dinda²⁶⁷ shown in Scheme 44. An electrocyclic reaction is an intramolecular reaction in which a σ bond is formed between the ends of a conjugated system, or the reverse of this process, by means of thermal or photochemical conversion. This is a concerted process and one which is reversible in nature. The stereochemical outcome of an electrocyclic reaction can be predicted based on the Woodward-Hoffmann rules.²⁶⁸



Scheme 44. Electrocyclization of *trans, cis, trans*-2,4,6-octatriene or *trans, cis, cis*-2,4,6-octatriene to *trans*-5,6-dimethyl-1,3-cyclohexadiene. The transformation can be photochemically or thermally induced, respectively. Adapted from the work of Dinda.²⁶⁷

Woodward and Hoffmann, in their paper in 1965,²⁶⁸ introduced the terms ‘conrotatory’ and ‘disrotatory’ to explain the mechanism and stereospecificity of electrocyclic reactions. These terms referred to the motion of the groups at the ends of an acyclic conjugated system which, when they proceeded in the same direction in either a clockwise or anticlockwise manner, it was termed ‘conrotatory’. Conversely, if the motion of one of these substituents was clockwise while the other was anticlockwise, this was termed ‘disrotatory’ motion. Woodward and Hoffmann deduced that the stereochemical outcome of electrocyclic reactions was controlled by the symmetry of the HOMO (highest occupied molecular orbital) of the open chain conjugated system, and in their paper they gave two examples. The first example was an open-chain system containing $4n$ π -electrons, where the symmetry of the HOMO meant that the bonding interaction between the termini of the acyclic conjugated system must involve overlap between the orbitals on opposite faces of this system. In this case, it can only be achieved via a conrotatory process. The second example was an open-chain system containing $(4n + 2)$ π -electrons, 1,3,5-hexatriene being an example of such a system. The symmetry of the HOMO means that the overlap between orbitals on the same face of the system is necessary for the terminal bonding interaction to occur, which can only be achieved by a disrotatory process.²⁶⁸

As the $(4n + 2)$ π -electron conjugated system relates to the type of conjugated systems that will be discussed in this chapter, it is this type that will be discussed further. In cases of thermal reactions of these conjugated systems, ψ_3 would be the HOMO as it has the minimum number of even nodes (two nodes).²⁶⁷ Hence, the disrotatory motion of the groups on terminal carbons brings the lobes of same phase together for bonding, involving a Hückel-type transition state that is said to be a ‘symmetry allowed’ path. The conrotatory motion would be ‘symmetry forbidden’ as it leads to a transition-state of high activation energy. For their photochemical reactions, ψ_4 would be the HOMO and hence, conrotatory motion would be the symmetry allowed path,²⁶⁷ Figure 80.

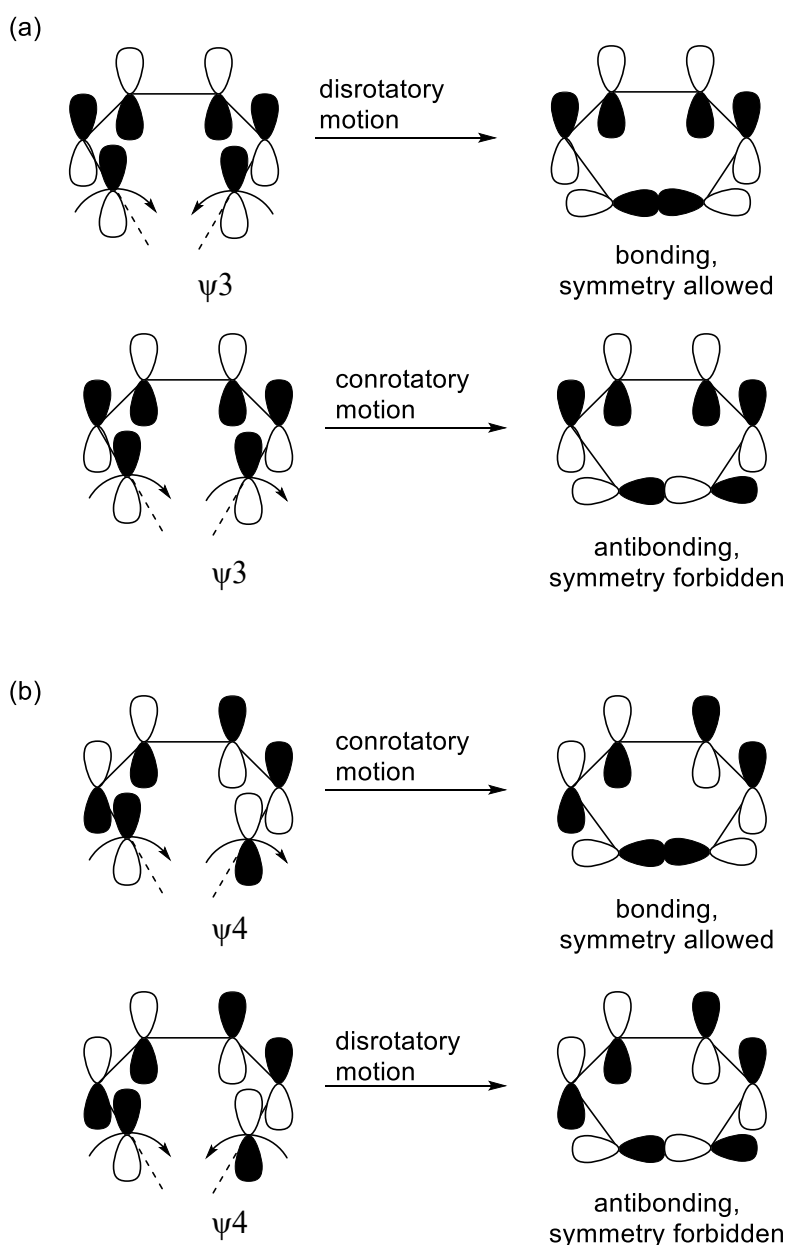


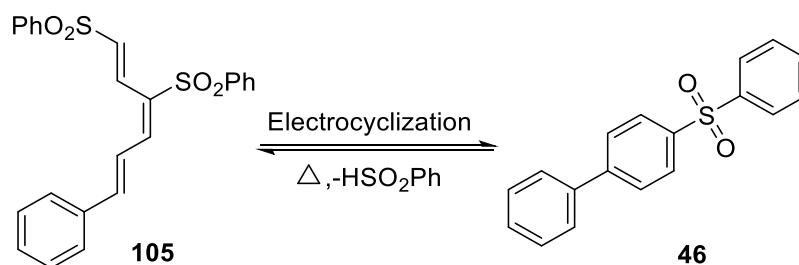
Figure 80. Graphical representations of (a) thermal electrocyclizations of $4n + 2$ π -electron conjugated systems; (b) photochemical electrocyclizations of $(4n + 2)$ π -electron conjugated systems, adapted from the work of Dinda.²⁶⁷

The Woodward–Hoffmann rules for electrocyclic reactions can therefore be summarized as per Table 18.

Table 18. Summary of the Woodward-Hoffmann rules of electrocyclic reactions, adapted from the work of Dinda.²⁶⁷

Acyclic conjugated system	Reaction allowed	Motion
$4n$ π -electron	Thermal	Conrotatory
	Photochemical	Disrotatory
$(4n + 2)$ π -electron	Thermal	Disrotatory
	Photochemical	Conrotatory

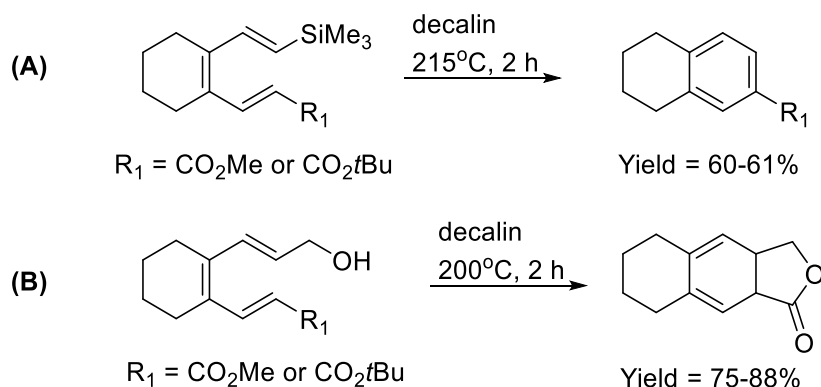
Given the range of 1,3,5-hexatrienes we had accessed, see Chapter Two, and particularly with respect to the $(1E,3E,5E)$ -1,3-bis-phenylsulfonyl-6-phenyl-hexa-1,3,5-trienes, we became interested in exploring whether these trienes could undergo a 6π electrocyclization. Our interest was triggered when collaborators at NUI Galway (Prof. Patrick McArdle and Dr Jolanta Karpinska) were attempting to generate an x-ray crystal structure of one of our $(1E,3E,5E)$ -1,3-bis-phenylsulfonyl-6-phenyl-hexa-1,3,5-trienes.^{226, 227} The thermal process they employed resulted in the 6π electrocyclization of $(1E,3E,5E)$ -1,3-bis-phenylsulfonyl-6-phenyl-hexa-1,3,5-triene, **105**, and formed 4-(phenylsulfonyl)-1,1'-biphenyl, **46**, in small amounts, Scheme 45.



Scheme 45. Thermal electrocyclization of $(1E,3E,5E)$ -1,3-bis-phenylsulfonyl-6-phenyl-hexa-1,3,5-triene, **105**, to give the corresponding biaryl product, **46**.

Numerous examples of thermal electrocyclization of 1,3,5-hexatrienes have been reported in the literature. Typical products obtained from these thermal electrocyclizations of 1,3,5-hexatrienes include functionalized ring-annulated cyclohexa-1,3-dienes,²⁶⁹ poly-substituted tricyclic products,²⁷⁰ and various other cyclic products including tricyclic lactones,¹⁸² and tetracycles.²⁷¹ A good example can be found in the work of von Zezschwitz *et al.*¹⁸² who transformed 1,3,5-hexatrienes substrates to various cyclic products, Scheme 46. The tetrahydronaphthalenes obtained (**A**, Scheme 46) result from a formal dehydrodesilylation which accompanied the thermal electrocyclization. The tricyclic lactones obtained (**B**, Scheme 46) result from an intramolecular

transesterification post electrocyclization. From our search of the per-reviewed literature, we could not find any reports that employ a single step 6π electrocyclization approach for the metal-free synthesis of biaryl systems.

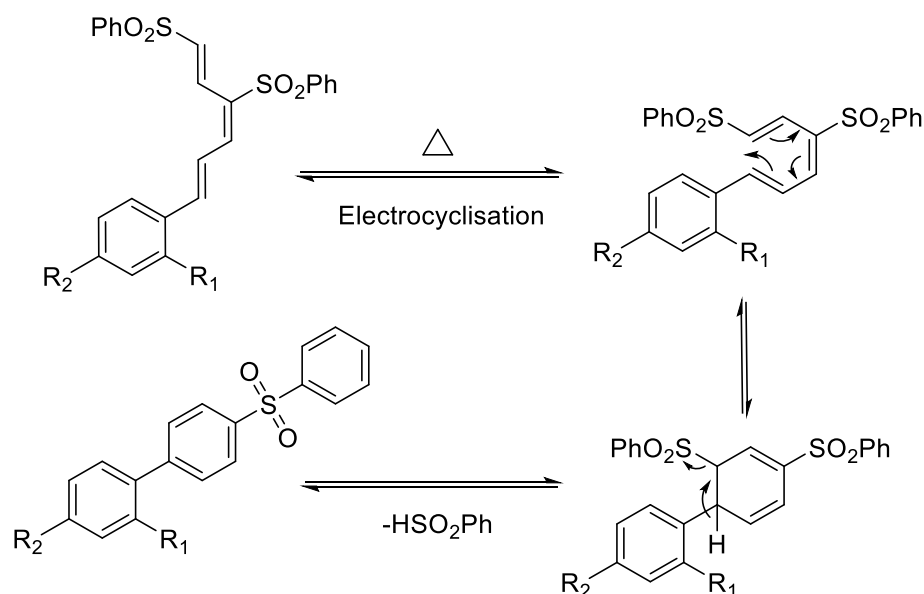


Scheme 46. Adapted from the work of von Zezschwitz *et al.*,¹⁸² a representation of how 1,3,5-hexatrienes have been used to access a variety of cyclic products.

On this basis, we considered an investigation into the thermal electrocyclization of our trienes. We first attempted an exploratory experiment where neat solid **105** (Scheme 45, 25 mg, 0.057 mmol) was heated quickly to high temperatures using a Bosch heat gun (set at the maximum temperature for approximately 10 seconds). We used NMR spectroscopy to analyze the crude product obtained and could determine that the desired biaryl **46** had been formed, Scheme 45 previously.

Compound **46** is a known literature compound and has been synthesized previously by groups such as Cho *et al.*²⁷². This group utilized a Suzuki-Miyaura coupling reaction of an aryl chloride with phenylboronic acid, using novel air stable phenyl backbone-derived 4'-(3-aminopropionic) phosphopantetheine (PN₂) ligands. This approach generated the biaryl **46** in 97% yield after a 12-hour reaction. Our NMR spectroscopic analysis (¹H and ¹³C NMR data) was consistent with that of Cho *et al.*²⁷², and hence confirmed our determination that **46** was the product formed in our thermal electrocyclization.

The mass of the crude biaryl **46** was 12.6 milligrams, corresponding to a crude yield of 75%. The proposed mechanism for this reaction is given in Scheme 47. The electrocyclization of our 1,3,5-hexatrienes is an example of a thermal, disrotatory, 6π electrocyclization that is allowed for by the Woodward-Hoffmann rules.²⁶⁸



Scheme 47. Biaryl synthesis via a thermally driven electrocyclozation.

3.2.2 Application of Woodward-Hoffman rules to our thermally induced electrocyclozation

As discussed previously, the occurrence of electrocyclic reactions is governed by the Woodward-Hoffman rules.^{267, 268} The 1,3-bis-phenylsulfonyl-6-phenyl-hexa-1,3,5-trienes synthesized as per Chapter Two are an example of open-chain system containing $(4n + 2)$ π -electrons, as characterised by Woodward and Hoffmann in their original publication.²⁶⁸ As such, in Figure 80(a) in section 3.2.1 above, 1,3,5-hexatriene was used as an example, in which it was observed that ψ_3 would be the HOMO, having the minimum number of even nodes (two). Therefore, the disrotatory motion of the substituents on terminal carbons was the symmetry allowed path by the Woodward-Hoffman rules.^{267, 268} Examining the proposed mechanism of our thermally-induced electrocyclic reaction, Scheme 47 above, using the conversion of (1*E*,3*E*,5*E*)-1,3-bis-phenylsulfonyl-6-phenyl-hexa-1,3,5-triene, **105**, as an example, the conversion to the corresponding cyclic diene is the step governed by the Woodward-Hoffman rules, Figure 81.

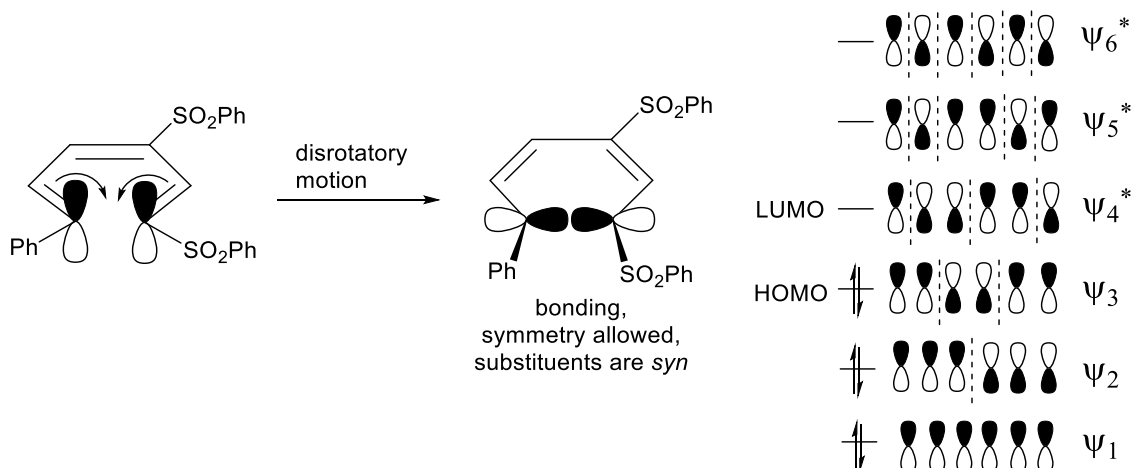


Figure 81. Analysis of the molecular orbitals involved in the thermally-induced electrocyclization that occurs as part of the formation of the desired biaryl **46**

As is evident by Figure 81, the molecular orbital analysis of compound **105** is very similar to that of 1,3,5-hexatriene (Section 3.2.1 previously) because they are both $(4n + 2)$ π -electron-containing acyclic systems with 3 conjugated π -bonds (therefore 6 π electrons). The substituents present on our triene have no effect on the application of the Woodward-Hoffman rules and so, its HOMO can also be predicted to be ψ_3 . Therefore the disrotatory motion of the substituents on the terminal carbons is the symmetry allowed pathway.^{267, 268} This disrotatory motion predicts that the formation of the *syn* diastereomer as the intermediate cyclic diene will occur, in which both the phenyl and phenylsulfonyl substituents end up on the same face of the diene product. However, this cyclic diene was not isolated during our studies and so, it is not possible to confirm whether this reaction is indeed a Woodward-Hoffman ‘symmetry allowed’ transformation, though it is likely.

If the electrocyclic reaction had occurred under photochemical conditions, a different mechanism would have ensued in that the conrotatory motion of substituents on the terminal carbons would be the symmetry allowed path. In addition, because of the promotion of an electron from the HOMO of the ground state (ψ_3) to its LUMO (ψ_4) due to the absorption of light, the HOMO of the excited state would be predicted to be ψ_4 and its LUMO ψ_5 , Figure 82.

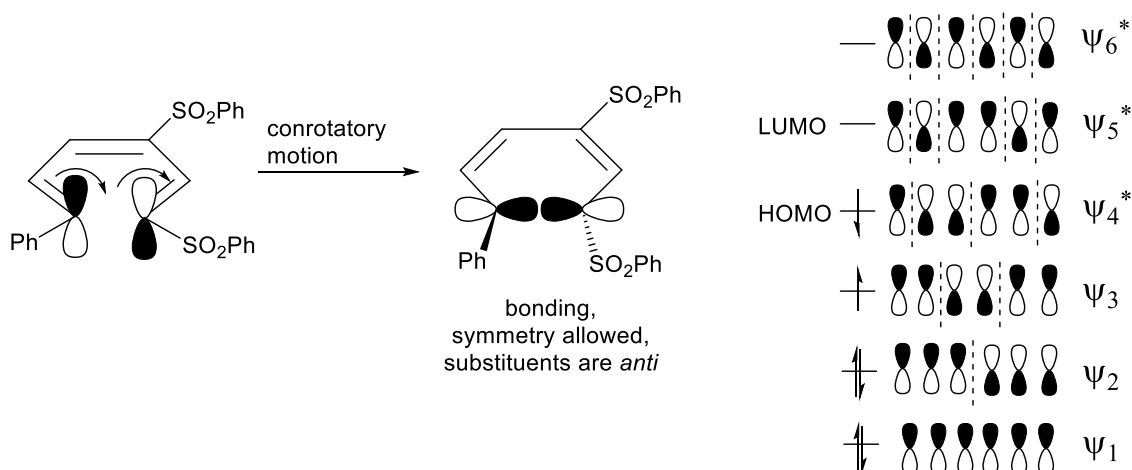


Figure 82. Analysis of the molecular orbitals involved in the alternative photochemically-induced electrocyclization step in the formation of the desired biaryl **46**

This conrotatory motion predicts that the *anti* diastereomer of the intermediate cyclic diene would form in this case, in which the phenyl and phenylsulfonyl substituents end up on the opposite face of the diene product. Photochemical conditions were investigated as part of our reaction optimisation study, see section 3.2.3.4. Biaryl formation did not occur under the photochemical conditions we attempted. As such, we favour the proposed thermal 6 π electrocyclization mechanism as shown in Scheme 47 and Figure 81.

3.2.3 Investigation of optimal procedure for biaryl synthesis

With preliminary results in hand, and a proposed mechanism, we now wanted to undertake an optimization study in order to determine preferred reaction conditions for our electrocyclization. As such, we investigated a number of different experimental set-ups that will be discussed in the following sub-sections.

3.2.3.1 Optimization study: Investigation of heating methodology

We firstly investigated different heating methods and applied these to the attempted electrocyclization of compound **105**, Scheme 45. In each case, neat solid **105** (25 mg, 0.057 mmol) was placed in a 25 gram round-bottom flask and subjected to each heating methodology for 1.5 hours unless specified otherwise, see Table 19. Conversion to biaryl **46** was determined by assessment of the ¹H NMR spectra, and the associated spectra can be found in Appendix 3, Figures A336-A340. As described in Section 3.2.1, our initial attempt at this procedure included the use of a Bosch heat gun set at the maximum temperature for 10 seconds and gave a 75% crude yield of **46** (12.6 mg). The additional attempts at improving the heating method included the use of an oil bath

heated to 175 °C, which gave a much superior 94% crude yield of **46** (15.8 mg). The use of a Pyrex bowl filled with Lab Armour metallic beads, into which our round-bottom flask containing triene was placed, and subsequently heated to 175 °C gave a crude yield of 70% (11.8 mg). Additionally, the use of sand was explored, firstly heated to 175 °C which gave an 80% crude yield of **46** (13.4 mg), and separately, heated to 200 °C gave **46** in 60% crude yield (10.1 mg). The higher temperature appeared to generate a more complex mixture and thus increasing temperature did not increase the conversion to biaryl.

Another version of the experimental set-up incorporated a Binder vacuum oven. In this case, **105** (25 mg, 0.057 mmol) was spread across a clock glass which was placed under the lid of a petri dish with tin foil wrapped underneath it to hold the clock glass and lid in place. This assembly was placed in the vacuum oven, which had been heated to 180 °C, and was left for 24 hours with the pressure approaching 0 millibar for the duration. Only 10% crude yield of **46** was observed after this time (1.7 mg). The use of an oil bath heated to 175 °C was therefore deemed as the optimal heating method in which a 94% crude yield of **46** was generated, and a summary of the percentage crude yield of biaryl **46** obtained from each method explored is given in Table 19.

Table 19. Conversion of neat **105** (25 mg, 0.057 mmol) to biaryl **46** for different heating methods.

Heating method	% Crude yield of biaryl obtained
Oil bath at 175 °C for 1.5 h	94
Metallic beads at 175 °C for 1.5 h	70
Sand at 175 °C for 1.5 h	80
Sand at 200 °C for 1.5 h	60
Heat gun for 10 seconds	75
Heating in a vacuum oven	10

3.2.3.2 Optimization study: Purification attempts using sublimation

After investigating different heating methods, we next explored purification methods that avoided the need for column chromatography. With the best heating method, **46** in a crude yield of 94% was obtained. Subsequent purification using column chromatography resulted in an isolated yield of 88%. The column chromatography procedure required a gradient mobile phase system employing 100% petroleum ether, followed by 95:5 petroleum ether/ ethyl acetate and increasing the polar phase by one percent every 100 mL (i.e. 94:6 petroleum ether/ ethyl acetate, then 93:7, then 92:8 etc.) until a final ratio of 84:16 petroleum ether/ ethyl acetate. This process was somewhat laborious and hence

we explored options to avoid the need for column chromatography. As confirmed by x-ray crystallography, the triene molecules are composed of stacks with good van der Waals interactions between neighbours.²²⁶ Van der Waals interactions are weak,²⁷³ and can be easily broken by heat. On this basis, we hypothesized that sublimation to the pure desired biaryl may be possible.

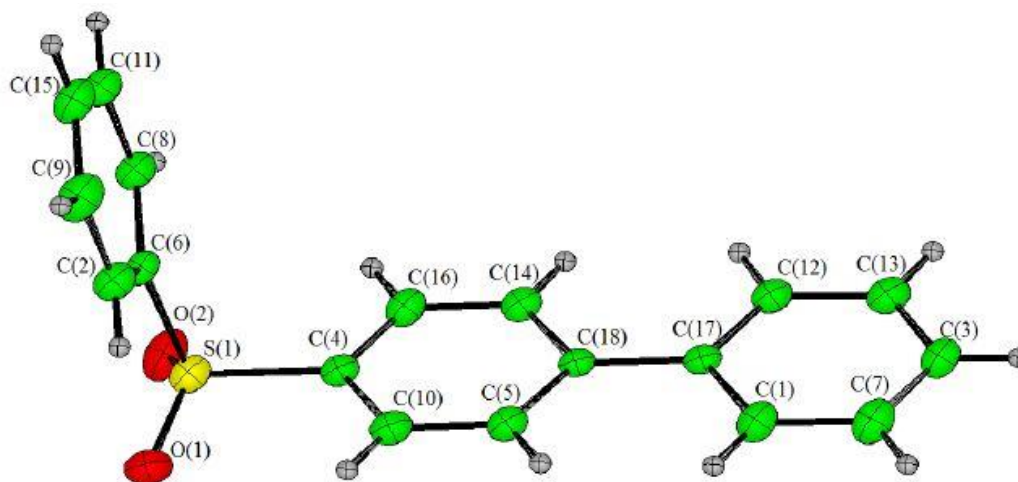


Figure 83. Crystal structure of **46**, obtained by collaborators Prof McArdle and Jolanta Karpinska.^{226, 227}

Two sublimation apparatus set-ups were attempted. The first attempt incorporated a sublimation apparatus, attached to an aspirator, which was fitted onto to a round-bottom flask containing **105** (25 mg, 0.057 mmol). This was heated using an oil bath set to 175 °C for 1.5 hours. After this time, there were 2 milligrams of material sublimed to the cold finger (which had cold water constantly running through it) and 6 milligrams of non-sublimed brown residue. The ¹H NMR spectra of both, Appendix 3, Figure A341(a) and (b), indicated that they both contained the same product – impure biaryl. Taking both the sublimed and remaining residue together, a total crude yield for **46** of 48% was obtained.

The second attempt changed the sublimation apparatus for one that required liquid nitrogen to be added to the cold finger, and this was inserted into a Schlenk tube containing **105** (25 mg, 0.057 mmol). This was heated using an oil bath set to 175 °C for 2 hours. The Schlenk tube was attached to a Schlenk line which achieved a vacuum of 0.1 mbar. The process of adding liquid nitrogen to the cold finger occurred over the course of 2 hours to ensure sufficient quantities of liquid nitrogen remained on the cold finger. A colourless material (4 mg) sublimed onto the cold finger and 13 milligrams of a brown residue remained on the bottom of the round bottom flask after the 2 hours of heating had elapsed. However, the sublimed material contained only trace amounts of biaryl **46** ($\leq 10\%$) and instead, was composed largely of an unidentified by-product. Thus, the crude yield of **46** was accounted for by the brown residue only, corresponding to a 77% crude yield. The ¹H NMR spectra of both the sublimed and non-sublimed material have been included in Appendix 3, Figure A342(a) and (b).

On this basis, the use of sublimation for biaryl isolation was not successful and discontinued as a method of purification.

3.2.3.3 Optimization study: Microwave heating

The use of microwave irradiation was then investigated as a heating method to see could this increase conversion to biaryl and generate a cleaner reaction with fewer by-products. A number of different solvents, temperatures, and concentrations of substrate were investigated, which will be discussed separately in the following sub-sections.

3.2.3.3.1 Microwave heating and choice of solvent

To investigate if solvent had an effect, 0.0025 M (5 mL) solutions of compound **105** were made up in respective solvents and each solution was exposed to microwave heating at 170 °C for 5 minutes. The crude ¹H NMR spectrum for each experiment attempted is included in Appendix 3, Figures A343-A346. The first solvent used was toluene, and in this case a white solid, which was not the desired product and whose structure could not be determined, precipitated at the end of the reaction. The remaining solution contained impure biaryl as well as unidentified side products, corresponding to 40% crude yield of biaryl **46**. An experiment using DMF as solvent was next attempted, resulting in a complex mixture and 50% crude yield of biaryl **46**. When chloroform was employed as the solvent, no conversion to biaryl was observed after 5 minutes. A complex mixture was formed and evidence of unconverted triene was found in the crude ¹H NMR spectrum. When acetonitrile was used as the solvent, very little conversion to biaryl was observed after 5 minutes and instead, like for chloroform, a complex mixture was formed. The crude yields of biaryl **46** obtained as part of our solvent screen process are given in Table 20, with DMF giving the best result.

Table 20. Conversion of **105** (0.0025 M, 5 mL) to biaryl **46** under microwave heating (175 °C, 5 min) using different solvents.

Solvent	% Crude yield of biaryl
Toluene	40
DMF	50
Chloroform	0
Acetonitrile	0

3.2.3.3.2 Microwave heating and variations in temperature used

To investigate whether the temperature could affect the conversion to biaryl, 0.0025 M solutions (5 mL) of compound **105** were made up in DMF (deemed to be the best solvent of those examined). Each solution was exposed to microwave heating at a different temperature for 5 minutes. The crude ^1H NMR spectrum for each experiment attempted is included in Appendix 3, Figures A347-A351. After microwave heating at 85 °C, no conversion from triene **105** to biaryl **46** was observed and this mixture consisted largely of unconverted triene **105**. Similarly, at 110 °C very little conversion from triene **105** to biaryl **46** was observed. Some evidence of its conversion could be seen in the crude ^1H NMR spectrum via a small multiplet at approximately 8 ppm (Appendix 3, Figure A348) but the yield was too low to accurately quantify. At 140 °C, a 30% crude yield (1.10 mg) of biaryl **46** was obtained (the remainder consisted of unconverted triene and a complex mixture). After exposure to microwave heating at 150 °C, a 40% crude yield (1.47 mg) of biaryl **46** was obtained, the remainder consisted of unconverted triene and a complex mixture. At 170 °C, a 50% crude yield (1.84 mg) of biaryl **46** was obtained and again, the remainder consisted of a complex mixture. A summary of results obtained as part of the temperature study can be found in Table 21. The best result was obtained for microwave heating at 170 °C for 5 minutes.

Table 21. Conversion of **105** (0.0025 M, 5 mL) to biaryl **46** under microwave heating for 5 min at different temperatures.

Temperature (°C)	% Conversion to biaryl
85	0
110	≤5
140	30
150	40
170	50

3.2.3.3.3 Microwave heating and concentration of triene

We next investigated whether the concentration of triene **105**, subjected to microwave irradiation, could have an effect on conversion to biaryl **46**. The same solvent, DMF, was used as it was deemed the preferred solvent. Different concentrations of compound **105** were made up to a volume of 5 mL and heated to 170 °C, deemed the preferred temperature, for 5 minutes. As reported in Section 3.2.3.3.1, a 0.0025 M solution of triene **105** corresponded to the generation of 50% crude yield of biaryl **46** under these conditions. A 0.01 M solution of triene **105** corresponded to the generation of 60% (8.8 mg) crude yield of biaryl **46** (the remainder consisted of a complex mixture), whereas

increasing the concentration to a 0.1 M solution of triene **105** did not increase the crude percentage yield of biaryl **46** obtained, with the remainder consisting of a complex mixture. The crude ¹H NMR spectrum for each experiment attempted is included in Appendix 3, Figures A351-A353.

Table 22. Conversion of **105** (5 mL) to biaryl **46** under microwave heating (170 °C, 5 min) at different concentrations.

Concentration of triene solution (M)	% Conversion to biaryl
0.0025	50
0.01	60
0.1	60

As none of these microwave experiments improved the crude yield of biaryl **46**, compared to neat conventional heating, no further investigation was conducted using microwave irradiation.

3.2.3.4 Optimisation study: UV experiment

Finally, a photochemical rather than a thermal conversion of triene **105** to biaryl **46** was attempted. Theoretically, the occurrence of this type of photochemical 6 π electrocyclicization is ‘symmetry allowed’ by the Woodward-Hoffmann rules, once a conrotatory overlap of molecular orbitals occurs.²⁶⁸ Our first attempt at applying a photochemical conversion involved dissolving triene **105** (11 mg, 0.03 mmol) in 10 mL of deuterated chloroform and placing this solution, stirring, in an ultraviolet (UV) box under a lamp emitting 365 nm wavelength light. After 7 days, no conversion to biaryl was observed by NMR and no physical changes appeared in the solution. The ¹H NMR spectrum of this solution is given in Appendix 3, Figure A354. Alternatively, the same set up was used but 254 nm wavelength light was employed. Despite a change in appearance at the end of 18.5 hours stirring, to a red solution from a yellow one, this did not correspond to the formation of biaryl **46**, as determined based on analysis of the ¹H NMR spectrum (Appendix 3, Figure A355). As we did not find success using this method via emission of UV light at the two wavelengths we had access to, in that, biaryl formation was not detected in either case, this method was not investigated further.

Thus, of all our efforts to find an optimal method for biaryl synthesis, heating the triene neat to 175 °C using an oil bath gave the best conversion to biaryl and therefore was deemed the preferred method. This method was then used to explore the substrate scope, employing a selection of our triene substrates, section 3.2.4.

3.2.4 Substrate scope investigation of the thermal electrocyclization of 1,3,5-hexatrienes

Our preferred reaction conditions were applied to a selection of the 1,3,5-hexatrienes with both electron-donating and electron-withdrawing substituents on the phenyl ring. Biaryl formation was successful in all cases, with isolated yields obtained varying from 40-88%, Figure 84. The biaryls formed were purified by column chromatography and recrystallization.

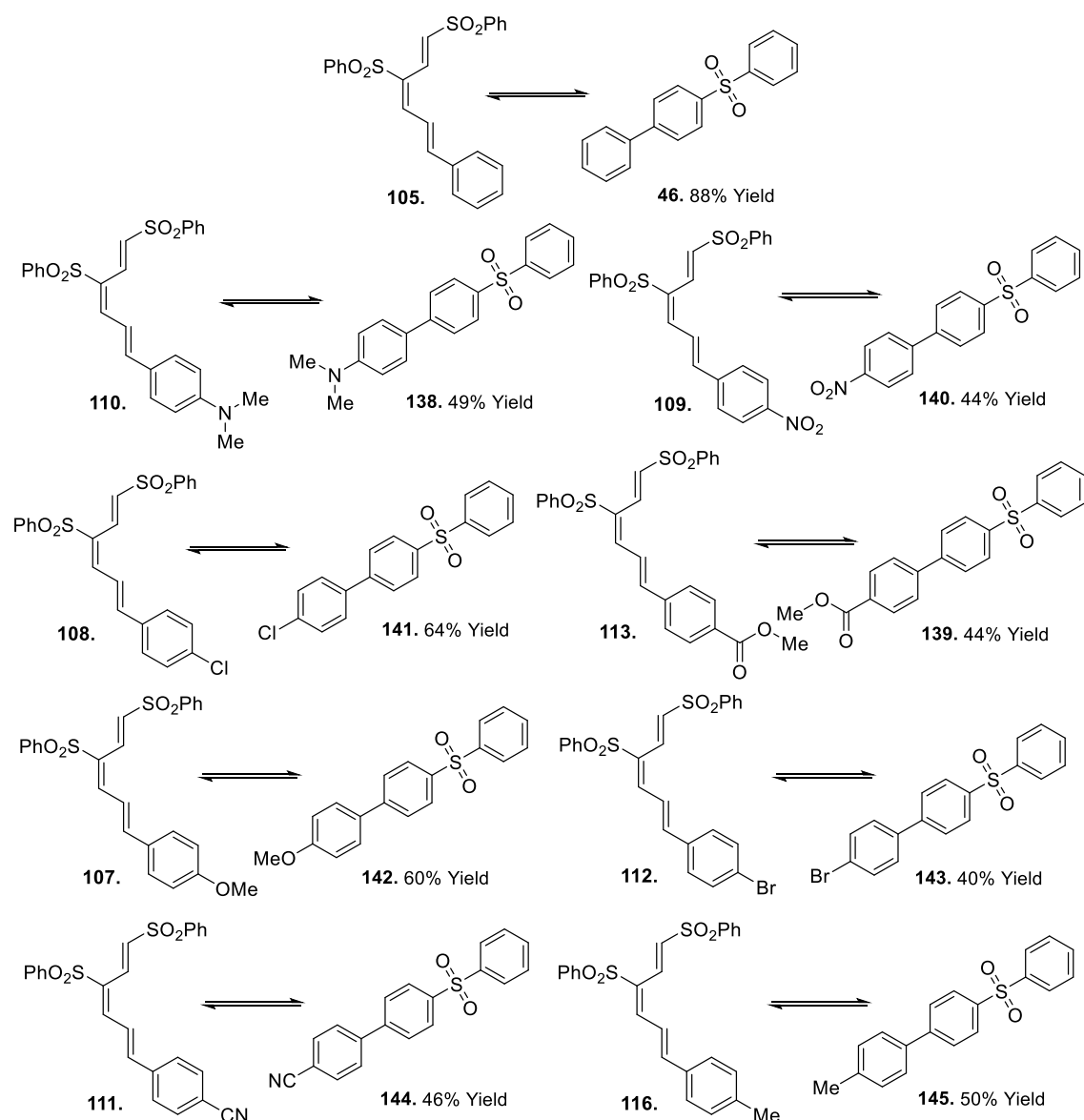


Figure 84. Biaryls obtained using the thermal electrocyclization methodology (neat 1,3,5-hexatriene, 175°C, 1.5 h. Purification by column chromatography and subsequent recrystallization.

Examining the yields obtained, there are no obvious trends with respect to the substituent effects on the yield. The non-substituted triene **105** gave the highest yield of biaryl (**46**)

at 88%. It appears that electron-donating or electron-withdrawing groups that have strong inductive or mesomeric effects are not as well tolerated by this methodology. For example, the 1-(4-dimethylaminophenyl)-4-(phenylsulfonyl)benzene product, **138**, was recorded with 49% yield and the dimethylamino substituent is an example of a strong electron-donating group. Similarly, a low yield for 1-(4-nitrophenyl)-4-(phenylsulfonyl)benzene, **140**, of 44% was recorded, and here, the nitro substituent is an example of a strong electron-withdrawing group. Those that exhibit moderate electron withdrawing/donating characteristics have varying levels of tolerance by this method, where both the 4-methyl ester and 4-methoxy substituents would be expected to be moderately electron-withdrawing and -donating, respectively but the yields recorded of their respective biaryl products, **139** and **142** were very different at 60% and 44%, respectively. Even examination of the halo-substituents does not lead to clarity regarding their effect on the yield, where the 4-chloro substituent was much better tolerated than its 4-bromo substituted analogue.

Aside from the occurrence of the thermal electrocyclization process, the difficulties encountered in terms of purification by column chromatography and subsequent recrystallization must be considered as factors influencing the yield. The crude mixtures of these compounds are quite complex, given that the vast majority of signals relating to these products and potential side products, namely the hydrosulfonylbenzene (HSO_2Ph) that is driven off during the electrocyclization process, appear within 7-8 ppm in the ^1H NMR spectra. They behave very similarly on a TLC plate and, because of this, separation can be difficult. The necessity to purify the product further by recrystallization using DCM/*n*-hexane in order to obtain crystal products leads to further loss of yield, although it does give access to a pure, crystalline product in all cases and this purity is an important attribute.

While there is room for improvement in terms of the yields recorded for the products of this synthetic methodology, it does give access to pure biaryl products which, because they are novel in all but one case, require full characterization and purity is important to do this accurately. In addition, in line with the interest in the development of more environmentally friendly protocols, while this procedure cannot be considered 'green' in light of the use of high temperatures, the requirement for these high temperatures is only for a short time at 1.5 hours. Additionally, the procedure does not require a solvent, nor a transition metal as a catalyst, and hence, there are some environmentally friendly attributes.

3.2.5 Structural characterization of 1-(4-methyl ester phenyl)-4-(phenylsulfonyl)benzene **139**

Full structural characterization was carried out for all biaryls synthesised. A lot of structural information can be obtained through analysis of the associated ^1H NMR, ^{13}C

NMR and 2D NMR spectra. The structural characterization of compound **139**, Figure 85, will be discussed as an example in the following sections.

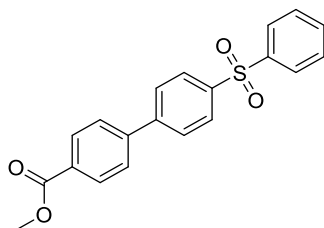


Figure 85. The structure of compound **139**

3.2.5.1 NMR analysis of 1-(4-methyl ester phenyl)-4-(phenylsulfonyl)benzene **139**

Comparing the DEPT-135 and ^{13}C spectra (Figure 86 and 87, respectively), the quaternary carbons can be identified at 166.6 (which corresponds to the C=O in the structure as this signal is the most deshielded due to the doubly bonded oxygen atom), 145.0, 143.5, 141.6, 141.1 and 130.2 ppm. These signals can be identified as quaternary carbon signals as they disappear in the DEPT-135 but are present in the ^{13}C NMR.

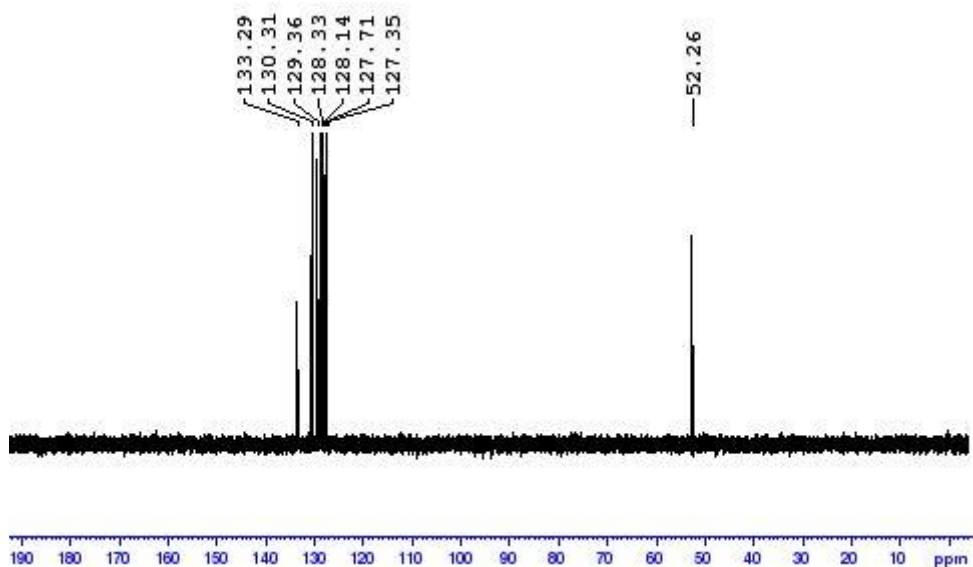


Figure 86. Full DEPT-135 spectrum of biaryl **139**.

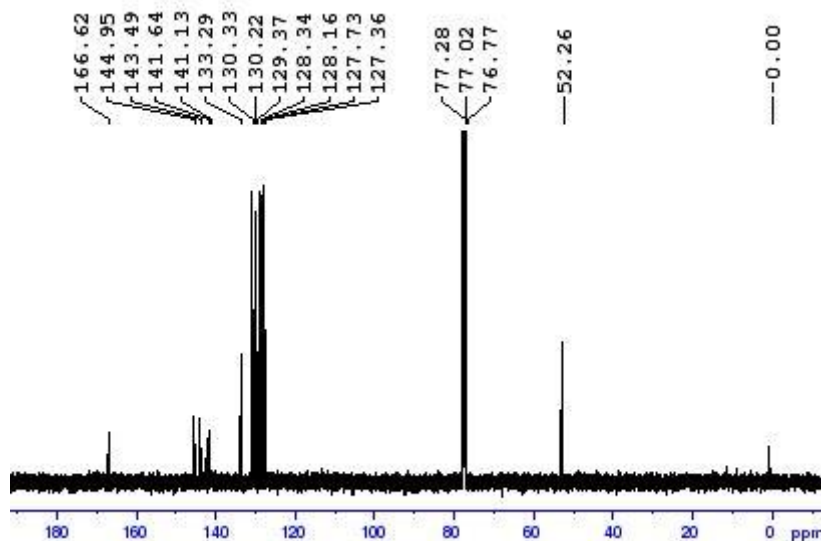


Figure 87. Full ^{13}C spectrum of biaryl **139**.

Six quaternary carbons can be identified in this way and this corresponds with the number expected by examination of the compound structure, where quaternary carbons that are part of the phenyl rings are labelled as C1-C5, plus the carbonyl C, Figure 88. The structure of this biaryl has 20 carbon atoms and there are only 14 carbon signals in the ^{13}C NMR spectrum. This is as expected due to the plane of symmetry within the aromatic rings and hence the number of signals arising from the aromatic rings is halved, Figure 88.

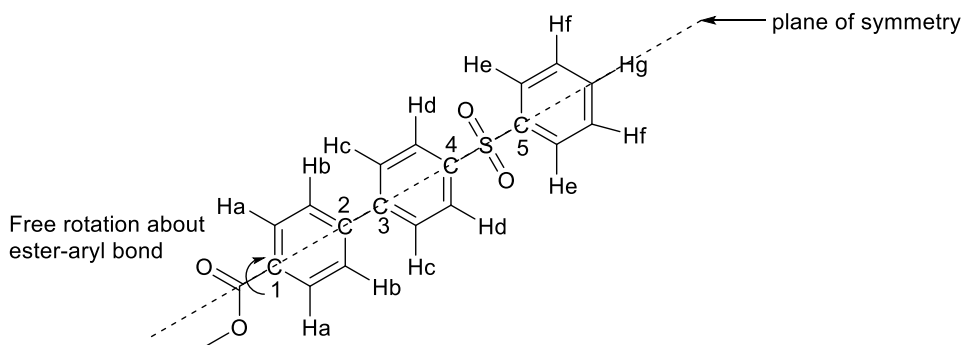


Figure 88. The structure of 1-(4-methyl ester phenyl)-4-(phenylsulfonyl)benzene **139**, with relevant protons labelled for ease of discussion and the plane of symmetry highlighted.

The methoxy carbon and hydrogens can be easily identified as the most shielded signal in both the ^{13}C and ^1H NMR spectra. Thus, the methoxy carbon appears at 52.3 ppm, Figure 89, and these hydrogens correspond to the singlet at 3.94 ppm, Figure 90, integrating for 3 protons in the ^1H NMR spectrum.

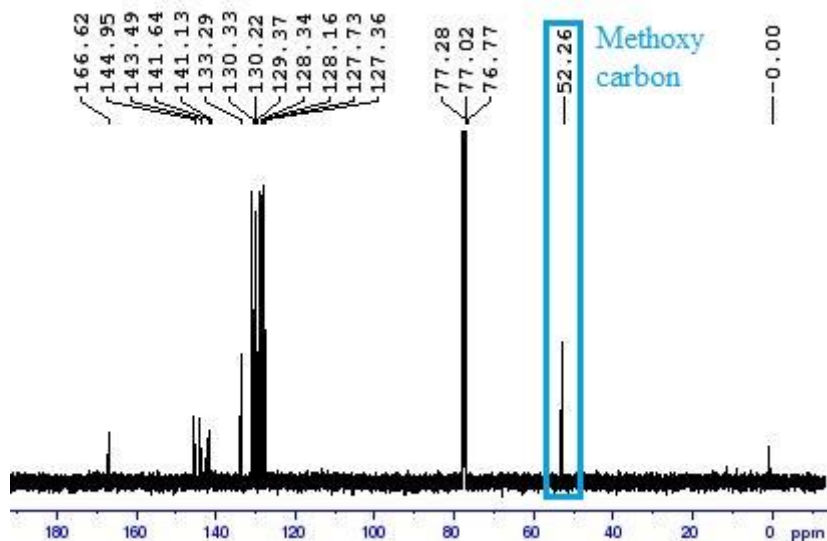


Figure 89. ^{13}C NMR spectrum showing the methoxy carbon within biaryl **139**

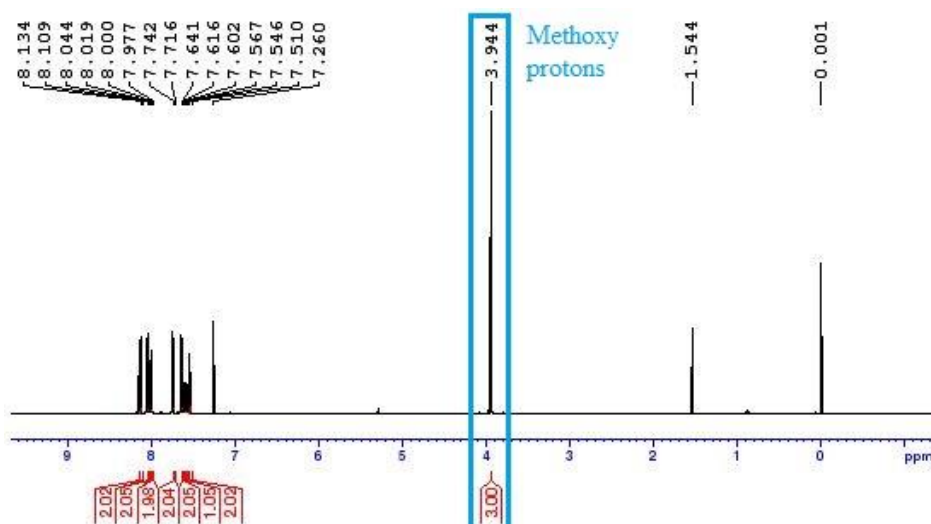


Figure 90. ^1H NMR spectrum showing the methoxy hydrogens within biaryl **139**

The carbonyl carbon signal at 166.6 ppm shows coupling in the HMBC spectrum to the most deshielded protons at 8.13-8.11 ppm (integrating for 2H) and to OCH_3 . This implies that the multiplet at 8.13-8.11 ppm is the peak of Ha shown in Figure 88 above. The high chemical shift of this signal is expected due to *ortho* relationship of these protons to the electron-withdrawing ester group.

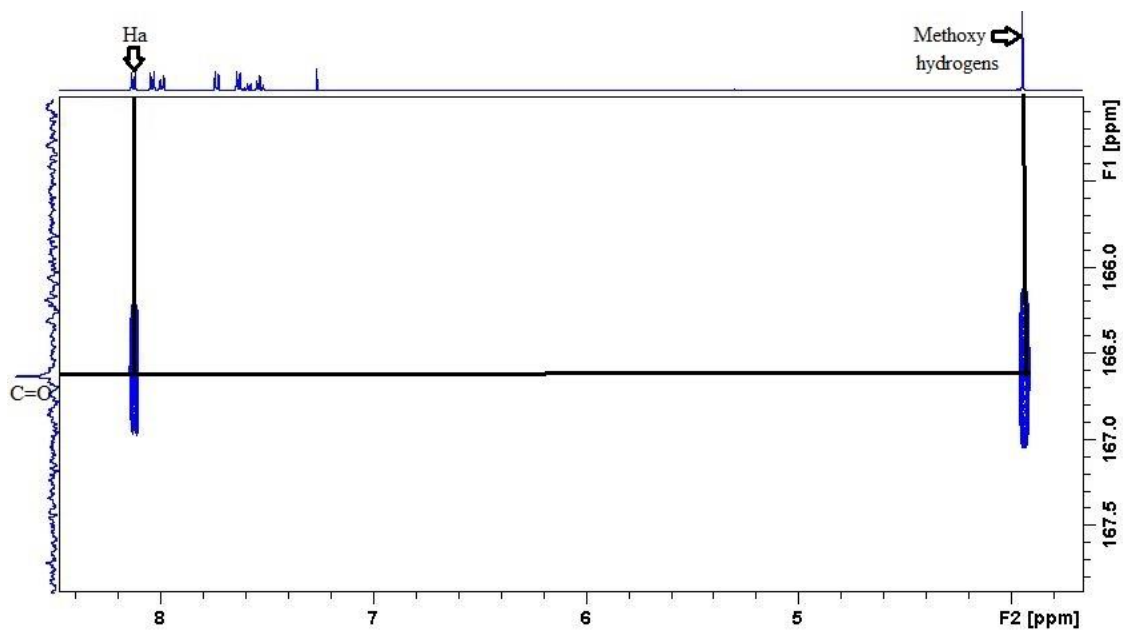


Figure 91. Expanded HMBC spectrum of **139** showing the coupling between the carbonyl carbon and Ha, as well as the methoxy protons.

Ha is coupled to 130.3 ppm in the HSQC, making this signal that of Ca.

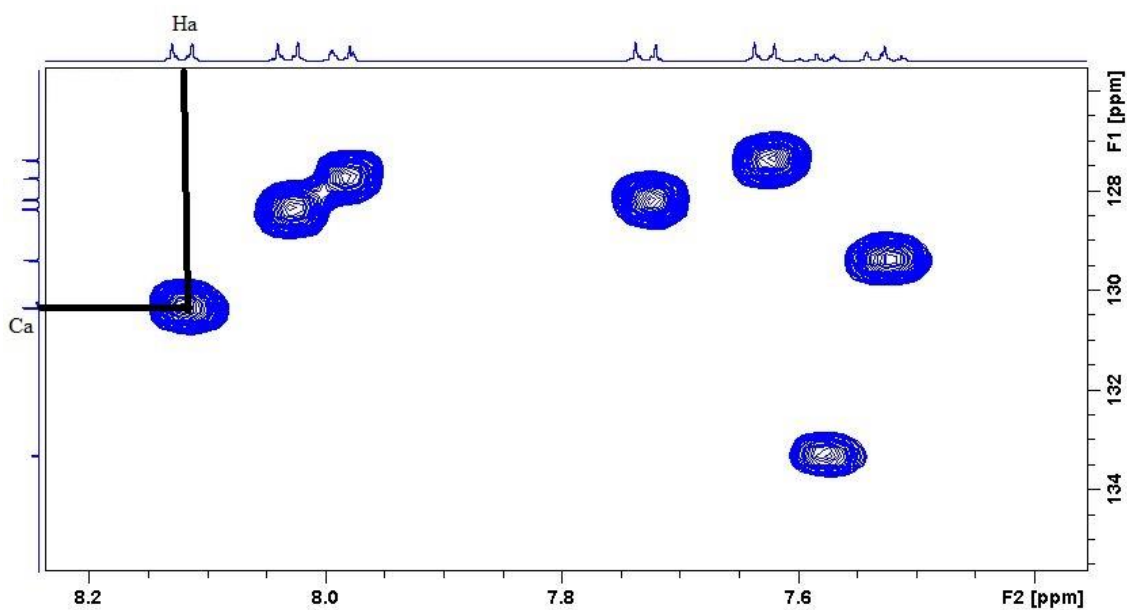


Figure 92. Expanded HSQC spectrum of **139** showing the coupling between Ha and Ca

Ha is coupled to only one other proton in COSY which implies that the peak at 7.64-7.62 ppm is Hb.

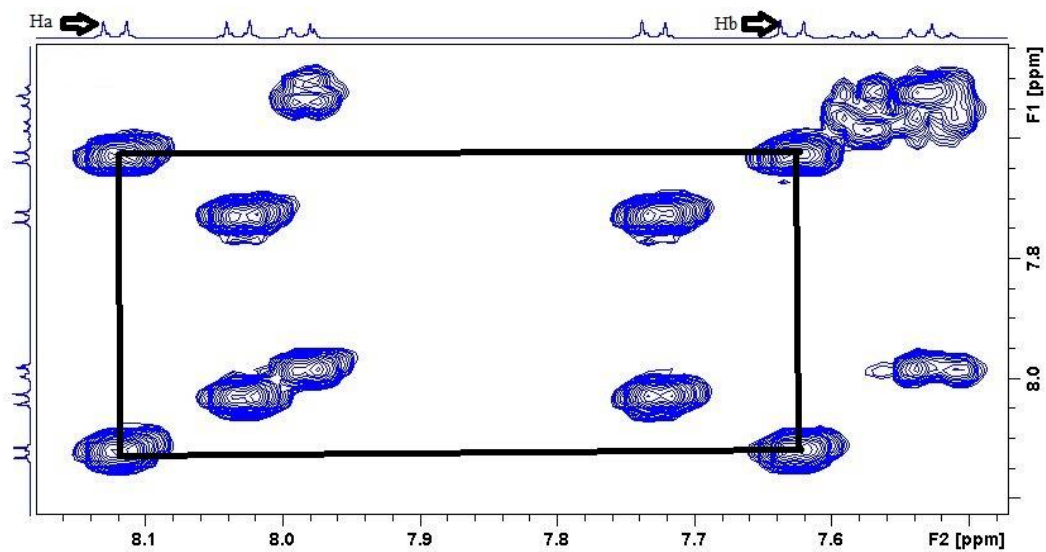


Figure 93. Expanded COSY spectrum showing the coupling between Ha and Hb in compound **139**

Hb is coupled to 127.4 ppm in the HSQC, making this signal that of Cb.

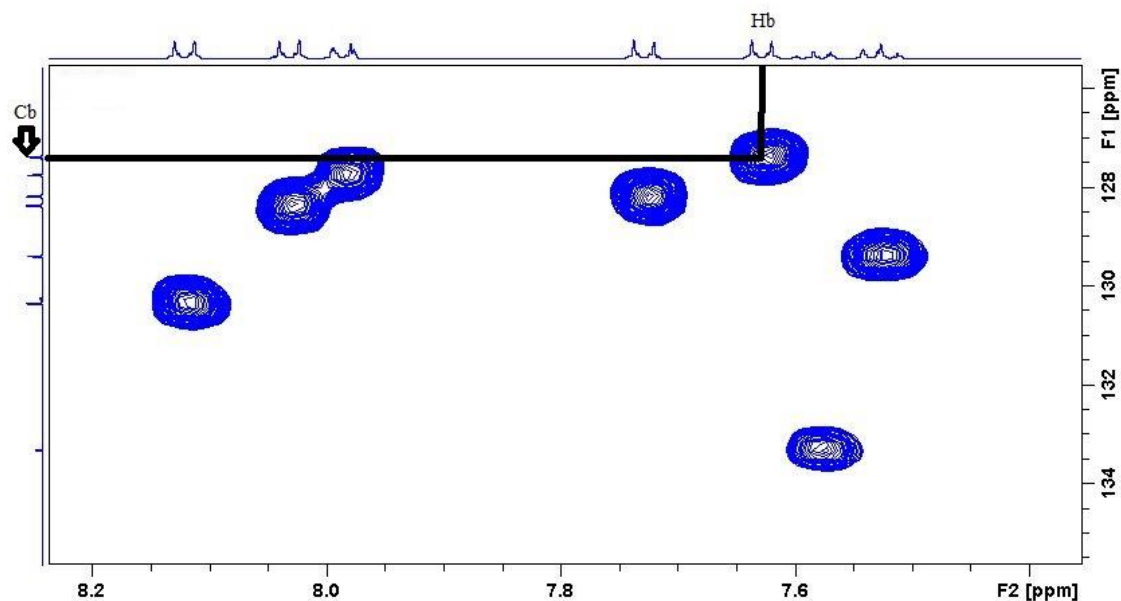


Figure 94. Expanded HSQC spectrum showing the coupling between Hb and Cb in **139**

Looking at the HMBC spectrum, Ha shows coupling to Ca and to another carbon at 143.5 ppm, which we know is a quaternary carbon. Hb shows coupling to Cb, a quaternary carbon at 130.2 ppm and another at 145.0 ppm.

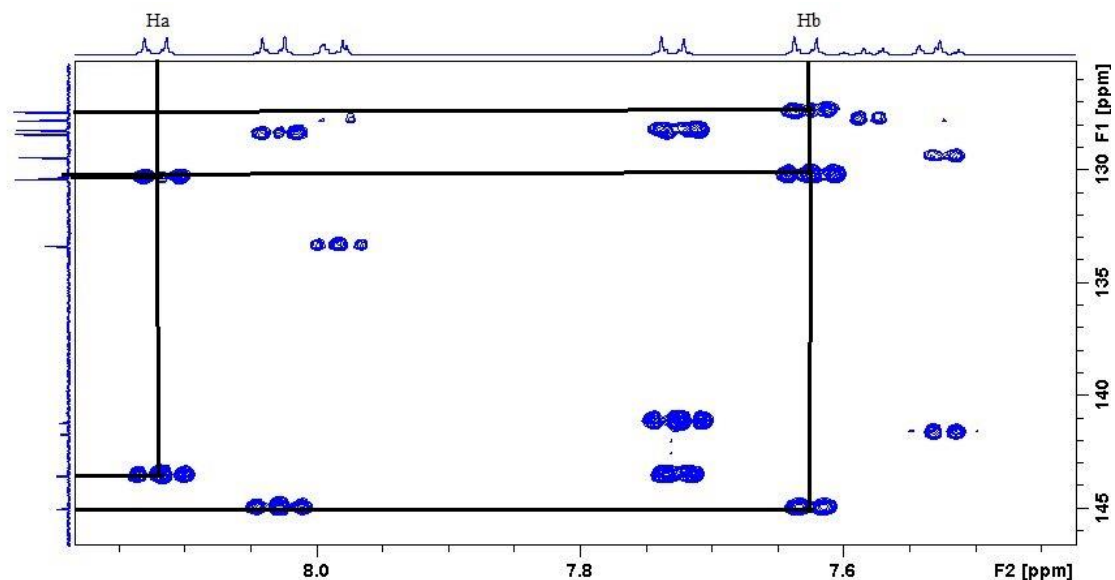


Figure 95. Expanded HMBC spectrum showing the long-range couplings of Ha and Hb in **139**

The fact that the carbon at 143.5 ppm shows coupling to Ha and another proton, that is not Hb (later assigned as Hc), means that this carbon could be either C2 or C3, as both carbons are within 4 bonds of the relevant proton groups. Similarly, the fact that the carbon at 145.0 ppm shows coupling to Hb and another proton, that is not Ha (later assigned as Hd), means that this carbon could be either C2 or C3, as both carbons are within 4 bonds of the relevant proton groups. Due to C3 being closer to a stronger electron-withdrawing group than C2 (a sulfone is more electron-withdrawing than the ester in this molecule), perhaps we could assign the carbon at the higher ppm of 145.0 as C3 on this basis, making C2 that at 143.5 ppm, but this is not a definitive assignment. The quaternary carbon that only shows coupling to Hb at 130.2 ppm is likely to be C1.

At the other end of the structure, the proton Hg is the only signal that integrates for one proton and this appears at 7.60-7.57 ppm. Examination of the HSQC shows that it couples to the carbon at 133.3 ppm, making this Cg.

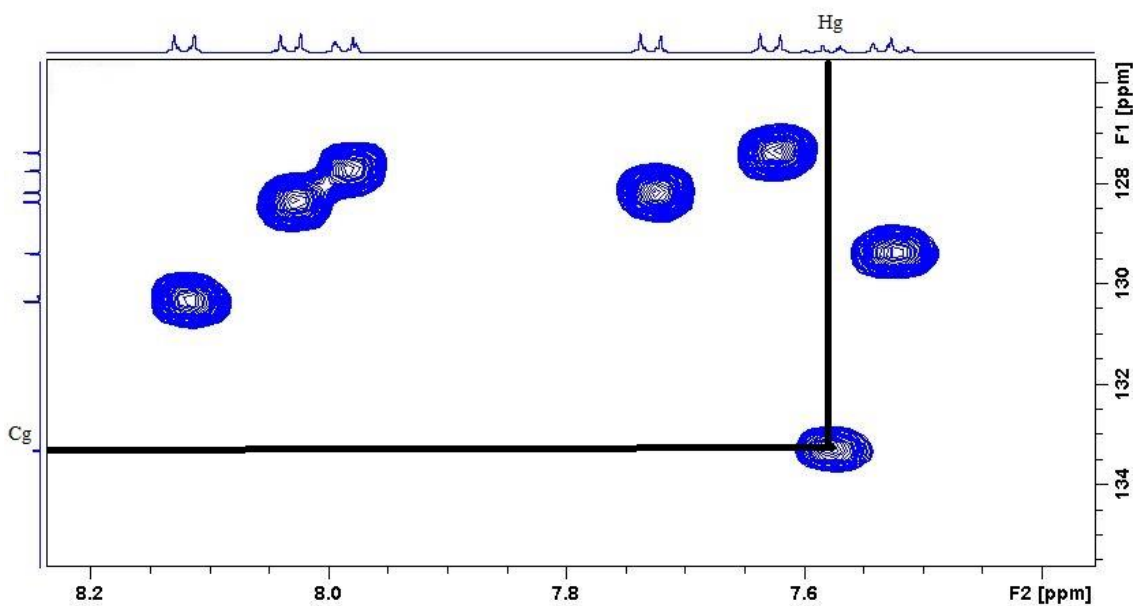


Figure 96. Expanded HSQC spectrum of **139** showing the coupling between Hg and Cg

The COSY spectrum shows that Hg is coupled to the protons at 7.55-7.51 ppm, which makes this signal that of Hf, and by HSQC these protons are coupled to the carbon at 129.4 ppm, Figures 97 and 98, respectively.

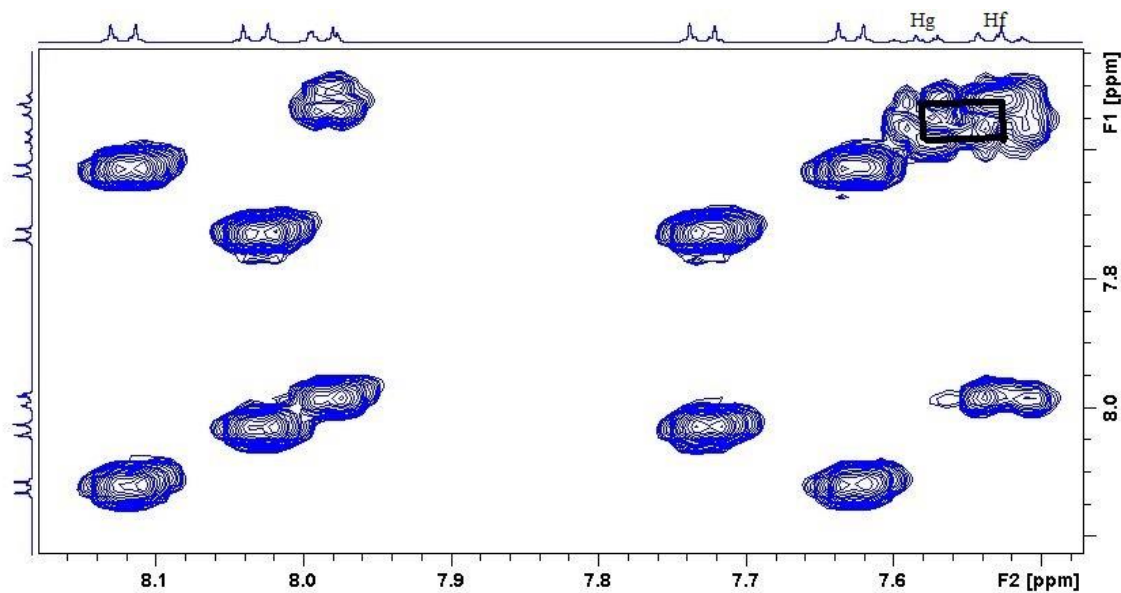


Figure 97. Expanded COSY spectrum of **139** showing the coupling between Hg and Hf

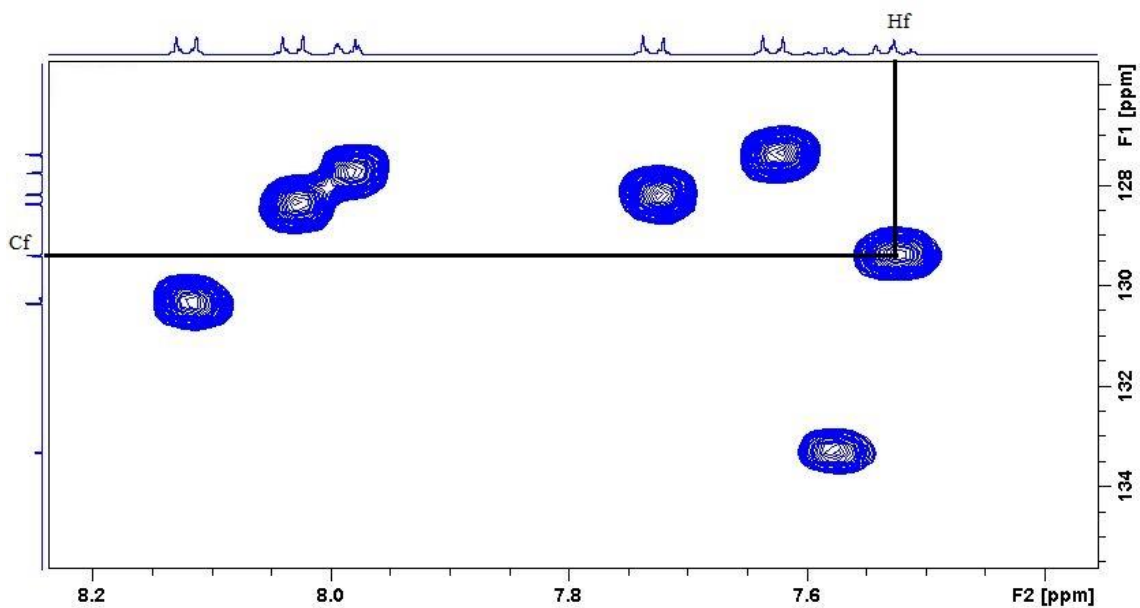


Figure 98. Expanded HSQC spectrum of **139** showing the coupling between Hf and Cf

The HMBC shows that Hf is coupled to the quaternary carbon at 141.6 ppm, thus it is likely this is C5.

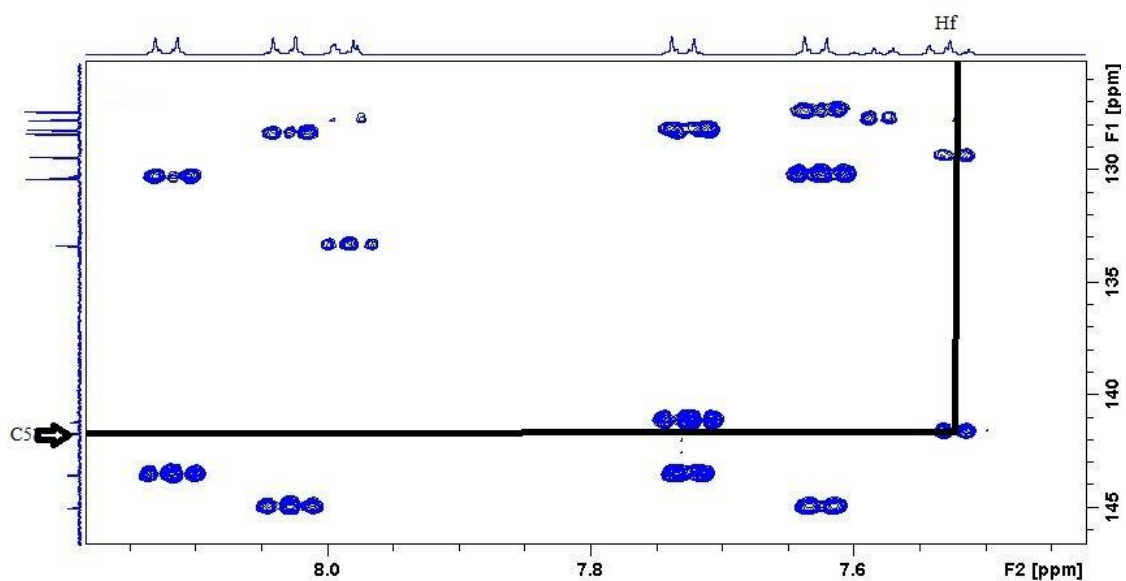


Figure 99. Expanded HMBC spectrum of **139** showing the long-range coupling of Hf

The COSY spectrum shows that Hf is coupled to the protons at 8.00-7.98 ppm, making this signal He, Figure 100.

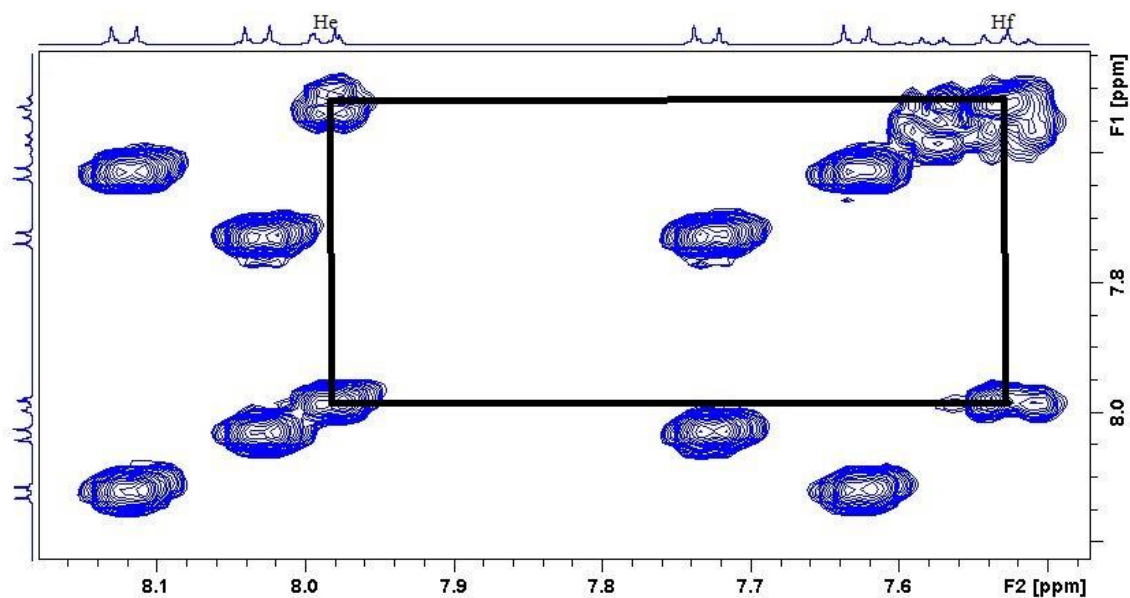


Figure 100. Expanded COSY spectrum of **139** showing the coupling between Hf and He

The HSQC shows that the He protons are coupled to the carbon at 127.7 ppm, making this Ce, Figure 101.

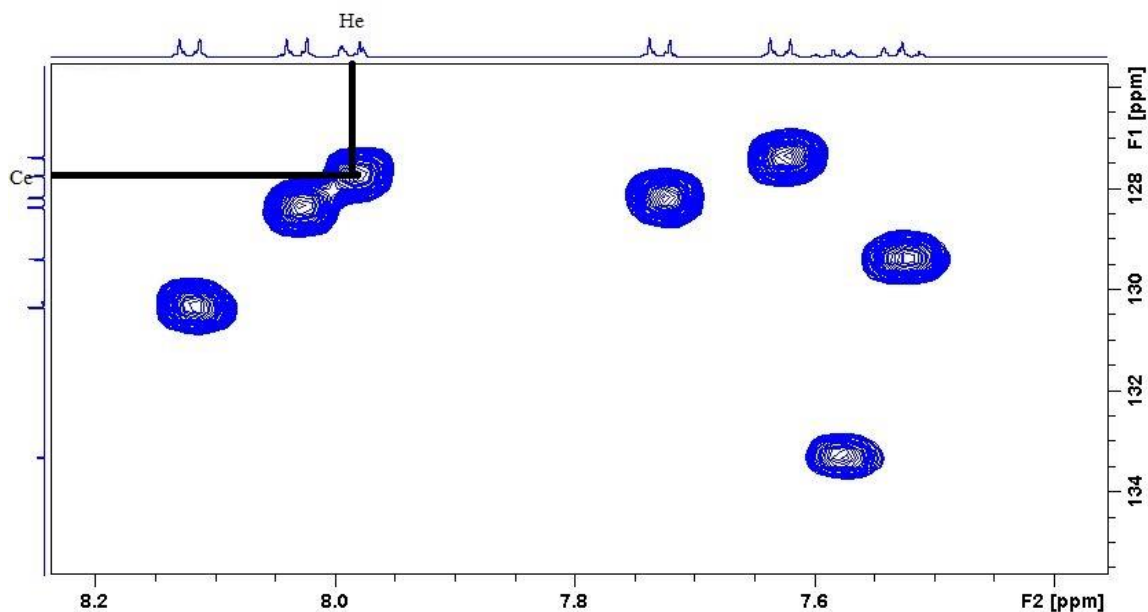


Figure 101. Expanded HSQC spectrum of **139** showing the coupling between He and Ce

This leaves two proton signals left to assign, those at 8.04-8.02 ppm and 7.74-7.72 ppm, both of which are coupled in the COSY spectrum.

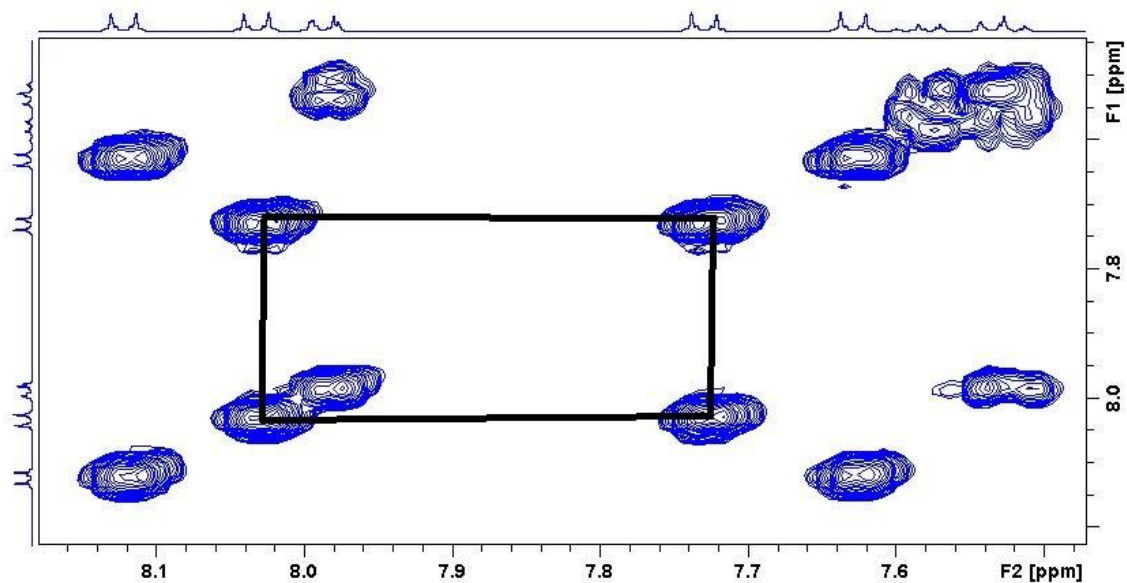


Figure 102. Expanded COSY spectrum of **139** showing the coupling between Hc and Hd

Hd is likely to be more deshielded than Hc due to its *ortho* relationship with the electron withdrawing SO₂Ph. Thus, Hd can be assigned as the signal at 8.04-8.02 ppm on this basis, which is coupled to the carbon at 128.3 ppm by the HSQC spectrum.

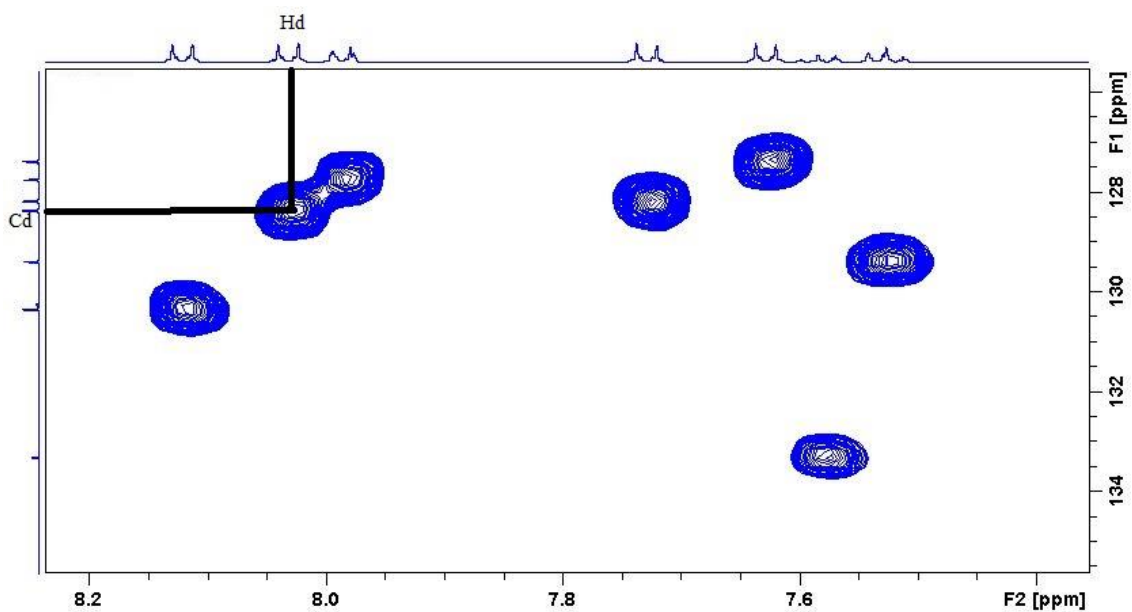


Figure 103. Expanded HSQC spectrum of **139** showing the coupling between Hd and Cd

Hc therefore is the peak at 7.74-7.72 ppm and is coupled to 128.2 ppm by the HSQC spectrum.

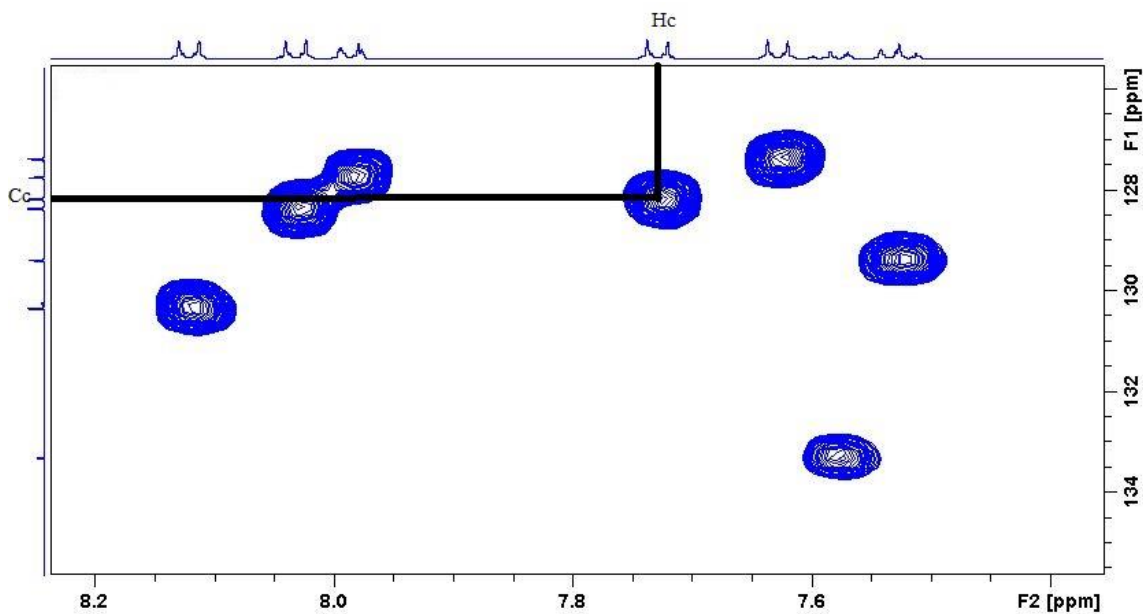


Figure 104. Expanded HSQC spectrum of **139** showing the coupling between Hc and Cc

This leaves the quaternary carbon at 141.1 ppm, which is coupled to Hc in the HMBC spectrum and is therefore likely to be C4.

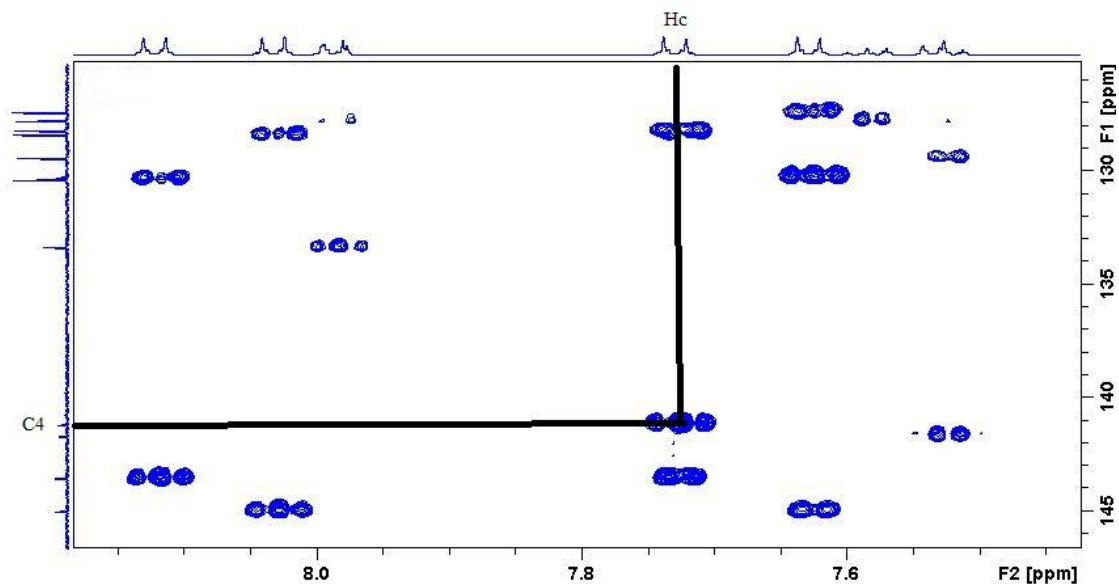


Figure 105. Expanded HMBC spectrum of **139** showing the long-range couplings of Hc

A summary of the assignments is shown in Figure 106.

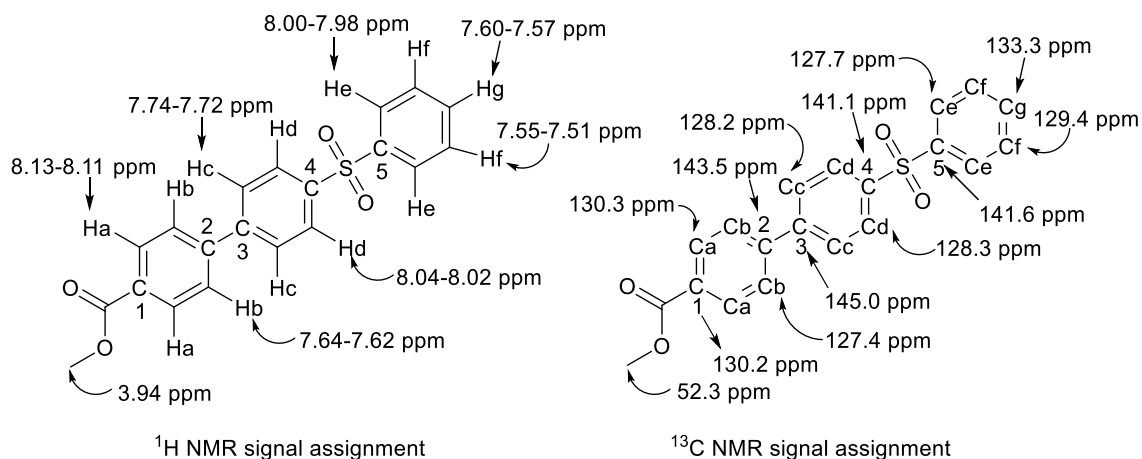


Figure 106. Summary of NMR spectroscopy signal assignment for 1-(4-methyl ester phenyl)-4-(phenylsulfonyl)benzene **139**.

3.2.5.2 IR spectroscopy and MS analysis used to fully characterize 1-(4-methyl ester phenyl)-4-(phenylsulfonyl)benzene **139**

In addition to the use of NMR spectroscopy, IR spectroscopy and MS analysis were used to fully characterize 1-(4-methyl ester phenyl)-4-(phenylsulfonyl)benzene **139**. The IR spectrum of **139**, is included as Figure 107.

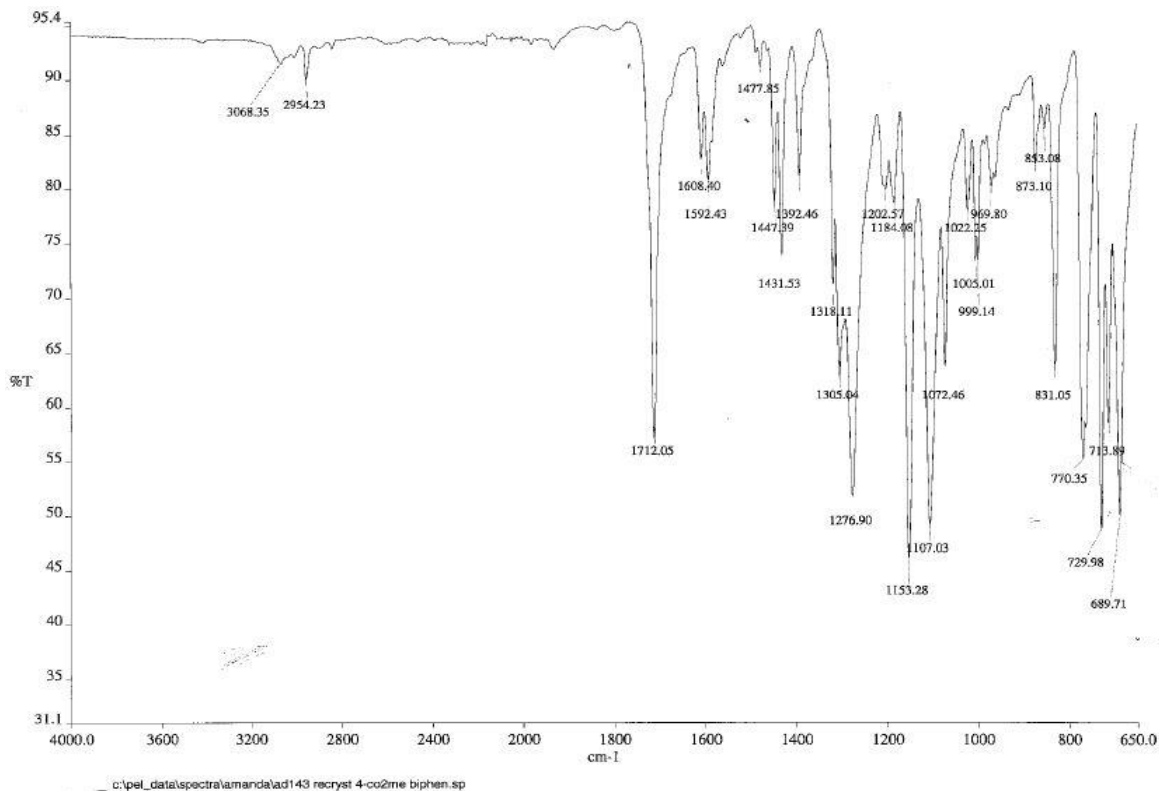


Figure 107. IR spectrum of 1-(4-methyl ester phenyl)-4-(phenylsulfonyl)benzene **139**.

As expected from the structure of compound **139**, there are a series of bands associated with the presence of aromatic C=C, C-C and =C-H bonds. These include the band at 3068 cm^{-1} , characteristic of an aromatic C-H stretch and the bands at 1608, 1592, and 1432 cm^{-1} which are characteristic of aromatic C-C stretches. There are overtones associated with the presence of aromatic rings that occur between 2000-1750 cm^{-1} also. The sulfone S=O asymmetric stretch is apparent at 1305 cm^{-1} and its symmetric stretch at 1153 cm^{-1} . The bands mentioned so far can be expected to be present in all of the phenylsulfonyl-substituted biaryls we synthesized. Specific to compound **139**, the presence of a methyl group also causes certain bands, such as that at 2954 cm^{-1} as a result of a C-H stretch, 1447 cm^{-1} associated with C-H scissoring and 1393 cm^{-1} corresponds to C-H rocking. The band at 1005 cm^{-1} is associated with in plane C-H bending and out of plane C-H bending is apparent at 730 cm^{-1} , all of which are attributed to the presence of a methyl group (as part of the ester). Additionally, the C=O bond of **139** produces the strong band at 1712 cm^{-1} and the C-O bond causes bands at 1277 and 1073 cm^{-1} .

The MS analysis can be broken down into LC-MS and HR-MS. The LC-ESI-MS spectrum of compound **139** showed it has m/z $[\text{M}+\text{Na}]^+$ 375.1 and the LC chromatogram obtained indicated the purity of this compound as 95.8%, and had a retention time of 30.7 minutes. The corresponding data can be found in Appendix 3, Figures A377 and A378. HR-MS was also applied to compound **139** in order to confirm the molecular formula assigned. A mass error of 2.16 ppm was found and, as before with respect to triene characterization, a mass error of less than 5.00 ppm means it is likely that the molecular formula assigned is that of the molecule analyzed. The corresponding data can be found in Appendix 3 Figure A379. Taken together, all of the data generated by NMR spectrometry, IR spectroscopy, and MS analysis confirmed the structural characterization of compound **139**.

All the 1-(4-substituted phenyl)-4-(phenylsulfonyl)benzene compounds synthesized were analyzed in the same manner using a combination of the analytical techniques at our disposal. It is beyond the scope of this thesis to fully explain the analysis of each member of this family of biaryls, but all the data is available and reported in the experimental section, with spectra available in Appendix 3, Figures A356-A439. As compound **139** is an example of a biaryl possessing an electron-withdrawing group, a brief explanation of the structural characterization for a biaryl with an electron-donating substituent (dimethylamino) is given below.

3.2.6 Structural characterization of 1-(4-dimethylaminophenyl)-4-(phenylsulfonyl)benzene **138**

In terms of NMR spectroscopic data, the major difference between the spectra of this compound and those of 1-(4-methyl ester phenyl)-4-(phenylsulfonyl)benzene, **139**, is the chemical shift of the *ipso*-carbon (C1, Figure 108), which now occurs at 150.7 ppm. This

is due to the significant deshielding effect of the *para*-dimethylamino group on its *ipso* carbon. The chemical shift of the *ipso* carbon is determined primarily by the inductive effect of the substituent.²³¹ Electronegative atoms directly bonded to the *ipso* carbon have a strong inductive effect on the *ipso* carbon and the result is a significant downfield shift for the *ipso* carbon.²³¹ The carbon *ortho* to the dimethylamino substituent (Ca, Figure 108) can be identified at 112.5 ppm and is shielded due to the ability of the lone pair on the nitrogen of the dimethylamino group to delocalize. This increases the electron density at Ca, which also has a shielding effect on Ha, the attached protons, which appear as the multiplet at 6.78-6.76 ppm, integrating for two protons. Ha can be identified from the HSQC additionally (Appendix 3, Figure A373). This shielding effect is also seen at C2 (Figure 108), which is different to C2 in compound **139**, with a lower ppm of 126.4 ppm. The full list of peaks observed in both the ¹H NMR and ¹³C NMR spectra of this compound can be found in the experimental section, with all NMR spectra relevant to the compound available in Appendix 3, Figures A370-A375.

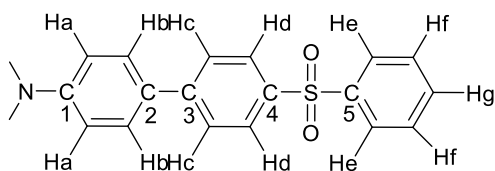


Figure 108. The structure of compound **138**

IR spectroscopy and MS (LCMS and HRMS) analysis was also completed, with the expected signals and data obtained, see experimental section and Appendix 3, Figures A366-A369.

3.2.7 Fluorescence

Luminescence refers to the emission of light from any substance and occurs because of electronically excited states.²⁷⁴ After absorbing an initial radiation, which can be termed ‘excitation light’, a molecule goes from a lower energetic state (commonly ground state) to an excited state by absorbing energy. The emission process that takes place by the molecule bouncing back to the initial state results in luminescence.²⁷⁵ Luminescence can be divided into two types, fluorescence and phosphorescence, depending on the nature of the excited state.²⁷⁴ A molecular electronic state in which all electron spins are paired is called a singlet state,²⁷⁶ and all associated electronic energy levels have the same energy. However, when one of a pair of electrons of a molecule is excited to a higher energy level, a singlet or a triplet state is formed. In the excited singlet state, the spin of the promoted electron is still paired with the ground-state electron. In the triplet state, the spins of the two electrons become unpaired and are thus parallel. These states can be represented as in Figure 109. It is interesting that the excited triplet state is less energetic than the corresponding excited singlet state.²⁷⁶

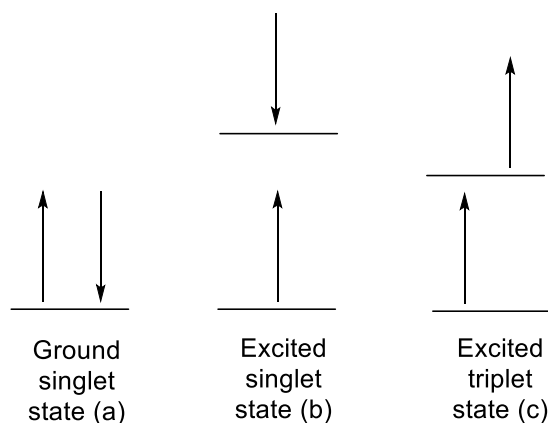


Figure 109. A graphical depiction of the different electronic spin states of molecules. (a) This depicts the ground state of a molecule (a singlet state). (b) This depicts the excited singlet state, in which the spins remain paired. (c) This depicts the excited triplet state, in which the spins are unpaired. Adapted from the work of Skoog *et al.*²⁷⁶

Phosphorescence is the emission of light from triplet excited states, whereas fluorescence is the emission of light from excited singlet states.²⁷⁴ The average lifetime of an excited triplet state may range from 10^{-4} to several seconds, compared with an average lifetime of $\sim 10^{-8}$ seconds for an excited singlet state,²⁷⁶ assuming it is undisturbed by collisions,²⁷⁵ and fluorescence can occur within this length of time.²⁷⁵ The lifetime (τ) of a fluorophore is the average time between its excitation and its return to the ground state.²⁷⁴ An electronically excited molecule ordinarily returns to its lowest excited state by a series of rapid vibrational relaxations and internal conversions that produce no emission of radiation. Thus, fluorescence most commonly arises from a transition from the lowest vibrational level of the first excited electronic state to one of the vibrational levels of the electronic ground state. This can be represented graphically, as per Figure 110.

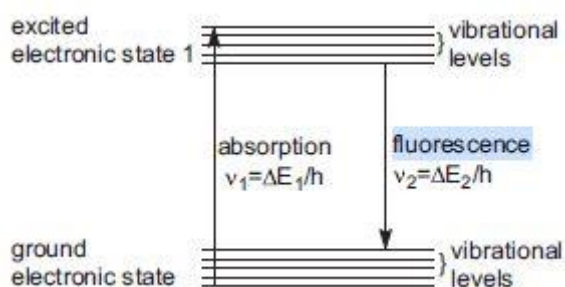


Figure 110. A simplified representation depicting electronic transitions during fluorescence, taken from the work of Moldoveanu and David.²⁷⁵

For most fluorescent compounds, radiation is produced by either a $\pi^* \rightarrow n$ or a $\pi^* \rightarrow \pi$ transition, depending on which of these is the less energetic.²⁷⁶ However, the most intense and useful fluorescence is found in compounds containing aromatic functional groups with low-energy $\pi^* \rightarrow \pi$ transitions.²⁷⁶ One well-known example is quinine, Figure 111,

which is present in tonic water and is the first known fluorophore.²⁷⁴ A glass of tonic water which is exposed to sunlight will have the appearance of a faint blue glow at the surface. This occurs as a result of electrons in the quinine molecule being excited by the ultraviolet (UV) light from the sun and then returning to its ground state, consequently emitting blue light with a wavelength near 450 nm.²⁷⁴

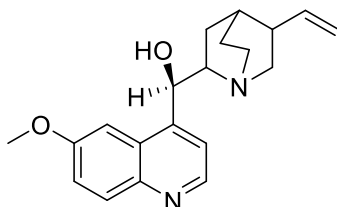


Figure 111. Structure of quinine

Different substituents on a phenyl ring results in different fluorescent properties being observed. For example, using benzene (wavelength of fluorescence of 270-310 nm) as a reference point and setting its relative intensity of fluorescence to 10, one can see that adding a nitrile substituent generates benzonitrile with a relative intensity of fluorescence of 20 (wavelength of fluorescence of 280-360 nm), and adding a carboxylic acid group generates benzoic acid with a relative intensity of fluorescence of 3 (wavelength of fluorescence of 310-390 nm). Looking more closely at benzoic acid, the substitution of a carboxylic acid on the aromatic ring inhibits fluorescence because the energy of the $n \rightarrow \pi^*$ transition is less than in the $\pi^* \rightarrow \pi$ transition, and the fluorescence yield from the $n \rightarrow \pi^*$ transition is usually low.²⁷⁶

3.2.7.1 Fluorescence reported for structurally similar biaryls

The fluorescent properties of biaryls have been investigated in the literature. For example, the work of Maus and Rettig,^{277, 278} assessed the fluorescent and photophysical properties of differently twisted donor-acceptor biphenyls, Figure 112.

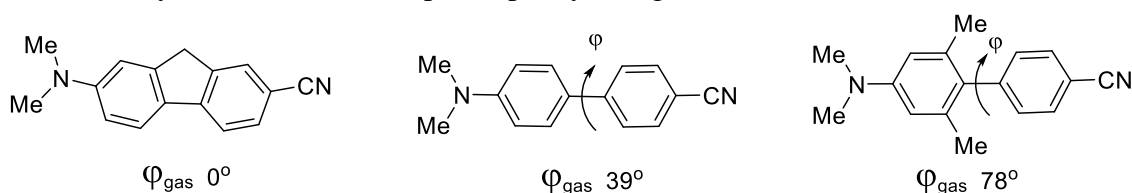


Figure 112. The molecular structures of the donor-acceptor biphenyls investigated in this work and their corresponding equilibrium ground state twist angles ϕ_{gas} obtained computationally, adapted from the work of Maus and Rettig.²⁷⁸

This publication provides insights into the electronic and conformational structure in the ground-state S_0 and the first excited singlet state S_1 reached after photoinduced intramolecular charge transfer,²⁷⁸ with charge being transferred from the HOMO (of the

donor component) to the LUMO (of the acceptor component) across the interannular bond. As a comparison, in unsubstituted biphenyl, charge-transfer interactions can be neglected. This group²⁷⁷ had previously investigated the intramolecular charge-transfer processes in these same donor-acceptor biphenyls after photoexcitation and drew numerous conclusions on the basis of, for example, the appearance of four bands in the steady-state spectra. These bands mainly corresponded to electronic transitions from the ground state S^0 into the terminal states.²⁷⁷

Examining the range of biaryls we synthesized, we strongly suspected that the 4-dimethylamino substituted biaryl, **138**, would exhibit interesting fluorescent properties as a structurally similar donor-acceptor molecule to those reported by Maus and Rettig.^{277, 278} Biaryl **138** consists of an electron-donating dimethylamino substituent and an electron-withdrawing sulfone group, which should give rise to an intramolecular “push-pull” effect. Building on some preliminary studies conducted by a previous member of the Stephens group,²⁷⁹ we undertook a study into the fluorescent properties of our biaryl systems.

3.2.7.2 Investigation of fluorescent properties of our biaryls

Each of the biaryls were made up as 35 μM solutions in both chloroform and methanol. Chloroform and methanol were chosen as representative polar aprotic and polar protic solvents, respectively. A serial dilution was performed on each solution, and the UV-absorption spectrum was recorded over a number of different concentrations. Once an absorbance of approximately 0.1 a.u. was recorded for a given concentration, then the emission and excitation spectra of each biaryl was recorded at that concentration. A summary of all three spectra recorded for each biaryl in chloroform is shown in Figures 113(a)-(i). The same experiments were performed in methanol and these results can be found in Appendix 3, Figures A440(a)-(i).

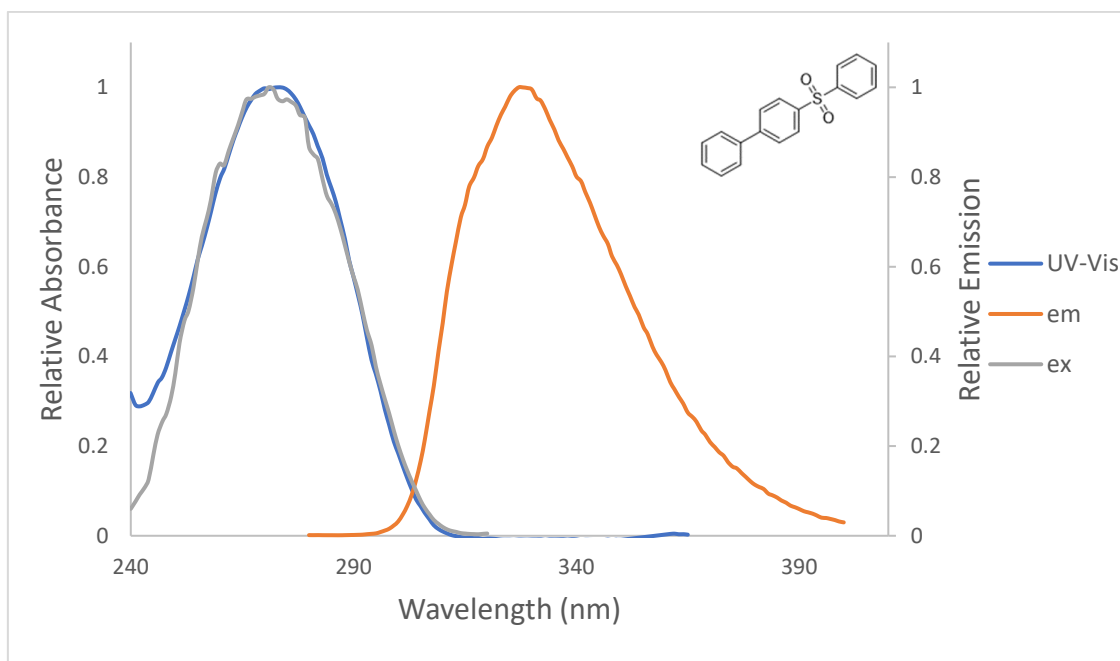


Figure 113 (a). Overlapped UV-Vis, emission, and excitation spectra of biaryl **46** in chloroform. Absorbance λ_{max} , emission λ_{max} , and excitation λ_{max} values of 273, 326, and 272 nm were found, respectively. The absorbance λ_{max} and emission/ excitation λ_{max} were recorded using 17.86 μM and 4.56 μM solutions, respectively.

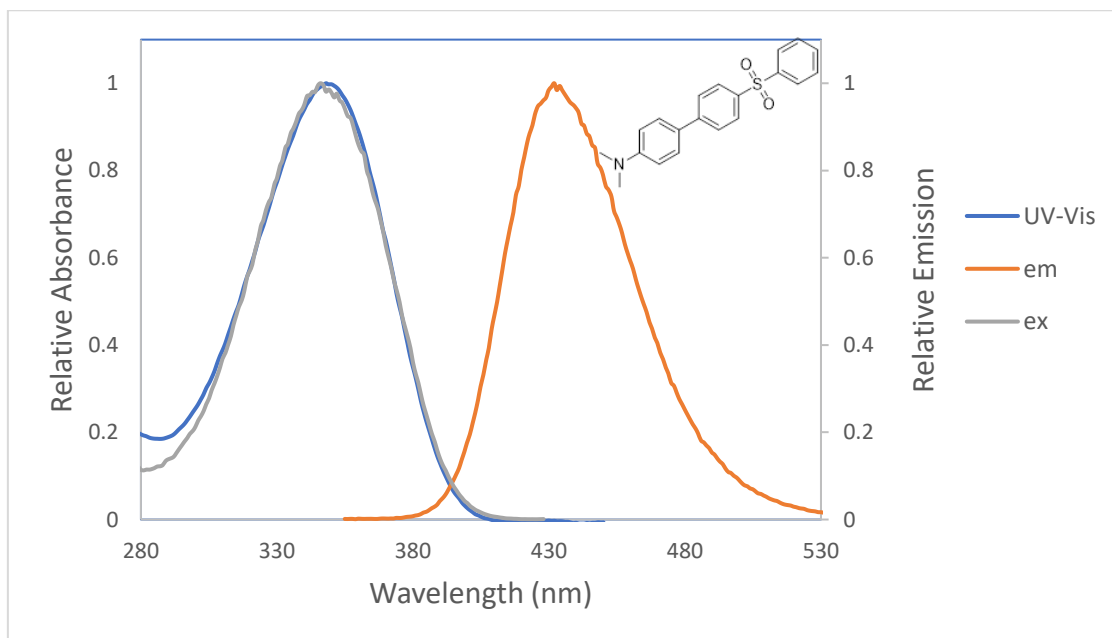


Figure 113(b). Overlapped UV-Vis, emission, and excitation spectra of biaryl **138** in chloroform. Absorbance λ_{max} , emission λ_{max} , and excitation λ_{max} values of 348, 433, and 346 nm were found, respectively. The absorbance λ_{max} and emission/ excitation λ_{max} were recorded using 17.86 μM and 5.58 μM solutions, respectively.

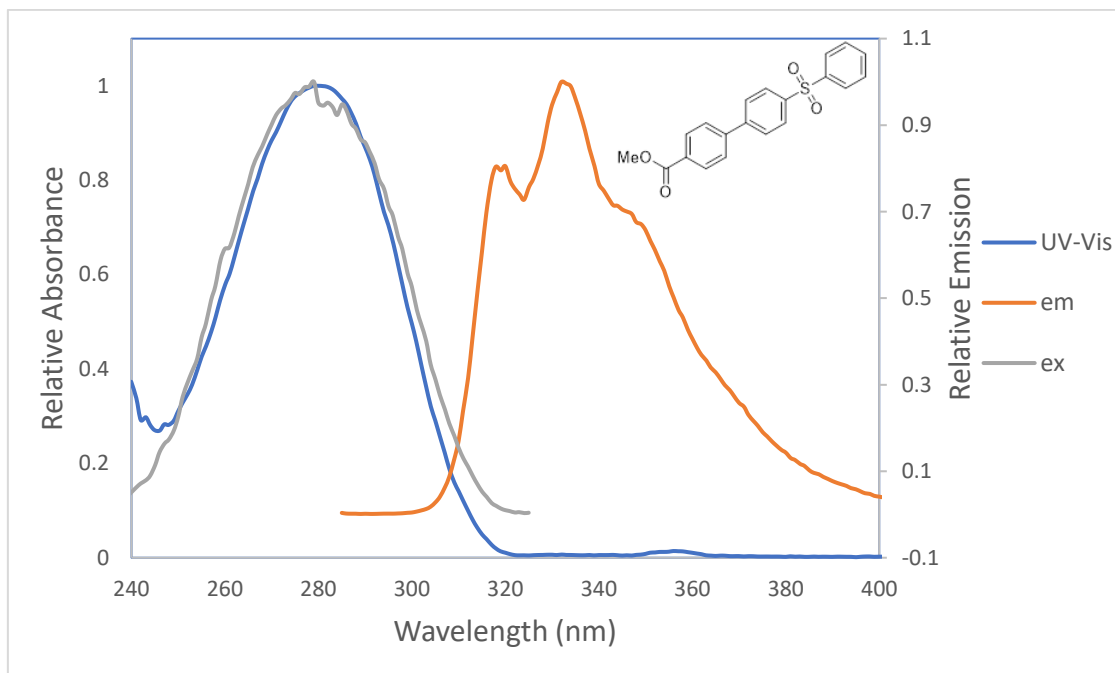


Figure 113(c). Overlapped UV-Vis, emission, and excitation spectra of biaryl **139** in chloroform. Absorbance λ_{max} , emission λ_{max} , and excitation λ_{max} values of 281, 332, and 280 nm were found, respectively. Shoulders at 318, 320, and 348 nm were evident in the emission spectrum of compound **139** additionally. The absorbance λ_{max} and emission/ excitation λ_{max} were recorded using 17.86 μM and 3.32 μM solutions, respectively.

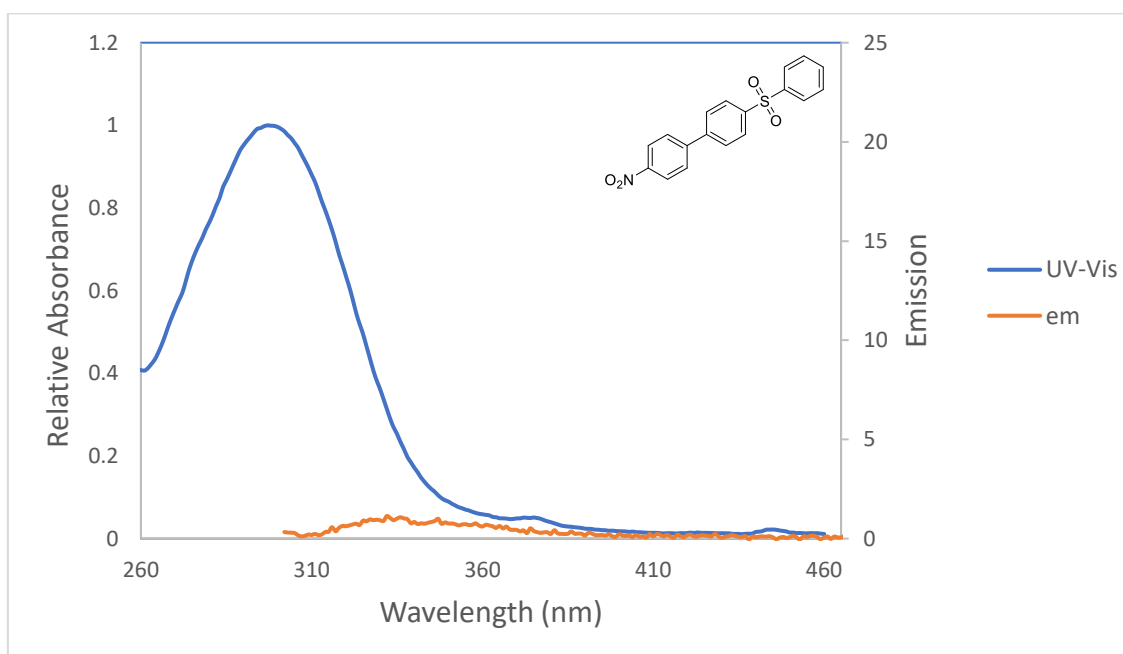


Figure 113(d). Overlapped UV-Vis and emission spectra of biaryl **140** in chloroform. An absorbance λ_{max} value of 297 nm was found. An emission λ_{max} (and therefore excitation λ_{max}) could not be found due to low emission intensity. The absorbance λ_{max} and emission/ excitation λ_{max} were recorded using 17.86 μM and 4.56 μM solutions, respectively.

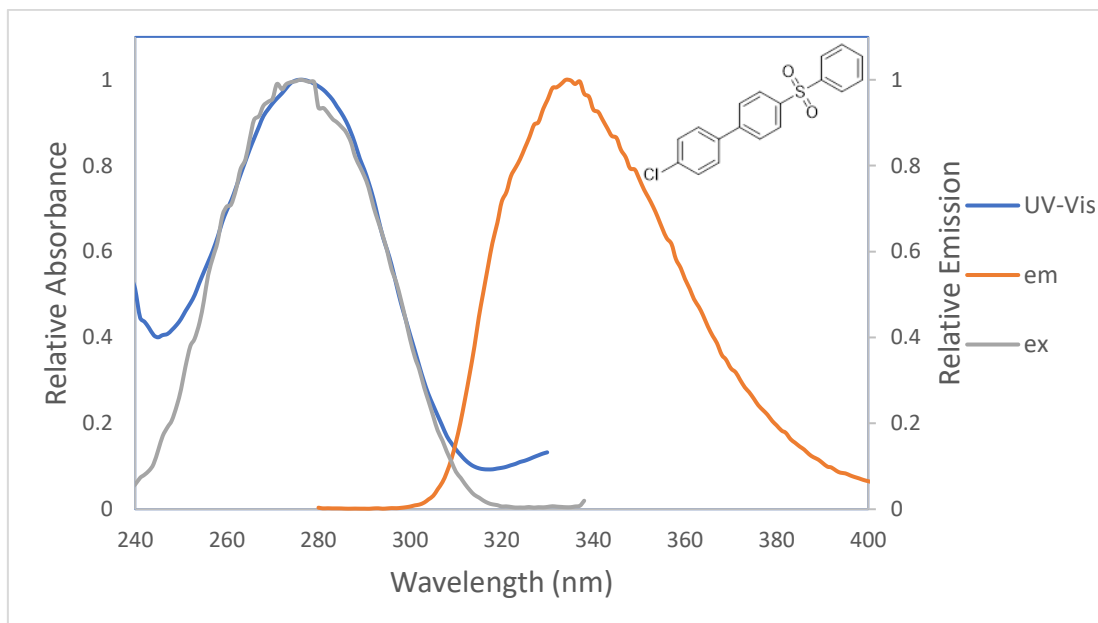


Figure 113(e). Overlapped UV-Vis, emission, and excitation spectra of biaryl **141** in chloroform. Absorbance λ_{max} , emission λ_{max} , and excitation λ_{max} values of 276, 334, and 277 nm were found, respectively. The absorbance λ_{max} and emission/ excitation λ_{max} were recorded using 17.86 μM and 2.79 μM solutions, respectively.

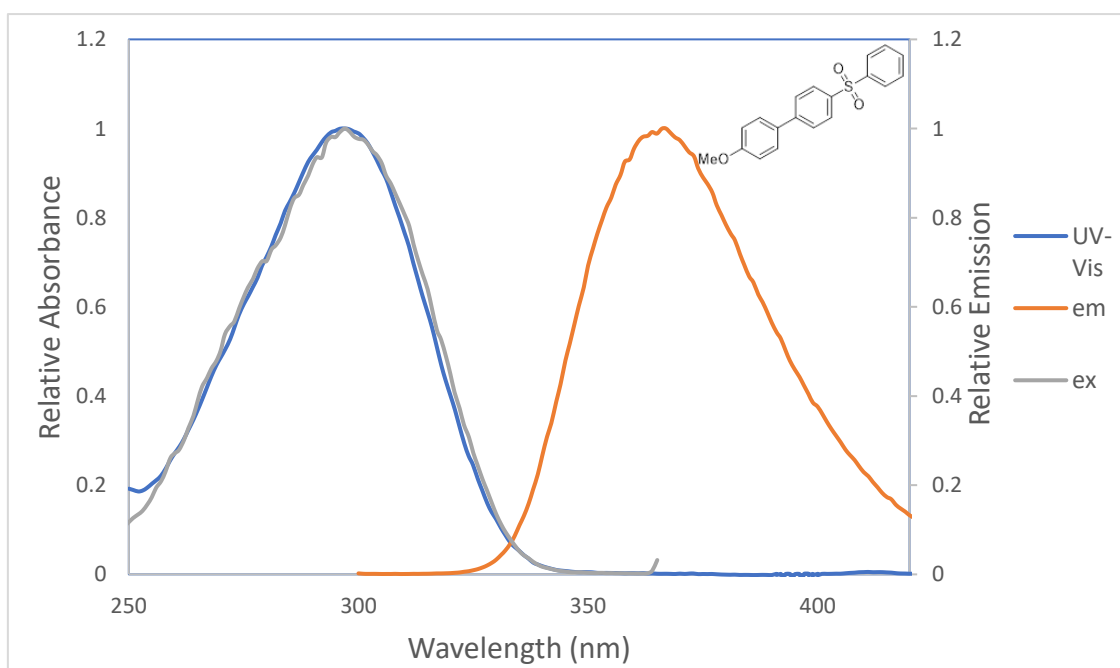


Figure 113(f). Overlapped UV-Vis, emission, and excitation spectra of biaryl **142** in chloroform. Absorbance λ_{max} , emission λ_{max} , and excitation λ_{max} values of 297, 367, and 298 nm were found, respectively. The absorbance λ_{max} and emission/ excitation λ_{max} were recorded using 17.86 μM and 2.32 μM solutions, respectively.

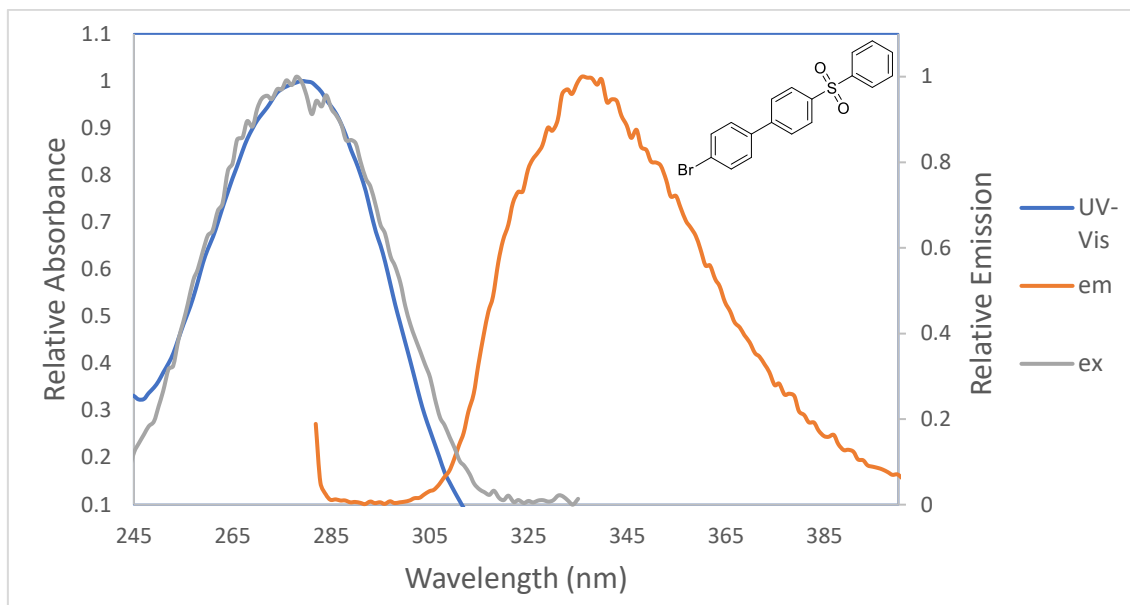


Figure 113(g). Overlapped UV-Vis, emission, and excitation spectra of biaryl **143** in chloroform. Absorbance λ_{max} , emission λ_{max} , and excitation λ_{max} values of 278, 336, and 277 nm were found, respectively. The absorbance λ_{max} and emission/ excitation λ_{max} were recorded using 17.86 μM and 3.32 μM solutions, respectively.

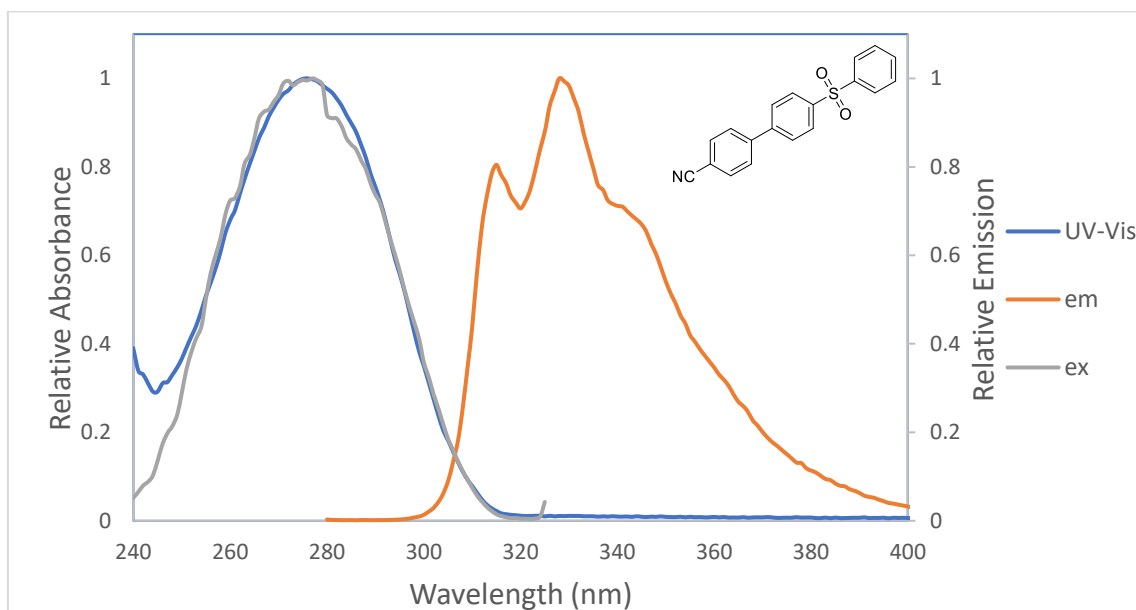


Figure 113(h). Overlapped UV-Vis, emission and excitation spectra of biaryl **144** in chloroform. Absorbance λ_{max} , emission λ_{max} , and excitation λ_{max} values of 276, 328, and 278 nm were found, respectively. Shoulders at 315 and 346 nm were evident in the emission spectrum of compound **144** additionally. The absorbance λ_{max} and emission/ excitation λ_{max} were recorded using 17.86 μM and 3.25 μM solutions, respectively.

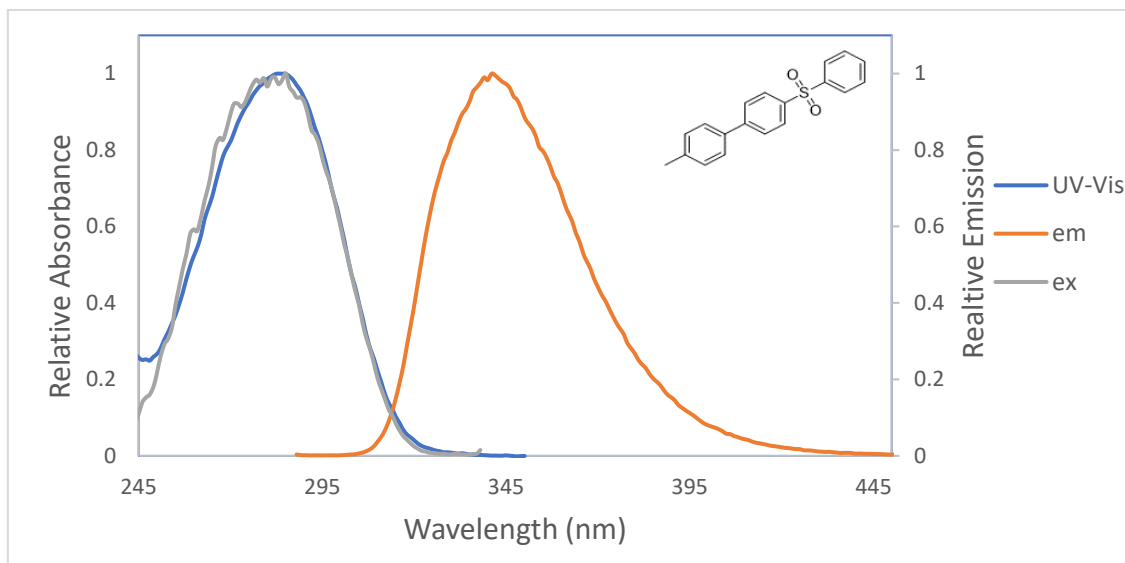


Figure 113(i). Overlapped UV-Vis, emission, and excitation spectra of biaryl **145** in chloroform. Absorbance λ_{max} , emission λ_{max} , and excitation λ_{max} values of 284, 341, and 286 nm were found, respectively. The absorbance λ_{max} and emission/ excitation λ_{max} were recorded using 17.86 μM and 3.25 μM solutions, respectively.

Of the biaryls investigated in this study, one did not exhibit any detectable fluorescence, and that was the 4-nitro substituted biaryl, **140**. This is a common occurrence for aromatic hydrocarbons possessing this substituent.²⁸⁰ It can be explained by the existence of a low-lying $n \rightarrow \pi^*$ transition and the resulting high rate of $S_1 \rightarrow S_0$ internal conversion in light of the strong electron-withdrawing nature of the nitro substituent.²⁸⁰ As predicted, of all the biaryls examined, the 4-dimethylamino substituted biaryl, **138**, exhibited the largest λ_{max} in both the UV-absorbance and emission spectra. This was followed by the 4-methoxy substituted biaryl, **142**.

The Stokes shift is another photophysical parameter that was considered as part of our preliminary photophysical investigation of the biaryls. The Stokes shift is simply the gap between the maximum of the absorption band (UV-absorbance λ_{max}) and the maximum of the fluorescence spectrum (emission λ_{max}), expressed in wavelengths.²⁸⁰ As can be observed from Figures 113(a)-(i), the Stokes shift varied greatly depending on the biaryl and was affected by the nature of the substituent. Compound **138** had the highest Stokes shift of 85 nm, followed by compound **142** of 70, and the other biaryls had a Stokes shift between 51 and 58 nm. Thus, generally the greater the electron-donating character of the substituent on the phenyl ring, the higher the absorbance λ_{max} observed. This effect that the nature of the substituent has on the absorbance spectra can be visualized by plotting all the relative absorbances on one plot, see Figure 114. This same trend is observed with the absorbance spectra recorded in methanol, and also with respect to the emission spectra recorded in both solvents. These spectra and plots can be found in Appendix 3, Figures A441-A443. From examining Figure 114, and as stated previously, it is evident that the

higher the electron-donating character of the substituent, the more red-shifted the corresponding absorbance.

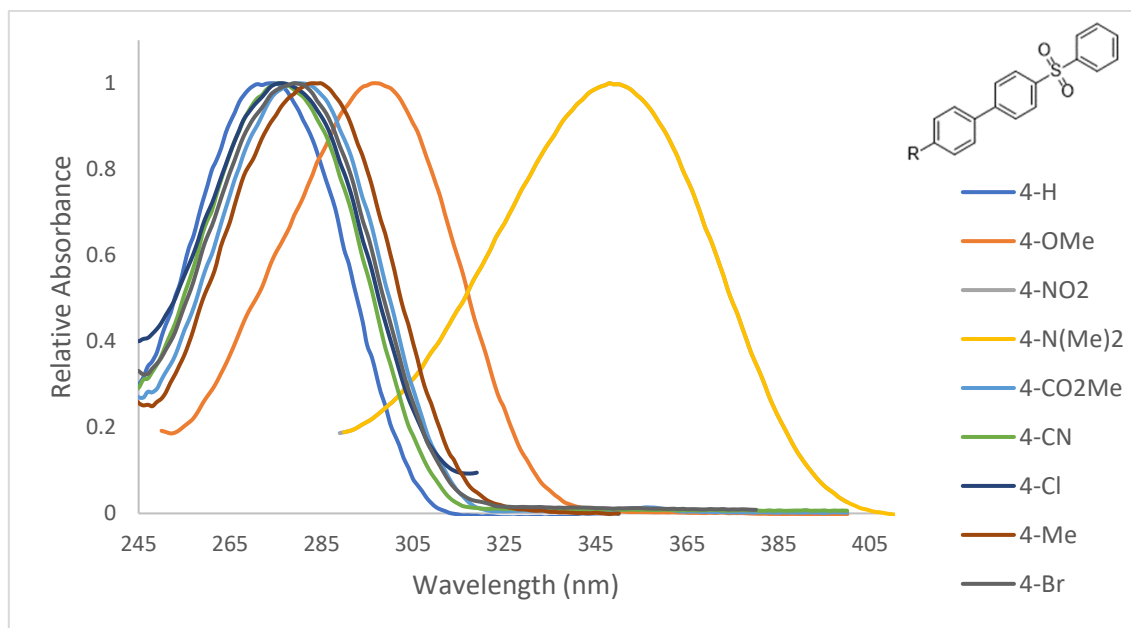


Figure 114. Relative absorbance spectra of all biaryls in chloroform, recorded using 17.86 μM solutions

3.2.7.3 Effect of solvent on emission spectra

The effect of solvent on the emission spectra varied depending on the biaryl examined. A comparison of the emission λ_{max} recorded in both solvents is included as Figures 115(a)-(h). As apparent above, Figure 113(d), the emission intensity of the 4-nitro substituent, **139**, was extremely low in both solvents and, as such, the emission spectra associated with this compound has not been included below, but can be found in Appendix 3, Figure A448. The effect of solvent on the absorbance spectra of all biaryls synthesized was also investigated. However, in this case the effect was minimal across all biaryls examined and as such, the relevant spectra have not been included below, but can be found in Appendix 3, Figure A444(a)-(i).

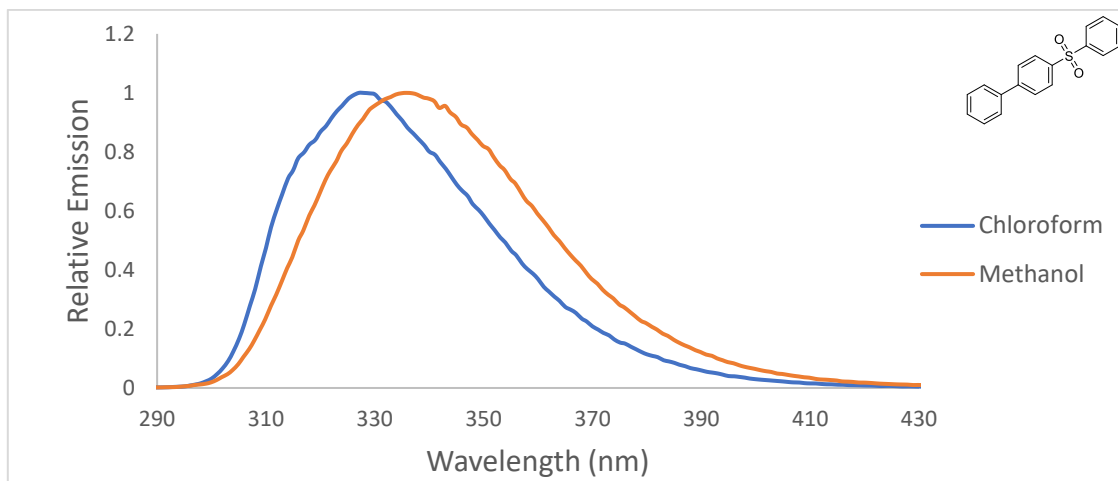


Figure 115(a). Effect of solvent on emission λ_{max} for biaryl **46**. Emission λ_{max} values of 326 and 336 nm were found using chloroform and methanol as solvent, respectively. The emission λ_{max} was recorded using a 4.56 μM and 2.85 μM solution using chloroform and methanol as solvent, respectively.

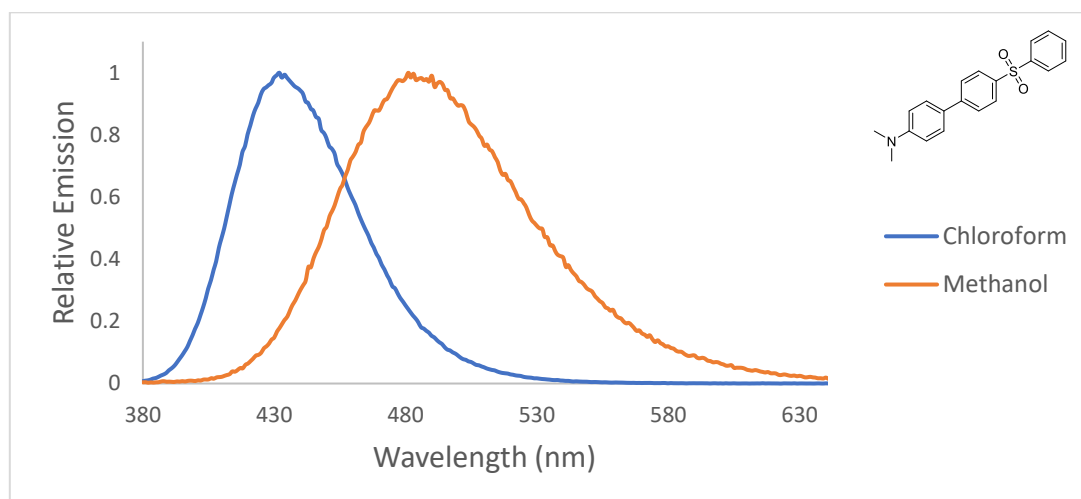


Figure 115(b). Effect of solvent on emission λ_{max} for biaryl **138**. Emission λ_{max} values of 432 and 481 nm were found using chloroform and methanol as solvent, respectively. The emission λ_{max} was recorded using a 5.58 μM and 6.51 μM solution using chloroform and methanol as solvent, respectively.

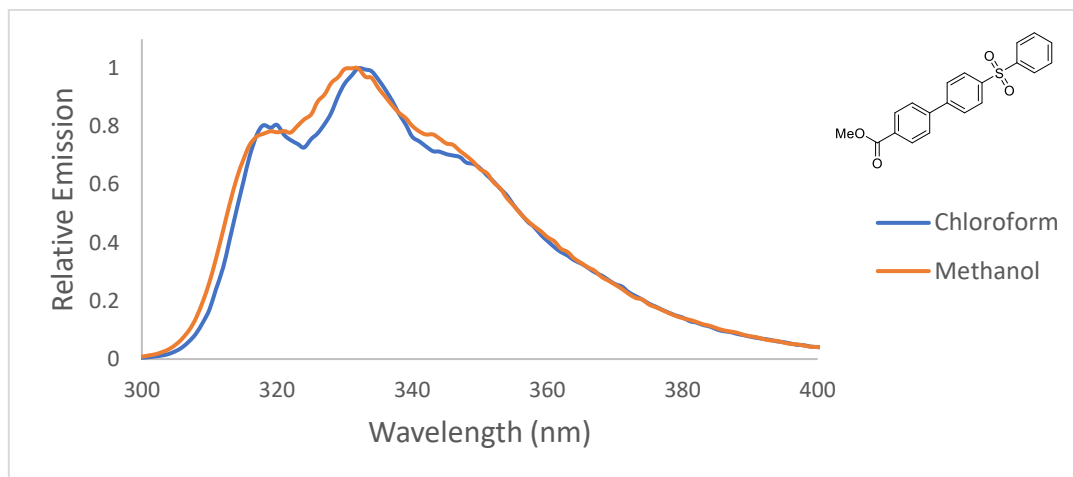


Figure 115(c). Effect of solvent on emission λ_{max} for biaryl **139**. Emission λ_{max} values of 332 and 331 nm were found using chloroform and methanol as solvent, respectively. Shoulders at 318, 320, and 348 nm were evident when the emission spectrum was recorded in chloroform, whereas these occurred at 319 & 344 nm in methanol. The emission λ_{max} was recorded using a 3.32 μM solution in both cases.

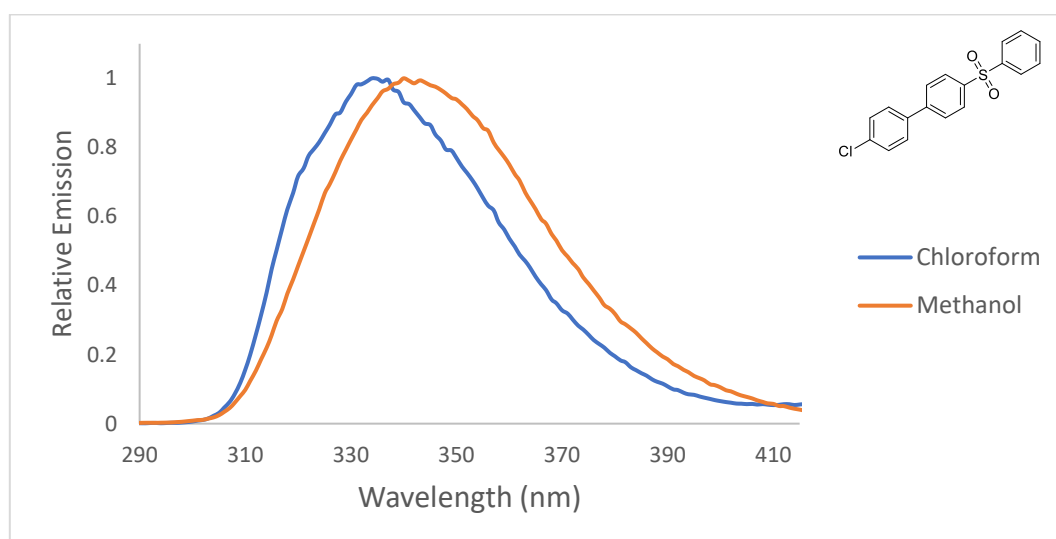


Figure 115(d). Effect of solvent on emission λ_{max} for biaryl **141**. Emission λ_{max} values of 334 and 340 nm were found using chloroform and methanol as solvent, respectively. The emission λ_{max} was recorded using a 2.79 μM and 2.85 μM solution using chloroform and methanol as solvent, respectively.

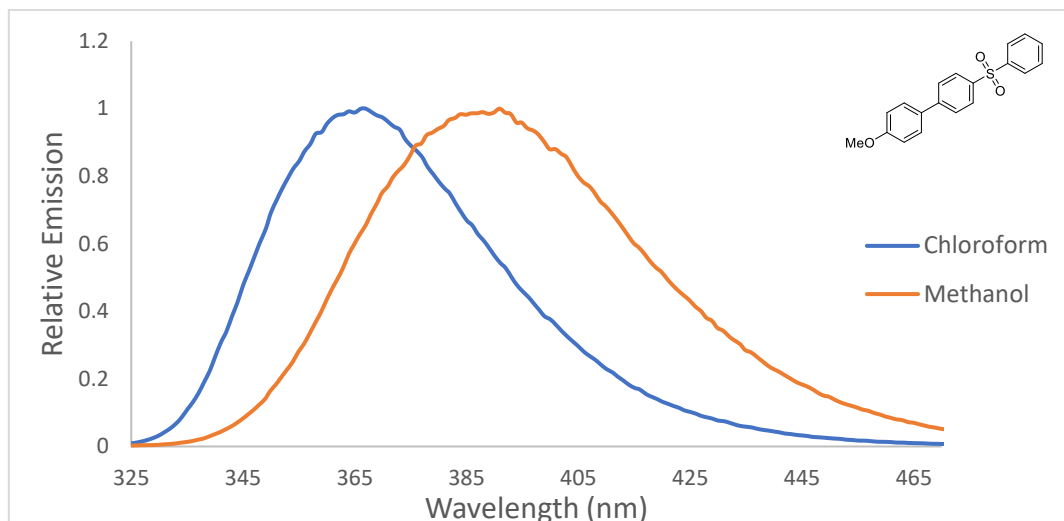


Figure 115(e). Effect of solvent on emission λ_{max} for biaryl **142**. Emission λ_{max} values of 367 and 391 nm were found using chloroform and methanol as solvent, respectively. The emission λ_{max} was recorded using a 2.32 μM and 4.65 μM solution using chloroform and methanol as solvent, respectively.

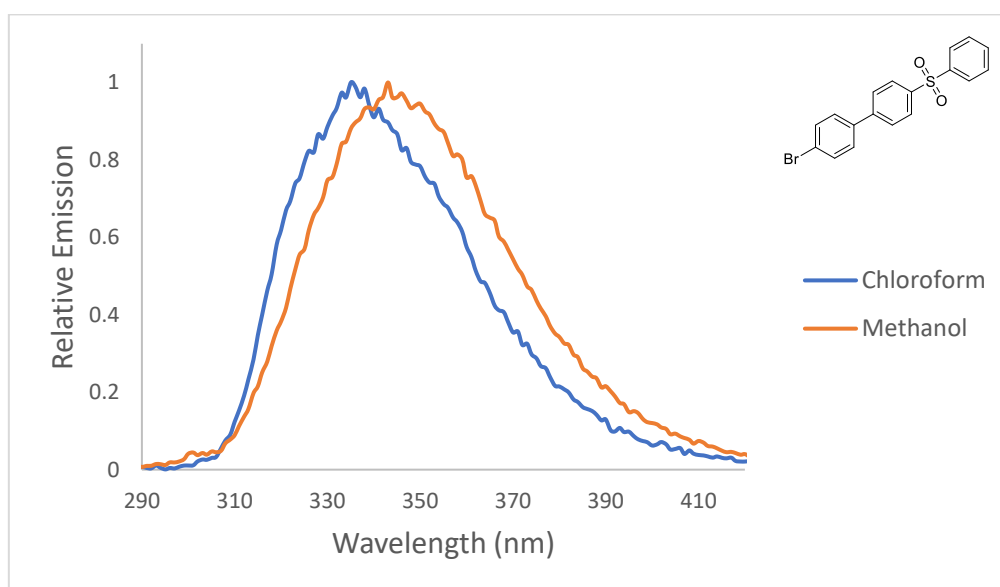


Figure 115(f). Effect of solvent on emission λ_{max} for biaryl **143**. Emission λ_{max} values of 335 and 343 nm were found using chloroform and methanol as solvent, respectively. The emission λ_{max} was recorded using a 3.32 μM and 3.98 μM solution using chloroform and methanol as solvent, respectively.

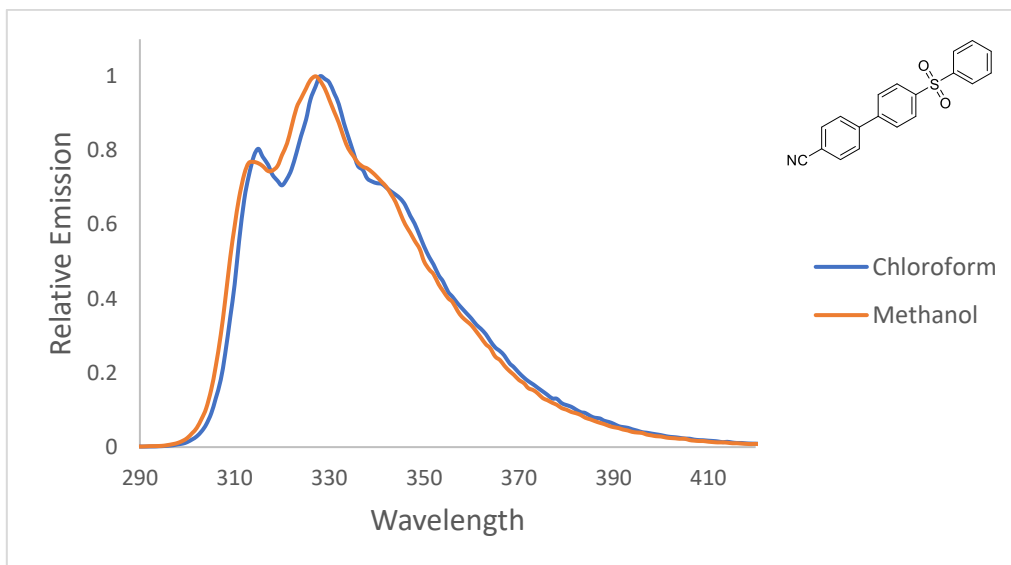


Figure 115(g). Effect of solvent on emission λ_{max} for biaryl **144**. Emission λ_{max} values of 328 and 327 nm were found using chloroform and methanol as solvent, respectively. Shoulders at 315 and 346 nm were evident when the emission spectrum was recorded in chloroform, whereas these occurred at 314 and 343 nm in methanol. The emission λ_{max} was recorded using a 3.25 μM and 2.85 μM solution using chloroform and methanol as solvent, respectively.

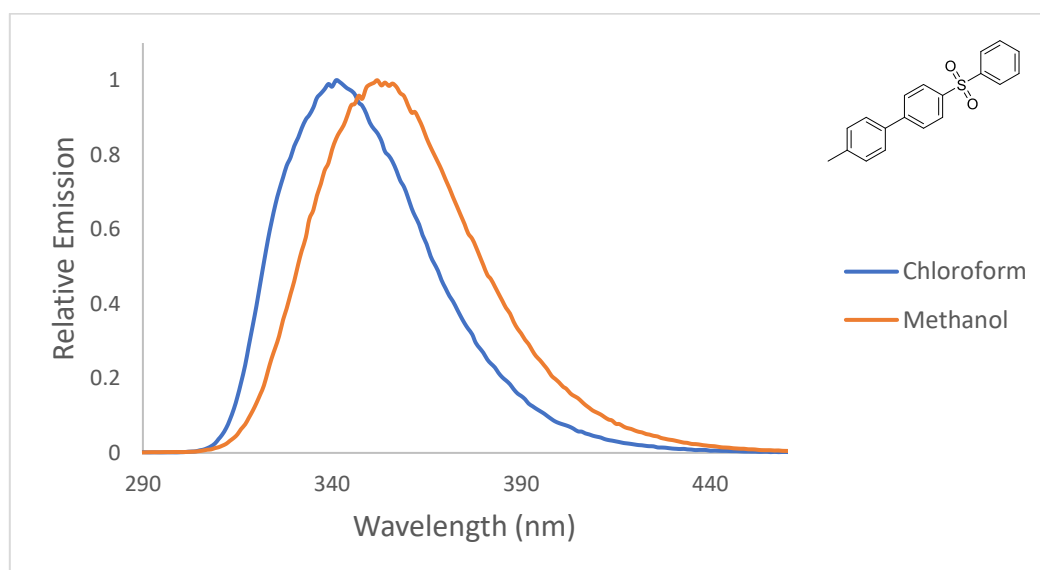


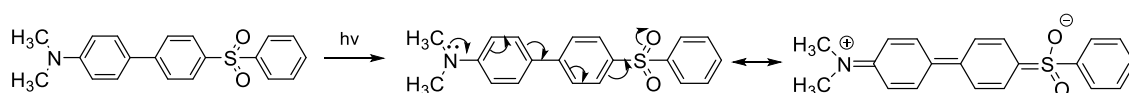
Figure 115(h). Effect of solvent on emission λ_{max} for biaryl **145**. Emission λ_{max} values of 341 and 352 nm were found using chloroform and methanol as solvent, respectively. The emission λ_{max} was recorded using a 3.25 μM and 3.32 μM solution using chloroform and methanol as solvent, respectively.

As is evident from the above spectra, the effect of the solvent employed on the emission λ_{max} depended greatly on the nature of the substituent on the phenyl ring. A difference of just 1 nm was observed in the case of an electron-withdrawing substituent, specifically a

cyano or ester in the *para*- position. A difference of 6 and 8 nm was recorded for a chloro or bromo substituent, respectively in this position and of 10 nm when this was simply a hydrogen. Replacement of a hydrogen with a methyl group increased this slightly to 11 nm, with a methoxy to 24 nm and finally with a dimethylamino to a 48 nm difference between the two solvents. The dimethylamino derivative, **138**, showed the greatest difference in the emission λ_{max} recorded in the two solvents. Thus, as electron-donating character increases, so does the effect of the solvent on the emission λ_{max} .

Correspondingly, the Stokes shift observed across the majority of the biaryls examined was affected by solvent, in that when the same samples were run in methanol (a more polar, protic solvent relative to chloroform) the Stokes shift increased (Appendix 3, Figures A440(a)-(i)). These results are consistent with the literature, and occur when the dipole moment of a fluorescent molecule is higher in the excited state than in the ground state.²⁸⁰ Biaryls with an electron-donating substituent showed a substantial increase in Stokes shift when changing solvent from chloroform to methanol. For example, compound **138** had a Stokes shift of 134 nm and compound **142** had a Stokes shift of 94 nm in methanol, compared with 85 nm and 70 nm in chloroform, respectively. The majority of other biaryls had Stokes shifts of between 51 and 69 in methanol. However, there was only a Stokes shift of 1 nm (essentially none) observed for compounds **139** and **144**, which bear electron-withdrawing groups of methyl ester and cyano, respectively.

All of these observations are consistent with the occurrence of an intramolecular charge transfer (ICT) process,²⁸⁰ Scheme 48, and given the nature of the biaryls we were examining, we specifically propose the occurrence of a twisted intramolecular charge transfer (TICT) process as the mechanism of fluorescence.



Scheme 48. Proposed ICT mechanism of fluorescence using biaryl **138** as an example.

A TICT mechanism is a particular phenomenon wherein the intramolecular charge transfer is accompanied by internal rotation within the fluorophore.²⁸⁰ A prominent example of this in the literature occurs with respect to 4-*N,N*-dimethylaminobenzonitrile, Figure 116 (a). In the ground state, this molecule is almost planar, which corresponds to the maximum conjugation between the dimethylamino substituent and the phenyl ring. According to the Franck-Condon principle, the locally excited (LE) state is still planar, but solvent relaxation takes place with a corresponding rotation of the dimethylamino substituent that occurs to such an extent that the molecule becomes twisted at right angles and the conjugation is lost. In the consequential TICT state, stabilized by polar solvent molecules, there is a complete charge separation between the dimethylamino and the cyanophenyl substituent,²⁸⁰ which can be depicted graphically as per Figure 116 (b).

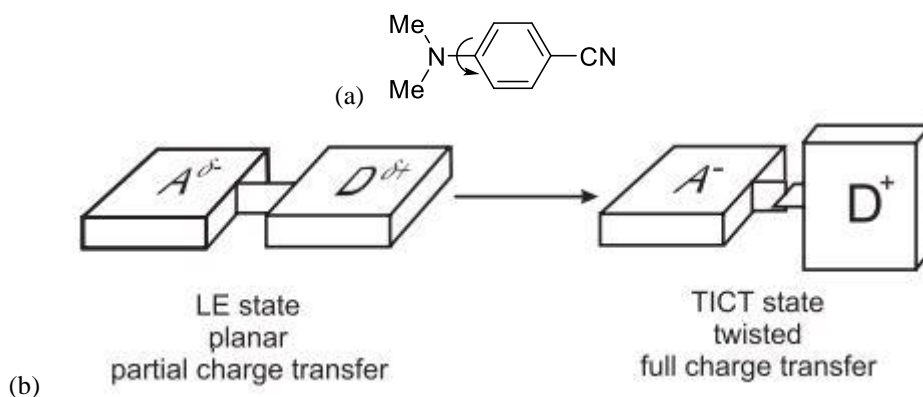


Figure 116(a). Structure of 4-*N,N*-dimethylaminobenzonitrile, **(b)** Structural representation of the occurrence of the TICT mechanism, with respect to 4-*N,N*-dimethylaminobenzonitrile.

Given the structural similarity between our biaryl **138** and 4-*N,N*-dimethylaminobenzonitrile, and the composition of both molecules in terms of possession of this donor/acceptor motif, it is very plausible that this same TICT mechanism applies to our biphenyl, and gives rise to the observed fluorescent activity.

3.2.7.4 Measurement of molar extinction coefficient (ϵ)

As part of our investigation of the preliminary photophysical properties of these biaryls, the molar extinction coefficient (ϵ) was also investigated. This was examined using chloroform as the solvent only. Here, two separate solutions of each biaryl were prepared using 35 μM and 17.5 μM concentrations. A serial dilution was performed in each case so as to ensure accurate and precise weighting and dilution, and consequently a good approximation of ϵ when the data was combined. Once the UV-absorbances across a number of different concentrations were recorded, the optical density at the respective absorbance λ_{max} was plotted against the relevant concentrations (expressed as molarity) and an equation of the line was generated for each biaryl. The slope of this line corresponds to the molar extinction coefficient (ϵ). Figure 117(a) is used as a representative example, the graphs relevant to biaryls **46**, **138-142**, and **144-145** can be found in Appendix 3, Figures A445(a)-(h).

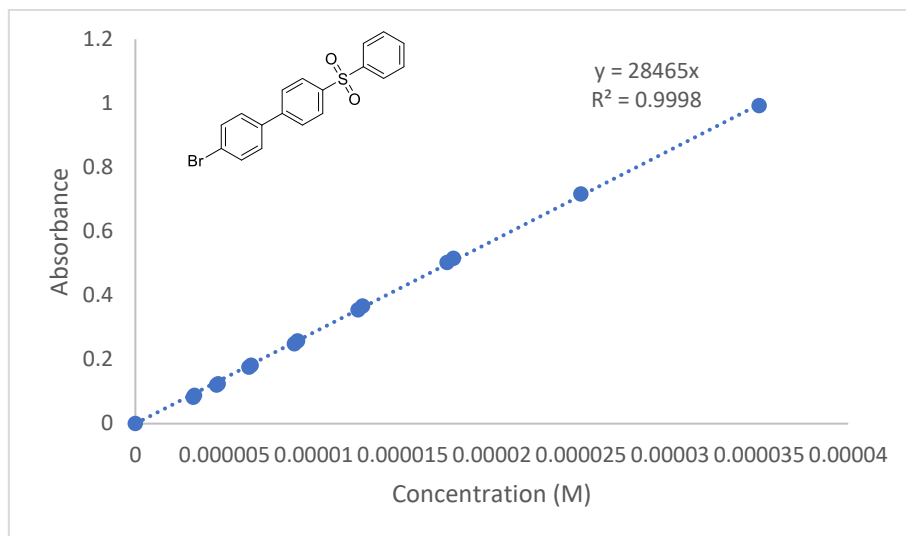


Figure 117. Graph of UV-absorbance intensity versus concentration, using data collected by analyzing solutions between 0-35 μM concentration. The ϵ for biaryl **143** was found to be $28465 \text{ M}^{-1} \text{ cm}^{-1}$.

The absorbance (A) of a sample generally follows the Beer-Lambert law: $A = \epsilon lc$, where ϵ is the molar extinction coefficient, c is the concentration (in molarity) of the absorbing species, and l is the absorption path length (thickness of the absorbing medium, generally the width of the cuvette) in cm .²⁸⁰ The molar extinction coefficient (ϵ) expresses the ability of a molecule to absorb light of wavelength λ in any given solvent. A high value of ϵ implies a probable transition.²⁸⁰ The values recorded for each of the biaryls range from 17332 - $37964 \text{ M}^{-1} \text{ cm}^{-1}$ in chloroform. This is consistent with the occurrence of $\pi \rightarrow \pi^*$ transitions, for which values of ϵ have been recorded up to the order of 10^5 .²⁸⁰ The highest value obtained for ϵ , of $37964 \text{ M}^{-1} \text{ cm}^{-1}$, was obtained with respect to 1-(4-chlorophenyl)-4-(phenylsulfonyl)benzene, **141**, and the lowest value ϵ , of $17332 \text{ M}^{-1} \text{ cm}^{-1}$, was obtained with respect to 4-dimethylamino substituted derivative **138**.

3.2.7.5 Quantum yield calculation

The quantum yield (ϕ) refers to the ratio of the number of molecules that fluoresce to the total number of excited molecules,²⁷⁶ and is another photophysical property of the biaryls that we examined. For highly fluorescent molecules, the quantum yield approaches one, whereas chemical species that do not fluoresce have quantum yields that approach zero.²⁷⁶ The ϕ of each biaryl was recorded in both chloroform and methanol, with the exception of the 4-nitro substituted biaryl, **140**, for which the emission intensity was too low to record a curve in either solvent. In each case, the concentration of each biaryl was sufficiently low such that an optical density of approximately $0.1 (\pm 0.05)$ was recorded. The absorbance λ_{max} was then chosen as the wavelength at which to excite the respective sample and this generated an emission spectrum curve. The area under this curve was

calculated using MATLAB® and used in the following formula to calculate the quantum yield.

$$\phi = \phi_R \frac{F A_R n^2}{F_R A n_R^2}$$

Figure 118. Equation for ϕ where ϕ_R is the quantum yield of the reference, F and F_R are the integrated emission intensities of the sample and the reference, respectively. A and A_R are the optical densities of the sample and the reference, respectively, and n and n_R are the refractive indexes of the solvent in which the measurement was performed for the sample and the reference, respectively.²⁸¹

In the majority of cases, the reference used was 2-aminopyridine, which has a literature quantum yield of 0.60 when made up using 0.1 M sulfuric acid as the solvent.²⁸² This was an appropriate reference because its emission range covers 315-480 nm, which is the range within which the emission λ_{\max} was recorded for the majority of the biaryls examined. The exception was the dimethylamino-substituted biaryl **138**, which had an emission λ_{\max} of 481 nm when recorded in methanol, and so quinine sulfate was used as the reference in this case. Quinine sulfate has a quantum yield of 0.54 when made up using 0.1 M sulfuric acid as the solvent,²⁸³ and covers an emission range of 400-600 nm. The following data was recorded in relation to obtaining the quantum yields of biaryl **138** in chloroform and methanol, Figure 119, and is used as an example of the data collected. The data relating to the other biaryls, **46**, and **139-145** can be found in Appendix 3, Figures A446(a)-(g), and the data relevant to the two standards is included in Appendix 3, Figures A447(a) and (b).

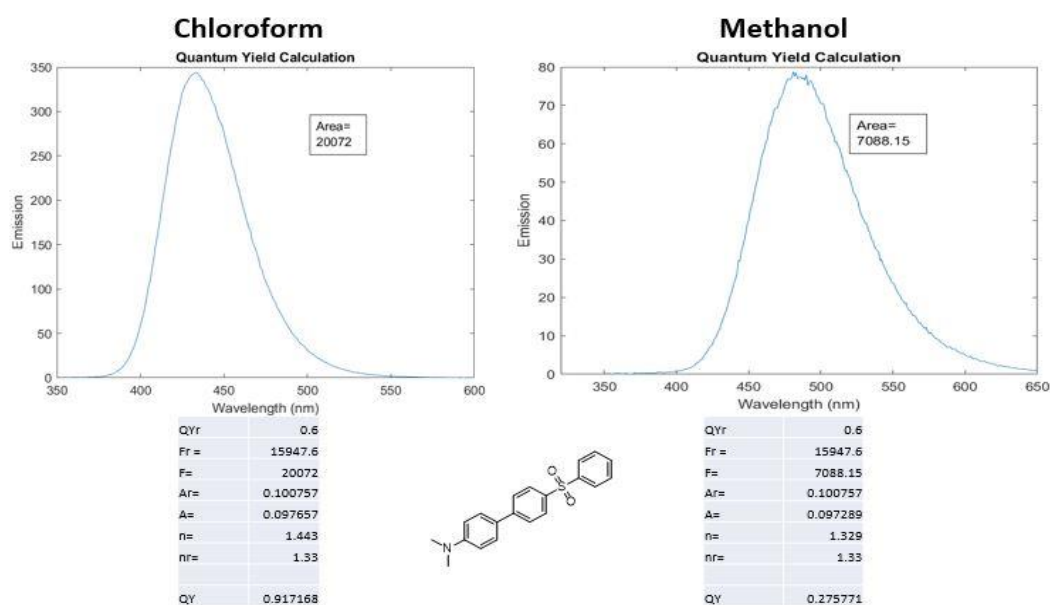


Figure 119. Data relevant to the calculation of quantum yield of biaryl **138** in chloroform (left) and methanol (right), using the equation displayed above in Figure 118. A quantum yield of 0.92 and 0.28 was recorded in chloroform and methanol, respectively using a 5.58 μM and 6.61 μM solution, respectively.

Generally, the quantum yields for the biaryls ranged between 0.35-0.62 across the two solvents examined. Some exceptions to this were evident, notably the 4-bromo substituted biaryl, **143**, which had a very low quantum yield of less than 0.05 in both solvents. This is expected from the literature, being attributed to the internal heavy atom effect.²⁸⁰ Essentially, the presence of a heavy atom, such as bromine, as the substituent of an aromatic molecule causes fluorescence quenching, and hence, the very low quantum yield consequently. Another anomaly was observed with respect to the 4-dimethylamino substituted biaryl, **138**, in that the highest quantum yield of 0.92 was recorded in chloroform and yet, one of the lowest quantum yields of 0.28 was recorded in methanol. As mentioned previously, chloroform is an aprotic solvent whereas methanol is a protic solvent. It has been noted in the literature that the occurrence of hydrogen bonding within a solvent may be sufficient to significantly change the fluorescence spectrum of a fluorophore.²⁸⁰ Valeur²⁸⁰ uses 4-aminophthalimide, Figure 120, to exemplify this, noting that this compound possesses a high quantum yield in aprotic solvents but a very low quantum yield in protic solvents, and attributes this to the occurrence of hydrogen bonding.²⁸⁰ Based on the quantum yields we observed with respect to biaryl **138**, we can hypothesize that the occurrence of hydrogen bonding in methanol has a similar effect on our dimethylamino biaryl, **138**, as that which occurs in the case of 4-aminophthalimide.

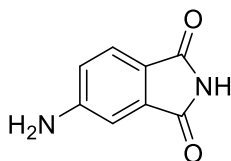


Figure 120. Chemical structure of 4-aminophthalimide

With respect to the 4-methyl ester substituted derivative **139**, a different solvent effect was observed in that a lower quantum yield was recorded in chloroform than that in methanol of 0.36 and 0.44 respectively. Some aromatic carbonyl compounds often have low-lying, closely spaced $\pi \rightarrow \pi^*$ and $n \rightarrow \pi^*$ states.²⁸⁰ Inversion of these two states can be observed when the polarity and the hydrogen-bonding ability of the solvent increases, because the $n \rightarrow \pi^*$ state shifts to higher energy whereas the $\pi \rightarrow \pi^*$ state shifts to lower energy, something which can be represented graphically, Figure 121.

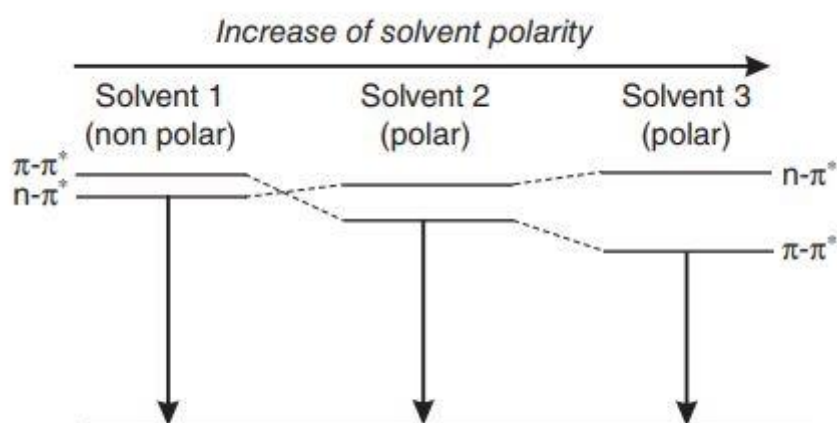
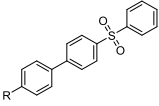


Figure 121. The effect of polarity-induced inversion of $n \rightarrow \pi^*$ and $\pi \rightarrow \pi^*$ states, taken from the work of Valeur.²⁸⁰

The result is in an increase in fluorescence quantum yield in more polar solvents that are capable of hydrogen bonding. A similar effect was observed with respect to the 4-methoxy-substituted biaryl, **142**, having a quantum yield of 0.62 in chloroform and 0.75 in methanol.

A summary of the photophysical properties of this family of biaryls, that we investigated as part of this study, can be summarized by the following table, Table 23.

Table 23. Summary of the preliminary photophysical properties of the biaryls **46**, **138-145** investigated in our study

	Solvent (Conc. = 35 μM)	$\lambda_{\text{max abs}}$ (nm)	$\lambda_{\text{max em}}$ (nm)	Stoke's shift (nm)	$\lambda_{\text{max ex}}$ (nm)	ϵ ($\text{M}^{-1} \text{cm}^{-1}$)	Φ
R =							
H	Chloroform	273	326	53	272	22034	0.41
H	Methanol	272	336	64	209 & 272		0.43
$\text{N}(\text{CH}_3)_2$	Chloroform	348	433	85	251 & 346	17332	0.92
$\text{N}(\text{CH}_3)_2$	Methanol	240 & 347	481	134	240 & 346		0.28
CO_2Me	Chloroform	281	332 ^a	51	280	34033	0.36
CO_2Me	Methanol	279	331 ^b	52	208 & 280		0.44
OMe	Chloroform	297	367	70	298	37703	0.62
OMe	Methanol	297	391	94	228 & 298		0.75
Me	Chloroform	284	341	57	286	29738	0.42

Me	Methanol	283	352	69	210 & 280		0.58
Cl	Chloroform	276	334	58	277	37964	0.37
Cl	Methanol	275	340	65	210 & 278		0.41
Br	Chloroform	278	335	57	277	28465	0.032
Br	Methanol	277	343	66	212 & 272		0.048
CN	Chloroform	276	328 ^e	52	278	30435	0.40
CN	Methanol	276	327 ^d	51	211 & 273		0.35
NO ₂	Chloroform	297	N/A	N/A	N/A	24730	N/A
NO ₂	Methanol	297	N/A	N/A	N/A		N/A

To summarize, interesting photophysical results were obtained with respect to the family of phenylsulfonyl biaryls analyzed. The largest Stokes shift of 134 nm was observed for the dimethylamino derivative, **138** in methanol. Compound **138** showed the greatest sensitivity to solvent choice and manifested itself in changes to the emission λ_{max} . In terms of the molar extinction coefficient (ϵ), the values recorded for each of the biaryls ranged from 17332-37964 M⁻¹ cm⁻¹ in chloroform, the largest being recorded with respect to the *p*-chloro derivative, **141**, and the lowest corresponded to compound **138**. The biaryl with the highest quantum yield of 0.92 was **138**, but this was only observed in the aprotic solvent chloroform. In methanol the quantum yield of **138** dropped dramatically to 0.28, due to a suspected hydrogen bonding effect. The results and structure of our biaryls, most notably the dimethylamino derivative **138**, suggests the occurrence of a twisted intramolecular charge transfer (TICT), which involves an intramolecular charge transfer process accompanied by internal rotation within the fluorophore.

3.3 Conclusion

To conclude, a selection of (1*E*,3*E*,5*E*)-1,3-bis-phenylsulfonyl-6-phenyl-hexa-1,3,5-trienes, synthesized as described in Chapter Two, were used as substrates in a thermal electrocyclization reaction. This reaction is symmetry allowed by the Woodward-Hoffman rules via disrotatory orbital overlap of the substituents on the terminal carbon atoms and resulted in the generation of a family of biaryls. An optimization study was carried out in order to determine preferred reaction conditions for this synthetic protocol. The conversion of (1*E*,3*E*,5*E*)-1,3-bis-phenylsulfonyl-6-phenyl-hexa-1,3,5-triene, **105**, to give 4-(phenylsulfonyl)-1,1'-biphenyl, **46**, was employed as a model reaction. As part of this study, a number of experimental set-ups were investigated including the choice of heat source for the electrocyclization process, the use of microwave irradiation, and the possibility of using sublimation as a purification method. The highest conversion to biaryl was recorded using neat heating (via an oil bath) of compound **105**, at 175 °C for 1.5 hours. This synthetic protocol gave an 88% yield of pure biaryl **46**, after column chromatography and subsequent re-crystallization. The application of thermal electrocyclization using the preferred reaction conditions resulted in the synthesis of eight 1-(4-substituted phenyl)-4-(phenylsulfonyl)benzene products in 40-64% yield. To the best of our knowledge, none of these eight biaryls have been reported in the peer reviewed literature. All biaryls synthesized were structurally characterized in full using NMR and IR spectroscopy, as well as LC-MS and HR-MS. There were no obvious trends observed relating substituent effects with yields obtained. Although yields of only 40-64% were achieved for the substituted biaryl products, the developed protocol has the advantages of being solvent-free and not requiring a transition metal catalyst. Furthermore, a short reaction time of 1.5 hours and use of simple apparatus is advantageous.

A preliminary investigation of the family of 1-(4-substituted phenyl)-4-(phenylsulfonyl)benzene compounds was conducted to determine some of their photophysical properties. As such, we collected data on the UV-absorbance λ_{max} , emission λ_{max} , excitation λ_{max} , Stokes' shift, molar extinction coefficient (ϵ) and quantum yield (ϕ). As expected, the 1-(4-dimethylaminophenyl)-4-(phenylsulfonyl)benzene derivative, **138**, exhibited the most potent fluorescent activity. For example, compound **138** had the largest observed UV-absorbance λ_{max} and emission λ_{max} , 348 and 433 nm, respectively of all biaryls (in chloroform). The effect the substituent had on absorbance and emission was examined and it was observed that the stronger the electron-donating character of the substituent then the higher the corresponding absorbance λ_{max} and emission λ_{max} . The 1-(4-nitrophenyl)-4-(phenylsulfonyl)benzene derivative, **140**, was the only biaryl for which fluorescent activity was not observed. This can be explained by a low-lying $n \rightarrow \pi^*$ transition, due to the presence of the strongly electron-withdrawing nitro substituent.

The effect of solvent was investigated by running samples in chloroform, a polar aprotic solvent, and in methanol, a polar protic solvent. While this did not have a significant effect on the absorbance λ_{max} , the effect on emission λ_{max} was more pronounced. This depended on the substituent found on the phenyl ring, with the emission λ_{max} of compound **138**, with a *para*-dimethylamino group, being red-shifted the most to 481 nm. This was followed by 1-(4-methoxyphenyl)-4-(phenylsulfonyl)benzene, compound **142**, with an emission λ_{max} of 391 nm. This effect decreased as the electron-donating character of the substituent diminished. Compound **138** had the largest Stokes' shift of all biaryls investigated (determined in methanol) of 134 nm. This was followed by compound **142**, with a Stokes' shift of 94 nm (also in methanol). The other biaryls had Stokes' shifts of between 51 and 69 in methanol.

The molar extinction coefficient (ϵ) varied greatly between biaryls. For example, a value of $17332 \text{ M}^{-1} \text{ cm}^{-1}$ was determined for compound **138** and of $37964 \text{ M}^{-1} \text{ cm}^{-1}$ for 1-(4-chlorophenyl)-4-(phenylsulfonyl)benzene **141**. The quantum yield (ϕ) also varied greatly, from 0.032 for the 1-(4-bromophenyl)-4-(phenylsulfonyl)benzene derivative, **143** in chloroform, to 0.92 for compound **138**, in chloroform. The large value for ϕ of 0.92 for **138** demonstrates its strong fluorescent activity. Interestingly, ϕ of biaryl **138** in methanol was much lower at 0.28 and this is consistent with literature reports for a structurally similar compound and can be explained by the effect of hydrogen bonding, not present in chloroform, and the consequential reduction in fluorescence. The effect of protic versus aprotic solvents is consistent with our proposed mechanism of fluorescence, which consists of a twisted intramolecular charge transfer (TICT). A TICT mechanism of fluorescence involves an intramolecular charge transfer process accompanied by internal rotation within the fluorophore.

Future work might entail further photophysical studies including an examination of the lifetime of this fluorophore (compound **138**). Additionally, the application of some of these biaryls as sensor molecules could be considered. For example the non-fluorescence of compound **140** could be useful in a nitroreductase sensor. Nitroreductase is one of a series of biomarkers that have been shown to be significantly upregulated in cells under hypoxic stress. Hypoxia has been reported to play a role in a number of diseases including in tumour development and resistance to therapy. The reaction of **140** with nitroreductase enzyme would result in the reduction of the nitro group to an amino group, fluorescence would be 'turned on', and hence one would have sensed the presence of nitroreductase. This example, as well as the preliminary photophysical properties we have completed, shows that these biaryls are potentially useful and versatile fluorescent small molecules.

3.4 Experimental Procedure

3.4.1 General information for chemical synthesis

See section 2.4.1 for full details. Additionally, the UV-Vis spectrum of each biaryl in solution was obtained using a Unicam UV 540 spectrometer. The emission and excitation spectra for each solution was obtained using a JASCO FP-6300 spectrofluorometer.

3.4.2 Optimization study to determine preferred reaction conditions for biaryl synthesis

3.4.2.1 Initial test reaction to confirm conversion of (1*E*,3*E*,5*E*)-1,3-bis-phenylsulfonyl-6-phenyl-hexa-1,3,5-triene, **105** using a heat gun

Neat solid (1*E*,3*E*,5*E*)-1,3-bis-phenylsulfonyl-6-phenyl-hexa-1,3,5-triene, **105**, (25 mg, 0.057 mmol) in a 25 mL round-bottom flask was heated quickly using a Bosch heat gun set at the maximum temperature for approximately 10 seconds. Heating in this way caused the contents to melt and a brown oil was visible, with some charring evident on the side of the round-bottom flask. The round-bottom flask was weighed before the addition of the triene and after heating the triene in this way, and the mass this corresponded to was assigned as the crude mass of 4-(phenylsulfonyl)-1,1'-biphenyl, **46**, obtained. This was then subjected to ¹H NMR spectroscopic analysis to confirm the formation of **46** (12.6 mg, 75%).

3.4.2.2 Optimization study: Investigation of optimal heating methodology

We investigated different heating methods and applied these to the attempted electrocyclization of **105** in each case.

3.4.2.2.1 Use of an oil bath (at 175 °C)

Neat solid **105** (25 mg, 0.057 mmol) was placed in a 25-gram round-bottom flask and the top was covered in parafilm with a pin-sized hole in the centre. The bottom half of the flask was immersed in an oil bath that had been heated to 175 °C and then left for 1.5 hours. Approximately 5 minutes into this time, the yellow-coloured powdered consistency of **105** changed to a brown oil. Once the 1.5 hours had elapsed, the outside of the flask was cleaned thoroughly with tissue, and then the flask weighed to obtain the crude mass of **46** (15.8 mg, 94%).

3.4.2.2.2 Use of a pyrex bowl full of Lab Armour metallic beads (at 175 °C)

As per section 3.4.2.2.1, replacing the oil bath with a pyrex bowl filled with Lab Armour metallic beads. Crude **46** was obtained (11.8 mg, 70%).

3.4.2.2.3 Use of a pyrex bowl full of sand (at 175 °C)

As per section 3.4.2.2.1, replacing the oil bath with a pyrex bowl filled with sand that had been pre-dried in an oven overnight. Crude **46** was obtained (13.4 mg, 80%).

3.4.2.2.4 Use of a pyrex bowl full of sand (at 200 °C)

As per section 3.4.2.2.3, but instead heated to 200 °C. Crude **46** was obtained (10.1 mg, 60%).

3.4.2.2.5 Use of a vacuum oven (at 180 °C)

Compound **105** (25 mg, 0.057 mmol) was spread across a clock glass which was placed under the lid of a petri dish with tin foil wrapped underneath it to hold the clock glass and lid in place. This assembly was placed in a Binder vacuum oven (Mason Technology), which had been heated to 180 °C, that was attached to a RV5 Edwards pump fitted with an oil mist filter EMF10. The petri dish was left inside the vacuum oven for 24 hours with the pressure approaching 0 mbar atm for the duration. Crude **46** was obtained (1.7 mg, 10%).

3.4.2.3 Optimization study: Purification attempts using sublimation

3.4.2.3.1 Sublimation attempt one – use of water for cooling

A sublimation apparatus was attached to an aspirator and fitted onto to a 50 mg round-bottom flask containing **105** (25 mg, 0.057 mmol). This was heated using an oil bath set to 175 °C for 1.5 hours. After this time, there was some material sublimed to the cold finger which consisted of a colourless solid (2 mg) and non-sublimed brown residue in the round-bottom flask (6 mg). The ¹H NMR spectra indicated they contained the same product – crude **46** (8 mg, 48%).

3.4.2.3.2 Sublimation attempt two - use of liquid nitrogen for cooling

The second attempt changed the sublimation apparatus from that used in section 3.2.3.3.1 to one that allowed liquid nitrogen to be added to the cold finger. This was inserted into a Schlenk tube containing **105** (25 mg, 0.057 mmol) which was heated using an oil bath set to 175 °C for 2 hours. The Schlenk tube was attached to a Schlenk line which achieved a vacuum of 0.1 mbar. The process of adding liquid nitrogen to the cold finger occurred

over the course of 2 hours to ensure sufficient quantities of liquid nitrogen remained on the cold finger. A colourless material (4 mg) sublimed onto the cold finger and 13 mg of a brown residue remained on the bottom of the round bottom flask after the 2 hours of heating had elapsed. However, the sublimed material contained only trace amounts of the biaryl ($\leq 10\%$) and instead, was composed largely of an unidentified by-product. Thus, the crude yield of **46** was accounted for by the brown residue only (13 mg, 77%)

3.4.2.4 Optimization study: Microwave heating

3.4.2.4.1 Microwave heating and choice of solvent

To investigate if solvent had an effect, 0.0025 M (5 mL) solutions of **105**, were made up by dissolving 5.46 mg of **105** in respective solvent, and each solution was exposed to microwave heating at 170 °C for 5 minutes. This solution was then transferred to a round-bottom flask, the contents reduced *in vacuo* to dryness and then subjected to ^1H NMR after dissolving in deuterated chloroform.

3.4.2.4.1.1 Use of toluene

As per section 3.4.2.4.1, using toluene. A white solid, which was not the desired product and whose structure could not be determined, precipitated at the end of the reaction. The remaining solution contained crude biaryl **46** (1.47 mg, 40%)

3.4.2.4.1.2 Use of DMF

As per section 3.4.2.4.1, using DMF. Crude biaryl **46** (1.84 mg, 50%)

3.4.2.4.1.3 Use of chloroform

As per section 3.4.2.4.1, using chloroform. No formation of biaryl **46** detected by ^1H NMR spectroscopy, only unreacted triene and a complex mixture.

3.4.2.4.1.4 Use of acetonitrile

As per section 3.4.2.4.1, using acetonitrile. No formation of biaryl **46** detected by ^1H NMR spectroscopy, only a complex mixture.

3.4.2.4.2 Microwave heating and variations in temperature used

As per section 3.4.2.4.1, using DMF but varying the temperature.

3.4.2.4.2.1 Use of 85 °C

As per section 3.4.2.4.2, using 85 °C. No conversion from triene **105** to biaryl **46** was observed and this mixture consisted largely of unconverted triene.

3.4.2.4.2.2 Use of 110 °C

As per section 3.4.2.4.2, using 110 °C. Very little conversion from triene **105** to biaryl **46** was observed. Some evidence of its conversion could be seen in the crude ¹H NMR spectrum but the yield was too low to accurately quantify.

3.4.2.4.2.3 Use of 140 °C

As per section 3.4.2.4.2, using 140 °C. Crude biaryl **46** (1.10 mg, 30%) and the remainder consisted of unconverted triene and a complex mixture.

3.4.2.4.2.4 Use of 150 °C

As per section 3.4.2.4.2, using 150 °C. Crude biaryl **46** (1.47 mg, 40%) and the remainder consisted of unconverted triene and a complex mixture.

3.4.2.4.2.5 Use of 170 °C

As per section 3.4.2.4.2, using 170 °C. Crude biaryl **46** (1.84 mg, 50%) and the remainder consisted of a complex mixture.

3.4.2.4.3 Microwave heating and concentration of triene

3.4.2.4.3.1 Use of 0.0025 M solution

Exactly as per section 3.4.2.4.2.5, crude biaryl **46** (1.84 mg, 50%) and the remainder consisted of a complex mixture.

3.4.2.4.3.2 Use of 0.01 M solution

A 0.01 M (5 mL) solution of **105**, was made up by dissolving 21.83 mg of **105** in DMF, and this solution was exposed to microwave heating at 170 °C for 5 minutes. This solution was then transferred to a round-bottom flask, the contents reduced *in vacuo* to dryness and then subjected to ¹H NMR after dissolving in deuterated chloroform. Crude biaryl **46** (8.83 mg, 60%) and the remainder consisted of a complex mixture.

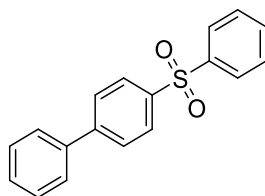
3.4.2.4.3.2 Use of 0.1 M solution

A 0.1 M (5 mL) solution of **105**, was made up by dissolving 218 mg of **105** in DMF, and this solution was exposed to microwave heating at 170 °C for 5 minutes. This solution was then transferred to a round-bottom flask, the contents reduced *in vacuo* to dryness and then subjected to ¹H NMR after dissolving in deuterated chloroform. Crude biaryl **46** (88.3 mg, 60%) and the remainder consisted of a complex mixture.

3.4.3 General procedure for synthesis of biaryls

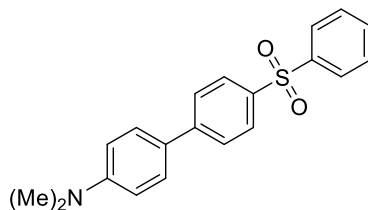
Neat 1,3,5-hexatriene (150 mg) was heated at 170 °C for 1.5 hours. The resulting brown residue was cooled to room temperature and purified using flash chromatography on silica gel with ethyl acetate/petroleum ether in different ratios to give the best separation as indicated by TLC. The resulting solid was then recrystallised using a minimum amount of DCM/*n*-hexane to give the final product.

Synthesis of 4-(phenylsulfonyl)-1,1'-biphenyl, **46**



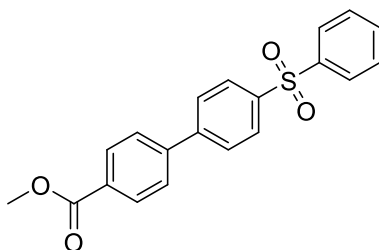
Neat **105** (150 mg, 0.34 mmol) was used as per the general procedure. The mobile phase for flash chromatography consisted of ethyl acetate/petroleum ether (100:0 petroleum ether, then 100 mL 95:5 petroleum ether: ethyl acetate, followed by a 1% increase in polar mobile phase every 100 mL. Column finished at 86:14 petroleum ether: ethyl acetate). An off-white solid was obtained as the final product, 88 % yield (89 mg). M.P. 144-146°C, Lit. 148-149°C.²⁷² ¹H NMR (500 MHz, CDCl₃) δ 8.02-7.98 (m, 4 H), 7.71-7.69 (m, 2 H), 7.59-7.50 (m, 5 H), 7.47-7.39 (m, 3 H); ¹³C NMR (125 MHz, CDCl₃) δ 146.2, 141.8, 140.2, 139.2, 133.2, 129.3, 129.1, 128.6, 128.2, 127.9, 127.7, 127.4 ppm. NMR data consists with literature.²⁷²; LC-MS: purity 98.8% t_R = 31.24 min, (ESI) m/z [M+H]⁺ 295.8.

Synthesis of 1-(4-dimethylaminophenyl)-4-(phenylsulfonyl)benzene, 138



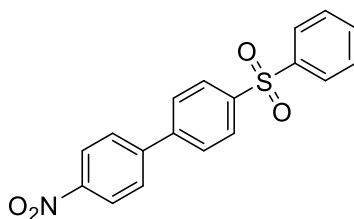
Neat (1*E*,3*E*,5*E*)-1,3-bis-phenylsulfonyl-(4-*p*-dimethylaminophenyl)-hexa-1,3,5-triene, **110** (150 mg, 0.31 mmol) was used as per the general procedure. The mobile phase for flash chromatography consisted of ethyl acetate/petroleum ether (100:0 petroleum ether, then 100 mL 95:5 petroleum ether: ethyl acetate, followed by a 1% increase in polar mobile phase every 100 mL. Column finished at 86:14 petroleum ether: ethyl acetate). An off-white solid was obtained as the final product, 49% yield (52 mg) ¹H NMR (500 MHz, CDCl₃) δ 7.98-7.96 (m, 2 H), 7.94-7.92 (m, 2 H), 7.66-7.64 (m, 2 H), 7.57-7.54 (m, 1 H), 7.52-7.48 (m, 4 H), 6.78-6.76 (m, 2 H), 3.01 (s, 6 H); ¹³C NMR (125 MHz, CDCl₃) δ 150.8, 146.2, 142.2, 138.3, 133.0, 129.2, 128.2, 128.0, 127.6, 126.5, 126.4, 112.5, 40.3 ppm; HRMS (ESI-MS) Calc. for C₂₀H₁₉O₂SN (M+Na)⁺: 337.1136; found: 337.1143; IR (ATR): ν_{max} 3063, 2920, 2851, 2815, 1611, 1587, 1538, 1492, 1446, 1369, 1306, 1288, 1146, 1106, 1072, 1023, 845, 807, 788, 738, 724, 685 cm⁻¹; LC-MS: purity 96.3% t_R= 31.78 min, (ESI) m/z [M+H]⁺ 338.1.

Synthesis of 1-(4-methyl ester phenyl)-4-(phenylsulfonyl)benzene, 139



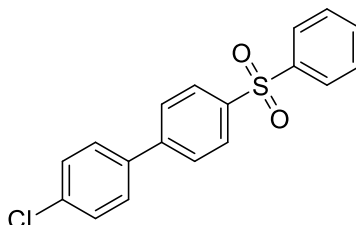
Neat (1*E*,3*E*,5*E*)-1,3-bis-phenylsulfonyl-(6-*p*-(methyl ester)phenyl)-hexa-1,3,5-triene **113** (150 mg, 0.30 mmol) was used as per the general procedure. The mobile phase for flash chromatography consisted of ethyl acetate/petroleum ether (75:25). Colourless crystals were obtained as the final product, 44% yield (47 mg). ¹H NMR (500 MHz, CDCl₃) δ 8.13-8.11 (m, 2 H), 8.04-8.02 (m, 2 H), 8.00-7.98 (m, 2 H), 7.74-7.72 (m, 2 H), 7.64-7.62 (m, 2 H), 7.60-7.57 (m, 1 H), 7.55-7.51 (m, 2 H), 3.94 (s, 3 H); ¹³C NMR (125 MHz, CDCl₃) δ 166.6, 145.0, 143.5, 141.6, 141.1, 133.3, 130.3, 130.2, 129.4, 128.3, 128.2, 127.7, 127.4, 52.3 ppm; HRMS (ESI-MS) Calc. for C₂₀H₁₆O₄S (M+H)⁺: 352.0769; found: 352.0777; IR (ATR): ν_{max} 3068, 2954, 1712, 1608, 1592, 1447, 1432, 1393, 1305, 1277, 1153, 1107, 1073, 1022, 1005, 873, 831, 770, 730, 714, 690 cm⁻¹; LC-MS: purity 95.8% t_R= 30.66 min, (ESI) m/z [M+Na]⁺ 375.1.

Synthesis of 1-(4-nitrophenyl)-4-(phenylsulfonyl)benzene, 140



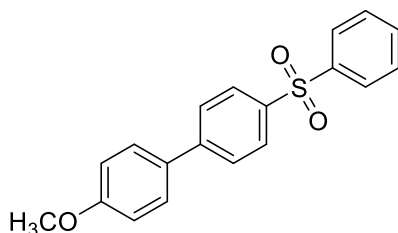
Neat (1*E*,3*E*,5*E*)-1,3-bis-phenylsulfonyl-(6-*p*-nitrophenyl)-hexa-1,3,5-triene **109** (150 mg, 0.31 mmol) was used as per the general procedure. The mobile phase for flash chromatography consisted of ethyl acetate/petroleum ether (2:8) until the top two spots were removed, followed by 4:6 of the same component mixture. White crystals were obtained as the final product, 44% yield (47 mg). ¹H NMR (500 MHz, CDCl₃) δ 8.33-8.31 (m, 2 H), 8.08-8.06 (m, 2 H), 8.00-7.98 (m, 2 H), 7.74-7.71 (m, 4 H), 7.62-7.59 (m, 1 H), 7.56-7.53 (m, 2 H); ¹³C NMR (125 MHz, CDCl₃) δ 148.0, 145.5, 143.6, 142.0, 141.4, 133.5, 129.4, 128.5, 128.3, 128.26, 127.8, 124.3 ppm; HRMS (ESI-MS) Calc. for C₁₈H₁₃O₄SN (M-H)⁺: 339.0565; found: 339.0561; IR (ATR): ν_{max} 3098, 3073, 1592, 1515, 1449, 1392, 1336, 1313, 1296, 1153, 1107, 1072, 1022, 1000, 873, 854, 831, 774, 755, 726, 713, 689, 678 cm⁻¹; LC-MS: purity 97.2% t_R= 30.59 min, (ESI) m/z [M+H]⁺ 340.2.

Synthesis of 1-(4-chlorophenyl)-4-(phenylsulfonyl)benzene, 141



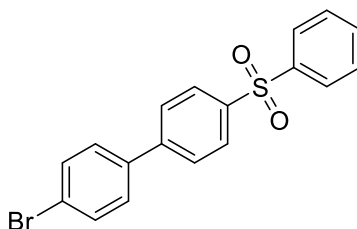
Neat (1*E*,3*E*,5*E*)-1,3-bis-phenylsulfonyl-(6-*p*-chlorophenyl)-hexa-1,3,5-triene **108** (150 mg, 0.32 mmol) was used as per the general procedure. The mobile phase for flash chromatography consisted of ethyl acetate/petroleum ether (15:85). White crystals were obtained as the final product, 64% yield (67 mg). Also performed on 1 mmol scale, 62% yield (203 mg). ¹H NMR (500 MHz, CDCl₃) δ 8.02-7.97 (m, 4 H), 7.67-7.65 (m, 2 H), 7.60-7.56 (m, 1 H), 7.54-7.52 (m, 2 H), 7.51-7.49 (m, 1 H), 7.485-7.48 (m, 1 H), 7.44-7.41 (m, 2 H); ¹³C NMR (125 MHz, CDCl₃) δ 144.9, 141.7, 140.6, 137.6, 134.9, 133.2, 129.4, 129.3, 128.6, 128.3, 127.8, 127.7 ppm; HRMS (ESI-MS) Calc. for C₁₈H₁₃O₂SCl (M+Na)⁺: 328.0325; found: 328.0330; IR (ATR): ν_{max} 3073, 1592, 1510, 1477, 1389, 1359, 1317, 1284, 1184, 1155, 1106, 1073, 1012, 1000, 973, 858, 829, 814, 780, 750, 734, 715, 681 cm⁻¹; LC-MS: purity 98.0% t_R= 33.64 min, (ESI) m/z [M+Na]⁺ 352.0.

Synthesis of 1-(4-methoxyphenyl)-4-(phenylsulfonyl)benzene, 142



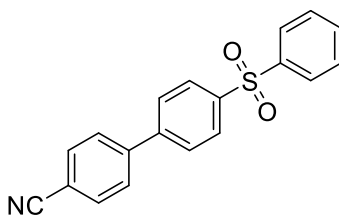
Neat (1*E*,3*E*,5*E*)-1,3-bis-phenylsulfonyl-(6-*p*-methoxyphenyl)-hexa-1,3,5-triene **107** (150 mg, 0.32 mmol) was used as per the general procedure. The mobile phase for flash chromatography consisted of ethyl acetate/petroleum ether (33:67). White crystals were obtained as the final product, 60% yield (62 mg). ¹H NMR (500 MHz, CDCl₃) δ 7.99-7.96 (m, 4 H), 7.67-7.65 (m, 2 H), 7.58-7.55 (m, 1 H), 7.53-7.50 (m, 4 H), 7.00-6.97 (m, 2 H), 3.85 (s, 3 H); ¹³C NMR (125 MHz, CDCl₃) δ 160.2, 145.8, 141.9, 139.4, 133.1, 131.5, 129.3, 128.5, 128.2, 127.6, 127.3, 114.5, 55.4 ppm; HRMS (ESI-MS) Calc. for C₁₉H₁₆O₃S (M+Na)⁺: 324.0820; found: 324.0824; IR (ATR): ν_{max} 3067, 3008, 2959, 2932, 2838, 1604, 1589, 1521, 1448, 1392, 1318, 1305, 1292, 1252, 1182, 1148, 1106, 1071, 1032, 1013, 998, 847, 824, 808, 763, 746, 717, 685 cm⁻¹; LC-MS: purity 96.9% t_R= 38.07 min, (ESI) m/z [M+H]⁺ 326.1.

Synthesis of 1-(4-bromophenyl)-4-(phenylsulfonyl)benzene 143



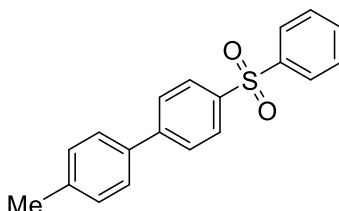
Neat (1*E*,3*E*,5*E*)-1,3-bis-phenylsulfonyl-6-(*p*-bromophenyl)-hexa-1,3,5-triene **112** (150 mg, 0.29 mmol) was used as per the general procedure. The mobile phase for flash chromatography consisted of ethyl acetate/petroleum ether (33:67). White crystals were obtained as the final product, 40% yield (44 mg). ¹H NMR (500 MHz, CDCl₃) δ 8.02-7.97 (m, 4 H), 7.67-7.65 (m, 2 H), 7.60-7.56 (m, 3 H), 7.54-7.51 (m, 2 H), 7.44-7.41 (m, 2 H); ¹³C NMR (125 MHz, CDCl₃) δ 144.9, 141.7, 140.6, 138.1, 133.3, 132.3, 129.4, 128.9, 128.4, 127.7, 127.68, 123.1 ppm; HRMS (ESI-MS) Calc. for C₁₈H₁₃O₂SBr (M+Na)⁺: 371.9820; found: 371.9820; IR (ATR): ν_{max} 3058, 1592, 1474, 1448, 1386, 1316, 1156, 1107, 1071, 1025, 1000, 963, 928, 858, 830, 813, 777, 749, 734, 716, 688, 679 cm⁻¹; LC-MS: purity 98.8% t_R= 34.07 min, (ESI) m/z [M+H]⁺ 373.9.

Synthesis of 1-(4-cyanophenyl)-4-(phenylsulfonyl)benzene 144



Neat (1*E*,3*E*,5*E*)-1,3-bis-phenylsulfonyl-(6-*p*-cyanophenyl)-hexa-1,3,5-triene **111** (150 mg, 0.32 mmol) was used as per the general procedure. The mobile phase for flash chromatography consisted of ethyl acetate/petroleum ether (25:75) until the top spot was removed, followed by 4:6 of the same component mixture. White crystals were obtained as the final product, 46% yield (48 mg). ¹H NMR (500 MHz, CDCl₃) δ 8.06-8.04 (m, 2 H), 8.00-7.98 (m, 2 H), 7.76-7.75 (m, 2 H), 7.71-7.69 (m, 2 H), 7.67-7.65 (m, 2 H), 7.61-7.58 (m, 1 H), 7.55-7.52 (m, 2 H); ¹³C NMR (125 MHz, CDCl₃) δ 144.0, 143.6, 141.7, 141.4, 133.4, 132.9, 129.4, 128.5, 128.2, 128.1, 127.8, 118.4, 112.4 ppm; HRMS (ESI-MS) Calc. for C₁₉H₁₃O₂SN (M+Na)⁺: 319.0667; found: 319.0669; IR (ATR): ν_{max} 3065, 2227, 1980, 1932, 1590, 1488, 1447, 1392, 1320, 1308, 1287, 1189, 1154, 1107, 1072, 998, 865, 837, 822, 760, 732, 717, 687 cm⁻¹; LC-MS: purity 99.3% t_R= 29.32 min, (ESI) m/z [M+K]⁺ 357.7.

Synthesis of 1-(4-methylphenyl)-4-(phenylsulfonyl)benzene 145



Neat (1*E*,3*E*,5*E*)-1,3-bis-phenylsulfonyl-(6-*p*-methylphenyl)-hexa-1,3,5-triene **116** (150 mg, 0.33 mmol) was used as per the general procedure. The mobile phase for flash chromatography consisted of ethyl acetate/petroleum ether (12:88). White crystals were obtained as the final product, 50% yield (51 mg). ¹H NMR (500 MHz, CDCl₃) δ 8.42-8.41 (m, 1 H), 7.60-7.53 (m, 2 H), 7.41-7.38 (m, 1 H), 7.26-7.24 (m, 2 H), 7.21-7.18 (m, 3 H), 7.00-6.99 (m, 2 H), 6.85-6.84 (m, 2 H), 2.38 (s, 3H); ¹³C NMR (125 MHz, CDCl₃) δ 142.4, 141.0, 139.8, 137.4, 135.2, 132.9, 132.8, 132.5, 129.9, 128.6, 128.2, 128.0, 127.8, 127.5, 21.3 ppm; HRMS (ESI-MS) Calc. for C₁₉H₁₆O₂S (M+H)⁺: 308.0871; found: 308.0879; IR (ATR): ν_{max} 3069, 3031, 2921, 2853, 1738, 1594, 1485, 1448, 1393, 1378, 1320, 1308, 1290, 1180, 1151, 1106, 1073, 998, 851, 804, 768, 746, 724, 711, 685 cm⁻¹; LC-MS: purity 97.4% t_R= 33.27 min, (ESI) m/z [M+H]⁺ 309.0.

3.4.4 General methods for the photophysical study of biaryls

3.4.4.1 Preparation of solutions

Compound **46** (0.24 mg) was weighed out using a five-figure balance and dissolved in chloroform (100 mL) using a 100 mL volumetric flask. The resulting solution, which corresponded to a concentration of 35 μM , was then examined for UV-absorbance. This was done for all biaryls, with the mass weighed out changed accordingly, and for all solutions alternatively made using methanol as the solvent. Alternatively, compound **46** (0.17 mg) was weighed out and dissolved in the same manner to give a 17.5 μM , and then for UV-absorbance. This was applied to all other biaryls but only using chloroform as the solvent.

2-Aminopyridine (0.94 mg) was weighed out using a five-figure balance and dissolved in 0.1 M sulfuric acid (100 mL) using a 100 mL volumetric flask. The resulting solution, which corresponded to a concentration of 100 μM , was then examined in the fluorescence study. A solution of quinine sulfate dihydrate (3.92 mg) was also prepared in the same way. These references were used for establishing the quantum yield only.

3.4.4.2 Fluorescence study

A UV-Vis spectrum of each 35 μM solution (in chloroform) was obtained in order to establish the absorbance λ_{max} and a serial dilution was performed in order to study each biaryl over a number of concentrations, the information from which was used to obtain the molar extinction coefficient (ϵ). For this purpose, the solutions of 17.5 μM concentration were assessed in the same way, in order to generate more data sets for establishing ϵ more precisely. The emission and excitation spectra for each solution was obtained, once the concentration of the respective solution was sufficiently low such that it corresponded to an optical density of approximately 0.1 (± 0.05). The absorbance λ_{max} for each solution was used as the excitation parameter to generate the emission spectrum, the data from which was used in the determination of the quantum yield. This emission maximum was in turn used as the emission parameter to generate the excitation spectrum. This method was applied to solutions of each biaryl in methanol additionally.

References

1. Langeveld, W. T.; Veldhuizen, E. J. A.; Burt, S. A., Synergy between essential oil components and antibiotics: a review. *Critical Reviews in Microbiology* **2014**, *40* (1), 76-94.
2. Guzman, J. D., Natural cinnamic acids, synthetic derivatives and hybrids with antimicrobial activity. *Molecules (Basel, Switzerland)* **2014**, *19* (12), 19292-19349.
3. Silva, L. N.; Zimmer, K. R.; Macedo, A. J.; Trentin, D. S., Plant Natural Products Targeting Bacterial Virulence Factors. *Chemical reviews* **2016**, *116* (16), 9162-9236.
4. Cassini, A.; Högberg, L. D.; Plachouras, D.; Quattrocchi, A.; Hoxha, A.; Simonsen, G. S.; Colomb-Cotinat, M.; Kretzschmar, M. E.; Devleeschauwer, B.; Cecchini, M.; Ouakrim, D. A.; Oliveira, T. C.; Struelens, M. J.; Suetens, C.; Monnet, D. L.; Strauss, R.; Mertens, K.; Struyf, T.; Catry, B.; Latour, K.; Ivanov, I. N.; Dobрева, E. G.; Tambic Andrašević, A.; Soprek, S.; Budimir, A.; Paphitou, N.; Žemlicková, H.; Schytte Olsen, S.; Wolff Sönksen, U.; Märtin, P.; Ivanova, M.; Lyytikäinen, O.; Jalava, J.; Coignard, B.; Eckmanns, T.; Abu Sin, M.; Haller, S.; Daikos, G. L.; Gikas, A.; Tsiodras, S.; Kontopidou, F.; Tóth, Á.; Hajdu, Á.; Guólaugsson, Ó.; Kristinsson, K. G.; Murchan, S.; Burns, K.; Pezzotti, P.; Gagliotti, C.; Dumpis, U.; Liuimiene, A.; Perrin, M.; Borg, M. A.; de Greeff, S. C.; Monen, J. C. M.; Koek, M. B. G.; Elstrøm, P.; Zabicka, D.; Deptula, A.; Hryniewicz, W.; Caniça, M.; Nogueira, P. J.; Fernandes, P. A.; Manageiro, V.; Popescu, G. A.; Serban, R. I.; Schréterová, E.; Litvová, S.; Štefkovicová, M.; Kolman, J.; Klavs, I.; Korošec, A.; Aracil, B.; Asensio, A.; Pérez-Vázquez, M.; Billström, H.; Larsson, S.; Reilly, J. S.; Johnson, A.; Hopkins, S., Attributable deaths and disability-adjusted life-years caused by infections with antibiotic-resistant bacteria in the EU and the European Economic Area in 2015: a population-level modelling analysis. *The Lancet Infectious Diseases* **2019**, *19* (1), 56-66.
5. Burt, S., Essential oils: their antibacterial properties and potential applications in foods—a review. *International Journal of Food Microbiology* **2004**, *94* (3), 223-253.
6. Calo, J. R.; Crandall, P. G.; O'Bryan, C. A.; Ricke, S. C., Essential oils as antimicrobials in food systems – A review. *Food Control* **2015**, *54*, 111-119.
7. Brewer, M. S.; Rojas, M., Consumer attitudes toward issues in food safety. *Journal of Food Safety* **2008**, *28* (1), 1-22.
8. Yossa, N.; Patel, J.; Millner, P.; Lo, Y. M., Essential oils reduce Escherichia coli O157:H7 and Salmonella on spinach leaves. *Journal of Food Protection* **2012**, *75* (3), 488-496.
9. Visvalingam, J.; Hernandez-Doria, J. D.; Holley, R. A., Examination of the Genome-Wide Transcriptional Response of Escherichia coli O157:H7 to Cinnamaldehyde Exposure. *Applied and Environmental Microbiology* **2013**, *79* (3), 942-950.
10. Nazzaro, F.; Fratianni, F.; De Martino, L.; Coppola, R.; De Feo, V., Effect of essential oils on pathogenic bacteria. *Pharmaceuticals (Basel, Switzerland)* **2013**, *6* (12), 1451-1474.
11. Shreaz, S.; Wani, W. A.; Behbehani, J. M.; Raja, V.; Irshad, M.; Karched, M.; Ali, I.; Siddiqi, W. A.; Hun, L. T., Cinnamaldehyde and its derivatives, a novel class of antifungal agents. *Fitoterapia* **2016**, *112*, 116-131.
12. Vasconcelos, N. G.; Croda, J.; Simionatto, S., Antibacterial mechanisms of cinnamon and its constituents: A review. *Microbial Pathogenesis* **2018**, *120*, 198-203.
13. Kwon, J. A.; Yu, C. B.; Park, H. D., Bacteriocidal effects and inhibition of cell separation of cinnamic aldehyde on Bacillus cereus. *Letters in Applied Microbiology* **2003**, *37* (1), 61-65.
14. Gill, A. O.; Holley, R. A., Mechanisms of Bacteriocidal Action of Cinnamaldehyde against Listeria monocytogenes and of Eugenol against L. monocytogenes and Lactobacillus sakei. *Applied and Environmental Microbiology* **2004**, *70* (10), 5750-5755.
15. Baskaran, S. A.; Amalaradjou, M. A. R.; Hoagland, T.; Venkitanarayanan, K., Inactivation of Escherichia coli O157:H7 in apple juice and apple cider by trans-cinnamaldehyde. *International Journal of Food Microbiology* **2010**, *141* (1), 126-129.

16. Firmino, D. F.; Cavalcante, T. T. A.; Gomes, G. A.; Firmino, N. C. S.; Rosa, L. D.; de Carvalho, M. G.; Catunda, F. E. A., Jr., Antibacterial and Antibiofilm Activities of Cinnamomum Sp. Essential Oil and Cinnamaldehyde: Antimicrobial Activities. *TheScientificWorldJournal* **2018**, *2018*, 7405736-7405736.
17. Friedman, M., Chemistry, Antimicrobial Mechanisms, and Antibiotic Activities of Cinnamaldehyde against Pathogenic Bacteria in Animal Feeds and Human Foods. *Journal of Agricultural and Food Chemistry* **2017**, *65* (48), 10406-10423.
18. Gill, A. O.; Holley, R. A., Disruption of Escherichia coli, Listeria monocytogenes and Lactobacillus sakei cellular membranes by plant oil aromatics. *International Journal of Food Microbiology* **2006**, *108* (1), 1-9.
19. Ashakirin, S. N.; Tripathy, M.; Patil, U. K.; Majeed, A. B. A., Chemistry and bioactivity of Cinnamaldehyde: a natural molecule of medicinal importance. *International Journal of Pharmaceutical Sciences and Research* **2017**, *8* (6), 2333.
20. Zhu, L.; Olsen, C.; McHugh, T.; Friedman, M.; Jaroni, D.; Ravishankar, S., Apple, Carrot, and Hibiscus Edible Films Containing the Plant Antimicrobials Carvacrol and Cinnamaldehyde Inactivate Salmonella Newport on Organic Leafy Greens in Sealed Plastic Bags. *Journal of Food Science* **2014**, *79* (1), M61-M66.
21. He, T. F.; Zhang, Z. H.; Zeng, X. A.; Wang, L. H.; Brennan, C. S., Determination of membrane disruption and genomic DNA binding of cinnamaldehyde to Escherichia coli by use of microbiological and spectroscopic techniques. *Journal of Photochemistry & Photobiology, B: Biology* **2018**, *178*, 623-630.
22. Reddy, A. M.; Seo, J. H.; Ryu, S. Y.; Kim, Y. S.; Kim, Y. S.; Min, K. R.; Kim, Y., Cinnamaldehyde and 2-methoxycinnamaldehyde as NF- κ B inhibitors from Cinnamomum cassia. *Planta Medica* **2004**, *70* (9), 823-827.
23. Guo, S.-Y.; Guo, J.-Y.; Huo, H.-R.; Zhao, B.-S.; Liu, H.-B.; Li, L.-F.; Ma, Y.-Y.; Jiang, T.-L., Cinnamaldehyde reduces IL-1 β -induced cyclooxygenase-2 activity in rat cerebral microvascular endothelial cells. *European Journal of Pharmacology* **2006**, *537* (1), 174-180.
24. Liao, J.-C.; Deng, J.-S.; Chiu, C.-S.; Hou, W.-C.; Huang, S.-S.; Shie, P.-H.; Huang, G.-J., Anti-inflammatory activities of Cinnamomum cassia constituents in vitro and in vivo. *Evidence-based Complementary and Alternative Medicine* **2012**, *2012*, 429320-429320.
25. Wei, Q.-Y.; Xiong, J.-J.; Jiang, H.; Zhang, C.; Ye, W., The antimicrobial activities of the cinnamaldehyde adducts with amino acids. *International Journal of Food Microbiology* **2011**, *150* (2), 164-170.
26. Bhatia, R.; Shreaz, S.; Khan, N.; Muralidhar, S.; Basir, S. F.; Manzoor, N.; Khan, L. A., Proton pumping ATPase mediated fungicidal activity of two essential oil components. *Journal of basic microbiology* **2012**, *52* (5), 504-512.
27. Morozumi, S., Isolation, purification, and antibiotic activity of o-methoxycinnamaldehyde from cinnamon. *Applied and Environmental Microbiology* **1978**, *36* (4), 577-583.
28. Jiang, J.; Emont, M. P.; Jun, H.; Qiao, X.; Liao, J.; Kim, D.-i.; Wu, J., Cinnamaldehyde induces fat cell-autonomous thermogenesis and metabolic reprogramming. *Metabolism* **2017**, *77*, 58-64.
29. Camacho, S.; Michlig, S.; de Senarclens-Bezençon, C.; Meylan, J.; Meystre, J.; Pezzoli, M.; Markram, H.; le Coutre, J., Anti-obesity and anti-hyperglycemic effects of cinnamaldehyde via altered ghrelin secretion and functional impact on food intake and gastric emptying. *Scientific reports* **2015**, *5* (1), 7919.
30. Tamura, Y.; Iwasaki, Y.; Narukawa, M.; Watanabe, T., Ingestion of Cinnamaldehyde, a TRPA1 Agonist, Reduces Visceral Fats in Mice Fed a High-Fat and High-Sucrose Diet. *Journal of Nutritional Science and Vitaminology* **2012**, *58* (1), 9-13.

31. Masamoto, Y.; Kawabata, F.; Fushiki, T., Intragastric Administration of TRPV1, TRPV3, TRPM8, and TRPA1 Agonists Modulates Autonomic Thermoregulation in Different Manners in Mice. *Bioscience, Biotechnology, and Biochemistry* **2009**, *73* (5), 1021-1027.
32. Michlig, S.; Merlini, J. M.; Beaumont, M.; Ledda, M.; Tavenard, A.; Mukherjee, R.; Camacho, S.; le Coutre, J., Effects of TRP channel agonist ingestion on metabolism and autonomic nervous system in a randomized clinical trial of healthy subjects. *Scientific reports* **2016**, *6* (1), 20795.
33. Chen, B.-J.; Fu, C.-S.; Li, G.-H.; Wang, X.-N.; Lou, H.-X.; Ren, D.-M.; Shen, T., Cinnamaldehyde Analogues as Potential Therapeutic Agents. *Mini reviews in medicinal chemistry* **2017**, *17* (1), 33-43.
34. Rao, P. V.; Gan, S. H., Cinnamon: a multifaceted medicinal plant. *Evidence-based complementary and alternative medicine : eCAM* **2014**, *2014*, 642942-12.
35. Zhang, Y.; Li, S.; Kong, X., Relationship between antimold activity and molecular structure of cinnamaldehyde analogues. *Bioorganic & Medicinal Chemistry Letters* **2013**, *23* (5), 1358-1364.
36. Lee, H.-S.; Kim, S.-Y.; Lee, C.-H.; Ahn, Y.-J., Cytotoxic and mutagenic effects of Cinnamomum cassia bark-derived materials. *Journal of Microbiology and Biotechnology* **2004**, *14* (6), 1176-1181.
37. Imai, T.; Yasuhara, K.; Tamura, T.; Takizawa, T.; Ueda, M.; Hirose, M.; Mitsumori, K., Inhibitory effects of cinnamaldehyde on 4-(methylnitrosamino)-1-(3-pyridyl)-1-butanone-induced lung carcinogenesis in rasH2 mice. *Cancer Letters* **2002**, *175* (1), 9-16.
38. Wu, S.-J.; Ng, L.-T.; Lin, C.-C., Cinnamaldehyde-induced apoptosis in human PLC/PRF/5 cells through activation of the proapoptotic Bcl-2 family proteins and MAPK pathway. *Life Sciences* **2005**, *77* (8), 938-951.
39. Banjerdpongchai, R.; Punyati, P.; Nakrob, A.; Pompimon, W.; Kongtawelert, P., 4'-hydroxycinnamaldehyde from *Alpinia galanga* (Linn.) induces human leukemic cell apoptosis via mitochondrial and endoplasmic reticulum stress pathways. *Asian Pacific Journal of Cancer Prevention* **2011**, *12* (3), 593-598.
40. Kim, S.-A.; Sung, Y.-K.; Kwon, B.-M.; Yoon, J.-H.; Lee, H.; Ahn, S.-G.; Hong, S.-H., 2'-Hydroxycinnamaldehyde shows antitumor activity against oral cancer in vitro and in vivo in a rat tumor model. *Anticancer Research* **2010**, *30* (2), 489-494.
41. Kang, H.-S.; Ock, J.; Lee, H.-J.; Lee, Y.-J.; Kwon, B.-M.; Hong, S.-H., Early growth response protein 1 upregulation and nuclear translocation by 2'-benzoyloxycinnamaldehyde induces prostate cancer cell death. *Cancer Letters* **2012**, *329* (2), 217-227.
42. Lee, M. A.; Park, H. J.; Chung, H.-J.; Kim, W. K.; Lee, S. K., Antitumor Activity of 2-Hydroxycinnamaldehyde for Human Colon Cancer Cells through Suppression of β -Catenin Signaling. *Journal of Natural Products* **2013**, *76* (7), 1278-1284.
43. Shin, D.-S.; Kim, H.-M.; Kim, J.-H.; Kim, K.-R.; Lee, S. J.; Lee, S.-K.; Han, D. C.; Son, K.-H.; Cheon, H.-G.; Sung, N.-D.; Kang, S. K.; Kwon, B.-M., Synthesis and biological evaluation of dimeric cinnamaldehydes as potent antitumor agents. *Bioorganic & Medicinal Chemistry* **2006**, *14* (8), 2498-2506.
44. Hong, S. H.; Kim, J.; Kim, J.-M.; Lee, S.-Y.; Shin, D.-S.; Son, K.-H.; Han, D. C.; Sung, Y. K.; Kwon, B.-M., Apoptosis induction of 2'-hydroxycinnamaldehyde as a proteasome inhibitor is associated with ER stress and mitochondrial perturbation in cancer cells. *Biochemical Pharmacology* **2007**, *74* (4), 557-565.
45. Gan, F. F.; Chua, Y. S.; Scarmagnani, S.; Palaniappan, P.; Franks, M.; Poobalasingam, T.; Bradshaw, T. D.; Westwell, A. D.; Hagen, T., Structure-activity analysis of 2'-modified cinnamaldehyde analogues as potential anticancer agents. *Biochemical and Biophysical Research Communications* **2009**, *387* (4), 741-747.

46. Chew, E.-H.; Nagle, A. A.; Zhang, Y.; Scarmagnani, S.; Palaniappan, P.; Bradshaw, T. D.; Holmgren, A.; Westwell, A. D., Cinnamaldehydes inhibit thioredoxin reductase and induce Nrf2: potential candidates for cancer therapy and chemoprevention. *Free Radical Biology and Medicine* **2010**, *48* (1), 98-111.
47. Nagle, A. A.; Gan, F.-F.; Jones, G.; So, C.-L.; Wells, G.; Chew, E.-H., Induction of Tumor Cell Death through Targeting Tubulin and Evoking Dysregulation of Cell Cycle Regulatory Proteins by Multifunctional Cinnamaldehydes. *PLOS ONE* **2012**, *7* (11), e50125.
48. Min, G.; Lee, S.-K.; Lee, R.-H.; Kim, H.-N.; Han, Y.-M.; Han, D. C.; Jeong, D. G.; Kwon, B.-M., Rhodanine-based PRL-3 inhibitors blocked the migration and invasion of metastatic cancer cells. *Bioorganic & Medicinal Chemistry Letters* **2013**, *23* (13), 3769-3774.
49. Cabello, C. M.; Bair, W. B.; Lamore, S. D.; Ley, S.; Bause, A. S.; Azimian, S.; Wondrak, G. T., The cinnamon-derived Michael acceptor cinnamic aldehyde impairs melanoma cell proliferation, invasiveness, and tumor growth. *Free Radical Biology and Medicine* **2009**, *46* (2), 220-231.
50. Motohashi, N.; Yamagami, C.; Tokuda, H.; Okuda, Y.; Ichiishi, E.; Mukainaka, T.; Nishino, H.; Saito, Y., Structure–activity relationship in potentially anti-tumor promoting benzalacetone derivatives, as assayed by the Epstein–Barr virus early antigen activation. *Mut.Res.-Genetic Toxicology and Environmental Mutagenesis* **2000**, *464* (2), 247-254.
51. Jeong, H.-W.; Kim, M.-R.; Son, K.-H.; Young Han, M.; Ha, J.-H.; Garnier, M.; Meijer, L.; Kwon, B.-M., Cinnamaldehydes inhibit cyclin dependent kinase 4/cyclin D1. *Bioorganic & Medicinal Chemistry Letters* **2000**, *10* (16), 1819-1822.
52. Li, X. Q.; Liu, X. X.; Wang, X. Y.; Xie, Y. H.; Yang, Q.; Ding, Y. Y.; Gao, W.; Wang, S. W., Cinnamaldehyde Derivatives Inhibit Coxsackievirus B3-Induced Viral Myocarditis. *BIOMOLECULES & THERAPEUTICS* **2017**, *25* (3), 279-287.
53. Song, F.; Li, H.; Sun, J.; Wang, S., Protective effects of cinnamic acid and cinnamic aldehyde on isoproterenol-induced acute myocardial ischemia in rats. *Journal of Ethnopharmacology* **2013**, *150* (1), 125-130.
54. Hwa, J. S.; Jin, Y. C.; Lee, Y. S.; Lee, J. H.; Ko, Y. S.; Kim, Y. S.; Kim, Y. M.; Kim, H. J.; Shi, L. Y.; Ngoc, T. M.; Bae, K. H.; Chang, K. C., 2-Methoxycinnamaldehyde from *Cinnamomum cassia* reduces rat myocardial ischemia and reperfusion injury in vivo due to HO-1 induction. *Journal of Ethnopharmacology* **2012**, *139* (2), 605-615.
55. Xue, Y.-L.; Shi, H.-X.; Murad, F.; Bian, K., Vasodilatory effects of cinnamaldehyde and its mechanism of action in the rat aorta. *Vascular Health and Risk Management* **2011**, *7* (1), 273-280.
56. Kwon, B.-M.; Kwon, J.-Y.; Hong, S.-H.; Park, S.-D.; Ahn, S.-G.; Yoon, J.-H.; Kim, S.-A., 2'-Benzoyloxycinnamaldehyde inhibits nitric oxide production in lipopolysaccharide-stimulated RAW 264.7 cells via regulation of AP-1 pathway. *European Journal of Pharmacology* **2012**, *696* (1-3), 179-186.
57. Shreaz, S.; Bhatia, R.; Khan, L. A.; Khan, N.; Maurya, I. K.; Ahmad, S. I.; Muralidhar, S.; Manzoor, N., Cinnamic aldehydes affect hydrolytic enzyme secretion and morphogenesis in oral *Candida* isolates. *Microbial Pathogenesis* **2012**, *52* (5), 251-258.
58. Shreaz, S.; Bhatia, R.; Khan, N.; Muralidhar, S.; Manzoor, N.; Khan, L. A., Influences of cinnamic aldehydes on H⁺ extrusion activity and ultrastructure of *Candida*. *Journal of Medical Microbiology* **2013**, *62* (2), 232-240.
59. Brackman, G.; Celen, S.; Hillaert, U.; Van Calenbergh, S.; Cos, P.; Maes, L.; Nelis, H. J.; Coenye, T., Structure-Activity Relationship of Cinnamaldehyde Analogs as Inhibitors of AI-2 Based Quorum Sensing and Their Effect on Virulence of *Vibrio* spp. *PLOS ONE* **2011**, *6* (1), e16084.

60. Sadofsky, L. R.; Boa, A. N.; Maher, S. A.; Birrell, M. A.; Belvisi, M. G.; Morice, A. H., TRPA1 is activated by direct addition of cysteine residues to the N-hydroxysuccinyl esters of acrylic and cinnamic acids. *Pharmacological Research* **2011**, *63* (1), 30-36.
61. Autelitano, A.; Minassi, A.; Pagani, A.; Tagliatela-Scafati, O.; Appendino, G., The reaction of cinnamaldehyde and cinnam(o)yl derivatives with thiols. *Acta Pharmaceutica Sinica B* **2017**, *7* (4), 523-526.
62. Avonto, C.; Avonto, C.; Tagliatela-Scafati, O.; Pollastro, F.; Minassi, A., An NMR Spectroscopic Method to Identify and Classify Thiol-Trapping Agents: Revival of Michael Acceptors for Drug Discovery? *Angewandte Chemie (International ed.)* **2011**, *50* (2), 467-471.
63. Ye, H.; Shen, S.; Xu, J.; Lin, S.; Yuan, Y.; Jones, G. S., Synergistic interactions of cinnamaldehyde in combination with carvacrol against food-borne bacteria. *Food Control* **2013**, *34* (2), 619-623.
64. Upadhyay, A.; Arsi, K.; Wagle, B. R.; Upadhyaya, I.; Shrestha, S.; Donoghue, A. M.; Donoghue, D. J., Trans-Cinnamaldehyde, Carvacrol, and Eugenol Reduce *Campylobacter jejuni* Colonization Factors and Expression of Virulence Genes in Vitro. *Frontiers in Microbiology* **2017**, *8*, 713.
65. Wang, H.; Yuan, H.; Li, S.; Li, Z.; Jiang, M., Synthesis, antimicrobial activity of Schiff base compounds of cinnamaldehyde and amino acids. *Bioorganic & Medicinal Chemistry Letters* **2016**, *26* (3), 809-813.
66. Liu, T.-T.; Tseng, Y.-W.; Yang, T.-S., Functionalities of conjugated compounds of γ -aminobutyric acid with salicylaldehyde or cinnamaldehyde. *Food Chemistry* **2016**, *190*, 1102-1108.
67. Shen, Q.; Zhou, W.; Hu, L.; Qi, Y.; Ning, H.; Chen, J.; Mo, H., Bactericidal activity of alpha-bromocinnamaldehyde against persisters in *Escherichia coli*. *PLoS one* **2017**, *12* (7), e0182122.
68. Doyle, A. A.; Stephens, J. C., A review of cinnamaldehyde and its derivatives as antibacterial agents. *Fitoterapia* **2019**, *139*, 104405.
69. Zhang, S.; Xie, H.; Song, A.; Wu, D.; Zhu, J.; Zhao, S.; Li, J.; Yu, X.; Wang, W., Efficient preparation of trans- α,β -unsaturated aldehydes from saturated aldehydes by oxidative enamine catalysis. *Science China Chemistry* **2011**, *54* (12), 1932-1936.
70. Chen, X.; Zhang, Y.; Wan, H.; Wang, W.; Zhang, S., Stereoselective organocatalytic oxidation of alcohols to enals: A homologation method to prepare polyenes. *Chemical Communications* **2016**, *52* (17), 3532-3535.
71. Liu, J.; Zhu, J.; Jiang, H.; Wang, W.; Li, J., Pd-catalyzed cascade Heck-Saegusa: Direct synthesis of enals from aryl iodides and allyl alcohol. *Chemical Communications* **2010**, *46* (3), 415-417.
72. Kim, E.; Koh, M.; Lim, B. J.; Park, S. B., Emission wavelength prediction of a full-color-tunable fluorescent core skeleton, 9-aryl-1,2-dihydropyrrolo[3,4-b]indolizin-3-one. *Journal of the American Chemical Society* **2011**, *133* (17), 6642-6649.
73. Morack, T.; Mück-Lichtenfeld, C.; Gilmour, R., Bioinspired Radical Stetter Reaction: Radical Umpolung Enabled by Ion-Pair Photocatalysis. *Angewandte Chemie International Edition* **2019**, *58* (4), 1208-1212.
74. Zhang, S.-L.; Xie, H.-X.; Zhu, J.; Li, H.; Zhang, X.-S.; Li, J.; Wang, W., Organocatalytic enantioselective β -functionalization of aldehydes by oxidation of enamines and their application in cascade reactions. *Nature Communications* **2011**, *2* (1), 211.
75. Zhu, J.; Liu, J.; Ma, R.; Xie, H.; Li, J.; Jiang, H.; Wang, W., A Direct Amine-Palladium Acetate Cocatalyzed Saegusa Oxidation Reaction of Unmodified Aldehydes to α,β -Unsaturated Aldehydes. *Advanced Synthesis & Catalysis* **2009**, *351* (9), 1229-1232.

76. Dess, D. B.; Martin, J. C., Readily accessible 12-I-5 oxidant for the conversion of primary and secondary alcohols to aldehydes and ketones. *The Journal of Organic Chemistry* **1983**, *48* (22), 4155-4156.
77. Byrne, P. A.; Gilheany, D. G., The modern interpretation of the Wittig reaction mechanism. *Chemical Society Reviews* **2013**, *42* (16), 6670-6696.
78. Wittig, G.; Geissler, G., Zur Reaktionsweise des Pentaphenyl-phosphors und einiger Derivate. *Justus Liebigs Annalen der Chemie* **1953**, *580* (1), 44-57.
79. Rodrigo, E.; García Ruano, J. L.; Cid, M. B., Organocatalytic Michael Addition/Intramolecular Julia–Kocienski Olefination for the Preparation of Nitrocyclohexenes. *The Journal of Organic Chemistry* **2013**, *78* (21), 10737-10746.
80. Challa, C.; Vellekkatt, J.; Ravindran, J.; Lankalapalli, R. S., A metal-free one-pot cascade synthesis of highly functionalized biaryl-2-carbaldehydes. *Organic & Biomolecular Chemistry* **2014**, *12* (43), 8588-8592.
81. Šagud, I.; Faraguna, F.; Marinić, Ž.; Šindler-Kulyk, M., Photochemical Approach to Naphthoxazoles and Fused Heterobenzoxazoles from 5-(Phenyl/heteroarylethenyl)oxazoles. *The Journal of Organic Chemistry* **2011**, *76* (8), 2904-2908.
82. I, I. B. W.; G, K. H.; W, N. V. D. M. A.; G, K. C.; ARNOLD, L. V.; JAN, Z. SULFONYLPYRAZOLE AND SULFONYLPYRAZOLINE CARBOXAMIDINE DERIVATIVES AS 5-HT6 ANTAGONISTS. 2008.
83. Paul, S.; Gorai, T.; Koley, A.; Ray, J. K., A simple route to 9-fluorenylidenes by domino Suzuki/Heck coupling reactions. *Tetrahedron Letters* **2011**, *52* (31), 4051-4055.
84. Cresp, T. M.; Sargent, M. V.; Vogel, P., A synthesis of $\alpha\beta$ -unsaturated aldehydes. *J. Chem. Soc., Perkin Trans. 1* **1974**, 37-41.
85. Takekuma, S.-I.; Matsuoka, H.; Ogawa, S.; Shibasaki, Y.; Minematsu, T., Preparation, crystal structures, and spectroscopic and chemical properties of 2,4,6-trifluorophenyl-or 4-(methoxycarbonyl)-Phenyl-substituted (E)-1-(3-guaiazulenyl)ethylene and (2E,4E)-1-(3-guaiazulenyl)-1,3-butadiene derivatives. *Bulletin of the Chemical Society of Japan* **2010**, *83* (10), 1248-1263.
86. McGarraugh, P. G.; Jones, J. H.; Brenner-Moyer, S. E., A general organocatalyzed Michael-Michael cascade reaction generates functionalized cyclohexenes. *Journal of Organic Chemistry* **2011**, *76* (15), 6309-6319.
87. Knolker, H. J.; Baum, G.; Foitzik, N.; Goesmann, H.; Gonser, P.; Jones, P. G.; Rottele, H., Transition metal complexes in organic synthesis. 41 - Synthesis, molecular structure, fluxional behavior, and tricarbonyliron transfer reactions of (eta(4)-1-azabuta-1,3-diene)tricarbonyliron complexes. *European Journal of Inorganic Chemistry* **1998**, (7), 993-1007.
88. Mathur, S.; Hoskins, C., Drug development: Lessons from nature. *Biomedical reports* **2017**, *6* (6), 612-614.
89. Calixto, J. B., Efficacy, safety, quality control, marketing and regulatory guidelines for herbal medicines (phytotherapeutic agents). *Brazilian Journal of Medical and Biological Research* **2000**, *33*, 179-189.
90. Karimi, A.; Majlesi, M.; Rafieian-Kopaei, M., Herbal versus synthetic drugs; beliefs and facts. *Journal of nephro pharmacology* **2015**, *4* (1), 27-30.
91. Kelada, M.; Walsh, J. M. D.; Devine, R. W.; McArdle, P.; Stephens, J. C., Synthesis of pyrazolopyrimidinones using a "one-pot" approach under microwave irradiation. *Beilstein Journal of Organic Chemistry* **2018**, *14*, 1222-1228.
92. Gavrin, L. K.; Lee, A.; Provencher, B. A.; Massefski, W. W.; Huhn, S. D.; Ciszewski, G. M.; Cole, D. C.; McKew, J. C., Synthesis of Pyrazolo[1,5- α]pyrimidinone Regioisomers. *The Journal of Organic Chemistry* **2007**, *72* (3), 1043-1046.

93. Bondock, S.; Fadaly, W.; Metwally, M. A., Synthesis and antimicrobial activity of some new thiazole, thiophene and pyrazole derivatives containing benzothiazole moiety. *European Journal of Medicinal Chemistry* **2010**, *45* (9), 3692-3701.
94. Abdallah, A.; Elgemeie, G., Design, synthesis, docking, and antimicrobial evaluation of some novel pyrazolo[1,5-a]pyrimidines and their corresponding cycloalkane ring-fused derivatives as purine analogs. *Drug Des Devel Ther.* **2018**, *12*, 1785-1798.
95. Shaikh, B. M.; Konda, S. G.; Chobe, S. S.; Mandawad, G. G.; Yemul, O. S.; Dawane, B. S., PEG-400 : prompted eco-friendly synthesis of some novel pyrazolo[1,5-a]pyrimidine derivatives and their in vitro antimicrobial evaluation. *J. Chem. Pharm. Res.* **2011**, *3* (2), 435-443.
96. Dorman, H. J. D.; Deans, S. G., Antimicrobial agents from plants: antibacterial activity of plant volatile oils. *Journal of Applied Microbiology* **2000**, *88* (2), 308-316.
97. Mousavi, F.; Bojko, B.; Bessonneau, V.; Pawliszyn, J., Cinnamaldehyde Characterization as an Antibacterial Agent toward E. coli Metabolic Profile Using 96-Blade Solid-Phase Microextraction Coupled to Liquid Chromatography-Mass Spectrometry. *Journal of Proteome Research* **2016**, *15* (3), 963-975.
98. Doyle, A. A.; Krämer, T.; Kavanagh, K.; Stephens, J. C., Cinnamaldehydes: Synthesis, antibacterial evaluation, and the effect of molecular structure on antibacterial activity. *Results in Chemistry* **2019**, *1*, 100013.
99. Frigerio, M.; Santagostino, M.; Sputore, S., A User-Friendly Entry to 2-Iodoxybenzoic Acid (IBX). *The Journal of Organic Chemistry* **1999**, *64* (12), 4537-4538.
100. Uyanik, M.; Ishihara, K., Hypervalent iodine-mediated oxidation of alcohols. *Chemical Communications* **2009**, (16), 2086-2099.
101. Huang, H.; Yu, C.; Li, X.; Zhang, Y.; Zhang, Y.; Chen, X.; Mariano, P. S.; Xie, H.; Wang, W., Synthesis of Aldehydes by Organocatalytic Formylation Reactions of Boronic Acids with Glyoxylic Acid. *Angewandte Chemie International Edition* **2017**, *56* (28), 8201-8205.
102. Yamazaki, S.; Sugiura, H.; Ohashi, S.; Ishizuka, K.; Saimu, R.; Mikata, Y.; Ogawa, A., Intramolecular [2 + 2] and [4 + 2] Cycloaddition Reactions of Cinnamylamides of Ethenetricarboxylate in Sequential Processes. *Journal of Organic Chemistry* **2016**, *81* (22), 10863-10886.
103. Vedejs, E.; Meier, G. P.; Snoble, K. A. J., Low-temperature characterization of the intermediates in the Wittig reaction. *Journal of the American Chemical Society* **1981**, *103* (10), 2823-2831.
104. Vedejs, E.; Marth, C. F., Mechanism of Wittig reaction: evidence against betaine intermediates. *Journal of the American Chemical Society* **1990**, *112* (10), 3905-3909.
105. Wittig, G.; Schöllkopf, U., Über Triphenyl-phosphin-methylene als olefinbildende Reagenzien (I. Mitteil. *Chemische Berichte* **1954**, *87* (9), 1318-1330.
106. Byrne, P. A.; Gilheany, D. G., Unequivocal Experimental Evidence for a Unified Lithium Salt-Free Wittig Reaction Mechanism for All Phosphonium Ylide Types: Reactions with β -Heteroatom-Substituted Aldehydes Are Consistently Selective for cis-Oxaphosphetane-Derived Products. *Journal of the American Chemical Society* **2012**, *134* (22), 9225-9239.
107. Robiette, R.; Richardson, J.; Aggarwal, V. K.; Harvey, J. N., On the Origin of High E Selectivity in the Wittig Reaction of Stabilized Ylides: Importance of Dipole-Dipole Interactions. *Journal of the American Chemical Society* **2005**, *127* (39), 13468-13469.
108. Sunnerheim, K.; Nordqvist, A.; Nordlander, G.; Borg-Karlson, A. K.; Unelius, C. R.; Bohman, B.; Nordenhem, H.; Hellqvist, C.; Karlen, A.; Högskolan i, K.; Naturvetenskapliga, i., Quantitative structure-activity relationships of pine weevil antifeedants, a Multivariate approach. *Journal of Agricultural and Food Chemistry* **2007**, *55* (23), 9365-9372.

109. Patil, N. T.; Singh, V., Synthesis of 1,3,5-trisubstituted pyrazolines via Zn(II)-catalyzed double hydroamination of enynes with aryl hydrazines. *Chemical Communications* **2011**, 47 (39), 11116-11118.
110. Fischer, E.; Speier, A., Darstellung der Ester. *Berichte der deutschen chemischen Gesellschaft* **1895**, 28 (3), 3252-3258.
111. Zimmermann, H.; Rudolph, J., Protonic States and the Mechanism of Acid-Catalysed Esterification. *Angewandte Chemie International Edition in English* **1965**, 4 (1), 40-49.
112. Bruice, P. Y., *Organic chemistry*. . Pearson/Prentice Hall.: Upper Saddle River, NJ, 2004.
113. Miller, A. E. G.; Biss, J. W.; Schwartzman, L. H., Reductions with Dialkylaluminum Hydrides. *The Journal of Organic Chemistry* **1959**, 24 (5), 627-630.
114. Taylor, R. J. K.; Reid, M.; Foot, J.; Raw, S. A., Tandem Oxidation Processes Using Manganese Dioxide: Discovery, Applications, and Current Studies. *Accounts of Chemical Research* **2005**, 38 (11), 851-869.
115. Fatiadi, A. J., Active manganese dioxide oxidation in organic chemistry — Part I. *Synthesis (Germany)* **1976**, 1976 (2), 65-104.
116. Ncube, N. S.; Afolayan, A. J.; Okoh, A. I., Assessment techniques of antimicrobial properties of natural compounds of plant origin: current methods and future trends. *African Journal of Biotechnology* **2008**, 7 (12), 1797-1806.
117. Jorgensen, J. H.; Ferraro, M. J., Antimicrobial Susceptibility Testing: A Review of General Principles and Contemporary Practices. *Clinical Infectious Diseases* **2009**, 49 (11), 1749-1755.
118. Schumacher, A.; Vranken, T.; Malhotra, A.; Arts, J. J. C.; Habibovic, P., In vitro antimicrobial susceptibility testing methods: agar dilution to 3D tissue-engineered models. *European Journal of Clinical Microbiology & Infectious Diseases* **2018**, 37 (2), 187-208.
119. Mounyr Balouiri Moulay Sadiki Saad Koraiçlai, I., Methods for in vitro evaluating antimicrobial activity : A review. *药物分析学报 : 英文版* **2016**, 6 (2), 71-79.
120. Das, K.; Tiwari, R. K. S.; Shrivastava, D. K., Techniques for evaluation of medicinal plant products as antimicrobial agent: Current methods and future trends. *Journal of Medicinal Plants Research* **2010**, 4 (2), 104-111.
121. *CLSI. Performance Standards for Antimicrobial Disk Susceptibility Tests; Approved Standard—Eleventh Edition. Wayne, PA: Clinical and Laboratory Standards Institute. 2012; CLSI document M02-A11 32(1). 2012.*
122. Parr, R. G.; Szentpály, L. v.; Liu, S., Electrophilicity Index. *Journal of the American Chemical Society* **1999**, 121 (9), 1922-1924.
123. Rowan, R.; Moran, C.; McCann, M.; Kavanagh, K., Use of *Galleria mellonella* larvae to evaluate the in vivo anti-fungal activity of [Ag₂(mal)(phen)₃]. *BioMetals* **2009**, 22 (3), 461-467.
124. Au - Ramarao, N.; Au - Nielsen-Leroux, C.; Au - Lereclus, D., The Insect *Galleria mellonella* as a Powerful Infection Model to Investigate Bacterial Pathogenesis. *JoVE* **2012**, (70), e4392.
125. Fuchs, B. B.; O'Brien, E.; El Khoury, J. B.; Mylonakis, E., Methods for using *Galleria mellonella* as a model host to study fungal pathogenesis. *Virulence* **2010**, 1 (6), 475-482.
126. Mukherjee, K.; Altincicek, B.; Hain, T.; Domann, E.; Vilcinskis, A.; Chakraborty, T., *Galleria mellonella* as a Model System for Studying *Listeria* Pathogenesis. *Applied and Environmental Microbiology* **2010**, 76 (1), 310.
127. Brennan, M.; Thomas, D. Y.; Whiteway, M.; Kavanagh, K., Correlation between virulence of *Candida albicans* mutants in mice and *Galleria mellonella* larvae. *FEMS Immunology & Medical Microbiology* **2002**, 34 (2), 153-157.

128. Peleg, A. Y.; Monga, D.; Pillai, S.; Mylonakis, E.; Moellering, R. C., Jr.; Eliopoulos, G. M., Reduced Susceptibility to vancomycin influences pathogenicity in *Staphylococcus aureus* infection. *The Journal of Infectious Diseases* **2009**, *199* (4), 532-536.
129. McCann, M.; Santos, A. L. S.; da Silva, B. A.; Romanos, M. T. V.; Pyrrho, A. S.; Devereux, M.; Kavanagh, K.; Fichtner, I.; Kellett, A., In vitro and in vivo studies into the biological activities of 1,10-phenanthroline, 1,10-phenanthroline-5,6-dione and its copper(ii) and silver(i) complexes. *Toxicology Research* **2012**, *1* (1), 47-54.
130. Kellett, A.; O'Connor, M.; McCann, M.; Howe, O.; Casey, A.; McCarron, P.; Kavanagh, K.; McNamara, M.; Kennedy, S.; May, D. D.; Skell, P. S.; O'Shea, D.; Devereux, M., Water-soluble bis(1,10-phenanthroline) octanedioate Cu²⁺ and Mn²⁺ complexes with unprecedented nano and picomolar in vitro cytotoxicity: promising leads for chemotherapeutic drug development. *MedChemComm* **2011**, *2* (7), 579-584.
131. Desbois, A. P.; Coote, P. J., Wax moth larva (*Galleria mellonella*): an in vivo model for assessing the efficacy of antimicrobial agents. *Journal of Antimicrobial Chemotherapy* **2011**, *66* (8), 1785-1790.
132. Piatek, M.; Sheehan, G.; Kavanagh, K., Utilising *Galleria mellonella* larvae for studying in vivo activity of conventional and novel antimicrobial agents. *Pathogens and Disease* **2020**.
133. Dolan, N.; Gavin, D. P.; Eshwika, A.; Kavanagh, K.; McGinley, J.; Stephens, J. C., Synthesis, antibacterial and anti-MRSA activity, in vivo toxicity and a structure-activity relationship study of a quinoline thiourea. *Bioorganic & Medicinal Chemistry Letters* **2016**, *26* (2), 630-635.
134. Domadia, P.; Swarup, S.; Bhunia, A.; Sivaraman, J.; Dasgupta, D., Inhibition of bacterial cell division protein FtsZ by cinnamaldehyde. *Biochemical Pharmacology* **2007**, *74* (6), 831-840.
135. Ferro, T. A. F.; Araújo, J. M. M.; Pinto, B. L. d. S.; dos Santos, J. S.; Souza, E. B.; da Silva, B. L. R.; Colares, V. L. P.; Novais, T. M. G.; Filho, C. M. B.; Struve, C.; Calixto, J. B.; Monteiro-Neto, V.; da Silva, L. C. N.; Fernandes, E. S., Cinnamaldehyde inhibits *Staphylococcus aureus* virulence factors and protects against infection in a *Galleria mellonella* model. *Frontiers in Microbiology* **2016**, *7*.
136. Nowotarska, S. W.; Nowotarski, K.; Grant, I. R.; Elliott, C. T.; Friedman, M.; Situ, C., Mechanisms of Antimicrobial Action of Cinnamon and Oregano Oils, Cinnamaldehyde, Carvacrol, 2,5-Dihydroxybenzaldehyde, and 2-Hydroxy-5-Methoxybenzaldehyde against *Mycobacterium avium* subsp. *paratuberculosis* (Map). *Foods (Basel, Switzerland)* **2017**, *6* (9), 72.
137. Rao, J.; Chen, B.; McClements, D. J., Improving the Efficacy of Essential Oils as Antimicrobials in Foods: Mechanisms of Action. *Annual Review of Food Science and Technology* **2019**, *10* (1), 365-387.
138. Zhang, Y.; Liu, X.; Wang, Y.; Jiang, P.; Quek, S., Antibacterial activity and mechanism of cinnamon essential oil against *Escherichia coli* and *Staphylococcus aureus*. *Food Control* **2016**, *59*, 282-289.
139. Turgis, M.; Han, J.; Caillet, S.; Lacroix, M., Antimicrobial activity of mustard essential oil against *Escherichia coli* O157:H7 and *Salmonella typhi*. *Food Control* **2009**, *20* (12), 1073-1079.
140. Moghimi, R.; Ghaderi, L.; Rafati, H.; Aliahmadi, A.; McClements, D. J., Superior antibacterial activity of nanoemulsion of *Thymus daenensis* essential oil against *E. coli*. *Food Chemistry* **2016**, *194*, 410-415.
141. Oussalah, M.; Caillet, S.; Lacroix, M., Mechanism of Action of Spanish Oregano, Chinese Cinnamon, and Savory Essential Oils against Cell Membranes and Walls of *Escherichia coli* O157:H7 and *Listeria monocytogenes*. *Journal of Food Protection* **2006**, *69* (5), 1046-1055.
142. Shen, S.; Zhang, T.; Yuan, Y.; Lin, S.; Xu, J.; Ye, H., Effects of cinnamaldehyde on *Escherichia coli* and *Staphylococcus aureus* membrane. *Food Control* **2015**, *47*, 196-202.
143. He, F., Bradford Protein Assay. *Bio-protocol* **2011**, *1* (6), e45.

144. Kon, K. V.; Rai, M. K., Plant essential oils and their constituents in coping with multidrug-resistant bacteria. *Expert Review of Anti-infective Therapy* **2012**, *10* (7), 775-790.
145. Abdel Reheim, M. A. M.; Baker, S. M., Synthesis, characterization and in vitro antimicrobial activity of novel fused pyrazolo[3,4-c]pyridazine, pyrazolo[3,4-d]pyrimidine, thieno[3,2-c]pyrazole and pyrazolo[3',4':4,5]thieno[2,3-d]pyrimidine derivatives. *Chemistry Central journal* **2017**, *11* (1), 112-112.
146. Clancy, C. J.; Yu, V. L.; Morris, A. J.; Snyderman, D. R.; Nguyen, M. H., Fluconazole MIC and the fluconazole dose/MIC ratio correlate with therapeutic response among patients with candidemia. *Antimicrobial agents and chemotherapy* **2005**, *49* (8), 3171-3177.
147. Frazee, B. W.; Lynn, J.; Charlebois, E. D.; Lambert, L.; Lowery, D.; Perdreau-Remington, F., High Prevalence of Methicillin-Resistant Staphylococcus aureus in Emergency Department Skin and Soft Tissue Infections. *Annals of Emergency Medicine* **2005**, *45* (3), 311-320.
148. Lister, P. D.; Wolter, D. J.; Hanson, N. D., Antibacterial-Resistant Pseudomonas aeruginosa: Clinical Impact and Complex Regulation of Chromosomally Encoded Resistance Mechanisms. *Clinical Microbiology Reviews* **2009**, *22* (4), 582.
149. Jander, G.; Rahme, L. G.; Ausubel, F. M., Positive Correlation between Virulence of *Pseudomonas aeruginosa* Mutants in Mice and Insects. *Journal of Bacteriology* **2000**, *182* (13), 3843.
150. Washington, J. A., Discrepancies between in vitro activity of and in vivo response to antimicrobial agents. *Diagnostic Microbiology and Infectious Disease* **1983**, *1* (1), 25-31.
151. Trevijano-Contador, N.; Zaragoza, O., Immune Response of Galleria mellonella against Human Fungal Pathogens. *Journal of fungi (Basel, Switzerland)* **2018**, *5* (1), 3.
152. Smith, A.; McCann, M.; Kavanagh, K., Proteomic analysis of the proteins released from Staphylococcus aureus following exposure to Ag(I). *Toxicology in Vitro* **2013**, *27* (6), 1644-1648.
153. Pang, Z.; Raudonis, R.; Glick, B. R.; Lin, T.-J.; Cheng, Z., Antibiotic resistance in Pseudomonas aeruginosa: mechanisms and alternative therapeutic strategies. *Biotechnology Advances* **2019**, *37* (1), 177-192.
154. Čarský, P.; Hünig, S.; Stemmler, I.; Scheutzow, D., über zweistufige Redoxsysteme, XXVII. Vinyloge Bipyridyle und Bichinolye; Synthesen und UV/VIS-Spektren. *Liebigs Annalen der Chemie* **1980**, *1980* (2), 291-304.
155. Haraguchi, R.; Tanazawa, S. g.; Tokunaga, N.; Fukuzawa, S. i., Palladium-Catalyzed Formylation of Alkenylzinc Reagents with S-(4-Nitrophenyl) Thioformate. *European Journal of Organic Chemistry* **2018**, *2018* (15), 1761-1764.
156. Craig, D.; Slavov, N. K., A quantitative structure-reactivity relationship in decarboxylative Claisen rearrangement reactions of allylic tosylmalonate esters. *Chemical Communications* **2008**, (45), 6054-6056.
157. Yang, L.; Zeng, Q. L., Metal- and Acid-Free Methyl Triflate Catalyzed Meyer-Schuster Rearrangement. *SYNTHESIS-STUTTGART* **2017**, *49* (14), 3149-3156.
158. Nordqvist, A.; Björkelid, C.; Andaloussi, M.; Jansson, A. M.; Mowbray, S. L.; Karlén, A.; Larhed, M.; Medicinska och farmaceutiska, v.; Struktur- och, m.; Institutionen för cell- och, m.; Farmaceutiska, f.; Avdelningen för organisk farmaceutisk, k.; Teknisk-naturvetenskapliga, v.; Institutionen för, l.; Biologiska, s.; Uppsala, u., Synthesis of functionalized cinnamaldehyde derivatives by an oxidative heck reaction and their use as starting materials for preparation of Mycobacterium tuberculosis 1-deoxy-d-xylulose-5-phosphate reductoisomerase inhibitors. *Journal of Organic Chemistry* **2011**, *76* (21), 8986-8998.
159. Killoran, P. M.; Rossington, S. B.; Wilkinson, J. A.; Hadfield, J. A., Expanding the scope of the Babler–Dauben oxidation: 1,3-oxidative transposition of secondary allylic alcohols. *Tetrahedron Letters* **2016**, *57* (35), 3954-3957.
160. Gregerson, C. E.; Trentadue, K. N.; Phipps, E. J. T.; Kirsch, J. K.; Reed, K. M.; Dyke, G. D.; Jansen, J. H.; Otteman, C. B.; Stachowski, J. L.; Johnson, J. B., Oxidative coupling of Michael

- acceptors with aryl nucleophiles produced through rhodium-catalyzed C-C bond activation. *Organic & Biomolecular Chemistry* **2017**, *15* (28), 5944-5948.
161. Lehmann, J.; Lloyd-Jones, G. C., Regiocontrol and Stereoselectivity in Tungsten-Bipyridine Catalysed Allylic Alkylation. *Tetrahedron* **1995**, *51* (32), 8863-8874.
162. Maguire, R.; Duggan, O.; Kavanagh, K., Evaluation of *Galleria mellonella* larvae as an in vivo model for assessing the relative toxicity of food preservative agents. *Cell Biology and Toxicology* **2016**, *32* (3), 209-216.
163. Stauffer, E.; Dolan, J. A.; Newman, R., CHAPTER 3 - Review of Basic Organic Chemistry. In *Fire Debris Analysis*, Stauffer, E.; Dolan, J. A.; Newman, R., Eds. Academic Press: Burlington, 2008; pp 49-83.
164. McNulty, J.; Das, P., Aqueous Wittig reactions of semi-stabilized ylides. A straightforward synthesis of 1,3-dienes and 1,3,5-trienes. *Tetrahedron Letters* **2009**, *50* (41), 5737-5740.
165. Capperucci, A.; Degl'Innocenti, A.; Dondoli, P.; Nocentini, T.; Reginato, G.; Ricci, A., Acetylenic silyl ketone as polysynthetic equivalent of useful building blocks in organic synthesis. *Tetrahedron* **2001**, *57* (29), 6267-6276.
166. Hadfield, M. S.; Lee, A.-L., Gold(i)-catalysed synthesis of conjugated trienes. *Chemical Communications* **2011**, *47* (4), 1333-1335.
167. Thirsk, C.; Whiting, A., Polyene natural products. *Journal of the Chemical Society, Perkin Transactions 1* **2002**, (8), 999-1023.
168. Miranda, J.; Arias, N.; Fernández-Quintela, A.; Portillo, M. d. P., Are conjugated linolenic acid isomers an alternative to conjugated linoleic acid isomers in obesity prevention? *Endocrinología y nutrición : organo de la Sociedad Espanola de Endocrinología y Nutricion* **2014**, *61*(4), 209-19.
169. Lansky, E. P.; Harrison, G.; Froom, P.; Jiang, W. G., Pomegranate (*Punica granatum*) pure chemicals show possible synergistic inhibition of human PC-3 prostate cancer cell invasion across Matrigel™. *Investigational New Drugs* **2005**, *23* (2), 121-122.
170. Oh, J.; Kim, J.; Jang, J. H.; Lee, S.; Park, C. M.; Kim, W.-K.; Kim, J.-S., Novel (1E,3E,5E)-1,6-bis(Substituted phenyl)hexa-1,3,5-triene Analogs Inhibit Melanogenesis in B16F10 Cells and Zebrafish. *International journal of molecular sciences* **2018**, *19* (4), 1067.
171. Ha, Y. M.; Lee, H. J.; Park, D.; Jeong, H. O.; Park, J. Y.; Park, Y. J.; Lee, K. J.; Lee, J. Y.; Moon, H. R.; Chung, H. Y., Molecular Docking Studies of (1*E*,3*E*,5*E*)-1,6-Bis(substituted phenyl)hexa-1,3,5-triene and 1,4-Bis(substituted *trans*-styryl)benzene Analogs as Novel Tyrosinase Inhibitors. *Biological and Pharmaceutical Bulletin* **2013**, *36* (1), 55-65.
172. Diels, O.; Alder, K., Synthesen in der hydroaromatischen Reihe. *Justus Liebigs Annalen der Chemie* **1928**, *460* (1), 98-122.
173. Woodward, R. B.; Katz, T. J., The mechanism of the Diels-Alder reaction. *Tetrahedron* **1959**, *5* (1), 70-89.
174. Yang, B.; Gao, S., Recent advances in the application of Diels–Alder reactions involving o-quinodimethanes, aza-o-quinone methides and o-quinone methides in natural product total synthesis. *Chemical Society Reviews* **2018**, *47* (21), 7926-7953.
175. Burshtein, K. Y.; Anikin, N. A.; Yanovskaya, L. A.; Veliev, M. G.; Guseinov, M. M., 1,3,5-Hexatrienes as dienophiles in their reactions with hexachlorocyclopentadiene. *Bulletin of the Academy of Sciences of the USSR, Division of chemical science* **1984**, *33* (8), 1743-1745.
176. Ohno, M.; Mori, K.; Eguchi, S., Site selective cycloaddition reaction of 1-methoxy-1-trimethylsiloxy-1,3,5-hexatriene with dienophile. *Tetrahedron Letters* **1986**, *27* (29), 3381-3384.

177. Veliev, M. G.; Guseinov, M. M.; Yanovskaya, L. A.; Burstein, K. Y., Some new dienophiles in the diels-alder reaction with active cyclic dienes. *Tetrahedron* **1985**, *41* (4), 749-761.
178. Schmid, T. E.; Drissi-Amraoui, S.; Crévisy, C.; Baslé, O.; Mauduit, M., Copper-catalyzed asymmetric conjugate addition of organometallic reagents to extended Michael acceptors. *Beilstein journal of organic chemistry* **2015**, *11*, 2418-2434.
179. Jacobsen, S.; Jart, A.; Kindt-Larsen, T.; Andersen, I. G. K.; Munch-Petersen, J., Conjugate additions of Grignard reagents to alpha, beta-unsaturated esters. XV Reactions with octa-2,4,6-trienoic ester. General discussion of the conjugate addition reaction. *Acta Chemica Scandinavica* **1963**, *17*, 2423-2436.
180. Jin, C. K.; Yamada, T.; Sano, S.; Shiro, M.; Nagao, Y., Stereoselective synthesis of unsymmetrical conjugated dienes and trienes utilizing silacyclobutenes. *Tetrahedron Letters* **2007**, *48* (21), 3671-3675.
181. Zhang, X.; Larock, R. C., Synthesis of highly substituted 1,3-dienes, 1,3,5-trienes, and 3,6-disubstituted cyclohexenes by the palladium-catalyzed coupling of organic halides, internal alkynes or 1,3-cyclohexadienes, and organoboranes. *Tetrahedron* **2010**, *66* (24), 4265-4277.
182. von Zezschwitz, P.; Petry, F.; de Meijere, A., A One-Pot Sequence of Stille and Heck Couplings: Synthesis of Various 1,3,5-Hexatrienes and Their Subsequent 6 π -Electrocyclizations. *Chemistry – A European Journal* **2001**, *7* (18), 4035-4046.
183. Sünnemann, H. W.; de Meijere, A., Steroids and Steroid Analogues from Stille–Heck Coupling Sequences. *Angewandte Chemie International Edition* **2004**, *43* (7), 895-897.
184. Mohamed, Y. M. A.; Hansen, T. V., Z-Stereoselective semi-reduction of alkynes: modification of the Boland protocol. *Tetrahedron* **2013**, *69* (19), 3872-3877.
185. Boland, W.; Schroer, N.; Sieler, C.; Feigel, M., Sterospecific Syntheses and Spectroscopic Properties of Isomeric 2,4,6,8-Undecatetraenes. New Hydrocarbons from the Marine Brown Alga *Giffordia mitchellae*. Part IV. *Helvetica Chimica Acta* **1987**, *70* (4), 1025-1040.
186. Oger, C.; Balas, L.; Durand, T.; Galano, J.-M., Are Alkyne Reductions Chemo-, Regio-, and Stereoselective Enough To Provide Pure (Z)-Olefins in Polyfunctionalized Bioactive Molecules? *Chemical Reviews* **2013**, *113* (3), 1313-1350.
187. Dayaker, G.; Durand, T.; Balas, L., A Versatile and Stereocontrolled Total Synthesis of Dihydroxylated Docosatrienes Containing a Conjugated E,E,Z-Triene. *Chemistry – A European Journal* **2014**, *20* (10), 2879-2887.
188. Chan, T.-L.; Fong, S.; Li, Y.; Man, T.-O.; Poon, C.-D., A new one-flask Ramberg–Bäcklund reaction. *Journal of the Chemical Society, Chemical Communications* **1994**, (15), 1771-1772.
189. Taylor, R. J. K.; Casy, G., The Ramberg–Bäcklund Reaction. *Organic Reactions* **2003**, *62*, 357-476.
190. Meyers, C. Y.; Malte, A. M.; Matthews, W. S., Ionic reactions of carbon tetrachloride. Survey of reactions with ketones, alcohols, and sulfones. *Journal of the American Chemical Society* **1969**, *91* (26), 7510-7512.
191. Cao, X.-P.; Chan, T.-L.; Chow, H.-F.; Tu, J., Stereoselective synthesis of substituted 1,3,5-hexatrienes from diallylic sulfones. *Journal of the Chemical Society, Chemical Communications* **1995**, (12), 1297-1299.
192. Seyferth, D., The Grignard Reagents. *Organometallics* **2009**, *28* (6), 1598-1605.
193. Dell'Erba, C.; Gabellini, A.; Mugnoli, A.; Novi, M.; Petrillo, G.; Tavani, C., From 3,4-dinitrothiophene to 1,2-diaryl-4-nitrobenzenes through (E,E,E)-1,6-diaryl-3-nitro-1,3,5-hexatrienes. *Tetrahedron* **2001**, *57* (43), 9025-9031.
194. Zhang, A.-Q.; Zhang, N.; Hong, S.; Zhang, M., Leucoemeraldine-Base-Catalyzed Knoevenagel Condensation. *Synthetic Communications* **2009**, *39* (17), 3024-3030.

195. Sylla, M.; Joseph, D.; Chevallier, E.; Camara, C.; Dumas, F., A Simple and Direct Access to Ethylidene Malonates. *Synthesis* **2006**, 2006 (06), 1045-1049.
196. Knoevenagel, E., Ueber eine Darstellungsweise des Benzylidenacetessigesters. *Berichte der deutschen chemischen Gesellschaft* **1896**, 29 (1), 172-174.
197. Knoevenagel, E., Ueber eine Darstellungsweise der Glutarsäure. *Berichte der deutschen chemischen Gesellschaft* **1894**, 27 (2), 2345-2346.
198. Knoevenagel, E., 1,5-Diketone. *Justus Liebigs Annalen der Chemie* **1894**, 281 (1), 25-126.
199. Jones, G., The Knoevenagel Condensation. *Organic Reactions* **1967**, 15.
200. List, B., Emil Knoevenagel and the Roots of Aminocatalysis. *Angewandte Chemie International Edition* **2010**, 49 (10), 1730-1734.
201. Knoevenagel, E., Condensationen zwischen Malonester und Aldehyden unter dem Einfluss von Ammoniak und organischen Aminen. *Berichte der deutschen chemischen Gesellschaft* **1898**, 31 (3), 2585-2595.
202. Knoevenagel, E.; Ruschhaupt, W., Synthesen in der Pyridinreihe. Ueber einige acetylierte Pyridine und Dihydropyridine. *Berichte der deutschen chemischen Gesellschaft* **1898**, 31 (1), 1025-1033.
203. Tietze, L. F.; Beifuss, U., 1.11 - The Knoevenagel Reaction. In *Comprehensive Organic Synthesis*, Trost, B. M.; Fleming, I., Eds. Pergamon: Oxford, 1991; pp 341-394.
204. Knoevenagel, E., Ueber den Chemismus der condensirenden Wirkung des Ammoniaks und organischer Amine bei Reactionen zwischen Aldehyden und Acetessigesters. *Berichte der deutschen chemischen Gesellschaft* **1898**, 31 (1), 738-748.
205. Knoevenagel, E., Condensation von Malonsäure mit aromatischen Aldehyden durch Ammoniak und Amine. *Berichte der deutschen chemischen Gesellschaft* **1898**, 31 (3), 2596-2619.
206. Rand, L.; Swisher, J. V.; Cronin, C. J., Reactions Catalyzed by Potassium Fluoride. III. The Knoevenagel Reaction. *The Journal of Organic Chemistry* **1962**, 27 (10), 3505-3507.
207. Lehnert, W., Knoevenagel-Kondensationen mit TiCl₄/Base - V1. 3-Alkyliden- und 3-Aryliden-2,4-pentandione aus Aldehyden und Acetylaceton. *Synthesis* **1974**, 1974 (09), 667-669.
208. Courtheyn, D.; Verhe, R.; De Kimpe, N.; De Buyck, L.; Schamp, N., Synthesis of electrophilic allyl dichlorides. *The Journal of Organic Chemistry* **1981**, 46 (16), 3226-3229.
209. Texier-Boullet, F.; Foucaud, A., Knoevenagel condensation catalysed by aluminium oxide. *Tetrahedron Letters* **1982**, 23 (47), 4927-4928.
210. Burate PA; Javle BR; Desale PH; AK, K., Solvent-free Knoevenagel Condensation over Amino Acid Amide based Ionic Liquid as an Efficient and Eco-friendly Catalyst. *Synth Catal* **2018**, 3 (3:6).
211. Ren, Z.; Cao, W.; Tong, W., THE KNOEVENAGEL CONDENSATION REACTION OF AROMATIC ALDEHYDES WITH MALONONITRILE BY GRINDING IN THE ABSENCE OF SOLVENTS AND CATALYSTS. *Synthetic Communications* **2002**, 32 (22), 3475-3479.
212. Kabalka, G. W.; Pagni, R. M., Organic reactions on alumina. *Tetrahedron* **1997**, 53 (24), 7999-8065.
213. Ivanova, A. S., Aluminum oxide and systems based on it: Properties and applications. *Kinetics and Catalysis* **2012**, 53 (4), 425-439.
214. Carrier, X.; Royer, S.; Marceau, E., 2 - Synthesis of metal oxide catalysts. In *Metal Oxides in Heterogeneous Catalysis*, Védrine, J. C., Ed. Elsevier: 2018; pp 43-103.
215. Vít, Z.; Vala, J.; Málek, J., Acid-base properties of aluminium oxide. *Applied Catalysis* **1983**, 7 (2), 159-168.

216. Huang, J.; Li, Y., BN Embedded Polycyclic π -Conjugated Systems: Synthesis, Optoelectronic Properties, and Photovoltaic Applications. *Frontiers in chemistry* **2018**, *6*, 341-341.
217. Grimsdale, A. C.; Leok Chan, K.; Martin, R. E.; Jokisz, P. G.; Holmes, A. B., Synthesis of Light-Emitting Conjugated Polymers for Applications in Electroluminescent Devices. *Chemical Reviews* **2009**, *109* (3), 897-1091.
218. Benavides, C. M.; Murto, P.; Chochos, C. L.; Gregoriou, V. G.; Avgeropoulos, A.; Xu, X.; Bini, K.; Sharma, A.; Andersson, M. R.; Schmidt, O.; Brabec, C. J.; Wang, E.; Tedde, S. F., High-Performance Organic Photodetectors from a High-Bandgap Indacenodithiophene-Based π -Conjugated Donor–Acceptor Polymer. *ACS Applied Materials & Interfaces* **2018**, *10* (15), 12937-12946.
219. Murphy, J. J.; Quintard, A.; McArdle, P.; Alexakis, A.; Stephens, J. C., Asymmetric Organocatalytic 1,6-Conjugate Addition of Aldehydes to Dienic Sulfones. *Angewandte Chemie International Edition* **2011**, *50* (22), 5095-5098.
220. Pezzati, B.; Chellat, M. F.; Murphy, J. J.; Besnard, C.; Reginato, G.; Stephens, J. C.; Alexakis, A., Organocatalytic Asymmetric Annulation of 1,3-Bis(alkoxycarbonyl)buta-1,3-dienes and Aldehydes. *Organic Letters* **2013**, *15* (12), 2950-2953.
221. Jungnickel, J. L.; Forbes, J. W., Quantitative Measurement of Hydrogen Types by Intergrated Nuclear Magnetic Resonance Intensities. *Analytical Chemistry* **1963**, *35* (8), 938-942.
222. Hollis, D. P., Quantitative Analysis of Aspirin, Phenacetin, and Caffeine Mixtures by Nuclear Magnetic Resonance Spectrometry. *Analytical Chemistry* **1963**, *35* (11), 1682-1684.
223. Bharti, S. K.; Roy, R., Quantitative ¹H NMR spectroscopy. *TrAC Trends in Analytical Chemistry* **2012**, *35*, 5-26.
224. Rundlöf, T.; Mathiasson, M.; Bekiroglu, S.; Hakkarainen, B.; Bowden, T.; Arvidsson, T., Survey and qualification of internal standards for quantification by ¹H NMR spectroscopy. *Journal of Pharmaceutical and Biomedical Analysis* **2010**, *52* (5), 645-651.
225. Elbagary, R. I.; Fouad, M. A.; Ezzeldin, M. I., Quantitative Nuclear Magnetic Resonance Spectroscopic Analysis of Two Commonly Used Gastrointestinal Tract Drugs. *Journal of AOAC INTERNATIONAL* **2020**.
226. Murphy, J. J. Studies in Synthesis and Organocatalysis: (i) The Design and Synthesis of Novel Electron Deficient Dienes and their Application in the First Enamine Activated Organocatalytic 1,6-Conjugate Addition. (ii) The Development of a New Organocatalytic Methodology through the Combination of DNA-Based Catalysis and Organocatalysis. National University of Ireland, Maynooth, Faculty of Science and Engineering, 2012.
227. Karpinska, J. Crystal Growth Using Low Temperature Gradient Sublimation in Vacuo. National University of Ireland, Galway, 2012.
228. Giral, Angela L.; Mahuteau-Betzer, F.; Gateau-Olesker, A.; Marazano, C., Knoevenagel Adducts from Reactions between Glutaconate Moieties and Aldehydes and Their Adducts with Primary Amines and Enamines. *European Journal of Organic Chemistry* **2003**, *2003* (10), 1859-1867.
229. Joseph, D., A Simple and Direct Access to Ethylidene Malonates. *Synthesis* **2006**, (6), 1045-1049.
230. Patai, S.; Zabicky, J., 412. The kinetics and mechanisms of carbonyl–methylene condensations. Part VIII. The reaction of ethyl cyanoacetate with aromatic aldehydes in ethanol, in water, and in ethanol–water mixtures. *Journal of the Chemical Society (Resumed)* **1960**, (0), 2030-2038.
231. Jacobsen, N. E., *NMR data interpretation explained : understanding 1D and 2D NMR spectra of organic compounds and natural products*. 2017.

232. Robinson, J. W.; Frame, E. S. F., G.W., *Undergraduate Instrumental Analysis*. CRC Press: 2014.
233. Pitt, J. J., Principles and applications of liquid chromatography-mass spectrometry in clinical biochemistry. *The Clinical biochemist. Reviews* **2009**, *30* (1), 19-34.
234. Rodríguez-Moreno, J.; Navarrete-Astorga, E.; Dalchiale, E. A.; Schrebler, R.; Ramos-Barrado, J. R.; Martín, F., Vertically aligned ZnO@CuS@PEDOT core@shell nanorod arrays decorated with MnO₂ nanoparticles for a high-performance and semi-transparent supercapacitor electrode. *Chem Commun (Camb)* **2014**, *50* (42), 5652-5.
235. Gallagher, E. T.; Grayson, D. H., Reactions of lithiated (E)-3-halo-1-phenylsulfonylprop-1-enes and (Z)-1-halo-3-phenylsulfonylprop-1-enes with aldehydes. *Organic & Biomolecular Chemistry* **2003**, *1* (8), 1374-1381.
236. Tang, X.-z.; Tong, L.; Liang, H.-j.; Liang, J.; Zou, Y.; Zhang, X.-j.; Yan, M.; Chan, A. S. C., Facile synthesis of substituted diaryl sulfones via a [3 + 3] benzannulation strategy. *Organic & Biomolecular Chemistry* **2018**, *16* (19), 3560-3563.
237. Horiguchi, H.; Hirano, K.; Satoh, T.; Miura, M., Palladium-Catalyzed Three-Component 1:2:1 Coupling of Aryl Iodides, Alkynes, and Alkenes to Produce 1,3,5-Hexatriene Derivatives. *Advanced Synthesis & Catalysis* **2009**, *351* (9), 1431-1436.
238. Diallo, A.; Zhao, Y.-L.; Wang, H.; Li, S.-S.; Ren, C.-Q.; Liu, Q., Base-Catalyzed Efficient Tandem [3 + 3] and [3 + 2 + 1] Annulation-Aerobic Oxidative Benzannulations. *Organic Letters* **2012**, *14* (22), 5776-5779.
239. Joshi, P. R.; Undeela, S.; Reddy, D. D.; Singarapu, K. K.; Menon, R. S., Regioselective Synthesis of Substituted Arenes via Aerobic Oxidative [3 + 3] Benzannulation Reactions of α,β -Unsaturated Aldehydes and Ketones. *Organic Letters* **2015**, *17* (6), 1449-1452.
240. Couhert, A.; Delagrangé, P.; Caignard, D.-H.; Chartier, A.; Suzenet, F.; Guillaumet, G., Synthesis of 2-arylfuro[3,2-b]pyridines: Effect of the C2-aryl group on melatonergic activity. *European Journal of Medicinal Chemistry* **2016**, *109*, 268-275.
241. Sarrazin, L.; Mauzé, B., An Efficient Indium-Mediated Synthesis of α -Cyano- β -Ethylene Secondary Alcohols in Water. *Synthetic Communications* **1996**, *26* (17), 3179-3191.
242. Jain, Z. J.; Gide, P. S.; Kankate, R. S., Biphenyls and their derivatives as synthetically and pharmacologically important aromatic structural moieties. *Arabian Journal of Chemistry* **2017**, *10*, S2051-S2066.
243. Stanforth, S. P., Catalytic cross-coupling reactions in biaryl synthesis. *Tetrahedron* **1998**, *54* (3), 263-303.
244. Holden, C. M.; Sohel, S. M. A.; Greaney, M. F., Metal Free Bi(hetero)aryl Synthesis: A Benzyne Truce–Smiles Rearrangement. *Angewandte Chemie International Edition* **2016**, *55* (7), 2450-2453.
245. Iranpoor, N.; Panahi, F.; Jamedi, F., Nickel-catalyzed one-pot synthesis of biaryls from phenols and arylboronic acids via C–O activation using TCT reagent. *Journal of Organometallic Chemistry* **2015**, *781*, 6-10.
246. Lloyd-Williams, P.; Giralt, E., Atropisomerism, biphenyls and the Suzuki coupling: peptide antibiotics. *Chemical Society Reviews* **2001**, *30* (3), 145-157.
247. Horton, D. A.; Bourne, G. T.; Smythe, M. L., The Combinatorial Synthesis of Bicyclic Privileged Structures or Privileged Substructures. *Chemical Reviews* **2003**, *103* (3), 893-930.
248. Kour, D.; Rana, K. L.; Kumar, R.; Yadav, N.; Rastegari, A. A.; Yadav, A. N.; Singh, K., Chapter 1 - Gene Manipulation and Regulation of Catabolic Genes for Biodegradation of Biphenyl Compounds. In *New and Future Developments in Microbial Biotechnology and Bioengineering*, Singh, H. B.; Gupta, V. K.; Jogaiah, S., Eds. Elsevier: Amsterdam, 2019; pp 1-23.
249. William Andrew, P., B. In *Pharmaceutical Manufacturing Encyclopedia (Third Edition)*, William Andrew, P., Ed. William Andrew Publishing: Oxford, 2007; pp 508-782.

250. William Andrew, P., D. In *Pharmaceutical Manufacturing Encyclopedia (Third Edition)*, William Andrew, P., Ed. William Andrew Publishing: Oxford, 2007; pp 1187-1413.
251. William Andrew, P., F. In *Pharmaceutical Manufacturing Encyclopedia (Third Edition)*, William Andrew, P., Ed. William Andrew Publishing: Oxford, 2007; pp 1546-1736.
252. William Andrew, P., V. In *Pharmaceutical Manufacturing Encyclopedia (Third Edition)*, William Andrew, P., Ed. William Andrew Publishing: Oxford, 2007; pp 3385-3463.
253. William Andrew, P., X. In *Pharmaceutical Manufacturing Encyclopedia (Third Edition)*, William Andrew, P., Ed. William Andrew Publishing: Oxford, 2007; pp 3466-3491.
254. Vardanyan, R. S.; Hruby, V. J., 32 - Antibiotics. In *Synthesis of Essential Drugs*, Vardanyan, R. S.; Hruby, V. J., Eds. Elsevier: Amsterdam, 2006; pp 425-498.
255. Muangpaisal, R.; Hung, W.-I.; Lin, J. T.; Ting, S.-Y.; Chen, L.-Y., Binaphthalene bridged bipolar transporting materials for blue electroluminescence: toward high EL efficiency via molecular tuning. *Tetrahedron* **2014**, *70* (18), 2992-2998.
256. Prachumrak, N.; Thangthong, A. m.; Tarsang, R.; Keawin, T.; Jungsuttiwong, S.; Sudyoadsuk, T.; Promarak, V., Synthesis, characterization, physical properties, and applications of highly fluorescent pyrene-functionalized 9,9-bis(4-diarylamino-phenyl)fluorene in organic light-emitting diodes. *Tetrahedron Letters* **2012**, *53* (41), 5492-5496.
257. Jin, R.-f.; Tang, S.-s.; Sun, W.-d., Rational design of donor- π -acceptor n-butyl-1,8-naphthalimide-cored branched molecules as charge transport and luminescent materials for organic light-emitting diodes. *Tetrahedron* **2014**, *70* (1), 47-53.
258. Thejo Kalyani, N.; Dhoble, S. J., Organic light emitting diodes: Energy saving lighting technology—A review. *Renewable and Sustainable Energy Reviews* **2012**, *16* (5), 2696-2723.
259. Xu, Z.; Gao, L.; Wang, L.; Gong, M.; Wang, W.; Yuan, R., Visible Light Photoredox Catalyzed Biaryl Synthesis Using Nitrogen Heterocycles as Promoter. *ACS Catalysis* **2015**, *5* (1), 45-50.
260. Walia, P. K.; Kumar, M.; Bhalla, V., Empowering Transition-Metal-Free Cascade Protocol for the Green Synthesis of Biaryls and Alkynes. *ACS Omega* **2018**, *3* (2), 1983-1990.
261. Finkelstein, H., Darstellung organischer Jodide aus den entsprechenden Bromiden und Chloriden. *Berichte der deutschen chemischen Gesellschaft* **1910**, *43* (2), 1528-1532.
262. Negishi, E.-i., Historical Background of Organopalladium Chemistry. In *Handbook of Organopalladium Chemistry for Organic Synthesis*, Wiley Online Books: 2002.
263. Yang, X.; Xu, G.; Tang, W., Efficient synthesis of chiral biaryls via asymmetric Suzuki-Miyaura cross-coupling of ortho-bromo aryl triflates. *Tetrahedron* **2016**, *72* (34), 5178-5183.
264. Barbero, M.; Dughera, S., Gold catalysed Suzuki-Miyaura coupling of arenediazonium o-benzenedisulfonimides. *Tetrahedron* **2018**, *74* (39), 5758-5769.
265. Wang, D.-Y.; Kawahata, M.; Yang, Z.-K.; Miyamoto, K.; Komagawa, S.; Yamaguchi, K.; Wang, C.; Uchiyama, M., Stille coupling via C-N bond cleavage. *Nature Communications* **2016**, *7* (1), 12937.
266. Wang, L.; Liu, G., One-pot Negishi cross-coupling reaction of aryldiazonium salts via Ni catalysis induced by visible-light. *Catalysis Communications* **2019**, *131*, 105785.
267. Dinda, B., Electrocyclic Reactions. In *Essentials of Pericyclic and Photochemical Reactions*, Dinda, B., Ed. Springer International Publishing: Cham, 2017; pp 13-35.
268. Woodward, R. B.; Hoffmann, R., Stereochemistry of Electrocyclic Reactions. *Journal of the American Chemical Society* **1965**, *87* (2), 395-397.
269. Voigt, K.; von Zezschwitz, P.; Rosauer, K.; Lansky, A.; Adams, A.; Reiser, O.; de Meijere, A., The Twofold Heck Reaction on 1,2-Dihalocycloalkenes and Subsequent 6π -Electrocyclization of the Resulting (E, Z, E)-1,3,5-Hexatrienes: A New Formal {2+2+2}-Assembly of Six-Membered Rings. *European Journal of Organic Chemistry* **1998**, *1998* (8), 1521-1534.
270. von Essen, R.; Frank, D.; Sünemann, H. W.; Vidović, D.; Magull, J.; de Meijere, A., Domino 6π -Electrocyclization/Diels-Alder Reactions on 1,6-Disubstituted (E,Z,E)-1,3,5-

- Hexatrienes: Versatile Access to Highly Substituted Tri- and Tetracyclic Systems. *Chemistry – A European Journal* **2005**, *11* (22), 6583-6592.
271. Sünneemann, H. W.; Banwell, M. G.; de Meijere, A., Synthesis and Use of New Substituted 1,3,5-Hexatrienes in Studying Thermally Induced 6π -Electrocyclizations. *European Journal of Organic Chemistry* **2007**, *2007* (23), 3879-3893.
272. Cho, S.-D.; Kim, H.-K.; Yim, H.-s.; Kim, M.-R.; Lee, J.-K.; Kim, J.-J.; Yoon, Y.-J., Suzuki–Miyaura coupling reaction of aryl chlorides using di(2,6-dimethylmorpholino)phenylphosphine as ligand. *Tetrahedron* **2007**, *63* (6), 1345-1352.
273. Frommhold, L., Collision-Induced Spectroscopy. In *Encyclopedia of Physical Science and Technology (Third Edition)*, Meyers, R. A., Ed. Academic Press: New York, 2003; pp 269-287.
274. Lakowicz, J. R., Introduction to Fluorescence. In *Principles of Fluorescence Spectroscopy*, Lakowicz, J. R., Ed. Springer US: Boston, MA, 1999; pp 1-23.
275. Moldoveanu, S. C.; David, V., Chapter 1 - Basic Information about HPLC. In *Essentials in Modern HPLC Separations*, Moldoveanu, S. C.; David, V., Eds. Elsevier: 2013; pp 1-51.
276. Skoog, D. A.; Crouch, S. R.; Holler, F. J., *Principles of instrumental analysis*. Thomson Brooks/Cole: Belmont, CA, 2007.
277. Maus, M.; Rettig, W.; Jonusauskas, G.; Lapouyade, R.; Rullière, C., Subpicosecond Transient Absorption of Donor–Acceptor Biphenyls. Intramolecular Control of the Excited State Charge Transfer Processes by a Weak Electronic Coupling. *The Journal of Physical Chemistry A* **1998**, *102* (38), 7393-7405.
278. Maus, M.; Rettig, W.; Bonafoux, D.; Lapouyade, R., Photoinduced Intramolecular Charge Transfer in a Series of Differently Twisted Donor–Acceptor Biphenyls As Revealed by Fluorescence. *The Journal of Physical Chemistry A* **1999**, *103* (18), 3388-3401.
279. Qiu, X. Synthesis and Evaluation of New Antimicrobial Agents and Novel Organic Fluorophores. National University of Ireland, Maynooth, 2013.
280. Valeur, B.; Berberan-Santos, M. N., *Molecular Fluorescence: Principles and Applications*. Wiley: 2012.
281. Mata, G.; Luedtke, N. W., Synthesis and Solvatochromic Fluorescence of Biaryl Pyrimidine Nucleosides. *Organic Letters* **2013**, *15* (10), 2462-2465.
282. Rusakowicz, R.; Testa, A. C., 2-Aminopyridine as a standard for low-wavelength spectrofluorimetry. *The Journal of Physical Chemistry* **1968**, *72* (7), 2680-2681.
283. Melhuish, W. H., QUANTUM EFFICIENCIES OF FLUORESCENCE OF ORGANIC SUBSTANCES: EFFECT OF SOLVENT AND CONCENTRATION OF THE FLUORESCENT SOLUTE1. *The Journal of Physical Chemistry* **1961**, *65* (2), 229-235.

Studies in organic and medicinal chemistry:
(i) Synthesis, antimicrobial evaluation, and photophysical studies of novel conjugated systems; (ii) Antimicrobial evaluation of pyrazolopyrimidinone heterocycles.

A thesis submitted by

Amanda Doyle B.Sc. (Hons.)

to

Maynooth University

for the degree of Doctor of Philosophy.



**Maynooth
University**
National University
of Ireland Maynooth

Volume 2 of 2

Based on the research carried out in the
Department of Chemistry, Faculty of Science and Engineering,
Maynooth University
under the supervision of
Prof. John C. Stephens
October 2020

Appendix 1

NMR & LCMS spectra of cinnamaldehydes synthesized

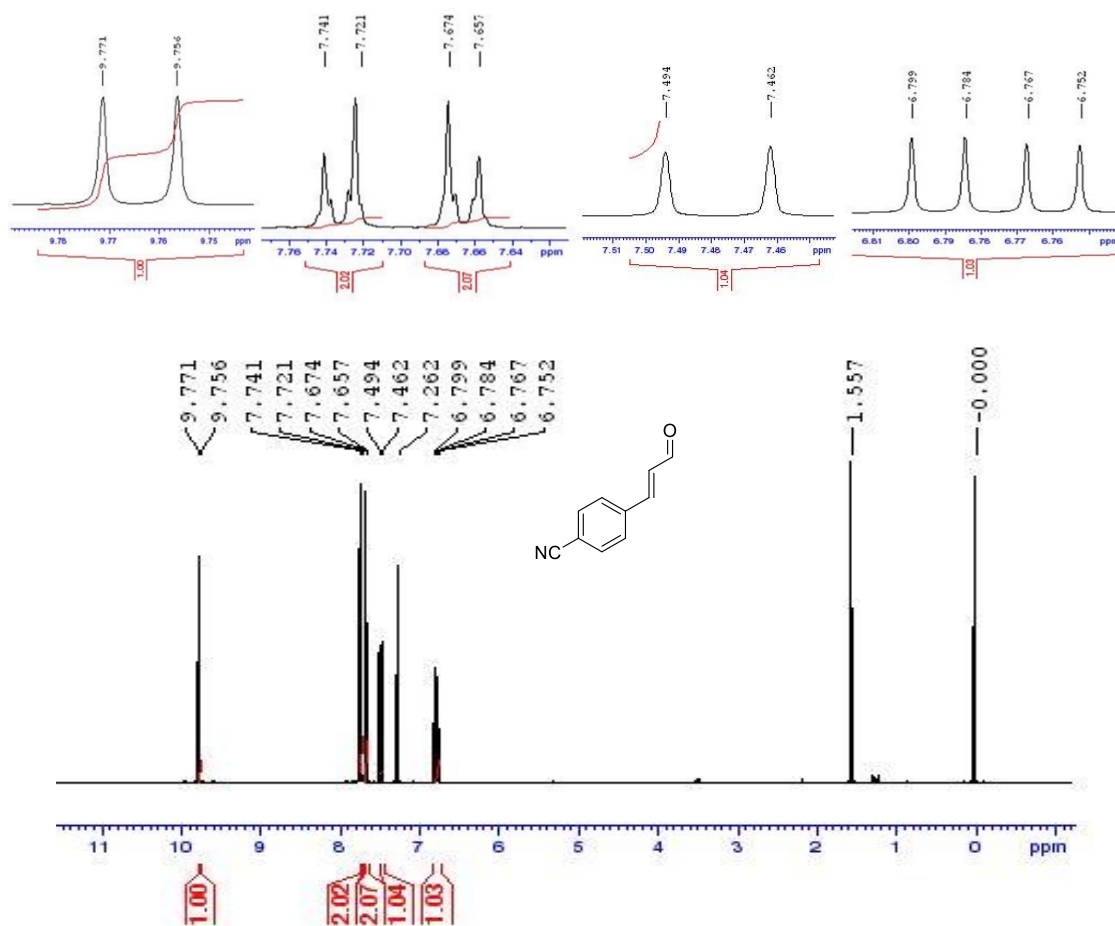


Figure A1. ^1H NMR spectrum of (*E*)-*p*-cyanocinnamaldehyde, **38**

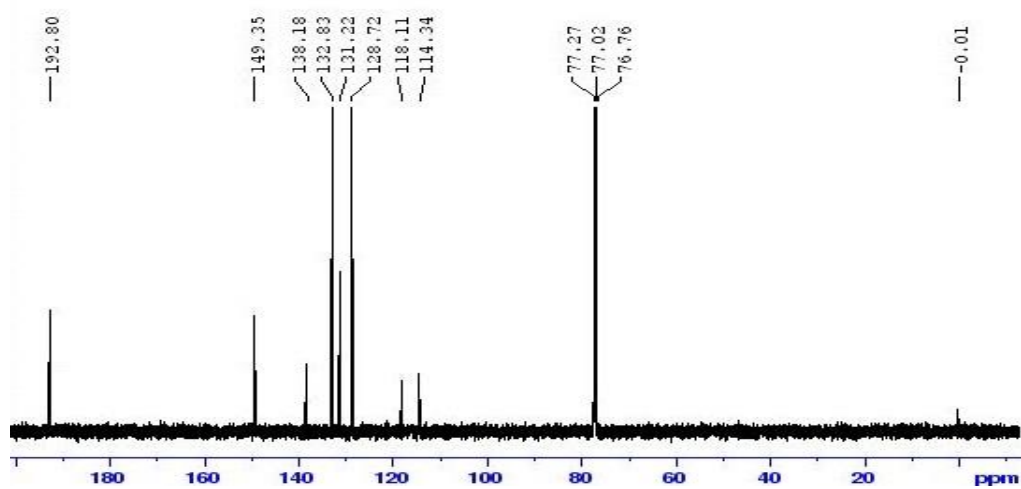


Figure A2. ^{13}C NMR spectrum of (*E*)-*p*-cyanocinnamaldehyde, **38**

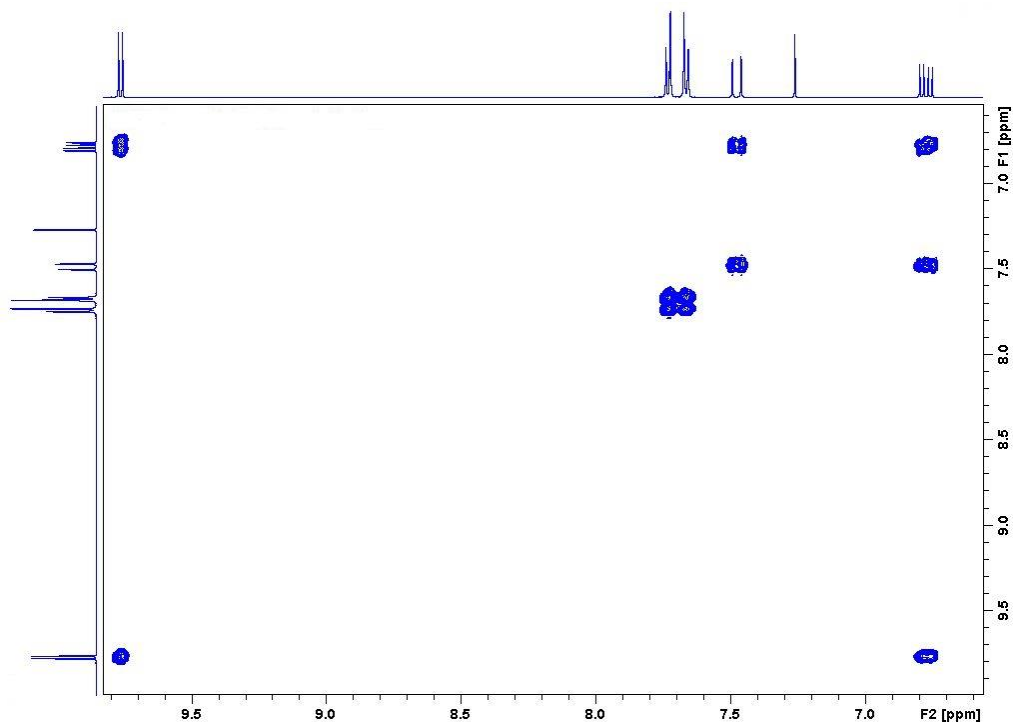


Figure A3. COSY spectrum of (*E*)-*p*-cyanocinnamaldehyde, **38**

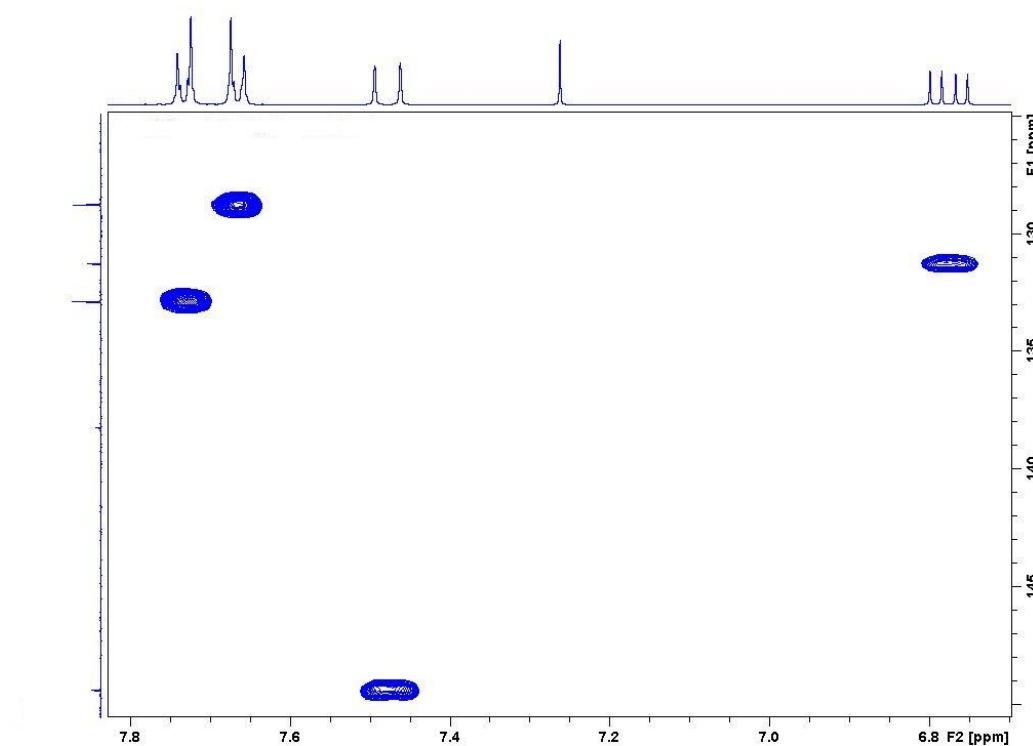


Figure A4. HSQC spectrum of (*E*)-*p*-cyanocinnamaldehyde, **38**

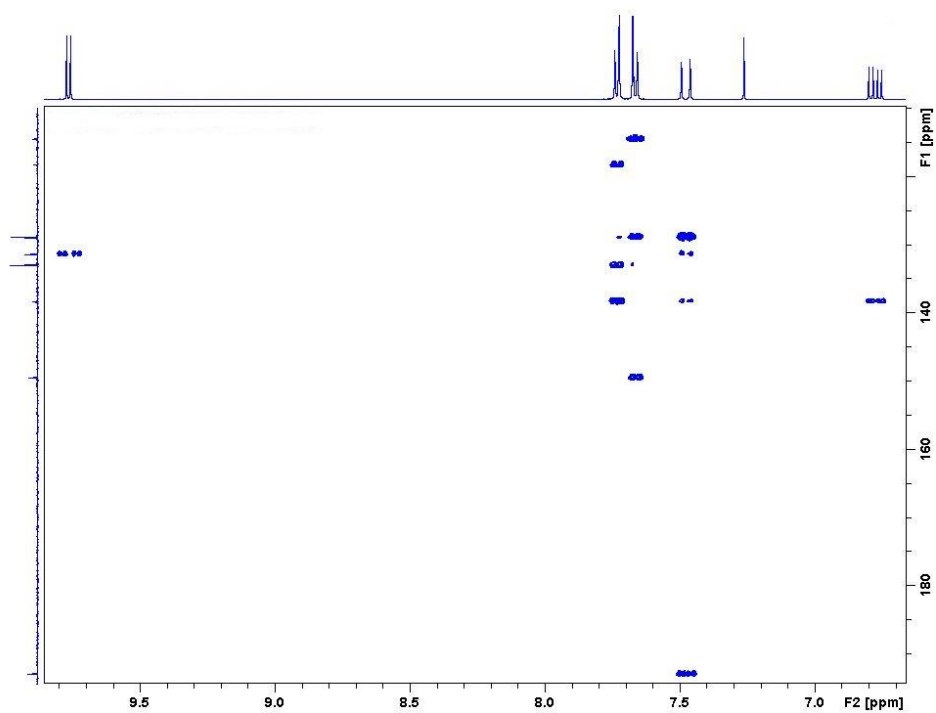


Figure A5. HMBC spectrum of (*E*)-*p*-cyanocinnamaldehyde, **38**

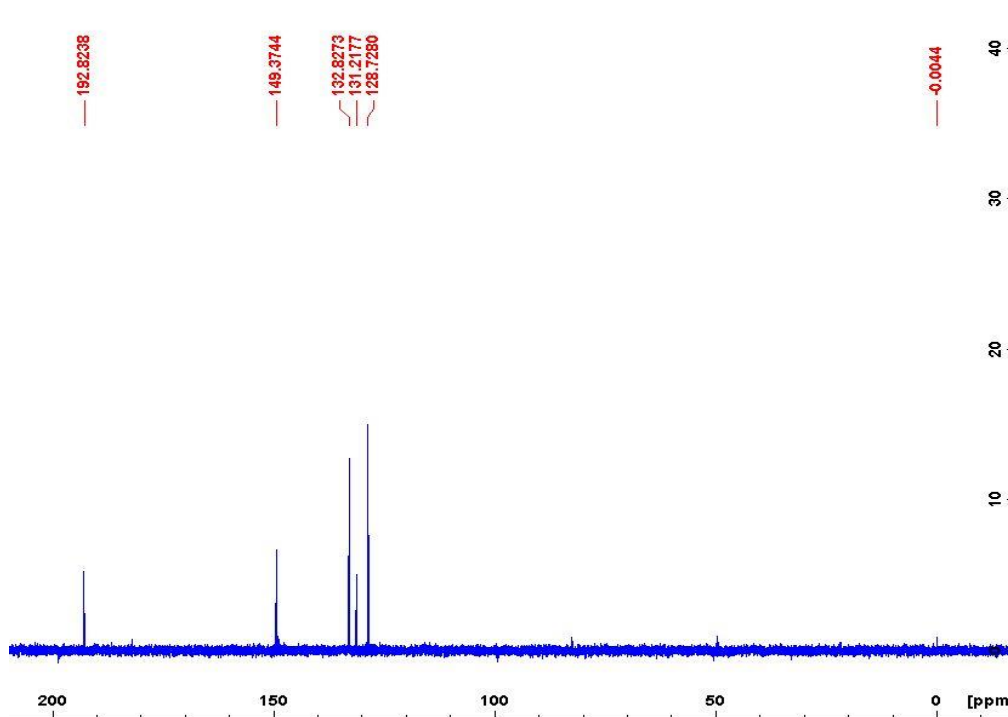
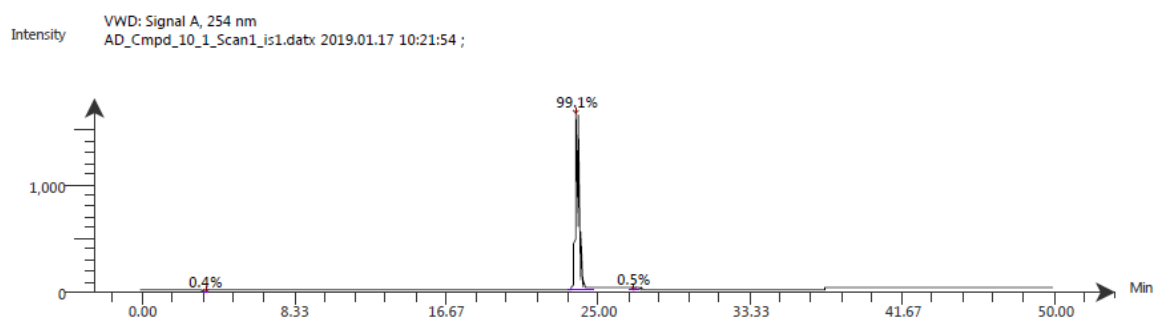


Figure A6. DEPT-135 spectrum of (*E*)-*p*-cyanocinnamaldehyde, **38**



Time (Peak Maximum M:S/Minutes)	Maximum Intensity (c/s)	Time (Peak Centroid M:S/Minutes)	Peak Area	% Peak Area	Peak Resolution Label
3.53	6.6E0	3.52	8.9E1	0.4	16.2
23.80	1.6E3	23.80	2.2E4	99.1	11.9
27.00	6.8E0	26.94	1E2	0.5	15.5

Figure A7. LCMS spectrum of (*E*)-*p*-cyanocinnamaldehyde, **38**

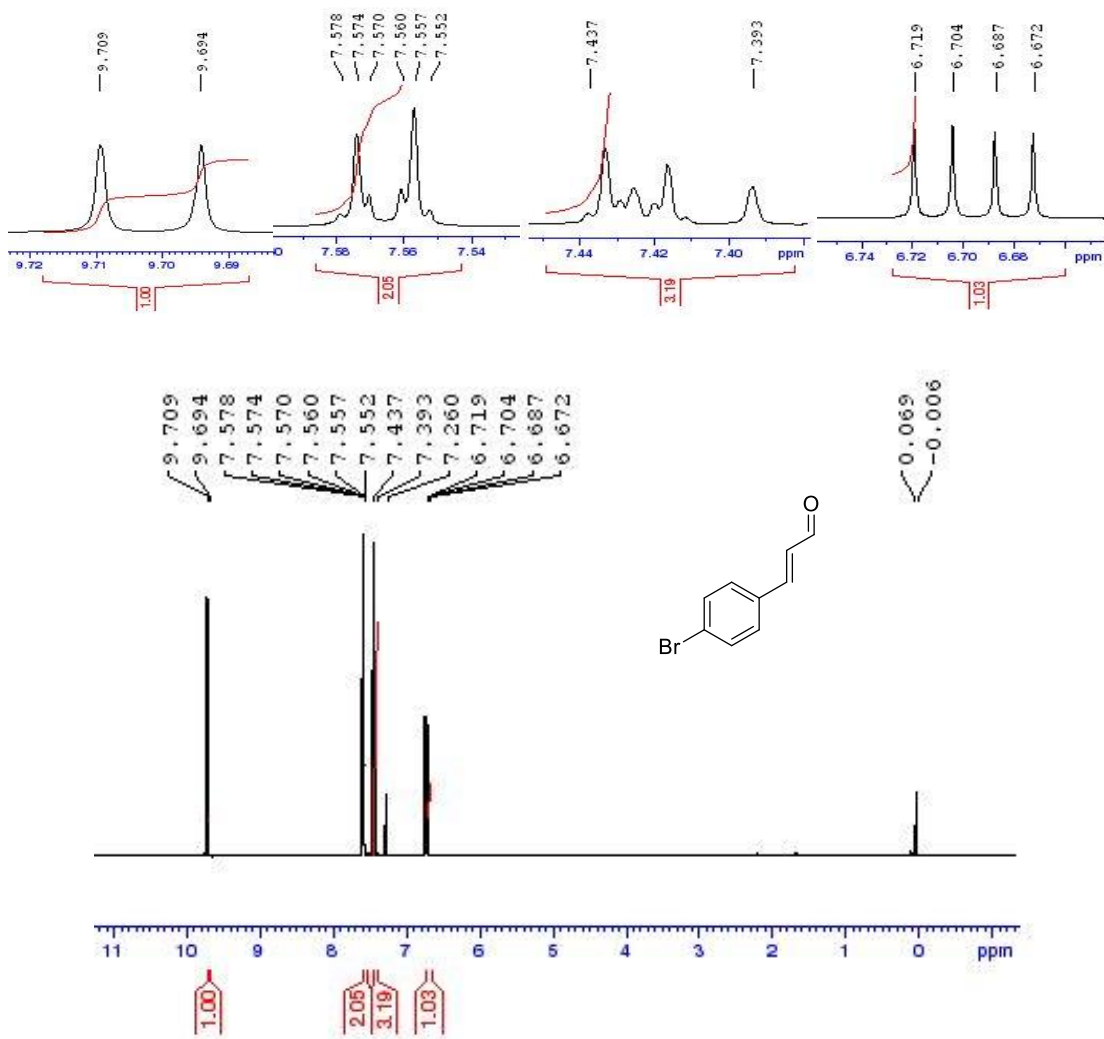


Figure A8. ¹H NMR spectrum of (*E*)-*p*-bromocinnamaldehyde, **40**

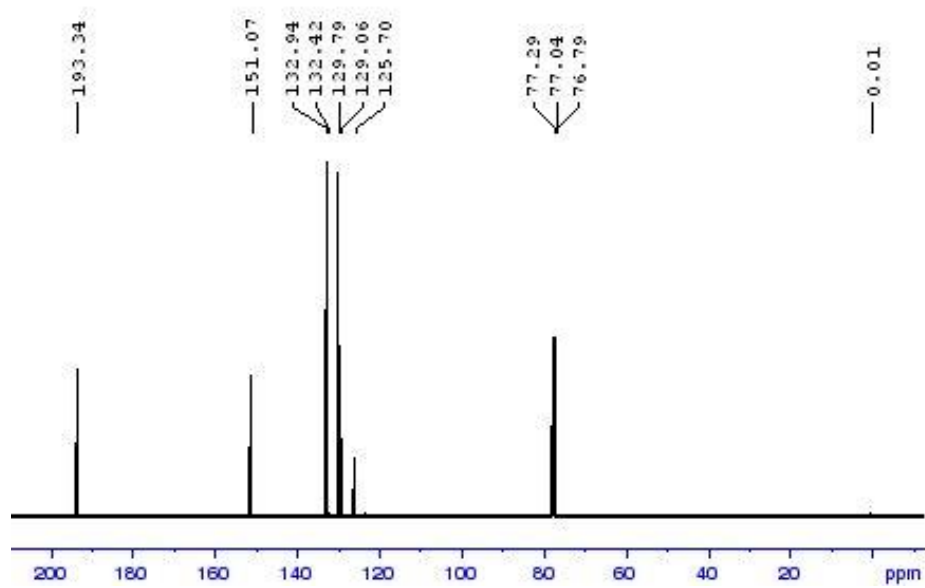
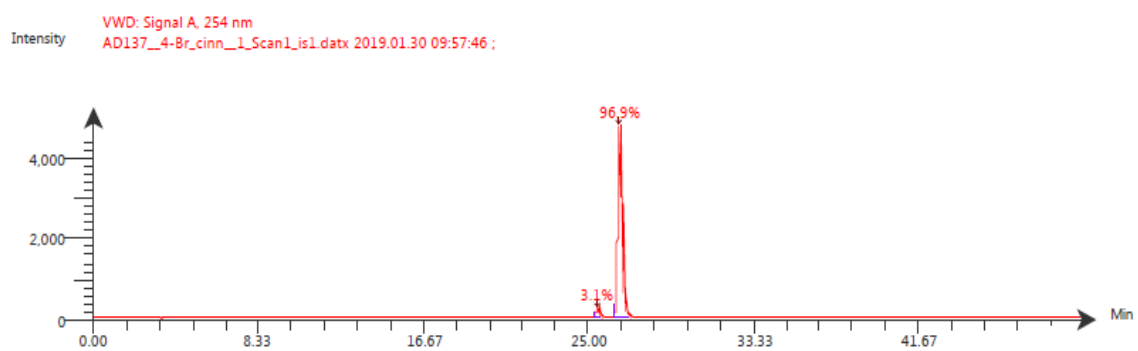


Figure A9. ^{13}C NMR spectrum of (*E*)-*p*-bromocinnamaldehyde, **40**



Time (Peak Maximum M:S/Minutes)	Maximum Intensity (c/s)	Time (Peak Centroid M:S/Minutes)	Peak Area	% Peak Area	Peak Resolution Label
25.41	2.7E2	25.44	2.3E3	3.1	16.6
26.56	4.7E3	26.56	7.2E4	96.9	14.4

Figure A10. LCMS spectrum of (*E*)-*p*-bromocinnamaldehyde, **40**

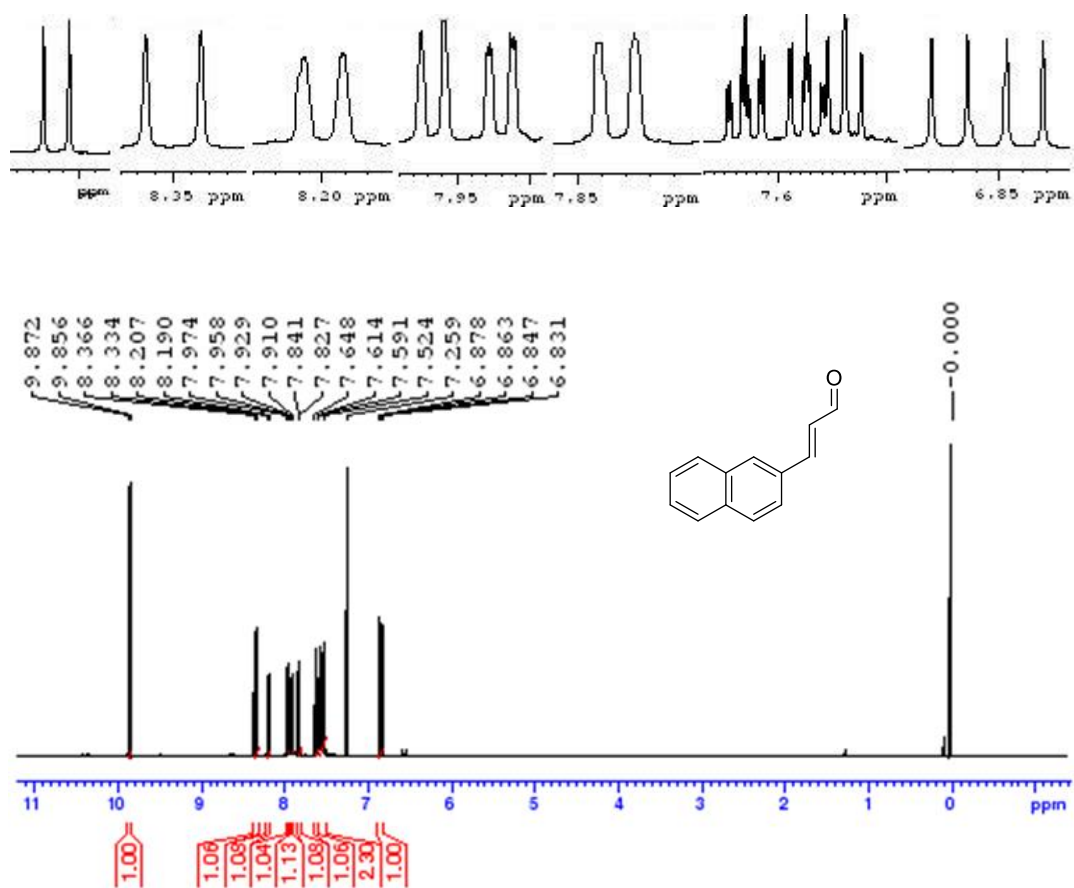


Figure A11. ¹H NMR spectrum of *(E)*-3-(naphthalen-1-yl)acrylaldehyde, **37**

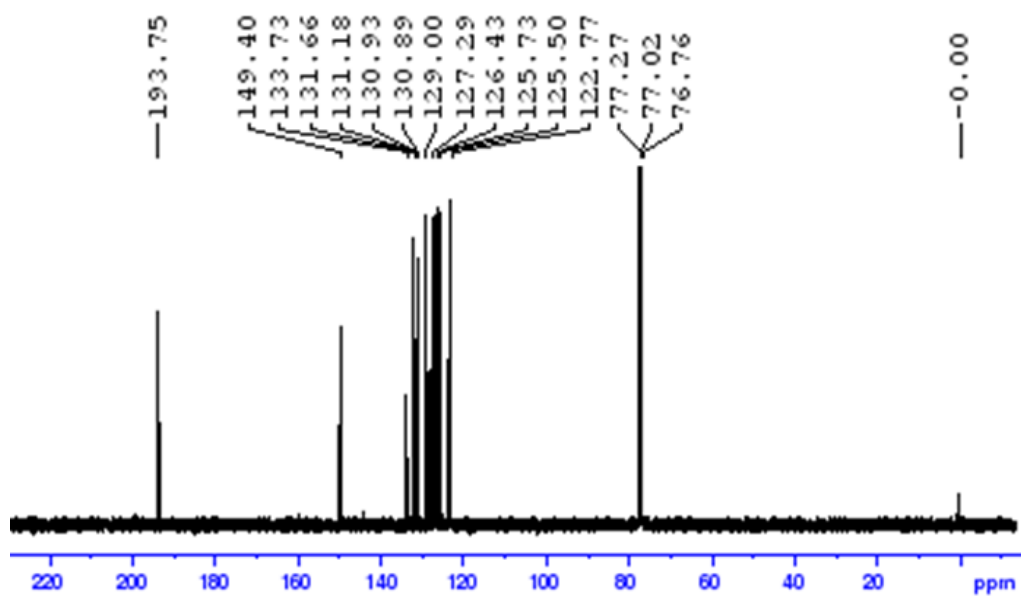
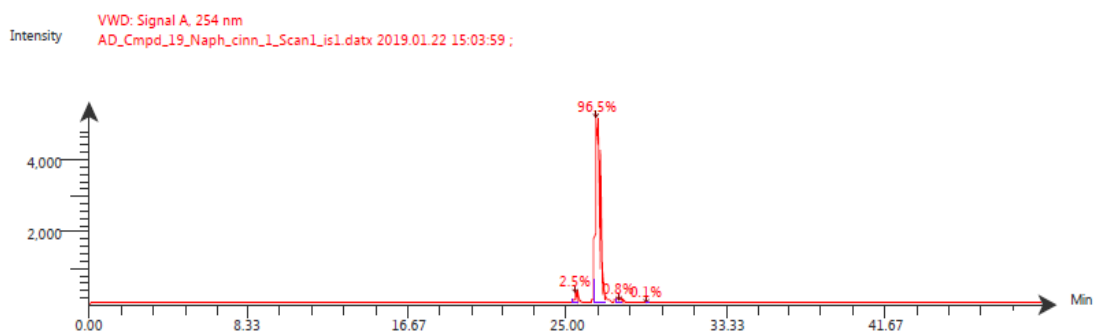


Figure A12. ¹³C NMR spectrum of *(E)*-3-(naphthalen-1-yl)acrylaldehyde, **37**



Time (Peak Maximum M:S/Minutes)	Maximum Intensity (c/s)	Time (Peak Centroid M:S/Minutes)	Peak Area	% Peak Area	Peak Resolution Label
25.45	2.8E2	25.46	2.3E3	2.5	8.4
26.54	5.1E3	26.58	8.6E4	96.5	16.4
27.66	6.5E1	27.68	7.4E2	0.8	16.3
29.18	1.3E1	29.21	8.9E1	0.1	11.6

Figure A13. LCMS spectrum of (*E*)-3-(naphthalen-1-yl)acrylaldehyde, **37**

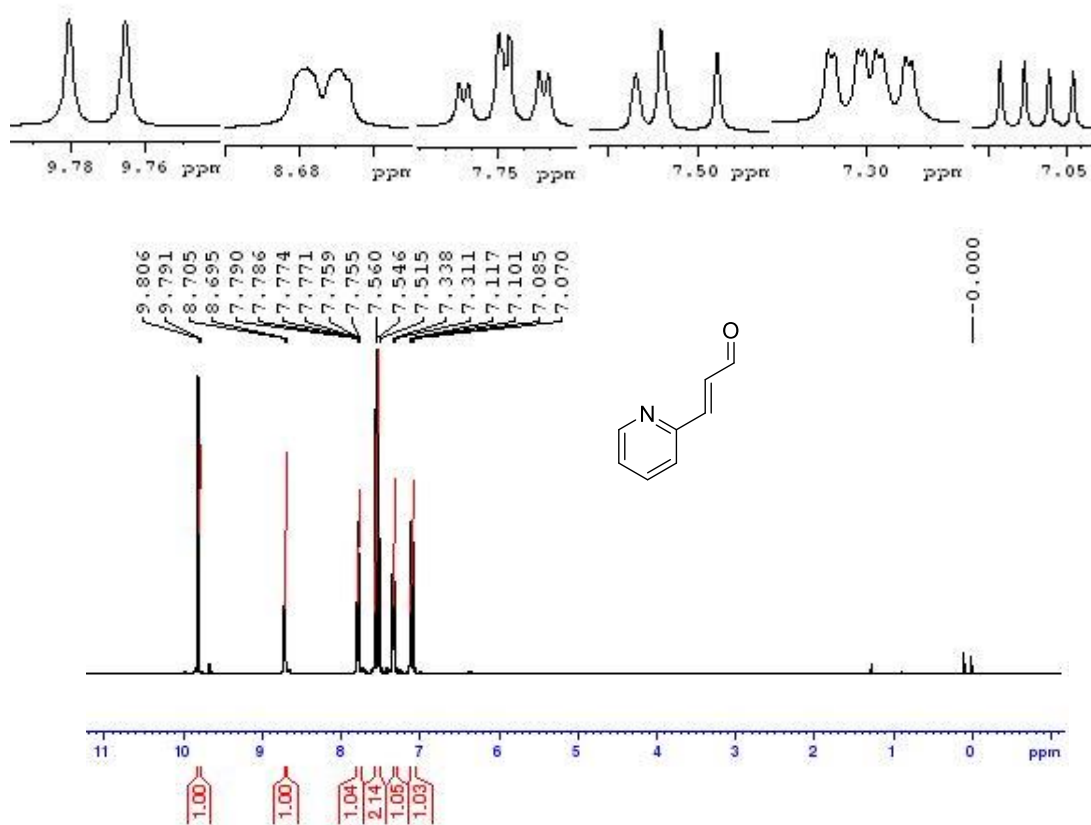


Figure A14. ¹H NMR spectrum of (*E*)-3-(pyridin-2-yl)acrylaldehyde, **35**

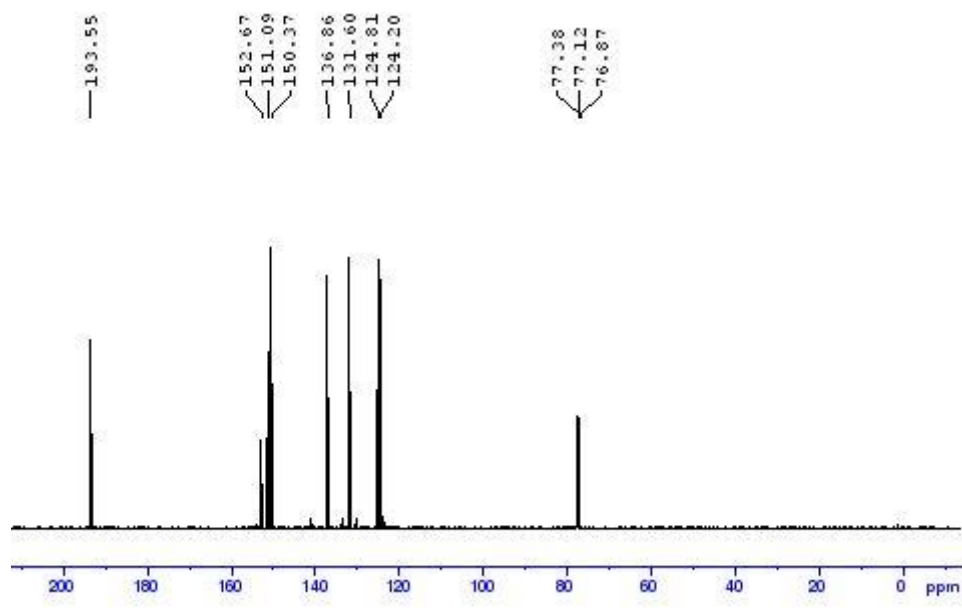


Figure A15. ^{13}C NMR spectrum of (*E*)-3-(pyridin-2-yl)acrylaldehyde, **35**

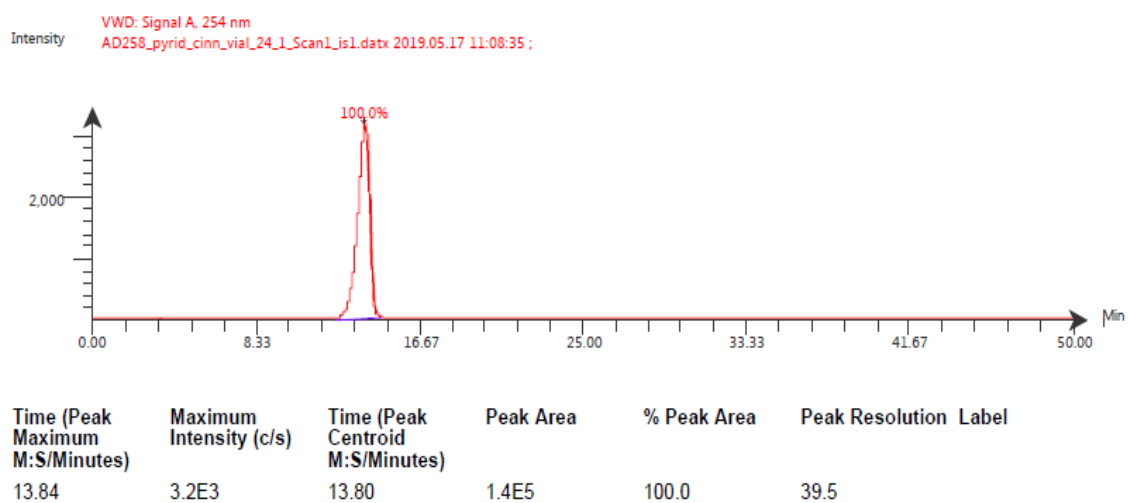


Figure A16. LCMS spectrum of (*E*)-3-(pyridin-2-yl)acrylaldehyde, **35**

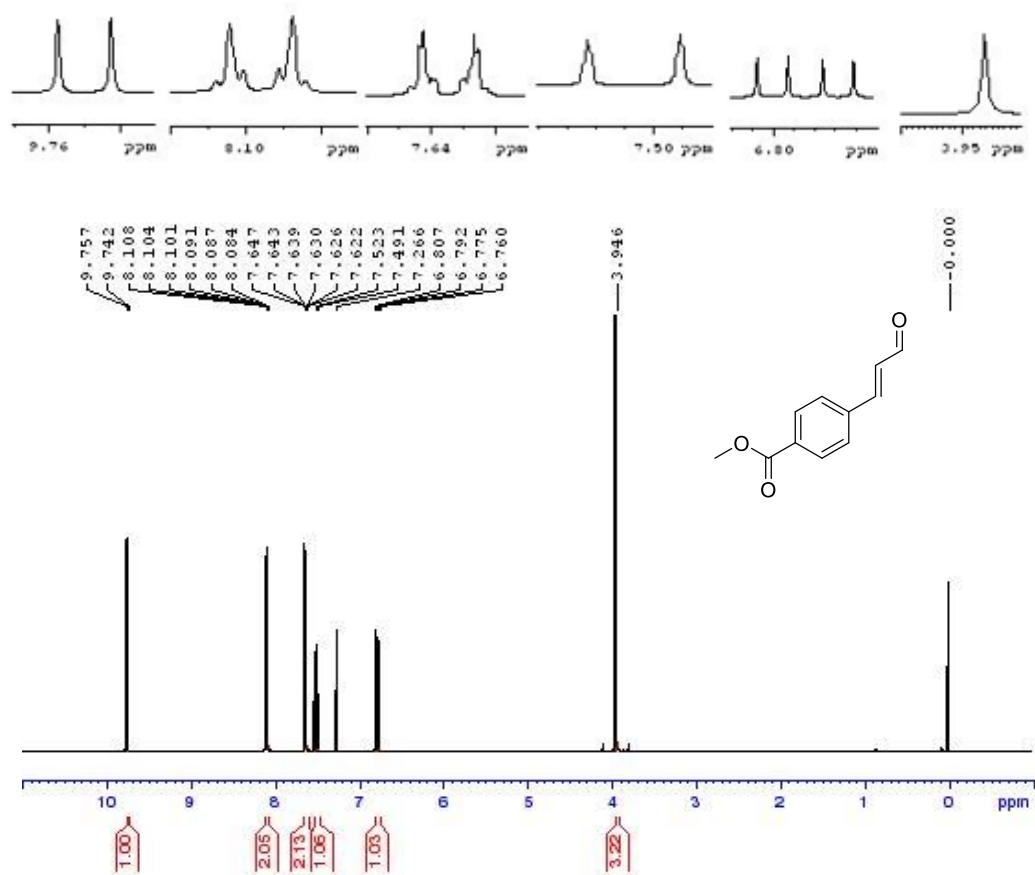


Figure A17. ¹H NMR spectrum of *(E)*-*p*-(methyl ester)cinnamaldehyde, **39**

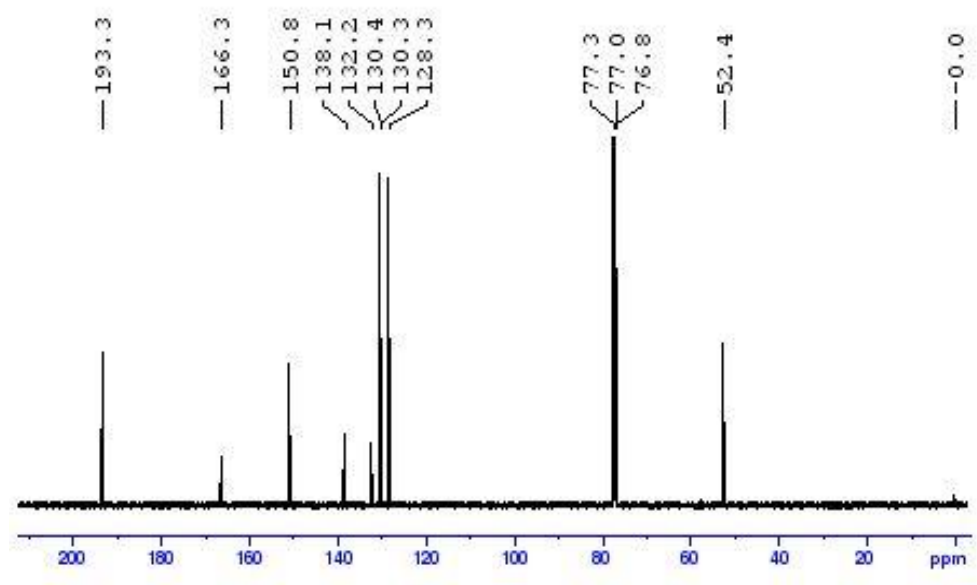
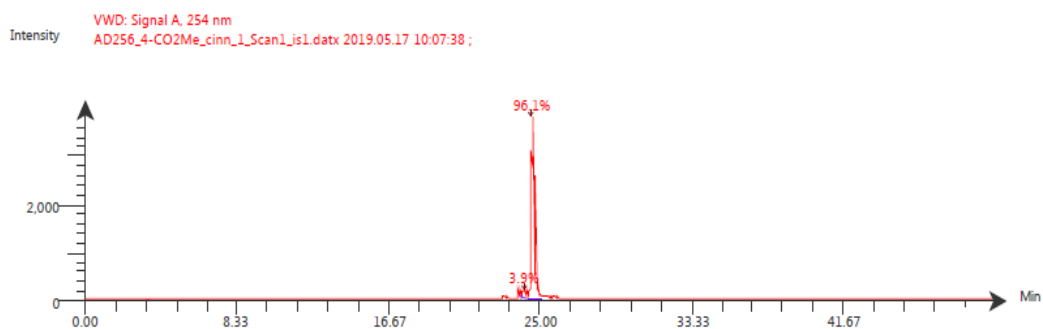


Figure A18. ¹³C NMR spectrum of *(E)*-*p*-(methyl ester)cinnamaldehyde, **39**



Time (Peak Maximum M:S/Minutes)	Maximum Intensity (c/s)	Time (Peak Centroid M:S/Minutes)	Peak Area	% Peak Area	Peak Resolution Label
24.10	1.8E2	24.09	1.8E3	3.9	9.9
24.55	3.8E3	24.55	4.5E4	96.1	10.7

Figure A19. LCMS spectrum of (*E*)-*p*-(methyl ester)cinnamaldehyde, **39**

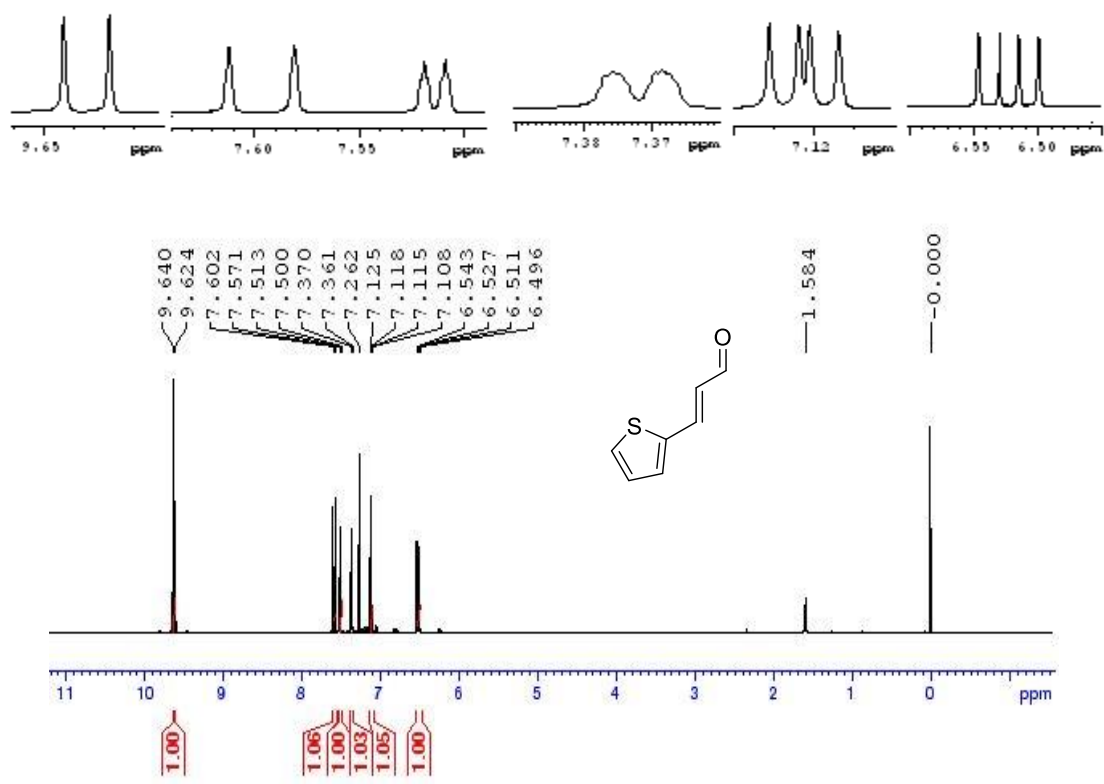


Figure A20. ^1H NMR spectrum of (*E*)-3-(thiophen-2-yl)acrylaldehyde, **36**

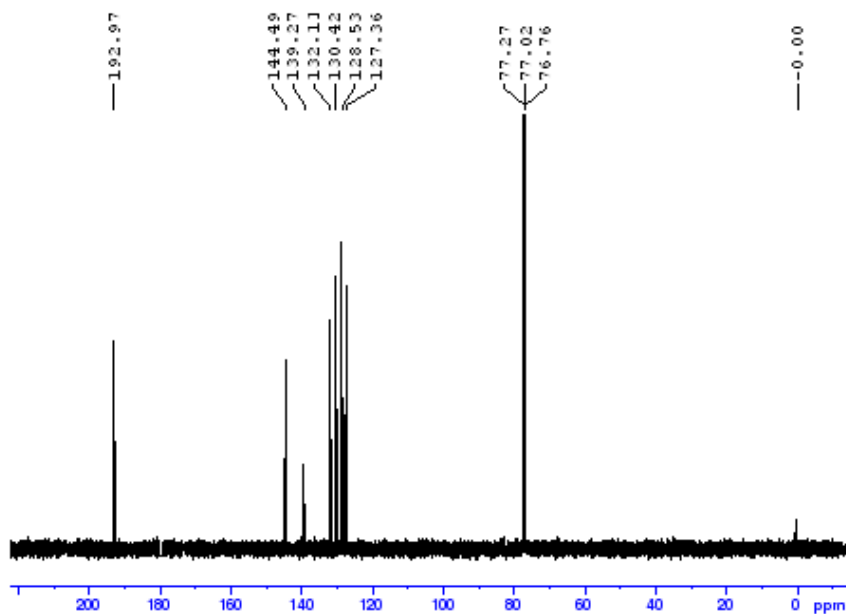
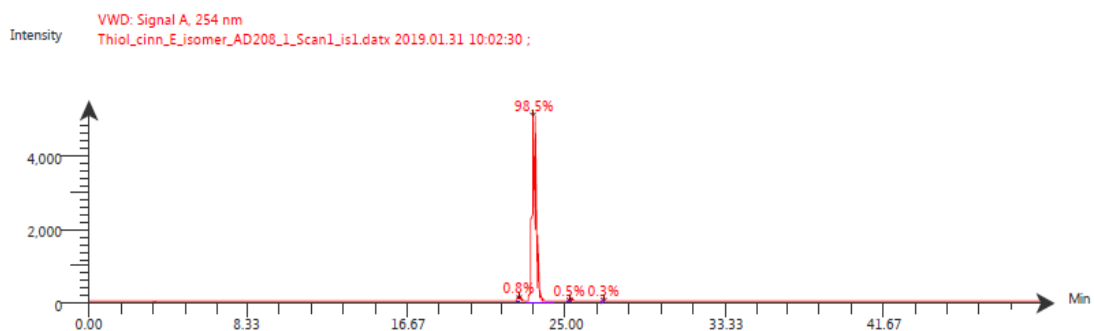


Figure A21. ^{13}C NMR spectrum of (*E*)-3-(thiophen-2-yl)acrylaldehyde, **36**



Time (Peak Maximum M:S/Minutes)	Maximum Intensity (c/s)	Time (Peak Centroid M:S/Minutes)	Peak Area	% Peak Area	Peak Resolution	Label
22.52	7.7E1	22.52	5.5E2	0.8	8.0	
23.29	5.1E3	23.29	7.1E4	98.5	12.6	
25.22	4.1E1	25.22	3.5E2	0.5	9.5	
26.99	2.1E1	26.98	2E2	0.3	6.4	

Figure A22. LCMS spectrum of (*E*)-3-(thiophen-2-yl)acrylaldehyde, **36**

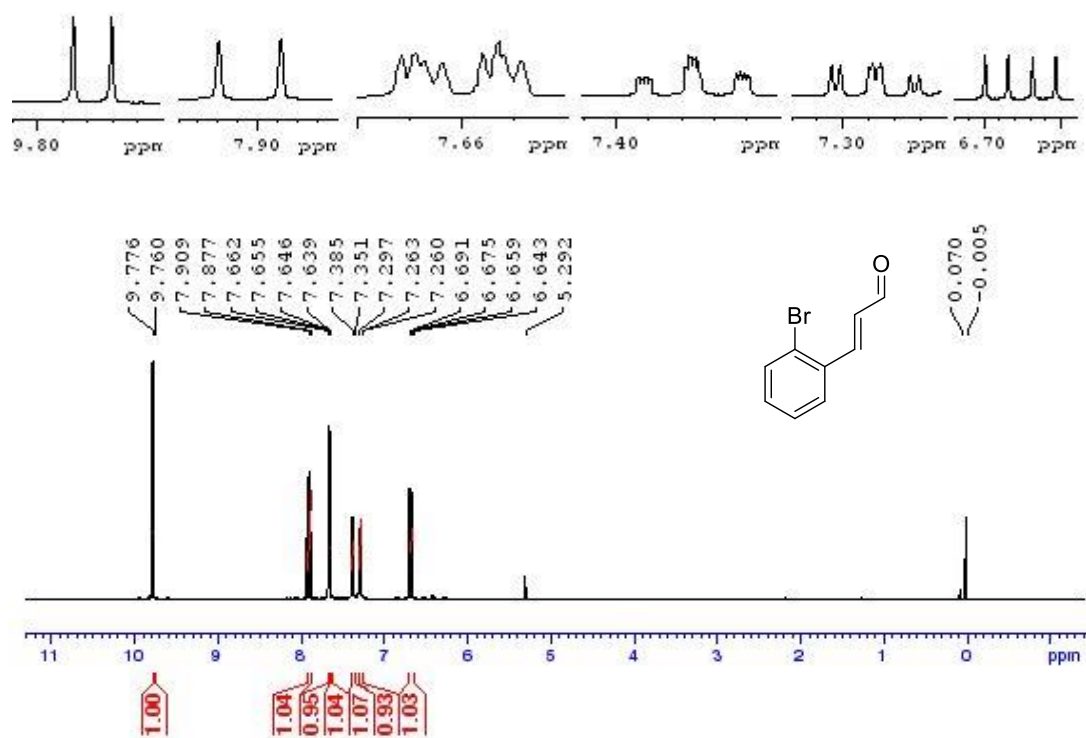


Figure A23. ¹H NMR spectrum of *(E)*-*o*-bromocinnamaldehyde, 5

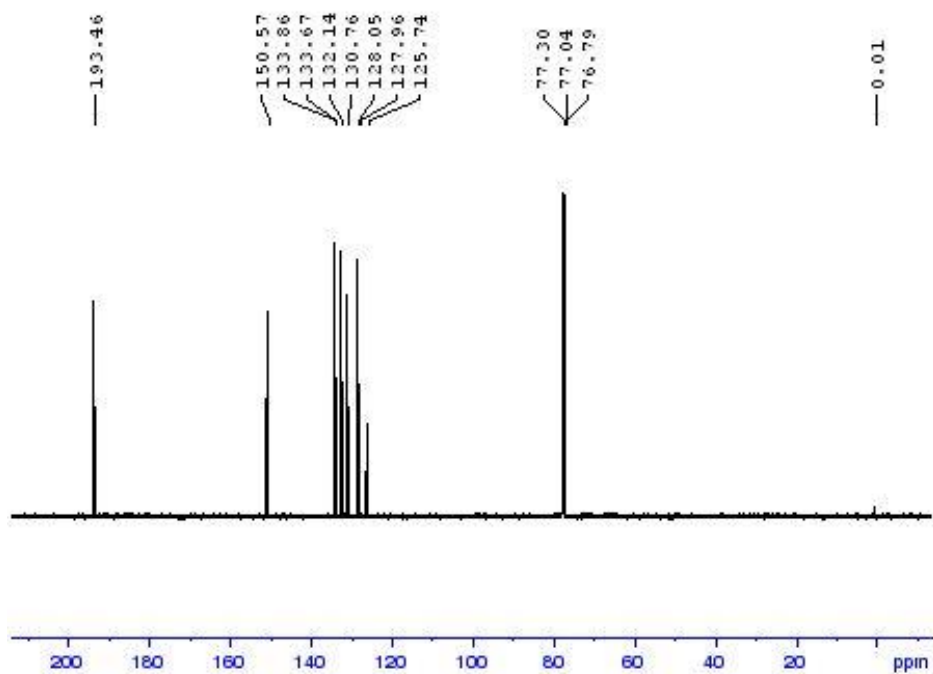
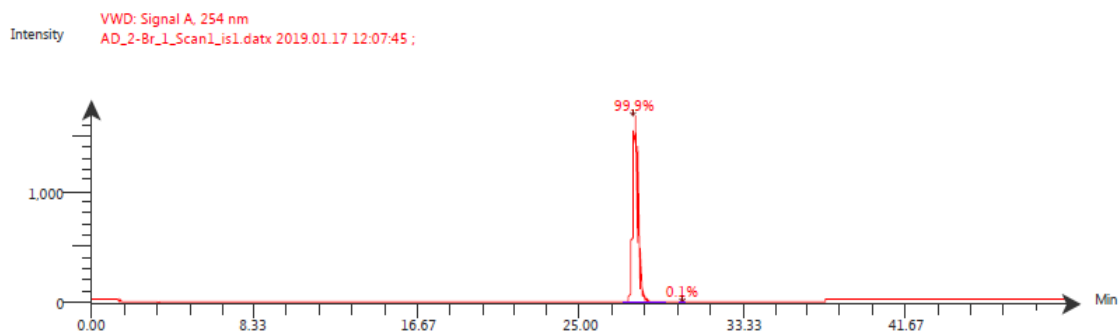


Figure A24. ¹³C NMR spectrum of *(E)*-*o*-bromocinnamaldehyde, 5



Time (Peak Maximum M:S/Minutes)	Maximum Intensity (c/s)	Time (Peak Centroid M:S/Minutes)	Peak Area	% Peak Area	Peak Resolution Label
27.79	1.7E3	27.79	3.1E4	99.9	16.5
0.00	1.6E1	30.22	2.7E1	0.1	18.3

Figure A25. LCMS spectrum of (*E*)-*o*-bromocinnamaldehyde, 5

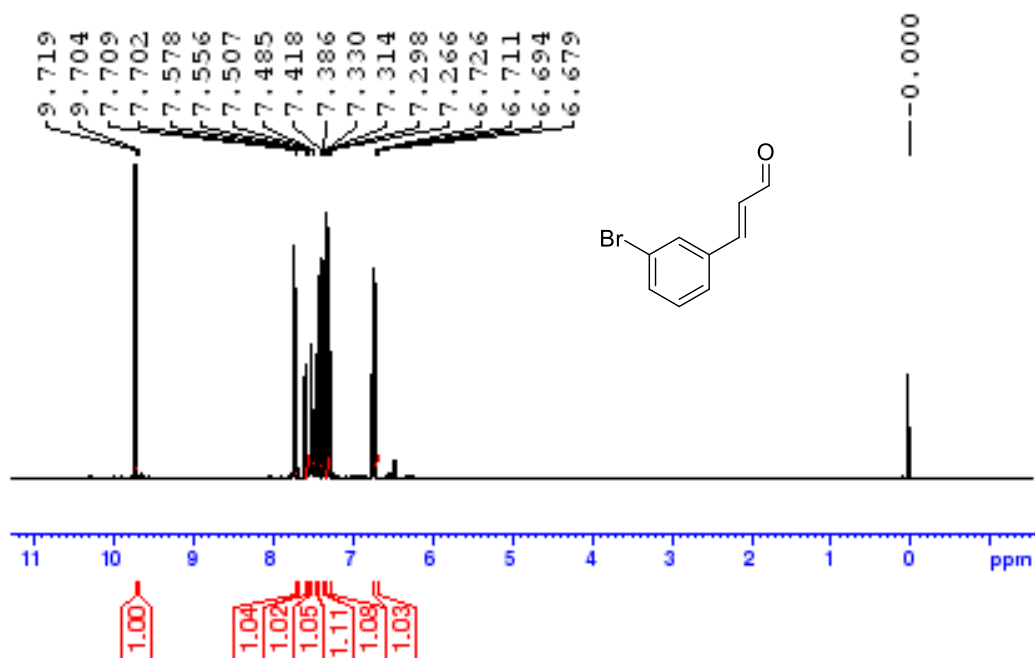
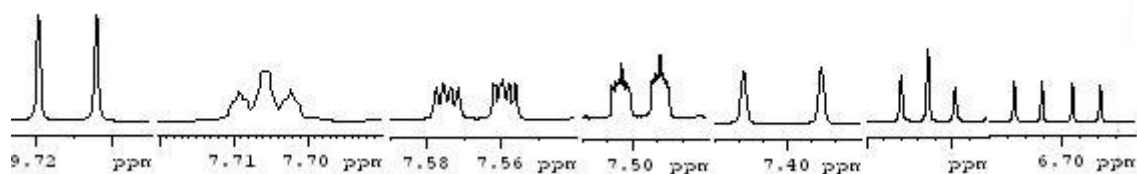


Figure A26. ¹H NMR spectrum of (*E*)-*m*-bromocinnamaldehyde, 34

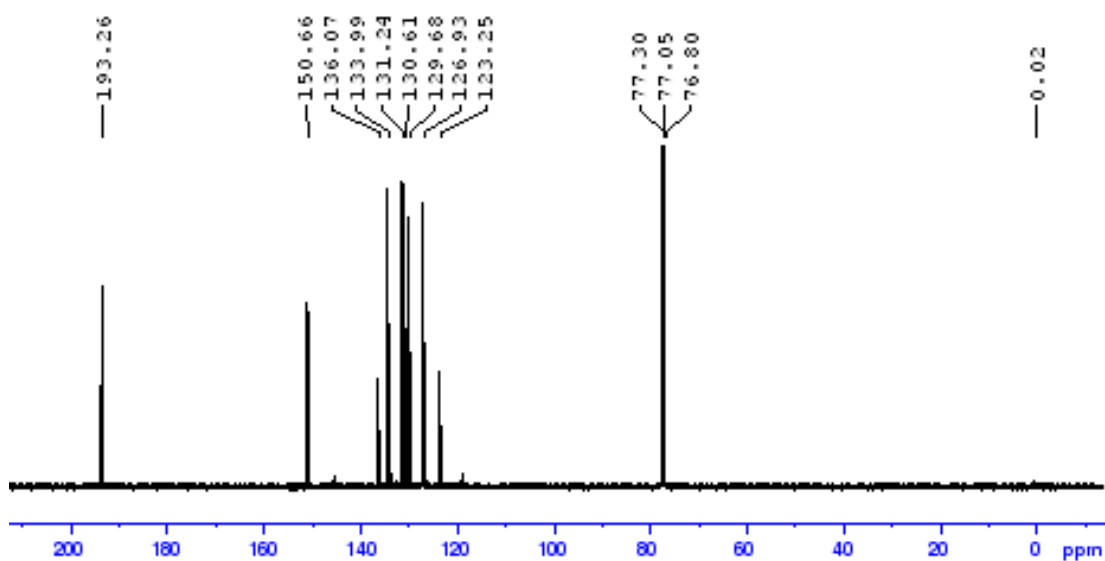


Figure A27. ¹³C NMR spectrum of (*E*)-*m*-bromocinnamaldehyde, **34**

Note: A HPLC chromatogram of **34** could not be obtained as it degraded on the HPLC column.

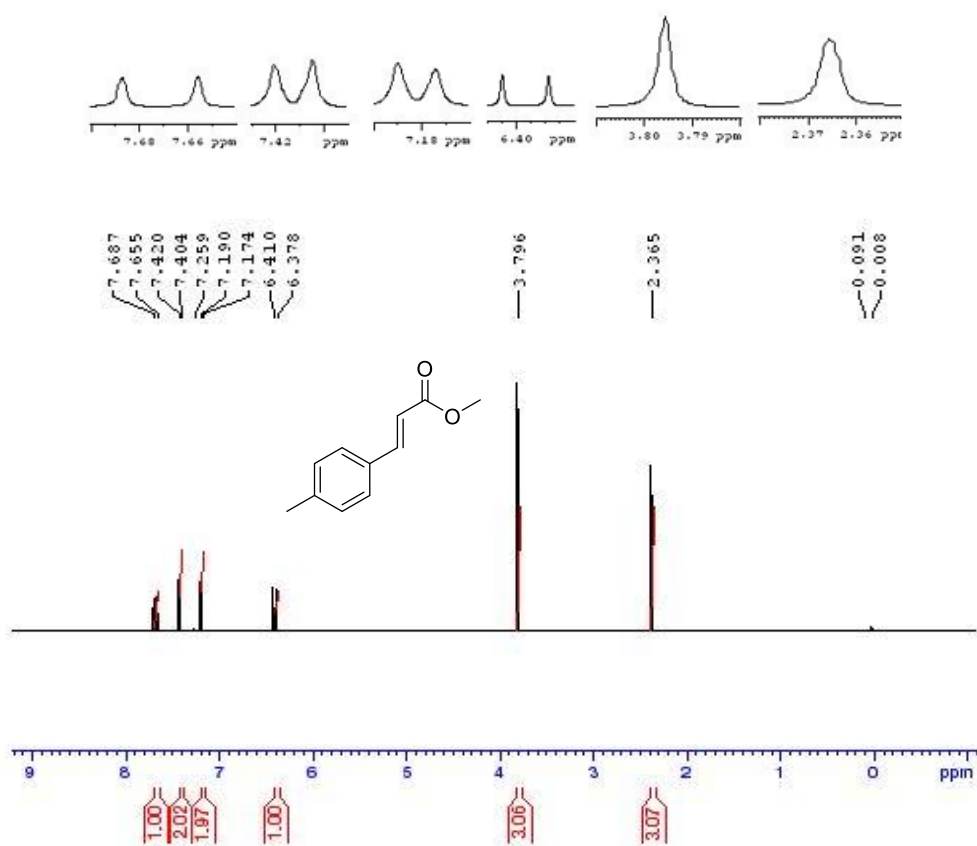


Figure A28. ¹H NMR spectrum of (*E*)-*p*-methyl cinnamate, **42**

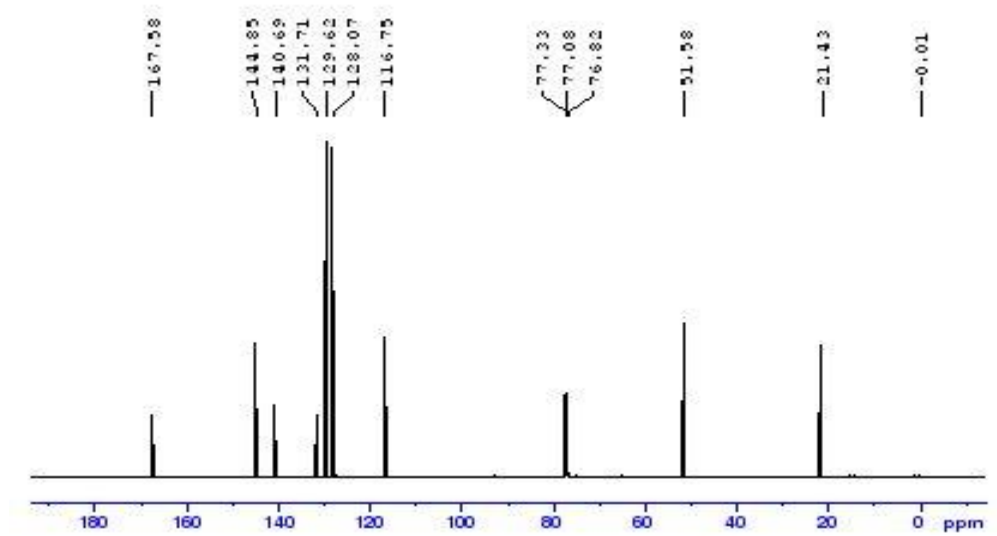


Figure A29. ^{13}C NMR spectrum of *(E)*-*p*-methyl cinnamate, 42

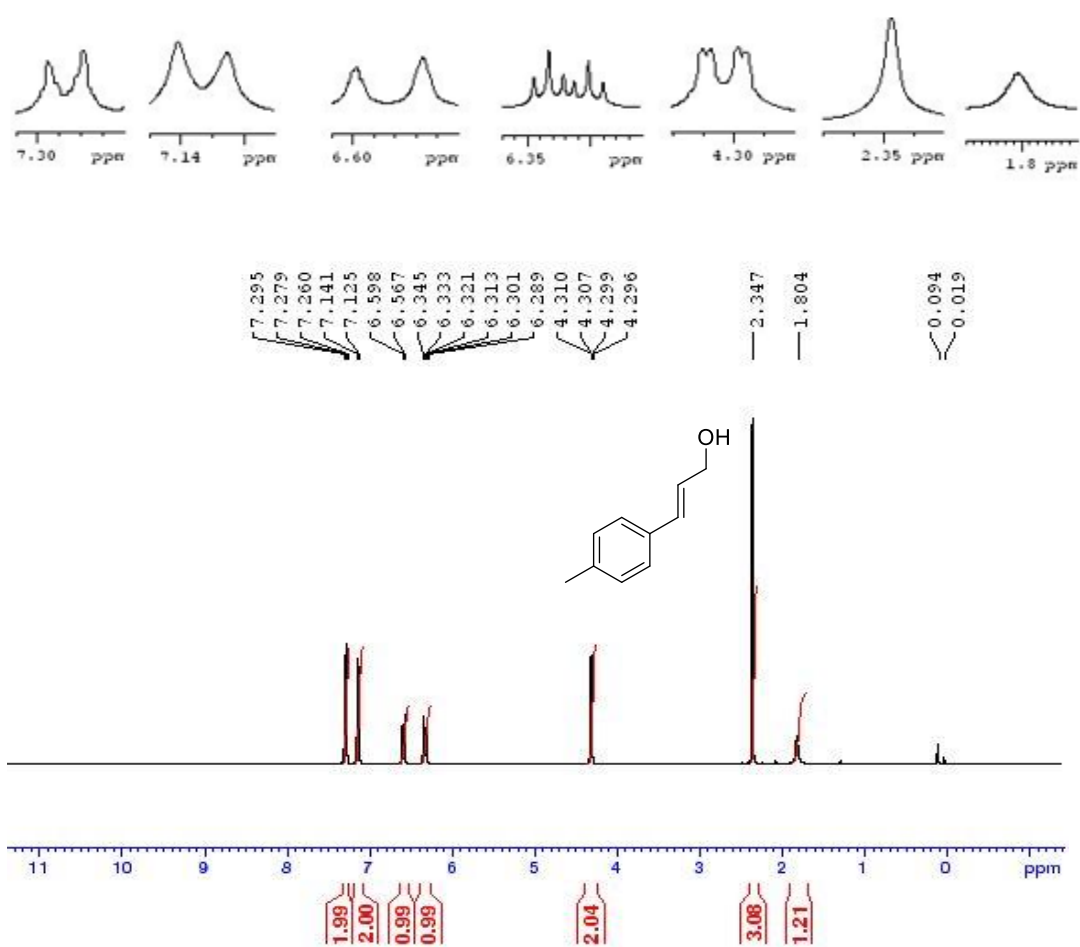


Figure A30. ^1H NMR spectrum of *(E)*-3-*p*-tolylprop-2-en-1-ol, 43

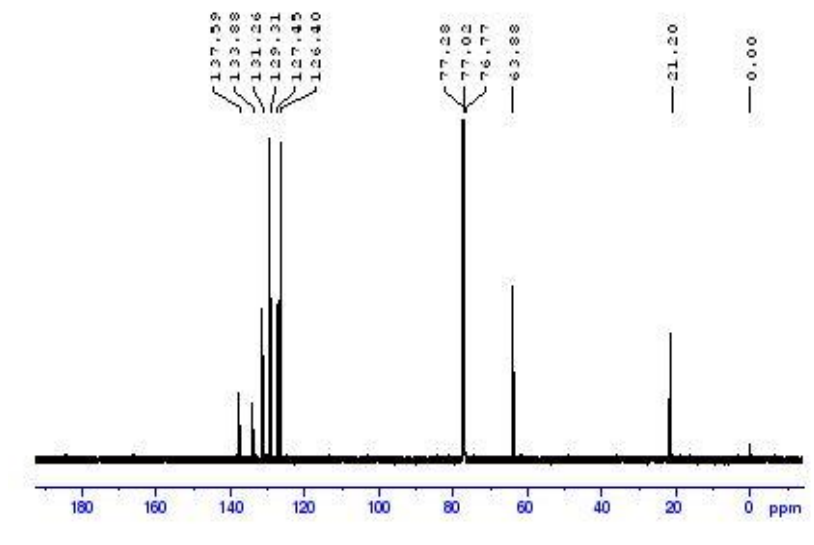


Figure A31. ^{13}C NMR spectrum of (*E*)-3-*p*-tolylprop-2-en-1-ol, **43**

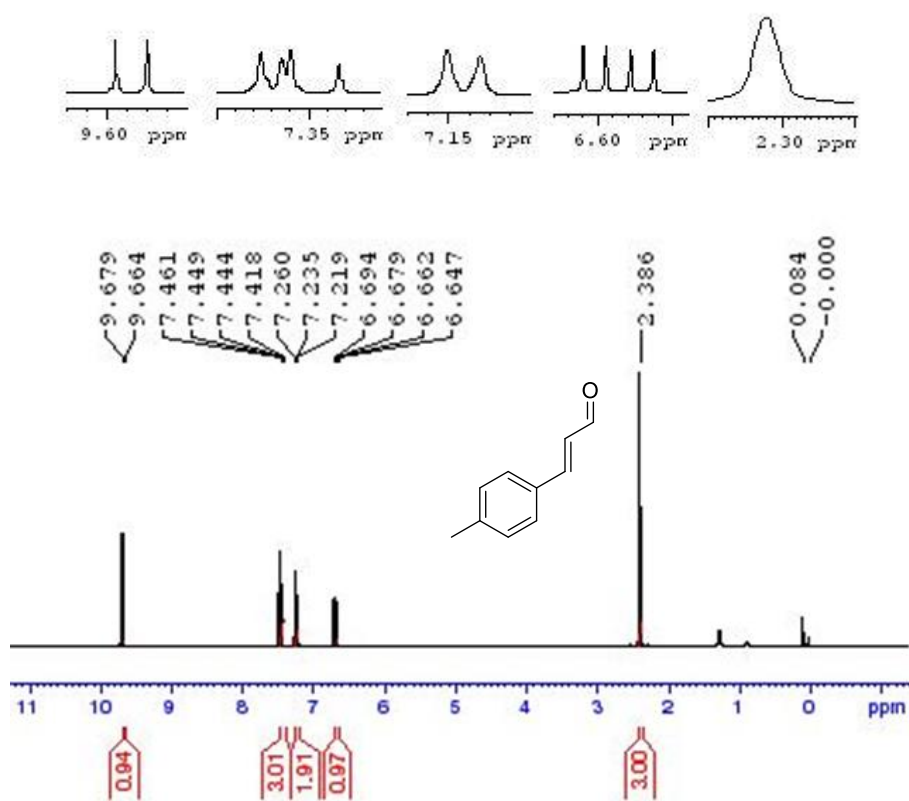


Figure A32. ^1H NMR spectrum of (*E*)-*p*-methyl cinnamaldehyde, **41**

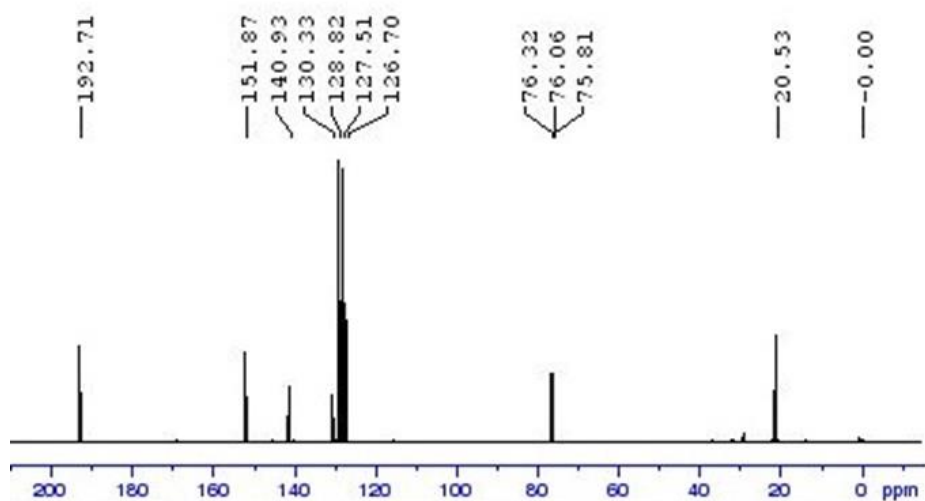
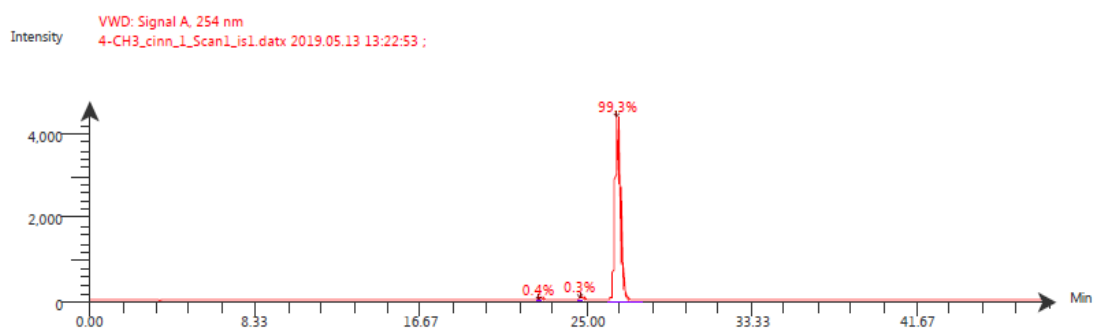


Figure A33. ^{13}C NMR spectrum of (*E*)-*p*-methyl cinnamaldehyde, **41**



Time (Peak Maximum M:S/Minutes)	Maximum Intensity (c/s)	Time (Peak Centroid M:S/Minutes)	Peak Area	% Peak Area	Peak Resolution Label
22.67	3.8E1	22.67	3E2	0.4	9.1
24.74	3.7E1	24.74	2.7E2	0.3	8.3
26.53	4.4E3	26.54	8.4E4	99.3	17.4

Figure A34. LCMS spectrum of (*E*)-*p*-methyl cinnamaldehyde, **41**

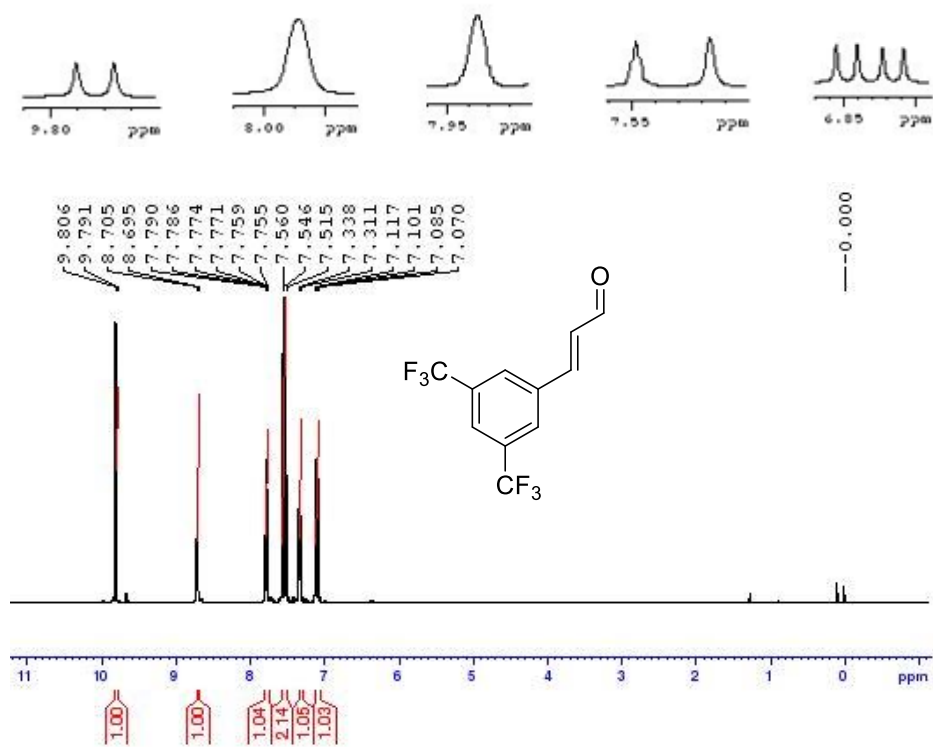


Figure A35. ¹H NMR spectrum of (*E*)-3,5-bis(trifluoromethyl)cinnamaldehyde, **86**

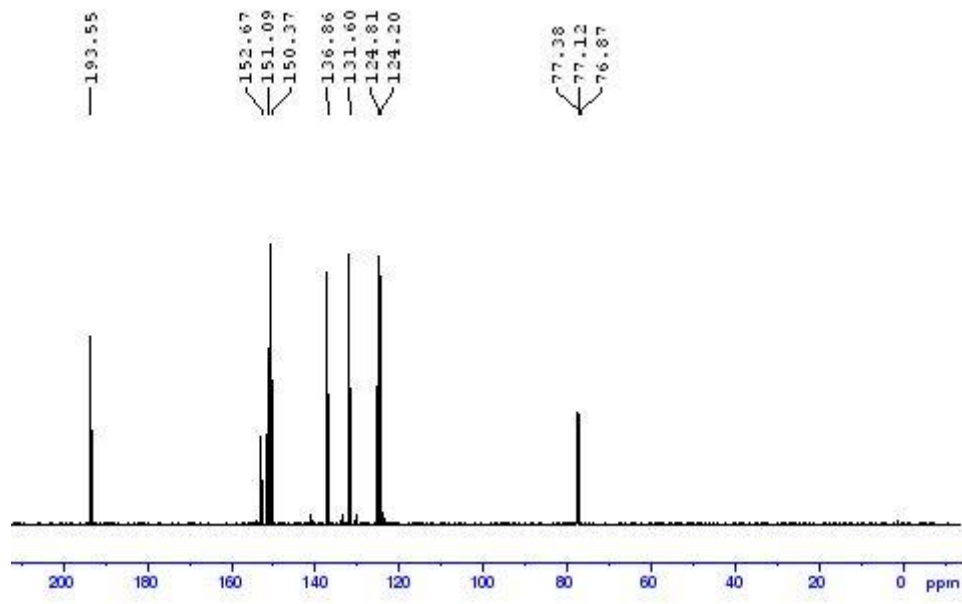


Figure A36. ¹³C NMR spectrum of (*E*)-3,5-bis(trifluoromethyl)cinnamaldehyde, **86**

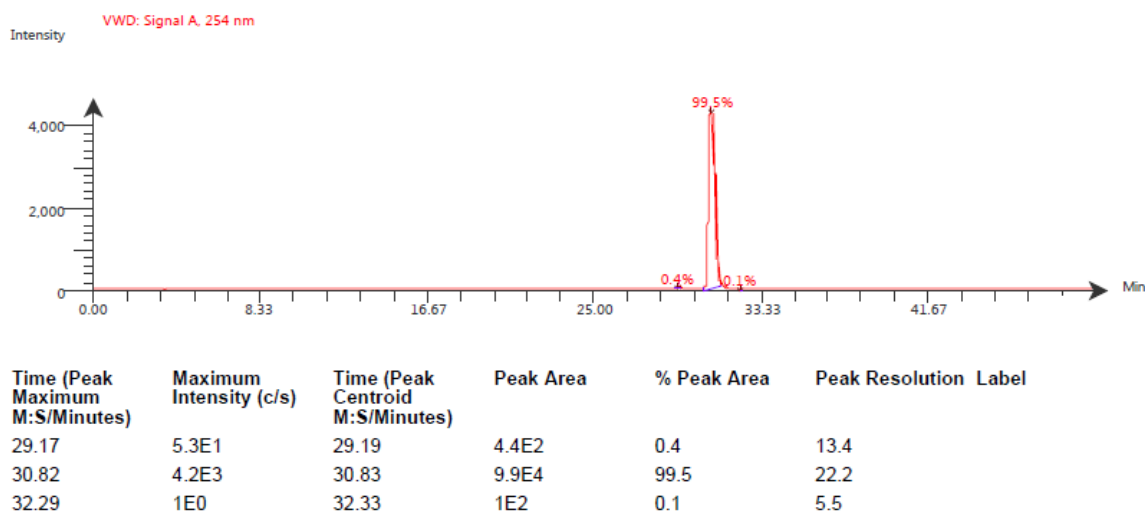


Figure A37. LCMS spectrum of (*E*)-3,5-bis(trifluoromethyl)cinnamaldehyde, **86**

^1H NMR spectra of example crude cinnamaldehyde mixtures.

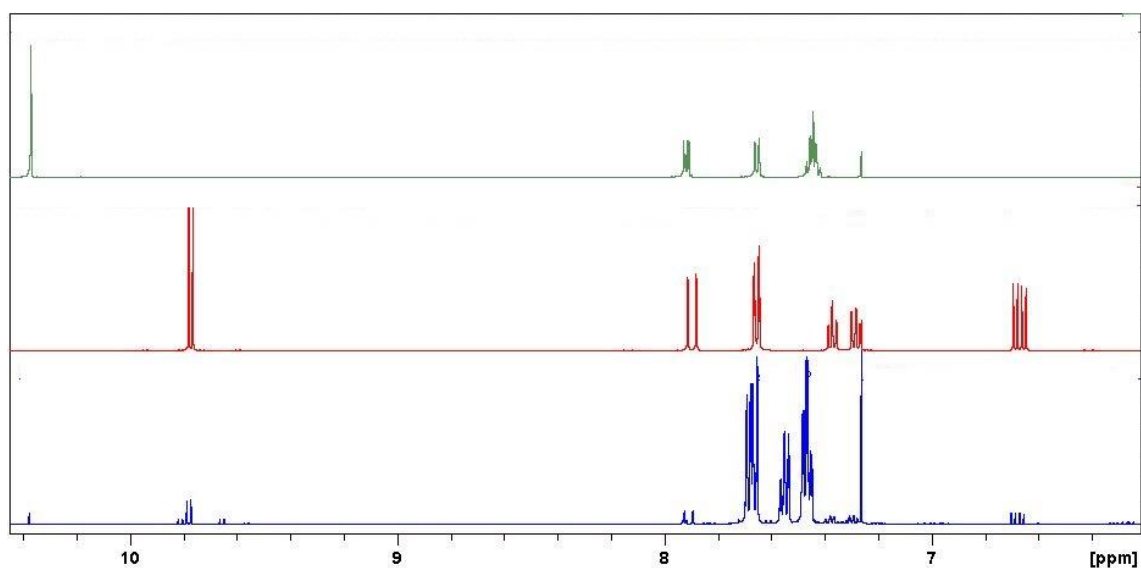


Figure A38. (a) The ^1H NMR of 2-bromobenzaldehyde (starting material, green), (b) the ^1H NMR of isolated (*E*)-2-bromocinnamaldehyde, **5** (product, red) and (c) the ^1H NMR of the crude mixture after reacting 2-bromobenzaldehyde and (triphenylphosphoranylidene)acetaldehyde for 24 hours in toluene at 80°C (blue).

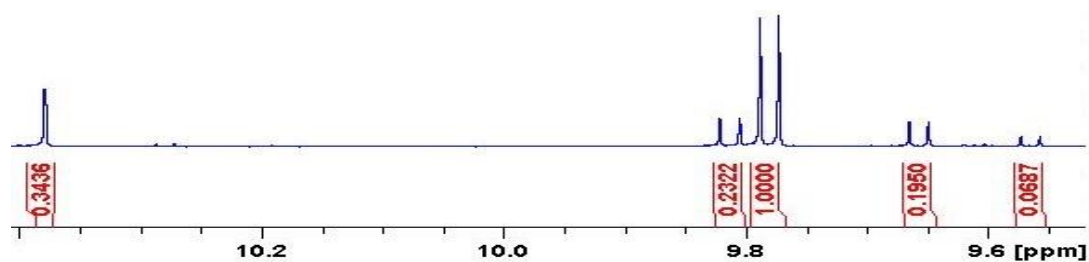


Figure A39. Zoomed in ^1H NMR of the crude mixture in Figure A38(c), showing *E:Z* cinnamaldehyde: starting aldehyde ratio, we well as formation of other aldehyde species as side products.

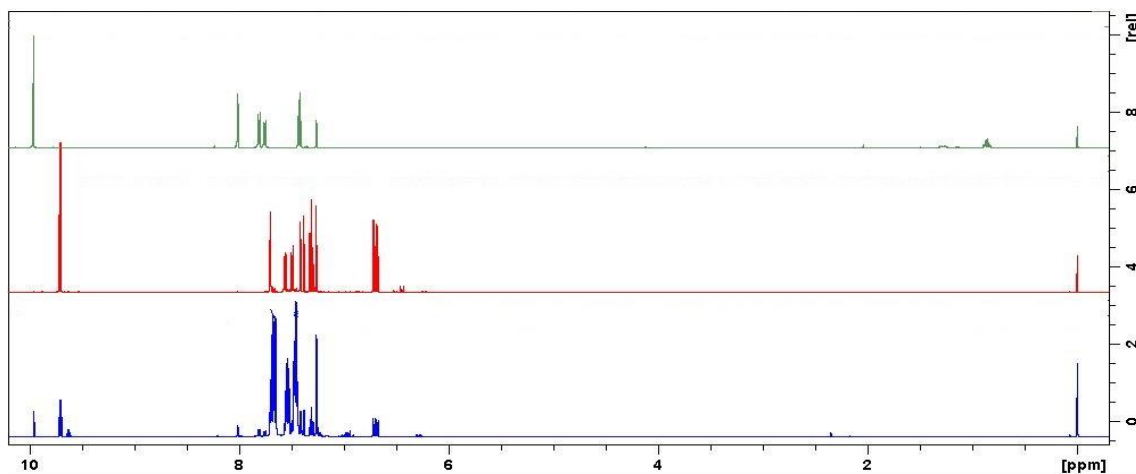


Figure A40. (a) The ^1H NMR of 3-bromobenzaldehyde (starting material, green), (b) the ^1H NMR of isolated (*E*)-3-bromocinnamaldehyde, **34** (product, red) and (c) the ^1H NMR of the crude mixture after reacting 3-bromobenzaldehyde and (triphenylphosphoranylidene)acetaldehyde for 24 hours in toluene at 80°C (blue).

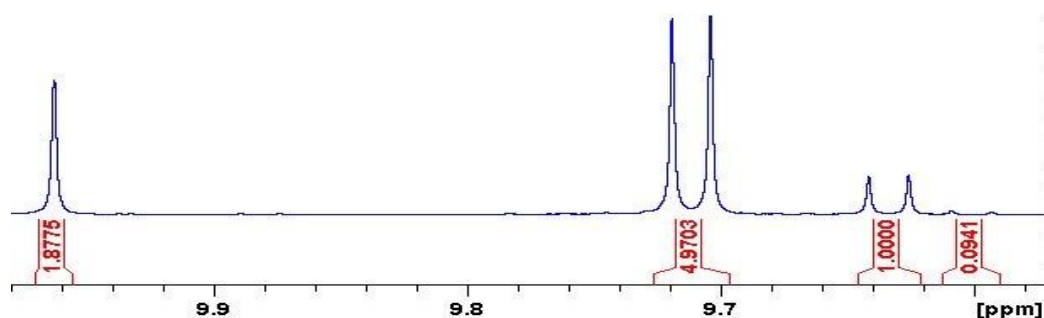


Figure A41. Zoomed in ^1H NMR of the crude mixture in Figure A40(c), showing *E:Z* cinnamaldehyde: starting aldehyde ratio, we well as formation of other aldehyde species as side products.

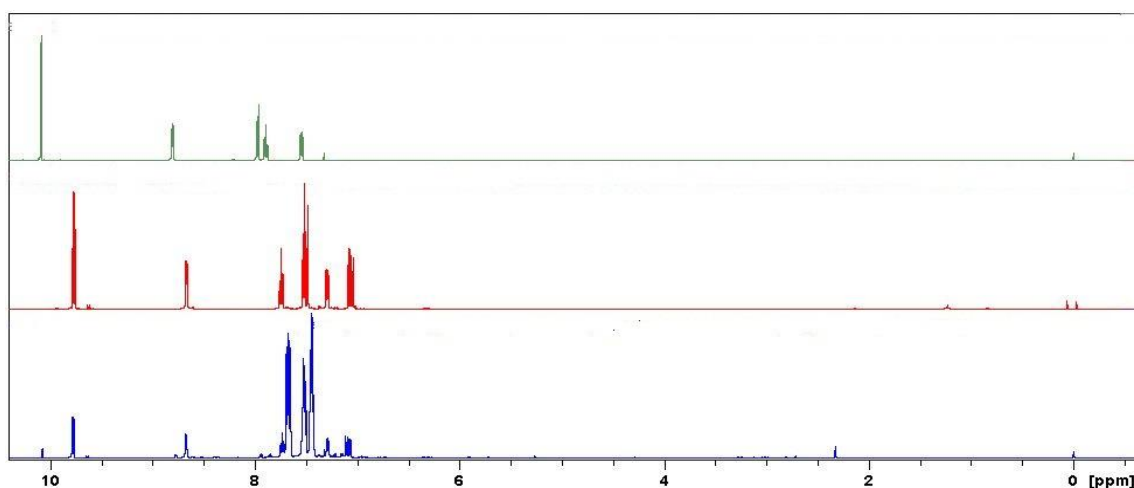


Figure A42. (a) The ^1H NMR of (*E*)-2-pyridine carboxaldehyde (green), (b) the ^1H NMR of isolated (*E*)-3-(pyridin-2-yl)acrylaldehyde, **35** (red) and (c) the ^1H NMR of the crude mixture after reacting (*E*)-2-pyridine carboxaldehyde and (triphenylphosphoranylidene)acetaldehyde for 24 hours in toluene at 80°C

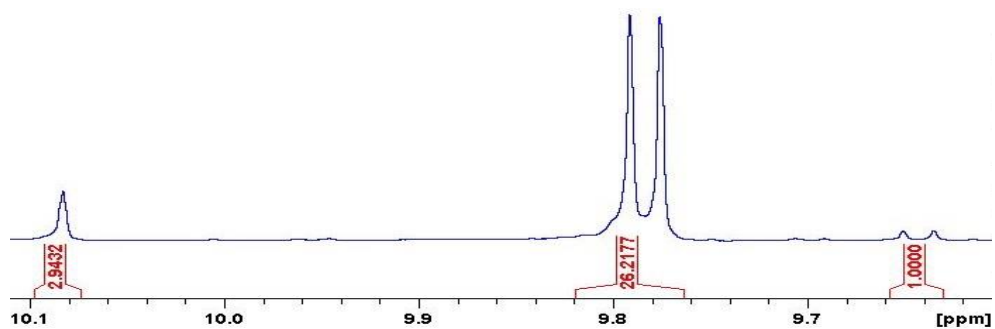


Figure A43. Zoomed in ^1H NMR of the crude mixture in Figure A42(c), showing *E:Z* cinnamaldehyde: starting aldehyde ratio, we well as formation of other aldehyde species as side products.

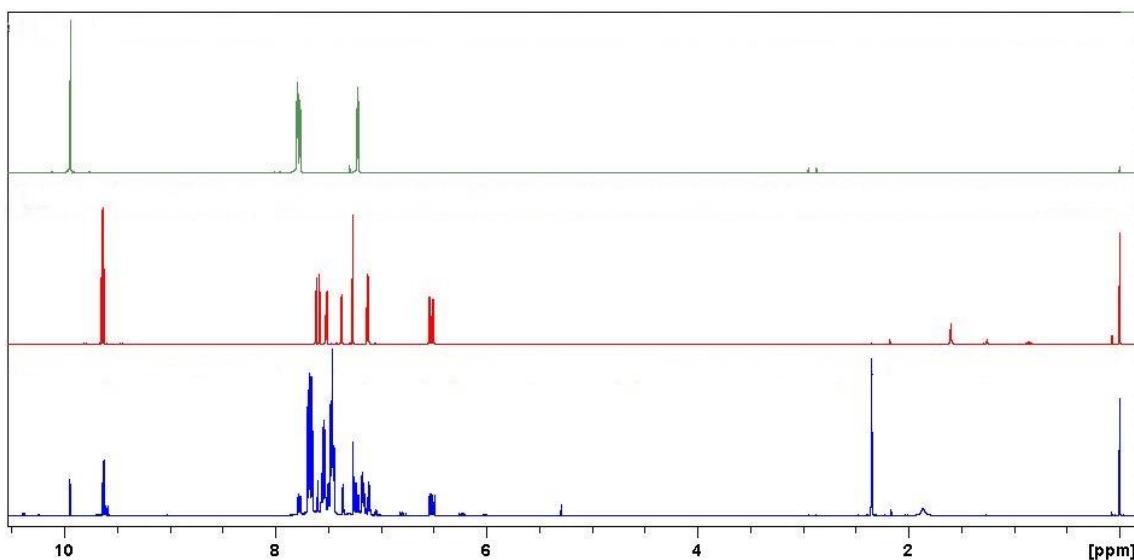


Figure A44. (a) The ^1H NMR of (*E*)- 2-thiophenecarboxaldehyde (green), (b) the ^1H NMR of isolated (*E*)-3-(thiophen-2-yl)acrylaldehyde, **36** (red) and (c) the ^1H NMR of the crude mixture after reacting (*E*)-2-thiophenecarboxaldehyde and (triphenylphosphoranylidene)acetaldehyde for 24 hours in toluene at 80°C

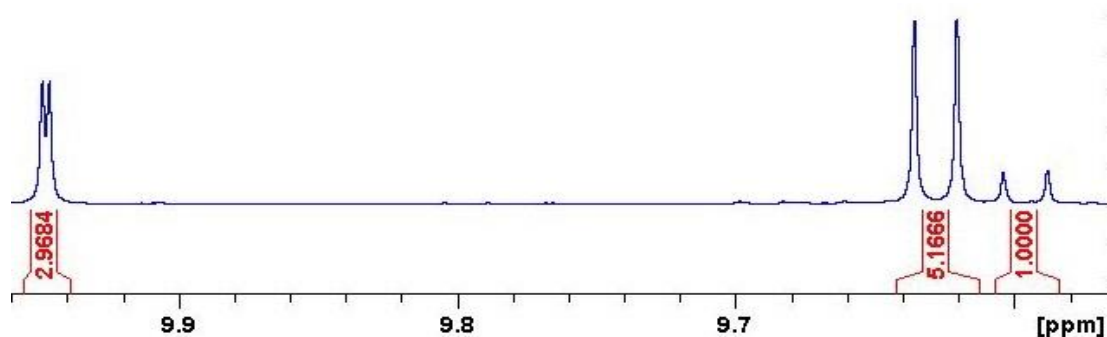


Figure A45. Zoomed in ^1H NMR of the crude mixture in Figure A44(c), showing *E:Z* cinnamaldehyde: starting aldehyde ratio, we well as formation of other aldehyde species as side products

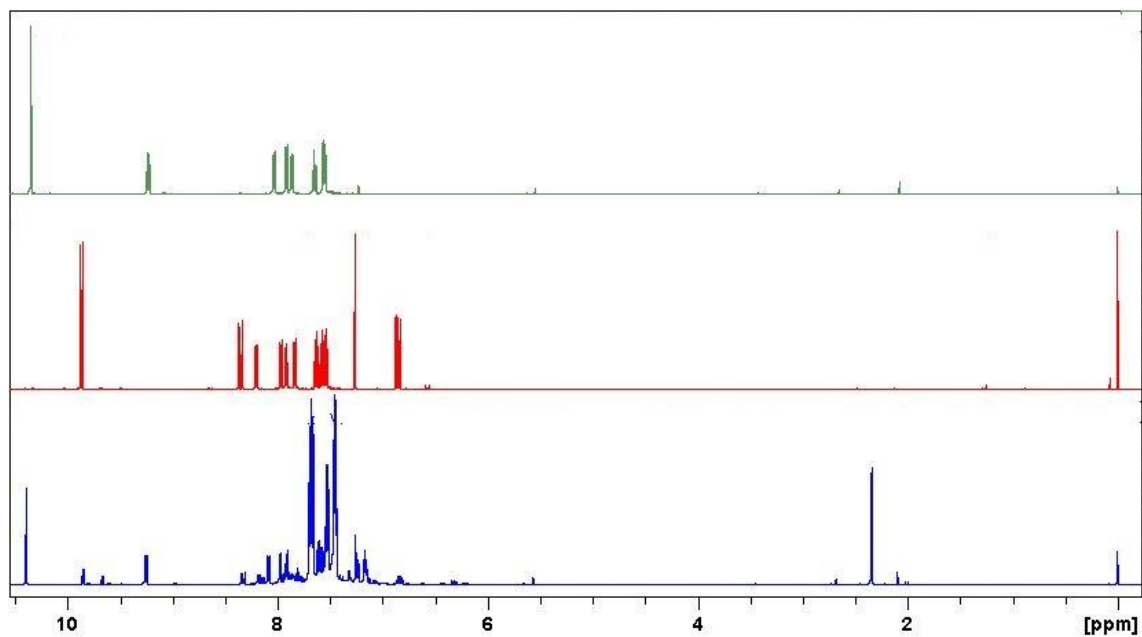


Figure 46. (a) The ^1H NMR of (*E*)- α -naphthaldehyde (green), (b) the ^1H NMR of isolated (*E*)-3-(naphthalen-1-yl)acrylaldehyde, **37** (red) and (c) the ^1H NMR of the crude mixture after reacting α -naphthaldehyde and (triphenylphosphoranylidene)acetaldehyde for 24 hours in toluene at 80°C

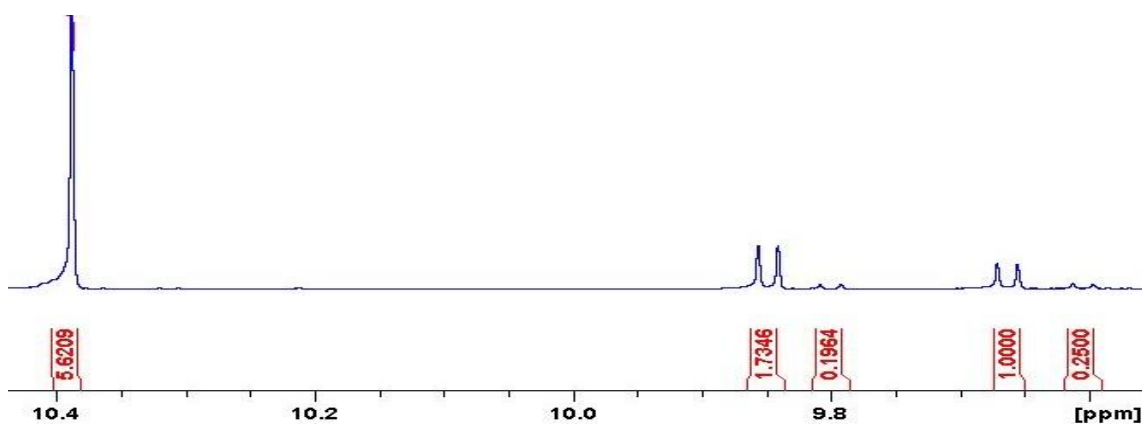


Figure A47. Zoomed in ^1H NMR of the crude mixture in Figure A46(c), showing *E*:*Z* cinnamaldehyde: starting aldehyde ratio, as well as formation of other aldehyde species as side products

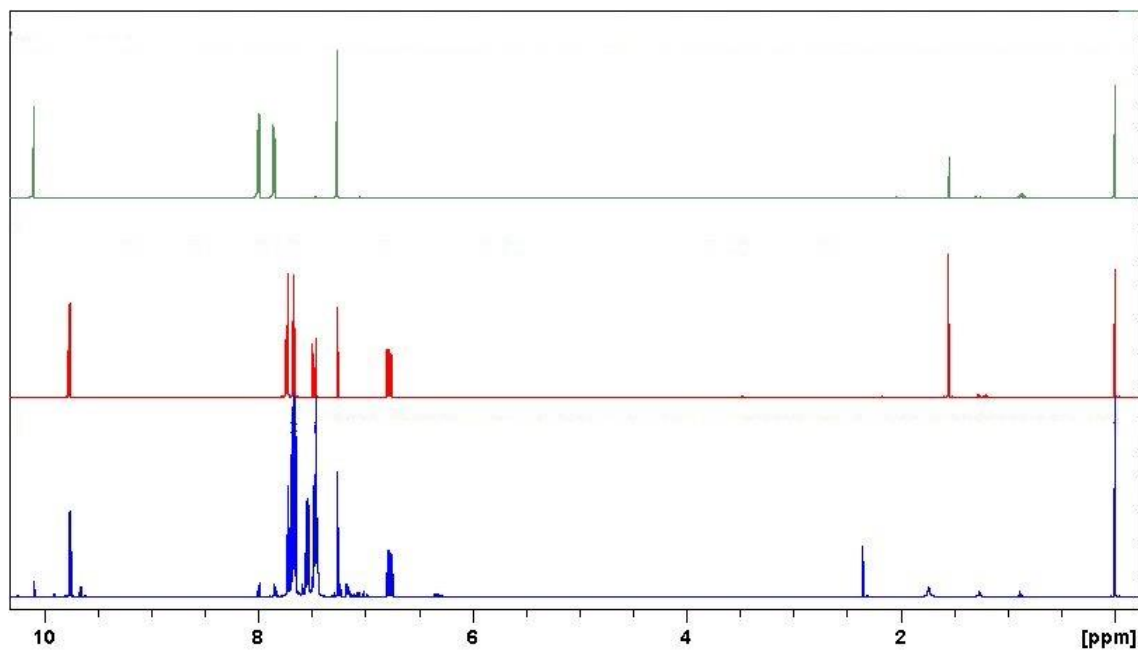


Figure A48. (a) The ^1H NMR of 4-formylbenzonitrile (green), (b) the ^1H NMR of isolated (*E*)-4-cyanocinnamaldehyde, **38** (red) and (c) the ^1H NMR of the crude mixture after reacting 4-formylbenzonitrile and (triphenylphosphoranylidene)acetaldehyde for 24 hours in toluene at 80°C

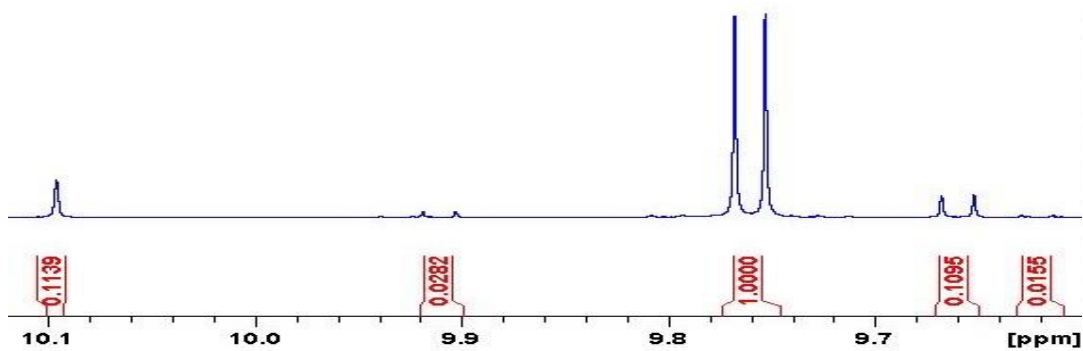


Figure A49. Zoomed in ^1H NMR of the crude mixture in Figure A48(c), showing *E*:*Z* cinnamaldehyde: starting aldehyde ratio, we well as formation of other aldehyde species as side products

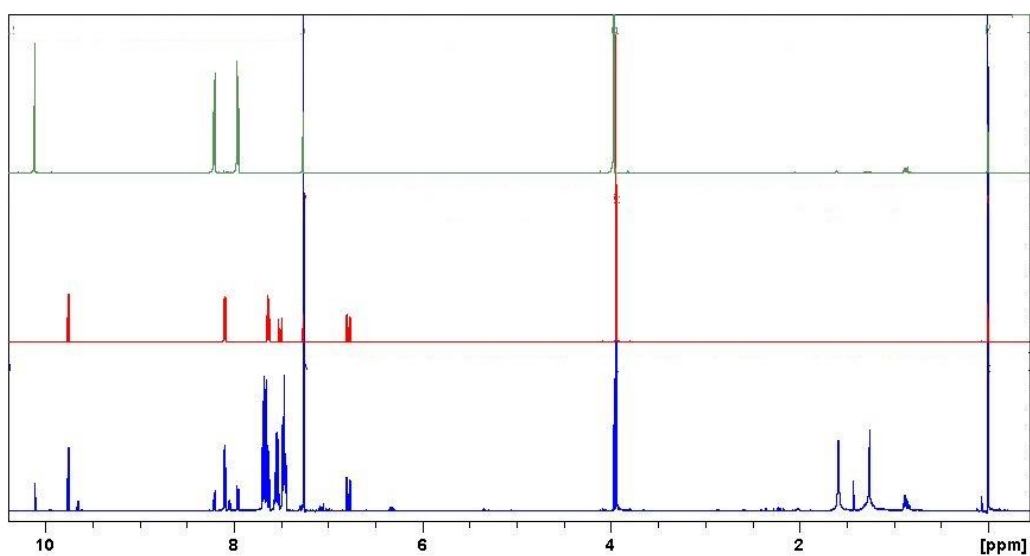


Figure A50. (a) The ^1H NMR of methyl 4-formylbenzoate, (b) the ^1H NMR of isolated (*E*)-4-(methyl ester)cinnamaldehyde, **39** (red) and (c) the ^1H NMR of the crude mixture after reacting 4-(methyl ester)benzaldehyde and (triphenylphosphoranylidene)acetaldehyde for 24 hours in toluene at 80°C

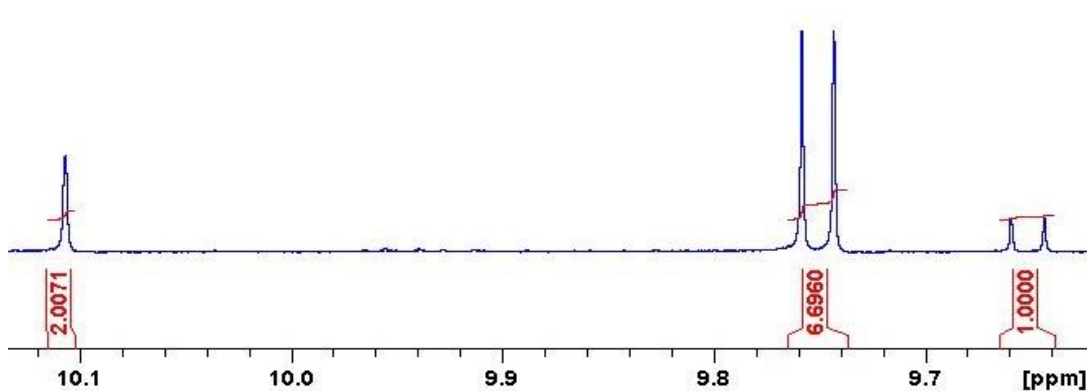


Figure A51. Zoomed in ^1H NMR of the crude mixture in Figure A50(c), showing *E*:*Z* cinnamaldehyde: starting aldehyde ratio, we well as formation of other aldehyde species as side products

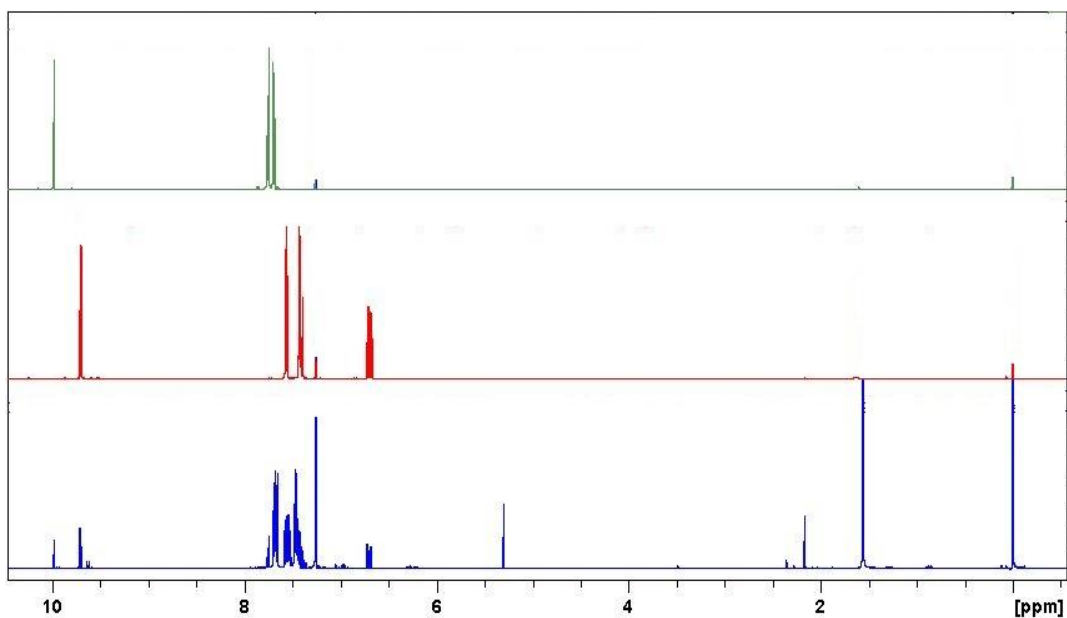


Figure 52. (a) The ^1H NMR of 4-bromobenzaldehyde (green), (b) the ^1H NMR of isolated (*E*)-4-bromocinnamaldehyde, **40** (red) and (c) the ^1H NMR of the crude mixture after reacting 4-bromobenzaldehyde and (triphenylphosphoranylidene)acetaldehyde for 24 hours in toluene at 80°C

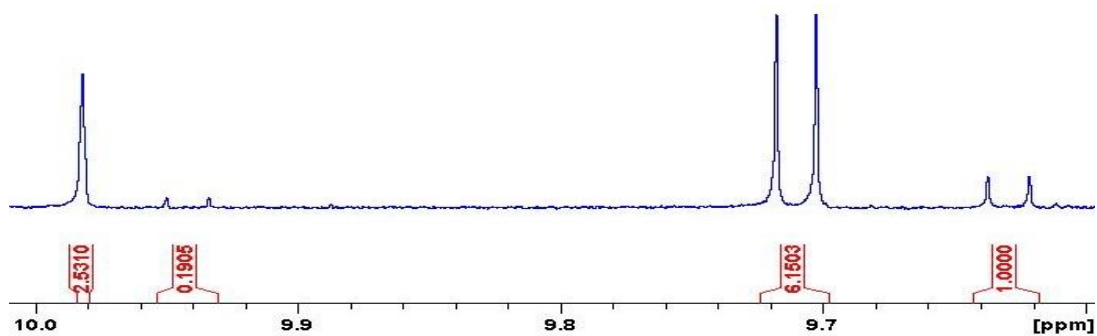


Figure A53. Zoomed in ^1H NMR of the crude mixture in Figure A52(c), showing *E:Z* cinnamaldehyde: starting aldehyde ratio, we well as formation of other aldehyde species as side products

NMR spectra relevant to cysteamine assay:

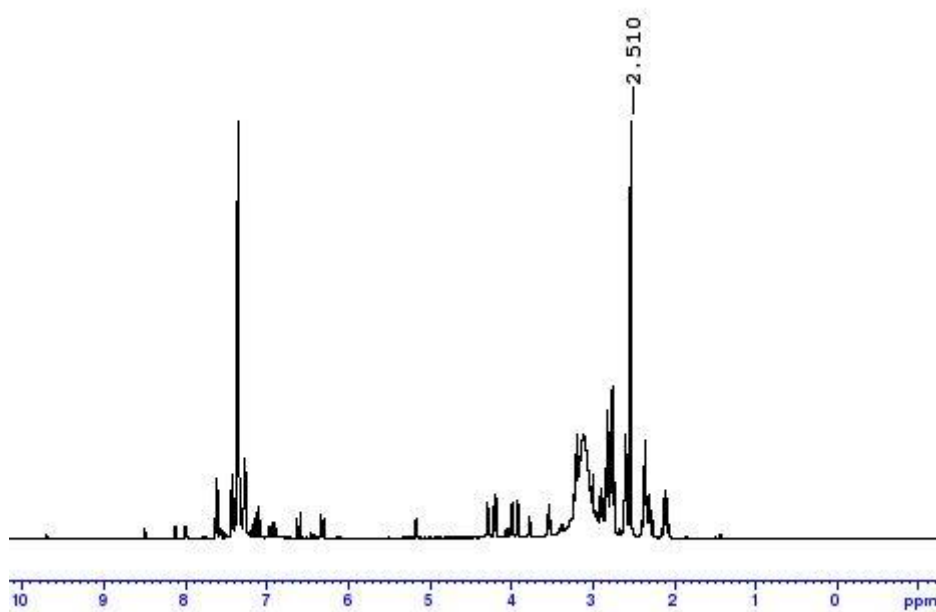


Figure A54. ^1H NMR spectrum acquired after reaction of *trans*-cinnamaldehyde, **1**, and cysteamine

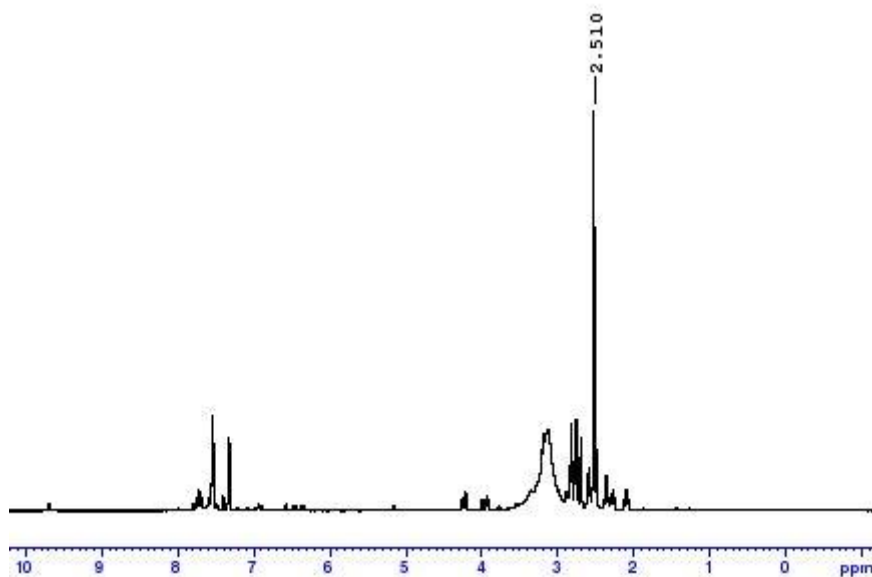


Figure A55. ^1H NMR spectrum acquired after reaction of (*E*)-4-bromocinnamaldehyde, **40**, and cysteamine

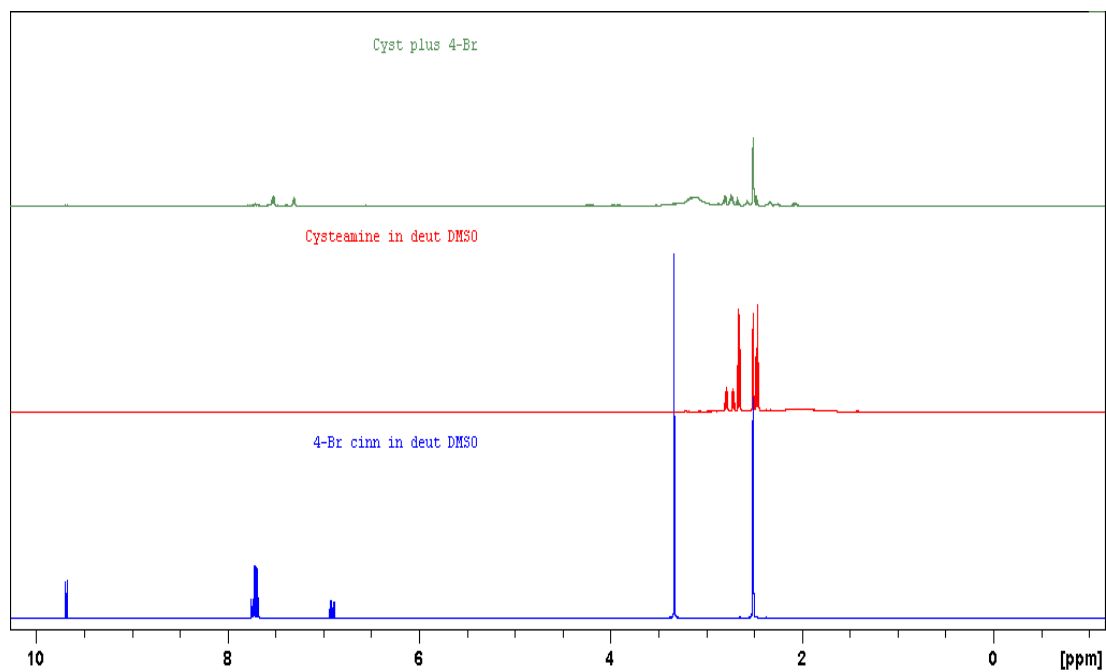


Figure A56. ¹H NMR of (a) The reaction between cysteamine and (*E*) 4-bromocinnamaldehyde, **40**, at room temperature (green), where there is no evidence of **40** remaining (c, blue) or cysteamine (b, red).

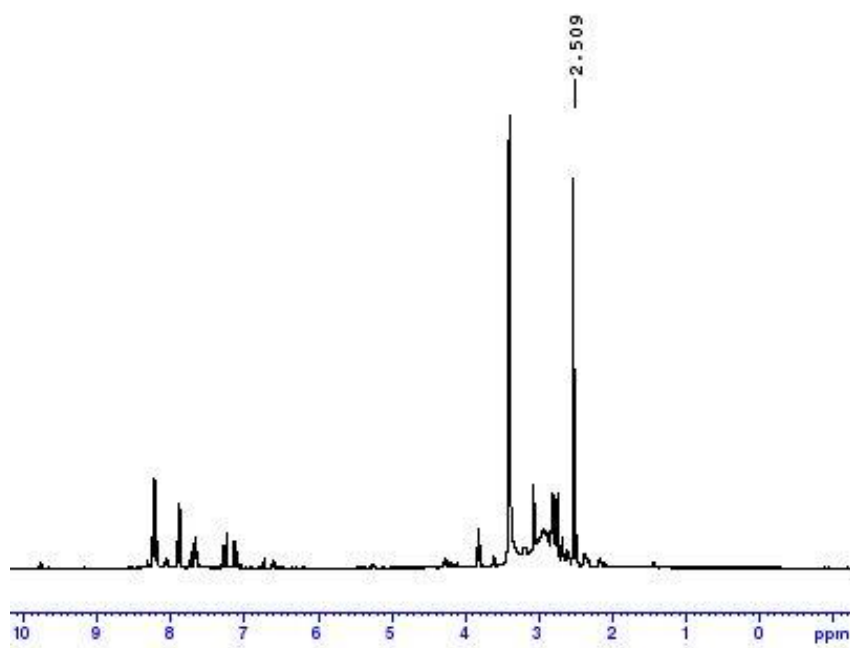


Figure A57. ¹H NMR spectrum acquired after reaction of (*E*) 4-nitrocinnamaldehyde, **44**, and cysteamine

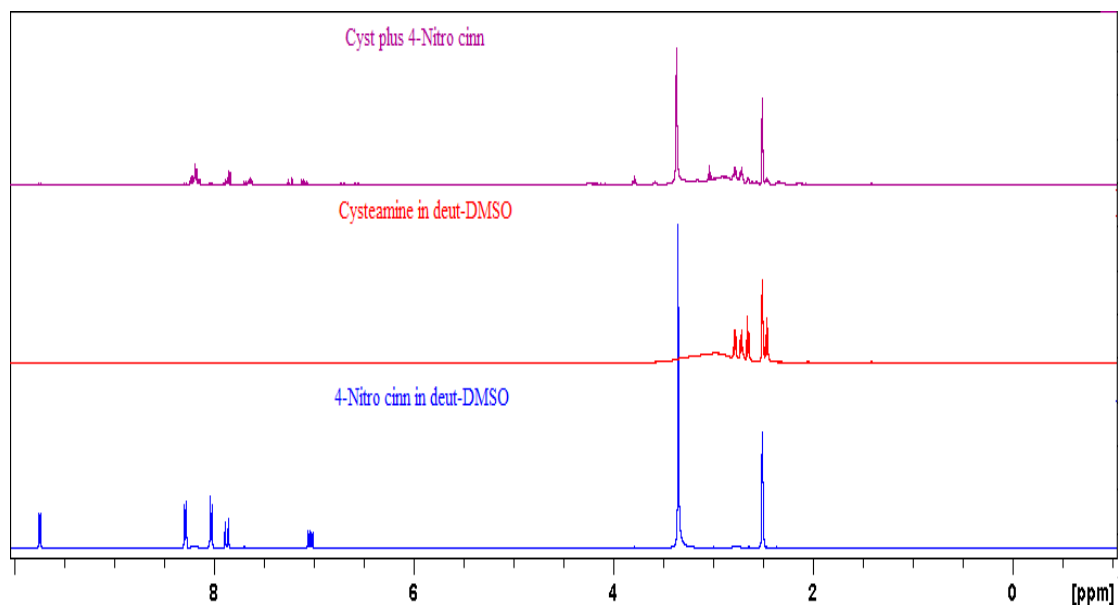


Figure A58. ^1H NMR of (a) The reaction between cysteamine and (*E*) 4-nitrocinnamaldehyde, **44**, at room temperature (purple), where there is no evidence of **44** remaining (c, blue) or cysteamine (b, red).

Data relevant to antibacterial evaluation of *trans*-cinnamaldehydes

Growth Relative to Control (%)	25.99758	27.99274	41.41475	124.7279	164.2684	162.2733	170.9794	172.9141	189.5405	100
Sample concentration (mM)	10	5	2.5	1.25	0.625	0.3125	0.15625	0.078125	0.039063	0

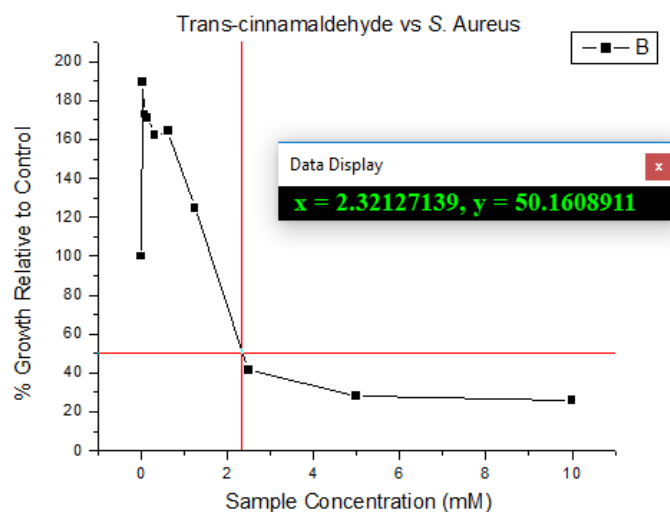


Figure A59. Graph showing antibacterial activity of *trans*-cinnamaldehyde, **1**, over a concentration of 0-10 mM.

Growth Relative to Control (%)	32.36293	93.88646	128.6754	128.3843	132.2659	125.1334	129.9369	135.1771	167.8311	100
Sample concentration (mM)	10	5	2.5	1.25	0.625	0.3125	0.15625	0.078125	0.039063	0

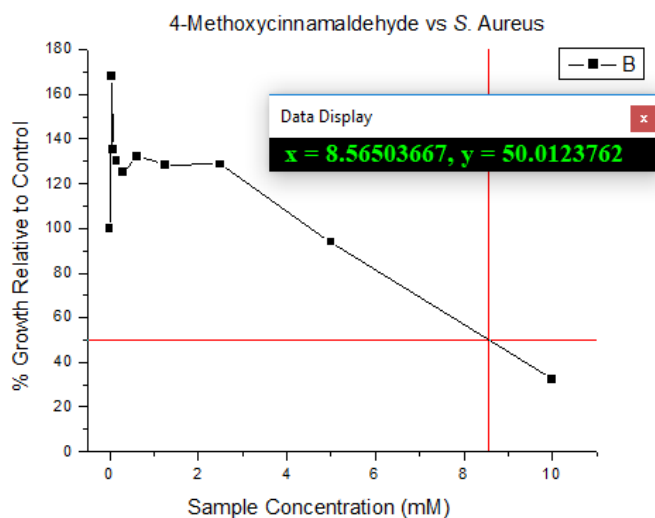


Figure A60. Graph showing antibacterial activity of (*E*)-4-methoxycinnamaldehyde, **14**, over a concentration of 0-10 mM.

Growth Relative to Control (%)	299.144	211.0775	166.6667	161.8832	155.287	133.3837	137.4119	135.0453	158.7613	100
Sample concentration (mM)	10	5	2.5	1.25	0.625	0.3125	0.15625	0.078125	0.039063	0

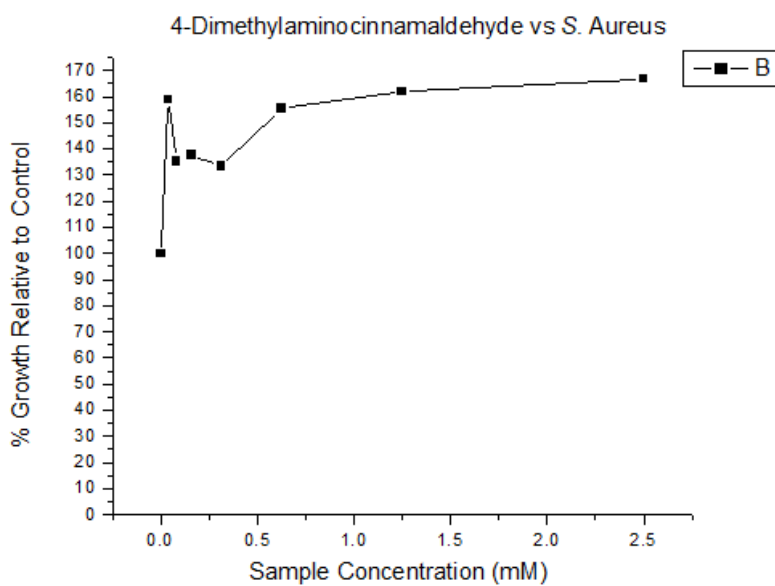


Figure A61. Graph showing antibacterial activity of (*E*)-4-dimethylaminocinnamaldehyde, **45**, over a concentration of 0-10 mM.

Growth Relative to Control (%)	326.5777	188.4962	36.99964	19.54562	23.76488	93.58096	110.3137	120.4111	119.3653	100
Sample concentration (mM)	10	5	2.5	1.25	0.625	0.3125	0.15625	0.078125	0.039063	0

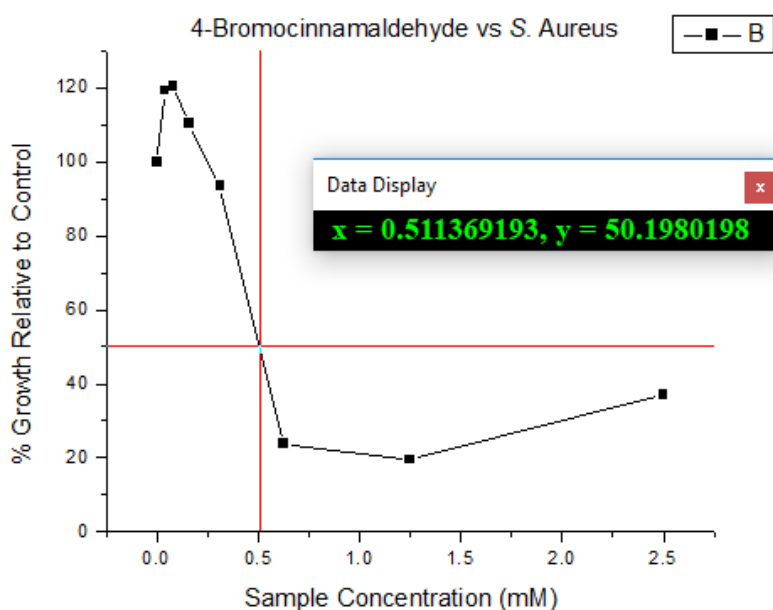


Figure A62. Graph showing antibacterial activity of (*E*)-4-bromocinnamaldehyde, **40**, over a concentration of 0-10 mM.

Growth Relative to Control (%)	19.1776	65.01241	101.1343	119.7093	121.7299	115.1719	109.3584	101.7015	92.80397	100
Sample concentration (mM)	10	5	2.5	1.25	0.625	0.3125	0.15625	0.078125	0.039063	0

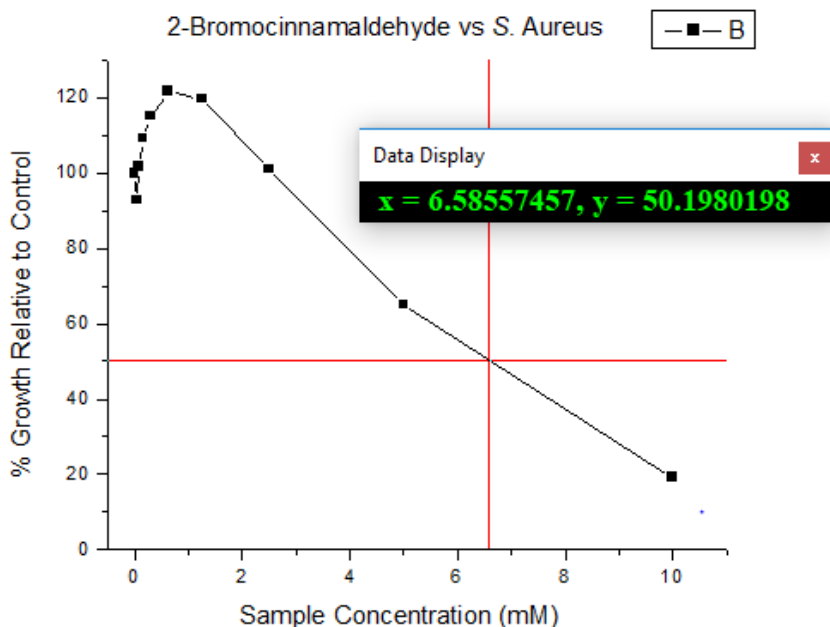


Figure A63. Graph showing antibacterial activity of (*E*)-2-bromocinnamaldehyde, **5**, over a concentration of 0-10 mM.

Growth Relative to Control (%)	259.8297	134.67	65.01065	34.77644	34.42158	131.3343	131.9375	129.9503	124.4855	100
Sample concentration (mM)	10	5	2.5	1.25	0.625	0.3125	0.15625	0.078125	0.039063	0

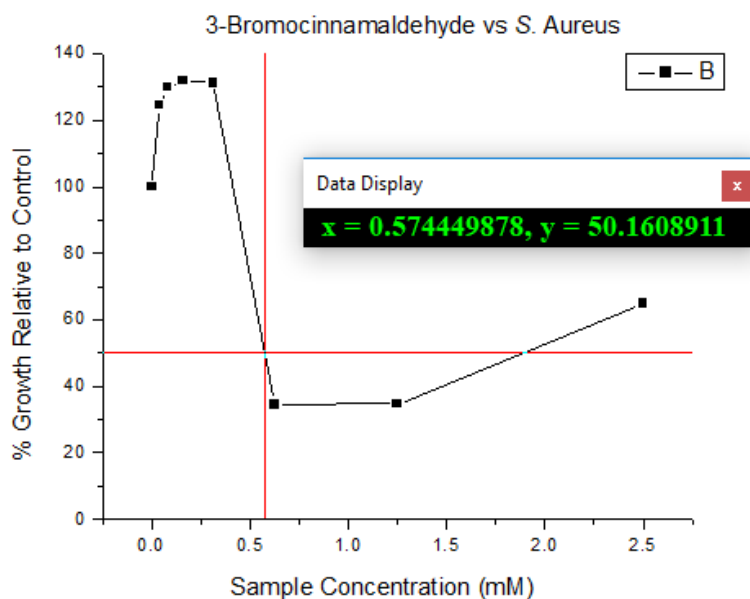


Figure A64. Graph showing antibacterial activity of (*E*)-3-bromocinnamaldehyde, **34**, over a concentration of 0-10 mM.

Data relevant to antimicrobial evaluation of pyrazolopyrimidinones

% Growth Relative to Control	127.2335	123.5893	111.3636	96.04232	104.663	104.0752	114.4984	118.221	116.5752	100
Sample concentration (mg/mL)	1.25	0.625	0.3125	0.15625	0.078125	0.039063	0.019531	0.009766	0.004883	0

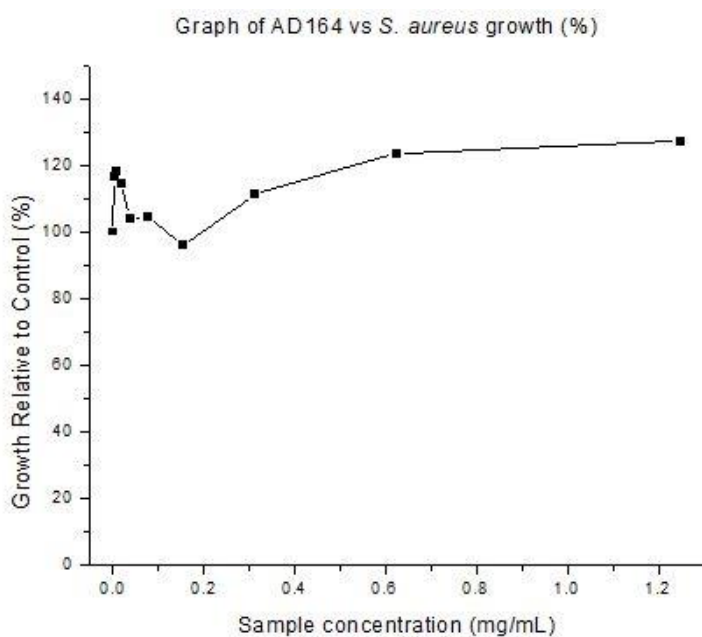


Figure A65. Graph showing antibacterial activity of 4-phenylsulfonyl-1,1'-biphenyl, **46**, against *S. aureus* over a concentration of 0-1.25 mg/mL.

% Growth relative to control	122.6728	163.2228	201.3047	217.4542	181.2412	136.9887	125.5642	120.0282	112.6939	100
Sample concentration (mg/ml)	1.25	0.625	0.3125	0.15625	0.078125	0.039063	0.019531	0.009766	0.004883	0

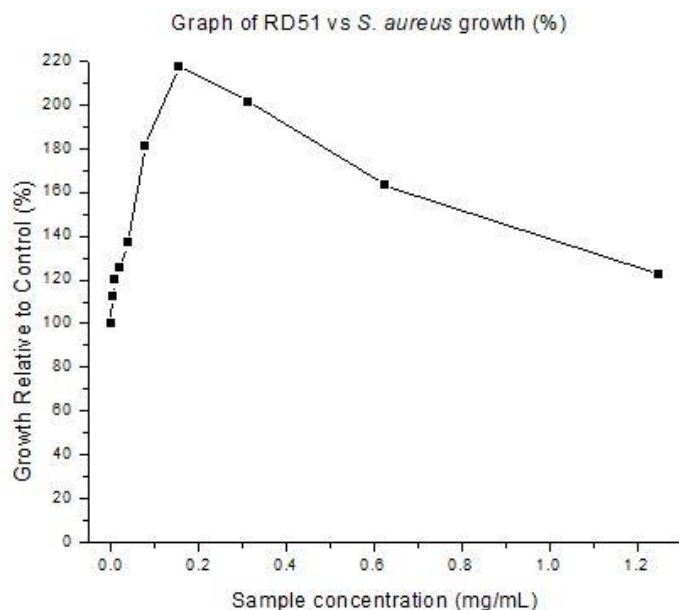


Figure A66. Graph showing antibacterial activity of ethyl 2-cyano-3'-fluoro-6-propyl-[1,1'-biphenyl]-4-carboxylate, **47**, against *S. aureus* over a concentration of 0-1.25 mg/mL.

% Growth relative to control	258.6789	248.844	150.0183	88.58716	59.26606	44.47706	38.31193	31.37615	26.56881	100
Sample concentration (mg/mL)	1.25	0.625	0.3125	0.15625	0.078125	0.039063	0.019531	0.009766	0.004883	0

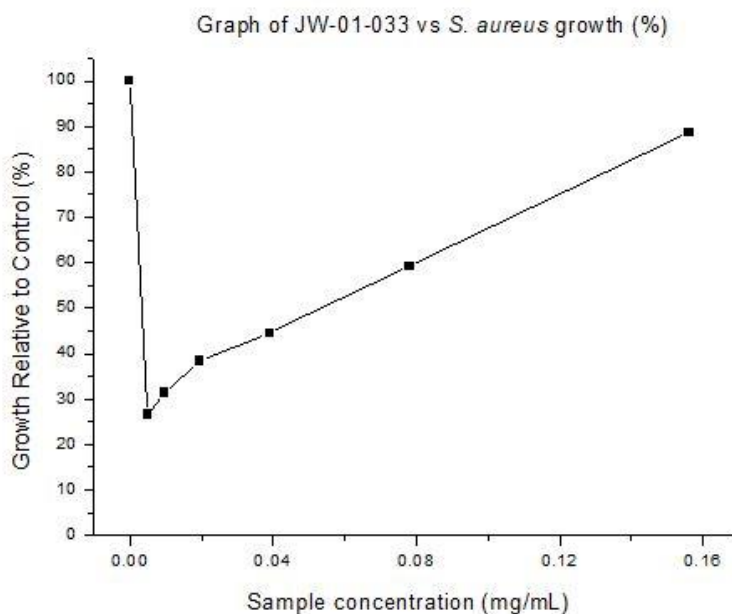


Figure A67. Graph showing antibacterial activity of 2-butyl-5-(3,5-bis(trifluoromethyl)phenyl)pyrazolo[1,5-a]pyrimidin-7(4H)-one, **48**, against *S. aureus* over a concentration of 0-0.15625 mg/mL.

% Growth relative to control	92.99964	161.9514	156.6921	155.0236	132.7167	111.6068	106.1299	103.9898	101.8498	100
Sample concentration (mg/mL)	1.25	0.625	0.3125	0.15625	0.078125	0.039063	0.019531	0.009766	0.004883	0

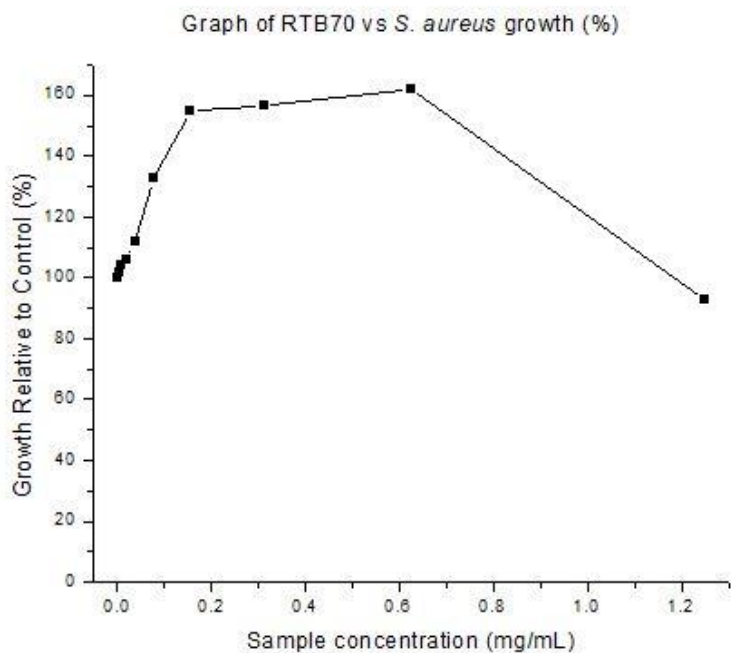


Figure A68. Graph showing antibacterial activity of 1-(4-(2-chloro-4-(trifluoromethyl) pyridin-2-yl)piperazin-1-yl)-4-(thiophen-2-yl)butan-1-one, **49**, over a concentration of 0-1.25 mg/mL.

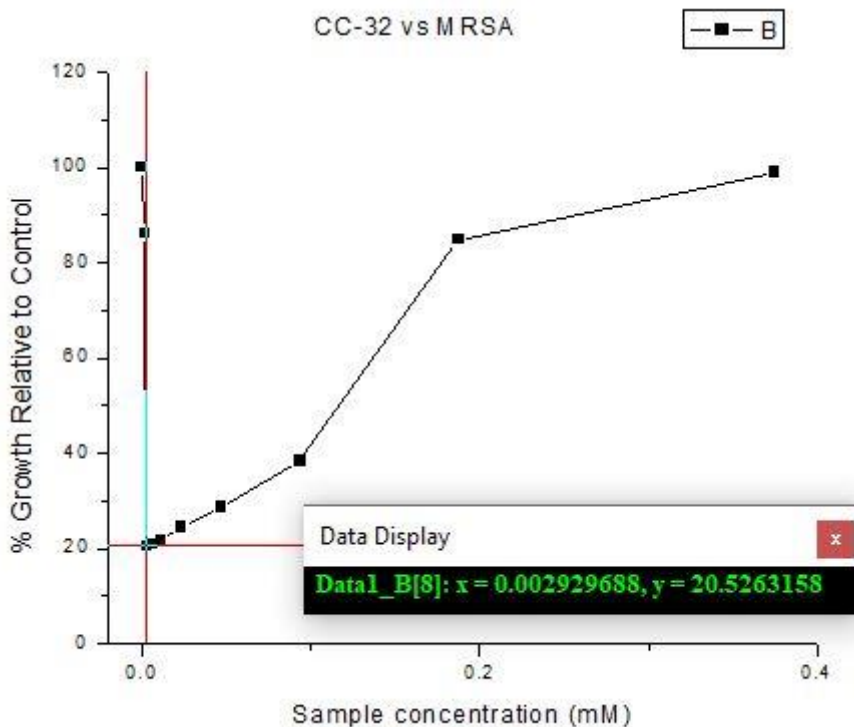


Figure A69. Example graph showing antibacterial activity of compound **57** against MRSA, to demonstrate how MIC₈₀ was obtained.

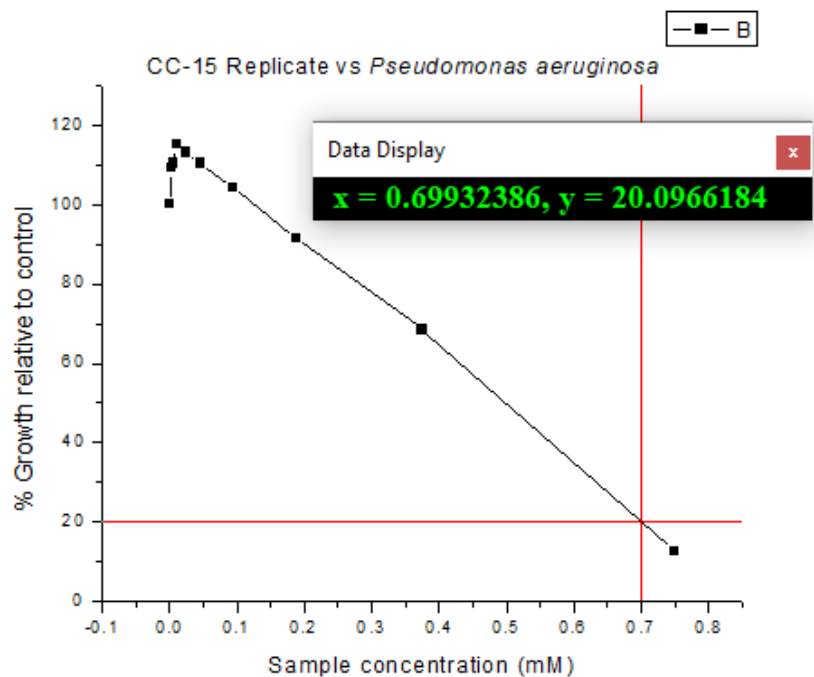


Figure A70. Example graph showing antibacterial activity of compound **71** against *P. aeruginosa*, to demonstrate how MIC₈₀ was obtained.

Antimicrobial evaluation of commercial antibiotics:

Growth Relative to Control (%)	22.51931	21.98455	21.86572	21.8063	42.12715	22.87582	22.1628	44.38503	45.51396	100
Sample concentration (mg/mL)	1.25	0.625	0.3125	0.15625	0.078125	0.039063	0.019531	0.009766	0.004883	0

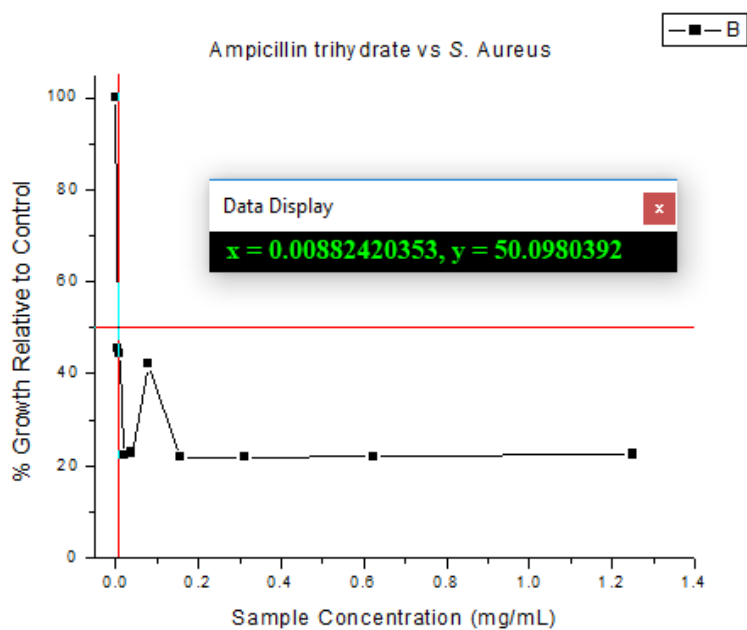


Figure A71. Graph showing antibacterial activity of ampicillin trihydrate against *S. aureus* over a concentration of 0-1.25 mg/mL.

Growth Relative to Control (%)	81.75218	52.03291	33.59148	27.49274	24.24976	22.84608	21.78122	20.81317	19.99032	100
Sample concentration (mg/mL)	1.25	0.625	0.3125	0.15625	0.078125	0.039063	0.019531	0.009766	0.004883	0

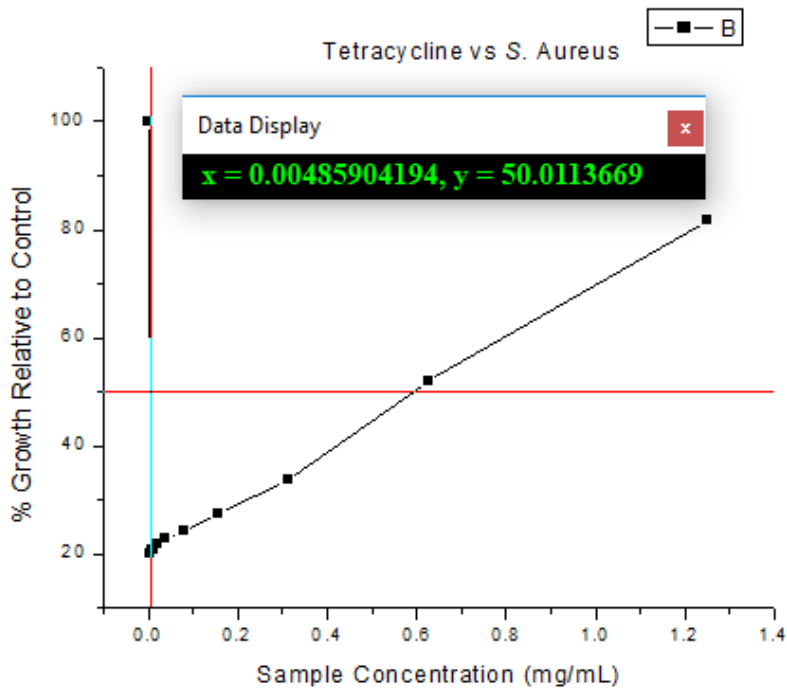


Figure A72. Graph showing antibacterial activity of tetracycline against *S. aureus* over a concentration of 0-1.25 mg/mL.

Growth Relative to Control (%)	26.79394	27.32061	26.72811	27.58394	27.32061	27.5181	27.78144	27.5181	27.97893	100
Sample concentration (mg/mL)	1.25	0.625	0.3125	0.15625	0.078125	0.039063	0.019531	0.009766	0.004883	0

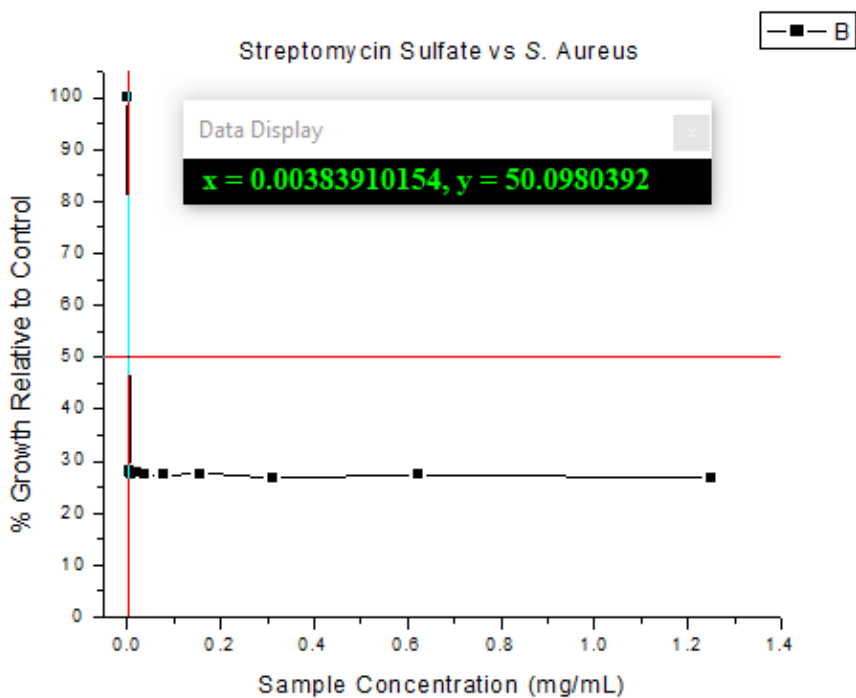


Figure A73. Graph showing antibacterial activity of streptomycin sulfate against *S. aureus* over a concentration of 0-1.25 mg/mL.

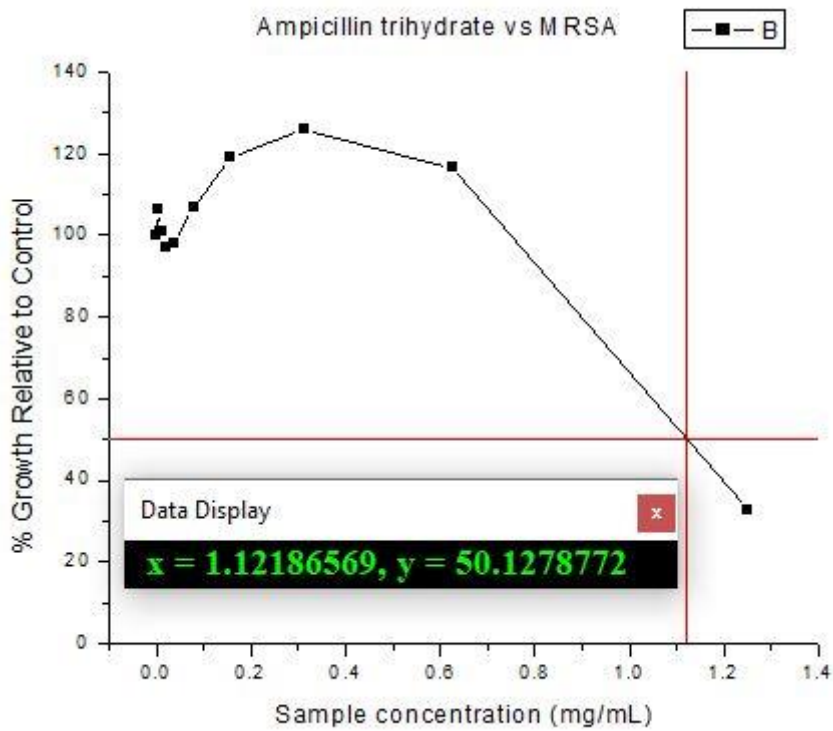


Figure A74. Graph showing antibacterial activity of ampicillin trihydrate against MRSA over a concentration of 0-1.25 mg/mL.

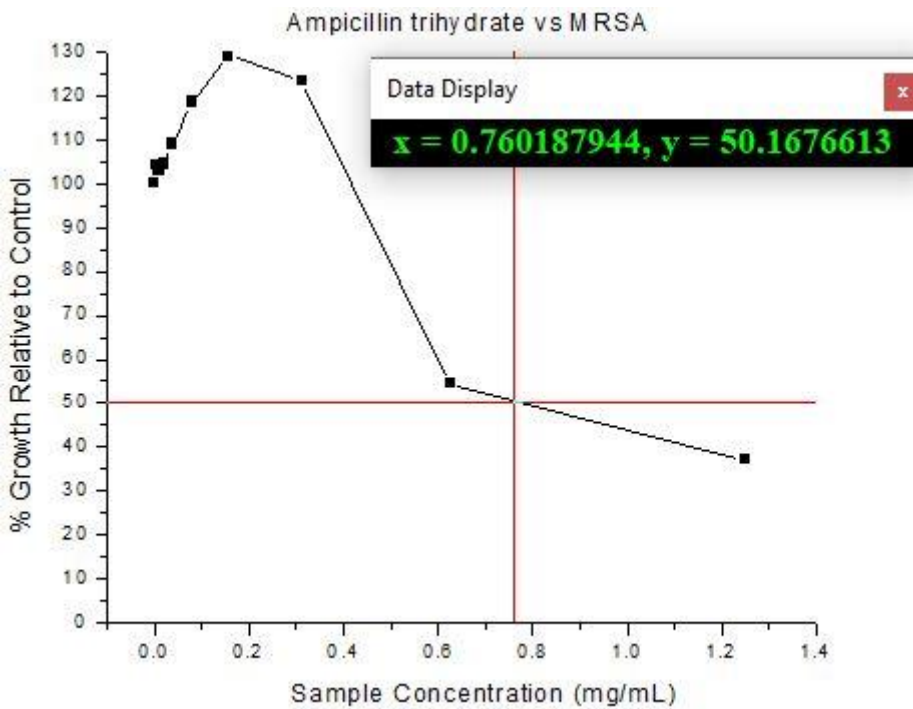


Figure A75. Graph showing antibacterial activity of ampicillin trihydrate against MRSA over a concentration of 0-1.25 mg/mL.

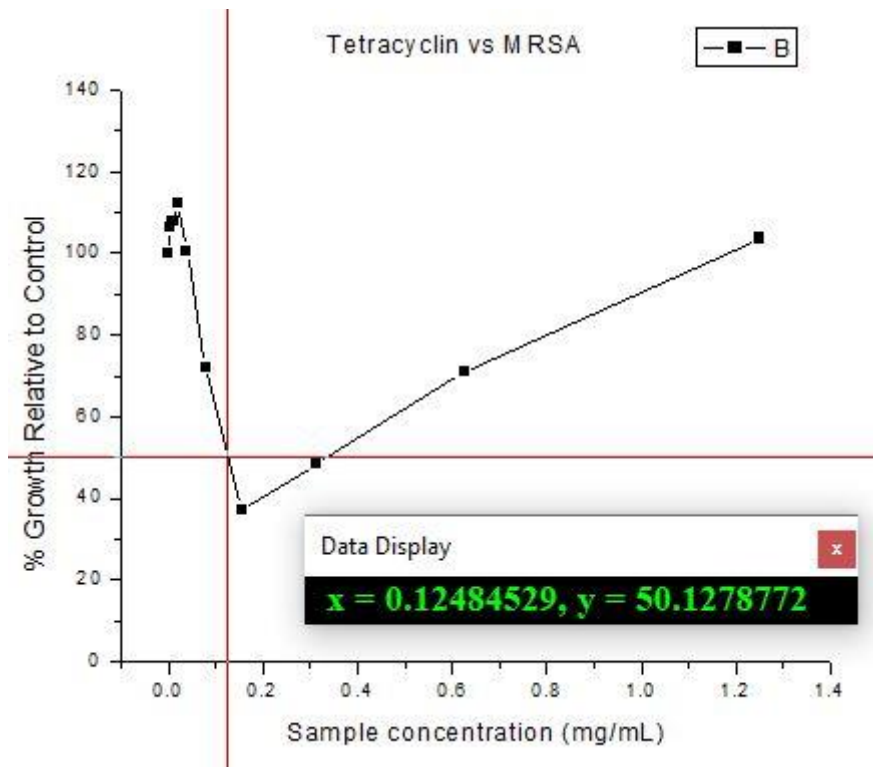


Figure A76. Graph showing antibacterial activity of tetracycline against MRSA over a concentration of 0-1.25 mg/mL.

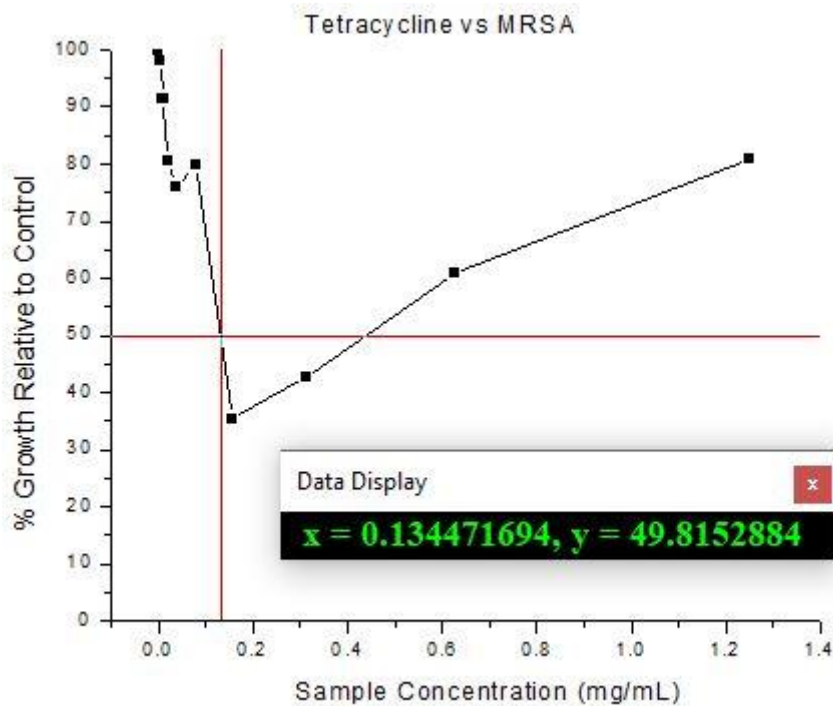


Figure A77. Graph showing antibacterial activity of tetracycline against MRSA over a concentration of 0-1.25 mg/mL.

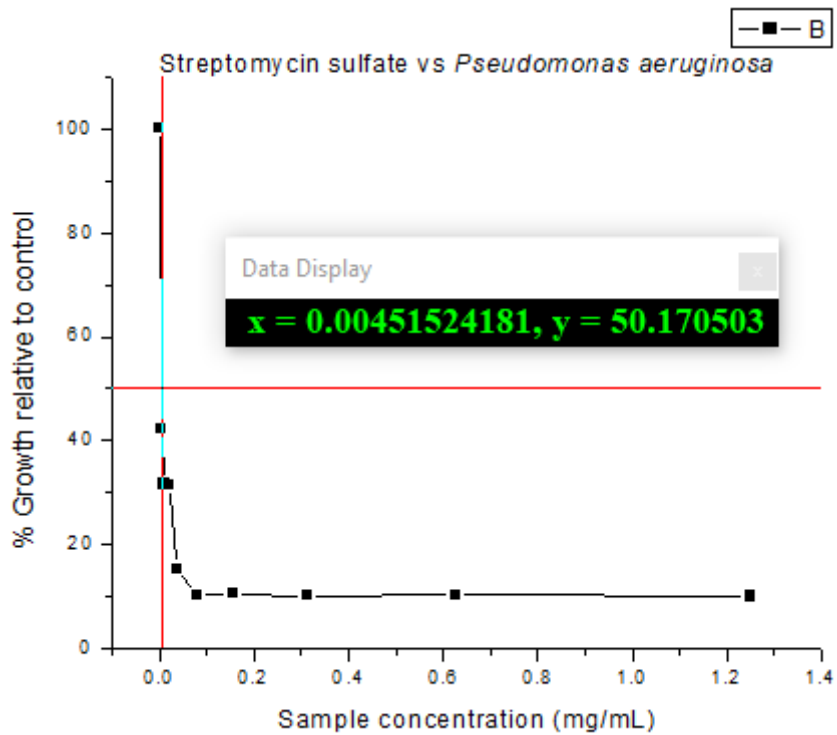


Figure A78. Graph showing antibacterial activity of tetracycline against *P. aeruginosa* over a concentration of 0-1.25 mg/mL.

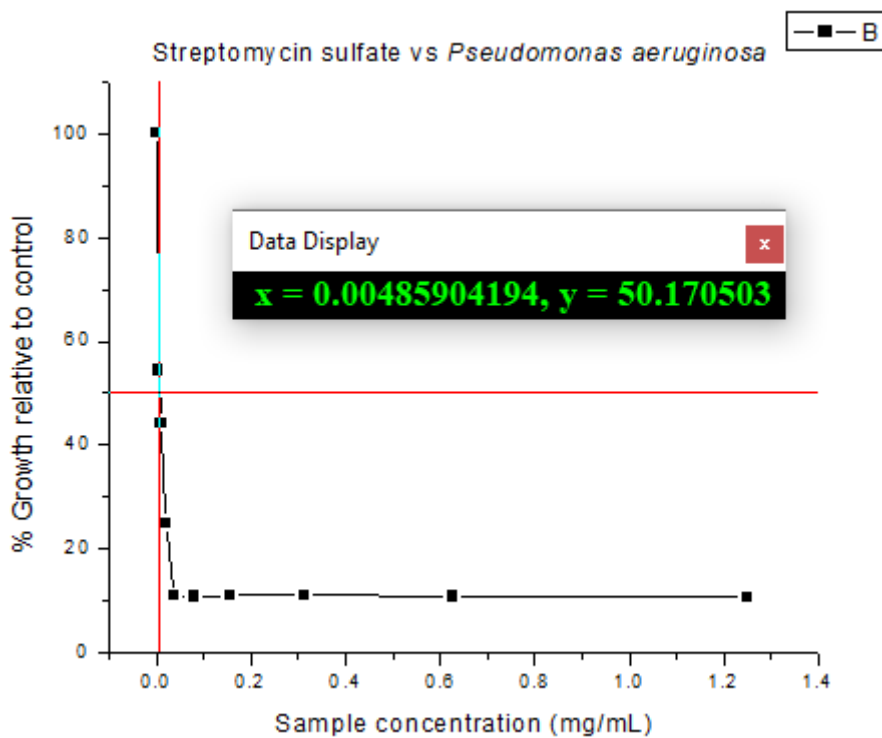


Figure A79. Graph showing antibacterial activity of tetracycline against *P. aeruginosa* over a concentration of 0-1.25 mg/mL

Appendix 2

NMR spectra & LCMS spectra

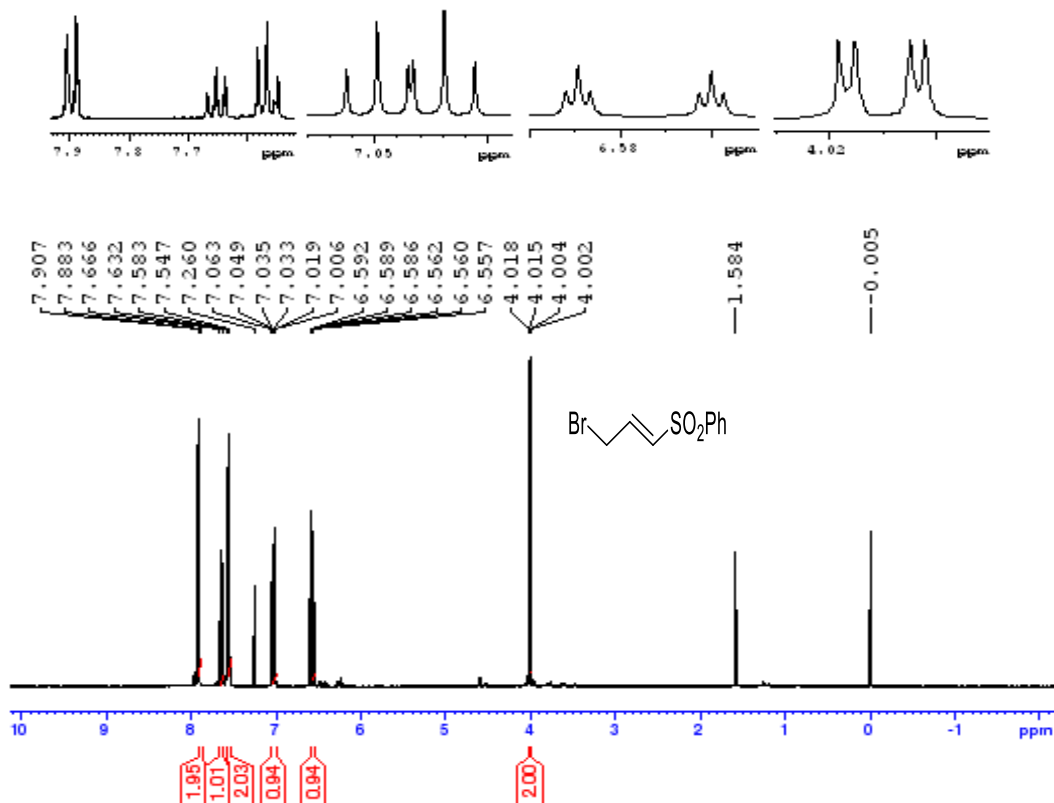


Figure A80. ¹H NMR spectrum of (*E*)-3-Bromo-1-phenylsulfonylprop-1-ene, **103**

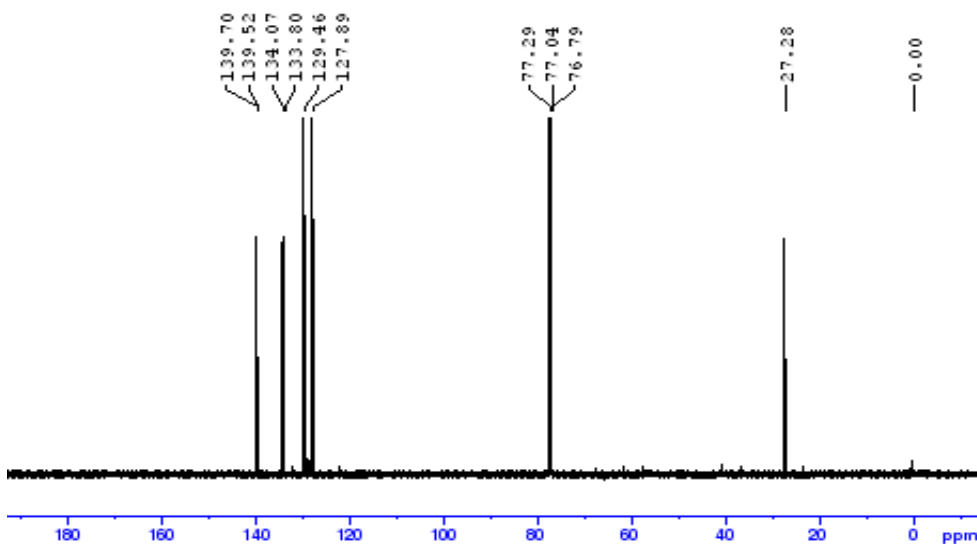
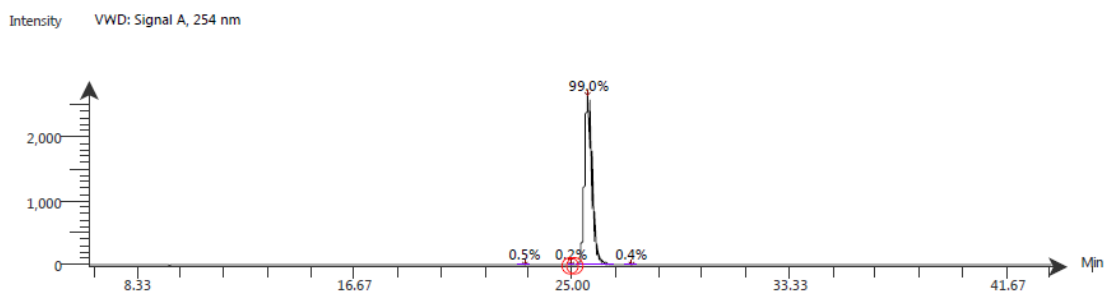


Figure A81. ¹³C NMR spectrum of (*E*)-3-Bromo-1-phenylsulfonylprop-1-ene, **103**



Time (Peak Maximum M:S/Minutes)	Maximum Intensity (c/s)	Time (Peak Centroid M:S/Minutes)	Peak Area	% Peak Area	Peak Resolution Label
23.16	1.7E1	23.20	2.4E2	0.5	14.5
0.00	1.3E1	24.96	1E2	0.2	11.4
25.59	2.7E3	25.59	5.3E4	99.0	17.9
0.00	1.9E2	27.28	2E2	0.4	26.8

Figure A82. LCMS spectrum of (*E*)-3-Bromo-1-phenylsulfonylprop-1-ene, **103**

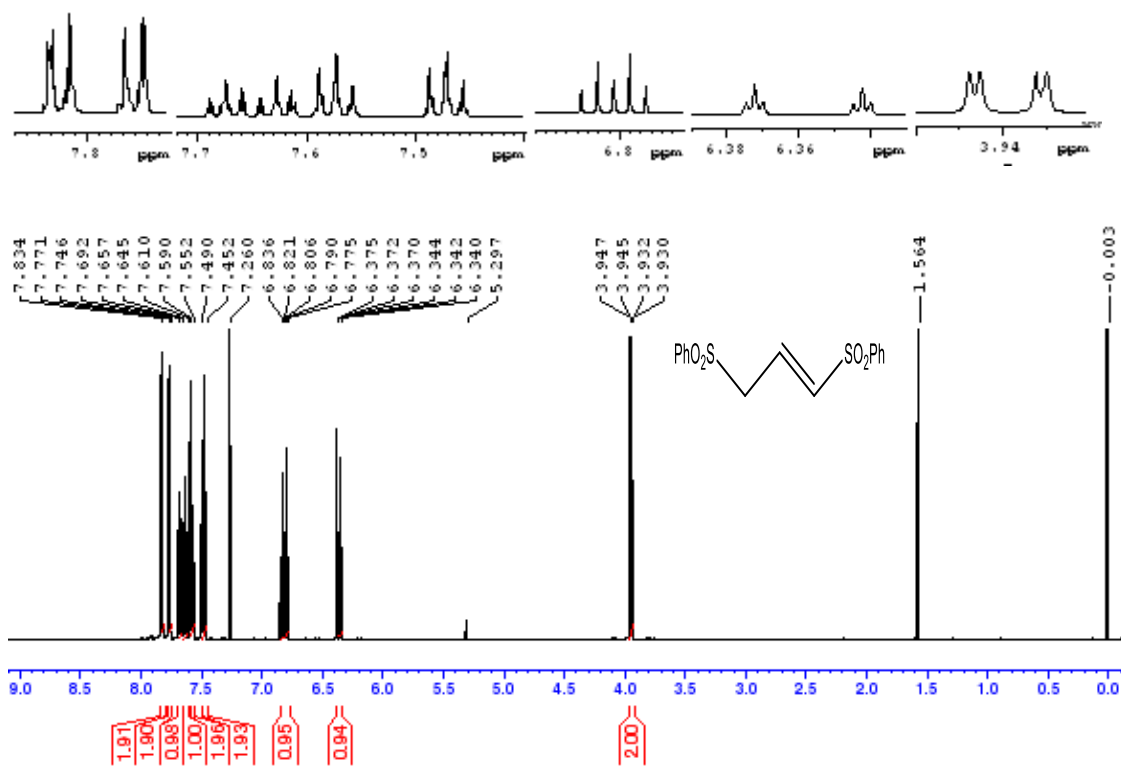


Figure A83. ¹H NMR spectrum of (*E*)-1,3-bis-phenylsulfonylprop-1-ene, **104**

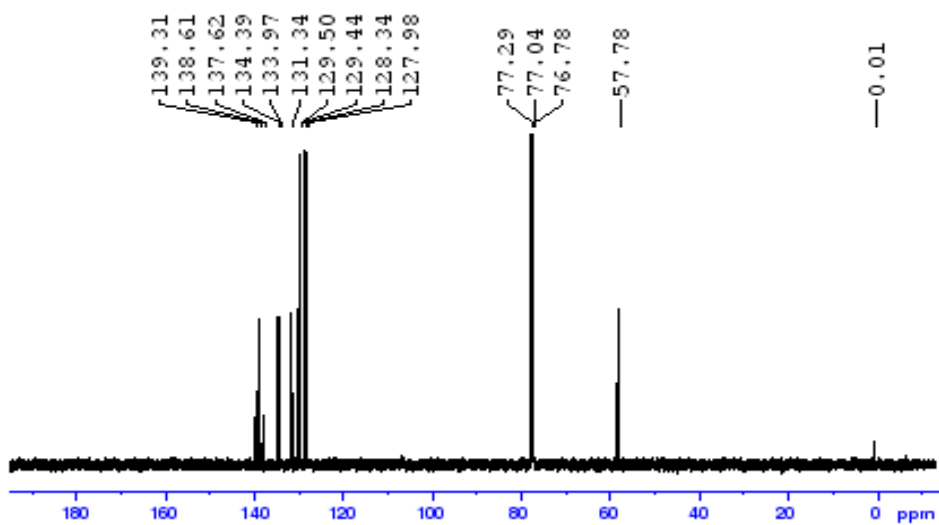
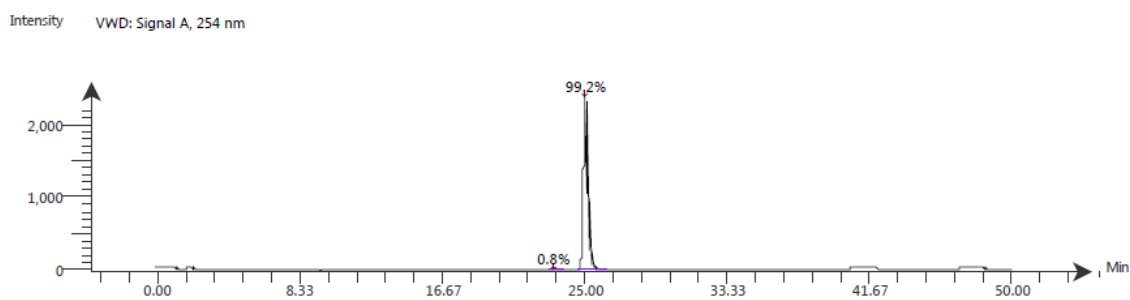


Figure A84. ^{13}C NMR spectrum of (*E*)-1,3-bis-phenylsulfonylprop-1-ene, **104**



Time (Peak Maximum M:S/Minutes)	Maximum Intensity (c/s)	Time (Peak Centroid M:S/Minutes)	Peak Area	% Peak Area	Peak Resolution Label
23.11	1.9E1	23.19	3.6E2	0.8	16.3
24.97	2.4E3	24.97	4.4E4	99.2	16.6

Figure A85. LCMS spectrum of (*E*)-1,3-Bis-phenylsulfonylprop-1-ene, **104**

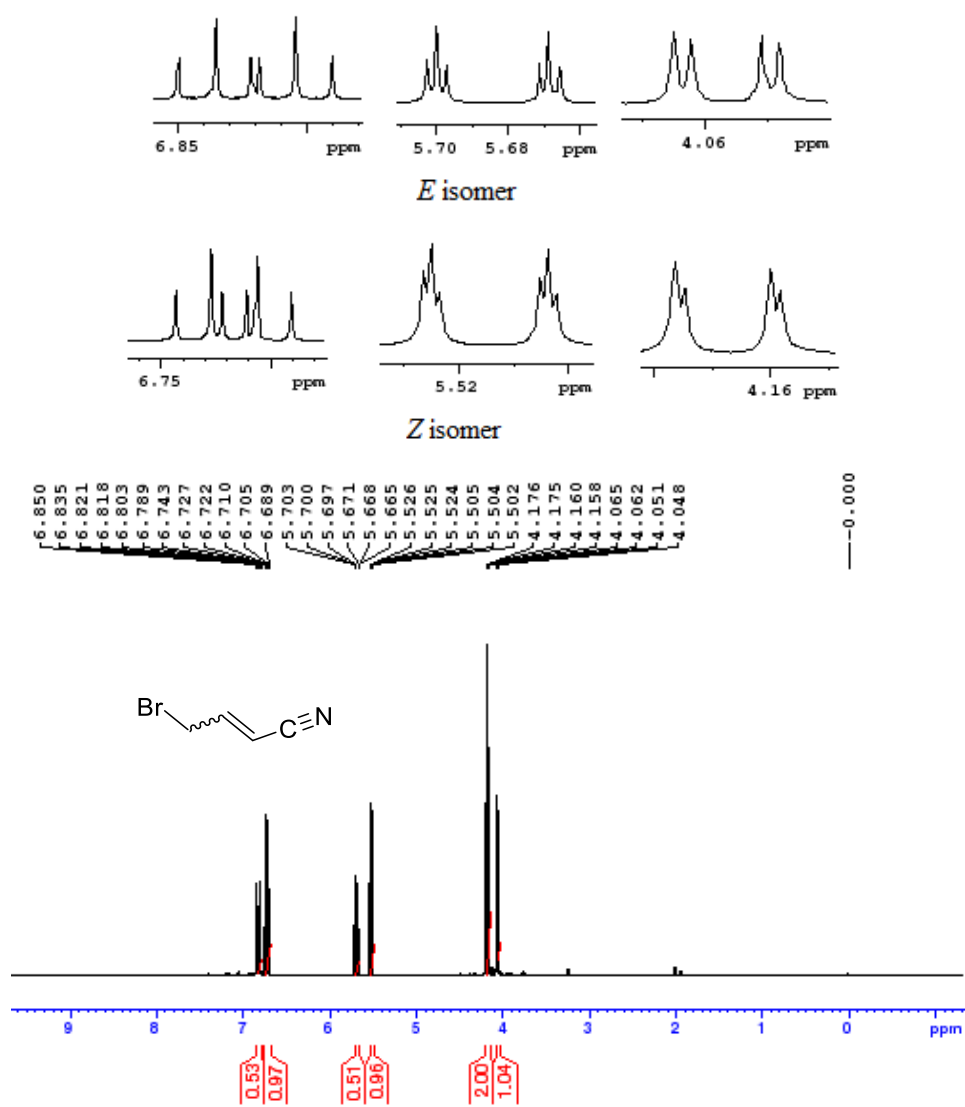


Figure A86. ^1H NMR spectrum of (*E/Z*)-4-bromobut-2-enitrile, **121**

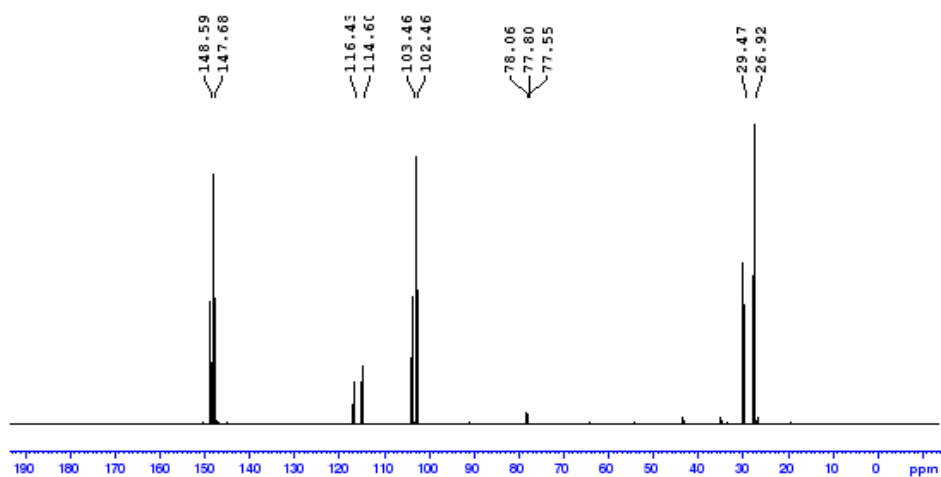


Figure A87. ^{13}C NMR spectrum of (*E/Z*)-4-bromobut-2-enitrile, **121**

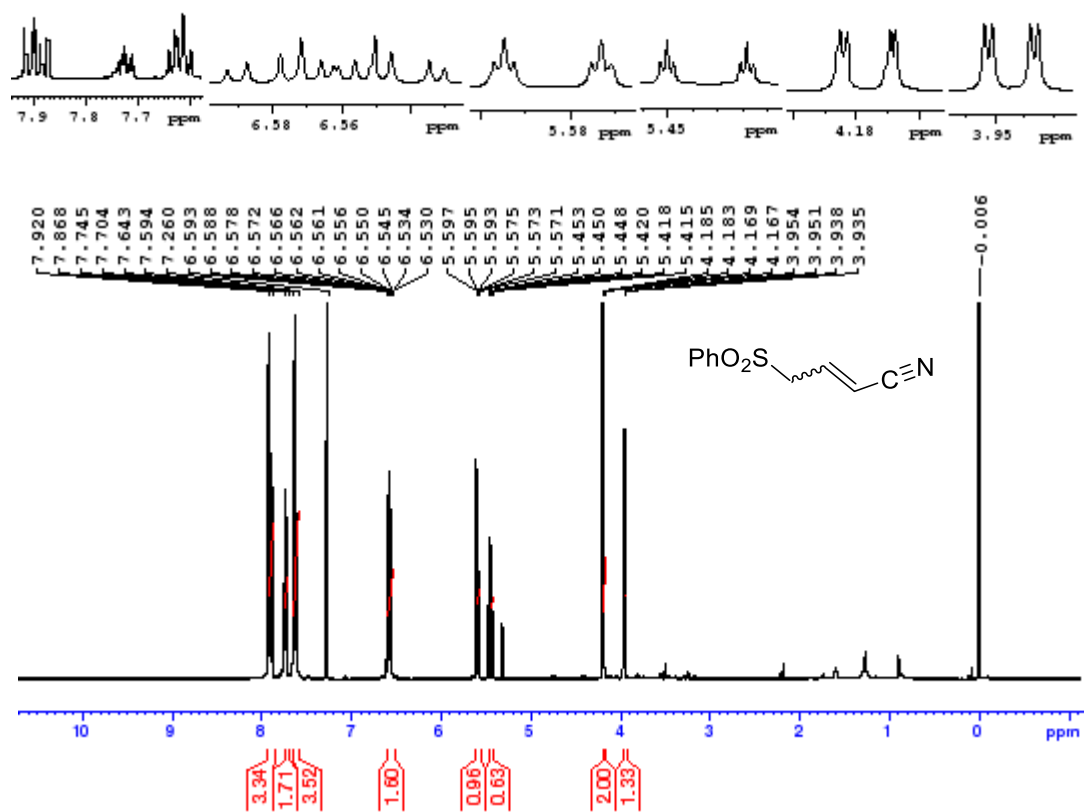


Figure A88. ^1H NMR spectrum of (*E/Z*)-4-(phenylsulfonyl)but-2-enenitrile, **122**

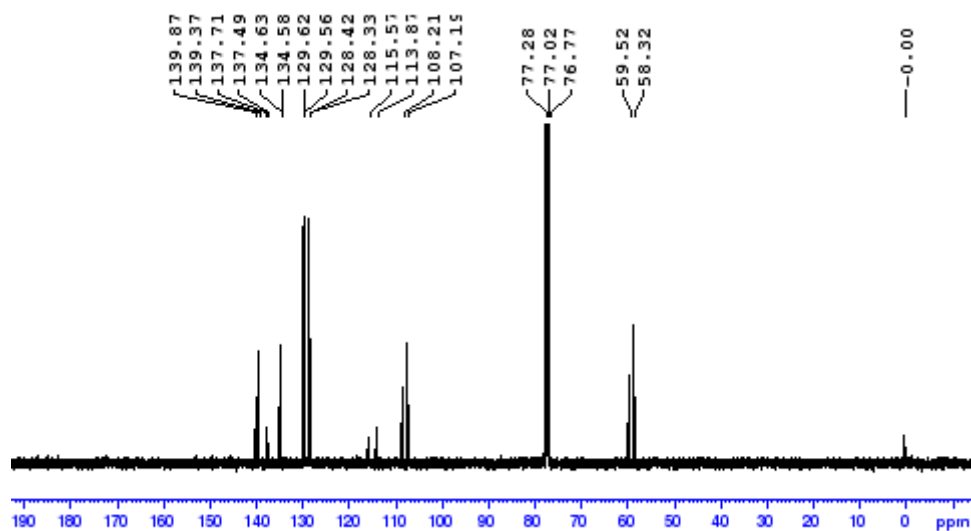


Figure A89. ^{13}C NMR spectrum of (*E/Z*)-4-(phenylsulfonyl)but-2-enenitrile, **122**

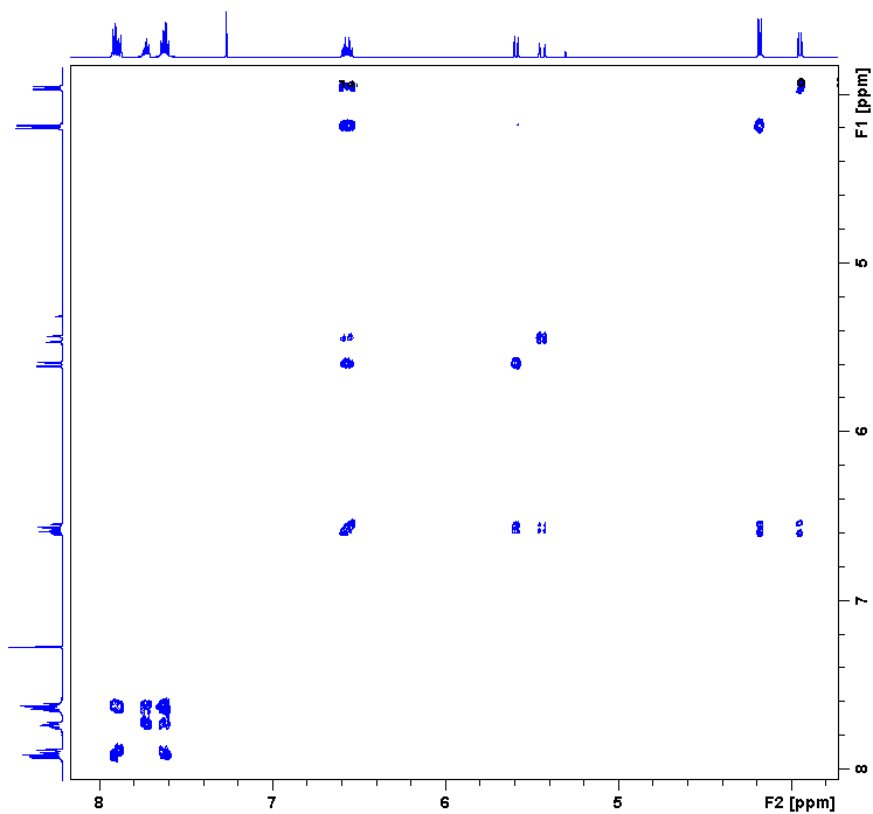


Figure A90. Zoomed in COSY spectrum of (*E/Z*)-4-(phenylsulfonyl)but-2-enitrile, **122**

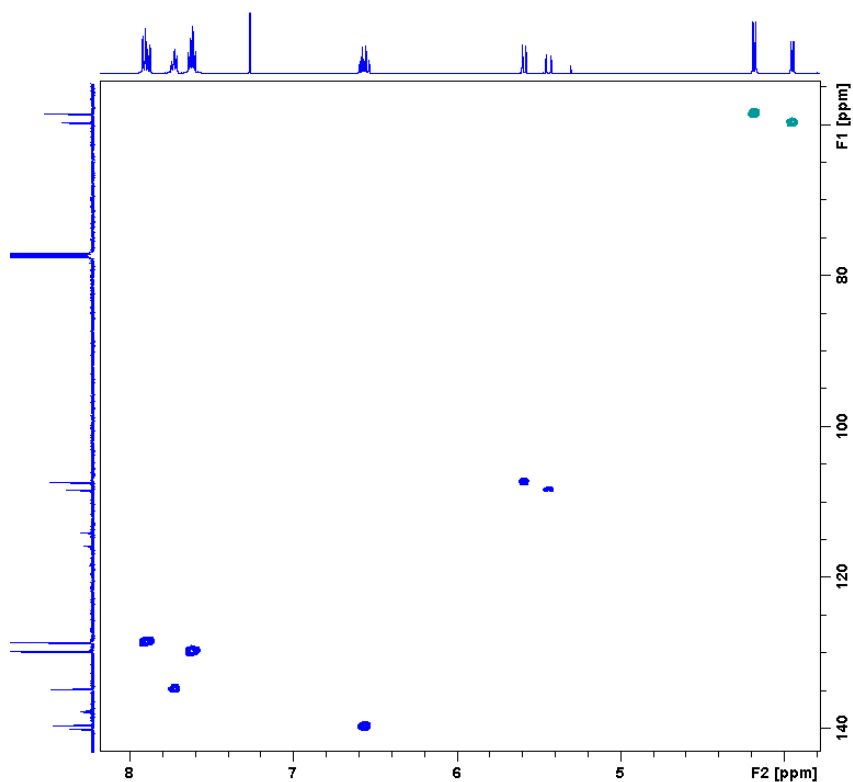


Figure A91. Zoomed in HSQC spectrum of (*E/Z*)-4-(phenylsulfonyl)but-2-enitrile, **122**

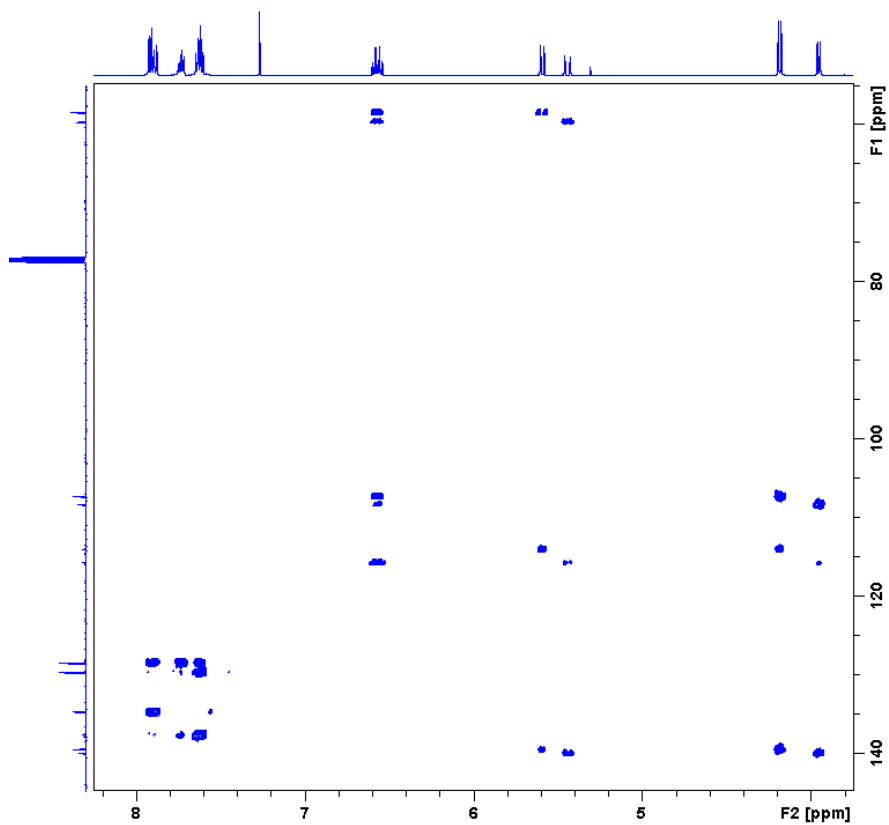


Figure A92. Zoomed in HMBC spectrum of (*E/Z*)-4-(phenylsulfonyl)but-2-enitrile, **122**

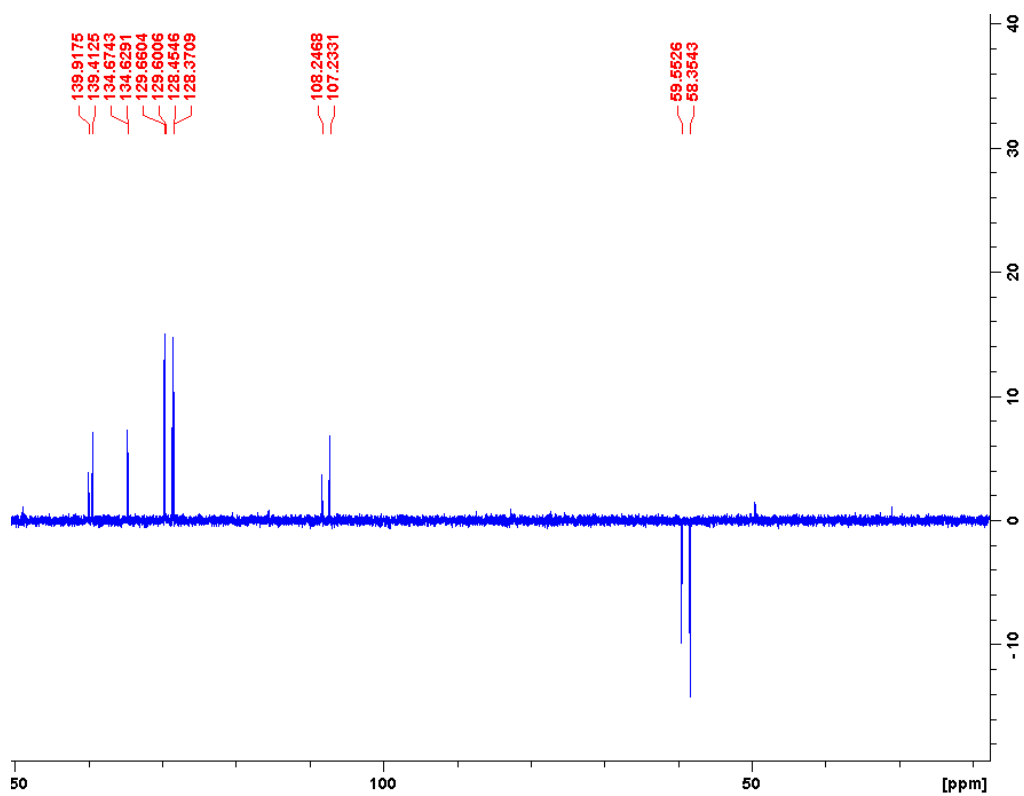


Figure A93. Zoomed in COSY spectrum of (*E/Z*)-4-(phenylsulfonyl)but-2-enitrile, **122**

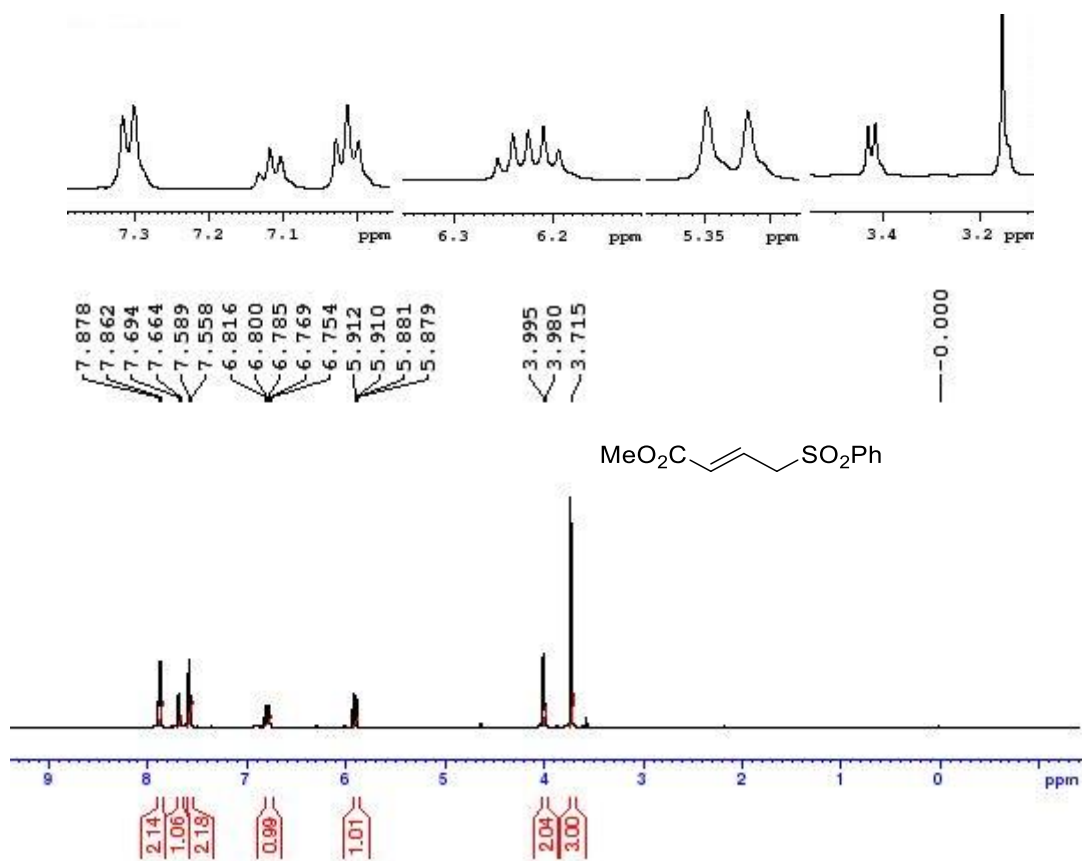


Figure A94. ¹H NMR spectrum of (*E*)-methyl 4-bromobut-2-enoate, **123**

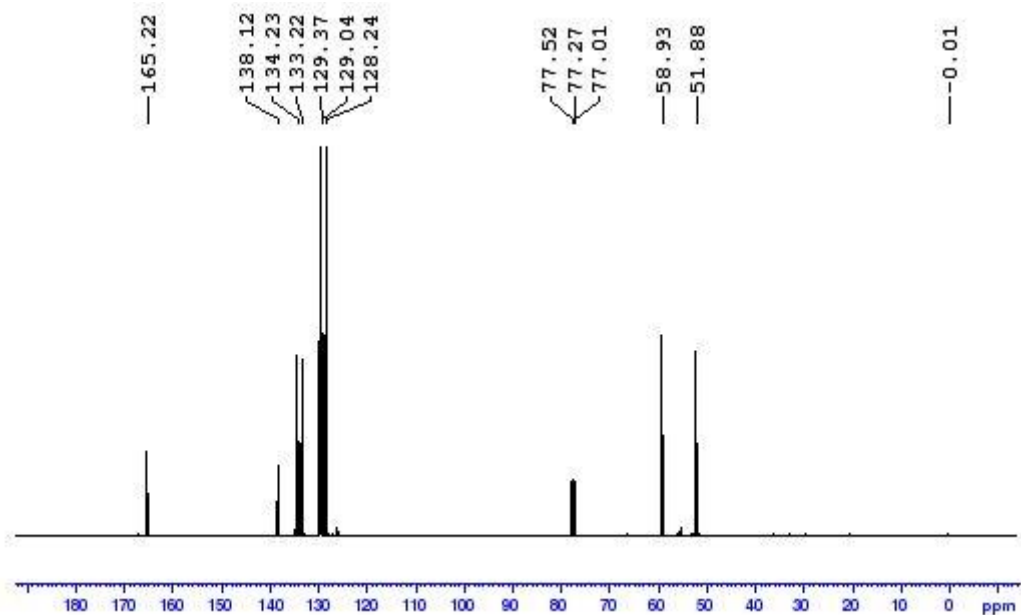


Figure A95. ¹³C NMR spectrum of (*E*)-methyl 4-bromobut-2-enoate, **123**

Reaction Optimisation Spectra: Preferred base

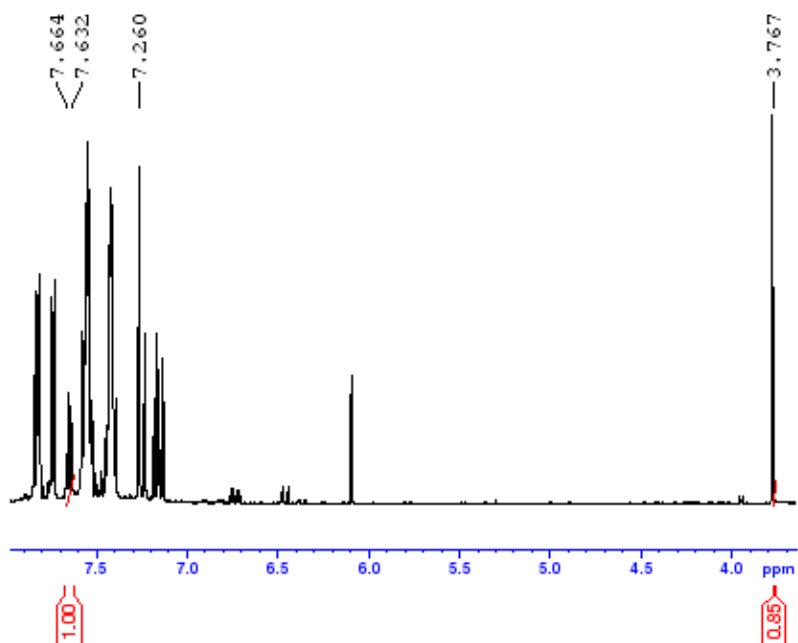


Figure A96. ¹H NMR spectrum of crude mixture containing (1*E*,3*E*,5*E*)-1,3-bis-phenylsulfonyl-6-phenyl-hexa-1,3,5-triene, **105**, and 1,3,5-trimethoxybenzene using 15 equivalents of Al₂O₃ as base, DCM as solvent at room temperature.

Reaction Optimisation Spectra: Solvent screen

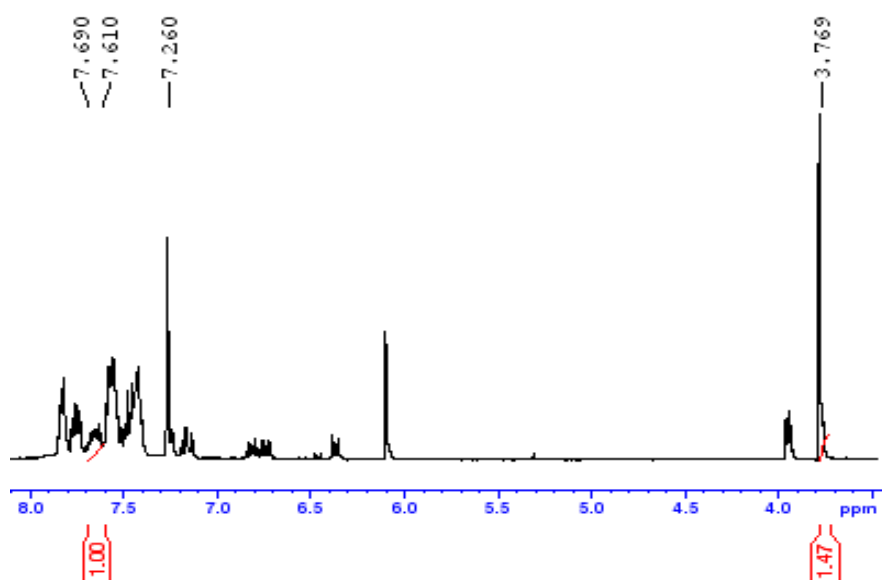


Figure A97. ¹H NMR spectrum of crude mixture containing (1*E*,3*E*,5*E*)-1,3-bis-phenylsulfonyl-6-phenyl-hexa-1,3,5-triene and 1,3,5-trimethoxybenzene using toluene as the solvent.

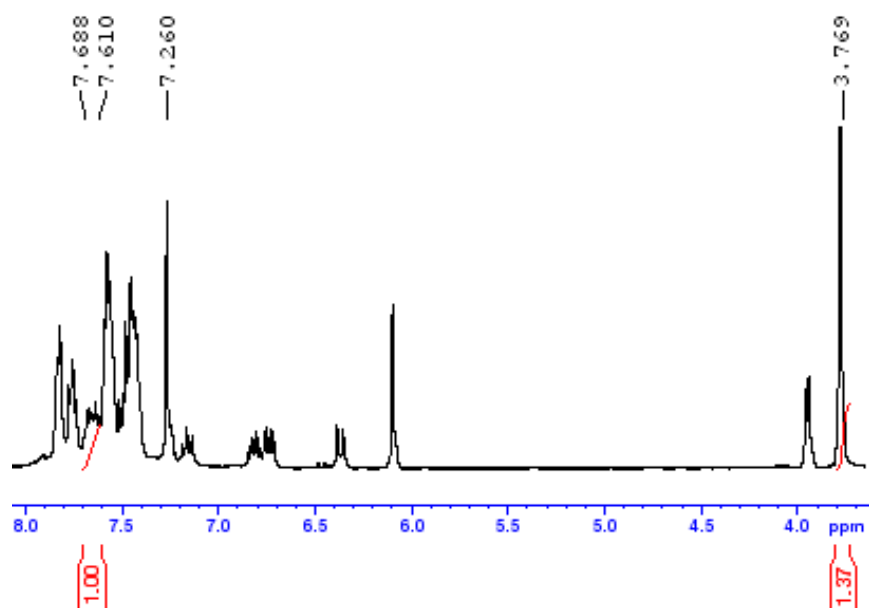


Figure A98. ^1H NMR spectrum of crude mixture containing (1*E*,3*E*,5*E*)-1,3-bis-phenylsulfonyl-6-phenyl-hexa-1,3,5-triene, **105**, and 1,3,5-trimethoxybenzene. This was obtained where methanol was used as the solvent at room temperature.

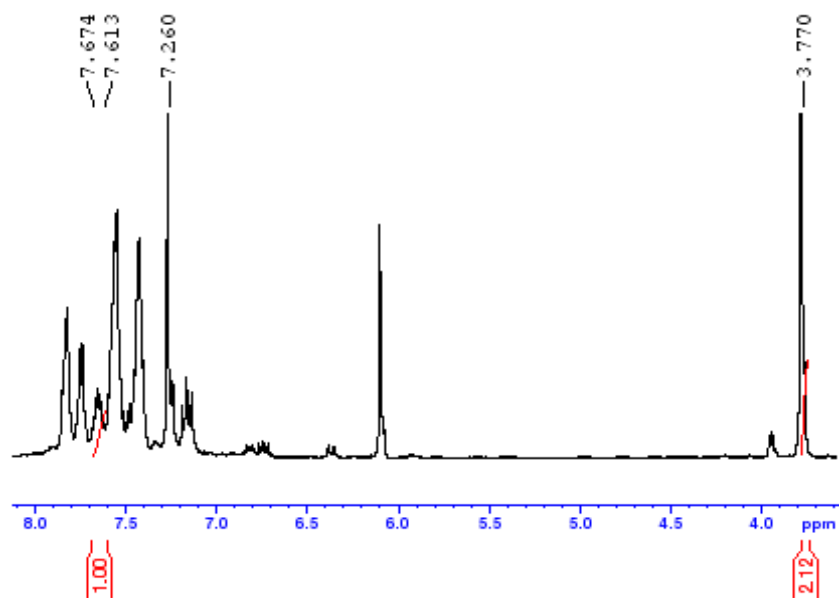


Figure A99. ^1H NMR spectrum of crude mixture containing (1*E*,3*E*,5*E*)-1,3-bis-phenylsulfonyl-6-phenyl-hexa-1,3,5-triene, **105**, and 1,3,5-trimethoxybenzene using acetonitrile as the solvent.

Reaction Optimisation Spectra: Equivalents of base

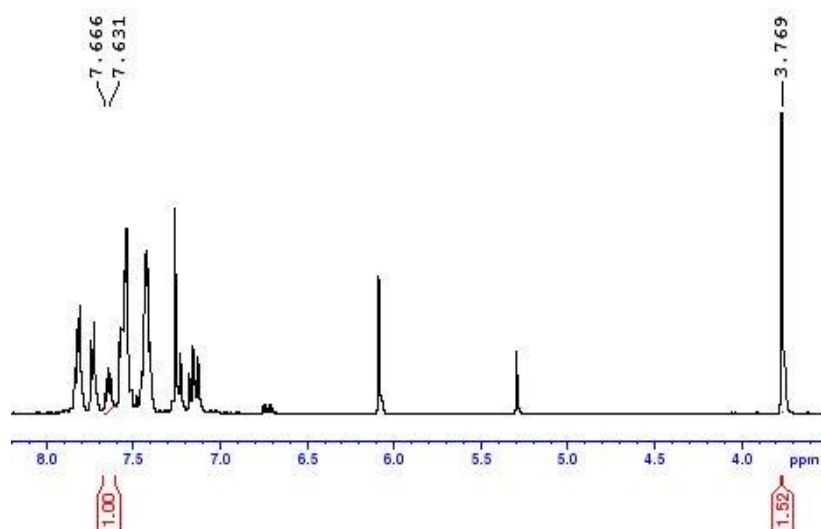


Figure A100. ¹H NMR spectrum of crude mixture containing (1*E*,3*E*,5*E*)-1,3-bis-phenylsulfonyl-6-phenyl-hexa-1,3,5-triene, **105**, and 1,3,5-trimethoxybenzene using 30 equivalents of Al₂O₃.

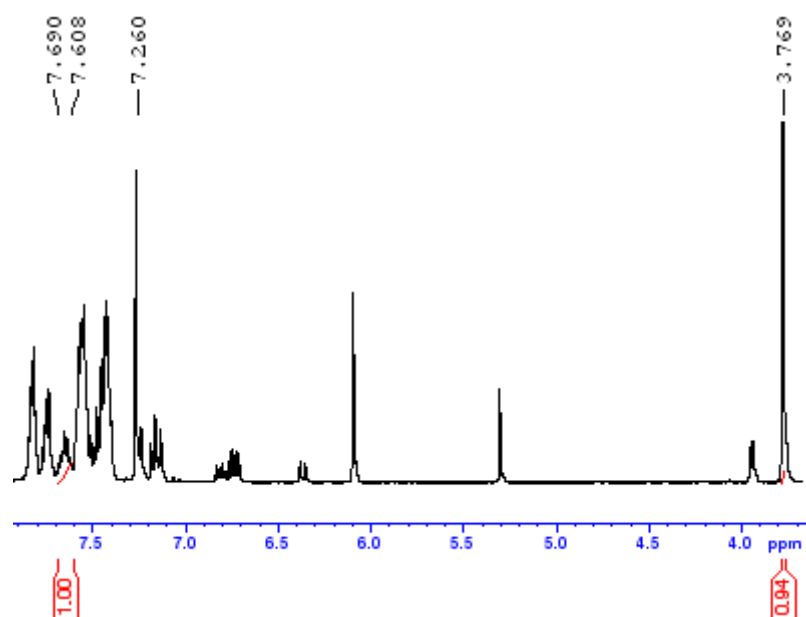


Figure A101. ¹H NMR spectrum of crude mixture containing (1*E*,3*E*,5*E*)-1,3-bis-phenylsulfonyl-6-phenyl-hexa-1,3,5-triene, **105**, and 1,3,5-trimethoxybenzene using 5 equivalents of Al₂O₃.

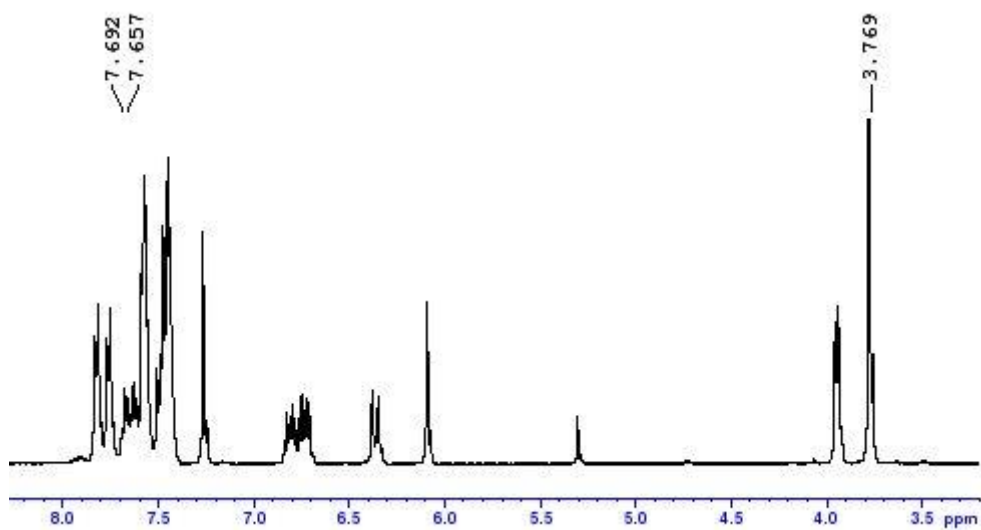


Figure A102. ^1H NMR spectrum of crude mixture containing (*1E,3E,5E*)-1,3-bis-phenylsulfonyl-6-phenyl-hexa-1,3,5-triene, **105**, and 1,3,5-trimethoxybenzene using 1 equivalent of Al_2O_3 . qNMR analysis was not applied here due to the overlap of the triene signal with others appearing between 7.5-7.65 ppm.

Reaction Optimisation Spectra: Preferred temperature

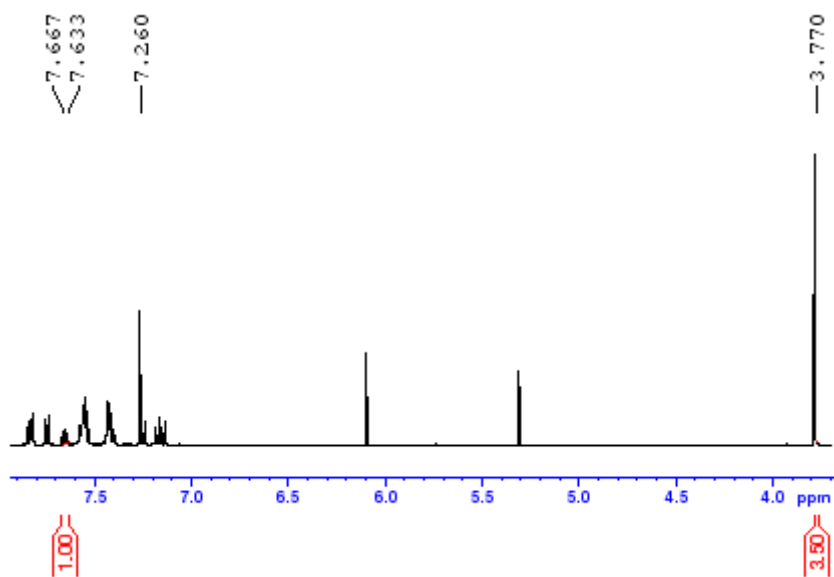


Figure A103. ^1H NMR spectrum of crude mixture containing (*1E,3E,5E*)-1,3-bis-phenylsulfonyl-6-phenyl-hexa-1,3,5-triene, **105**, and 1,3,5-trimethoxybenzene obtained when the reaction is conducted at reflux.

NMR Spectra of trienes

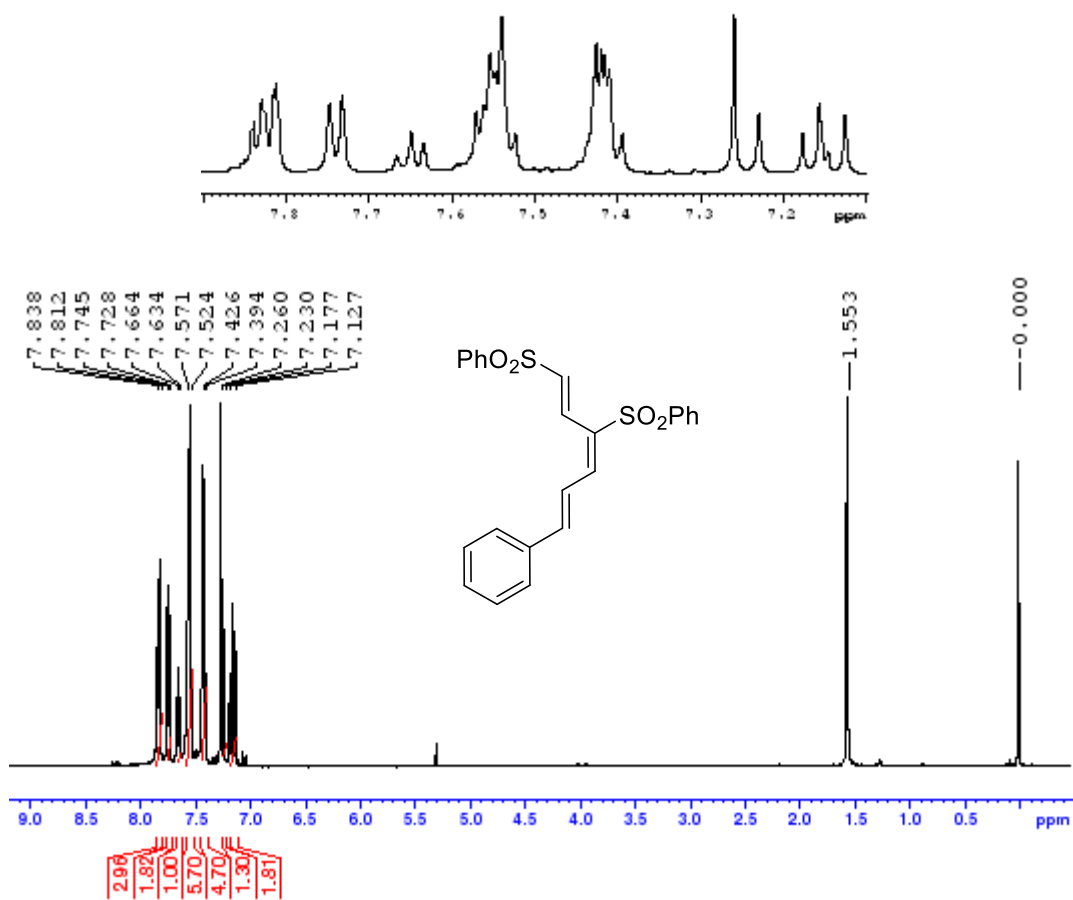


Figure A104. ¹H NMR spectrum of (1E,3E,5E)-1,3-bis-phenylsulfonyl-6-phenyl-hexa-1,3,5-triene, 105

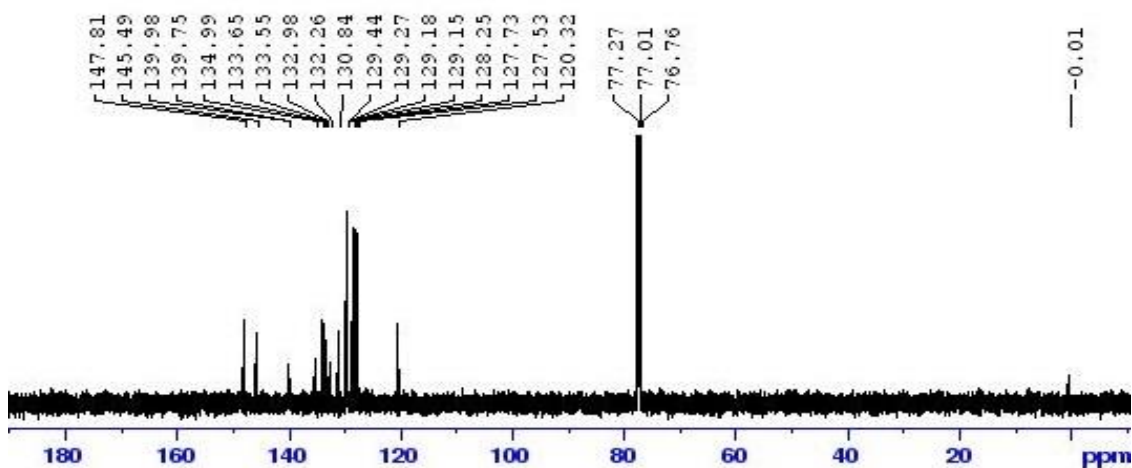


Figure A105. ¹³C NMR spectrum of (1E,3E,5E)-1,3-bis-phenylsulfonyl-6-phenyl-hexa-1,3,5-triene, 105

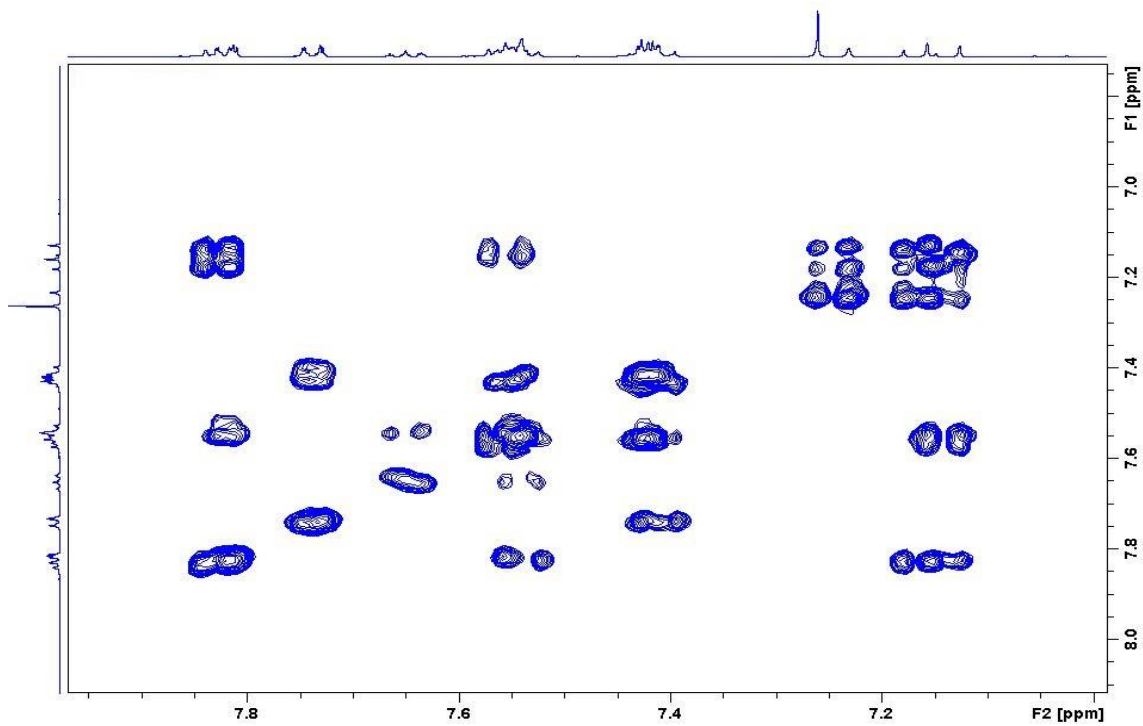


Figure A106. Zoomed in COSY spectrum of (1*E*,3*E*,5*E*)-1,3-bis-phenylsulfonyl-6-phenyl-hexa-1,3,5-triene, **105**

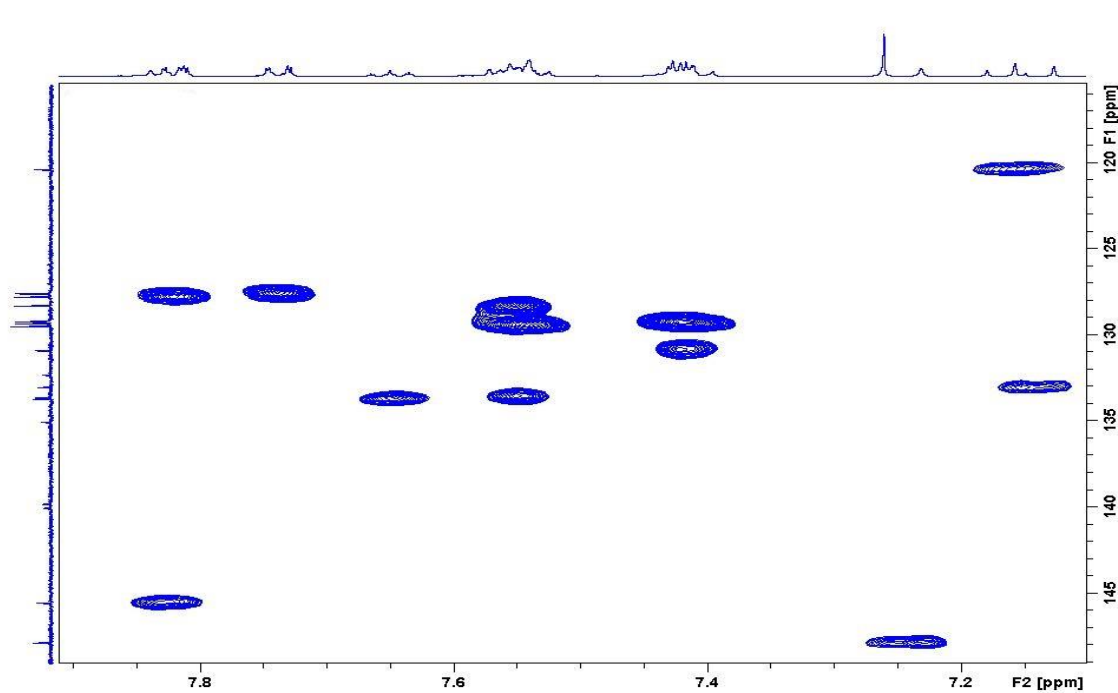


Figure A107. Zoomed in HSQC spectrum of (1*E*,3*E*,5*E*)-1,3-bis-phenylsulfonyl-6-phenyl-hexa-1,3,5-triene, **105**

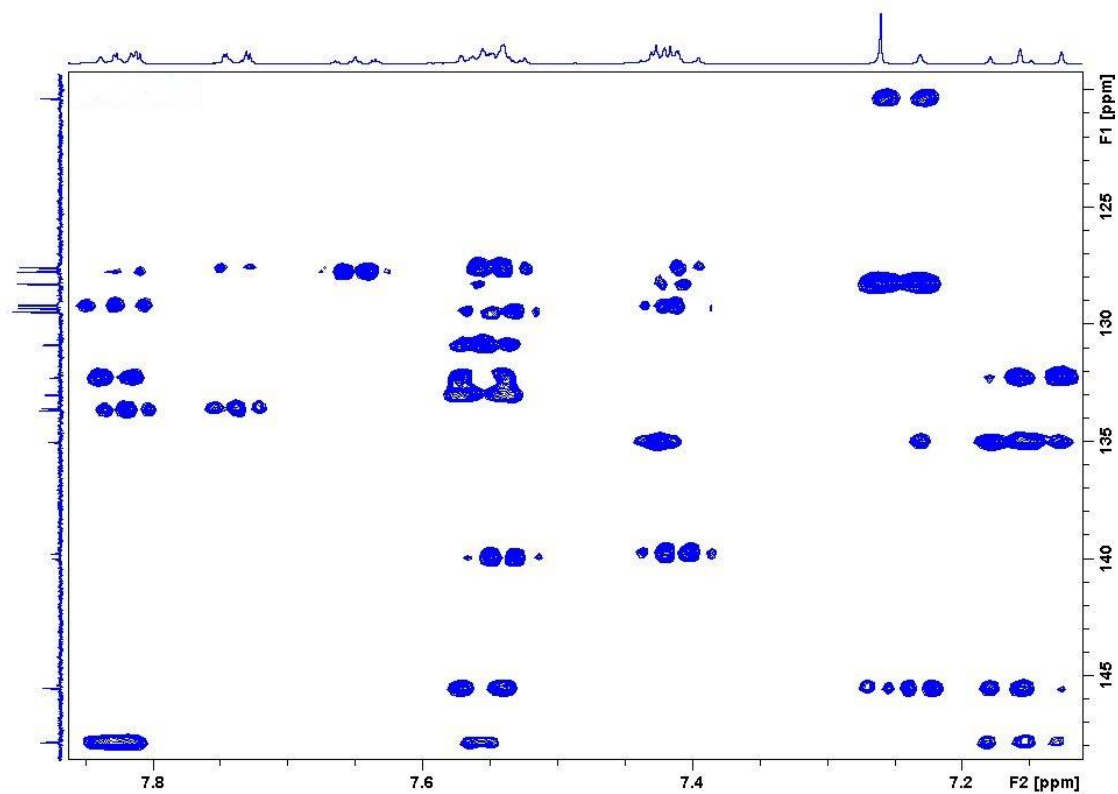


Figure A108. Zoomed in HMBC spectrum of (1*E*,3*E*,5*E*)-1,3-bis-phenylsulfonyl-6-phenyl-hexa-1,3,5-triene, **105**

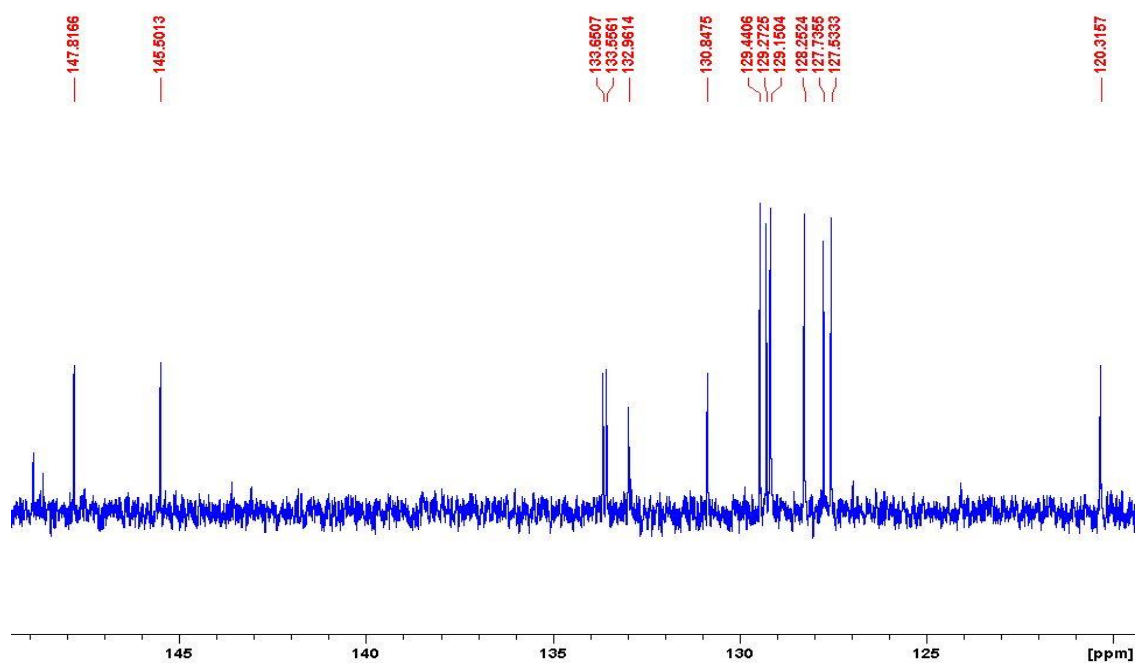


Figure A109. DEPT-135 spectrum of (1*E*,3*E*,5*E*)-1,3-bis-phenylsulfonyl-6-phenyl-hexa-1,3,5-triene, **105**

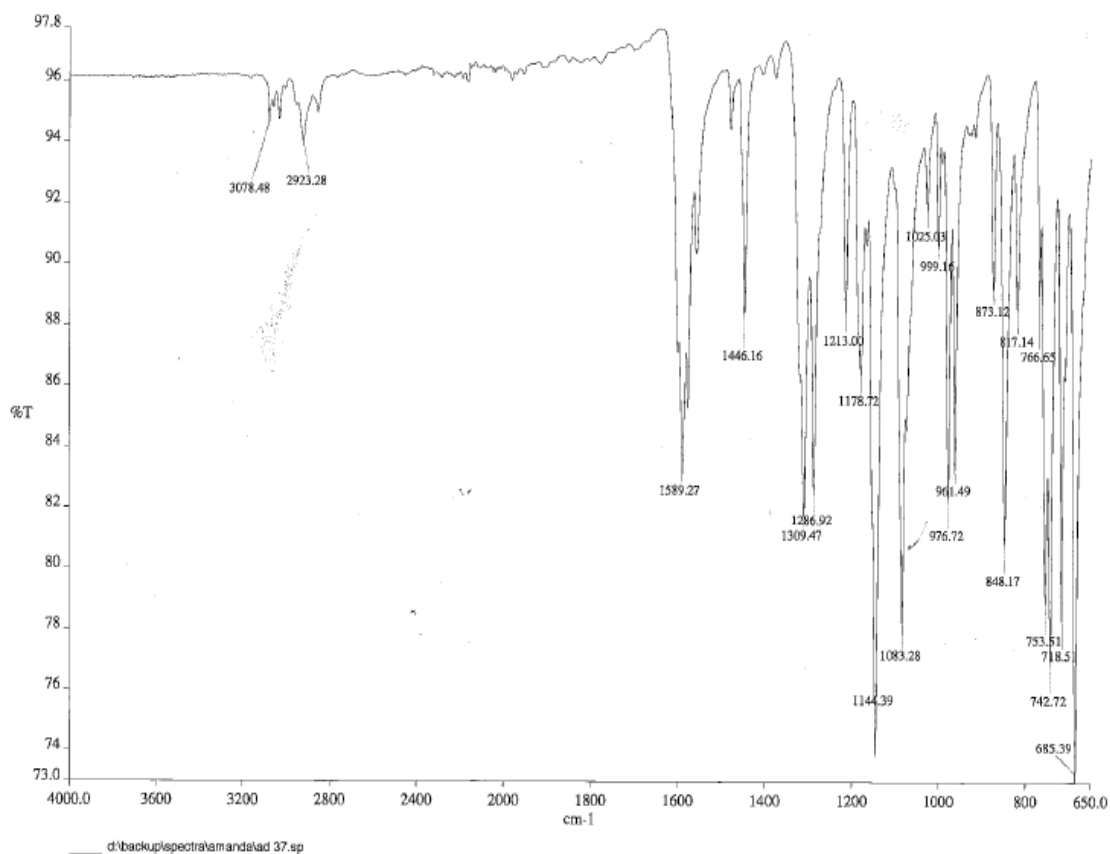


Figure A110. IR spectrum of (1*E*,3*E*,5*E*)-1,3-bis-phenylsulfonyl-6-phenyl-hexa-1,3,5-triene, **105**

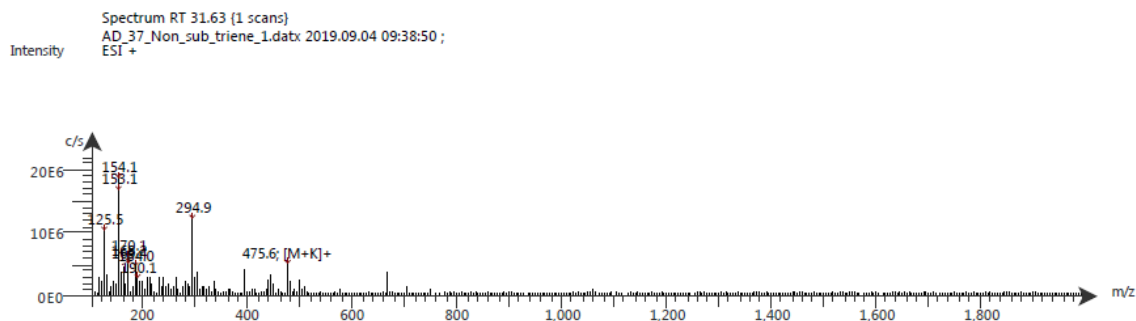


Figure A111. LC-ESI-MS spectrum of (1*E*,3*E*,5*E*)-1,3-bis-phenylsulfonyl-6-phenyl-hexa-1,3,5-triene, **105**. The ESI spectrum shows it has m/z [M+K]⁺ 475.6.

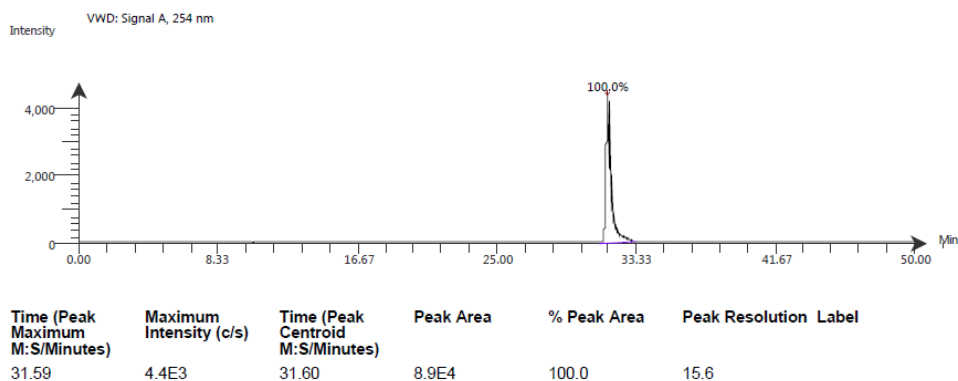


Figure A112. LC-UV-MS spectrum of (1*E*,3*E*,5*E*)-1,3-bis-phenylsulfonyl-6-phenyl-hexa-1,3,5-triene, **105**.

Compound Table

Compound Label	RT	Mass	Abund	Formula	Tgt Mass	Diff (ppm)
Cpd 1: C24 H20 O4 S2	0.203	436.0788	1936273	C24 H20 O4 S2	436.0803	-3.48

Figure A113. HR-MS analysis of (1*E*,3*E*,5*E*)-1,3-bis-phenylsulfonyl-6-phenyl-hexa-1,3,5-triene, **105**

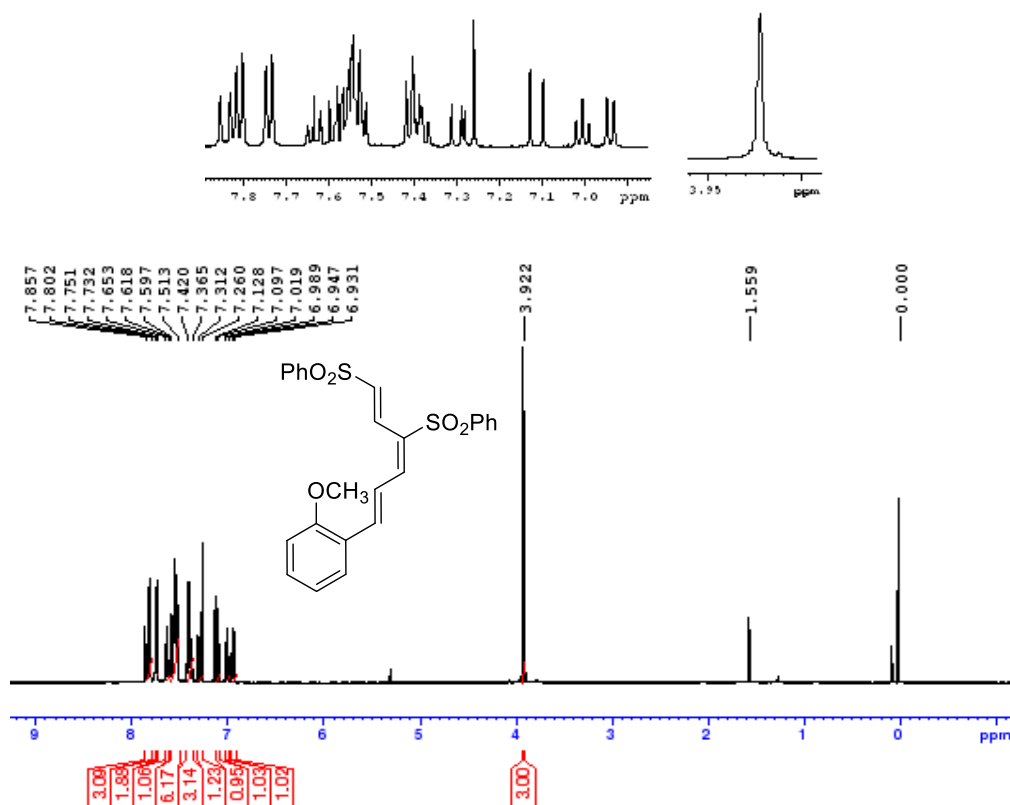


Figure A114. ¹H NMR spectrum of (1*E*,3*E*,5*E*)-1,3-bis-phenylsulfonyl-(6-*o*-methoxyphenyl)-hexa-1,3,5-triene, **106**.

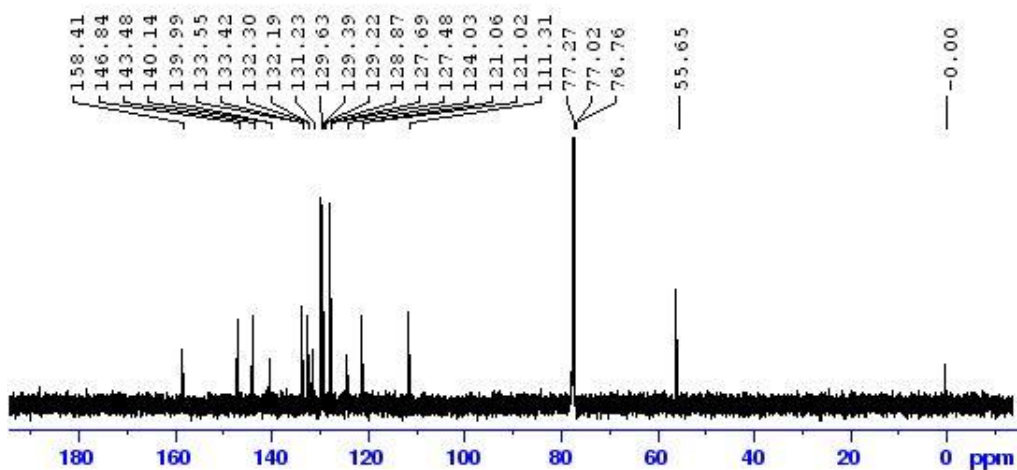


Figure A115. ^{13}C NMR spectrum of (1*E*,3*E*,5*E*)-1,3-bis-phenylsulfonyl-(6-*o*-methoxyphenyl)-hexa-1,3,5-triene, **106**

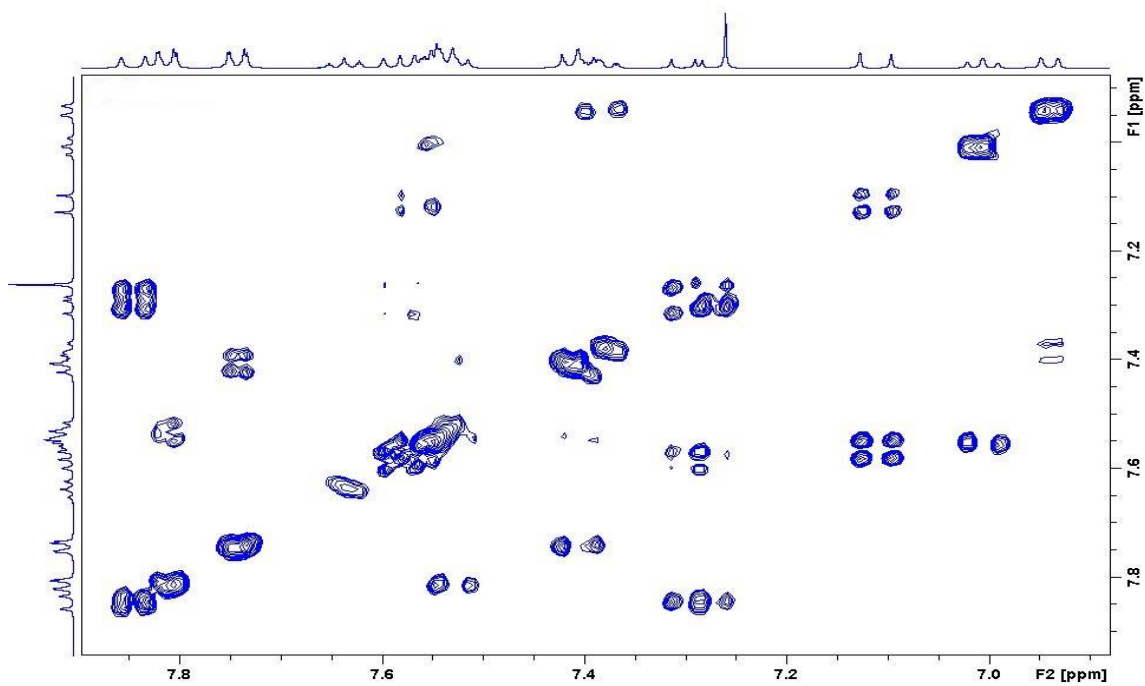


Figure A116. Zoomed in COSY spectrum of (1*E*,3*E*,5*E*)-1,3-bis-phenylsulfonyl-(6-*o*-methoxyphenyl)-hexa-1,3,5-triene, **106**

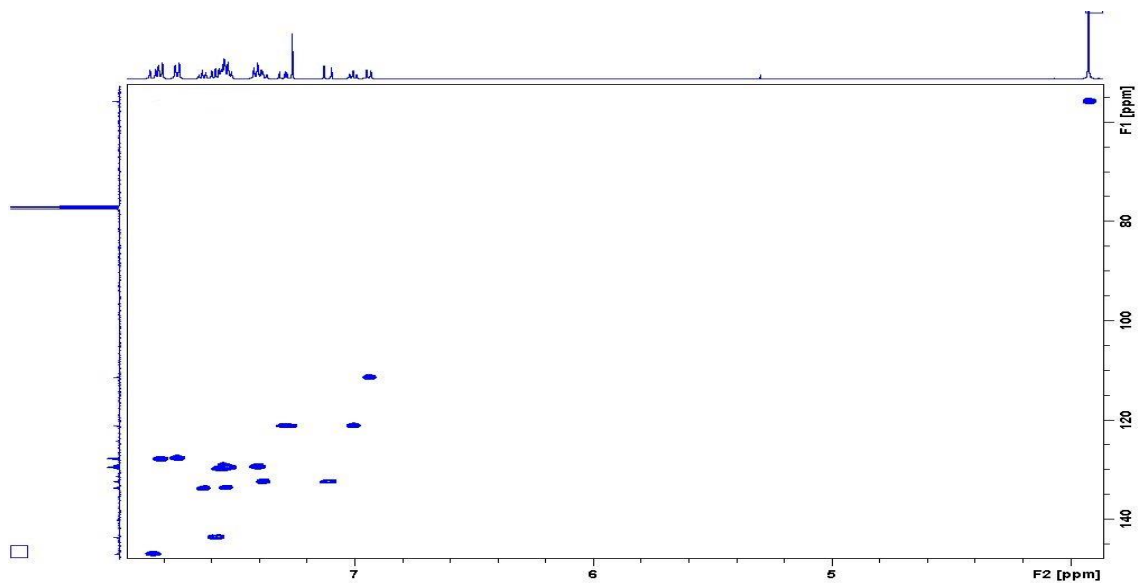


Figure A117. Zoomed in HSQC spectrum of (1*E*,3*E*,5*E*)-1,3-bis-phenylsulfonyl-(6-*o*-methoxyphenyl)-hexa-1,3,5-triene, **106**

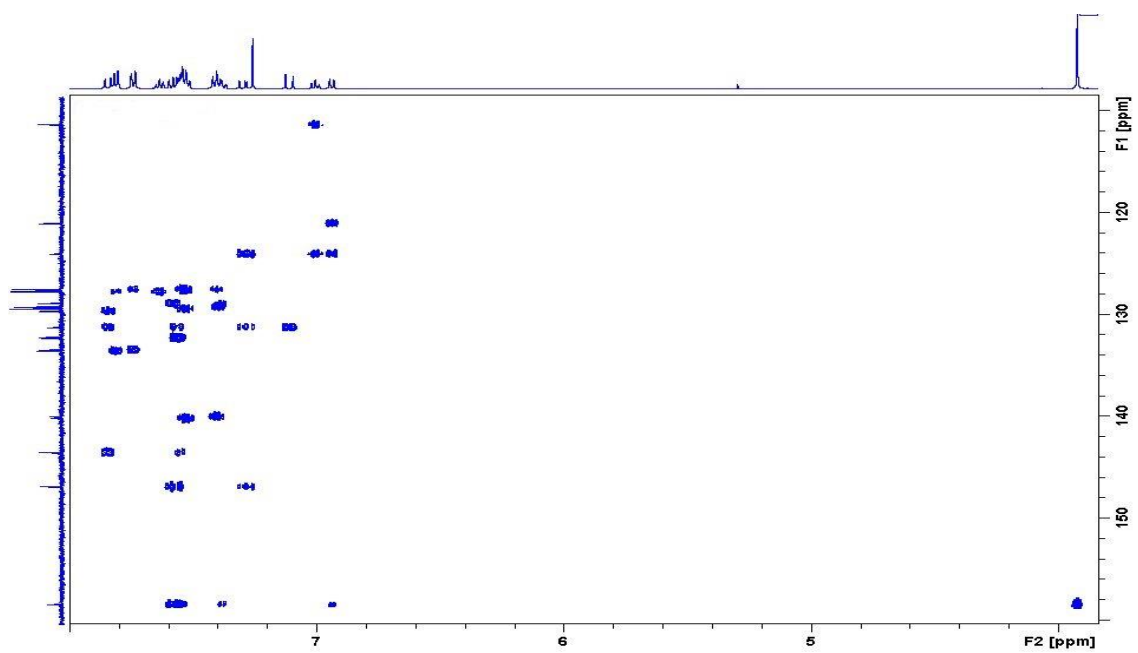


Figure A118. Zoomed in HMBC spectrum of (1*E*,3*E*,5*E*)-1,3-bis-phenylsulfonyl-(6-*o*-methoxyphenyl)-hexa-1,3,5-triene, **106**

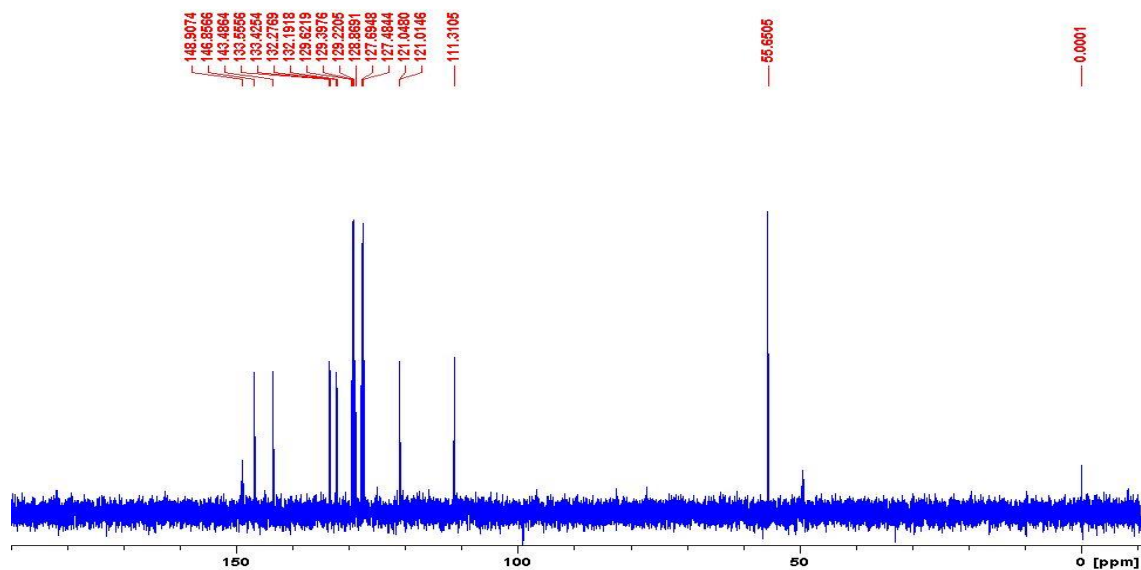


Figure A119. DEPT-135 spectrum of (1E,3E,5E)-1,3-bis-phenylsulfonyl-(6-o-methoxyphenyl)-hexa-1,3,5-triene, 106

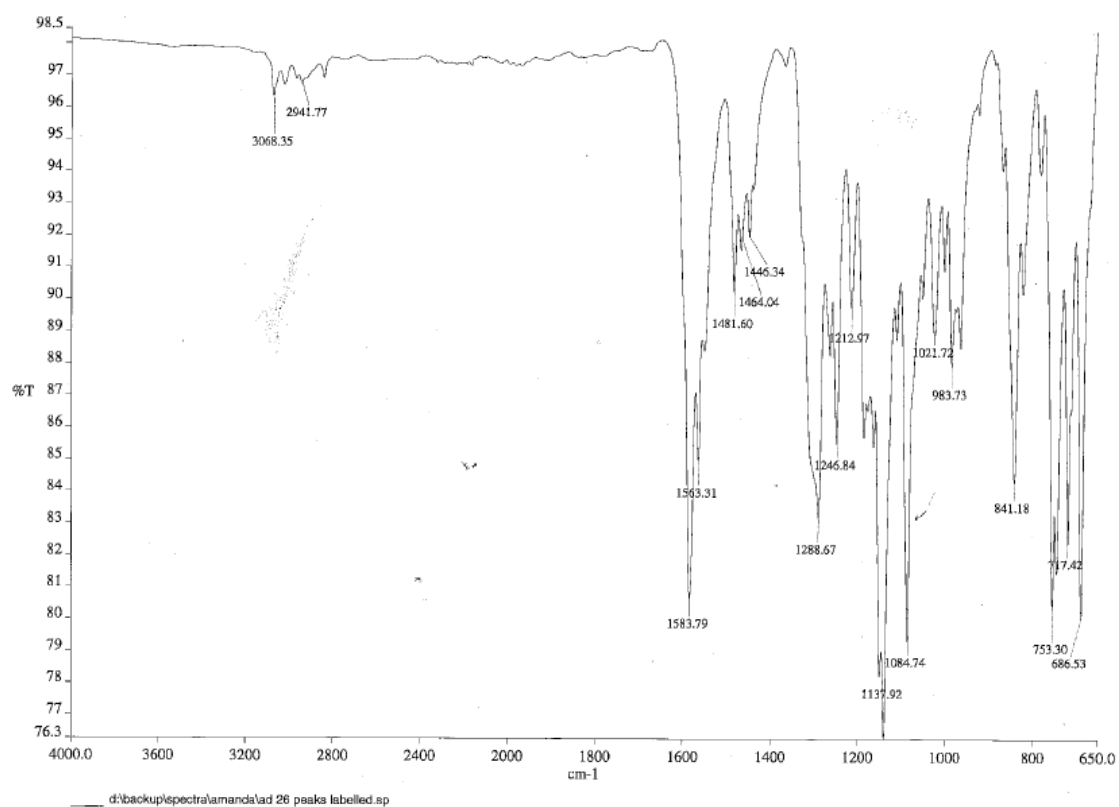


Figure A120. IR spectrum of (1E,3E,5E)-1,3-bis-phenylsulfonyl-(6-o-methoxyphenyl)-hexa-1,3,5-triene, 106

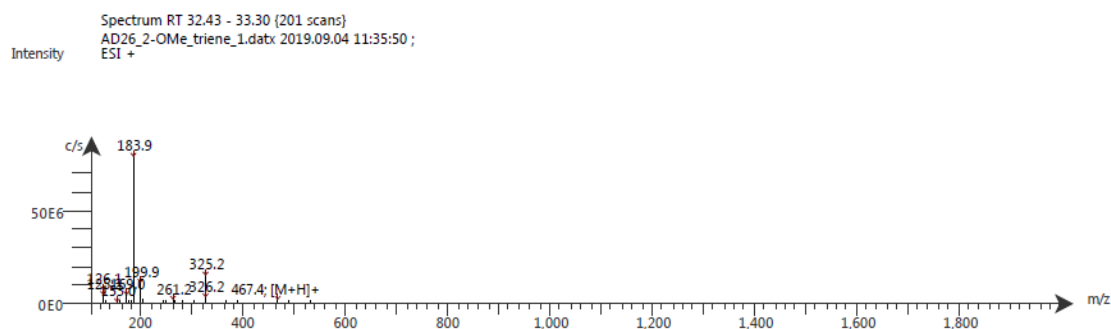
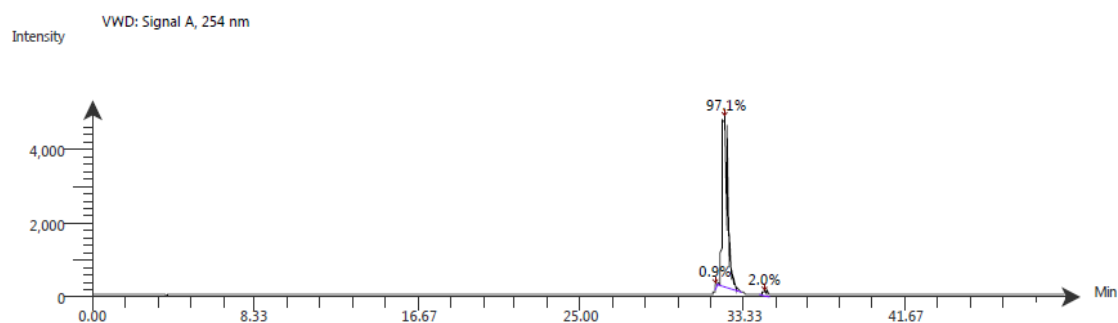


Figure A121. LC-ESI-MS spectrum of (1*E*,3*E*,5*E*)-1,3-bis-phenylsulfonyl-(6-*o*-methoxyphenyl)-hexa-1,3,5-triene, **106**. The ESI spectrum shows it has m/z $[M+H]^+$ 467.4



Time (Peak Maximum M:S/Minutes)	Maximum Intensity (c/s)	Time (Peak Centroid M:S/Minutes)	Peak Area	% Peak Area	Peak Resolution Label
31.98	1.2E2	31.99	8.2E2	0.9	11.4
32.34	4.7E3	32.36	8.6E4	97.1	16.1
34.42	1.6E2	34.42	1.8E3	2.0	10.4

Figure A122. LC-UV-MS spectrum of (1*E*,3*E*,5*E*)-1,3-bis-phenylsulfonyl-(6-*o*-methoxyphenyl)-hexa-1,3,5-triene, **106**

Compound Table

Compound Label	RT	Mass	Abund	Formula	Tgt Mass	Diff (ppm)
Cpd 1: C25 H22 O5 S2	0.193	466.0896	1662291	C25 H22 O5 S2	466.0909	-2.81

Figure A123. HR-MS analysis of (1*E*,3*E*,5*E*)-1,3-bis-phenylsulfonyl-(6-*o*-methoxyphenyl)-hexa-1,3,5-triene, **106**

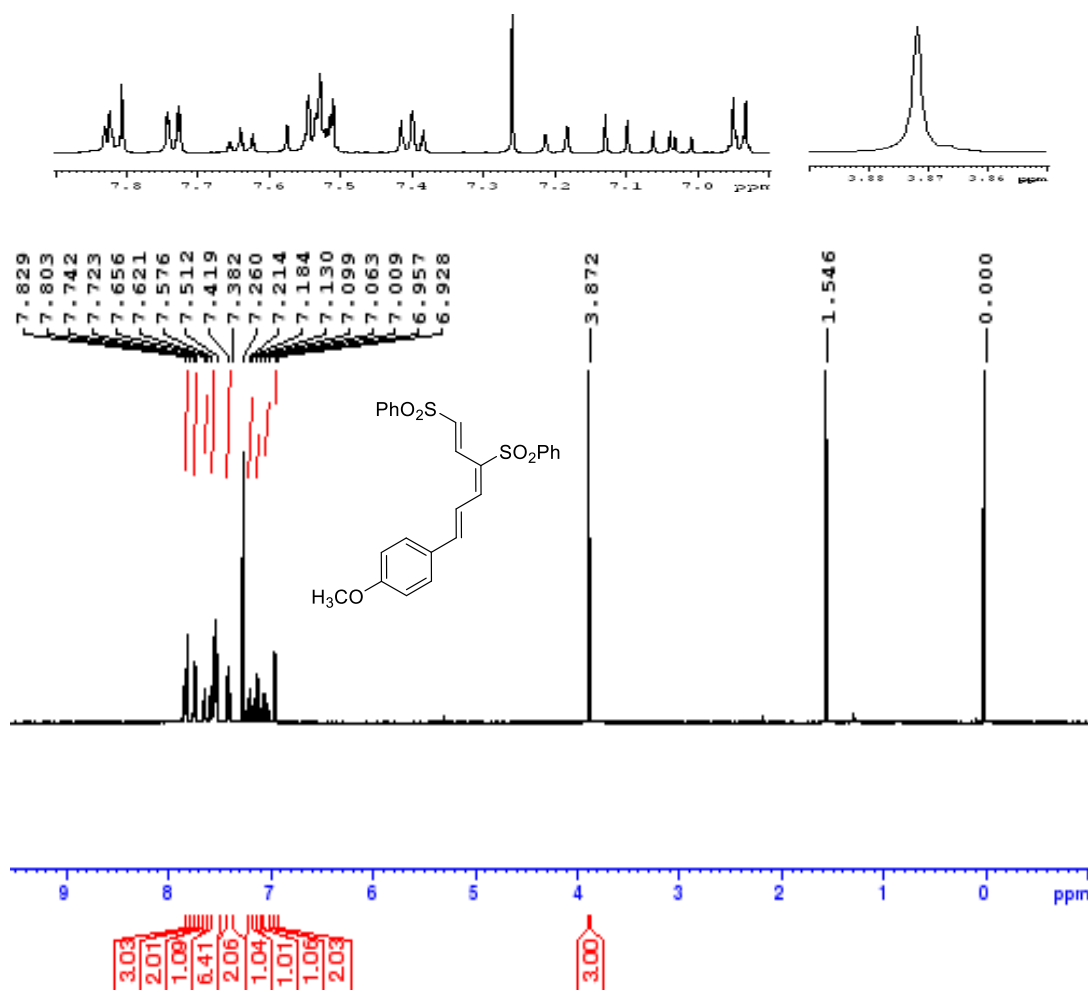


Figure A124. ¹H NMR spectrum of (1E,3E,5E)-1,3-bis-phenylsulfonyl-(6-p-methoxyphenyl)-hexa-1,3,5-triene, **107**

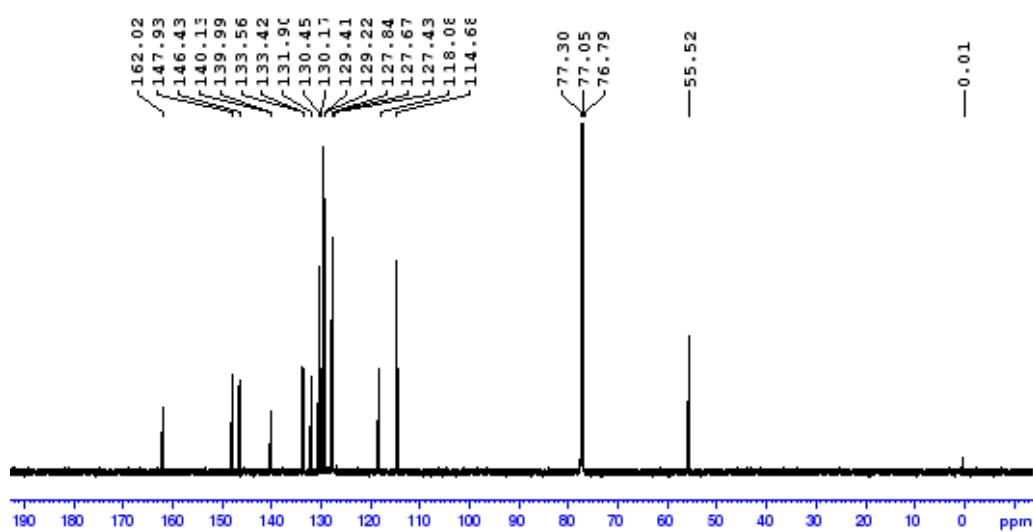


Figure A125. ¹³C NMR spectrum of (1E,3E,5E)-1,3-bis-phenylsulfonyl-(6-p-methoxyphenyl)-hexa-1,3,5-triene, **107**

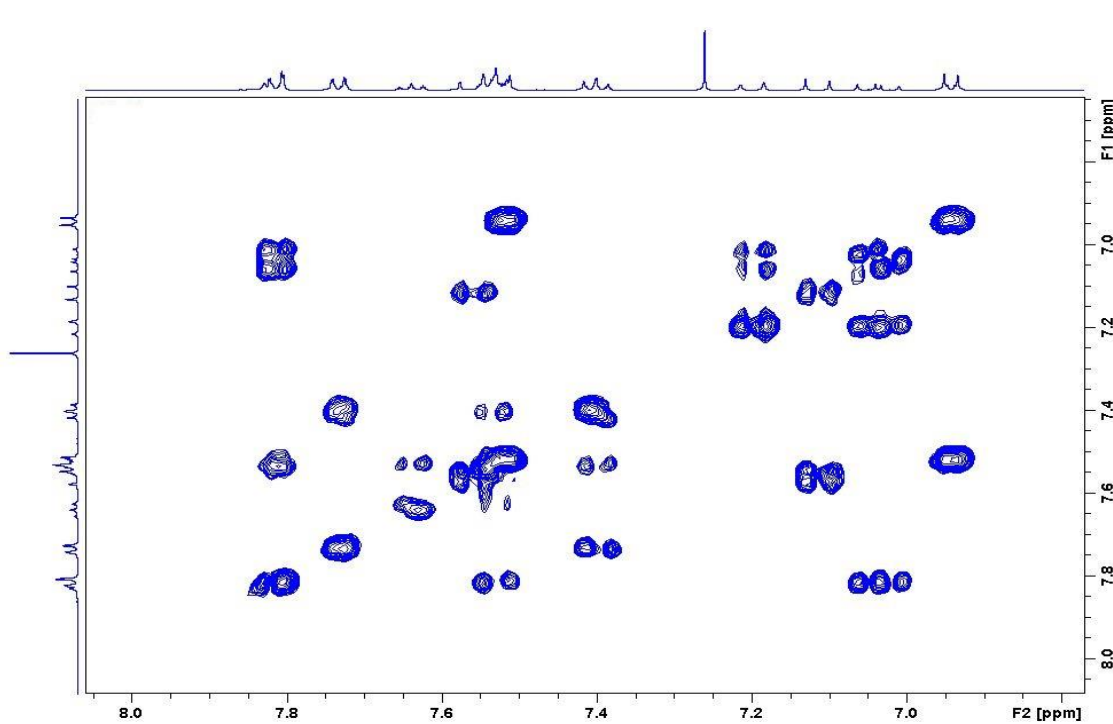


Figure A126. Zoomed in COSY spectrum of (1*E*,3*E*,5*E*)-1,3-bis-phenylsulfonyl-(6-*p*-methoxyphenyl)-hexa-1,3,5-triene, **107**

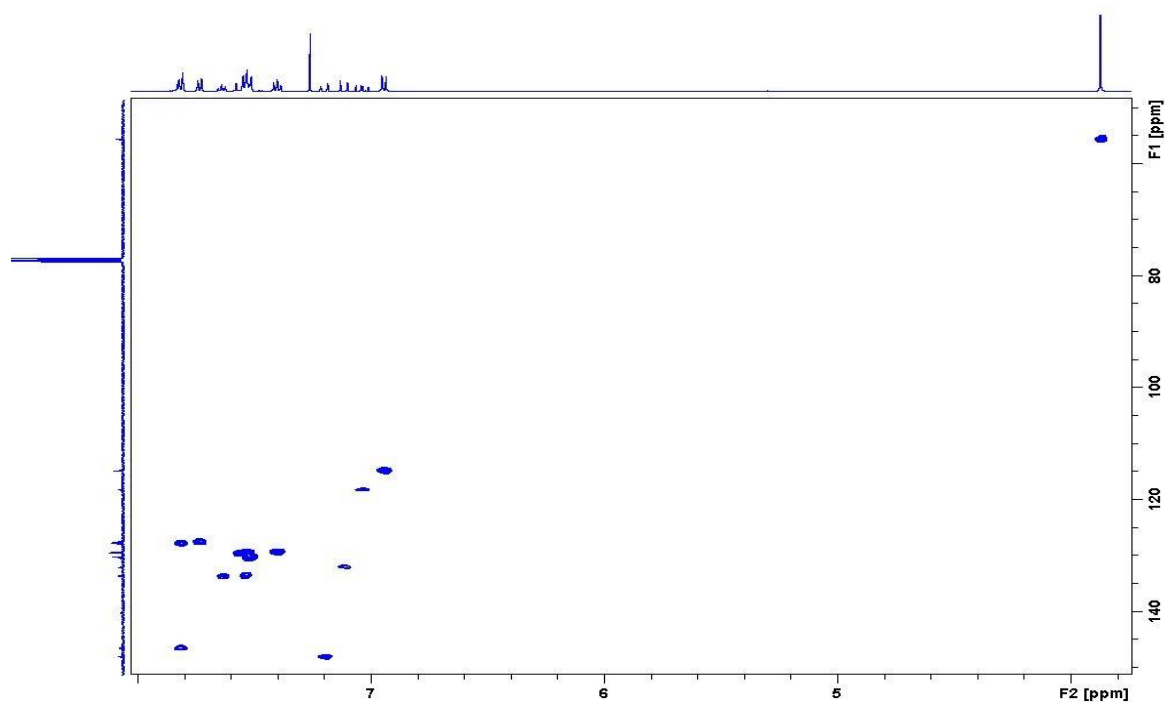


Figure A127. Zoomed in HSQC spectrum of (1*E*,3*E*,5*E*)-1,3-bis-phenylsulfonyl-(6-*p*-methoxyphenyl)-hexa-1,3,5-triene, **107**.

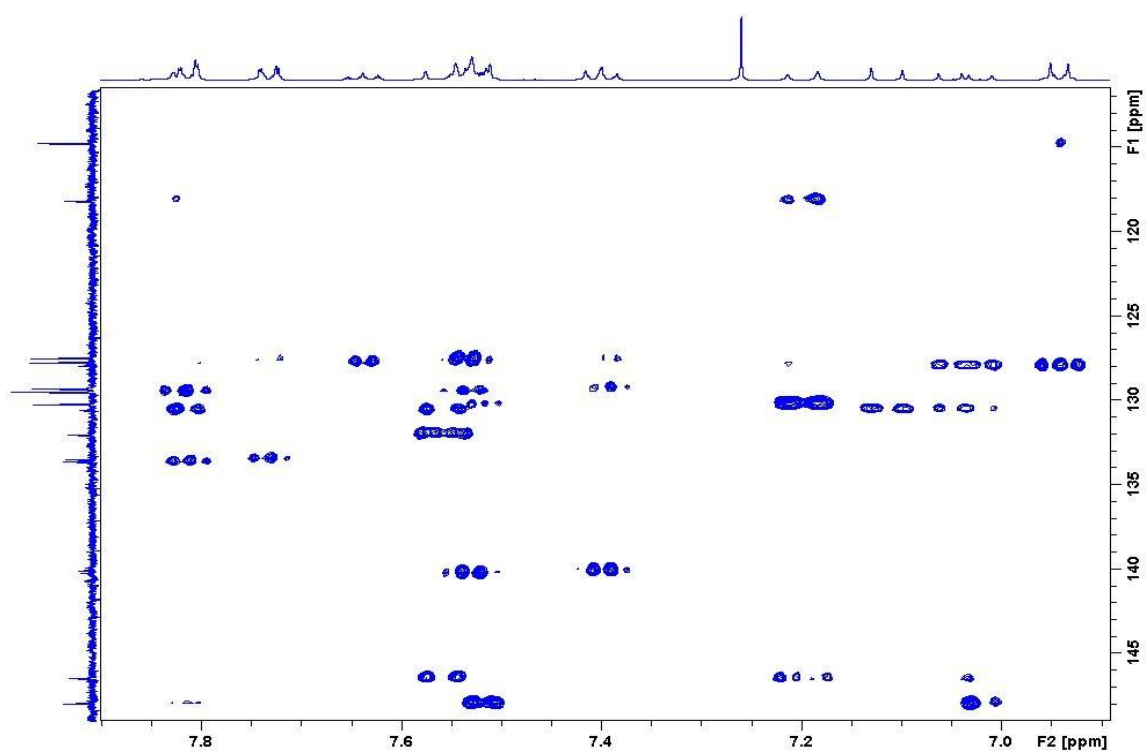


Figure A128. HMBC spectrum of (1*E*,3*E*,5*E*)-1,3-bis-phenylsulfonyl-(6-*p*-methoxyphenyl)-hexa-1,3,5-triene, **107**

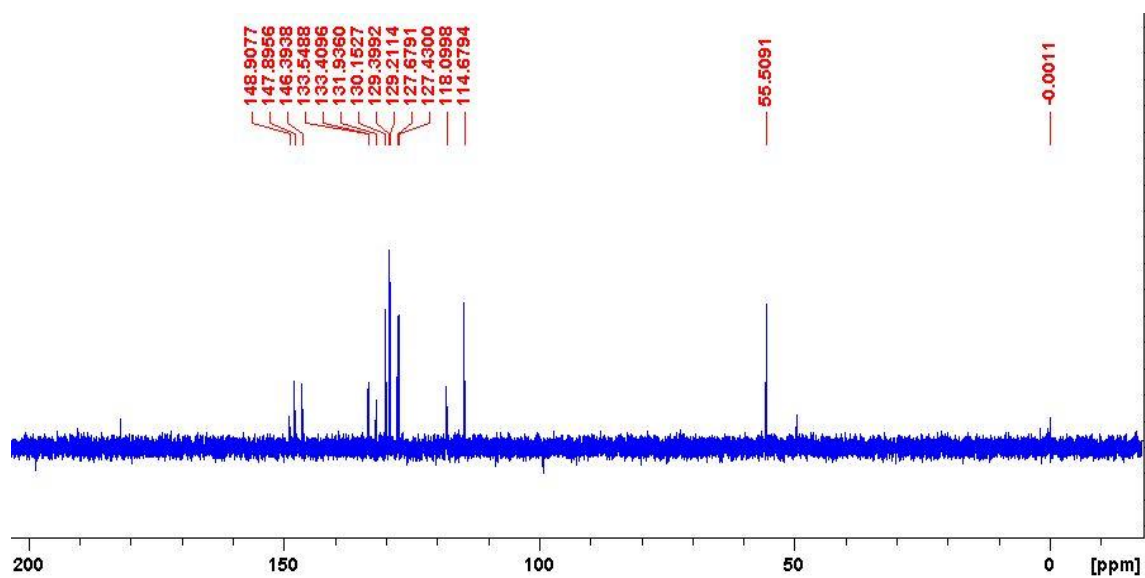


Figure A129. DEPT-135 spectrum of (1*E*,3*E*,5*E*)-1,3-bis-phenylsulfonyl-(6-*p*-methoxyphenyl)-hexa-1,3,5-triene, **107**

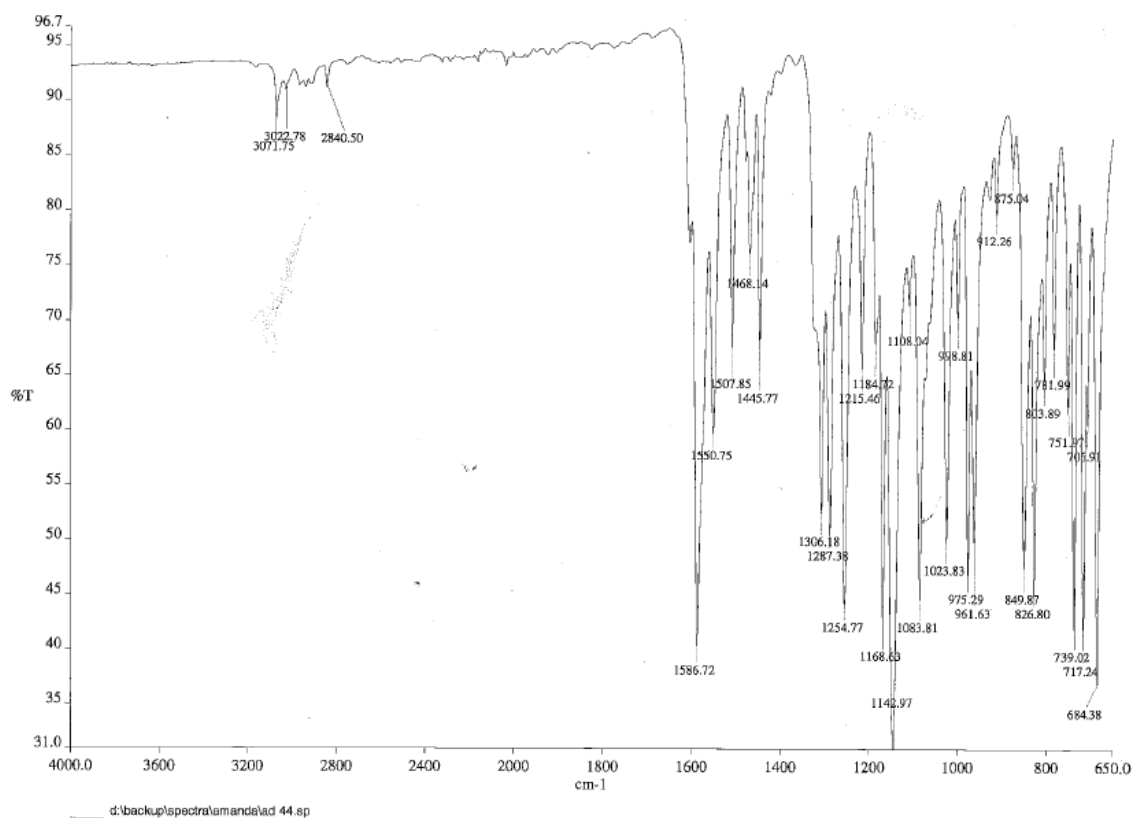


Figure A130. IR spectrum of (1*E*,3*E*,5*E*)-1,3-bis-phenylsulfonyl-(6-*p*-methoxyphenyl)-hexa-1,3,5-triene, **107**

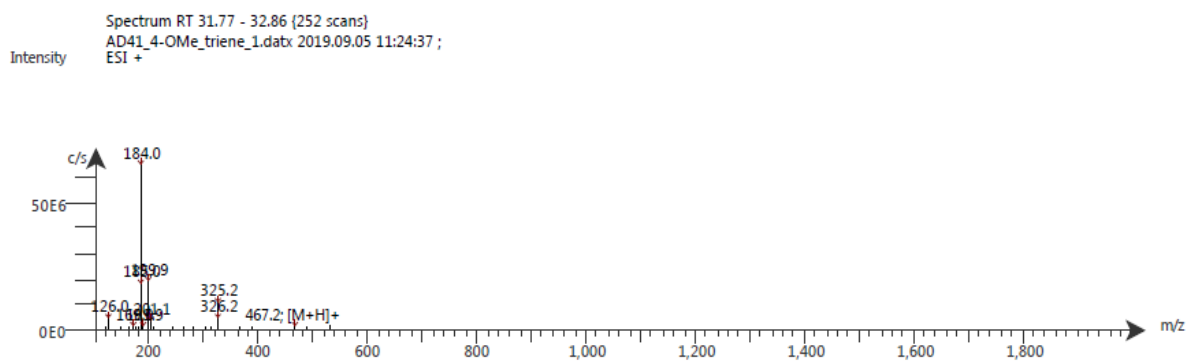


Figure A131. LC-ESI-MS spectrum of (1*E*,3*E*,5*E*)-1,3-bis-phenylsulfonyl-(6-*p*-methoxyphenyl)-hexa-1,3,5-triene, **107**. The ESI spectrum shows it has m/z [M+H]⁺ 467.2

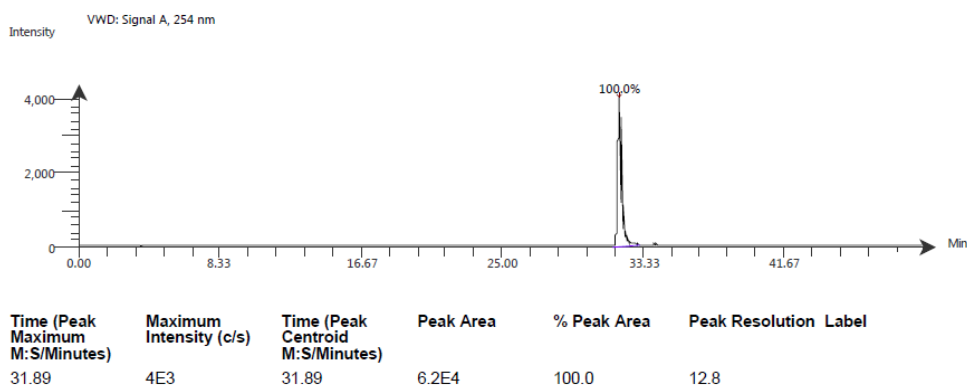


Figure A132. LC-UV-MS spectrum of (1*E*,3*E*,5*E*)-1,3-bis-phenylsulfonyl-(6-*p*-methoxyphenyl)-hexa-1,3,5-triene, **107**

Compound Table

Compound Label	RT	Mass	Abund	Formula	Tgt Mass	Diff (ppm)
Cpd 1: C25 H22 O5 S2	0.144	466.0907	905199	C25 H22 O5 S2	466.0909	-0.31

Figure A133. HR-MS analysis of (1*E*,3*E*,5*E*)-1,3-bis-phenylsulfonyl-(6-*p*-methoxyphenyl)-hexa-1,3,5-triene, **107**

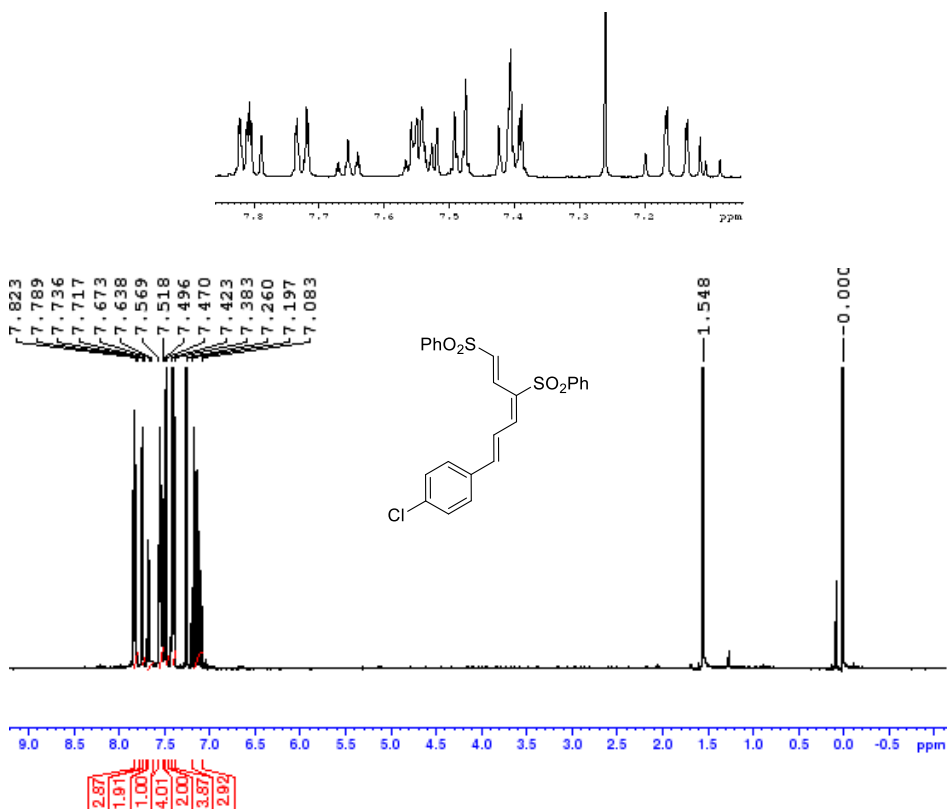


Figure A134. ¹H NMR spectrum of (1*E*,3*E*,5*E*)-1,3-bis-phenylsulfonyl-(6-*p*-chlorophenyl)-hexa-1,3,5-triene, **108**

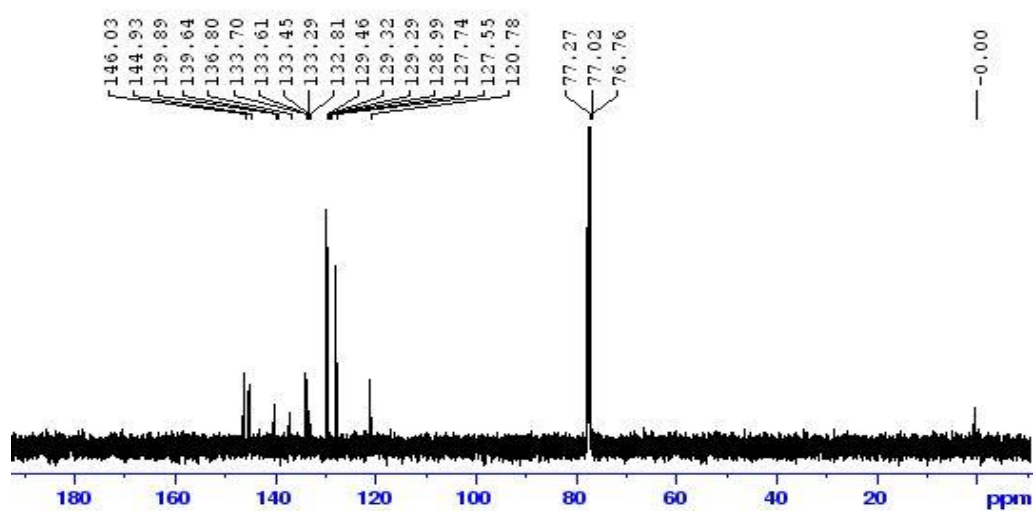


Figure A135. ^{13}C NMR spectrum of (1*E*,3*E*,5*E*)-1,3-bis-phenylsulfonyl-(6-*p*-chlorophenyl)-hexa-1,3,5-triene, **108**

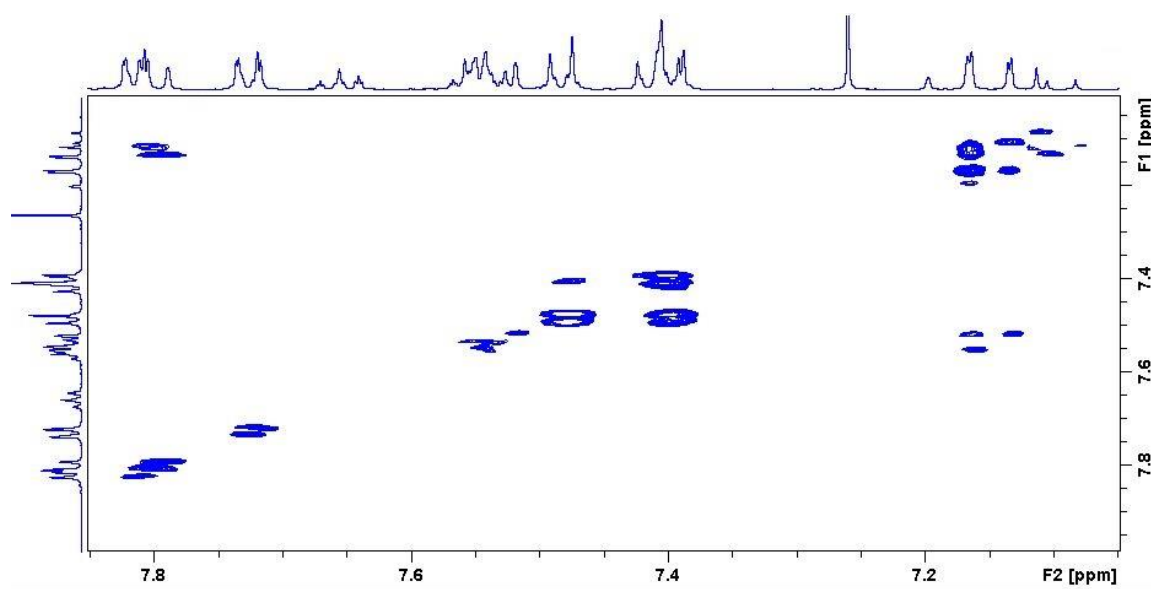


Figure A136. Zoomed in COSY spectrum of (1*E*,3*E*,5*E*)-1,3-bis-phenylsulfonyl-(6-*p*-chlorophenyl)-hexa-1,3,5-triene, **108**

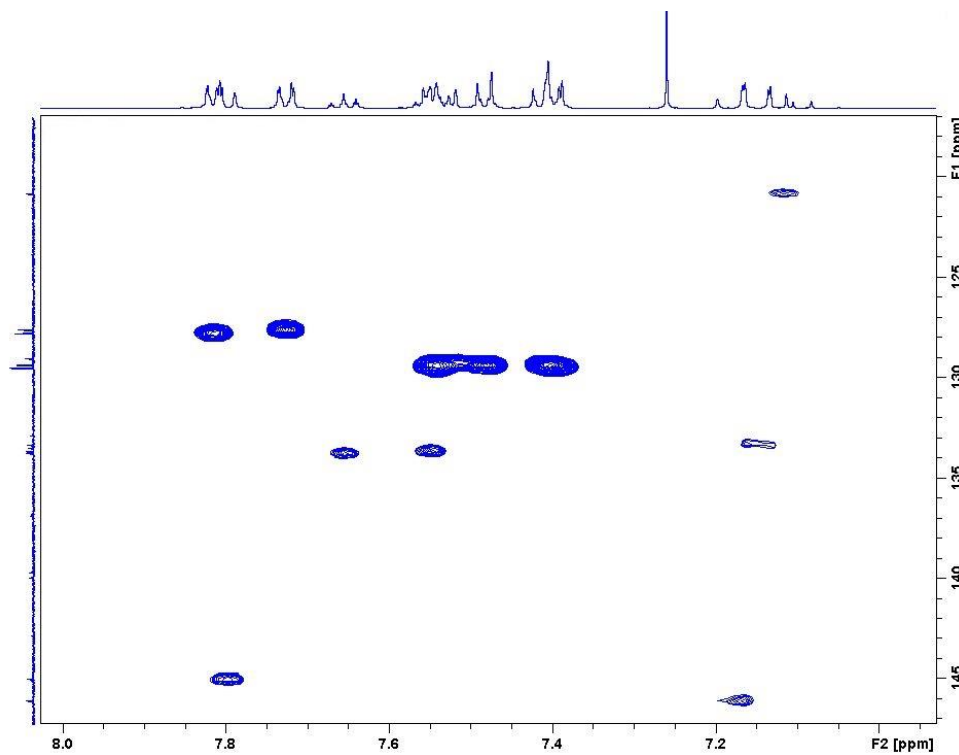


Figure A137. Zoomed in HSQC spectrum of (1*E*,3*E*,5*E*)-1,3-bis-phenylsulfonyl-(6-*p*-chlorophenyl)-hexa-1,3,5-triene, **108**

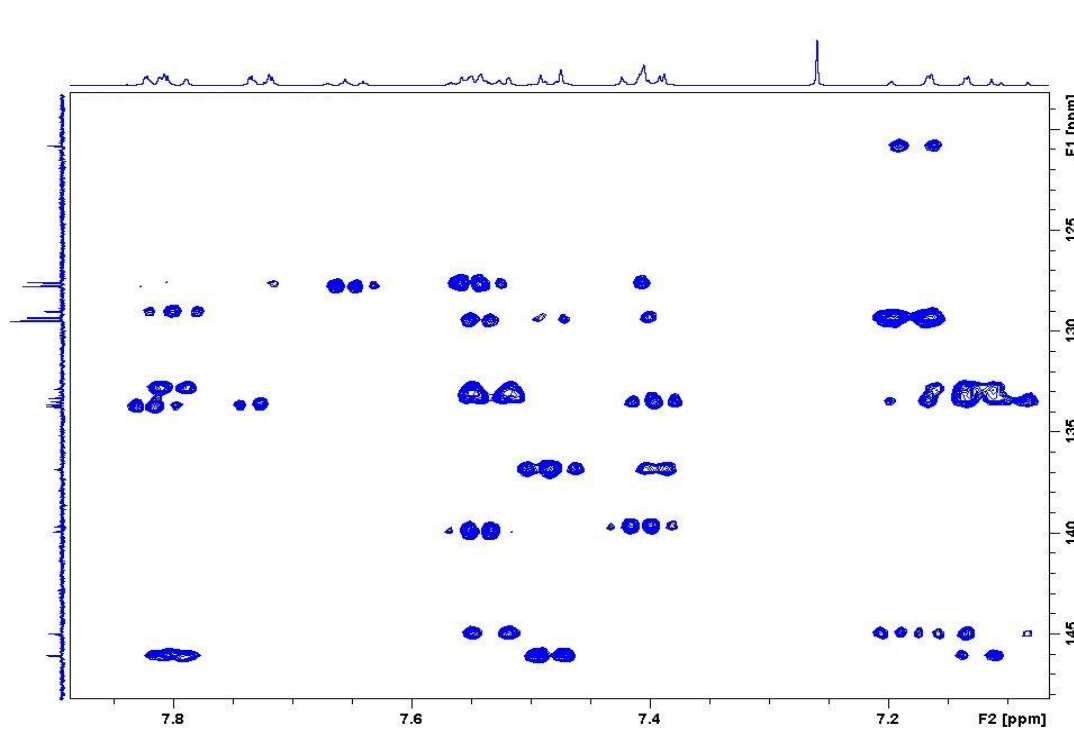


Figure A138. Zoomed in HMBC spectrum of (1*E*,3*E*,5*E*)-1,3-bis-phenylsulfonyl-(6-*p*-chlorophenyl)-hexa-1,3,5-triene, **108**

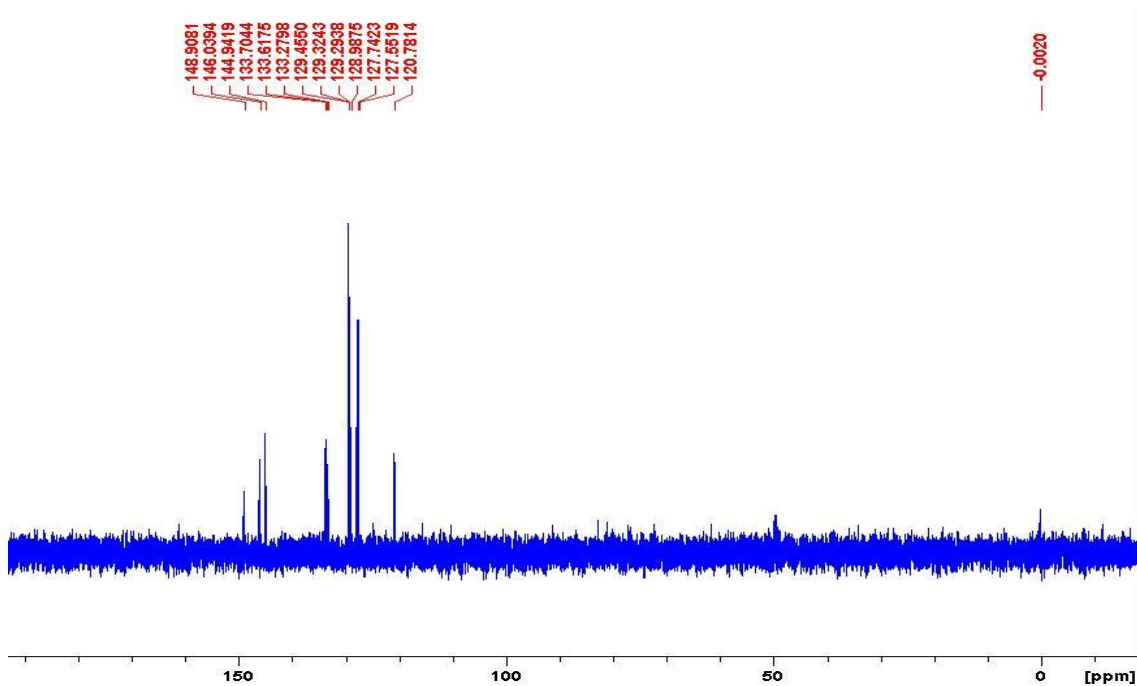


Figure A139. DEPT-135 spectrum of (1*E*,3*E*,5*E*)-1,3-bis-phenylsulfonyl-(6-*p*-chlorophenyl)-hexa-1,3,5-triene, **108**

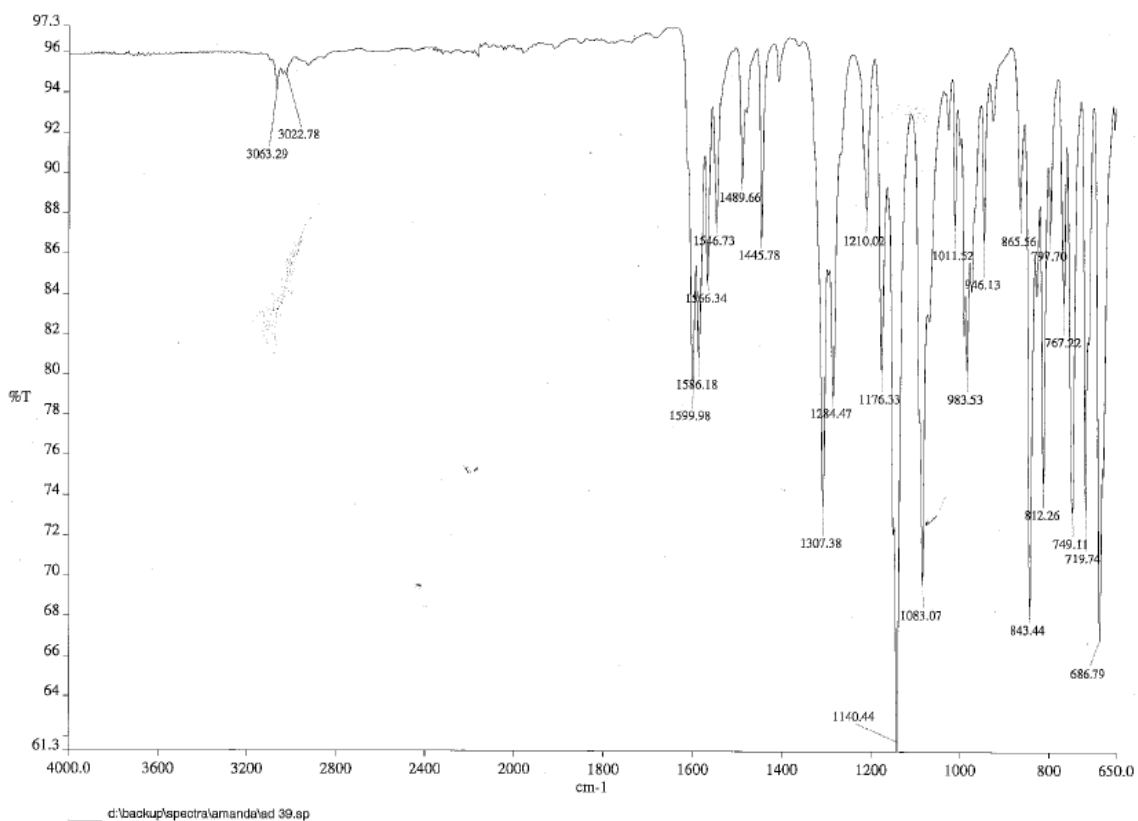


Figure A140. IR spectrum of (1*E*,3*E*,5*E*)-1,3-bis-phenylsulfonyl-(6-*p*-chlorophenyl)-hexa-1,3,5-triene, **108**

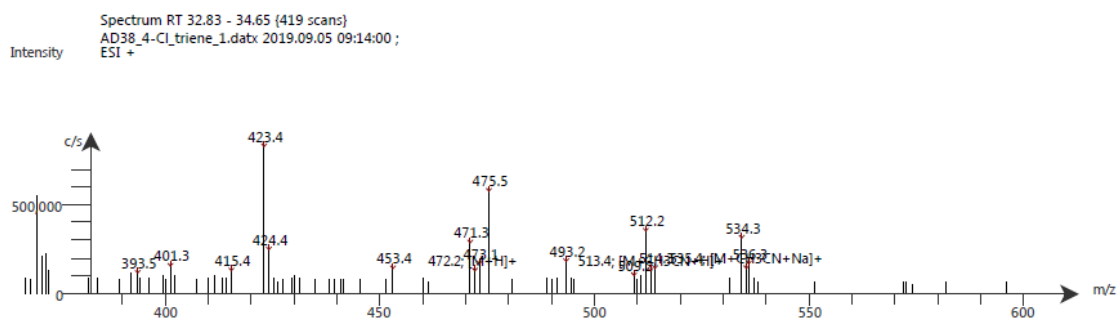
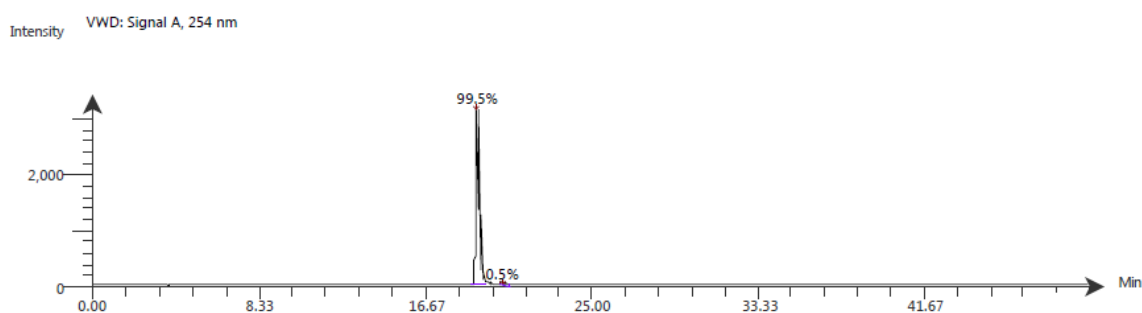


Figure A141. LC-ESI-MS spectrum of (1*E*,3*E*,5*E*)-1,3-bis-phenylsulfonyl-(6-*p*-chlorophenyl)-hexa-1,3,5-triene, **108**. The ESI spectrum shows it has m/z $[M+H]^+$ 472.2



Time (Peak Maximum M:S/Minutes)	Maximum Intensity (c/s)	Time (Peak Centroid M:S/Minutes)	Peak Area	% Peak Area	Peak Resolution Label
19.21	3.1E3	19.21	3.7E4	99.5	10.6
20.47	1.3E1	20.51	1.7E2	0.5	28.5

Figure A142. LC-UV-MS spectrum of (1*E*,3*E*,5*E*)-1,3-bis-phenylsulfonyl-(6-*p*-chlorophenyl)-hexa-1,3,5-triene, **108**

m/z	Calc m/z	Diff (ppm)	z	Abund	Formula	Ion
471.0469	471.0486	-3.62	1	80834	C ₂₄ H ₂₀ ClO ₄ S ₂	(M+H) ⁺

Figure A143. HR-MS analysis of (1*E*,3*E*,5*E*)-1,3-bis-phenylsulfonyl-(6-*p*-chlorophenyl)-hexa-1,3,5-triene, **108**

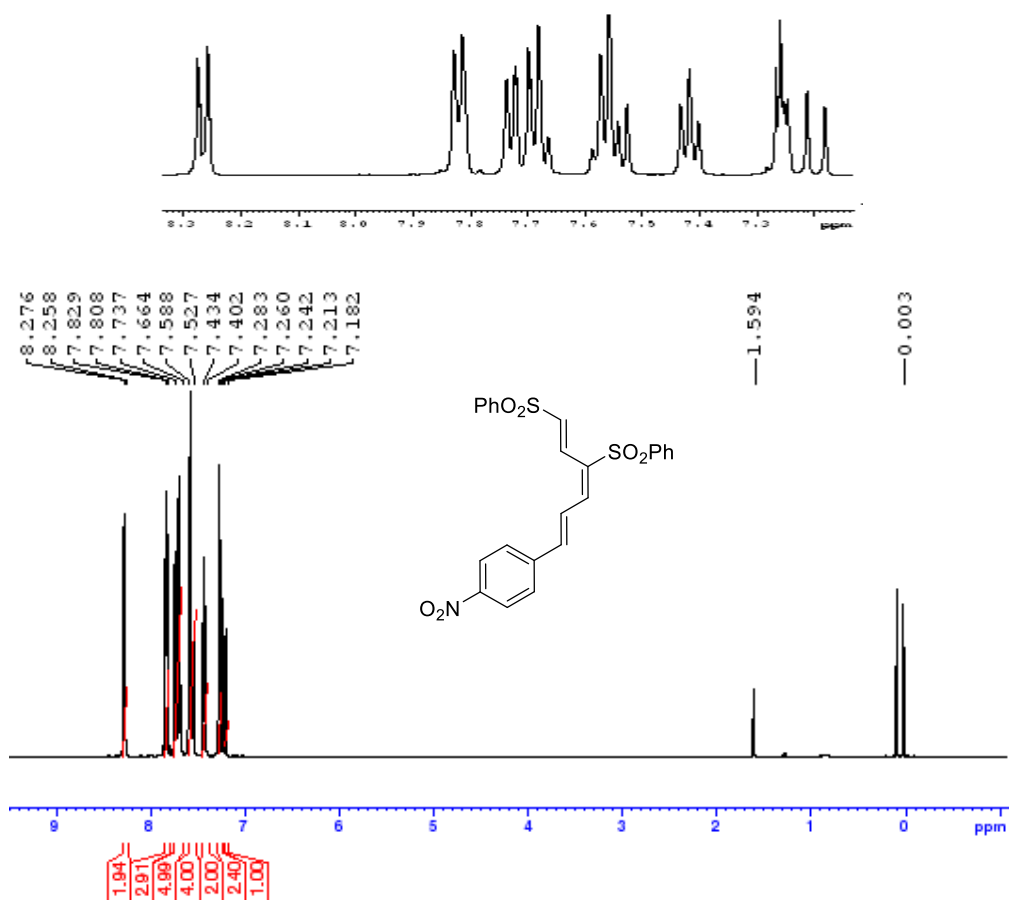


Figure A144. ¹H NMR spectrum of (1E,3E,5E)-1,3-bis-phenylsulfonyl-(6-*p*-nitrophenyl)-hexa-1,3,5-triene, **109**

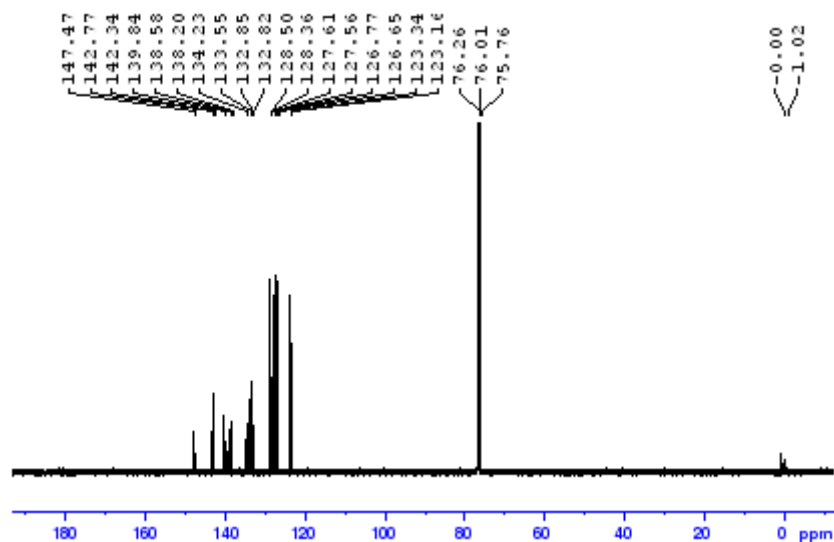


Figure A145. ¹³C NMR spectrum of (1E,3E,5E)-1,3-bis-phenylsulfonyl-(6-*p*-nitrophenyl)-hexa-1,3,5-triene, **109**

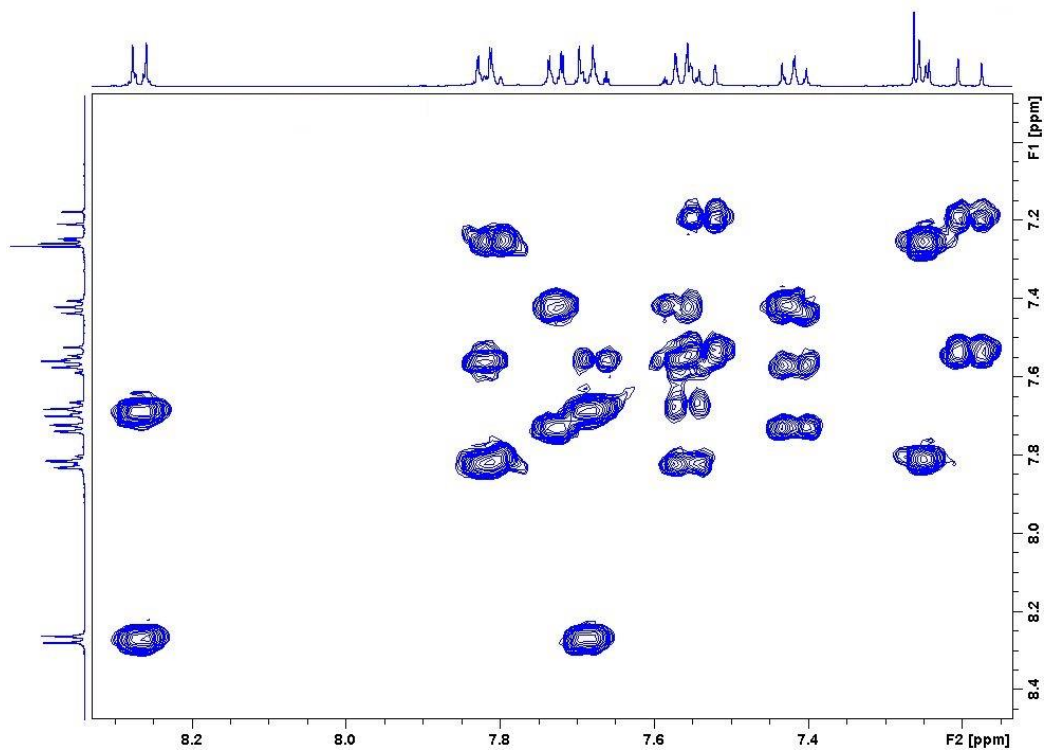


Figure A146. Zoomed in COSY spectrum of (1*E*,3*E*,5*E*)-1,3-bis-phenylsulfonyl-(6-*p*-nitrophenyl)-hexa-1,3,5-triene, **109**

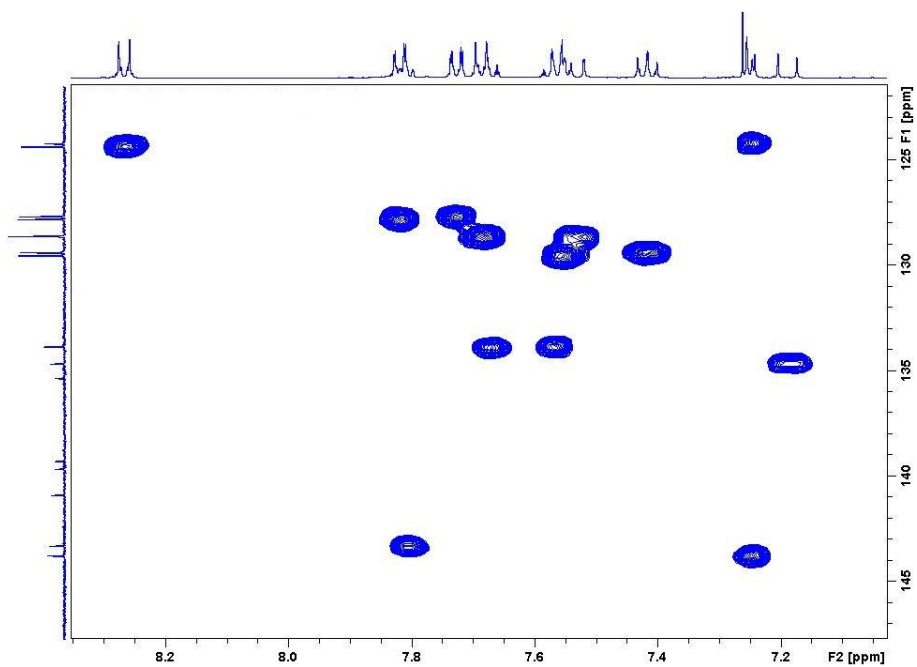


Figure A147. Zoomed in HSQC spectrum of (1*E*,3*E*,5*E*)-1,3-bis-phenylsulfonyl-(6-*p*-nitrophenyl)-hexa-1,3,5-triene, **109**

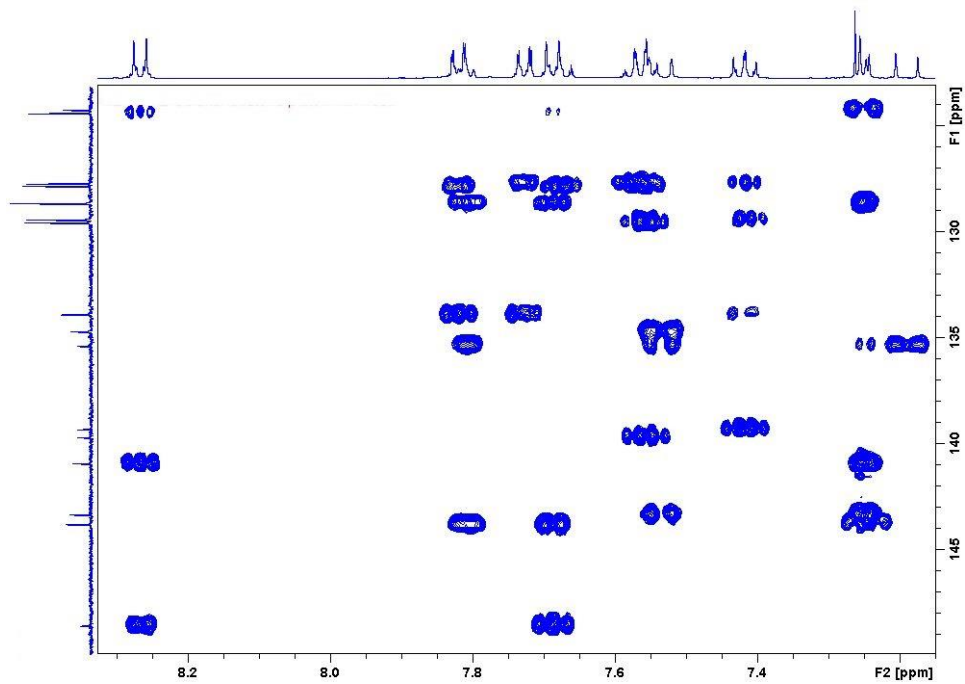


Figure A148. Zoomed in HMBC spectrum of (1*E*,3*E*,5*E*)-1,3-bis-phenylsulfonyl-(6-*p*-nitrophenyl)-hexa-1,3,5-triene, **109**

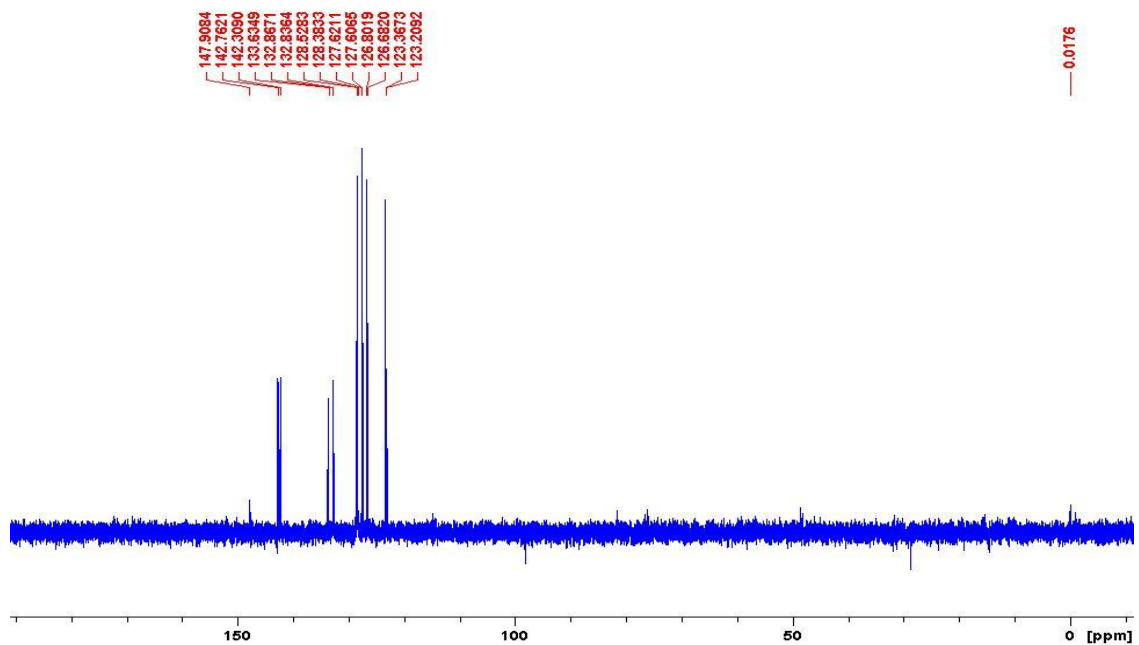


Figure A149. DEPT-135 spectrum of (1*E*,3*E*,5*E*)-1,3-bis-phenylsulfonyl-(6-*p*-nitrophenyl)-hexa-1,3,5-triene, **109**

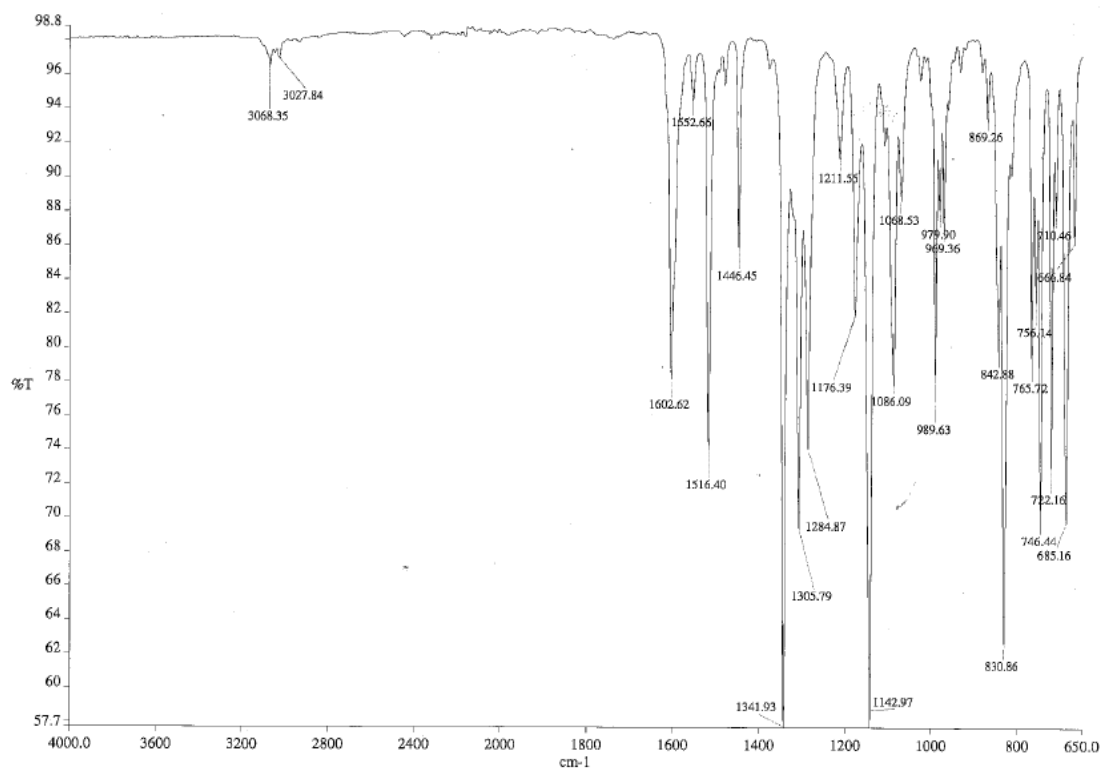


Figure A150. IR spectrum of (1*E*,3*E*,5*E*)-1,3-bis-phenylsulfonyl-(6-*p*-nitrophenyl)-hexa-1,3,5-triene, **109**

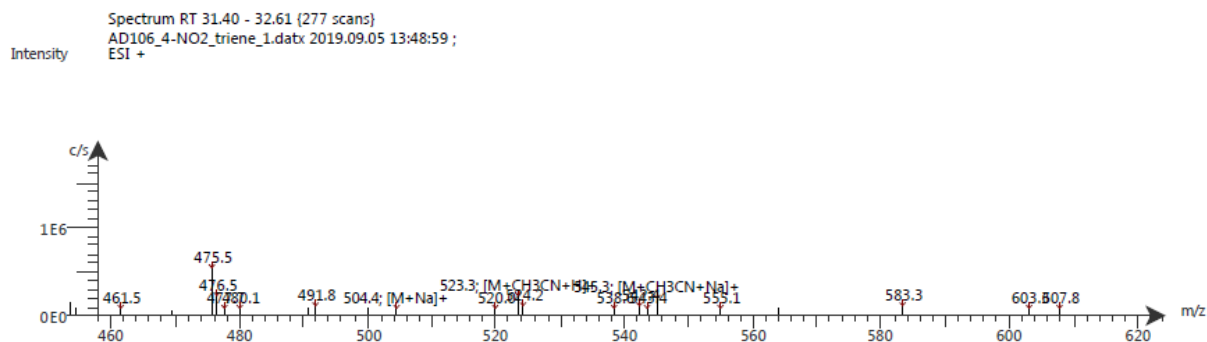
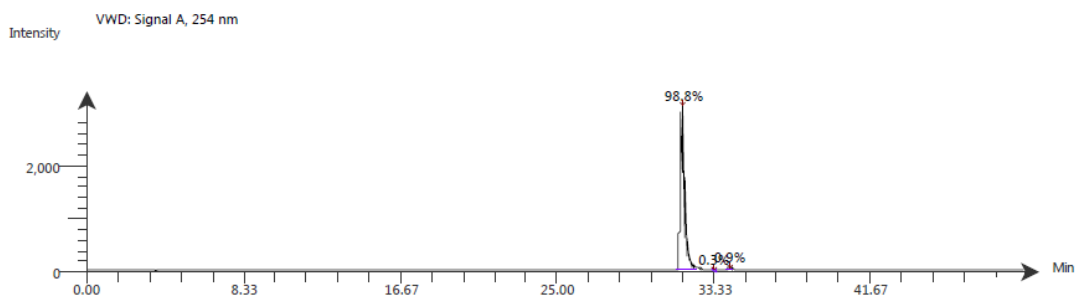


Figure A151. LC-ESI-MS spectrum of (1*E*,3*E*,5*E*)-1,3-bis-phenylsulfonyl-(6-*p*-nitrophenyl)-hexa-1,3,5-triene, **109**. The ESI spectrum shows it has m/z [M+Na]⁺ 504.4



Time (Peak Maximum M:S/Minutes)	Maximum Intensity (c/s)	Time (Peak Centroid M:S/Minutes)	Peak Area	% Peak Area	Peak Resolution Label
31.60	3.1E3	31.65	4.7E4	98.8	12.7
33.25	3.7E-1	33.31	1.5E2	0.3	11.6
34.18	3.3E1	34.16	4.1E2	0.9	12.5

Figure A152. LC-UV-MS spectrum of *(1E,3E,5E)*-1,3-bis-phenylsulfonyl-(6-*p*-nitrophenyl)-hexa-1,3,5-triene, **109**

Compound Table

Compound Label	RT	Mass	Abund	Formula	Tgt Mass	Diff (ppm)
Cpd 1: C ₂₄ H ₁₉ O ₆ N ₂ S ₂	0.146	481.0638	118910	C ₂₄ H ₁₉ O ₆ N ₂ S ₂	481.0654	-3.26

Figure A153. HR-MS analysis of *(1E,3E,5E)*-1,3-bis-phenylsulfonyl-(6-*p*-nitrophenyl)-hexa-1,3,5-triene, **109**

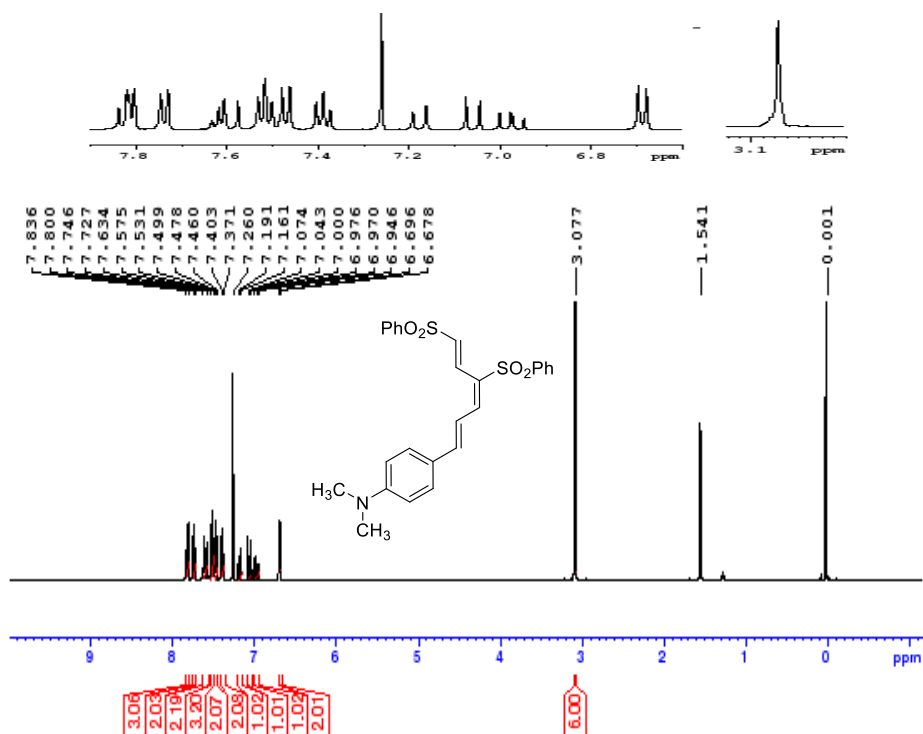


Figure 154. ¹H NMR spectrum of *(1E,3E,5E)*-1,3-bis-phenylsulfonyl-(6-*p*-dimethylaminophenyl)-hexa-1,3,5-triene, **110**

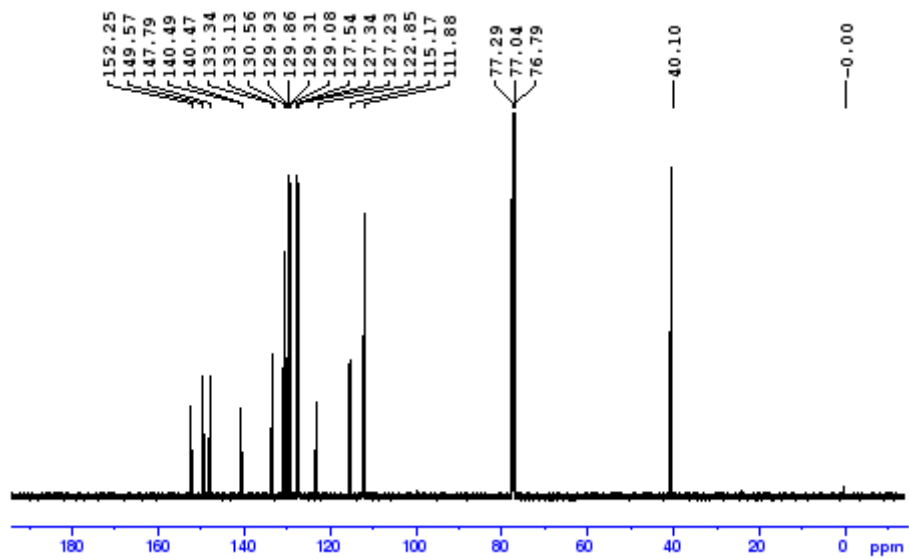


Figure A155. ^{13}C NMR spectrum of (1*E*,3*E*,5*E*)-1,3-bis-phenylsulfonyl-(6-*p*-dimethylaminophenyl)-hexa-1,3,5-triene, **110**

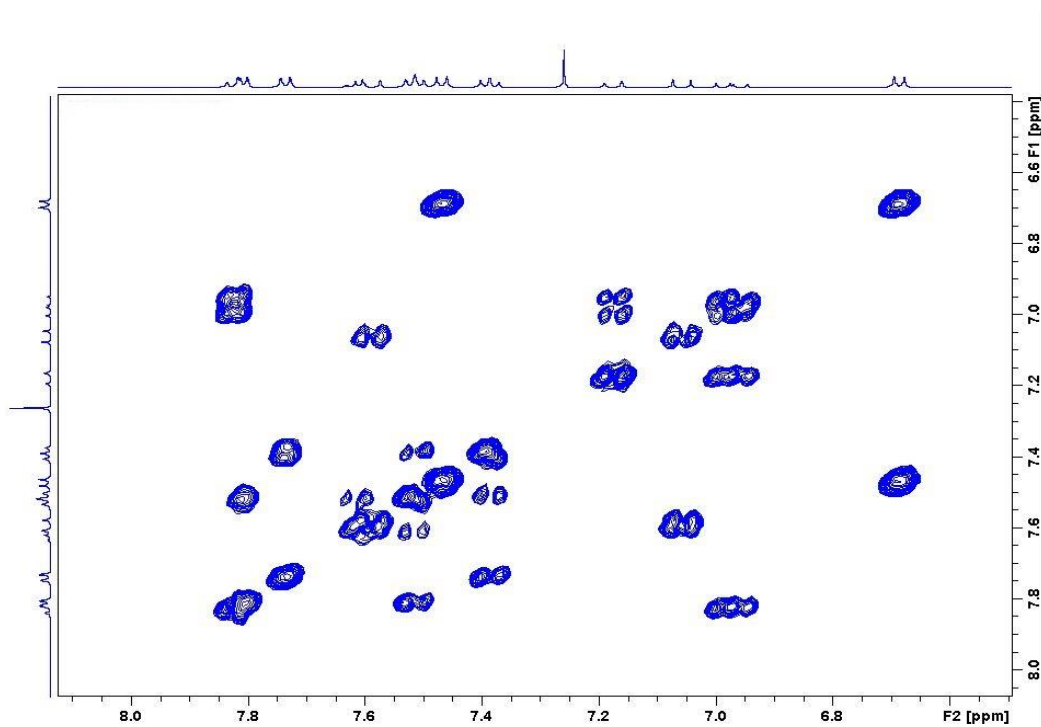


Figure A156. COSY spectrum of (1*E*,3*E*,5*E*)-1,3-bis-phenylsulfonyl-(6-*p*-dimethylaminophenyl)-hexa-1,3,5-triene, **110**

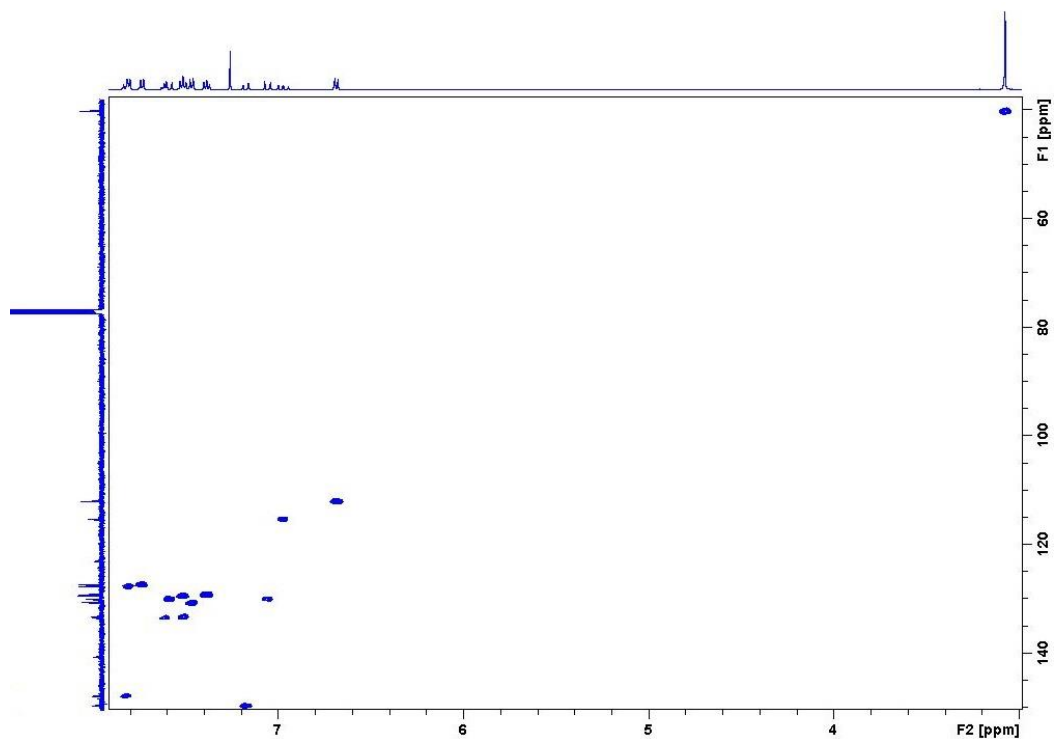


Figure A157. HSQC spectrum of *(1E,3E,5E)*-1,3-bis-phenylsulfonyl-(6-*p*-dimethylaminophenyl)-hexa-1,3,5-triene, **110**

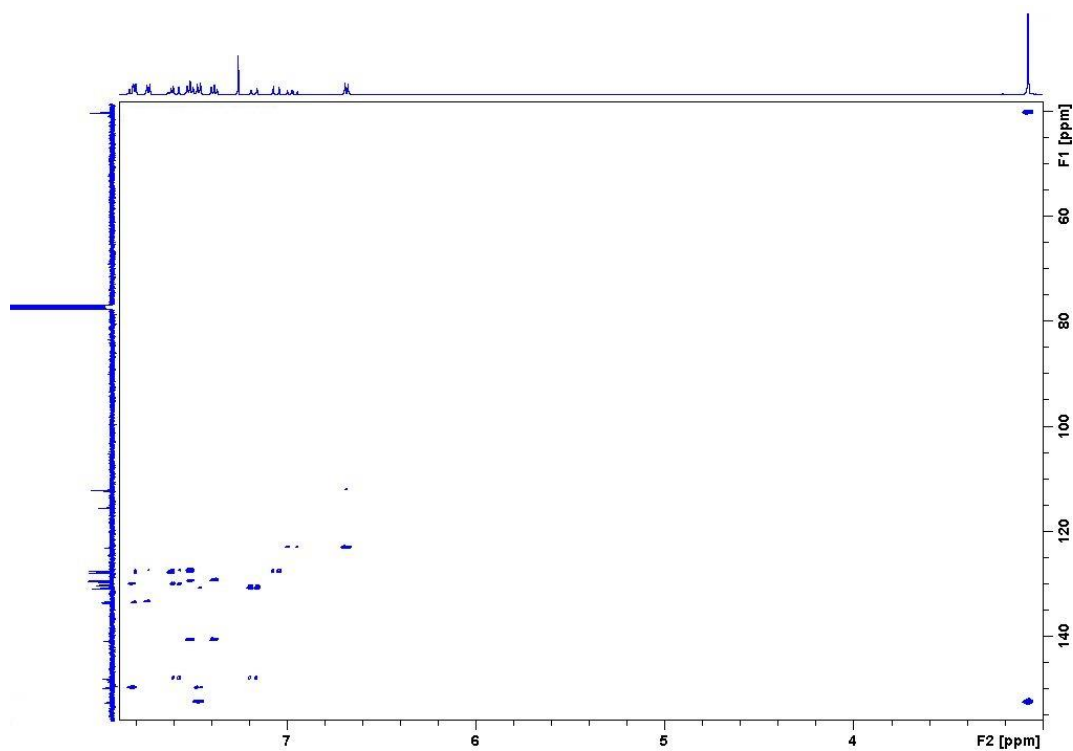


Figure A158. HMBC spectrum of *(1E,3E,5E)*-1,3-bis-phenylsulfonyl-(6-*p*-dimethylaminophenyl)-hexa-1,3,5-triene, **110**

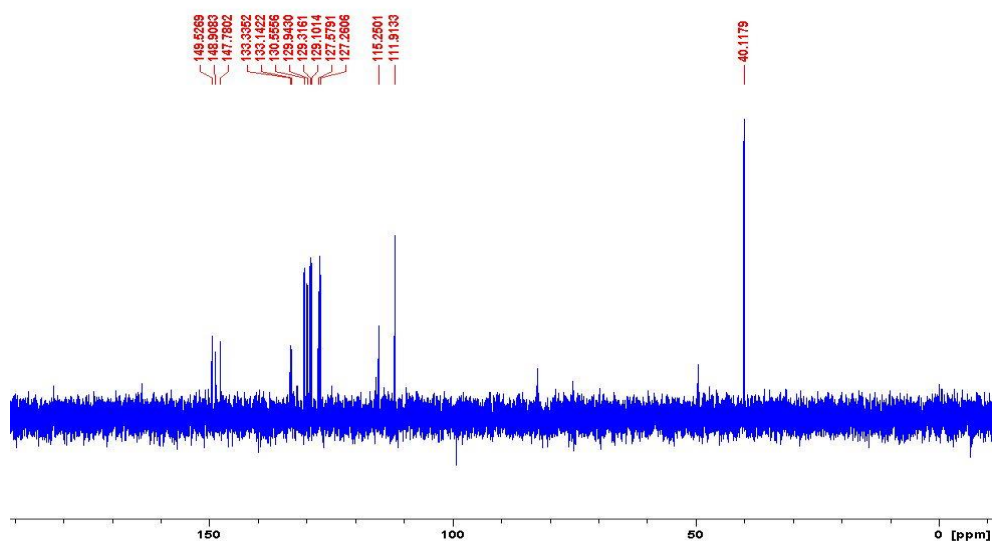


Figure A159. DEPT-135 spectrum of (1*E*,3*E*,5*E*)-1,3-bis-phenylsulfonyl-(6-*p*-dimethylaminophenyl)-hexa-1,3,5-triene, **110**

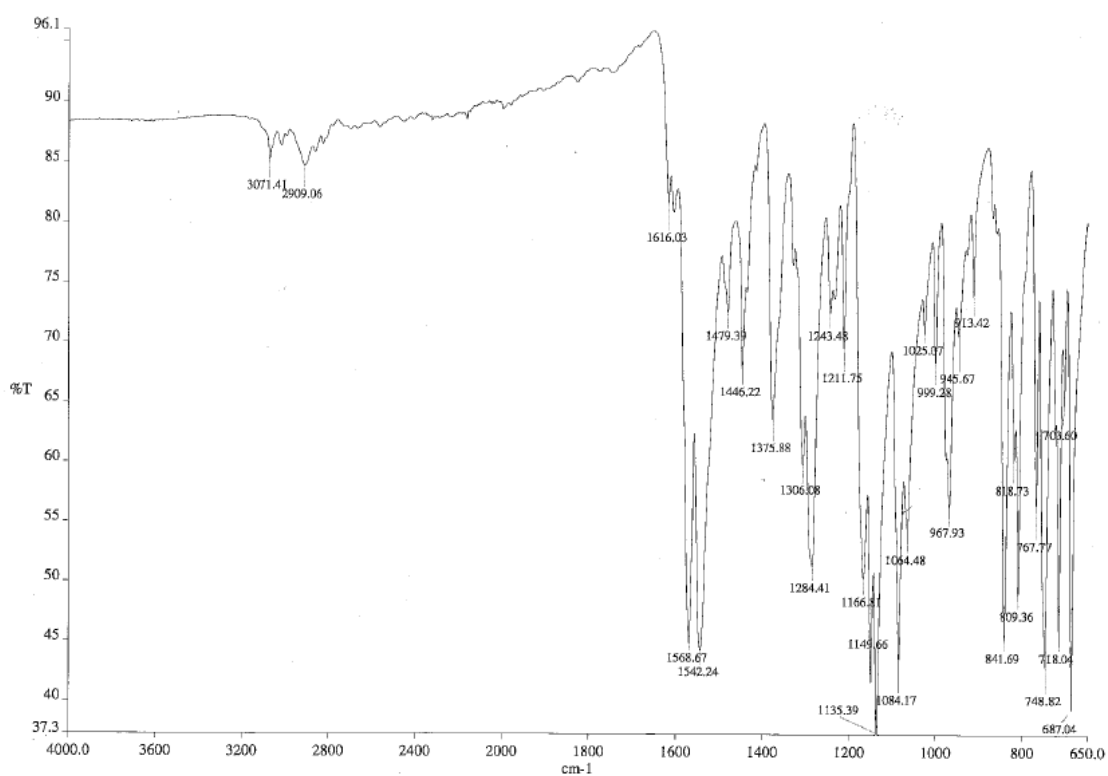


Figure A160. IR spectrum of (1*E*,3*E*,5*E*)-1,3-bis-phenylsulfonyl-(6-*p*-dimethylaminophenyl)-hexa-1,3,5-triene, **110**

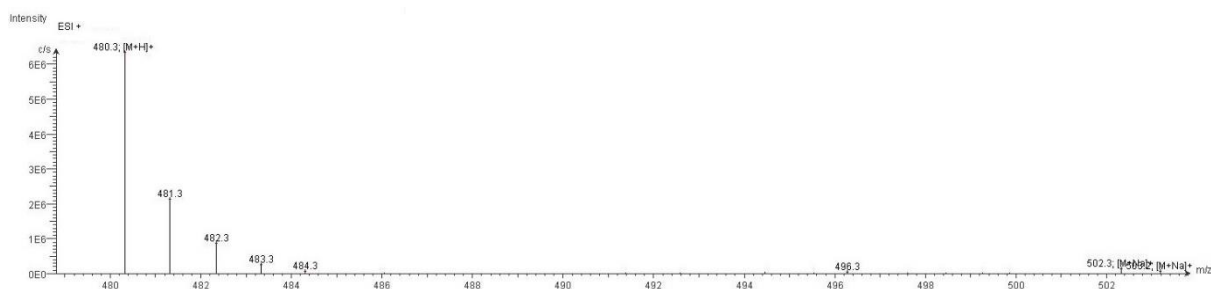
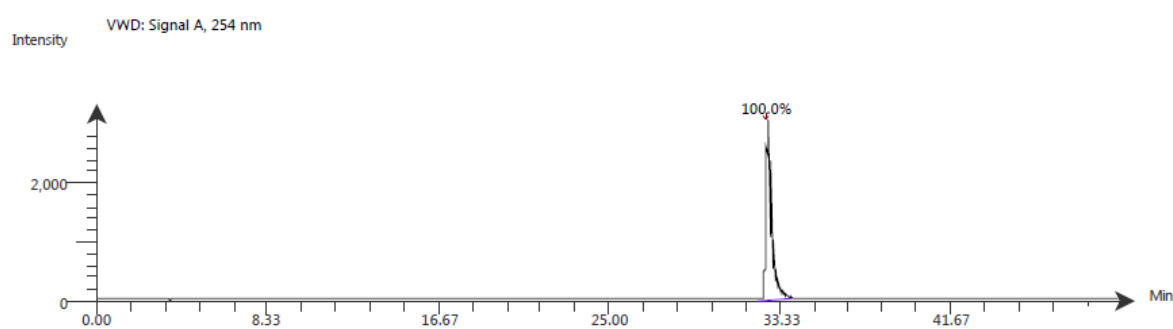


Figure A161. LC-ESI-MS spectrum of (1*E*,3*E*,5*E*)-1,3-bis-phenylsulfonyl-(6-*p*-dimethylaminophenyl)-hexa-1,3,5-triene, **110**. The ESI spectrum shows it has m/z $[M+H]^+$ 480.3



Time (Peak Maximum M:S/Minutes)	Maximum Intensity (c/s)	Time (Peak Centroid M:S/Minutes)	Peak Area	% Peak Area	Peak Resolution Label
32.71	3.1E3	32.72	5.6E4	100.0	14.3

Figure A162. LC-UV-MS spectrum of (1*E*,3*E*,5*E*)-1,3-bis-phenylsulfonyl-(6-*p*-dimethylaminophenyl)-hexa-1,3,5-triene, **110**

Compound Table

Compound Label	RT (min)	Observed mass (m/z)	Neutral observed mass (Da)	Theoretical mass (Da)	Mass error (ppm)	Isotope match score (%)
Cpd 1: C ₂₆ H ₂₅ N O ₄ S ₂	0.81	480.1296	479.1224	479.1225	-0.22	96.71

Mass errors of between -5.00 and 5.00 ppm with isotope match scores above 60% are considered confirmation of molecular formulae

Figure A163. HR-MS analysis of (1*E*,3*E*,5*E*)-1,3-bis-phenylsulfonyl-(6-*p*-dimethylaminophenyl)-hexa-1,3,5-triene, **110**

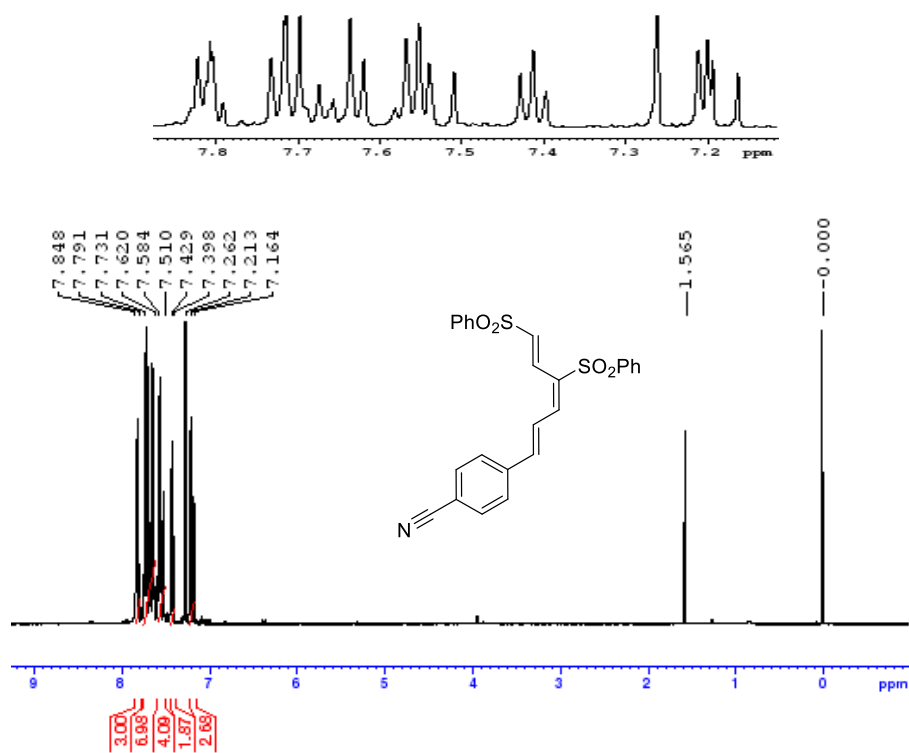


Figure A164. ¹H NMR spectrum of (1E,3E,5E)-1,3-bis-phenylsulfonyl-(6-p-cyanophenyl)-hexa-1,3,5-triene, **111**

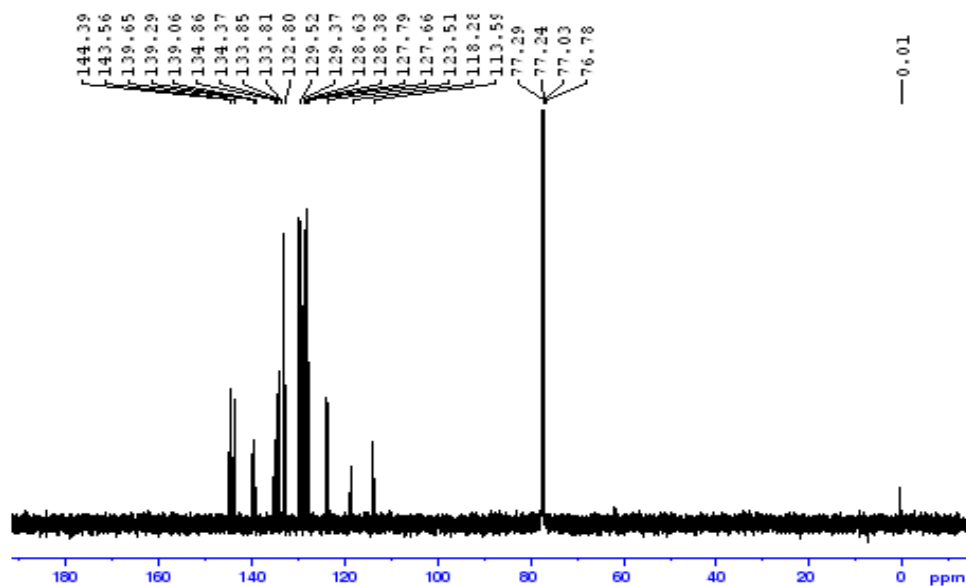


Figure A165. ¹³C NMR spectrum of (1E,3E,5E)-1,3-bis-phenylsulfonyl-(6-p-cyanophenyl)-hexa-1,3,5-triene, **111**

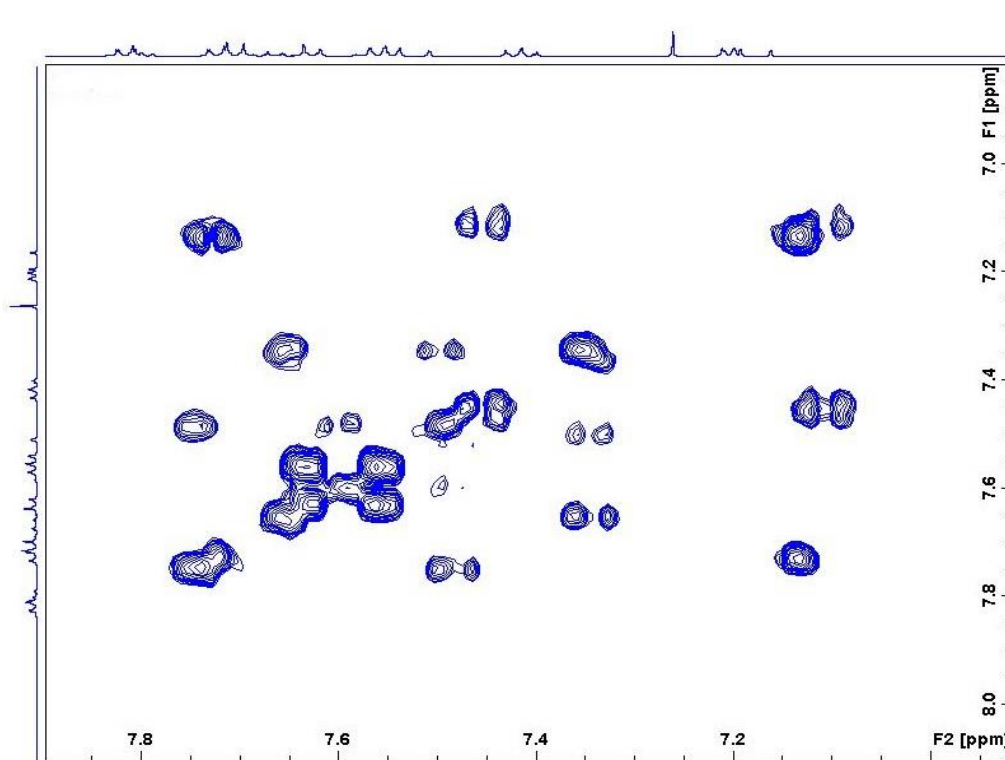


Figure A166. COSY spectrum of (1*E*,3*E*,5*E*)-1,3-bis-phenylsulfonyl-(6-*p*-cyanophenyl)-hexa-1,3,5-triene,
111

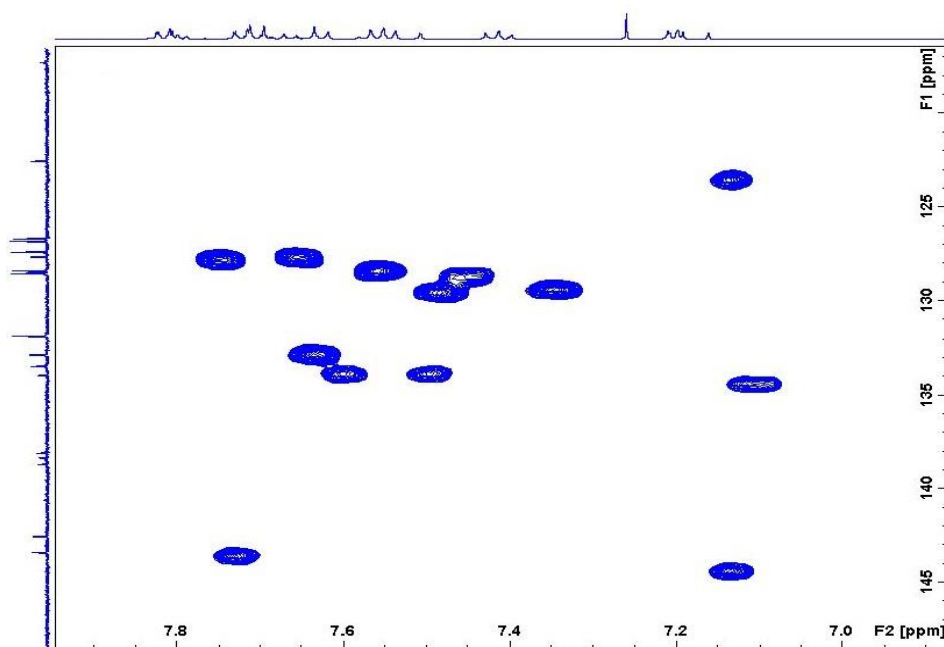


Figure A167. HSQC spectrum of (1*E*,3*E*,5*E*)-1,3-bis-phenylsulfonyl-(6-*p*-cyanophenyl)-hexa-1,3,5-triene,
111

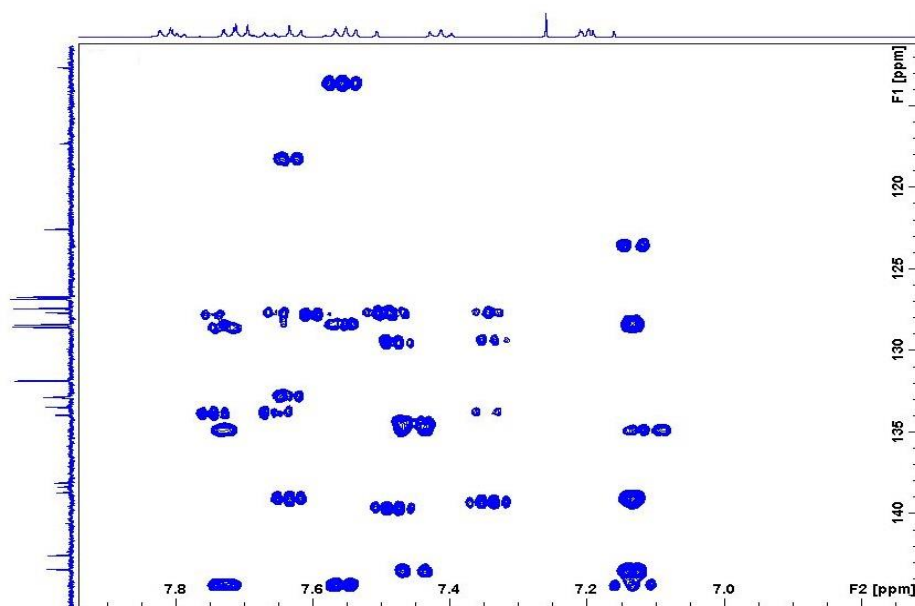


Figure A168. HMBC spectrum of (1*E*,3*E*,5*E*)-1,3-bis-phenylsulfonyl-(6-*p*-cyanophenyl)-hexa-1,3,5-triene, **111**

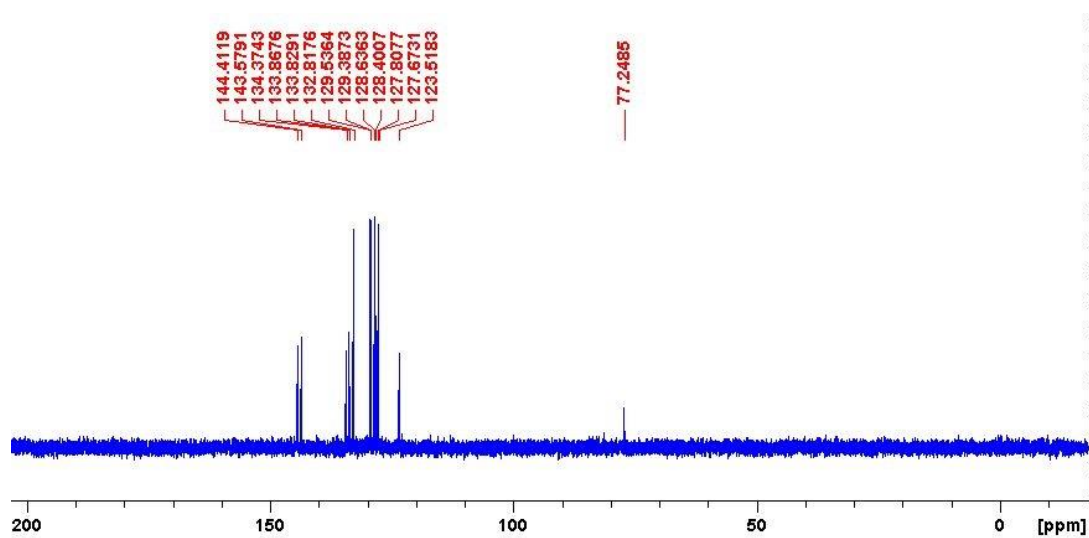


Figure A169. DEPT-135 spectrum of (1*E*,3*E*,5*E*)-1,3-bis-phenylsulfonyl-(6-*p*-cyanophenyl)-hexa-1,3,5-triene, **111**

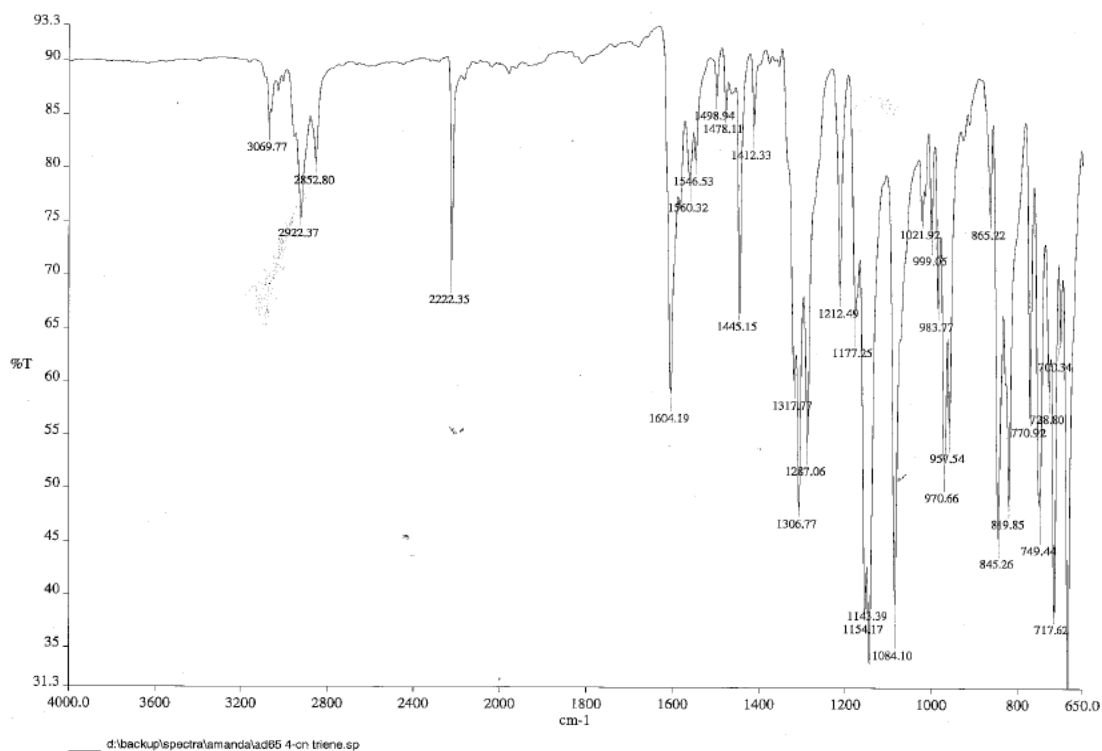


Figure A170. IR spectrum of (1*E*,3*E*,5*E*)-1,3-bis-phenylsulfonyl-(6-*p*-cyano)-hexa-1,3,5-triene, **111**

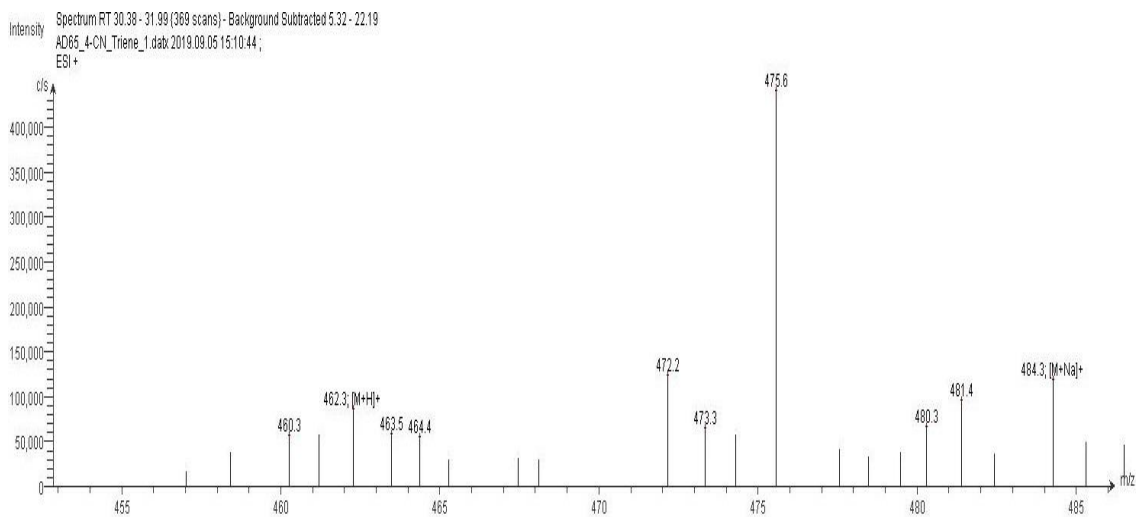
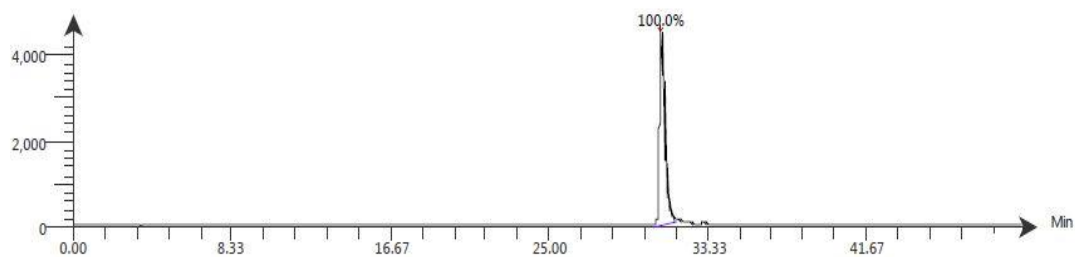


Figure A171. LC-ESI-MS spectrum of (1*E*,3*E*,5*E*)-1,3-bis-phenylsulfonyl-(6-*p*-cyano)-hexa-1,3,5-triene, **111**. The ESI spectrum shows it has m/z [M+Na]⁺ 484.3

VWD: Signal A, 254 nm
 Intensity AD65_4-CN_Triene_1.datx 2019.09.05 15:10:44 ;



Time (Peak Maximum M:S/Minutes)	Maximum Intensity (c/s)	Time (Peak Centroid M:S/Minutes)	Peak Area	% Peak Area	Peak Resolution Label
30.86	4.5E3	30.88	9.1E4	100.0	17.7

Figure A172. LC-UV-MS spectrum of (1*E*,3*E*,5*E*)-1,3-bis-phenylsulfonyl-(6-*p*-cyano)-hexa-1,3,5-triene, **111**

Compound Table

Compound Label	RT (min)	Observed mass (m/z)	Neutral observed mass (Da)	Theoretical mass (Da)	Mass error (ppm)	Isotope match score (%)
Cpd 1: C25 H19 N O4 S2	0.78	462.0819	461.0749	461.0755	-1.36	93.67

Figure A173. HR-MS analysis of (1*E*,3*E*,5*E*)-1,3-bis-phenylsulfonyl-(6-*p*-cyano)-hexa-1,3,5-triene, **111**

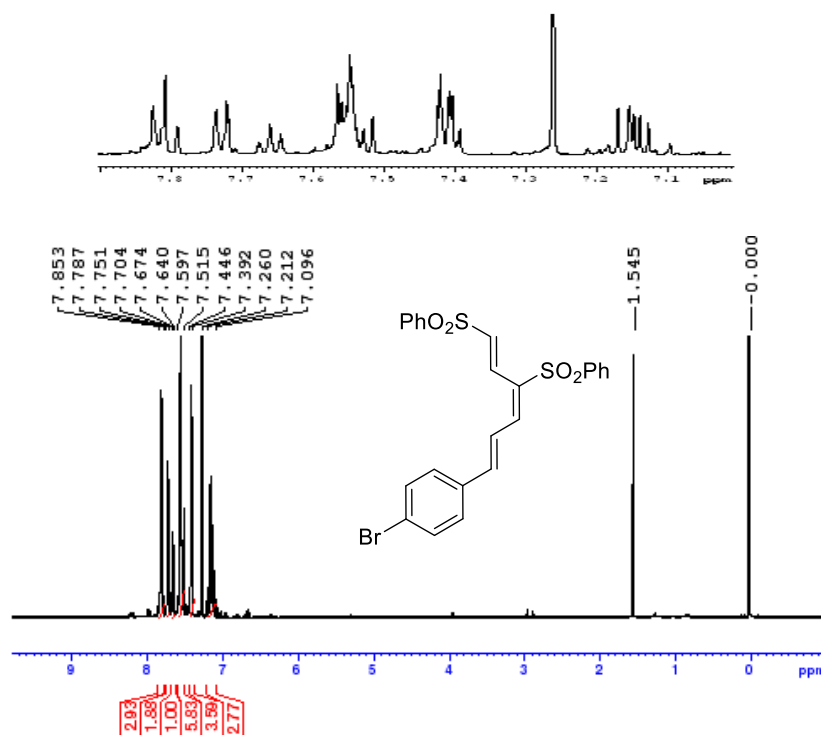


Figure A174. ¹H NMR spectrum of (1*E*,3*E*,5*E*)-1,3-bis-phenylsulfonyl-(6-*p*-bromophenyl)-hexa-1,3,5-triene, **112**

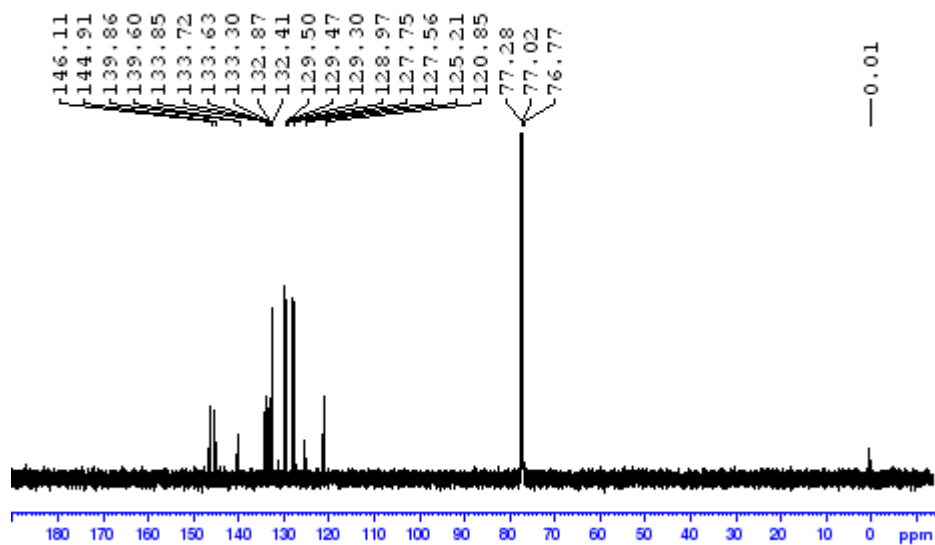


Figure A175. ^{13}C NMR spectrum of (1*E*,3*E*,5*E*)-1,3-bis-phenylsulfonyl-(6-*p*-bromophenyl)-hexa-1,3,5-triene, **112**

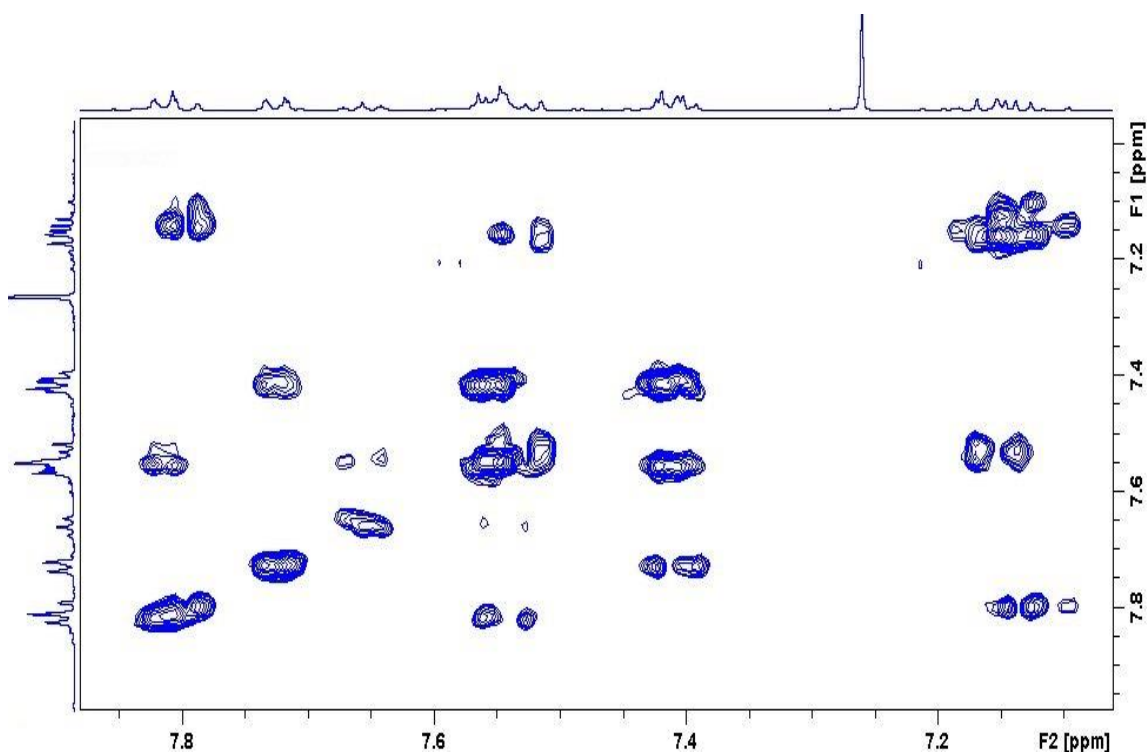


Figure A176. Zoomed in COSY spectrum of (1*E*,3*E*,5*E*)-1,3-bis-phenylsulfonyl-(6-*p*-bromophenyl)-hexa-1,3,5-triene, **112**

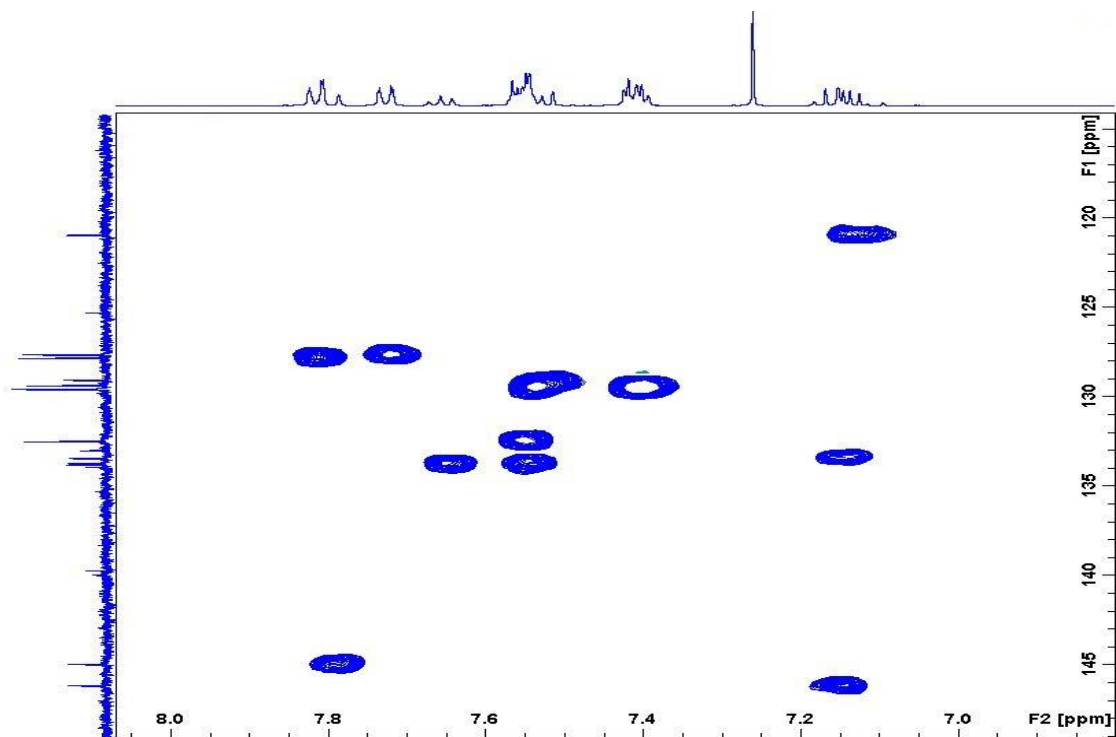


Figure A177. HSQC spectrum of (1*E*,3*E*,5*E*)-1,3-bis-phenylsulfonyl-(6-*p*-bromophenyl)-hexa-1,3,5-triene, **112**

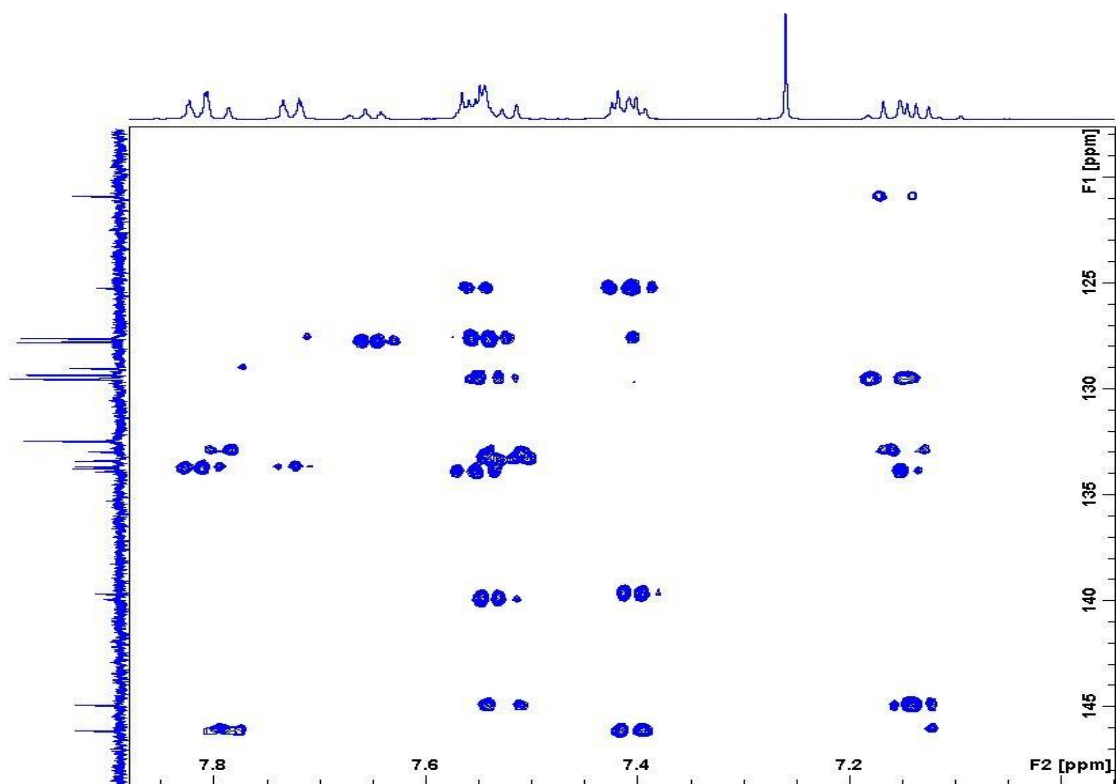


Figure A178. HMBC spectrum of (1*E*,3*E*,5*E*)-1,3-bis-phenylsulfonyl-(6-*p*-bromophenyl)-hexa-1,3,5-triene, **112**

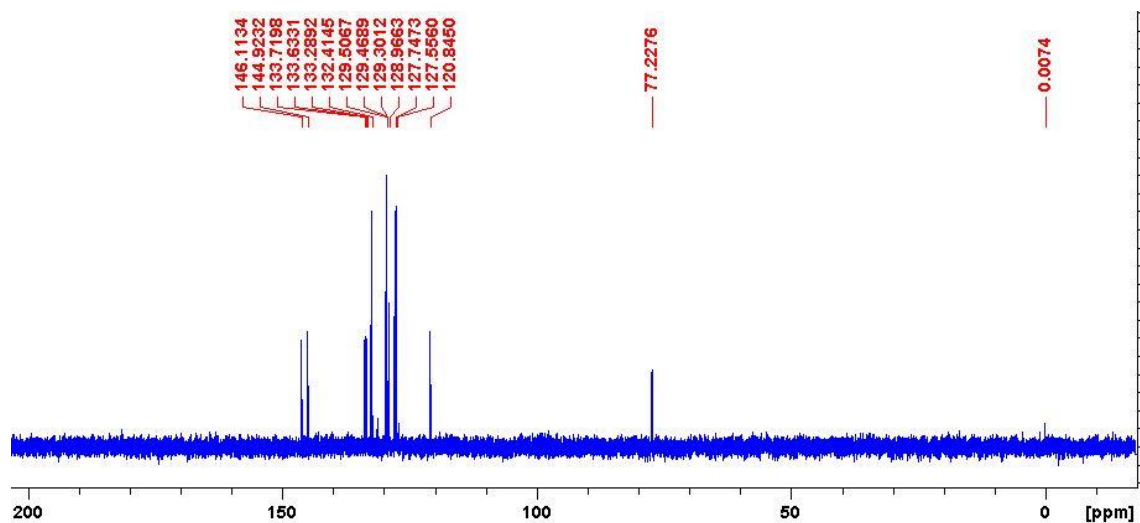


Figure A179. DEPT-135 spectrum of (1*E*,3*E*,5*E*)-1,3-bis-phenylsulfonyl-(6-*p*-bromophenyl)-hexa-1,3,5-triene, **112**

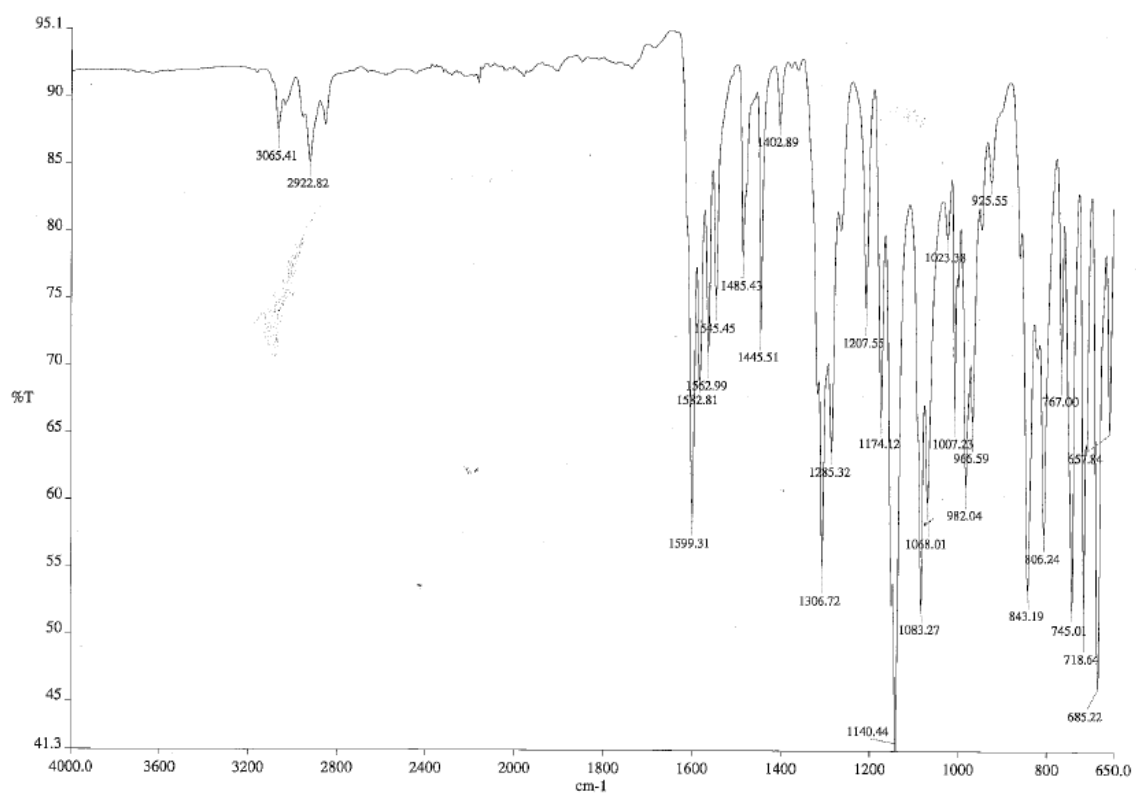


Figure A180. IR spectrum of (1*E*,3*E*,5*E*)-1,3-bis-phenylsulfonyl-(6-*p*-bromo)-hexa-1,3,5-triene, **112**

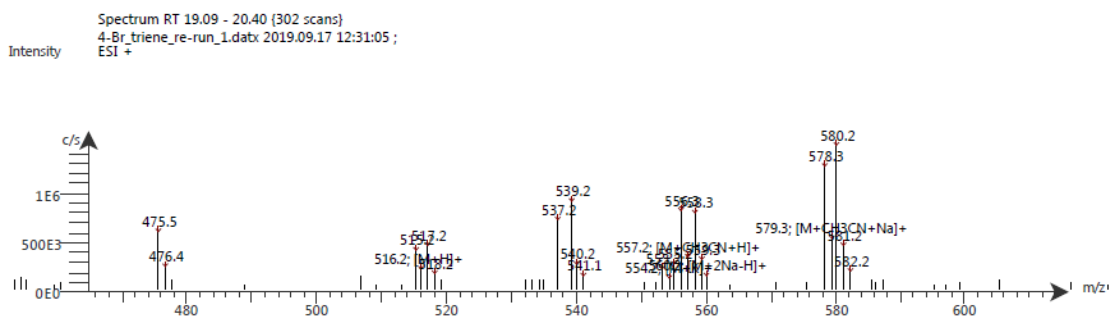


Figure A181. LC-ESI-MS spectrum of (1*E*,3*E*,5*E*)-1,3-bis-phenylsulfonyl-(6-*p*-bromophenyl)-hexa-1,3,5-triene, **112**. The ESI spectrum shows it has m/z $[M+H]^+$ 516.2

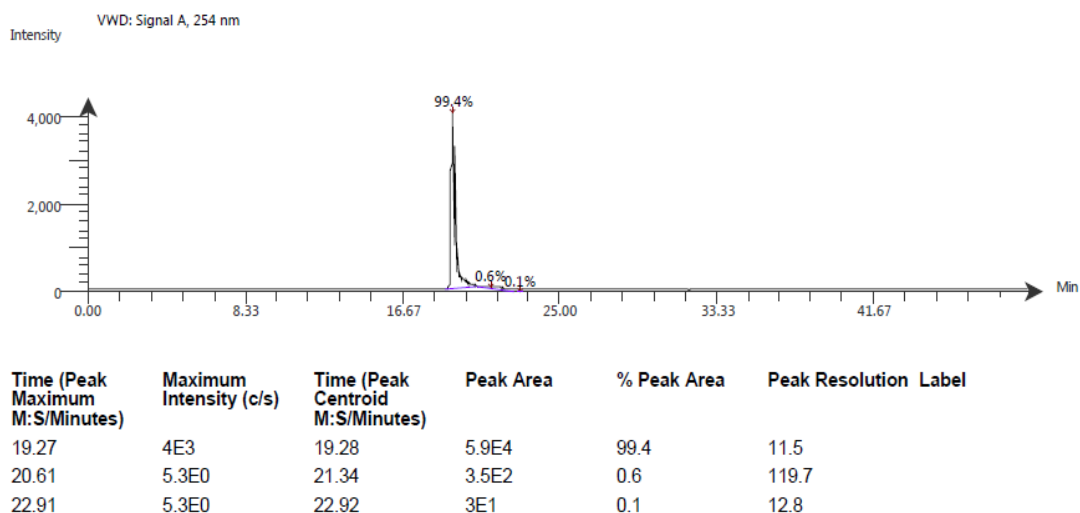


Figure A182. LC-UV-MS spectrum of (1*E*,3*E*,5*E*)-1,3-bis-phenylsulfonyl-(6-*p*-bromophenyl)-hexa-1,3,5-triene, **112**

Expected formula	Ionization mode		Bath admin: date processed and data	Manually reprocessed, detected?
	X	NEG		
C24H19S2O4Br	POS	NEG	30-May-18	Yes, -1.5 ppm mass error for reprocessed. See spectra with simulation

Figure A183. HR-MS analysis of (1*E*,3*E*,5*E*)-1,3-bis-phenylsulfonyl-(6-*p*-bromo)-hexa-1,3,5-triene, **112**

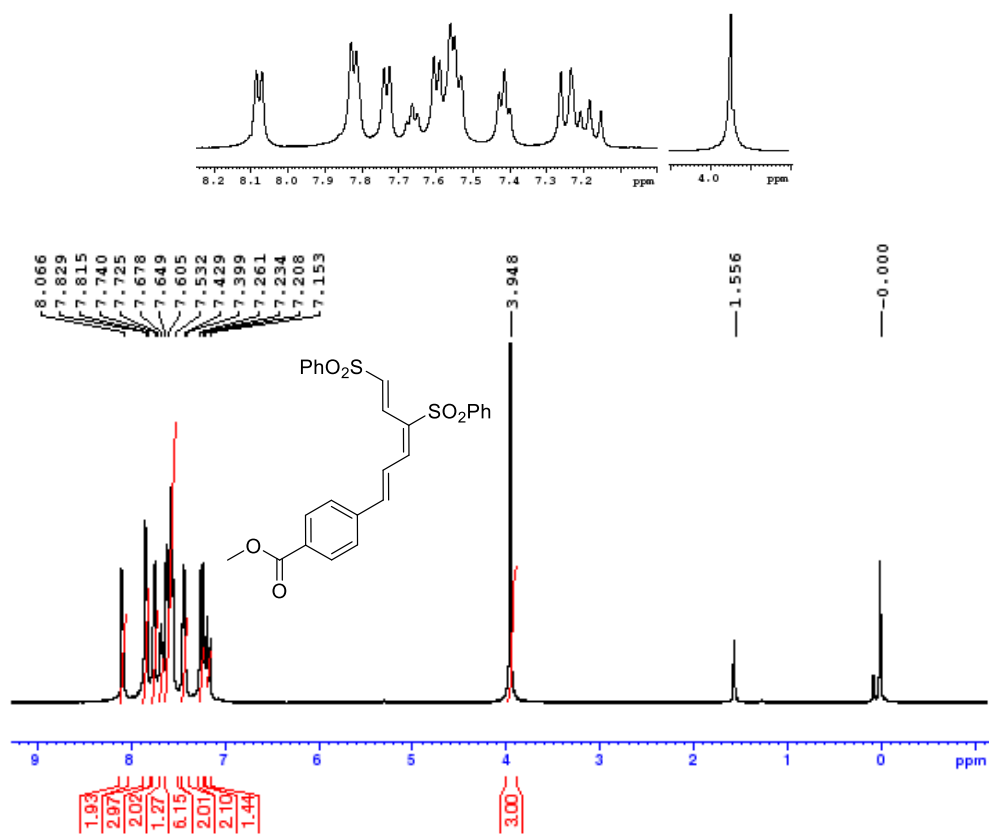


Figure A184. ¹H NMR spectrum of (1E,3E,5E)-1,3-bis-phenylsulfonyl-6-(p-methyl benzoate)-hexa-1,3,5-triene, **113**

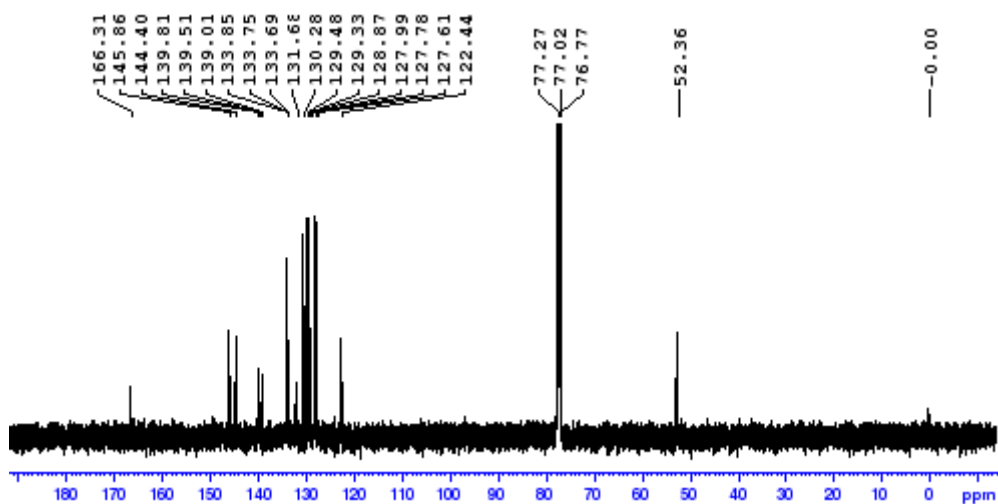


Figure A185. ¹³C NMR spectrum of (1E,3E,5E)-1,3-bis-phenylsulfonyl-6-(p-methyl benzoate)-hexa-1,3,5-triene, **113**

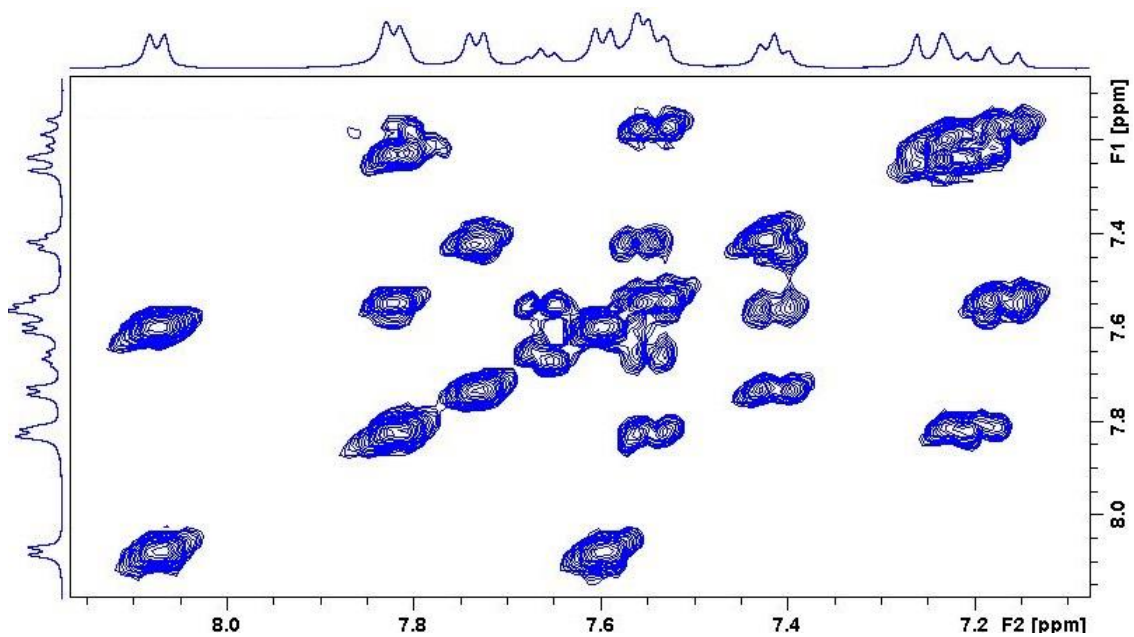


Figure A186. Zoomed in COSY spectrum of (1*E*,3*E*,5*E*)-1,3-bis-phenylsulfonyl-6-(*p*-methyl benzoate)-hexa-1,3,5-triene, **113**

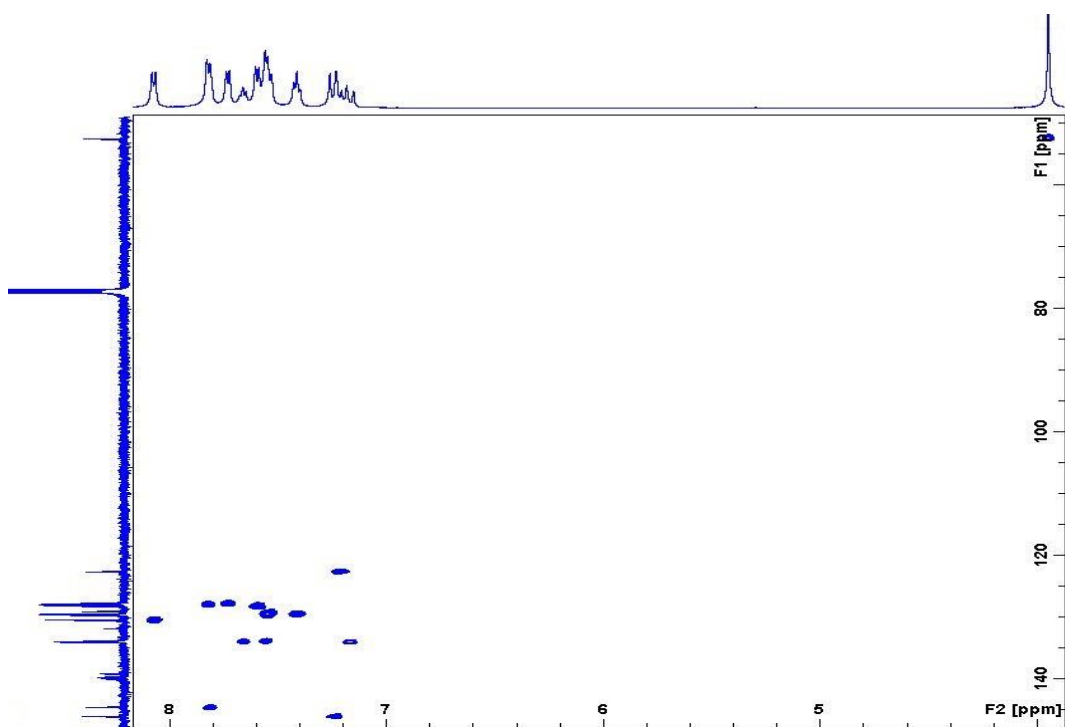


Figure A187. HSQC spectrum of (1*E*,3*E*,5*E*)-1,3-bis-phenylsulfonyl-6-(*p*-methyl benzoate)-hexa-1,3,5-triene, **113**

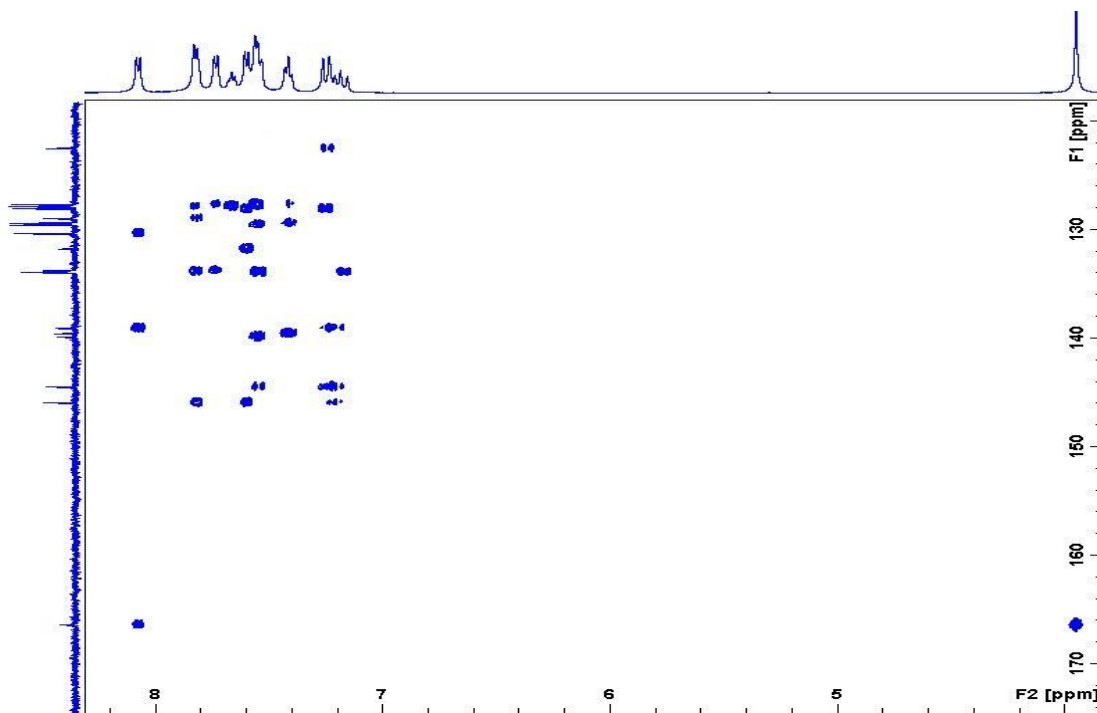


Figure A188. HMBC spectrum of (1*E*,3*E*,5*E*)-1,3-bis-phenylsulfonyl-6-(*p*-methyl benzoate)-hexa-1,3,5-triene, **113**

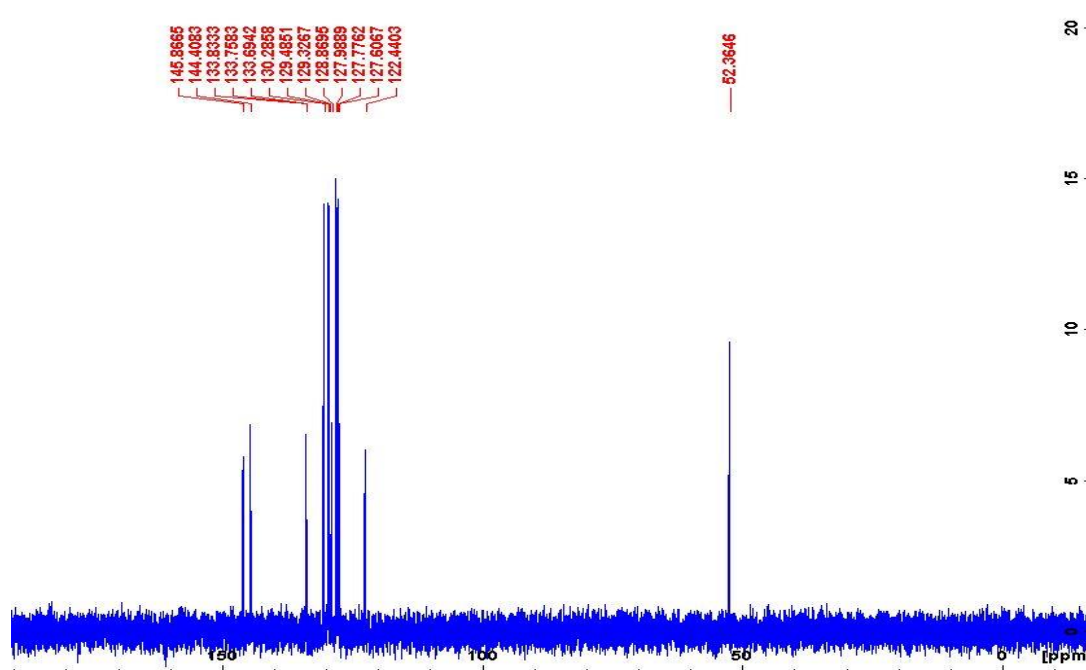


Figure A189. DEPT-135 spectrum of (1*E*,3*E*,5*E*)-1,3-bis-phenylsulfonyl-6-(*p*-methyl benzoate)-hexa-1,3,5-triene, **113**

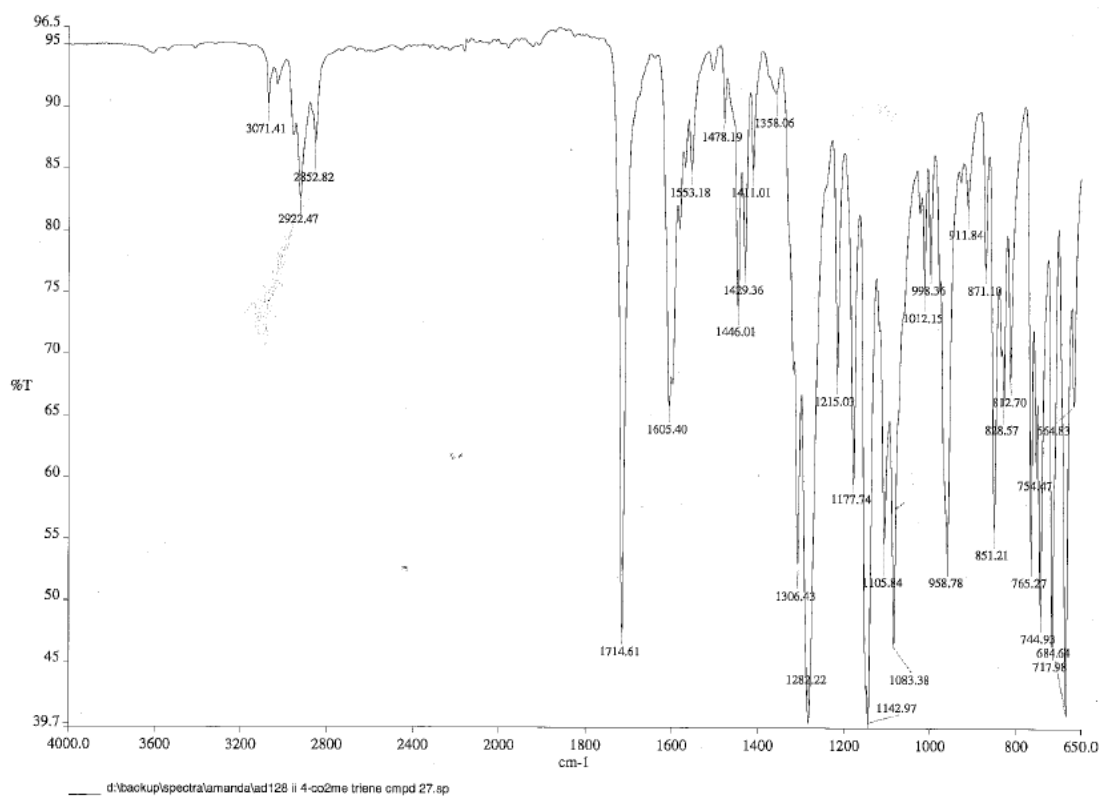


Figure A190. IR spectrum of (1*E*,3*E*,5*E*)-1,3-bis-phenylsulfonyl-(*p*-methyl benzoate)-hexa-1,3,5-triene, **113**

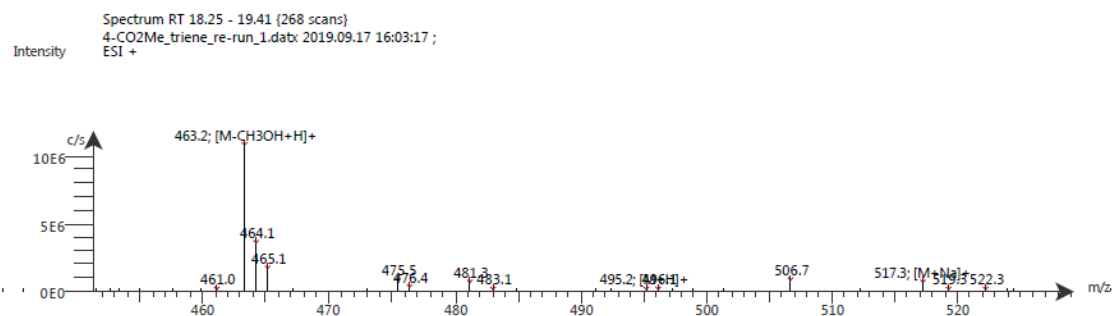
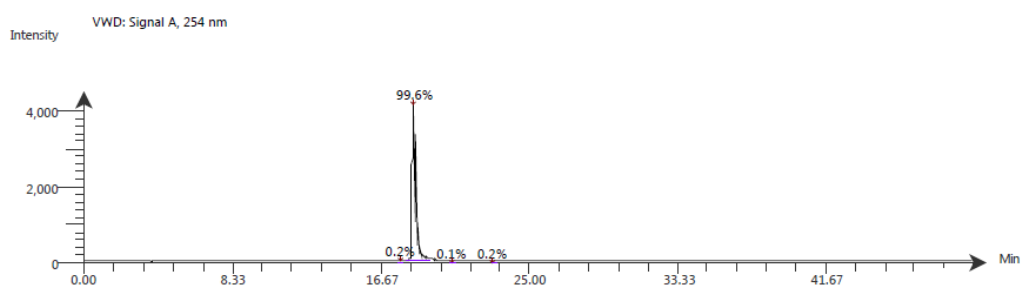


Figure A191. LC-ESI-MS spectrum of (1*E*,3*E*,5*E*)-1,3-bis-phenylsulfonyl-(*p*-methyl benzoate)-hexa-1,3,5-triene, **113**. The ESI spectrum shows it has m/z [M+Na]⁺ 517.3



Time (Peak Maximum M:S/Minutes)	Maximum Intensity (c/s)	Time (Peak Centroid M:S/Minutes)	Peak Area	% Peak Area	Peak Resolution Label
17.74	1.2E1	17.76	8.9E1	0.2	10.0
18.43	4.1E3	18.44	5.5E4	99.6	11.2
20.50	2.2E0	20.60	4.5E1	0.1	20.1
22.90	6.7E0	22.95	9.6E1	0.2	17.8

Figure A192. LC-UV-MS spectrum of (1*E*,3*E*,5*E*)-1,3-bis-phenylsulfonyl-(*p*-methyl benzoate)-hexa-1,3,5-triene, **113**

#	meas. m/z	theo. m/z	Err[ppm]	Sigma	Formula
1	517.0738	517.0750	-2.40	0.0091	C 26 H 22 Na 1 O 6 S 2

Figure A193. HR-MS analysis of (1*E*,3*E*,5*E*)-1,3-bis-phenylsulfonyl-(*p*-methyl benzoate)-hexa-1,3,5-triene, **113**

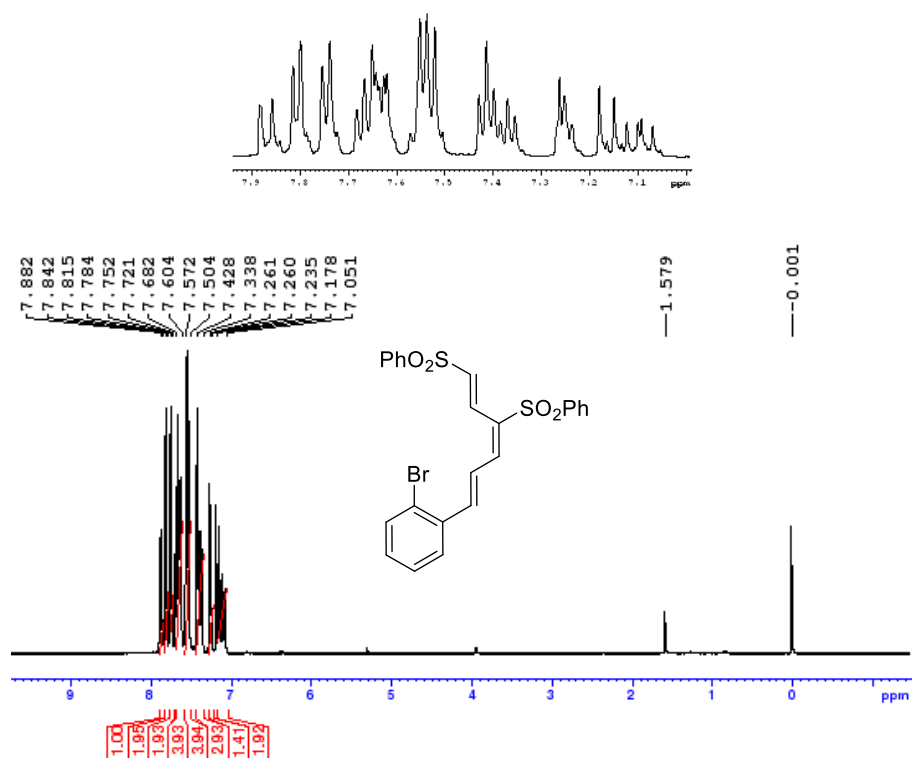


Figure A194. ¹H NMR spectrum of (1*E*,3*E*,5*E*)-1,3-bis-phenylsulfonyl-(6-*o*-bromophenyl)-hexa-1,3,5-triene, **114**

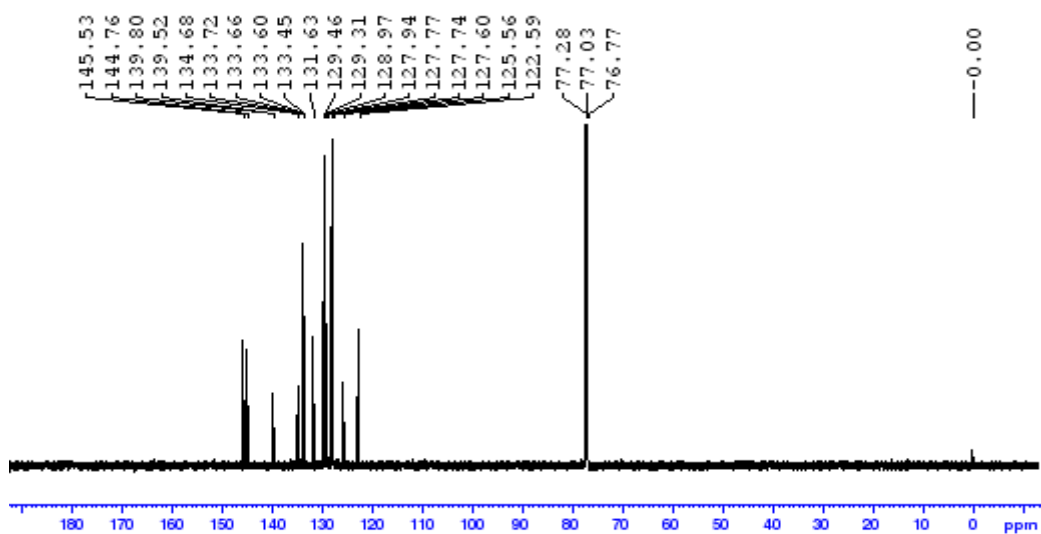


Figure A195. ^{13}C NMR spectrum of (1*E*,3*E*,5*E*)-1,3-bis-phenylsulfonyl-(6-*o*-bromophenyl)-hexa-1,3,5-triene, **114**

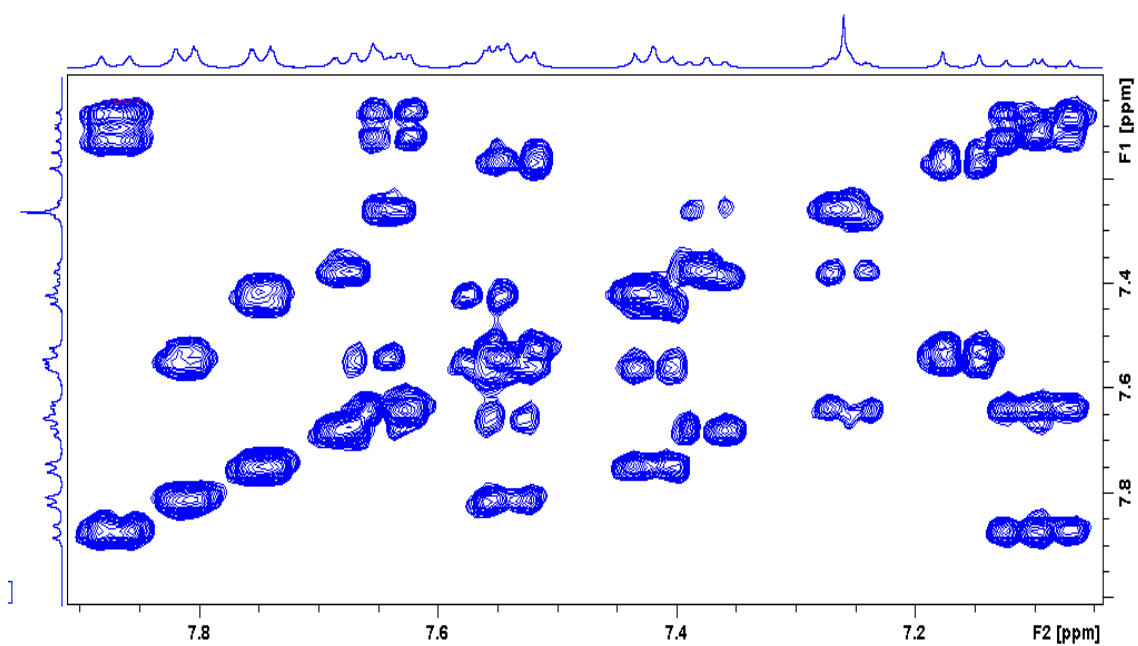


Figure A196. Zoomed in COSY spectrum of (1*E*,3*E*,5*E*)-1,3-bis-phenylsulfonyl-(6-*o*-bromophenyl)-hexa-1,3,5-triene, **114**

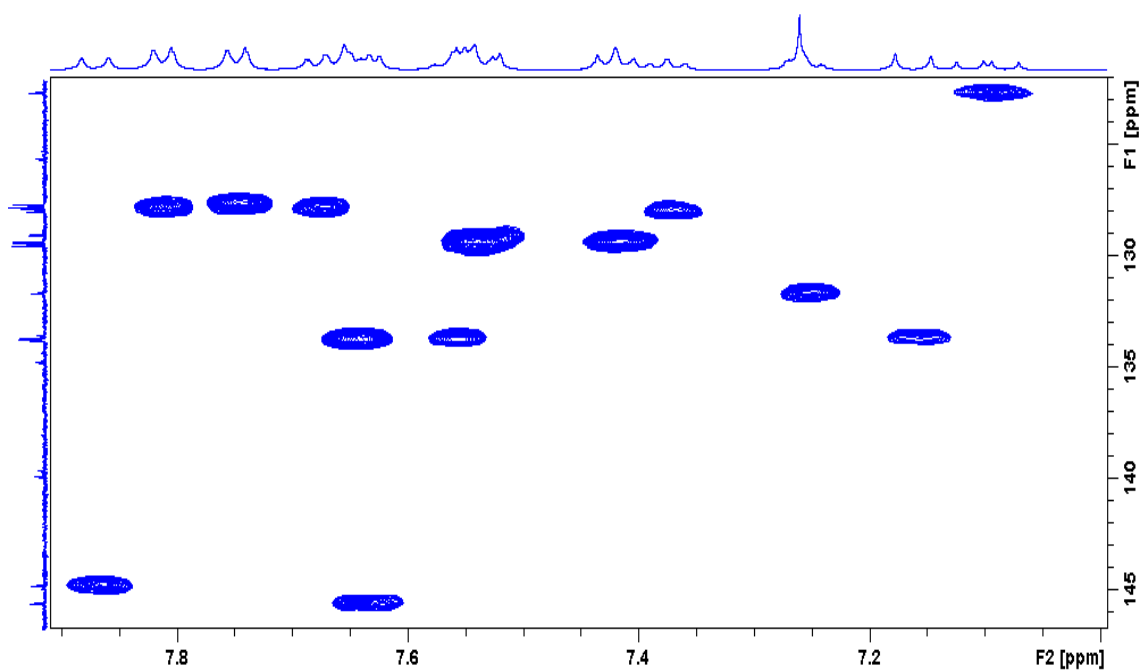


Figure A197. Zoomed in HSQC spectrum of (1*E*,3*E*,5*E*)-1,3-bis-phenylsulfonyl-(6-*o*-bromophenyl)-hexa-1,3,5-triene, **114**

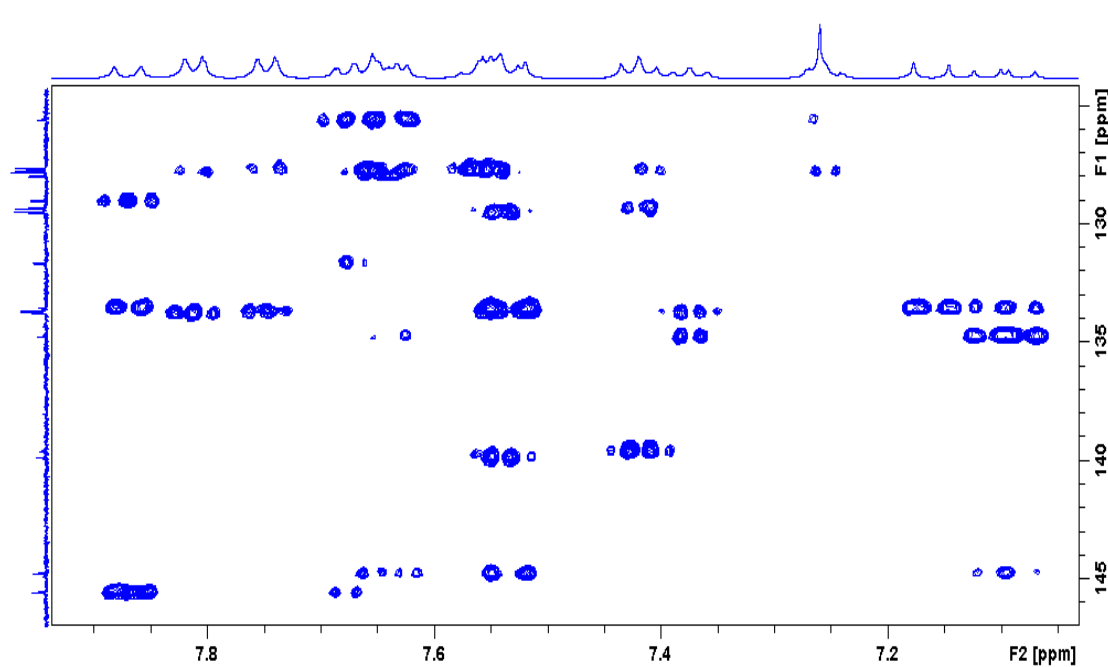


Figure A198. Zoomed in HMBC spectrum of (1*E*,3*E*,5*E*)-1,3-bis-phenylsulfonyl-(6-*o*-bromophenyl)-hexa-1,3,5-triene, **114**

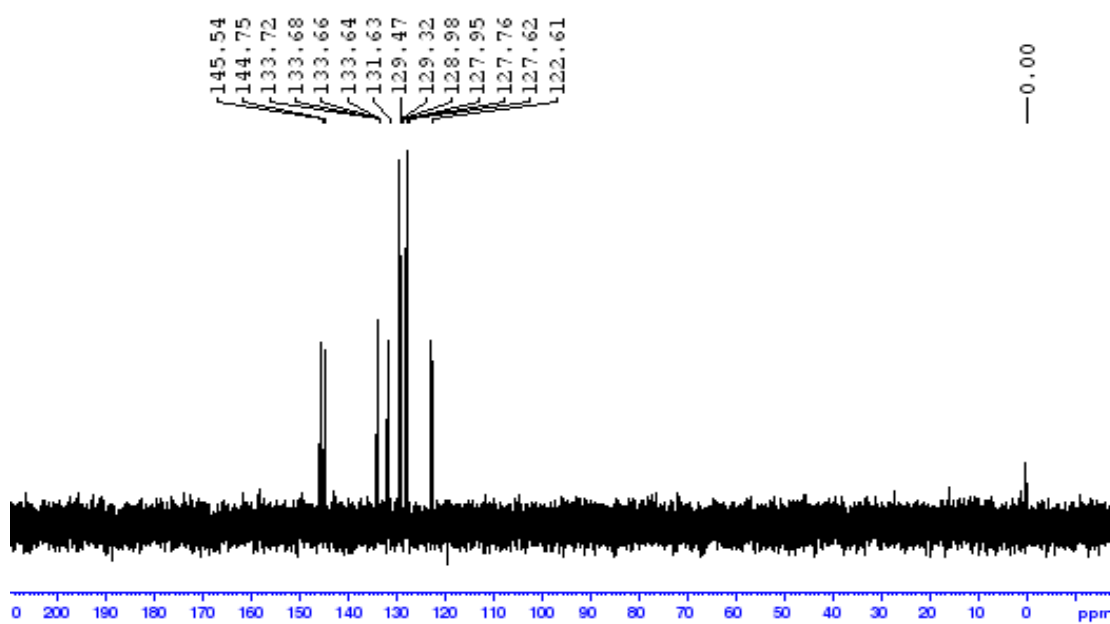


Figure A199. DEPT-135 spectrum of (1*E*,3*E*,5*E*)-1,3-bis-phenylsulfonyl-(6-*o*-bromophenyl)-hexa-1,3,5-triene, **114**

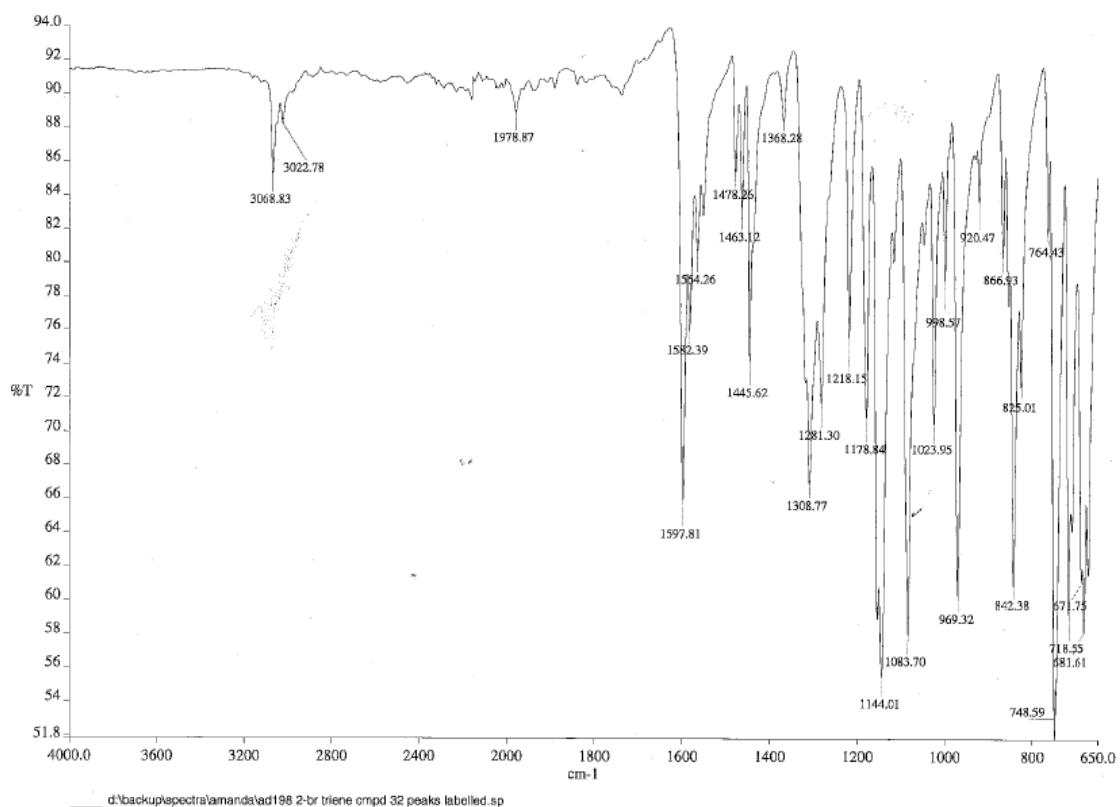


Figure A200. IR spectrum of (1*E*,3*E*,5*E*)-1,3-bis-phenylsulfonyl-(6-*o*-bromophenyl)-hexa-1,3,5-triene, **114**

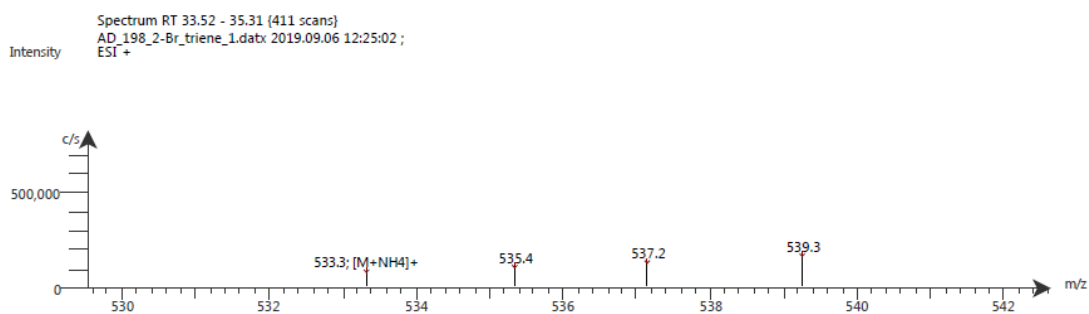
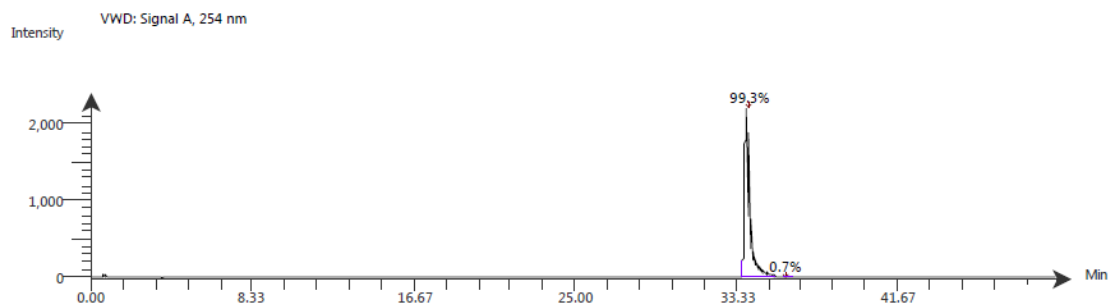


Figure A201. LC-ESI-MS spectrum of (1*E*,3*E*,5*E*)-1,3-bis-phenylsulfonyl-(6-*o*-bromophenyl)-hexa-1,3,5-triene, **114**. The ESI spectrum shows it has m/z $[M+NH_4]^+$ 533.3



Time (Peak Maximum M:S/Minutes)	Maximum Intensity (c/s)	Time (Peak Centroid M:S/Minutes)	Peak Area	% Peak Area	Peak Resolution Label
33.80	2.2E3	33.92	4.2E4	99.3	14.2
0.00	1.4E3	35.93	3.1E2	0.7	28.0

Figure A202. LC-UV-MS spectrum of (1*E*,3*E*,5*E*)-1,3-bis-phenylsulfonyl-(6-*o*-bromophenyl)-hexa-1,3,5-triene, **114**

Compound Table

Compound Label	RT (min)	Observed mass (m/z)	Neutral observed mass (Da)	Theoretical mass (Da)	Mass error (ppm)	Isotope match score (%)
Cpd 1: C ₂₄ H ₁₉ Br O ₄ S ₂	0.79	538.9780	513.9906	513.9908	-0.44	98.59

Mass errors of between -5.00 and 5.00 ppm with isotope match scores above 60% are considered confirmation of molecular formulae

Figure A203. HR-MS analysis of (1*E*,3*E*,5*E*)-1,3-bis-phenylsulfonyl-(6-*o*-bromophenyl)-hexa-1,3,5-triene, **114**

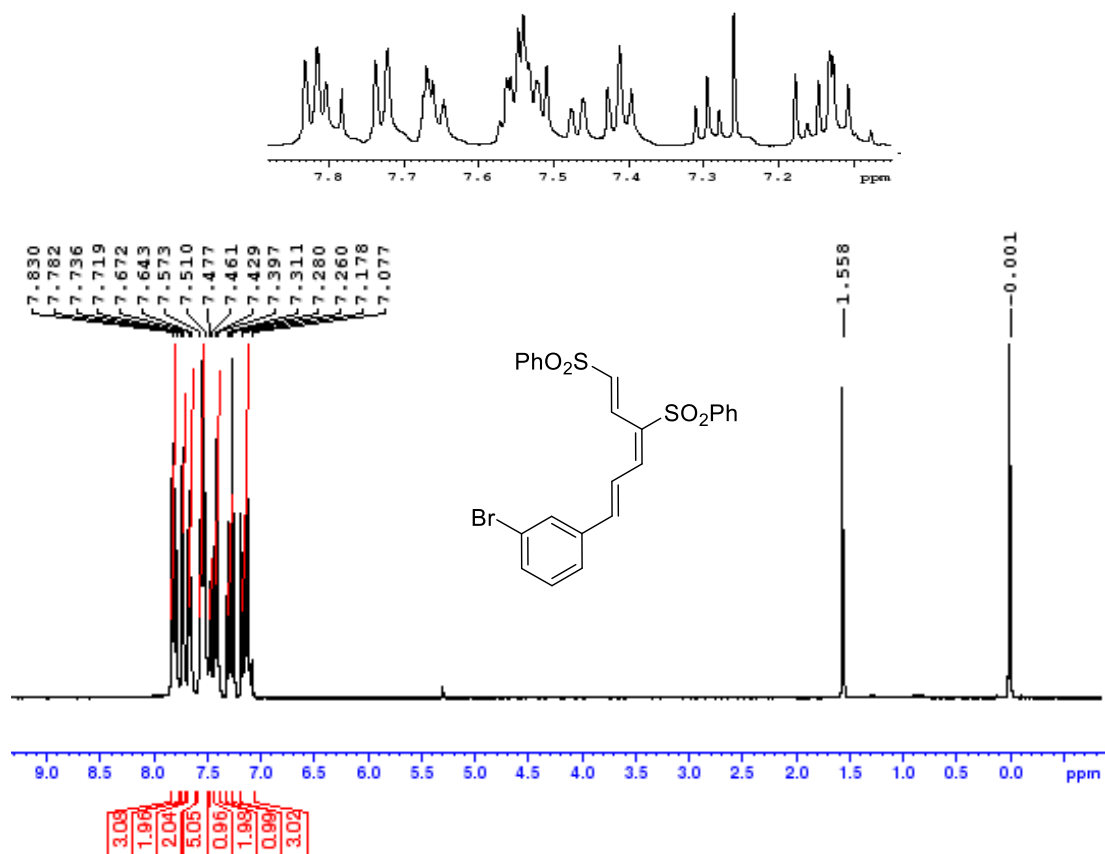


Figure A204. ¹H NMR spectrum of (1E,3E,5E)-1,3-bis-phenylsulfonyl-(6-m-bromophenyl)-hexa-1,3,5-triene, **115**

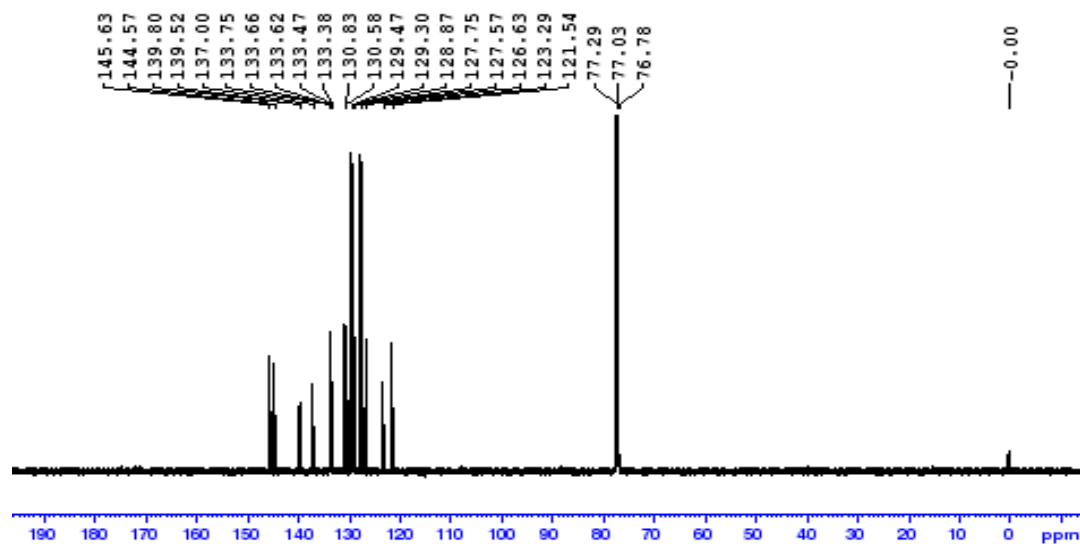


Figure A205. ¹³C NMR spectrum of (1E,3E,5E)-1,3-bis-phenylsulfonyl-(6-m-bromophenyl)-hexa-1,3,5-triene, **115**

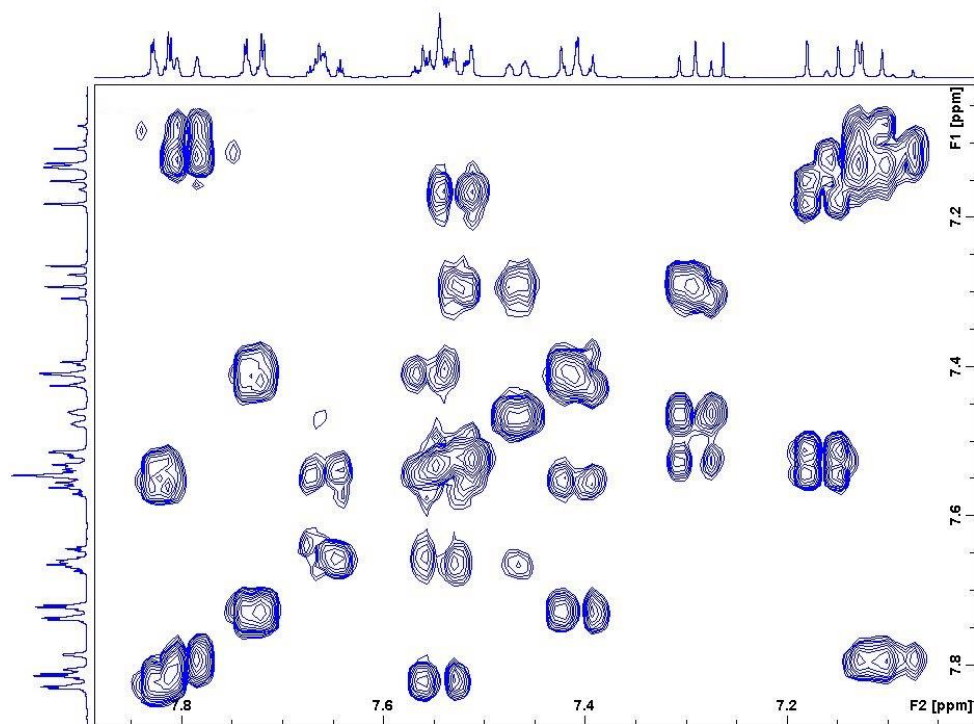


Figure A206. Zoomed in COSY spectrum of (1*E*,3*E*,5*E*)-1,3-bis-phenylsulfonyl-(6-*m*-bromophenyl)-hexa-1,3,5-triene, **115**

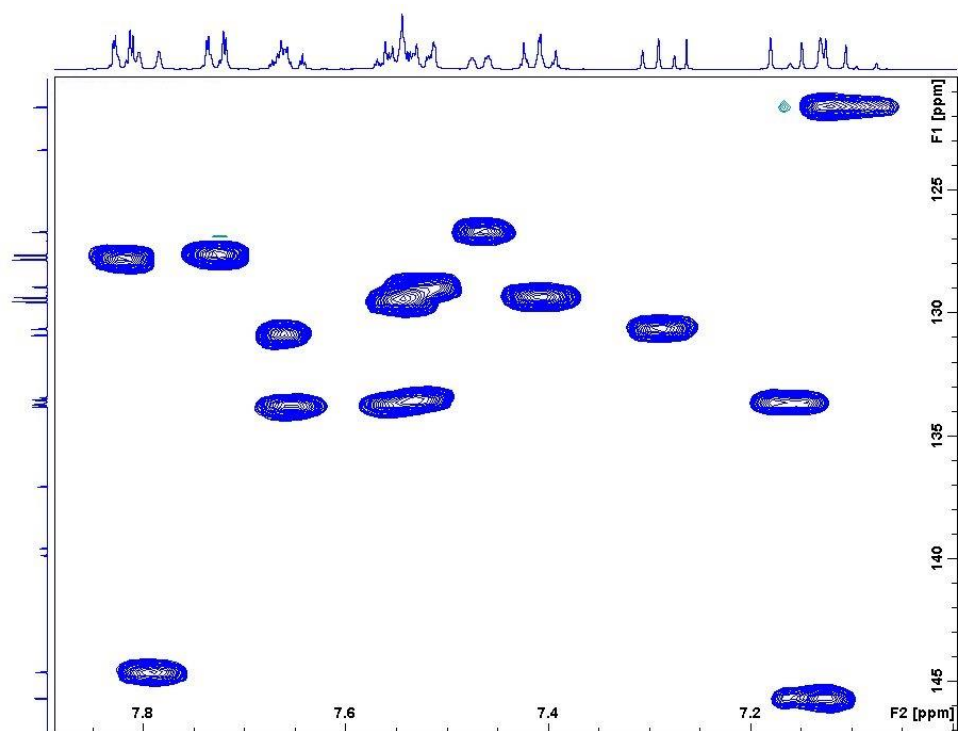


Figure A207. Zoomed in HSQC spectrum of (1*E*,3*E*,5*E*)-1,3-bis-phenylsulfonyl-(6-*m*-bromophenyl)-hexa-1,3,5-triene, **115**

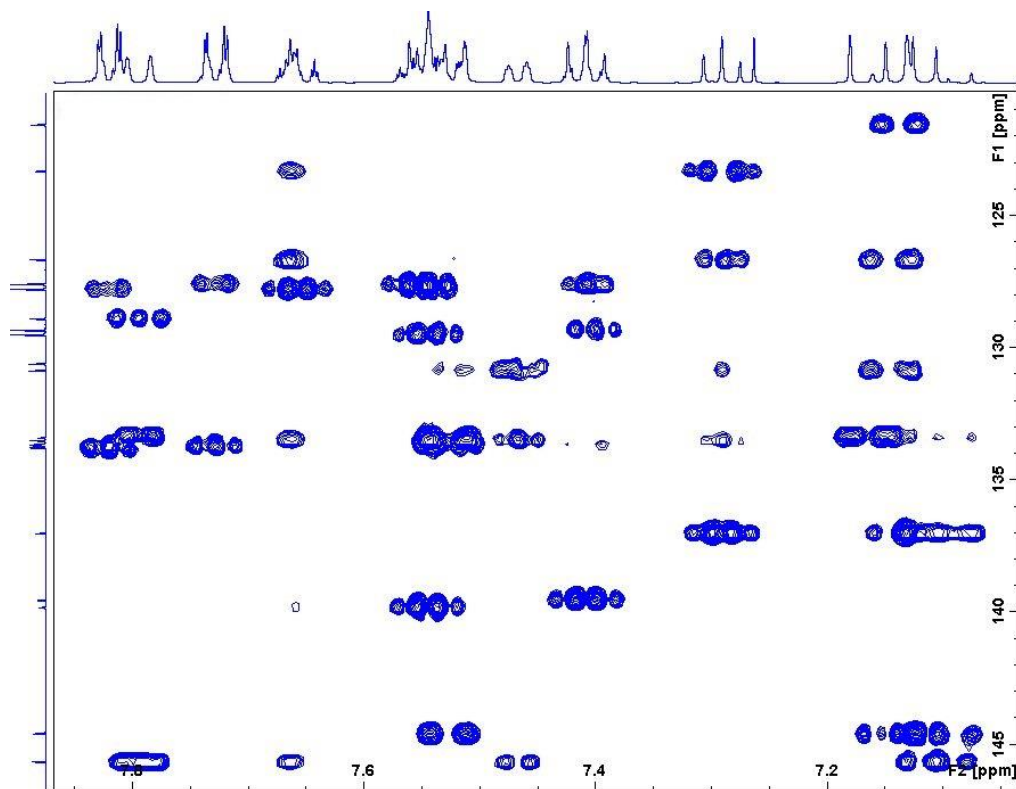


Figure A208. Zoomed in HMBC spectrum of (1*E*,3*E*,5*E*)-1,3-bis-phenylsulfonyl-(6-*m*-bromophenyl)-hexa-1,3,5-triene, **115**

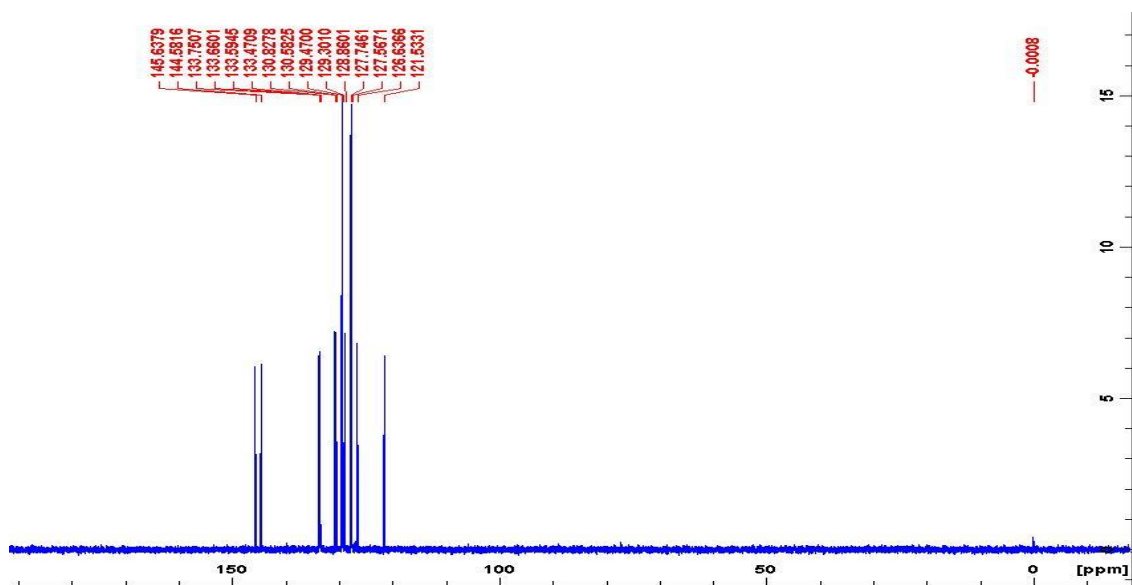


Figure A209. DEPT-135 spectrum of (1*E*,3*E*,5*E*)-1,3-bis-phenylsulfonyl-(6-*m*-bromophenyl)-hexa-1,3,5-triene, **115**

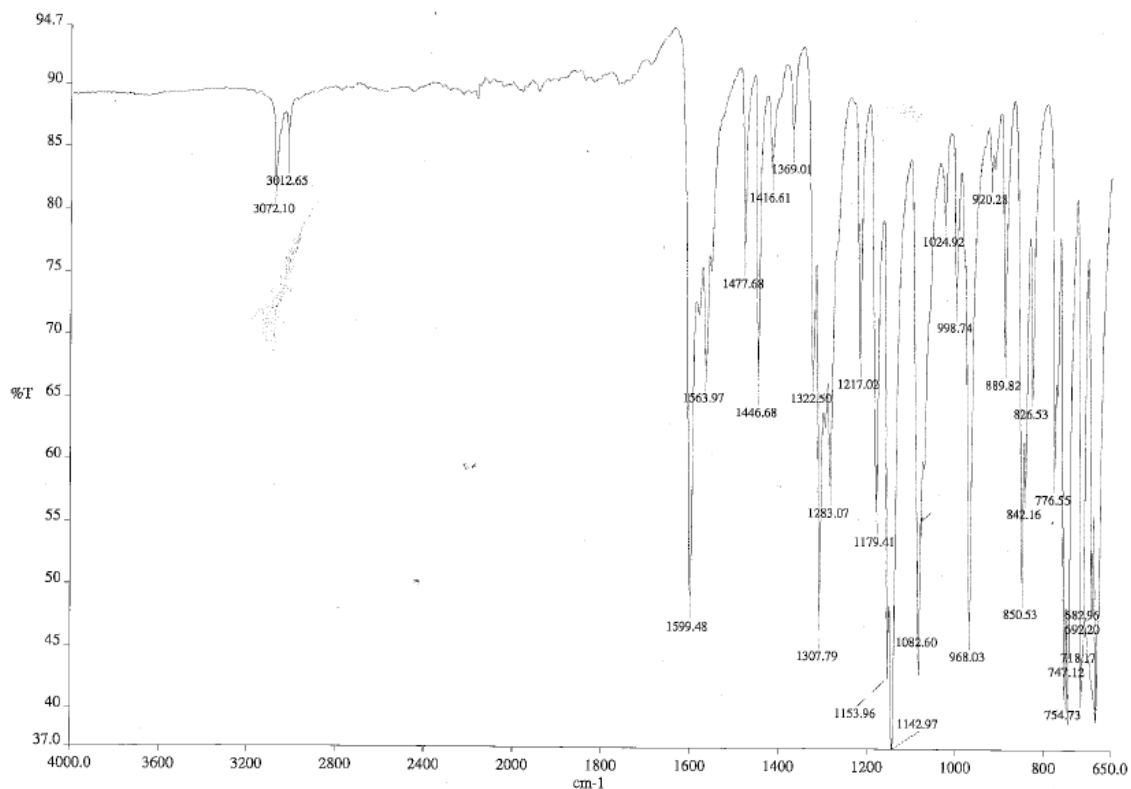


Figure A210. IR spectrum of (1*E*,3*E*,5*E*)-1,3-bis-phenylsulfonyl-(6-*m*-bromophenyl)-hexa-1,3,5-triene, **115**

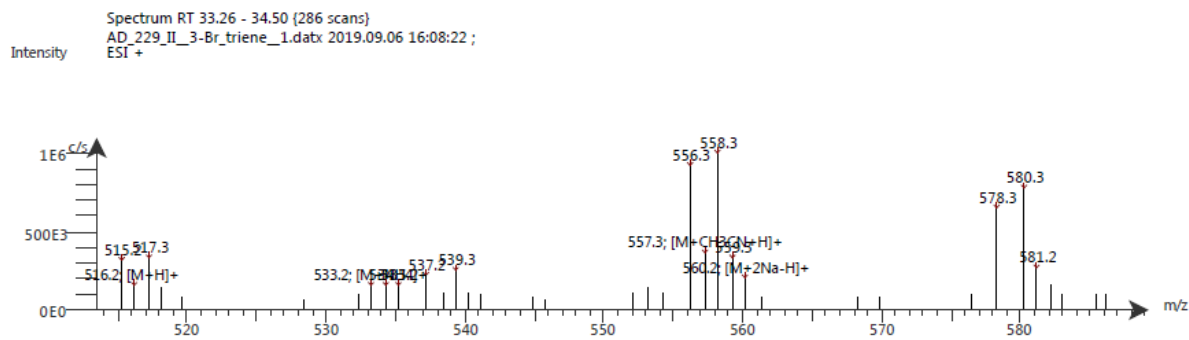


Figure A211. LC-ESI-MS spectrum of (1*E*,3*E*,5*E*)-1,3-bis-phenylsulfonyl-(6-*m*-bromophenyl)-hexa-1,3,5-triene, **115**. The ESI spectrum shows it has m/z [M+H]⁺ 516.2

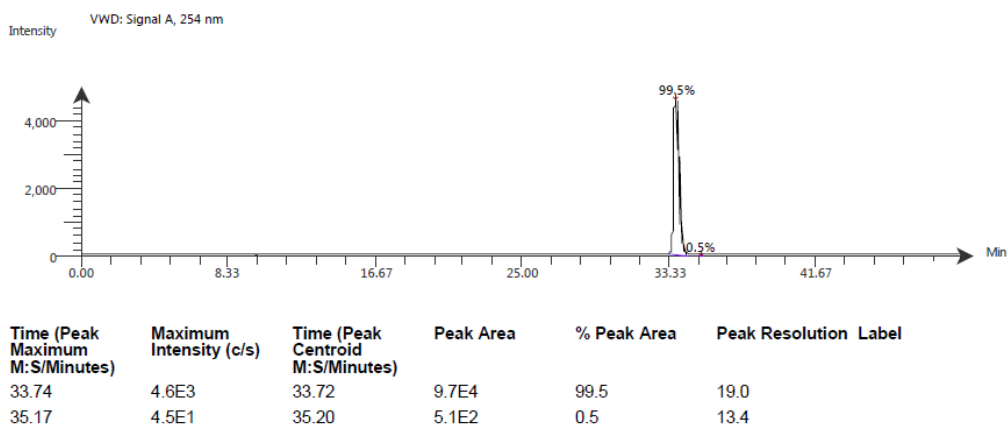


Figure A212. LC-UV-MS spectrum of (1*E*,3*E*,5*E*)-1,3-bis-phenylsulfonyl-(6-*m*-bromophenyl)-hexa-1,3,5-triene, **115**

Compound Table

Compound Label	RT (min)	Observed mass (m/z)	Neutral observed mass (Da)	Theoretical mass (Da)	Mass error (ppm)	Isotope match score (%)
Cpd 1: C ₂₄ H ₁₉ BrO ₄ S ₂	0.80	516.9957	513.9906	513.9908	-0.50	98.41

Mass errors of between -5.00 and 5.00 ppm with isotope match scores above 60% are considered confirmation of molecular formulae

Figure A213. HR-MS analysis of (1*E*,3*E*,5*E*)-1,3-bis-phenylsulfonyl-(6-*m*-bromophenyl)-hexa-1,3,5-triene, **115**

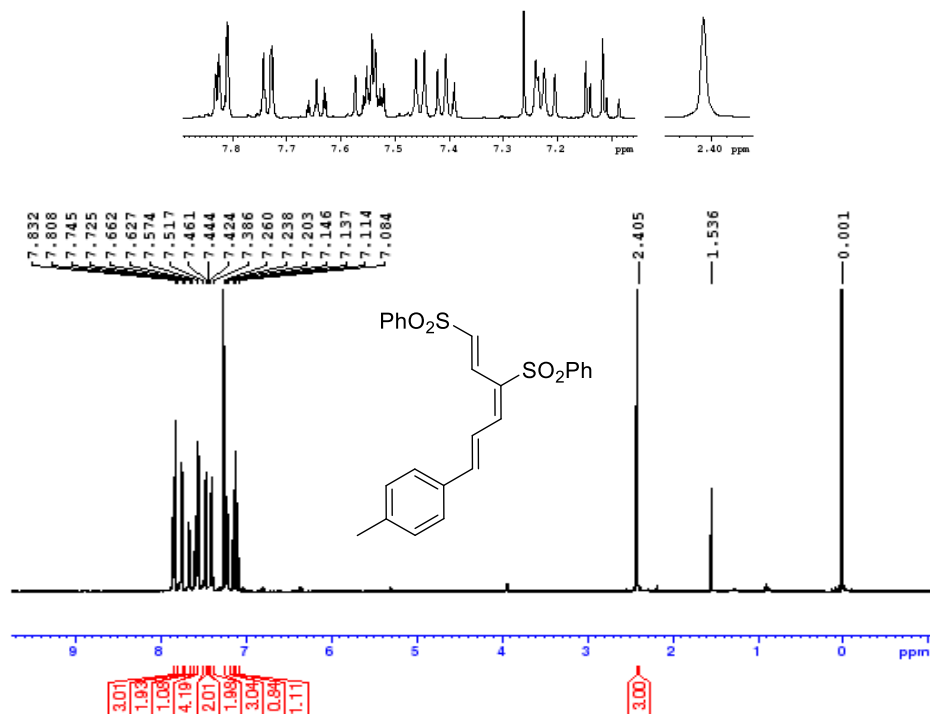


Figure A214. ¹H NMR spectrum of (1*E*,3*E*,5*E*)-1,3-bis-phenylsulfonyl-6-(*p*-methylphenyl)-hexa-1,3,5-triene, **116**

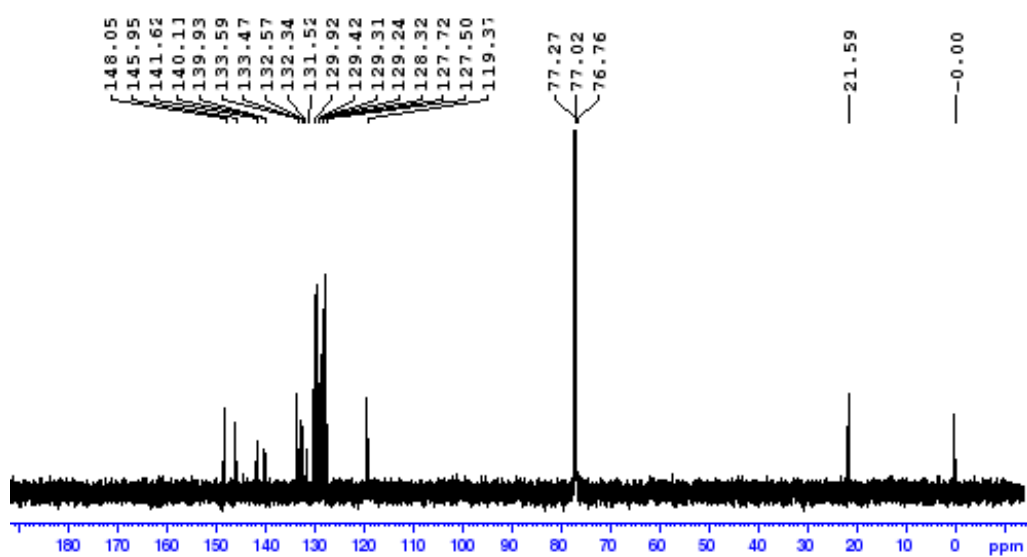


Figure A215. ^{13}C NMR spectrum of $(1E,3E,5E)$ -1,3-bis-phenylsulfonyl-6-(*p*-methylphenyl)-hexa-1,3,5-triene, **116**

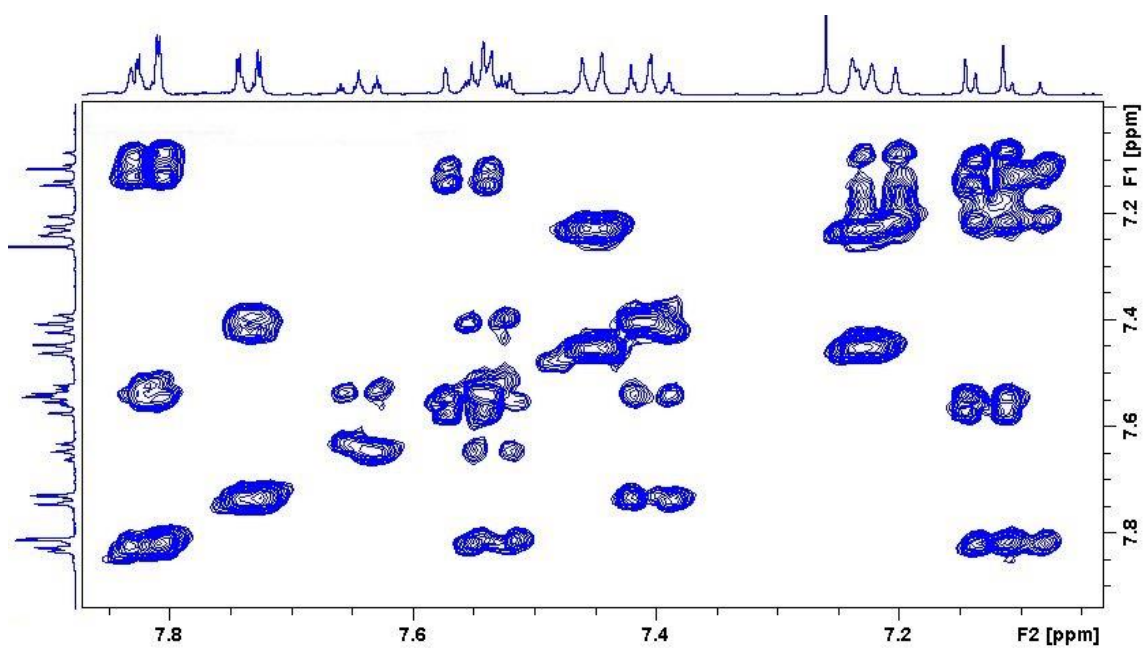


Figure A216. COSY spectrum of $(1E,3E,5E)$ -1,3-bis-phenylsulfonyl-6-(*p*-methylphenyl)-hexa-1,3,5-triene, **116**

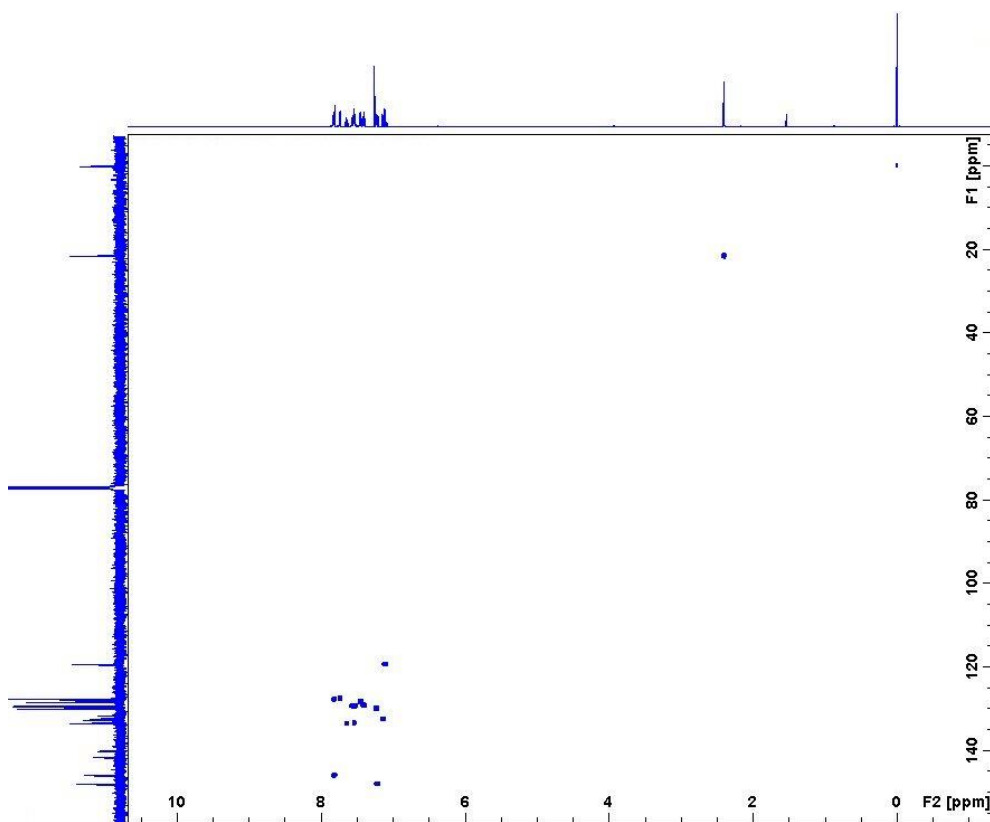


Figure A217. HSQC spectrum of (1*E*,3*E*,5*E*)-1,3-bis-phenylsulfonyl-6-(*p*-methylphenyl)-hexa-1,3,5-triene, **116**.

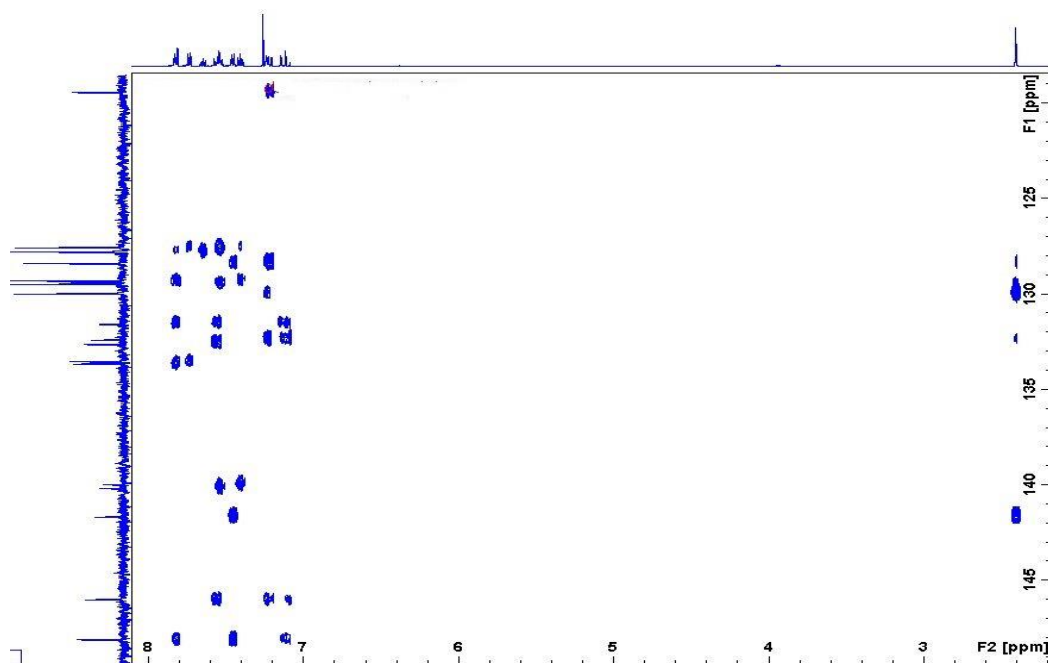


Figure A218. HMBC spectrum of (1*E*,3*E*,5*E*)-1,3-bis-phenylsulfonyl-6-(*p*-methylphenyl)-hexa-1,3,5-triene, **116**.

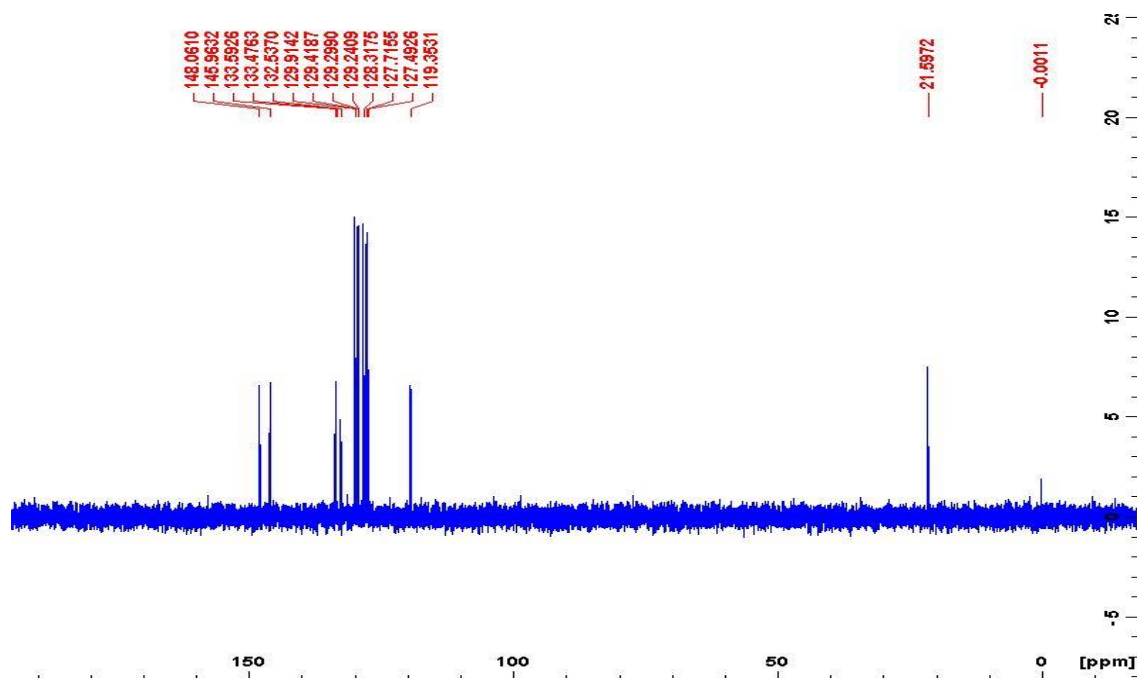


Figure A219. DEPT-135 spectrum of (1*E*,3*E*,5*E*)-1,3-bis-phenylsulfonyl-6-(*p*-methylphenyl)-hexa-1,3,5-triene, **116**

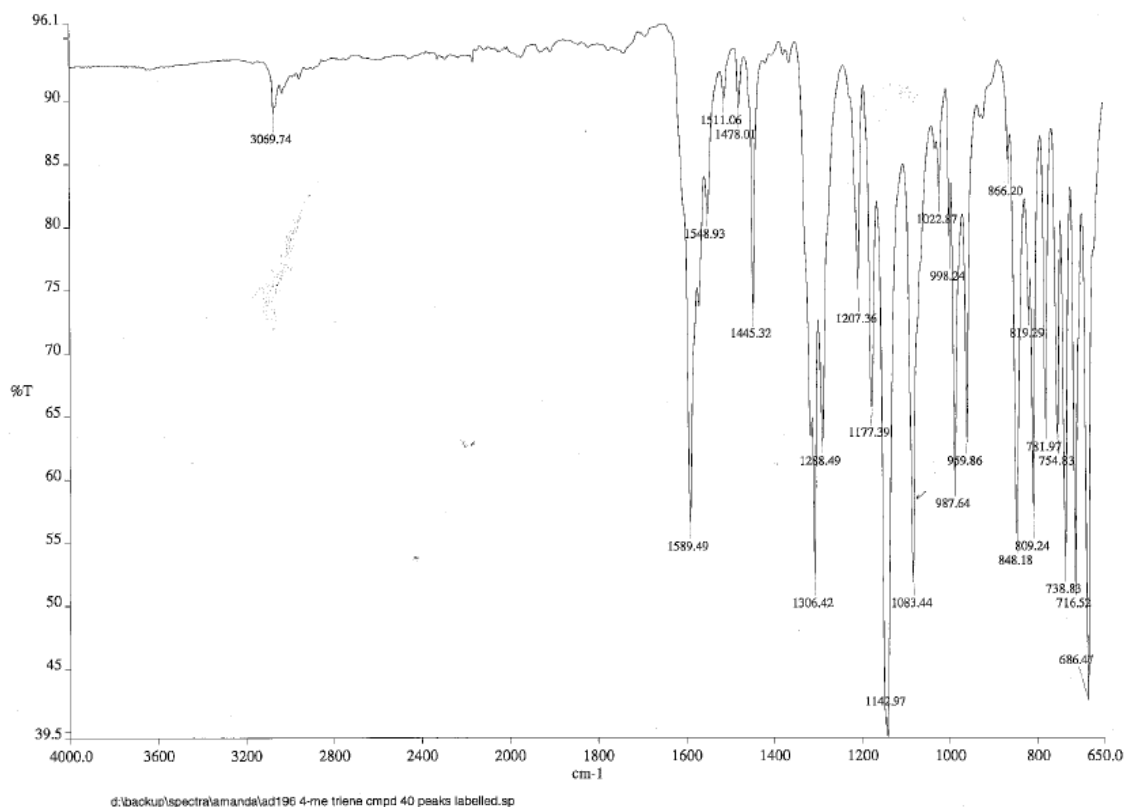


Figure A220. IR spectrum of (1*E*,3*E*,5*E*)-1,3-bis-phenylsulfonyl-(*p*-methylphenyl)-hexa-1,3,5-triene, **116**

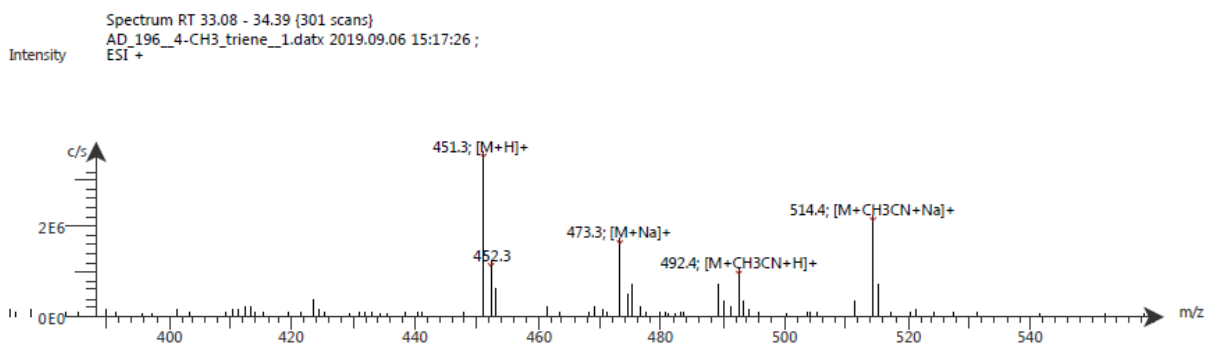
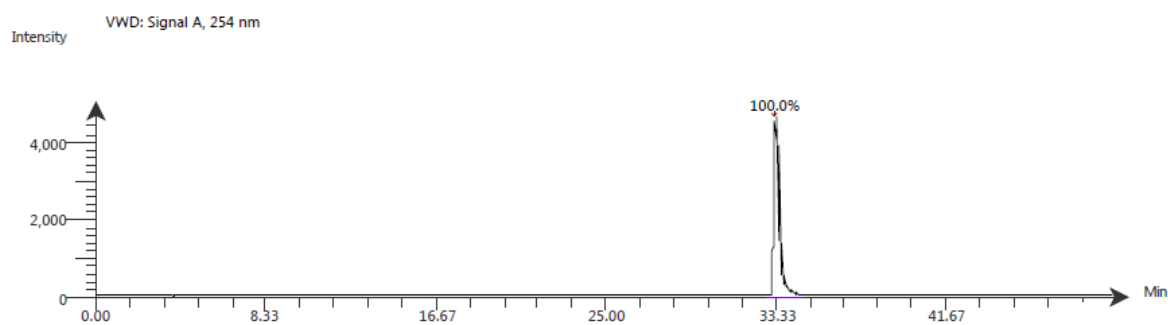


Figure A221. LC-ESI-MS spectrum of (1*E*,3*E*,5*E*)-1,3-bis-phenylsulfonyl-(*p*-methylphenyl)-hexa-1,3,5-triene, **116**. The ESI spectrum shows it has m/z $[M+H]^+$ 451.3



Time (Peak Maximum M:S/Minutes)	Maximum Intensity (c/s)	Time (Peak Centroid M:S/Minutes)	Peak Area	% Peak Area	Peak Resolution Label
33.31	4.7E3	33.31	8.7E4	100.0	15.9

Figure A222. LC-UV-MS spectrum of (1*E*,3*E*,5*E*)-1,3-bis-phenylsulfonyl-(*p*-methylphenyl)-hexa-1,3,5-triene, **116**

Compound Table

Compound Label	RT (min)	Observed mass (m/z)	Neutral observed mass (Da)	Theoretical mass (Da)	Mass error (ppm)	Isotope match score (%)
Cpd 1: C25 H22 O4 S2	0.80	473.0852	450.0960	450.0960	0.12	92.56

Mass errors of between -5.00 and 5.00 ppm with isotope match scores above 60% are considered confirmation of molecular formulae

Figure A223. HR-MS analysis of (1*E*,3*E*,5*E*)-1,3-bis-phenylsulfonyl-(*p*-methylphenyl)-hexa-1,3,5-triene, **116**

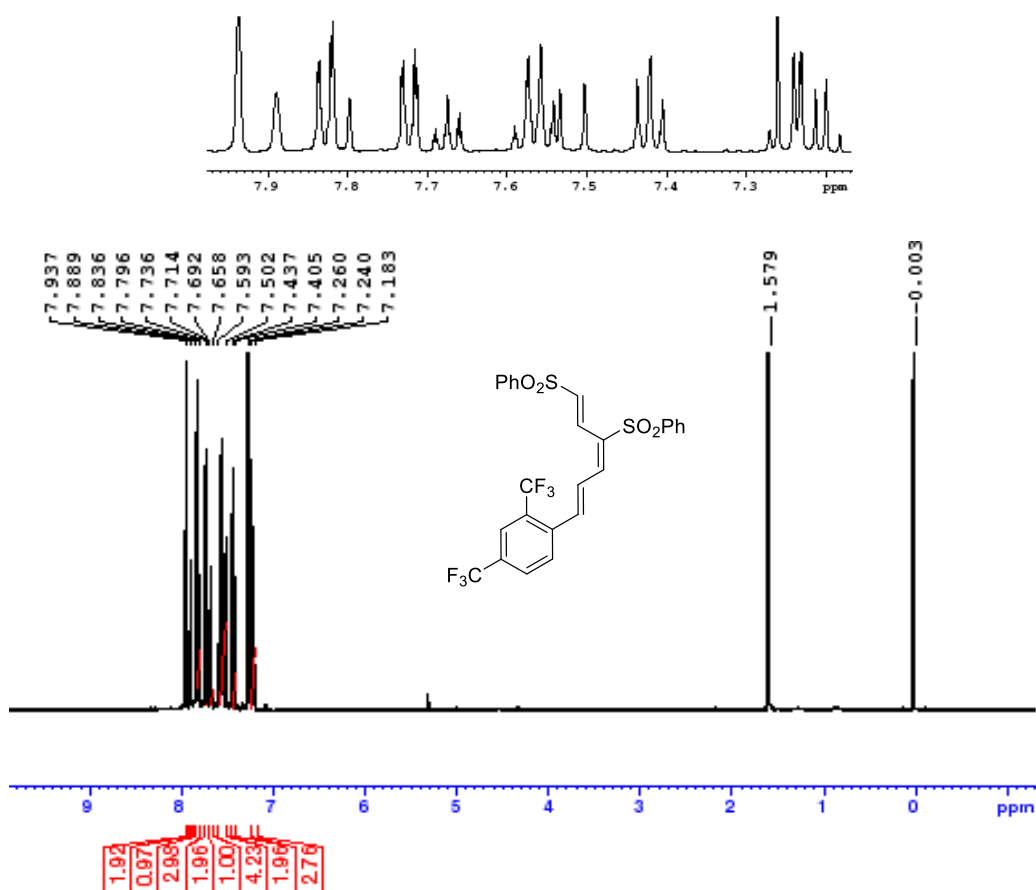


Figure A224. ¹H NMR spectrum of (1E,3E,5E)-1,3-bis-phenylsulfonyl-6-(3,5-bis(trifluoromethyl)phenyl)-hexa-1,3,5-triene, **117**

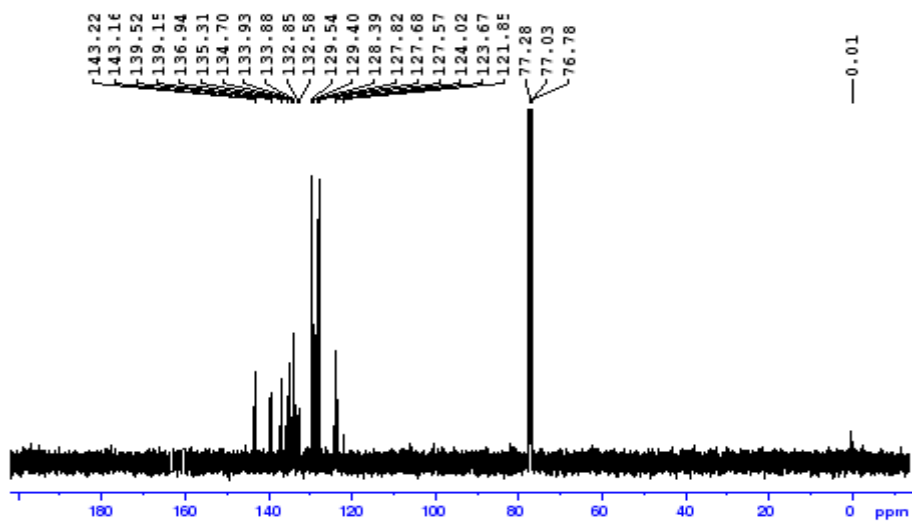


Figure A225. ¹³C NMR spectrum of (1E,3E,5E)-1,3-bis-phenylsulfonyl-6-(3,5-bis(trifluoromethyl)phenyl)-hexa-1,3,5-triene, **117**

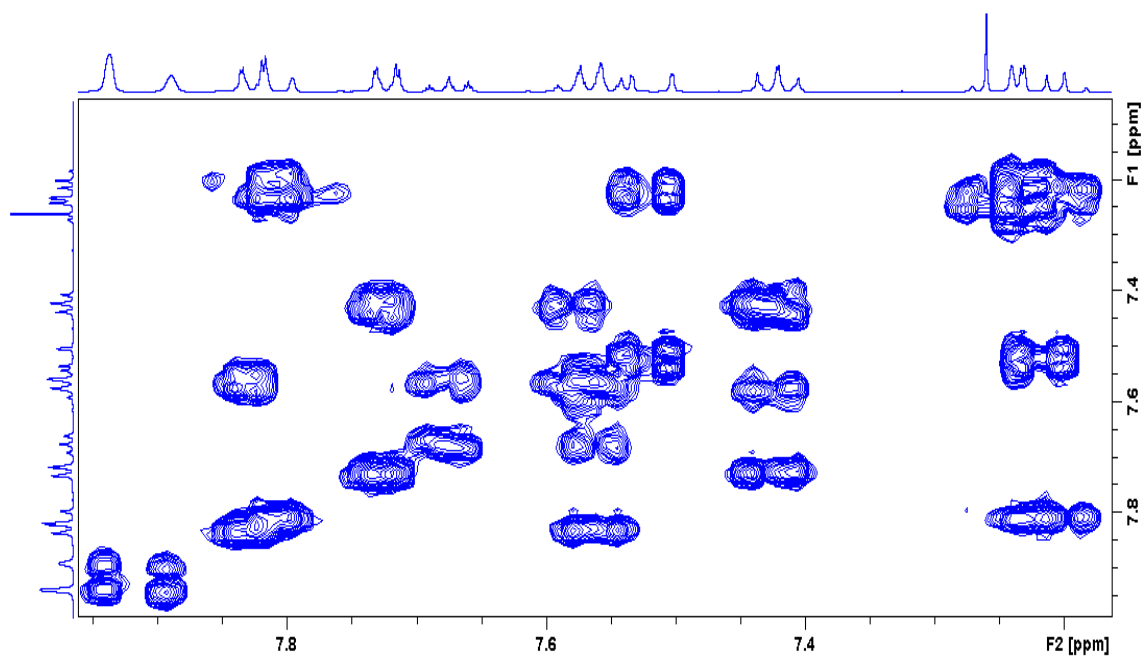


Figure A226. Zoomed in COSY spectrum of (1*E*,3*E*,5*E*)-1,3-bis-phenylsulfonyl-6-(3,5-bis(trifluoromethyl)phenyl)-hexa-1,3,5-triene, **117**

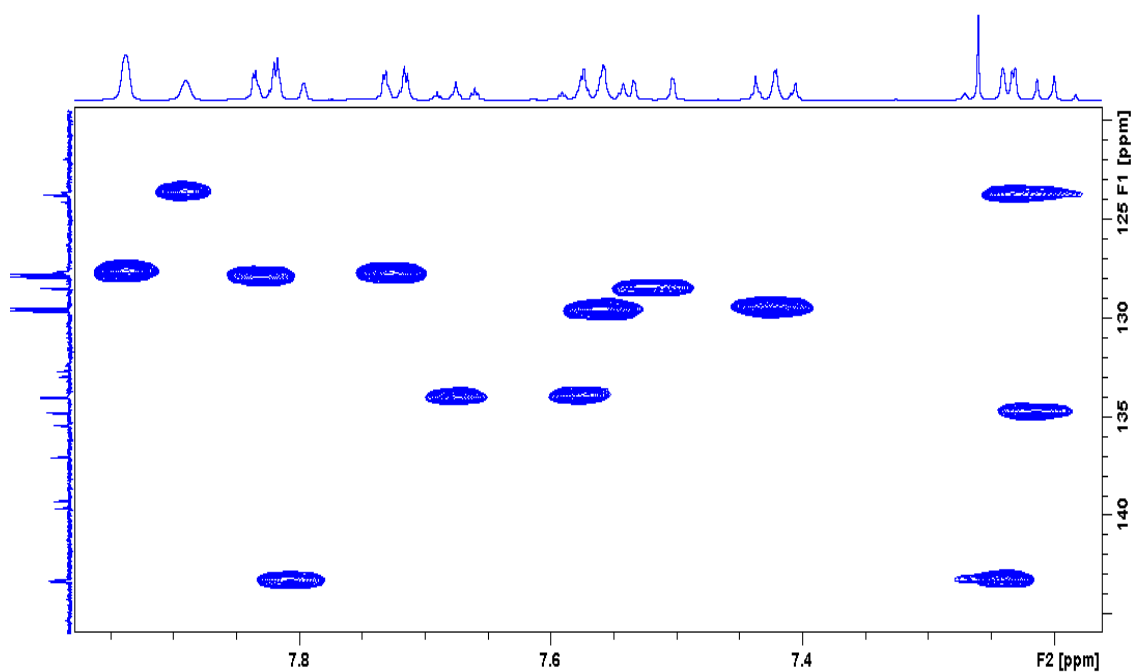


Figure A227. Zoomed in HSQC spectrum of (1*E*,3*E*,5*E*)-1,3-bis-phenylsulfonyl-6-(3,5-bis(trifluoromethyl)phenyl)-hexa-1,3,5-triene, **117**

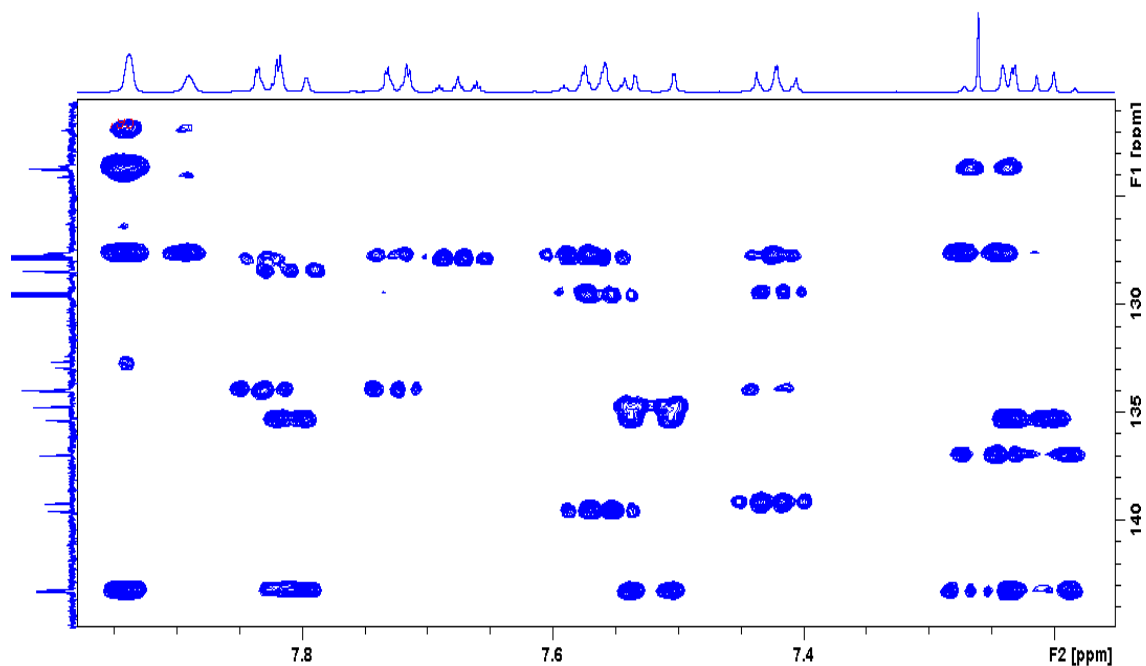


Figure A228. Zoomed in HMBC NMR spectrum of (1*E*,3*E*,5*E*)-1,3-bis-phenylsulfonyl-6-(3,5-bis(trifluoromethyl)phenyl)-hexa-1,3,5-triene, **117**

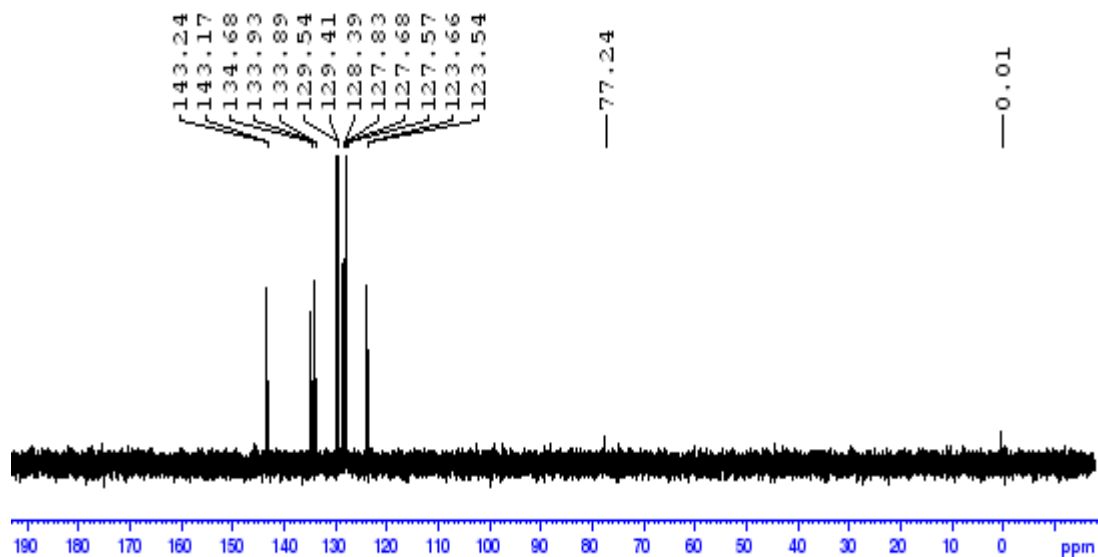


Figure A229. DEPT-135 NMR spectrum of (1*E*,3*E*,5*E*)-1,3-bis-phenylsulfonyl-6-(3,5-bis(trifluoromethyl)phenyl)-hexa-1,3,5-triene, **117**

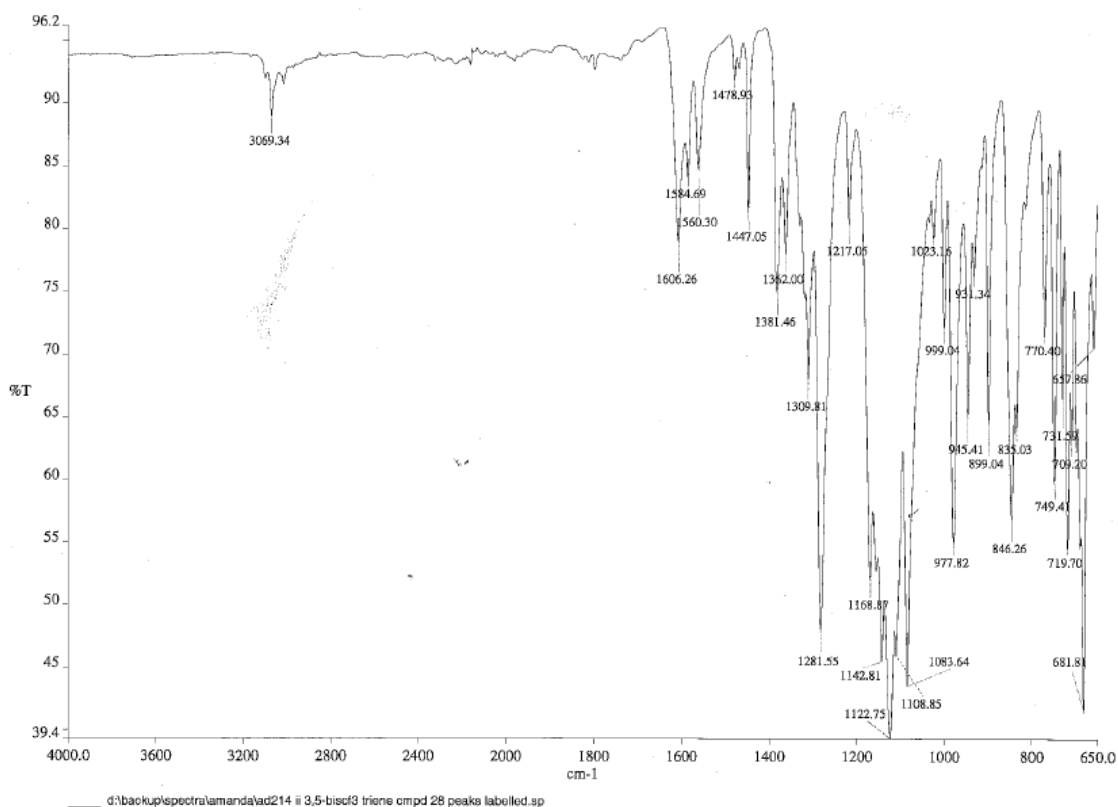


Figure A230. IR spectrum of (1*E*,3*E*,5*E*)-1,3-bis-phenylsulfonyl-6-(3,5-bis(trifluoromethyl)phenyl)-hexa-1,3,5-triene, **117**

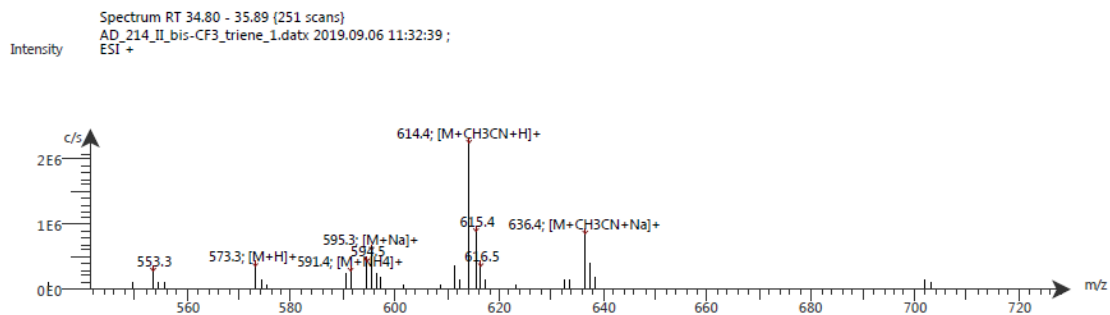


Figure A231. LC-ESI-MS spectrum of (1*E*,3*E*,5*E*)-1,3-bis-phenylsulfonyl-6-(3,5-bis(trifluoromethyl)phenyl)-hexa-1,3,5-triene, **117**. The ESI spectrum shows it has m/z [M+H]⁺ 595.3.

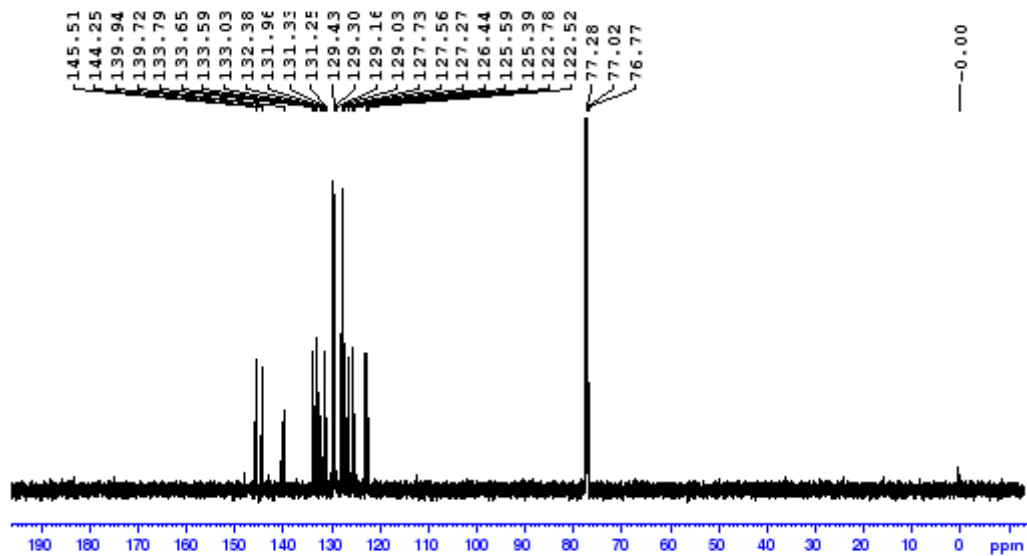


Figure A235. ^{13}C NMR spectrum of (1*E*,3*E*,5*E*)-1,3-bis-phenylsulfonyl-6-(α -naphthalene)-hexa-1,3,5-triene, **118**

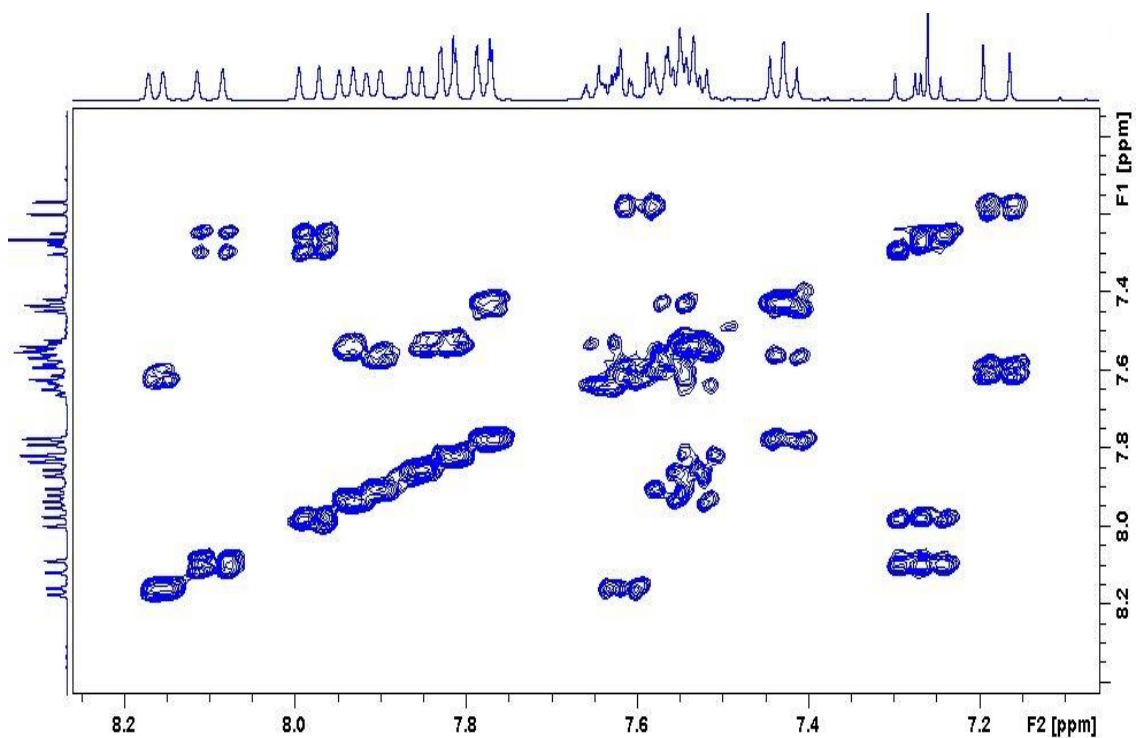


Figure A236. Zoomed in COSY spectrum of (1*E*,3*E*,5*E*)-1,3-bis-phenylsulfonyl-6-(α -naphthalene)-hexa-1,3,5-triene, **118**

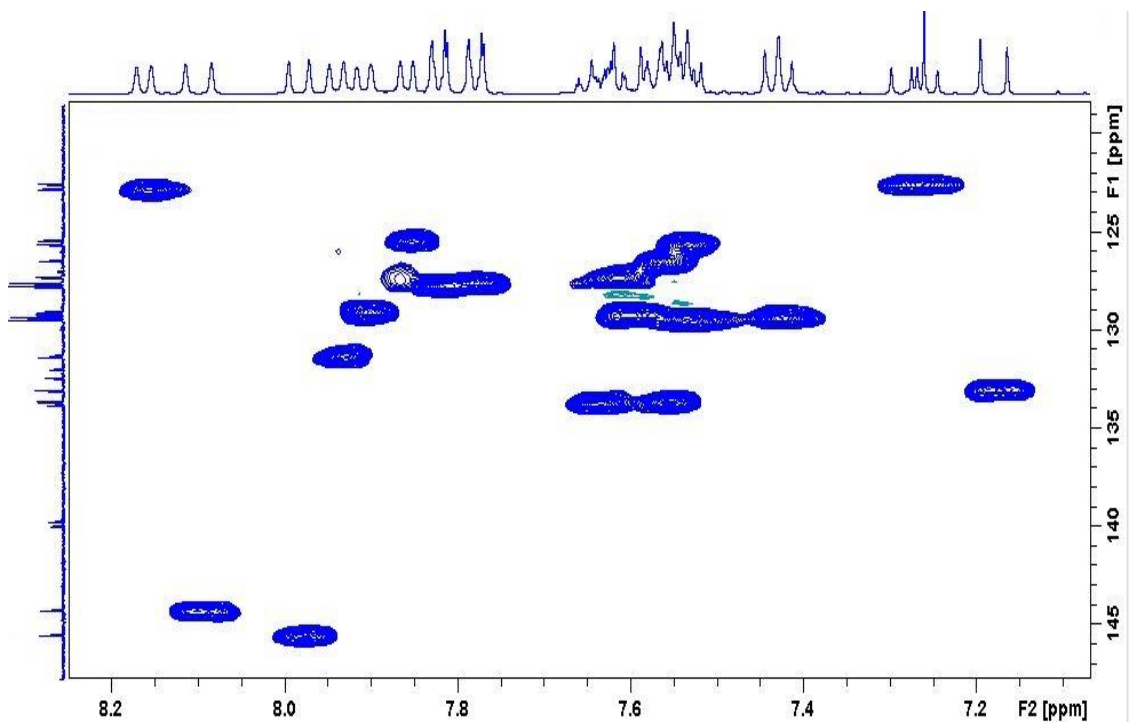


Figure A237. Zoomed in HSQC spectrum of (1*E*,3*E*,5*E*)-1,3-bis-phenylsulfonyl-6-(α -naphthalene)-hexa-1,3,5-triene, **118**

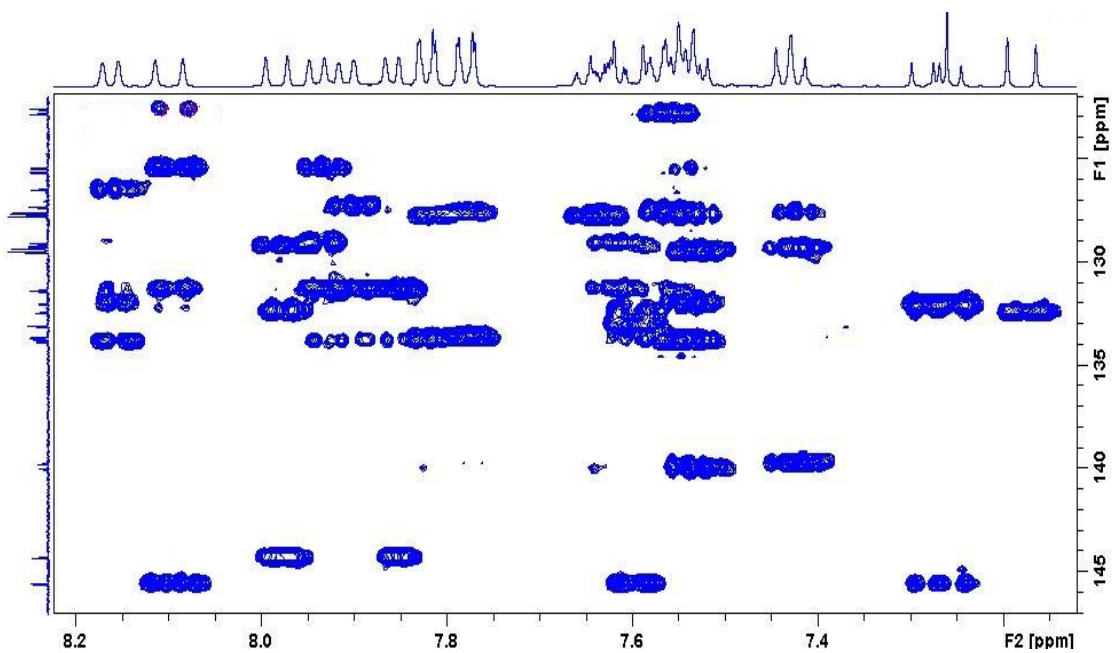


Figure A238. Zoomed in HMBC spectrum of (1*E*,3*E*,5*E*)-1,3-bis-phenylsulfonyl-6-(α -naphthalene)-hexa-1,3,5-triene, **118**

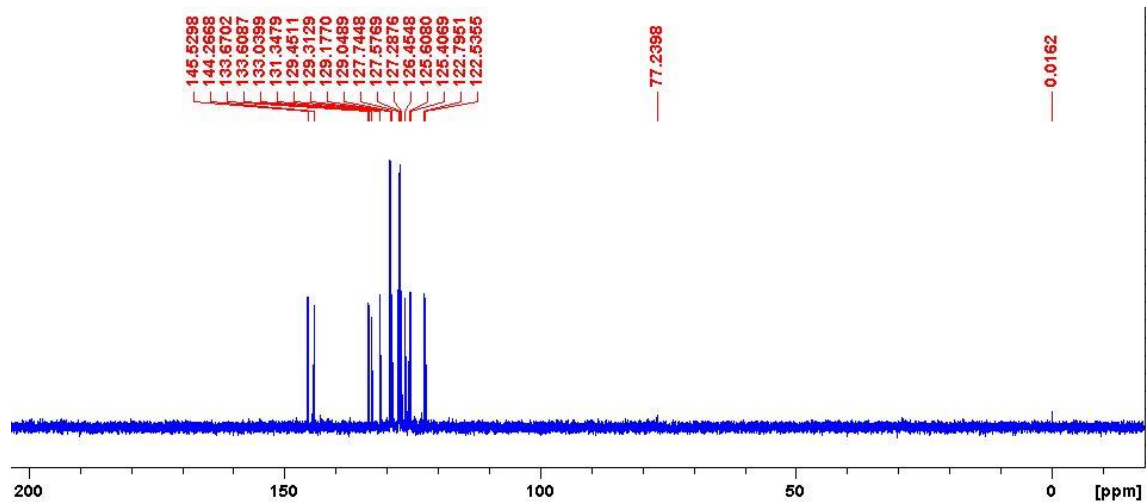


Figure A239. DEPT-135 spectrum of (1E,3E,5E)-1,3-bis-phenylsulfonyl-6-(α -naphthalene)-hexa-1,3,5-triene, **118**

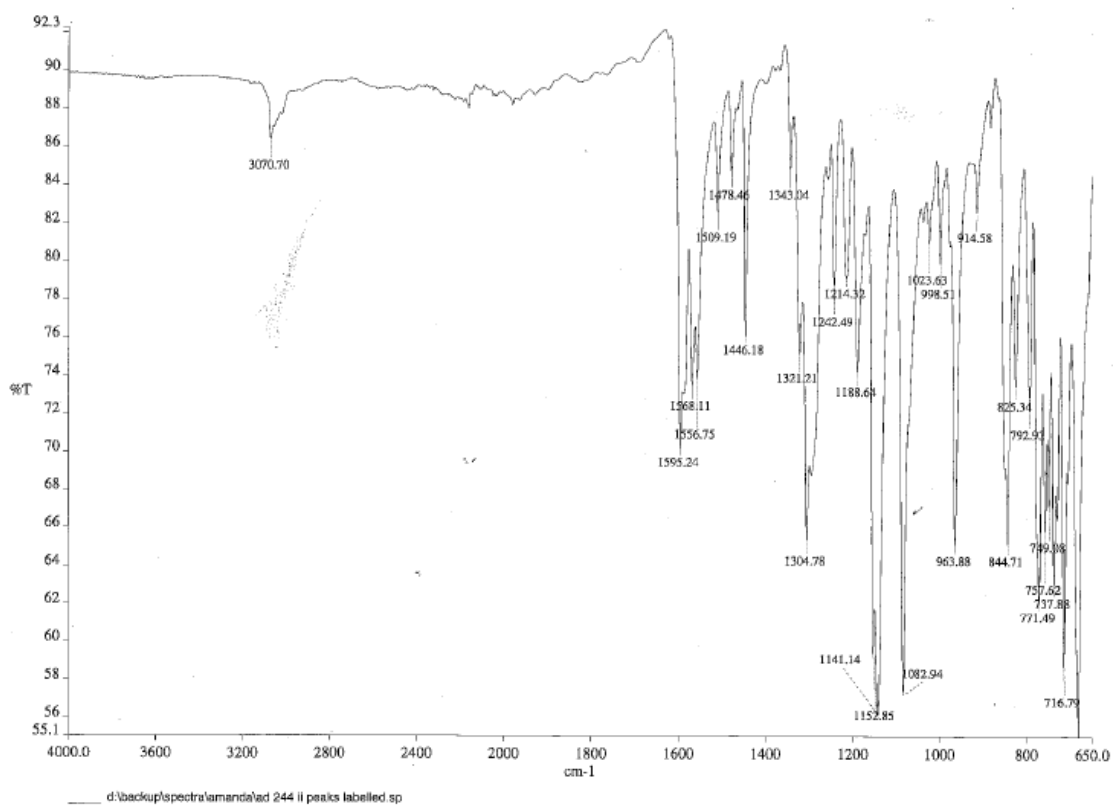


Figure A240. IR spectrum of (1E,3E,5E)-1,3-bis-phenylsulfonyl-6-(α -naphthalene)-hexa-1,3,5-triene, **118**

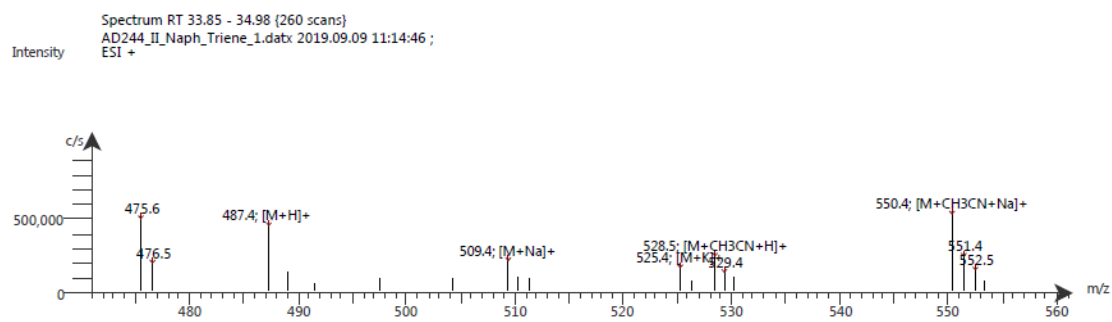
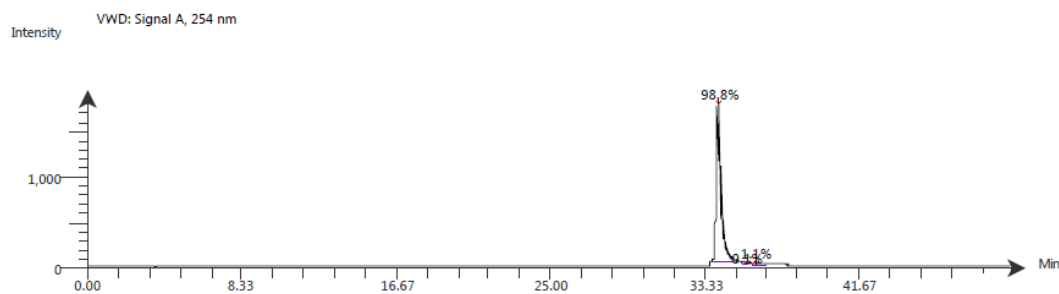


Figure A241. LC-ESI-MS spectrum of (1*E*,3*E*,5*E*)-1,3-bis-phenylsulfonyl-6-(α -naphthalene)-hexa-1,3,5-triene, **118**. The ESI spectrum shows it has m/z $[M+H]^+$ 487.4



Time (Peak Maximum M:S/Minutes)	Maximum Intensity (c/s)	Time (Peak Centroid M:S/Minutes)	Peak Area	% Peak Area	Peak Resolution	Label
34.00	1.7E3	34.07	2.9E4	98.8	13.8	
35.44	7.4E0	35.53	2.7E1	0.1	14.9	
35.84	1.5E1	36.08	3.1E2	1.1	44.8	

Figure A242. LC-UV-MS spectrum of (1*E*,3*E*,5*E*)-1,3-bis-phenylsulfonyl-6-(α -naphthalene)-hexa-1,3,5-triene, **118**

Compound Table

Compound Label	RT (min)	Observed mass (m/z)	Neutral observed mass (Da)	Theoretical mass (Da)	Mass error (ppm)	Isotope match score (%)
Cpd 1: C ₂₈ H ₂₂ O ₄ S ₂	0.80	487.1026	486.0958	486.0960	-0.38	93.27

Mass errors of between -5.00 and 5.00 ppm with isotope match scores above 60% are considered confirmation of molecular formulae

Figure A243. HR-MS analysis of (1*E*,3*E*,5*E*)-1,3-bis-phenylsulfonyl-6-(α -naphthalene)-hexa-1,3,5-triene, **118**

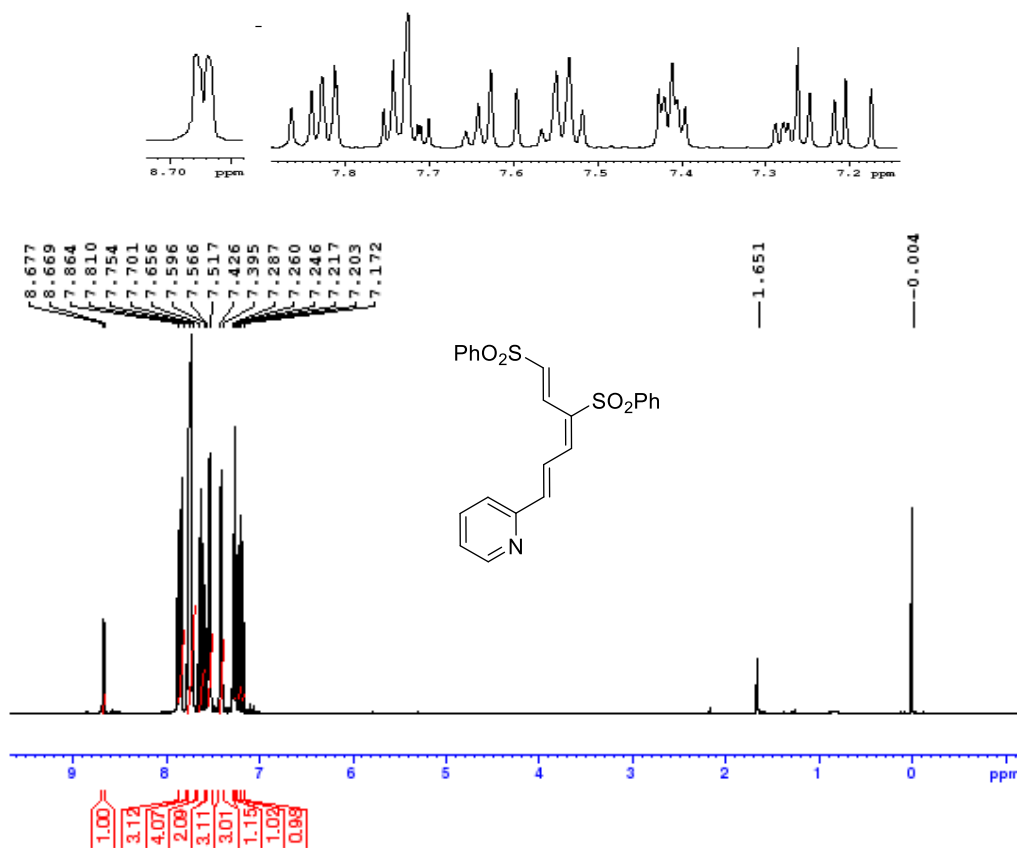


Figure A244. ¹H NMR spectrum of (1*E*,3*E*,5*E*)-1,3-bis-phenylsulfonyl-6-(2-pyridine)-hexa-1,3,5-triene, 119

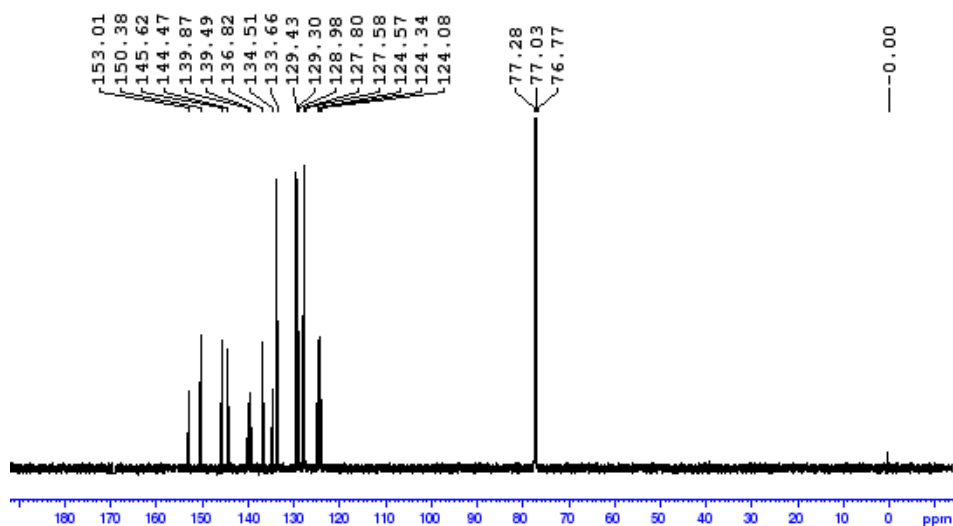


Figure A245 ¹³C NMR spectrum of (1*E*,3*E*,5*E*)-1,3-bis-phenylsulfonyl-6-(2-pyridine)-hexa-1,3,5-triene, 119

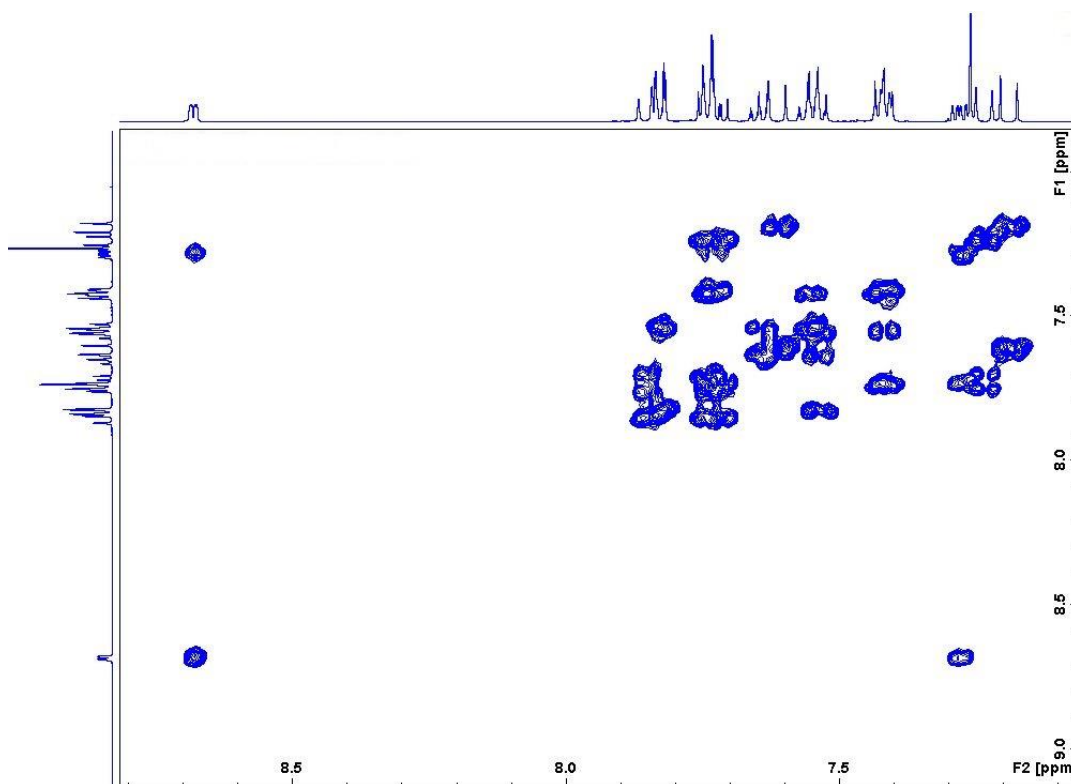


Figure A246. Zoomed in COSY spectrum of (1*E*,3*E*,5*E*)-1,3-bis-phenylsulfonyl-6-(2-pyridine)-hexa-1,3,5-triene, **119**

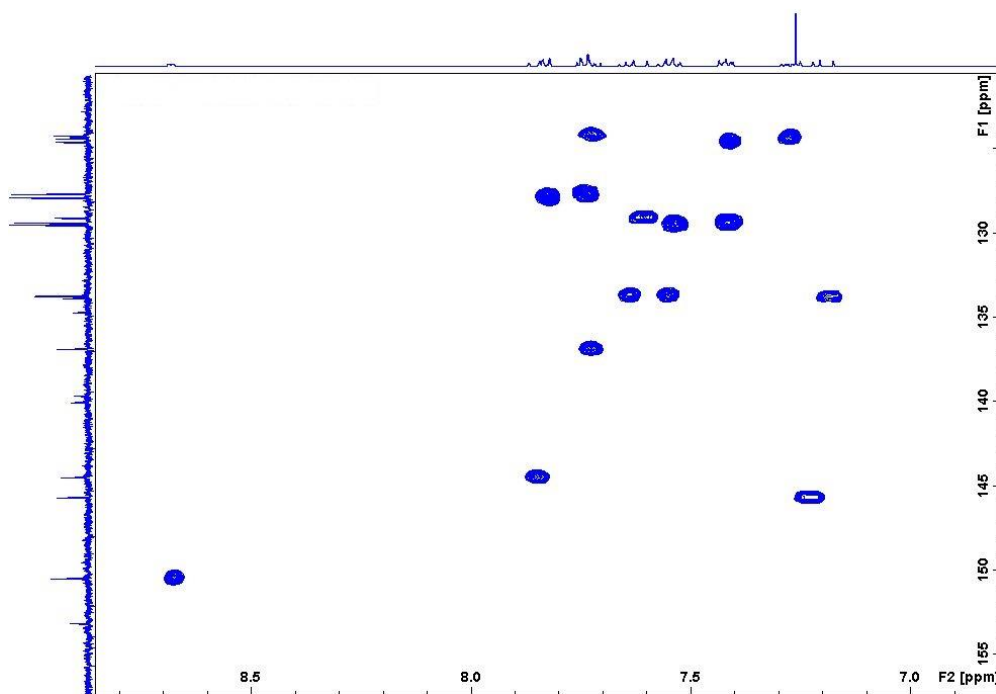


Figure A247. Zoomed in HSQC spectrum of (1*E*,3*E*,5*E*)-1,3-bis-phenylsulfonyl-6-(2-pyridine)-hexa-1,3,5-triene, **119**

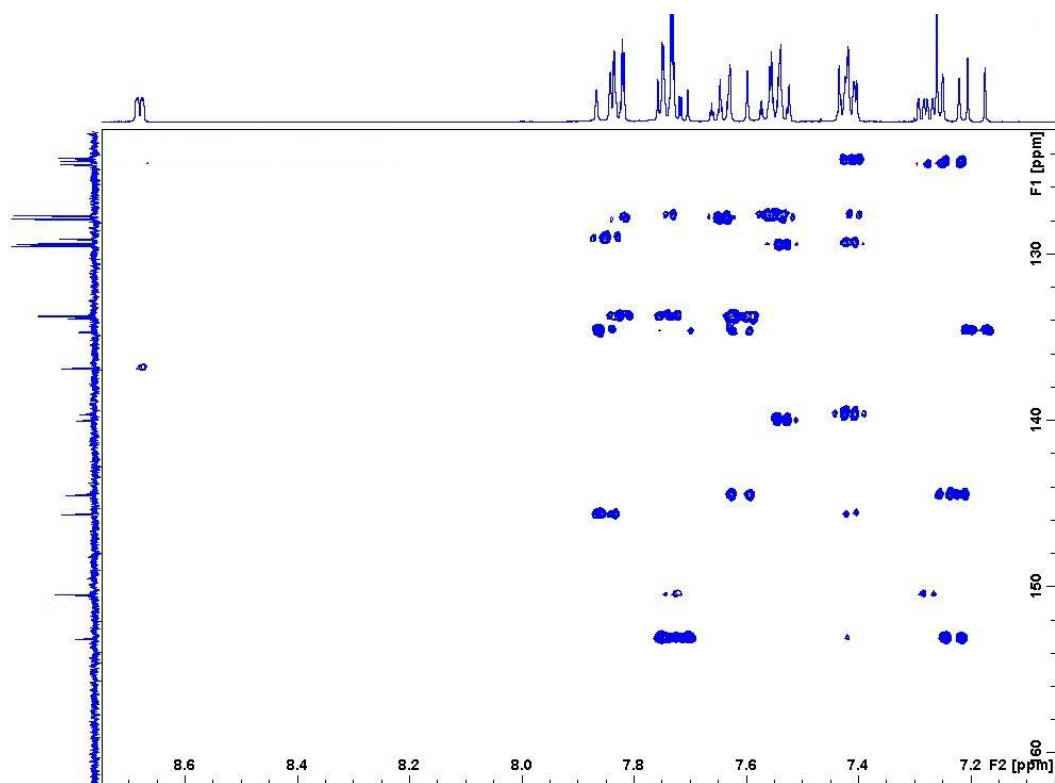


Figure A248. Zoomed in HMBC spectrum of *(1E,3E,5E)*-1,3-bis-phenylsulfonyl-6-(2-pyridine)-hexa-1,3,5-triene, **119**

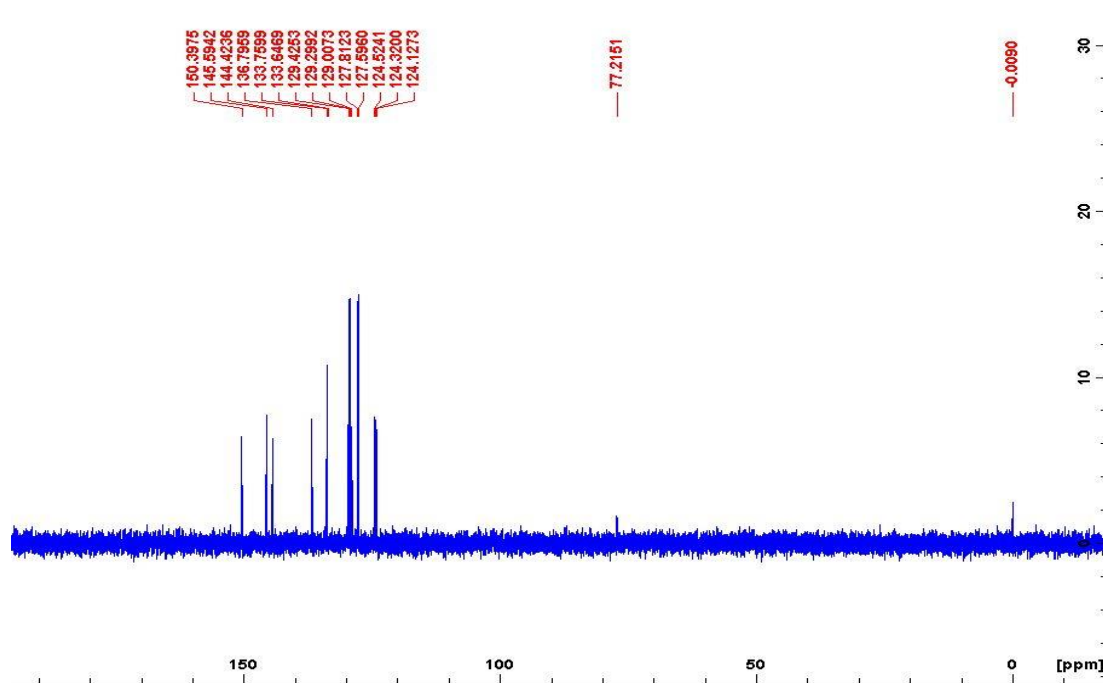


Figure A249. DEPT-135 spectrum of *(1E,3E,5E)*-1,3-bis-phenylsulfonyl-6-(2-pyridine)-hexa-1,3,5-triene, **119**

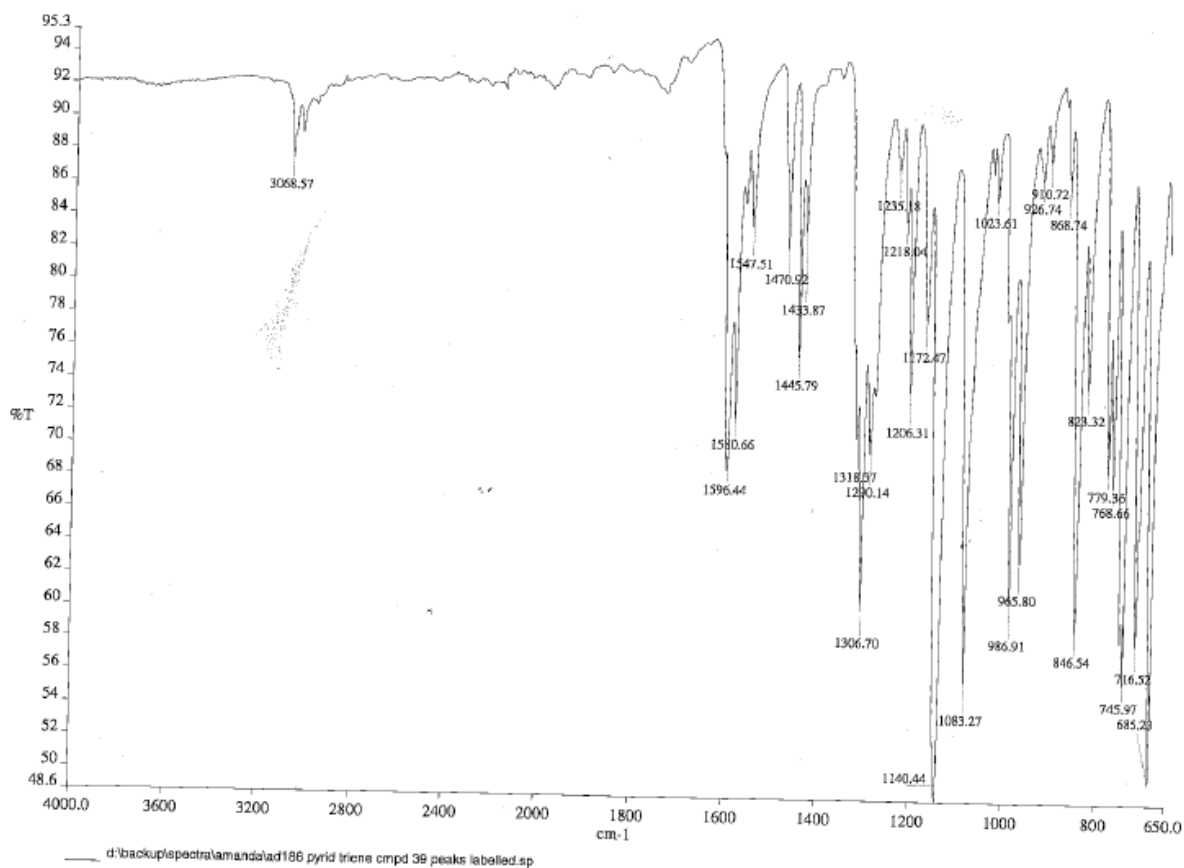


Figure S250. IR spectrum of (1*E*,3*E*,5*E*)-1,3-bis-phenylsulfonyl-6-(2-pyridine)-hexa-1,3,5-triene, **119**

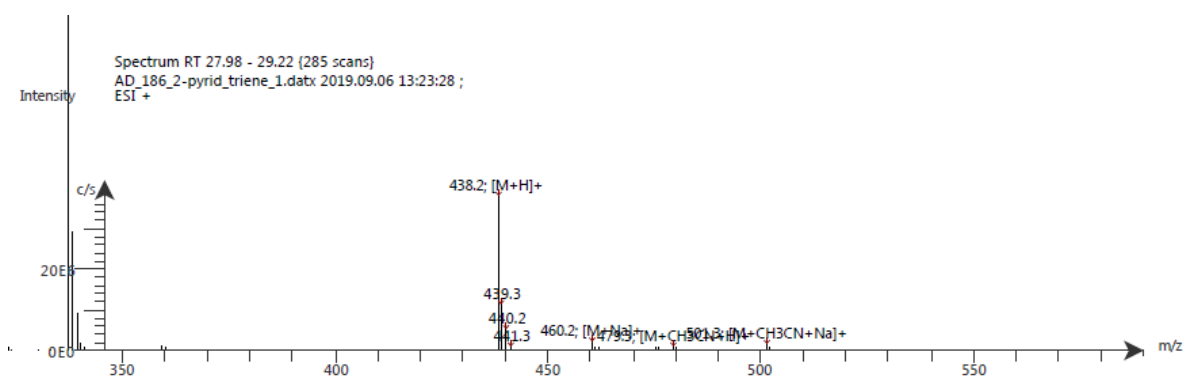


Figure A251. LC-ESI-MS spectrum of (1*E*,3*E*,5*E*)-1,3-bis-phenylsulfonyl-6-(2-pyridine)-hexa-1,3,5-triene, **119**. The ESI spectrum shows it has m/z [M+H]⁺ 438.2

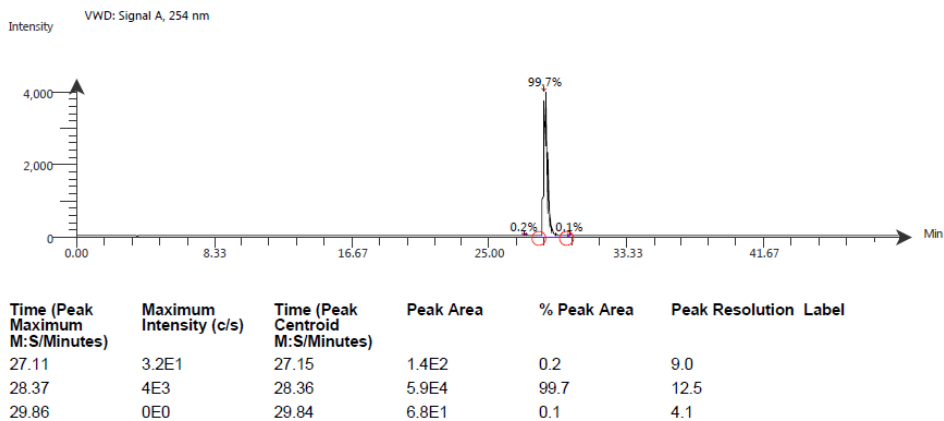


Figure A252. LC-UV-MS spectrum of (1*E*,3*E*,5*E*)-1,3-bis-phenylsulfonyl-6-(2-pyridine)phenyl)-hexa-1,3,5-triene, **119**

Compound Table

Compound Label	RT (min)	Observed mass (m/z)	Neutral observed mass (Da)	Theoretical mass (Da)	Mass error (ppm)	Isotope match score (%)
Cpd 1: C23 H19 N O4 S2	0.79	460.0648	437.0757	437.0755	0.45	94.44

Mass errors of between -5.00 and 5.00 ppm with isotope match scores above 60% are considered confirmation of molecular formulae

Figure A253. HR-MS analysis of (1*E*,3*E*,5*E*)-1,3-bis-phenylsulfonyl-6-(2-pyridine)-hexa-1,3,5-triene, **119**

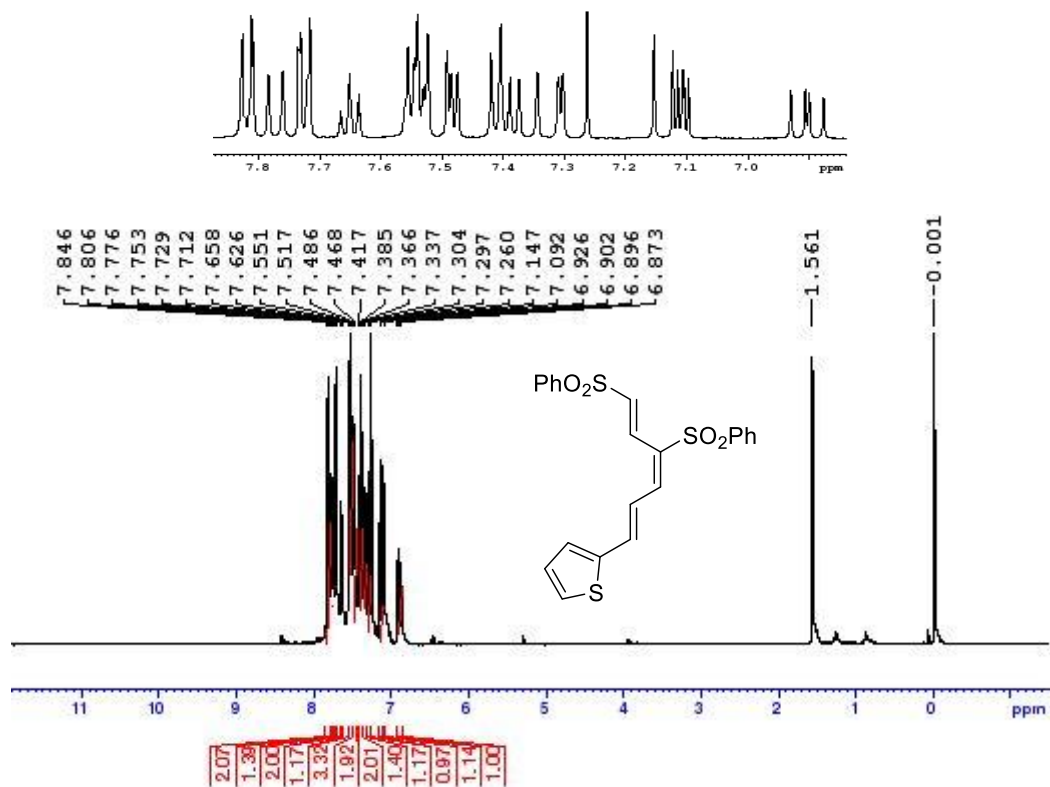


Figure A254. ¹H NMR spectrum of (1*E*,3*E*,5*E*)-1,3-bis-phenylsulfonyl-6-(2-thiophene)-hexa-1,3,5-triene, **120**

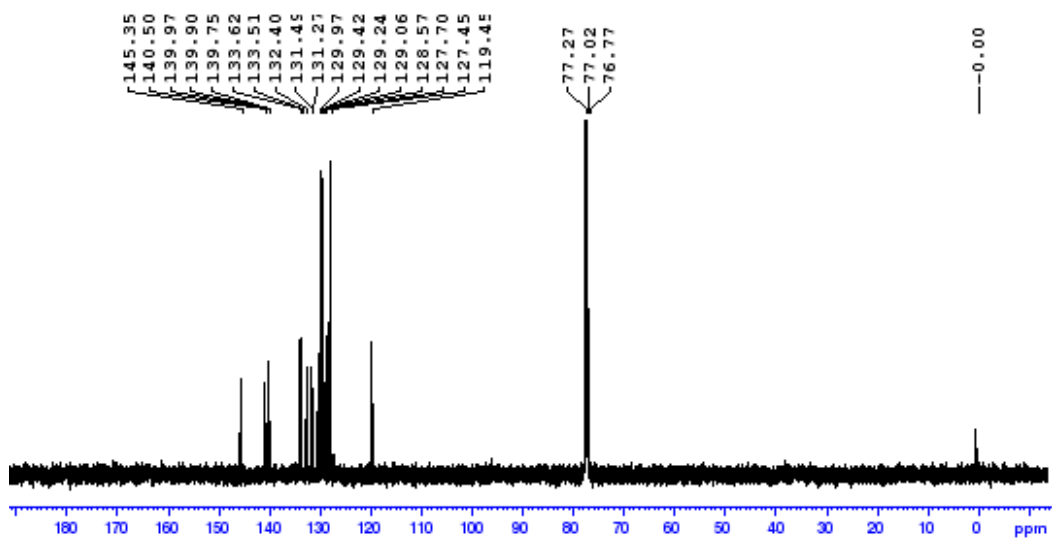


Figure A255. ^{13}C NMR spectrum of (1*E*,3*E*,5*E*)-1,3-bis-phenylsulfonyl-6-(2-thiophene)-hexa-1,3,5-triene, 120

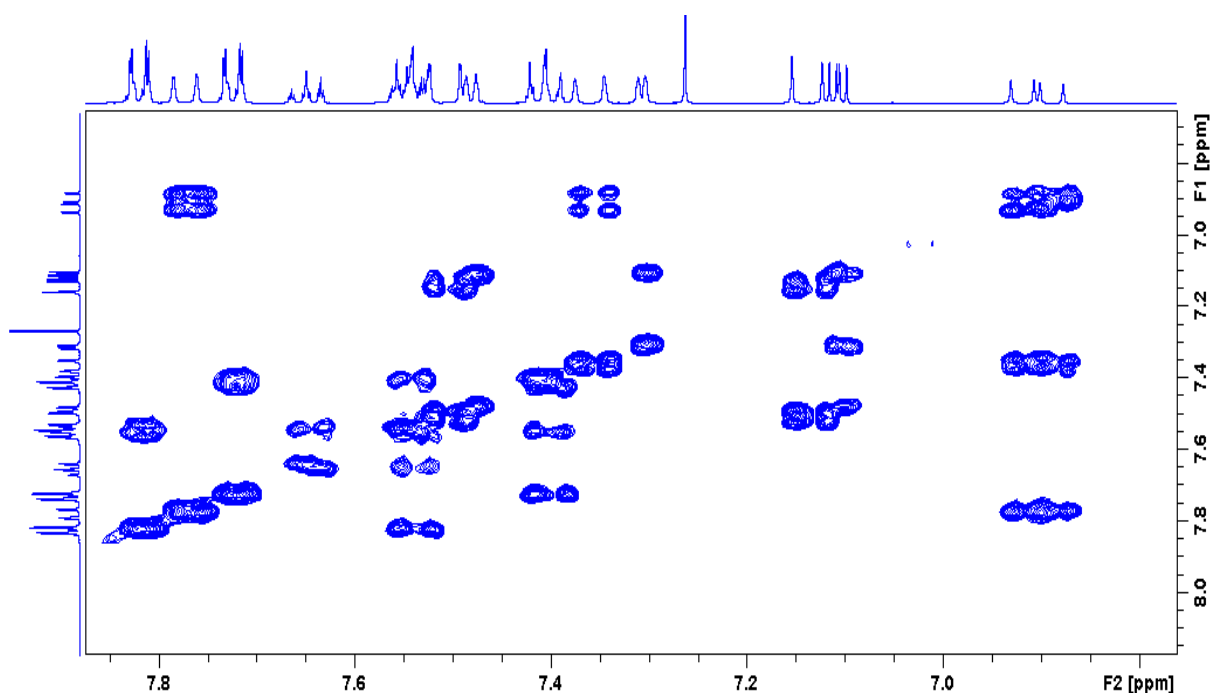


Figure A256 Zoomed in COSY spectrum of (1*E*,3*E*,5*E*)-1,3-bis-phenylsulfonyl-6-(2-thiophene)-hexa-1,3,5-triene, 120

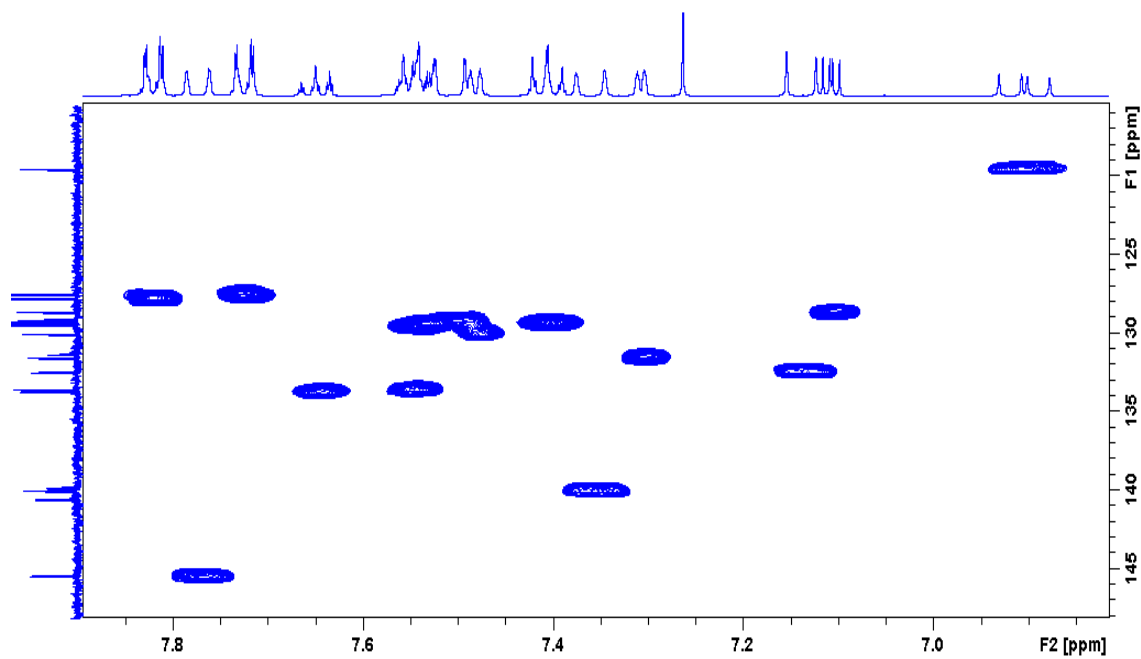


Figure A257. Zoomed in HSQC spectrum of (1*E*,3*E*,5*E*)-1,3-bis-phenylsulfonyl-6-(2-thiophene)-hexa-1,3,5-triene, **120**

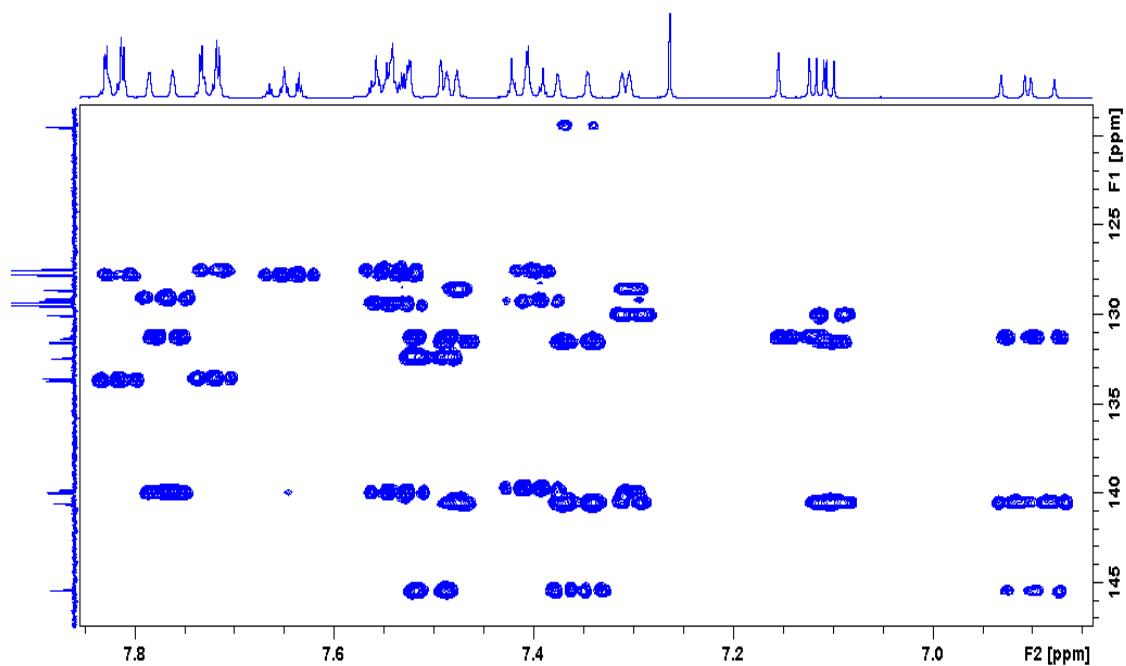


Figure A258. Zoomed in HMBC spectrum of (1*E*,3*E*,5*E*)-1,3-bis-phenylsulfonyl-6-(2-thiophene)-hexa-1,3,5-triene, **120**

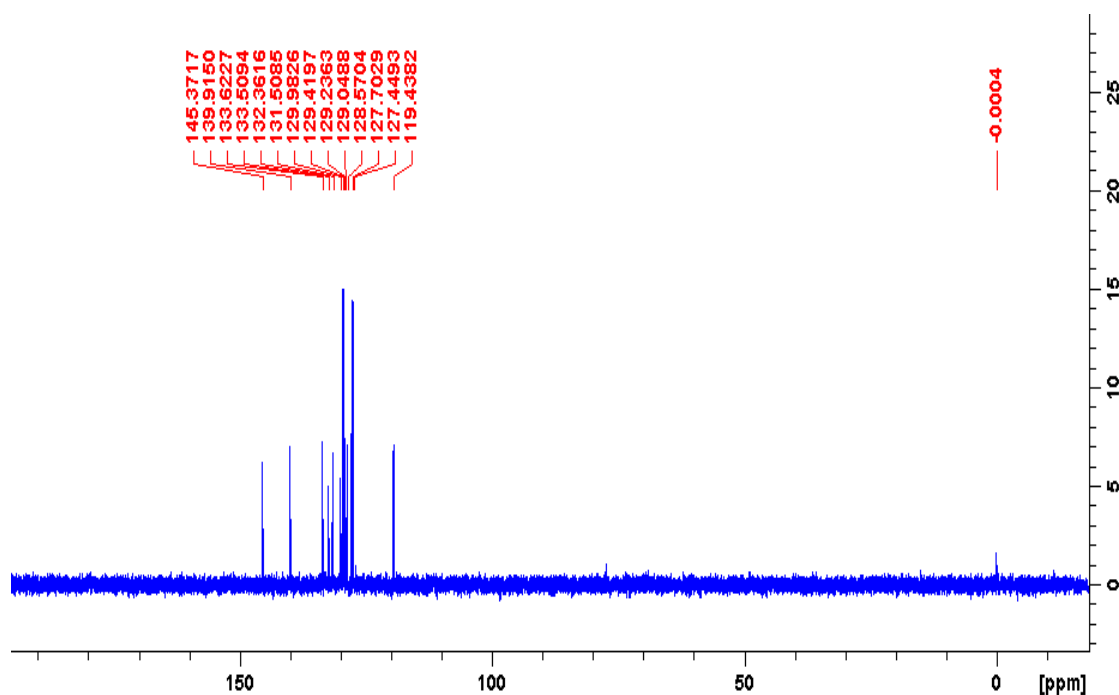


Figure A259. DEPT-135 spectrum of (1*E*,3*E*,5*E*)-1,3-bis-phenylsulfonyl-6-(2-thiophene)-hexa-1,3,5-triene, **120**

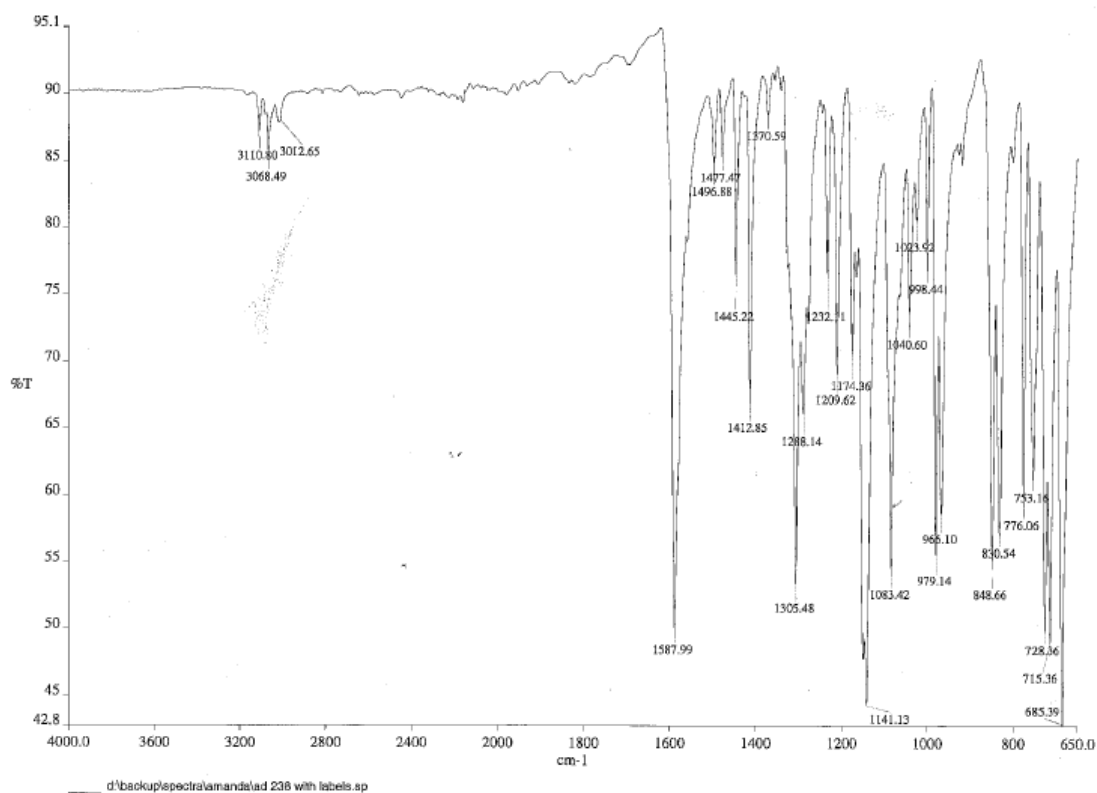


Figure A260. IR spectrum of (1*E*,3*E*,5*E*)-1,3-bis-phenylsulfonyl-6-(2-thiophene)-hexa-1,3,5-triene, **120**

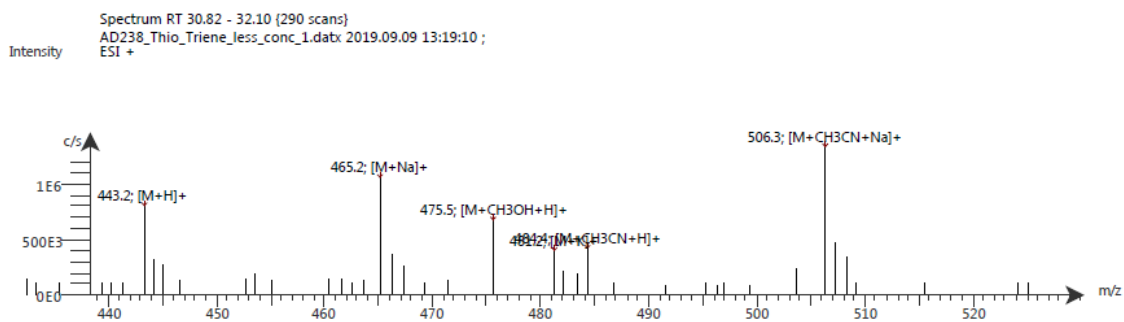
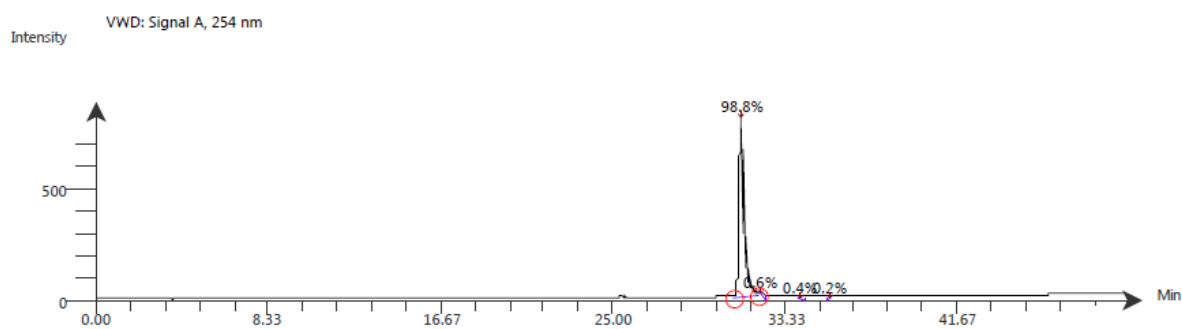


Figure A261. LC-ESI-MS spectrum of (1*E*,3*E*,5*E*)-1,3-bis-phenylsulfonyl-6-(2-thiophene)-hexa-1,3,5-triene, **120**. The ESI spectrum shows it has m/z $[M+Na]^+$ 465.2



Time (Peak Maximum M:S/Minutes)	Maximum Intensity (c/s)	Time (Peak Centroid M:S/Minutes)	Peak Area	% Peak Area	Peak Resolution Label
31.16	8E2	31.17	1.3E4	98.8	13.9
32.13	6.9E-2	32.20	8.1E1	0.6	15.4
34.03	1.3E-1	34.12	5.6E1	0.4	19.5
35.45	7.3E0	35.48	2.5E1	0.2	6.1

Figure A262. LC-UV-MS spectrum of (1*E*,3*E*,5*E*)-1,3-bis-phenylsulfonyl-6-(2-thiophene)-hexa-1,3,5-triene, **120**

Compound Table

Compound Label	RT (min)	Observed mass (m/z)	Neutral observed mass (Da)	Theoretical mass (Da)	Mass error (ppm)	Isotope match score (%)
Cpd 1: C22 H18 O4 S3	0.79	465.0262	442.0369	442.0367	0.46	92.26

Mass errors of between -5.00 and 5.00 ppm with isotope match scores above 60% are considered confirmation of molecular formulae

Figure A263. HR-MS analysis of (1*E*,3*E*,5*E*)-1,3-bis-phenylsulfonyl-6-(2-thiophene)-hexa-1,3,5-triene

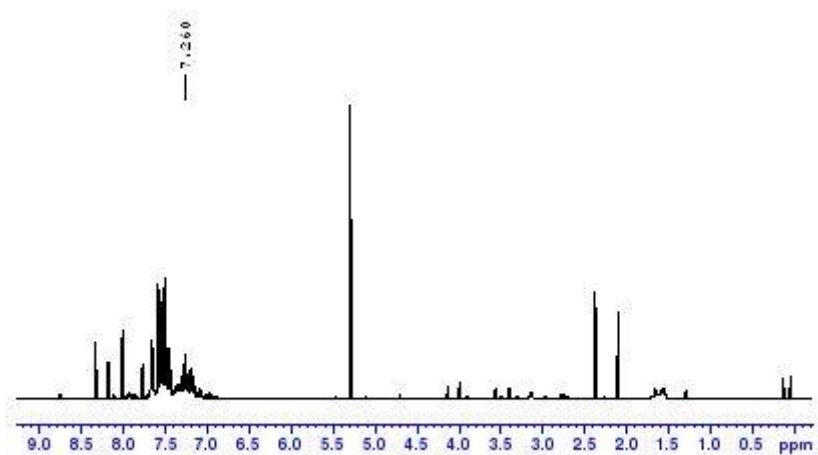


Figure A264. Crude ^1H NMR spectrum containing impure $(2E,4E,6E)$ -1-cyano-4-phenylsulfonyl-7-phenyl-hepta-2,4,6-triene, **125**, as part of a complex mixture.

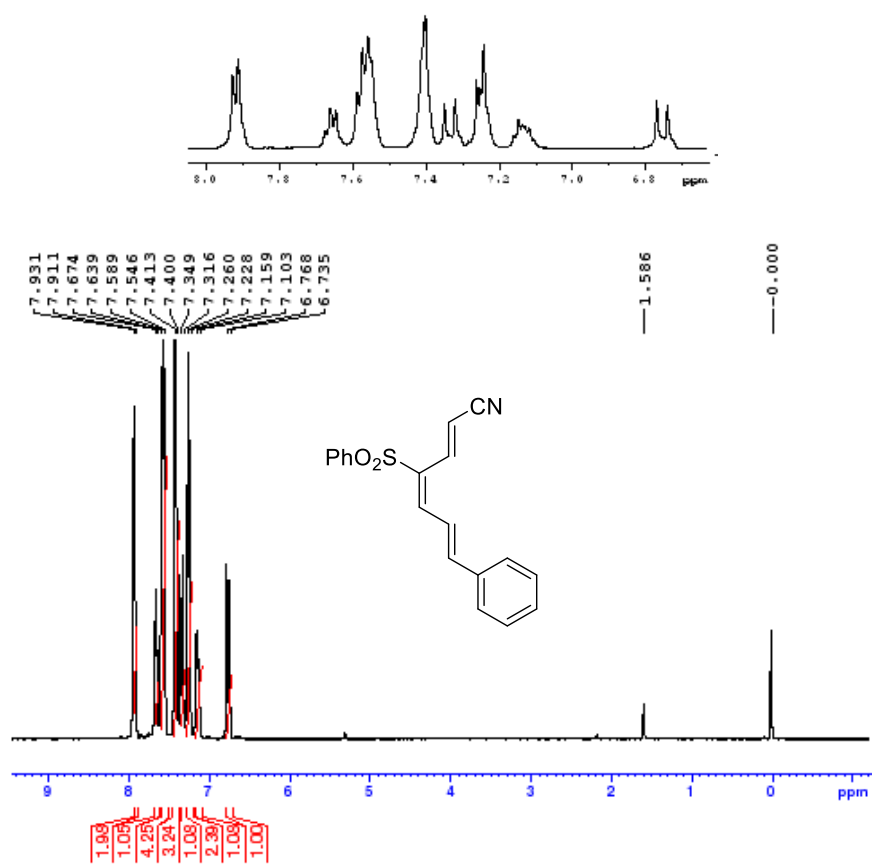


Figure A265. ^1H NMR spectrum of $(2E,4E,6E)$ -1-cyano-4-phenylsulfonyl-7-phenyl-hepta-2,4,6-triene, **125**

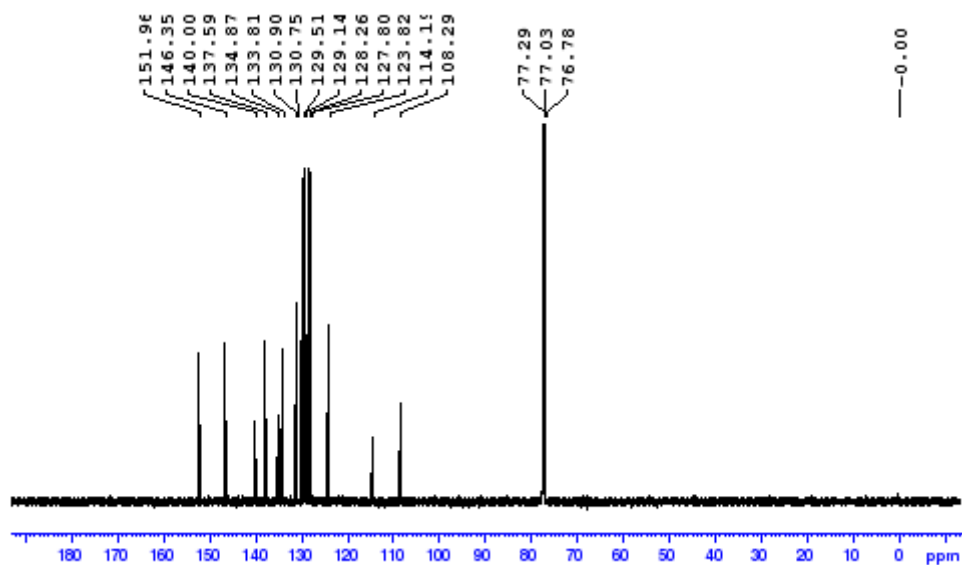


Figure A266. ^{13}C NMR spectrum of (2*E*,4*E*,6*E*)-1-cyano-4-phenylsulfonyl-7-phenyl-hepta-2,4,6-triene, **125**

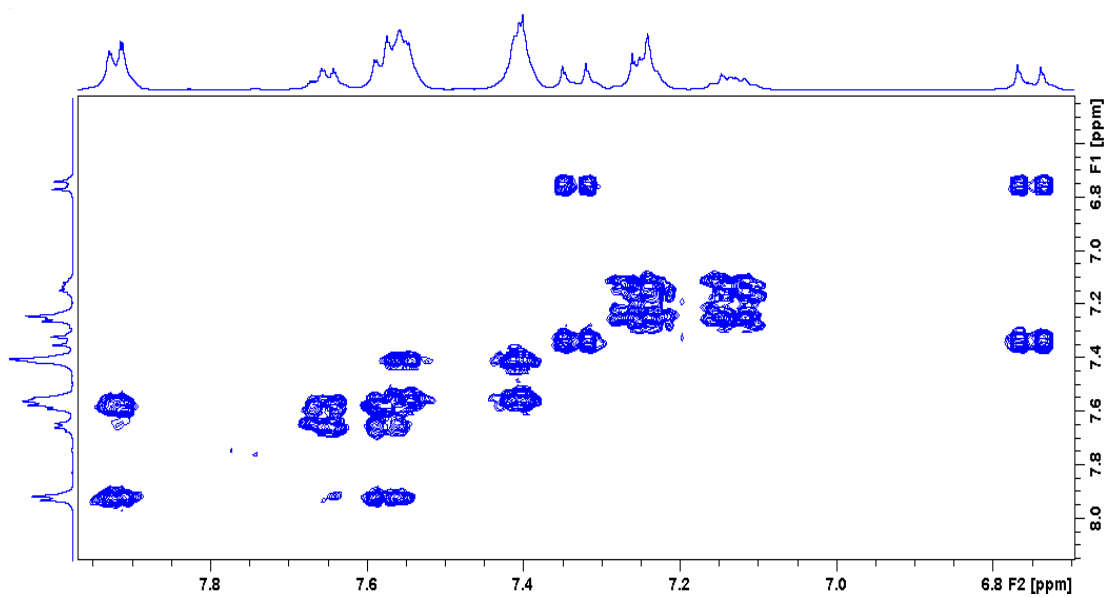


Figure A267. Zoomed in COSY spectrum of (2*E*,4*E*,6*E*)-1-cyano-4-phenylsulfonyl-7-phenyl-hepta-2,4,6-triene, **125**

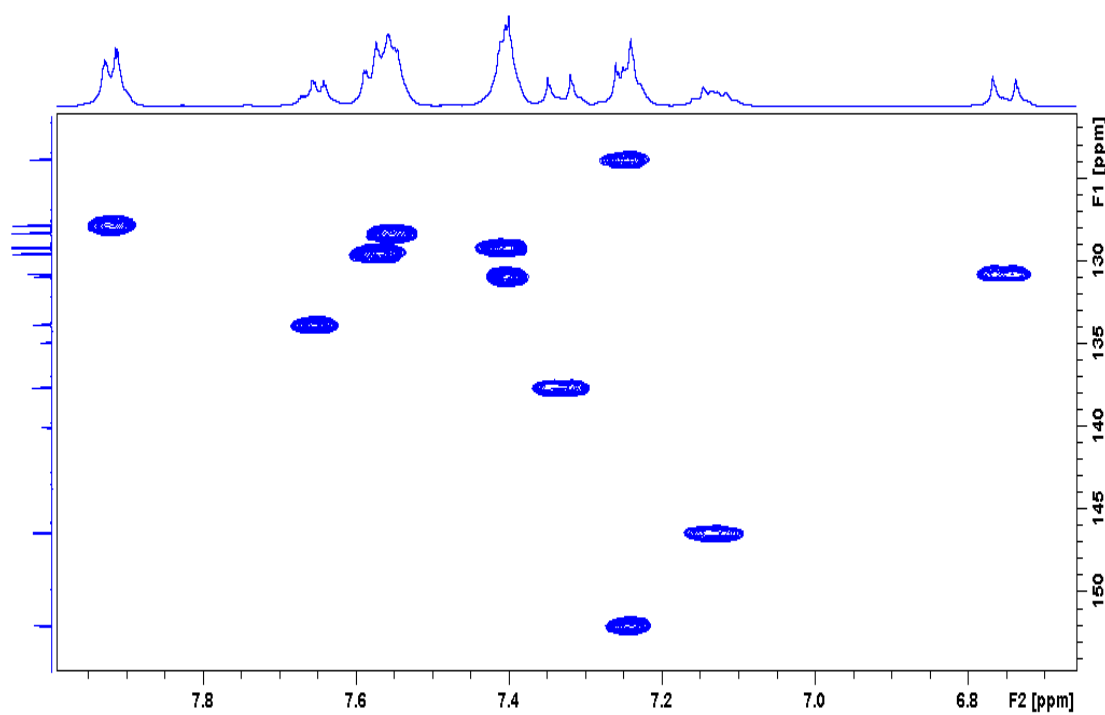


Figure A268. Zoomed in HSQC spectrum of *(2E,4E,6E)*-1-cyano-4-phenylsulfonyl-7-phenyl-hepta-2,4,6-triene, **125**

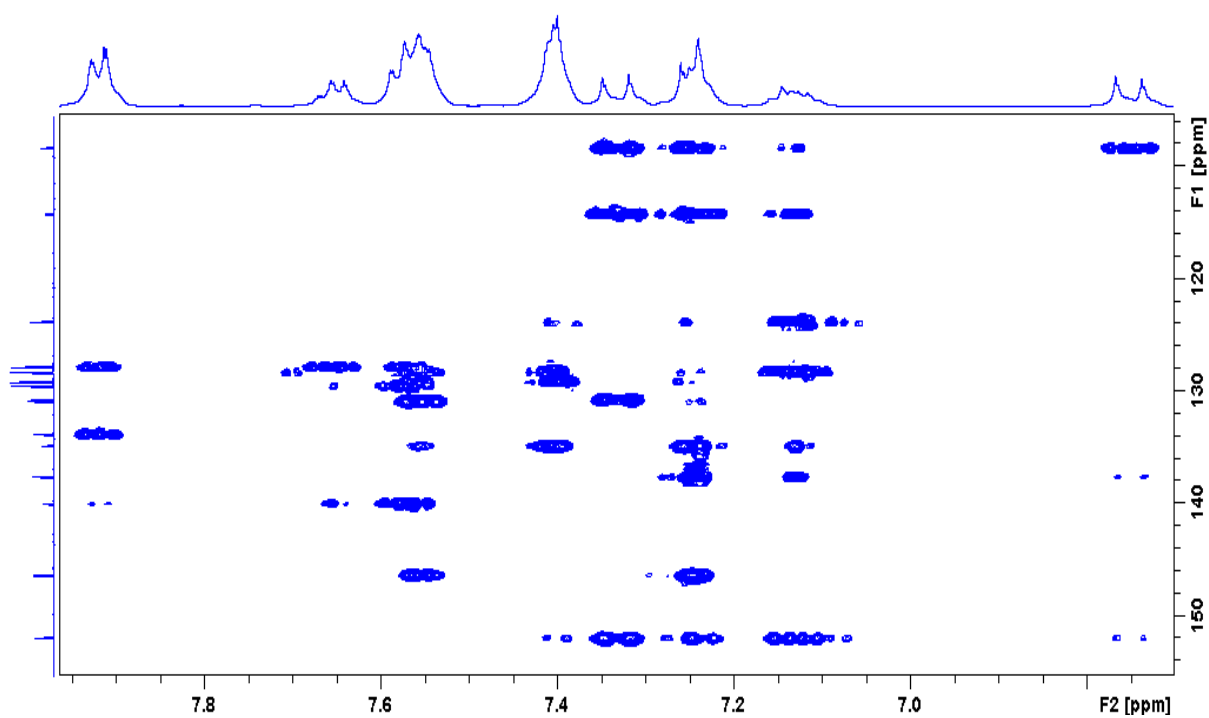


Figure A289. Zoomed in HMBC spectrum of *(2E,4E,6E)*-1-cyano-4-phenylsulfonyl-7-phenyl-hepta-2,4,6-triene, **125**

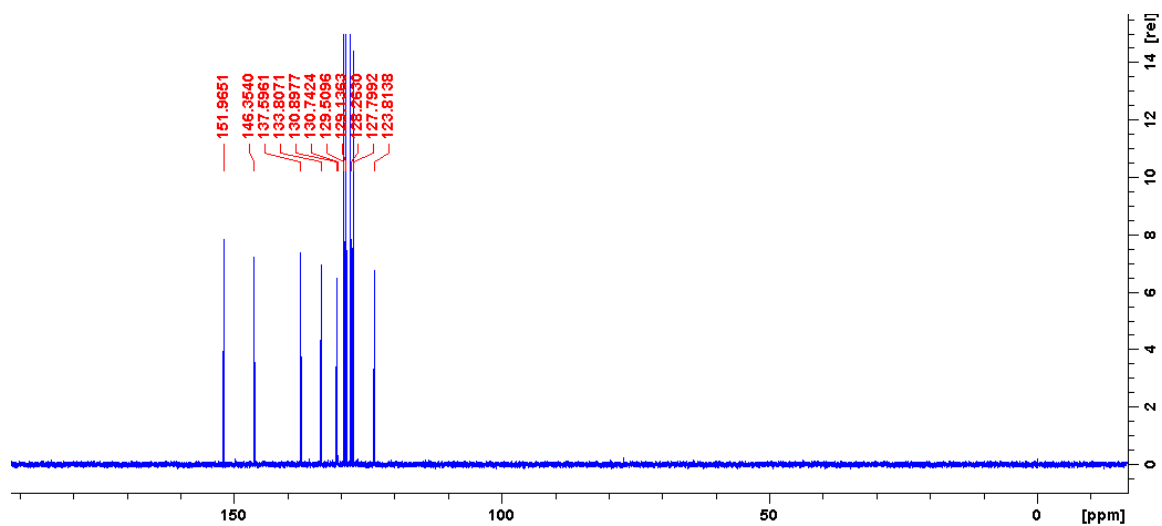


Figure A290. DEPT-135 spectrum of *(2E,4E,6E)*-1-cyano-4-phenylsulfonyl-7-phenyl-hepta-2,4,6-triene, **125**

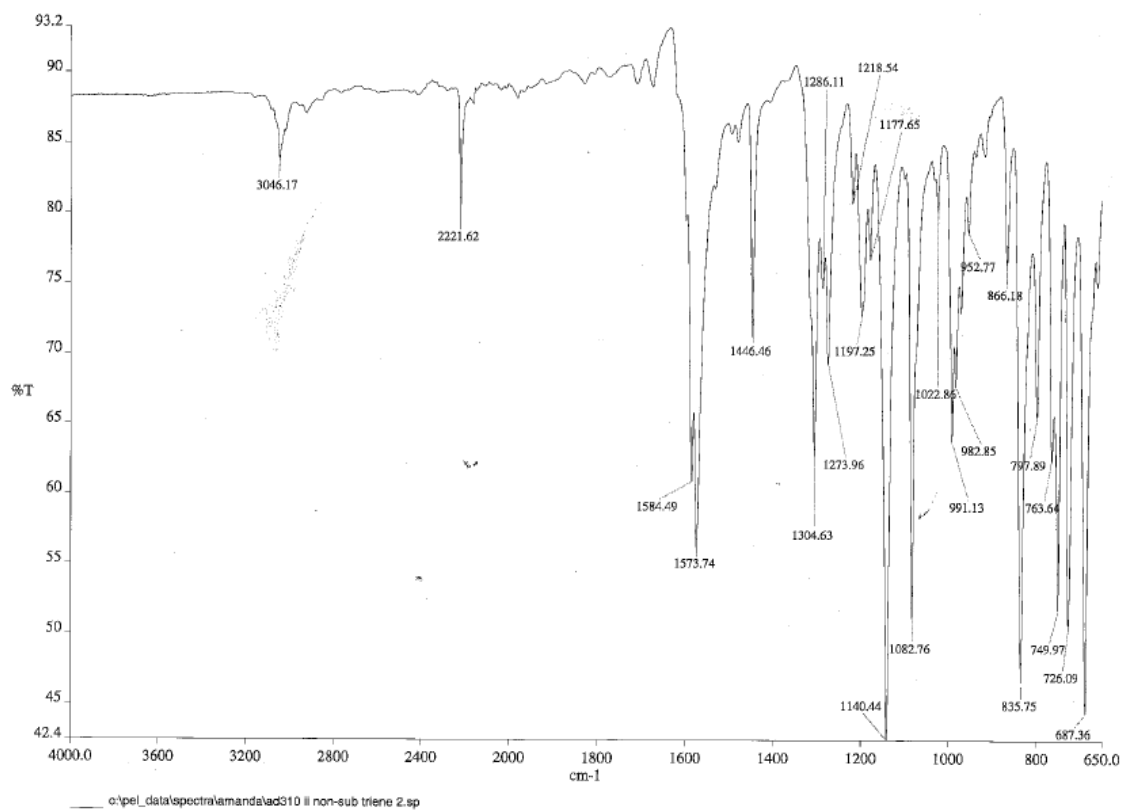


Figure A291. IR spectrum of *(2E,4E,6E)*-1-cyano-4-phenylsulfonyl-7-phenyl-hepta-2,4,6-triene, **125**

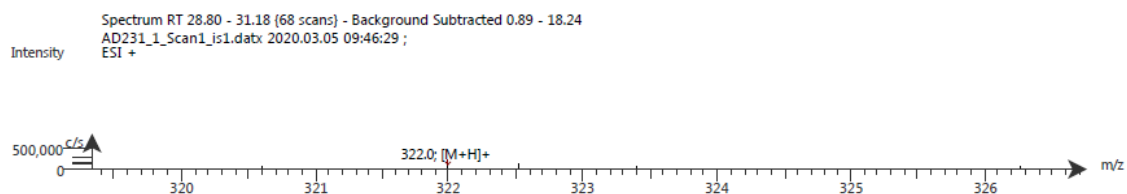
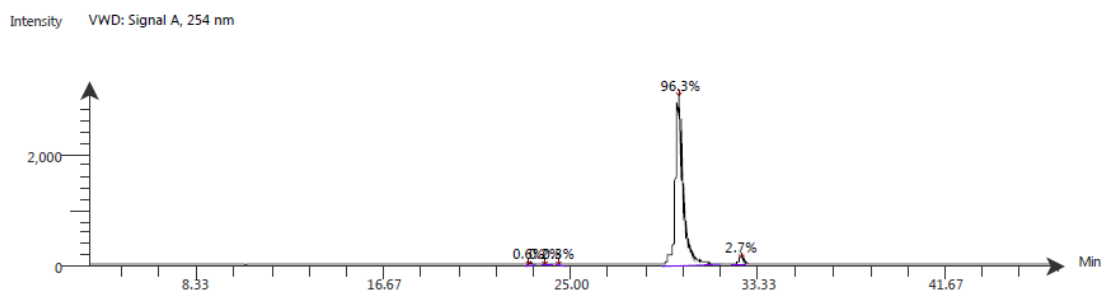


Figure A292. LC-ESI-MS spectrum of (2*E*,4*E*,6*E*)-1-cyano-4-phenylsulfonyl-7-phenyl-hepta-2,4,6-triene, **125**. The ESI spectrum shows it has m/z $[M+H]^+$ 322.0



Time (Peak Maximum M:S/Minutes)	Maximum Intensity (c/s)	Time (Peak Centroid M:S/Minutes)	Peak Area	% Peak Area	Peak Resolution Label
23.11	2.7E1	23.16	4.1E2	0.6	15.4
23.84	9.1E0	23.88	1.1E2	0.2	13.8
24.50	1.6E1	24.52	1.9E2	0.3	12.5
29.76	3E3	29.84	7.1E4	96.3	18.2
32.56	1.5E2	32.55	2E3	2.7	12.6

Figure A293. LC-UV-MS spectrum of (2*E*,4*E*,6*E*)-1-cyano-4-phenylsulfonyl-7-phenyl-hepta-2,4,6-triene, **125**

Compound Table

Compound Label	RT (min)	Observed mass (m/z)	Neutral observed mass (Da)	Theoretical mass (Da)	Mass error (ppm)	Isotope match score (%)
Cpd 1: C19 H15 N O2 S	0.72	344.0719	321.0826	321.0823	0.84	96.49

Figure A294. HR-MS analysis of (2*E*,4*E*,6*E*)-1-cyano-4-phenylsulfonyl-7-phenyl-hepta-2,4,6-triene, **125**

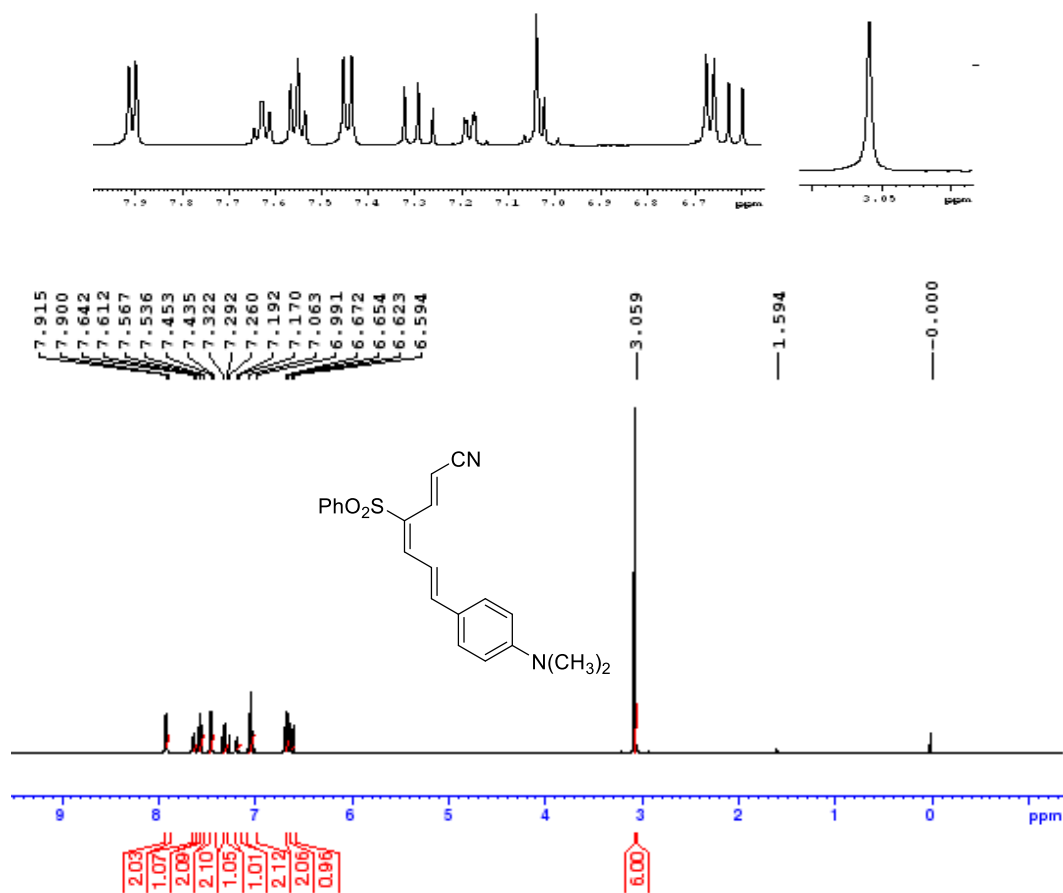


Figure A295. ¹H NMR spectrum of (2E,4E,6E)-1-cyano-4-phenylsulfonyl-7-(p-dimethylaminophenyl)-hepta-2,4,6-triene, **126**

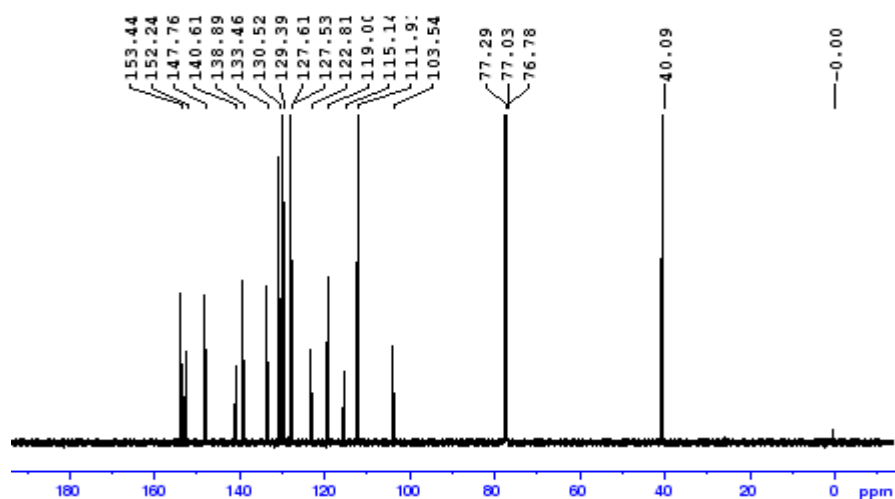


Figure A296. ¹³C NMR spectrum of (2E,4E,6E)-1-cyano-4-phenylsulfonyl-7-(p-dimethylaminophenyl)-hepta-2,4,6-triene, **126**

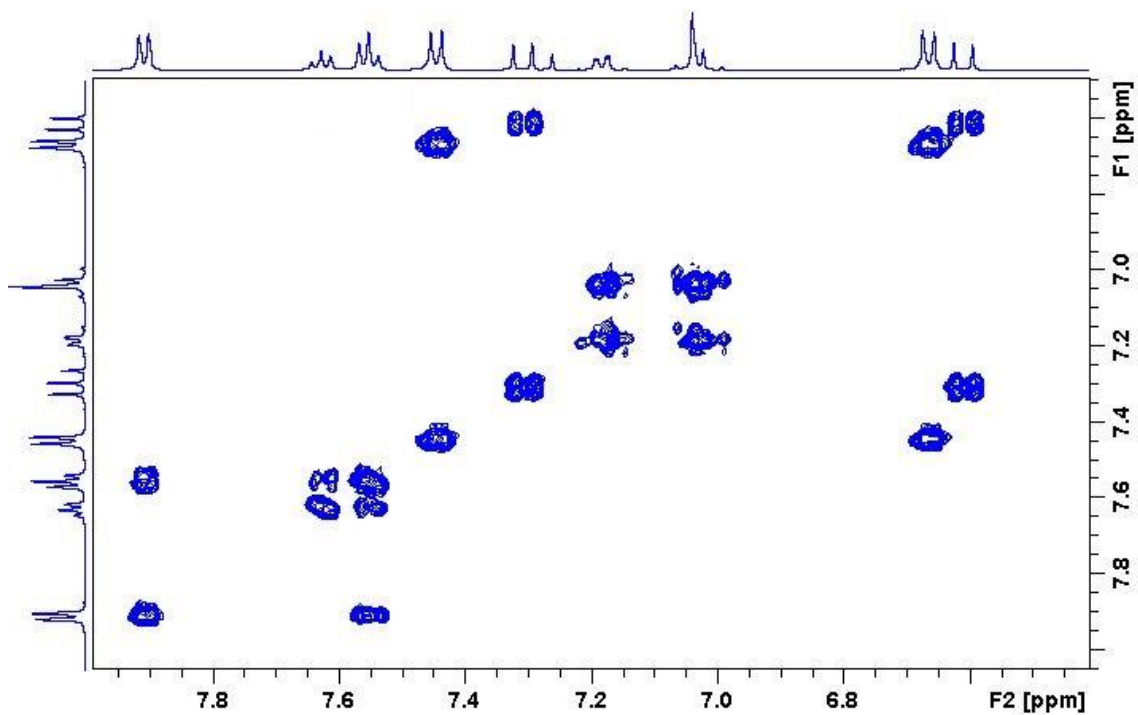


Figure A297. COSY spectrum of *(2E,4E,6E)*-1-cyano-4-phenylsulfonyl-7-(*p*-dimethylaminophenyl)-hepta-2,4,6-triene, **126**

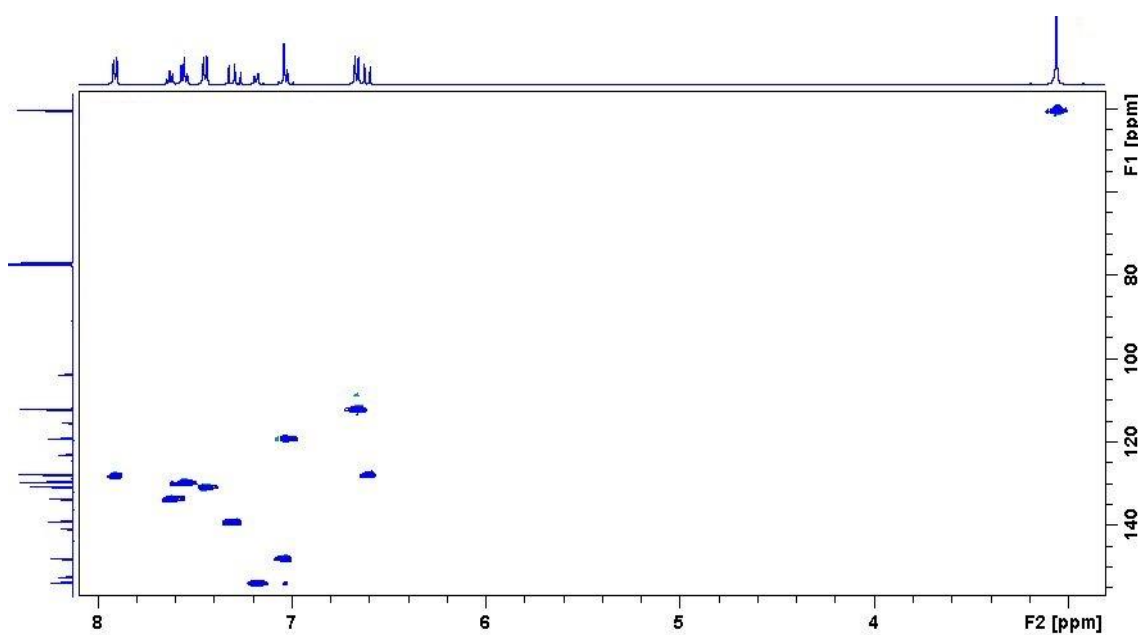


Figure A298. HSQC spectrum of *(2E,4E,6E)*-1-cyano-4-phenylsulfonyl-7-(*p*-dimethylaminophenyl)-hepta-2,4,6-triene, **126**

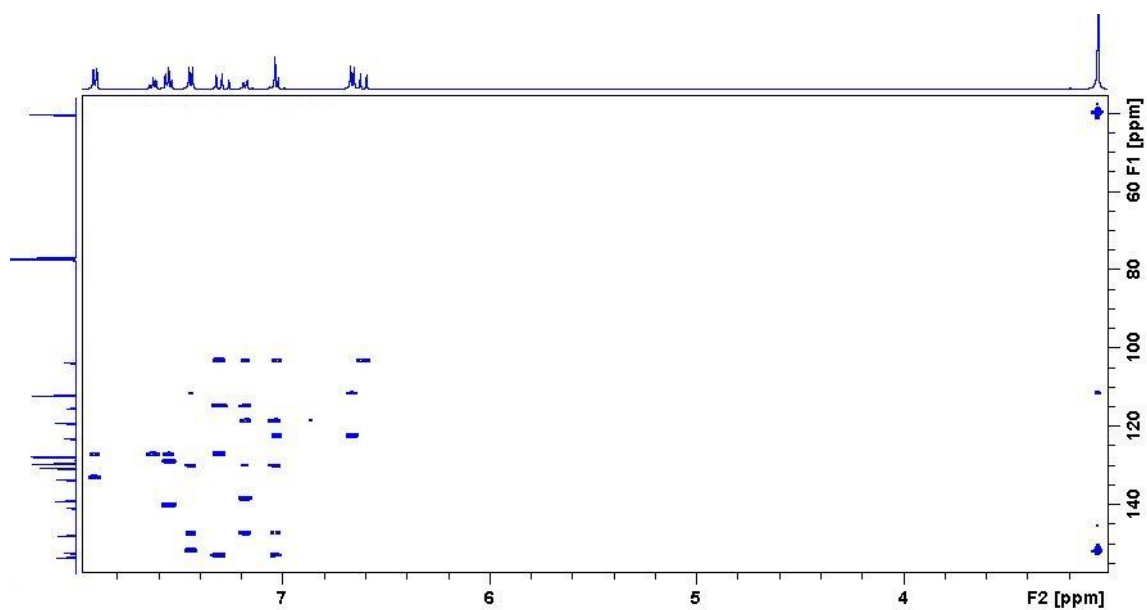


Figure A299. HMBC spectrum of *(2E,4E,6E)*-1-cyano-4-phenylsulfonyl-7-(*p*-dimethylaminophenyl)hepta-2,4,6-triene, **126**

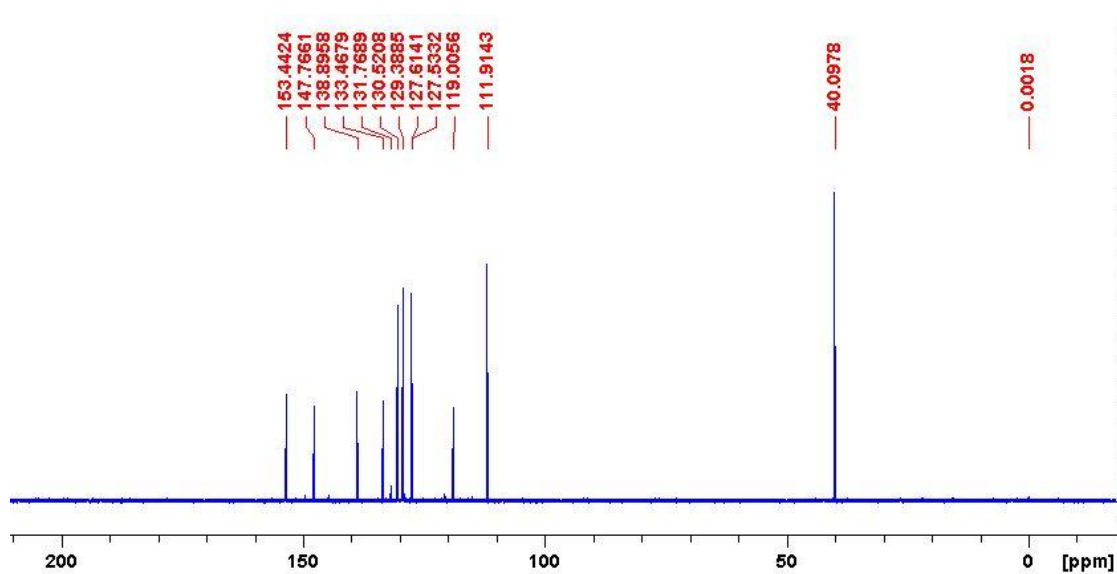


Figure A300. DEPT-135 spectrum of *(2E,4E,6E)*-1-cyano-4-phenylsulfonyl-7-(*p*-dimethylaminophenyl)hepta-2,4,6-triene, **126**

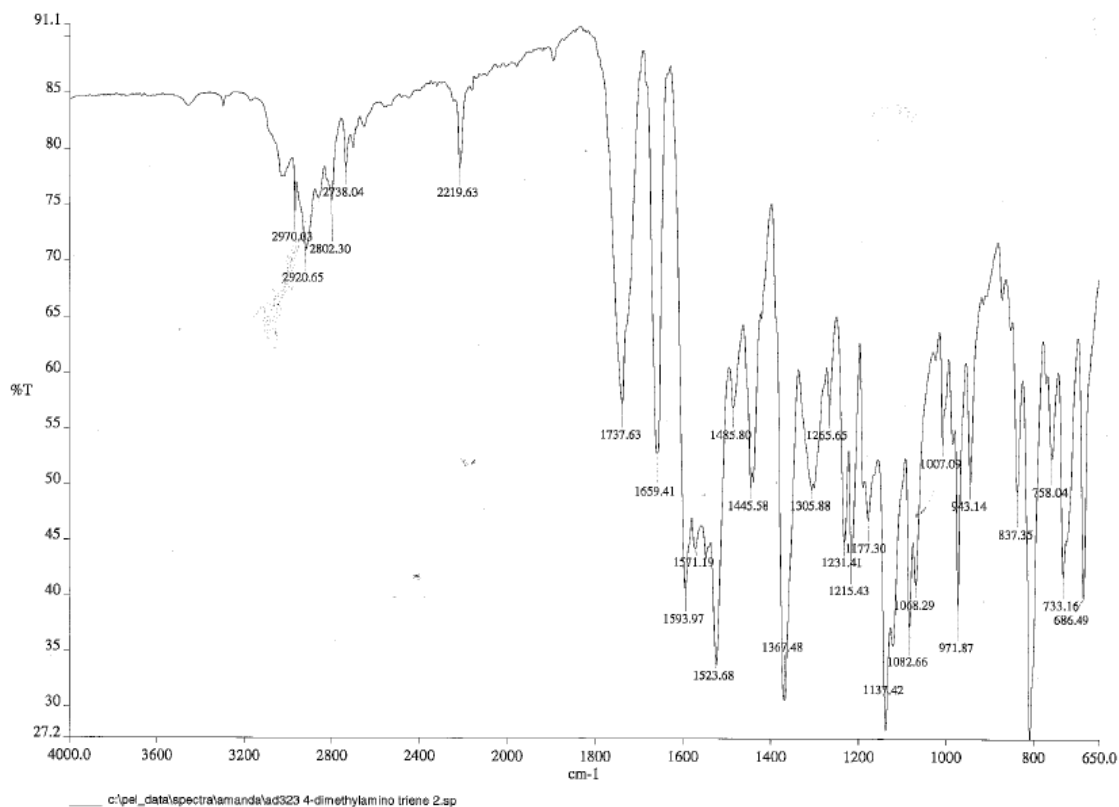


Figure A301. IR spectrum of (2E,4E,6E)-1-cyano-4-phenylsulfonyl-7-(p-dimethylaminophenyl)-hepta-2,4,6-triene, **126**

Compound Table

Compound Label	RT (min)	Observed mass (m/z)	Neutral observed mass (Da)	Theoretical mass (Da)	Mass error (ppm)	Isotope match score (%)
Cpd 1: C21 H20 N2 O2 S	0.73	365.1319	364.1246	364.1245	0.11	95.58

Figure A302. HR-MS analysis of (2E,4E,6E)-1-cyano-4-phenylsulfonyl-7-(p-dimethylamino)-hepta-2,4,6-triene, **126**

LC-MS data for compound **126** is not included because this compound degraded on the column, therefore the associated data could not be obtained.

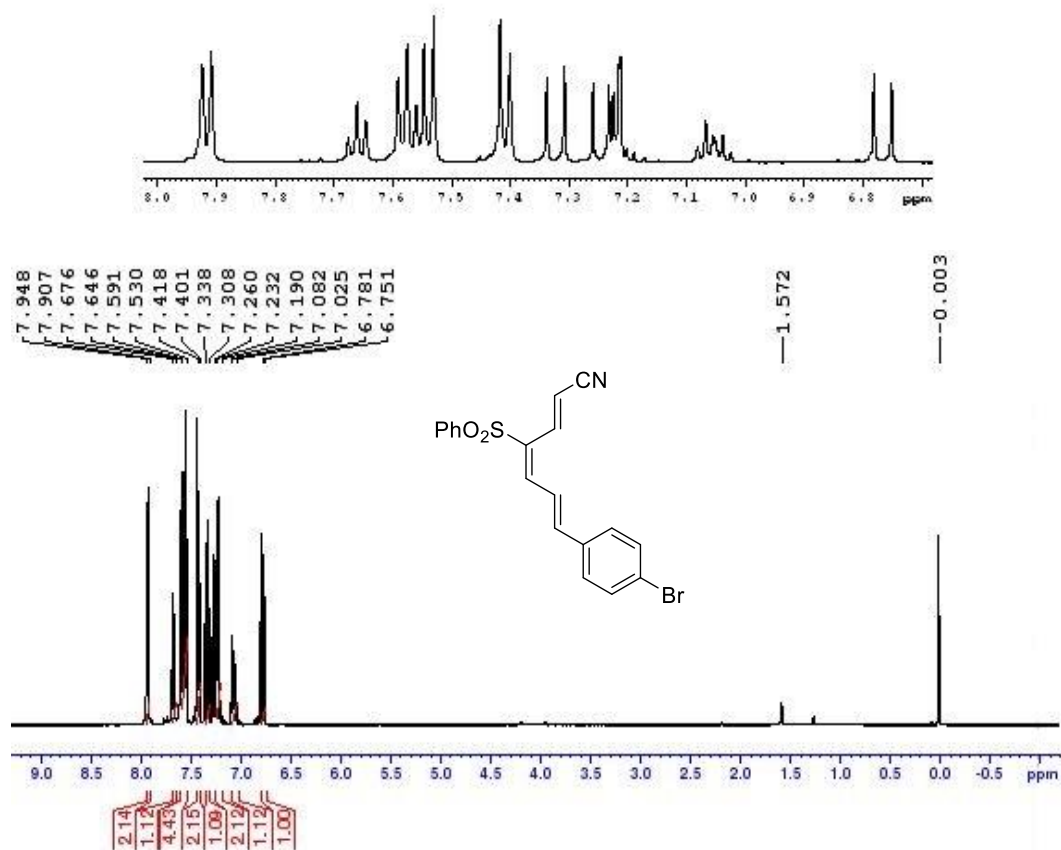


Figure A303. ¹H NMR spectrum of (2E,4E,6E)-1-cyano-4-phenylsulfonyl-7-(p-bromophenyl)-hepta-2,4,6-triene, **127**

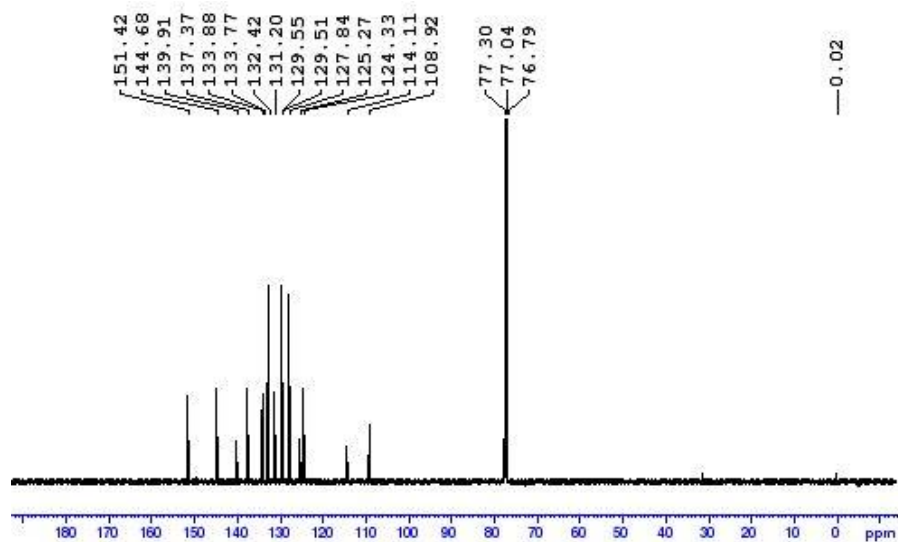


Figure A304. ¹³C NMR spectrum of (2E,4E,6E)-1-cyano-4-phenylsulfonyl-7-(p-bromophenyl)-hepta-2,4,6-triene, **127**

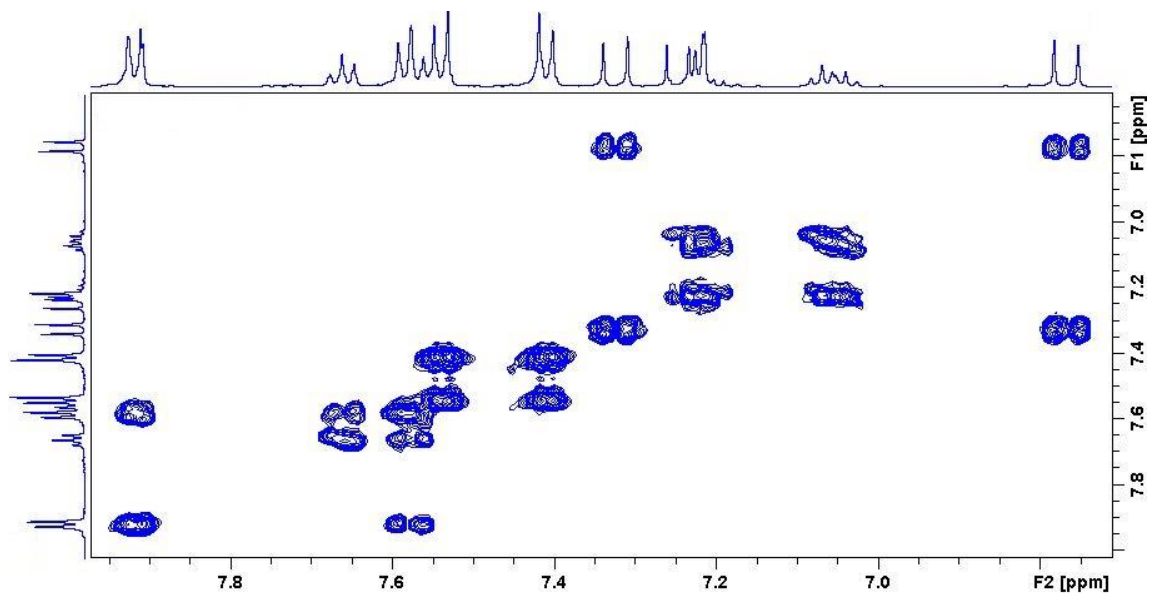


Figure A305. COSY spectrum of *(2E,4E,6E)*-1-cyano-4-phenylsulfonyl-7-(*p*-bromophenyl)-hepta-2,4,6-triene, **127**

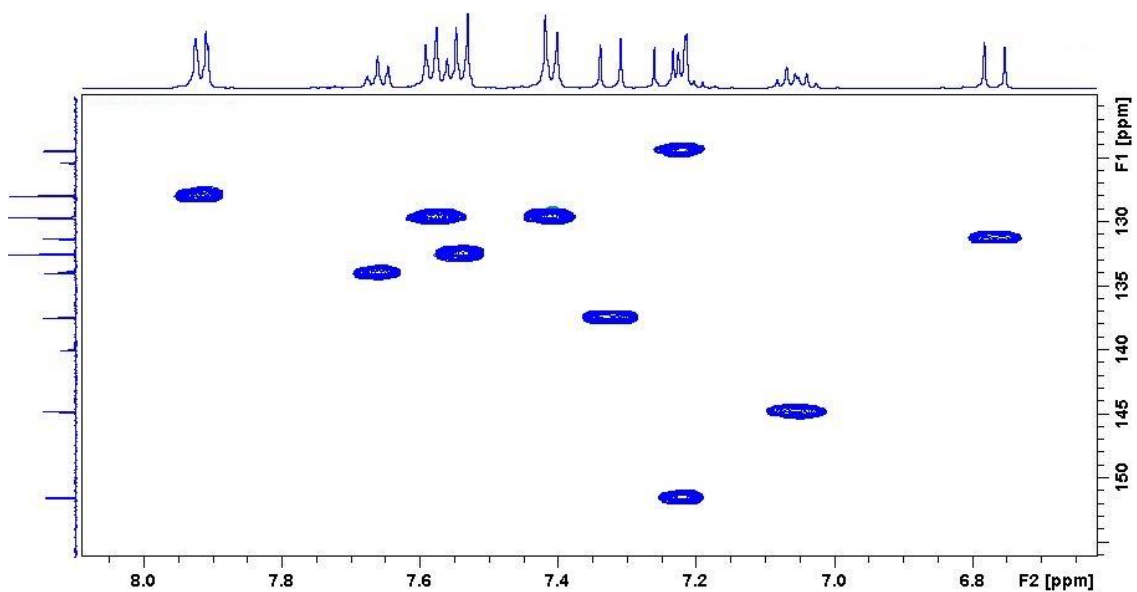


Figure A306. HSQC spectrum of *(2E,4E,6E)*-1-cyano-4-phenylsulfonyl-7-(*p*-bromophenyl)-hepta-2,4,6-triene, **127**

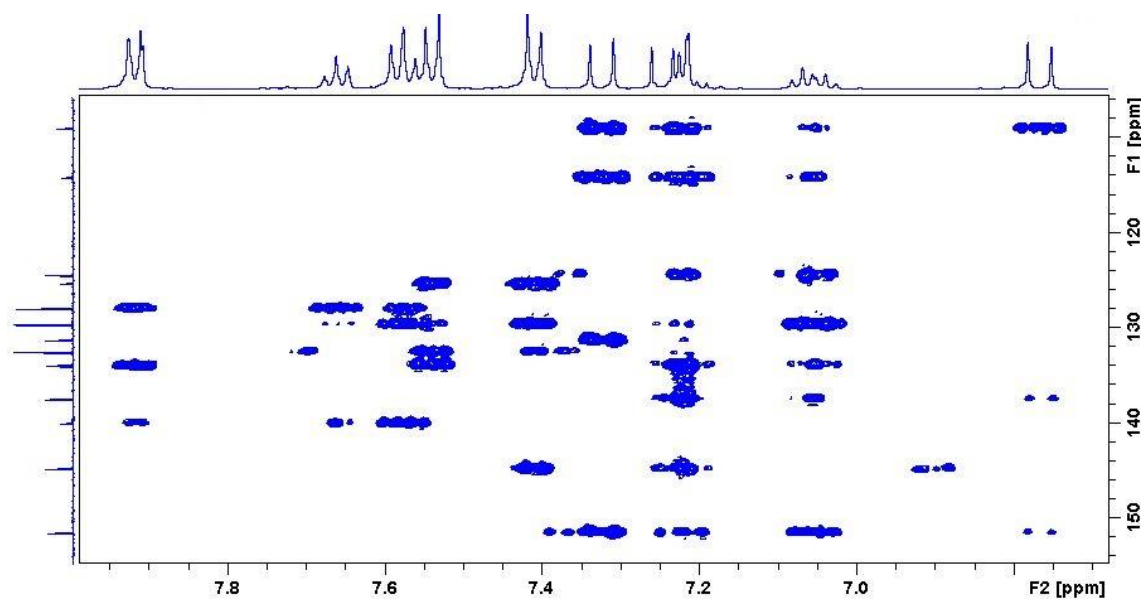


Figure A307. HMBC spectrum of *(2E,4E,6E)*-1-cyano-4-phenylsulfonyl-7-(*p*-bromophenyl)-hepta-2,4,6-triene, **127**

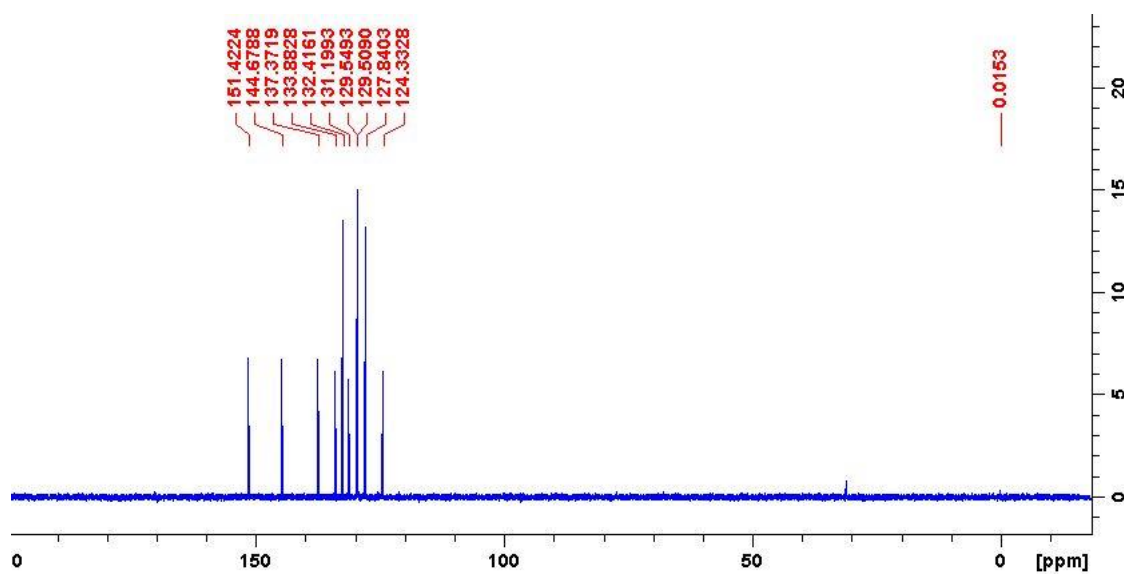


Figure A308. DEPT-135 spectrum of *(2E,4E,6E)*-1-cyano-4-phenylsulfonyl-7-(*p*-bromophenyl)-hepta-2,4,6-triene, **127**

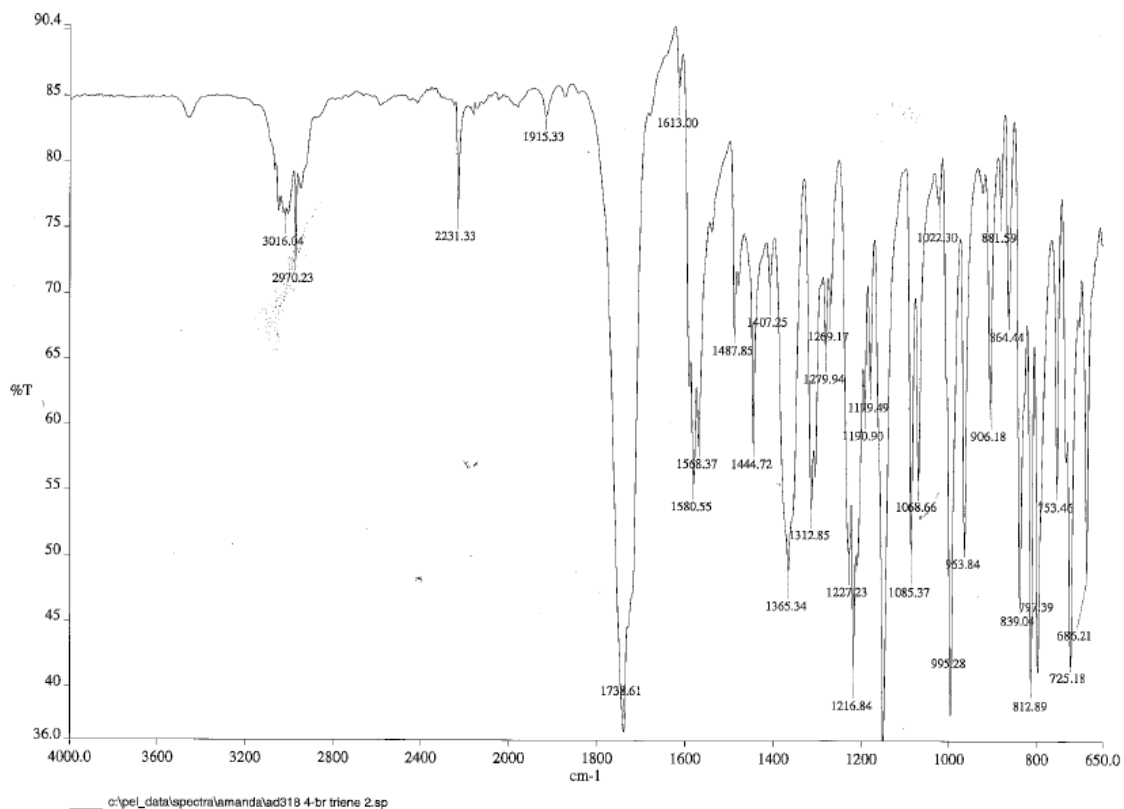


Figure A309. IR spectrum of (2*E*,4*E*,6*E*)-1-cyano-4-phenylsulfonyl-7-(*p*-bromophenyl)-hepta-2,4,6-triene, **127**

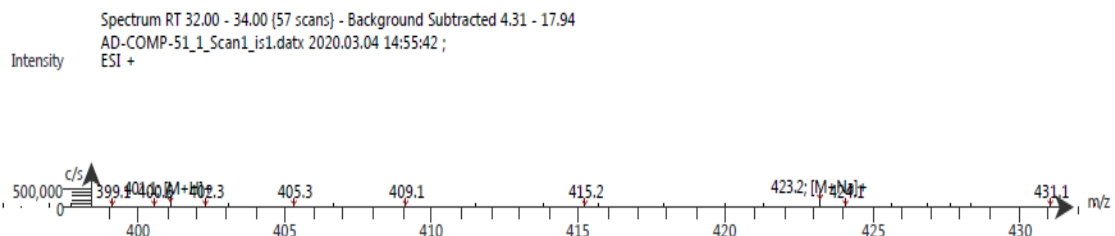


Figure A310. LC-ESI-MS spectrum of (2*E*,4*E*,6*E*)-1-cyano-4-phenylsulfonyl-7-(*p*-bromophenyl)-hepta-2,4,6-triene, **127**. The ESI spectrum shows it has m/z [M+Na]⁺ 423.2

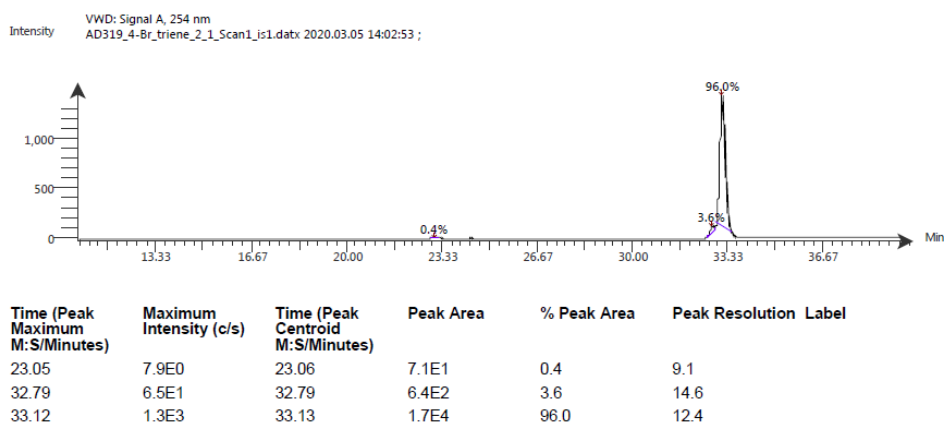


Figure A311. LC-UV-MS spectrum of (2*E*,4*E*,6*E*)-1-cyano-4-phenylsulfonyl-7-(*p*-bromophenyl)-hepta-2,4,6-triene, **127**

Compound Table

Compound Label	RT (min)	Observed mass (m/z)	Neutral observed mass (Da)	Theoretical mass (Da)	Mass error (ppm)	Isotope match score (%)
Cpd 1: C19 H14 Br N O2 S	0.71	423.9800	398.9927	398.9929	-0.40	98.65

Figure A312. HR-MS analysis of (2*E*,4*E*,6*E*)-1-cyano-4-phenylsulfonyl-7-(*p*-bromophenyl)-hepta-2,4,6-triene, **127**

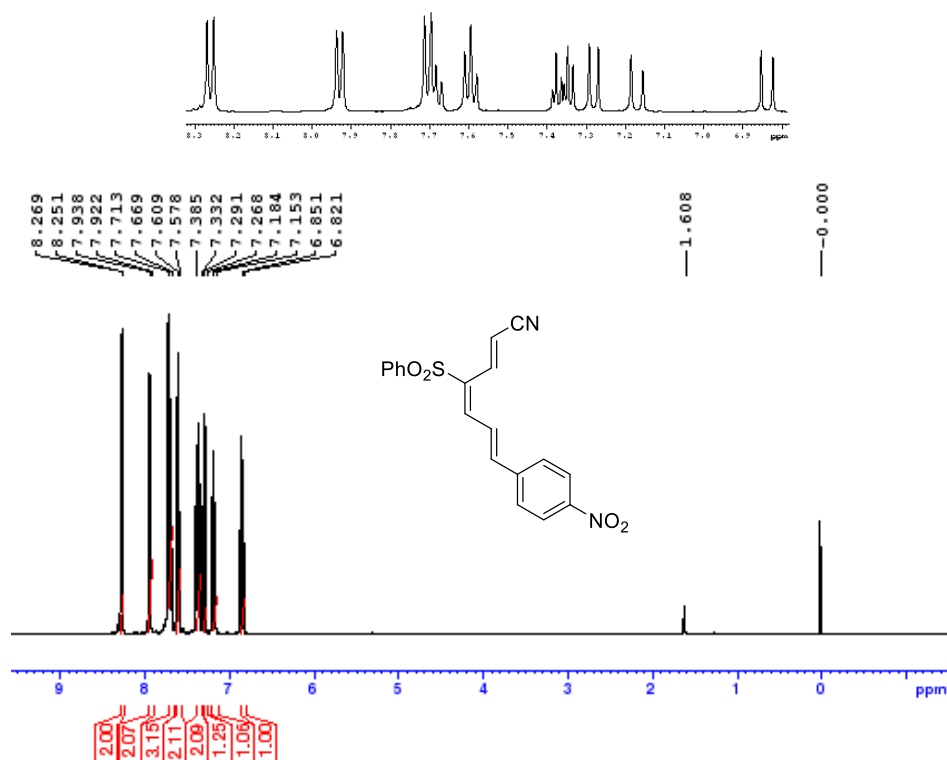


Figure A313. ¹H NMR spectrum of (2*E*,4*E*,6*E*)-1-cyano-4-phenylsulfonyl-7-(*p*-nitrophenyl)-hepta-2,4,6-triene, **128**

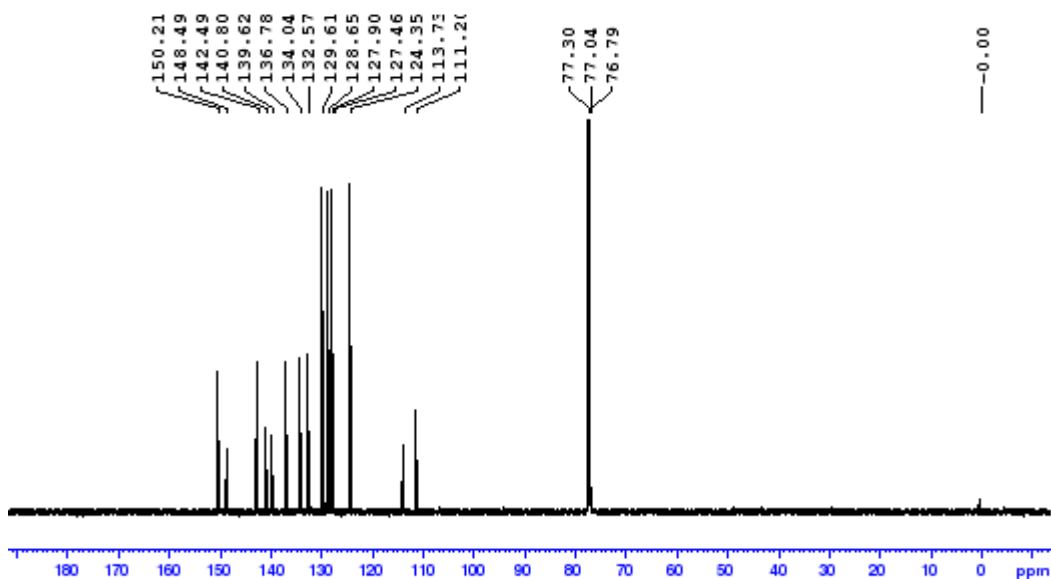


Figure A314. ^{13}C NMR spectrum of $(2E,4E,6E)$ -1-cyano-4-phenylsulfonyl-7-(*p*-nitrophenyl)-hepta-2,4,6-triene, **128**

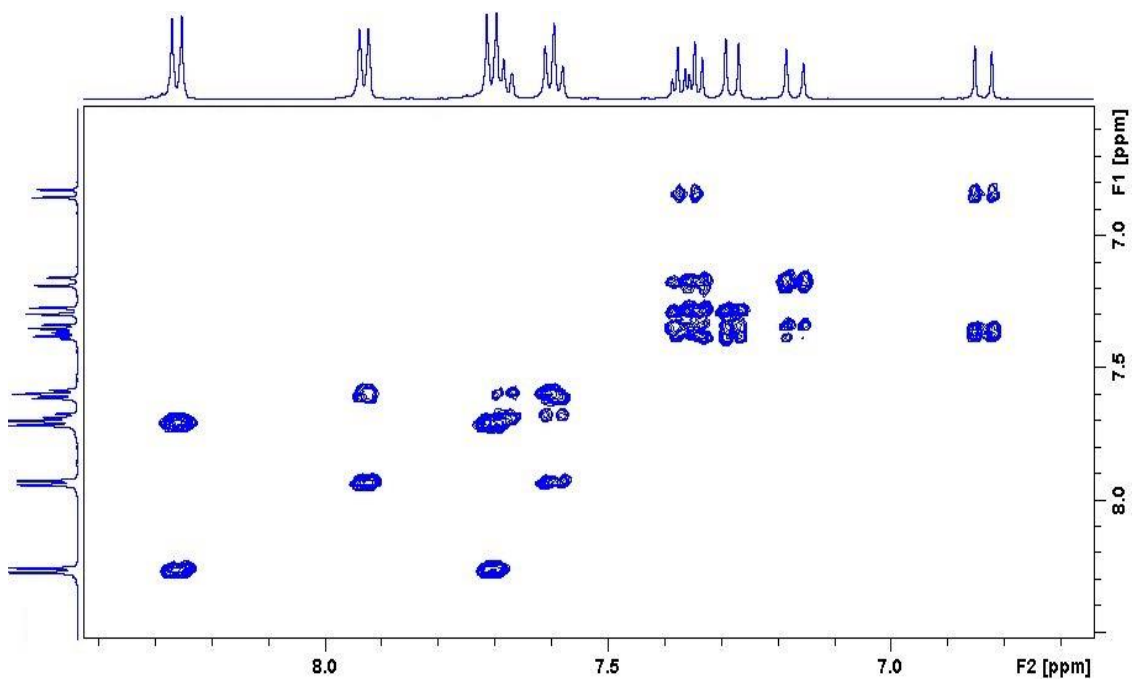


Figure A315. Zoomed in COSY spectrum of $(2E,4E,6E)$ -1-cyano-4-phenylsulfonyl-7-(*p*-nitrophenyl)-hepta-2,4,6-triene, **128**

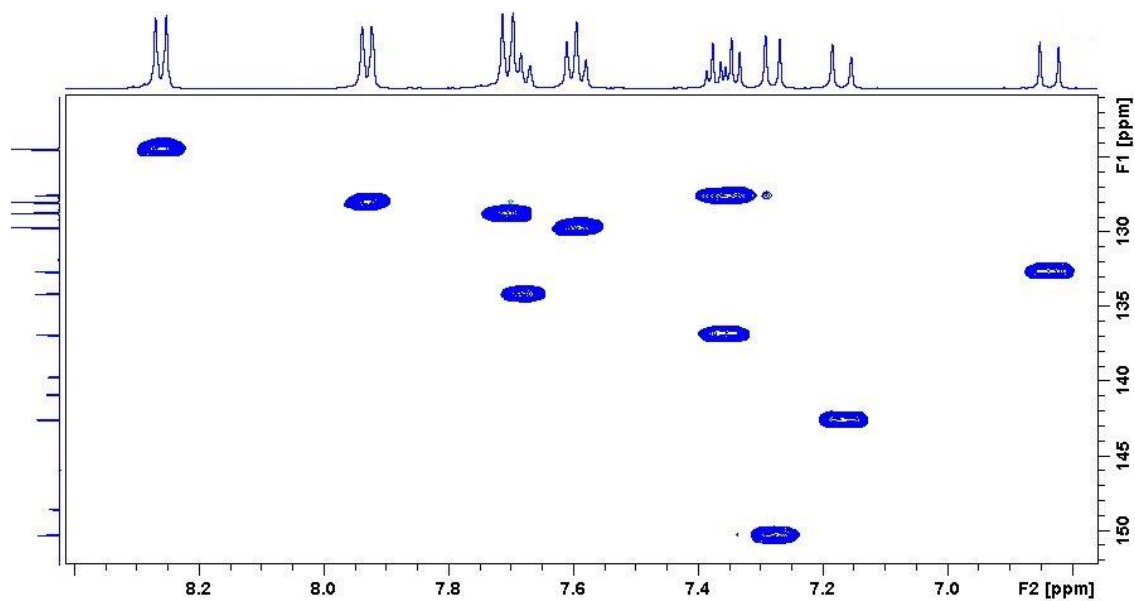


Figure A316. Zoomed in HSQC spectrum of (2*E*,4*E*,6*E*)-1-cyano-4-phenylsulfonyl-7-(*p*-nitrophenyl)-hepta-2,4,6-triene, **128**

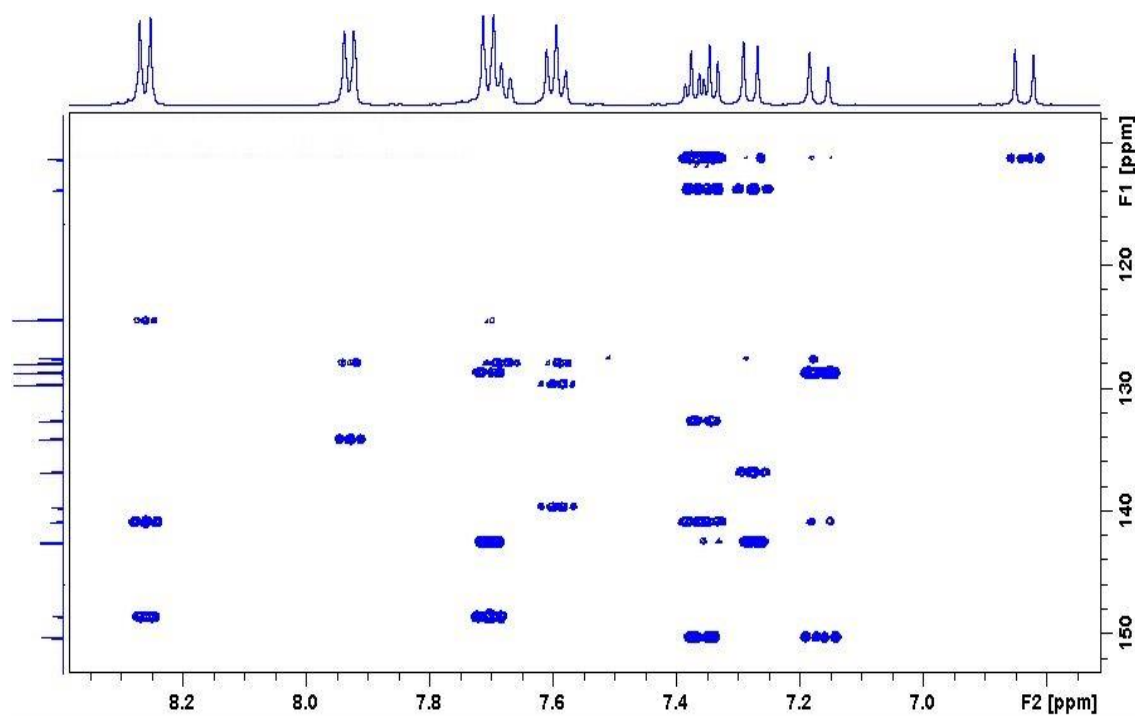


Figure A317. Zoomed in HMBC spectrum of (2*E*,4*E*,6*E*)-1-cyano-4-phenylsulfonyl-7-(*p*-nitrophenyl)-hepta-2,4,6-triene, **128**

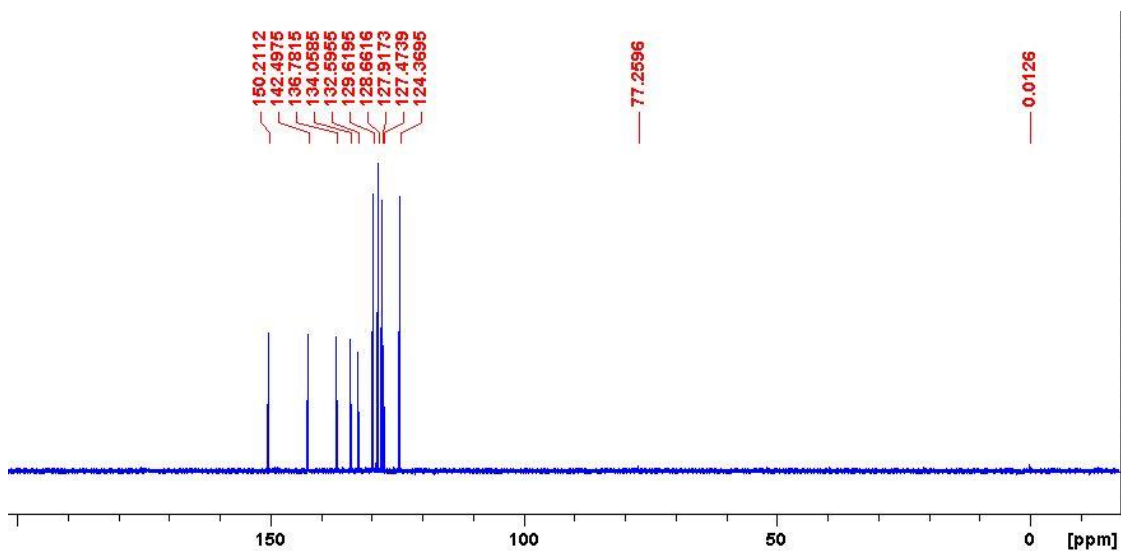


Figure A318. DEPT-135 spectrum of (2*E*,4*E*,6*E*)-1-cyano-4-phenylsulfonyl-7-(*p*-nitrophenyl)-hepta-2,4,6-triene, **128**

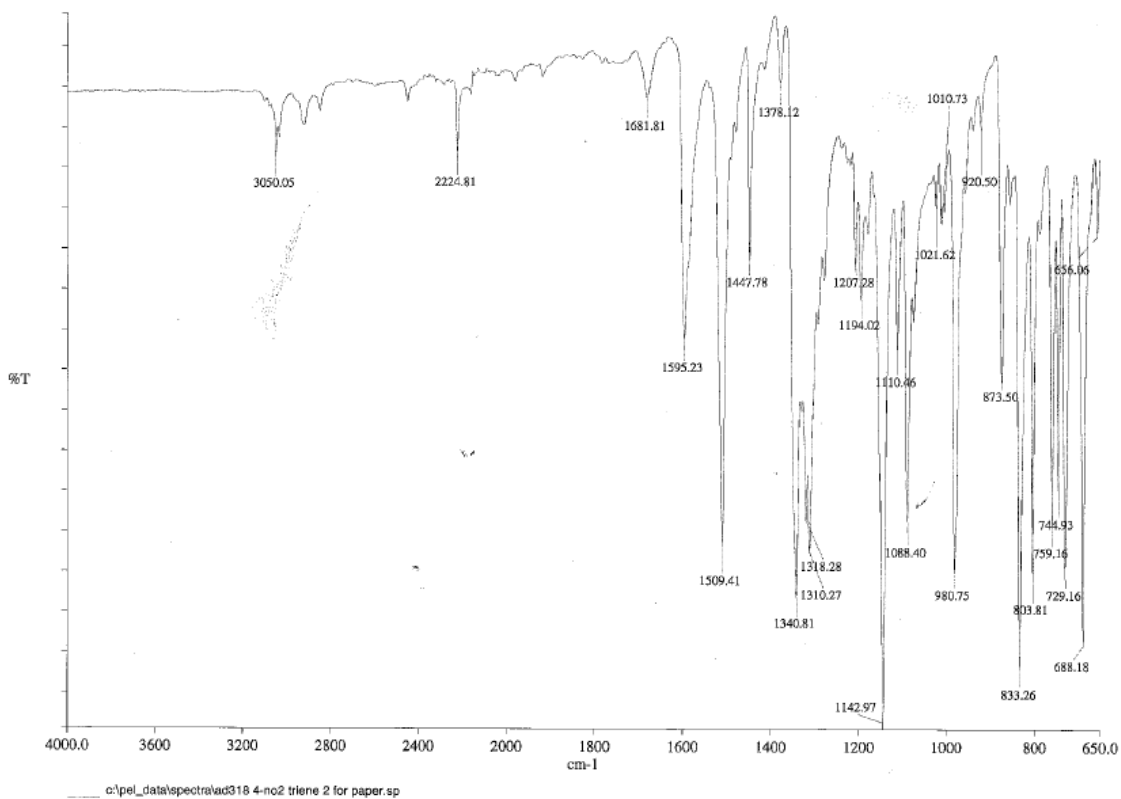


Figure A319. IR spectrum of (2*E*,4*E*,6*E*)-1-cyano-4-phenylsulfonyl-7-(*p*-nitrophenyl)-hepta-2,4,6-triene, **128**

Spectrum RT 29.71 - 31.70 (57 scans) - Background Subtracted 2.28 - 16.29
 AD-COMP-50_1_Scan1_is1.datx 2020.03.04 13:58:48 ;
 Intensity ESI +

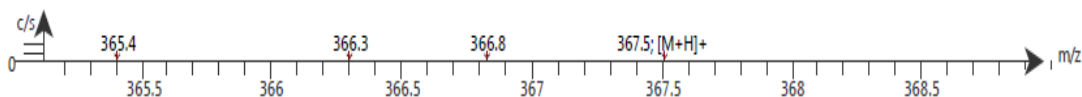
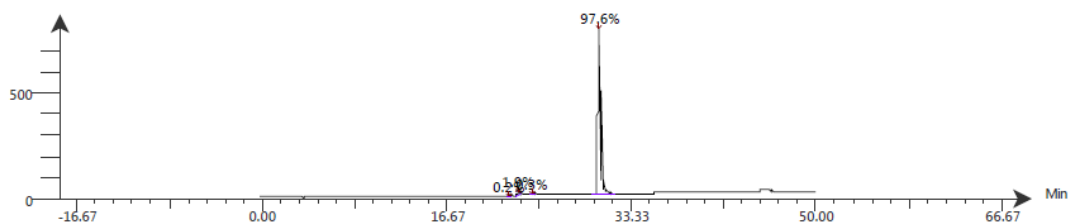


Figure A320. LC-ESI-MS spectrum of (2*E*,4*E*,6*E*)-1-cyano-4-phenylsulfonyl-7-(*p*-nitrophenyl)-hepta-2,4,6-triene, **128**. The ESI spectrum shows it has m/z $[M+H]^+$ 367.5

Intensity VWD: Signal A, 254 nm



Time (Peak Maximum M:S/Minutes)	Maximum Intensity (c/s)	Time (Peak Centroid M:S/Minutes)	Peak Area	% Peak Area	Peak Resolution Label
22.37	1.9E0	22.39	2.2E1	0.2	15.1
23.05	1.7E1	23.10	2.4E2	1.9	15.2
24.35	3.5E0	24.37	3.5E1	0.3	12.8
30.29	7.9E2	30.30	1.2E4	97.6	13.6

Figure A321. LC-UV-MS spectrum of (2*E*,4*E*,6*E*)-1-cyano-4-phenylsulfonyl-7-(*p*-nitrophenyl)-hepta-2,4,6-triene, **128**

Compound Table

Compound Label	RT (min)	Observed mass (m/z)	Neutral observed mass (Da)	Theoretical mass (Da)	Mass error (ppm)	Isotope match score (%)
Cpd 1: C19 H14 N2 O4 S	0.68	366.0681	366.0676	366.0674	0.59	96.40

Figure A322. HR-MS analysis of (2*E*,4*E*,6*E*)-1-cyano-4-phenylsulfonyl-7-(*p*-nitrophenyl)-hepta-2,4,6-triene, **128**

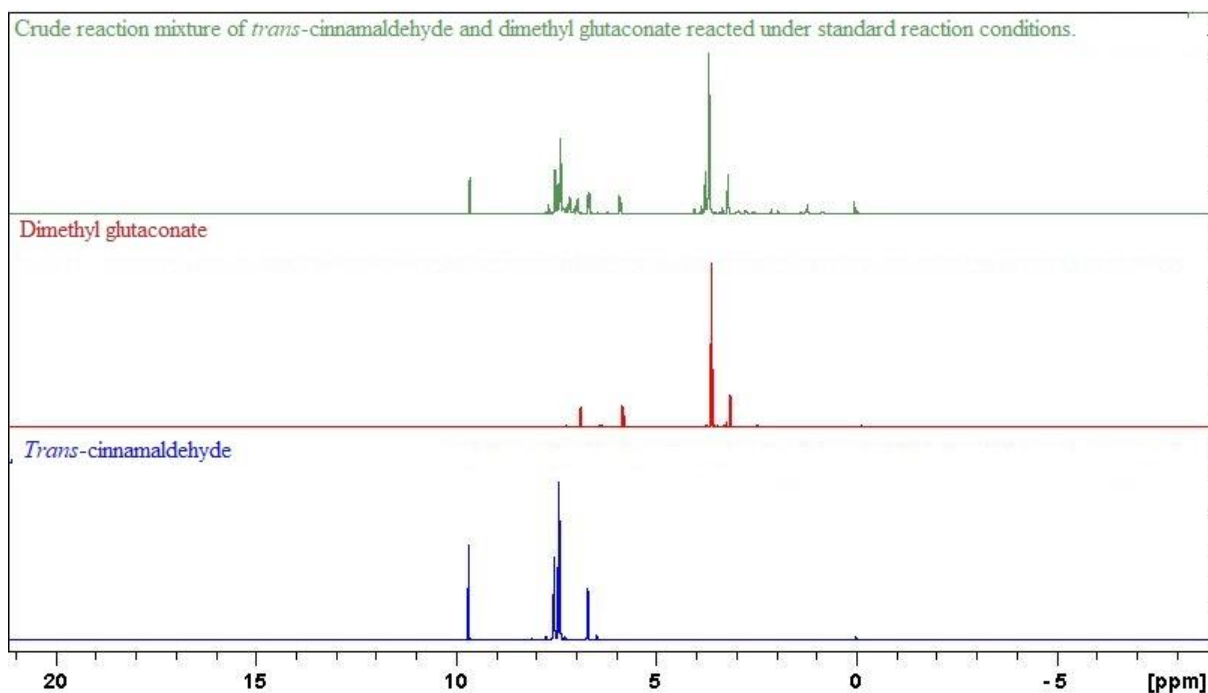


Figure A323. Crude ^1H NMR spectrum of attempted synthesis of bis(methyl ester) triene obtained under standard reaction conditions, showing no reaction occurred.

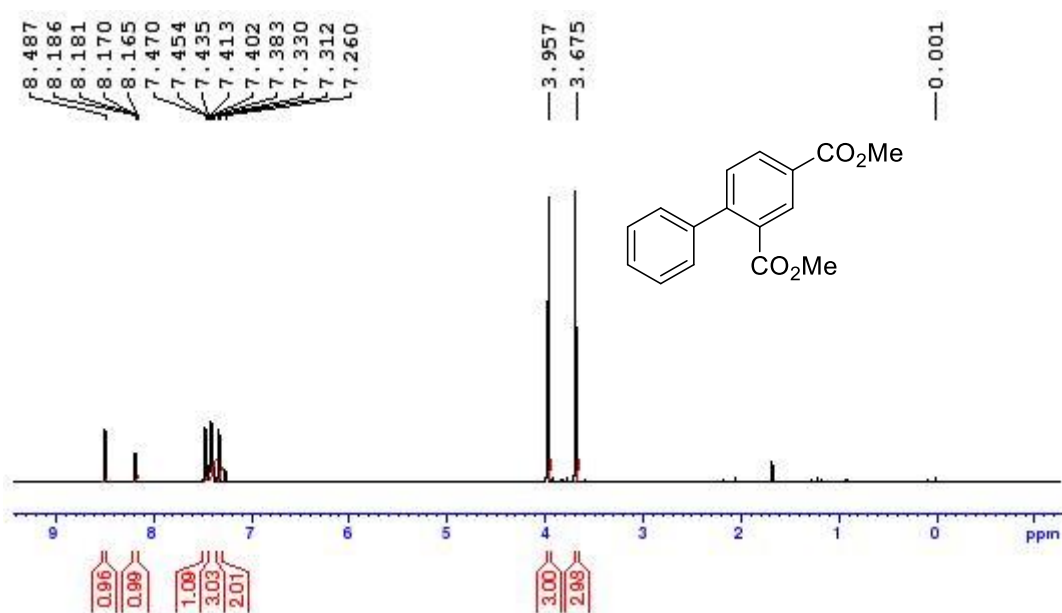


Figure A324. ^1H NMR spectrum of dimethyl biphenyl-2,4-dicarboxylate, **129**, obtained when dimethyl glutaconate and *trans*-cinnamaldehyde, **1**, reacted under traditional Knoevenagel condensation reaction conditions.

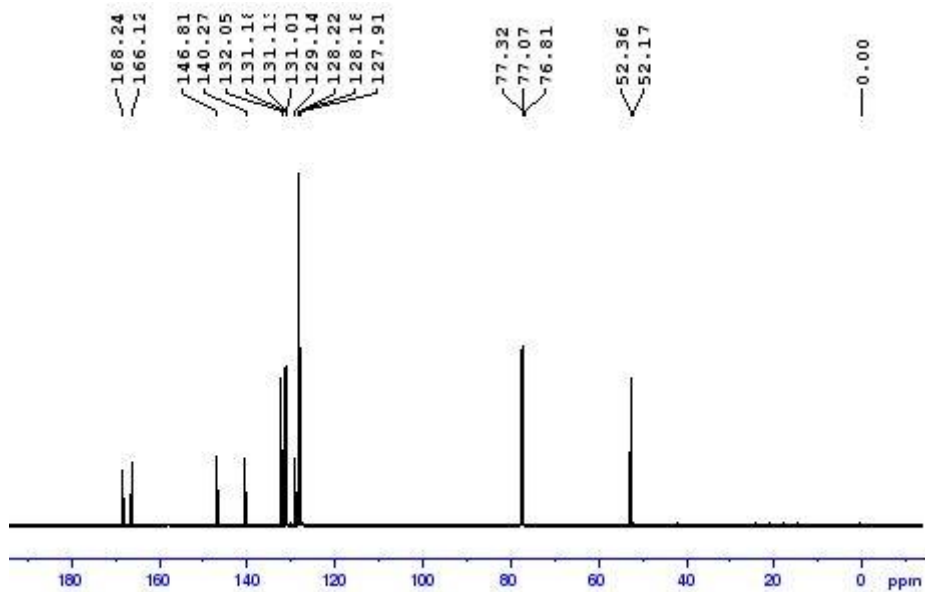


Figure A325. ^{13}C NMR spectrum of dimethyl biphenyl-2,4-dicarboxylate, **129**

Compound Table

Compound Label	RT (min)	Observed mass (m/z)	Neutral observed mass (Da)	Theoretical mass (Da)	Mass error (ppm)	Isotope match score (%)
Cpd 1: C ₁₆ H ₁₄ O ₄	0.71	293.0789	270.0897	270.0892	1.67	99.00

Figure A326. HR-MS analysis of dimethyl biphenyl-2,4-dicarboxylate, **129**

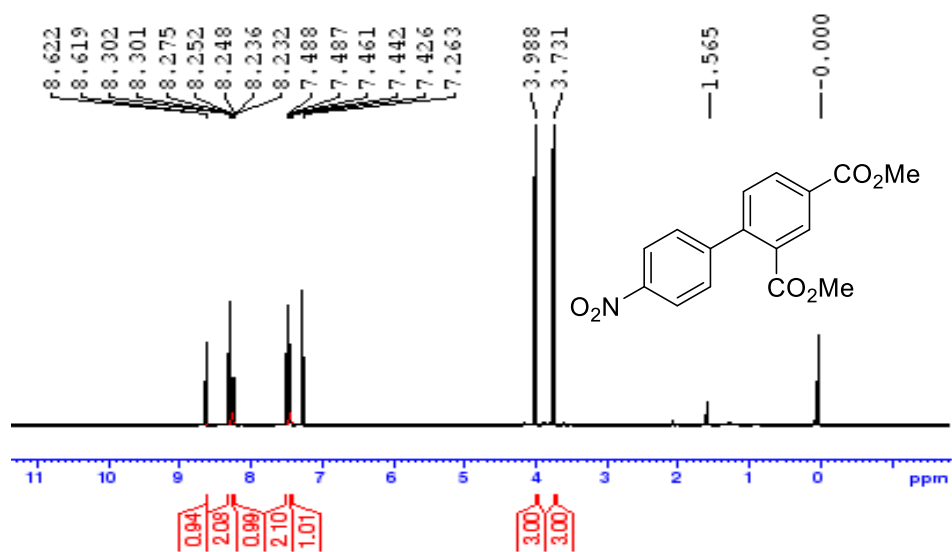


Figure A327. ¹H NMR spectrum of dimethyl 4'-nitrobiphenyl-2,4-dicarboxylate, **130**

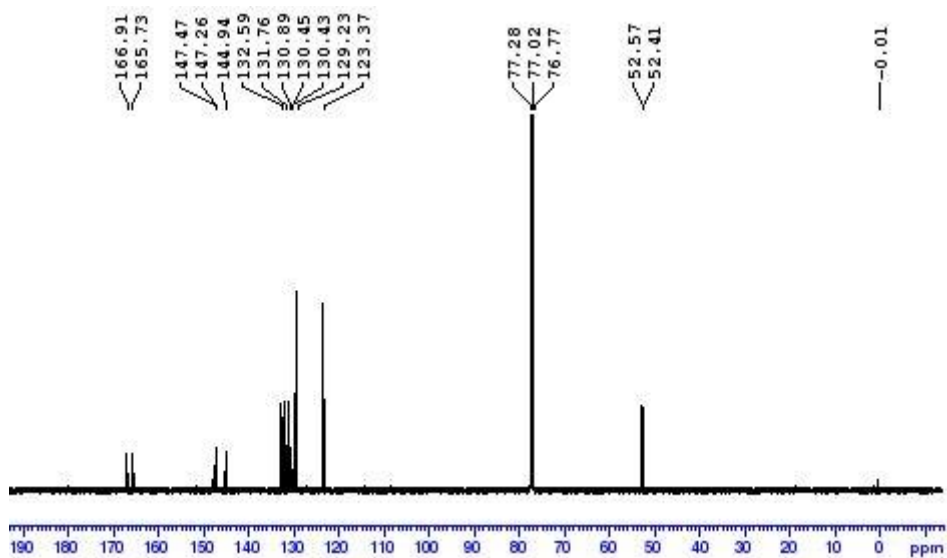


Figure A328. ¹³C NMR spectrum of dimethyl 4'-nitrobiphenyl-2,4-dicarboxylate, **130**

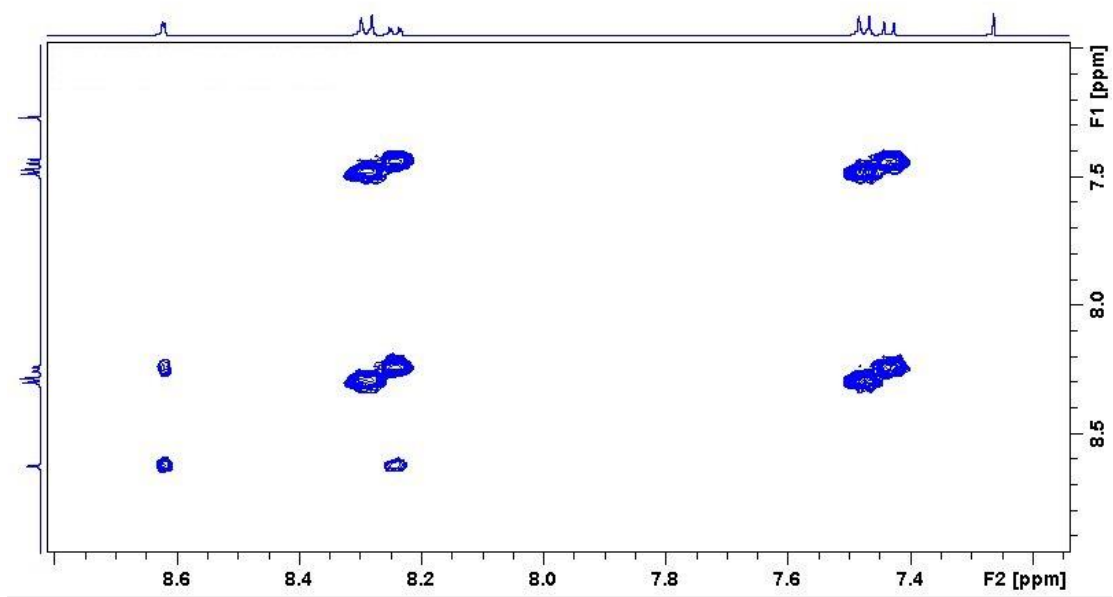


Figure A329. COSY spectrum of dimethyl 4'-nitrophenyl-2,4-dicarboxylate, **130**

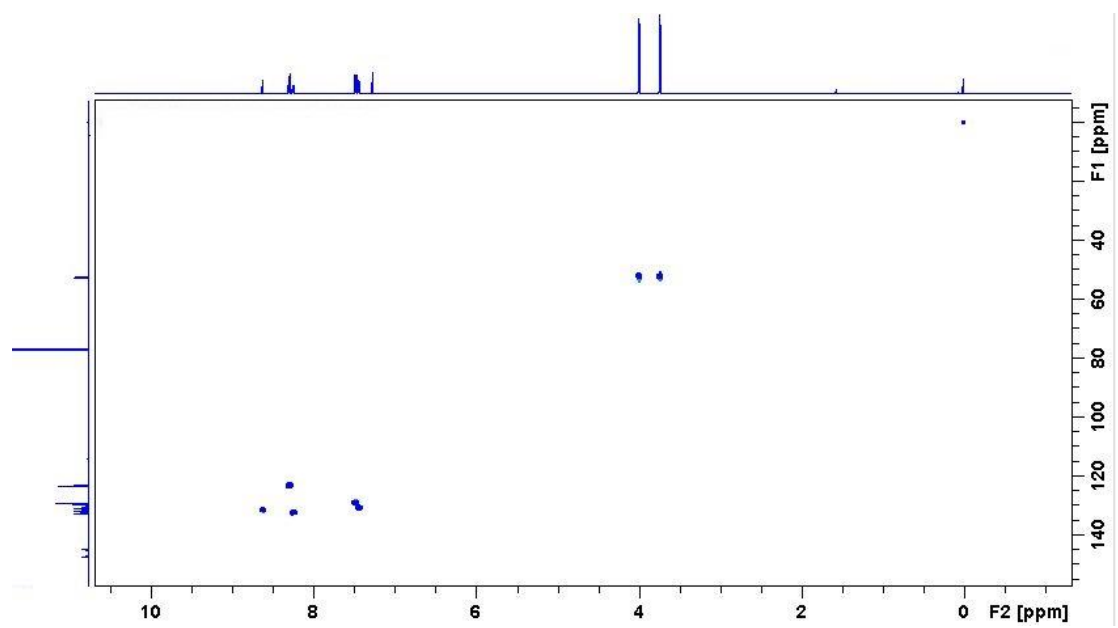


Figure A330. HSQC spectrum of dimethyl 4'-nitrophenyl-2,4-dicarboxylate, **130**

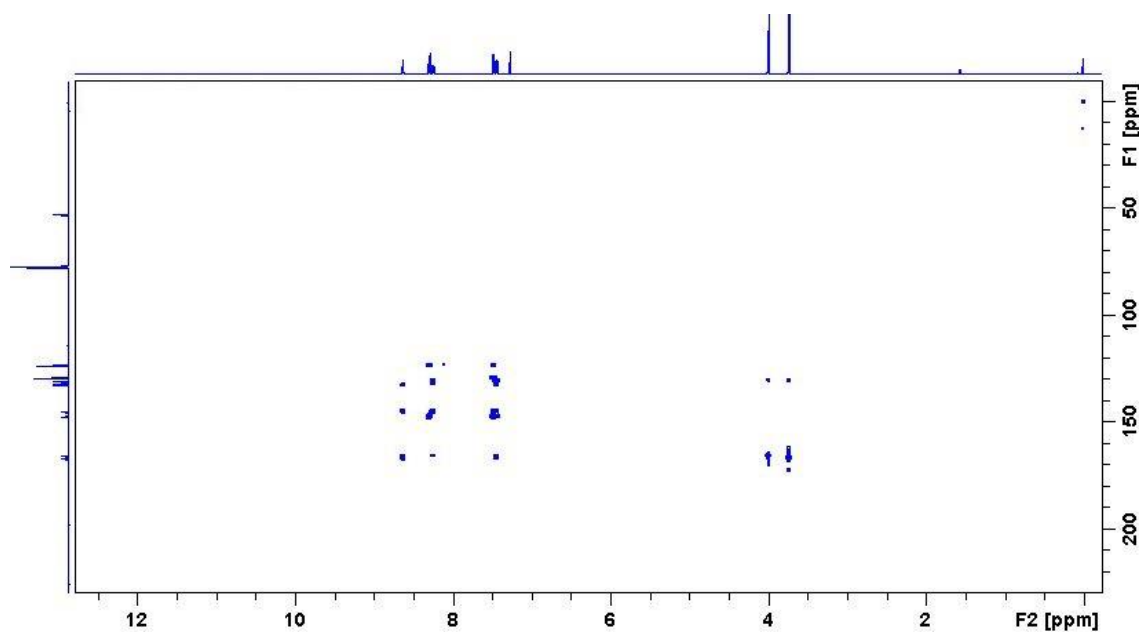


Figure A331. HMBC spectrum of dimethyl 4'-nitrophenyl-2,4-dicarboxylate

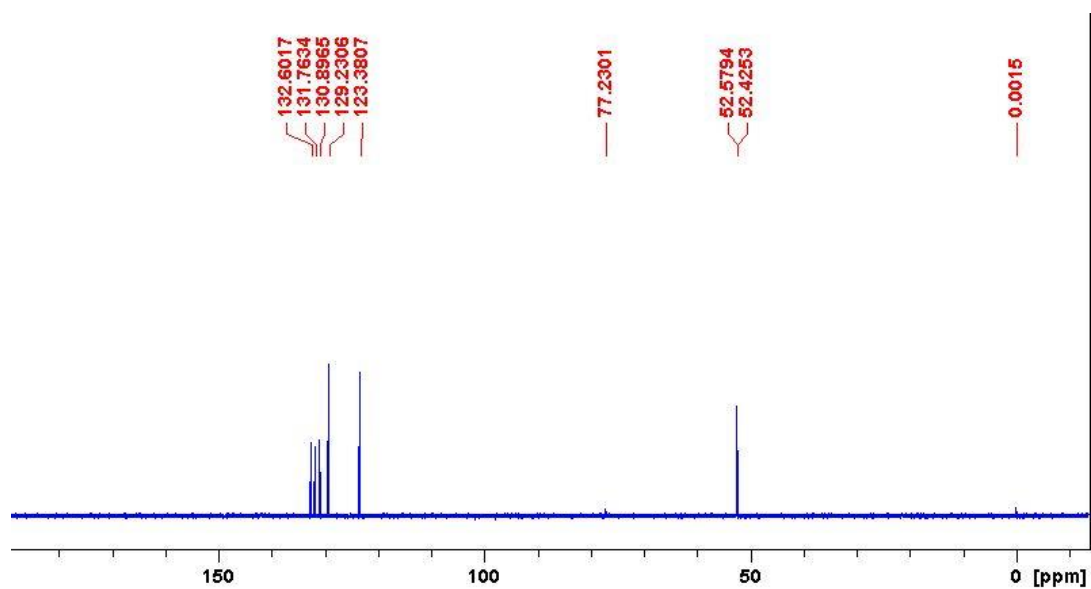


Figure A332. DEPT-135 spectrum of dimethyl 4'-nitrophenyl-2,4-dicarboxylate

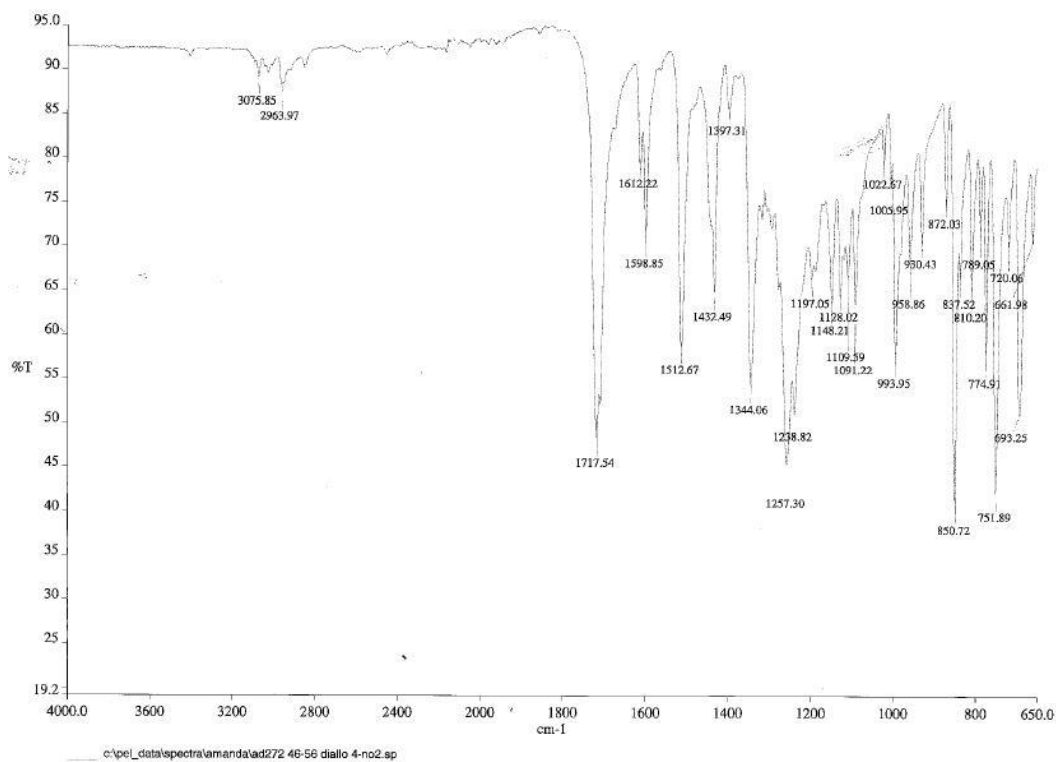


Figure A333. IR spectrum of dimethyl 4'-nitrobiphenyl-2,4-dicarboxylate, **130**

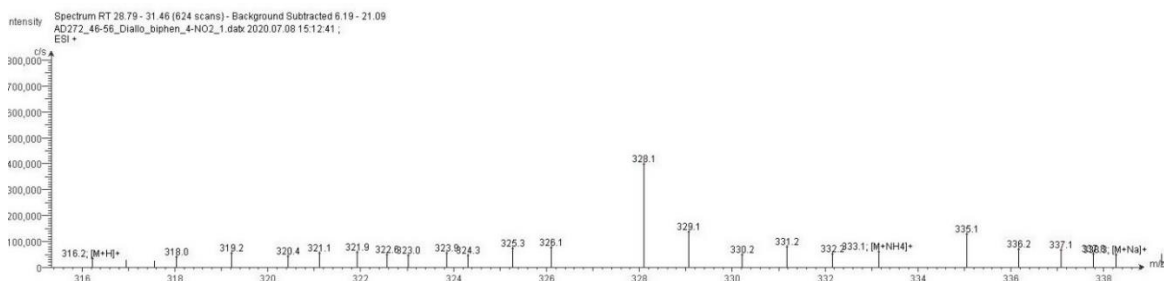


Figure A334. LC-ESI-MS spectrum of dimethyl 4'-nitrobiphenyl-2,4-dicarboxylate, **130**. The ESI spectrum shows it has m/z [M+NH₄]⁺ 333.1

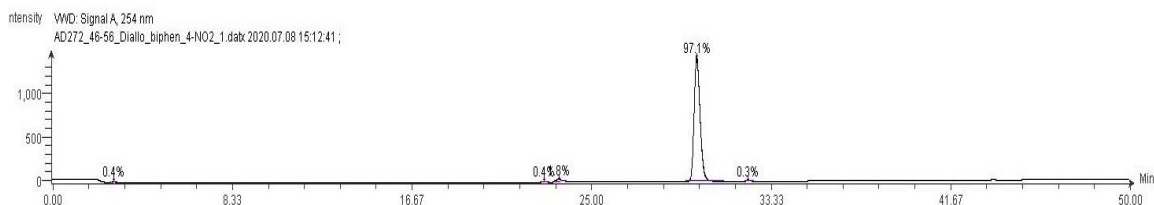


Figure A335. LC-UV-MS spectrum of dimethyl 4'-nitrobiphenyl-2,4-dicarboxylate, **130**

Appendix 3

Spectra related to method optimization

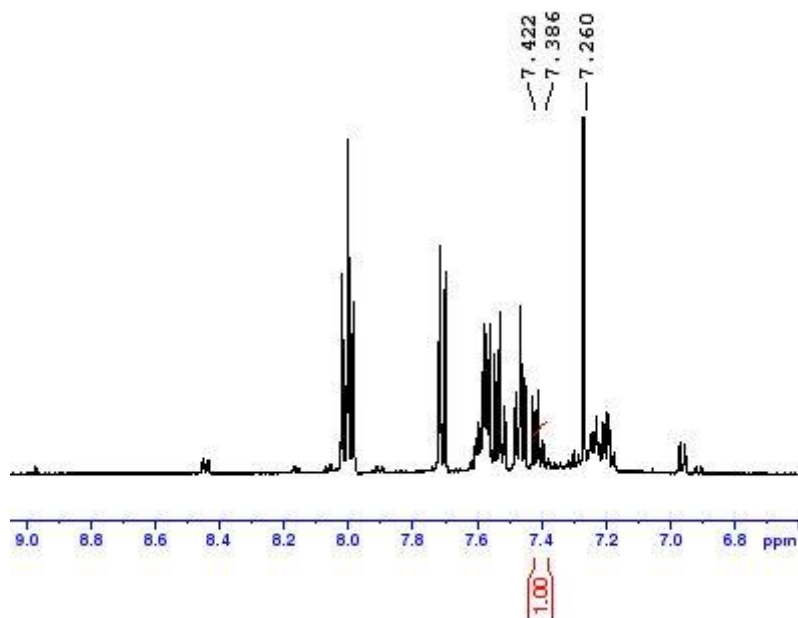


Figure A336. ¹H NMR spectrum of crude mixture containing 4-(phenylsulfonyl)-1,1'-biphenyl **46**, obtained from heating neat (1*E*,3*E*,5*E*)-1,3-bis-phenylsulfonyl-6-phenyl-hexa-1,3,5-triene **105** using a heat gun at its maximum setting for 10 seconds.

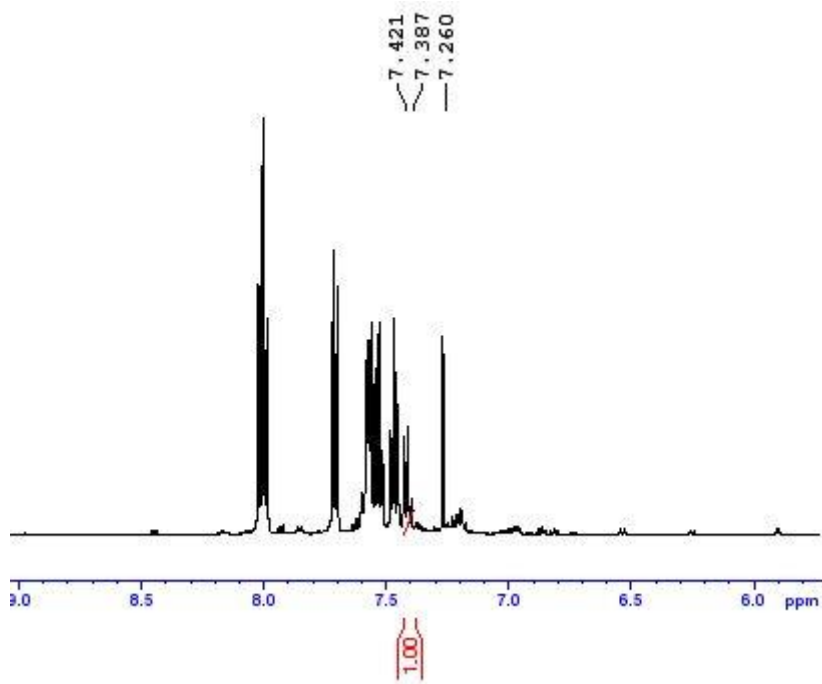


Figure A337. ¹H NMR spectrum of crude mixture containing biaryl **46**, obtained from heating **105** neat in an oil bath at 175 °C for 1.5 h

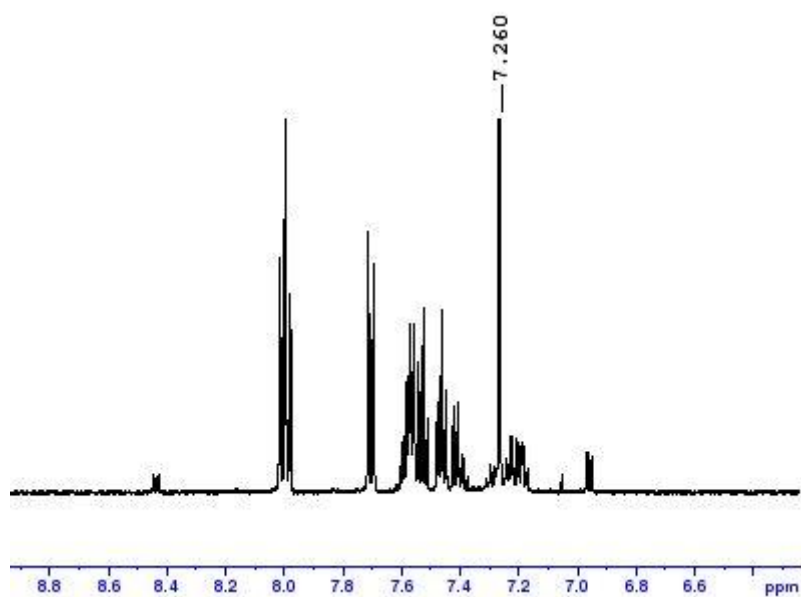


Figure A338. ^1H NMR spectrum of crude mixture containing biaryl **46**, obtained from heating the **105** neat in bath of Lab Armour metallic beads at 175 °C for 1.5 h

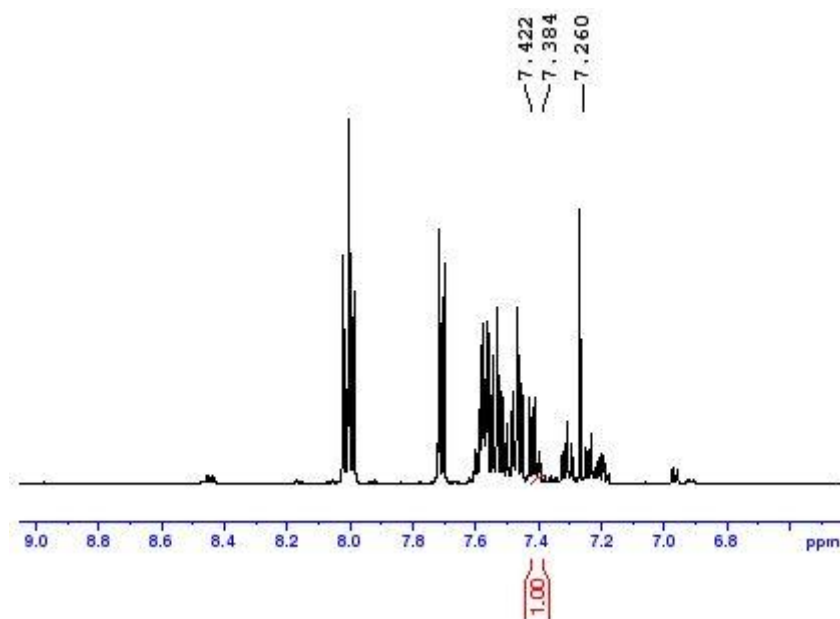


Figure A339 (a). ^1H NMR spectrum of crude mixture containing biaryl **46**, obtained from heating **105** neat in a sand bath at 175 °C for 1.5 h

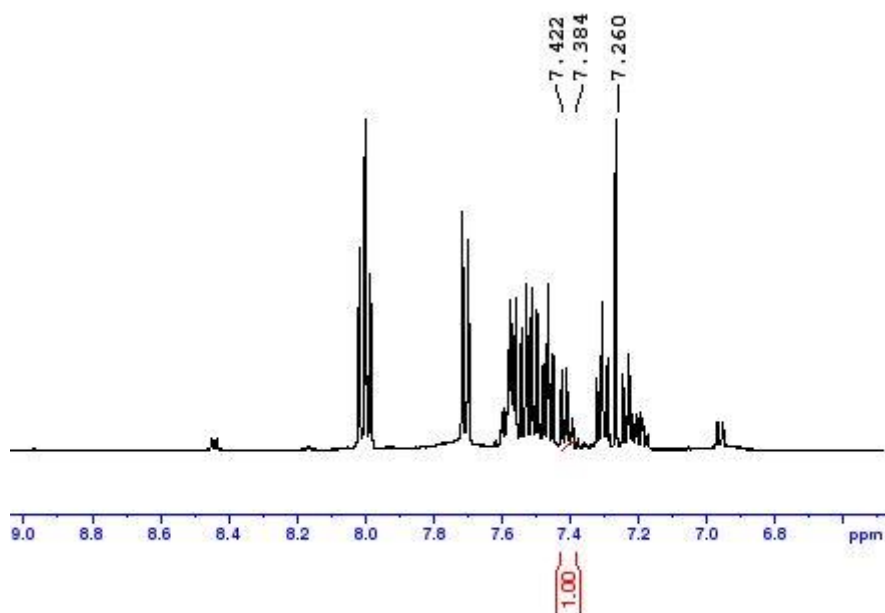


Figure A339 (b). ^1H NMR spectrum of crude mixture containing biaryl **46**, obtained from heating **105** neat in a sand bath at 200 °C for 1.5 h

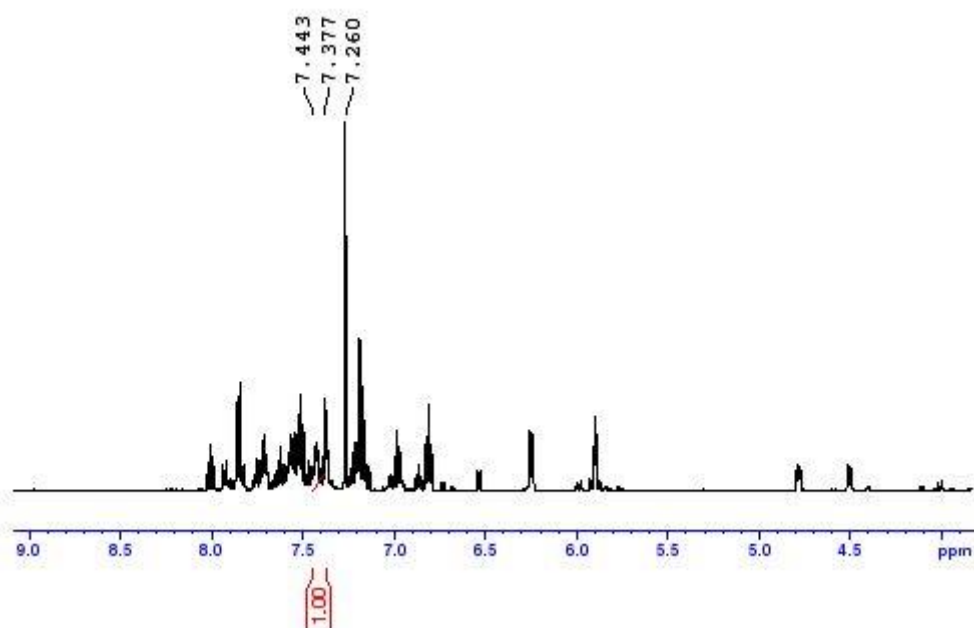


Figure A340. ^1H NMR spectrum of crude mixture containing biaryl **46**, obtained from heating **105** neat in a vacuum oven at 180 °C below 0 mbar atm for 24 h

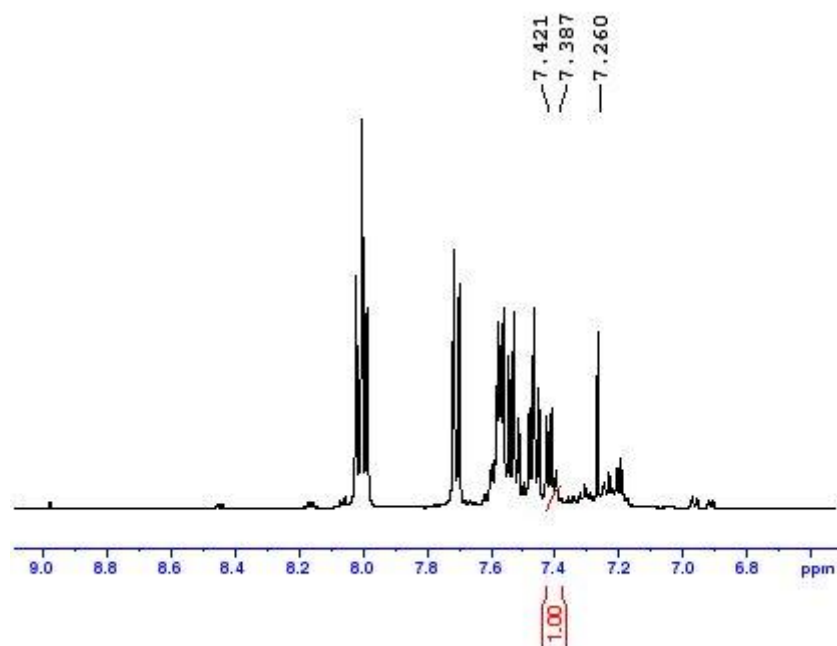


Figure A341 (a). ^1H NMR spectrum of non-sublimed material containing biaryl **46**, obtained from the use of sublimation apparatus using water for cooling and heating **105** neat in an oil bath at 175 °C for 1.5 h

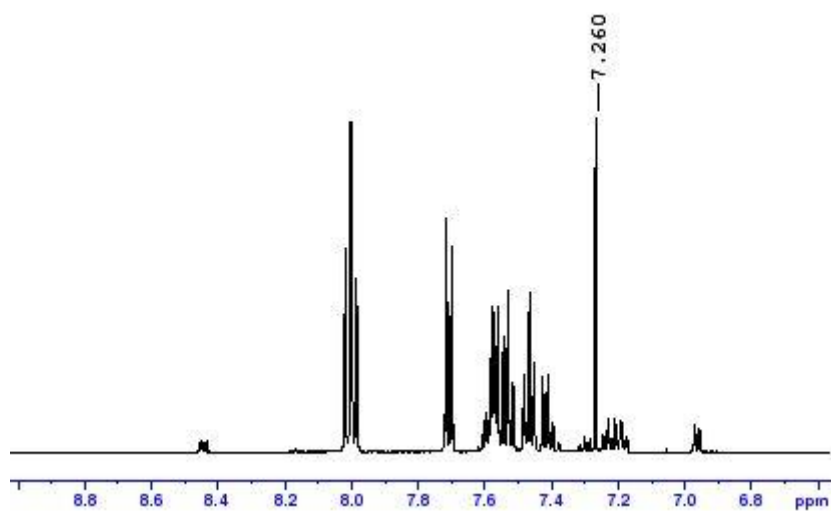


Figure A341 (b). ^1H NMR spectrum of sublimed material containing biaryl **46**, obtained from the use of sublimation apparatus using water for cooling and heating **105** neat in an oil bath at 175 °C for 1.5 h

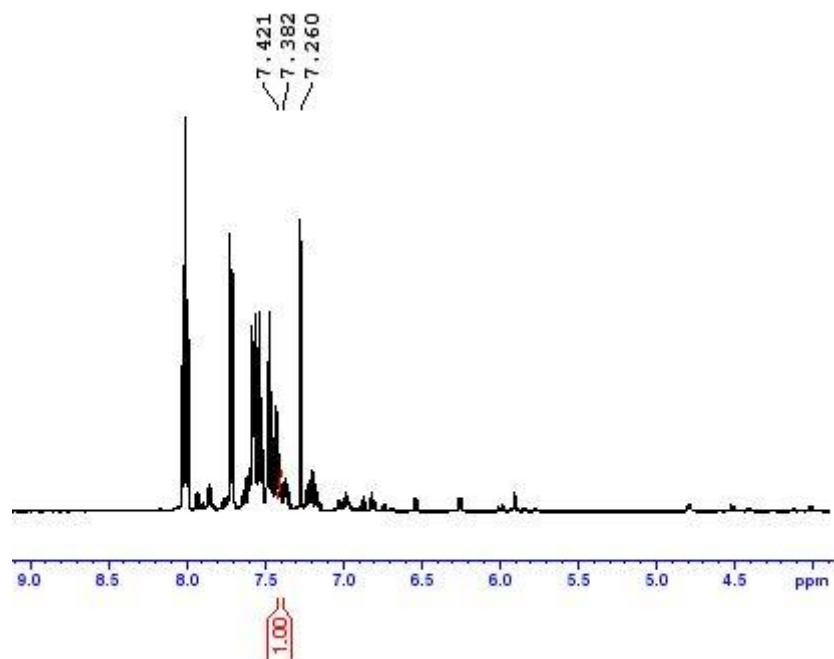


Figure A342 (a). ¹H NMR spectrum of non-sublimed material containing biaryl **46**, obtained from the use of sublimation apparatus using liquid N₂ for cooling and heating **105** neat in an oil bath at 175 °C for 2 h

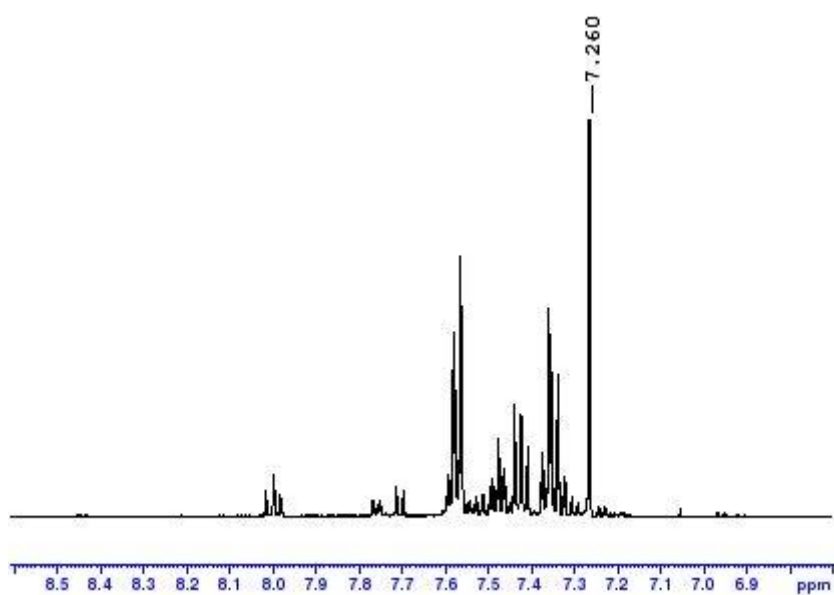


Figure A342 (b). ¹H NMR spectrum of sublimed material containing biaryl **46**, obtained from the use of sublimation apparatus using liquid N₂ for cooling and heating **105** neat in an oil bath at 175 °C for 2 h.

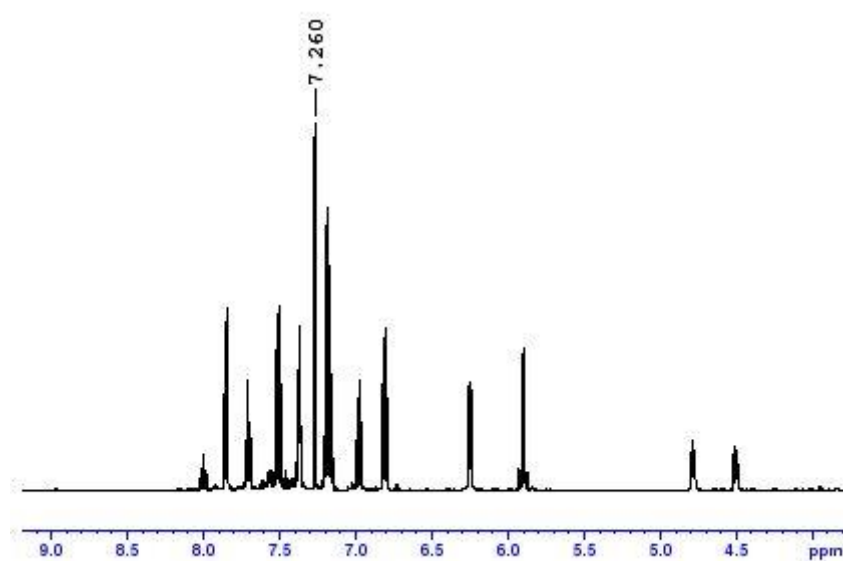


Figure A343 (a). ¹H NMR spectrum of the solid that precipitated after 0.0025 M solution of triene **105** was exposed to microwave irradiation for 5 minutes, where toluene was used as a solvent

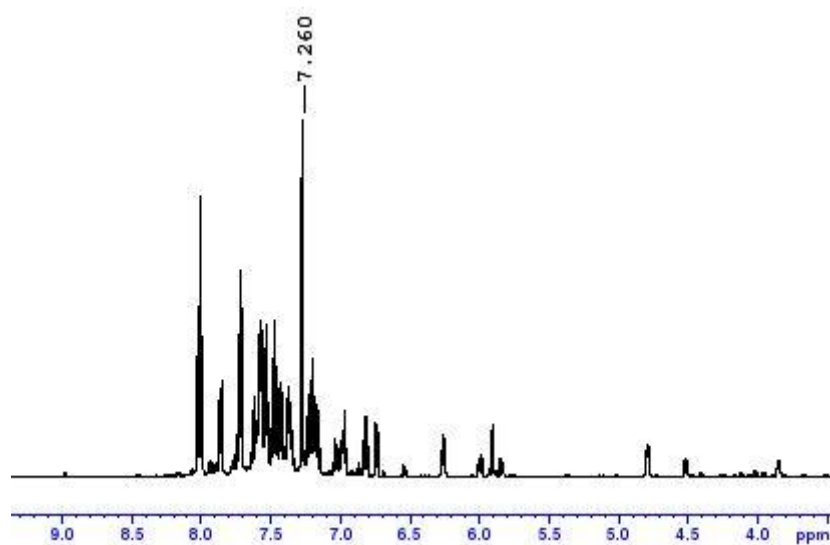


Figure A343 (b). ¹H NMR spectrum of the solution obtained after 0.0025 M solution of triene **105** was exposed to microwave irradiation for 5 minutes, where toluene was used as a solvent

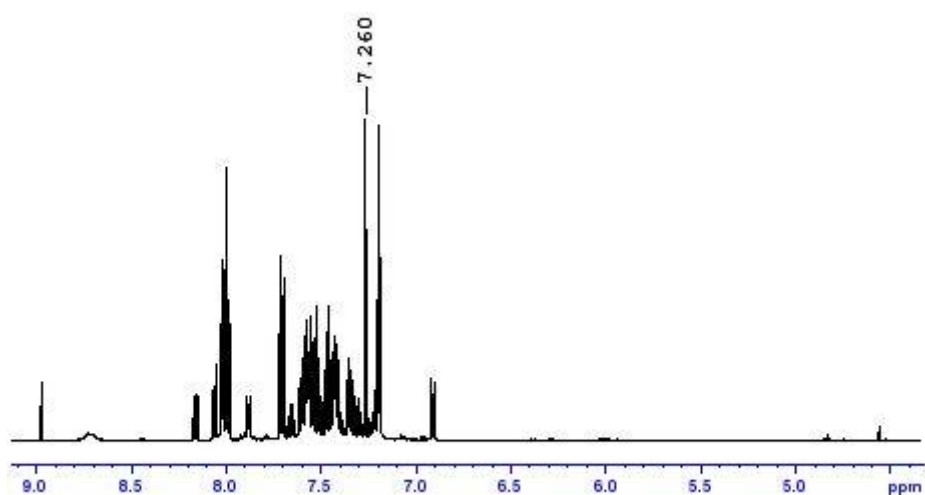


Figure A344. ¹H NMR spectrum of the solution obtained after 0.0025 M solution of triene **105** was exposed to microwave irradiation for 5 minutes, where DMF was used as a solvent

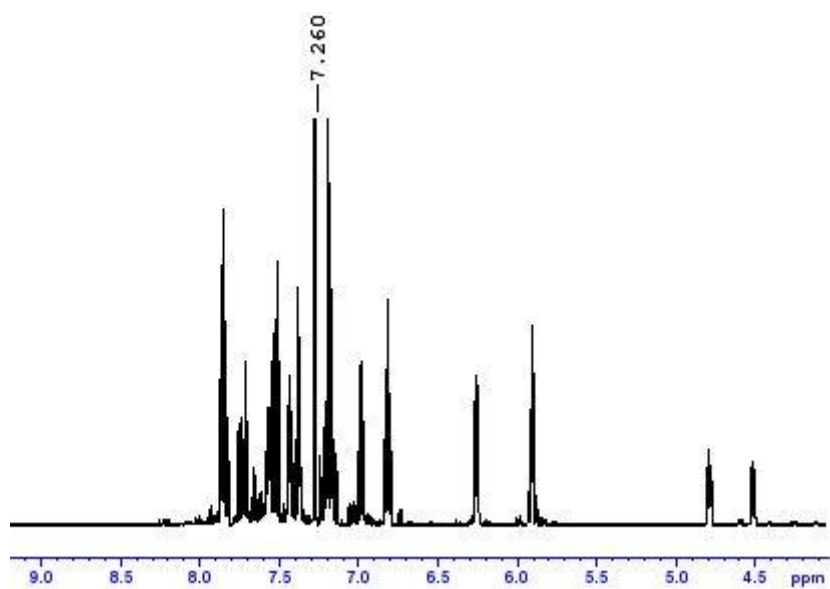


Figure A345. ¹H NMR spectrum of the solution obtained after 0.0025 M solution of triene **105** was exposed to microwave irradiation for 5 minutes, where chloroform was used as a solvent

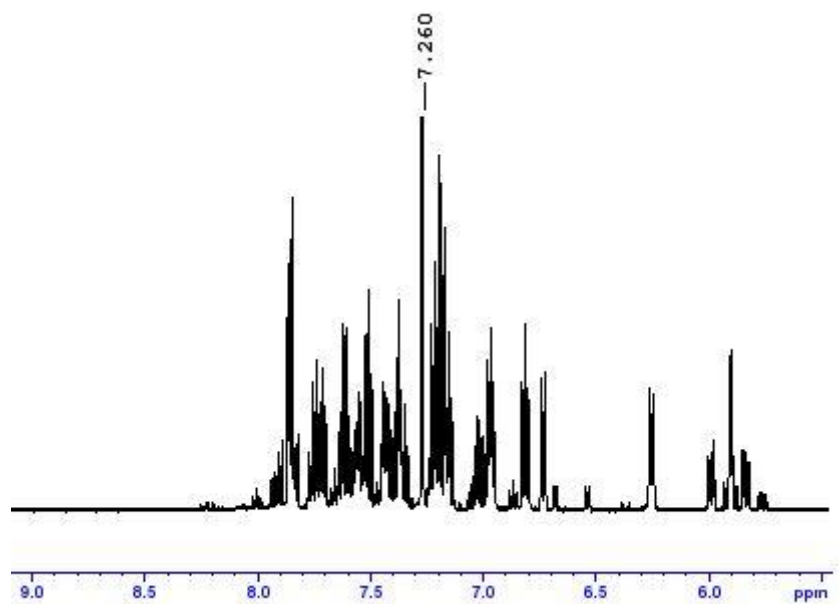


Figure A346. ¹H NMR spectrum of the solution obtained after 0.0025 M solution of triene **105** was exposed to microwave irradiation for 5 minutes, where acetonitrile was used as a solvent

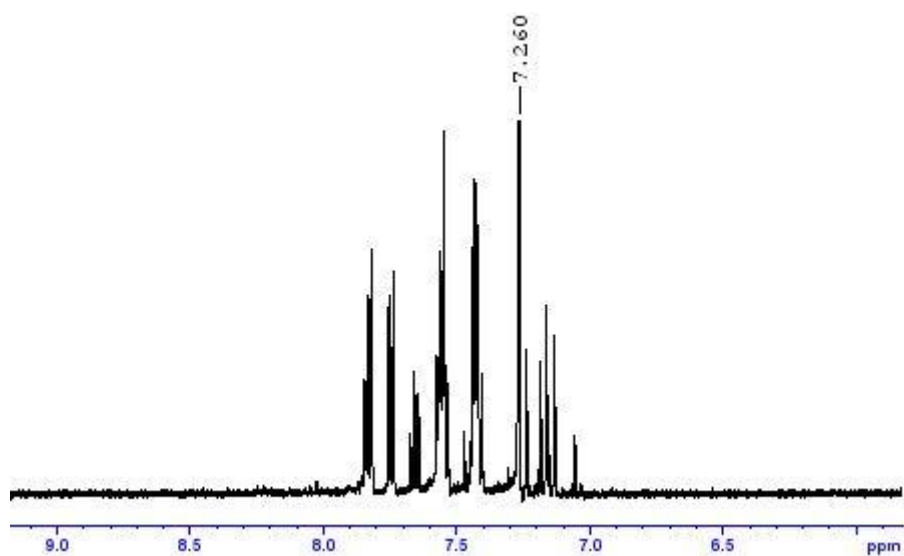


Figure A347. ¹H NMR spectrum of the solution obtained after 0.0025 M solution of triene **105** was exposed to microwave irradiation and 85 °C for 5 minutes, using DMF as a solvent.

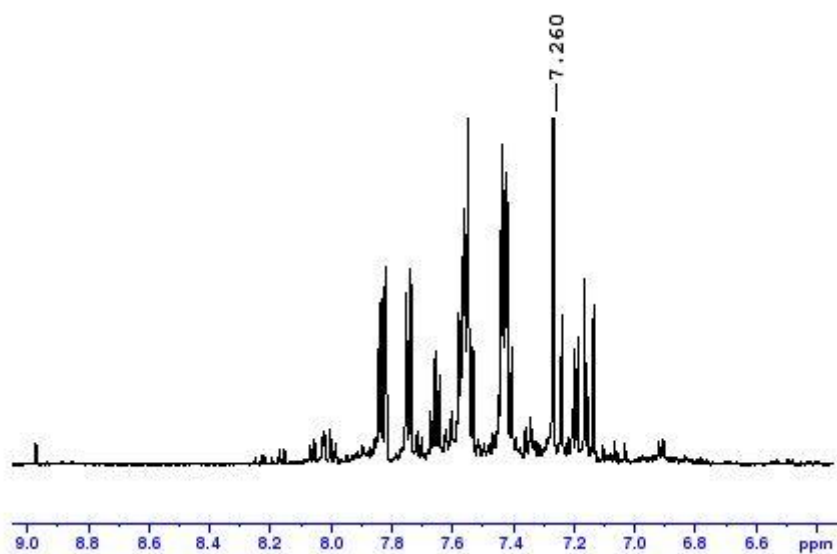


Figure A348. ¹H NMR spectrum of the solution obtained after 0.0025 M solution of triene **105** was exposed to microwave irradiation and 110 °C for 5 minutes, using DMF as a solvent.

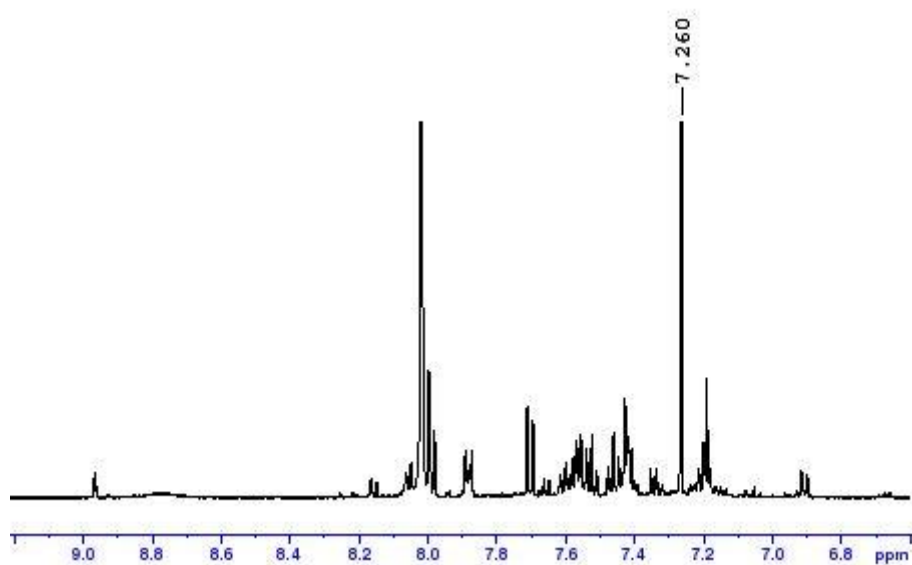


Figure A349. ¹H NMR spectrum of the solution obtained after 0.0025 M solution of triene was exposed to microwave irradiation and 140 °C for 5 minutes, using DMF as a solvent.

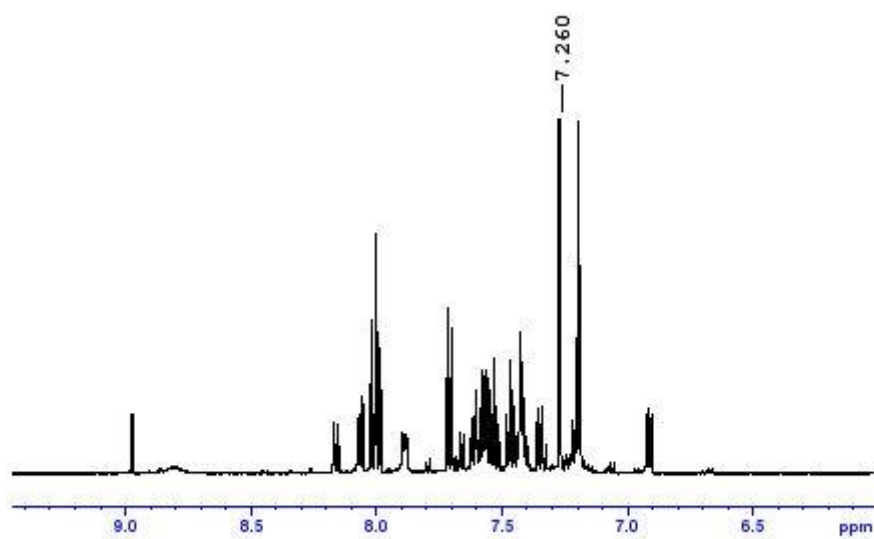


Figure A350. ¹H NMR spectrum of the solution obtained after 0.0025 M solution of triene **105** was exposed to microwave irradiation and 150 °C for 5 minutes, using DMF as a solvent.

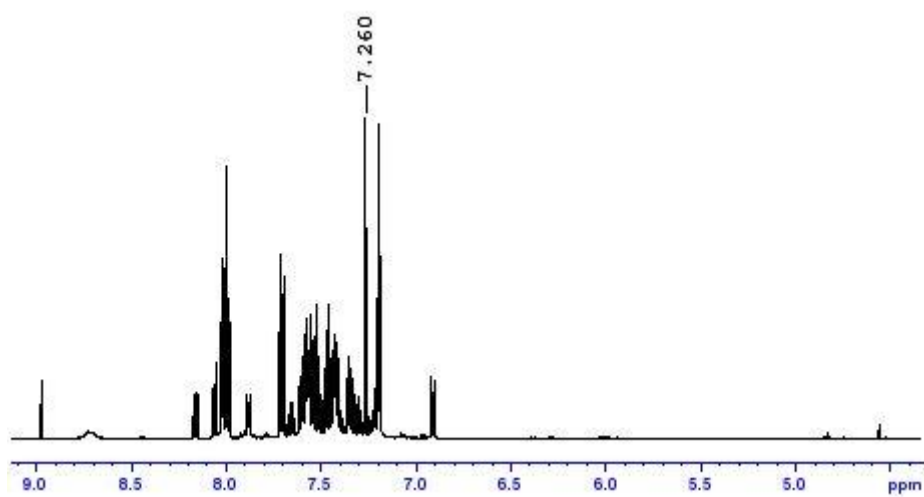


Figure A351. ¹H NMR spectrum of the solution obtained after 0.0025 M solution of triene **105** was exposed to microwave irradiation and 170 °C for 5 minutes, using DMF as a solvent.

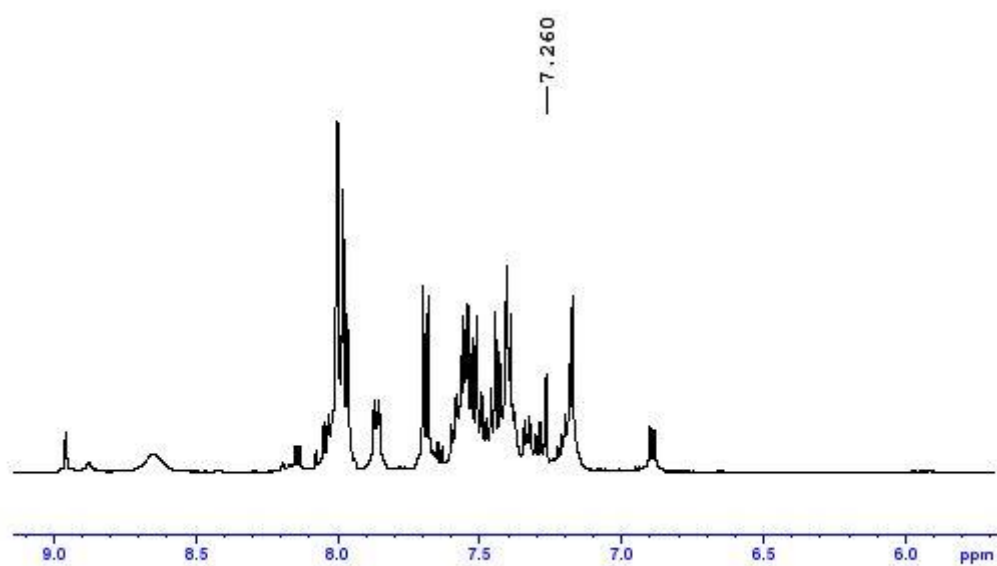


Figure A352. ¹H NMR spectrum of the solution obtained after 0.01 M solution of triene **105** was exposed to microwave irradiation and 170 °C for 5 minutes, using DMF as a solvent.

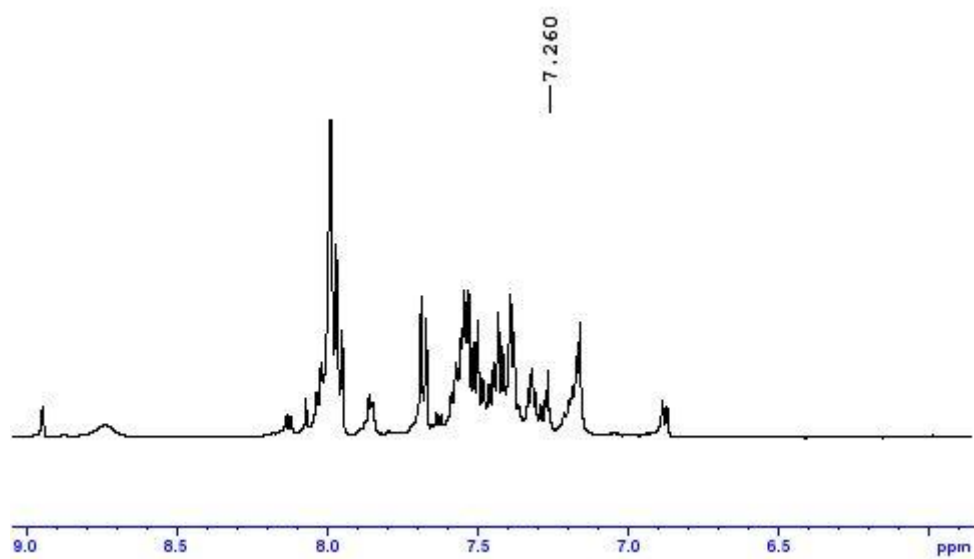


Figure A353. ¹H NMR spectrum of the solution obtained after 0.1 M solution of triene **105** was exposed to microwave irradiation and 170 °C for 5 minutes, using DMF as a solvent.

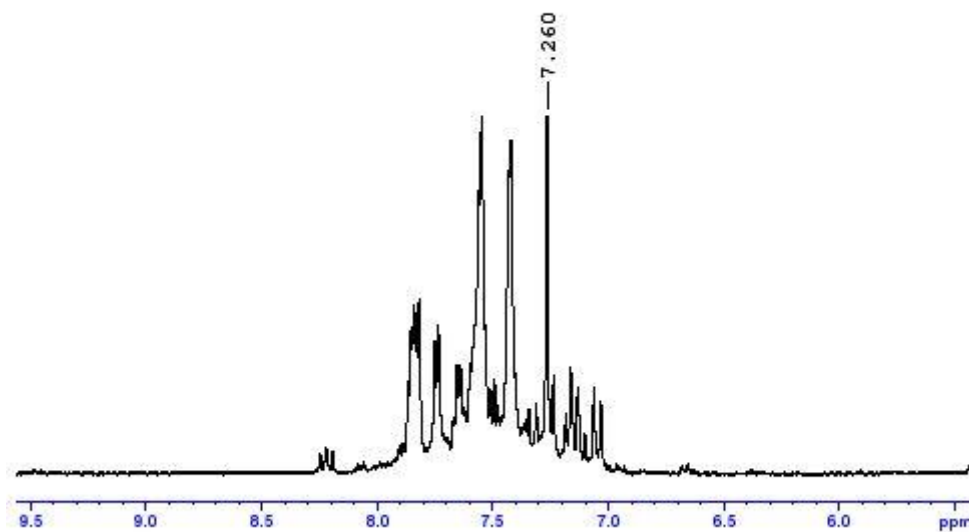


Figure A354. The ¹H NMR spectrum of the solution obtained after 0.03 mol of triene **105** was left stirring in a UV box under a lamp emitting 365 nm wavelength light for 7 days.

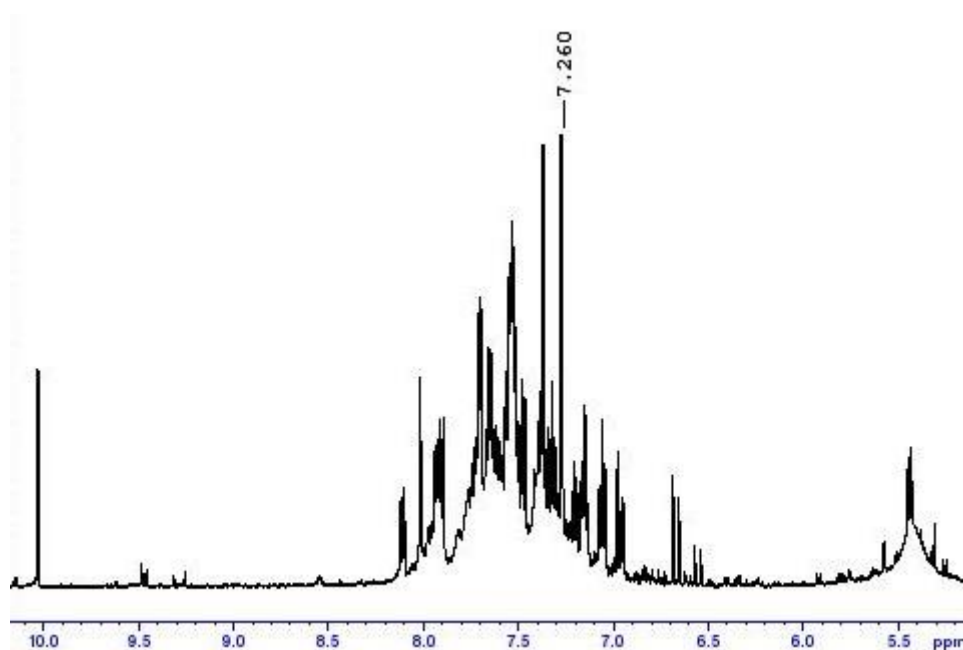


Figure A355. The ¹H NMR spectrum of the solution obtained after 0.03 mol of triene **105** was left stirring in a UV box under a lamp emitting 254 nm wavelength light for 18.5 hrs.

NMR/IR/LC-MS/HR-MS Spectra of biaryls synthesized by preferred method

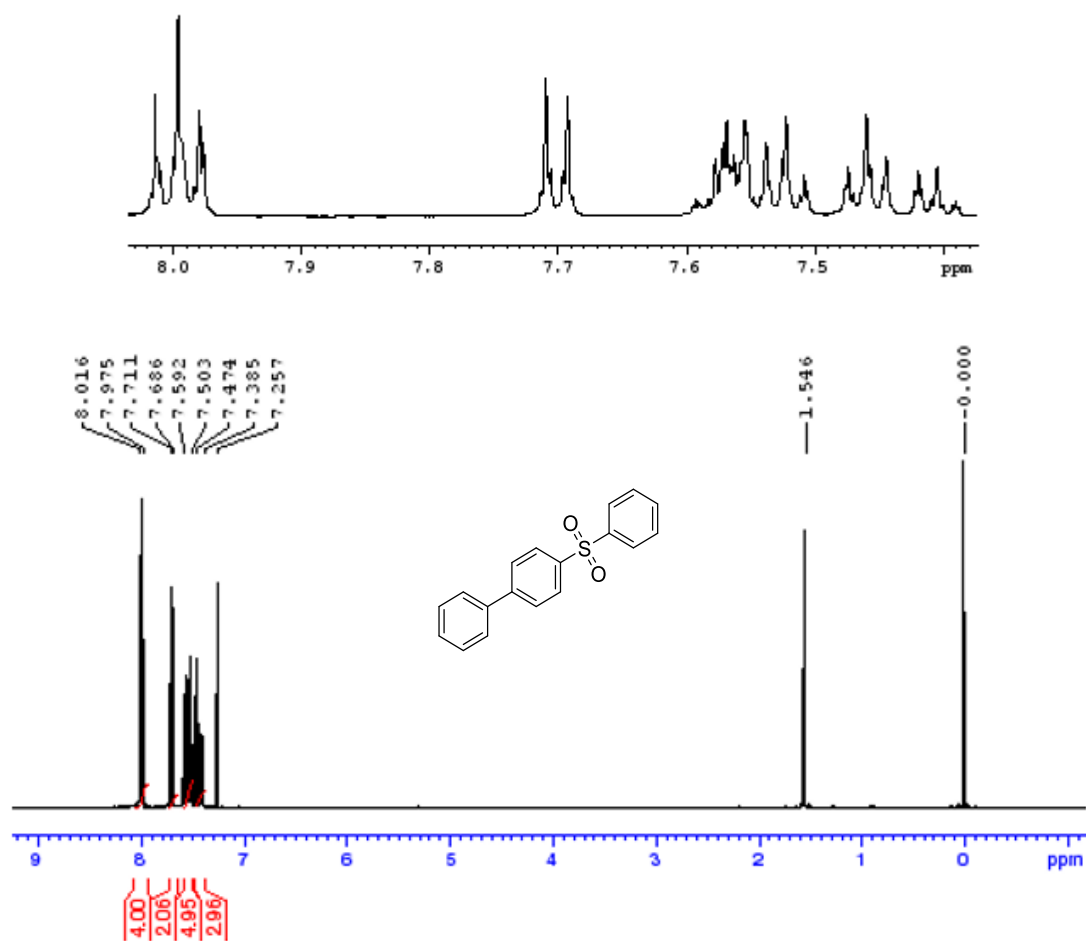


Figure A356. ¹H NMR spectrum of 4-(phenylsulfonyl)-1,1'-biphenyl, 46.

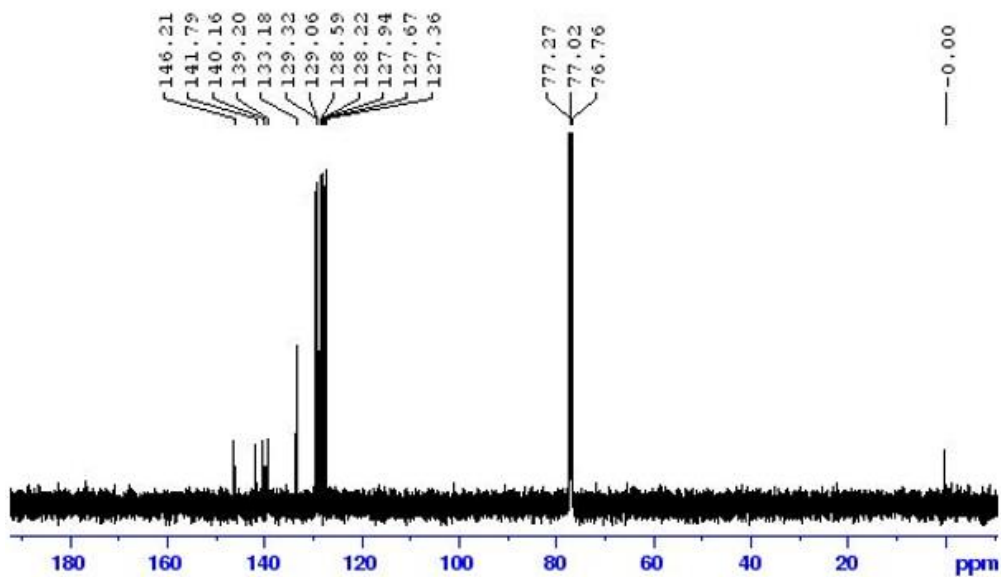


Figure A357. ^{13}C NMR spectrum of 4-(phenylsulfonyl)-1,1'-biphenyl, **46**

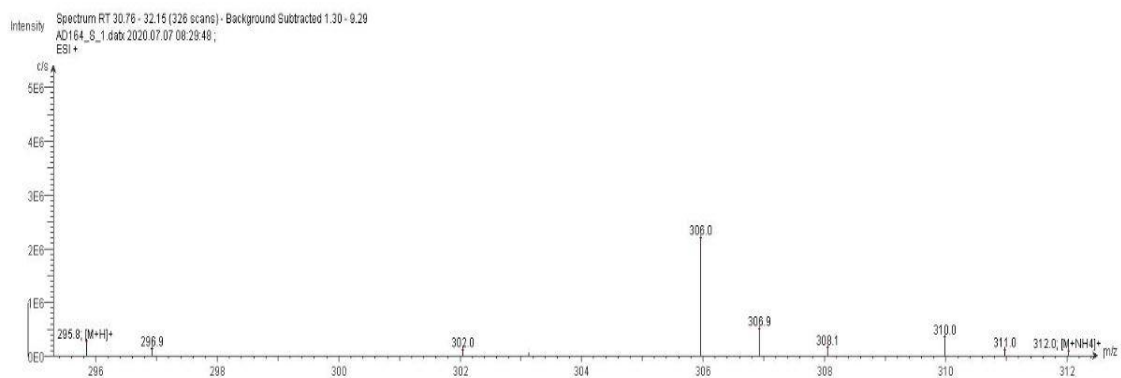
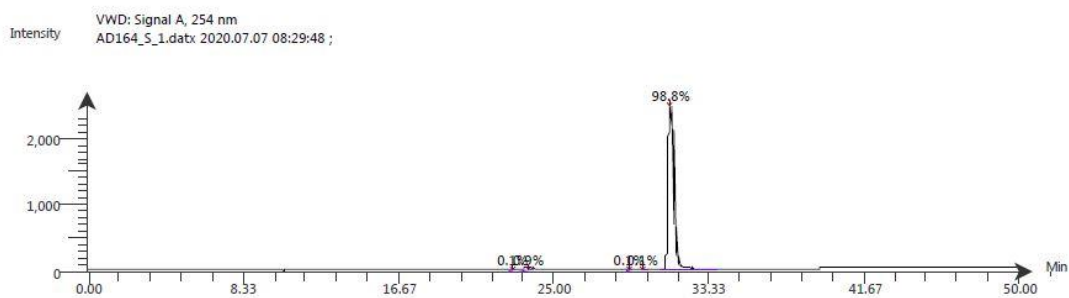


Figure A358. LC-ESI-MS spectrum of 4-(phenylsulfonyl)-1,1'-biphenyl, **46**. The ESI spectrum shows it has m/z $[\text{M}+\text{H}]^+$ 295.8.



Time (Peak Maximum M:S/Minutes)	Maximum Intensity (c/s)	Time (Peak Centroid M:S/Minutes)	Peak Area	% Peak Area	Peak Resolution Label
22.89	9.5E-1	22.77	4.5E1	0.1	25.3
23.52	2.9E1	23.59	5.2E2	0.9	17.9
29.01	5.6E0	29.02	6.9E1	0.1	18.6
29.80	3.5E0	29.84	4.4E1	0.1	17.8
31.23	2.5E3	31.24	5.7E4	98.8	20.9

Figure A359. LC-UV-MS chromatogram of 4-(phenylsulfonyl)-1,1'-biphenyl, **46**

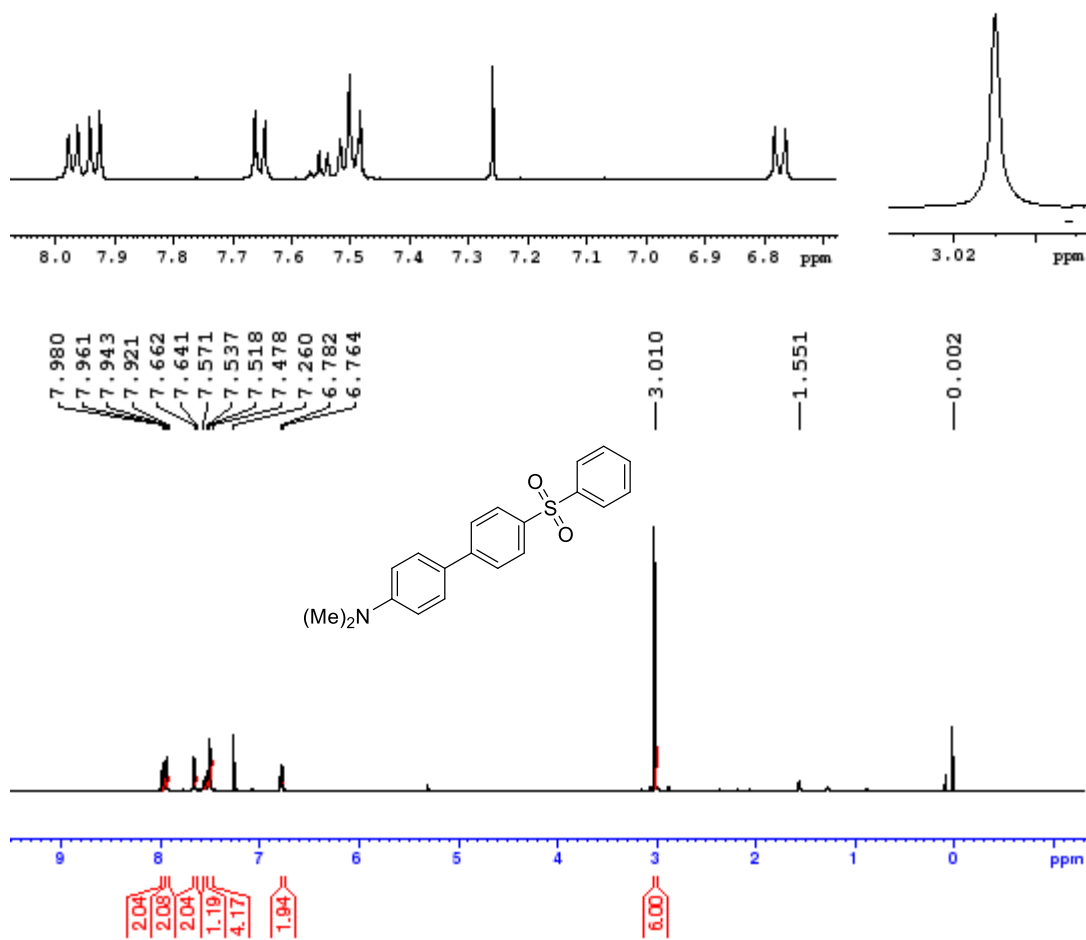


Figure A360. ¹H NMR spectrum of 1-(4-dimethylaminophenyl)-4-(phenylsulfonyl)benzene **138**

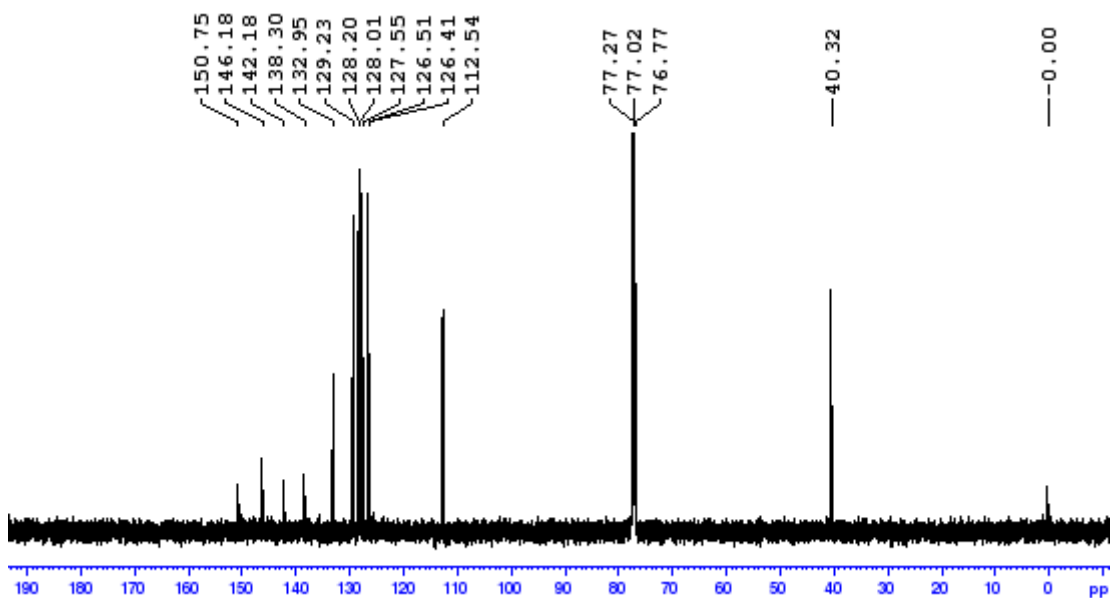


Figure A361. ^{13}C NMR spectrum of ^1H NMR spectrum of 1-(4-dimethylaminophenyl)-4-(phenylsulfonyl)benzene **138**

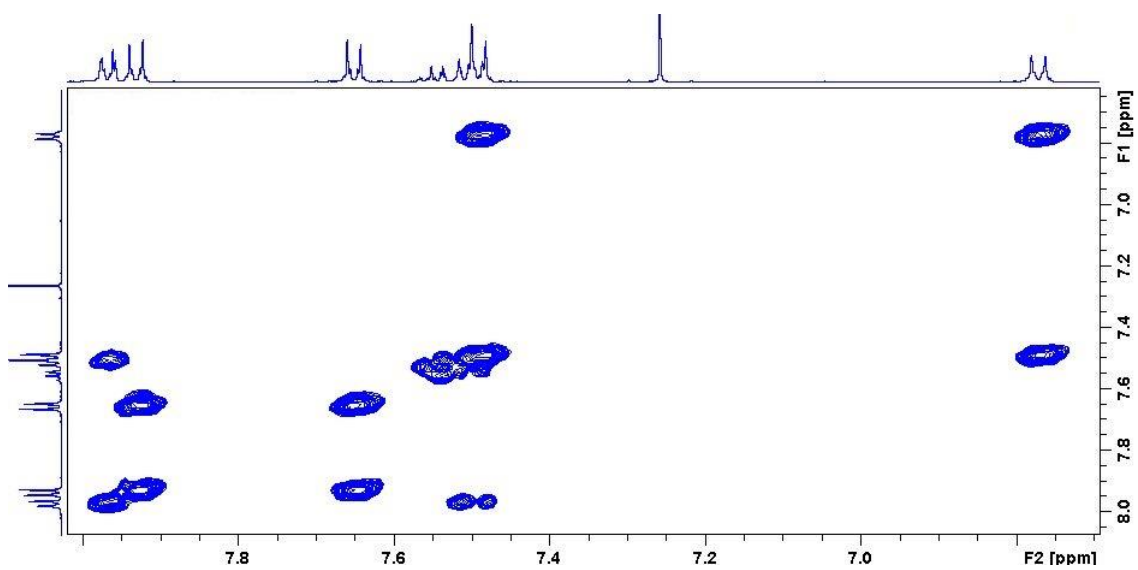


Figure A362. Zoomed in COSY spectrum of ^1H NMR spectrum of 1-(4-dimethylaminophenyl)-4-(phenylsulfonyl)benzene **138**

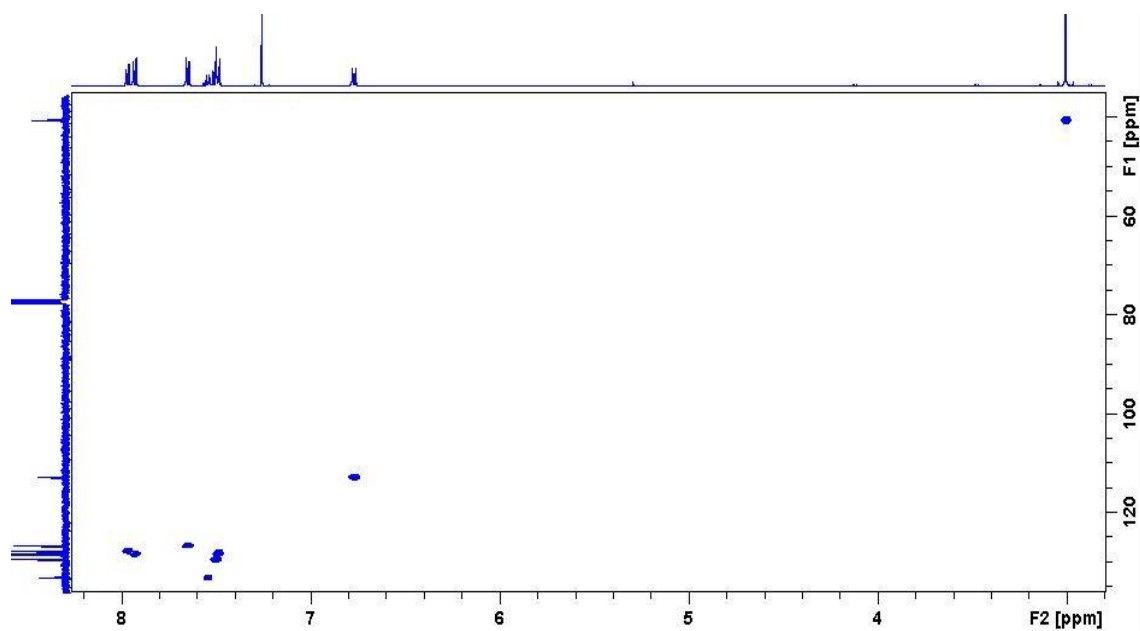


Figure A363. Zoomed in HSQC spectrum of ^1H NMR spectrum of 1-(4-dimethylaminophenyl)-4-(phenylsulfonyl)benzene **138**

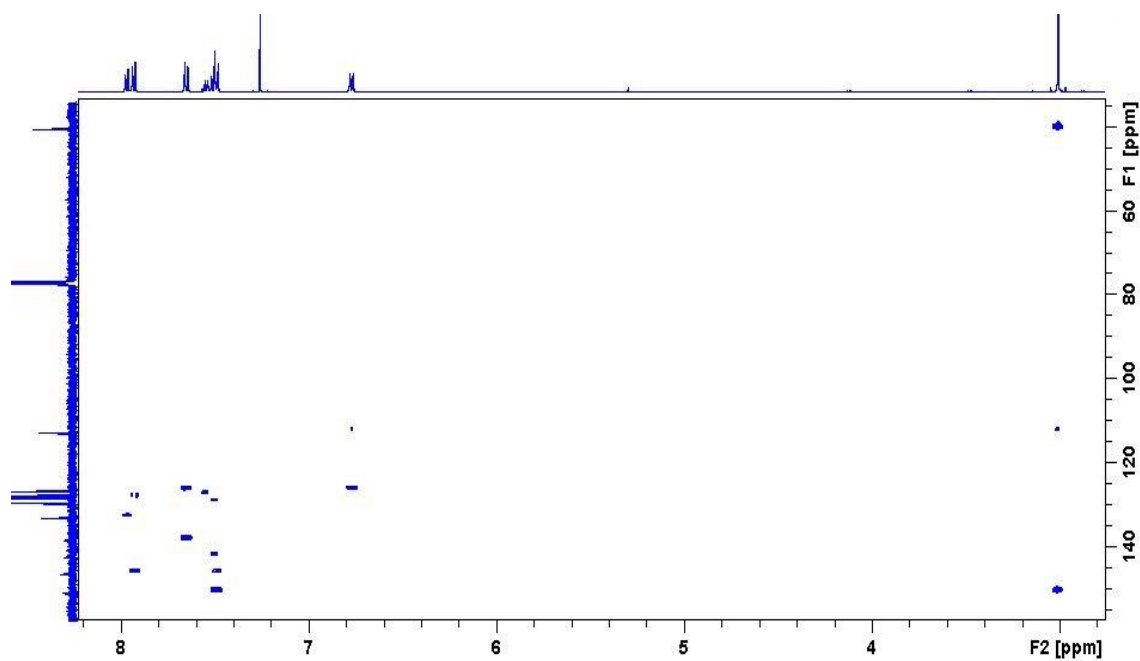


Figure A364. Zoomed in HMBC spectrum of ^1H NMR spectrum of 1-(4-dimethylaminophenyl)-4-(phenylsulfonyl)benzene **138**.

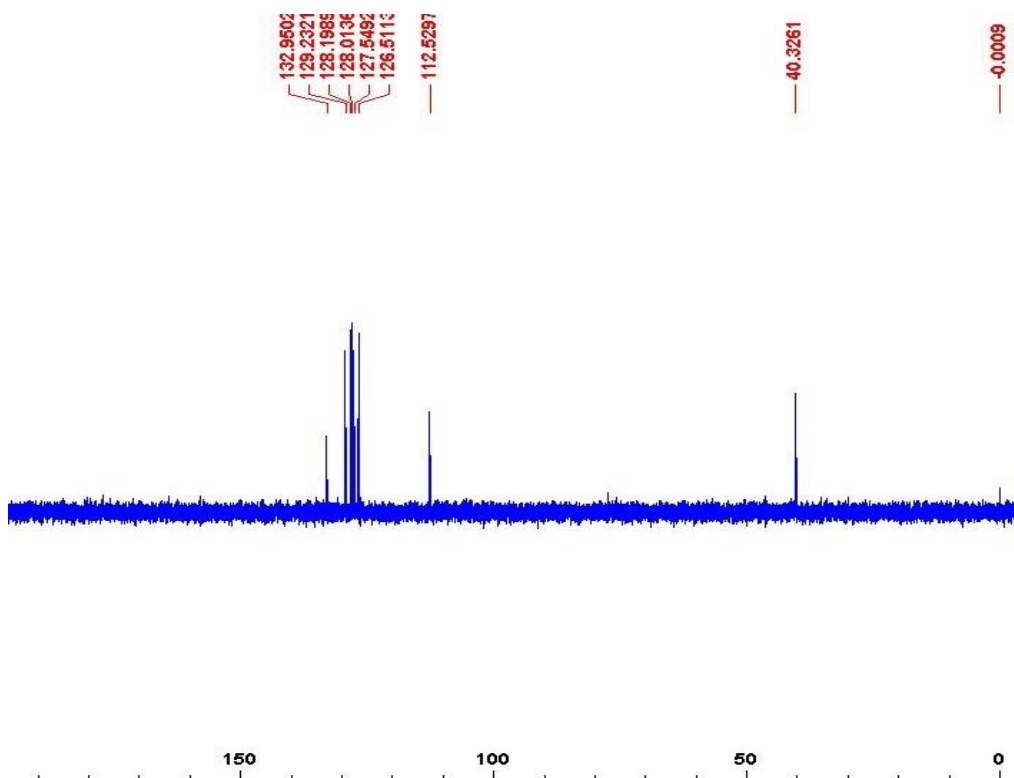


Figure A365. DEPT-135 spectrum of ^1H NMR spectrum of 1-(4-dimethylaminophenyl)-4-(phenylsulfonyl)benzene **138**

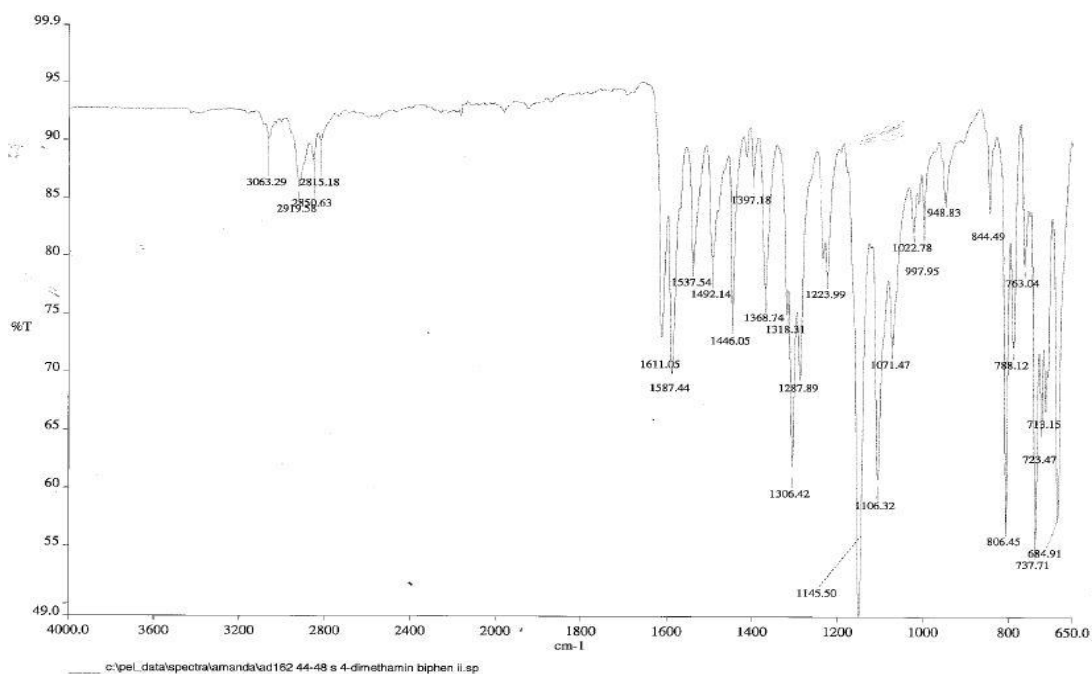


Figure A366. IR spectrum of ^1H NMR spectrum of 1-(4-dimethylaminophenyl)-4-(phenylsulfonyl)benzene **138**

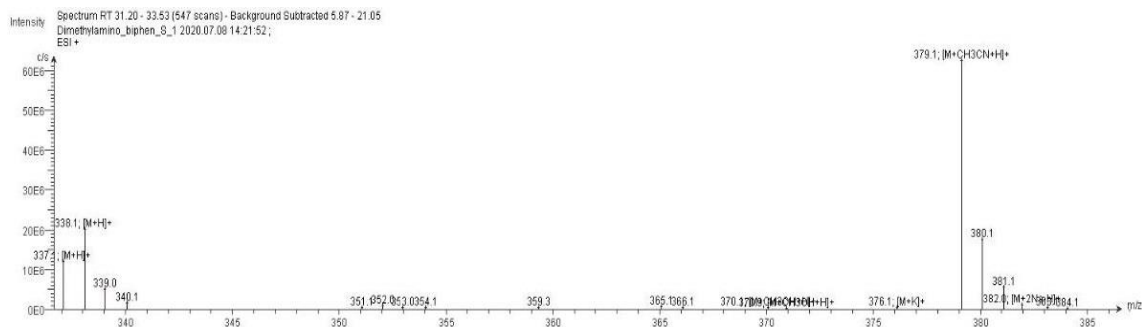
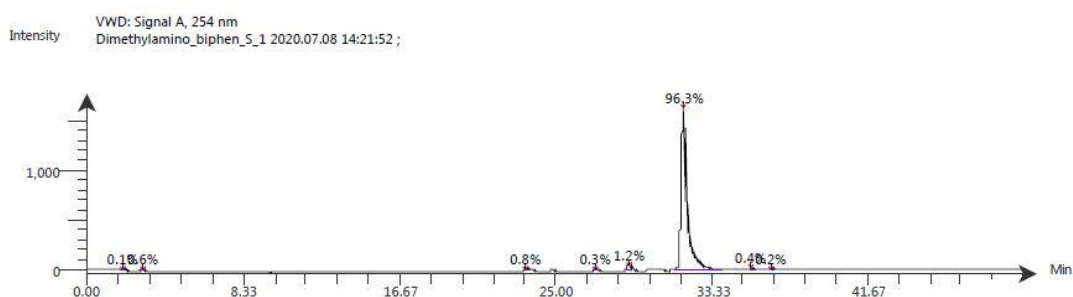


Figure A367. LC-ESI-MS spectrum of ^1H NMR spectrum of 1-(4-dimethylaminophenyl)-4-(phenylsulfonyl)benzene **138**. The ESI spectrum shows it has m/z $[\text{M}+\text{H}]^+$ 338.1.



Time (Peak Maximum M:S/Minutes)	Maximum Intensity (c/s)	Time (Peak Centroid M:S/Minutes)	Peak Area	% Peak Area	Peak Resolution	Label
1.90	8.5E0	1.88	5.4E1	0.1	10.8	
0.00	8.9E1	2.92	2.4E2	0.6	24.5	
23.41	2.3E1	23.43	3.1E2	0.8	14.0	
27.10	1.5E1	27.13	1.1E2	0.3	11.1	
28.87	4.7E1	28.89	4.8E2	1.2	16.6	
31.77	1.7E3	31.78	3.8E4	96.3	16.5	
35.47	2.1E1	35.49	1.7E2	0.4	12.8	
36.54	9.3E0	36.55	7.1E1	0.2	11.4	

Figure A368. LC-UV-MS chromatogram of ^1H NMR spectrum of 1-(4-dimethylaminophenyl)-4-(phenylsulfonyl)benzene **138**

Compound Table

Compound Label	RT (min)	Observed mass (m/z)	Neutral observed mass (Da)	Theoretical mass (Da)	Mass error (ppm)	Isotope match score (%)
Cpd 1: C ₂₀ H ₁₉ N O ₂ S	0.70	360.1030	337.1143	337.1136	1.87	97.77

Figure A369. HR-MS analysis of ^1H NMR spectrum of 1-(4-dimethylaminophenyl)-4-(phenylsulfonyl)benzene **138**

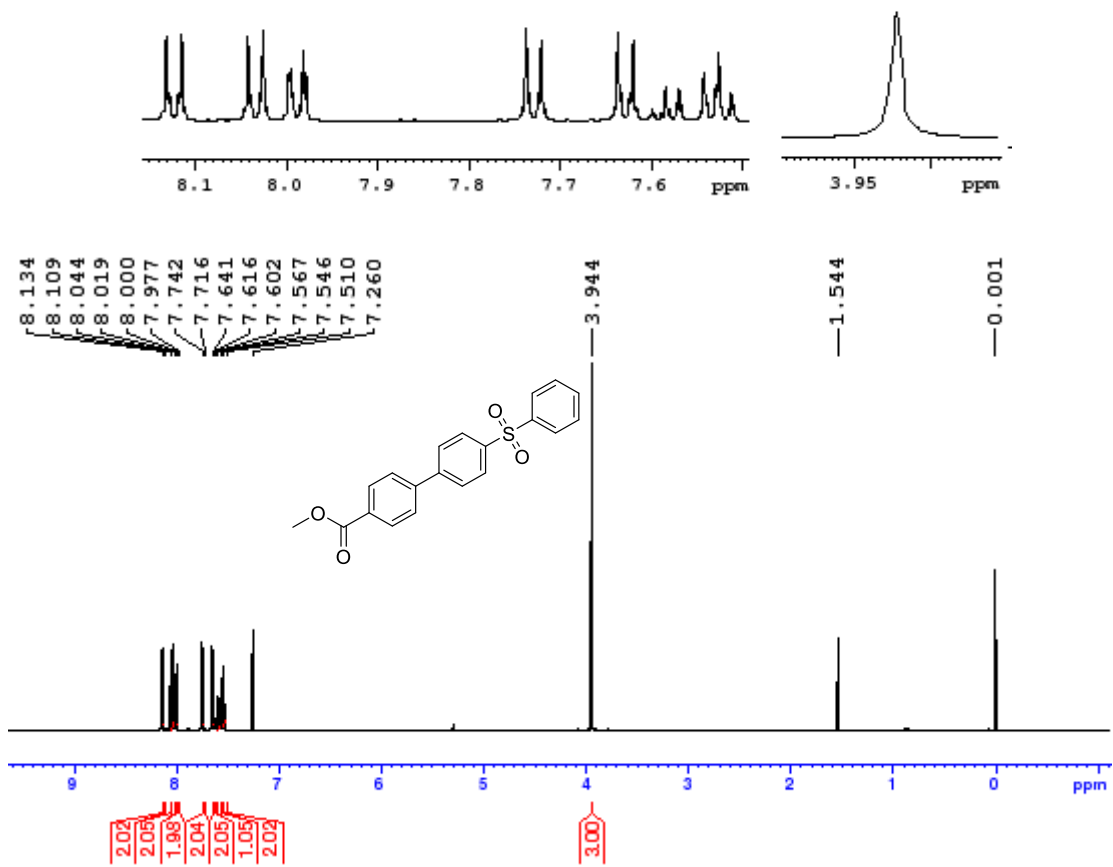


Figure A370. ¹H NMR spectrum of 1-(4-methyl ester phenyl)-4-(phenylsulfonyl)benzene **139**

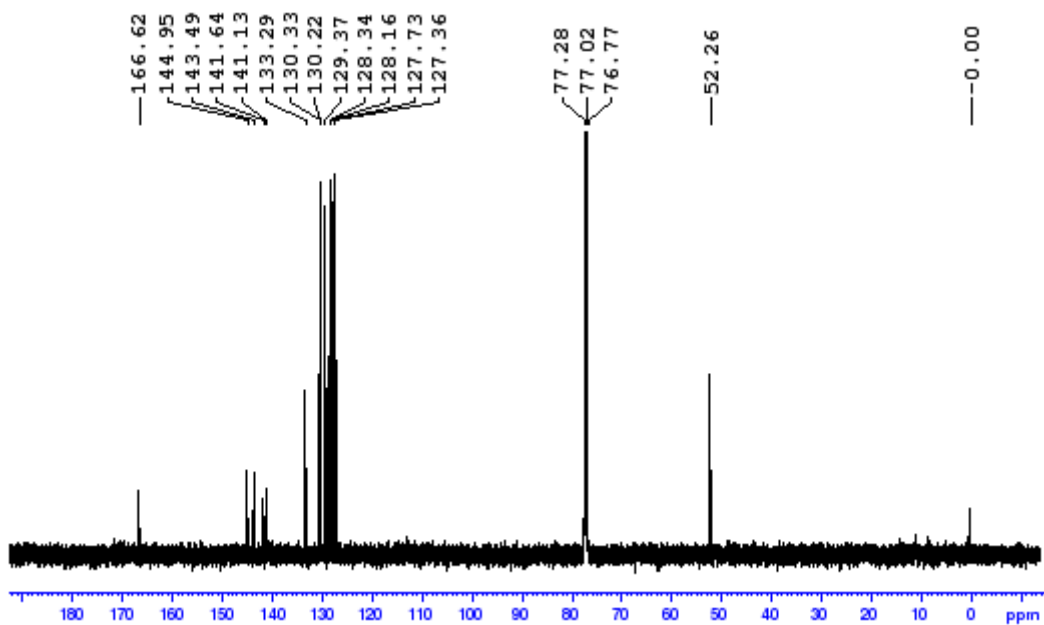


Figure A371. ¹³C NMR spectrum of 1-(4-methyl ester phenyl)-4-(phenylsulfonyl)benzene **139**

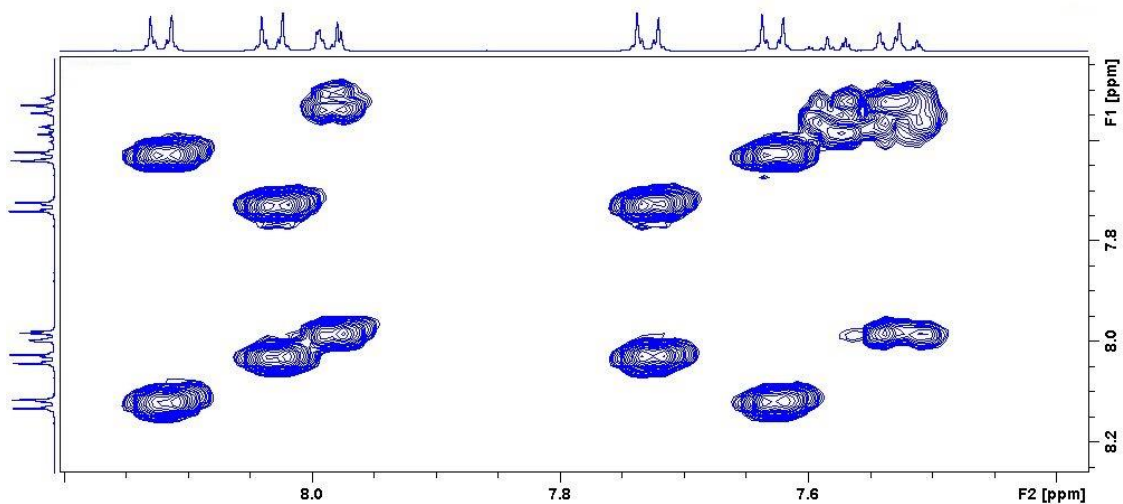


Figure A372. Zoomed in COSY spectrum of 1-(4-methyl ester phenyl)-4-(phenylsulfonyl)benzene **139**

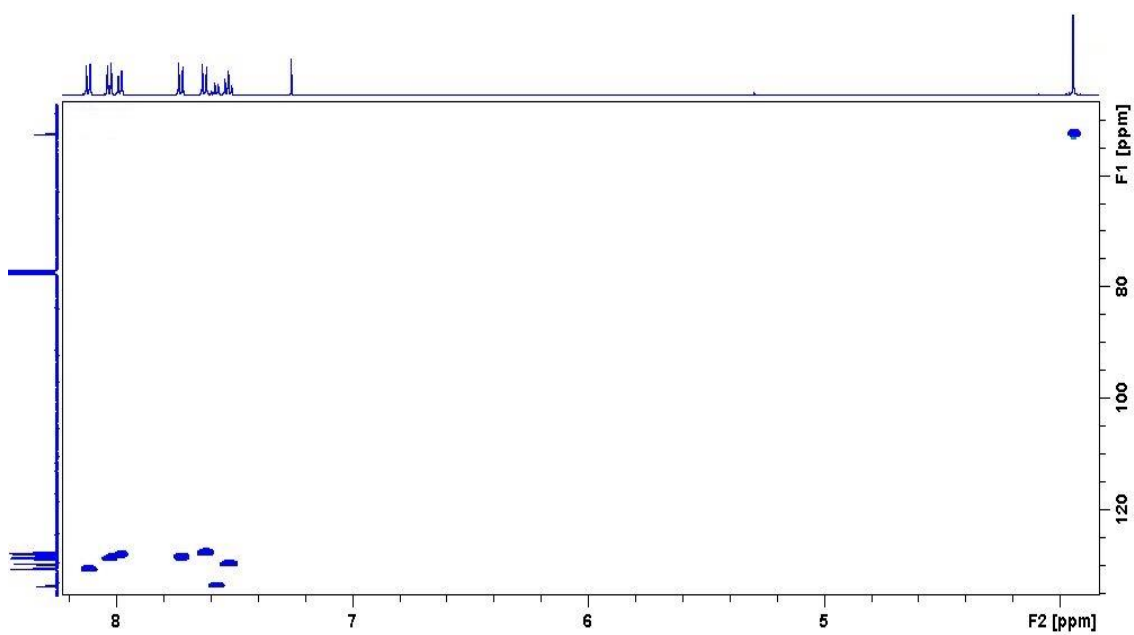


Figure A373. Zoomed in HSQC spectrum of 1-(4-methyl ester phenyl)-4-(phenylsulfonyl)benzene **139**

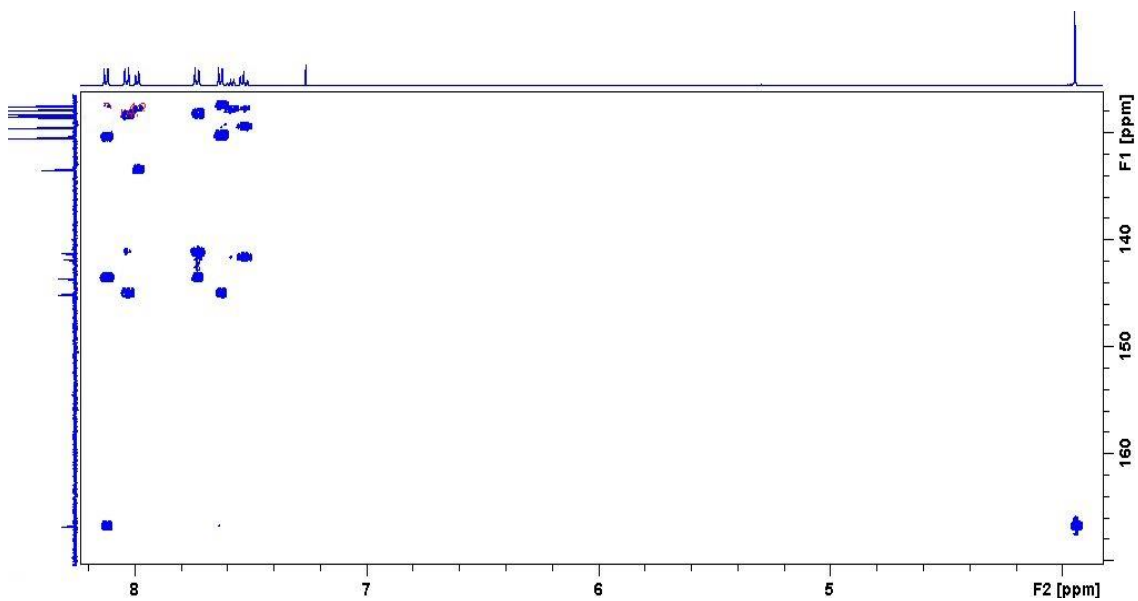


Figure A374. Zoomed in HMBC spectrum of 1-(4-methyl ester phenyl)-4-(phenylsulfonyl)benzene **139**

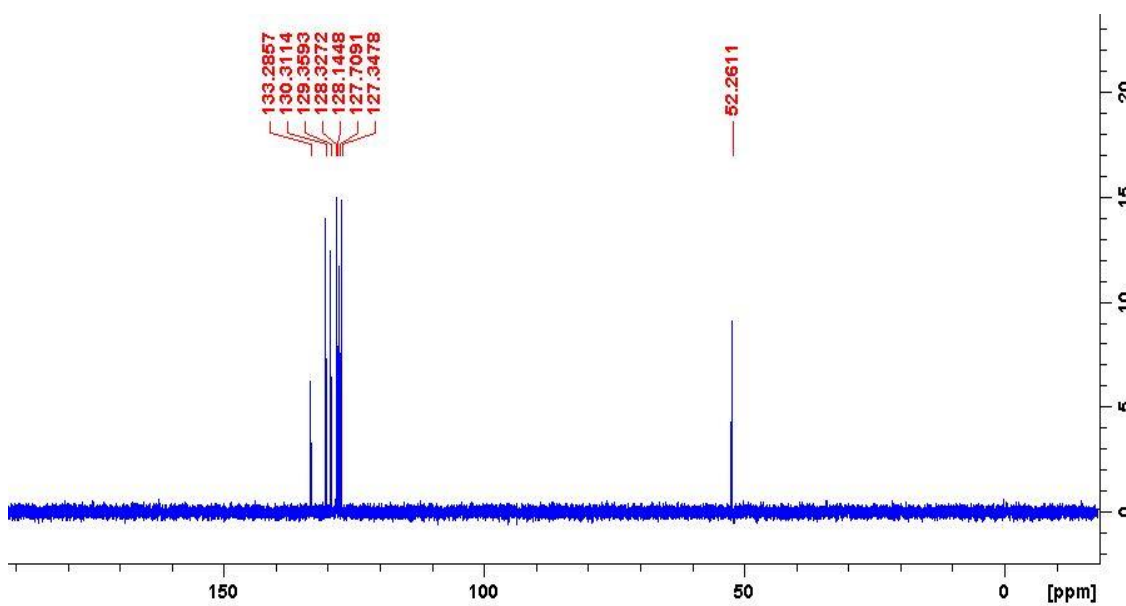


Figure A375. DEPT-135 spectrum of 1-(4-methyl ester phenyl)-4-(phenylsulfonyl)benzene **139**

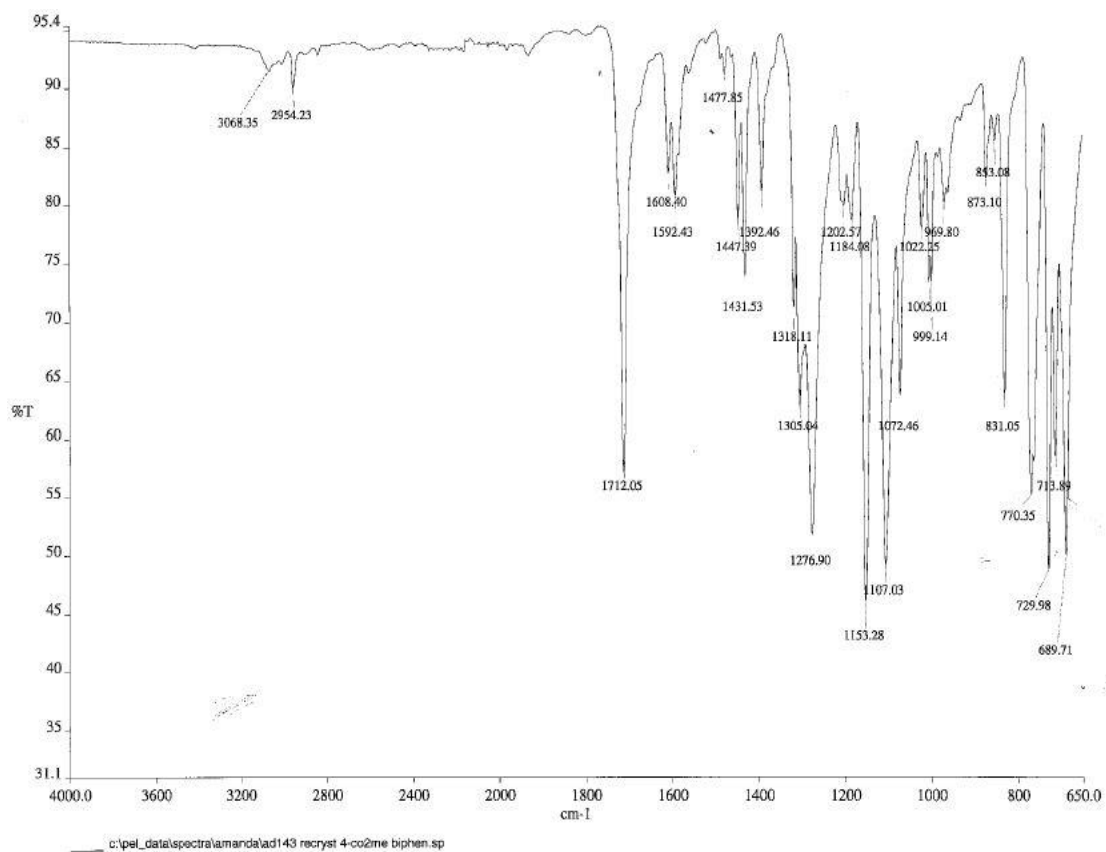


Figure A376. IR spectrum of 1-(4-methyl ester phenyl)-4-(phenylsulfonyl)benzene **139**

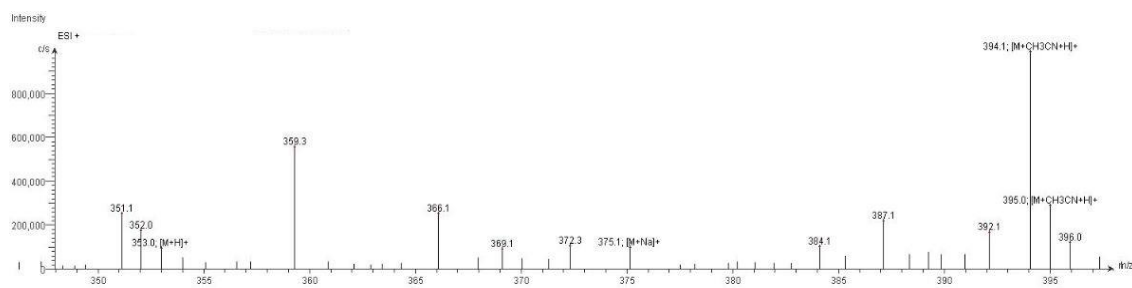


Figure A377. LC-ESI-MS spectrum of 1-(4-methyl ester phenyl)-4-(phenylsulfonyl)benzene **139**. The ESI spectrum shows it has m/z $[M+Na]^+$ 375.1.

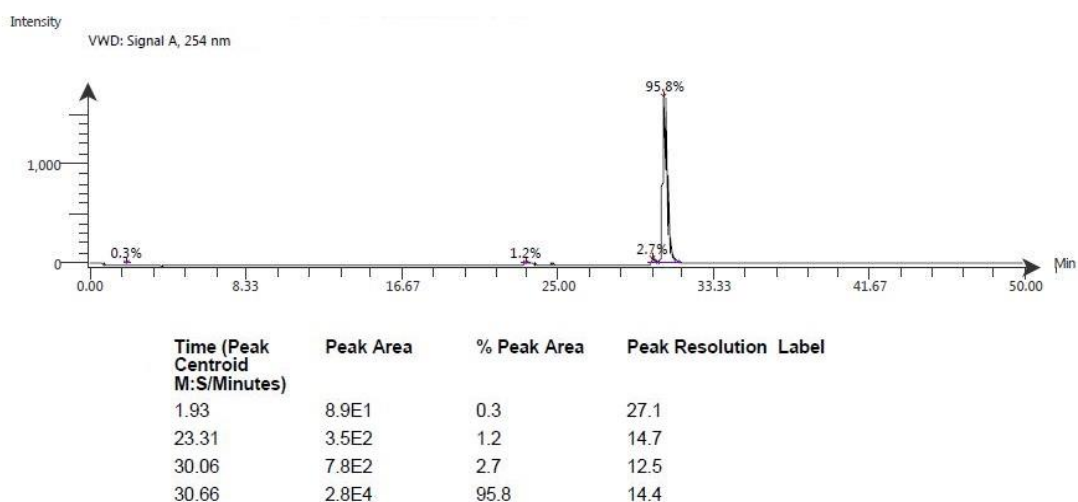


Figure A378. LC-UV-MS chromatogram of 1-(4-methyl ester phenyl)-4-(phenylsulfonyl)benzene **139**

Compound Table

Compound Label	RT (min)	Observed mass (m/z)	Neutral observed mass (Da)	Theoretical mass (Da)	Mass error (ppm)	Isotope match score (%)
Cpd 1: C20 H16 O4 S	0.69	353.0844	352.0777	352.0769	2.16	96.95

Figure A379. HR-MS analysis of 1-(4-methyl ester phenyl)-4-(phenylsulfonyl)benzene **139**

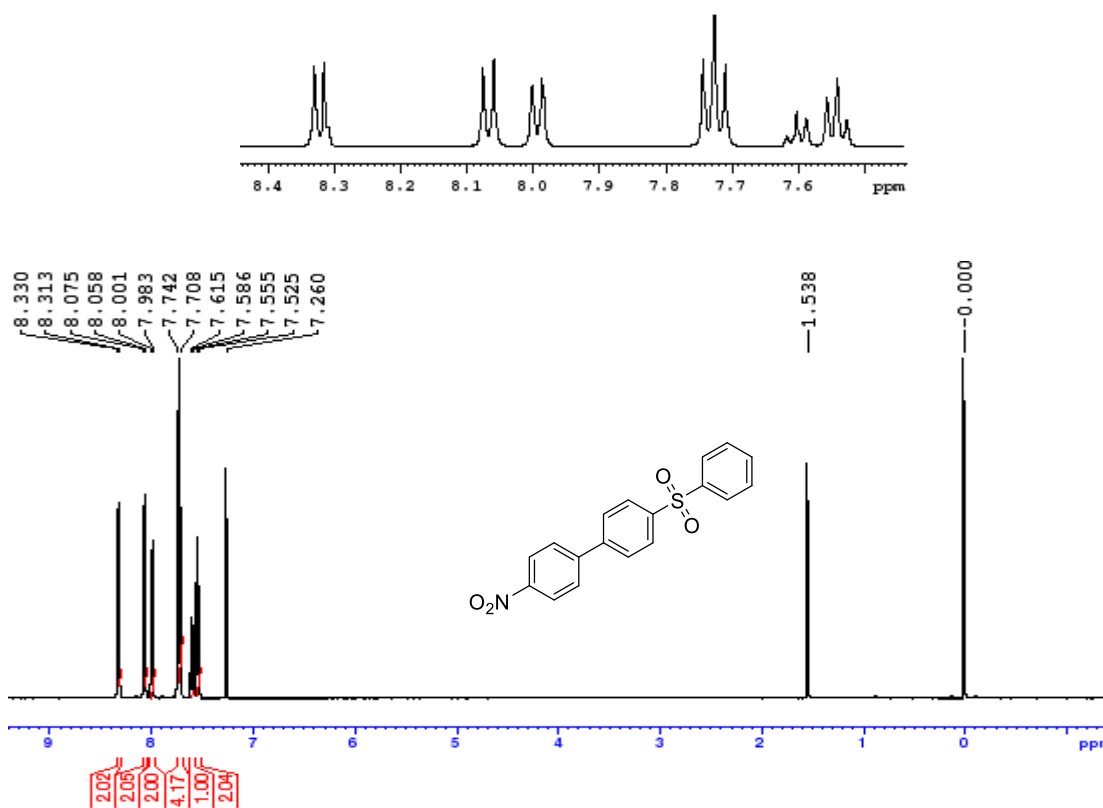


Figure A380. ^1H NMR spectrum of 1-(4-nitrophenyl)-4-(phenylsulfonyl)benzene **140**

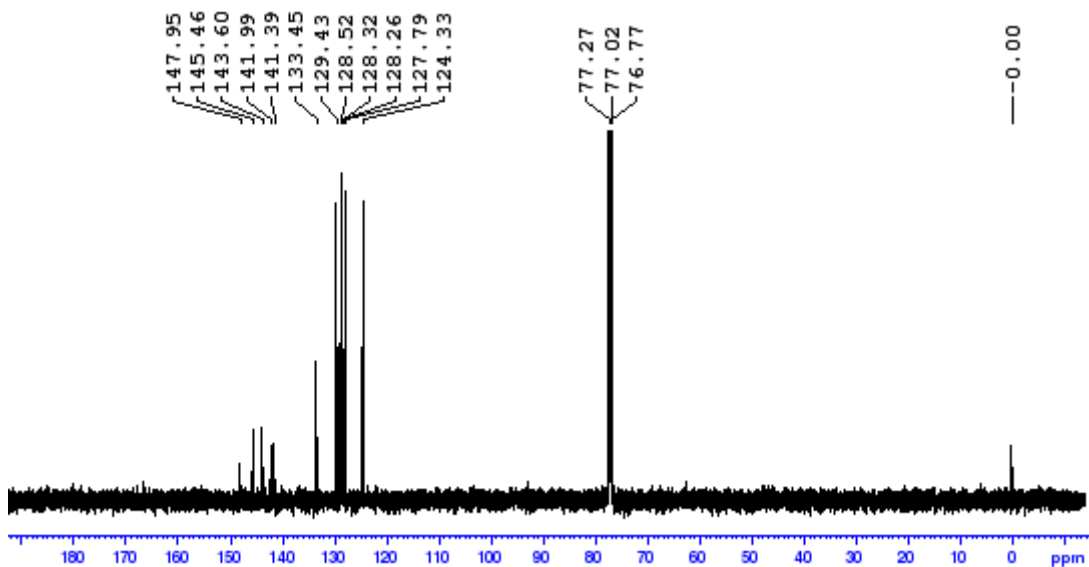


Figure A381. ^{13}C NMR spectrum of 1-(4-nitrophenyl)-4-(phenylsulfonyl)benzene **140**

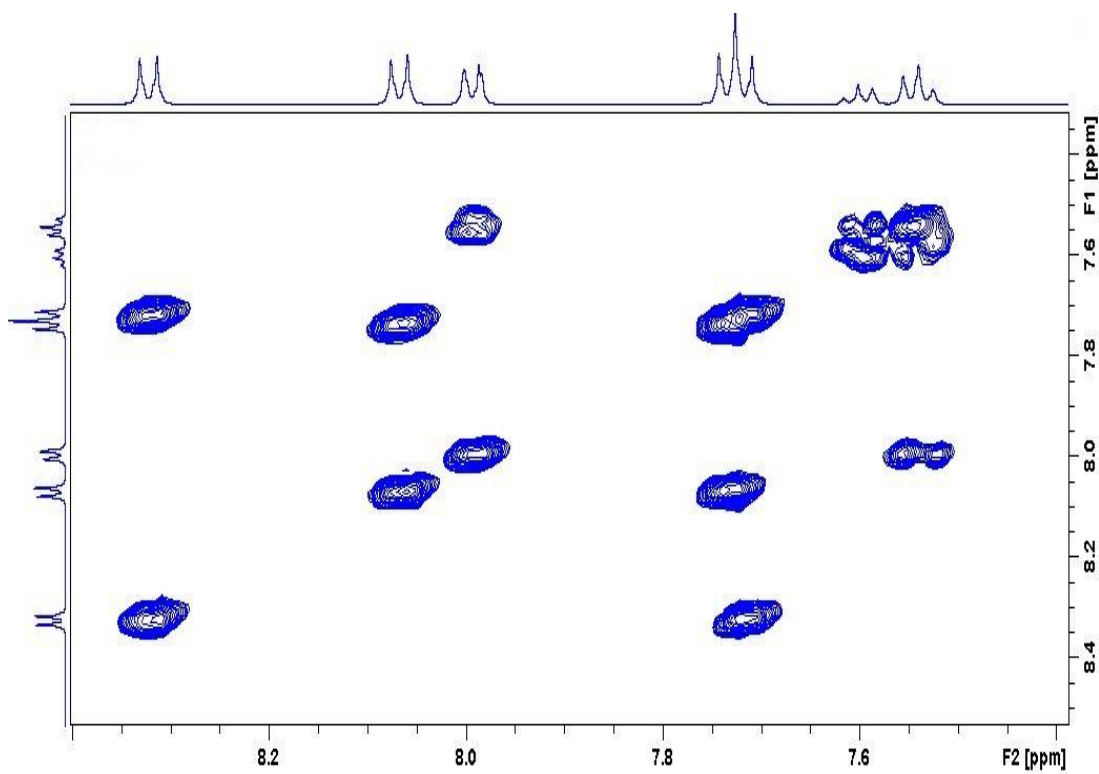


Figure A382. Zoomed in COSY spectrum of 1-(4-nitrophenyl)-4-(phenylsulfonyl)benzene **140**

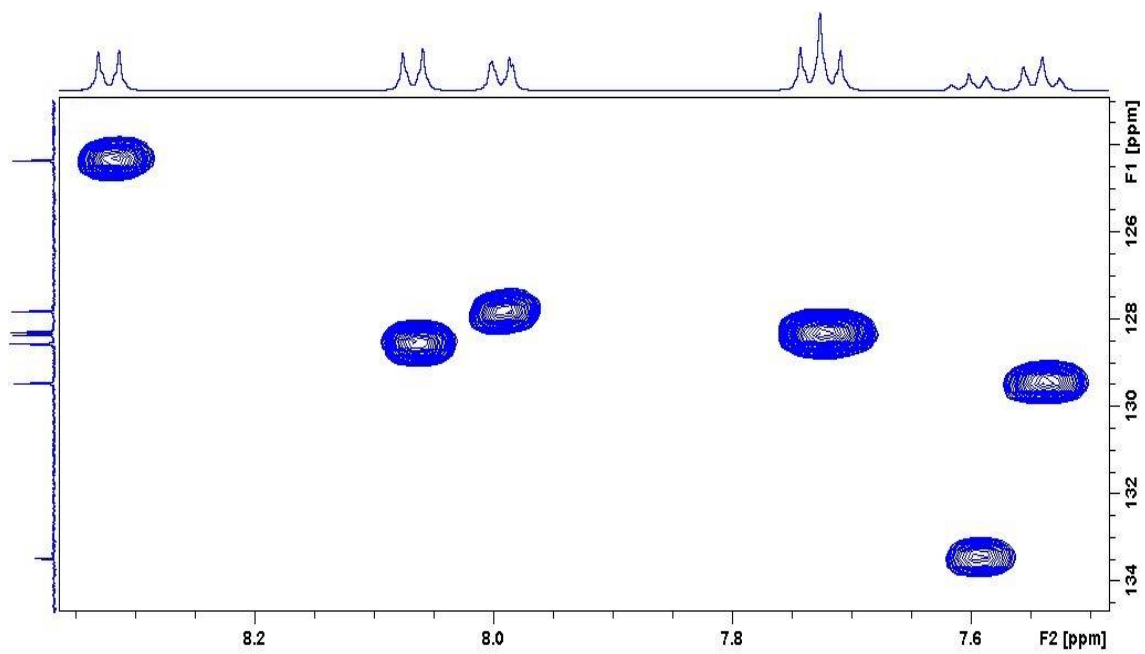


Figure A383. Zoomed in HSQC spectrum of 1-(4-nitrophenyl)-4-(phenylsulfonyl)benzene **140**

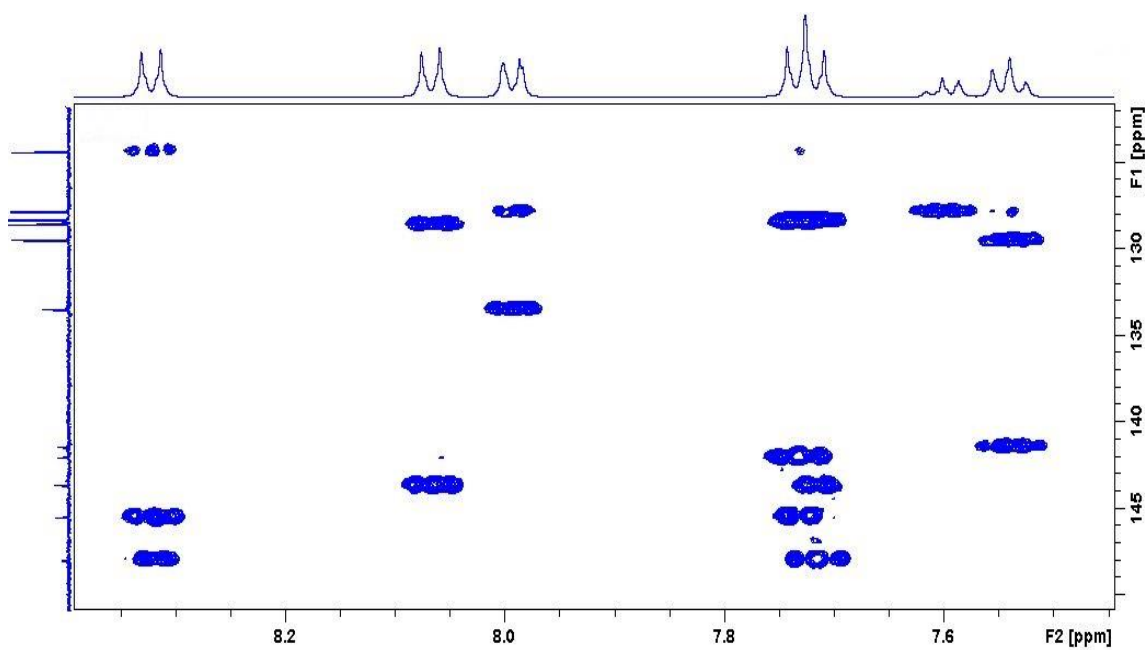


Figure A384. Zoomed in HMBC spectrum of 1-(4-nitrophenyl)-4-(phenylsulfonyl)benzene **140**

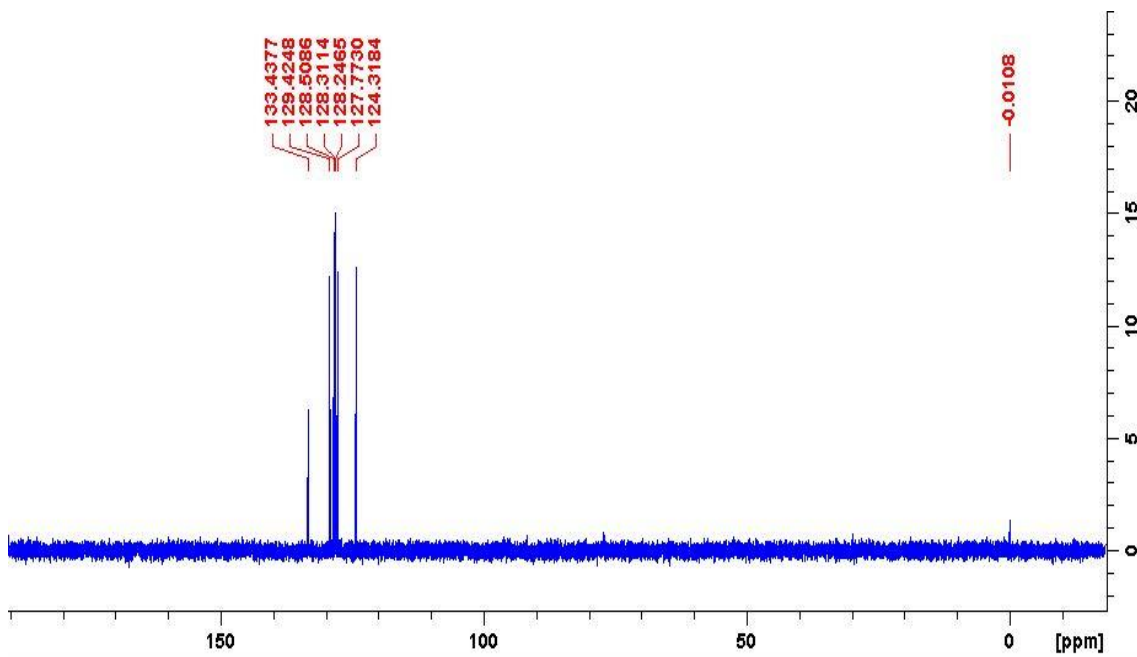


Figure A385. DEPT-135 spectrum of 1-(4-nitrophenyl)-4-(phenylsulfonyl)benzene **140**

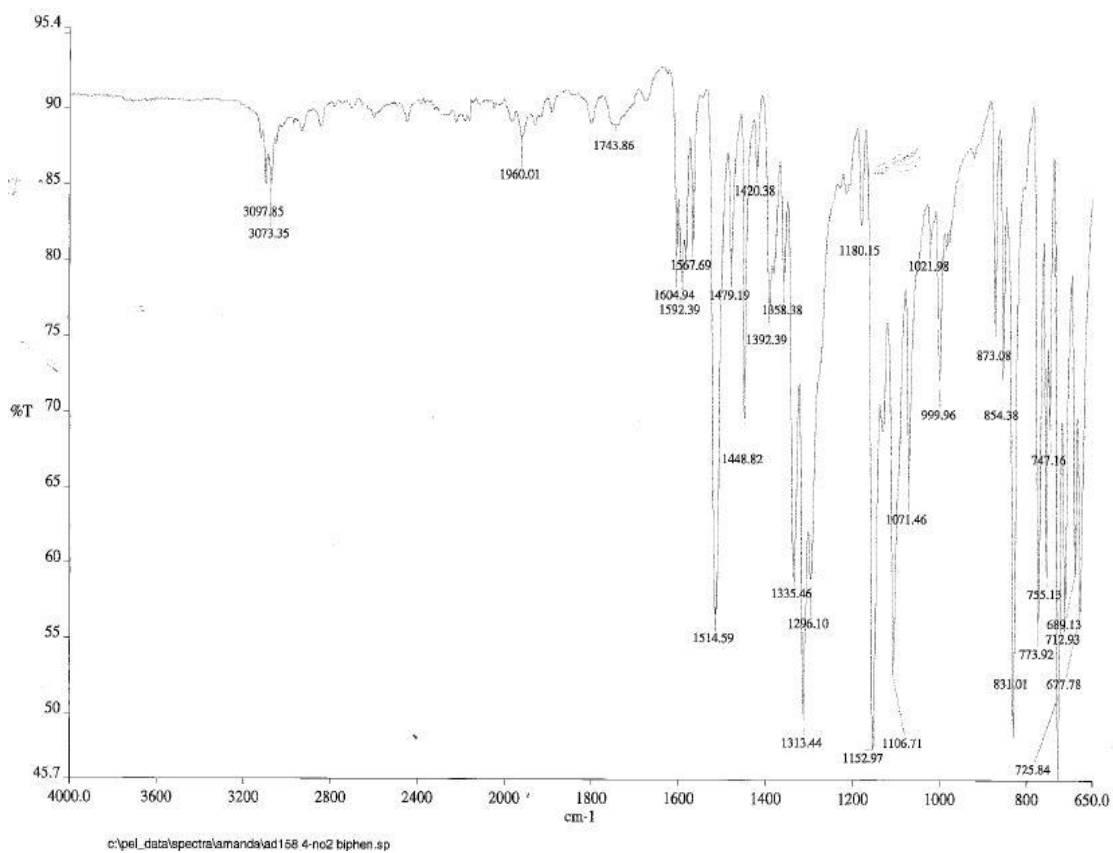


Figure A386. IR spectrum of 1-(4-nitrophenyl)-4-(phenylsulfonyl)benzene **140**

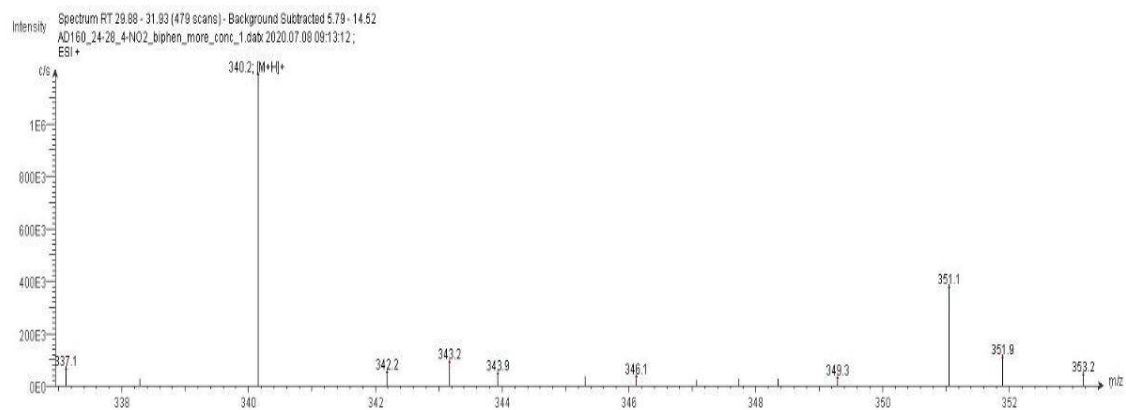
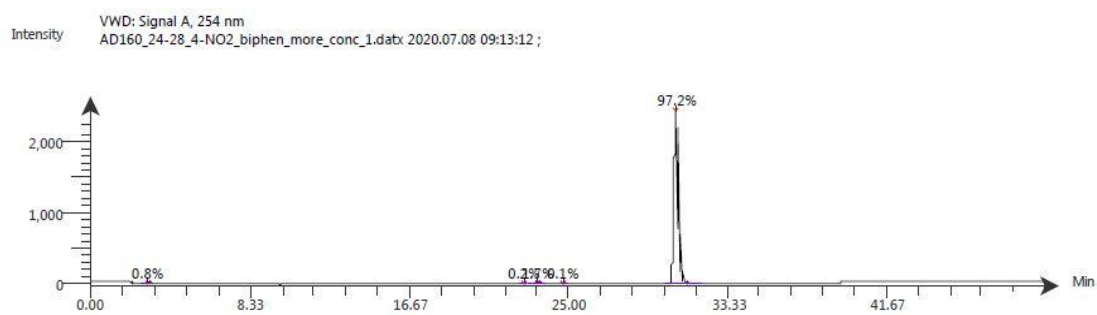


Figure A387. LC-ESI-MS spectrum of 1-(4-nitrophenyl)-4-(phenylsulfonyl)benzene **140**. The ESI spectrum shows it has m/z $[M+H]^+$ 340.2



Time (Peak Maximum M:S/Minutes)	Maximum Intensity (c/s)	Time (Peak Centroid M:S/Minutes)	Peak Area	% Peak Area	Peak Resolution Label
2.97	2.5E1	2.95	3E2	0.8	10.7
0.00	3.4E2	22.65	8.1E1	0.2	21.8
23.30	3E1	23.41	6.4E2	1.7	19.4
0.00	1.9E1	24.72	4.6E1	0.1	17.8
30.59	2.4E3	30.59	3.7E4	97.2	13.8

Figure A388. LC-UV-MS chromatogram of 1-(4-nitrophenyl)-4-(phenylsulfonyl)benzene **140**

Compound Table

Compound Label	RT (min)	Observed mass (m/z)	Neutral observed mass (Da)	Theoretical mass (Da)	Mass error (ppm)	Isotope match score (%)
Cpd 1: C18 H13 N O4 S	0.90	339.0566	339.0561	339.0565	-1.23	97.10

Figure A389. HR-MS analysis of 1-(4-nitrophenyl)-4-(phenylsulfonyl)benzene **140**

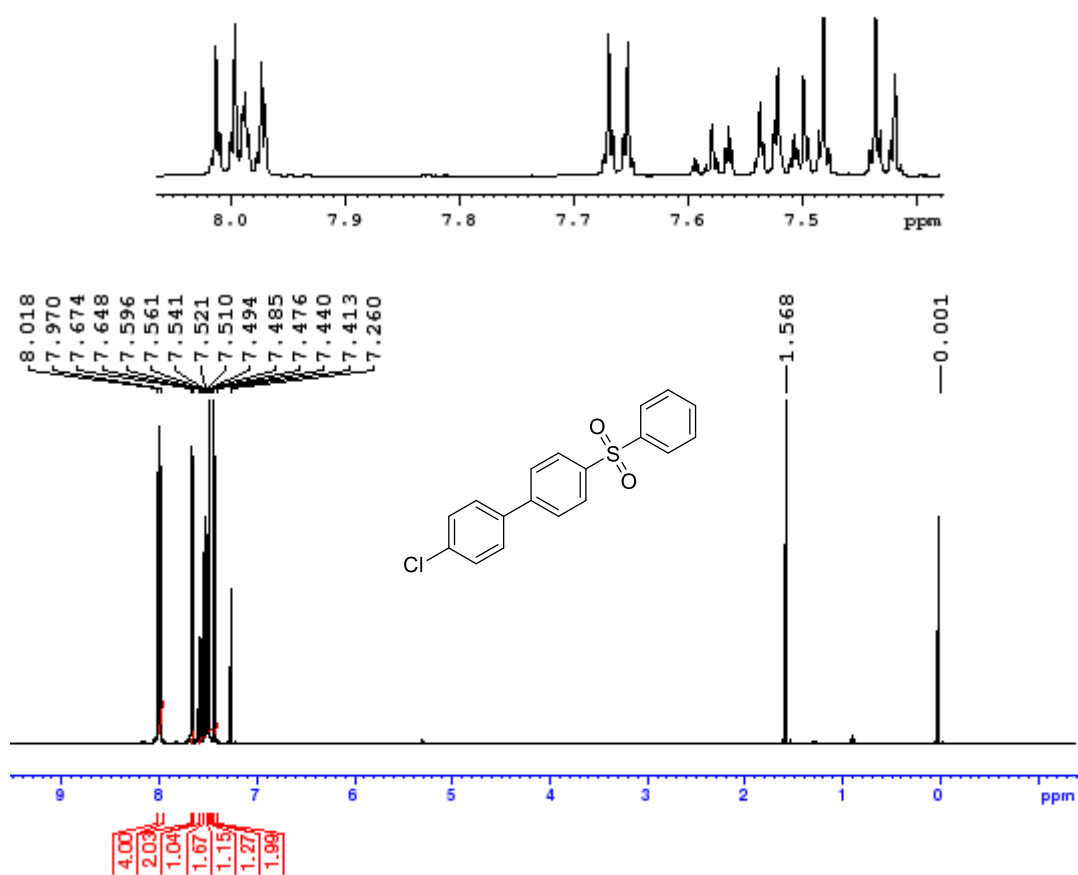


Figure A390. ¹H NMR spectrum of 1-(4-chlorophenyl)-4-(phenylsulfonyl)benzene **141**

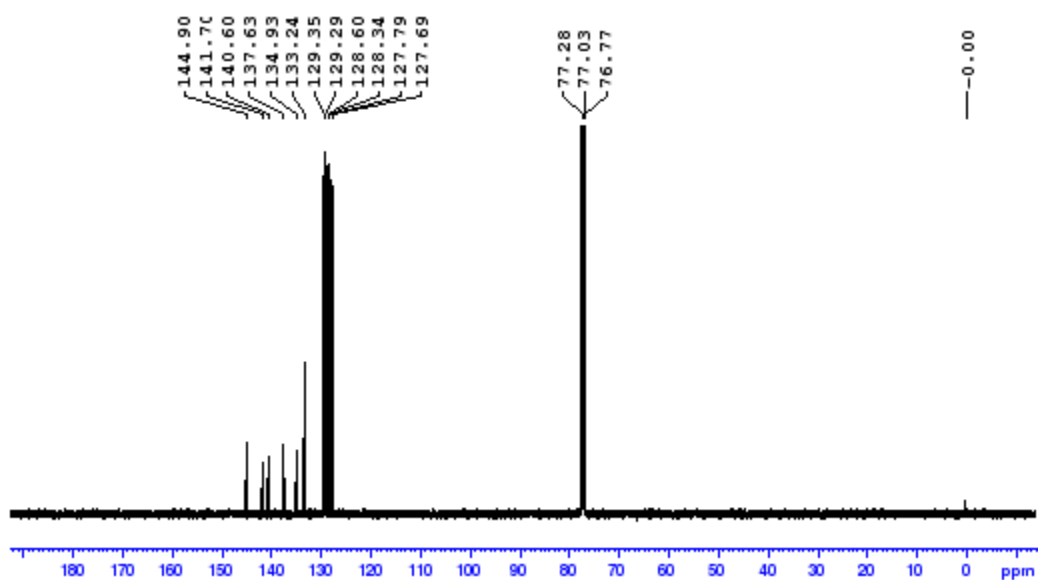


Figure A391. ¹³C NMR spectrum of 1-(4-chlorophenyl)-4-(phenylsulfonyl)benzene **141**

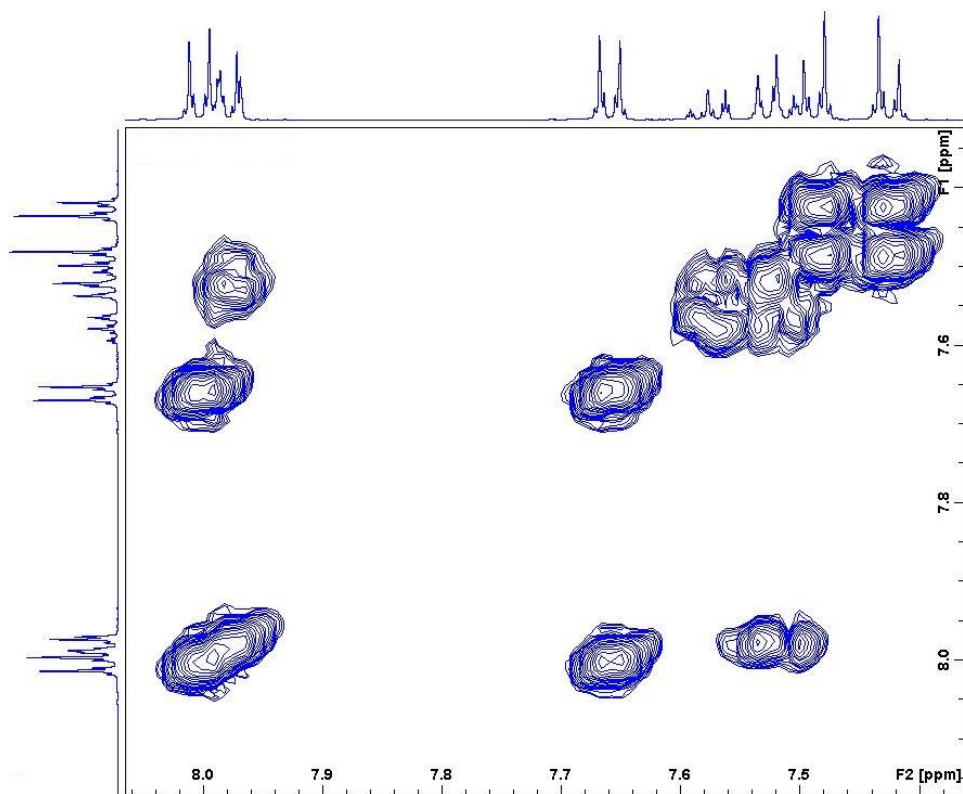


Figure A392. Zoomed in COSY spectrum of 1-(4-chlorophenyl)-4-(phenylsulfonyl)benzene **141**

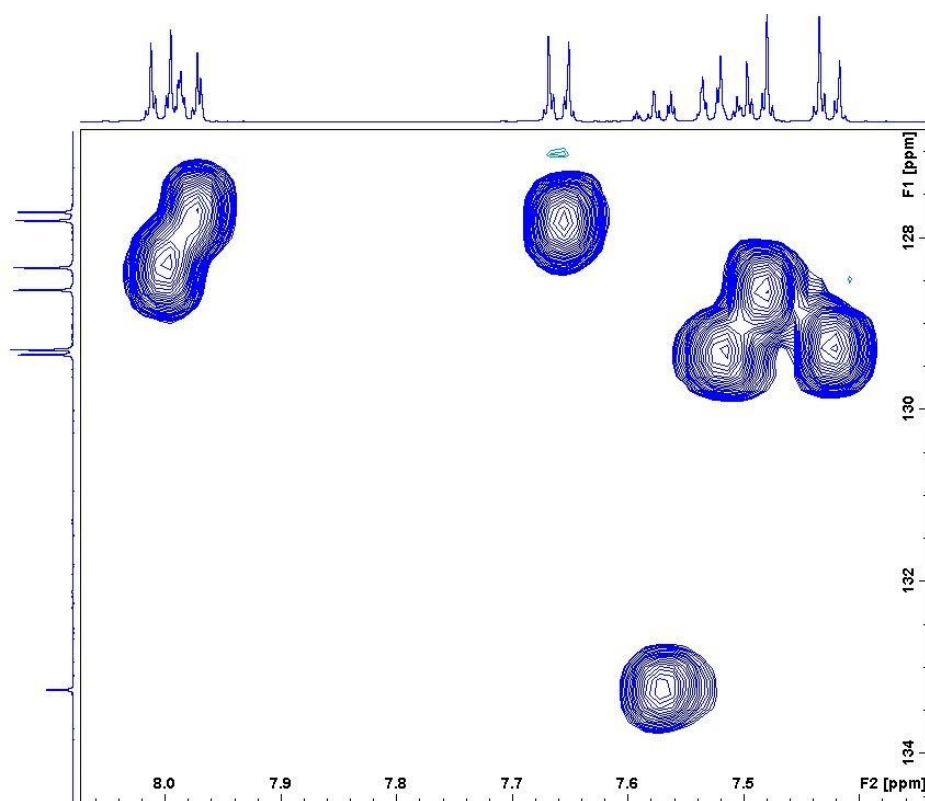


Figure A393. Zoomed in HSQC spectrum of 1-(4-chlorophenyl)-4-(phenylsulfonyl)benzene **141**

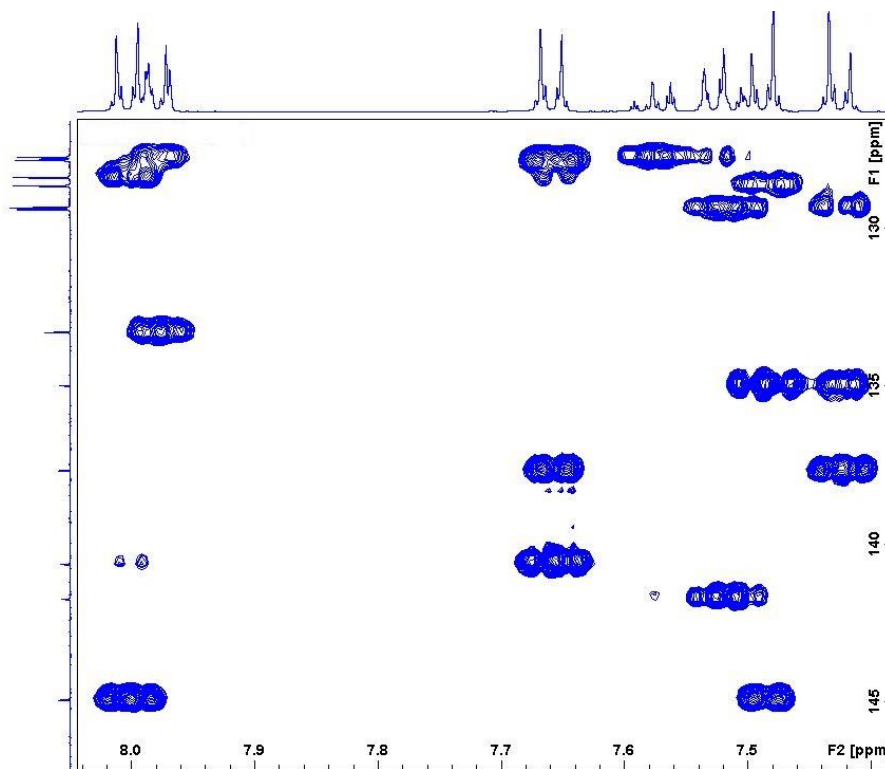


Figure A394. Zoomed in HMBC spectrum of 1-(4-chlorophenyl)-4-(phenylsulfonyl)benzene **141**

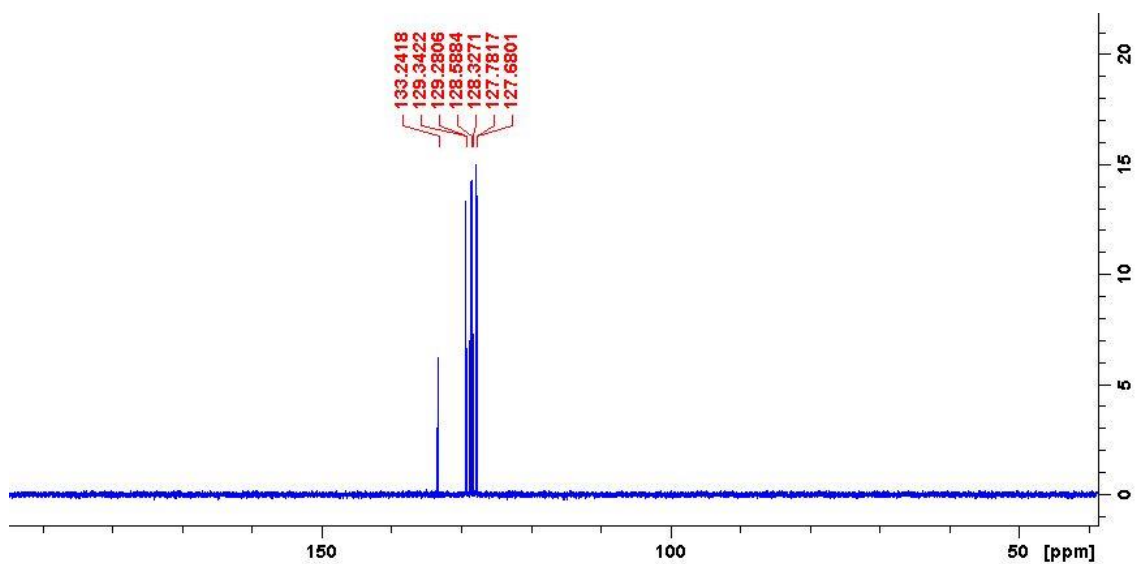


Figure A395. DEPT-135 spectrum of 1-(4-chlorophenyl)-4-(phenylsulfonyl)benzene **141**

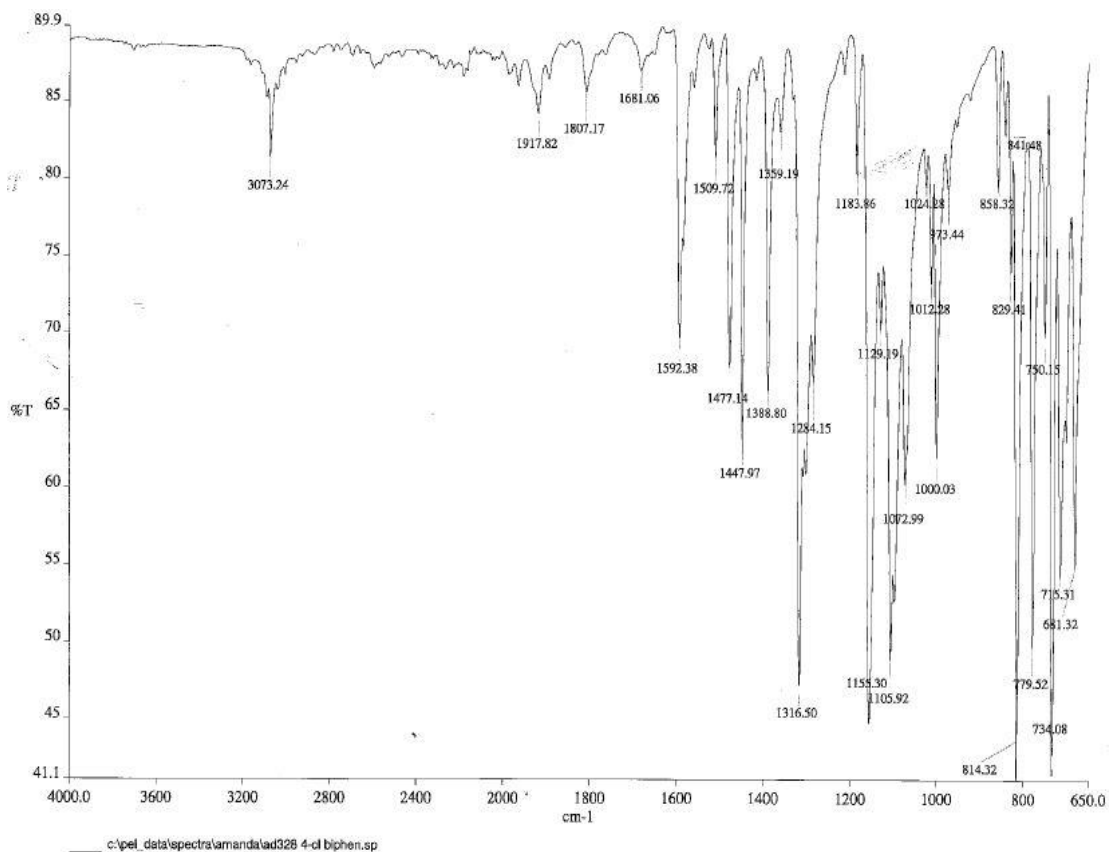


Figure A396. IR spectrum of 1-(4-chlorophenyl)-4-(phenylsulfonyl)benzene **141**

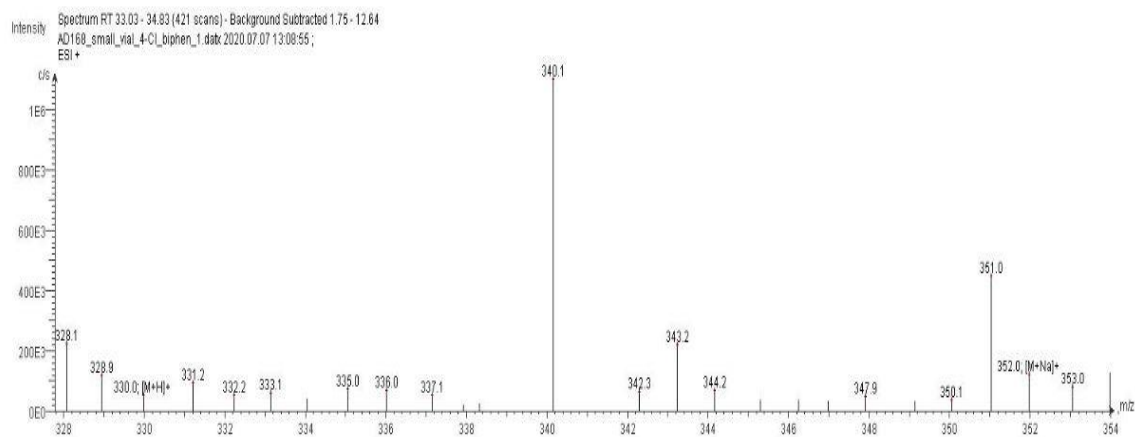
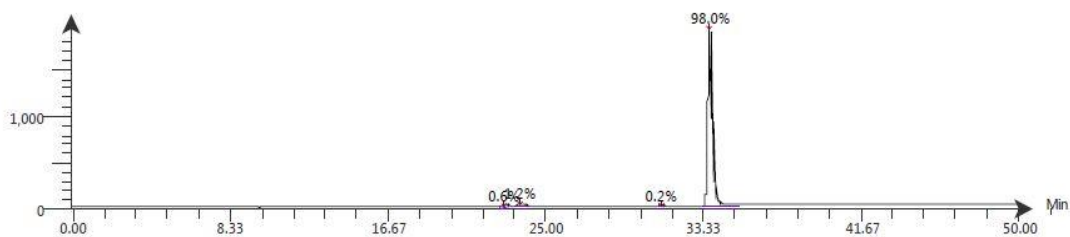


Figure A397. LC-ESI-MS spectrum of 1-(4-chlorophenyl)-4-(phenylsulfonyl)benzene **141**. The ESI spectrum shows it has m/z [M+Na]⁺ 352.0.

VWD: Signal A, 254 nm
 Intensity AD168_small_vial_4-Cl_biphen_1.datx 2020.07.07 13:08:55 ;



Time (Peak Maximum M:S/Minutes)	Maximum Intensity (c/s)	Time (Peak Centroid M:S/Minutes)	Peak Area	% Peak Area	Peak Resolution	Label
22.84	1.2E1	22.84	1.9E2	0.6	16.5	
23.56	2.7E1	23.61	4.1E2	1.2	14.9	
31.08	6.9E0	31.09	5E1	0.2	9.8	
33.63	1.9E3	33.64	3.3E4	98.0	15.3	

Figure A398. LC-UV-MS chromatogram of 1-(4-chlorophenyl)-4-(phenylsulfonyl)benzene **141**

Compound Table

Compound Label	RT (min)	Observed mass (m/z)	Neutral observed mass (Da)	Theoretical mass (Da)	Mass error (ppm)	Isotope match score (%)
Cpd 1: C18 H13 Cl O2 S	0.70	351.0224	328.0330	328.0325	1.63	99.00

Figure A399. HR-MS analysis of 1-(4-chlorophenyl)-4-(phenylsulfonyl)benzene **141**

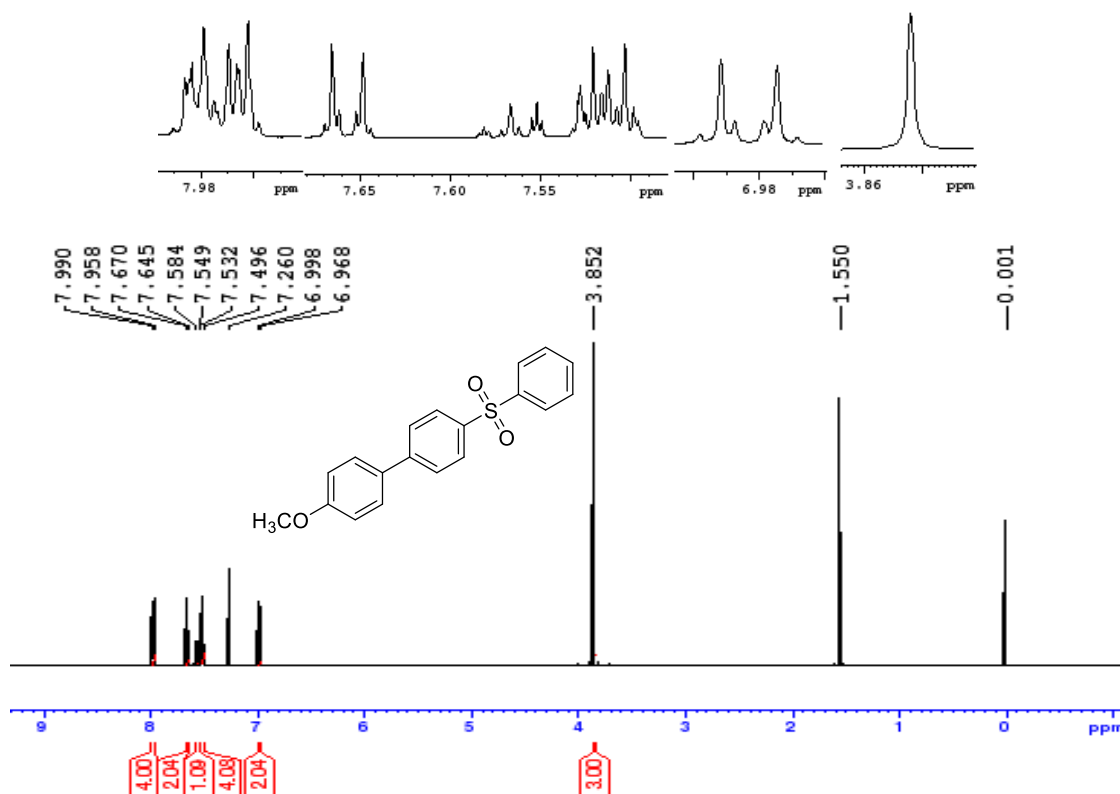


Figure A400. ¹H NMR spectrum of 1-(4-methoxyphenyl)-4-(phenylsulfonyl)benzene **142**

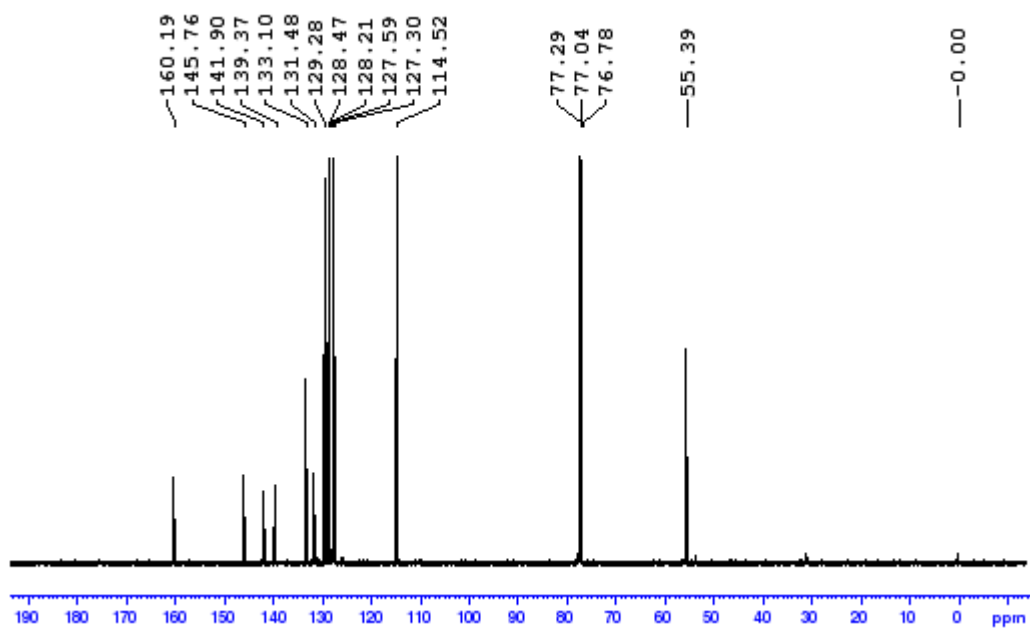


Figure A401. ^{13}C NMR spectrum of 1-(4-methoxyphenyl)-4-(phenylsulfonyl)benzene **142**

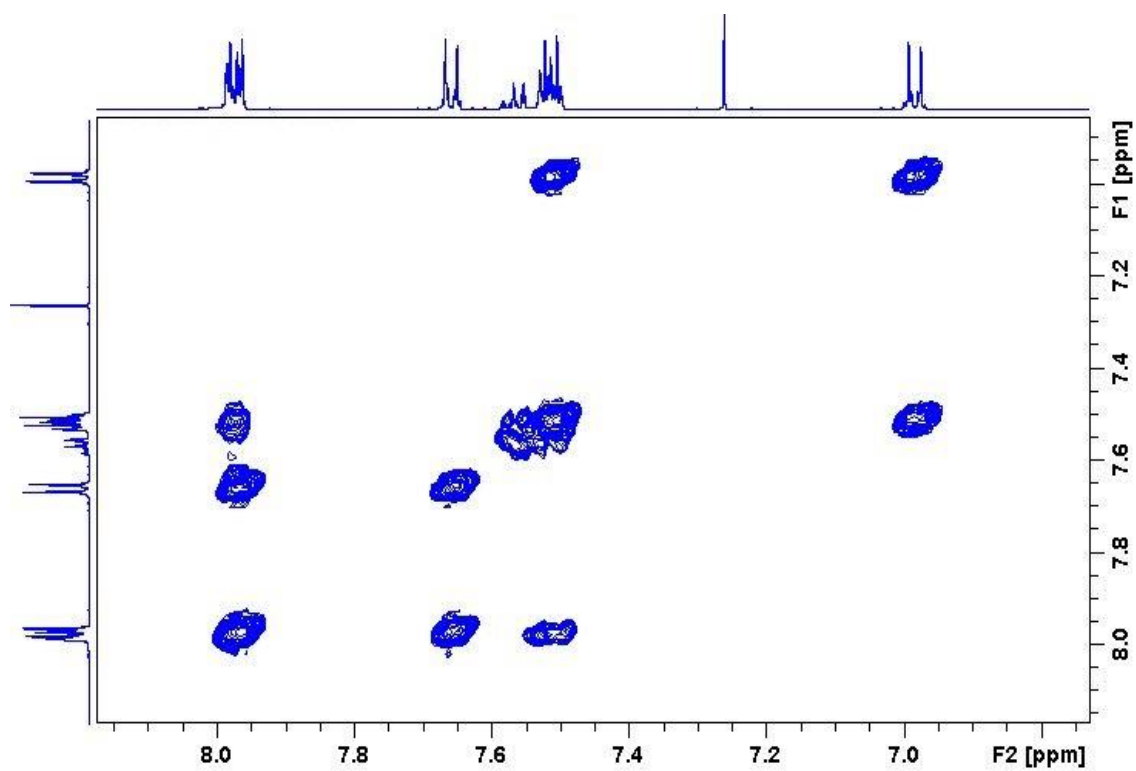


Figure A402. Zoomed in COSY spectrum of 1-(4-methoxyphenyl)-4-(phenylsulfonyl)benzene **142**

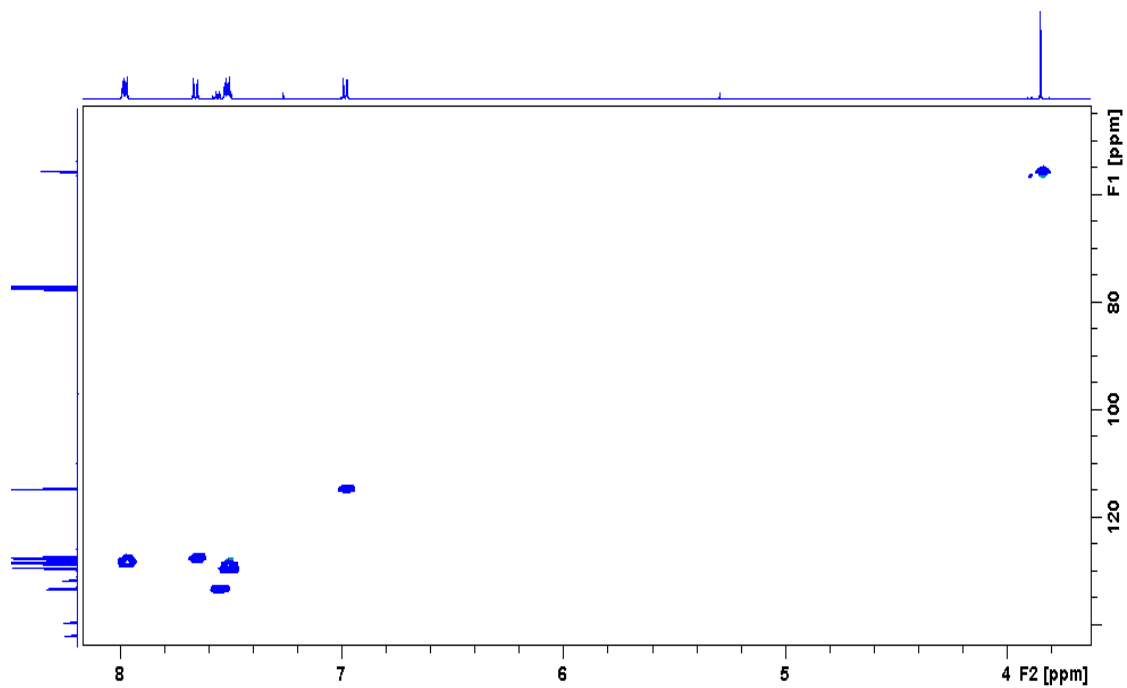


Figure A403. Zoomed in HSQC spectrum of 1-(4-methoxyphenyl)-4-(phenylsulfonyl)benzene **142**

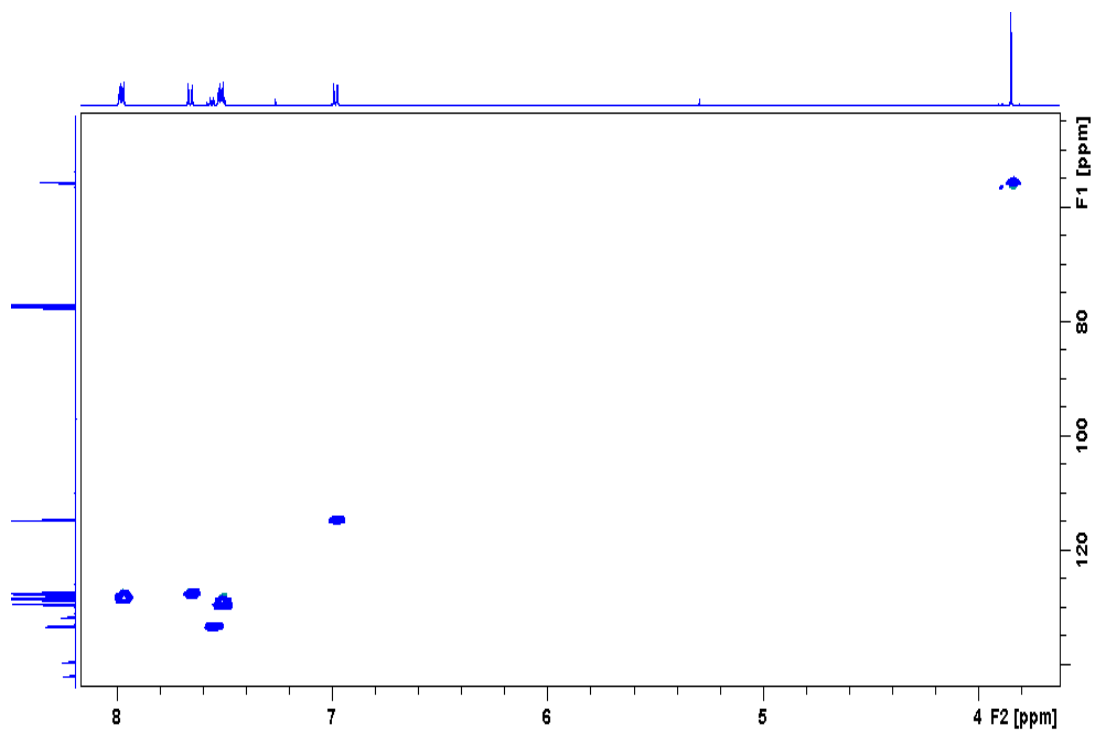


Figure A404. Zoomed in HMBC spectrum of 1-(4-methoxyphenyl)-4-(phenylsulfonyl)benzene **142**

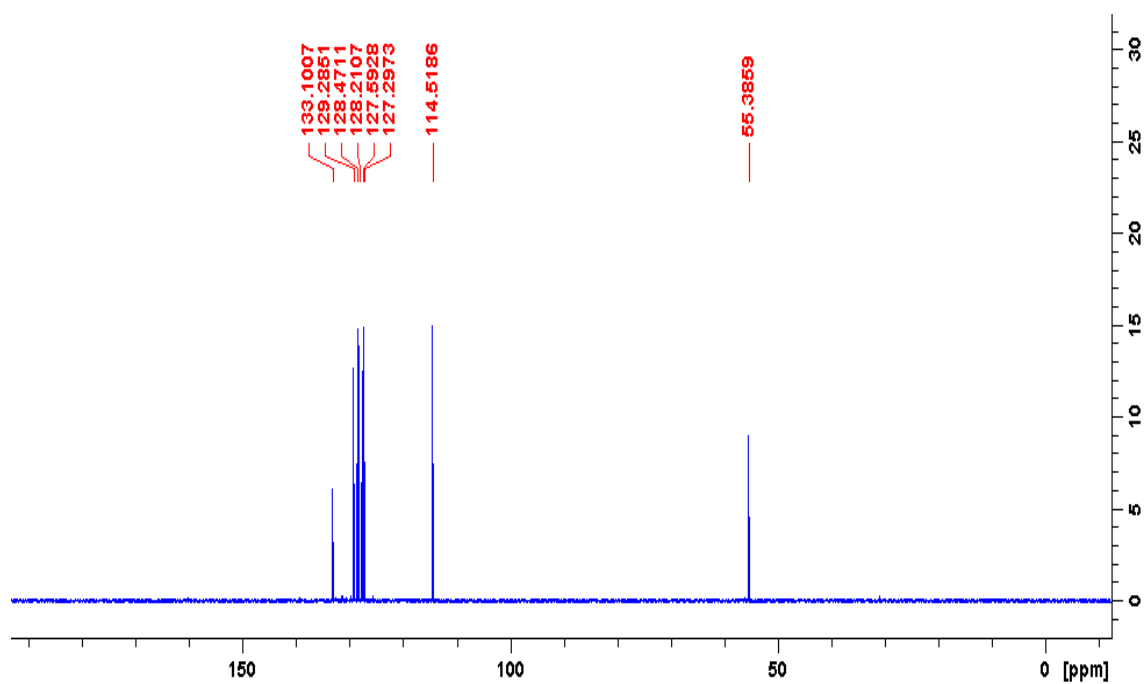


Figure A405. DEPT-135 spectrum of 1-(4-methoxyphenyl)-4-(phenylsulfonyl)benzene, 1-(4-methoxyphenyl)-4-(phenylsulfonyl)benzene **142**

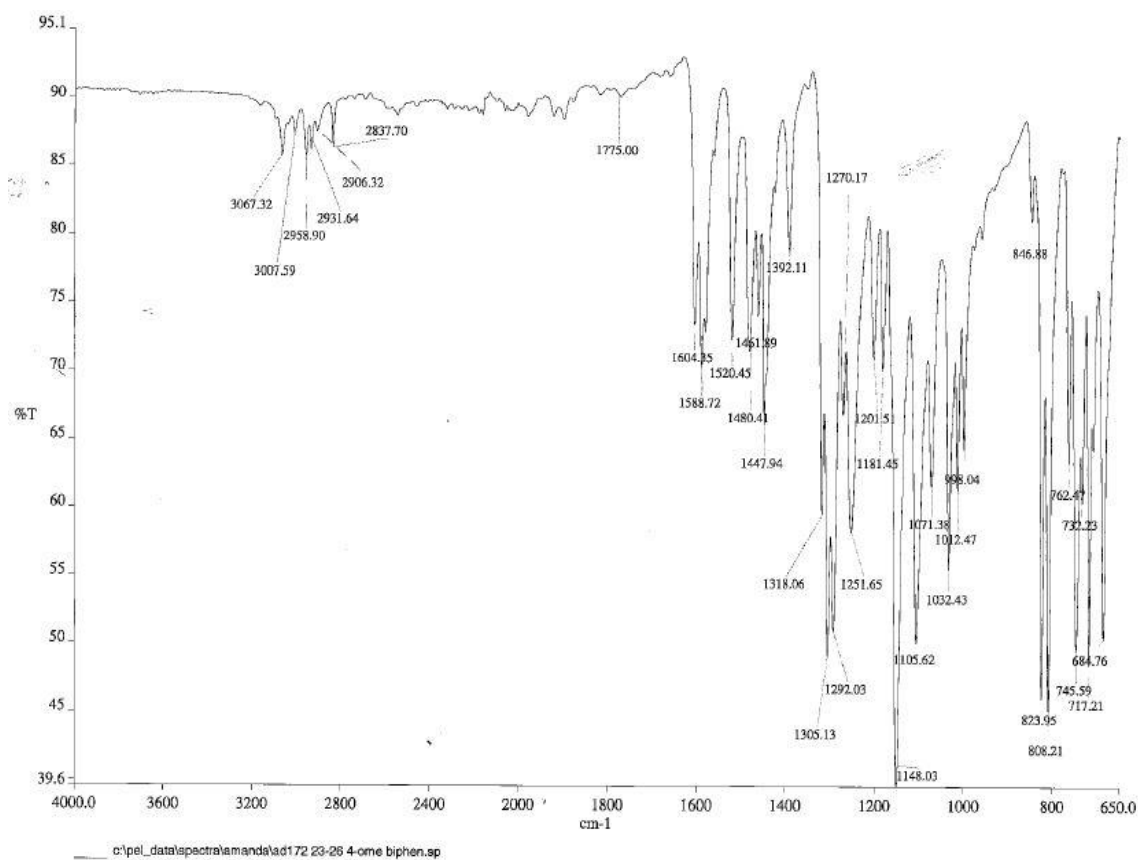


Figure A406. IR spectrum of 1-(4-methoxyphenyl)-4-(phenylsulfonyl)benzene **142**

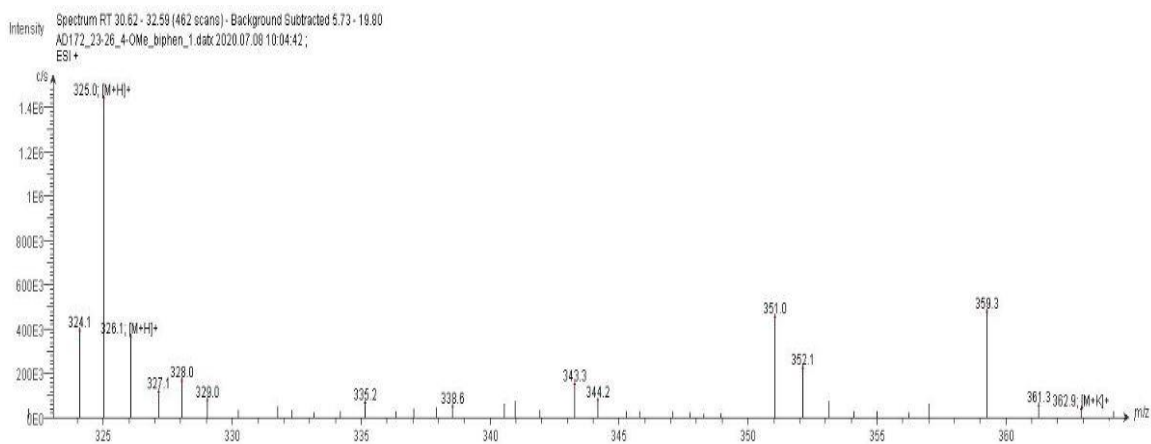
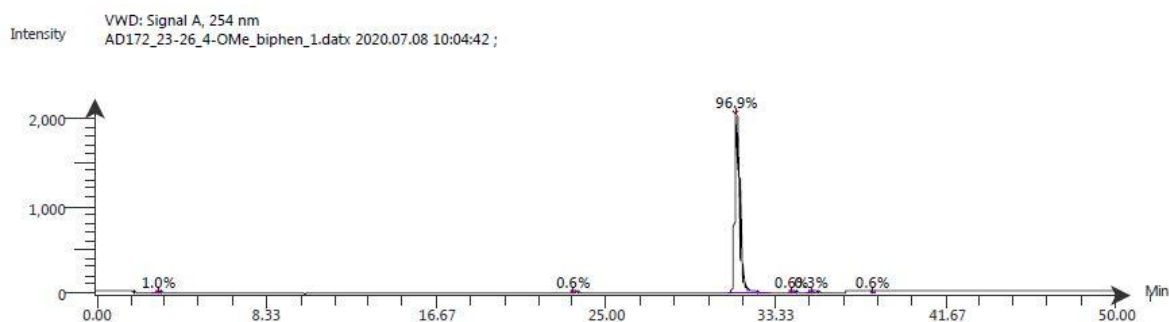


Figure A407. LC-ESI-MS spectrum of 1-(4-methoxyphenyl)-4-(phenylsulfonyl)benzene **142**. The ESI spectrum shows it has m/z $[M+K]^+$ 362.9.



Time (Peak Maximum M:S/Minutes)	Maximum Intensity (c/s)	Time (Peak Centroid M:S/Minutes)	Peak Area	% Peak Area	Peak Resolution Label
0.00	6E1	3.00	3.7E2	1.0	28.0
23.34	2.1E1	23.37	2.2E2	0.6	16.6
31.38	2.1E3	31.38	3.4E4	96.9	15.1
34.14	1.7E1	34.15	2.1E2	0.6	12.2
0.00	3.9E2	35.09	1E2	0.3	23.9
38.07	1.7E1	38.07	2E2	0.6	12.1

Figure A408. LC-UV-MS chromatogram of 1-(4-methoxyphenyl)-4-(phenylsulfonyl)benzene **142**

Compound Table

Compound Label	RT (min)	Observed mass (m/z)	Neutral observed mass (Da)	Theoretical mass (Da)	Mass error (ppm)	Isotope match score (%)
Cpd 1: C19 H16 O3 S	0.73	347.0715	324.0824	324.0820	1.12	97.81

Figure A409. HR-MS analysis 1-(4-methoxyphenyl)-4-(phenylsulfonyl)benzene **142**.

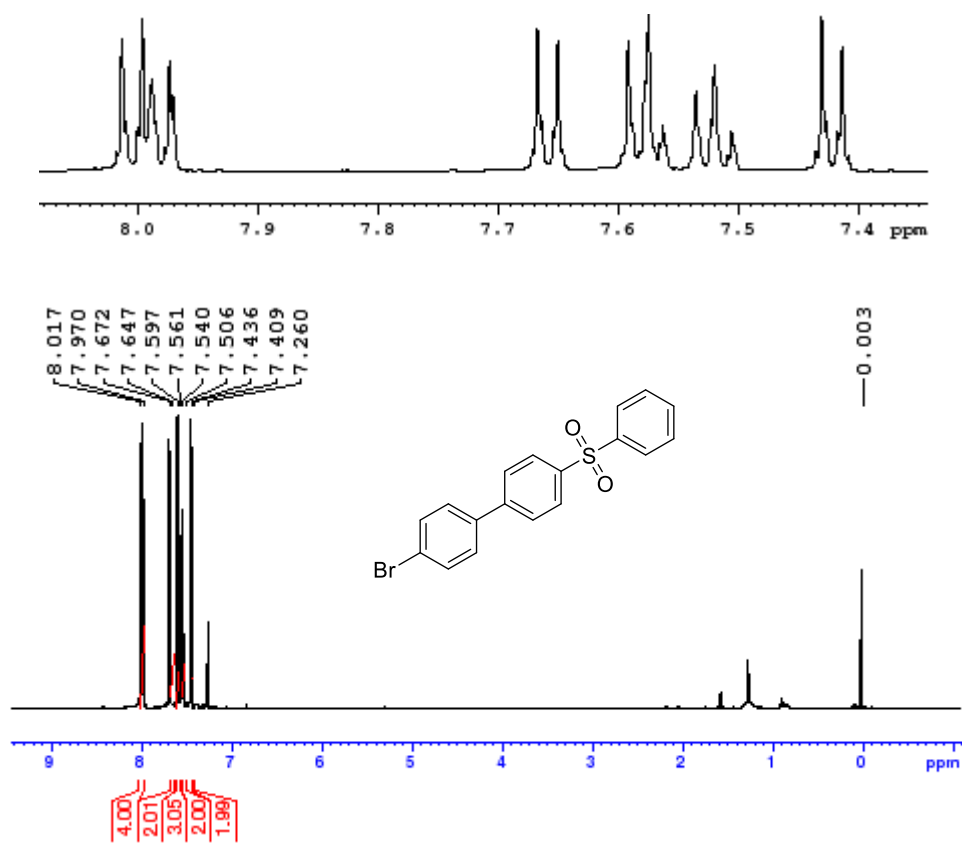


Figure A410. ¹H NMR spectrum of 1-(4-bromophenyl)-4-(phenylsulfonyl)benzene **143**.

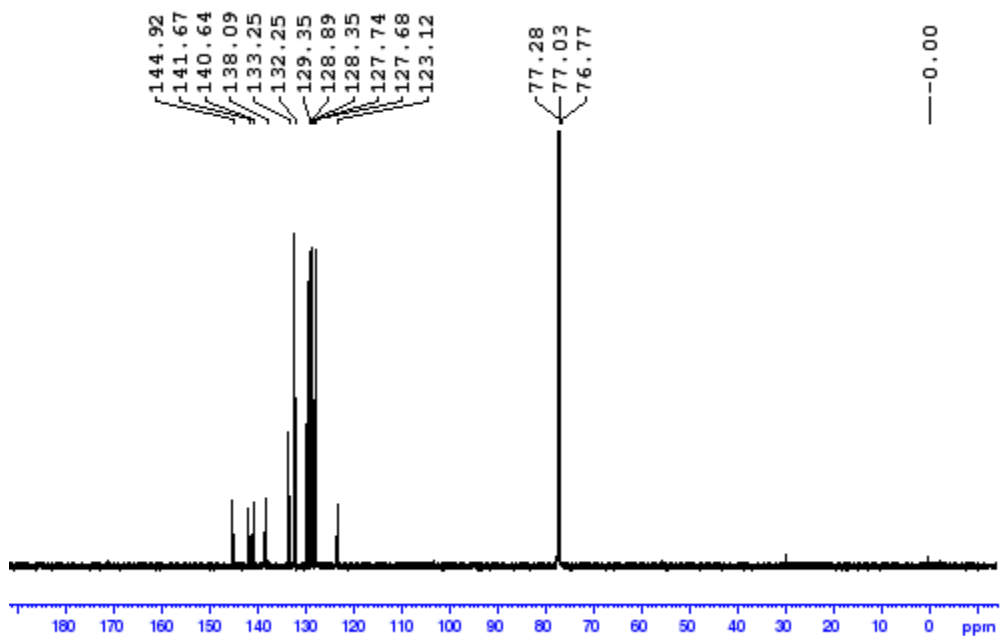


Figure A411. ¹³C NMR spectrum of 1-(4-bromophenyl)-4-(phenylsulfonyl)benzene **143**.

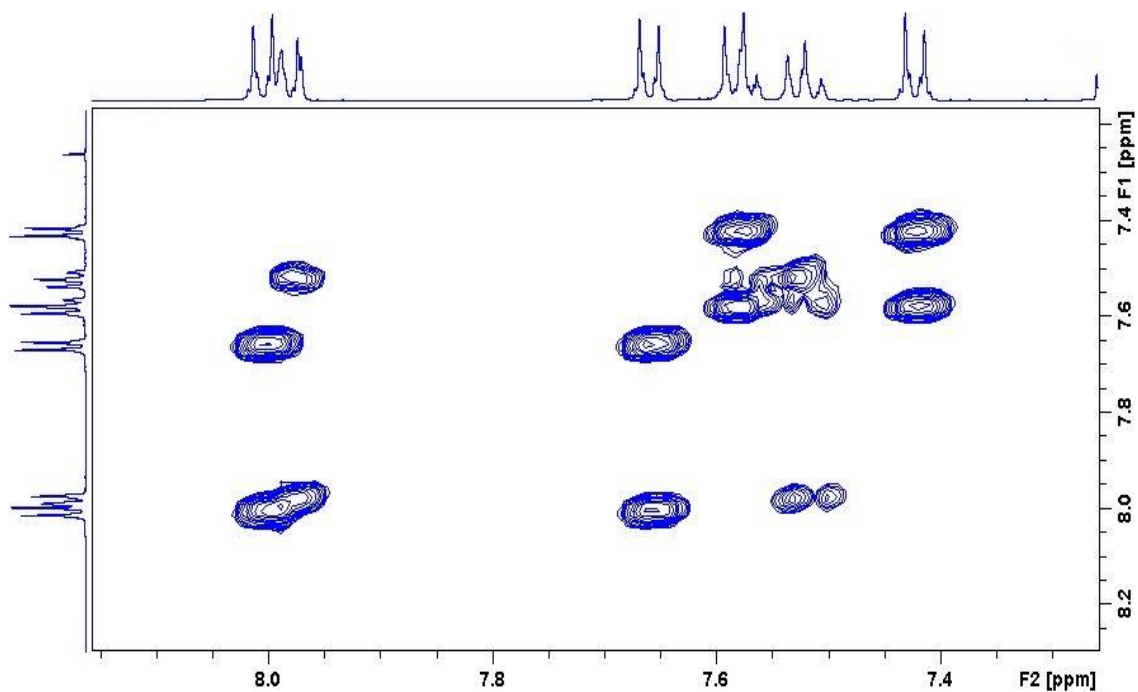


Figure A412. Zoomed in COSY spectrum of 1-(4-bromophenyl)-4-(phenylsulfonyl)benzene **143**.

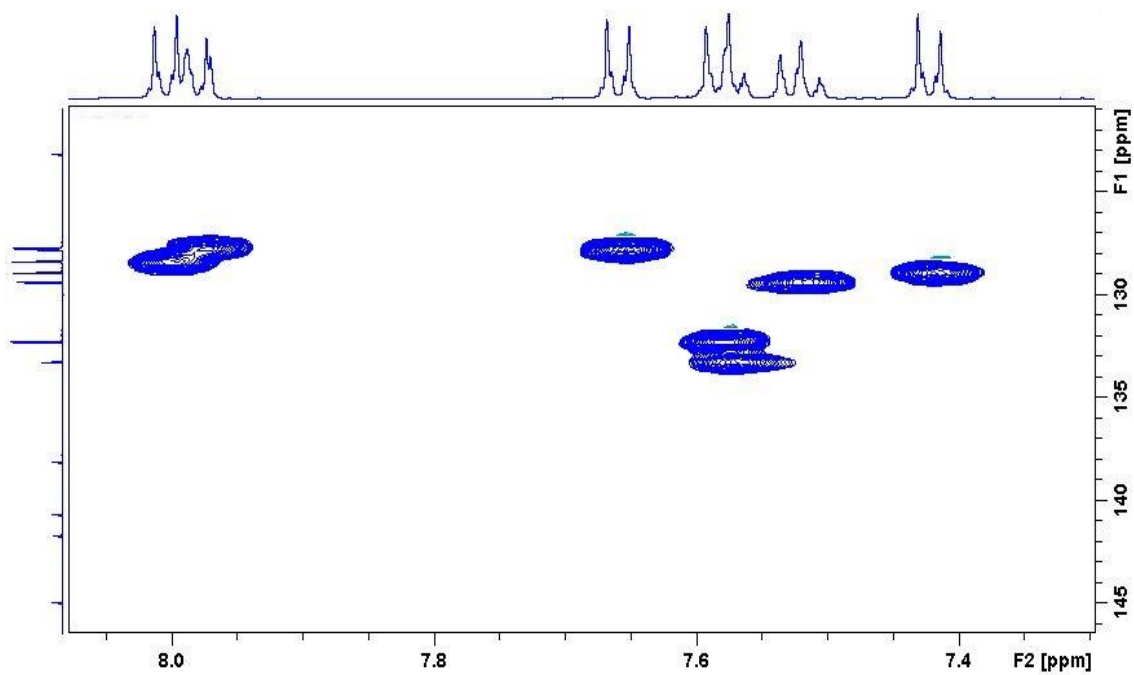


Figure A413. Zoomed in HSQC spectrum of 1-(4-bromophenyl)-4-(phenylsulfonyl)benzene **143**.

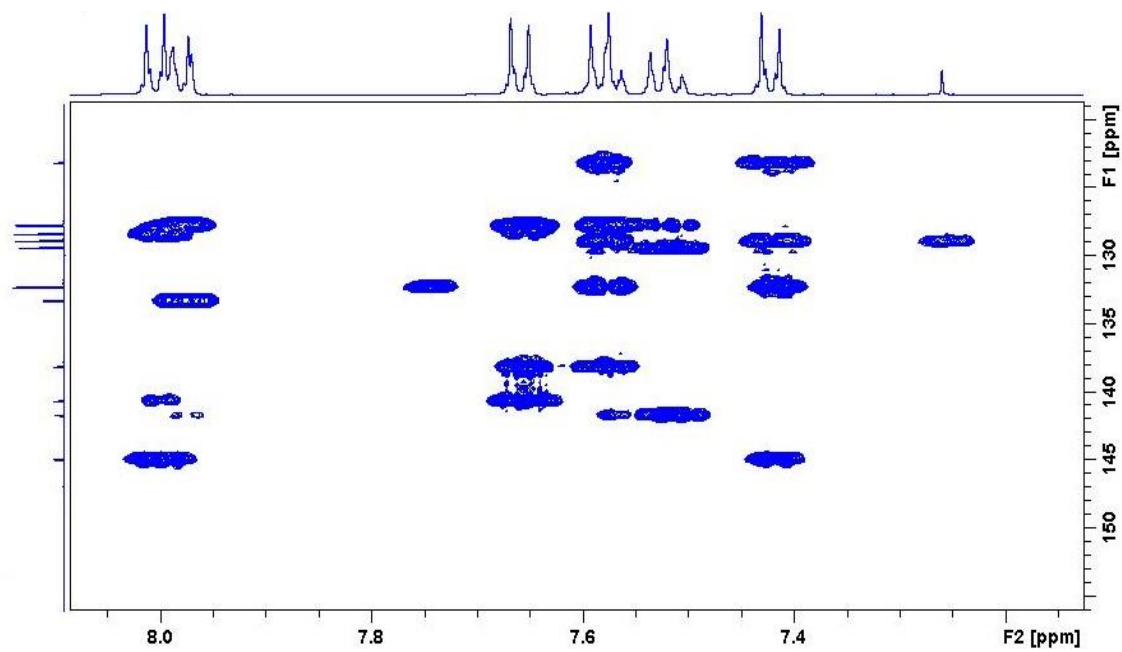


Figure A414. Zoomed in HMBC spectrum of 1-(4-bromophenyl)-4-(phenylsulfonyl)benzene **143**.

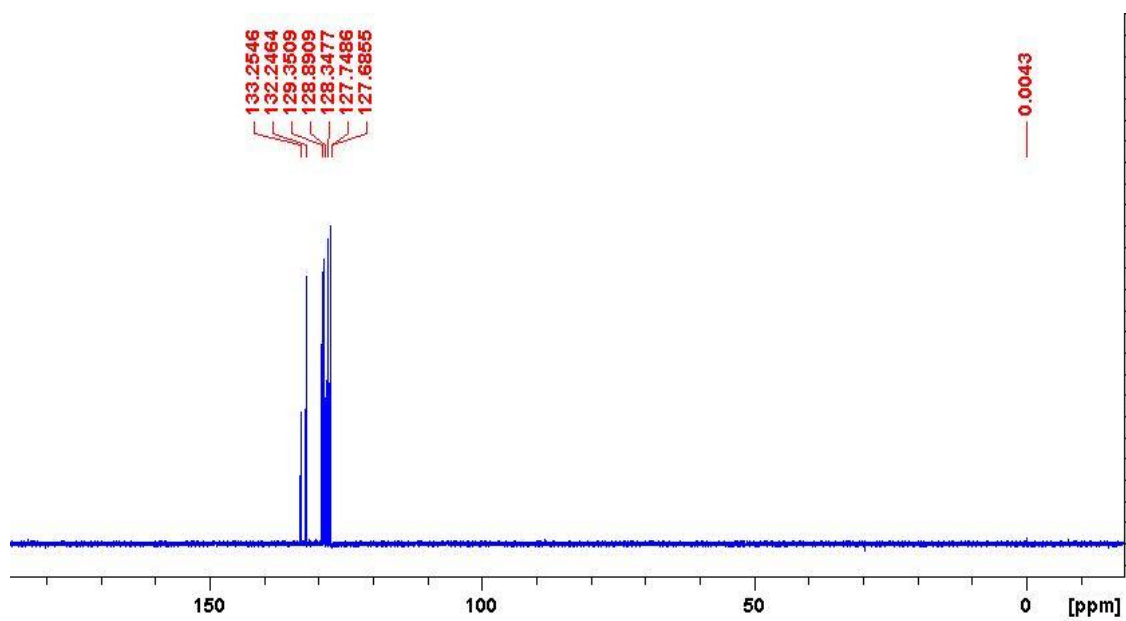


Figure A415. DEPT-135 spectrum of 1-(4-bromophenyl)-4-(phenylsulfonyl)benzene **143**.

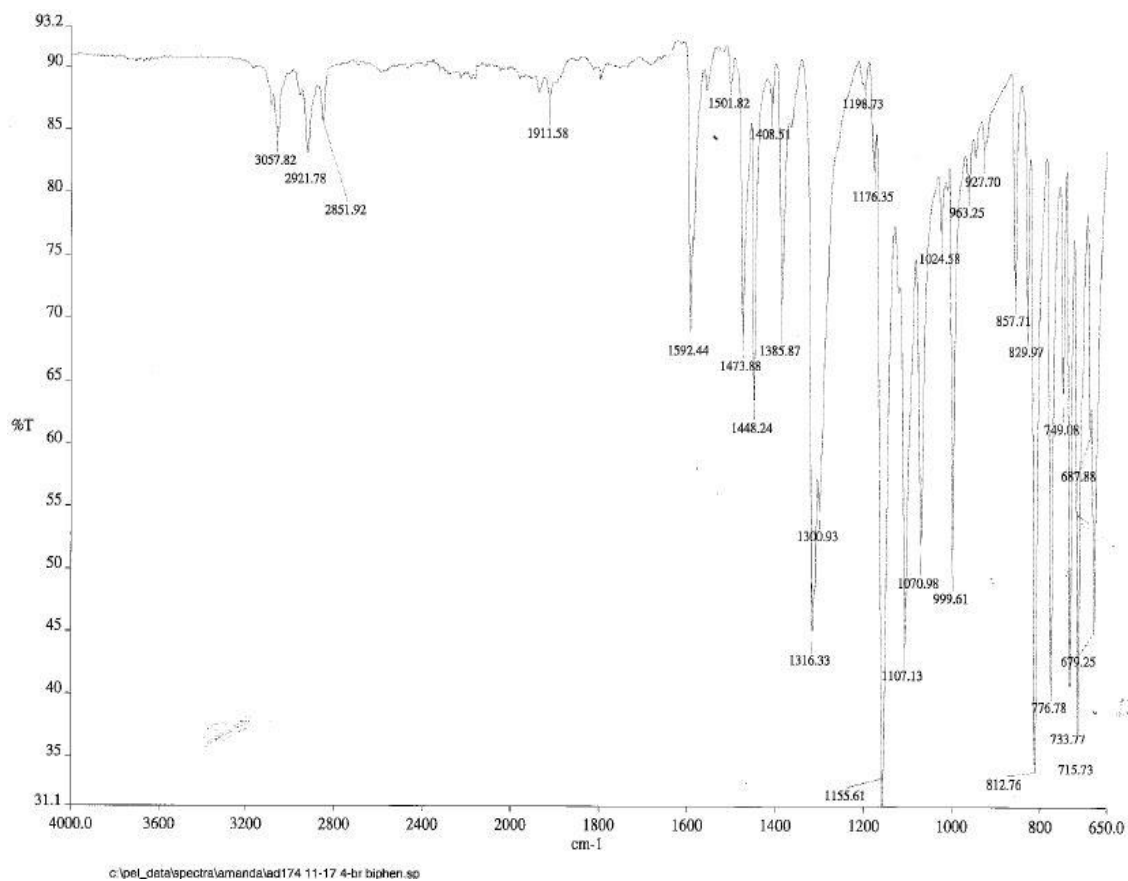


Figure A416. IR spectrum of 1-(4-bromophenyl)-4-(phenylsulfonyl)benzene **143**.

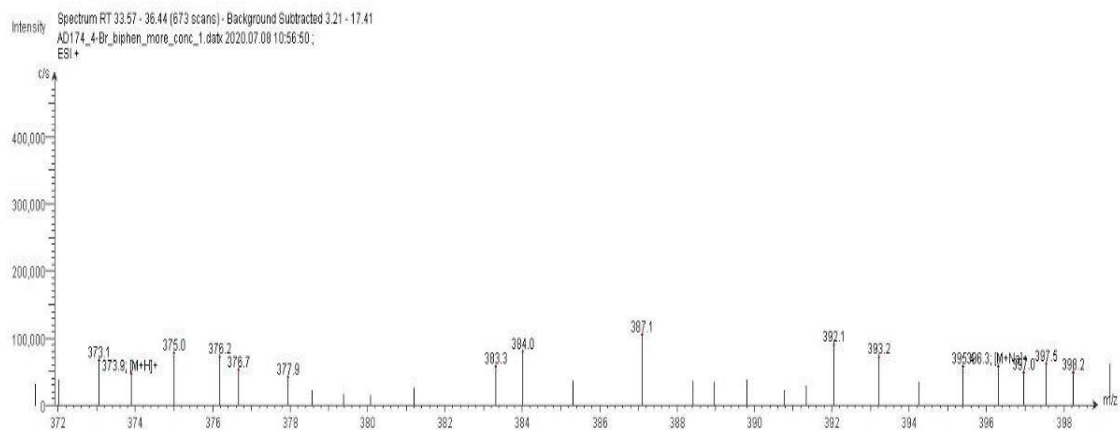
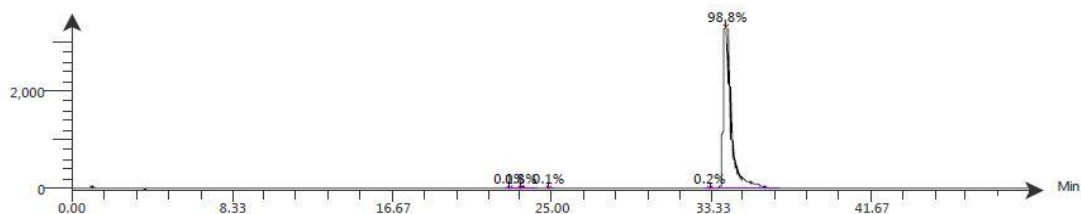


Figure A417. LC-ESI-MS spectrum of 1-(4-bromophenyl)-4-(phenylsulfonyl)benzene **143**. The ESI spectrum shows it has m/z [M+H]⁺ 373.9.

VWD: Signal A, 254 nm
 Intensity AD174_4-Br_biphen_more_conc_1.datx 2020.07.08 10:56:50 ;



Time (Peak Maximum M:S/Minutes)	Maximum Intensity (c/s)	Time (Peak Centroid M:S/Minutes)	Peak Area	% Peak Area	Peak Resolution Label
0.00	4.2E2	22.77	1.4E2	0.1	23.3
23.39	3.2E1	23.41	7.4E2	0.8	19.9
0.00	3.3E2	24.84	1.3E2	0.1	21.5
0.00	6.9E2	33.30	1.6E2	0.2	26.5
34.05	3.3E3	34.07	9.7E4	98.8	22.5

Figure A418. LC-UV-MS chromatogram of 1-(4-bromophenyl)-4-(phenylsulfonyl)benzene **143**.

Compound Table

Compound Label	RT (min)	Observed mass (m/z)	Neutral observed mass (Da)	Theoretical mass (Da)	Mass error (ppm)	Isotope match score (%)
Cpd 1: C18 H13 Br O2 S	0.72	394.9712	371.9820	371.9820	0.16	97.95

Figure A419. HR-MS analysis 1-(4-bromophenyl)-4-(phenylsulfonyl)benzene **143**.

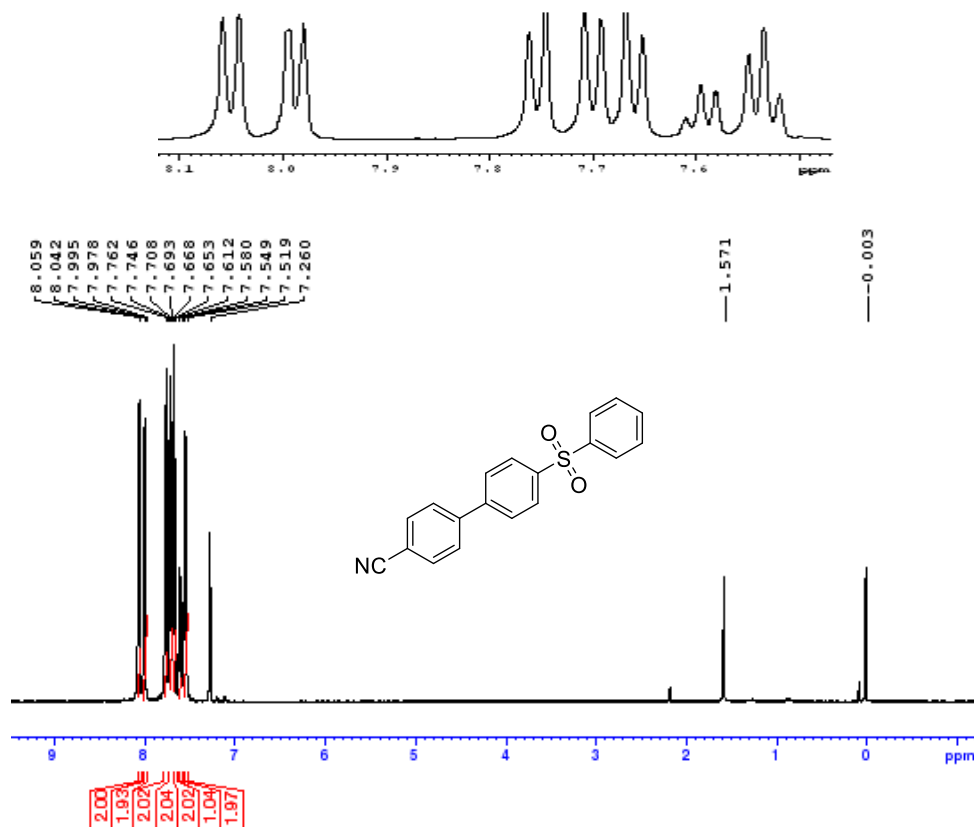


Figure A420. ¹H NMR spectrum of 1-(4-cyanophenyl)-4-(phenylsulfonyl)benzene **144**

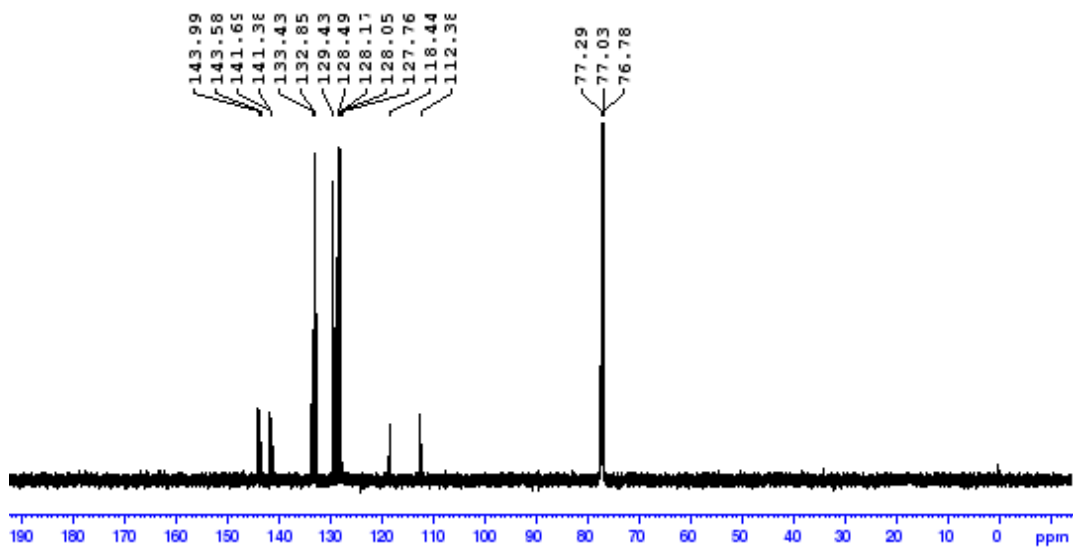


Figure A421. ^{13}C NMR spectrum of 1-(4-cyanophenyl)-4-(phenylsulfonyl)benzene **144**.

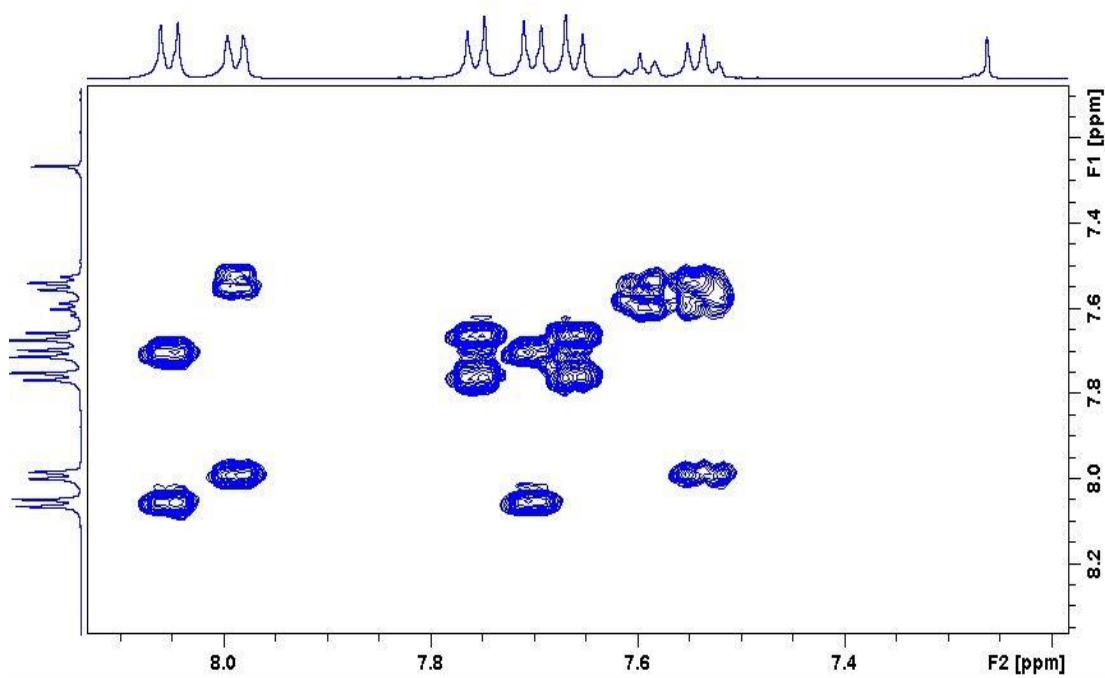


Figure A422. Zoomed in COSY spectrum of 1-(4-cyanophenyl)-4-(phenylsulfonyl)benzene **144**

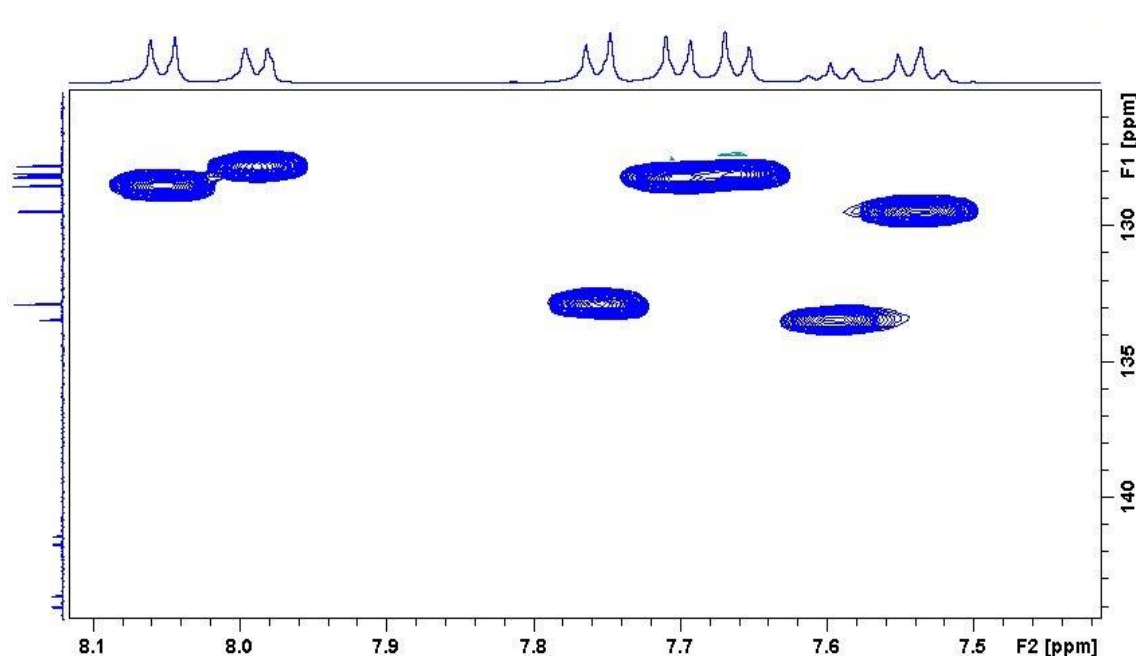


Figure A423. Zoomed in HSQC spectrum of 1-(4-cyanophenyl)-4-(phenylsulfonyl)benzene **144**

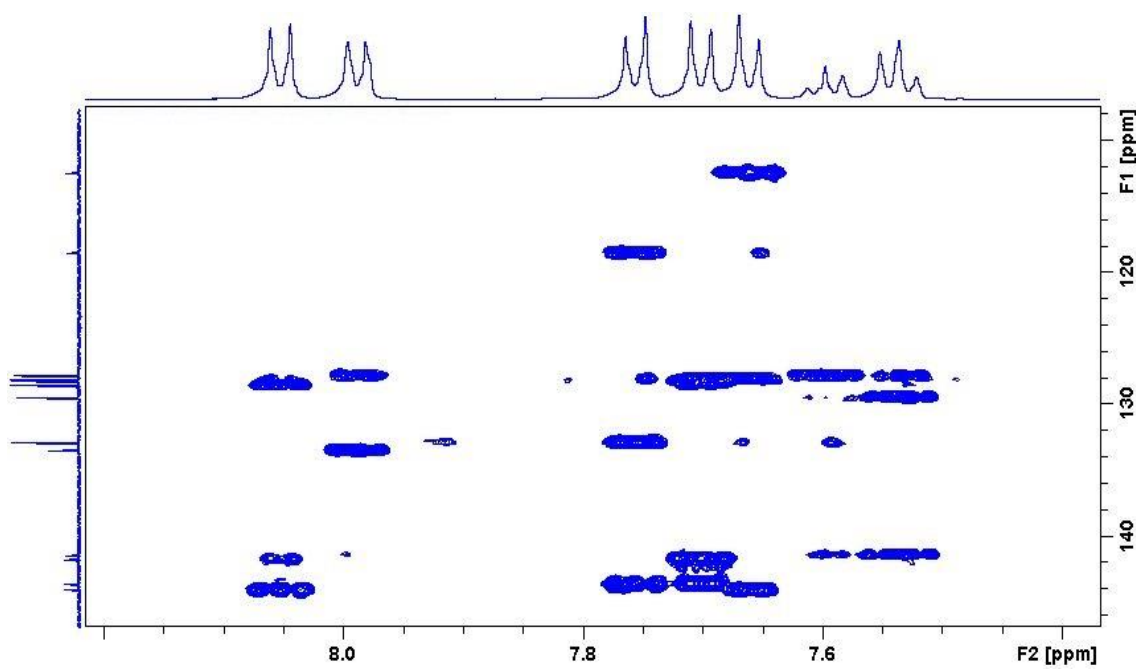


Figure A424. Zoomed in HMBC spectrum of 1-(4-cyanophenyl)-4-(phenylsulfonyl)benzene **144**

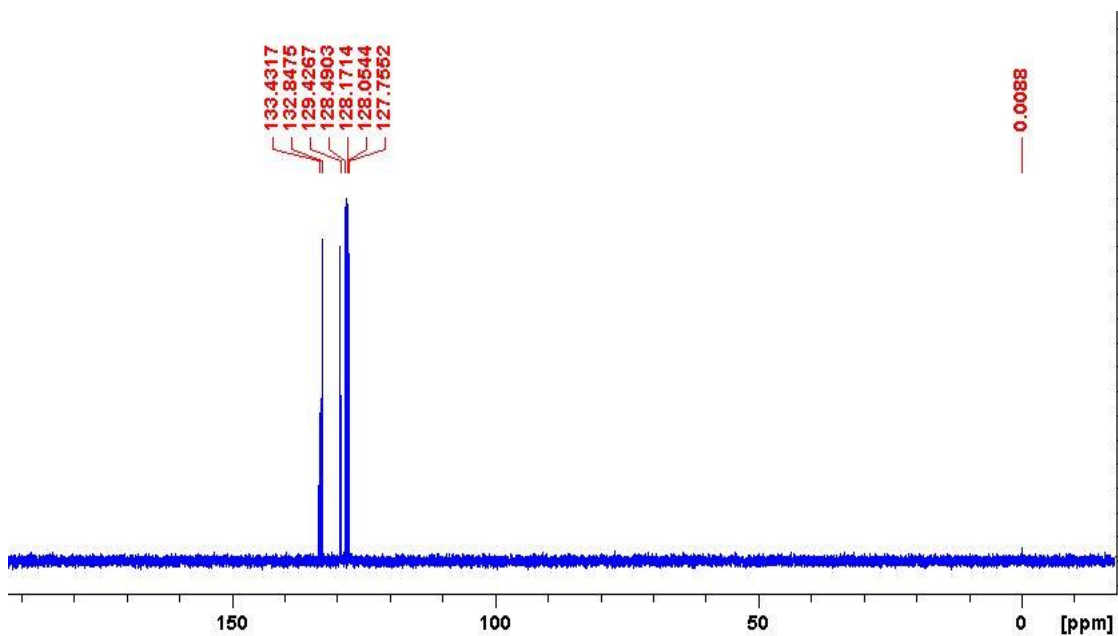


Figure A425. DEPT-135 spectrum of 1-(4-cyanophenyl)-4-(phenylsulfonyl)benzene **144**

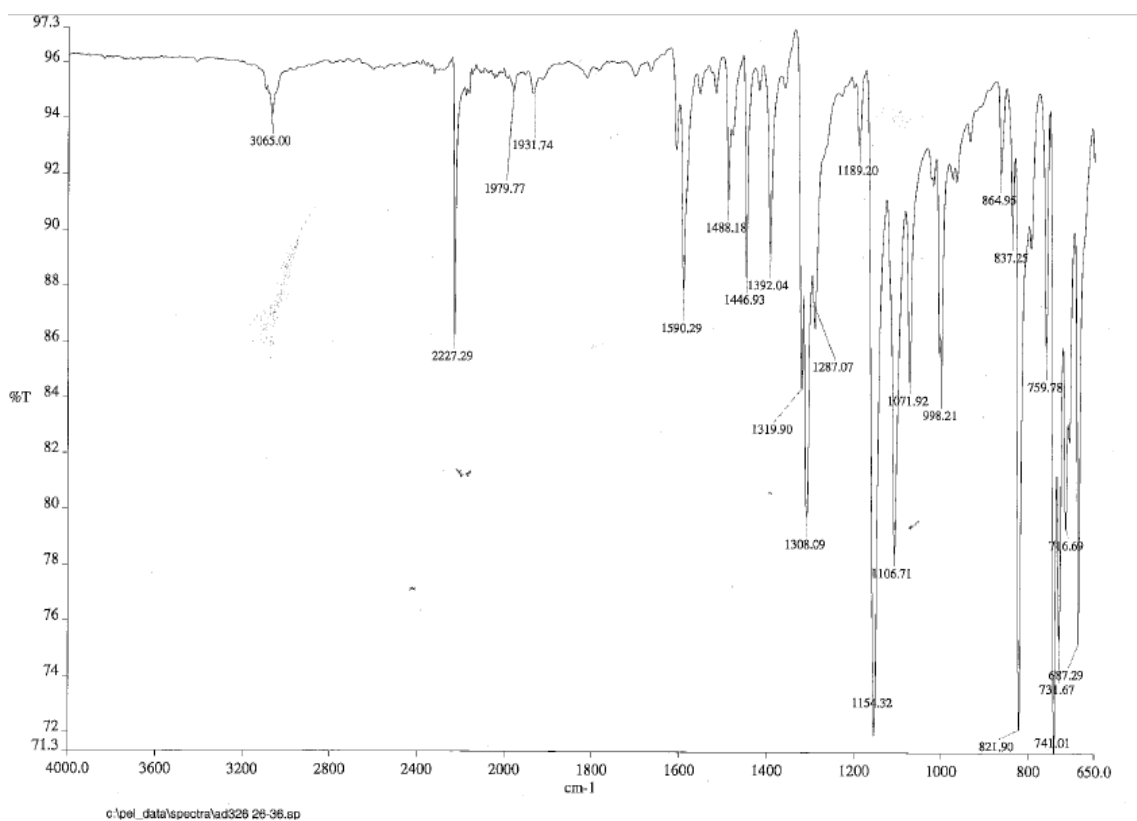


Figure A426. IR spectrum of 1-(4-cyanophenyl)-4-(phenylsulfonyl)benzene **144**

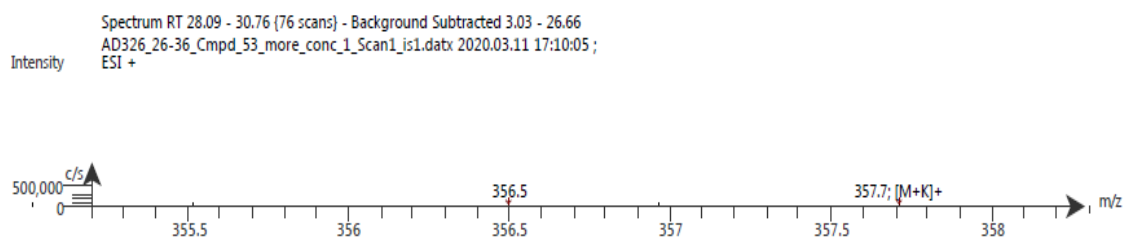
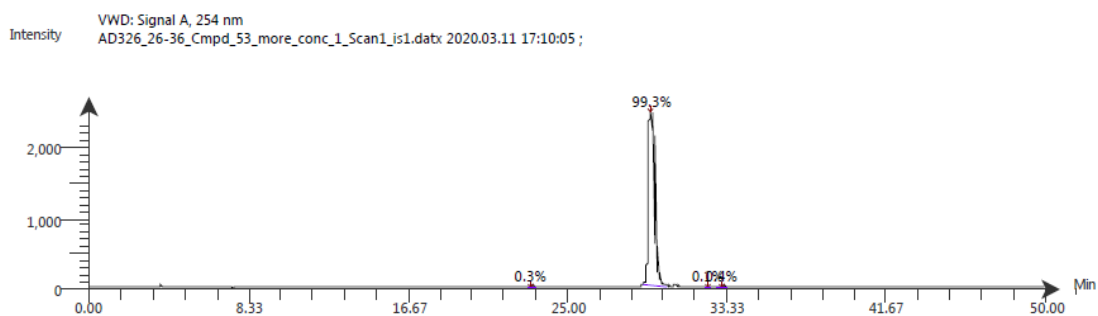


Figure A427. LC-ESI-MS spectrum of 1-(4-cyanophenyl)-4-(phenylsulfonyl)benzene **144**. The ESI spectrum shows it has m/z $[M+K]^+$ 357.7.



Time (Peak Maximum M:S/Minutes)	Maximum Intensity (c/s)	Time (Peak Centroid M:S/Minutes)	Peak Area	% Peak Area	Peak Resolution	Label
23.11	1.3E1	23.14	1.6E2	0.3	12.5	
29.32	2.4E3	29.34	5.6E4	99.3	21.3	
32.37	4.9E0	32.37	4.2E1	0.1	11.2	
33.03	1.5E1	33.09	2.2E2	0.4	14.8	

Figure A428. LC-UV-MS chromatogram of 1-(4-cyanophenyl)-4-(phenylsulfonyl)benzene **144**

Compound Table

Compound Label	RT (min)	Observed mass (m/z)	Neutral observed mass (Da)	Theoretical mass (Da)	Mass error (ppm)	Isotope match score (%)
Cpd 1: C ₁₉ H ₁₃ N O ₂ S	0.72	342.0561	319.0669	319.0667	0.77	94.63

Figure A429. HR-MS analysis 1-(4-cyanophenyl)-4-(phenylsulfonyl)benzene **144**.

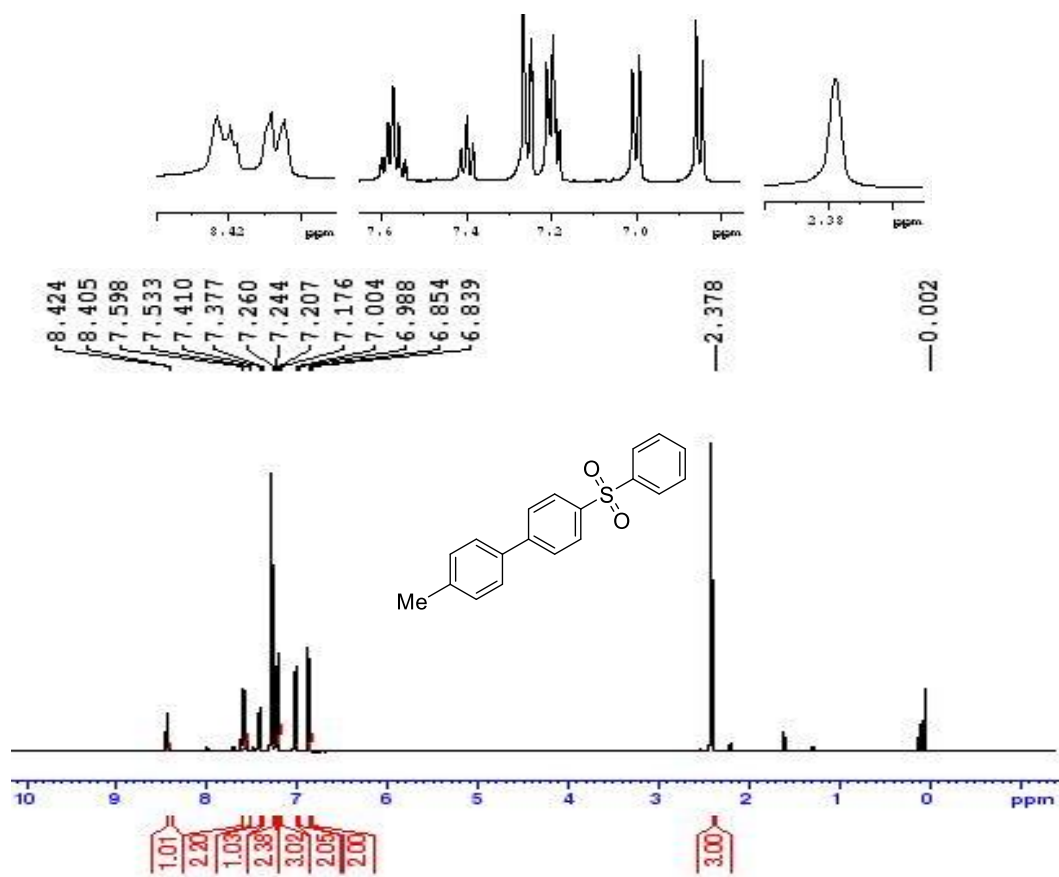


Figure A430. ¹H NMR spectrum of 1-(4-methylphenyl)-4-(phenylsulfonyl)benzene **145**

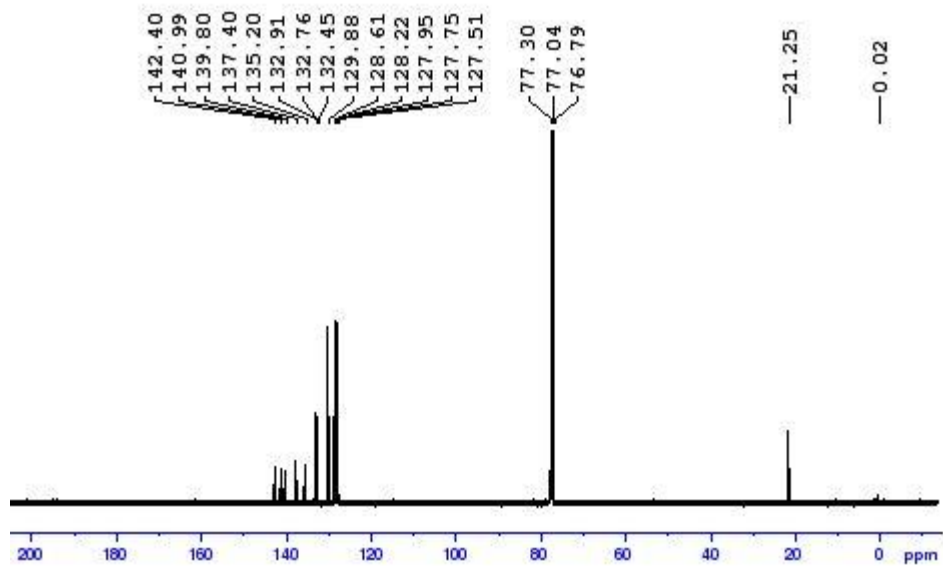


Figure A431. ¹³C NMR spectrum of 1-(4-methylphenyl)-4-(phenylsulfonyl)benzene **145**.

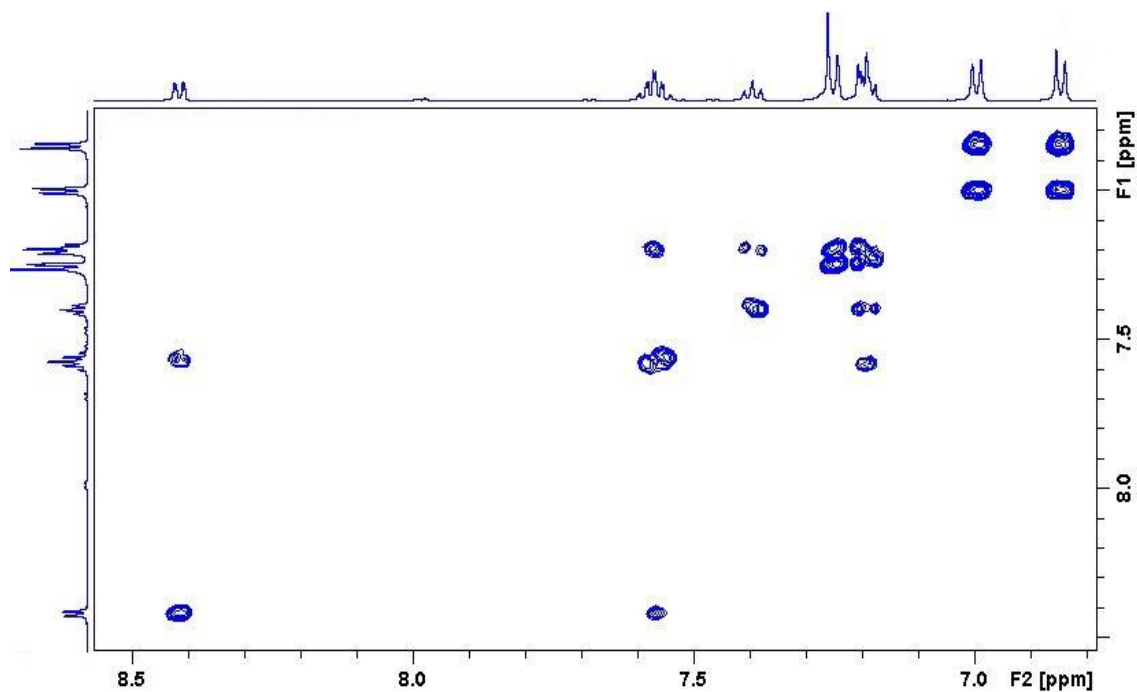


Figure A432. Zoomed in COSY spectrum of 1-(4-methylphenyl)-4-(phenylsulfonyl)benzene **145**

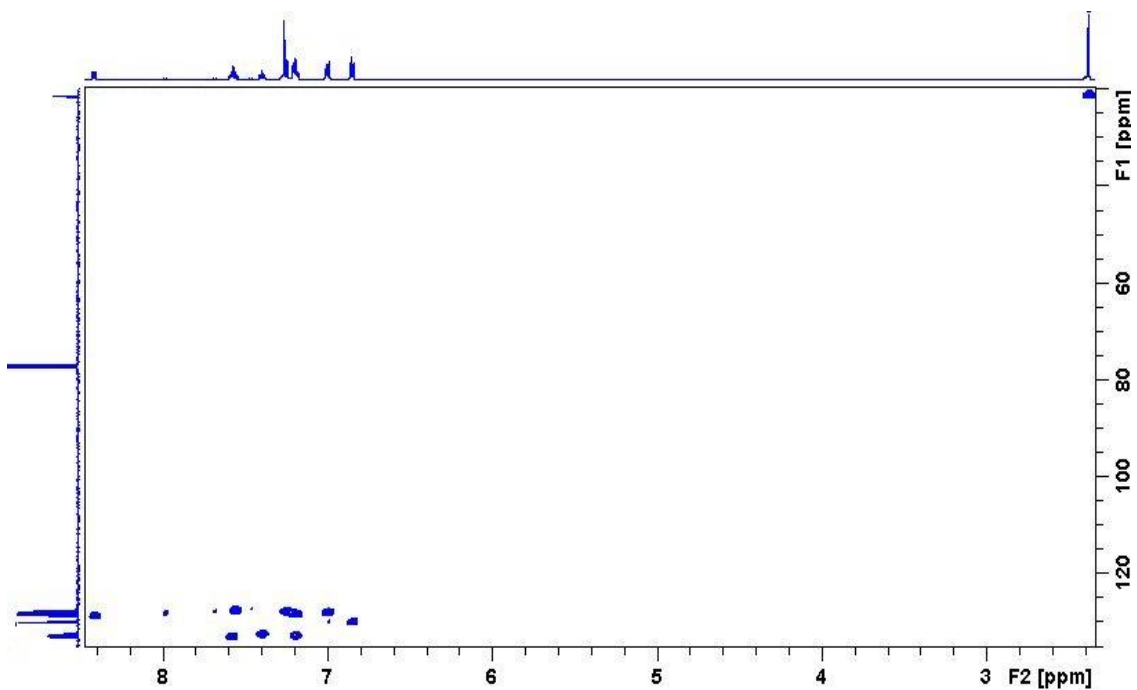


Figure A433. Zoomed in HSQC spectrum of 1-(4-methylphenyl)-4-(phenylsulfonyl)benzene **145**

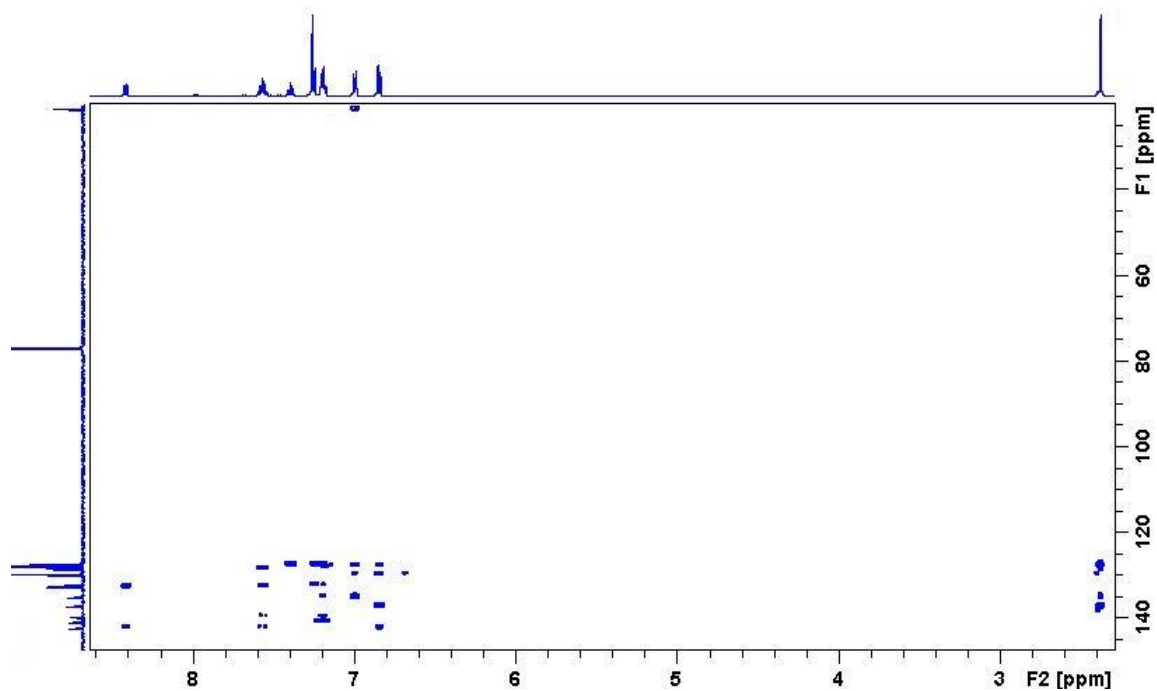


Figure A434. Zoomed in HMBC spectrum of 1-(4-methylphenyl)-4-(phenylsulfonyl)benzene **145**

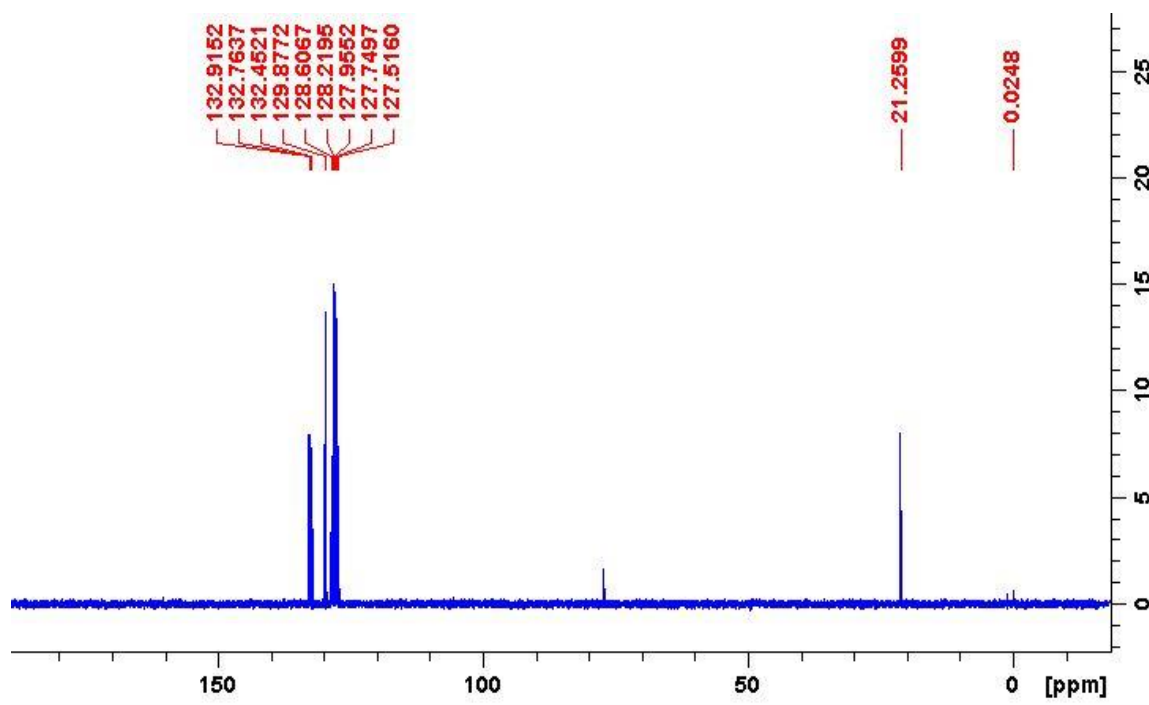


Figure A435. DEPT-135 spectrum of 1-(4-methylphenyl)-4-(phenylsulfonyl)benzene **145**

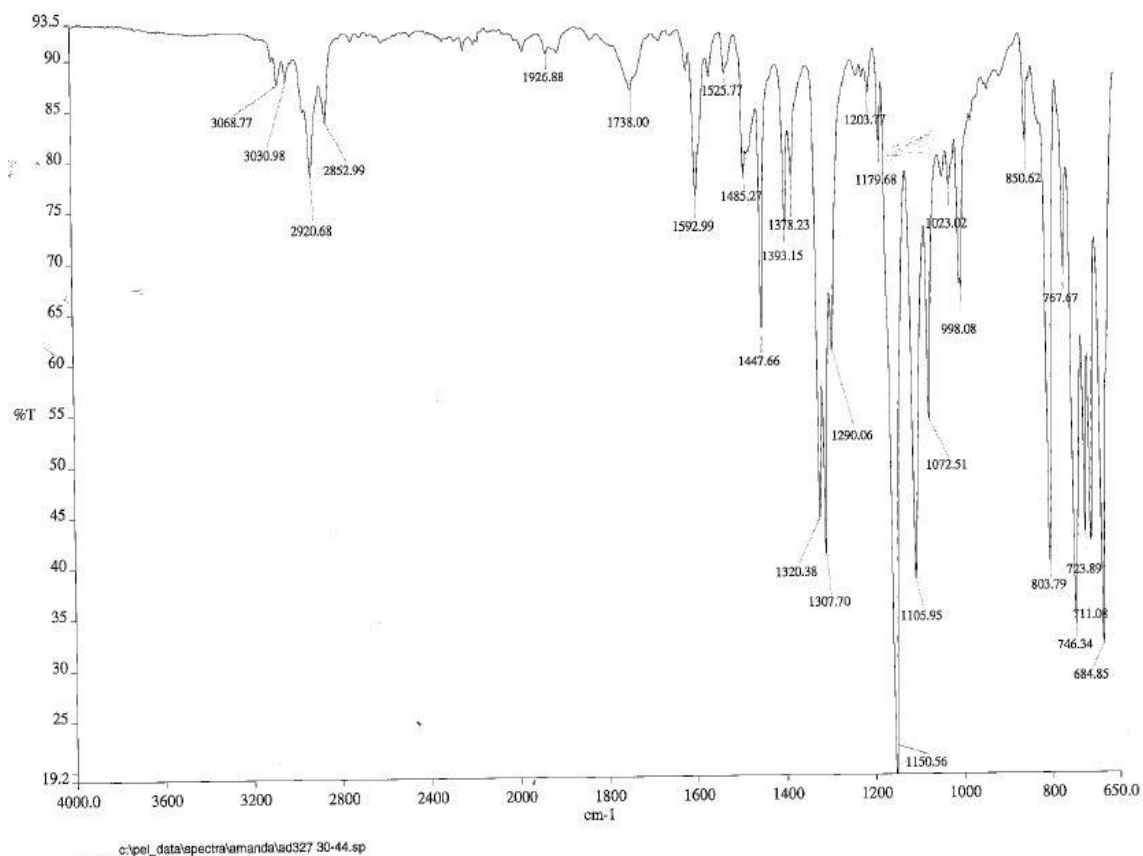


Figure A436. IR spectrum of 1-(4-methylphenyl)-4-(phenylsulfonyl)benzene **145**

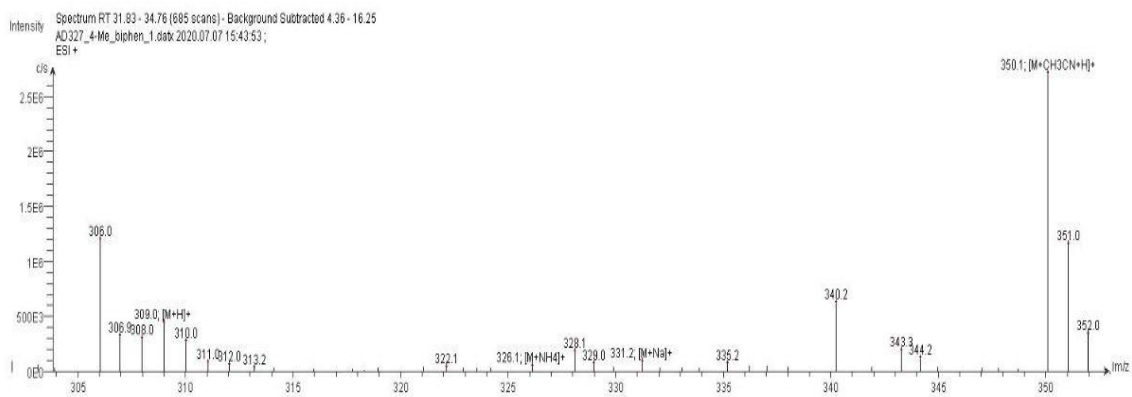
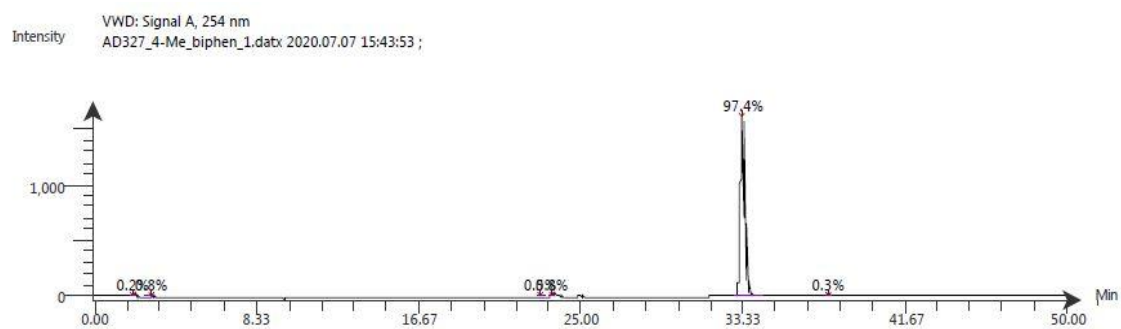


Figure A437. LC-ESI-MS spectrum of 1-(4-methylphenyl)-4-(phenylsulfonyl)benzene **145**. The ESI spectrum shows it has m/z [M+Na]⁺ 331.2.



Time (Peak Maximum M:S/Minutes)	Maximum Intensity (c/s)	Time (Peak Centroid M:S/Minutes)	Peak Area	% Peak Area	Peak Resolution Label
2.00	8.5E0	1.94	6.5E1	0.2	15.1
0.00	6.9E1	2.90	2.3E2	0.8	27.4
0.00	1.4E2	22.87	1.2E2	0.5	26.5
23.49	1.9E1	23.52	2.2E2	0.8	12.1
33.26	1.6E3	33.27	2.6E4	97.4	14.8
37.72	8.9E0	37.72	7.4E1	0.3	8.6

Figure A438. LC-UV-MS chromatogram of 1-(4-methylphenyl)-4-(phenylsulfonyl)benzene **145**

Compound Table

Compound Label	RT (min)	Observed mass (m/z)	Neutral observed mass (Da)	Theoretical mass (Da)	Mass error (ppm)	Isotope match score (%)
Cpd 1: C19 H16 O2 S	0.74	309.0947	308.0879	308.0871	2.54	96.69

Figure A439. HR-MS analysis 1-(4-methylphenyl)-4-(phenylsulfonyl)benzene **145**

Spectra relating to fluorescent studies

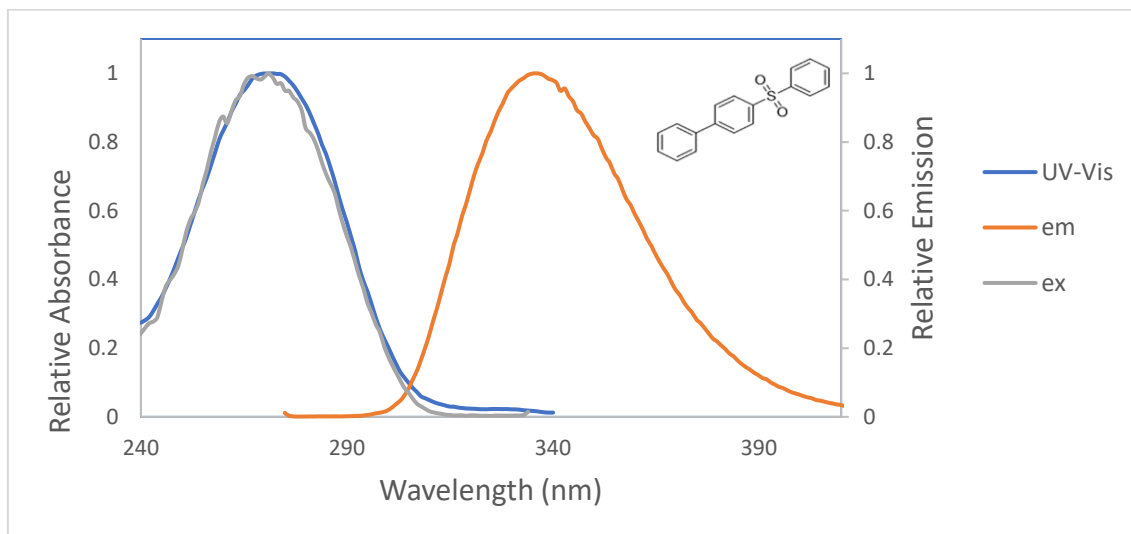


Figure A440 (a). Overlapped UV-Vis, emission, and excitation spectra of biaryl **46** in methanol, in which absorbance λ_{max} , emission λ_{max} and excitation λ_{max} values of 272, 336, and 272 nm were found, respectively. The absorbance λ_{max} and emission/excitation λ_{max} were recorded using 17.86 μM and 2.85 μM solutions, respectively.

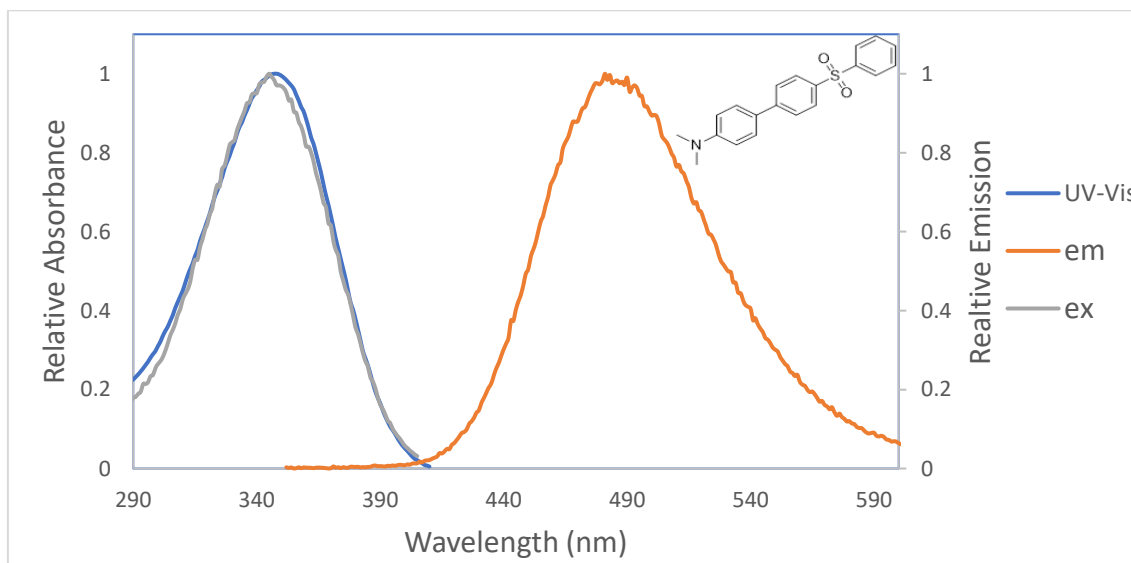


Figure A440 (b). Overlapped UV-Vis, emission, and excitation spectra of biaryl **138** in methanol, in which absorbance λ_{max} , emission λ_{max} and excitation λ_{max} values of 347, 481, and 346 nm were found, respectively. The absorbance λ_{max} and emission/excitation λ_{max} were recorded using 17.86 μM and 6.51 μM solutions, respectively.

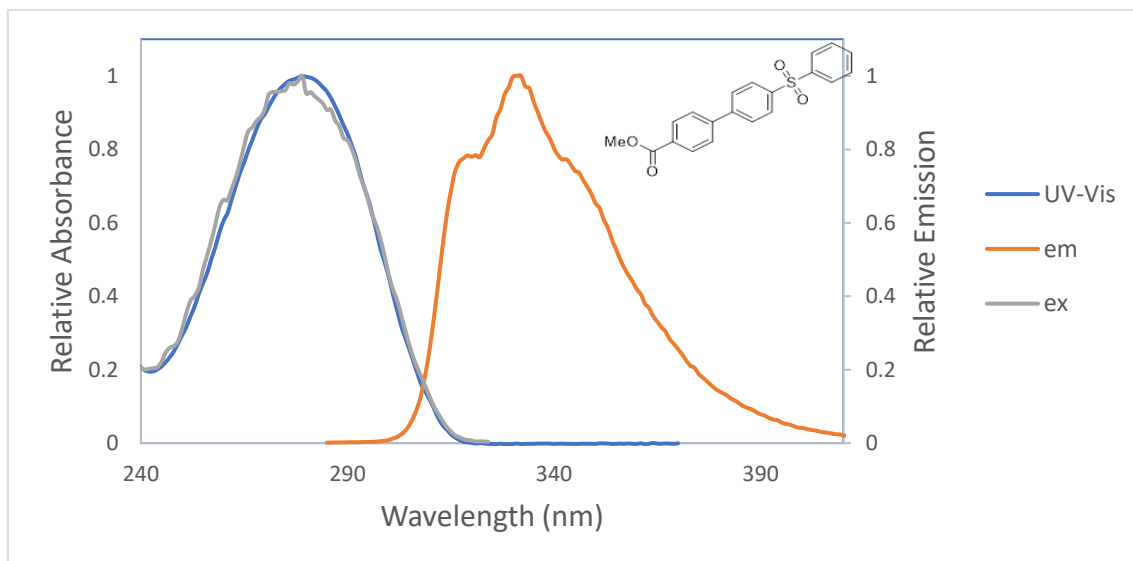


Figure A440 (c). Overlapped UV-Vis, emission, and excitation spectra of biaryl **139** in methanol, in which absorbance λ_{max} , emission λ_{max} and excitation λ_{max} values of 279, 331, and 280 nm were found, respectively. Shoulders at 319 & 344 nm were evident in the emission spectrum of compound **139** additionally. The absorbance λ_{max} and emission/excitation λ_{max} were recorded using 17.86 μM and 3.32 μM solutions, respectively.

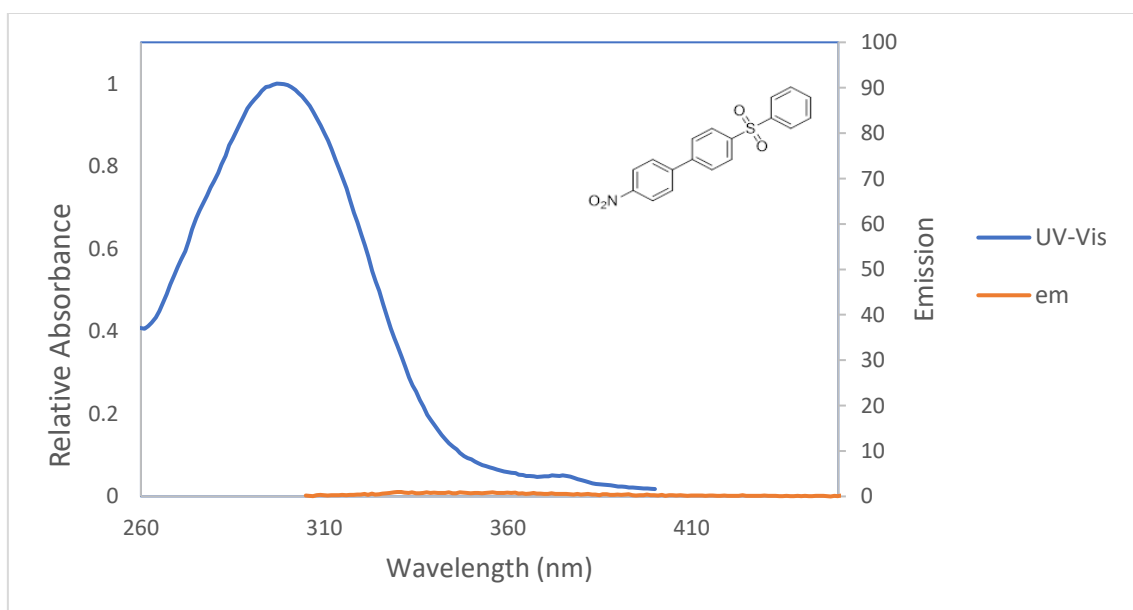


Figure A440 (d). Overlapped UV-Vis and emission spectra of biaryl **140** in methanol, in which an absorbance λ_{max} value of 297 nm was found. An emission λ_{max} (and therefore excitation λ_{max}) could not be found due to low emission intensity. The absorbance λ_{max} was recorded using a 17.86 μM solution and the emission spectrum was run using a 4.65 μM solution.

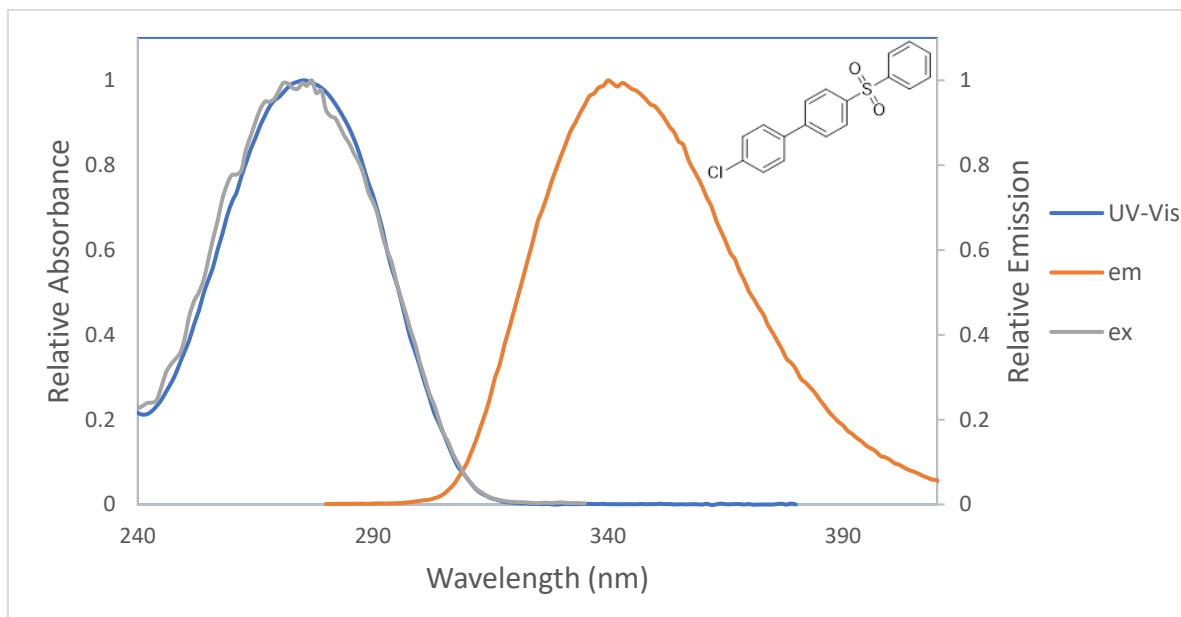


Figure A440 (e). Overlapped UV-Vis, emission, and excitation spectra of biaryl **141** in methanol, in which absorbance λ_{max} , emission λ_{max} and excitation λ_{max} values of 275, 340, and 278 nm were found, respectively. The absorbance λ_{max} and emission/excitation λ_{max} were recorded using 17.86 μM and 2.85 μM solutions, respectively.

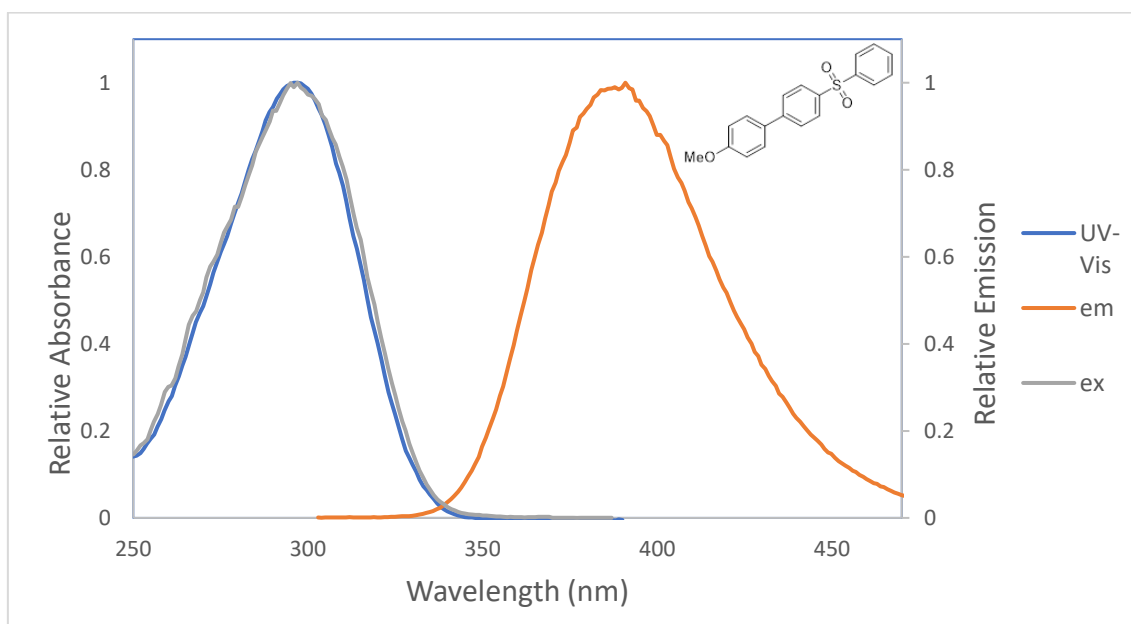


Figure A440 (f). Overlapped UV-Vis, emission, and excitation spectra of biaryl **142** in methanol, in which absorbance λ_{max} , emission λ_{max} and excitation λ_{max} values of 297, 391, and 298 nm were found, respectively. The absorbance λ_{max} and emission/excitation λ_{max} were recorded using 17.86 μM and 4.65 μM solutions, respectively.

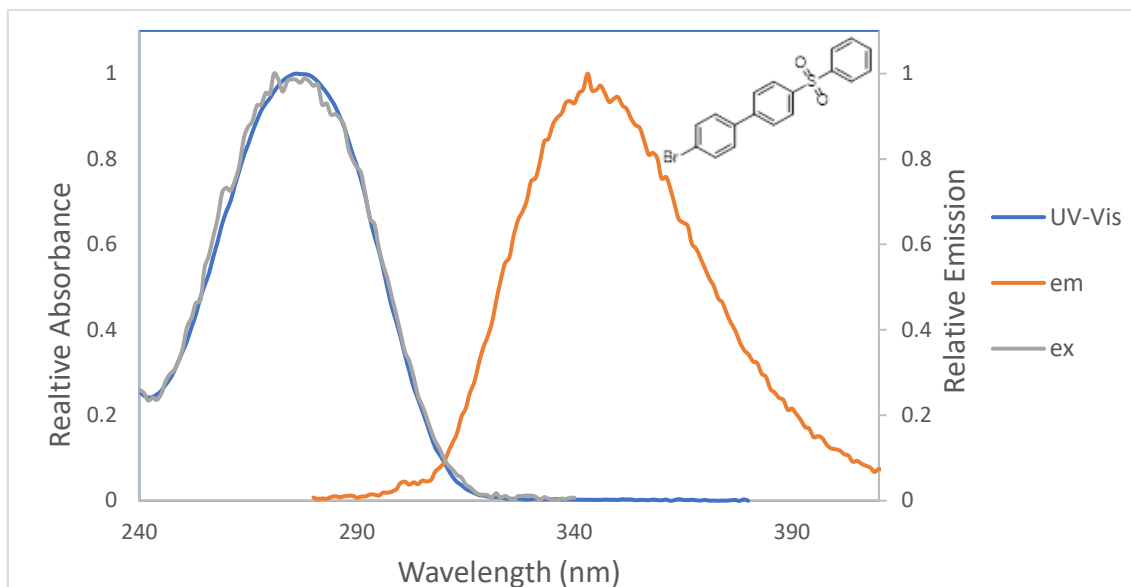


Figure A440 (g). Overlapped UV-Vis, emission, and excitation spectra of biaryl **143** in methanol, in which absorbance λ_{max} , emission λ_{max} and excitation λ_{max} values of 277, 343, and 272 nm were found, respectively. The absorbance λ_{max} and emission/excitation λ_{max} were recorded using 17.86 μM and 3.98 μM solutions, respectively.

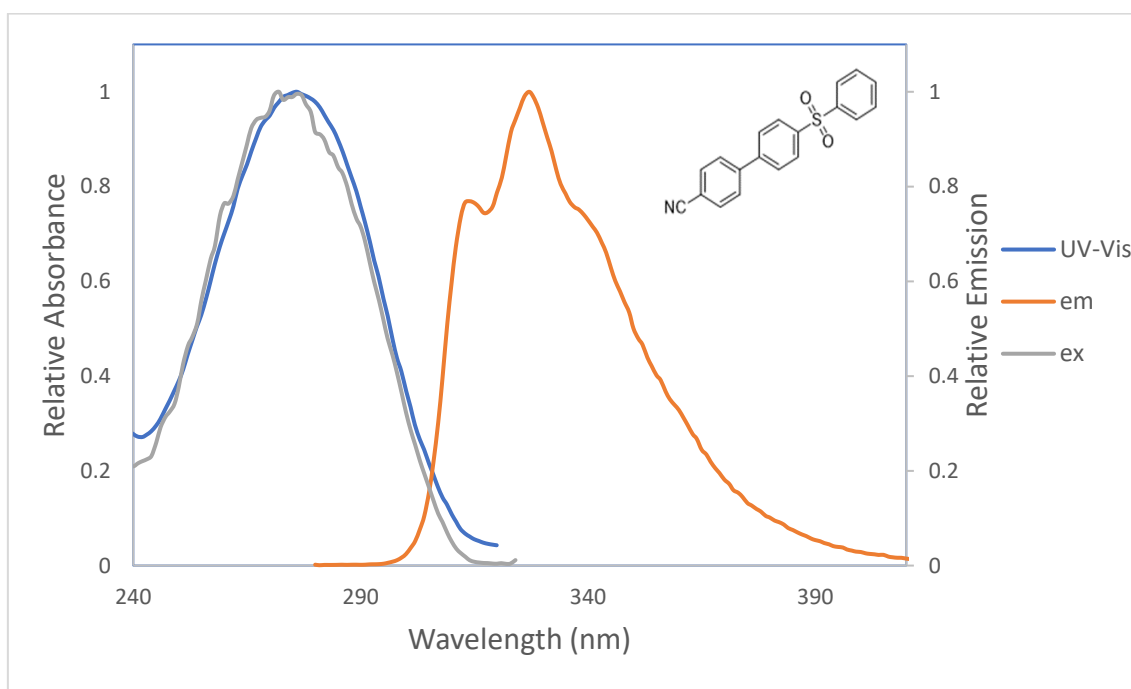


Figure A440 (h). Overlapped UV-Vis, emission, and excitation spectra of biaryl **144** in methanol, in which absorbance λ_{max} , emission λ_{max} and excitation λ_{max} values of 276, 327, and 273 nm were found, respectively. Shoulders at 314 & 343 nm were evident in the emission spectrum of compound **144** additionally. The absorbance λ_{max} and emission/excitation λ_{max} were recorded using 17.86 μM and 2.85 μM solutions, respectively.

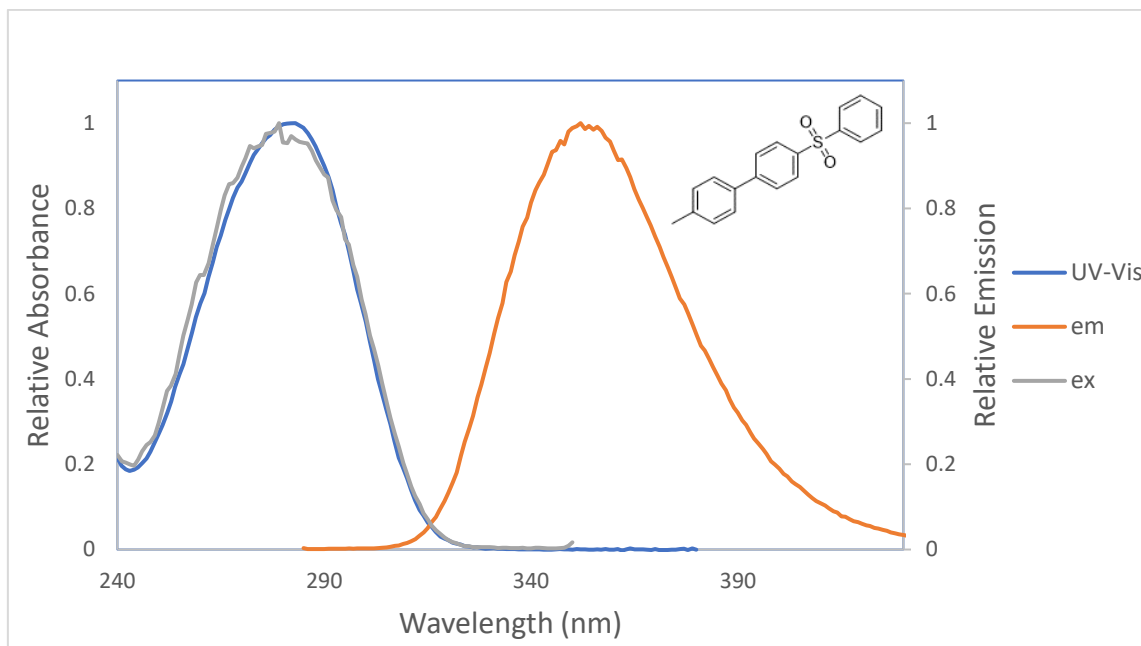


Figure A440 (i). Overlapped UV-Vis, emission, and excitation spectra of biaryl **145** in methanol. Absorbance λ_{max} , emission λ_{max} and excitation λ_{max} values of 283, 352, and 280 nm were found, respectively. The absorbance λ_{max} and emission/excitation λ_{max} were recorded using 17.86 μM and 3.32 μM solutions, respectively.

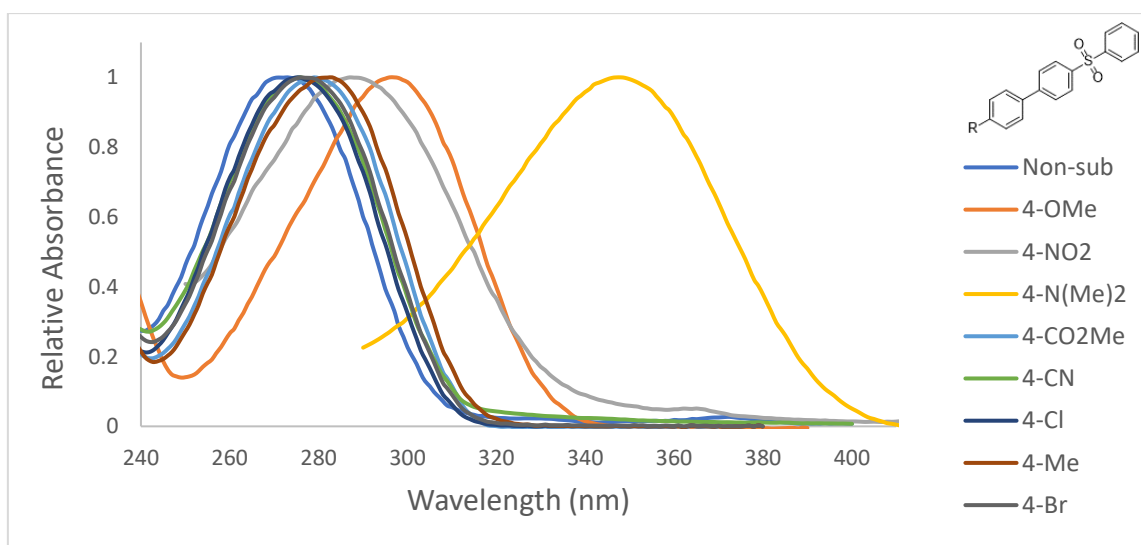


Figure A441. Relative absorbance spectra of all biaryls in methanol, using a 17.86 μM solution in each case.

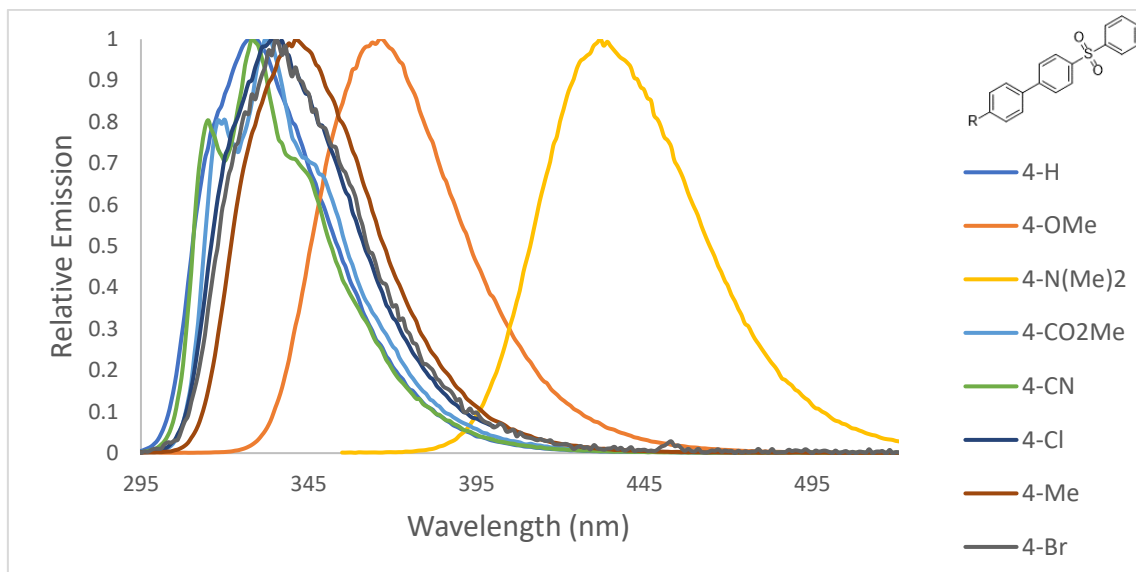


Figure A442. Relative emission spectra of all biaryls in chloroform, recorded using solutions between 2.32 and 5.58 μM concentration.

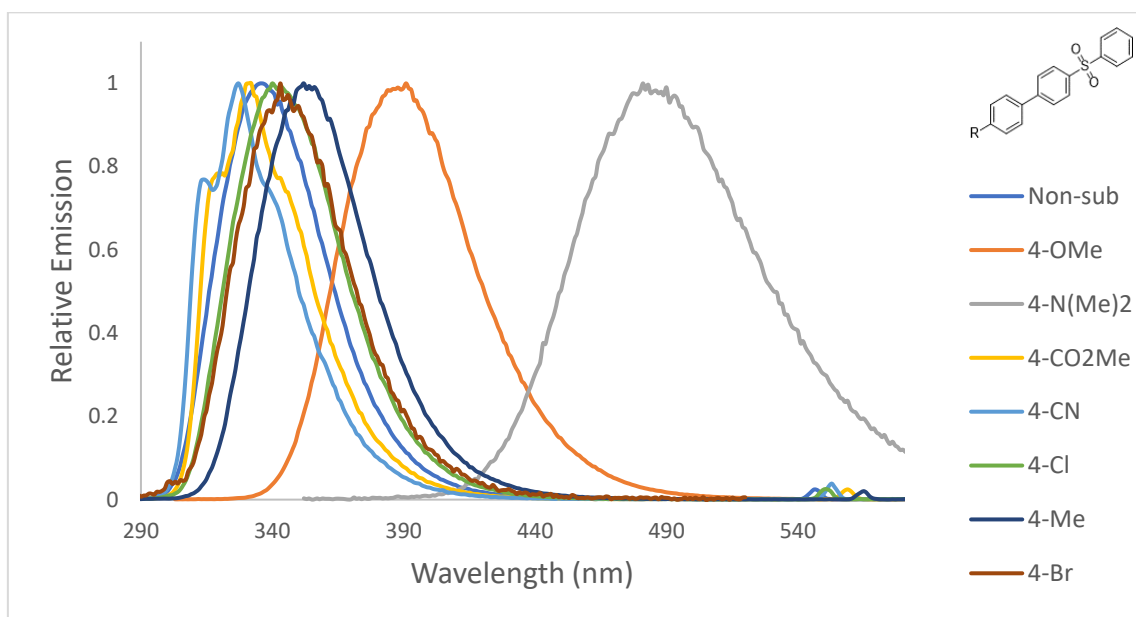


Figure A443. Relative emission spectra of all biaryls in methanol, recorded using solutions between 2.85 and 6.51 μM concentration.

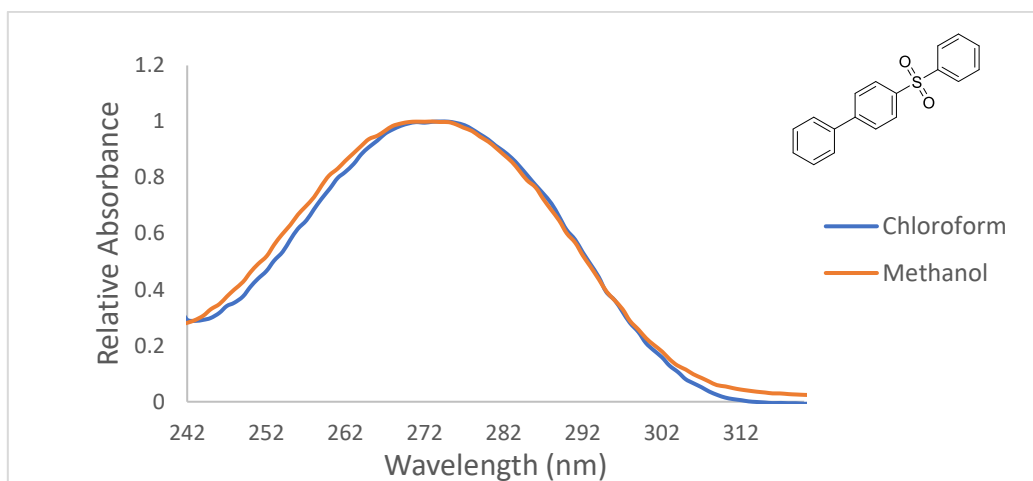


Figure A444 (a). Effect of solvent on absorbance λ_{\max} for biaryl **46**. Absorbance λ_{\max} values of 273 and 272 nm were found using chloroform and methanol as solvent, respectively, using a 17.86 μM solution in both cases.

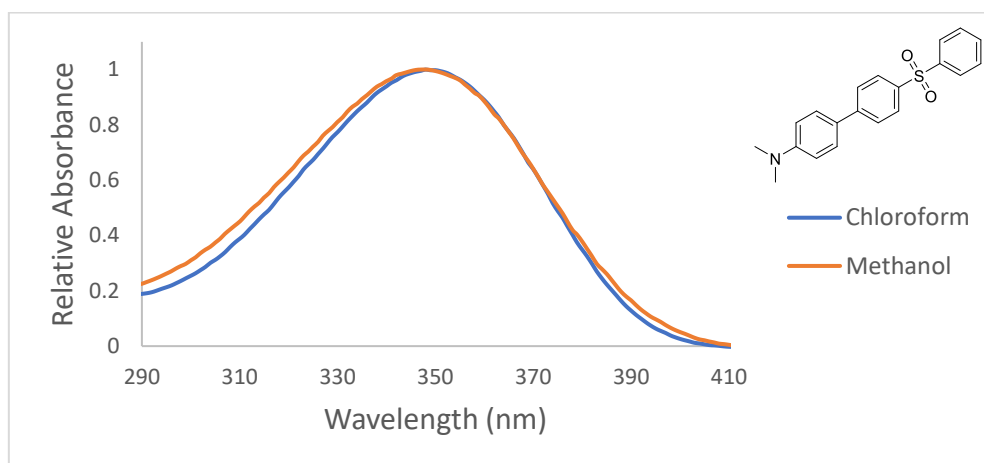


Figure A444 (b). Effect of solvent on absorbance λ_{\max} for biaryl **138**. Absorbance λ_{\max} values of 348 and 347 nm were found using chloroform and methanol as solvent, respectively, using a 17.86 μM solution in both cases.

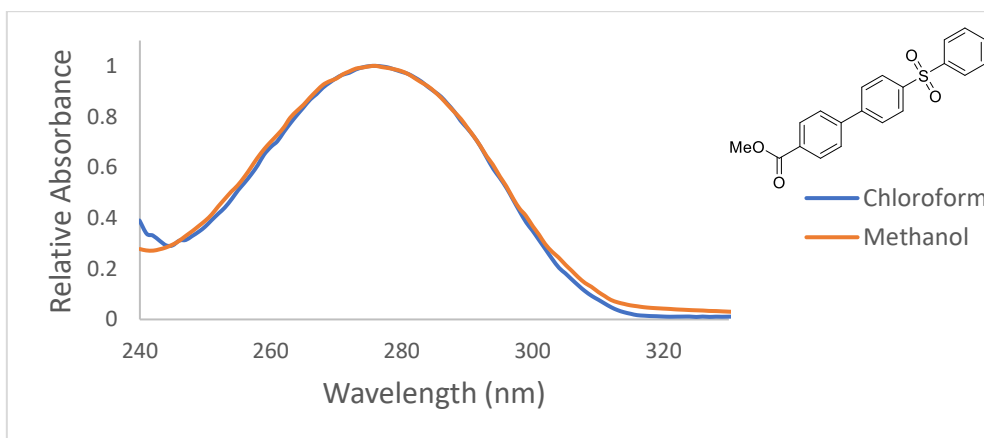


Figure A444 (c). Effect of solvent on absorbance λ_{\max} for biaryl **139**. Absorbance λ_{\max} values of 281 and 279 nm were found using chloroform and methanol as solvent, respectively, using a 17.86 μM solution in both cases.

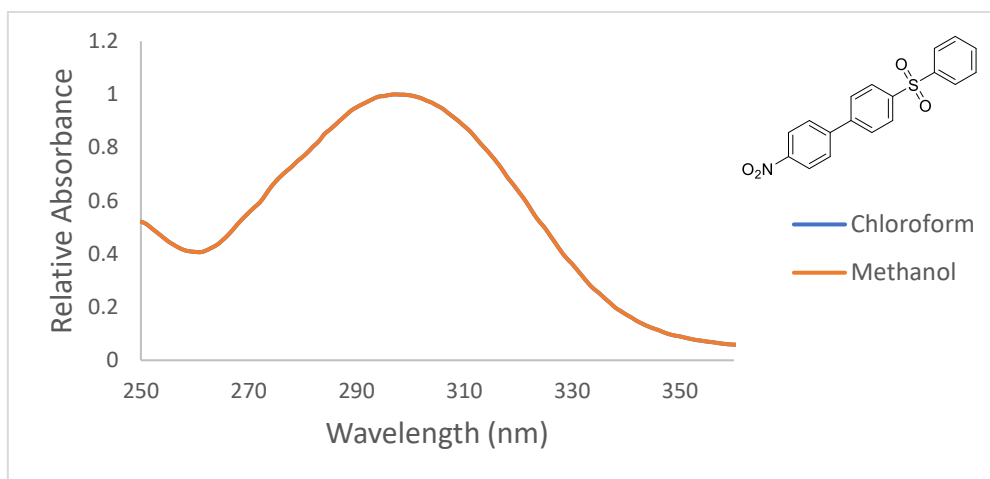


Figure A444 (d). Effect of solvent on absorbance λ_{\max} for biaryl **140**. An absorbance λ_{\max} value of 297 nm was found using both chloroform and methanol as the solvent, using a 17.86 μM solution in both cases.

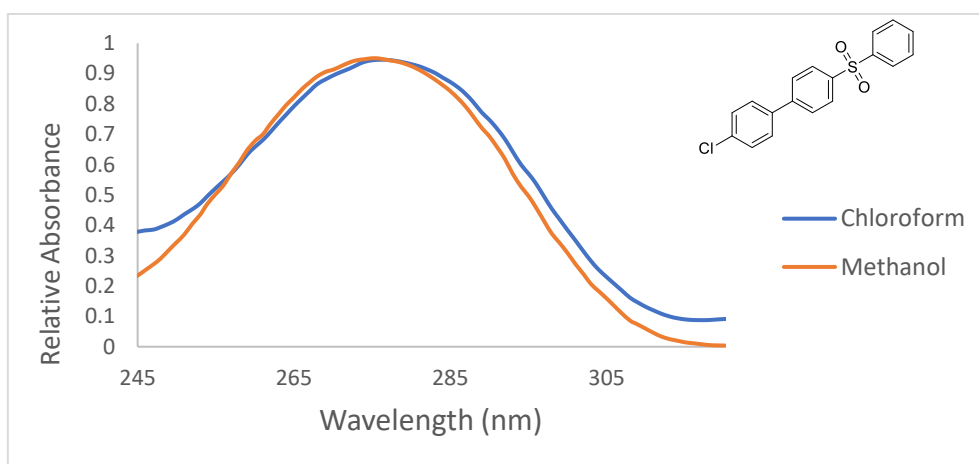


Figure A444 (e). Effect of solvent on absorbance λ_{\max} for biaryl **141**. Absorbance λ_{\max} values of 276 and 275 nm were found using chloroform and methanol as solvent, respectively, using a 17.86 μM solution in both cases.

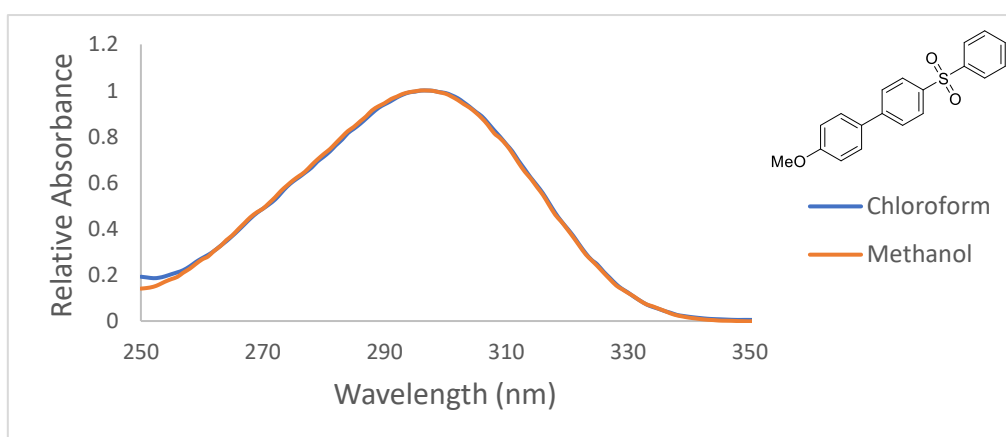


Figure A444 (f). Effect of solvent on absorbance λ_{\max} for biaryl **142**. An absorbance λ_{\max} value of 297 nm was found using both chloroform and methanol as the solvent, using a 17.86 μM solution in both cases.

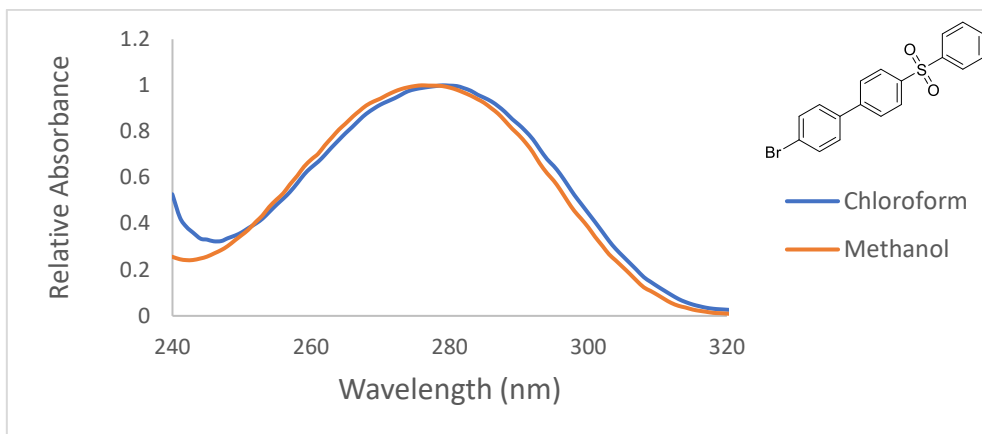


Figure A444 (g). Effect of solvent on absorbance λ_{\max} for biaryl **143**. Absorbance λ_{\max} values of 278 and 277 nm were found using chloroform and methanol as solvent, respectively, using a 17.86 μM solution in both cases.

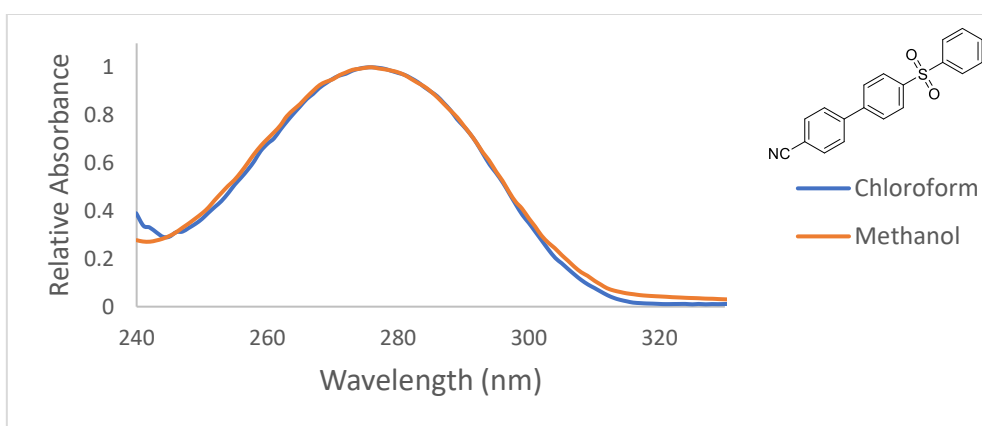


Figure A444 (h). Effect of solvent on absorbance λ_{\max} for biaryl **144**. An absorbance λ_{\max} value of 276 nm was found using both chloroform and methanol as solvent, using a 17.86 μM solution in both cases.

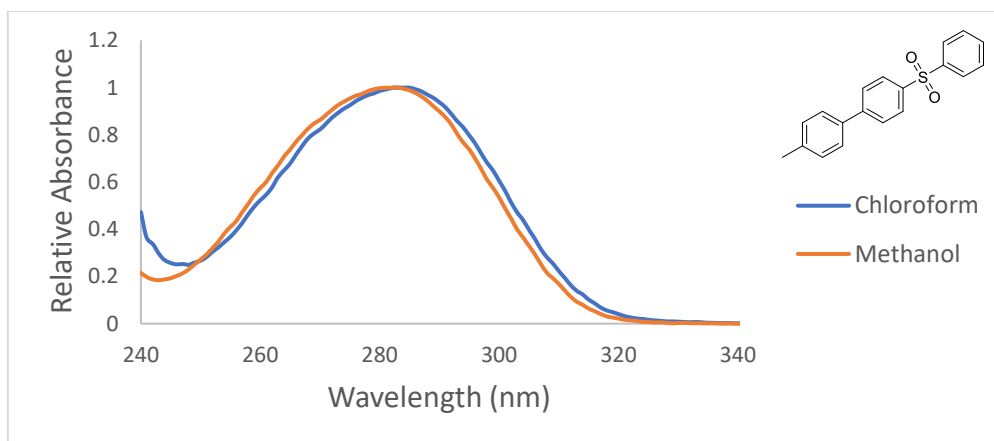


Figure A444 (i). Effect of solvent on absorbance λ_{\max} for biaryl **145**. Absorbance λ_{\max} values of 284 and 283 nm were found using chloroform and methanol as solvent, respectively, using a 17.86 μM solution in both cases.

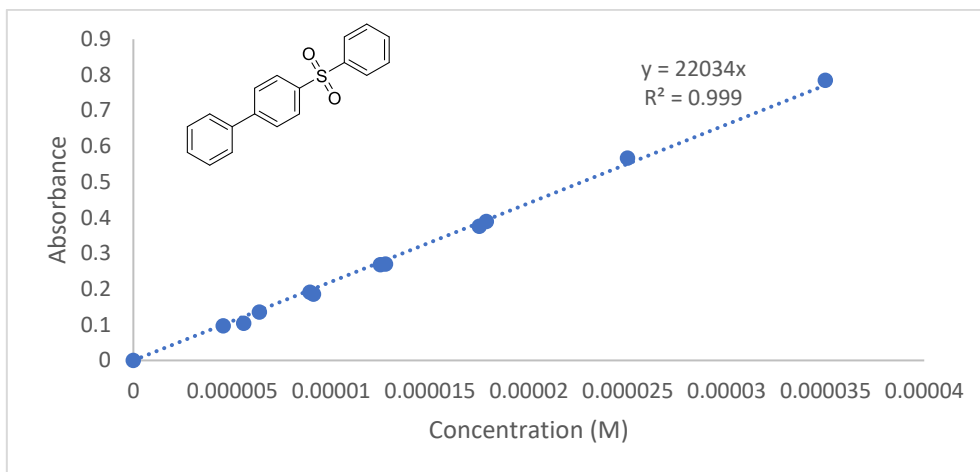


Figure A445 (a). Graph of UV-absorbance intensity versus concentration, using data collected from the dilution of both the 35 μM and 17.5 μM solutions. The molar extinction coefficient (ϵ) for biaryl **46** was found to be 22034 $\text{M}^{-1} \text{cm}^{-1}$

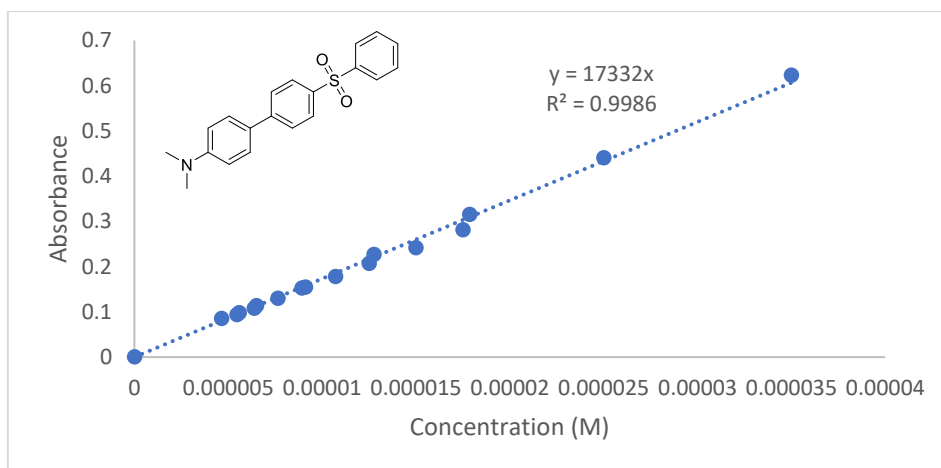


Figure A445 (b). Graph of UV-absorbance intensity versus concentration, using data collected from the dilution of both the 35 μM and 17.5 μM solutions. The ϵ for biaryl **138** was found to be 17332 $\text{M}^{-1} \text{cm}^{-1}$

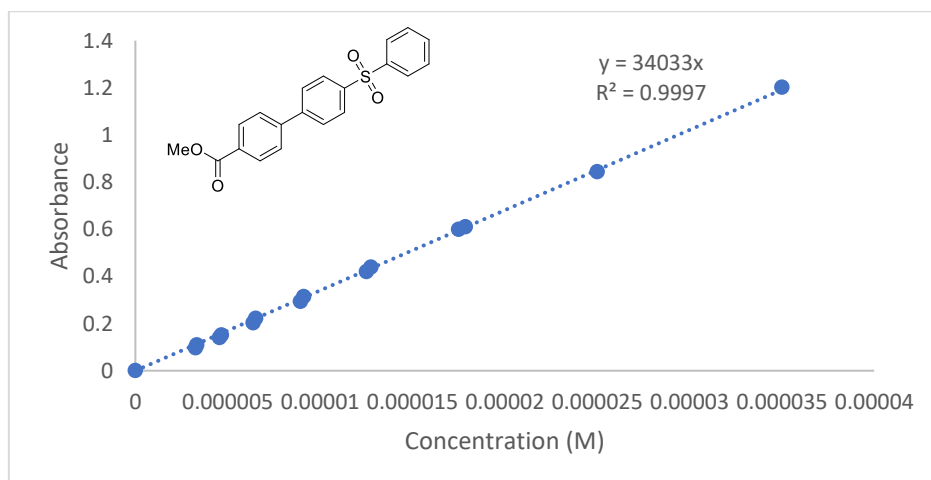


Figure A445 (c). Graph of UV-absorbance intensity versus concentration, using data collected from the dilution of both the 35 μM and 17.5 μM solutions. The ϵ for biaryl **139** was found to be 34033 $\text{M}^{-1} \text{cm}^{-1}$

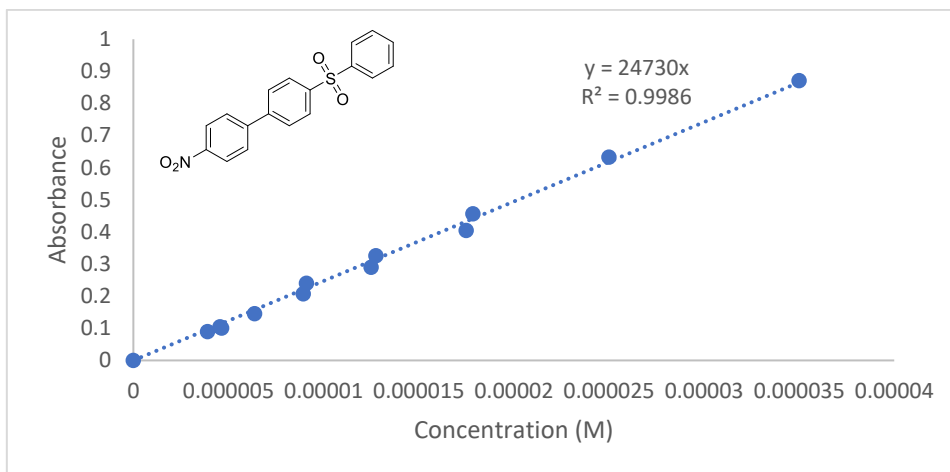


Figure A445 (d). Graph of UV-absorbance intensity versus concentration, using data collected from the dilution of both the 35 μM and 17.5 μM solutions. The ϵ for biaryl **140** was found to be 24730 $\text{M}^{-1} \text{cm}^{-1}$

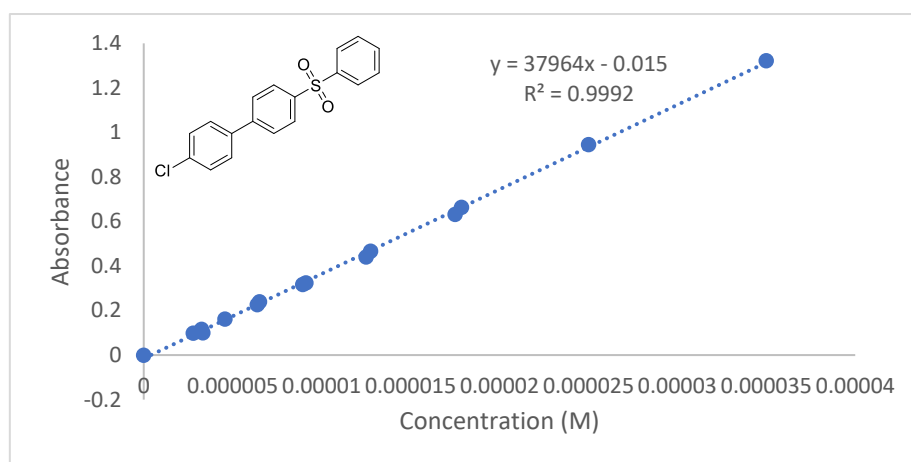


Figure A445 (e). Graph of UV-absorbance intensity versus concentration, using data collected from the dilution of both the 35 μM and 17.5 μM solutions. The ϵ for biaryl **141** was found to be 37964 $\text{M}^{-1} \text{cm}^{-1}$

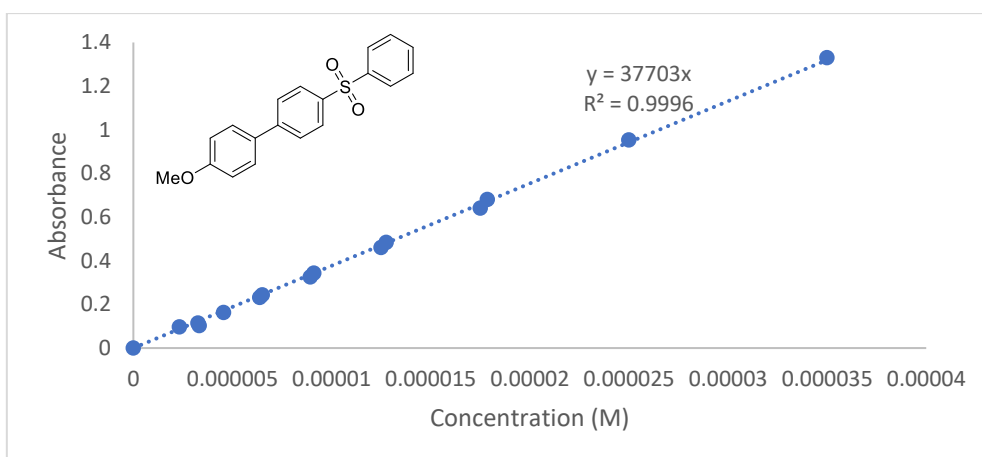


Figure A445 (f). Graph of UV-absorbance intensity versus concentration, using data collected from the dilution of both the 35 μM and 17.5 μM solutions. The ϵ for biaryl **442** was found to be 37703 $\text{M}^{-1} \text{cm}^{-1}$

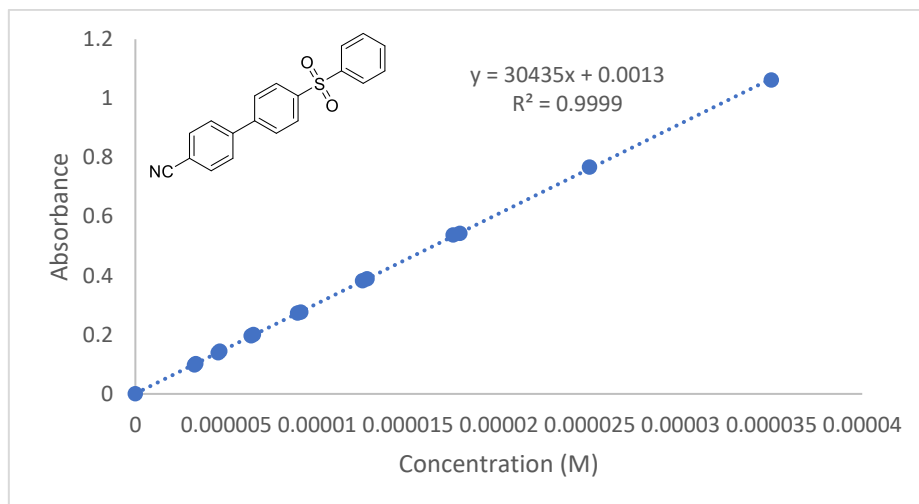


Figure A445 (g). Graph of UV-absorbance intensity versus concentration, using data collected from the dilution of both the 35 μM and 17.5 μM solutions. The ϵ for biaryl **144** was found to be $30435 \text{ M}^{-1} \text{ cm}^{-1}$

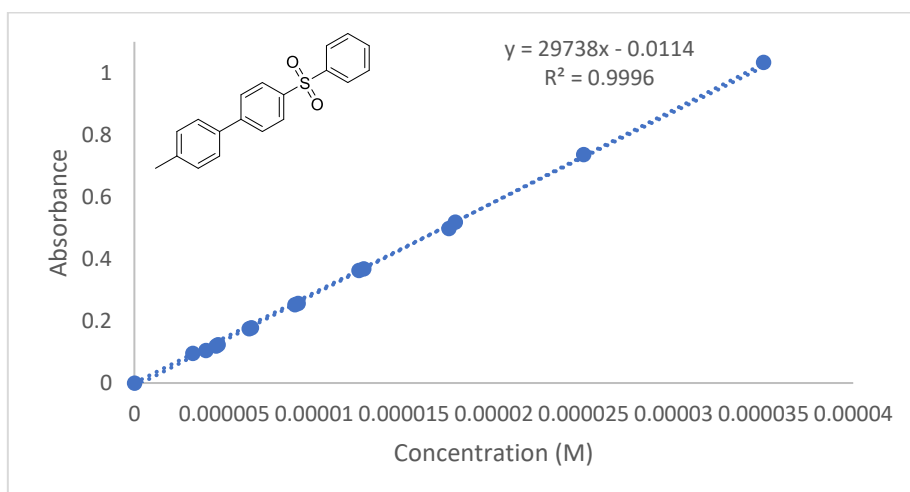


Figure A445 (h). Graph of UV-absorbance intensity versus concentration, using data collected from the dilution of both the 35 μM and 17.5 μM solutions. The ϵ for biaryl **145** was found to be $29738 \text{ M}^{-1} \text{ cm}^{-1}$

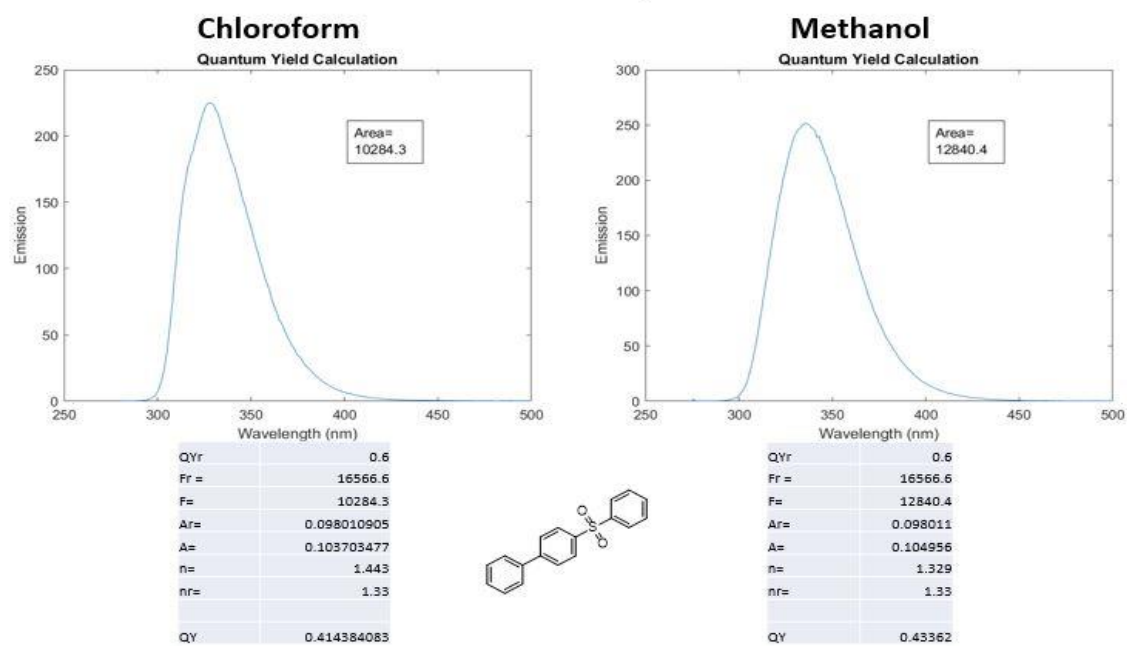


Figure A446 (a). Data relevant to the calculation of quantum yield of biaryl **46** in chloroform (left) and methanol (right). A quantum yield of 0.41 and 0.43 was recorded in chloroform and methanol, respectively, using a 4.56 μM and 2.85 μM solution, respectively.

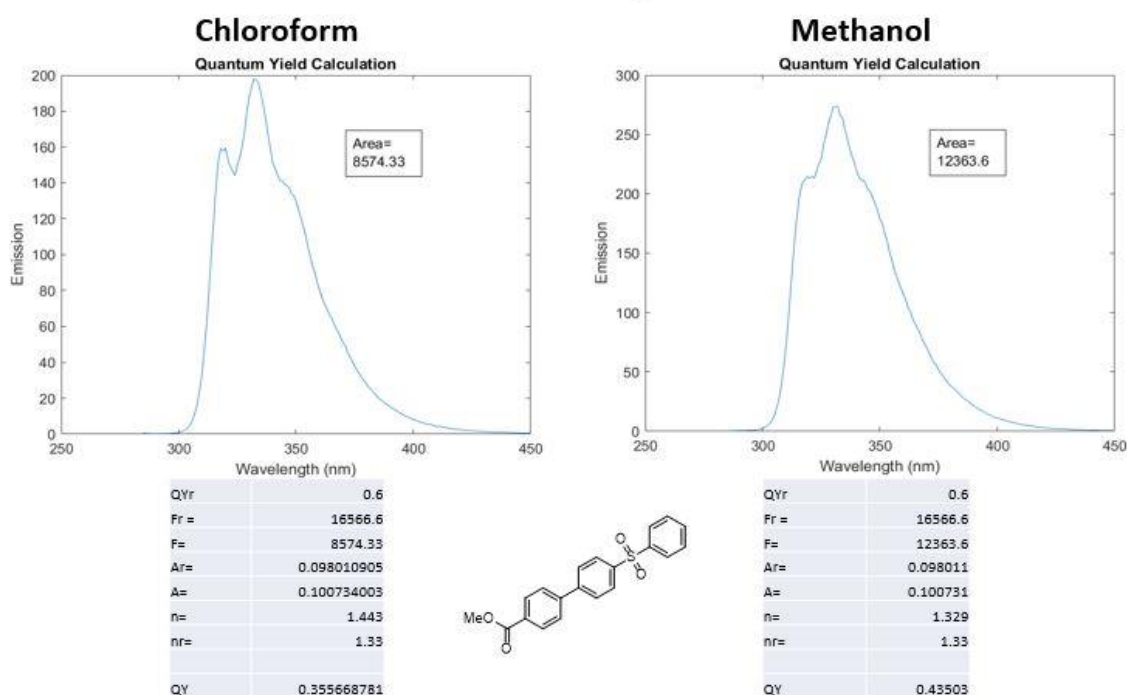


Figure A446 (b). Data relevant to the calculation of quantum yield of biaryl **139** in chloroform (left) and methanol (right). A quantum yield of 0.36 and 0.44 was recorded in chloroform and methanol, respectively, using a 3.32 μM solution in both cases.

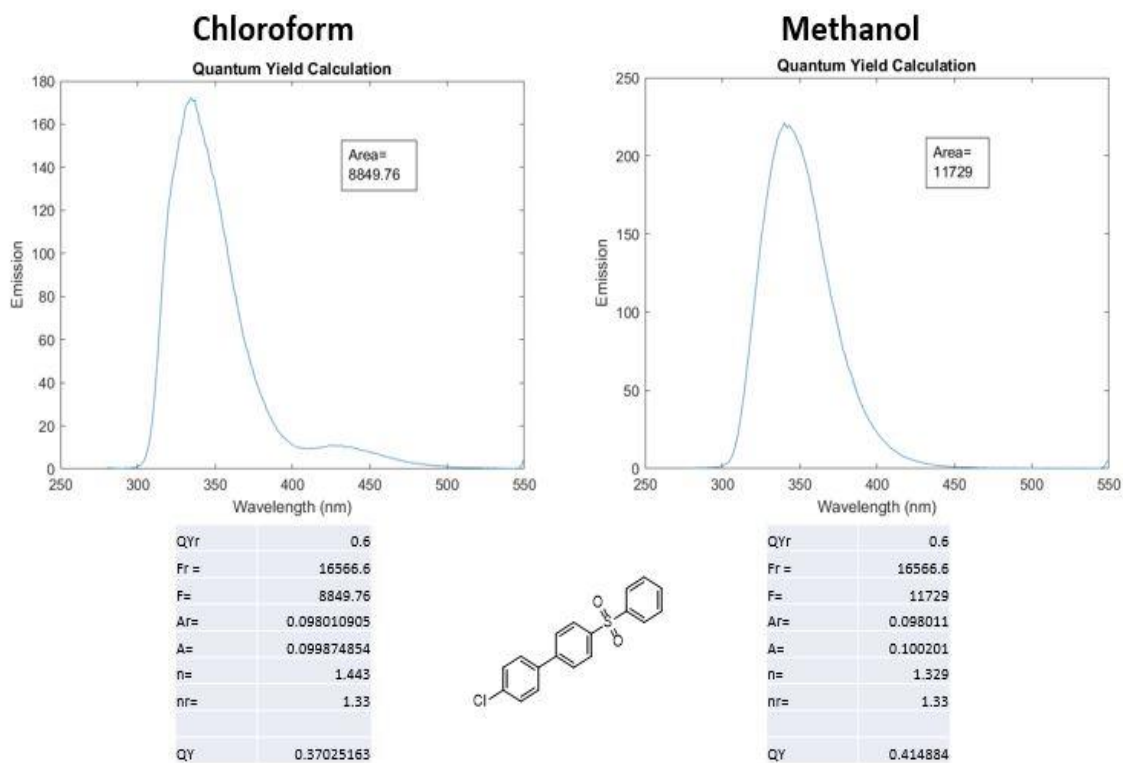


Figure A446 (c). Data relevant to the calculation of quantum yield of biaryl **141** in chloroform (left) and methanol (right). A quantum yield of 0.37 and 0.41 was recorded in chloroform and methanol, respectively, using a 2.79 μM and 2.85 μM solution, respectively.

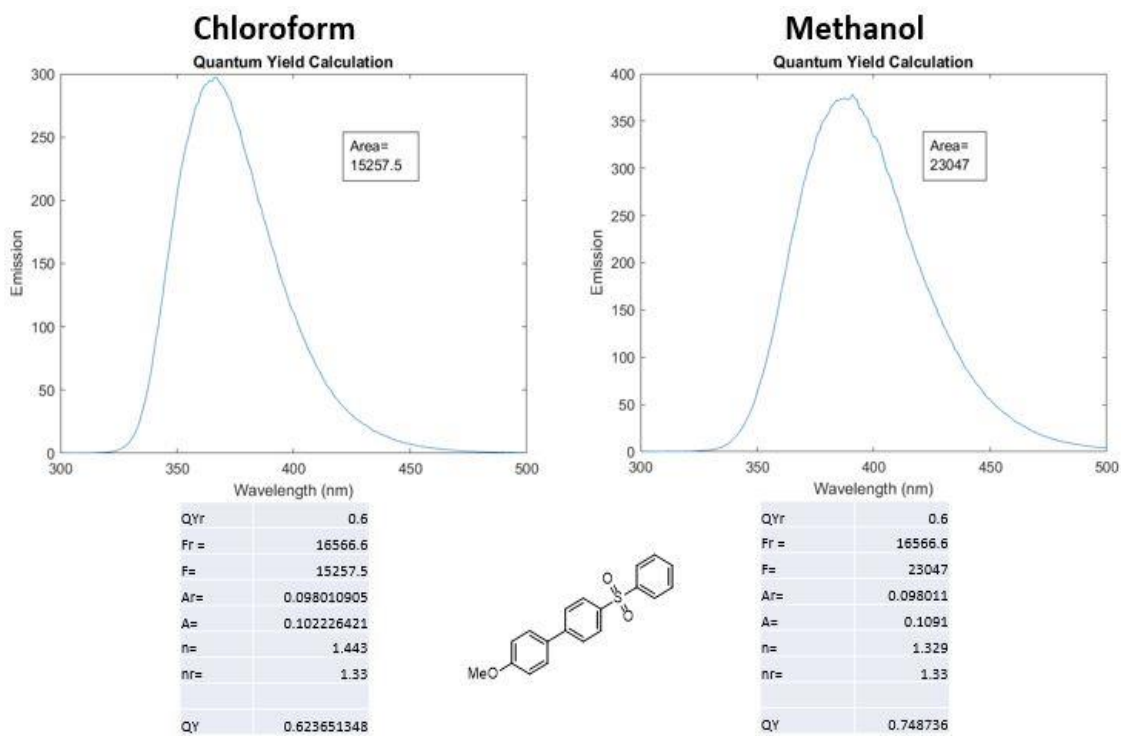


Figure A446 (d). Data relevant to the calculation of quantum yield of biaryl **142** in chloroform (left) and methanol (right). A quantum yield of 0.62 and 0.75 was recorded in chloroform and methanol, respectively, using a 2.32 μM and 4.65 μM solution, respectively.

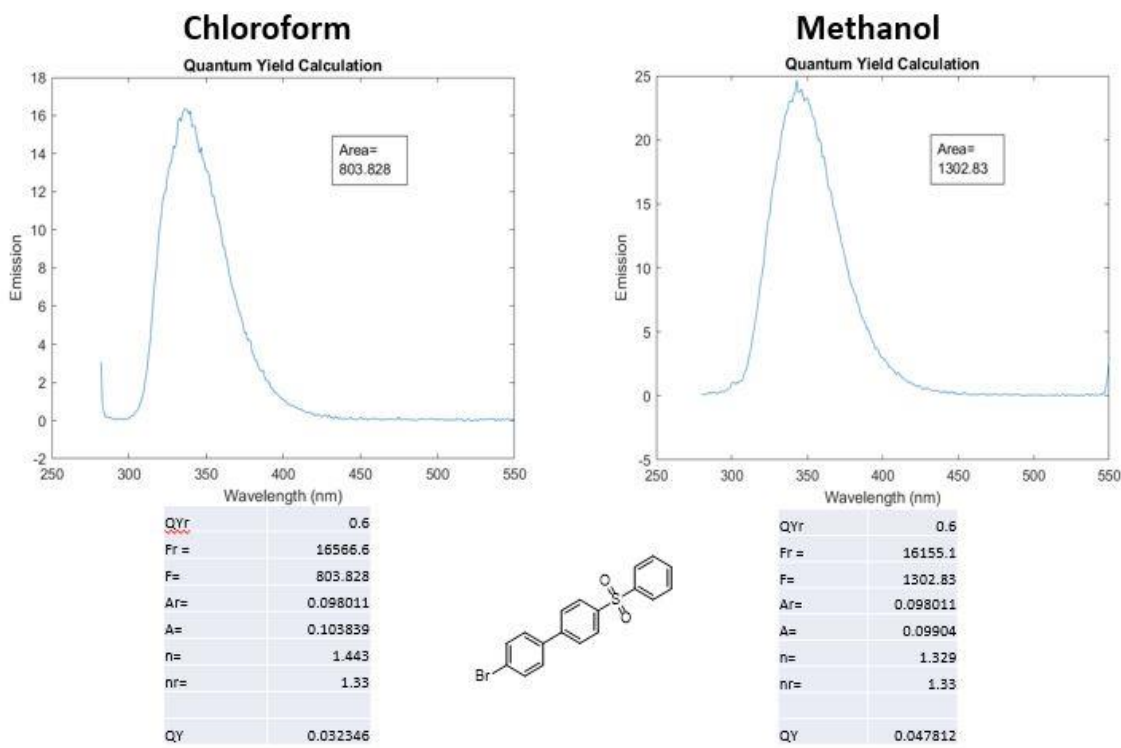


Figure A446 (e). Data relevant to the calculation of quantum yield of biaryl **143** in chloroform (left) and methanol (right). A quantum yield of 0.032 and 0.048 was recorded in chloroform and methanol, respectively, using a 3.32 μM and 3.98 μM solution, respectively.

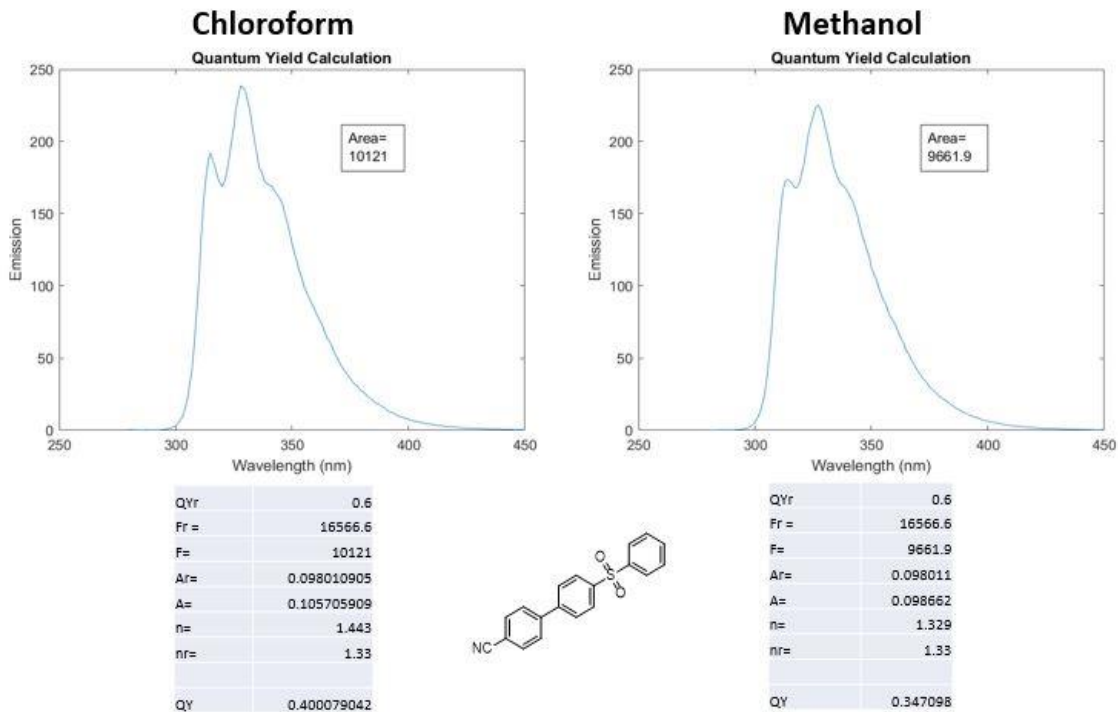


Figure A446 (f). Data relevant to the calculation of quantum yield of biaryl **144** in chloroform (left) and methanol (right). A quantum yield of 0.40 and 0.35 was recorded in chloroform and methanol, respectively, using a 3.25 μM and 2.85 μM solution, respectively.

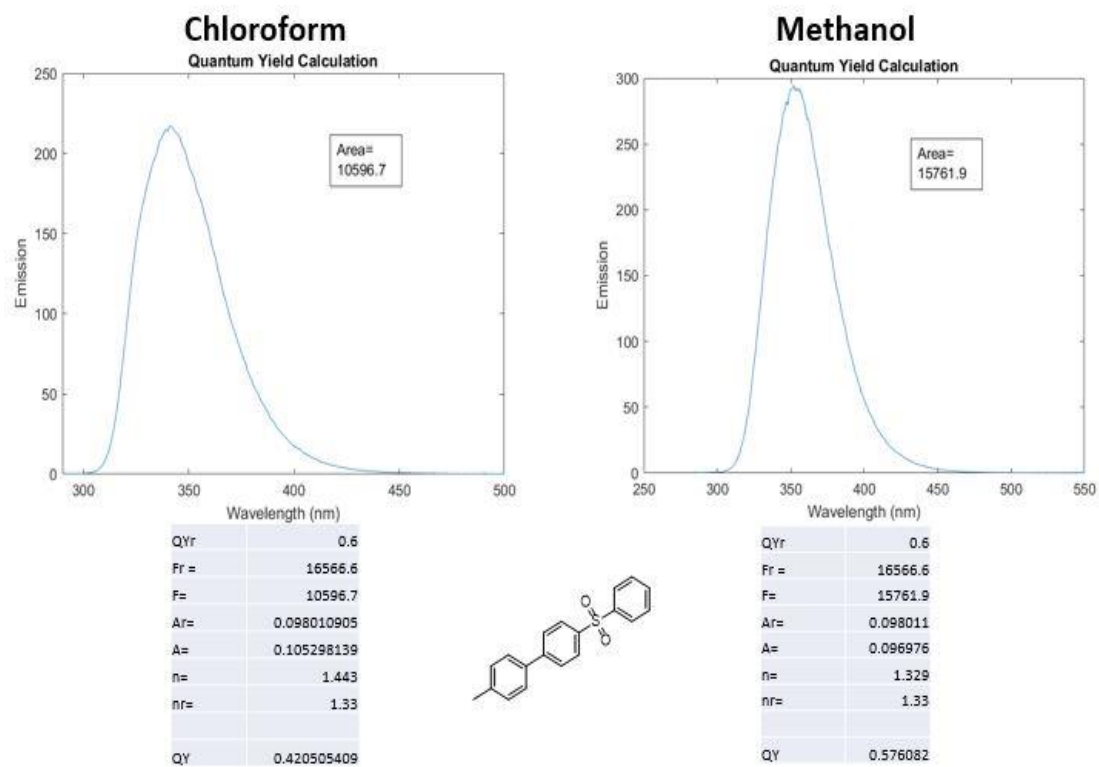
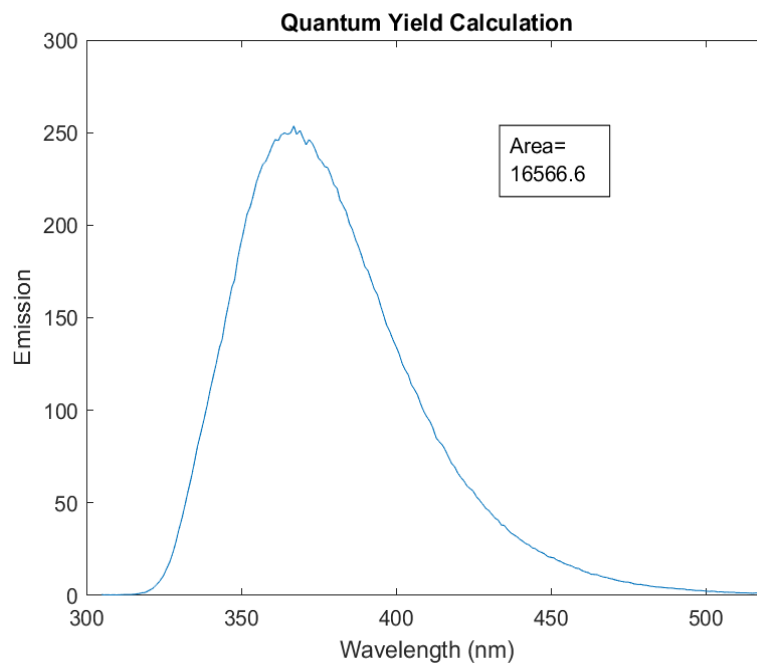
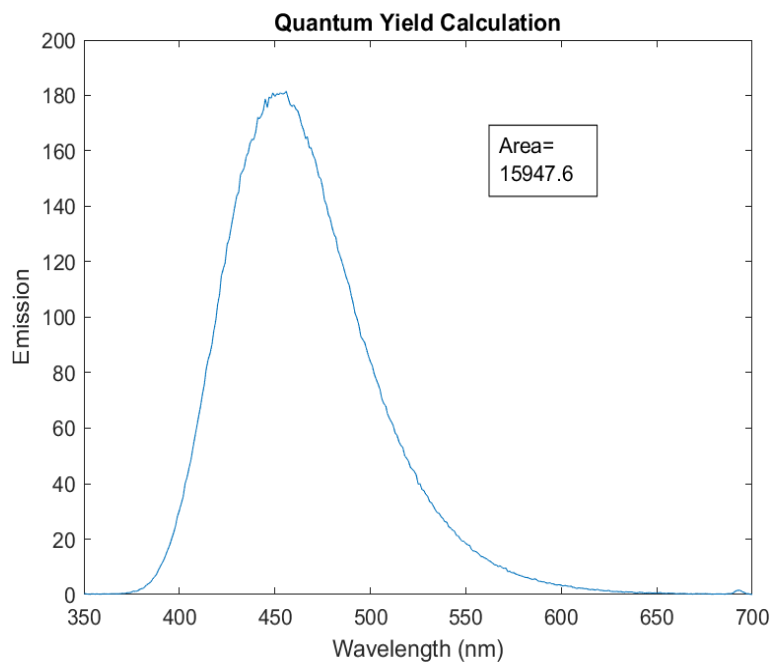


Figure A446 (g). Data relevant to the calculation of quantum yield of biaryl **145** in chloroform (left) and methanol (right). A quantum yield of 0.42 and 0.58 was recorded in chloroform and methanol, respectively, using a 3.25 μM and 3.32 μM solution, respectively.



QYr	0.54
Fr =	15947.6
F=	16566.6
Ar=	0.100757472
A=	0.098010905
n=	1.33
nr=	1.33
QY	0.64075524
Lit QY for 2-aminopyridine	0.6

Figure A447 (a). Data relevant to the calculation of quantum yield of the standard 2-aminopyridine, using a 13.28 μM solution, for which quinine sulfate at a concentration of 9.49 μM was used as the reference standard to ensure accuracy of the method employed.



QYr	0.6
Fr =	16566.6
F=	15947.6
Ar=	0.098010905
A=	0.100757472
n=	1.33
nr=	1.33
QY	0.561836997
Lit for QS	0.54

Figure A447 (b). Data relevant to the calculation of quantum yield of the standard quinine sulfate dihydrate, using a 9.49 μM solution, for which 2-aminopyridine at a concentration of 13.28 μM was used as the reference standard to ensure accuracy of the method employed.

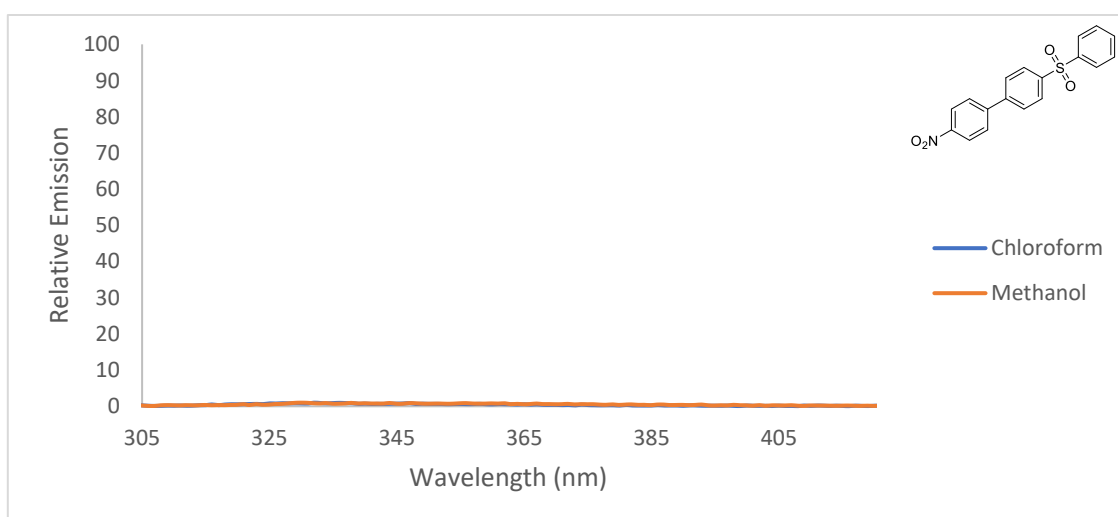


Figure A448. Effect of solvent on emission λ_{max} for biaryl **140**. An emission λ_{max} could not be found due to low emission intensity when either chloroform or methanol were used as the solvent. A 4.65 μM solution of **140** in both cases was used.